To the Graduate Council:

I am submitting herewith a dissertation written by Arthur James Merschat entitled "Assembling the Blue Ridge and Inner Piedmont: Insights into the nature and timing of terrane accretion in the southern Appalachian orogen from geologic mapping, stratigraphy, kinematic analysis, petrology, geochemistry, and modern geochronology." I have examined the final electronic copy of the dissertation for form and content and recommend that it be accepted in partial fulfillment of the requirements for the degree of Doctor of Philosophy with a major in Geology.

Robert D. Hatcher, Jr., Major Professor

We have read this dissertation and
recommend its acceptance:

Theodore C. Labotka

Calvin F. Miller

John B. Wilkerson

J. Wright Horton, Jr.

Accepted for the Council:

Carolyn R. Hodges
Vice Provost and Dean of the Graduate School

(Original Signatures are on file with official student records.)

ASSEMBLING THE BLUE RIDGE AND INNER PIEDMONT: INSIGHTS INTO THE NATURE AND TIMING OF TERRANE ACCRETION IN THE SOUTHERN APPALACHIAN OROGEN FROM GEOLOGIC MAPPING, STRATIGRAPHY, KINEMATIC ANALYSIS, PETROLOGY, GEOCHEMISTRY, AND MODERN GEOCHRONOLOGY

A Dissertation
Presented for the
Doctor of Philosophy Degree
The University of Tennessee

Arthur James Merschat
August, 2009

DEDICATION

This dissertation is dedicated to my parents,
Carl and Holley Merschat,
and wife and son,
Carrie and James Evan.
Thank you for the endless love, encouragement, and support.

ACKNOWLEDGMENTS

Foremost, I would like to thank my advisor Dr. Robert D. Hatcher, Jr., for his scientific and porfessional guidance over the past nine years. His emphasis on geologic mapping and field-based geologic studies, willingness to incorporate new ideas and techniques, enthusiasm for Appalachian geology, and open-door policy have prFoundly influenced me. My committee members Drs. Theodore Labotka, Calvin Miller, John Wilkerson, and Wright Horton are thanked for their discussions about geology, thorough reviews and comments, and for being patient as proposed dates to finish came and went. Finally, no Hatchery thesis or dissertation is complete or correct with out expressing my great appreciation to Nancy "Damama" Meadows, who truly lives up to her name. She keeps the Hatchery students in line; edits early drafts, provides pep talks and interesting lunch conversations, maintains an endless bowl of candy (I have tested its limits), and on a few rare occasions she even provided a bandage.

For all the past and present Hatchery students I have enjoyed the friendship and discussions of Appalachian geology. It is a long list: Jay Kalbas, Milan Heath, David Settles, Camilo Montes, Chris Whisner, Jennifer Whisner, Brendan Bream, Jonathan Evenick, John Bultman, Ryan Thigpen, Neil Whitmer, Crystal Wilson, Don Stahr, Shawna Cyphers, Mary Varnell, Heather Byars, William Gilliam, Brittany Davis, Matt Heubner, and Philip Derryberry. Special thanks to Jonathan Evenick for the after-lunch football throwing sessions, Brendan Bream (my academic big brother) for his thoughtful discussions of Appalachian geology and reassuring insight, and fellow Blue Ridge mappers Don Stahr and Shawna Cyphers for numerous hours of discussion of Blue Ridge geology.

I would also like to acknowledge several other individuals outside the University of Tennessee for their help, support, discussions, and encouragement. Joe Wooden and Frank Mazdab at the SUMAC SHRIMP lab are greatly appreciated for their time, instruction, and assistance using the SHRIMP. Chris Fisher is thanked for orchestrating two marathon zircon separation sessions. I would like to thank two of my previous professors from Appalachian State University, Fred Webb and Loren Raymond, for always encouraging me to continue doing field work. Loren is also greatly appreciated for his many discussions of Blue Ridge and Inner Piedmont geology, and his excellent wine selections. Richard Harrison, Wright Horton, Scott Southworth, Greg Walsh, and Michelle Alexander of the U.S. Geological Survey Eastern Geology and Climate Center are greatly appreciated for patiently answering numerous questions on everything

from geology to travel authorizations. Many former and present members of the North Carolina Geological Survey are acknowledged for discussions about North Carolina geology including Leonard Wiener, Carl Merschat, Mark Carter, Bart Cattanach, Ken Gillon, and Rick Wooten. Leonard Wiener is also thanked for his tough questions, and bison feed (day-old delicious breads, muffins, and other bakery treats) he provided on several field reviews.

Research for this dissertation was supported by the U.S. Geological Survey National Cooperative Geologic Mapping Program EDMAP awards 05HQAG00004 and 06HQAG0056 to Robert D. Hatcher, Jr., University of Tennessee Science Alliance Center of Excellence, and U. S. Geological Survey Student Career Experience Program.

Finally, I would like to thank my family: my wife and son, Carrie and James Evan; parents, Carl and Holley Merschat; and brother, Michael Merschat. This dissertation would not have been completed without their support, love, and encouragement.

Thank you.

ABSTRACT

Detailed geologic mapping, SHRIMP U-Pb zircon geochronology, geochemistry, petrology, and structural and kinematic analyses were applied to decipher the structure, tectonic heredity, and Paleozoic accretionary history of suspect terranes of the southern Appalachian Blue Ridge (BR) and Inner Piedmont (IP). Detailed geologic mapping in the Waynesville and Sam Knob 7.5-minute quadrangles recognized the Great Balsam Mountains window cored by sillimanite I and II zone Dahlonega gold belt rocks, overthrust by migmatitic biotite gneiss of the Cartoogechaye terrane to the northwest, and migmatitic Tallulah Falls Formation of the Tugaloo terrane to the southeast. Suspect terranes of the BR and IP consist of peri-Laurentian and mixed Laurentian and peri-Gondwanan heredities and were accreted to the Laurentian margin during the Taconian, 465–450 Ma, and Neoacadian, 365–340 Ma, orogenies. Detrital zircon populations of 1.3–0.9 Ga, 1.5–1.3 Ga, and 750–700 Ma from the Cartoogechaye, Cowrock, Dahlonega gold belt, and Tugaloo terranes indicate a dominantly Laurentian provenance. Minor Paleoproterozoic populations in these terranes suggest input from distal terranes of the Laurentian mid-continent or the Amazonian craton. Detrital Paleozoic zircons, 460–430 Ma, occur only in samples from the Cat Square terrane and Smith River allochthon. Ordovician and 600–500 Ma detrital zircons from the Cat Square terrane document the first occurrence of peri-Gondwanan material deposited in a convergent setting between Laurentia and the approaching Carolina superterrane during the Late Silurian to Early Devonian. Palinspastic reconstruction of the Cat Square basin suggests a paleogeographic location in the Pennsylvania embayment and links deformation in the crystalline core with progradation of the Devonian clastic wedge.

Metamorphic zircons from central BR terranes yield U-Pb ages of 465–450 Ma, and delimit accretion to the Laurentian margin and metamorphism to amphibolite and granulite facies during the Taconian orogeny. U-Pb ages of metamorphic zircons from the IP yield ages of 392–344 Ma corresponding to upper amphibolite facies metamorphism associated with the Devonian–Mississippian collision of the Carolina superterrane during the Neoacadian orogeny. The IP and parts of the eastern BR flowed west and southwest out from beneath the overthrust Carolina superterrane as an orogenic channel.

TABLE OF CONTENTS

Introduction 1
REFERENECES CITED 4

PART I

Geology of the Waynesville and Sam Knob 7.5-minute quadrangles, Haywood, Jackson, and Transylvania Counties, North Carolina 5
ABSTRACT 6
INTRODUCTION 7
LOCATION 11
GENERAL GEOLOGIC SETTING 13
LITHOSTRATIGRAPHY 17
SURFICIAL UNITS 27
METAMORPHISM 32
STRUCTURE 43
DEFORMATIONS 52
CONCLUSIONS 55
REFERENCES CITED 58

PART II

Summary of the Geology of part of the Blue Ridge of southwestern North Carolina and northeastern Georgia: Integrating detailed geologic mapping and SHRIMP U-Pb zircon geochronologic studies 66
ABSTRACT 67
INTRODUCTION 68
TECTONIC SETTING 75
TERRANES AND LITHOSTRATIGRAPHY 76
PROVENANCE 90
MAGMATISM 91
METAMORPHISM 95
STRUCTURE 102
TECTONIC SUMMARY 112
REFERENCES CITED 118

PART III

Thrice-Baked Appalachia: Delimiting the temporal and spatial distribution of Paleozoic metamorphism in the southern Appalachian Blue Ridge and Inner Piedmont with SHRIMP U-Pb ages of metamorphic zircon 131

ABSTRACT 132
INTRODUCTION 133
TECTONIC SETTING 134
METAMORPHIC ISOGRAD MAP OF THE SOUTHERN APPALACHIANS ... 140
SAMPLING AND METHODOLOGY 145
SAMPLE DESCRIPTION AND ZIRCON MORPHOLOGY 146
RESULTS 149
DISCUSSION: TECTONIC IMPLICATIONS 154
TECTONIC MODELS 173
CONCLUSIONS 175
REFERENCES CITED 177

PART IV

Detrital zircon geochronology and provenance of southern Appalachian Blue Ridge and Inner Piedmont crystalline terranes 192

ABSTRACT 193
INTRODUCTION 194
REGIONAL GEOLOGIC SETTING 196
METHODOLOGY 204
SAMPLE DESCRIPTIONS 206
MAJOR AND TRACE ELEMENT WHOLE-ROCK GEOCHEMISTRY 213
DETRITAL ZIRCON GEOCHRONOLOGY 218
DETRITAL ZIRCON TRACE ELEMENT CONCENTRATIONS 223
AGE OF DEPOSITION 225
PROVENANCE 230
PALEOGEOGRAPHY AND TECTONIC MODELS 238
CONCLUSIONS 244
ACKNOWLEDGMENTS 246
REFERENCES CITED 248

PART V

The Cat Square terrane: Possible Siluro-Devonian remnant ocean basin in the Inner Piedmont, southern Appalachians, USA 264

ABSTRACT 265
INTRODUCTION 266
TECTONIC SETTING 267
CAT SQUARE TERRANE 271
SILURO-DEVONIAN CAT SQUARE REMNANT OCEAN BASIN 274
TECTONIC SYNTHESIS 282
CONCLUSIONS 282
ACKNOWLEDGMENTS 283
REFERENCES CITED 285

PART VI

The Appalachian Inner Piedmont: An Exhumed Strike-Parallel, Tectonically Forced Orogenic Channel 292

ABSTRACT 293
INTRODUCTION 294
TECTONIC SETTING 296
ATTRIBUTES OF THE INNER PIEDMONT: FACILITATING CONDITIONS OF MID-PALEOZOIC DUCTILE FLOW 299
APPLICATION OF THE CHANNEL FLOW CONCEPT TO THE INNER PIEDMONT 315
CONCLUSIONS 321
REFERENCES CITED 324

PART VII

Inner Piedmont Geo-traverse from the Brushy Mountains to Lincolnton, North Carolina: Architecture of the Cat Square and Tugaloo Terranes 336

INTRODUCTION 337
TECTONIC SETTING AND ATTRIBUTES OF THE NORTHERN IP 340
METAMORPHISM 349
INNER PIEDMONT TERRANES: CONTRASTING LITHOSTRATIGRAPHIES AND MAGMATISM 352
NATURE OF THE TUGALOO-CAT SQUARE CONTACT: THE BRINDLE CREEK FAULT 358
TECTONIC SYNTHESIS 372

ACKNOWLEDGMENTS 379
REFERENCES CITED 380

APPENDIX I
Structural Measurements and Outcrop Descriptions from the Waynesville 7.5-minute Quadrangle 391

APPENDIX II
Structural Measurements and Outcrop Descriptions from the Sam Knob 7.5-minute Quadrangle 411

APPENDIX III
SHRIMP-RG U-Pb Analyses and Trace Element Concentrations of Detrital Zircons 437

Vita 455

LIST OF TABLES

PART I

Table 1–1. U-Pb SHRIMP-RG analytical data for zircons from trondhjemite. 28
Table 1–2. Description of recognized landslide deposits..... 33
Table 1–3. Summary of major Paleozoic and younger deformational events 45

PART II

Table 2–1. Sources of compiled geologic maps 77
Table 2–3. Comparison of thrust sheets, terranes and lithostratigraphic 82
Table 2–4. SHRIMP U-Pb zircon ages 85
Table 2–5. Compilation of recent U-Pb zircon ages of Paleozoic plutons 87
Table 2–6. Compiled ages of detrital zircons..... 92
Table 2–7. U-Pb ages of zircon, monazite, and monazite. 100
Table 2–8. Summary of major Paleozoic and younger deformational events 103

PART III

Table 3–1. Sample locations and descritpions. 137
Table 3–2. Ion microprobeU-Pb analayses of metamorphic zircons. 150
Table 3–2. Continued. 151

PART IV

Table 4–1. Sample descriptions and locations. 207
Table 4–2. Whole-rock chemical analyses 214
Table 4–3. Whole-rock trace element analyses of metasedimentary samples. 214

PART VI

Table 6–1. Hypothetical subduction zone parameters required for different dip*.. 320

PART VII

Table 7–1. Tectonic summary for the northern IP. 341
Table 7–2. Summary of recent SHRIMP U-Pb. 353
Table 7–2. Continued. 354
Table 7–3. Locations and descriptions of amphibolite samples. 366
Table 7–4. Whole-rock major and trace element data 368
Table 7–5. U-Pb SHRIMP-RG analytical data for zircons from the Reepsville ... 373

LIST OF FIGURES

PART I

Figure 1–1. Simplified tectonic map of part of the Blue Ridge 8
Figure 1–2. Simplified geologic map of the Waynesville and Sam Knob 9
Figure 1–2. Continued. 10
Figure 1–3. Shaded relief map of the Great Balsam Mountains 12
Figure 1–4. Field photographs of typical rock types 19
Figure 1–5. Typical field exposure of the magnetite-bearing 25
Figure 1–6. Concordia diagrams and weighted average 29
Figure 1–7. SHRIMP U-Pb analyses of a fine-grained trondhjemite 30
Figure 1–8. Metamorphic isograd map of the Waynesville and Sam Knob 7 35
Figure 1–9. Photomicrographs of different mineral assemblages 37
Figure 1–10. CL images of selected zircon with metamorphic rims 42
Figure 1–11. Form-line map of S_2 foliation 46
Figure 1–12. Equal-area, lower-hemisphere stereonets of poles to regional S_2 47
Figure 1–13. Linear mesoscopic structures 49
Figure 1–14. Equal-area, lower-hemisphere stereonets of measured mesoscopic fold axes 50

PART II

Figure 2–1. Simplified tectonic map of the southern Appalachians 69
Figure 2–2. Simplified geologic map of the part of the western, central, and eastern Blue Ridge 71
Figure 2–2. Continued. 73
Figure 2–3. Simplified lithostratigraphy and terranes 78
Figure 2–4. Stratigraphic column of western, central and eastern Blue Ridge 83
Figure 2–5. Compiled metamorphic isograd map 97
Figure 2–6. U-Pb ages of metamorphic zircon 101
Figure 2–7. Graph of tectonothermal events 113

PART III

Figure 3–1. Simplified tectonic map of the southern Appalachians 135
Figure 3–2. Metamorphic isograd map of the southern Appalachian 141
Figure 3–3. CL images of various metamorphic zircon rim morphologies 148
Figure 3–4. Plots of SHRIMP U-Pb metamorphic zircon data. 152
Figure 3–5. Metamorphic isograd map of the Blue Ridge and Inner Piedmont 155
Figure 3–6. Plots of thermochronometers age versus distance 157
Figure 3–7. Comparison of Ordovician to Silurian U-Pb ages 158
Figure 3–8. Comparison of Silurian to Mississippian U-Pb ages 162
Figure 3–9. Metamorphic domains 164

PART IV

Figure 4–1. Simplified tectonic map of the southern Appalachians 195
Figure 4–2. Tectonic map of part of the Blue Ridge and Inner Piedmont 198

Figure 4–3. Cathodoluminescence images of selected detrital zircons. 209
Figure 4–4. Multi-element variation diagrams of REE 216
Figure 4–5. CIA ternary plot. 216
Figure 4–6. Tectonic discriminant diagrams for graywackes 217
Figure 4–7. Relative probability plots with histograms of U-Pb ages 219
Figure 4–7. Continued. 220
Figure 4–8. Chondrite normalized rare earth element multi-element variation diagrams of zircon. 224
Figure 4–9. Discriminant plots based on Hf, U, and Yb concentrations 226
Figure 4–10. Depositional age based 227
Figure 4–11. Relative probability plots with histograms of U-Pb ages 231
Figure 4–12. Possible source areas 233

PART V

Figure 5–1. Conceptual diagram of a remnant ocean basin 267
Figure 5–2. Simplified tectonic map of the southern Appalachians 268
Figure 5–3. Simplified geologic map of the Cat Square terrane 272
Figure 5–4. Possible palinspastic location of the Inner Piedmont 277
Figure 5–5. Maps representing the sequential tectonic history 280
Figure 5–6. (a) Idealized stratigraphic column of a remnant ocean basin 281

PART VI

Figure 6–1. Simplified tectonic map of the southern Appalachians 297
Figure 6–2. Tugaloo and Cat Square terranes lithologic components. 298
Figure 6–3. Pattern of dominant (S_2) foliation and lineation 301
Figure 6–4. 3D structure of part of the northern IP. 304
Figure 6–5. Folded stromatic migmatite in saprolite 305
Figure 6–6. Ductile flow orientation and shear-sense data 307
Figure 6–7. Mineral stretching lineation and tight fold pattern 308
Figure 6–8. Orientation of mineral stretching lineations and fold hinges. 309
Figure 6–9. Geologic map and orientations of lineations and tight folds 310
Figure 6–10. Neoacadian metamorphic isograd map 311
Figure 6–11. Agmatite (blocky migmatite) in saprolite 313
Figure 6–12. Tectonothermal time line for the Inner Piedmont. 314
Figure 6–13. Comparison of a cross section (a) through part of the Inner Piedmont in North Carolina 317
Figure 6–14. Relationships in 3D 319
Figure 6–15. Composite cross-section cartoon 322

PART VII

Figure 7–1. Index map of the U.S. 338
Figure 7–2. Pattern of dominant (S_2) foliation and lineation 342
Figure 7–3. Simplified geologic maps of (a) northwestern IP 345
Figure 7–4. 3D sturcture of part of the northern Inner Piedmont. 348

Figure 7–5. Metamorphic isograd map of the northern Inner Piedmont 350
Figure 7–6. Simplified detailed geologic map of the South Mountains 356
Figure 7–7. Tectonothermal time line for the Inner Piedmont. 359
Figure 7–8. Simplified detailed geologic map of the Brushy Mountains 361
Figure 7–9. Geologic map and cross section of the Newton window 364
Figure 7–10. Tectonic discriminant diagrams for mafic rocks..... 369
Figure 7–11. Tectonic discrimant diagrams for mafic rocks using REE 370
Figure 7–12. Relative probability plots and histograms of 204-corrected $^{207}Pb/^{206}Pb$ SRHIMP ages of detrital zircons from different IP paragneisses 371
Figure 7–13. Concordia diagrams of 204-corrected SHRIMP U-Pb data from the Reepsville gneiss. 374
Figure 7–14. Possible location of the southern termination of the Brindle 375
Figure 7–15. Maps representing the sequential tectonic history of the Cat Square terrane 377

LIST OF PLATES

Plate 1. Geologic Map of the Waynesville and Sam Knob 7.5-Minute Quadrangles, Haywood, Jackson, and Transylvania Counties, North Carolina ..... *attached*

Plate 2. Station Geologic Map of the Waynesville and Sam Knob 7.5-Minute Quadrangles, Haywood, Jackson, and Transylvania Counties, North Carolina..... *attached*

Plate 3. Geologic map of part of the western, central, and eastern Blue Ridge, southwestern North Carolina and northeastern Georgia ..... *attached*

Plate 4. Geologic Map of the northern half of the Inner Piedmont, NC-SC-GA ..... *attached*

Introduction

Plate tectonics is a theory that describes the interaction of lithospheric plates and explains the motions of continents and smaller landmasses, formation of mountain belts and oceans basins, and the occurrence of most earthquakes and volcanism. Plate tectonics directly or indirectly affects most earth and biological systems and cycles including: magmatism, metamorphism, sedimentation, biological development, and long-term climate patterns. Likewise, this dissertation integrates various techniques and data sets to address the structure and tectonic history of the southern Appalachian Blue Ridge and Inner Piedmont. This research was conducted from 2003–2009 and involved: detailed geologic mapping, compilation of existing detailed geologic maps, structural and kinematic analysis, SHRIMP U-Pb zircon geochronology, metamorphic petrology, geochemistry, and stratigraphy and basin analysis. The dissertation consists of seven parts, each an independent paper that has been or will be submitted to a peer-reviewed journal, USGS report, or is part of a field trip guidebook. The four plates included with the dissertation are geologic maps of the Blue Ridge and Inner Piedmont—the most fundamental data set incorporated in this dissertation—and will accompany the papers. Research for these papers represents both new research conducted for my Ph.D. and a continuation of research from my Master of Science at the University of Tennessee. I have shared writing responsibilities and contributed data for all included papers, guides, and maps, and my contributions are indicated at the beginning of each part.

The dissertation can be separated into three categories; Blue Ridge geology, Parts I and II; U-Pb zircon geochronology, Parts III and IV; and Inner Piedmont geology, Parts V, VI, and VII. Part I consists of a description of the bedrock geology and surficial units of the Waynesville and Sam Knob 7.5–minute quadrangles, North Carolina, mapped between 2004-2008 (Plates 1 and 2). Part II is a summary of the geology of part of the southwestern North Carolina and northeastern Georgia Blue Ridge. It incorporates over three decades of geologic mapping (Plate 3) with modern geochronology to better understand the tectonic history of the area. Part III addresses the temporal and spatial distribution of Paleozoic metamorphism in the Blue Ridge and Inner Piedmont using U-Pb ages of metamorphic zircons. It is anticipated that this paper will be submitted to a peer-reviewed journal in late summer of early fall 2009. A manuscript version of Part IV was submitted in April 2009 to a proposed Geological Society of America Memoir "From Rodinia to Pangea: The Lithotectonic Record of the Appalachian Region" edited by R. P. Tollo, P. Karabinos, M. J. Bartholomew, and J. P. Hibbard. The paper addresses the provenance of various metasedimentary terranes of the Blue Ridge and Inner Piedmont through SHRIMP U-Pb zircon geochronology. Part V was published

by Merschat and Hatcher (2007) in the Geological Society of America Memoir 200 and discusses the relationship between Siluro–Devonian sedimentation in the Cat Square terrane, Devonian–Mississippian deformation and metamorphism in the Inner Piedmont, accretion of the Carolina superterrane, and parallel development of Devonian clastic wedges in the Appalachian foreland. Part VI was published by Hatcher and Merschat (2005) in the Geological Society Special Paper 268 on orogenic channel flow, edited by R. D. Law, M. P. Searle, and L. Godin. This paper related the Devonian to early Mississippian west- and southwest-directed mid-crustal flow recognized in the Inner Piedmont and eastern Blue Ridge to the orogenic channel flow concept proposed for the Himalayas and the India-Asia collision. Part VII is a field trip guidebook by Merschat et al. (2008) that examines the Brindle Creek fault and the geology of the Cat Square terrane in the Brushy Mountains, and near Lincolnton, North Carolina. The guidebook was published for the Southeastern Section of the Geological Society of America meeting in April 2008.

Plates included are: (1) geologic map of the Waynesville and Sam Knob 7.5-minute quadrangles, North Carolina; (2) accompanying station map of the Waynesville and Sam Knob quadrangles; (3) compiled geologic map of part of the Blue Ridge in southwestern North Carolina and northeastern Georgia; and (4) compiled geologic map of the northern half of the Inner Piedmont, North Carolina, South Carolina, Georgia. Appendices I and II contain the structural measurements and rock descriptions from the Waynesville and Sam Knob 7.5-minute quadrangles, respectively. Appendix III contains SHRIMP U-Pb analyses and trace-element concentrations of detrital zircons.

REFERENECES CITED

Hatcher, R. D., Jr., and Merschat, A. J., 2006, The Appalachian Inner Piedmont: An exhumed strike-parallel, tectonically forced orogenic channel, *in* Law, R. D., Searle, M., and Godin, L., eds., Channel flow, ductile extrusion and exhumation of lower-mid crust in continental collision zones: London, Geological Society of London Special Publication 268, p. 517-540.

Merschat, A. J., and Hatcher, R. D., Jr., 2007, The Cat Square terrane: Possible Siluro-Devonian remnant ocean basin in the Inner Piedmont, southern Appalachians, USA, *in* Hatcher, R. D., Jr., Carlson, M. P., McBride, J. H., and Martínez Catalán, J. R., eds., 4-D Framework of Continental Crust: Geological Society of America Memoir 200, p. 553–565.

Merschat, A. J., Hatcher, R. D., Jr., Byars, H. E., and Gilliam, W. G., 2008, Inner Piedmont geo-traverse from the Brushy Mountains to Lincolnton, North Carolina: Architecture of the Cat Square and Tugaloo terranes: Geological Society of America Southeastern Section, Field trip guidebook, 64 p. http://segsa2008.uncc.edu/fieldtrips.html

PART I

Geology of the Waynesville and Sam Knob 7.5-minute quadrangles, Haywood, Jackson, and Transylvania Counties, North Carolina

All writing, data, and interpretation in this part is my own. A modified version of the manuscript will be submitted to the U.S. Geological Survey with Plates 1 and 2 to be published as part of Scientific Investigations Map and report.

ABSTRACT

Detailed geologic mapping of the Waynesville and Sam Knob 7.5-minute quadrangles (~340 km^2) in the central and eastern Blue Ridge of western North Carolina recognizes the Dahlonega gold belt, Cartoogechaye, and Tugaloo terranes exposed as three thrust sheets framing the Great Balsam Mountains window (GBMW). The lowest thrust sheet exposed in the core of the GBMW contains Otto Formation sillimanite-garnet-biotite-muscovite schist and metagraywacke of the Dahlonega gold belt. Rare mafic and ultramafic rocks occur as small lenticular bodies. The inner window extends from near Sylva to Canton, North Carolina, with several smaller windows along its NW flank, Raccoon Valley and Ratcliff Mountain windows. The Soque River fault transported migmatitic rocks of the Cartoogechaye terrane above the Dahlonega gold belt. These rocks are pervasively migmatitic and include amphibolite, felsic gneiss (Grenville basement?), and dominant biotite gneiss. No ultramafic rocks were observed here, despite common occurrences throughout the terrane. The Tugaloo terrane is the southeasternmost and highest thrust sheet. It juxtaposes migmatitic Tallulah Falls Formation against Dahlonega gold belt rocks, and Cartoogechaye terrane further to the NE and SW by the Chattahoochee-Holland Mountain fault. Tallulah Falls Formation consists of lower metagraywacke-schist-amphibolite and upper metagraywacke-schist members separated by aluminous schist. A magnetite-bearing, chlorite muscovite schist was recognized in the upper member and locally contains quartz tourmaline schist along its contact with metagraywacke. Several small bodies of magnetite-bearing muscovite-biotite granitoid and the medium-grained Horseshoe Rock granite intrude the Tallulah Falls Formation.

Foliations preserved in amphibolite boudins and inclusion trails in garnets occur in all terranes, and represent the earliest deformation, D_1, and evidence of earlier amphibolite grade metamorphism M_1. The dominant structures throughout the field area are D_2, including penetrative S_2 foliation defined by micas, sillimanite ± kyanite, hornblende, and migmatitic layering. The core of the GBMW is folded into the NE-plunging Lickstone antiform and S_2 trends NNW, E-W, to N-S, and dips steeply to the N and E. Southeast of this fold is a uniform domain of NE-SW-trending structures

S_2, F_2, and L_2. S_2 parallels the E-W trend and subvertical dip of the Soque River fault, suggesting it is a D_2 structure. Metamorphic grade reaches sillimanite II in the GBMW and sillimanite I extends southeast into the Tugaloo terrane before decreasing to kyanite-staurolite grade. Trondhjemite dikes from the Cartoogechaye and GBMW yielded SHRIMP U-Pb lower intercept ages of ~450 Ma, indicating that S_2 developed prior to this. SHRIMP U-Pb zircon metamorphic rim ages of ~455 Ma from the GBMW, indicate D_2 and associated upper amphibolite M_2 is Taconic. D_3 is characterized by a weak S_3 foliation, NE-trending tight to closed folds, F_3. Kyanite-staurolite grade rocks in the southeastern part of the Tugaloo terrane may have formed during M_3. Upright NNE to E-W folds superposed on the Soque River fault are interpreted as F_3. The Chattahoochee-Holland Mountain fault juxtaposes rocks of similar grade, is isoclinally folded, and oriented parallel to S_2 suggesting a Taconic age. Along-strike truncation of the ~335 Ma Rabun Granodiorite indicates that the fault is Mississippian, early Alleghanian D_4. The NW-dipping Dill Falls shear zone is an Alleghanian reverse oblique-slip fault in the southeastern part of the Tugaloo terrane.

INTRODUCTION

The Blue Ridge records part of the Neoproterozoic to late Paleozoic tectonic history of the southern Appalachian orogen. The Blue Ride is a composite of polydeformed metasedimentary crystalline terranes that represent both the early Paleozoic Laurentian margin and accreted terranes (Fig. 1–1). The composite Blue Ridge terranes record the late Neoproterozic opening and middle Paleozoic closing of the Iapetus ocean, and subsequent modifications during later Paleozoic orogenesis. Multiple deformations and orogenies have juxtaposed the Blue Ridge terranes into a west-verging thrust stack. Metamorphic facies ranges from greenschist to granulite with amphibolite facies being the most extensive throughout the Blue Ridge. To help unravel the complex tectonic history of the Blue Ridge, detailed geologic mapping of the Waynesville and Sam Knob 7.5-minute quadrangles (Fig. 1–2; Plates 1 and 2) was conducted to describe the structural, metamorphic, and lithostratigraphic histories of the prominent Blue Ridge terranes.

Detailed 1:24,000-scale geologic mapping of the Waynesville and Sam Knob 7.5-minute quadrangles was conducted during the winter through summers of 2004-2008. Mapping was supported by University of Tennessee Science Alliance Center of Excellence (2004), EDMAP grants to Prof. Robert D. Hatcher, Jr. (2005, 2006), and

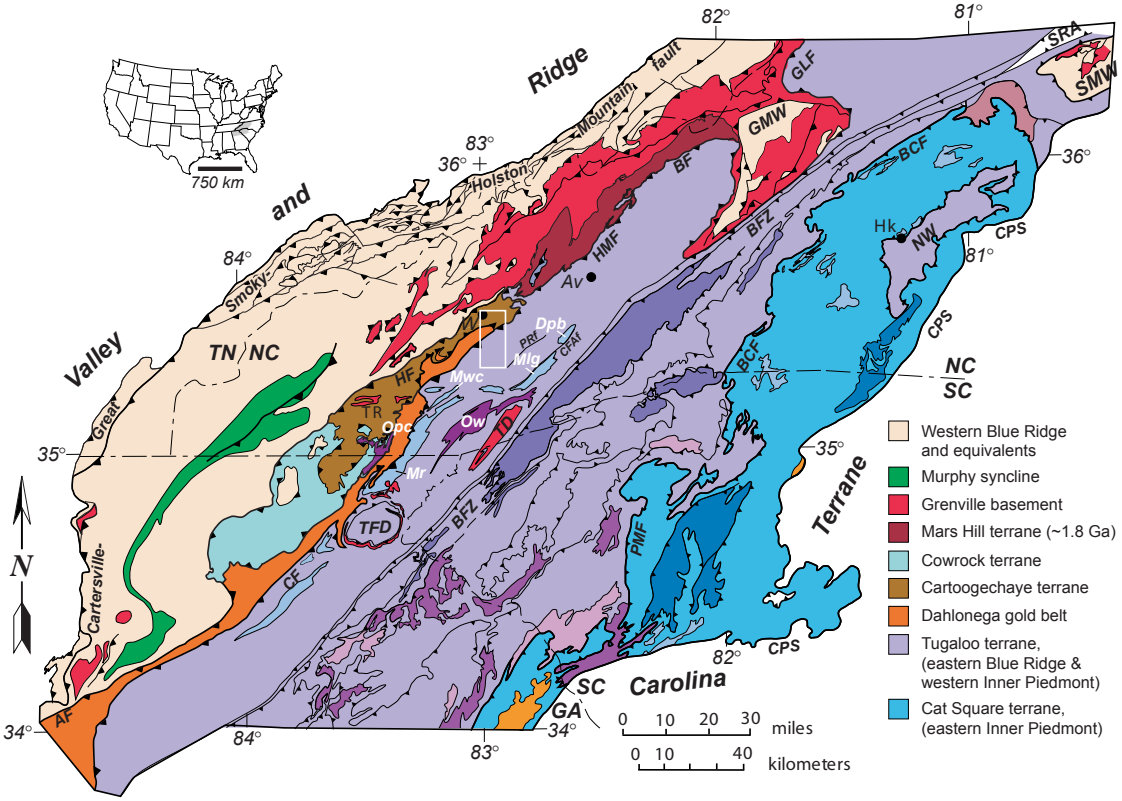

Figure 1–1. Simplified tectonic map of part of the Blue Ridge and Inner Piedmont of Georgia, North Carolina, South Carolina and Tennessee with location of Waynesville and Sam Knob 7.5-minute quadrangles. Map modified from Bream (2003) and Hatcher et al. (2004). BCF– Brindle Creek fault. BF–Burnsville fault. BFZ–Brevard fault zone. CF–Chattahoochee fault. CFAf–Cradle-of-Forestry-in-America fault. Dpb–Pink Beds granodiorite. GLF–Gossan Lead fault. GMW–Grandfather Mountain window. HF–Hayesville fault. HMF–Holland Mountain fault. Mlg–Looking Glass granodiorite. Mr–Rabun granodiorite. Mwc–Walnut Creek granodiorite. NW–Newton window. Opc–Persimmon Creek Gneiss. Ow–Whiteside granodiorite. PMF–Paris Mountain fault. PRf–Pisgah Ridge fault. SMW–Sauratown Mountains window. SRA–Smith River allochthon. TD–Toxaway dome. TFD–Tallulah Falls dome. TR–Trimont Ridge complex. Cities: Av–Asheville. Hk–Hickory. W–Waynesville.

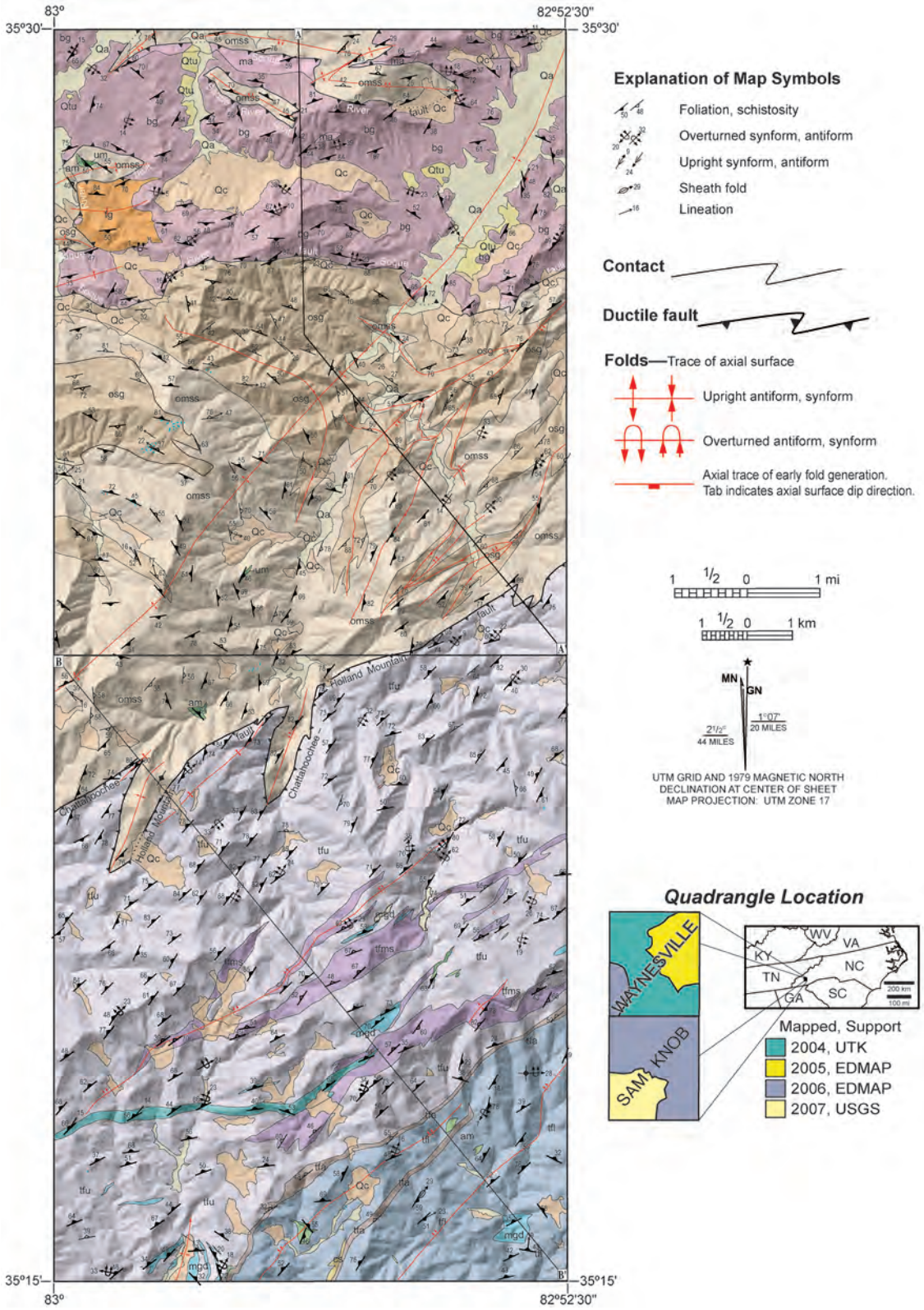

Figure 1–2. Simplified geologic map of the Waynesville and Sam Knob 7.5-minute quadrangles with random representative data.

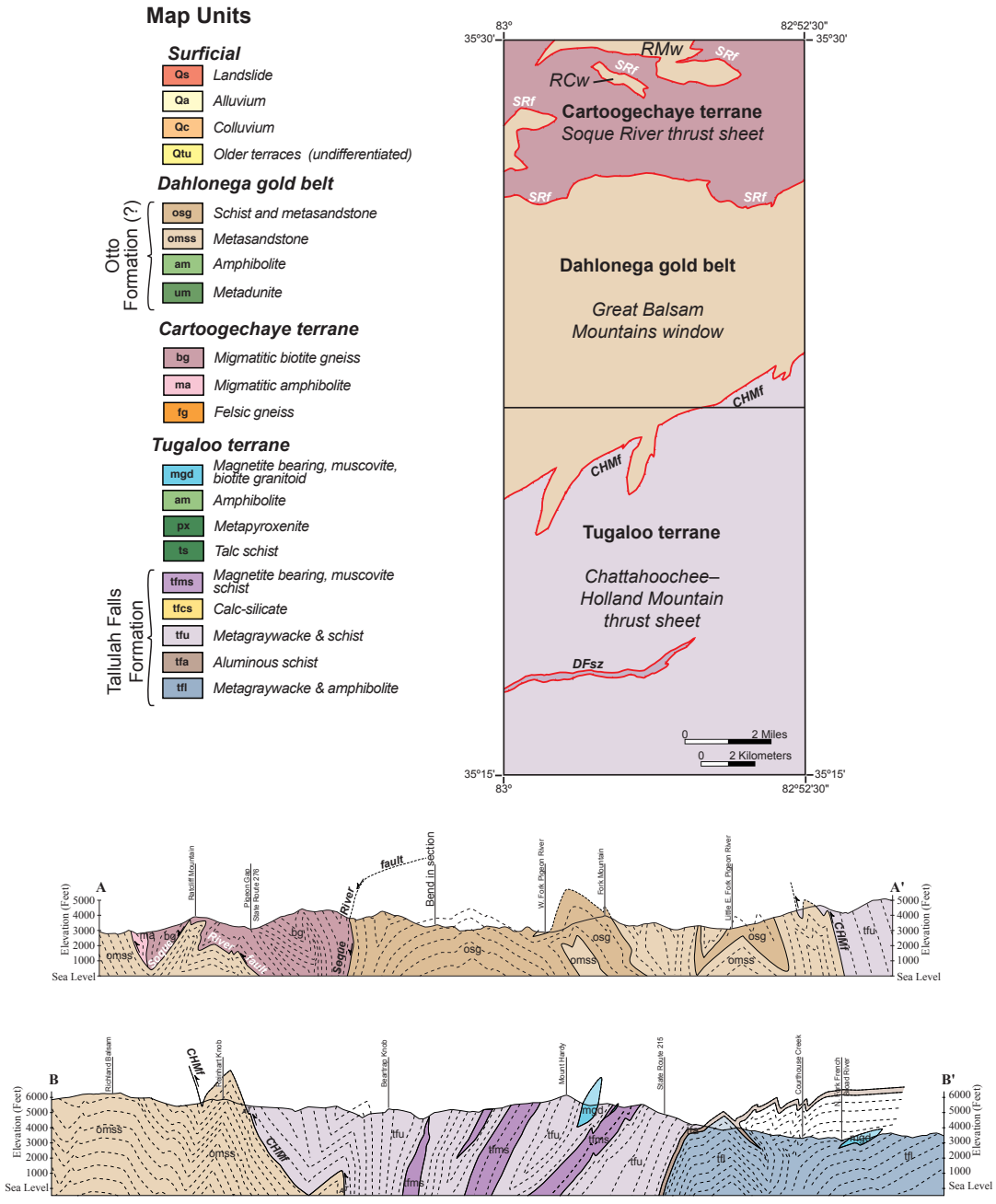

Figure 1–2. Continued. CHMf–Chattahoochee–Holland Mountain fault. RCw–Raccoon Creek window. RMw–Ratcliff Mountain window.

FEDMAP (2007, 2008). Detailed geologic mapping recognized the Soque River and Chattahoochee-Holland Mountain faults separating three different distinct lithotectonic stratigraphies of the Cartoogechaye, Dahlonega gold belt, and Tugaloo terranes, exposed in the northeast end of a ductile eyelid window (Fig. 1–2; Plate 1). Sensitive High-Resolution Ion MicroProbe (SHRIMP) U-Pb geochronology of two trondhjemite dikes and several detrital samples was supported by funding from University of Tennessee Science Alliance Center of Excellence and FEDMAP. 5–10 kg samples were collected and zircons were separated following standard mineral separation techniques (see Parts III and IV). SHRIMP U-Pb zircon analyses were conducted during four sessions at the Standford University–U.S Geological Survey Micro Analysis Center from May, 2005 to September, 2007. Routine operating contions and well characterized zircon standards were used as described in Parts III and IV.

This paper provides an in-depth discussion of the geology of the Waynesville and Sam Knob 7.5-minute quadrangles including: (1) description of surficial units and deposits; (2) description of recognized terranes and their distinct lithotectonic stratigraphies; (3) descriptions of the major tectonic boundaries; (4) comparison of structural and metamorphic histories; and (5) a summary of the Blue Ridge tectonics incorporating observations and data from this study.

LOCATION

The study area is located in the Great Balsam Mountains in the Blue Ridge Mountains, ~48 km (~30 mi) west of Asheville, North Carolina (Figs. 1–1 and 1–3). The area extends south from Waynesville North Carolina, and consists of a 340 km^2 (132 mi^2) area encompassing the Waynesville, and Sam Knob 7.5 minute quadrangles. Over 1 km (3780 ft) of vertical relief and deeply incised valleys and gorges cut by the headwaters of the Pigeon, Tuckasegee, and French Broad Rivers provide excellent exposure and rugged terrain. The area also includes significant land holdings of both federal agencies and local municipalities. The National Park Service Blue Ridge Parkway winds through the Sam Knob quadrangle from mileposts 421–430, reaching its highest elevations along its entire length, including the highest point on the parkway, Richland Balsam. Significant portions of the Waynesville quadrangle consist of Pisgah National Forest and the east half of the Town of Waynesville watershed. The Sam Knob quadrangle is almost entirely Pisgah and Nantahala National Forests with minor private land in the southwest quarter. National Forest land holdings in Waynesville and Sam Knob quadrangles includes part of the Shining Rock and all of the Middle Prong Wilderness Areas.

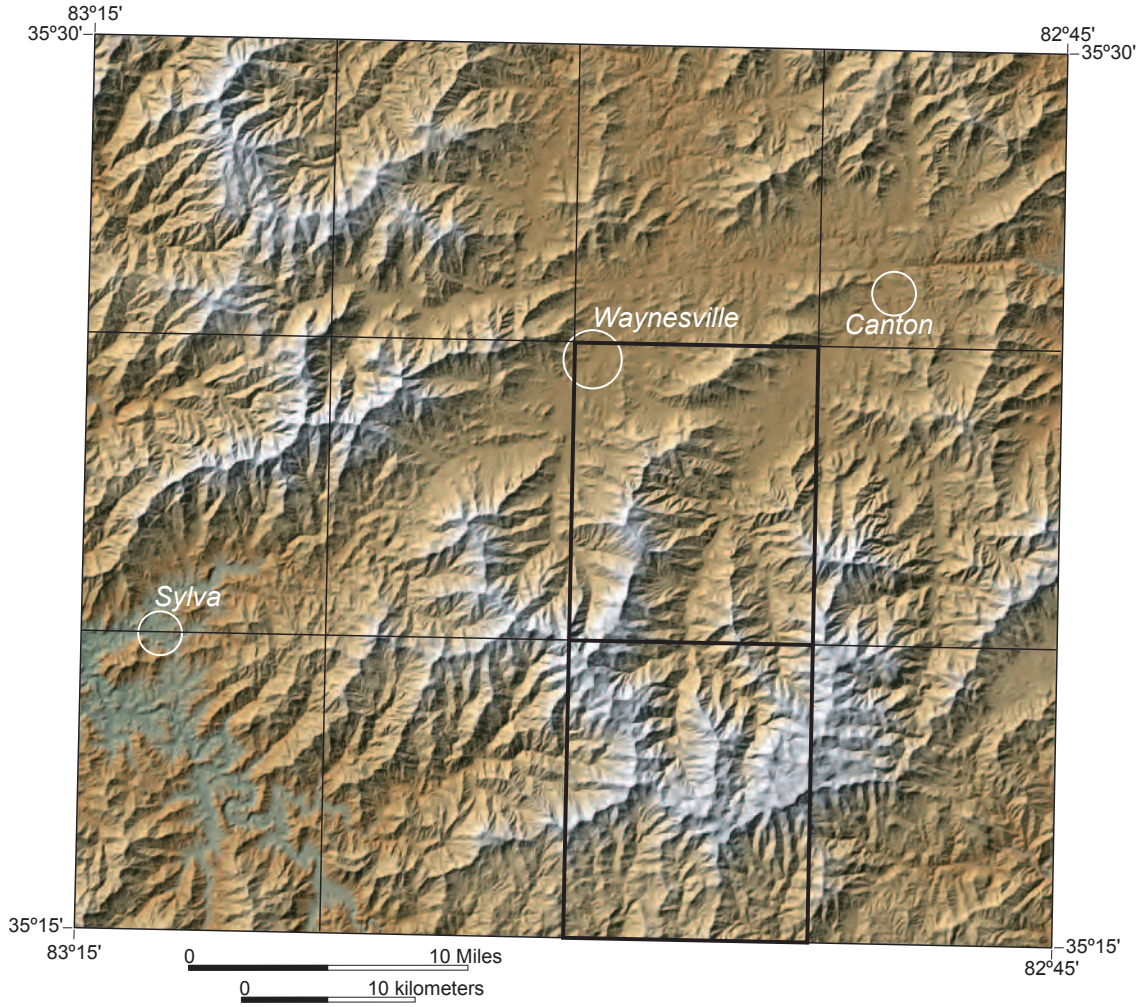

Figure 1–3. Shaded relief map of the Great Balsam Mountains, western North Carolina with the location of the Waynesville and Sam Knob 7.5-minute quadrangles outlined with a thick black line. Larger towns are indicated.

GENERAL GEOLOGIC SETTING

The southern Appalachian Blue Ridge is a composite thrust stack of polydeformed, crystalline terranes (Fig. 1–1). Collectively the Blue Ridge was affected by the Proterozoic Grenville orogeny and three Paleozoic orogenies, although the degree to which each orogeny affected each terrane varies. Although the thermal overprint of the Alleghanian orogeny is weak to moderate, it is poorly understood (Hatcher et al., 2005; Miller et al., 2006, Stahr et al., 2006). This culminating event decapitated previous Blue Ridge structures and transported all terranes westward as part of the Blue Ridge-Piedmont megathrust sheet (Hatcher, 1989; Hatcher and Hooper, 1992).

The Sam Knob and Waynesville 7.5-minute quadrangles are surrounded by areas of detailed geologic mapping, but the geology of these quadrangles was only known from three generations of reconnaissance geologic mapping: Keith (1907), Hadley and Nelson (1971), and Brown et al. (1985). Most workers have generally recognized similar lithologic contacts, but the nature of the contacts and rocks have varied. Hadley and Nelson (1971) traced rocks correlative with the Dahlonega gold belt from the Georgia-North Carolina border to near Canton, North Carolina. Brown et al. (1985) did not recognize the Dahlonega gold belt, and indicated the main contact existed between the Ashe/Tallulah Falls Formation rocks and migmatitic biotite gneisses of the Cartoogechaye terrane. Surrounding detailed geologic mapping consists of contributions from the USGS (e.g., Hadley and Goldsmith, 1963; King et al., 1968; Southworth et al., 2005), North Carolina Geological Survey (e.g., Merschat and Wiener, 1988), and projects supported by different academic institutions (e.g., Acker, 1982; Eckert, 1984; Eckert et al., 1989; Quinn, 1991; Davidson, 1995; Montes, 1997; Edelman, unpublished mapping). Merschat and Wiener (1988) recognized Ashe/Tallulah Falls rocks thrust over migmatitic rocks of the Cartoogechaye terrane in the Canton, North Carolina, 7.5-minute quadrangle. Quinn (1991) suggested that mica schist and gneiss near Sylva, North Carolina belonged to the Otto Formation of the Dahlonega gold belt. Edelman (unpublished mapping) continued the same lithotectonic units described by Quinn (1991) into the Hazelwood quadrangle adjacent to the Waynesville quadrangle to the west. Morrow (1977) and Acker (1982) mapped mica gneisses and schists correlative with the units of Hadley and Nelson (1971) in the Cruso and Shining Rock quadrangles, east of the Waynesville and Sam Knob quadrangles, respectively. Southeast of the Sam Knob quadrangle, Horton (1982) mapped Tallulah Falls Formation, the northern tip of the Toxaway dome, and parts of the Whiteside and Looking Glass plutons in the northwest part of the Rosman

quadrangle. Additionally, various studies regarding structural analysis, petrology, geochronology, and geochemistry provide additional information about the tectonics of the area (Cameron, 2001; Berquist, 2005; Massey and Moecher, 2005). These detailed studies yield a tectonic framework related to the tectonic evolution of the Blue Ridge.

The Blue Ridge can be separated into western, central, and eastern subdivisions in western North Carolina, northwestern South Carolina, and northeastern Georgia. These subdivisions combine terranes with similar tectonic affinities and tectonothermal histories.

Western Blue Ridge

The western Blue Ridge is bound by the Cartersville-Great Smoky-Iron Mountain-Holston Mountain fault to the northwest and the Hayesville and Allatoona faults to the southeast (Fig. 1–1). It consists of Neoproterozoic to Cambrian-age rocks deposited on Mesoproterozoic Grenvillian crust and represents the early Paleozoic Laurentian margin (Hatcher et al., 2005). Neoproterozoic metasedimentary components include the Ocoee Supergroup, and Grandfather Mountain, Mount Rogers, and Mechum River Formations, which represent a series of failed rift basins throughout the western Blue Ridge (Hatcher et al., 2005). The Ocoee Supergroup contains nearly 15 km of sediment, dwarfing the other basins, but lacks significant volcanic and mafic-ultramafic components. The Cambrian Chilhowee Group overlies both Neoproterozoic failed rift facies rocks and Mesoproterozoic basement (King and Ferguson, 1960; Hadley and Nelson, 1971). The Chilhowee Group and overlying Shady Dolomite and Rome Formation represent the rift-to-drift-to-passive margin transition (Hatcher et al., 2005). The Murphy syncline consists of a sequence of sandstones and slates to schists of the Murphy Group, overlain by the Murphy marble, and the Mineral Bluff Formation. Crinoid stems from a marble near the base of the Mineral Bluff Formation constrain minimum age of deposition to the Ordovician (Tull et al., 1993).

The western Blue Ridge contains a complete progression of Barrovian series isograds, from chlorite in the west, increasing southeastward to sillimanite zone rocks (Hadley and Goldsmith, 1963; Parts II, and III). Corrie and Kohn (2007) reported ~450 Ma ID-TIMS monazite age from staurolite to kyanite grade Great Smoky Group rocks near the southeastern end of the Great Smoky Mountains National Park.

Central Blue Ridge

The central Blue Ridge consists of several enigmatic terranes sandwiched between the western and eastern Blue Ridge in northeastern Georgia and western North Carolina. The central Blue Ridge consists of the Cartoogechaye, Cowrock, and Dahlonega gold belt terranes in a west-verging antiformal-synformal thrust stack (Hatcher et al., 2005).

The Cartoogechaye terrane extends from north of Canton, North Carolina, to near Blairsville, Georgia, and overlies the Cowrock terrane (Fig. 1–1) The terrane is bounded by the Hayesville fault to the northwest and the Soque River and Chunky Gal Mountain faults on the southeast and southwest, respectively (Fig. 1–1). Migmatitic biotite gneiss dominates, with lesser amounts of the garnet-biotite-muscovite-sillimanite schist of the Shooting Creek Schist, felsic gneiss, and minor quartzite (Hatcher et al., 2005). The ~1103 Ma Trimont Ridge meta-igneous complex consisting of orthopyroxene-bearing felsic gneiss and minor amphibolite is the only documented basement in the Cartoogechaye terrane (Hatcher et al., 2004); however, several other undated felsic gneisses remain suspect basement massifs. Numerous and often large amphibolite and ultramafic bodies occur in the Cartoogechaye terrane including the Buck Creek-Chunky Gal Mountain complex and Webster-Addie ultramafic body, the best candidates for ophiolites in the southern Appalachians (Swanson et al., 2005). Miller et al. (1998) reported detrital zircons ages of 1200-1000 Ma from pelitic schist at Winding Stair Gap. Hatcher (1980) initially correlated these rocks with the Tallulah Falls Formation, but they are now recognized as part of a separate lithotectonic terrane (Hatcher et al., 2004, 2005). Metamorphic grade ranges from amphibolite to granulite facies conditions (Absher and McSween, 1985; Eckert et al., 1989; Moecher et al., 2004) and locally may have reached eclogite facies conditions (Anderson and Moecher, 2006). U-Pb ages of zircon rims indicate peak metamorphism occurred at ~460 Ma (Moecher et al., 2004; Berquist, 2005; Merschat et al., 2006).

The Cowrock terrane is bounded by the Hayesville, Soque River, Shope Fork, and Chunky Gal Mountain faults and is located below and to the southwest of the Cartoogechaye terrane (Hatcher et al., 2005). The Coweeta Group of the Cowrock terrane consists of metasandstone and schist of Coleman River Formation overlain by biotite schist, metagraywacke, and quartzite of the Ridgepole Mountain Formation (Hatcher et al., 2005). Detrital zircons from the Coleman River Formation display a peak at 1200–900, 1400–1200 Ma, and single peaks at 1600 and 2700 Ma (Bream, 2002, 2003; Bream et al., 2004; Part IV). Dunite and mafic bodies are small and the largest occur proximal to the Hayesville fault (Swanson et al., 2005). Coweeta Group

rocks are intruded by the ~468 Ma Persimmon Creek Gneiss, a dominantly tonalitic arc-related pluton (McDowell et al., 2002). SHRIMP U-Pb analysis of zircon rims indicate these rocks were metamorphosed to kyanite and sillimanite conditions by 460–450 Ma (Merschat et al., 2006; Part III).

The Dahlonega gold belt extends as a continuous belt from south of Canton, Georgia, to just northeast of Franklin, North Carolina, and is interpreted to be exposed again between Sylva and Canton North Carolina, in the Great Balsam Mountains window (Fig. 1–1) (Hatcher et al., 2005; Merschat et al., 2006). The Dahlonega gold belt consists of metasandstone and schist interlayered with several mafic and felsic meta-igneous rocks (Hopson et al., 1989). The Dahlonega gold belt displays the typical Grenville peak at 1200–900 Ma, but Bream (2002, 2003) and Bream et al. (2004) noted smaller peaks at 2900, 2700, 2100–2000, 1800 and 1600 Ma that are typical of a Gondwanan signature (Fig. 1–2). Thomas (2001) and Settles (2002) reported SHRIMP U-Pb ages from 482–458 Ma for several felsic gneisses of the Dahlonega gold belt (see Part II), including the Lake Burton felsic metatuff (468±6 Ma). Hopson et al. (1989; their Table 1–1) noted that the complex stratigraphic nomenclature of this terrane is the result of along-strike variations of lithologic units, particularly the greater abundance of felsic gneisses near Canton, Georgia. Geochemical analyses of felsic gneisses from the Dahlonega gold belt generally indicate a volcanic arc signature (Spell and Norrell, 1990; Thomas, 2001; Settles, 2002), while mafic samples suggest a mixed MORB to volcanic-arc signature (Spell and Norrell, 1990; Thomas, 2001; Settles, 2002). Relict amygdules and pillows are reported in the mafic rocks of the gold belt suggesting these are flows interfingering with sediment (Spell and Norrell, 1990). Settles (2002) suggested that the Dahlonega gold belt was deposited in an Early Ordovician back-arc basin and metamorphosed during the Acadian.

Eastern Blue Ridge

The highest thrust sheet in the Blue Ridge thrust stack is the eastern Blue Ridge, the western Tugaloo terrane. It is bound to the northwest by the Chattahoochee-Holland Mountain-Burnsville fault, and separated from the eastern Tugaloo terrane by the Brevard fault zone (Figs. 1–1, and 1–2). Correlation of the faults along different segments of the western boundary of the Tugaloo terrane is complicated by the contrasting descriptions of the timing and kinematics of the Chattahoochee, Holland Mountain, and Burnsville faults. The Tugaloo terrane consists of Neoproterozoic to Cambrian Ashe/Tallulah Falls Formation, intruded by several Paleozoic plutons, and rare internal

massifs of Mesoproterozoic basement. The Tallulah Falls Formation consists of a lower metagraywacke and amphibolite member, middle aluminous schist member, and upper metagraywacke containing minor amphibolite (Hatcher, 1971, 1977, 1978; Hatcher et al., 2005). Detrital zircons from the TF largely display a single broad population of 1300–900 Ma ages interpreted as a Laurentian source (Bream, 2003; Bream et al., 2004). Plutonism in the western Tugaloo terrane can be separated into three pulses: Ordovician, Whiteside trondhjemite-granodiorite; Devonian, Pink Beds granodiorite, and Spruce Pine pegmatites; and Mississippian, Round Mountain granite, Looking Glass granodiorite, Rabun Granodiorite, Mount Airy granodiorite, Stone Mountain granodiorite, Walnut Creek granodiorite, and Yonah Mountain tonalite (Miller et al., 1998; Miller et al., 2000; Mapes, 2002; Miller et al., 2006; Stahr, 2007; Varnell et al., 2008). Inliers of Mesoproterozoic basement occur in the core of the Toxaway and on the flanks of the Tallulah Falls domes (Hatcher, 1977, 1984; Hatcher et al., 2004). Hatcher et al. (2004) interpreted the Tallulah Falls Formation to have been deposited nonconformably on blocks of Grenvillian and oceanic crust. In northwestern North Carolina, the Ashe/ Tallulah Falls Formation is interpreted to be overlain by the Alligator Back Formation (Rankin et al., 1973). In the eastern Tugaloo terrane the Tallulah Falls Formation is overlain by the Chauga River and Poor Mountain Formations (Hatcher, 2002).

Metamorphic grade remains kyanite and sillimanite grade until it decreases to garnet to kyanite grade north of the Grandfather Mountain window (Butler, 1991; Hatcher and Goldberg, 1991). Timing of metamorphism is complex, with evidence of three episodes of Paleozoic metamorphism (Parts II and III). A fourth episode, a product of the Grenville orogeny, is recognized when the internal Grenville basement massifs are considered (Carrigan et al., 2003; Ownby et al., 2004).

LITHOSTRATIGRAPHY

The Waynesville and Sam Knob 7.5-minute quadrangles are dominated by upper-amphibolite facies metasedimentary units and lesser meta-igneous rocks. These units comprise three separate thrust sheets and terranes exposed in the Great Balsam Mountains window (GBMW) bound by the Soque River fault to the north and Chattahoochee-Holland Mountain fault to the southeast. The Dahlonega gold belt comprises the lowest thrust sheet exposed in the GBMW, and smaller Raccoon Valley and Ratcliff Mountain windows in the north. This study has subdivided the Otto Formation of the Dahlonega gold belt into a metasandstone, and schist and metasandstone units. In the northern part of the study area, the Soque River thrust sheet placed migmatitic biotite

gneiss and amphibolite of the Cartoogechaye terrane structurally above the Dahlonega gold belt. The southeast side of the GBMW is bound by the Chattahoochee-Holland Mountain fault and juxtaposes Tallulah Falls Formation of the Tugaloo terrane above the lower thrust sheets of the GBMW. The Tugaloo terrane consists of the distinct, mappable lithostratigraphy of the Tallulah Falls Formation. The map units recognized in this study are described in detail below according to terrane and thrust sheet.

Dahlonega gold belt, Great Balsam Mountains window

The GBMW consists of aluminous metagraywacke, and mica schist (Fig. 1–4), with minor amounts of amphibolite and ultramafic rocks. These rock types share similarities with many of the Blue Ridge metasedimentary units including the rocks of the Great Smoky Group, Dahlonega gold belt, or Ashe-Tallulah Falls Formation. Based on correlations with detailed mapping to the southwest (Quinn, 1991; Edelman, unpublished mapping; Cyphers, 2009) these rocks are correlated the with Dahlonega gold belt, Otto Formation. Hatcher (1988) first defined the Otto Formation as metasandstone, and schist near Otto, North Carolina. This study, like others (e.g. Lamb, 2001; Eckert, unpublished mapping), subdivided the Otto Formation into a metasandstone and schist and metasandstone unit. Stratigraphic relationships between the schist and metasandstone units cannot be resolved due to absence of facing criteria. Minor lenticular bodies of amphibolite and altered mafic bodies occur, similar to mapping in the southwest part of the GBMW (Quinn, 1991; Cyphers, 2009; Edelman, unpublished mapping).

Otto Formation

Metasandstone. Light to medium gray, fine- to medium-grained muscovite, garnet, biotite, potassium feldspar, plagioclase, quartz gneiss with interlayers of sillimanite, garnet, biotite, muscovite schist and lenses of medium-grained calc-silicate comprise one of the major units of the Otto Formation in the northeast end of the GBMW (Fig. 1–4). Several occurrences of an inequigranular metasandstone with layers containing 0.5–2 cm porphyroclasts of quartz, and plagioclase are likely metaconglomerate. Locally, the metasandstones are sulfidic and characterized by orange yellow weathering stains. Transposed layering ranges from 1 cm to greater than 2 m, is generally parallel to foliation, and locally migmatitic. Exposures vary in size, and often produce large exfoliation cliffs to domes. The metasandstone unit corresponds with the high (>1500m; ~5000'), steep topography in the southern part of the Waynesville 7.5-minute quadrangle, including most of Lickstone Ridge and Fork Mountain.

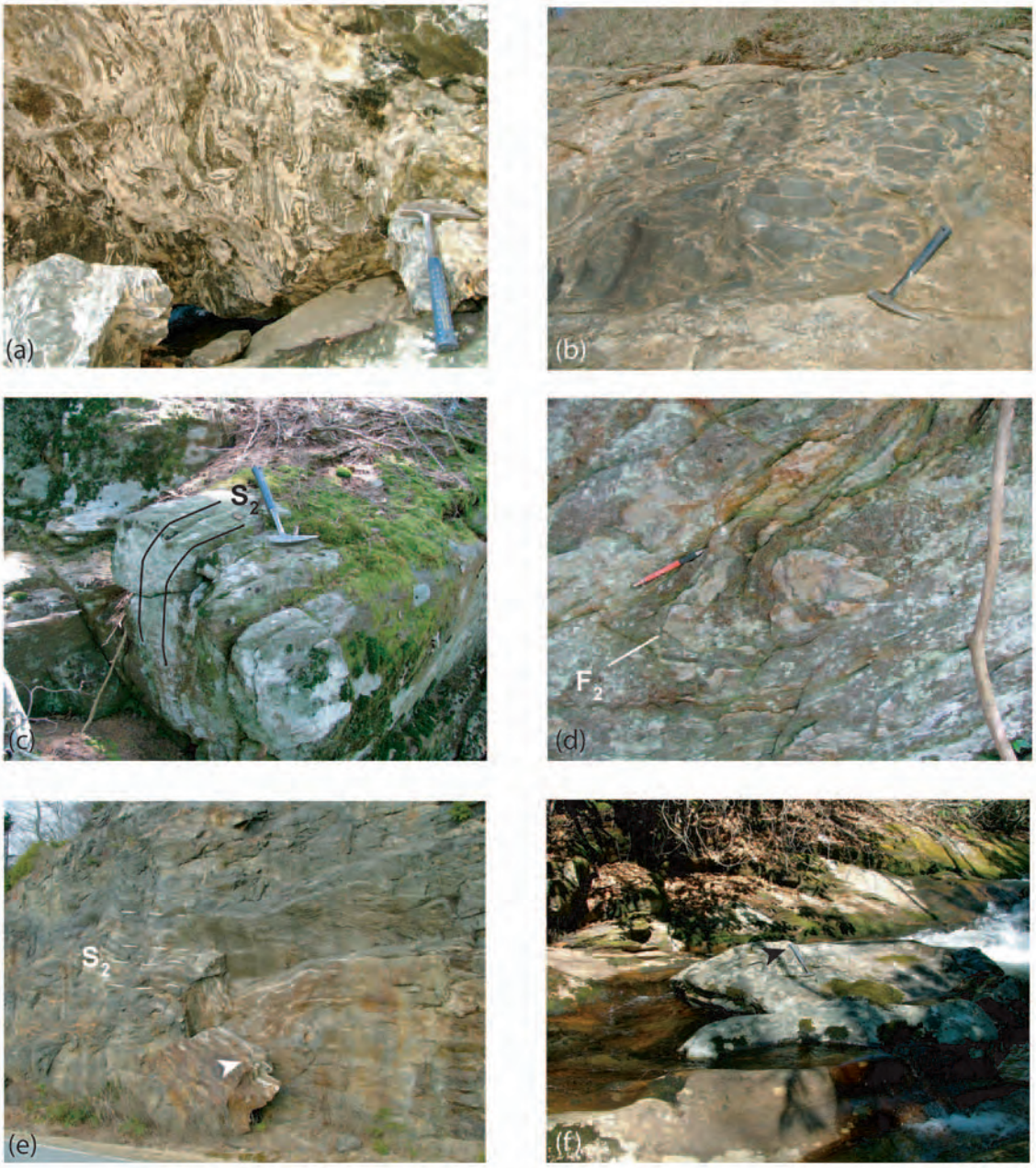

Figure 1–4. Field photographs of typical rock types of the GBMW. (a) Cartoogechaye terrane migmatitic biotite gneiss with tight to isoclinal folds and sheath folds from Wolfpen Mountain, Waynesville quadrangle. (b) Agmatite in amphibolite of the Cartoogechaye terrane from Wolfpen Mountain, Waynesville quadrangle. Leucosomes are composed of quartz, feldspar, and hornblende surround irregular blocks of amphibolite (c) Typical exposure of two-mica metasandstone of the Otto Formation from Cold Spring knob, Waynesville quadrangle. (d) Otto Formation migmatitic sillimanite schist and isoclinal F_2 fold from Deep Cove Gap, Fork Mountain, Waynesville quadrangle. (e) Road cut exposure of interlayered metagraywacke and schist of the upper Tallulah Falls member on NC 215 near Tanasee Bald, Sam Knob quadrangle. Arrow points to hammer for scale. (f) Large amphibolite boudin in metagraywacke of the lower Tallulah Falls Formation, in Tanasee Creek, Sam Knob quadrangle.

Ratcliff Mountain and Raccoon Valley windows in the northern part of the Waynesville 7.5-minute quadrangle are smaller elliptical windows exposing Dahlonega gold belt Otto Formation. These windows are dominated by metagraywacke and schist of the metasandstone unit. Merschat and Wiener (1988) mapped a klippe Ashe/Tallulah Falls Formation in the southern parts of Canton and Clyde 7.5-minute quadrangles. An alternative interpretation of the Ratcliff Mountain and Raccoon Valley windows is they expose Great Smoky Group rocks similar to the Shooting Creek and Brasstown Bald windows (Nelson et al., 1998; Hatcher, unpublished mapping; Edelman, unpublished mapping). There are no distinguishing criteria to determine which correlation is correct.

Schist and Metasandstone. Silvery gray to light gray, fine- to medium-grained, porphyroblastic, lepidoblastic, ±sillimanite, garnet, quartz, biotite, muscovite schist to garnet, quartz, alkali feldspar, plagioclase, biotite, sillimanite schist interlayered with lesser amounts of medium gray, migmatitic, fine- to medium-grained ±muscovite, garnet, biotite plagioclase quartz gneiss comprises the other major map unit recognized in the northeast end of the GBMW (Fig. 1–4). Schist may be variably migmatitic and/or sulfidic with bright yellow to orange-yellow stains. Subordinate metasandstone layers range from a few centimeters to several meters thick. Layers and boudins of medium-grained calc-silicate occur in both schist and metasandstone, but are more common in the latter. The schist units underlie several areas of high topography (>1500 m, ~5000 ft) as well, but are characterized by a more jagged topography than the metasandstone.

Amphibolite. The Otto Formation of the GBMW does not contain as many amphibolite bodies as the *sensu stricto* Dahlonega gold belt to the southwest in Georgia. In the GBMW several small bodies were recognized near Tuckaseege, North Carolina (Cyphers, 2009), and two small bodies occur in the Waynesville 7.5-minute quadrangle. These bodies consist of medium gray to black, medium-grained, plagioclase, hornblende gneiss to hornblende schist.

Metadunite. Located in a subdivison approximately 1 km southwest of downtown Waynesville are exposures of light to medium grayish-green, fine- to medium-grained, granoblastic to weakly foliated metadunite. The metadunite contains minor chromite and talc and is weakly foliated. The extent of the metadunite is only ~500 m^2 and is enclosed by a small amphibolite body on its north and west sides.

Cartoogechaye terrane

The Hayesville-Soque River thrust sheet is comprised of the migmatitic gneisses and schists of the Cartoogechaye terrane. The most abundant rock type of the Cartoogechaye terrane is migmatitic biotite gneiss (Fig. 1–4), and Merschat and Cattanach (2008) have suggested the in formal name Cartoogechaye gneiss for this rock type. Lesser units within the Cartoogechaye terrane include the Shooting Creek Schist, felsic gneiss, ~1.0 Ga Trimont Ridge complex, amphibolite, and metadunite. The Cartoogechaye terrane is only exposed in the northern third of the Waynesville 7.5-minute quadrangle, and only the southern boundary, the Soque River fault, is recognized (Fig. 1–2). Only three rock types were recognized; the abundant migmatitic biotite gneiss, migmatitic amphibolite, and felsic gneiss.

Migmatitic biotite gneiss. The dominant and characteristic rock type of the Cartoogechaye terrane is migmatitic biotite gneiss. In the Waynesville 7.5-minute quadrangle, this unit consists of medium to dark gray, migmatitic biotite gneiss consisting of dark-colored layers of medium- to coarse-grained inequigranular ±hornblende, ±garnet, epidote, biotite, quartz, plagioclase gneiss to porphyroblastic garnet, quartz, plagioclase, biotite schist, and light-colored, medium- to coarse-grained, granoblastic, biotite, quartz, feldspar-rich layers. Stromatic migmatitic layering ranges from 1–70 cm. It contains lenses and layers of medium-grained amphibolite, garnet amphibolite, and biotite granitic gneiss. Layering is often intricately folded and may have a wavy appearance the result of abundant open to isoclinal folds.

Migmatitic felsic orthogneiss(?). Light to medium gray, fine- to medium-grained, migmatitic garnet, biotite, quartz, plagioclase gneiss occurs in the northwestern part of the Waynesville 7.5-minute quadrangle, near the Soque River fault. Transposed layering ranges from 10 cm – >1 m. It commonly contains thin layers of porphyroblastic garnet, quartz, plagioclase, biotite schist. Stromatic migmatitic layering ranges from 1–20 cm. Rare lenses and layers of medium- to coarse-grained, migmatitic garnet amphibolite occur in the orthogneiss. Layering is commonly intricately folded and may have a wavy appearance. This unit is similar to the felsic gneiss mapped by Hatcher (unpublished mapping) to the southwest in the Rainbow Springs 7.5-minute quadrangle. Although both of these felsic units are not pyroxene bearing, they may be correlative with the felsic

orthogneiss of the ~1103 Ma Trimont Ridge complex (Hatcher et al., 2004) and represent internal Grenville basement massifs.

Migmatitic amphibolite. Amphibolite is common in the Cartoogechaye terrane either as smaller boudins, lenses, and layers in the dominant migmatitic biotite gneiss or as larger map-scale bodies. Amphibolite bodies mapped in the Waynesville 7.5-minute quadrangle consist of medium to dark gray, medium- to coarse-grained, migmatitic, ± biotite, ± garnet, quartz, plagioclase, hornblende gneiss. Common migmatite structures observed include stromatic, agmatite, schlieren, and nebulitic structures. Agmatite consisting of eliptical to subangular blocks of amphibolite in ±hornblende, quartz, feldspar leucosome (1–50 cm thick) is the most common structure (Fig. 1–4). Minor interlayers of migmatitic biotite gneiss are common and are frequently complexly folded around amphibolite blocks and lenses.

Tugaloo terrane

The Chattahoochee-Holland Mountain fault juxtaposes migmatitic, sillimanite-bearing schists and metagraywackes of the Tugaloo terrane over sillimanite grade metasandstones and schists of the Dahlonega gold belt, Otto Formation in the GBMW (Fig. 1–2). The Tugaloo terrane consists of paragneiss, schist, and amphibolite of the Ashe/Tallulah Falls Formation (Hatcher, 2002). The Ashe/Tallulah Falls Formation consists of a lower metagraywacke-amphibolite member, middle aluminous schist, and upper metagraywacke and schist member with minor amphibolite (Hatcher, 1978, 1993). These units have been intruded by various Paleozoic granitoids. Detailed mapping in this study recognized a similar tripartite stratigraphy of the Tallulah Falls Formation and an additional map unit, a magnetite bearing, chlorite,-muscovite schist delineated in the upper member of the Tallulah Falls Formation.

Tallulah Falls Formation

Metagraywacke-Schist-Amphibolite Member. The lower member of the Tallulah Falls Formation consists of medium to dark gray, fine- to medium-grained, migmatitic, muscovite, garnet, biotite, plagioclase, quartz gneiss with interlayers of garnet, biotite, muscovite schist. Boudins and pods of fine- to medium-grained amphibolite and garnet amphibolite are common and vary from 10 cm to greater than several meters thick including several map-scale bodies (Fig. 1–4). The largest body of amphibolite/

metagabbro and metapyroxenite occur just north of the confluence of the Tanasee and Pinehook Creeks in southern part of the Sam Knob quadrangle. Transposed layering ranges from 1 cm to greater than 2 m and is generally parallel to foliation. Stromatic migmatite is most common with lesser amounts of agmatite.

Aluminous schist. The critical marker unit of the Tallulah Falls stratigraphy is the middle aluminous schist. This unit is a silvery gray to light gray fine- to medium-grained, porphyroblastic, lepidoblastic, migmatitic, garnet, sillimanite, staurolite, kyanite, quartz, biotite, muscovite schist. Locally, the unit displays a scaly texture, likely the result of the partial replacement of kyanite by muscovite, or an S–C fabric. The unit is typically only 100-200 m thick but locally may be thicker (Fig. 1–2, Plate 1). Minor interlayers of amphibolite are common.

Metagraywacke-Schist Member. The upper member of the Tallulah Falls Formation consists of light to medium gray, fine- to medium-grained, migmatitic, muscovite, garnet, biotite, plagioclase, quartz metagraywacke with interlayers of garnet, biotite, muscovite schist, and minor boudins and pods of medium-grained calc-silicate and amphibolite (Fig. 1–4). Layering ranges from 1 cm to greater than 2 m, and is generally parallel to foliation. Stromatic migmatite is most common with lesser amounts of agmatite.

Dill Falls Shear Zone Mylonitic Metagraywacke-Schist. Light to medium gray, medium-grained, migmatitic, porphyroclastic, muscovite, garnet, biotite, plagioclase, quartz gneiss with interlayers of porphyrolcastic garnet, biotite, muscovite schist, and muscovite, biotite, granitoid gneiss occur in the Dill Falls shear zone. Rocks in the shear zone vary from protomylonite to mylonite. Interlayered gneiss schist and migmatite in the shear zone ranges from 1 – 10 cm. Migmatite and thin schistose layers display a wispy S-C fabric. Garnets are strongly deformed, often fragmented and recrystallized.

Magnetite-bearing, chlorite-muscovite schist. This study recognizes a distinct schist unit in the upper member of the Tallulah Falls Formation. Excellent exposures of the unit occur at Devils Courthouse and the parking lot for the foot trail to Devils Courthouse on the Blue Ridge Parkway. The schist consists of silvery gray to light greenish gray, migmatitic, fine- to medium-grained, porphyroblastic, lepidoblastic ±sillimanite, ±staurolite, ±kyanite, magnetite, garnet, quartz, biotite, chlorite, muscovite schist interlayered with lesser amounts of medium gray, migmatitic, fine- to medium-

grained ±muscovite, ±chlorite, garnet, biotite, plagioclase, quartz paragneiss. Magnetite porphyroblasts, diagnostic of the schist unit, range from 0.25–3 cm in diameter, and are subhedral to euhedral. The schist is also variably migmatitic, with quartz-feldspar leucosome that commonly contain magnetite porphyroblasts (Fig. 1–5). Subordinate metasandstone layers range from a few centimeters to several meters thick. Fine- to medium-grained massive tourmaline schist occurs locally near the contact with Tallulah Falls Formation metagraywacke.

Tourmaline schist. The southeast contact of the magnetite-bearing, chlorite, muscovite schist is marked by a dark greenish black to black, fine- to medium-grained massive quartz, plagioclase, tourmaline schist. This unit occurs as a 0.10 to 2 m-thick layer that is parallel to the regional foliation, and commonly contains quartz veins, and weathers orangeish-yellow. The contact is exposed on NC 215 just south of Beech Gap and has been mapped elsewhere by presence of float along the contact of magnetite-bearing, chlorite, muscovite schist and Tallulah Falls Formation metagraywacke.

Calc-silicate granofels. Light greenish-gray, medium- to coarse-grained, granoblastic to foliated, ±garnet, diopside, epidote, quartz granoblastite is mappable in the lower member of the Tallulah Falls. The unit is not very extensive, and appears to occupy a stratigraphic position near the top of the lower member of the Tallulah Falls Formation. Hatcher (1971) traced a continuous layer of calc-silicate near the contact of the Wiley Gneiss on the northern flank of the Tallulah Falls dome, Georgia. Stahr (2007) and Cyphers (2009), however, recognized calc-silicate in the upper member of the Tallulah Falls Formation often closely associated with the Mississippian Rabun and Walnut Creek Granodiorites.

Igneous–Metaigneous

Pegmatite. Located in the northern part of the Franklin-Sylva pegmatite district (Lesure, 1968), white, unfoliated biotite, muscovite pegmatite dikes, ~1m thick or greater occur throughout the study area. The distribution of the pegmatite dikes varies from none to only a single dike observed, to multiple pegmatite dikes occurring in an area. Areas where multiple pegmatite dikes were observed is indicated with a stipple pattern (Fig. 1–2, Plate 1). Locations of pegmatite prospect and mines are indicated (Fig. 1–2, Plate 1), although considerably fewer pegmatite mines and prospects were observed than reported by Lesure (1968).

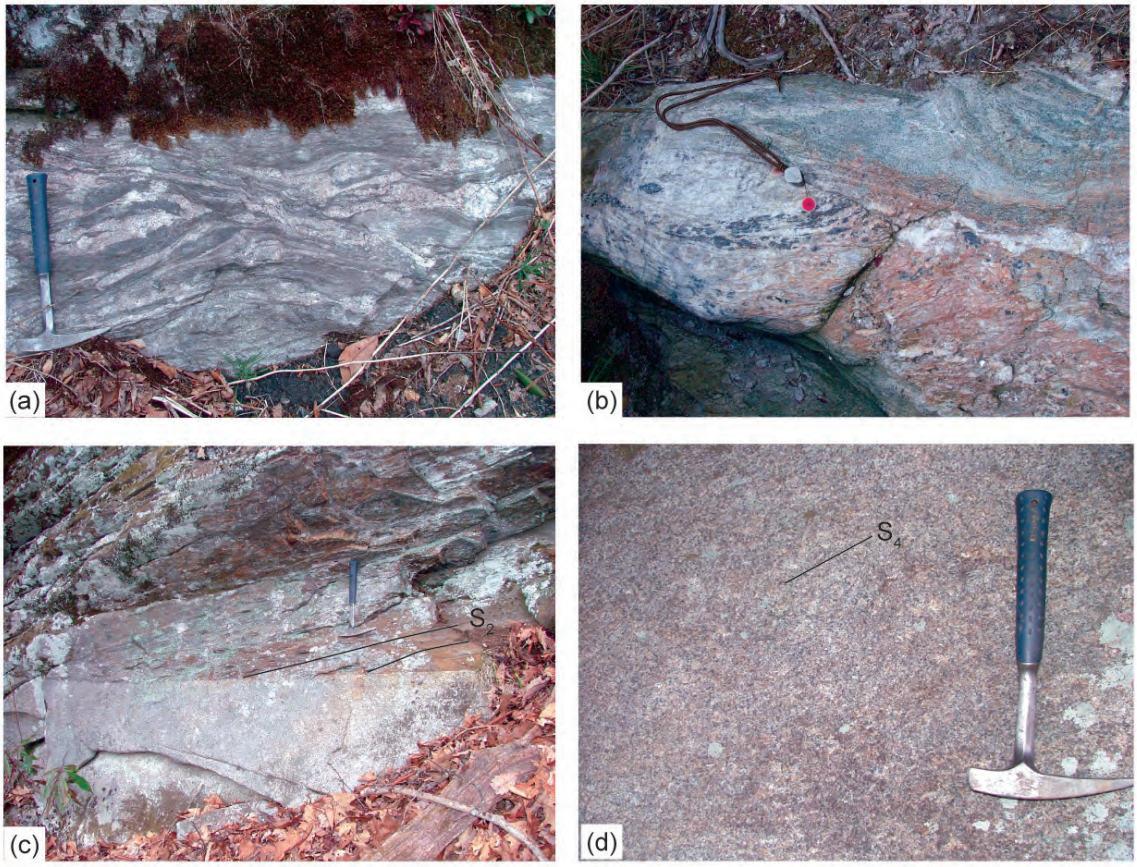

Figure 1–5. Typical field exposure of the magnetite-bearing, chlorite-muscovite schist and contact relationships of Horseshoe Rock granitoid. (a) Exposure of migmatitic magnetite-bearing chlorite-muscovite schist. (b) Sheared magnetite bearing leucosome from within the chlorite-muscovite schist. Small magnet for scale is ~ 1cm in diameter. (c) Contact of the Horseshoe Rock granitoid with the metagraywacke and schist of the upper Tallulah Falls Formation. The regional S_2 foliation is truncated along the contact. (d) A weak S_4 foliation is present in the medium-grained Horseshoe Rock granitoid.

Muscovite-Biotite Granitoid. Light gray, migmatitic, medium- to coarse-grained, weakly foliated to banded, porphyritic to equigranular, ± magnetite, garnet, muscovite-biotite, granitoid to granitoid gneiss occur in the Chattahoochee thrust sheet in the Sam Knob 7.5-minute quadrangle. Three main bodies exist and several smaller sill- to sheet-like intrusions. These are only smaller bodies of numerous Paleozoic granitoid plutons of the Tugaloo terrane/Chattahoochee thrust sheet in southwestern North Carolina. In the smaller bodies located on the southeast face of Mount Hardy and in the headwaters of the North Fork of the French Broad River, biotite gneiss xenoliths and schlieren are common and are usually parallel to foliation. Subhedral to euhedral magnetite phenocrysts vary from 0.25–2 cm and occur in leucocratic layers in the smaller lens-shaped intrusion in the northern part of the quadrangle.

The largest granitoid body occurs on Wolf Creek near the southern end of the Sam Knob 7.5-minute quadrangle. This pluton consists of white to very light gray, medium-grained, weakly foliated to massive, locally porphyritic, muscovite, biotite granitoid. It consists of several gently north dipping, 5–20 m-thick granitoid sheets and the approximately 300 m-thick main pluton. M. G. Varnell (in progress) proposed the name Horseshoe Rock granite for exposures at this locality in the Lake Toxaway 7.5-minute quadrangle. The Horseshoe Rock granite truncates the foliation in the surrounding country rock of upper Tallulah Falls Formation schist and metagraywacke (Fig. 1–5). The Horseshoe Rock granite is folded into a north-plunging, open antiform. Based on similar textures, composition, map relationships, and proximity, this granite is correlated with the ~342 Ma Round Mountain granite of Varnell et al. (2008). Smaller ~1 m-thick medium-grained granitoid dikes and sills occur in the vicinity of the Horseshoe Rock granite and are assumed to be related based on similar textures, composition, and structural relationships, but were not mapped because of there small size.

***Trondhjemite Dikes*.** Although these ~10 cm to 1–2 m-thick dikes and lesser sills are not large enough to map, they do occur in all three terranes in the Waynesville and Sam Knob 7.5-minute quadrangles. The dikes are white to very light gray, fine- to medium-grained locally foliated, or porphyritic, ±muscovite, biotite granitoid. Foliations where developed are generally parallel to dike margins and commonly thought to be magmatic (Merschat and Wiener, 1988). Porphyritic textures contain 0.5–1 cm plagioclase phenocrysts with concentric zoning. Mapes (2002) reported an age of ~402 Ma from a trondhjemite dike that intrudes the Otto Formation of the GBMW at Cove Field Ridge overlook on the Blue Ridge Parkway.

Two additional trondhjemite dikes were sampled and dated using the SHRIMP-RG. Sample W637, intruded Cartoogechaye terrane felsic gneiss in the northwestern corner of the Waynesville quadrangle. The dike is medium-grained and truncates foliations in the felsic gneiss. A second sample from the southeastern end of GBMW, SS1, was a fine-grained, biotite-bearing trondhjemite. Both dikes contain xenocrystic zircons with inherited cores and thin dark magmatic rims. Inherited cores ranged from 1300–900 Ma (Table 1–1; Figs. 1–6 and 1–7). Analyses of dark rims were discordant and lower intercept ages were interpreted for both dikes with large errors (Figs. 1–6, and 1–7). W637 yield a lower intercept age of 444±25 Ma and a weighted average 449±4 Ma from eight Paleozoic rims analyses (Fig. 1–6). Data from SS1 were limited, and selected analyses yielded an age of 451±25 Ma (Fig 1–7). The errors associated with these ages are large and overlap metamorphic ages from the western and central Blue Ridge (see Part III). The age are also significantly older than other ages of Blue Ridge trondhjemite dikes (Miller et al., 2000; Mapes, 2002) making these new ages questionable.

Metapyroxenite. Dark olive green, medium-grained, weakly foliated, hornblende, plagioclase, clinopyroxene gneiss occur locally as thin discontinuous blocks and foliation parallel layers. Amphibolite is commonly associated with the metapyroxenite.

Talc schist. White to silvery gray, fine- to medium-grained talc schist is associated with a metapyroxenite body on the lower west slops of Little Sam Knob. The unit is thin, ~10 m thick, and occurs as a layer generally parallel to the regional foliation. It is likely an altered dunite body.

Amphibolite. Several small bodies of amphibolite, often pod-shaped, occur in the Tallulah Falls Formation, commonly in the lower member. They consist of medium gray to black, medium- to coarse-grained migmatitic ±biotite, ±garnet, plagioclase, hornblende gneiss to hornblende schist. The largest body, near the confluence of Tanasse and Pinehook Creeks, has an asymmetric shape, and is bound on the north by a thin layer of metapyroxenite.

SURFICIAL UNITS

Increased development of steep mountain land in western North Carolina has increased the need for understanding the surficial geology to help planning and remittance of potential geologic hazards. Surficial deposits were mapped on the Waynesville and

Table 1–1. U-Pb SHRIMP-RG analytical data for zircons from trondhjemite dikes of central Blue Ridge. Gray shading indicates inherited cores.

Spot Name	204 /206	% err	% comm 206	ppm U	ppm Th	232Th /238U	204corr 206Pb /238U Age	1s err	207corr 206Pb /238U Age	1s err	204corr 207Pb /206Pb Age	1s err	% Dis-cor-dant	Total 238 /206	% err	Total 207 /206	% err	238/ 206r	% err	207r /206r	% err	207r /235	% err	206r /238	% err	err corr
W637-1.2R	2.8E-4	18	**0.49**	**1818**	**8**	0.00	**427.5**	**1.3**	**427.6**	**1.3**	**420**	**35**	-2	14.51	0.3	.0593	0.7	14.59	0.3	.0552	1.6	0.52	1.6	.0686	0.3	.200
W637-14.1R	2.3E-4	26	**0.32**	**1493**	**38**	0.03	**433.2**	**1.7**	**433.6**	**1.7**	**406**	**41**	-6	14.33	0.4	.0582	0.9	14.39	0.4	.0549	1.8	0.53	1.9	.0695	0.4	.218
W637-11.1R	5.8E-7	99	**0.13**	**922**	**8**	0.01	**438.4**	**2.9**	**437.8**	**2.9**	**479**	**30**	9	14.21	0.7	.0567	1.3	14.21	0.7	.0567	1.4	0.55	1.5	.0704	0.7	.447
W637-2.1R	2.3E-4	22	**0.50**	**1363**	**44**	0.03	**444.6**	**1.6**	**444.2**	**1.5**	**475**	**33**	7	13.95	0.3	.0599	0.8	14.01	0.4	.0566	1.5	0.56	1.6	.0714	0.4	.233
W637-19.1R	4.3E-5	32	**0.03**	**2835**	**44**	0.02	**446.1**	**1.0**	**446.3**	**1.1**	**429**	**15**	-4	13.94	0.2	.0561	0.5	13.96	0.2	.0554	0.7	0.55	0.7	.0717	0.2	.347
W637-15.1R	2.6E-5	50	**0.09**	**735**	**31**	0.04	**450.9**	**2.0**	**450.7**	**2.1**	**466**	**24**	3	13.80	0.5	.0567	1.0	13.80	0.5	.0563	1.1	0.56	1.2	.0725	0.5	.395
W637-12.1R	9.0E-4	18	**1.44**	**911**	**106**	0.12	**450.7**	**2.3**	**451.5**	**2.0**	**393**	**109**	-13	13.59	0.4	.0676	1.6	13.81	0.5	.0545	4.9	0.54	4.9	.0724	0.5	.109
W637-13.1R	8.6E-4	14	**1.48**	**1000**	**100**	0.10	**451.7**	**2.1**	**452.1**	**2.0**	**429**	**91**	-5	13.56	0.4	.0680	2.1	13.78	0.5	.0554	4.1	0.55	4.1	.0726	0.5	.115
W637-17.1R	2.4E-5	45	**0.21**	**996**	**88**	0.09	**454.9**	**1.8**	**454.2**	**1.8**	**506**	**20**	11	13.67	0.4	.0577	0.9	13.68	0.4	.0574	0.9	0.58	1.0	.0731	0.4	.407
W637-16.1R	1.4E-5	50	**-0.02**	**3463**	**12**	0.00	**455.6**	**1.1**	**455.9**	**1.1**	**441**	**12**	-3	13.65	0.3	.0559	0.5	13.65	0.3	.0557	0.6	0.56	0.6	.0732	0.3	.415
W637-8.1R	2.5E-5	41	**-0.01**	**2099**	**6**	0.00	**456.8**	**1.3**	**457.1**	**1.3**	**441**	**15**	-4	13.61	0.3	.0561	0.6	13.62	0.3	.0557	0.7	0.56	0.7	.0734	0.3	.395
W637-7.1R	2.7E-4	27	**1.05**	**960**	**112**	0.12	**623.4**	**2.8**	**620.0**	**2.7**	**779**	**37**	25	9.80	0.4	.0691	0.7	9.85	0.5	.0651	1.8	0.91	1.8	.1015	0.5	.255
W637-18.1INT	4.4E-5	50	**0.09**	**290**	**78**	0.28	**912.4**	**5.4**	**912.2**	**5.6**	**917**	**23**	0	6.57	0.6	.0702	1.0	6.58	0.6	.0696	1.1	1.46	1.3	.1520	0.6	.491
W637-9.1R	---	0	**0.30**	**528**	**187**	0.37	**956.7**	**4.2**	**954.1**	**4.4**	**1024**	**15**	7	6.25	0.5	.0734	0.7	6.25	0.5	.0734	0.7	1.62	0.9	.1600	0.5	.546
W637-6.1R	9.9E-5	21	**0.94**	**1148**	**277**	0.25	**963.0**	**2.9**	**956.1**	**3.0**	**1132**	**12**	18	6.20	0.3	.0788	0.5	6.21	0.3	.0774	0.6	1.72	0.7	.1611	0.3	.459
W637-4.1R	3.4E-5	50	**-0.06**	**264**	**47**	0.18	**1034.9**	**6.2**	**1036.0**	**6.6**	**1009**	**21**	-3	5.74	0.7	.0733	1.0	5.74	0.7	.0728	1.0	1.75	1.2	.1741	0.7	.535
W637-3.2R	2.2E-5	48	**0.17**	**583**	**43**	0.08	**1050.2**	**9.7**	**1048.9**	**10.1**	**1079**	**13**	3	5.65	1.0	.0757	0.6	5.65	1.0	.0754	0.7	1.84	1.2	.1769	1.0	.831
W637-1.1C	---	0	**0.23**	**207**	**71**	0.36	**1052.5**	**7.4**	**1050.2**	**7.7**	**1102**	**22**	5	5.64	0.8	.0763	1.1	5.64	0.8	.0763	1.1	1.86	1.3	.1773	0.8	.572
W637-5.1int	1.1E-4	47	**-0.30**	**140**	**57**	0.42	**1072.7**	**8.9**	**1077.5**	**9.4**	**964**	**35**	-10	5.51	0.9	.0728	1.3	5.52	0.9	.0712	1.7	1.78	1.9	.1810	0.9	.467
W637-10.1C	3.7E-4	16	**1.03**	**487**	**175**	0.37	**1091.4**	**4.9**	**1087.4**	**5.0**	**1175**	**27**	8	5.39	0.5	.0844	0.7	5.42	0.5	.0791	1.3	2.01	1.4	.1845	0.5	.340
W637-3.1C	---	0	**0.10**	**231**	**100**	0.45	**1099.4**	**8.2**	**1098.4**	**8.7**	**1121**	**22**	2	5.38	0.8	.0770	1.1	5.38	0.8	.0770	1.1	1.97	1.4	.1860	0.8	.591
W637-9.2C	2.4E-4	44	**0.07**	**89**	**38**	0.45	**1170.7**	**13.7**	**1174.3**	**14.5**	**1102**	**51**	-6	5.00	1.3	.0797	1.5	5.02	1.3	.0763	2.6	2.09	2.9	.1991	1.3	.449
SS1-2.1R	5.7E-4	84	**0.72**	**134**	**61**	0.47	**373.9**	**6.6**	**375.1**	**6.0**	**265**	**332**	-29	16.57	1.6	.0599	3.9	16.74	1.8	.0515	14.4	0.42	14.6	.0597	1.8	.125
SS1-10.1R	2.5E-3	21	**2.72**	**203**	**24**	0.12	**407.8**	**5.7**	**414.9**	**4.3**	**-312**	**511**	-177	14.64	1.0	.0770	2.4	15.31	1.4	.0406	19.9	0.37	20.0	.0653	1.4	.072
SS1-1.1R	2.1E-4	18	**0.32**	**2242**	**24**	0.01	**443.7**	**1.2**	**443.9**	**1.2**	**427**	**26**	-4	13.98	0.3	.0584	0.6	14.03	0.3	.0554	1.2	0.54	1.2	.0713	0.3	.231
SS1-9.1R	3.6E-4	45	**0.10**	**447**	**504**	1.17	**455.2**	**4.4**	**457.6**	**4.4**	**274**	**118**	-40	13.58	1.0	.0569	2.2	13.67	1.0	.0517	5.1	0.52	5.2	.0732	1.0	.193
SS1-7.1R	1.7E-3	19	**2.33**	**251**	**19**	0.08	**513.0**	**5.2**	**516.9**	**4.4**	**249**	**239**	-51	11.70	0.8	.0766	2.2	12.07	1.1	.0512	10.4	0.58	10.4	.0828	1.1	.102
SS1-4.1R	2.5E-3	7	**5.43**	**1038**	**101**	0.10	**625.9**	**3.6**	**619.5**	**3.1**	**904**	**93**	44	9.38	0.4	.1048	1.7	9.81	0.6	.0692	4.5	0.97	4.6	.1020	0.6	.133
SS1-6.1R	2.3E-3	9	**4.69**	**433**	**94**	0.22	**718.6**	**4.8**	**714.1**	**4.7**	**887**	**133**	23	8.14	0.5	.1018	3.0	8.48	0.7	.0686	6.4	1.12	6.5	.1179	0.7	.109
SS1-11.1R	2.9E-4	38	**0.59**	**287**	**86**	0.31	**762.5**	**6.6**	**761.9**	**6.7**	**784**	**64**	3	7.92	0.9	.0695	1.8	7.96	0.9	.0653	3.1	1.13	3.2	.1256	0.9	.286
SS1-5.1R	4.9E-5	45	**0.54**	**431**	**170**	0.41	**867.2**	**4.1**	**863.6**	**4.6**	**974**	**50**	12	6.94	0.5	.0723	2.4	6.94	0.5	.0716	2.5	1.42	2.5	.1440	0.5	.200
SS1-8.1R	3.2E-5	55	**0.12**	**1400**	**294**	0.22	**1031.3**	**3.3**	**1030.7**	**3.5**	**1045**	**12**	1	5.76	0.3	.0746	0.5	5.76	0.3	.0741	0.6	1.77	0.7	.1735	0.3	.499
SS1-3.1C	3.6E-5	50	**0.00**	**202**	**69**	0.35	**1253.9**	**8.2**	**1254.6**	**8.8**	**1242**	**30**	-1	4.65	0.7	.0823	1.5	4.66	0.7	.0818	1.5	2.42	1.7	.2147	0.7	.420
SS1-7.2C	7.2E-5	51	**-0.74**	**362**	**113**	0.32	**1310.0**	**7.7**	**1320.2**	**8.5**	**1145**	**39**	-13	4.43	0.6	.0789	1.8	4.44	0.6	.0779	1.9	2.42	2.1	.2253	0.6	.316

Errors are 1s unless otherwise specified

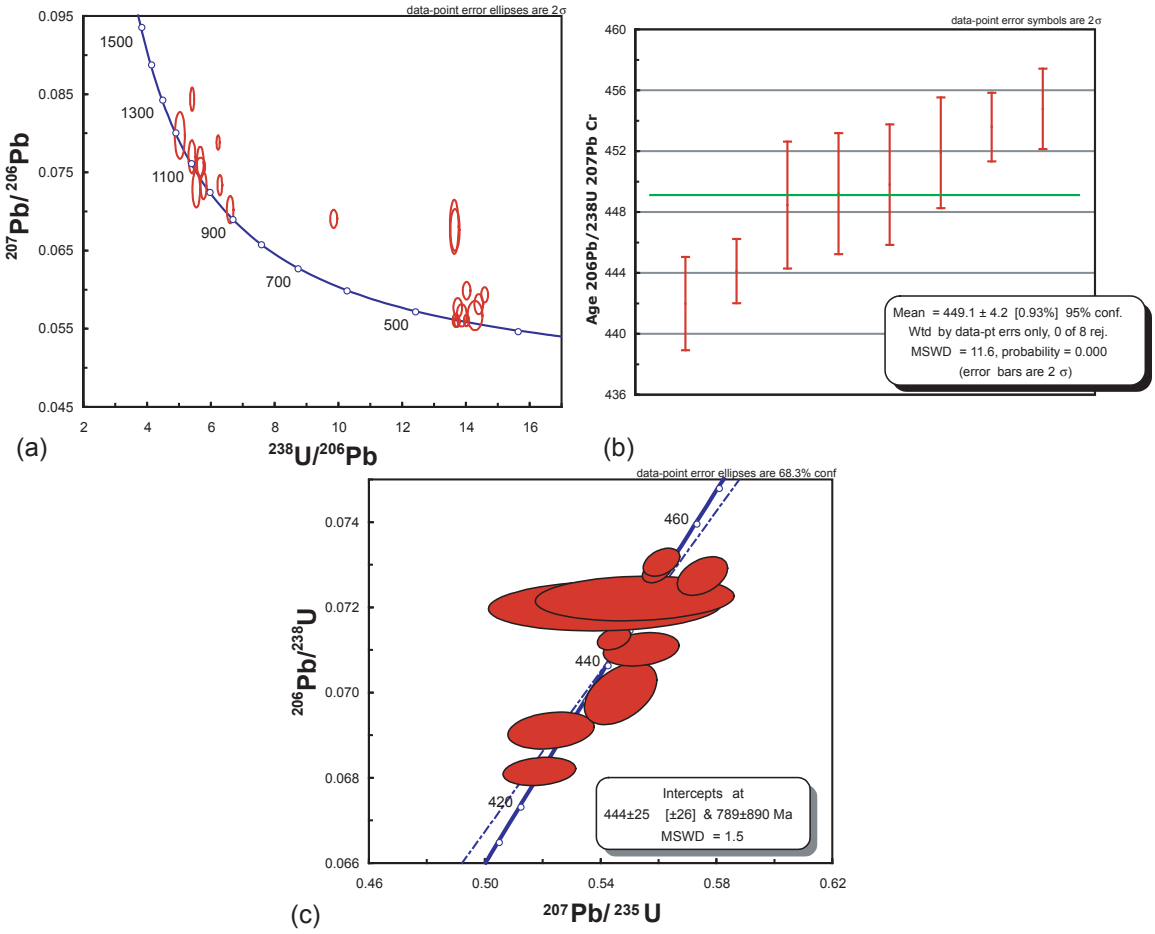

Figure 1–6. Concordia diagrams and weighted average of SHRIMP U-Pb analyses of a medium-grained trondhjemite dike from Wolfpen Mountain, Waynesville quadrangle (W637). (a) Terra-Wasserburg concordia diagram of all data. Ages 1250–900 Ma ages are inherited. (b) Weighted average of dark rims yields an age of 449±4.2 Ma. (c) Calculated concordia age of Paleozic rims yields a lower intercept of 444±25 Ma with an MSWD = 1.5 and probability of fit = 0.14. Plots generated using Isoplot v. 3.0 (Ludwig, 2003).

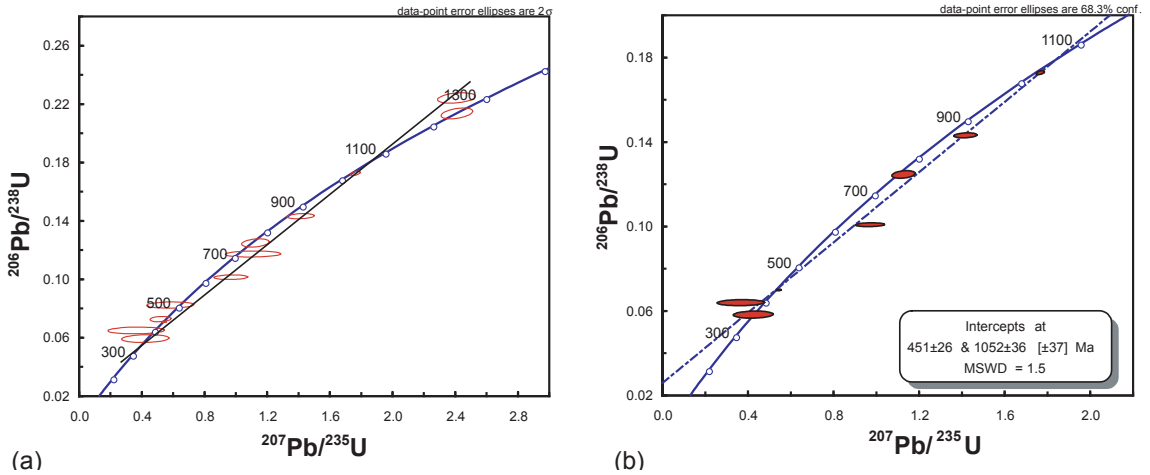

Figure 1–7. SHRIMP U-Pb analyses of a fine-grained trondhjemite dike from the GBMw near Cullowhee, North Carolina, in the Slyva South quadrangle. (a) Conventional concordia diagram of all analyses, (b) only selected analyses that define a discordia, and a lower intercept of 451±26 Ma with a MSWD of 1.5 and 0.18 probablity of fit. A single concordant analysis at 442±1 Ma may represent the age of the dike. Plots generated using Isoplot v. 3.0 (Ludwig, 2003).

Sam Knob 7.5-minute quadrangles during fieldwork, and augmented with interpretation of 7.5-minute topographic maps, digital-elevation models, and aerial photographs. The primary focus of this study was to map the larger surficial deposits and slides. This study separates the surficial deposits into the following units: alluvial terraces, alluvium, colluvium, alluvium and colluvium undifferentiated, and landslides. Additional detailed study could resolve more Quaternary surficial deposits and their complicated history.

Alluvium. This unit mainly includes the modern floodplain deposits of the Pigeon River and its West and East Forks; however, deposits have been mapped along several smaller tributary streams in the Waynesville and Sam Knob 7.5-minute quadrangles. The largest deposits occur along the West Fork of the Pigeon River, and at the confluence of the East and West Forks, forming the Pigeon River in the northeastern part of the Waynesville quadrangle. The alluvium consists of poorly to well-sorted, massive to bedded, unconsolidated sediments ranging from silt to boulders. Some areas are well stratified consisting of beds of medium gray clay to silt shale, interlayered with conglomeratic sands. Pebbles, cobbles, and boulders are sub-rounded to rounded. Modern river terraces and possible abandoned meanders are included in this unit. Thickness ranges from 0–20 m.

Older Alluvial terraces (undifferentiated). A wide floodplain exists along the Pigeon River and the confluence of its West and East Forks in the northeastern part of the Waynesville 7.5-minute quadrangle. Older alluvial terrace deposits are recognized by gentle to flat topographic surfaces, located above the current floodplain elevation, and the occurrence of well-rounded quartz gravels and weathered cobbles. The ages of terraces are related to elevation, with the oldest terrace at higher elevation, and the commonly contain the most weathered quartz pebbles. These deposits consist of poorly sorted, unconsolidated sediments ranging from silt to boulders and likely do not exceed a few meters in thickness. Terraces are composite and are modified by subsequent erosion. Similar deposits were recognized by Hadley and Goldsmith (1963) along the flanks of the floodplain of Jonathans Creek.

Colluvium. The steep topography of the Great Balsam Mountains yields numerous and prominent colluvial features. These features were mapped by combined field observations and interpretation of topographic maps. This unit includes talus deposits, block fields, and alluvial-colluvial fans. The colluvium generally consists of poorly sorted, unconsolidated large boulders to clay-sized material. Large boulders to cobbles are angular and variably weathered. Many of the colluvial fan deposits may represent the accumulations of multiple ancient debris flows. Thickness ranges from 0–40 m, and the larger deposits occur at the base of cliff and exfoliation domes, and on the flanks of steep ridges. Some of the largest deposits occur along flanks of Lickstone Ridge including Francis Cove at it northern end, just of south of Waynesville, and Big Creek Cove near Burnett Siding (Plate 1).

Colluvium-Alluvium undifferentiated. The distinction between colluvium and alluvium is not easily recognized in many places. Commonly where streams incur a local decrease in gradient it becomes difficult the differentiate deposits of strictly colluvium, alluvium, or colluvium reworked by alluvial processes. These deposits are mapped as undifferentiated colluvium and alluvium.

Landslide. Potentially the most dangerous geologic hazards in the western North Carolina Blue Ridge are landslides. Landslides are the result of multiple contributing factors including geology, climate, and anthropogenic activities. The hurricane season of 2004 was especially devastating to parts of western North Carolina. During September 2004, the remnants of hurricanes Frances and Ivan inundated western North Carolina

with rain and triggered over 130 reported slope movements, resulting in the destruction of 27 homes, and 5 deaths (NCGS website). All landslides encountered in the field were mapped, and older landslides were mapped using aerial photographs and interpretation of topographic maps. Most of the recent landslides mapped are interpreted to be the result of the remnants of hurricanes Frances and Ivan. Landslide deposits consist of undifferentiated debris flow, slide, and rock slide deposits of poorly sorted colluvial soils to angular boulders. The bedrock scarp and slide track are included. Table 1–2 lists the observed and interpreted landslides, possible age, and scarp.

METAMORPHISM

The western North Carolina Blue Ridge is largely an amphibolite facies metamorphic core (Carpenter, 1970; Hadley and Nelson, 1971; Butler, 1991; Hatcher and Goldberg, 1991). Hadley and Nelson (1971) indicated that most of the rocks in the study area are in the sillimanite zone, with several areas of migmatite. Later regional metamorphic isograd maps display a narrower distribution of the sillimanite zone and slight broader distribution of kyanite zone rocks (Butler, 1991; Hatcher and Goldberg, 1991). Further to the southwest in northeastern Georgia and southwestern North Carolina, the Dahlonega gold belt is dominantly kyanite to kyanite-staurolite zone, leading Hatcher and Goldberg (1991) to extend a fault bounded domain of kyanite-staurolite zone rocks into parts of the Waynesville and Sam Knob 7.5-minute quadrangles. To the northeast, Merschat and Wiener (1988) recognized that the rocks of the Holland Mountain thrust sheet, Tugaloo terrane, are largely in the sillimanite zone with the kyanite-sillimanite isograd located in a klippe to the northwest. East of the Sam Knob quadrangle, the sillimanite-kyanite isograd in Tugaloo terrane was mapped trending NE-SW into the study area (Acker, 1982), the Tugaloo terrane likely remains in or below the kyanite zone to the Brevard fault zone (Hatcher, 1973; Horton, 1982).

Metamorphism in the western North Carolina Blue Ridge is generally attributed to three Paleozoic orogenies: the Taconic, 480-460 Ma; Neoacadian-Acadian, 380-360 Ma (Carrigan et al., 2001; Hatcher, 2002; Hatcher and Merschat, 2006), and Alleghanian, 320-260 Ma (Hatcher, 1989; Hatcher et al., 2007). Various studies have attempted to demarcate the timing of metamorphism in the Blue Ridge (Dallmeyer, 1988; Connelly and Dallmeyer, 1993; Goldberg and Dallmeyer, 1997; Moecher et al., 2004; Corrie and Kohn, 2007), often with conflicting results. SHRIMP U-Pb ages of zircon rims (see Part III) further support the polymetamorphic history of the Blue Ridge, and attempts to separate the orogen into domains of similar metamorphic histories. To help resolve the

Table 1–2. Description of recognized landslide deposits.

Number*	Quadrangle	Location	Type	Scarp	Age	Reference/Indentification
1	Waynesville	Francis Cove, Wolfpen Mountain	Debris Flow	Jeep trail	Sept. 2004	Field
2	Waynesville	N.C. Hwy 276, Pigeon Gap	Slump	Highway fill	Active	Field
3	Waynesville	Smoky Cove	Debris Flow	Jeep trail	Fall, 2003	Ray Griffin, personal comm.
4	Waynesville	Marge Mountain	Debris flow	Bedrock	~15-20 yrs old	Munroe Miller, personal comm.
5	Waynesville	Big Ridge	Debris Flow	Logging road	20+ years	Field
6	Waynesville	Murray Cove	Debris flow	Logging road	20+ years	Field
7	Waynesville	Big Ridge	Debris flow track	Bedrock	1941-1979	Topo revisions
8	Waynesville	Big Creek Cove	Debris Flow	USFS Rd. 97	Sept. 2004	Field
9	Waynesville	Big Creek Cove	Debris Flow track	Bedrock	1941-1979	Topo revision
10	Waynesville	Laurel Branch	Debris Flow	USFS Rd. 97	Sept. 2004	Field
11	Waynesville	Spruce Ridge	Debris Flow Track	Bedrock	20+ years	Aerial Photo
12	Waynesville	Spruce Ridge	Debris flow track	Bedrock	20+ years	Aerial Photo
13	Waynesville	Spruce Ridge	Debris Flow Track	Bedrock	20+ years	Aerial Photo
14	Waynesville	Spruce Ridge	Debris Flow Track	Bedrock	20+ years	Aerial Photo
15	Waynesville	Queen Creek	Debris Flow	USFS Rd. 97	Sept. 2004	Field
16	Waynesville	Hwy. 215	Debris Flow	Hwy. 215	Sept. 2004	Field
17	Waynesville	Cathey Cove	Slump	Bedrock	Active	Field
18	Sam Knob	Hwy. 215	Debris Flow	Hwy. 215	Sept. 2004	Field
19	Sam Knob	Green Ridge	Debris Flow	Bedrock	Sept. 2004	Field
20	Sam Knob	Green Ridge	Debris Flow	Bedrock	Sept. 2004	Field
21	Sam Knob	Green Knob	Debris flow track	Bedrock		Aerial Photo
22	Sam Knob	Green Knob	Debris flow track	Bedrock		Aerial Photo
23	Sam Knob	Green Knob	Debris flow track	Bedrock	Sept. 2004	Field
24	Sam Knob	Flat Laurel Creek	Debris Flow	Bedrock	Sept. 2004	Field
25	Sam Knob	Chestnut Ridge	Debris Flow	Logging Road	Sept. 2004	Field
26	Sam Knob	Charley Creek	Debris Flow	Development Road	Sept. 2004	Field

*Number corresponds to landslide identified on Plate 1.

metamorphic history of this study area and part of the central and eastern Blue Ridge, this study identified metamorphic index minerals and textures in the field. Timing is delimited by crosscutting relationships of undeformed igneous bodies and quantitatively by SHRIMP U-Pb metamorphic zircon ages.

Field identification of metamorphic index minerals, textures, and petrography were combined to create a metamorphic isograd map of the Waynesville and Sam Knob 7.5-minute quadrangles (Fig. 1–8). Rocks in the study area are all in the upper amphibolite facies, ranging from kyanite-staurolite to sillimanite II zones. Metamorphic index minerals, sillimanite, kyanite, and staurolite were observed in pelitic rocks of the Dahlonega gold belt in the GBMW, and Tugaloo terrane. No metamorphic index minerals were observed in the Cartoogechaye terrane, probably a function of bulk composition. Rocks of the GBMW are mostly sillimanite I and II zones, with a minor area of kyanite zone rocks. In the Chattahoochee-Holland Mountain thrust sheet Tallulah Falls Formation, grade decreases southward from sillimanite I to kyanite-staurolite zone.

Cartoogechaye terrane

The Cartoogechaye terrane contains a sillimanite II and granulite facies metamorphic assemblages to the southwest (Hatcher and Butler, 1979; Eckert et al., 1989), but in the Waynesville quadrangle contains only upper amphibolite facies assemblages. The rocks commonly contain biotite, garnet, and hornblende, but no key metamorphic index minerals were observed in the field or in thin section. The rocks are characteristically migmatitic. The mineral assemblage of the dominant rock type, migmatitic biotite gneiss includes:

± muscovite ± epidote/clinozoisite ± garnet + biotite + quartz + K-feldspar + plagioclase + opaques

Migmatitic amphibolites from the Cartoogechaye terrane contain the assemblage:

± garnet ± biotite + plagioclase + hornblende + opaques

Garnets in the amphibolite vary in size from 0.5 cm to 2 cm in diameter. Locally, garnet amphibolites were observed with plagioclase coronas surrounding garnets.

Various migmatite structures were observed in the Cartoogechaye terrane during fieldwork. Migmatite structures observed include stromatic (layered), schollen (raft), fold , phlebitic (vein), agmatite (breccia), and schlieren. Migmatite structures developed in amphibolite units commonly displayed agmatitic, stromatic, and schlieren. Leucosomes developed in the amphibolite contain hornblende, suggesting higher-temperature of metamorphism.

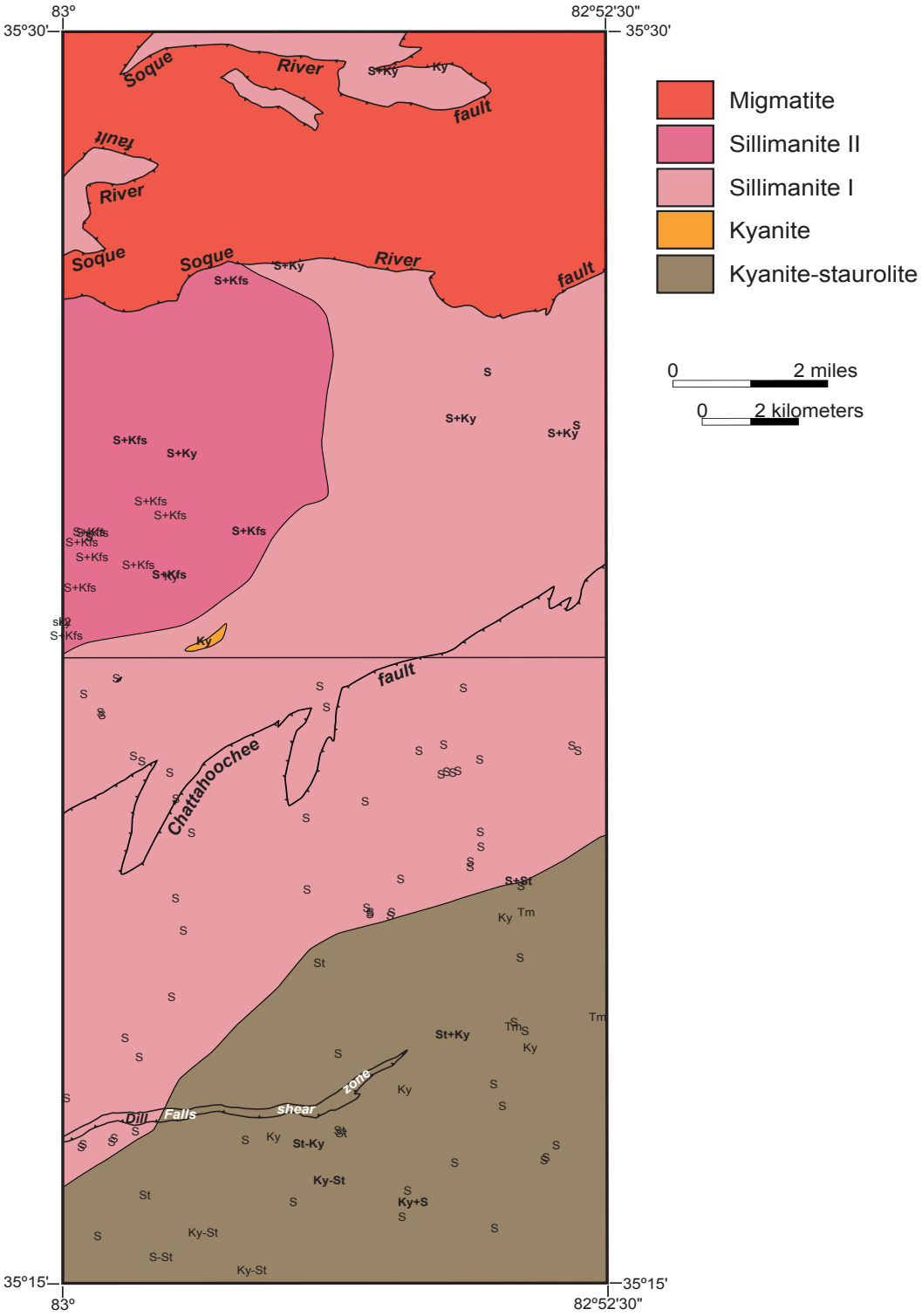

Figure 1–8. Metamorphic isograd map of the Waynesville and Sam Knob 7.5-minute quadrangles based on field and petrographic (bold face) observations of key index minerals and mineral assemblages. Mineral abbreviations are Kfs, potassium feldspar; Ky, kyanite; S, sillimanite; St, staurolite; and Tm, tourmaline.

Great Balsam Mountains window: Otto Formation

The northern end of the GBMW consists of mostly sillimanite I and II zone rocks with a small area of kyanite zone rocks (Fig. 1–8). Aluminous pelitic schists of the Otto Formation generally contain sillimanite, and locally kyanite, which were readily visible using a 10x hand lens. The second sillimanite isograd was mapped based on presence of sillimanite and K-feldspar and absence of muscovite in the pelitic rocks of the Otto Formation. The two assemblages observed in the schist include:

muscovite + biotite + garnet + sillimanite + quartz + plagioclase (A1)

biotite + garnet + sillimanite + K-feldspar + plagioclase +quartz (A2)

Sillimanite in both assemblages consists of small to large prismatic needles, aligned to the dominant foliation and often defining a lineation. Garnet porphyroclasts are commonly surrounded by sillimanite or have sillimanite tails (Fig. 1–9). Quartz often has sillimanite growing through or over it. Kyanite occurs in several samples, but is often kinked, bent, and overgrown with sillimanite (Fig. 1–9), except from samples from within the kyanite zone. Field and petrographic observations revealed that large kyanite porphyroblasts are the only aluminum silicate in this zone. Rocks from this narrow zone contain the assemblage

muscovite + biotite + kyanite + quartz + plagioclase (A3)

Garnets from throughout the GBMW are optically zoned, indicating two stages of growth. Garnet cores generally contain inclusions of biotite, quartz, sillimanite, plagioclase, and kyanite, while rims are inclusion free. Some garnets, however, contain late often radial fibrolitic sillimanite needles.

Rocks of the GBMW are migmatitic, although the character and amount of migmatization present is considerably less than in the Cartoogechaye and Tugaloo terranes. Migmatite structures observed in the GBMW include stromatic (layered), schlieren, and augen structures. Leucosomes generally contain quartz, K-feldspar, and minor biotite, muscovite, garnet, and Fe-sulfides. Larger, 10–30 cm thick, leucosome layers are often coarse-grained to pegmatitic.

Assemblages of the mafic and ultramafic rocks observed in the GBMW are consistent upper amphibolite facies. The few amphibolite, ultramafic, and metadunite bodies contain the respective assemblages

quartz + plagioclase + hornblende (A4)

anthyopholite + talc + opaques (A5)

olivine + tremolite + talc + chromite (A6)

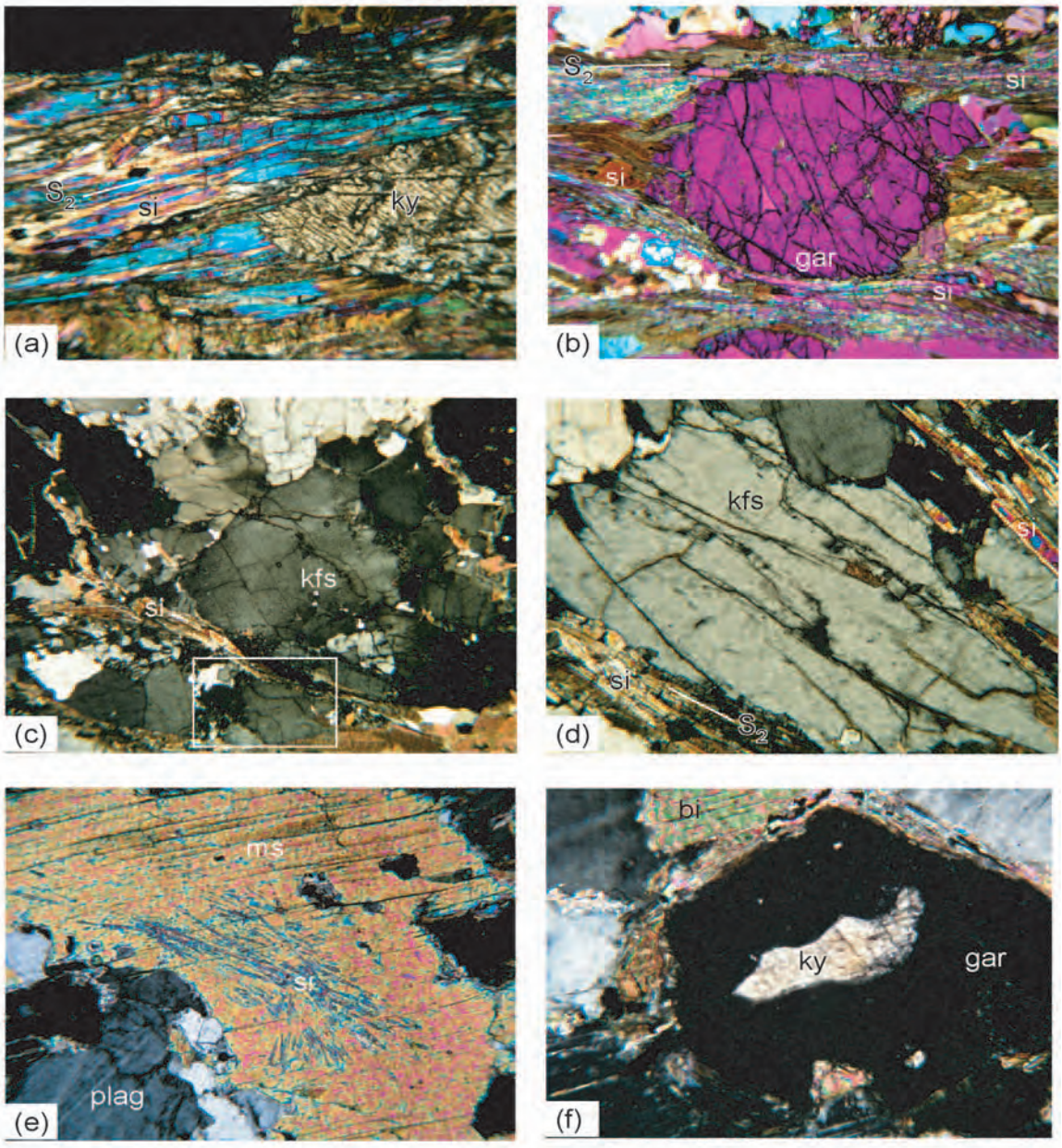

Figure 1–9. Photomicrographs of different mineral assemblages from the GBMW. (a) Prismatic sillimanite surrounding a kyanite porphyroblast from Otto Formation schist. (b) Optically zoned garnet with tails of garnet, biotite, and prismatic sillimanite. S_2 foliation surrounding garnet defined by prismatic sillimanite, biotite, quartz and potassium feldspar. Gypsum plate is inserted. (c) Sillimanite II assemblage of perthitic potassium feldspar + sillimanite + biotite + quartz, observed in Otto Formation aluminous schist. Inset white box indicates location of (d). (d) Perthitic potassium feldspar and prismatic sillimanite from the Otto Formation aluminous schist as sillimanite II. (e) Muscovite with inclusions of sillimanite needles from the Tallulah Falls Formation. (f) Subhedral garnet with inclusion of kyanite from the Tallulah Falls Formation metagraywacke. Mineral abbreviations are: bi–biotite, gar–garnet, kfs–potassium feldspar, ky–kyanite, ms–muscovite, plag–plagioclase, and si–sillimanite.

Locally, agmatite and stromatic migmatite have been observed in these amphibolite bodies. No migmatite structures were observed in the ultramafic bodies. Mineral assemblages of both mafic and ultramafic rocks are consistent with sillimanite I and II grade metamorphism observed in the GBMW.

Retrograde textures and assemblages recognized in the GBMW include the replacement of minerals by sericite and chlorite, and growth of late coarse-grained muscovite. The replacement of prograde minerals by retrogade metamorphism is sparse and localized, but seems more common toward the southeast. Sericite and chlorite (pinite) are the dominant retrograde minerals observed. Sericite occurs as a fine-grained groundmass or mats, usually parallel to the relict foliation, surrounding porphyroclasts of garnet, sillimanite, quartz, and occasional plagioclase. Chlorite developed locally, replacing chlorite and garnet along cleavage planes and fractures, respectively. Some mats of chlorite exist, likely representing an entirely replaced porphyroblast. Coarse-grained poikiloblastic muscovite occurs throughout the GBMW. Muscovite poikiloblasts often contain inclusions of sillimanite, biotite, quartz, and opaques. Some muscovite poikiloblasts are lath-shaped, suggesting replacement of kyanite, but most are subhedral and subparallel to foliation making it difficult to determine the mineral(s) replaced.

Tugaloo Terrane

Based on field and petrographic identification of index metamorphic minerals, the sillimanite I zone continues southward across the Chattahoochee-Holland Mountain fault and into Tugaloo terrane (Fig. 1–8). Metamorphic grade decreases to kyanite and kyanite-staurolite zone to the southeast in the Sam Knob quadrangle. Despite being the same grade as parts of the GBMW, the Tallulah Falls Formation is generally more migmatitic, with common stromatic (layered) migmatite and lesser agmatite.

Similar rock types and grade results in similar assemblages and textures as observed in the GBMW. Typical assemblages observed in the pelitic rocks of the Tallulah Falls Formation include:

garnet + sillimanite + muscovite + biotite + quartz + plagioclase + opaques (A7)

garnet ± sillimanite + kyanite + muscovite + biotite + quartz + plagioclase + opaques (A8)

garnet ± sillimanite + kyanite + staurolite + muscovite + biotite + quartz + plagioclase + opaques (A9)

Sillimanite occurs as prismatic needles that help define the dominant foliation, in the sillimanite zone. In the kyanite-staurolite zone, sillimanite occurs as isolated clusters and trails of small prismatic sillimanite needles. These isolated sillimanite needles

occur as inclusion trails in coarse-grained muscovite (Fig. 1–9), along plagioclase grain boundaries, and as inclusions in garnet and quartz. In these same samples kyanite occurs as sub- to euhedral porphyroblasts. Staurolite occurs as sub- to euhedral poikiloblasts, occasionally twinned, and usually visible in hand specimen.

Garnets show significant variation in the Tallulah Falls Formation. Most garnets are 0.5–1 cm in diameter, subhedral to anhedral, and often embayed, although some samples contain 0.1 –0.25-cm diameter euhedral inclusion-free garnets. Optically, two stages of garnet growth can be discerned: inclusion-rich cores surrounded by clean rims. Garnets commonly contain inclusions of quartz, biotite, muscovite, plagioclase, sillimanite, and opaques.

The magnetite-bearing, chlorite-muscovite schist, although similar to the other metapelitic rocks of the Tallulah Falls Formation, remains distinct because of the number of Fe-phases present.

± garnet ± sillimanite ± staurolite + kyanite + chlorite + muscovite + biotite + quartz + plagioclase + magnetite (A10)

Magnetite occurs as euhedral to subhedral grains from 0.25 – 2 cm in length, and are roughly aligned with the foliation. The largest magnetite grains, 1–2 cm, occur in muscovite-quartz-feldspar leucosomes. Pleochroic green to greenish yellow to brown chlorite is medium- to coarse-grained are both parallel and oblique to the foliation. Chlorite frequently replaces biotite. Garnets from the chlorite, muscovite schist vary in size from 0.25 cm to 2 cm in diameter, and are less abundant than in other metapelitic units of the Tallulah Falls Formation. Large, euhedral, 2 cm diameter garnets contain inclusion trails of magnetite, biotite, chlorite, and quartz aligned parallel to the surrounding foliation, suggesting late garnet growth.

Mafic and ultramafic rocks contain similar assemblages as in the GBMW (A4, A5, and A6), consistent with upper amphibolite facies metamorphism. Amphibolites of the Chattahoochee-Holland Mountain thrust sheet, however, can be coarse-grained, contain less migmatite, and commonly contain garnet.

Rocks of the Chattahoochee-Holland Mountain thrust sheet are migmatitic, and locally display two episodes of migmatization. Stromatic migmatite parallel to the regional foliation is common in most exposures with lesser amounts of agmatite (breccia) occurring locally. Leucosomes are generally medium- to coarse-grained and consist of quartz, K-feldspar, ±muscovite, and ±biotite. At some locations, stromatic leucosomes are cut by coarse-grained, quartz-feldspar leucosomes that are slightly oblique to the regional foliation, suggesting a second or late stage of migmatization. Areas with

agmatite structures are present at the mesoscopic scale and produce areas of chaotically oriented foliations.

Retrograde assemblages and textures involving the replacement of different minerals by sericite and chlorite, and growth of late coarse-grained muscovite, similar to those observed in the GBMW, are also observed in the Tugaloo terrane.

Summary of Metamorphic Events

Observations of metamorphism and relative age suggest at least three metamorphic events have affected parts of the central and eastern Blue Ridge in western North Carolina. The earliest metamorphic event M_1 is preserved in boudins and pods of amphibolite. Similar assemblages as recognized in amphibolite map-scale bodies suggest that M_1 was likely the early stage of M_2, the dominant metamorphic event in the terranes. M_2 is characterized by upper amphibolite facies assemblages, including kyanite to sillimanite II (A1-A6). The kyanite-staurolite zone in the southern part of the Sam Knob quadrangle could represent decreasing grade during M_2. The presence of sillimanite needles preserved as inclusion trails in coarse-grained poikiloblastic muscovite, between plagioclase grain boundaries, and as inclusion in garnet and quartz suggest this is a later event M_3, defined by the growth of kyanite + staurolite + muscovite, replacing an earlier assemblage in which sillimanite was present. Later retrograde fabrics and textures involving the replacement of M_2 and M_3 assemblages with sericite and chlorite are combined into M_4.

Relative and Absolute Ages of Metamorphism: Field Relationships and SHRIMP U-Pb ages

Metamorphism in the terranes of the Waynesville and Sam Knob 7.5-minute quadrangles is bracketed by known ages of intrusive units and U-Pb ages of metamorphic zircon rims to provide an absolute age of metamorphism. Together these suggest the terranes are affected by a Middle to Late Ordovician (Llandeilan to Caradocian) amphibolite metamorphism, and a later Mississippian event.

The Cartoogechaye, GBMW, and Tugaloo terranes are all intruded by similar trondhjemite dikes and local sills. These dikes are not as common in the Tugaloo terrane as the other two terranes, but a few occurrences were recognized. These dikes both truncate the dominant regional foliation defined by peak mineral assemblages and stromatic migmatite, where developed. At several locations, however, the foliation in the country rock is deflected and transposed into the dike contact. Trondhjemite dikes from

three locations in the Great Balsam Mountains have been sampled and dated. Mapes (2002) yielded a U-Pb age of 402±4 Ma from a trondhjemite dike that intruded Otto Formation of the GBMW at Cove Field Ridge overlook on the Blue Ridge Parkway. Two additional trondhjemite dikes sampled in this study yielded U-Pb ages of 449±4 Ma from a dike in the Cartoogechaye terrane near Waynesville, and a U-Pb age of ~451 Ma from the southern end of the GBMW in the Sylva South quadrangle. Although the dikes are not as common in the Tugaloo terrane, the trondhjemite dikes suggest the M_2 occurred prior to ~449 Ma in the study area.

The Horseshoe Rock granite, and several texturally and compositionally similar 1–2 m dikes that occur in the vicinity of the main body, intruded M_3 kyanite-staurolite zone Tallulah Falls Formation. Foliation in the schist and gneisses of the Tallulah Falls Formation are truncated along the intrusions (Fig. 1–5). Although this unit is not dated, it is correlated with the ~342 Ma Round Mountain granite (Varnell et al., 2008), and suggests M_3 is pre-342 Ma. The formation of kyanite after sillimanite suggests crustal loading, and M_3 is interpreted to be the result of Devonian-Mississippian tectonothermal event.

SHRIMP U-Pb ages of metamorphic rims of zircons from the Cartoogechaye and GBMW provide an absolute age of the time of near-peak metamorphism, M_2. Cathodoluminescence images of zircons from the Cartoogechaye terrane migmatitic biotite gneiss (W18) contain abundant bright white metamorphic rims (Fig. 1–10). The rims were low in U, as indicated by the bright white color, and yielded an age of 494±35 Ma (Fig. 1–10; see also Part III). Metamorphic rims analyzed from the GBMW at Cove Field Ridge overlook yielded ages of between 465–450 Ma with an average of 455±12 Ma (Fig. 1–8), and is consistent with field relationships of the regional S_2 foliation truncated against ~407 Ma dikes. The large error associated with the age determined from the low-U rims in W18 overlaps the metamorphic ages obtained from the GBMW, and does not preclude these events are the same. The age of ~455 Ma is interpreted as the timing of near-peak M_2 metamorphism in the GBMW, Cartoogechaye, and Tugaloo terranes.

Additional U-Pb ages zircon rims from the central and eastern Blue Ridge, including published U-Pb zircon ages, monazite chemical ages, and Ar-Ar cooling ages, are presented and described in detail in Part III. These ages support a 465–450 Ma timing of peak metamorphism in western North Carolina Blue Ridge, particularly in the terranes of the western and central Blue Ridge. No zircon rim ages have been reported from the western Blue Ridge, although several monazite ages exist. Moecher et al. (2005) reported

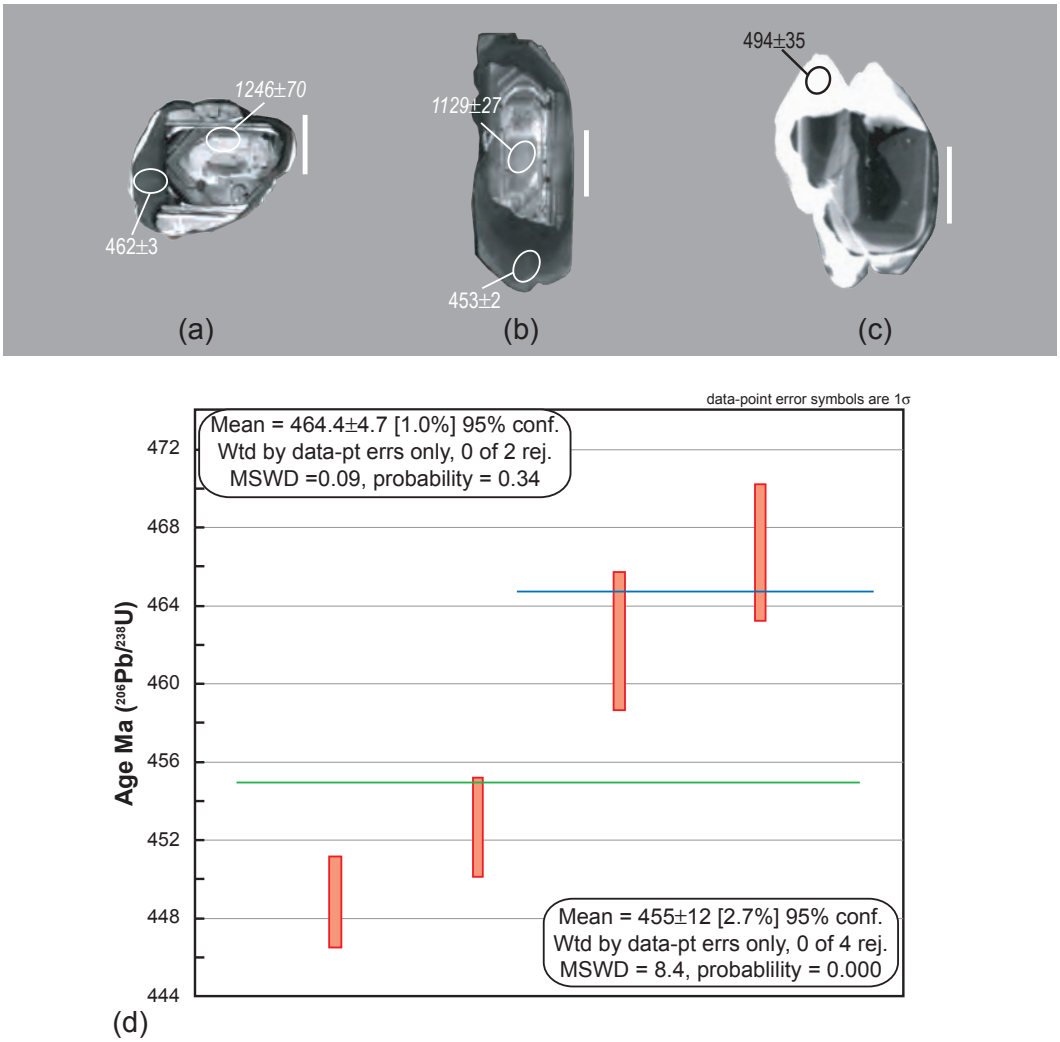

Figure 1–10. CL images of selected zircon with metamorphic rims from the Cartoogechayee and GBMW (a)-(c). Scale bars are 100 mm; italicized ages are Pb/Pb, all others are 206Pb/238U ages. (a)-(b) Dark gray to black roughly concentric, metamorphic rims surrounding core and truncating interior oscillatory zoning fro HAZ2 (see Part III for discussion and location). (c) Anhedral zircon with bright white metamorphic rims from sample W18. Note the white reabsorption feature between rim and core. (d) Weighted average of 206Pb/238U ages of metamorphic rims from HAZ2, Otto Formation, Great Balsam Mountains window at Cove Field Ridge Overlook on the Blue Ridge Parkway.

a chemical monazite age from Great Smoky Group rocks of ~459 Ma just meters below the Hayesville fault, and ~467 Ma further to the west. Corrie and Kohn (2007) reported a TIMS U-Pb age of microdrilled monazite of ~450 Ma from staurolite to kyanite zone Great Smoky Group rocks just south of the Great Smoky Mountains. U-Pb zircon ages include ~453 Ma from the granulite at Winding Stair Gap (Moecher et al., 2004). Several other U-Pb SHRIMP analyses of zircon rims from different locations in the Cowrock and Cartoogechaye terranes range from 490–440 Ma (Part III). Collectively, these suggest the terranes of the central and western Blue Ridge were amalgated and subjected to a regional upper amphibolite to granulite facies event during the Middle Ordovician Taconian orogeny (460–450 Ma).

Metamorphism in the Tugaloo terrane is more complicated, with several different ages yielded by different geochronometers. The Lick Ridge ecologite yields a U-Pb age of ~459 Ma (Miller et al., 2006), while metamorphic zircon rims have yielded ages of 365 and 359 Ma (Carrigan et al., 2001, 2003; Bream, 2003; Part III). Stahr (2007) recognized that a migmatitic contact aureole surrounds the ~466 Ma Whiteside Granite, and suggested that metamorphism in the Tugaloo terrane has similar age. Ar/Ar hornblende and muscovite ages from the Tugaloo terrane near Highlands, North Carolina indicate Mississippian cooling (Burton and Kunk, 2006). The Tugaloo terrane is polymetamorphic; overprinted by similar amphibolite facies metamorphisms during the Ordovician, M_2, and again during the Devonian to Mississippian, M_3 and possibly M_4.

The relative and absolute ages presented suggest that M_2 produced the regional upper amphibolite facies metamorphism, kyanite to sillimanite II zone at 465–450 Ma. This event affected the Cartoogechaye terrane and GBMW, and likely the Tugaloo terrane as well. M_3 recognized by the stable assemblage of muscovite + kyanite ± staurolite with relict sillimanite needles preserved as inclusions in muscovite, garnet, and quartz, likely occurred during the Devonian to Mississippian. This event likely corresponds to the Neoacadian orogeny as the eastern Blue Ridge was overthrust by the Inner Piedmont and Carolina superterrane, and locally remobilized. Although M_3 is recognized as kyanite-staurolite grade in the Sam Knob quadrangle, it may increase to sillimanite grade along strike.

STRUCTURE

The Blue Ridge has generally been described as a polydeformed crystalline thrust stack (e.g., Hatcher and Goldberg, 1991), an adequate description of the structure of the geology in the Waynesville and Sam Knob 7.5-minute quadrangles. The three

thrust sheets recognized in this study are exposed in a ductile eyelid duplex and contain polydeformed upper amphibolite facies rocks. Structural data and field observations presented here support a similar polydeformational history of the Blue Ridge as described by previous studies in this area (e.g., Hadley and Goldsmith, 1963; Hatcher, 1977; Hatcher and Butler, 1979; Merschat and Wiener, 1988: Quinn, 1991; Massey and Moecher, 2005; Stahr, 2007) (Table 1–3). Evidence of the polydeformational history includes multiple transposed foliations, different fold orientations and geometries, superposed folds, crenulations, and late brittle faults and joints. These deformations extend from early ductile deformations to late brittle deformation associated with uplift. Most of the deformational events are common to all three terranes, but some of the events are more pronounced or developed in a particular terrane or area. Stahr (2007) noted that in the vicinity of large plutons in the Tugaloo terrane deformational styles and possible timing differed from the regional deformations observed.

Form-lines drawn parallel to the regional foliation, S_2, are used to separate the study area into seven different homogenous domains (Fig. 1–11). The majority of the domains, I–V, and variation in structural trends occur in the Waynesville quadrangle. Domain VI, the largest domain, includes almost the entire Sam Knob quadrangle and the southeastern part of the Waynesville quadrangle, and is characterized by NE–SW trends and steep NW dips (Figs. 1–11 and 1–12). Although strike varies significantly, dip remains moderate to steep in all domains. Saddle-shaped patterns displayed by the contoured poles to foliation (Fig. 1–12) is common of superposed folds, but the variation in the beta axes suggests it may be the result of local fluctuations of the steep dips common throughout all the domains.

The form-line map and domains help accentuate map-scale fold patterns and relationships between faults and other structures. Domains I-V define the NE-plunging Lickstone Ridge antiform. Foliations in the Cartoogechaye terrane trend NE–SW, E–W, and NW–SE, and define a broad antiformal structure. In the core of the window, the Lickstone Ridge antiform tightens to a closed fold, and foliations in domains IV and V trend WNW–ESE and N–S. The large domain VI characterized by NE-SE trending, and NW dipping foliations defines the southeastern limb of the fold in the Waynesville quadrangle. Foliations are parallel across both the Soque River and Chattahoochee–Holland Mountain faults, and are superposed by later NE-trending tight folds, and closed to open E-W trending folds. Map-scale folds delineated from the formlines include the NNE-plunging Lickstone Ridge and Wolf Creek antiforms. Local variations in foliation orientations are the result of superposed folds, but are not map scale.

Table 1–3. Summary of major Paleozoic and younger deformational events and related structures and metamorphisms that have affected the Blue Ridge. Modified from Hopson et al. (1989) and Merschat et al. (2005).

EVENTS	STRUCTURES			METAMORPHIC CONDITIONS	REGIONAL EVENTS	OROGENY & TIMING
	Fabrics	Folds	Faults	*Z* *PP* *Gs* *A* *G*		
D_1	S_1 Early foliation preserved in amphiboolite and calc-silicate boudins	F_1 Intrafolial folds and isoclinal folds preserved in boudins	Greenbrier fault, Hayesville fault (?)	M_1 Moderate to high pressure and temperature	Initial collision of central and eastern BR terranes with western BR	Pre- to early Taconian pre~465 Ma
D_2	S_2 Penetrative foliation L_2 Mineral lineation	F_2 Inclined to recumbent, tight to isoclinal passive and flexural flow folds, and sheath folds;	Shope Fork-Chunky Gal Mountain, Soque River, Chattahoochee-Holland Mountain faults	M_2 Peak metamorphism, greenschist (middle amphibolite in map area) to granulite facies	Continued collision of BR terranes, intrusion of synkinematic plutons (Whiteside, Persimmon Creek)	Taconian 465 – 450 Ma
D_3	S_3 Reactivates S_2 L_3 Mineral and intersection lineations, NE-SW	F_3 Inclined to upright, tight to open folds, trend NE-SW, & E-W	Dextral strike-slip kinematics, Burnsville fault, Chattahoochee fault, NE GA	M_3 Middle amphibolite facies; new growth of muscovite, kyanite, and staurolite	Collision of Carolina superterrane; mobilizes IP and parts of eastern BR as SW-directed orogenic channel flow	Neoacadian 365 – 345 Ma
D_4	S_4 reactivation of S_3, solid-state fabrics in Miss. plutons, S-C fabrics in faults Mineral lineations	F_4 Upright, open folds, trend NW-SE, & NE; crenulations plunge SE & NE	Ductile reactivation of Chattahoochee, BFZ, Dills Falls, and CFAF	Greenschist to middle amphibolite facies (retrogressive)	Intrusion of Miss. synkinematic plutons & initial emplacement of the BR-IP thrust sheet	Alleghanian: Early 335–320 Ma; Middle ~300 Ma; Late ~260 Ma
D_5	Joints Mineralized (?)	Regional broad, open folds, most trend NE & NW	Brittle NW-directed thrusts; Great Smoky, Rosman faults	Brittle conditions	Cont'd. emplacement and exhumation of the BR-IP thrust sheet	
$D_{6...}$	Filled joints Unfilled joints	Regional broad, open folds, trend NE	Meso- and macroscale normal faults	M_4 Brittle conditions	Rifting — ? — Uplift	Mesozoic extension — ? — Cenozoic uplift

Shaded gray boxes indicates range of metamorphic conditions associated with each event.
Metamorhpic facies: *Z* – Zeolite, *PP* – Prehnite-Pumpellyite, *Gs* – Greenschist, *A* – Amphibolite, *G* – Granulite.
BFZ—Brevard fault zone. BR–Blue Ridge. CFAF–Cradle or Forestry-in-America fault. IP–Inner Piedmont.

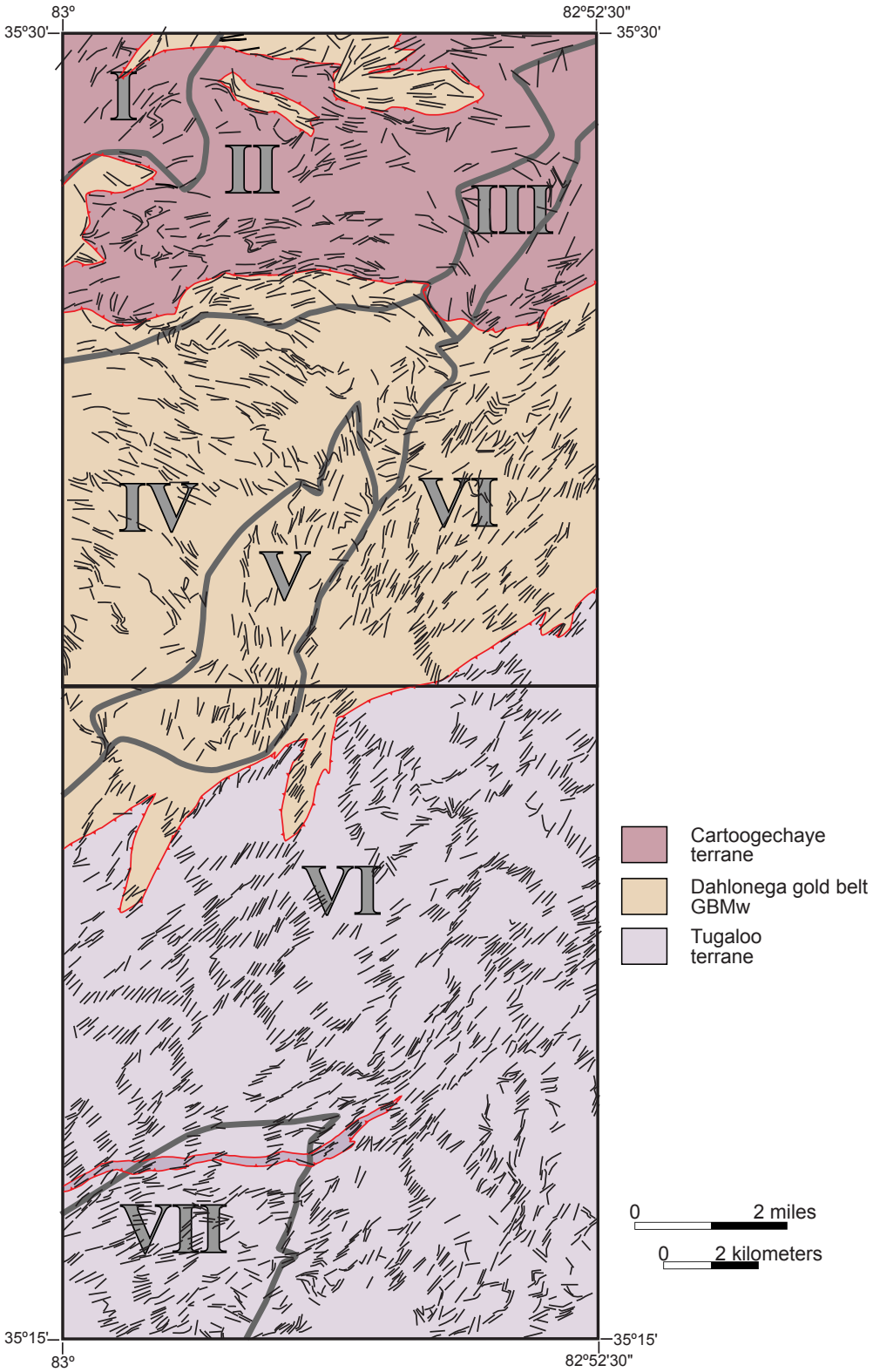

Figure 1–11. Form-line map of S_2 foliation and defined homogeneous domains. Faults are in red.

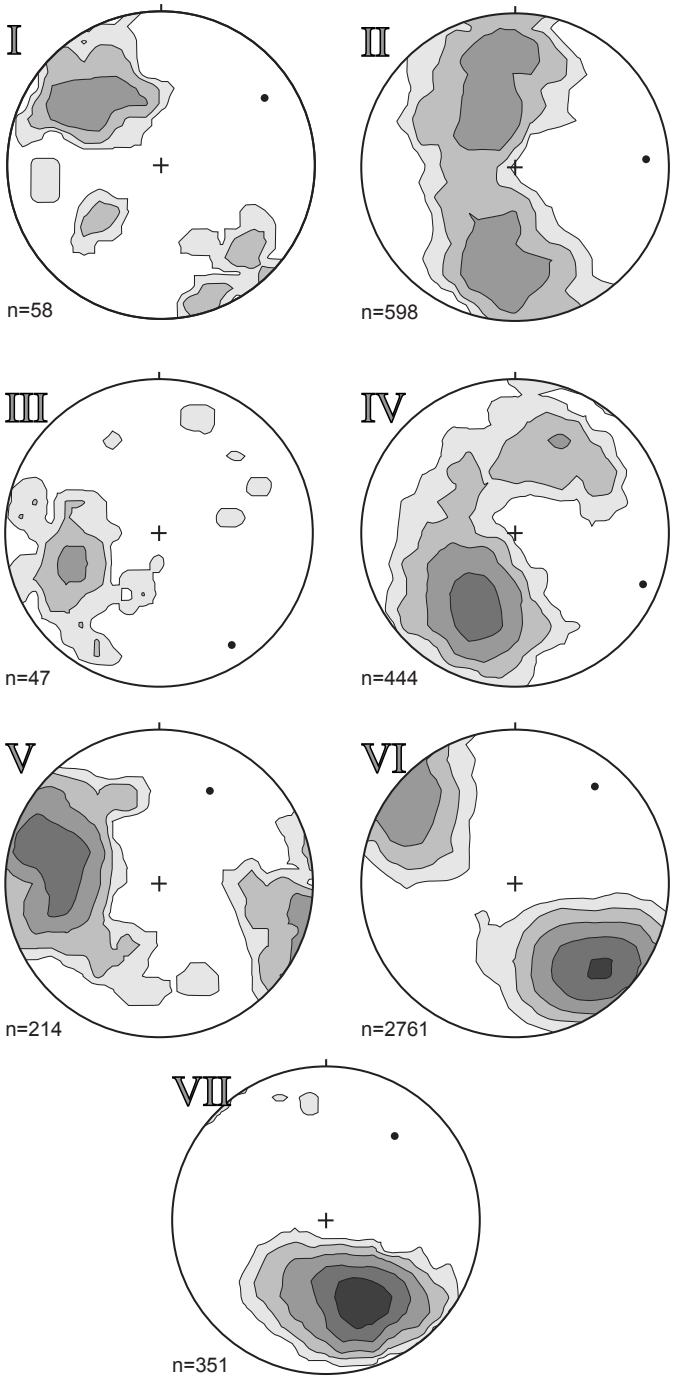

Figure 1–12. Equal-area, lower-hemisphere stereonets of poles to regional S_2 foliation and calculated beta-axes for each domain. Contour intervals are 1, 2, 4, and 8%.

Linear structures, mineral lineations, and fold axes also display a similar variation of orientation according to domain (Figs. 1–13, and 1–14). Mineral lineations throughout most of the terranes are subparallel to the dominant strike of the foliation. In the GBMW, mineral lineations are commonly defined by aligned prismatic sillimanite and plunge gently sub-parallel to the strike of foliation. Multiple fold generations are recognized in the area, the most common are tight to isoclinal F_2 and F_3 folds trend subparallel to the general foliation strike in each domain (Figs. 1–12 and 1–14). Axial surfaces of most F_2 folds (isoclinal to tight folds) are parallel to foliation. In domains II, VI, and VII the L_2 mineral lineations are subparallel to F_2 and F_3 folds (Figs, 12 and 14). Late closed to open subvertical to inclined folds, F_4 to F_5, plunge gently NE in most domains. Crenulations, most common in the Tugaloo terrane and domains VI-VII, also plunge gently NE–SW, coaxial to F_4 to F_5 folds.

Faults

Three ductile faults recognized in the Waynesville and Sam Knob 7.5–minute quadrangles are the Soque River, Chattahoochee-Holland Mountain faults, and the Dill Falls shear zone (Fig. 1–2). The Soque River and Chattahoochee-Holland Mountain faults separate the terranes of the central and eastern Blue Ridge. The Dill Falls shear zone is recognized and described by this report, and is an intraterrane fault within the Tugaloo terrane. The geometries, and kinematics of the faults are discussed further below.

Soque River fault

Gillon (1982) and Nelson (1982) first recognized that the northwest boundary of the Dahlonega gold belt was a fault. In northeast Georgia and parts of southwestern North Carolina, a significant metamorphic break is associated with this fault. Although Hatcher (1980) did not initially recognize the Soque River fault in the Prentiss quadrangle, later revaluations of the geology indicated that it truncates the Shope Fork fault and the Cowrock terrane, and migmatitic biotite gneiss of the Cartoogechaye terrane overlies the Dahlonega gold belt to the northwest (e.g., Hopson et al., 1989; Part II). This relationship continues to the northeast and in the GBMW where the Soque River fault separates migmatitic biotite gneiss of the Cartoogechaye terrane and the sillimanite I and II grade aluminous schists and metasandstones of the Otto Formation.

The Soque River fault occurs in the northern part of the Waynesville 7.5-minute quadrangle and is a subvertical fault that traces nearly east-west. Foliations adjacent to

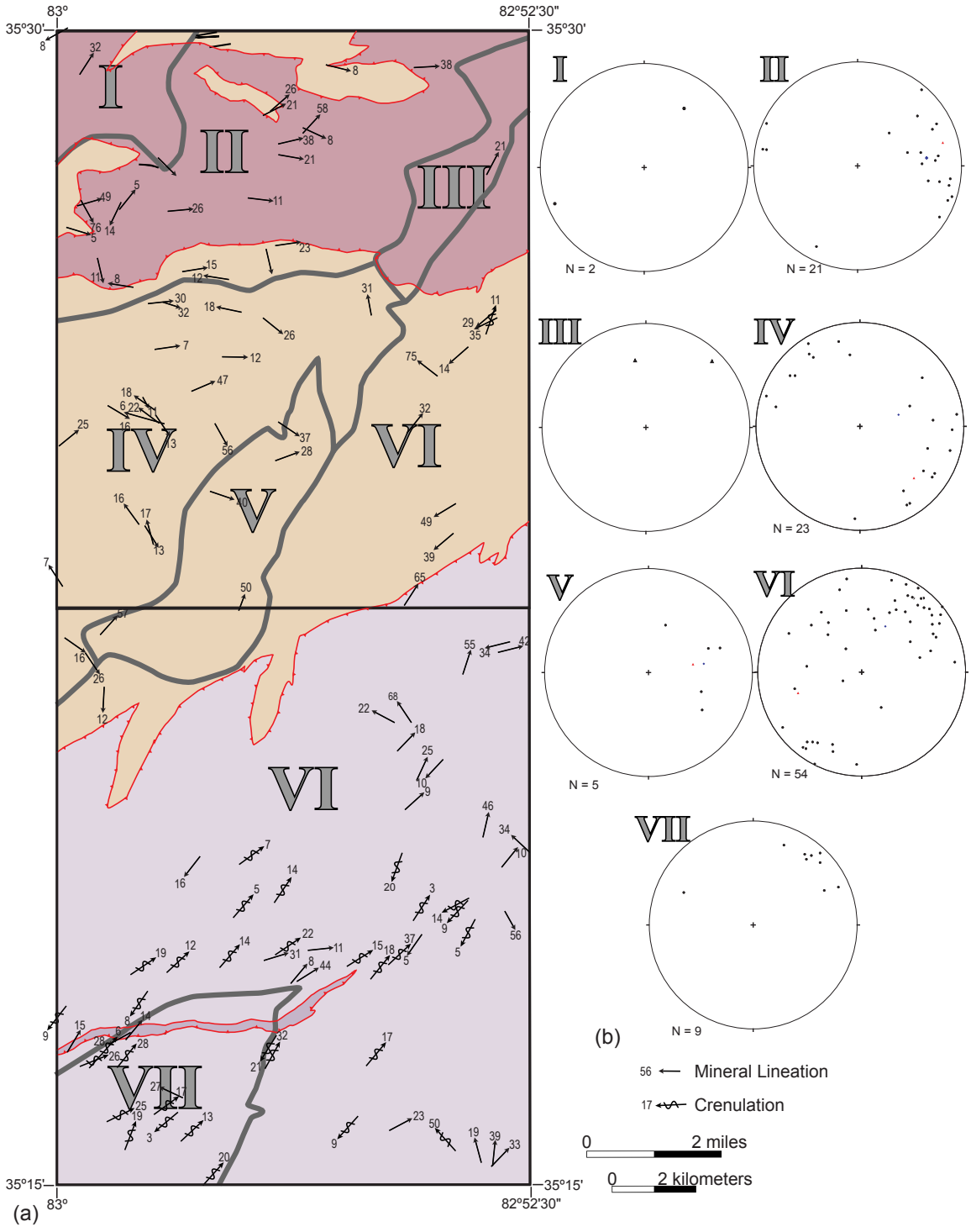

Figure 1–13. Linear mesoscopic structures from the Waynesville and Sam Knob quadrangles. (a)Lineation and crenulation map with faults and terranes indicated. (b) Equal-area, lower-hemisphere stereonets of mineral lineations separated by domain.

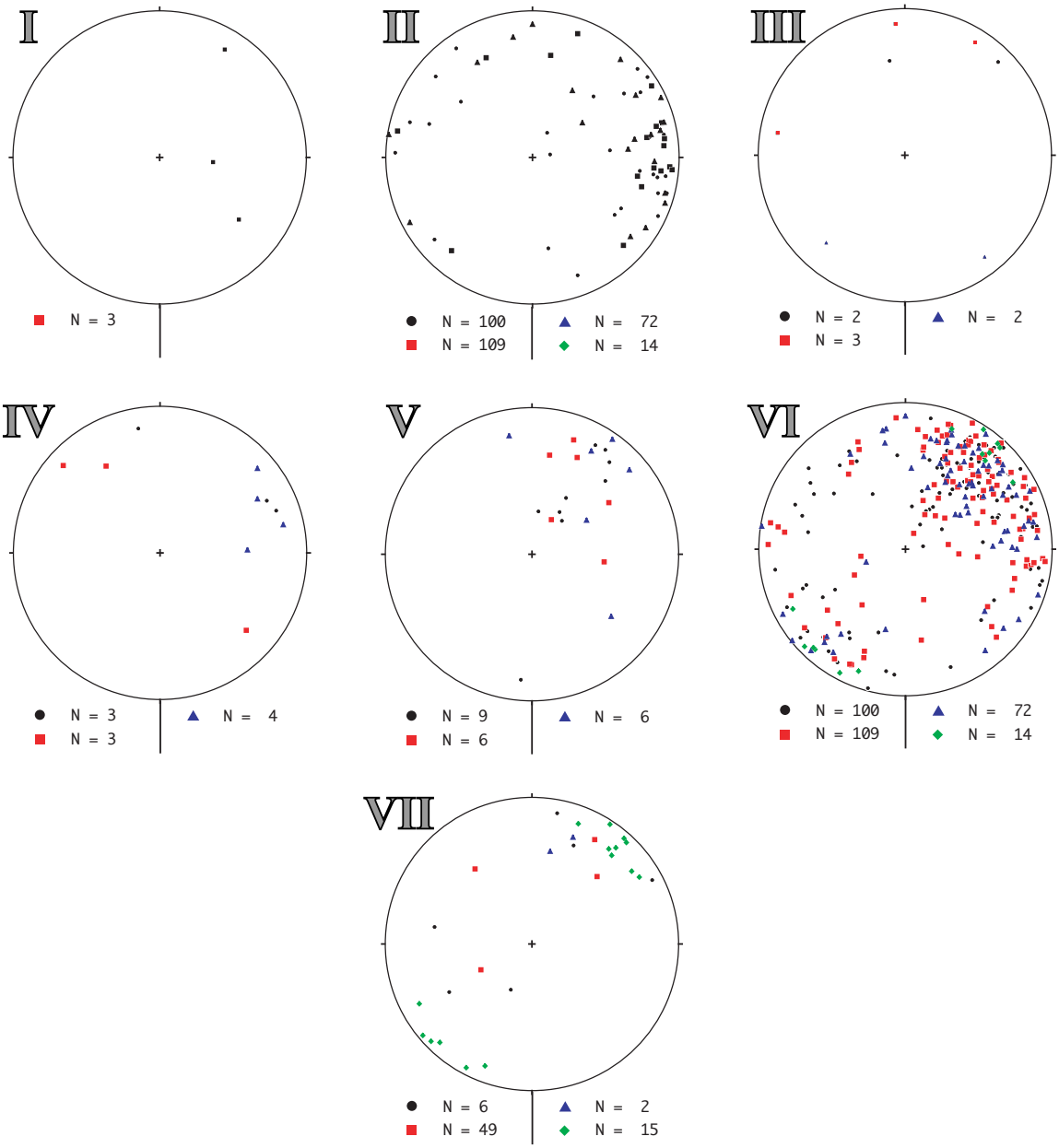

Figure 1–14. Equal-area, lower-hemisphere stereonets of measured mesoscopic fold axes separated by domain. Black circles represent tight to isoclinal F_2 folds; F_3 folds are represented by red squares, blue triangles include closed to open F_{4-5} folds, and crenulations are indicated by green diamonds.

the fault dip steeply southeast and northwest, and the fault is folded by east-northeast and east-west-trending open folds. The fault re-emerges to the north producing the elliptical-shaped, east-west-trending Raccoon Valley and Ratcliff Mountain windows. Mylonite occurs locally along the fault and varies from 1 m to several tens of meters thick. Migmatitic biotite gneiss of the Cartoogechaye terrane in the hanging wall commonly becomes finer-grained and develops thin planar banding. This may represent an additional method of strain accommodation associated with movement of the Soque River fault.

Chattahoochee-Holland Mountain Fault

The boundary between the Tugaloo terrane and lower terranes and thrust sheets to the northwest has been described as the Chattahoochee fault (Hurst, 1973) and the Holland Mountain fault (Merschat and Wiener, 1988). The Chattahoochee fault trends northeast, dips steeply southeast, and is folded by NE–trending tight to open folds. It occurs in homogeneous domain VI, and the regional foliation is parallel to the fault. The mylonite zone associated with the fault varies from 1 m to 50 m thick. At Reinhart Gap the Chattahoochee–Holland Mountain fault is exposed in a large roadcut along the Blue Ridge Parkway, and is characterized by a mylonite zone at least 50 m wide with a local zone of ultramylonite up to 10 cm wide. Migmatite and pegmatite dikes occur at the exposure and are mylonitic. Microstructures observed in mylonitic Tallulah Falls Formation metagraywacke include undulose quartz with sweeping extinctions, recrystallized quartz, undulose plagioclase porphyroclasts with mantled boundaries and subgrains, and small areas of recrystallized plagioclase. Asymmetric porphyroclasts indicate top-to-the-NW shear sense. Microstructures and field and map relationships suggest the Chattahoochee fault here is a synmetamorphic, amphibolite grade thrust fault.

Dill Falls shear zone

A ~300 m-thick zone of mylonitic migmatitic metagraywacke and garnet, muscovite, biotite schist in the southern part of the Sam Knob 7.5-minute quadrangle is here informally named the Dill Falls shear zone for the exposure at Dill Falls. The shear zone trends ~N 80º E, and dips ~60º NW. It occurs within the Tallulah Falls Formation, Tugaloo terrane, and does not displace or truncate any unit. The porphyroclastic metagraywacke displays a wispy S–C fabric. Garnet porphyroclasts in the schist are ~0.5 cm in diameter but occur as small clusters of 0.1–0.4 cm garnets in the mylonitic metagraywacke in the shear zone. Asymmetric feldspar porphyroclasts yield both top-to-

the SE and top-to-the NE shear sense, suggesting it is a reverse-oblique-slip shear zone. Plagioclase porphyroclasts with recrystallized mantles, recrystallization of garnets, and occurrence of migmatite in the shear zones suggest it is an amphibolite grade shear zone.

The Dill Falls shear zone was recognized by Cyphers (2009) and begins to trend more NE–SW in the Tuckasegee 7.5-minute quadrangle. The southern termination of the shear zone is uncertain, but it is along-strike to the southeastern margin of the Rabun pluton. Lamb (2001) and Stahr (2007) did not recognize a shear zone along the southeastern boundary of the Rabun pluton. Steep, northwest-dipping dextral faults also have been recognized in the Shining Rock quadrangle and include the Pisgah Ridge (Acker, 1982) and Cradle-of-Forestry-in-America faults (Dockal, 2007). The orientation, oblique-slip kinematics, and close spatial relationship of these faults with Mississippian plutons raises the question of whether the Dill Falls shear zone and other NW-dipping shear zones are related to the emplacement of the Mississippian plutons or to the early Alleghanian Brevard fault as suggested by Dockal (2007).

DEFORMATIONS

Six deformations, D_1–D_6, were recognized in the terranes of the Great Balsam Mountains (Table 1–3). Evidence of some deformations are limited; either early structures completely transposed or similar orientations of later structures hinders separation of structures into different deformation events. Regardless, all terranes were affected by an early progressive upper amphibolite grade deformation D_1-D_2, followed by two separate middle to lower amphibolite grade deformations, D_3 and D_4, which overprint and superpose previous structures, and late deformations involving the final emplacement of the Blue Ridge-Piedmont megathrust sheet and Mesozoic extension and Cenozoic uplift.

D_1

The earliest deformation is often the most difficult to recognize. Although several occurrences of metaconglomerate, porphyroclastic quartz feldspar gneiss occur in the GBMW and Tugaloo terrane, no primary sedimentary structures were observed. D_1 structures in all three terranes are rare, and usually preserved as oblique foliations and folds in amphibolite boudins, intrafolial folds, and linear inclusion trails preserved in the cores of garnets. These structures are most common in the amphibolite boudins in the Cartoogechaye and Tugaloo terranes. The mineral assemblages defining the foliations and folds in amphibolite boudins, and linear inclusion trails are similar to near-peak

assemblages throughout the terranes, and suggest D_1 may have been an early stage of D_2. In the GBMW, map-scales folds of schist and metasandstone of the Otto Formation may represent early F_1folds.

D_2

The principal deformational event in the study area is interpreted to be D_2. This event includes the development of the regional S_2 foliation (Fig. 1–11), mineral lineation, L_2, map- and mesoscale folds, F_2, and activation of the Soque River fault. M_2 mineral assemblages commonly define the S_2 and L_2 fabrics, indicating this D_2 correlates with upper amphibolite facies M_2 metamorphism at ~455 Ma.

In the Cartoogechaye terrane, S_2 is defined by gneissic and migmatitic layering. F_2 folds show significant variation in style, and are often noncylindrical, non-plane, inclined to reclined tight to isoclinal folds, and sheath folds. Polyharmonic folds are common (Quinn, 1991) resulting from contrasts between the mica-rich and quartz-feldspar or amphibole dominated layers. Viscosity contrasts between the mica-rich and quartz-feldspar dominated layers results in significant thickening of fold hinges. Several mesoscopic sheath folds were recognized in the Cartoogechaye terrane (Fig. 1–4), and plunge gently to the east.

Sillimanite and phyllosilicates, biotite and muscovite, commonly define the dominant S_2 foliation in the GBMW. Locally, stromatic migmatite layers are also parallel to S_2. The northern end of the GBMW is folded into a NE plunging Lickstone Ridge antiform, and S_2 changes orientation from N–S, E–W to NW–SE trends along the limbs of the fold (domain II, IV, and V). The L_2 mineral lineation where developed is commonly defined by aligned prismatic sillimanite, which often dominates the S_2 foliation and wraps garnets and other porphyroclasts (Fig. 1–9). The lack of easily recognizable layers, like the migmatitic layering in the Cartoogechaye terrane, makes recognition of F_2 folds in the GBMW difficult, but they do occur. Folds observed are cylindrical, planar, inclined, tight-to-isoclinal folds (Fig. 1–4); hinges show minor to moderate thickening. Commonly, F_2 and L_2 are coaxial and vary in orientation according to their location on the limbs of the Lickstone Ridge antiform.

The Tugaloo terrane occurs almost completely within domain VI, with the exception of domain VII in the southwestern corner of the study area, and the fabrics developed are relatively uniform. The regional foliation S_2 generally strikes NE and dips moderately to steeply NW. Domain VII also dips moderately to steeply NW, but the strike is more E-W. S_2 is defined by aligned phyllosilicates, sillimanite, and kyanite, and

stromatic migmatite. L_2 is developed locally and defined by rodded quartz and streaked muscovite and biotite. Tight-to-isoclinal F_2 folds plunge gently to moderately NE-SW, and verge SE. The Chattahoochee-Holland fault occurs in domain VI, and parallel fabrics across the fault imply a ~455 Ma development. This early Taconic phase is here referred to as the Holland Mountain phase, based on the description of Merschat and Wiener (1988).

D_3

Overprinting the dominant deformation are D_3 structures that are fairly common throughout the map area and all three terranes. Development of the D_3 structures is more pronounced in certain locations, especially toward the southeast in the Tugaloo terrane.

Reclined to inclined, tight-to-closed F_3 folds are common throughout the Cartoogechaye terrane. Fold geometries and orientations are similar to F_2 folds, making it difficult to recognize F_3 folds with superposed structures. Axial planar S_3 foliations are often defined by biotite and are developed in cores of some F_3 folds. In the Dahlonega gold belt exposed in the core of the GBMW, D_3 is not well developed. S_3 foliations are not common and difficult to recognize. Upright, tight-to-closed F_3folds superpose earlier fold and foliations. In the Tugaloo terrane, D_3 structures become more pronounced to the southeast and corresponds with areas of M_3 and new growth of kyanite and staurolite. Upright to inclined, tight to open folds, F_3, superpose S_2. Locally S_3 reactivates S_2, as suggested by Stahr (2007); elsewhere S_3 defines a new steep SE-dipping foliation.

D_4

Crenulations and upright open cylindrical folds in all three terranes superposed previous structures and are interpreted to be the result of D_4. Although the orientation of fold axes are similar to earlier fold axes (F_2 and F_3), F_4 folds are cylindrical and upright to steeply inclined. Crenulations are coaxial to the upright, closed-to-open F_4 folds. Foliations associated with this event are not common, but micas (primarily muscovite) aligned parallel to the axial planes of crenulations may represent S_4. This deformation is correlated with regional deformation associated with the emplacement of Mississippian plutons (~335 Ma Rabun and Walnut Creek granodiorites, Stahr, 2007), and is referred to as early Alleghanian. The Wolf Creek antiform in the southern part of the Sam Knob quadrangle is a north-plunging, upright, open-to-gentle F_4 fold. The Horseshoe Rock granite is correlated with the ~342 Ma Round Mountain granite (Varnell et al., 2008), and suggests this structure developed post ~342 Ma, an Alleghanian structure. Varnell

et al. (2008) reported an age of ~337 Ma for the Looking Glass pluton, which delimits the movement of the Cradle-of-Forestry-in-America fault to post ~337 Ma. Based on similar geometry, kinematics, and grade of deformation the Dill Falls shear zone is also interpreted as a Mississippian early Alleghanian ductile shear zone. To the southwest, the Chattahoochee–Holland Mountain fault truncates the ~335 Ma Rabun Granodiorite (Lamb, 2001; Acker and Hatcher, unpublished mapping), and implies the final movement of the Chattahoochee–Holland Mountain fault was post ~335 Ma.

D_5 and D_6 . . .

The youngest deformations to affect the Blue Ridge (D_5, D_6, and $D_{7?}$) are often recognized from map-scale or regional folds, and brittle structures including both faults and fractures (Hopson et al., 1989). Regional structures that Hopson et al. (1989) interpreted to be D_5 included the formation of the Tallulah Falls dome, movement on the Rosman and Blue Ridge-Great Smoky faults, and formation of joints.

The youngest structures recognized in the Waynesville and Sam Knob 7.5-minute quadrangle are joints. They are present in all units including the youngest undeformed Paleozoic granitoids. Joints are both unfilled and filled, usually with quartz and/or chlorite, and some pegmatite dikes. Slickenlines, usually down dip, were observed on some joint surfaces, but are not common. These joints may have formed from either Mesozoic extension or Cenozoic uplift (Merschat et al., 2005), and are similarly combined as a D_6 event.

CONCLUSIONS

1. Detailed geologic mapping in the Waynesville and Sam Knob 7.5-minute quadrangles recognized the Cartoogechaye, Dahlonega gold belt, and Tugaloo terranes separated by the Soque River and Chattahoochee–Holland Mountain faults. Each terrane comprises a separate thrust sheet and frames the GBMW, a ductile eyelid window. The northwesternmost thrust sheet consists of Cartoogechaye terrane migmatitic biotite gneiss, minor felsic gneiss, and interlayers and pods of amphibolite. Aluminous schist and metagraywacke in the inner core of the window are correlated with the Otto Formation of the Dahlonega gold belt. The Tugaloo terrane is the southeasternmost and highest thrust sheet, and overthrust the terranes to the northwest. The tripartite stratigraphy of the Tallulah Falls Formation was mapped in the Tugaloo terrane.

2. Metamorphism ranges from kyanite–staurolite to sillimanite II grade in the Waynesville and Sam Knob quadrangles. In the inner window, rocks of the Dahlonega gold belt are sillimanite I and II and decrease to sillimanite I, then kyanite–staurolite to the southeast in the Tugaloo terrane. Cartoogechaye rocks are pervasively migmatitic, but metamorphic indicator minerals were not observed.
3. Three regional metamorphic events were recognized in these terranes. M_1, defined by relict porphyroclasts of kyanite, inclusion trails in garnet, and foliations preserved in amphibolite boudins contain assemblages similar to M_2, suggesting these events represent progressive metamorphism that reached sillimanite II grade in the GMBW. SHRIMP U-Pb ages of zircon indicate M_2 occurred ~455 Ma a product of the Taconian orogeny. M_3 is also an amphibolite facies regional metamorphism, but mostly affects the southeastern part of the Tugaloo terrane where kyanite and staurolite are forming after sillimanite. M_3 is related to the Neoacadian orogeny 365–345 Ma, and is the result of juxtaposing the Inner Piedmont and Carolina superterrane over the Blue Ridge. Retrograde textures defined by sericite and chlorite are interpreted as M_4.
4. Terranes of the Great Balsam Mountains are polydeformed. Six deformational events are recognized that include early high-temperature contractional structures to late brittle features. D_1 and D_2 events are the results of upper amphibolite deformation associated with the Taconian orogeny, 465–450 Ma. D_2 corresponds with near peak M_2 metamorphism, development of tight to isoclinal F_2 folds, and regional S_2 defined peak mineral assemblages. Parallelism of S_2 with the Soque River and Chattahoochee–Holland Mountain faults and microstructures in the fault compatible with the regional metamorphic grade indicate these faults are associated with D_2. D_3 is interpreted to be the result of the Neoacadian orogeny; these structures often have similar orientations as D_2 structures. M_3, resulting in the growth of new kyanite and staurolite, is interpreted to be associated with this event. D_4 and D_5, correlate with early and late stages of the Alleghanian orogeny, produced upright NW–SE trending open folds, crenulations, and regional broad open folds. During early Alleghanian, D_4, the Chattahoochee fault was reactivated as a dextral shear zone, however, this may not have strongly affected the rocks in the GBMW. The youngest structures in the Great Balsam Mountains, joints, fractures, and minor faults, are combined as D_6 and are the result of Mesozoic extension or Cenozoic uplift.

5. Surficial units recognized in the Great Balsam Mountains include modern flood plain alluvium, colluvium, alluvial–colluvial fans, and various landslide deposits.

REFERENCES CITED

Absher, B. S., and McSween, H. Y., 1985, Granulites at Winding Stair Gap, North Carolina: The thermal axis of Paleozoic metamorphism in the southern Appalachians: Geological Society of America Bulletin, v. 96, p. 588–599.

Acker, L. L., 1982, Geology of the Shining Rock quadrangle, North Carolina [M.S. thesis]: Chapel Hill, University of North Carolina, 110 p.

Anderson, E. D., and Moecher, D. P., 2006, Reaction textures in retrograde eclogites: Mechanisms and mass balance as a function of decompression and cooling rates: Geological Society of America Abstracts with Programs, v. 38, no. 7, p. 112.

Berquist, P. J., 2005, U–Pb geochronology and geochemistry of southern Appalachian basement: Tectonic implications and constraints on age, extent, and origin [M.S. thesis]: Nashville, Tennessee, Vanderbilt University, 91 p.

Bream, B. R., 2002, The southern Appalachian Inner Piedmont: New perspectives based on recent detailed geologic mapping, Nd isotopic evidence, and zircon geochronology, *in* Hatcher, R. D., Jr., and Bream, B. R., eds., Inner Piedmont geology in the South Mountains-Blue Ridge Foothills and the southwestern Brushy Mountains, central-western North Carolina: Carolina Geological Society Guidebook, p. 45–63.

Bream, B. R., 2003, Tectonic implications of geochronology and geochemistry of para- and orthogneisses from the southern Appalachian crystalline core [Ph.D. dissertation]: Knoxville, University of Tennessee, 296 p.

Bream, B. R., Hatcher, R. D., Jr., Miller, C. F., and Fullagar, P. D., 2004, Detrital zircon ages and Nd isotopic data from the southern Appalachian crystalline core, Georgia, South Carolina, North Carolina, and Tennessee: New provenance constraints for part of the Laurentian margin, *in* Tollo, R. P., Corriveau, L., McLelland, J., and Bartholomew, M. J., eds., Proterozoic tectonic evolution of the Grenville orogen in North America: Boulder, Colorado, Geological Society of America Memoir 197, p. 459–475.

Brown, P. M., Burt, E. R., II, Carpenter, P. A., Enos, R. M., Flynt, B. J., Jr., Gallagher, P. E., Horrman, C. W., Merschat, C. E., Wilson, W. F., and Parker, J. M., III, 1985,. Geologic map of North Carolina: North Carolina Geological Survey, scale 1:500,000.

Burton, W. C., and Kunk, M. J., 2006, Evidence for Taconian and Alleghanian orogenesis in the eastern Blue Ridge near Highlands, NC: Geological Society of America Abstracts with Programs, v. 38, no. 3, p. 20.

Butler, J. R., 1991, Metamorphism, *in* Horton, J. W., Jr., and Zullo, V. A., eds., The geology of the Carolinas: Knoxville, University of Tennessee Press, p. 127–141.

Cameron, M. L., 2001, Garnet zoning, mineral inclusions, and P-T paths: Evidence for a polymetamorphic history of the Cullowhee gneiss [M.S. thesis]: Knoxville, University of Tennessee, 240 p.

Carpenter, R. H., 1970, Metamorphic history of the Blue Ridge province of Tennessee and North Carolina: Geological Society of America Bulletin, v. 81, p. 749-762.

Carrigan, C. W., Bream, B. R., Miller, C. F., and Hatcher, R. D., Jr., 2001, Ion microprobe analyses of zircon rims from the eastern Blue Ridge and Inner Piedmont, NC-SC-GA: Implications for the timing of Paleozoic metamorphism in the southern Appalachians: Geological Society of America Abstracts with Programs (SE Section), v. 33, p. A–7.

Carrigan, C. W., Miller, C. F., Fullagar, P. D., Hatcher, R. D., Jr., Bream, B. R., and Coath C. D., 2003, Ion microprobe age and geochemistry of southern Appalachian basement, with implications for Proterozoic and Paleozoic reconstructions: Precambrian Research, v. 120, p. 1–36.

Connelly, J. B., and Dallmeyer, R. D., 1993, Polymetamorphic evolution of the western Blue Ridge: Evidence from $^{40}Ar/^{39}Ar$ whole-rock slate/phyllite and muscovite ages: American Journal of Science, v. 292, p. 322–359.

Corrie, S. L., and Kohn, M. J., 2007, Resolving the timing of orogenesis in the western Blue Ridge, southern Appalachians, via *in situ* ID-TIMS monazite geochronology: Geology, v. 35, p. 627–630.

Cyphers, S. R., 2009, Detailed mapping of a terrane boundary and structure and origin of block-in-matrix structures, central and eastern Blue Ridge, Jackson County, North Carolina [M.S. thesis]: Knoxville, Tennessee, University of Tennessee, 227 p.

Dallmeyer, R. D., 1988, Late Paleozoic tectonothermal evolution of the western Piedmont and eastern Blue Ridge, Georgia: Controls on the chronology of terrane accretion and transport in the southern Appalachian orogen: Geological Society of America Bulletin, v. 100, p. 702–713.

Davidson, G. L., 1995, The tectono-metamorphic history of a portion of the eastern Blue Ridge, Jackson county, North Carolina [M.S. thesis]: Knoxville, Tennessee, University of Tennessee, 157 p.

Dockal, J. A., 2007, Cradle-of-forestery-in-America fault an Acadian and Alleghanian dextral strike-slip fault within the eastern Blue Ridge, Transylvania County, North Carolina: Southeastern Geology, v. 44, p. 171–189.

Eckert, J. O., Jr., 1984, Stratigraphy, structure, and metamorphism of the east half of the Wayah Bald quadrangle, North Carolina: Evidence for Paleozoic granulite facies metamorphism in the southern Appalachians [M.S. thesis]: Columbia, South Carolina, University of South Carolina, 411 p.

Eckert, J. O., Hatcher, R. D., Jr., and Mohr, D. W., 1989, The Wayah granulite-facies metamorphic core, southwestern North Carolina: High-grade culmination of Taconic metamorphism in the southern Blue Ridge: Geological Society of America Bulletin, v. 101, p. 1434–1447.

Gillon, K. A., 1982, Stratigraphy, structural, and metamorphic geology of portions of the Cowrock and Helen, Georgia 7.5 minute quadrangles [M.S. thesis]: Athens, Georgia, University of Georgia, Athens, 236 p.

Goldberg, S. A., and Dallmeyer, R. D., 1997, Chronology of Paleozoic metamorphism and deformation in the Blue Ridge thrust complex, North Carolina and Tennessee: American Journal of Science, v. 297, p. 488–526.

Hadley, J. B., and Goldsmith, R., 1963, Geology of the eastern Great Smoky Mountains North Carolina and Tennessee: U. S. Geological Survey Professional Paper, 349-B, 117 p.

Hadley, J. B., and Nelson, A. E., 1971, Geologic map of the Knoxville quadrangle, North Carolina, Tennessee, and South Carolina: U. S. Geological Survey Map I–654, scale 1:250,000.

Hatcher, R. D., Jr., 1971, Geology of Rabun and Habersham counties, Georgia: A reconnaissance study: Georgia Geological Survey Bulletin 83, 48 p.

Hatcher, R. D., Jr., 1977, Macroscopic polyphase folding illustrated by the Toxaway dome, eastern Blue Ridge, South Carolina-North Carolina: Geological Society of America Bulletin, v. 88, p. 1678–1688.

Hatcher, R. D., Jr., 1978, Tectonics of the western Piedmont and Blue Ridge: Review and speculation: American Journal of Science, v. 278, p. 276–304.

Hatcher, R. D., Jr., 1980, Geologic map and mineral resources of the Prentiss quadrangle, North Carolina: North Carolina Geological Survey, GM 167–SW, scale 1/24,000.

Hatcher, R. D., Jr., 1984, Southern and central Appalachian basement massifs, *in* Bartholomew, M. J., ed., The Grenville event in the Appalachians and related topics: Boulder, Colorado, Geological Society of America Special Paper 194, p. 149–153.

Hatcher, R. D., Jr., 1987, Tectonics of the southern and central Appalachian internides: Annual Reviews in Earth and Planetary Sciences, v. 15, p. 337–362.

Hatcher, R. D., Jr., 1989, Tectonic synthesis of the U.S. Appalachians, Chapter 14, *in* Hatcher, R. D., Jr., Thomas, W. A., and Viele, G. W., eds., The Appalachian-Ouachita orogen in the United States: Boulder, Colorado, Geological Society of America, The Geology of North America, v. F-2, p. 511–535.

Hatcher, R. D., Jr., 1993, Perspective on the tectonics of the Inner Piedmont, southern Appalachians, *in* Hatcher, R. D., Jr., Davis, T. L., eds., Studies of Inner Piedmont geology with a focus on the Columbus Promontory: Carolina Geological Society Guidebook, North Carolina Geological Survey, pp. 17–43, http://carolinageologicalsociety.org/cgscdguide.htm.

Hatcher, R. D., Jr., 2002, An Inner Piedmont primer, *in* Hatcher, R. D., Jr., and Bream, B. R., eds., Inner Piedmont geology in the South Mountains-Blue Ridge Foothills and the southwestern Brushy Mountains, central-western North Carolina: Carolina Geological Society Guidebook, p. 1–18.

Hatcher, R. D., Jr., and Butler, J. R., 1979, Guidebook for southern Appalachian field trip in the Carolinas, Tennessee, and northeastern Georgia: International Geologic Correlation Program Project 27, University of North Carolina, Chapel Hill, 117 p.

Hatcher, R. D., Jr., and Goldberg, S. A., 1991, The Blue Ridge Geologic Province, *in* Horton, J. W., Jr., and Zullo, V. A., eds., The Geology of the Carolinas—Carolina Geological Society 50th Anniversary Volume: Knoxville, The University of Tennessee Press, p. 11–35.

Hatcher, R. D., Jr., and Hooper, R. J., 1992, Evolution of crystalline thrust sheets in the internal parts of mountain chains, *in* McClay, K. R., ed., Thrust tectonics: London, Chapman and Hall, p. 217–234.

Hatcher, R. D., Jr., and Merschat, A. J., 2006, The Appalachian Inner Piedmont: An exhumed strike-parallel, tectonically forced orogenic channel, *in* Law, R. D., Searle, M., and Godin, L., eds., Channel flow, ductile extrusion and exhumation of lower-mid crust in continental collision zones: London, Geological Society of London Special Publication 268, p. 517–540.

Hatcher, R. D., Jr., Bream, B. R., Miller, C. L., Eckert, J. O., Jr., Fullagar, P. D., and Carrigan, C. W., 2004, Paleozoic structure of internal basement massifs, southern Appalachian Blue Ridge, incorporating new geochronologic, Nd and Sr isotopic, and geochemical data, *in* Tollo, R. P., Corriveau, L., McLelland, J., and Bartholomew, M. J., eds., Proterozoic tectonic evolution of the Grenville orogen in North America: Boulder, Colorado, Geological Society of America Memoir 197, p. 525–547.

Hatcher, R. D., Jr., Bream, B. R., and Merschat, A. J., 2007, Tectonic map of the southern and central Appalachians: A tale of three orogens and a complete Wilson cycle, *in* Hatcher, R. D., Jr., Carlson, M. P., McBride, J. H., and Martínez Catalán, J. R., eds., 4-D Framework of Continental Crust: Geological Society of America Memoir 200, p. 595–632.

Hatcher, R. D., Jr., Merschat, A. J., and Thigpen, J. R., 2005, Blue Ridge Primer, *in* Hatcher, R. D., Jr., and Merschat, A. J., eds., Blue Ridge geology geotraverse east of the Great Smoky Mountains National Park, western North Carolina: Carolina Geological Society Guidebook, North Carolina Geological Survey, p. 1–24.

Hopson, J. L., Hatcher, R. D., Jr., and Stieve, A. L., 1989, Geology of the eastern Blue Ridge, northeastern Georgia and the adjacent Carolinas, *in* Fritz, W. J., Hatcher, R. D., Jr., and Hopson, J. L., eds., Geology of the eastern Blue Ridge of northeast Georgia and the adjacent Carolinas: Georgia Geological Society Guidebooks, v. 9, p. 1–40.

Horton, J. R., Jr., 1982, Geologic map of the Rosman quadrangle, North Carolina: North Carolina Geological Survey GM–185–NE, scale 1:24,000.

Hurst, V. J., 1973, Geology of the southern Blue Ridge belt: American Journal of Science, V. 273, p. 643–670.

Keith, A., 1907, Description of the Pisgah quadrangle (NC-SC): U. S. Geological Survey folio.

King, P. B., and Ferguson, H. W., 1960, Geology of northeasternmost Tennessee: U. S. Geological Survey Professional Paper 311, 136 p.

King, P. B., Neuman, R. B., and Hadley, J. B., 1968, Geology of the Great Smoky Mountains National Park, Tennessee and North Carolina: U. S. Geological Survey Professional Paper 587, 23 p.

Lamb, Dwight D., 2001, Geology of the Scaly Mountain quadrangle, emphasizing the structures, timing and emplacement mechanisms for the Rabun granodiorite, eastern Blue Ridge, southwestern north Carolina [M.S. thesis]: Knoxville, University of Tennessee, 86 p.

Lesure, F. G., 1968, Mica deposits of the Blue Ridge in North Carolina: U. S. Geological Survey Professional Paper 577, 124 p.

Ludwig, K. R., 2003, Isoplot v. 3.00, computer program.

Mapes, R. W., 2002, Geochemistry and geochronology of mid-Paleozoic granitic plutonism in the southern Appalachian Piedmont terrane, North Carolina-South Carolina-Georgia [M.S. thesis]: Nashville, Vanderbilt University, 150 p.

Massey, M. A., and Moecher, D. P., 2005, Deformation and metamorphic history of the western Blue Ridge-eastern Blue Ridge terrane boundary, southern Appalachian orogen: Tectonics, v. 24, p. TC5010, 1–18.

McDowell, S. M., Miller, C.F., Fullagar, P. D., Bream, B. R., and Mapes, R. W., 2002, The Persimmon Creek Gneiss, eastern Blue Ridge, North Carolina-Georgia: Evidence for the missing Taconic arc?: Southeastern Geology, v. 41, p. 103–117.

Merschat, A. J., Hatcher, R. D., Jr., and Davis, T. L., 2005, The northern Inner Piedmont, southern Appalachians, USA: Kinematics of transpression and SW-directed mid-crustal flow: Journal of Structural Geology, v. 27, p. 1252–1281.

Merschat, A. J., Hatcher, R. D., Jr., Miller, C. F., and Wooden, J. L., 2006, Provenance of central and western Blue Ridge paragneisses, southwestern North Carolina: Geological Society of America Abstracts with Programs, v. 38, no. 3, p. 63.

Merschat, C. E., and Cattanach, B. L., 2008, Bedrock geologic map of the west half of the Asheville 1:100,000-scale quadrangle, North Carolina and Tennessee: North Carolina Geological Survey, scale 1:100,000.

Merschat, C. E., and Wiener, L. S., 1988, Geology of the Sandymush and Canton Quadrangles, North Carolina: Raleigh, North Carolina Geological Survey Bulletin 90, 1:24,000 scale, 66 p.

Miller, B. V., Stewart, K. G., Miller, C. F., and Thomas, C. W., 2000, U-Pb ages from the Bakersville, North Carolina eclogite: Taconian eclogite metamorphism followed by Acadian and Alleghanian cooling: Geological Society of America Abstracts with Programs, v. 32, no. 2, p. 62.

Miller, B. V., Fetter, A. H., and Stewart, K. G., 2006, Plutonism in three orogenic pulses, eastern Blue Ridge Province, southern Appalachians: Geological Society of America Bulletin, v. 118, p. 171–184.

Miller, C. F., Hatcher, R. D., Jr., Harrison, T. M., Coath, C. D., and Gorisch, E. B., 1998, Cryptic crustal events elucidated through zone imaging and ion microprobe studies of zircon, southern Appalachian blue Ridge, North Carolina-Georgia: Geology, v. 26, p. 419–422.

Miller, C. F., Hatcher, R. D., Jr., Ayers, J. C., Coath, C. D., and Harrison, T. M., 2000, Age and zircon inheritance of eastern Blue Ridge plutons, southwestern North Carolina and Northeastern Georgia, with implications for magma history and evolution of the southern Appalachian orogen: American Journal of Science, v. 300, p. 142–172.

Moecher, D. P., Samson, S. D., and Miller, C. F., 2004, Precise time and conditions of peak Taconian granulite facies metamorphism in the southern Appalachian orogen, USA, with implications for zircon behavior during crustal melting events: Journal of Geology, v. 112, p. 289–304.

Moecher, D. P., Massey, M. A., and Tracy, R. J., 2005, Timing and pattern of metamorphism in the western and central Blue Ridge, TN and NC: Status and outstanding problems, *in* Hatcher, R. D., Jr., and Merschat, A. J., eds., Blue Ridge geology geotraverse east of the Great Smoky Mountains National Park, western North Carolina: Carolina Geological Society Guidebook, North Carolina Geological Survey, p. 57–66.

Montes, C., 1997, The Greenbrier and Hayesville faults in western North Carolina [M.S. thesis]: Knoxville, University of Tennessee, 145 p.

Morrow, H. B., 1977, Geologic map of the Cruso quadrangle, North Carolina [M.S. thesis]: Chapel Hill, University of North Carolina, scale 1:24,000.

Nelson, A. E., 1982, Geologic map of the Tray Mountain Roadless Area, northern Georgia: U. S. Geological Survey Miscellaneous Field Studies Map MF-1347-A, scale 1:30,000.

Ownby, S. E., Miller, C. F., Berquist, P. J., Carrigan, C. W., Wooden, J. L., and Fullagar, P. D., 2004, U-Pb geochronology and geochemistry of a portion of the Mars Hill terrane, North Carolina–Tennessee: Constraints on origin, history, and tectonic assembly, *in* Tollo, R. P., Corriveau, L., McLelland, J., and Bartholomew, M. J., eds., Proterozoic evolution of the Grenville orogen in North America: Boulder, Colorado, Geological Society of America Memoir 197, p. 609–632.

Quinn, M. J., 1991, Two lithotectonic boundaries in western North Carolina: Geologic interpretation of a region surrounding Sylva, Jackson County [unpublished M.S. thesis]: Knoxville, University of Tennessee, 223 p.

Rankin, D. W., Espenshade, G. H., and Shaw, K. W., 1973, Stratigraphy and structure of the metamorphic belt in northwestern North Carolina and southwestern Virginia: A study from the Blue Ridge across the Brevard Fault Zone to the Sauratown Mountains Anticlinorium: American Journal of Science, v. 273, p. 1–40.

Settles, D. J., 2002, Defining the Hayesville-Soque River and Allatoona faults and an Ordovician arc assemblage within the central Blue Ridge northwest of Dahlonega, Georgia [unpublished M.S. thesis]: Knoxville, University of Tennessee, 148 p.

Southworth, S., Schultz, A., and Denenny, D., 2005, Geologic map of the Great Smoky Mountains National Park Region, Tennessee and North Carolina: U.S. Geological Survey Open File Report 2005-2115, scale 1:100,000.

Spell, T. L., and Norrell, G. T., 1990, The Ropes Creek assemblage: Petrology, geochemistry, and tectonic setting of an ophiolitic thrust sheet in the southern Appalachians: American Journal of Science, v. 290, p. 811–842.

Stahr, D. W., III., 2007, Tectonometamorphic evolution of the eastern Blue Ridge: Differentiating multiple Paleozoic orogenic pulses in the Glenville and Big Ridge quadrangles, southwestern North Carolina [unpublished MS thesis]: Knoxville, Tennessee, University of Tennessee, 263 p.

Stahr, D. W., III, Hatcher, R. D., Jr., Miller, C. F., and Wooden, J. L., 2006, Alleghanian deformation in the Georgia and North Carolina eastern Blue Ridge: Insights from pluton ages and fabrics: Geological Society of America Abstracts with Programs, v. 38, no. 3, p. 20.

Swanson, S. E., Raymond, L. A., Warner, R. D., Ryan, J. G., Yurkovich, S. P., and Peterson, V. L., 2005, Petrotectonics of mafic and ultramafic rocks in Blue Ridge terranes of western North Carolina and northern Georgia, *in* Hatcher, R. D., Jr., and Merschat, A. J., eds., Blue Ridge geology geotraverse east of the Great Smoky Mountains National Park, western North Carolina: Carolina Geological Society Guidebook, North Carolina Geological Survey, p. 73–90.

Thomas, C. W., 2001, Origins of ultramafic complexes of the eastern Blue Ridge province, southern Appalachians: Geochronological and geochemical constraints [M.S. thesis]: Nashville, Tennessee, Vanderbilt University, 154 p.

Tull, J. F., Ausich, W. I., Groszos, M. S., and Thompson, T. W., 1993, Appalachian Blue Ridge cover sequence ranges at least into the Ordovician: Geology, v. 21, p. 215–218.

Varnell, M. G., in progress, Geology of the Lake Toxaway and east half of the Big Ridge 7.5-minute quadrangles, North Carolina [M.S. thesis]: Knoxville, Tennessee, Univeristy of Tennessee, xxx p.

Varnell, M. G., Hatcher, R. D., Jr., Merschat, A. J., and Wooden, J. L., 2008, Limits on timing of deformation and plutonism in the eastern Blue Ridge, southwestern North Carolina, from Geologic mapping and U-Pb zircon geochronology: Geological Society of America Abstracts with Programs, v. 40, no. 4, p. 28.

PART II

Summary of the Geology of part of the Blue Ridge of southwestern North Carolina and northeastern Georgia: Integrating detailed geologic mapping and SHRIMP U-Pb zircon geochronologic studies

This paper written by myself and Robert D. Hatcher, Jr., describes the geology of part of the southwestern North Carolina and northeastern Georgia Blue Ridge. It is anticipated that this paper and accompaning map, Plate 3, will be submitted to an appropriate peer-reviewed journal that publishes large maps or the U.S. Geological Survey. My contributions include the majority of writing, and compilation of the geologic map (Plate 3) and geochronologic data.

ABSTRACT

The Blue Ridge in southwestern North Carolina and northeastern Georgia consists of a polydeformed, thrust stack of amphibolite to granulite facies rocks of the western Blue Ridge/Laurentian margin, Cartoogechaye, Cowrock, and Dahlonega gold belt accreted terranes, which are truncated and overlain by the eastern Blue Ridge Tugaloo terrane. Several decades of detailed geologic mapping of an ~850 km^2 area between Waynesville, North Carolina, and Clayton, Georgia, attempts to resolve fundamental tectonic problems existing between central and eastern Blue Ridge terranes. The western Blue Ridge/Laurentian margin consists of kyanite to sillimanite zone metagraywackes and schists of the Great Smoky Group. The highest thrust sheet in the central Blue Ridge, the Cartoogechaye terrane, consists of upper amphibolite to granulite facies migmatitic biotite gneiss with map- to mesoscale lenses and pods of migmatitic amphibolite. Numerous ultramafic bodies occur throughout, including the dome-shaped Webster-Addie body. The ~1.10 Ga Trimont Ridge complex is the only documented Grenville basement massif, but several other migmatitic felsic orthogneisses exist. Below the Cartoogechaye terrane, the Cowrock terrane consists of metasandstones and schist of the Coleman River and Ridgepole Mountain Formations intruded by the ~468 Ma Persimmon Creek Gneiss, and mafic and ultramafic rocks including the Lake Chatuge mafic-ultramafic complex. Pelitic schist and metagraywacke of the DGB occur in the footwall of the folded, steeply NW-dipping Soque River fault, and in Great Balsam Mountains window (GBM) extending from Sylva to Canton, NC. Metamorphic grade of the Dahlonega gold belt remains kyanite-staurolite zone in GA and increases to sillimanite zone in the GBM. SHRIMP U-Pb ages of metamorphic zircons suggest peak metamorphism in the Cartoogechaye and Dahlonega gold belt terranes occurred ~460 Ma, suggesting the western and central Blue Ridge comprise the Taconic metamorphic core. The Chattahoochee fault juxtaposes migmatitic Tallulah Falls-Ashe Formation metagraywacke, amphibolite, and schist of the Tugaloo terrane against central Blue Ridge terranes, and truncates the Soque River fault. Truncation of the Mississippian

Rabun Granodiorite indicates final movement of the Chattahoochee fault was post-335 Ma. Evidence for multiple tectonothermal deformation events in the Tugaloo terrane includes (1) Taconic (~460 Ma); truncation of folded amphibolite layers by the ~466 Ma Whiteside Granite; (2) Neoacadian (360-350 Ma); reported metamorphic rims on zircon; and (3) Alleghanian (~330 Ma); truncation of ~335 Rabun granodiorite, parallelism of magmatic and country rock fabrics, and Ar/Ar cooling ages.

INTRODUCTION

The Blue Ridge of western North Carolina and northeastern Georgia consists of complex, polydeformed crystalline rocks that record the Mesoproterozoic through Paleozoic tectonic history of the southern Appalachians. Detailed geologic maps are a fundamental data set necessary to resolve the tectonic history of the Blue Ridge and southern Appalachians. This paper summarizes nearly 40 years of detailed geologic mapping in the western, central, and eastern Blue Ridge of southwestern North Carolina and northeastern Georgia, and incorporates recent geochronologic and geochemical data to refine our understanding of Blue Ridge geologic history.

This paper discusses the geology of a ~850 km^2 area of the Blue Ridge that extends diagonally from 35º 30' N, 82º 52' 30" W, near Waynesville, North Carolina, to its southernmost latitude of 34º 52' 30" N near Clayton, Georgia, and its westernmost boundary of 83º 45' W near Shooting Creek, North Carolina (Figs. 2–1 and 2–2; Plate 3). The width of the diagonal strip varies from three to four 7.5-minute quadrangles. Elevations range from 1954 m at Richland Balsam to 700 m in Clayton, Georgia, and the area includes several subsidiary ranges of the Blue Ridge province including the Plott, Great Balsam, Cowee, and Nantahala Mountains.

Geologic mapping was conducted at scale of 1:24,000 or larger. Research was supported by different academic institutions (University of Tennessee, University of South Carolina, Clemson University, and Western Carolina University), the Geological Survey of North and South Carolina, and several grants from the National Science Foundation, and National Cooperative Geologic Mapping Programs (EDMAP and FEDMAP). Compiled Geologic maps include published reports, Hatcher (1980); unpublished theses and dissertations, Eckert (1984, 1988), Quinn (1991), Lamb (2001), Stahr (2007), and Cyphers (2009), and unpublished maps by L. L. Acker, A. Burns, J. O. Eckert, Jr., S. H. Edelman, R. D. Hatcher, Jr., and S. E. Yurkovich (Table 2–1). These

Figure 2–1. Simplified tectonic map of the southern Appalachians with location of Figure 2 indicated by white box. The Laurentian platform contains the Alleghanian foreland fold-thrust belt driven in front of the Blue Ridge-Piedmont megathrust sheet (the Laurentian margin, gold with red inliers of Grenvillian, not necessarily Laurentian Grenville, and older inherited crust), and all components to the east. All terranes west of the Cat Square terrane have a Laurentian source (Bream et al., 2004). Cat Square terrane contains Siluro-Devonian metasedimentary rocks with a mixed Laurentian and Peri-Gondwanan source. Carolina superterrane is Peri-Gondwanan and exotic to Laurentia. BCF– Brindle Creek fault. BF–Burnsville fault. Cart. terr.–Cartoogechaye terrane. CHMF–Chattahoochee-Holland Mountain fault. Cow. terr.–Cowrock terrane. DGB–Dahlonega gold belt. FF–Forbush fault. GLF–Gossan Lead fault. GMW–Grandfather Mountain window. MH–Mars Hill terrane. NW–Newton window. SRA–Smith River allochthon, an outlier of Carolina superterrane rocks. SMW–Sauratown Mountains window. PMW–Pine Mountain window. Light gray–Probable western Tugaloo terrane rocks in Alabama and Georgia. Purple–Ordovician Elkahatchee Quartz Diorite. A–Athens. H–Hickory. S–Statesville. WS–Winston–Salem.

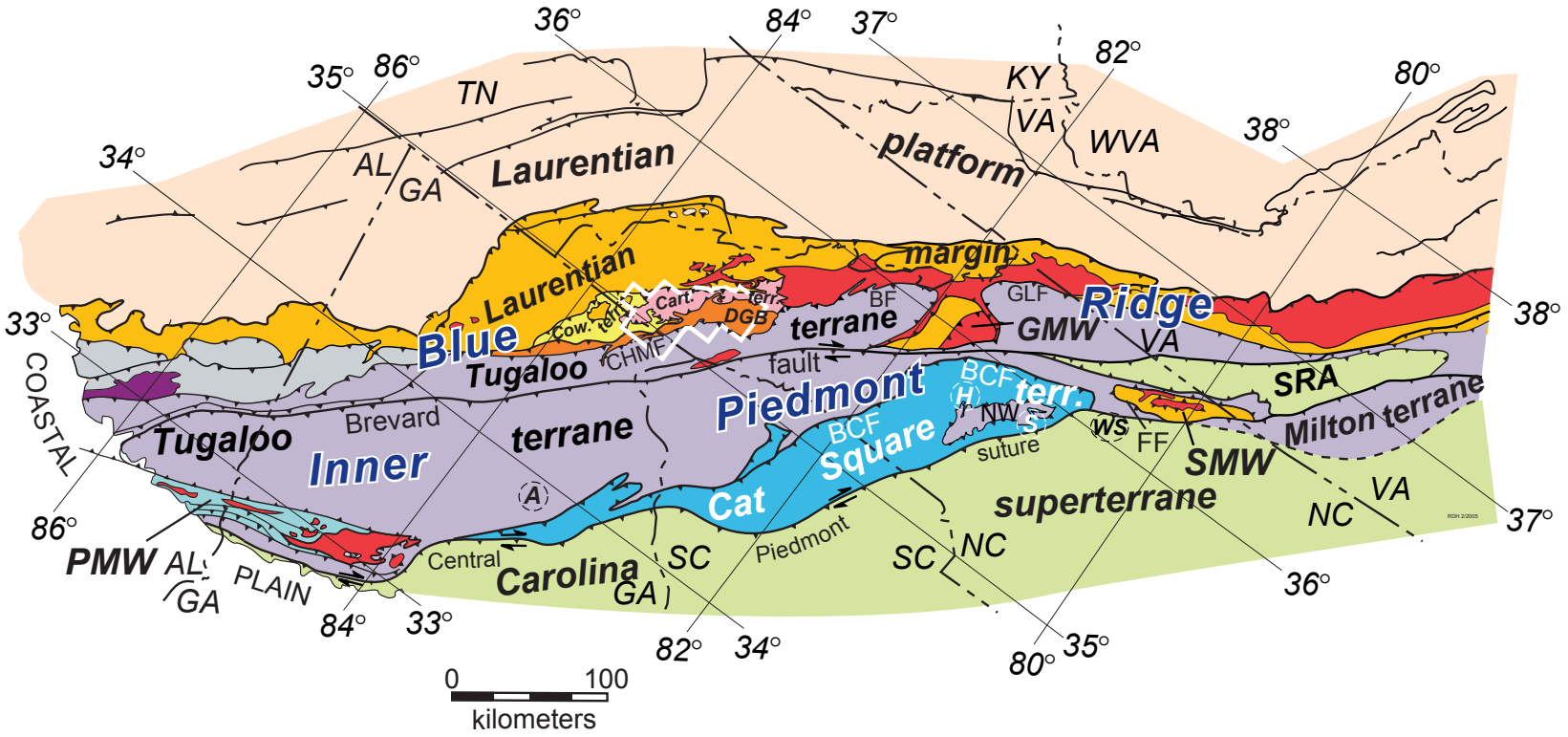
36°
84°
37°
82°
80°
35°
86°
TN
KY
VA
WVA
38°
34°
AL
GA
Laurentian
platform
margin
Laurentian
Blue
Ridge
Cow. terr.
Cart.
terr.
DGB
BF
terrane
GLF
GMW
VA
33°
38°
fault
CHME
Tugaloo
Piedmont
BCF
terr.
SRA
Brevard
Tugaloo
terrane
Inner
BCF
Square
NW
suture
FF
SMW
Milton terrane
COASTAL
Cat
superterrane
VA
NC
37°
86°
PMW
AL
GA
PLAIN
Central
Carolina
SC
GA
Piedmont
SC
NC
36°
84°
33°
82°
34°
80°
35°
0
100
kilometers

Figure 2–2. Simplified geologic map of the part of the western, central, and eastern Blue Ridge of southwestern North Carolina and northeastern Georgia. CFAf–Cradle-of-Forestry-in-America fault. CGMF–Chunky Gal Mountain fault. CHMf–Chattahoochee–Holland Mountain fault. Hf–Hayesville fault. Lw–Long Branch window. SCw–Shooting Creek window. SFf–Shope Fork fault. SRf–Soque River fault.

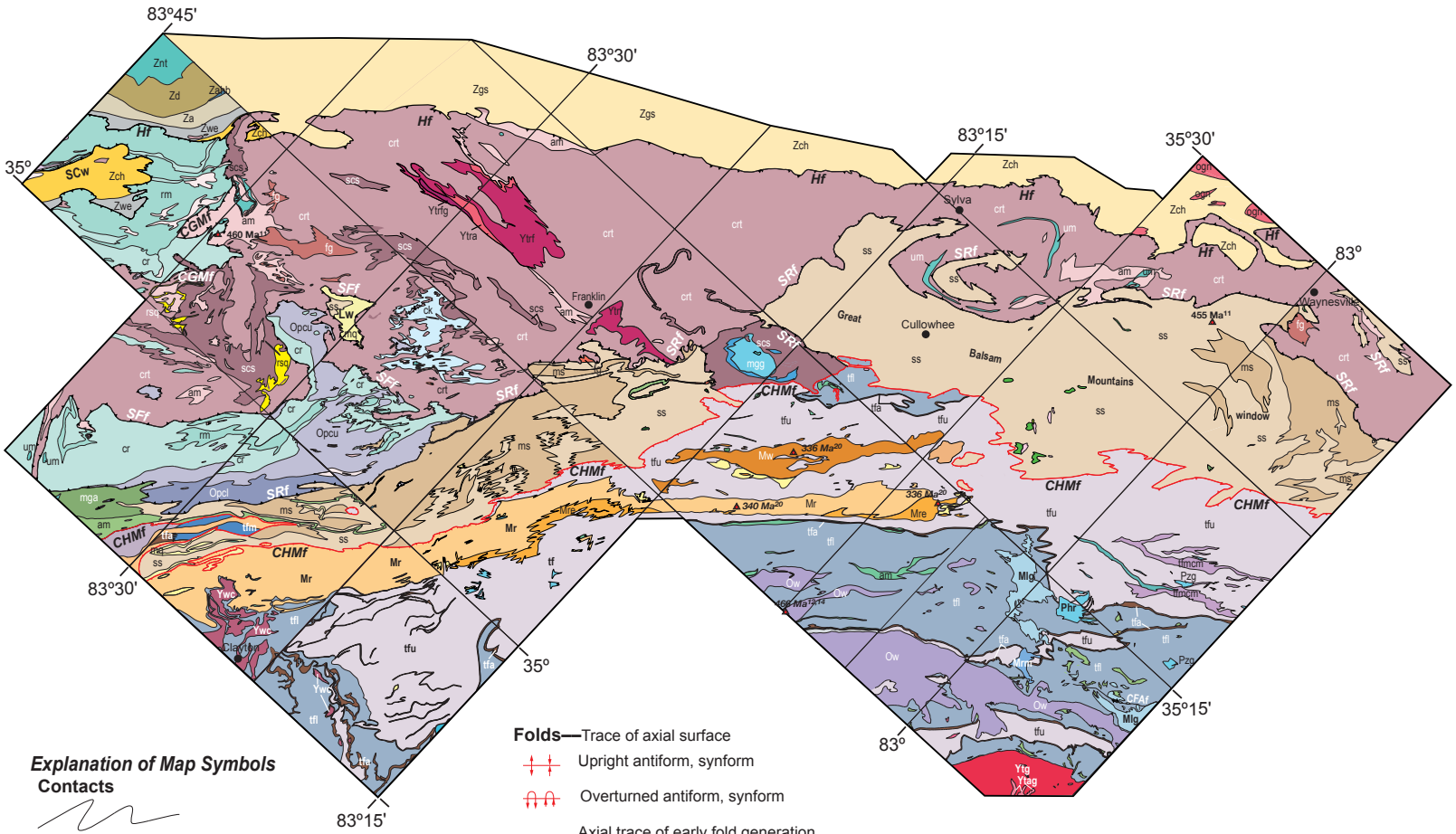

Explanation of Map Symbols

Contacts

Thrust fault

Teeth located on upper plate.

Taconic pre- to synmetamorphic fault.

Alleghanian syn- to postmetamorphic Chattahoochee-Holland Mountain fault.

Folds—Trace of axial surface

Upright antiform, synform

Overturned antiform, synform

Axial trace of early fold generation. Tab indicates axial surface dip direction.

Location of SHRIMP samples

Age of igneous crystallization
▲ ***336 Ma***

Age of zircon rim
▲ ***456 Ma***

Town

Block-in matrix

CONTOUR INTERVAL 50 METERS

Projection Universal Transverse Mercator, zone 17

0 10 20
Kilometers

0 10
Miles

Western Blue Ridge

Great Smoky Group

- Znt — Nantahala Formation
- Zd — Dean Formation
- Zahb — Horse Branch Member
- Zam — Ammons Formation
- Zwe — Wehutty Formation
- Zch — Copper Hill Formation
- Zgs — Great Smoky Group (undivided)

Basement (?)

- ogn — Augen gneiss

Central Blue Ridge

Cartoogechaye terrane

- crt — Metasandstone-pelitic schist
- scs — Shooting Creek schist
- mgg — Medium-grained granitoid
- am — Amphibolite
- um — Ultramafic
- CK — Carroll Knob Complex
- mg — Metagabbro
- fg — Felsic orthogneiss (basement ?)

Basement Orthogneiss

Trimont Ridge complex (1103 Ma)

- Ytrf — Felsic gneiss
- Ytrfa — Felsic gneiss and amphibolite
- Ytrfg — Felsic gneiss and metagabbro

Central Blue Ridge cont.

Cowrock terrane

Coweeta Group

- rm — Ridgepole Mountain Formation
- cr — Coleman River Formation
- Opcu — Persimmon Creek Tonalitic Gneiss (Upper)
- Opcl — Persimmon Creek Tonalitic Gneiss (Lower)
- am — Amphibolite
- um — Ultramafic

Dahlonega Gold belt

Otto Formation

- ss — Metasandstone
- ms — Muscovite schist
- mq — Muscovite quartzite
- am — Amphibolite
- um — Ultramafic bodies

Basement (?)

- ag — Augen gneiss (altered)

Index of Geologic Mapping

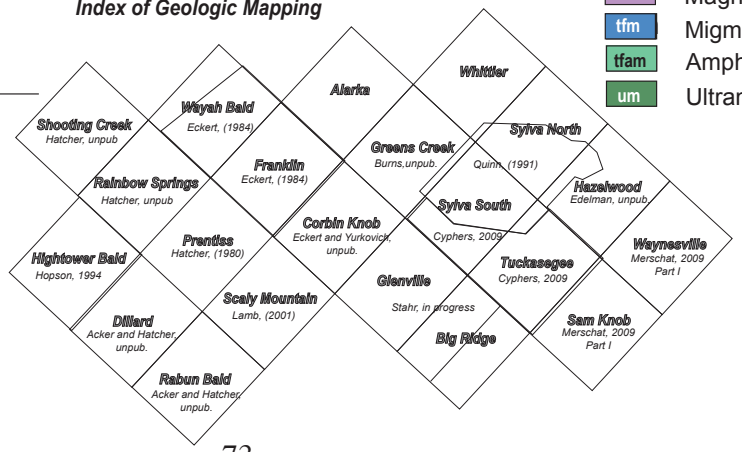

Eastern Blue Ridge

Tugaloo terrane

Plutonic Units

- Mr — Rabun Granodiorite (336 Ma) porphyritic phase
- Mre — Equigranular phase
- Mw — Walnut Creek pluton (335 Ma)
- Mlg — Looking Glass pluton (337 Ma)
- Mrm — Round Muntain pluton (342 Ma)
- Ow — Whiteside Granite (466 Ma)
- Pzg — Granitoid & Pegmatite

Basement

- Ywc — Wolf Creek Gneiss (1123 Ma)
- Ytg — Toxaway Gneiss (1156 Ma)

Tallulah Falls Formation

- tf — Tallulah Falls Formation (Undivided)
- ms — Muscovite schist
- tfu — Tallulah Falls Formation (Upper)
- tfa — Aluminous schist
- tfl — Tallulah Falls Formation (Lower)
- tfmcm — Magnetite-Chlorite-Muscovite schist
- tfm — Migmatite
- tfam — Amphibolite
- um — Ultramafic bodies

Figure 2–2. Continued.

Table 2–1. Sources of compiled geologic maps based on 7.5-minute quadrangle.

Quadrangle	Reference	Status	Support
Big Ridge, NC	Stahr, 2007	MS	UT-SA, EDMAP
Big Ridge, NC	Varnell, in progress	MS	UT-SA, EDMAP
Corbin Knob, NC	Echert, and Yurkovich, 2005	Unpub.	UTK, NCGS
Dillard, NC-GA	Acker and Hatcher, 2002	Unpub.	NSF
Franklin, NC	Eckert, 1984, 1988	MS, PhD	UT
Glenville, NC	Stahr, 2007	MS	UT-SA, EDMAP
Greens Creek, NC	Burns, 2005	Unpub.	UTK
Hazelwood, NC	Edelman and Hatcher, 2005	Unpub	UTK, NSF
Hightower Bald, NC-GA	Hopson, 1994	PhD	NSF
Prentiss, NC	Hatcher, 1980	NCGS GM 167	NCGS
Rabun Bald, NC-GA	Acker and Hatcher, 2003	Unpub.	NSF
Rainbow Springs, NC	Hatcher, 1978	Unpub.	NSF
Sam Knob, NC	This study, Plates 1 & 2	PhD	EDMAP, FEDMAP
Scaly Mountain, NC-GA	Lamb, 2001	MS	UTK
Shooting Creek, NC	Hatcher, 1978	Unpub.	NSF
Sylva North, NC	Quinn, 1991	MS	UTK
Sylva South, NC	Quinn, 1991	MS	UTK
Sylva South, NC	Davidson, 1995	MS	UTK
Sylva South, NC	Cyphers, 2009	MS	UT-SA, EDMAP
Topton, NC	Ausburn et al., 1998	NCGS GM-6	NCGS
Toxaway Lake, NC	Varnell, in progress	MS	UT-SA, EDMAP
Tuckasegee, NC	Cyphers, 2009	MS	UT-SA, EDMAP
Wayah Bald, NC	Eckert, 1984, 1988	MS, PhD	NCGS
Waynesville, NC	This study, Plates 1 & 2	PhD	UT-SA, EDMAP

Support for geologic mapping includes funding from: National Cooperative Geologic Mapping Program, EDMAP to Robert D. Hatcher, Jr., and FEDMAP components; NCGS, North Carolina Geological Survey; NSF, National Science Foundation; UTK, University of Tennessee; and UT-SA University of Tennessee Science Alliance Center of Excellence. Unpublished maps (Unpub.) are on file with the Tectonics and Structural Geology Research Group, University of Tennessee–Knoxville.

maps were digitally compiled at 1:24,000 scale and combined into a single map at 1:50,000 scale.

During the time in which the geologic mapping was completed, major advances in geochronology have improved our ability to obtain absolute ages of complex radiogenic minerals, especially zircon. Complex xenocrystic zircons and overprinting metamorphic events plagued early attempts to determine absolute ages of magmatism and metamorphism (e.g., Tull, 1980; C. F. Miller et al., 1997, 2000). The development of Sensitive High Resolution Ion MicroProbes (SHRIMP) enable *in situ* spot analyses of xenocrystic radiogenic minerals, like zircon, yielding multiples ages from different zones in the same crystal that record the chronology of the mineral's growth. Additionally, U-Pb zircon ages are not easily reset by later events, unlike other isotopic systems e.g., Rb-Sr, K-Ar, and Ar-Ar. The complex xenocrystic zircons can potentially yield information about inheritance, igneous crystallization, and age of metamorphism. The ability to make multiple precise measurements on a single crystal using the SHRIMP permits analysis of detrital zircons to address provenance and paleogeographic reconstructions for high-grade

metasedimentary terranes. Several recent studies obtained absolute ages of magmatism, metamorphism, and provenance from the study area using the SHRIMP or other ion microprobes (e.g., Miller et al., 1998; Carrigan et al., 2003; Bream et al., 2004; Stahr, 2007; Varnell et al., 2008). Other studies have reported traditional Isotope Dilution-Thermal Ionization Mass Spectormetry (ID-TIMS) U-Pb ages of zircon (e.g., Miller et al., 2006), and Ar-Ar mineral ages (e.g., Dallmeyer, 1988) provide important chronologic data. These recent geochronologic studies have refined the ages of Blue Ridge magmatic and metamorphic events.

Our goal here is to merge data sets —geologic map, petrology, U-Pb geochronology, and geochemical data — and provide a refined interpretation of the tectonic evolution of the Blue Ridge of southwestern North Carolina and northeastern Georgia. Descriptions of the geology, including lithostratigraphy, structure, and composition of Paleozoic magmatism, will follow that of previous summaries by Hatcher and Butler (1979), Hopson et al. (1989), Miller et al. (1997), and Hatcher et al. (2005). New data and field observations will be incorporated with these studies to present a more thorough understanding of the geology.

TECTONIC SETTING

The Blue Ridge of southwestern North Carolina and northeastern Georgia represents part of the Neoproterozoic to early Paleozoic rifted margin of eastern Laurentia, and the various metasedimentary terranes accreted during different middle Paleozoic orogenies. Polyphase deformation and metamorphism is well documented in the Blue Ridge by several previous studies (e.g., Hadley and Goldsmith, 1963; Hatcher, 1977; Hatcher and Butler, 1979; Hopson et al., 1989; Massey and Moecher, 2005). The Blue Ridge consists of a west-vergent stack of crystalline thrust sheets of polydeformed metasedimentary and metaigneous rocks (e.g., Hopson et al., 1989; Hatcher and Goldberg, 1991). Metamorphic grade ranges from anchizone to granulite facies in the Blue Ridge (Butler, 1991; Hatcher and Goldberg, 1991; Part III) and this study focuses on a section of middle amphibolite to granulite facies rocks intruded by several Paleozoic granitoids.

Metasandstone, metagraywacke, and metapelite are the most abundant rock types in the Blue Ridge, with lesser amounts of Mesoproterozoic metaigneous, Paleozoic granitoids, and mafic and ultramafic rocks. Recognition of contrasting lithostratigraphic sequences and tectonic boundares have led to the separation of five tectonostratigraphic terranes (Hatcher, 2002; Hatcher et al., 2004; Hatcher et al., 2007). Some of the

lithotectonic terranes, like those of the western Blue Ridge, contain sedimentary sequences correlative with the Laurentian platform and/or deposited on Laurentian crust (Williams and Hatcher, 1983; Hatcher et al., 2007). The remaining terranes to the east were grouped together as large suspect terrane by Williams and Hatcher (1983), recognizing the lack of evidence linking it to Laurentia. The stratigraphic, structural, metamorphic, and deformation histories of the these terranes will be discussed in detail below.

TERRANES AND LITHOSTRATIGRAPHY

Five tectonostratigraphic terranes recognized in the map area are the western Blue Ridge/Laurentian margin, Cartoogechaye, Cowrock, Dahlonega gold belt, and Tugaloo terranes (Fig. 2–2). Fundamental similarities and differences are present in the rock assemblages, stratigraphic sequences, and igneous rocks distributed throughout these terranes, as listed in Table 2–2. The Hayesville fault separates rocks deposited on Laurentian crust, and contains sedimentary sequences similar to the Laurentian platform from suspect terranes east of the fault. A suspect status is maintained for central and eastern Blue Ridge terranes, because the sedimentary sequences in these terranes cannot be directly correlated with sedimentary sequences of the Laurentian platform, despite significant geochemical and geochronologic data suggesting these terranes formed proximal to Laurentia (Bream, 2003; Beam et al., 2004; Hatcher et al., 2007). As recognized by Hatcher (1978a), the Hayesville fault is a suture between the Laurentian margin and several peri-Laurentian terranes. These terranes are separated by several ductile faults into a complex thrust stack (Fig. 2–3). The Hayesville fault separates the western Blue Ridge/Laurentian margin, the lowest thrust sheet, from the terranes of the central Blue Ridge. The central Blue Ridge terranes are exposed in a complex synform-antiform thrust stack between the western Blue Ridge and eastern Blue Ridge/western Tugaloo terrane. Migmatitic biotite gneiss and lesser lithologies of the Cartoogechaye terrane were thrust above the Cowrock and Dahlonega gold belt terranes. The Cowrock terrane sits in a lower synformal position beneath the Cartoogechaye terrane and west of the narrow antiformal Dahlonega gold belt. The Chattahoochee-Holland Mountain thrust sheet is the highest and overrides the terranes of the central Blue Ridge.

Western Blue Ridge/Laurentian margin

The western Blue Ridge contains a succession of Neoproterozoic to Cambrian rift-related clastic rocks overlain by Cambrian to Ordovician carbonate rocks following

Table 2–2. Summary of lithotectonic terranes in southwestern North Carolina and northeastern Georgia Blue Ridge.

Laurentian margin/Western Blue Ridge

Mesoproterozoic basement massifs and overlying Neoproterozoic to early Paleozoic clastic and carbonate rocks
2 sequences: ~730 Ma immature clastic intracratonic rift sediments, Ocoee Supergroup; 565–480 Ma rift to drift to passive margin sequence
Early Cambrian to Ordovician stratigraphy similar to Laurentian Platform rocks
Deposited nonconformably on Meso- and Neoproterozoic metaigneous rocks
Anchizone to sillimanite I zone metamorphism
No ultramafic rocks; minor mafic rocks occur as basaltic flows in early Cambrian rift facies
No Paleozoic plutons
Detrital zircons: 1.3–1.0 Ga abundant, lesser 1.5–1.3 Ga and Paleoproterozoic ages.
Sm-Nd model age of source material, T_{DM}: 1.46–1.37 Ga

Central Blue Ridge

Metasedimentary terranes with associated mafic and ultramafic rocks, Paleozoic igneous rocks, and minor internal Mesoproterozoic basement massifs
Amphibolite facies metamorphism: Kyanite-staurolite to hypersthene granulite

Cartoogechaye. Migmatitic biotite gneiss with common pods/interlayers of amphibolite, Shooting Creek schist, and Rainbow Springs quartzite
Mafic and ultramafic complexes: Webster-Addie, Buck Creek, & Carroll Knob
Detrital zircons: abun. 1.3–1.0 & 1.5–1.3 Ga, lesser 1.9, 1.8, 1.6, and 0.9, 0.8, and 0.7 Ga

Cowrock. Coweeta Group: Ridgepole Mountain and Coleman River Formations
Metasandstone and schist, minor siliceous marbles
Intruded by ~466 Ma Persimmon Creek gneiss
Mafic and ultramafic complexes: Lake Chatuge
Detrital zircons: 1.3–1.0 and 1.5–1.3 Ga abun., rare 0.7, 1.6, and 2.7 Ga
Sm-Nd model age of source material, T_{DM}: 1.60 Ga

Dahlonega gold belt. Otto Formation schist and metasandstone (2 mica, 2 feldspar)
Locally sulfidic and massive sulfides are present
Mafic and Ultramafic rocks are present: Lake Burton
Felsic to intermediate 480–460 Ma igneous rocks, some with arc-signatures
Kyanite-Staurolite majority and sillimanite I and II in Great Balsam Mountains window
Detrital zircons: 1.3–1.0 & 1.4 abun. Lesser 2.1, 2.0, 1.9, 1.8, 1.6 Ga, and rare 2.9 Ga
Sm-Nd model age of source material, T_{DM}: 1.91–1.43 Ga

Western Tugaloo terrane/ Eastern Blue Ridge

Chattahoochee-Holland Mountain-Burnsville-Gossan-Lead thrust sheet
Neoproterozoic to Ordovician Ashe-Tallulah Falls Formation: Upper metagraywacke-schist, aluminous schist, and lower metagraywacke-amphibolite-schist members
Middle Ordovician, Devonian, and Mississippian magmatism
Internal Mesoproterozoic basement massifs: Toxaway and Tallulah Falls domes
Mafic and ultramafic rocks: Laurel Creek complex and several smaller bodies
Detrital zircons: 1.3–1.0 Ga abundant, lesser 1.5–1.3 Ga, lesser 0.9–0.7 Ga
Sm-Nd model age of source material, T_{DM}: 1.61–1.24 Ga

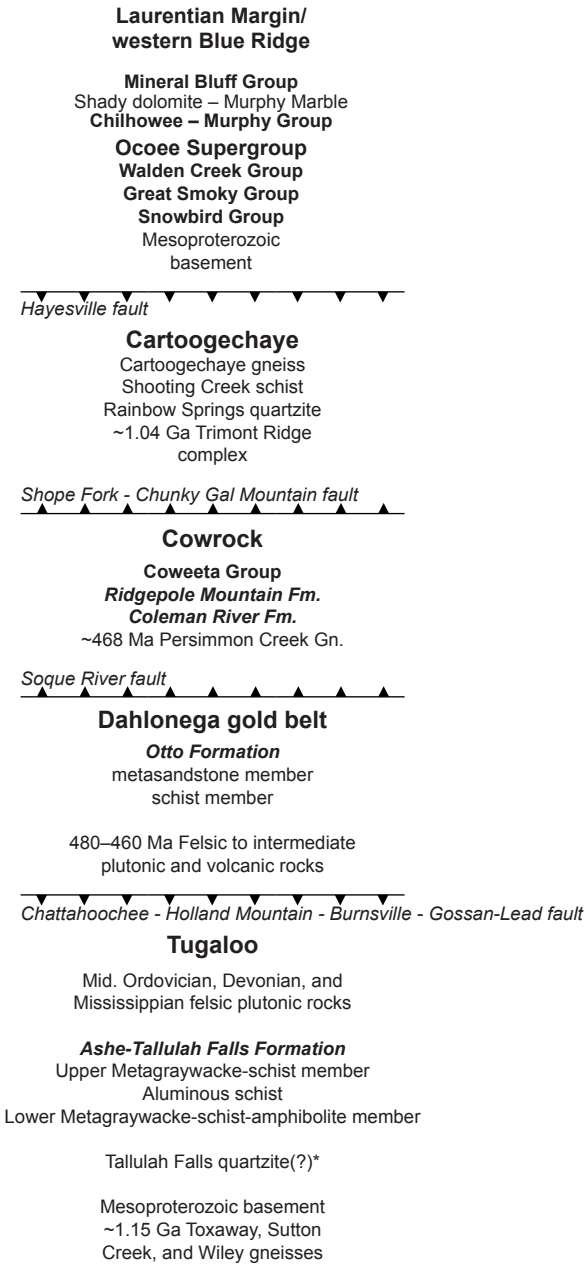

Figure 2–3. Simplified lithostratigraphy and terranes of southwestern North Carolina and northeastern Georgia Blue Ridge. Terranes are listed according to thrust sheet stacking order from northwest to southeast.

a transition to passive margin setting (Tull et al., 1992). The succession of rocks is the product of two rifting events, one between 750–700 Ma, and the second at 568 Ma responsible for the opening of the Iapetus (Aleinikoff et al., 1995; Brewer and Thomas, 2000). The basal units of both rifting events nonconformably overlie Mesoproterozoic basement rocks and indicate the western Blue Ridge is parautochthonous.

The stratigraphy of the western Blue Ridge is quite complex, and numerous studies have recognized different lithologies and formations. The literature surrounding the entire stratigraphy of the western Blue Ridge is quite extensive, and we will focus of the stratigraphy and formations recognized and compiled in this map, the Great Smoky Group. For more complete descriptions of the entire sedimentary package of the western Blue Ridge, we recommend the descriptions and summaries by: Hadley and Goldsmith (1963), King et al., (1968), Powers and Frost (1971), Rast and Kohles (1986), Wiener and Merschat (1992), Tull et al., (1992), and Southworth et al. (2005).

Great Smoky Group

The easternmost portion of the western Blue Ridge along the Hayesville fault is comprised of the Great Smoky Group. The Great Smoky Group is a monotonous sequence of impure and immature clastic sedimentary rocks that reaches a maximum thickness of ~7,600 m (25,000 ft) in the vicinity of the Great Smoky Mountains (King et al., 1968). It consists of two mica-two feldspar metasandstones, and two-mica schists and phyllites. At lower metamorphic grades to the west, the Great Smoky Group consists of fine- to coarse-grained sandstones, pebble conglomerates, and argillaceous rocks (King et al., 1968). The Great Smoky Group is subdivided into the Copperhill, Wehutty, Ammons, and Dean Formations (Hurst, 1955). Due to increased metamorphic grade, structural complexities, or other reasons, the Great Smoky Group was not subdivided consistently by different geologists and areas of undivided Great Smoky Group exist.

Great Smoky Group undivided. Areas of undivided Great Smoky Group consist of interlayered two-mica, two-feldspar metasandstones to gneisses and interlayered garnet-biotite-muscovite schists that may be correlative of several Great Smoky Group formations, but are most likely Copperhill Formation (Thunderhead Sandstone) equivalents (Quinn, 1991). They contain ±staurolite, garnet, aluminum silicate (kyanite or sillimanite, depending on grade), muscovite, biotite, quartz, plagioclase (An_{20-37}), and microcline (Quinn, 1991). Common accessory minerals include tourmaline, zircon, apatite, and sphene (Quinn, 1991). These rocks are commonly sulfidic, especially the

schist interlayers. Although these rocks contain penetrative fabrics, well-developed foliations and tight to isoclinal folds, locally graded beds and other sedimentary features can be recognized (Quinn, 1991; Montes, 1997; Massey and Moecher, 2005).

Copperhill Formation. The basal formation of the Great Smoky Group is the Copperhill Formation and is equivalent to the Thunderhead Sandstone (Hadley and Goldsmith, 1963). Northwest of the map area, Hadley and Goldsmith (1963) recognized that the base of the Great Smoky Group, Thunderhead Sandstone rests conformably above the Snowbird Group. It consists of gray to tan, medium- to coarse-grained metasandstone and lesser metaconglomerate and pelitic schist (Ausburn et al., 1998). Layering ranges from 20 cm to 3 m, while schist interlayers vary from 1 cm to 2 m thick. Mineralogy consists of quartz, plagioclase, biotite, opaque minerals, muscovite, and garnet with trace amounts of chlorite, sphene, sillimanite, zircon, apatite, epidote and tourmaline.

Wehutty Formation. Equivalent to the Anakeesta Formation of Hadley and Goldsmith (1963), the Wehutty consists of dark gray, graphitic, sulfidic slate to muscovite-biotite schist interbedded with lesser amounts of coarse-grained metasandstone, metaconglomerate, and calc-silicate granofels (Ausburn et al., 1998; Hatcher et al., 2005). The schist is generally composed of muscovite, biotite, quartz, plagioclase (An_{25-30}), and kyanite with accessory and trace amounts of garnet, apatite, chlorite, tourmaline, epidote, zircon, and sphene (Ausburn et al., 1998). In the Topton 7.5-minute quadrangle, the Wehutty ranges from 800-1000 m thick (Ausburn et al., 1998).

Ammons Formation. The Ammons Formation consists of phyllite, schist, medium-grained metagraywacke, and metasandstone. The total thickness of the unit may approach 5000 m and varies considerably (Ausburn et al., 1998). The Horse Branch Member is a distinctive unit of a gray to tan, interlayered graphitic and nongraphitic metasiltstone, phyllite and schist that marks the top of the Ammons Formation (Ausburn et al., 1998). Mineralogy of the Horse Branch Member consists of muscovite, quartz, opaque minerals, biotite, and plagioclase. Accessory minerals include chlorite, tourmaline, epidote, zircon, and apatite (Ausburn et al., 1998). The thickness of the Horse Branch Member varies from 300–1300 m (Ausburn et al., 1998). Informal units mapped in the Ammons include cross-biotite schist, phyllite-metagraywacke, and metasandstone-schist units, although these units could not be mapped continuously across the Topton 7.5-minute quadrangle (Ausburn et al., 1998).

Dean Formation. Metaconglomerates, metasandstones, and phyllites of the Dean Formation mark the top of the Great Smoky Group. The Dean Formation fines upward from metasandstones and pebble conglomerates near the base to dominantly phyllites at the top of the formation. The thickness ranges from 1300–450 m. Phyllite contains muscovite, biotite, quartz, plagioclase, opaque minerals (hematite, magnetite, and graphite), and chlorite. Accessory and trace minerals include garnet, staurolite, tourmaline, epidote, and apatite. Garnet, although minor, is common throughout the phyllite and schist horizons, and staurolite porphyroblasts up to 5 cm may be present. Metasandstone and metaconglomerate are poorly sorted and beds range up to 2 m thick. Metasandstone is commonly coarse-grained and composed of quartz, muscovite, plagioclase (An_{25-30}), biotite, and magnetite with accessory and trace amounts of chlorite, zircon, apatite, allanite, and sphene. Metaconglomerate consists of well-rounded pebbles of plagioclase, and vein and blue quartz. Description from Ausburn et al. (1998).

Central and Eastern Blue Ridge Terranes

East of the Hayesville fault the metasedimentary terranes of the Blue Ridge share many similarities: they are composed of dominantly clastic metasedimentary rocks, lack fossils, amphibolite to granulite facies metamorphism, polydeformed, occurrence of mafic and ultramafic rocks, and were intruded by several Paleozoic felsic igneous rocks (Table 2–2). The high metamorphic grade and polydeformed nature of the terranes has hindered unraveling detailed stratigraphic relationships. Table 2–3 lists some of proposed nomenclature used by various researchers working the same area, or in the same terranes along-strike to describe the stratigraphic relationships in the central and eastern Blue Ridge. The nomenclature of Hatcher (2002) and Hatcher et al. (2004, 2007) is used in the study and will be the primary focus of discussion. The terranes will be discussed from northwest to southeast: beginning at the top of the central Blue Ridge thrust stack, continuing to the lowest thrust sheet, the Dahlonega gold belt, and then the Tugaloo terrane/eastern Blue Ridge, the highest thrust sheet (Figs. 2–2, 2–3 and 2–4).

Cartoogechaye terrane

The Hayesville-Chunky Gal Mountain–Shope Fork thrust sheet is the highest in the central Blue Ridge and is composed of the Cartoogechaye terrane. This terrane consists of a nearly ubiquitous migmatitic biotite-quartz-plagioclase gneiss, the Shooting Creek Schist, Rainbow Springs quartzite, several mafic and ultramafic complexes, and

Table 2–3. Comparison of thrust sheets, terranes and lithostratigraphic units recognized east of the Hayesville fault.

Study:	Hadley and Goldsmith, 1963	Hadley and Nelson, 1971	Hatcher, 1979	Hatcher, 1988	Merschat and Weiner, 1988	Nelson et al. 1998	Merschat and Catanache, 2008	**This Study**
Hayesville-Chunky Gal Mountain-Shope Fork thrust sheet								
Cartoogechaye	Carolina gneiss	layered gneiss and migmatite	—	—	Earlies Gap Fm. Richard Russell Fm.	Richard Russell Fm.	Cartoogechaye Mig. Gneiss, metagraywacke, schist, amphibolite	Rainbow Springs quartzite, Shooting Creek Schist, Cartoogechaye Mig. Gneiss
Hayesville-Soque River thrust sheet								
Cowrock terrane	—	biotite schist and gneiss	**Coweeta Group:** Ridgepole Mountain Fm. Coleman River Fm. Persimmon Creek gn (basement)	—	—	Richard Russell Fm.	—	~468 Ma Presimmon Creek Gn. **Coweeta Group:** Ridgepole Mountain Fm. Coleman River Fm.
Soque River thrust sheet								
Dahlonega gold belt	—	muscovite schist and gneiss	—	Otto Fm. Metasandstone and schist	—	**Helen Group:** Nacooche Fm.(schist & mss) Horton Fm.(feld. mss) Roberston Fm. (mss)	—	Otto Fm. Aluminous schist member, Metasandstone member
Chattahoochee-Holland Mountain-Burnesville-Gossan Lead thrust sheet								
Tugaloo	—	Great Smoky undivided Biotite schist and gneiss	—	—	Ashe-Tallulah Falls Fm. schist and metagraywacke	—	Ashe-Tallulah Falls Fm. schist and metagraywacke	Ashe-Tallulah Falls Fm. Upper metagraywacke–schist, Aluminous schist, Lower Metagraywacke-amphibolite-schist

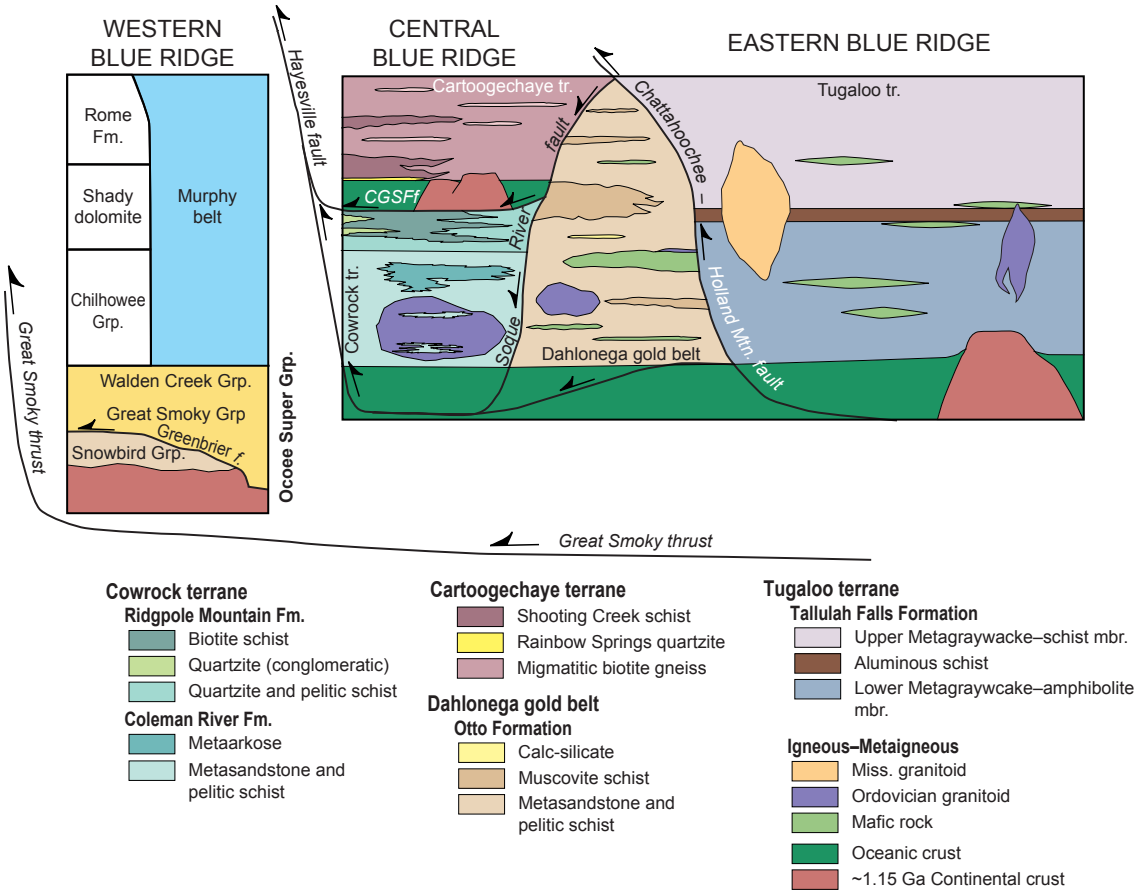

Figure 2–4. Stratigraphic column of western, central and eastern Blue Ridge terranes in southwestern North Carolina and northeastern Georgia. Terranes are shown in position according to thrust sheet from northwest to southeast. Stratigraphic thickness is not known for central and eastern Blue Ridge terranes and is not proportional. Modified from Hatcher et al. (1995). CGSFf–Chunky Gal Mountain–Shope Fork fault.

internal massifs of Mesoproterozoic basement. The main rock type of the Cartoogechaye terrane is homogeneously, heterogeneous migmatitic biotite-quartz-plagioclase gneiss. As indicated in Table 2–3, various names have been proposed for the units of this thrust sheet (including the Smackass Gap Formation), most recently the Cartoogechaye gneiss (Merschat and Cattanach, 2008). The migmatitic biotite gneiss consists of interlayered medium- to coarse-grained garnet biotite schist and metagraywacke. Two units largely recognized southwest of Franklin, North Carolina, include the Shooting Creek schist and the Rainbow Springs quartzite. The Shooting Creek Schist is an aluminous schist that contains garnet up to 1 cm in diameter, white mica, sillimanite, oligoclase, and K-feldspar with minor biotite, ilmenite, and rutile. At granulite facies, exposures of the this unit contain garnet, sillimanite, orthoclase, K-feldspar, rutile, and ilmenite (Force, 1976; Moecher et al., 2004), and have been prospected for rutile (Force, 1976). The Rainbow Springs quartzite is a thin unit, isoclinally folded with the migmatitic biotite gneiss, recognized by Hatcher (unpublished mapping) southwest of Franklin, North Carolina. The quartzite is medium-grained with 7–15 cm layers, and contains minor rutile, garnet, muscovite, and biotite. Amphibolite commonly occurs as interlayers or blocks, but also occurs as map-scale bodies to complexes, e.g., Kimsey Blad, Willets-Ochre Hill, and Carroll Knob complexes. The Cartoogechaye gneiss dominates in the northern part of the terrane, but near Franklin, North Carolina, the Shooting Creek Schist and Rainbow Springs quartzite have been recognized.

Mafic-ultramafic complexes. Several well-studied mafic-ultramafic complexes occur in the Cartoogechaye terrane including the Webster-Addie ultramafic body, Buck Creek dunite, Kimsey Bald, Carroll Knob mafic-ultramafic complex, Balsam Gap dunite, and Dark Ridge mafic-ultramafic complex. Raymond et al. (2003) and Swanson et al. (2005) provided thorough reviews of the different complexes and associated rocks, including their mineralogy, composition, and possible tectonic heredity.

Mesoproterozoic basement. The Trimont Ridge complex is the only documented body of Mesoproterozoic basement in the Cartoogechaye terrane (Hatcher et al., 2004); however, other felsic gneiss bodies mapped by Hatcher (unpublished) in the Rainbow Springs 7.5-minute quadrangle remain possible candidates. Eckert (1984, 1988) initially recognized the Trimont Ridge complex, which consists of othropyroxene bearing, granitic gneiss and two-pyroxene bearing amphibolite. Hatcher et al. (2004) reported a SHRIMP U-Pb zircon age of 1103±69 Ma from the Trimont Ridge complex (Table 2–4). It is the

Table 2–4. SHRIMP U-Pb zircon ages of central and eastern Blue Ridge internal basement massifs.

Terrane	Massif	Rock Unit	Lat. & Long.	Age (Ma)	Inheritance	Source
Tugaloo	Tallulah Falls dome	Wolf Creek Gneiss	—	1123±29	—	Hatcher et al., 2004
		Wiley Gneiss (GA)	34° 48.2 N 83° 25.3 W	1159±19	—	Carrigan et al., 2003
		Sutton Creek Gneiss (GA)	34° 44.2 N 83° 34.5 W	1156±23	—	Carrigan et al., 2003
	Toxaway dome	Toxaway Gneiss TOX-1 (SC) TOX-1B (SC) G-MA-2 (SC) B-TB-3 (SC) TXFL (NC)	 35° 0026 N 83° 04.29 W 35° 00.4 N 82° 59.6 W 35° 07.2 N 82° 55.5 W	 1151±17 1149±56 1157±36 1141±148 1149±32	—	Carrigan et al., 2003
Cartoogechaye	Trimont Ridge	Trimont Ridge felsic gneiss (NC)	—	1103±69 (207/206)	—	Bream, 2003; Hatcher et al., 2004

only documented occurrence of Mesoproterozoic crust in the Cartoogechaye terrane, although several bodies of augen and granitic gneiss occur in the Dellwood quadrangle, north of the map (Hadley and Goldsmith, 1963).

Cowrock terrane

Below and to the southwest of the Cartoogechaye terrane, the Hayesville-Soque River thrust sheet contains metasandstones and pelitic schists of the Cowrock terrane. The Cowrock terrane consists of the Coweeta Group, several mafic-ultramafic bodies and the ~468 Ma Persimmon Creek gneiss. The Coweeta Group, defined by Hatcher (1979, 1988), consists of metasandstone of the Coleman River Formation overlain by pelitic schist, metasandstones, and minor metaconglomerates of the Ridgepole Mountain Formation. The Coleman River Formation is dominated by metasandstone and interlayered pelitic schist, and locally becomes more arkosic. The Ridgepole Mountain Formation consists of biotite schist and interlayered quartzite and pelitic schist that locally become conglomeratic toward the west (Hatcher, 1979). Mafic and ultramafic rocks occur locally in the southeastern part of the Cowrock terrane (Nelson et al., 1998). The Lake Chatuge mafic-ultramafic complex occurs along the southern part of the Shooting Creek window and around the entire Brasstown Bald window to the south of the map area (Hopson et al., 1989; Nelson et al., 1998). The Lake Chatuge is the largest mafic-ultramafic body in the Cowrock terrane and consists of dunite, metagabbro, amphibolite, and lesser chlorite-talc schist (Hartley, 1973; Hopson et al., 1989; Hopson, 1994; Nelson et al., 1998; Thomas, 2001; Swanson et al., 2005).

Persimmon Creek Gneiss is the only large felsic plutonic unit in the Cowrock terrane. It occurs in the lower part of the Coleman River Formation and is lithologically diverse, consisting of granodiorite, tonalite, and hornblende gabbro (Hatcher, 1979; McDowell et al., 2002). Strongly foliated, coarse-grained, biotite tonalite gneiss is the most abundant lithology and contains biotite, oligoclase, quartz and minor amounts of muscovite, epidote/clinozoisite, chlorite, and garnet (Hatcher, 1979). Interlayering of the Coleman River Formation with the Persimmon Creek Gneiss led Hatcher (1979) to suggest a volcanic origin; however, Hopson (1994) recognized Coleman River Formation xenoliths in the gneiss and argued for a plutonic origin. McDowell et al. (2002) reported a SHRIMP U-Pb zircon age of ~468 Ma and several inherited cores varying in age from ~1.4 Ga, and 1.15–1.09 Ga (Table 2–5). The magmatic age of the Persimmon Creek Gneiss was reproduced using TIMS by B. V. Miller et al. (2006).

Dahlonega gold belt

In the footwall of the Soque River and the Chattahoochee faults is the linear antiformal Dahlonega gold belt (Figs. 2–2 and 2–3). In southwestern North Carolina, the Dahlonega gold belt plunges under a remnant of the Hayesville-Chunky Gal Mountain-Shope Fork fault and reemerges to the northeast in the Great Balsam Mountains window (A. Merschat et al., 2006; C. E. Merschat et al., 2006; Merschat and Hatcher, 2007). The Dahlonega gold belt is a metasedimentary terrane with several mafic-ultramafic complexes, and associated felsic gneisses (trondhjemitic–dacitic) (German, 1985; Thomas, 2001; Settles, 2002; Hatcher et al., 2005). The stratigraphic nomenclature of this terrane is more complicated than indicated in Table 2–3, likely the result of facies changes from the northeastern (this study) to southwestern end of the Dahlonega gold belt (see also discussion in Hopson et al., 1989). The northeastern end of the Dahlonega gold belt is lithologically less diverse, lacking mafic-ultramafic complexes, massive sulfides, banded-iron formations, and more arkosic lithologies recognized at the southwestern end. This study recognizes the Otto Formation (Hatcher, 1988), which is composed of two-mica, two-feldspar metasandstone and interlayered aluminous schist. Although Hatcher (1988) did not separate metasandstone and aluminous schist members, several subsequent studies have split out these members. Davidson (1995) described the garnet-quartz-feldspar Cullowhee gneiss in the Sylva South and parts of the Greens Creek quadrangle, which is correlative with the metasandstone member of the Otto Formation. In this same area, the Cullowhee gneiss contains several exposures of block-in-matrix structures characterized by amphibolite and garnet amphibolite in a quartzo-feldspathic matrix (e.g.,

Table 2–5. Compilation of recent U-Pb zircon ages of Paleozoic plutons in the western North Carolina and northeastern Georgia Blue Ridge.

Pluton	Country rock	Method	Age (Ma)	Inheritance	Comments	Ref.
Cartoogechaye						
Trondhj. dike (NC)	Mig. biotite gn.	SHRIMP	444±25	abun., 1.25-0.9 Ga	lower intercept	12
Cowrock						
Persimmon Creek Gneiss (NC-GA)	Coleman River/Ridgepole Fm.	SHRIMP	468±3	Common, 1.15-1.09 Ga; two 1.4 Ga cores		4
Persimmon Creek Gneiss (NC-GA)	Coleman River/Ridgepole Fm.	ID-TIMS	458±2	common	upper intercept	7
Dahlonega gold belt						
Cane Creek gneiss (GA)	Otto Fm.	SHRIMP	482±4	common		1, 8
Lake Burton felsic metatuff (GA)	Otto Fm.	SHRIMP	468±6	common 1.3-0.975 Ga & 1.3-1.2 Ga		10
Barlow gneiss (GA)	Otto Fm.	SHRIMP	466±6	None		10
Galts Ferry gneiss (GA)	Otto Fm.	SHRIMP	463±3	None		10
Villa Rica gneiss (GA)	Otto Fm.	SHRIMP	458±3	None		10
Trondhj. dike (NC)	Otto Fm.	SHRIMP	451±26	abun., 1.25-0.9 Ga	lower intercept	12
Trondhj. dike (NC)	Otto Fm.	SHRIMP	402±4	abun., 1.2-1.0 Ga		2
Tugaloo						
Whiteside Trondhj–granodi (NC)	Tallulah Falls/Ashe Fm.	SHRIMP	466±10	Common, 1.28-1.2 Ga; one 2.6 Ga		5, 6
Spruce Pine Pegmatite (NC)	Tallulah Falls/Ashe Fm.	SHRIMP	392±2	None		2
Pink Beds trondhjemite (NC)	Tallulah Falls/Ashe Fm.	SHRIMP	388±5	abun., 1.25-1.0 Ga, single cores of 720, 650, & 460 Ma		6
Pink Beds trondhjemite (NC)	Tallulah Falls/Ashe Fm.	SHRIMP	371±4			11
Looking Glass granodiorite (NC)	Tallulah Falls/Ashe Fm.	SHRIMP	380±3	abun., 1.2-1.0 Ga with one 1.42 Ga and 2 discordant 2.85 Ga.	3.2 Ga upper intercept of discord. core	6
Looking Glass granodiorite (NC)	Tallulah Falls/Ashe Fm.	SHRIMP	337+11/-23			11
Chalk Mountian granodiorite (NC)	Tallulah Falls/Ashe Fm.	ID-TIMS	378±3		Discordant, upper intercept. high U concen. Zr had accicular radiating form	7
Spruce Pine Pegmatite (NC)	Tallulah Falls/Ashe Fm.	SHRIMP	361±2	None	Zr had accicular fan-like form	2
Stone Mountain granodiorite (NC)	Tallulah Falls/Ashe Fm.	SHRIMP	353±6	abun. 1.2-0.9 Ga		2
Stone Mountain granodiorite (NC)	Tallulah Falls/Ashe Fm.	ID-TIMS	337±1		Discordant, upper intercept. 334±2 Ma U-Pb monazite	7
Mount Airy granodiotrite (NC)	Tallulah Falls/Ashe Fm.	SHRIMP	352±6			2*
Mount Airy granodiotrite (NC)	Tallulah Falls/Ashe Fm.	ID-TIMS	332±30	common	Discordant, lower intercept. 334±3 Ma U-Pb monazite	7
Yonah Mountain tonalite (GA)	Tallulah Falls/Ashe Fm.	SHRIMP	346±17	abun. 1.5-0.9 Ga, five core between 760-571 Ma		2
Round Mountain Granite (NC)	Tallulah Falls/Ashe Fm.	SHRIMP	343±2			10
Rabun Granodiorite	Tallulah Falls/Ashe Fm.	SHRIMP	374±4	abun. 1.2-1.0 Ga; one 1.41 Ga & two 2.7-2.6	15-20% Zr are acicular and lack core	5, 6
porphyritic (NC)	Tallulah Falls/Ashe Fm.	SHRIMP	340±12	1.2-1.0 Ga, and 950 Ma		9
porphyritic (NC)	Tallulah Falls/Ashe Fm.	ID-TIMS	335±3	common	334±1 Ma, U-Pb monazite	7
equigranular (NC)	Tallulah Falls/Ashe Fm.	SHRIMP	336±2	abun. 1.1-1.0 Ga; 1.35-1.3 Ga, single analysis ~450 Ma		9
Walnut Creek granodiorite (NC)	Tallulah Falls/Ashe Fm.	SHRIMP	336±2	abun. 1.2-1.0 Ga, and single 1.42 Ga		9
Walnut Creek granodiorite (NC)	Tallulah Falls/Ashe Fm.	SHRIMP	324±14	1.1-1.0 Ga, 1.44 Ga, 440-430 Ma		9
Talladega belt						
Hillabee metadacite (AL)	overlies Talladega Group	SHRIMP	470±4			3, 10
Mas Hill						
Trondhj. dike (NC)	Mig. biotite-hornblende gn.	SHRIMP	417±9	abun., 1.15-1.0 Ga		6

References. 1–Bream, 2003; 2–Mapes, 2002. 3–McClellan et al., 2007. 4–McDowell et al., 2002. 5–Miller et al., 1998. 6–C. F. Miller et al., 2000. 7–Miller et al., 2006. 8–Settles, 2002. 9–Stahr, 2007. 10–Thomas, 2001. 11–Varnell et al., 2008. 12–Part I. * Sinha personal communication in Mapes (2002).

Catamount Gap, Savannah Church–Tathum Creek) (Raymond et al., 1989; Cyphers, 2009). Minor rock types recognized in the northern extent of the Dahlonega gold belt include calc-silicate and muscovite quartzite (Acker and Hatcher, unpublished mapping).

Several mafic and mafic-ultramafic complexes occur throughout the Dahlonega gold belt, but few occur in the northern part of the belt. Associated with many of the complexes are low-potassium trondhjemitic/dacitic felsic gneisses that range from 482–458 Ma (Table 2–5) (Thomas, 2001; Settles, 2002; Bream, 2003). The Lake Burton mafic-ultramafic complex consists of amphibolite, metagabbro–amphibolite, and ultramafic rocks, and a ~100 m thick possible felsic tuff unit, but only amphibolite and metagabbro extend into the Hightower Bald 7.5–minute quadrangle in the southwestern part of the map (Hopson et al., 1989; Hopson, 1994; Thomas, 2001). Mafic and ultramafic rocks are sparse in the northeasternmost end of the Dahlonega gold belt and Great Balsam Mountains window. Cyphers (2009) mapped several small pods of altered ultramafic rocks in the Great Balsam Mountains window in the Tuckasegee quadrangle. Raymond et al., (1989) and Cyphers (2009) described amphibolite blocks in a metasandstone matrix at Tatum's Creek/Savannah Church exposure. No felsic gneisses similar to the Cane Creek or Villa Rica gneiss have been observed, although Eckert (unpublished mapping) recongnized an altered and deformed felsic gneiss in the Corbin Knob quadrangle as a possible Mesoproterozoic basement unit.

Tugaloo terrane

The structurally highest thrust sheet is the Chattahoochee-Holland Mountain thrust sheet, which juxtaposes the middle to upper amphibolite facies Tugaloo terrane against Dahlonega gold belt and Cartoogechaye terranes (Figs. 2–2 and 2–3). Northeast of the map, the Tugaloo terrane overrides ~1.8 Ga gneisses of the Mars Hill terrane and other external basement massifs of the western Blue Ridge (Fig. 2–1). The Tugaloo terrane was proposed by Hatcher (2002) and subdivided the Piedmont terrane of Williams and Hatcher (1983). The Tugaloo terrane includes both the eastern Blue Ridge and parts of the Inner Piedmont (Fig. 2–1). It is composed of psammitic and pelitic rocks of the Ashe-Tallulah Falls Formation, inliers of Mesoproterozoic basement, mafic and ultramafic rocks, and Ordovician, Devonian, and Mississippian granitoids.

The Tallulah Falls Formation consists of a lower metagraywacke-amphibolite member, aluminous schist-amphibolite member, and upper metagraywacke-schist member (Hatcher, 1971, 1978a, 1993). A conglomeratic, muscovite quartzite occurs in the core of the Tallulah Falls dome and was originally mapped as the highest unit in

the Tallulah Falls Formation (Hatcher, 1971; Hopson et al., 1989), but has since been separated (e.g., Hatcher et al., 2004). The lower metagraywacke-amphibolite member generally contains more outcrop- to map-scale pods, layers, and lenses of amphibolite and dunite than the upper member. Amphibolite and ultramafic rocks, however have also been mapped in the upper member, along with calc-silicate and magnetite-bearding, chlorite, muscovite schist (Plates 1, 3). In southwestern North Carolina and northeastern Georgia, small mappable pods of calc-silicate (clinopyroxene, plagioclase, quartz) occur in the upper member often in close proximity to Mississippian plutons (Stahr, 2007; Cyphers, 2009; Acker and Hatcher, unpublished mapping). In the Sam Knob 7.5-minute quadrangle a magnetite-bearing, chlorite-muscovite schist unit with minor interlayers of fine- to medium-grained quartz-feldspar gneiss was recognized in the upper member. A thin, ~0.2–1m thick, sulfidic, quartz, tourmaline schist occurs along the boundary with the metagraywacke.

Mesoproterozoic basement rocks. Mesoproterozoic basement rocks occur in the core of the Toxaway dome and several small massifs on the flanks of the Tallulah Falls dome (Fig. 2–1). The Toxaway Gneiss cores the Toxaway dome, and consists dominantly of layered biotite granitic gneiss and lesser augen gneiss (Hatcher, 1977; Merschat et al., 2003; Hatcher et al., 2004). Carrigan et al. (2003) reported SHRIMP U-Pb ages of ~1.15 Ga for three samples of layered Toxaway Gneiss (Table 2–4). Several Mesoproterozoic basement units are mapped around the flanks of the Tallulah Falls dome, including the Sutton Creek, Wolf Creek, and Wiley gneisses. The basement gneisses surrounding the Tallulah Falls dome also yields ~1.15 Ga (Table 2–5; Carrigan et al., 2003).

Mafic and Ultramafic rocks. Although mafic and ultramafic rocks volumetrically represent a minor component, they are common in the Tugaloo terrane. Common mafic rocks include amphibolite, metagabbro, and hornblende gneiss and schist. In the eastern Blue Ridge the largest mafic body is in northwestern North Carolina, both north and south of the Grandfather Mountain window (Abbott and Greenwood, 2001). Mafic bodies recognized in the map are mostly small pod to lens-shaped bodies, except for several continuous bodies mapped in the vicinity of the Whiteside pluton and Toxaway dome (Stahr, 2007; Varnell in progress). Ultramafic rocks consist of metadunite, metapyroxenite, and talc and serpentine schists. These bodies are small, < 1 km^2, uncommon, and may have only one or several mafic-ultramafic rock types associated with it, including amphibolite (Pratt and Lewis, 1905; Swanson et al., 2005). A few

mafic-ultramafic complexes, e.g., Laurel Creek, have been mapped in the Tugaloo terrane (Petty, 1982; Hatcher et al., 1984).

Paleozoic Plutons. Several Paleozoic granitoid plutons occur in the eastern Blue Ridge Tugaloo terrane of southwestern North Carolina and northeastern Georgia. These plutons vary in size from 120–20 km^2 and occur in a relatively limited area with Ordovician and Mississippian plutons in close proximity (a few kilometers or less). Compositionally all are peraluminous, low-potassium granodiorites to trondhjemites, but size, textures, and age vary. The Whiteside Granite was initially defined by Keith (1907), and included all of the other Paleozoic granodioritic to trondhjemitic plutons in southwestern North Carolina and northeastern Georgia. Hadley and Nelson (1971) and Hatcher (1977) refined the name to include only the granitoid intrusion and several surrounding smaller sheets whose main body was located near Highlands, North Carolina, just south of the map area. The ~466 Ma Whiteside pluton (Table 2–5) occupies an area of ~ 100 km^2 and consists of fine- to medium-grained, weak to strongly foliated, locally layered muscovite, biotite granodiorite to trondhjemite gneiss (the latter is more abundant [Miller et al., 1997; Stahr, 2007]). The Looking Glass gneiss, named by Acker (1982), is a coarse-grained, weakly to well-foliated, porphyritic granodiorite to trondhjemite (Acker, 1982; Miller et al., 1997). Acker (1982) noted a subhorizontal mineral lineation defined by biotite and muscovite was common in the Looking Glass. Mississippian plutons include the porphyritic and equigranular Rabun granodiorite, Walnut Creek trondhjemite, Round Mountain granodiorite-trondhjemite, and Pink Beds trondhjemite and range from 343–324 Ma (Table 2–4). The Tuckasegee pluton mapped by Cyphers (2009) has not been dated, but is included as a Mississippian pluton because of close proximity and textural similarity to the Rabun and Walnut Creek plutons.

PROVENANCE

The occurrences of mafic and ultramafic rocks and minor basement massifs in the terranes east of the Hayesville fault indicate these terranes were deposited on oceanic crust and minor fragments of continental crust (Hatcher, 1978a; Abbott and Raymond, 1984; Hatcher et al., 2004, 2007). However, the paleogeographic location of these terranes was only loosely delimited permitting significant variations in tectonic models regarding the heredity of these terranes (e.g., Rankin, 1975; Williams and Hatcher, 1983). Detrital zircon studies provide significant information regarding the provenance of the different terranes of the Georgia-North Carolina-South Carolina-Tennessee Blue Ridge

(Bream, 2003; Bream et al., 2004; Merschat et al., in review, Part IV). Twenty-two paragneiss samples from the different Blue Ridge terranes have been examined, including seven samples from lithotectonic units in the map area (Table 2–6). All samples contain abundant Mesoproterozoic zircons with the largest populations of 1.2–1.0 Ga, and lesser 1.5–1.3 Ga zircons. Minor populations include Paleoproterozoic 1.9–1.6 Ga and Neoproterozoic 0.8–0.7 Ga zircons, often represented by only a few grains analysesed per sample. Minor Archean zircons were identified in from the Georgia Dahlonega gold belt, Cowrock terrane (Bream et al., 2004), and the Mineral Bluff formation (Merschat et al., in review; Part V). A Laurentian provenance is preferred for all terranes based on the occurrence of 1.5–1.0 Ga with 0.7 Ga zircons in all terranes. Likely Laurentian sources include 1.3–1.0 Ga Grenvillian basement, 1.5–1.3 Ga granite-rhyolite province of the Laurentian Mid-continent, and 750–700 Ma Crossnore and Robertson River igneous suites in the western Blue Ridge. Possible sources of Paleoproterozoic zircons include the Mars Hill terrane in the western North Carolina Blue Ridge, or far-traveled zircons from either the Laurentian mid-continent or shed from Amazonia during the rifting of Rodinia and the opening of the Iapetus ocean.

Laurentian detrital zircon suites from the central and eastern Blue Ridge terranes confirm that these terranes are peri-Laurentian (Bream, 2003; Bream et al., 2004; Merschat et al., in review; Part IV). Late Neoproterozoic (750–700 Ma) detrital zircons found in all of the terranes suggest a maximum age, but the 570–560 Ma opening of the Iapetus ocean (Aleinikoff et al., 1995; Brewer and Thomas, 2000) suggests the terranes are latest Neoproterozoic to Early Cambrian. Ordovician metamorphism and magmatism, discussed below, brackets the upper age of the terranes. Similar to previous models (e.g., Hatcher et al., 2004), we conclude that the Cartoogechaye, Cowrock, Dahlonega gold belt and Tugaloo terranes were deposited during the latest Neoproterozoic to Early Ordovician, in parts of the Iapetus ocean proximal to Laurentia that were floored by oceanic crust and small continental basement fragments.

MAGMATISM

SHRIMP U-Pb ages obtained in the past 15 years have significantly improved our understanding of Paleozoic felsic igneous activity in the Blue Ridge. Previous isotopic studies yielded imprecise ages, causing some igneous units to be assigned an incorrect age. These problems were largely the result of complicated xenocrystic zircons and the tectonothermal history of the Blue Ridge. Complex zircons with inherited cores, magmatic interiors and metamorphic rims can now be deciphered with a combined

Table 2–6. Compiled ages of detrital zircons from Blue Ridge terranes. Ages are rounded to 0.1 Ga.

Terrane	Sample	Location	Ages (Ga)	Source
Laurentian Margin/ western Blue Ridge	Mineral Bluff Fm. metass & phylite (NC)	35.0953° N 84.0176°W	0.85, 1.0, 1.1, 1.3, 1.4, 1.5, 1.6, 1.7, 1.8, 1.9, 2.1, & 2.7	Part IV
	Walden Creek Grp. Sandsuck Fm. cgl. (TN)	35.548°N 84.050°W	1.1 ,1.2, 1.3,& 1.4	Bream et al., 2004
	Walden Creek Grp. Sandsuck Fm. ss. (TN)	35.248°N 84.444°W	1.1, 1.2, 1.3, & 1.4	Bream et al., 2004
	Great Smoky Grp. Deam Fm. ss (TN)	35.336°N 84.296°W	1.1, 1.2, 1.3, & 1.4	Bream et al., 2004
	Snowbird Grp. Longarm Quartzite (NC)	35.702°N 83.040°W	1.1, 1.2, 1.3, 1.4 7 1.5	Bream et al., 2004
Cowrock	Coleman River Fm. (NC)	34.908°N 83.612°W	1.1, 1.2, 1.3, 1.4, 1.6, & 2.7	Bream et al., 2004
	Coweeta Group, Chunky Gal Mountain (NC)	35.0588°N 83.6203°W	0.7, 0.9, 1.0. 1.1, 1.2, & 1.3	Part IV
Cartoogechaye	DEL1 Caldwell Gap (NC)	35.58122°N 82.98646°W	0.7, 0.8, 0.9, 1.0. 1.1, 1.2, 1.3, 1.6, & 1.8	Part IV
	Earlies Gap biotite gneiss (NC)	—	0.6, 1.0. 1.1, 1.2, 1.3, 1.4, 1.6, 1.8, 1.9, & 2.3	Part IV
	Rainbow Springs quartzite (NC)	35.0111°N 83.6189°W	0.8, 1.0. 1.1, 1.2, 1.3, 1.4, 1.6, 1.8, & 2.3	Part IV
	Winding Stair Gap (NC)	35.1224°N 83.5435°W	0.8, 1.0, 1.2	Miller et al., 1998
	Wolfpen migmatite (NC)	35.4709°N 82.8850°W	0.95, 1.1, 1.2, 1.7, & 1.8	Part IV
Dahlonega Gold Belt	Otto Fm. (GA)	34.560°N 84.074°W	1.1, 1.2, 1.3, 1.4, & 2.7	Bream et al., 2004
	Otto Fm. (GA)	34.533°N 84.018°W	1.1, 1.2, 1.3, 1.4, 1.8, 1.9, 2.0, 2.1, & 2.9	Bream et al., 2004
	Otto Fm. (NC)	35.060°N 83.453°W	1.1, 1.2, 1.3, 1.4, 1.5, & 1.6	Bream et al., 2004
	Otto Fm. (NC)	35.4308°N 83.093°W	1.0, 1.1, 1.2, & 1.3	Part IV
Tugaloo	Tallulah Falls quartzite (GA)	34.817°N 83.424°W	1.1, 1.2, & 1.3	Bream et al., 2004
	Tallulah Falls quartzite (GA)	34.736°N 83.391°W	1.1, 1.2, & 1.3	Bream et al., 2004
	Tallulah Falls mgw (GA)	34.838°N 83.422°W	1.1, 1.2, & 1.3	Bream et al., 2004
	Tallulah Falls mgw (NC)	35.454°N 82.661°W	1.1, 1.2, & 1.3	Bream et al., 2004
	Tallulah Falls mgw (NC)	35.600°N 82.538°W	1.1, 1.2, & 1.3	Bream et al., 2004
	Biotite schist xenolith in Wiley Gneiss (GA)	35.600°N 82.538°W	1.1, 1.2,1.3 & 1.5	Part IV

method of optical and CL imaging, and *in situ* spot analysis using the SHRIMP. Paleozoic magmatism in the Blue Ridge occurred during the Middle Ordovician, Devonian, and Mississippian. These studies have also documented one of the main culprits that produced imprecise dates early geochronologic dates: inherited cores. This sections discusses the recent SHRIMP U-Pb zircon ages of different felsic igneous units of the central and eastern Blue Ridge of southwestern North Carolina and northeastern Georgia.

Ordovician

Ordovician felsic igneous activity in the central and eastern Blue Ridge has been documented in the Cowrock, Dahlonega gold belt, and Tugaloo terranes, and spans a range of 483–458 Ma (Table 2–5). These granitoids are penetratively deformed and characterized by generally low-potassium, granodioritic, tonalitic, and trondhjemitic compositions (Miller et al., 1997; Thomas, 2001). Intrusive versus extrusive settings have been suggesed for several of the Ordovician granitoids (e.g., Hatcher, 1979; Hopson et al., 1989; Hopson, 1994; Thomas, 2001), but a definitive answer is obscured by the penetrative deformation present in the granitoids and surrounding rocks. Mafic rocks are closely associated with several Ordovician felsic plutons, but may not be genetically related.

South of the map area, the Dahlonega gold belt contains several low-potassium, trondhjemitic/dactic felsic gneisses commonly associated with mafic and mafic-ultramafic complexes. SHRIMP U-Pb zircon ages have been obtained for the ~463 Ma Galts Ferry and ~458 Ma Villa Rica felsic gneisses (Thomas, 2001), ~466 Ma Barlow (Thomas, 2001) and ~482 Ma Cane Creek (Settles, 2002; Bream, 2003) felsic gneisses of the Sally Free mafic complex, and ~468 Ma felsic metatuff(?) from the Lake Burton mafic-ultramafic complex (Thomas, 2001) (Table 2–5). Many workers have concluded that the felsic and mafic rocks of the Dahlonega gold belt are extrusive (McConnell and Abrams, 1984; Hopson, 1994; Thomas, 2001; Settles, 2002). North of the Lake Burton complex, south of the Georgia-North Carolina border, however, no major mafic complexes or felsic gneisses occur in the Dahlonega gold belt (Fig. 2–2, Plate 3; Hatcher, 1988; Cyphers, 2009; Eckert, unpublished mapping).

The only large felsic plutonic unit in the Cowrock terrane is the Persimmon Creek Gneiss, which yielded a SHRIMP U-Pb age of ~468 Ma and several inherited cores varying in age from ~1.4 Ga, and 1.15–1.09 Ga (Table 2–5; McDowell et al., 2002). The magmatic age of the Persimmon Creek Gneiss was reproduced using ID-TIMS

by Miller et al. (2006). Although dominantly tonalitic, the composition varies from gabbro to granodiorite and displays trace element concentrations unique from the other Ordovician plutons (McDowell et al., 2002). McDowell et al. (2002) concluded that the geochemistry, mineral assemblages, textures, and field relationships of Persimmon Creek Gneiss are consistent with a subduction-related, deep-seated pluton of a short-lived arc.

Several Ordovician granitoids occur throughout the Tugaloo terrane (e.g., Drummond et al., 1997; Bream, 2003; Steltenpohl, 2005), but the ~466 Ma Whiteside pluton is the only Ordovician pluton in the Tugaloo terrane in southwestern North Carolina and northeastern Georgia Blue Ridge. C. F. Miller et al. (1998, 2000) reported a SHRIMP U-Pb zircon age of 466±10 Ma, with inherited cores of 1.28–1.2 Ga and 2.6 Ga (Table 2–4). The Whiteside varies from granodiorite to torondhjemite, is low in potassium, incompatible, and high-field strength trace elements, but rich in Al, Na, and Sr (Miller et al,, 1997). The Whiteside formed in a primitive island arc to continental arc setting and requires a relatively mafic source (Miller et al., 1997).

Devonian

Several plutons that were previously thought to have Devonian ages were recently re-examined and determined to be Mississippian (Miller et al., 2006; Stahr, 2007; Varnell et al., 2008). The ~371 Ma Pink Beds trondhjemite is only remaining Devonian pluton in southwestern North Carolina and northeastern Georgia (Table 2–5; Varnell et al., 2008). It is the smallest pluton, ~20 km^2, and is compositionally and texturally uniform. Coarse-grained, weakly foliated to massive, porphyritic muscovite, biotite trondhjemite is characteristic of the Pink Beds pluton (Acker, 1982; Miller et al., 1997). Acker (1982) described anhedral microcline and plagioclase-microcline aggregate phenocrysts ~1–2 cm long in a biotite-quartz-plagioclase matrix from the Pink Beds. Inherited cores were observed and yielded ages of 1.25–1.0 Ga and single grain analyses of 720, 650, and 460 Ma (Table 2–5; C. F. Miller et al., 2000). Other Devonian plutons and granitoid intrusions in the Tugaloo terrane occur north of the map area and include the ~392, 377, and ~361 Ma Spruce Pine pegmatites (Mapes, 2002; Miller et al., 2006), and ~377 Ma Chalk Mountain granodiorite (B. V. Miller et al., 2006).

Mississippian

Like the Ordovician and Devonian plutons, the Mississippian plutons are low-potassium, peraluminous granodiorites to trondhjemites, including the largest pluton, the ~336 Ma Rabun granodiorite (Miller et al., 2006; Stahr, 2007). Other plutons included

in this group are the ~346 Ma Yonah Mountain tonalite (Mapes, 2002), ~ 342 Ma Round Mountain trondhjemite, ~337 Ma Looking Glass granodiorite (Varnell et al., 2008), and ~333 Ma Walnut Creek granodiorite (Stahr, 2007) (Table 2–5). Unlike the Ordovician granitoids, these plutons are not as penetratively deformed, not genetically associated with mafic rocks, and are clearly intrusive plutonic rocks. Chemically, all of the Mississippian plutons are similar and require a mixed source of both depleted mafic rocks and felsic igneous and/or sedimentary rocks (Miller et al., 1997; Stahr, 2007; Cyphers, 2009).

We propose the informal name Pisgah plutonic suite to describe the texturally, compositionally, and chemically similar peraluminous granodiorites to trondhjemites in the Tugaloo terrane. The Pisgah plutonic suite includes the Looking Glass, Rabun, Round Mountain, Tuckasegee and Walnut Creek plutons. Use of the Spruce Pine plutonic suite (e.g., McSween et al., 1991) should be restricted to the Devonian granodiorites and pegmatites of the Spruce Pine area. The Pink Beds pluton remains difficult to assign, and chronologically belongs with the Spruce Pine plutonic suite, but spatially is associated with the Pisgah plutonic suite. Additional geochronologic studies may further refine its age or delimit the relationship between the Devonian and Mississippian plutonism in the Tugaloo terrane/eastern Blue Ridge of North Carolina.

METAMORPHISM

Metamorphic grade in the Blue Ridge increases from anchizone to granulite facies, with a significant portion consisting of amphibolite and higher facies metamorphism (Hadley and Goldsmith, 1963; Force, 1976; Eckert et al., 1989; Butler, 1991; Hatcher and Goldberg, 1991). The area encompassed in this study includes the Wayah granulite core of the Blue Ridge, (Force, 1976; Hatcher and Butler, 1979; Absher and McSween, 1985; Eckert et al., 1989), and surrounding areas of upper to middle amphibolite facies metamorphism. In addition to the effects of regional metamorphism, recent studies have recognized contact metamorphism associated with the various granodioritic to trondhjemitic plutons in this area (Stahr, 2007).

Metamorphic grade varies from kyanite-staurolite to hypersthene granulite facies, and is interpreted to be the result of multiple Barrovian-type metamorphic events. Several isograds, including the kyanite, sillimanite I and II, and hypersthene-in are recognized and trend northeast-southwest parallel to the regional structural grain. The majority of the area is sillimanite or higher, but kyanite and staurolite-kyanite zone rocks occur to the northwest, in the Dahlonega gold belt, and the southeastern part of the

Tugaloo terrane. Northwest of the Hayesville fault to the core of the central Blue Ridge, a continuous gradient from kyanite to hypersthene granulite zone was recognized by Eckert et al. (1989), but elsewhere the isograds are folded or truncated by faults juxtaposing rocks of different grade (Fig. 2–5). The Wayah granulite core occurs near the center of the map area and defines a northeast-trending axis that links with sillimanite II zone rocks in the Great Balsam Mountains window (Fig. 2–5). Most of the rocks are migmatitic, except for staurolite-kyanite rocks of the Dahlonega gold belt.

Polymetamorphism in the middle to upper amphibolite facies terranes of the Blue Ridge has been documented by several workers based on textural relationships (Quinn, 1991; Davidson, 1995; Cameron, 2001; Massey and Moecher, 2005; Stahr, 2007), and geochronologic evidence (Kish, 1991; Connelly and Dallmeyer, 1993; Moecher et al., 2005; Part III). Blue Ridge terranes the show evidence of a prograde Barrovian series metamorphism, overprinted by at least one subsequent Barrovian series metamorphic event and the local affects of contact metamorphism (Davidson, 1995; Massey and Moecher, 2005; Moecher et al., 2005; Stahr, 2007).

The effects of contact metamorphism superposed on the regional metamorphism has been recognized by Miller et al. (1997) and Stahr (2007). Miller et al. (1997) noted the lack of chilled margins or distinct contact aureoles around the majority of plutons to indicate that the plutons were emplaced while the terrane was still hot. Migmatitic zones border the larger bodies of the Whiteside plutons and occur locally around the Rabun and Walnut Creek plutons (Miller et al., 1997; Stahr, 2007; Acker and Hatcher, unpublished mapping). Within 1 km from the margins of the ~466 Ma Whiteside pluton the Tallulah Falls Formation is substantially more migmatitic (Miller et al., 1997; Burton, 2007; Stahr, 2007). Acker and Hatcher (unpublished mapping) noted that the Tallulah Falls Formation was more migmatitic near the northwestern margin of the Rabun granodiorite pluton near its southeastern termination in the Dillard, Georgia 7.5-minute quadrangle. Near the northeastern termination of Rabun pluton, Stahr (2007) documented a migmatite zone sandwiched between the Rabun and Walnut Creek plutons, and the breakdown of staurolite and growth of sillimanite proximal to the plutons. Similar amphibolite facies assemblages and textures in contact aureoles surrounding both Ordovician and Mississippian plutons indicate that the Tugaloo terrane, and perhaps most the Blue Ridge, remained hot for over ~130 m.y.

The polymetamorphic history of the Blue Ridge has complicated efforts to delimit timing of peak metamorphism. Various K-Ar and Ar-Ar mineral and whole rock ages indicate a protracted metamorphic event that ranges from the early to middle

Figure 2–5. Compiled metamorphic isograd map of the part of the western, central, and eastern Blue Ridge of southwestern North Carolina and northeastern Georgia. Fault abbreviations and plutons are the same as Fig. 2–2.

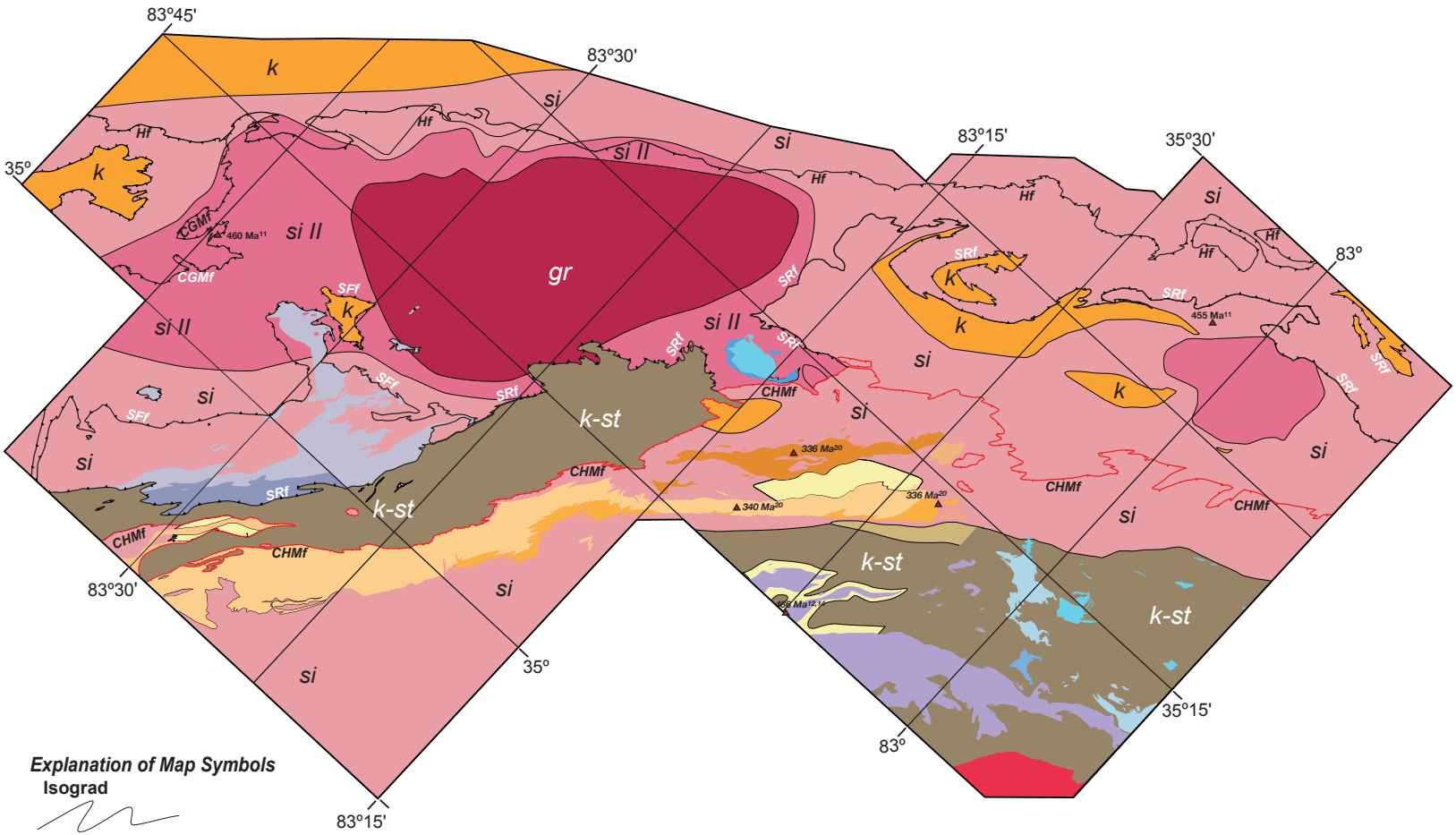

Explanation of Map Symbols

Isograd

Thrust fault

Teeth located on upper plate.

Taconic pre- to synmetamorphic fault.

Alleghanian syn- to postmetamorphic Chattahoochee-Holland Mountain fault.

	Contact aureole	*si*	Sillimanite
k-st	Kyanite + Staurolite	*si II*	Sillimanite II
k	Kyanite	*gr*	Granulite

CONTOUR INTERVAL 50 METERS

Projection Universal Transverse Mercator, zone 17

0 10 20

Kilometers

0 10

Miles

Paleozoic (Kish, 1991; Dallmeyer, 1988; Connelly and Dallmeyer, 1993; Burton and Kunk, 2006). Recent U-Pb geochronologic studies have refined both the relative and absolute ages of metamorphism in the Blue Ridge.

Relative ages of metamorphism and deformation are delimited by U-Pb ages of the various felsic igneous rocks of the Blue Ridge, although complex relationships exist. Deformed and undeformed crosscutting igneous bodies can be used to bracket the age of metamorphism and deformation. Unfortunately, Ordovician, Devonian, and Mississippian plutons are deformed, and paraconformable with the regional structural grain. Metamorphic fabrics observed in Mississippian plutons, like the Rabun and Walnut Creek (e.g., Stahr, 2007), suggest metamorphism may be younger than ~335 Ma. The numerous weakly deformed trondhjemite dikes that occur throughout the central Blue Ridge and into the Tugaloo terrane also truncate regional fabrics. Several U-Pb ages have been obtained for these trondhjemite dikes including: ~407 Ma in the Great Balsam Mountains window, ~444 Ma in the Cartoogechaye terrane, and ~412 Ma in the Mars Hill terrane. Peak metamorphism occurred prior to ~444 Ma intrusion of the oldest crosscutting dike. The syntectonic intrusion of several Ordovician plutons, 470–460 Ma, may correspond to near-peak metamorphic conditions as indicated by U-Pb age of metamorphic zircon rims. After Taconian metamorphism, the rocks remained at depth and were also affected by a Mississippian ~335 Ma or younger event.

Absolute ages of metamorphism including U-Pb ages of zircon and monazite, and monazite chemical ages support a Taconian metamorphic-peak (Table 2–7). SHRIMP U-Pb ages of metamorphic zircon rims from several para- and orthogneisses of the central and eastern Blue Ridge range from 520–365 Ma, and central Blue Ridge terranes yielded mostly Ordovician ages (Table 2–7, Fig. 2–6). The majority of the rims have Th/U ratios near or below 0.1 common of metamorphic rims (Rubatto and Herman, 2007)(Fig. 2–6). Relative probability plots of U-Pb ages of zircon rims display peaks at 465, 455, and 450 Ma (Fig. 2–6). The range of 465–450 Ma agrees well with other published zircon and monazite ages. Zircons separated from the garnet-bearing leucosomes from the granulite facies Shooting Creek schist at Winding Stair Gap yielded U-Pb zircon ages of 458±2 Ma (ID-TIMS) and U-Pb and 460±12 Ma (SHRIMP) (Moecher et al., 2004). No metamorphic zircon ages have been reported from the western Blue Ridge, although several studies have reported both conventional and chemical monazite ages. Corrie and Kohn (2007) reported an ID-TIMS U-Pb monazite age of ~450 Ma from staurolite to kyanite grade Great Smoky Group metasandstone and schist from west of the study area. Moecher et al. (2005) reported chemical monazite ages of ~467 and ~459 Ma from Great

Table 2–7. U-Pb ages of zircon, monazite, and monazite chemical ages from the southwestern North Carolina and northeastern Georgia Blue Ridge.

Terrane	Rock Unit	Lat. & Long.	Age (Ma)	Type	Source
Mars Hill	Bakersville metagabbro (gar.-am.) (NC)	—	~475	SHRIMP Zircon rim	Ownby et al., 2004
Laurentian Margin	Great Smoky Grp. (NC)	35.4525ºN 83.093ºW	459±6	EMP Monazite	Moecher et al., 2004, 2005
	Great Smoky Grp. (NC)	—	467±11	EMP Monazite	Moecher et al., 2005
	Great Smoky Grp. (NC)	(13 samples)	450±5	TIMS Monazite	Corrie and Kohn, 2007
Cowrock	Chunky Gal Mtn, (NC)	35.0588ºN 83.6203ºW	463±6	SHRIMP Zircon rim	Part III
Cartoogechaye	Winding Stair Gap, (NC)	35.1224ºN 83.5435ºW	460±12 458±1.0	SHRIMP Zircon rim	Moecher et al., 2004
	DEL1 Caldwell Gap (NC)	35.58122ºN 82.98646ºW	~442	SHRIMP/TIMS Zircon	Part III
	Rainbow Springs quartzite (NC)	35.0111ºN 83.6189ºW	439±3	SHRIMP Zircon rim	Part III
	Felsic gneiss, RS787 (NC)	35.0953ºN 83.5564ºW	467±3	SHRIMP Zircon rim	Part III
	Willets-Ochre Hill am., P22A (NC)	—	~450	SHRIMP Zircon rim	Berquist, 2005; Berquist et al., 2005
Dahlonega gold belt	Otto Fm. (NC)	35º 25.85' N 83º 05.58'W	455±12	SHRIMP Zircon rim	Part III
Tugaloo	Beaucatcher Mountain, I-40 roadcut (NC)	35.5997ºN 82.5377º W	365±4	SHRIMP Zircon rim	Bream, 2003 Merschat, 2009
	Toxaway Gneiss TOX-1 (SC) TOX-1B (SC)	35º 0026 N 83º 0429 W	~350	SHRIMP Zircon rim	Carrigan et al., 2001, 2003
	Tallulah Falls mig. am. P77D (NC)	—	~450	SHRIMP Zircon rim	Berquist, 2005; Berquist et al., 2005

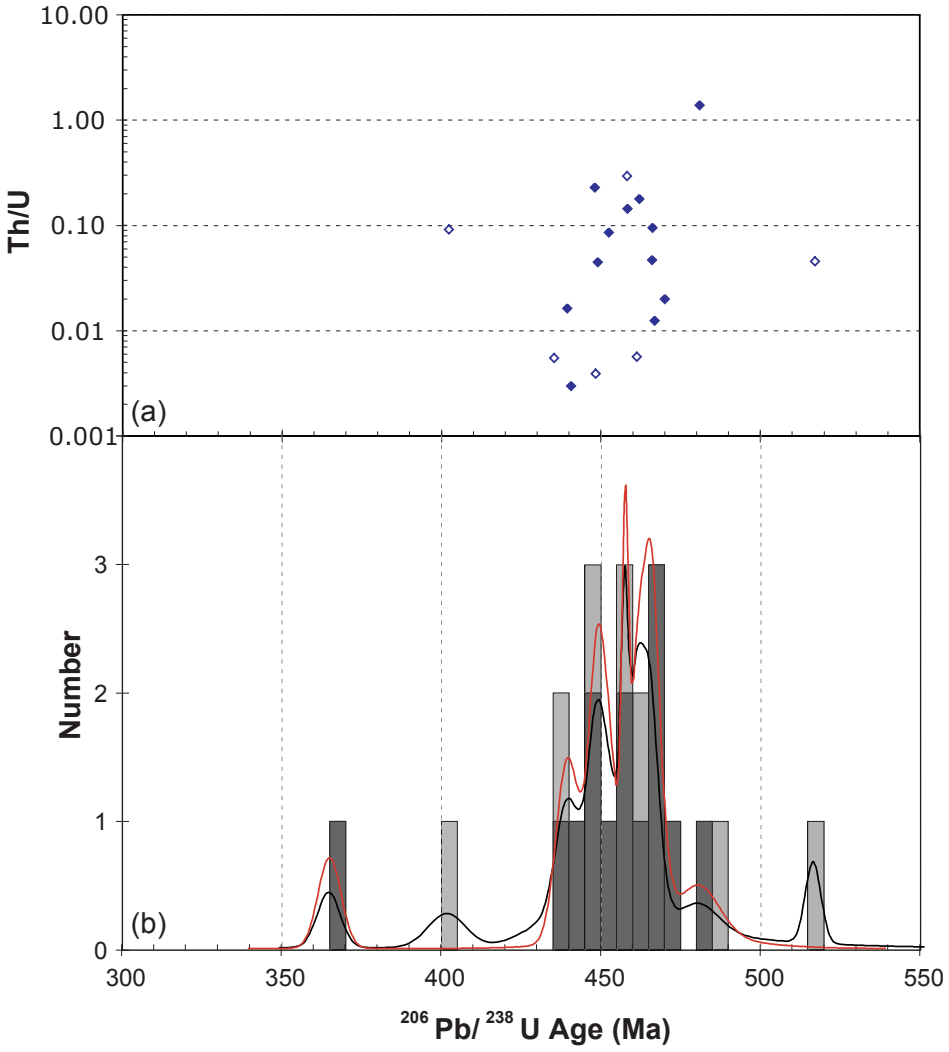

Figure 2–6. U-Pb ages of metamorphic zircon from the southwestern North Carolina and northeastern Georgia Blue Ridge. (a) Th/U ratios of measured metamorphic rims. Open diamonds indicate age is greater than ±10% discordant (b) Relative probability plot and histogram of 206Pb/238U ages of metamorphic zircon including all data (light gray and black line) and only ages that are ±10% discordant (dark gray and red line). Relative probability plot generated using Isoplot v. 3.00 (Ludwig, 2003).

Smoky Group metasandstone and schist from the eastern part of the western Blue Ridge. Overlapping metamorphic zircon and monazite ages from the western and central Blue Ridge further confirms these terranes were metamorphosed during the same 465–450 Ma event, during the Middle Ordovician Taconian orogeny. Zircon ages from the Tugaloo terrane are limited to three analyses (Table 2–7) and suggest a 450 Ma and a 365–350 Ma event. Combined with fabric and field observations regarding the polymetamorphic history of the Tugaloo terrane, it likely experienced two or three regional amphibolite facies metamorphic events at ~450 Ma, 365–350 Ma, and ~335 Ma. Finally, published Ar-Ar and K-Ar ages from the Blue Ridge indicate the terranes did not cool through 500 ºC and 350 ºC until ~330 and ~311 Ma, respectively (Dallmeyer, 1988; Kish, 1991; Connelly and Dallmeyer, 1993; Moecher et al., 2005). Zircon and apatite fission track ages further constrain cooling to ~280 Ma (zircon) and Mesozoic–Cenozoic cooling for apatite (Naeser et al., 2005).

STRUCTURE

Numerous studies have documented the polydeformed history of the Blue Ridge (e.g., Hadley and Goldsmith, 1963; Hatcher and Butler, 1979; Hatcher, 1977; Trupe et al., 2003; Massey and Moecher, 2005; Stahr, 2007). Recent geochronologic studies provide better age constraints of these deformations. Six deformations are recognized that represent major contractional and extensional orogenic events that affected part of the western, central, and eastern Blue Ridge (Table 2–8). Structures are grouped according to age to simplify the various deformations recognized by previous workers, and the variability of structural style with metamorphic grade over a large and complex area. Relative and absolute ages of the deformations are indicated, where possible, along with associated structures, and metamorphic and tectonic events. D_1 and D_2 are correlated with early and late stages of the Middle Ordovician Taconian orogeny, which was the prominent metamorphic and deformational event in southern Appalachian Blue Ridge. Effects of the Late Devonian to early Mississippian Neoacadian, and late Mississippian to Permian Alleghanian orogenies are manifested in a similar manner regarding orientation of structures and metamorphic grade; consequently, many of the D_3 and D_4 structures are difficult to separate. Deformation associated with the Late Alleghanian, D_5, is related to emplacement of the Blue Ridge-Piedmont megathrust sheet, development of map-scale domes, and joints (Hopson et al., 1989; Hatcher and Hooper, 1992). Mesozoic to Cenozoic extension and uplift of the Blue Ridge, here combined as D_6, resulted in local brittle faulting and formation of joints and fracture sets that influence modern topography.

Table 2–8. Summary of major Paleozoic and younger deformational events and related structures and metamorphisms that have affected the Blue Ridge. Modified from Hopson et al. (1989) and Merschat et al. (2005).

EVENTS	STRUCTURES			METAMORPHIC CONDITIONS	REGIONAL EVENTS	OROGENY & TIMING
	Fabrics	Folds	Faults	*Z* | *PP* | *Gs* | *A* | *G*		
D_1	S_1 Early foliation preserved in amphiboolite and calc-silicate boudins	F_1 Intrafolial folds and isoclinal folds preserved in boudins	Greenbrier fault, Hayesville fault (?)	M_1 Moderate to high pressure and temperature	Initial collision of central and eastern BR terranes with western BR	Pre- to early Taconian pre~465 Ma
D_2	S_2 Penetrative foliation L_2 Mineral lineation	F_2 Inclined to recumbent, tight to isoclinal passive and flexural flow folds, and sheath folds;	Shope Fork-Chunky Gal Mountain, Soque River, Chattahoochee-Holland Mountain faults	M_2 Peak metamorphism, greenschist (middle amphibolite in map area) to granulite facies	Continued collision of BR terranes, intrusion of synkinematic plutons (Whiteside, Persimmon Creek)	Taconian 465 – 450 Ma
D_3	S_3 Reactivates S_2 L_3 Mineral and intersection lineations, NE-SW	F_3 Inclined to upright, tight to open folds, trend NE-SW, & E-W	Dextral strike-slip kinematics, Burnsville fault, Chattahoochee fault, NE GA	M_3 Middle amphibolite facies; new growth of muscovite, kyanite, and staurolite	Collision of Carolina superterrane; mobilizes IP and parts of eastern BR as SW-directed orogenic channel flow	Neoacadian 365 – 345 Ma
D_4	S_4 reactivation of S_3, solid-state fabrics in Miss. plutons, S-C fabrics in faults Mineral lineations	F_4 Upright, open folds, trend NW-SE, & NE; crenulations plunge SE & NE	Ductile reactivation of Chattahoochee, BFZ, Dills Falls, and CFAF	Greenschist to middle amphibolite facies (retrogressive)	Intrusion of Miss. synkinematic plutons & initial emplacement of the BR-IP thrust sheet	Alleghanian: Early 335–320 Ma; Middle ~300 Ma; Late ~260 Ma
D_5	Joints Mineralized (?)	Regional broad, open folds, most trend NE & NW	Brittle NW-directed thrusts; Great Smoky, Rosman faults	Brittle conditions	Cont'd. emplacement and exhumation of the BR-IP thrust sheet	
$D_{6...}$	Filled joints Unfilled joints	Regional broad, open folds, trend NE	Meso- and macroscale normal faults	M_4 Brittle conditions	Rifting — ? — Uplift	Mesozoic extension — ? — Cenozoic uplift

Shaded gray boxes indicates range of metamorphic conditions associated with each event.
Metamorhpic facies: *Z* – Zeolite, *PP* – Prehnite-Pumpellyite, *Gs* – Greenschist, *A* – Amphibolite, *G* – Granulite.
BFZ—Brevard fault zone. BR–Blue Ridge. CFAF–Cradle or Forestry-in-America fault. IP–Inner Piedmont.

Due to the limited extent of Mesoproterozoic basement rocks in the map area, possible Mesoproterozoic deformation preserved in the basement massifs is not described. It is likely that additional deformation events associated with the Mesoproterozoic Grenville orogeny are preserved in the few internal basement massifs. Carrigan et al. (2003) reported 1050–1030 Ma metamorphic zircon rims from the Toxaway, Sutton Creek, and Wiley Gneisses. Crosscutting relationships indicate that significant amounts of Mesoproterozoic fabrics and structures are preserved in the larger external basement massifs to the northwest (Hatcher et al., 2006; C. E. Merschat et al., 2006).

Planar Fabrics

Original bedding, S_0, in the western Blue Ridge is common at greenschist to lower amphibolite facies conditions (Hadley and Goldsmith, 1963; Hatcher and Butler, 1979), but as grade and intensity of deformation increases, recognition of S_0 becomes difficult due to transposition. Kyanite to sillimanite grade Great Smoky Group rocks northwest of the Hayesville fault contain some original sedimentary structures (beds and graded beds), and interlayers of schistose and quartz-feldspar layers are often interpreted as representing parallelism between bedding and tectonic foliation $S_{1\text{-}2}$ (Quinn, 1991; Montes, 1997; Ausburn et al., 1998; Massey and Moecher, 2005). Southeast of the Hayesville fault in the central and eastern Blue Ridge terranes, sedimentary structures are rare and limited to isolated outcrops with sedimentary layers marked by graded conglomerate beds. Foliations preserved in amphibolite boudins and as inclusion trails in porphyroblasts of garnet or staurolite, represent the oldest foliations, S_1, in the central and eastern Blue Ridge terranes (e.g., Quinn, 1991; Davidson, 1995; Stahr, 2007). These boudins and porphyroblasts are surrounded by the dominant regional S_2 foliation defined by near-peak metamorphic minerals including, sillimanite, kyanite, and other minerals. Further, stromatic (layered) migmatite commonly occurs parallel to S_2 and supports near-peak development. S_2 generally trends NE-SW and dips steeply SE to subvertical, except near Franklin, North Carolina, and east of Waynesville, North Carolina, in the Great Balsam Mountains window where S_2 trends E-W.

Separation of later S_3 and S_4 fabrics is difficult, because they are not well developed, often similarly oriented to S_2, and comprised of similar amphibolite facies minerals as S_2. The development of the fabrics becomes more pronounced to the southeast in the Dahlonega gold belt and Tugaloo terranes. S_3 is defined by alignment of micas, and is axial planar cleavages to F_3 folds superposed on $S_{1/2}$ in the western

Blue Ridge (Hadley and Goldsmith, 1963; Quinn, 1991; Montes, 1997; Massey and Moecher, 2005). Similar relationships are present in the Waynesville quadrangle in the Cartoogechaye terrane north of the Great Balsam Mountains window. In the Dahlonega gold belt and the Tugaloo terrane, the late growth of staurolite (Davidson, 1995; Stahr, 2007), growth of new coarse-grained muscovite with sillimanite inclusion trails, and kyanite after sillimanite all support that S_3 and S_4 formed during an amphibolite facies event.

Original igneous textures have been observed in most Paleozoic plutons, regardless of age (Acker, 1982; Miller et al., 1997; Stahr, 2007), but are not discussed here. Solid-state foliations developed in all of the plutons in the central and eastern Blue Ridge parallel S_2 in the surrounding country rocks (Acker, 1982; Miller et al., 1997; Lamb, 2001; Stahr, 2007). However, similar age plutons are not equally deformed, suggesting possible inhomogeneous strain patterns (Miller et al., 1997). Comparison of the regional foliation with igneous and metamorphic fabrics in the various plutons provides relative age of the deformation. Recent SHIRMP U-Pb zircon ages indicate these plutons are Mississippian, and require that foliations in the pluton and possibly surrounding country rock are also Mississippian. Stahr (2007) observed that the tectonic foliation in the Rabun and Walnut Creek plutons is parallel to the foliation in the surrounding country rocks and suggested S_4 represents the localized reactivation of S_2 near the plutons. Truncation of ~335 Ma Rabun pluton by the Chattahoochee fault indicates the late development of mylonitic S_4 in and near the shear zone. Other late steeply dipping shear zones with associated mylonitic S_4 include the Pisgah Ridge fault (Acker, 1982), Cradle of Forestry-in-America fault (Dockal, 2007), and Dill Falls shear zone. The geometry, kinematics, and close proximity of the faults to Mississippian plutons raises the question if these faults are related to pluton emplacement.

Folds

Multiple fold generations are recognized at both the mesoscopic and map-scale. The fold history becomes more complex to the southeast. F_1 folds dominate in the Great Smoky Group in the western Blue Ridge (Hadley and Goldsmith, 1963; Massey and Moecher, 2005). In the central and eastern Blue Ridge terranes, F_1 folds are preserved in boudins, and recognized as refolds and intrafolial folds. Passive and flexural flow F_2 folds are the most abundant folds in the central and eastern Blue Ridge, and are axial planar to the regional S_2 foliation. F_2 folds are isoclinal to tight, trend NE-SW, and generally verge NW. Quinn (1991) described polyharmonic folding in the Cartoogechaye

terrane resulting from mechanical contrasts between the more gneissic and schistose layers. Superposed on these folds are tight to closed F_3 folds that have similar trends and styles to F_2 often making them difficult to distinguish. Late upright, closed to open F_4 folds are common in the central and eastern Blue Ridge. In the more schistose units NE-SW–trending F_4 crenulations are common. An axial planar foliation is not typical of F_4, but may locally be developed (Hopson et al., 1989). Near Mississippian plutons, F_4 folds become tighter and more common, but may not be directly related to the regional F_4 folds (Stahr, 2007). Finally, F_5 folds related to emplacement of the Blue Ridge-Piedmont thrust sheet are expressed as shear-zone related folds and map-scale open folds like the Tallulah Falls dome (Hopson et al., 1989).

Faults

Several large ductile faults have been traced throughout the Blue Ridge, and numerous other smaller shear zones have been recognized by different workers. Beginning in the northwest, the major faults recognized include the Hayesville, Shope Fork-Chunky Gal Mountain, Soque River, and the Chattahoochee–Holland Mountain fault (Fig. 2–3). In the northeastern part of the map the Chattahoochee–Holland Mountain fault truncates the Soque River fault, producing the Great Balsam Mountains window (Merschat and Hatcher, 2007). The late brittle Rosman fault, the youngest and westernmost part of the Brevard fault zone, occurs just southeast of the map area (Horton, 1982). Several steep, NW–dipping shear zones occur in the southeastern part of the Tugaloo terrane and their significance is not yet completely understood. Geometries, kinematics, and histories of the faults vary and will be summarized below, incorporating new information regarding timing and map relationships.

Hayesville fault

The Hayesville fault is a suture between the Laurentian margin/western Blue Ridge and the accreted suspect peri-Laurentian Cowrock and Cartoogechaye terranes of the central Blue Ridge (Hatcher, 1978a). Lithostratigraphic sequences in the footwall and hanging-wall units are truncated along the fault. The Hayesville fault trends NE-SW, dips steeply both SE and NW, and locally is subvertical. The fault surface is folded by NE-SW and E-W trending folds, and several windows occur just southeast of the fault, including the Brasstown Bald, Shooting Creek, and smaller unnamed windows (e.g., a window mapped by Edelman on the Hazelwood quadrangle). Map relationships that imply the fault is an early premetamorphic fault include a continuous progression of Barrovian series isograds

across the trace of the fault (Eckert et al., 1989), and the trace is folded by F_2 and younger generations of folds (Ausburn et al., 1998; Massey and Moecher, 2005). Mylonite has been described along segments of the fault (Eckert, 1988; Vauchez and Dallmeyer, 1989; Coble, 1996), but rocks adjacent to the fault are usually not strongly mylonitized, and display significant recrystallization fabrics. Moecher et al. (2005) reported a monazite chemical age of ~459 Ma from Great Smoky Group rocks a few meters below the Hayesville fault, and indicates emplacement of the Hayesville fault was prior to the regional metamorphism at ~459 Ma.

Other pre-metamorphic faults west of the study area include the Greenbrier and Dunn Creek faults (Hadley and Nelson, 1963; Connelly and Woodward, 1992). These faults are transected by the chlorite and biotite isograds, and regional cleavage. Recent ID-TIMS monazite ages from Great Smoky Group rocks (Corrie and Kohn, 2007) limit movement on these faults to prior to 450 Ma.

Shope Fork–Chunky Gal Mountain fault

The Shope Fork–Chunky Gal Mountain thrust sheet is the highest thrust sheet in the central Blue Ridge and sits in a northeast–plunging synform above the Cowrock and Dahlonega gold belt terranes. It is truncated to the northwest by the Hayesville fault and to the southeast by the Soque River fault; making its timing relationships complicated. The Chunky Gal Mountain fault was originally described on the northwestern side of the Cartoogechaye terrane (Hatcher, 1978b; Hatcher and Butler, 1979). The Chunky Gal Mountain fault in exposures on US 64 at Chunky Gal Mountain is marked by a mylonite zone up 12 m thick in the footwall, changes orientation of S_2 across the fault, and is folded by F_3 tight to isoclinal folds (Hatcher, 1978b; Hatcher and Butler, 1979). Interestingly, deformation is not equally partitioned between footwall and hanging wall lithologies. A zone of amphibolite ultramylonite a few centimeters thick occurs in the hanging wall. The mylonite is characterized by significant grain-size reduction of hornblende, formation of epidote, and a weakly developed S-C fabric. SHRIMP U-Pb ages of zircon rims from several meters below the mylonitic zone in the Coweeta Group Coleman River Formation yields a weighted average of ~463 Ma. Similar assemblages in the mylonite, as in metamorphic peak assemblages suggest synmetamorphic movement of the fault at ~463 Ma. The Shope Fork fault was originally mapped by Hatcher (1979, 1980) to explain truncations of the Coweeta Group and ~468 Ma Persimmon Creek gneiss against the migmatitic biotite gneiss of the Cartoogechaye terrane along an E–W trending segment of the fault in the Prentiss 7.5–minute quadrangle. The fault is folded

by NW– and NE–trending isoclinal folds, and E–W-trending open folds (Hatcher, 1979; 1980). Subsequent mapping eventually traced these faults southwestward where they merge in the Shooting Creek 7.5-minute quadrangles (Hatcher, unpub. mapping).

Soque River fault

The Soque River fault has been traced from Georgia into North Carolina along the northwest flank of the Dahlonega gold belt where it separates non-migmatitic, middle amphibolite facies rocks from higher grade rocks of the Cowrock and Cartoogechaye terranes. The fault traces northeast and dips northwest; and is folded by NE-trending F_3 folds, and E-W trending F_4 folds. Various geologists have concluded that the Soque River fault is post-metamorphic because of the distinct metamorphic break across the fault and the local truncations of S_2 (Gillon, 1982; Nelson, 1982; Hopson et al., 1989). Map relationships that bracket movement on the fault include truncation of S_2 and F_2 synforms in the Cowrock terrane and F_3 folds of the fault trace (Hopson et al., 1989). S_2 foliations in the Dahlonega gold belt and Cartoogechaye terranes are parallel across the fault in the Great Balsam Mountains (Merschat and Hatcher, 2007; Plate 1). Although Hopson et al. (1989) suggested the Soque River fault is Acadian becasue it truncates D_2 structures, map relationships and timing of metamorphism suggest it is a syn- to post-metamorphic D_2 Taconian fault.

Chattahoochee–Holland Mountain fault

The northwestern boundary of the Tugaloo terrane is the Chattahoochee–Holland Mountain fault in southwestern North Carolina and northeastern Georgia. The fault trends NE-SW and dips steeply SE, and is superposed by tight to open folds, F_{3-4}. Along the length of the fault, the regional foliations in the Dahlonega gold belt and Tugaloo terrane are parallel across the fault, although rock units are truncated at several localities. Mylonite zones associated with the fault vary from a few meters to tens of meters thick. The ~335 Ma Rabun pluton is truncated by the Chattahoochee fault in the Scaly Mountain (Lamb, 2001) and Dillard quadrangles (Acker and Hatcher, unpub. mapping). Rabun Granodiorite near the Chattahoochee fault is characterized by minor quartz ribbons, pods of undulose and recrystallized quartz, and mechanically bent feldspar grains consistent with lower amphibolite to greenschist facies deformation (Merschat et al., 2007; Stahr, 2007). A large exposure of Chattahoochee fault on the Blue Ridge Parkway near Reinhart Gap consists of migmatitic and mylonitic metagraywacke, metasandstone and several variably deformed granitic to pegmatitic intrusions. At this

exposure the fault is tightly to openly folded, contains ~50 m of mylonite, and several discrete zones of ultramylonite 5–10 cm wide. Microstructures include recrystallized and lesser undulose quartz, and bent and undulose plagioclase porphyroclasts with subgrains. Migmatitic rocks in the shear zone and observed mylonite microstructures support the Chattahoochee–Holland Mountain fault at Reinhart Gap is an amphibolite grade shear zone.

Along–strike variations in strain, reactivation, and overprinting of structures and metamorphism complicate the tectonic history of the Blue Ridge. From northeastern Georgia to northwestern North Carolina the northwestern boundary of the Tugaloo terranes consists of the Chattahoochee, Holland Mountain, Burnsville, and Gossan–Lead faults. Different segments along the northwestern boundary of the Tugaloo terrane and structures within the terrane have been interpreted as Taconic, Acadian/Neoacadian, and Alleghanian structures. The Chattahoochee fault was defined by Hurst (1973) near Gainesville, Georgia, and has been traced northward into the map area where it truncates the ~335 Ma Rabun Granodiorite (Fig. 2–2). Higgins et al. (2003) described the Chattahoochee fault as a post-metamorphic dextral fault.

North of the map area, the Holland Mountain, Burnsville, and Gossan–Lead faults define the northwestern boundary of the Tugaloo terrane and are described as older faults. In the Canton and Sandymush quadrangles immediately to the northeast of Waynesville, Merschat and Wiener (1988) described the Holland Mountain fault as a synmetamorphic thrust fault juxtaposing the Ashe Formation against central and western Blue Ridge rocks. A mylonite zone associated with the fault ranges from 10 m to 200 m wide and upright NE-trending open folds superpose the fault yielding several klippes (Merschat and Wiener, 1988). Additional studies by Merschat (1977; 1993), Burr (2002), and Cattanach and Merschat (2005) trace the Holland Mountain fault northeast to near Burnsville, North Carolina. North of the Grandfather Mountain window Abbott and Raymond (1984) concluded this contact is a Taconic thrust, the Gossan-Lead fault (Hatcher, 1978a). The ~459 Ma Lick Ridge eclogite (B. V. Miller et al., 2000, 2006) near Bakersville, North Carolina, supports a Taconican origin of this contact. Partially overlapping the work of C. E. Merschat (1977, 1993, unpublished data) from Weaverville to north of Burnsville, North Carolina, Trupe et al. (2003) interpreted the same contact between the eastern and western Blue Ridge as the dextral Burnsville fault. The contact is defined by a kilometer-scale shear zone and is not folded (Trupe et al., 2003). Movement on the Burnsville fault is bracketed by ~377 Ma sheared pegmatite and $^{40}Ar/^{39}Ar$ hornblende cooling ages of ~360 Ma from amphibolite from the fault zone (Trupe et al., 2003). $^{40}Ar/^{39}Ar$ ages of

retrograde hornblende from the Lick Ridge eclogite yields ages of ~360 Ma supporting a Neoacadian overprint (B. V. Miller et al., 2000, 2006).

The contrasting kinematics, mechanics, and timing of movement along the western boundary of the Tugaloo terrane led Merschat et al. (2007) to suggest separate phases of deformation: (1) Holland Mountain–Gossan–Lead phase, Middle Ordovician, Taconian accretionary phase; (2) Burnsville, Middle Devonian dextral strike slip phase, and (3) Chattahoochee phase, late Mississippian reactivation as a dextral shear zone. All of the northwestern boundary of the Tugaloo terrane was affected by the Holland Mountain–Gossan–Lead phase during Middle Ordovician accretion of the terrane to the southeastern margin of Laurentia. This tectonic boundary was then locally overprinted during the Devonian and Mississippian. Segments affected by younger deformation are closely related to recesses similar to the spatial distribution of metamorphism (see Part III).

Pisgah Ridge, Cradle-of-Forestry-in-America, and Dill Falls shear zones

Recent studies have recognized three similar NW-dipping dextral shear zones in the southeastern part of the Tugaloo terrane in southwestern North Carolina. These faults are close to several of the Mississippian plutons raising questions regarding their significance for pluton emplacement.

Acker (1982) recognized the NE-SW trending, moderate to steeply NW-dipping Pisgah Ridge fault. It extends from the northeastern part of the Shining Rock quadrangle into the Sam Knob and Lake Toxaway quadrangles. The fault truncates footwall units, and is characterized by schlieric structures and porphyroclastic textures in migmatitic biotite gneiss (Acker, 1982). Based on geometry, the fault was interpreted to be a southeast-directed thrust (Acker, 1982). Annealed mylonitic textures led Acker (1982) to suggest it was active during high-grade metamorphism.

On the southeast side of the Pink Beds pluton to the northwest margin of the Looking Glass pluton is a 300–600 m wide dextral shear zone named the Cradle-of-Forestry-in-America fault (Dockal, 2001, 2006, 2007). The following description of the shear zone is from Dockal (2007). The shear zone trends NE-SW and dips steeply NW, and consists of mylonitic porphyroclastic biotite gneiss and schist, and areas of tectonic mélange. Blocks in the tectonic mélanges consist of biotite gneiss, Looking Glass granitoid gneiss, Pink Beds granitoid gneiss, hornblende gneiss, and rare soapstone. Two episode of deformation are recognized along the fault; an early amphibolite grade deformation overprinted by a greenschist grade event. Dockal (2007) estimated ~15

km of right-lateral offset associated with the fault to restore the Looking Glass pluton to the northwest, adjacent to the Pink Beds pluton, but this may be an oversimplification considering different ages and compositions of the plutons (Miller et al., 1997; C.F., Miller et al., 200). Varnell et al. (2008) reported a SHRIMP U-Pb zircon age of ~337 Ma for the Looking Glass pluton, bracketing the maximum age of the shear zone.

The Dill Falls shear zones recognized on the Sam Knob 7.5-minute quadrangle is the structurally highest (northwesternmost), NW-dipping, dextral faults internal to the Tugaloo terrane (Fig. 2–2). Like the other shear zones, it trends WNW-ESE, dips steeply NW, and extends from the middle of the Sam Knob quadrangle into the southeast corner of the Tuckasegee quadrangle where it could not be mapped any further. It is characterized by a 400–300 m-thick shear zone of mylonitic Tallulah Falls Formation lithologies including porphyroclastic metagraywacke/biotite gneiss and porphyroclastic garnet-muscovite-biotite schist. A map-scale lens of mylonitic granitoid gneiss occurs in the shear zone just west of Dill Falls, but could not be traced along strike. A wispy S-C foliation is common in the mylonitic metagraywackes and schists. Mantled plagioclase sigma porphyroclasts indicate top-to-the-SW and lesser top-down-to-the-NW shear sense. Garnet occurs as 0.5 cm porphyroclasts in mylonitic schist, and as cluster of 0.1-0.4 cm garnets in the mylonitic metagraywacke. These may represent larger garnets that were fragmented during shearing, and then became the nuclei for new garnet growth. Mantled plagioclase porphyroclasts, recrystallization of garnet and occurrence of migmatite in the shear zones suggest this is an amphibolite grade fault. The geometry of the fault, and SE- and NE-directed shear sense suggest this is an oblique-slip fault with reverse and dextral shear sense.

Similar geometries, kinematics, and grade suggest these faults are related. Map relationships suggest the Cradle-of-Forestry-in-America and Pisgah Ridge faults are post emplacement of the ~371 Ma Pink Beds and ~337 Ma Looking Glass plutons (Varnell et al., 2008). The Dills Falls shear does not intersect a pluton, but is likely to be the same age as the other faults. The significance of these faults is not completely understood at this time. They may represent part of a late Neoacadian and early Alleghanian dextral shear zones (Dockal, 2007). Alternatively, the close proximity to and often surrounding Mississippian plutons, raises the question of whether or not these are faults along which the plutons were emplaced. This could help explain the dominance of Looking Glass and Pink Beds lithologies in the block-in-matrix structures.

TECTONIC SUMMARY

The complex tectonic history of the Blue Ridge began with two episodes of extension, followed by three contractional/collisional events that culminated with the formation of Pangea. These events are recorded in the Blue Ridge terranes as different periods of sedimentation, deformation, metamorphism, and magmatism (Fig. 2–7). These events correspond to the late Neoproterozoic opening of the Iapetus ocean, Middle Ordovician Taconian, Late Devonian to Mississippian Neoacadian, and late Mississippian to Permian Alleghanian orogenies.

All of the terranes of the southwestern North Carolina and northeastern Georgia Blue Ridge were affected by Middle Ordovician metamorphism, magmatism, and deformation associated with the Taconian orogeny (Fig. 2–7). The Tugaloo terrane and all terranes to the west of it were accreted to the Laurentian margin/western Blue Ridge during the Middle Ordovician Taconian orogeny. This event produced regional Barrovian series greenschist to granulite facies metamorphism in the Blue Ridge (M_1, M_2), including the middle amphibolite to granulite facies preserved in the study area as the result of accretion and loading the margin with the various suspect terranes of the central and eastern Blue Ridge. Pre-, syn-, and post-metamorphic structures have been separated into D_1 and D_2 events associated with the Taconian orogeny. However, D_1 and D_2 events may represent a continuum of deformation associated with the Taconian orogeny based on similar orientations of structures, and mineral assemblages defining the earlier fabrics. Arc-like magmatism lasted from 480–460 Ma, with felsic and mafic intrusives into Dahlonega gold belt, the Persimmon Creek Gneiss in the Cowrock terrane, and the ~466 Ma Whiteside pluton, Tugaloo terrane. Magmatism resulted from the westward subduction, closing the small ocean basins of the Cartoogechaye and Cowrock terranes. By ~460 Ma magmatism stepped further eastward into the Tugaloo terrane producing the remnants of the 460–450 Ma arc in the western Inner Piedmont (Bream, 2003). Peak metamorphism probably lasted from 465–450 Ma based on SHRIMP U-Pb metamorphic zircon ages from the granulitic and upper amphibolite core of the central Blue Ridge. Various pre- to synmetamorphic faults: Hayesville, Shope Fork–Chunky Gal Mountain, and syn- to post-metamorphic faults, Soque River and Chattahoochee faults, transported these terranes westward into the a west-verging, polydeformed thrust stack.

The transpressional Neoacadian orogeny, 365-345 Ma, reactivated parts of the Blue Ridge, resulting in superposed folds F_3, new foliations S_3, and dextral strike-slip faults. Deformation and metamorphism was most intense near the Brevard fault zone and decreased westward. In the map area Neoacadian deformation is manifested as

Figure 2–7. Graph of tectonothermal events in the Georgia-North Carolina Blue Ridge. Sources of data are Berquist (2005)[1], Bream (2003)[2], Burton and Kunk (2006)[3], Carrigan et al. (2003)[4], Connelly and Dallmeyer, (1993)[5], Corrie and Kohn, (2007)[6], Dallmeyer, (1988)[7], Goldberg and Dallmeyer (1997)[8], Mapes (2002)[9], McDowell et al. (2002)[10], Merschat et al. (2006)[11], Miller et al. (1998)[12], B. V. Miller et al. (2000)[13], C. F. Miller et al. (2000b)[14], Miller et al. (2006)[15], Moecher et al. (2003)[16], Moecher et al. (2004)[17], Moecher et al. (2005)[18], Settles, (2002)[19], Stahr et al. (2006)[20], Thomas, (2001)[21], Trupe et al. (2003)[22], and Varnell et al. (2008)[23] Plutons names are Dlg–Looking Glass granodiorite. Dpb–Pink Beds trondhjemite. Dsp–Spruce Pine pegmatites. Mma–Mount Airy granodiorite. Mrg–Rabun Granodiorite porphyritic. Mre–Rabun Granodiorite equigranular. Mrm–Round Mountain trondhjemite. Msm–Stone Mountain granodiorite. Mwc–Walnut Creek granodiorite. My–Yonah Mountain tonalite. Obg–Barlow gneiss. Occ–Cane Creek felsic gneiss. Ogf–Galts Ferry gneiss. Olbft–Lake Burton felsic metatuff. Opc–Persimmon Creek gneiss. Ow–Whiteside trondhjemite-granodiorite. Ovr–Vila Rica felsic gneiss. tdj–unamed trondhjemite dikes.

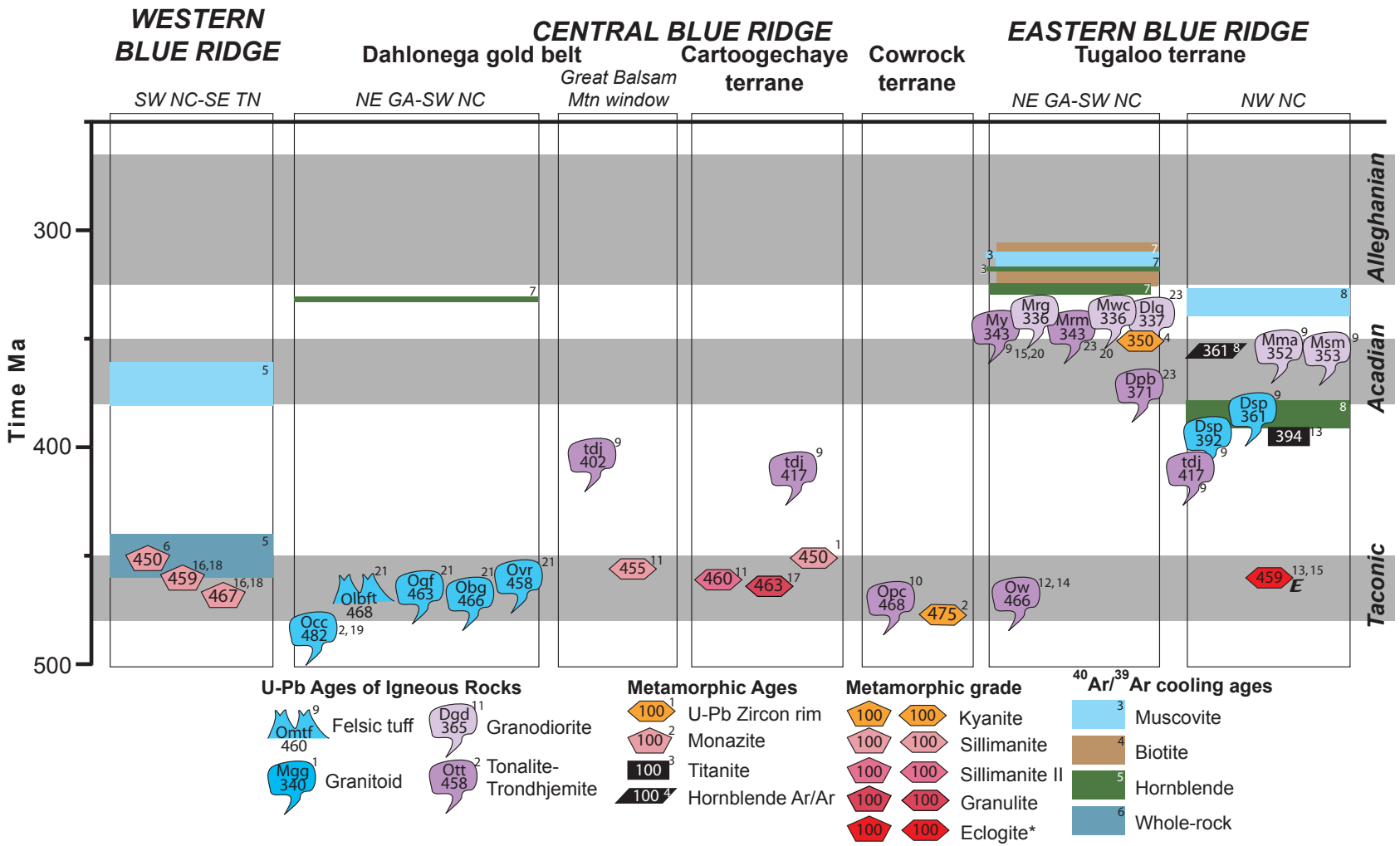
WESTERN BLUE RIDGE
CENTRAL BLUE RIDGE
EASTERN BLUE RIDGE
Dahlonega gold belt
Great Balsam Mtn window
Cartoogechaye terrane
Cowrock terrane
Tugaloo terrane
SW NC-SE TN
NE GA-SW NC
NE GA-SW NC
NW NC
Time Ma
300
400
500
Alleghanian
Acadian
Taconic
U-Pb Ages of Igneous Rocks
Felsic tuff
Granitoid
Granodiorite
Tonalite-Trondhjemite
Metamorphic Ages
U-Pb Zircon rim
Monazite
Titanite
Hornblende Ar/Ar
Metamorphic grade
Kyanite
Sillimanite
Sillimanite II
Granulite
Eclogite*
40Ar/39Ar cooling ages
Muscovite
Biotite
Hornblende
Whole-rock

tight to open F_3 folds, both meso- and map-scale, weakly developed S_3, and M_3 growth of kyanite and staurolite often associated with S_3. Dextral shear zones associated with the Neoacadian have not been recognized in the area. Massey and Moecher (2005) described mylonitic Great Smoky Group outcrops with dextral shear sense. To the northeast and southwest the western boundary of the Tugaloo terrane has been described as a dextral shear zone. The Burnsville shear zone is an amphibolite grade, Middle Devonian dextral shear zone (e.g., Trupe et al., 2003), but the southern continuation is uncertain. In northeastern Georgia, dextral shear sense has been documented for the Chattahoochee fault and parts of the Dahlonega gold belt (Albino, 1988, 1989). Hatcher and Merschat (2006) suggested that the Inner Piedmont and eastern Blue Ridge were part of an orogenic channel that flowed west and southwestward from underneath the Carolina superterrane. The channel flow model proposed by Hatcher and Merschat (2006) explains many aspects of the geology of the eastern Blue Ridge: reported Devonian SHRIMP U-Pb zircon ages (Table 2–7, Part III), Devonian to Mississippian Ar-Ar mineral ages, dextral kinematics associated with Devonian faults, and NE–SW-trending mineral lineations (Rankin et al., 1972; Higgins et al., 2003). Unlike the Inner Piedmont, Neoacadian deformation and metamorphism is not as pervasive throughout the eastern Blue Ridge and older Taconian structures and metamorphism are common (e.g. Burton and Kunk, 2006; Stahr, 2007). Merschat et al. (2005) suggested the eastern Blue Ridge was a footwall buttress to ductile flow in the Inner Piedmont, which may provide a better explanation of commonly preserved Taconian, D_2, structures and M_2 metamorphism in the eastern Blue Ridge. Deformation was partitioned along segments of the eastern Blue Ridge strongly overprinting and reactivating previous fabrics. Other areas may not have been strongly affected. Segments of the eastern Blue Ridge that correspond to promontories in the continental margin were reactivated, while segments in the salients, including most of the study area were not strongly affected. This is supported by metamorphic ages compiled in Part III. Additionally, M_3 growth of staurolite and kyanite in the southeastern part of the Tugaloo terrane suggest a later increase in pressure, which can be explained by juxtaposing the Carolina superterrane and Inner Piedmont orogenic channel above the eastern Blue Ridge.

The Alleghanian orogeny and the late Paleozoic formation of the supercontinent Pangea is the culmination of the Appalachian Wilson cycle (Hatcher et al., 2007). The effects of this final contractional event were variable experience by the southwestern North Carolina and northeastern Georgia Blue Ridge, and are separated into early and late phases. The early Alleghanian phase includes low-potassium granodioritic to

trondhjemitic plutonism and middle amphibolite to greenschist facies metamorphism and deformation. Mississippian plutons include the Round Mountain, Pink Beds, Yonah Mountain, Rabun, and Walnut Creek. Migmatitic contact aureoles have been recognized near the southern end of the Rabun and the area between the Rabun and Walnut Creek plutons (Stahr, 2007). Miller et al. (1997) noted that these plutons are variably deformed and often contain tectonic foliations, S_4. Additionally, additional detailed mapping has documented that the Chattahoochee fault truncates the ~335 Ma Rabun pluton along its western margin (Lamb, 2001; Acker and Hatcher, unpublished mapping). Quartz ribbons and bent or fractured feldspar grains suggest lower amphibolite to greenschist facies deformation associated with the fault (Merschat et al., 2007; Stahr, 2007). The distribution of early Alleghanian deformation is localized. Several late, steep NW– dipping shear zones have been documented in the southeastern part of the Tugaloo terrane (Acker, 1982; Dockal, 2007; this study). These faults may be related to early Alleghanian deformation along the Brevard fault zone, or to faults related to emplacement of the Mississippian plutons based on their close association, extensional nature, and observed blocks of granitoids in the shear zones.

Late Alleghanian deformation is interpreted as the final emplacement of the Blue Ridge-Piedmont megathrust sheet (Hatcher and Hooper, 1992). Emplacement of the Blue Ridge-Piedmont megathrust sheet produced regional dome-and-basin map patterns, possibly as a result of formation of antiformal stack duplexes in the footwall of the thrust sheet. The Tallulah Falls dome, which the northern flank of which extends into the southern part of the map area, is interpreted to have formed by doming of the thrust sheet above a footwall duplex of Paleozoic sedimentary rocks (Hatcher et al., 2004). Zircon fission track ages from across the Great Smoky Mountains, eastern Blue Ridge, and just across the Brevard fault indicate rapid emplacement of the thrust sheet and cooling through ~235ºC occurred by ~280 Ma (Naeser et al., 2005).

Mesozoic extension and Cenozoic uplift have had variable effects across the entire orogen, but structures formed during these events are limited to mostly joints and fractures. Mesozoic extension responsible for the opening of the Atlantic Ocean also produced numerous Triassic basins distributed throughout the Piedmont and beneath the Coastal Plain. Other structures commonly associated with Mesozoic extension, siliceous cataclasite, and Triassic diabase dikes are neither common nor absent in the map area. Several diabase dikes have been traced across the Tallulah Falls dome just south of the map area. Hopson (1994) mapped a ~300 m long dike in the southwest corner of the Hightower Bald quadrangle; the only Triassic diabase dike in the map area. Several E-W

and NNW trending lineaments have been recognized in the Blue Ridge, like the Fontana–Rhodhiss lineament (Hatcher et al., 2005) or the Warwoman lineament, Georgia-South Carolina (Hatcher, 1974). Although numerous topographic lineaments can be recognized in the map area, often of similar orientation to major lineaments that transect the Blue Ridge, no cataclasite or offset units has been recognized along these lineaments.

The steep topography of the Blue Ridge precludes it is the remnant topography of an ancient mountain range (Hatcher et al., 2005). Cosmogenic nuclide and apatite fission tracks studies suggest a slow continuous uplift and erosion rates persisting from the Late Triassic to Early Jurassic to present day (Matmon et al., 2003a, 2003b; Naeser et al., 2005). However, younger apatite fission track ages near Grandfather Mountain yield a more rapid erosion rate affecting part of the Blue Ridge (Naeser et al., 2005) and indicates all of the Blue Ridge has not experienced a uniform erosion rate. Alternatively, the uplift and development of the present topography of the Blue Ridge may be punctuated. Prowell and Christopher (2000) suggested that the truncation of the Appalachian orogen (including Blue Ridge along-strike equivalents) by the Alabama Coastal Plain indicates the mountain chain was eroded flat and uplifted again during the Tertiary. Regardless of whether the Blue Ridge has experienced a slow continuous or punctuated uplift history, the topography of the Blue Ridge remains enigmatic.

REFERENCES CITED

Abbott, R. N., Jr., and Greenwood, J. P., 2001, Retrograde metamorphism of eclogite in the southern Appalachian mountains, U.S.A.—A case involving seamount subduction: Journal of Metamorphic Geology, v. 19, p. 433–443.

Abbott, R. N., Jr., and Raymond, L. A., 1984, The Ashe Metamorphic Suite, northwest North Carolina: Metamorphism and observations on geologic history: American Journal of Science, v. 284, p. 350–375.

Absher, B. S., and McSween, H. Y., 1985, Granulites at Winding Stair Gap, North Carolina: The thermal axis of Paleozoic metamorphism in the southern Appalachians: Geological Society of America Bulletin, v. 96, p. 588–599.

Acker, L. L., 1982, Geology of the Shining Rock quadrangle, North Carolina [M.S. thesis]: Chapel Hill, University of North Carolina, 110 p.

Albino, G. V., 1988, Gold deposits of the Dahlonega belt, northeast Georgia: Mother-lode-type mineralization at mid crustal depths: Geological Society of America Abstracts with Programs, v. 20, no. 4, p. 251.

Albino, G. V., 1989, Shear zone-hosted gold deposits of the Dahlonega belt, NE Georgia: Geological Society of America Abstracts with Programs, v. 21, no. 2, p. 1.

Aleinikoff, J. N., Zartman, R. E., Walter, M., Rankin, D. W., Lyttle, P. T., and Burton, W. C., 1995, U–Pb ages of metarhyolites of the Catoctin and Mount Rodgers Formations, central and southern Appalachians: Evidence for two pulses of Iapetan rifting: American Journal of Science, v. 295, p. 428–454.

Ausburn, M. P., Hatcher, R. D., Jr., Bryan, J. G., Godfrey, S. C., and Acker, L. L., 1998, Geologic map of the Topton quadrangle, North Carolina: North Carolina Geological Survey, GMS–6, scale 1:24,000.

Berquist, P. J., 2005, U–Pb geochronology and geochemistry of southern Appalachian basement: Tectonic implications and constraints on age, extent, and origin [M.S. thesis]: Nashville, Tennessee, Vanderbilt University, 91 p.

Berquist, P. J., Fisher, C. M., Miller, C. F., Wooden, J. L., Fullagar, P. D., and Loewy, S. L., 2005, Geochemistry and U–Pb geochronology of Blue Ridge basement, western North Carolina and eastern Tennessee: Implications for tectonic assembly, *in* Hatcher, R. D., Jr., and Merschat, A. J., eds., Blue Ridge geology geotraverse east of the Great Smoky Mountains National Park, western North Carolina: Carolina Geological Society Guidebook, North Carolina Geological Survey, p. 33–44.

Bream, B. R., 2003, Tectonic implications of geochronology and geochemistry of para- and orthogneisses from the southern Appalachian crystalline core [Ph.D. dissertation]: Knoxville, University of Tennessee, 296 p.

Bream, B. R., Hatcher, R. D., Jr., Miller, C. F., and Fullagar, P. D., 2004, Detrital zircon ages and Nd isotopic data from the southern Appalachian crystalline core, Georgia, South Carolina, North Carolina, and Tennessee: New provenance constraints for part of the Laurentian margin, *in* Tollo, R. P., Corriveau, L., McLelland, J., and Bartholomew, M. J., eds., Proterozoic tectonic evolution of the Grenville orogen in North America: Boulder, Colorado, Geological Society of America Memoir 197, p. 459–475.

Brewer, M. C., and Thomas, W. A., 2000, Stratigraphic evidence for Neoproterozoic-Cambrian two-phase rifting of southern Laurentia: Southeastern Geology, v. 39, p. 91–106.

Burr, J. L., 2002, Manuscript geologic map and mineral resources summary of the Weaverville quadrangle, North Carolina: North Carolina Geological Survey, scale 1:24,000.

Burton, W. C., 2007, Bedrock geologic map of the headwaters region of the Cullasaja River, Macon and Jackson Counties, North Carolina: U. S. Geological Survey Scientific Investigations Map 2887, scale 1:24,000.

Burton, W. C., and Kunk, M. J., 2006, Evidence for Taconian and Alleghanian orogenesis in the eastern Blue Ridge near Highlands, NC: Geological Society of America Abstracts with Programs, v. 38, no. 3, p. 20.

Butler, J. R., 1991, Metamorphism, *in* Horton, J. W., Jr., and Zullo, V. A., eds., The geology of the Carolinas: Knoxville, University of Tennessee Press, p. 127–141.

Cameron, M. L., 2001, Garnet zoning, mineral inclusions, and P-T paths: Evidence for a polymetamorphic history of the Cullowhee gneiss [M.S. thesis]: Knoxville, University of Tennessee, 240 p.

Carrigan, C. W., Bream, B. R., Miller, C. F., and Hatcher, R. D., Jr., 2001, Ion microprobe analyses of zircon rims from the eastern Blue Ridge and Inner Piedmont, NC-SC-GA: Implications for the timing of Paleozoic metamorphism in the southern Appalachians: Geological Society of America Abstracts with Programs (SE Section), v. 33, p. A–7.

Carrigan, C. W., Miller, C. F., Fullagar, P. D., Hatcher, R. D., Jr., Bream, B. R., and Coath C. D., 2003, Ion microprobe age and geochemistry of southern Appalachian basement, with implications for Proterozoic and Paleozoic reconstructions: Precambrian Research, v. 120, p. 1–36.

Cattanach, B. L., and Merschat, C. E., 2005, An overview of the Mesoproterozoic basement complex on the west half of the Asheville 1:100,000 scale geologic map, *in* Hatcher, R. D., Jr., and Merschat, A. J., eds., Blue Ridge geology geotraverse east of the Great Smoky Mountains National Park, western North

Carolina: Carolina Geological Society Guidebook, North Carolina Geological Survey, p. 25–32.

Coble, J. F., 1996, Structural–metamorphic development of the Hayesville fault, Haywood and Jackson Counties, North Carolina [PhD dissertation]: University of Kentucky, Lexington, 180 p.

Connelly, J. B., and Dallmeyer, R. D., 1993, Polymetamorphic evolution of the western Blue Ridge: Evidence from $^{40}Ar/^{39}Ar$ whole-rock slate/phyllite and muscovite ages: American Journal of Science, v. 292, p. 322–359.

Connelly, J. B., and Woodward, N. B., 1992, Taconian foreland-style thrust system in the Great Smoky Mountains, Tennessee: Geology, v. 20, p. 177–180.

Corrie, S. L., and Kohn, M. J., 2007, Resolving the timing of orogenesis in the western Blue Ridge, southern Appalachians, via *in situ* ID-TIMS monazite geochronology: Geology, v. 35, p. 627–630.

Cyphers, S. R., 2009, Detailed mapping of a terrane boundary and structure and origin of block-in-matrix structures, central and eastern Blue Ridge, Jackson County, North Carolina [M.S. thesis]: Knoxville, Tennessee, University of Tennessee, 227 p.

Dallmeyer, R. D., 1988, Late Paleozoic tectonothermal evolution of the western Piedmont and eastern Blue Ridge, Georgia: Controls on the chronology of terrane accretion and transport in the southern Appalachian orogen: Geological Society of America Bulletin, v. 100, p. 702–713.

Davidson, G. L., 1995, The tectono-metamorphic history of a portion of the eastern Blue Ridge, Jackson County, North Carolina [M.S. thesis]: Knoxville, Tennessee, University of Tennessee, 157 p.

Dockal, J. A., 2001, Boundary relationships of the Looking Glass pluton, Shining Rock quadrangle, Transylvania County, North Carolina: Geological Society of America Abstracts with Programs, v. 33, no. 2, p. A–30.

Dockal, J. A., 2006, Dextral strike-slip faulting in the eastern Blue Ridge near Brevard, North Carolina: Observations, problems and speculations: Geological Society of America Abstracts with Programs, v. 38, no. 3, p. 20.

Dockal, J. A., 2007, Cradle-of-forestery-in-America fault an Acadian and Alleghanian dextral strike-slip fault within the eastern Blue Ridge, Transylvania County, North Carolina: Southeastern Geology, v. 44, p. 171–189.

Drummond, M. S., and Neilson, M. J., Allison, D. T., and Tull, J. F., 1997, Igneous petrogenesis and tectonic setting of granitic rocks from the eastern Blue Ridge and Inner Piedmont, Alabama Appalachians, *in* Sinha, A. K., Whalen, J. B., and Hogan, J. P., eds., The nature of magmatism in the Appalachian orogen: Boulder, Colorado, Geological Society of America Memoir 191, p. 147–164.

Eckert, J. O., Jr., 1984, Stratigraphy, structure, and metamorphism of the east half of the Wayah Bald quadrangle, North Carolina: Evidence for Paleozoic granulite facies metamorphism in the southern Appalachians [M.S. thesis]: Columbia, South Carolina, University of South Carolina, 411 p.

Eckert, J. O., 1988, Petrology and tectonic implications of the transition from staurolite-kyanite zone to the Wayah granulite-facies metamorphic core, southwest North Carolina Blue Ridge: Including quantitative analysis of mineral homogeneity [PhD dissertation]: College Station, Texas, Texas A&M University, 337 p.

Eckert and Lesure, F. G., (unpublished mapping), Geologic map of the Franklin quadrangle, North Carolina, scale 1:24,000.

Eckert and Yurkovich, S. P., (unpublished mapping), Geologic map of the Corbin Knob quadrangle, North Carolina, scale 1:24,000.

Edelman, S. H., and Hatcher, R. D., Jr., (unpublished mapping), Geologic map of the Hazelwood quadrangle, North Carolina: Knoxville, University of Tennessee, Tectonics and Structural Geology Research, scale 1:24,000.

Eckert, J. O., Hatcher, R. D., Jr., and Mohr, D. W., 1989, The Wayah granulite-facies metamorphic core, southwestern North Carolina: High-grade culmination of Taconic metamorphism in the southern Blue Ridge: Geological Society of America Bulletin, v. 101, p. 1434–1447.

Force, E. R., 1976, Metamorphic source rocks of titanium placer deposits—A geochemical cycle: U. S. Geological Survey Professional Paper 959-B, 16 p.

German, J. M., 1985, The geology of the northeastern portion of the Dahlonega gold belt: Georgia Geological Survey Bulletin v. 100, 41 p.

Gillon, K. A., 1982, Stratigraphy, structural, and metamorphic geology of portions of the Cowrock and Helen, Georgia 7.5 minute quadrangles [M.S. thesis]: Athens, Georgia, University of Georgia, Athens, 236 p.

Goldberg, S. A., and Dallmeyer, R. D., 1997, Chronology of Paleozoic metamorphism and deformation in the Blue Ridge thrust complex, North Carolina and Tennessee: American Journal of Science, v. 297, p. 488–526.

Hadley, J. B., and Goldsmith, R., 1963, Geology of the eastern Great Smoky Mountains North Carolina and Tennessee: U. S. Geological Survey Professional Paper, 349-B, 117 p.

Hadley, J. B., and Nelson, A. E., 1971, Geologic map of the Knoxville quadrangle, North Carolina, Tennessee, and South Carolina: U. S. Geological Survey Map I–654, scale 1:250,000.

Hartley, M. E. 1973, Ultramafic and related rocks in the vicinity of Lake Chatuge: Georgia Geological Survey Bulletin, v. 85, 61 p.

Hatcher, R. D., Jr., 1971, Geology of Rabun and Habersham counties, Georgia: A reconnaissance study: Georgia Geological Survey Bulletin 83, 48 p.

Hatcher, R. D., Jr., 1974, An Introduction to the Blue Ridge tectonic history of northeast Georgia: Georgia Geological Society Guidebook 13-A, 60 p.

Hatcher, R. D., Jr., 1977, Macroscopic polyphase folding illustrated by the Toxaway dome, eastern Blue Ridge, South Carolina-North Carolina: Geological Society of America Bulletin, v. 88, p. 1678–1688.

Hatcher, R. D., Jr., 1978a, Tectonics of the western Piedmont and Blue Ridge: Review and speculation: American Journal of Science, v. 278, p. 276–304.

Hatcher, R. D., Jr., 1978b, Field trips in the southern Appalachians: Tennessee Division of Geology Report of Investigations 37, 86 p.

Hatcher, R. D., Jr., 1979, The Coweeta Group and Coweeta syncline: Major features of the North Carolina–Georgia Blue Ridge: Southeastern Geology, v. 21, p. 17–29.

Hatcher, R. D., Jr., 1980, Geologic map and mineral resources of the Prentiss quadrangle, North Carolina: North Carolina Geological Survey, GM 167–SW, scale 1/24,000.

Hatcher, R. D., Jr., 1988, Bedrock geology and regional geologic setting of Coweeta Hydrologic Laboratory in the eastern Blue Ridge, with some discussion of Quaternary deposits and structural controls of topography, *in* Swank, W. T., and Crossley, D. A., Jr., eds., Coweeta Symposium Volume 66: New York, Springer–Verlag, p. 81–92.

Hatcher, R. D., Jr., 1989, Tectonic synthesis of the U.S. Appalachians, Chapter 14, *in* Hatcher, R. D., Jr., Thomas, W. A., and Viele, G. W., eds., The Appalachian-Ouachita orogen in the United States: Boulder, Colorado, Geological Society of America, The Geology of North America, v. F-2, p. 511–535.

Hatcher, R. D., Jr., 1993, Perspective on the tectonics of the Inner Piedmont, southern Appalachians, *in* Hatcher, R. D., Jr., Davis, T. L., eds., Studies of Inner Piedmont geology with a focus on the Columbus Promontory: Carolina Geological Society Guidebook, North Carolina Geological Survey, pp. 17–43, http://carolinageologicalsociety.org/cgscdguide.htm.

Hatcher, R. D., Jr., 2002, An Inner Piedmont primer, *in* Hatcher, R. D., Jr., and Bream, B. R., eds., Inner Piedmont geology in the South Mountains-Blue Ridge Foothills and the southwestern Brushy Mountains, central-western North Carolina: Carolina Geological Society Guidebook, p. 1–18.

Hatcher, R. D., Jr., Day 1, Transect from Laurentian rifted margin to suspect terranes and the upper crust to lower middle crust SE TN, western NC Blue Ridge: Ordovician greenschist to granulite facies Barrovian metamorphism, *in* Merschat, A. J., and

Hatcher, R. D., Jr., eds., Trans Appalachians Geotraverse: 17th International Basement Tectonics Association Field Trip Guidebook, p. 13–28.

Hatcher, R. D., Jr., and Butler, J. R., 1979, Guidebook for southern Appalachian field trip in the Carolinas, Tennessee, and northeastern Georgia: International Geologic Correlation Program Project 27, University of North Carolina, Chapel Hill, 117 p.

Hatcher, R. D., Jr., Bream, B. R., Miller, C. L., Eckert, J. O., Jr., Fullagar, P. D., and Carrigan, C. W., 2004, Paleozoic structure of internal basement massifs, southern Appalachian Blue Ridge, incorporating new geochronologic, Nd and Sr isotopic, and geochemical data, *in* Tollo, R. P., Corriveau, L., McLelland, J., and Bartholomew, M. J., eds., Proterozoic tectonic evolution of the Grenville orogen in North America: Boulder, Colorado, Geological Society of America Memoir 197, p. 525–547.

Hatcher, R. D., Jr., and Goldberg, S. A., 1991, The Blue Ridge Geologic Province, *in* Horton, J. W., Jr., and Zullo, V. A., eds., The Geology of the Carolinas—Carolina Geological Society 50th Anniversary Volume: Knoxville, The University of Tennessee Press, p. 11–35.

Hatcher, R. D., Jr., and Hooper, R. J., 1992, Evolution of crystalline thrust sheets in the internal parts of mountain chains, *in* McClay, K. R., ed., Thrust tectonics: London, Chapman and Hall, p. 217–234.

Hatcher, R. D., Jr., Hooper, R. J., Petty, S. M., and Willis, J. D., 1984, Structure and chemical petrology of three southern Appalachian mafic-ultramafic complexes and their bearing upon the tectonics of emplacement and origin of Appalachian ultramafic bodies: American Journal of Science, v. 284, p. 484–506.

Hatcher, R. D., Jr., and Merschat, A. J., 2006, The Appalachian Inner Piedmont: An exhumed strike-parallel, tectonically forced orogenic channel, *in* Law, R. D., Searle, M., and Godin, L., eds., Channel flow, ductile extrusion and exhumation of lower-mid crust in continental collision zones: London, Geological Society of London Special Publication 268, p. 517–540.

Hatcher, R. D., Jr., Merschat, A. J., and Thigpen, J. R., 2005, Blue Ridge Primer, *in* Hatcher, R. D., Jr., and Merschat, A. J., eds., Blue Ridge geology geotraverse east of the Great Smoky Mountains National Park, western North Carolina: Carolina Geological Society Guidebook, North Carolina Geological Survey, p. 1–24.

Hatcher, R. D., Jr., Merschat, A. J., and Raymond, L. A., 2006, Geotraverse: Geology of northeastern Tennessee and the Grandfather Mountain region, *in* Labotka, T. L., and Hatcher, R. D., Jr., eds., Geological Society of America Southeastern Section meeting Field Trip Guidebook: Knoxville, Tennessee, University of Tennessee, p. 129–184.

Hatcher, R. D., Jr., Bream, B. R., and Merschat, A. J., 2007, Tectonic map of the southern and central Appalachians: A tale of three orogens and a complete Wilson cycle, *in* Hatcher, R. D., Jr., Carlson, M. P., McBride, J. H., and Martínez Catalán, J. R., eds., 4-D Framework of Continental Crust: Geological Society of America Memoir 200, p. 595–632.

Higgins, M. W., Crawford, T. J., Atkins, R. L., and Crawford, R. F., 2003, Geologic map of the Atlanta 30' x 60' quadrangle, Georgia: U. S. Geologic Survey, Geologic Investigations Series Map I-2602, scale 1:100,000.

Hopson, J. L., 1994, Geology of part of the eastern Blue Ridge, northeast Georgia and the adjacent Carolinas [Ph.D. dissertation]: Knoxville, university of Tennessee, 350 p.

Hopson, J. L., Hatcher, R. D., Jr., and Stieve, A. L., 1989, Geology of the eastern Blue Ridge, northeastern Georgia and the adjacent Carolinas, *in* Fritz, W. J., Hatcher, R. D., Jr., and Hopson, J. L., eds., Geology of the eastern Blue Ridge of northeast Georgia and the adjacent Carolinas: Georgia Geological Society Guidebooks, v. 9, p. 1–40.

Horton, J. R., Jr., 1982, Geologic map of the Rosman quadrangle, North Carolina: North Carolina Geological Survey GM–185–NE, scale 1:24,000.

Hurst, V. J., 1955, Stratigraphy, structure, and mineral resources of the Mineral Bluff quadrangle, Georgia: Georgia Geological Survey Bulletin 63, 137 p.

Hurst, V. J., 1973, Geology of the southern Blue Ridge belt: American Journal of Science, V. 273, p. 643–670.

Keith, A., 1907, Description of the Pisgah quadrangle (NC-SC): U. S. Geological Survey folio.

King, P. B., Neuman, R. B., and Hadley, J. B., 1968, Geology of the Great Smoky Mountains National Park, Tennessee and North Carolina: U. S. Geological Survey Professional Paper 587, 23 p.

Kish, S. A., 1991, Potassium-Argon dating in the western Blue Ridge of North Carolina and Tennessee, *in* Kish, S. A., ed., Studies of Precambrian and Paleozoic stratigraphy in the western Blue Ridge: Carolina Geological Society Guidebook, North Carolina Geological Survey, p. 69–77.

Lamb, D. D., 2001, Geology of the Scaly Mountain quadrangle, emphasizing the structures, timing and emplacement mechanisms for the Rabun granodiorite, eastern Blue Ridge, southwestern north Carolina [M.S. thesis]: Knoxville, University of Tennessee, 86 p.

Lowey, S. L., Connely, J. N., Dalziel, I. W. D., Gower, C. F., 2003 Eastern Laurentia in Rodinia: constraints from whole-rock Pb and U/Pb geochronology: Tectophysics, v. 375, 169–197.

Ludwig, K. R., 2003, Isoplot v. 3.00, computer program.

Mapes, R. W., 2002, Geochemistry and geochronology of mid-Paleozoic granitic plutonism in the southern Appalachian Piedmont terrane, North Carolina-South Carolina-Georgia [M.S. thesis]: Nashville, Vanderbilt University, 150 p.

Massey, M. A., and Moecher, D. P., 2005, Deformation and metamorphic history of the western Blue Ridge-eastern Blue Ridge terrane boundary, southern Appalachian orogen: Tectonics, v. 24, p. TC5010, 1–18.

Matmon, A., Bierman, P. R., Larsen, J., Southworth, S., Pavich, M., Finkel, R., and Caffee, M., 2003b, Erosion of an ancient mountain range, the Great Smoky Mountains, North Carolina and Tennessee: American Journal of Science, v. 303, p. 817–855.

Matmon, A., Bierman, P. R., Larsen, J., Southworth, S., Pavich, M., and Caffee, M., 2003a, Temportally and spatially uniform rates of erosion in the southern Appalachian Great Smoky Mountains: Geology, v. 31, p. 155–158.

McClellan, E. A., Steltenpohl, M. G., Thomas, C., and Miller, C. F., 2007, Isotopic age constraints and metamorphic history of the Talladega belt: New evidence for timing of arc magmatism and terrane emplacement along the southern Laurentian margin: Journal of Geology, v. 115, p. 541–561.

McConnell, K. I., and Abrams, C. E., 1984, Geology of the greater Atlanta region: Georgia Geologic Survey Bulletin, v. 96, 150 p.

McDowell, S. M., Miller, C.F., Fullagar, P. D., Bream, B. R., and Mapes, R. W., 2002, The Persimmon Creek Gneiss, eastern Blue Ridge, North Carolina-Georgia: Evidence for the missing Taconic arc?: Southeastern Geology, v. 41, p. 103–117.

McSween, H. Y., Jr., Speer, J. A., and Fullagar, P. D., 1991, Plutonic rocks, *in* Horton, J. W., Jr., and Zullo, V. A., eds., The Geology of the Carolinas—Carolina Geological Society 50th Anniversary Volume: Knoxville, The University of Tennessee Press, p. 109–126.

Merschat, A. J., and Hatcher, R. D., Jr., 2007, Detailed geologic mapping of the central and eastern Blue Ridge contact in the Great Balsam Mountains, western North Carolina: Geological Society of America Abstracts with Programs, v. 39, no. 2, p. 78.

Merschat, A. J., Hatcher, R. D., Jr., and Davis, T. L., 2005, The northern Inner Piedmont, southern Appalachians, USA: Kinematics of transpression and SW-directed mid-crustal flow: Journal of Structural Geology, v. 27, p. 1252–1281.

Merschat, A. J., Stahr, D. W., III, Hatcher, R. D., Jr., and Cyphers, S. R., 2006, Detailed geologic mapping in the Great Balsam and Cowee Mountains, central and eastern Blue Ridge, southwestern North Carolina: Geological Society of America Abstracts with Programs, v. 38, no. 7, p. 166.

Merschat, A. J., Stahr, D. W., III, Hatcher, R. D., Jr., 2007, The Chattahoochee fault, USA: An Appalachian Ordovician terrane boundary reactivated in the Late Devonian and Early Carboniferous: The Geological Society, Continental Tectonics and Mountain Building Programme with Abstracts.

Merschat, C. E., 1977, Geologic map and mineral resources summary of the Mars Hill quadrangle, North Carolina: North Carolina Geological Survey, scale 1:24,000.

Merschat, C. E., 1993, Geologic map and mineral resources summary of the Barnardsville, North Carolina: North Carolina Geological Survey, scale 1:24,000.

Merschat, C. E., Carter, M. W., and Wooten, R. M., 2003, Bedrock geologic map of Gorges State Park, Transylvania County, North Carolina: North Carolina Geological Survey GMS–10A, scale 1:12,000.

Merschat, C. E., and Cattanach, B. L., 2008, Bedrock geologic map of the west half of the Asheville 1:100,000-scale quadrangle, North Carolina and Tennessee: North Carolina Geological Survey, scale 1:100,000.

Merschat, C. E., and Wiener, L. S., 1988, Geology of the Sandymush and Canton Quadrangles, North Carolina: Raleigh, North Carolina Geological Survey Bulletin 90, 1:24,000 scale, 66 p.

Merschat, C. E., Cattanach, B. L., Carter, M. W., and Wiener, L. S., 2006, Geology of the Mesoproterozoic basement and younger cover rocks in the west half of the Asheville 100,000 quadrangle, North Carolina and Tennessee—An updated look, *in* Labotka, T. L., and Hatcher, R. D., Jr., eds., Geological Society of America Southeastern Section meeting Field Trip Guidebook: Knoxville, Tennessee, University of Tennessee, p. 129–184.

Miller, B. V., Stewart, K. G., Miller, C. F., and Thomas, C. W., 2000, U-Pb ages from the Bakersville, North Carolina eclogite: Taconian eclogite metamorphism followed by Acadian and Alleghanian cooling: Geological Society of America Abstracts with Programs, v. 32, no. 2, p. 62.

Miller, B. V., Fetter, A. H., and Stewart, K. G., 2006, Plutonism in three orogenic pulses, eastern Blue Ridge Province, southern Appalachians: Geological Society of America Bulletin, v. 118, p. 171–184.

Miller, C. F., Fullagar, P. D., Sando, T. W., Kish, S. A., Solomon, G. C., Russell, G. S., and Steltenpohl, L. F. W., 1997, Low-potassium, trondhjemitic to granodioritic plutonism in the eastern Blue Ridge, southwestern North Carolina-northeastern

Georgia, *in* Sinha, A. K., Whalen, J. B., and Hogan, J. P., eds., The nature of magmatism in the Appalachian orogen: Boulder, Colorado, Geological Society of America Memoir 191, p. 235–254.

Miller, C. F., Hatcher, R. D., Jr., Harrison, T. M., Coath, C. D., and Gorisch, E. B., 1998, Cryptic crustal events elucidated through zone imaging and ion microprobe studies of zircon, southern Appalachian blue Ridge, North Carolina-Georgia: Geology, v. 26, p. 419–422.

Miller, C. F., Hatcher, R. D., Jr., Ayers, J. C., Coath, C. D., and Harrison, T. M., 2000b, Age and zircon inheritance of eastern Blue Ridge plutons, southwestern North Carolina and Northeastern Georgia, with implications for magma history and evolution of the southern Appalachian orogen: American Journal of Science, v. 300, p. 142–172.

Moecher, D. P., Tracy, R. J., and Anderson, E. D., 2003, Taconian metamorphism in eastern Great Smoky Mountains inferred from U–Th–Pb monazite chemical ages: Geological Society of America Abstracts with Programs, v. 35, no. 1, p. 20.

Moecher, D. P., Samson, S. D., and Miller, C. F., 2004, Precise time and conditions of peak Taconian granulite facies metamorphism in the southern Appalachian orogen, USA, with implications for zircon behavior during crustal melting events: Journal of Geology, v. 112, p. 289–304.

Moecher, D. P., Massey, M. A., and Tracy, R. J., 2005, Timing and pattern of metamorphism in the western and central Blue Ridge, TN and NC: Status and outstanding problems, *in* Hatcher, R. D., Jr., and Merschat, A. J., eds., Blue Ridge geology geotraverse east of the Great Smoky Mountains National Park, western North Carolina: Carolina Geological Society Guidebook, North Carolina Geological Survey, p. 57–66.

Montes, C., 1997, The Greenbrier and Hayesville faults in western North Carolina [M.S. thesis]: Knoxville, University of Tennessee, 145 p.

Naeser, C. W., Naeser, N. D., and Southworth, S., 2005, Tracking across the southern Appalachians, *in* Hatcher, R. D., Jr., and Merschat, A. J., eds., Blue Ridge geology geotraverse east of the Great Smoky Mountains National Park, western North Carolina: Carolina Geological Society Guidebook, North Carolina Geological Survey, p.67–72.

Nelson, A. E., 1982, Geologic map of the Tray Mountain Roadless Area, northern Georgia: U. S. Geological Survey Miscellaneous Field Studies Map MF-1347-A, scale 1:30,000.

Nelson, A. E., Horton, J. W., and Clarke, J. W., 1998, Geologic map of the Greenville 1ºx2º quadrangle, Georgia, South Carolina, and North Carolina: U.S. Geological Survey Map I-2175, scale 1:250,000.

Ownby, S. E., Miller, C. F., Berquist, P. J., Carrigan, C. W., Wooden, J. L., and Fullagar, P. D., 2004, U-Pb geochronology and geochemistry of a portion of the Mars Hill terrane, North Carolina–Tennessee: Constraints on origin, history, and tectonic assembly, *in* Tollo, R. P., Corriveau, L., McLelland, J., and Bartholomew, M. J., eds., Proterozoic evolution of the Grenville orogen in North America: Boulder, Colorado, Geological Society of America Memoir 197, p. 609–632.

Pratt, J. H., and Lewis, J. V., 1905, Corundum and the peridotites of western North Carolina: North Carolina Geological Survey, v. 1, 464 p.

Petty, S. M., 1982, The geology of the Laurel Creek mafic-ultramafic complex in northeast Georgia: Intrusive complex or ophiolite? [M.S. thesis]: Tallahassee, Florida, Florida State University, 147 p.

Power, W. R., and Forrest, J. T., 1971, Stratigraphy and structure of the Murphy belt, North Carolina: Carolina Geological Society Field Trip Guidebook, 29 p.

Prowell, D. C., and Christopher, R. A., 2000, The last Appalachian orogeny: Evidence for Cenozoic tectonism and uplift of mountains in the eastern United States: Geological Society of America Abstracts with Programs, v. 32, no. 2, p. A–67.

Quinn, M. J., 1991, Two lithotectonic boundaries in western North Carolina: Geologic interpretation of a region surrounding Sylva, Jackson County [unpublished M.S. thesis]: Knoxville, University of Tennessee, 223 p.

Rankin, D. W., 1975, The continental margin of eastern North America in the southern Appalachians: The opening and closing of the proto-Atlantic Ocean: American Journal of Science, v. 275-A, p. 298–336.

Rankin, D. W., Espenshade, G. J., and Neuman, R. B., 1972, Geologic map of the west half of the Winston-Salem quadrangle, North Carolina, Virginia, and Tennessee. U. S. Geological Survey Map I-709-A, scale 1:250,000.

Rast, N., and Kohles, K. M., 1986, The origin of the Ocoee Supergroup: American Journal of Science, v. 286, p. 593–616.

Raymond, L. A., Yurkovich, S. P., and McKinney, M., 1989, Block-in-matrix structures in the North Carolina Blue Ridge belt and their significance for the tectonic history of the southern Appalachian orogen, *in* Horton, J. W., Jr., and Rast, N., eds., Mélanges: Boulder, Colorado, Geological Society of America Special Paper, 228, p. 195–215.

Raymond, L. A., Swanson, S. E., Allan, J. F., and Love, A. B., 2003, Cr-spinel compositions, metadunite petrology, and the petrotectonic history of the Blue

Ridge ophiolites, southern Appalachian orogen, USA, *in* Dilek, Y., and Bobinson, P. T., eds., Ophiolites in Earth History: Geological Society of London Special Publication 218, p. 253–277.

Raymond, L. A., Yurkovich, S. P., and McKinney, M., 1989, Block-in-matrix structures in the North Carolina Blue Ridge belt and their significance for the tectonic history of the southern Appalachian orogen, *in* Horton, J. W., Jr., and Rast, N., eds., Mélanges and olistostromes of the U.S. Appalachians: Geological Society of America Special Paper 228, p. 195–215.

Rubatto, D., and Hermann, J., 2007, Zircon behavior in deeply subducted rocks: Elements, v. 3, p 31–35.

Settles, D. J., 2002, Defining the Hayesville-Soque River and Allatoona faults and an Ordovician arc assemblage within the central Blue Ridge northwest of Dahlonega, Georgia [unpublished M.S. thesis]: Knoxville, University of Tennessee, 148 p.

Southworth, S., Schultz, A., and Denenny, D., 2005, Geologic map of the Great Smoky Mountains National Park Region, Tennessee and North Carolina: U.S. Geological Survey Open File Report 2005–2115, scale 1:100,000.

Stahr, D. W., III., 2007, Tectonometamorphic evolution of the eastern Blue Ridge: Differentiating multiple Paleozoic orogenic pulses in the Glenville and Big Ridge quadrangles, southwestern North Carolina [unpublished MS thesis]: Knoxville, Tennessee, University of Tennessee, 263 p.

Stahr, D. W., III, Hatcher, R. D., Jr., Miller, C. F., and Wooden, J. L., 2006, Alleghanian deformation in the Georgia and North Carolina eastern Blue Ridge: Insights from pluton ages and fabrics: Geological Society of America Abstracts with Programs, v. 38, no. 3, p. 20.

Steltenpohl, M. G., 2005, An introduction to the terranes of the southernmost Appalachians of Alabama and Georgia, *in* Steltenpohl, M. G., ed., Southernmost Appalachian terranes, Alabama and Georgia: Southeastern Section of the Geological Society of America Field Trip Guidebook, p. 1–18.

Swanson, S. E., Raymond, L. A., Warner, R. D., Ryan, J. G., Yurkovich, S. P., and Peterson, V. L., 2005, Petrotectonics of mafic and ultramafic rocks in Blue Ridge terranes of western North Carolina and northern Georgia, *in* Hatcher, R. D., Jr., and Merschat, A. J., eds., Blue Ridge geology geotraverse east of the Great Smoky Mountains National Park, western North Carolina: Carolina Geological Society Guidebook, North Carolina Geological Survey, p. 73–90.

Thomas, C. W., 2001, Origins of ultramafic complexes of the eastern Blue Ridge province, southern Appalachians: Geochronological and geochemical constraints [M.S. thesis]: Nashville, Tennessee, Vanderbilt University, 154 p.

Trupe, C. H., Stewart, K. G., Adams, M. G., Waters, C. L., Miller, B. V., and Hewitt, L. K., 2003, The Burnsville fault: Evidence for the timing and kinematics of southern Appalachian Acadian dextral transform tectonics: Geological Society of America Bulletin, v. 115, p. 1365–1376.

Tull, J. F., 1980, Overview of the sequence and timing of deformational events in the southern Appalachians: Evidence from the crystalline rocks North Carolina to Alabama, *in* Wones, D. R., ed., "The Caledonides in the USA" IGCP project 27: Caledonide orogen: Blacksburg, Virginia, Memoir 2, p. 167–177.

Tull, J. F., Ausich, W. I., Groszos, M. S., and Thompson, T. W., 1992, Appalachian Blue Ridge cover sequence ranges at least into the Ordovician: Geology, v. 21, p. 215–218.

Varnell, M. G., in progress, Geologic map of the Lake Toxaway and east half of the Big Ridge 7.5-minute quadrangles, North Carolina.

Varnell, M. G., Hatcher, R. D., Jr., Merschat, A. J., and Wooden, J. L., 2008, Limits on timing of deformation and plutonism in the eastern Blue Ridge, southwestern North Carolina, from Geologic mapping and U-Pb zircon geochronology: Geological Society of America Abstracts with Programs, v. 40, no. 4, p. 28.

Vauchez, A. R., and Dallmeyer, R. D., 1989, Polyphase tectonic evolution of the Hayesville fault, Georgia–North Carolina: Geological Society of America Abstracts with Programs, v. 21, no. 3, p. 63.

Wiener, L. S., and Merschat, C. E., 1992, Geologic map of southwestern North Carolina including adjoining southeastern Tennessee and northern Georgia: North Carolina Geological Survey, scale 1:250,000.

Williams, H., and Hatcher, R. D., Jr., 1983, Appalachian suspect terranes, *in* Hatcher, R. D., Jr., Williams, H., and Zeitz, I., D., eds., Contributions to the tectonics and geophysics of mountain chains: Geological Society of America Memoir 158, p. 33–53.

PART III

Thrice-Baked Appalachia: Delimiting the temporal and spatial distribution of Paleozoic metamorphism in the southern Appalachian Blue Ridge and Inner Piedmont with SHRIMP U-Pb ages of metamorphic zircon

Part III is a spin-off from several recent SHRIMP U-Pb zircon geochronology studies in the Blue Ridge and Inner Piedmont. Metamorphic zircon ages were compiled from various studies and used address the age and distribution of high-temperature Paleozoic metamorphism. My coauthors are Brendan R. Bream, Robert D. Hatcher, Jr., Calvin F. Miller, and Charles W. Carrigan. A modified version of the manuscript will be submitted to a peer-reviewed journal later this year. My contributions include sample and data collection, compilation of metamorphic isograd map and published mineral ages, synthesis and interpretation of the data, and most of the writing.

ABSTRACT

The polydeformed, crystalline southern Appalachians consist of dominantly amphibolite-facies rocks with several sillimanite grade metamorphic highs, yet ambiguity exists regarding the areal extent and timing of peak metamorphism. This study presents SHRIMP U-Pb zircon rim ages from twenty-five samples across the Blue Ridge and Inner Piedmont to help delimit the timing and spatial extent of the superposed metamorphisms. Samples included both paragneisses and orthogneisses. Zircons are subhedral to anhedral, with occasional soccer ball-shaped morphologies. Zircon rims vary from 10–40 μm and are bright white, or dark gray to black in CL. Rims are mostly unzoned, and truncate and/or embay interior oscillatory zoning. Results of $^{206}Pb/^{238}U$ ages from 85 analyses range from 700–300 Ma and define a bimodal distribution with 95 percent of the data between 500–300 Ma. Ages greater than 500 Ma represent significant overlap with older zircon interiors. Th/U ratios range from 0.01–1.2, with the majority less than 0.1. Relative probability plots of the data define peaks at 460, 450, 425, 389, 362, 344, and 325 Ma. The following can be recognized by comparing the spatial occurrence of zircon rim ages from separate samples with metamorphic isograds and other published reliable ages of metamorphism. (1) All 460–450 Ma ages occur in the western and central Blue Ridge, and define a continuous section from greenschist to granulite facies that represents the intact Taconic core. (2) The Inner Piedmont contains 420–325 Ma zircon rim ages with peaks at 389, 362, 344, and 325 Ma and represents the Neoacadian metamorphic core. (3) The eastern Blue Ridge contains evidence of three possible tectonothermal events: 460 Ma, 360–340 Ma and 320 Ma. Implications for terrane accretion suggest that the central Blue Ridge terranes were accreted to the western Blue Ridge and metamorphosed during the Taconian orogeny. The eastern Blue Ridge/Tugaloo terrane may have also been affected by the Taconic orogeny, although no Ordovician ziron rims were analyzed. Published U-Pb ages of eclogite and granitoids, and Sm-Nd and Rb-Sr

mineral ages sugges that a Taconic event affected the terrane. The lack of a pervasive overprinting 360–350 Ma high-temperature metamorphism in the Carolina superterrane indicates it could not have been accreted prior to the Devonian. Instead, our data indicate that the Carolina superterrane was accreted during the Late Devonian to early Mississippian producing high-temperature metamorphism and migmatization of the Inner Piedmont and eastern Blue Ridge.

INTRODUCTION

Resolving the timing and areal extent of metamorphism is critical to unraveling the tectonic evolution of any orogen or mountain belt. Common thermochronometers employed to address orogenic histories include ^{40}Ar-^{39}Ar ages of muscovite, biotite, and hornblende; apatite and zircon fission tracks; Rb-Sr in garnet; and Sm-Nd in garnet and hornblende. Low closure temperatures (300 ºC–550 ºC) limit many thermochronometers to a cooling or uplift age that usually does not correspond to peak metamorphism in high-grade terranes. Additionally, overprinting events can reset thermochronometers and commonly record only the latest event. Application of these thermochronometers to various modern and ancient orogens has generated significant information (e.g., Dallmeyer et al., 1986; Goldberg and Dallmeyer, 1997; Wang et al., 2006; Robinson et al., 2007), but with often mixed results regarding actual timing of peak metamorphism.

Thermochronometers with high closure temperatures (>550ºC) such as sphene, monazite, and zircon can be used to delimit timing of near-peak metamorphism. Polyphase orogenic histories often produce complex growth patterns that can hinder the use of these minerals to resolve the timing of metamorphism (Harley et al., 2007); therefore, a combination of small spot size and detailed images or zoning maps are required. Sensitive High-Resolution Ion Microprobes (SHRIMP) provide the small spot size (20–40μm), precision, and accuracy required to analyze specific zones and to resolve different growth stages in a single mineral grain. Diffusion of Pb in zircon occurs at temperatures greater than 700ºC (Cherniak and Watson, 2000, 2003), which is significantly higher than closure temperatures of ^{40}Ar-^{39}Ar of muscovite, biotite, and hornblende, Sm-Nd, and Rb-Sr in garnet and hornblende. Furthermore, the high zircon closure temperature resists resetting by later lower-temperature events and preserves the time of earlier metamorphisms (Harley et al., 2007). Although zircon has a high closure temperature, in high-temperature metamorphic terranes multiple reactions and processes may produce pre-peak, peak, and post-peak metamorphic zircons with ages that often span 25 m.y. or more (Harley et al. 2007). Zircon zoning textures and patterns provide

insight into the processes related to their formation and relative position of formation on a P-T path, but are not conclusive (Harley et al., 2007). Minimum temperatures associated with zircon formation are approximately 650 ºC–750 ºC for formation of new zircon in late melts and fluids. High zircon closure temperatures suggest that rim formation likely coincides to near peak metamorphic conditions, and provides a tool to measure time of near peak metamorphism.

The southern Appalachian crystalline core consists of multiple amphibolite grade metamorphic belts, yet controversy still surrounds the timing of metamorphism (e.g., Carpenter, 1970; Drake et al., 1989; Osberg et al., 1989; Butler, 1991; Kohn and Malloy, 2004; Moecher et al., 2004, 2005; B. Miller et al., 2006; Corrie and Kohn, 2007). This study presents new ion microprobe U-Pb ages of zircon rims from 25 amphibolite to granulite facies samples from the southern Appalachian Blue Ridge and Inner Piedmont (Fig. 3–1; Table 3–1) and attempts to integrate these with existing data. The data were collected during several previous geochronologic studies that focused on the age of pre-Paleozoic Grenvillian basement massifs (Carrigan et al., 2003; Ownby et al., 2004), Paleozoic plutonism (Bream, 2003; Gatewood, 2007), and provenance of Blue Ridge and Inner Piedmont metasedimentary rocks (Bream, 2002, 2003; Bream et al., 2004; Gatewood, 2007; Merschat et al., 2007). Our objectives are to delimit the timing of near-peak metamorphism in the Blue Ridge and Inner Piedmont, define domains of common tectonothermal events, and combine spatial and temporal patterns of regional metamorphism to address timing of orogeny and terrane accretion in the southern Appalachian crystalline core.

TECTONIC SETTING

The southern Appalachian orogen is composed of undeformed Paleozoic strata, a late Paleozoic foreland fold-thrust belt, and several crystalline cores that are a collage of polydeformed terranes. The composite crystalline core (the focus of this study) consists of various Laurentian and suspect terranes of the Blue Ridge and Inner Piedmont, sandwiched between the foreland fold-thrust belt (Valley and Ridge) and the exotic, peri-Gondwanan Carolina superterrane (Williams and Hatcher, 1982; Hatcher et al., 2007; Fig. 3–1). These terranes are exposed in the composite Blue Ridge-Inner Piedmont megathrust sheet (Hatcher and Hooper, 1992). Erosion following post-Pangea-breakup has exposed crystalline rocks that were once buried tens of kilometers below the surface during several peaks of Paleozoic orogenesis.

Figure 3–1. Simplified tectonic map of the southern Appalachians showing the location of the Inner Piedmont, and the Tugaloo (lavender) and Cat Square (blue) terranes. The Laurentian platform contains the Alleghanian foreland fold-thrust belt driven in front of the Blue Ridge-Piedmont megathrust sheet (the Laurentian margin, gold with red inliers of Grenvillian, not necessarily Laurentian Grenville, and older inherited crust), and all components to the east. All terranes west of the Cat Square terrane have a Laurentian source (Bream et al., 2004). Cat Square terrane contains Siluro-Devonian metasedimentary rocks with a mixed Laurentian and Peri-Gondwanan source. Carolina superterrane is Peri-Gondwanan and exotic to Laurentia. BCF– Brindle Creek fault. BF–Burnsville fault. Cart. terr.–Cartoogechaye terrane. CHMF–Chattahoochee-Holland Mountain fault. Cow. terr.–Cowrock terrane. DGB–Dahlonega gold belt. FF–Forbush fault. GLF–Gossan Lead fault. GMW–Grandfather Mountain window. MH–Mars Hill terrane. NW–Newton window. SRA–Smith River allochthon, an outlier of Carolina superterrane rocks. SMW–Sauratown Mountains window. PMW–Pine Mountain window. Light gray–Probable western Tugaloo terrane rocks in Alabama and Georgia. Purple–Ordovician Elkahatchee Quartz Diorite. A–Athens. H–Hickory. S–Statesville. WS–Winston–Salem.

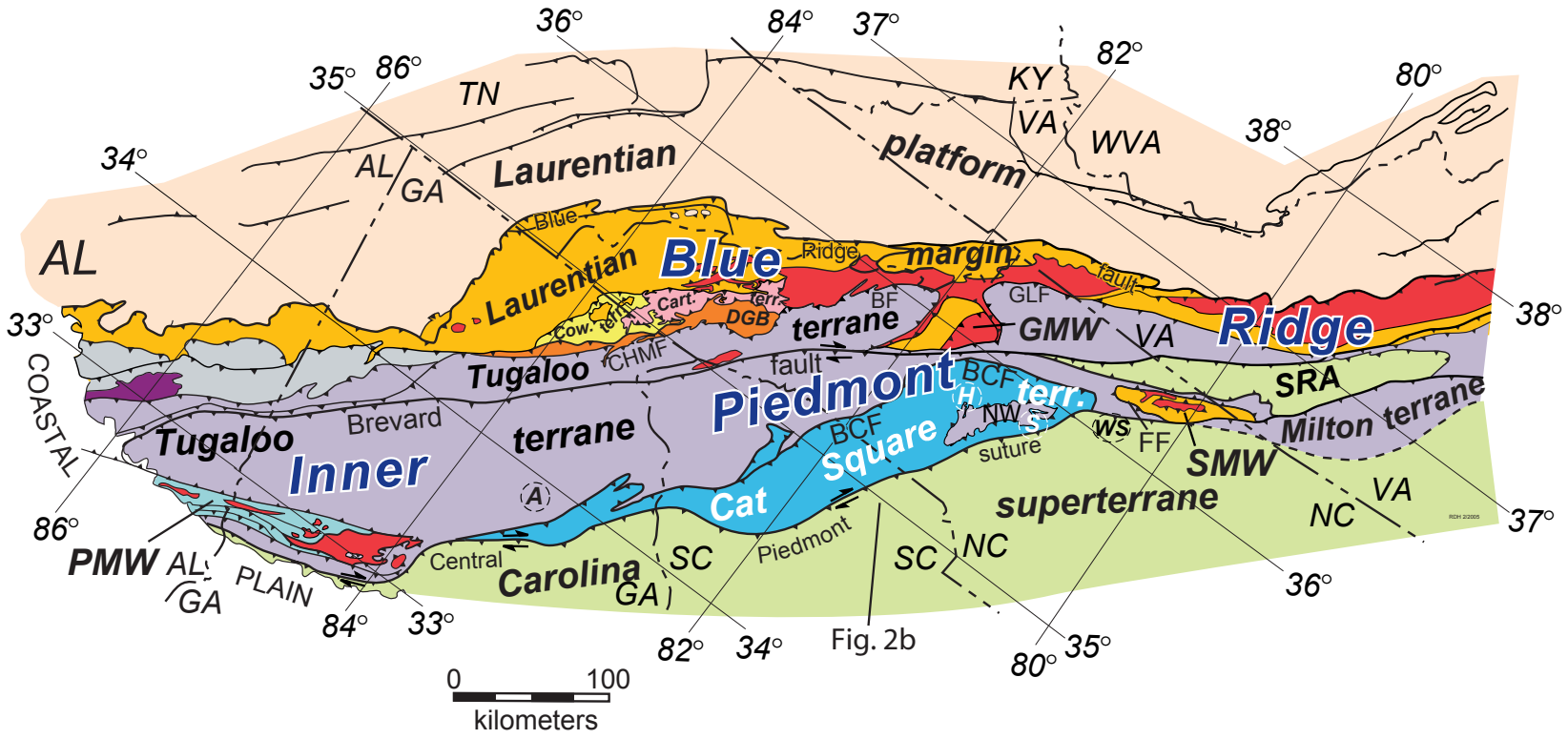
36°
84°
37°
82°
80°
35°
86°
TN
KY
VA
WVA
38°
34°
AL
GA
Laurentian
platform
AL
Blue
Ridge
margin
Laurentian
Blue
fault
Cart.
terr.
DGB
BF
GLF
33°
Cow. terr.
terrane
GMW
VA
Ridge
38°
COASTAL
Tugaloo
CHMF
fault
Piedmont
BCF
terr.
SRA
Brevard
Tugaloo
terrane
Inner
BCF
Square
NW
SE
WS
FF
Milton terrane
suture
SMW
Cat
superterrane
VA
NC
37°
86°
PMW
AL
GA
PLAIN
Central
Carolina
SC
GA
Piedmont
SC
NC
36°
84°
33°
82°
34°
Fig. 2b
80°
35°
0
100
kilometers

Table 3–1. Sample locations and descritpions.

Sample	Belt	Terrane	Formation or unit name	7.5-minute	County (State)	Latitude (°N)	Longitude (°W)	Lithology	Type	Metamorphic zone	Mineral assemblage*	Migmatite**
central Blue Ridge												
COLRAB	cBR	Cowrock	Coleman River Formation	Hightower Bald	Rabun (GA)	34.9076	-83.6120	Bi gn	Detrital	Sillimanite I	qtz-plag-akf	L
CGM	cBR	Cowrock	Coweeta group	Shooting Creek	Macon (NC)	35.0588	-83.6203	siliceous marble	Detrital	Sillimanite I	cc-qtz-bi-gar	L
RS711	cBR	Cartoogechaye	Rainbow Springs quartzite	Rainbow Springs	Macon (NC)	35.0111	-83.6189	quartzite	Detrital	Sillimanite I	qtz-plag-rut	L
RS 787	cBR	Cartoogechaye	felsic gneiss	Rainbow Springs	Macon (NC)	35.0952	-83.5564	mig. bi felsic gn	Detrital	Sillimanite I	gar-bi-qtz-plag-akf	L
W18	cBR	Cartoogechaye	Unnamed migmatitic biotite gneiss	Waynesville	Haywood (NC)	35.4709	-82.8850	Mig. Bi gn	Detrital	Migmatite	bi-qtz-plag-hbl	L, Ag
Dahlonega gold belt												
OTD	cBR	DGB	Otto Formation	Campbell Mountain	Lumpkin (GA)	34.5597	-84.0744	metasandstone	Detrital	Kyanite-Staurolite	ms-bi-qtz-plag-akf	L
HAZ2MSS	cBR	DGB	Otto Formation	Hazelwood	Haywood (NC)	35.4308	-83.0930	mgw, metacgl, and schist	Detrital	Sillimanite I	ms-bi-qtz-plag-akf-sil	L
eastern Blue Ridge												
BOCAT	eBR	Tugaloo	Tallulah Falls-Ashe Formation (metagraywacke member)	Asheville	Buncombe (NC)	35.5997	-82.5377	bi gn/mgw	Detrital	Sillimanite I	ms-bi-qtz-plag-akf	L
BTB3	eBR	Tugaloo	Toxaway gneiss	Reid	Oconee (SC)	35.0067	-82.9933	bi orthogn	Igneous	Kyanite	bi-qtz-plag	
GMA2	eBR	Tugaloo	Toxaway gneiss	Reid	Oconee (SC)	35.0067	-82.9933	bi orthogn	Igneous	Kyanite	bi-qtz-plag	
TOX, TOX-1B	eBR	Tugaloo	Toxaway gneiss	Cashiers	Oconee (SC)	35.0026	-83.0429	bi orthogn	Igneous	Kyanite	bi-qtz-plag	
TXFL	eBR	Tugaloo	Toxaway gneiss	Reid	Transylvania (NC)	35.1200	-82.9250	bi orthogn	Igneous	Kyanite	bi-qtz-plag	
western Inner Piedmont												
VM1782	wIP	Tugaloo	Dysartsville Tonalite	Glenwood	McDowell (NC)	35.5491	-81.9619	tonalite gn	Igneous	Sillimanite I	qtz-plag-bi-hbl	L
KC-1	wIP	Tugaloo	Hibriten mylonite	Kings Creek	Caldwell (NC)	35.9067	-81.4906	mylo ineq bi gn	Igneous	Sillimanite I	qtz-plag-bi	L
KEOTF	wIP	Tugaloo	Tallulah Falls-Ashe Formation (aluminous schist member)	Seneca	Oconee (SC)	34.6963	-82.8789	schist	Detrital	Sillimanite I	ms-bi-gar-sil-qtz	L
LVQ1	wIP	Tugaloo	Lenoir Quarry migmatite	Kings Creek	Caldwell (NC)	35.9308	-81.4794	mig am	Igneous	Sillimanite I	hbl-plag	L, Ag
MV-668	wIP	Tugaloo	Hibriten mylonite	Moravian Falls	Wilkes (NC)	36.0733	-81.1964	mylo ineq bi gn	Igneous	Sillimanite I	qtz-plag-bi	L
POMTN	wIP	Tugaloo	Poor Mountain Quartzite	Glenwood	McDowell (NC)	35.6048	-81.9548	am	Igneous	Sillimanite I	hbl-plag	L
SMTF	wIP	Tugaloo	Tallulah Falls-Ashe Formation (metagraywacke member)	Copeland	Surry (NC)	36.2753	-80.7316	bi gn/mgw	Detrital	Kyanite	ms-bi-qtz-plag-akf	L
UTF85	wIP	Tugaloo	Tallulah Falls-Ashe Formation (metagraywacke member)	Marion East	McDowell (NC)	35.6443	-81.9865	bi gn/mgw	Detrital	Kyanite	ms-bi-qtz-plag-akf	L
ZIRCONIA	wIP	Tugaloo	Zirconia Pegmatite	Zirconia	Henderson (NC)	35.2329	-82.4460	granitic peg	Igneous	???		L
Newton Window												
SW6	NW	Tugaloo	Tallulah Falls Fm.	Statesville West	Irdell (NC)	35.8038	-80.9217	mig bi gn	Detrital	Sillimanite I	ms-bi-qtz-plag-akf	L
WTR29	NW	Tugaloo	mylonitic orthogneiss	Reepsville	Lincoln (NC)	34.5556	-81.2939	mylo augen gn	Igneous	Sillimnaite I	bi-qtz-plag	L
R29	NW	Tugaloo	Reepsville gneiss	Reepsville	Lincoln (NC)	35.5155	-81.3540	ineq bi gn	Igneous	Sillimnaite I	ms-bi-qtz-plag-akf	L
eastern Inner Piedmont												
BCTF	eIP	Cat Square	unassigned mgw	Benn Knob	Rutherford (NC)	35.5392	-81.7024	bi gn/mgw	Detrital	Sillimanite II	ms-bi-qtz-plag-akf-hbl	L
GR1	eIP	Cat Square	unassigned mgw	Greer	Spartanburg (SC)	34.9166	-82.1389	bi gn/mgw	Detrital	Sillimanite I	ms-bi-qtz-plag-akf-hbl	L
EL2	eIP	Cat Square	unassigned mgw	Ellendale	Alexander (NC)	35.9519	-81.3242	Mig. metagraywacke	Detrital	Sillimanite II	ms-bi-qtz-plag-akf-hbl	L
MV336	eIP	Cat Square	unassigned mgw	Moravian Falls	Wilkes (NC)	36.0408	-81.1353	bi gn/mgw	Detrital	Sillimanite II	ms-bi-qtz-plag-akf-hbl	L

NAD27 CONUS coordinates

* Mineral assemblage abbrevations are akf-alkali feldspar; bi-biotite; cc-calcite; gar-garnet; hbl-hornblende; ms-muscovite; plag-plagioclase; rut - rutile; and sil- sillimanite.

** Migmatite abbreviations are L-stromatic or layered; and Ag-agmatite.

The orogen was assembled over six different orogenies culminating with the Late Carboniferous-Permian Alleghanian orogeny and formation of supercontinent Pangea (Hatcher, 1989, 2002a; Hatcher et al., 2007). These six orogenies extend from the Precambrian to late Paleozoic and include: Grenville, 1.25–0.9 Ga; Virgilina, 510 Ma; Taconian, 480–460 Ma; Salinian, 420–410 Ma; Acadian-Neoacadian, 410–380 Ma and 360–350 Ma; and Alleghanian, 320–260 Ma. The Blue Ridge is composed of low- to medium- to high-grade metamorphic rocks with inliers of older relict Grenville and pre-Grenville (Mars Hill terrane) metamorphism reaching granulite facies. The Inner Piedmont consists of high-grade rocks flanked by low- to medium-grade rocks, with Grenville basement exposed in the Newton, Sauratown Mountains, and Pine Mountain windows. Excluding the various basement massifs with relict Grenville metamorphism, regional metamorphism in the southern Appalachian metamorphic core is variably attributed to the three Paleozoic orogenies: Taconic, Acadian-Neoacadian, and Alleghanian (Hatcher, 1989; Butler, 1991; Hatcher and Goldberg, 1991; Hatcher et al., 2007). Laurentian metamorphism is flanked by older, exotic Virgilina metamorphic rocks of the Carolina superterrane, east of the central Piedmont suture (Dennis and Wright, 1997a; Hibbard et al., 2002). Younger metamorphism of the Alleghanian core (Kiokee-Raleigh-Goochland belts) overlaps Virgilina metamorphism to the east and extends beneath the Coastal Plain (Horton et al., 1991).

The Blue Ridge of western North Carolina, northwestern South Carolina, northeastern Georgia, and eastern Tennessee can be separated into western, central, and eastern subdivisions. Central Blue Ridge terranes end in west Georgia, and only the western and eastern division are recognized southward into Alabama (Steltenpohl, 2005). The central and eastern Blue Ridge and Inner Piedmont consist of suspect and peri-Laurentian terranes accreted to the western Blue Ridge Laurentian margin (Fig. 3–1). The Inner Piedmont is a composite terrane separated from the eastern Blue Ridge by the Brevard fault zone.

The western Blue Ridge/Laurentian margin extends from the Great Smoky fault to the Hayesville-Gossan Lead faults, and consists of Neoproterozoic to Ordovician rocks deposited nonconformably on ~1.15 Ga Grenvillian gneisses. The western Blue Ridge is cored by a thick sequence of Ocoee Super Group rocks flanked by younger rocks exposed in frontal duplexes exposing lower Cambrian Chilhowee Group rocks to the west and the sinuous Murphy syncline to the east. An Ordovician crinoid stem was obtained from the lower Mineral Bluff Formation, which cores the Murphy syncline (Tull and Groszos, 1988). The southern equivalent of the western Blue Ridge in southwestern

Georgia and Alabama is the Talladega belt, which is bound by the Talladega-Cartersville fault to the west and Hollins line fault to the east (Tull et al., 1988; Steltenpohl, 2005; McClellan et al., 2007). The Talladega belt consists of a sequence of Neoproterozoic to lower Cambrian clastics, Cambro-Orodvician carbonates, and Devonian to Mississippian clastics (Tull et al., 1988; Gastaldo et al., 1993; Steltenpohl, 2005). Fossils constrain the age and Laurentian affinity of both the middle Cambro-Ordovician carbonate package and the upper clastic units of Devonian to Mississippian age (Tull et al., 1988; Gastaldo et al., 1993).

The central Blue Ridge extends from near Waynesville, North Carolina southwest to near the Alabama-Georgia state line and consists of an antiform-synform thrust stack between the Hayesville and Chattahoochee-Holland Mountain-Burnsville-Gossan Lead faults. The Cowrock and Cartoogechaye terranes rest synformally above and to the west of the linear, antiformal Dahlonega gold belt. The occurrence of Grenville basement and paucity of mafic and ultramafic rocks in the western Blue Ridge, compared with the abundance of mafic and ultramafic rocks in the Cowrock and Cartoogechaye terranes, led Hatcher (1978) to suggest that the Hayesville fault represents a suture. In northeastern Georgia, the Hayesville fault wraps around the southern end of Cowrock terrane and truncates the Allatoona fault (Settles, 2002). From northeastern Georgia to the disappearance of the Blue Ridge beneath the Alabama Coastal Plain sediments, the suture is marked by three faults: Allatoona, Goodwater-Enitachopoco, and Hollins Line Faults (Fig. 3–1).

East of the Chattahoochee-Holland Mountain-Burnsville-Gossan Lead fault, the eastern Blue Ridge consists of the peri-Laurentian Tugaloo terrane, which continues across the Brevard fault zone into the Inner Piedmont (Hatcher, 2002b; Hatcher et al., 2007). The Tugaloo terrane is comprised principally of Neoproteozoic to Cambrian metasedimentary rocks of the Ashe/Tallulah Falls Formation and southern equivalents. The lithostratigraphy of the eastern Blue Ridge in southwestern Georgia and Alabama is more complicated and includes the Wedowee, Hatchet Creek, Higgins Ferry, Mad Indian, Poe Bridge, and Emuckfaw Groups (Steltenpohl, 2005). In the eastern Tugaloo/western Inner Piedmont the Ashe/Tallulah Falls Formation is unconformably overlain by Middle Ordovician biomodal volcaninc and sedimentary rocks of the Poor Mountain Formation (Hatcher, 2002b; Bream, 2003; Hatcher et al., 2007). Detrital zircon ages and Sm-Nd isotopic data indicate a Laurentian source of the Ashe/Tallulah Falls Formation (Bream et al., 2004), which is interpreted to have been deposited on oceanic crust with small massifs of Grenville continental crust (Hatcher, 1978, 1987, 1989, 2002b; Abbott

and Raymond, 1984; Hatcher et al., 2004). Tugaloo terrane rocks were intruded by Ordovician, Devonian, and Mississippian granitoids (C. Miller et al., 2000b; Mapes, 2002; Bream, 2003; B. Miller et al., 2006).

The Inner Piedmont is composed of the eastern Tugaloo terrane and the mixed Laurentian and Gondwanan affinity, Siluro-Devonian Cat Square terrane. The Cat Square terrane is juxtaposed against the Tugaloo terrane by the Brindle Creek fault (Giorgis, 1999; Hatcher, 2002b; Merschat and Kalbas, 2002; Merschat et al., 2005b). Numerous bodies of peraluminous, and megacrystic granitoids with concordant contacts with the surrounding gneisses and schists occur throughout the Cat Square terrane (Goldsmith et al., 1988; Merschat et al., 2005b). Several of the larger granitoid bodies yielded Late Devonian to Mississippian SHRIMP U-Pb ages (Giorgis et al., 2002; Mapes, 2002; Gatewood, 2007; Byars et al., 2008b).

Although the terranes of the Blue Ridge and Inner Piedmont are distinct and separable, frequently they will be referred to collectively as the western, central, and eastern Blue Ridge, and Inner Piedmont. This is to emphasize similarities in metamorphic and structural histories of the terranes and facilitate discussion by reducing lengthy lists of the terranes affected by different tectonothermal events. It is not to be interpreted as a replacement of terrane divisions. As will be the case, the combined metamorphic history and lithostratigraphy of several terranes have key bearings on resolving the metamorphic and tectonic history of the Appalachians.

METAMORPHIC ISOGRAD MAP OF THE SOUTHERN APPALACHIANS

The metamorphic isograd map presented here (Fig. 3–2) was compiled from various sources including: detailed geologic maps (1:24,000 scale or greater; Hadley and Goldsmith, 1963; Merschat and Wiener, 1988; Hopson et al., 1989; Settles, 2002; Merschat 2003), regional geologic maps (Bryant and Reed, 1970; Hadley and Nelson, 1971; Rankin et al., 1972; Espenshade et al., 1975; Goldsmith et al., 1988; Nelson et al., 1998), petrologic studies (Bentley and Neathety, 1970; Abbott and Raymond, 1984; Eckert et al., 1989), and previous compilations (Carpenter, 1970; Steltenpohl and Moore, 1988; Butler, 1991; Hatcher and Goldberg, 1991). As is customary, metamorphic grade is separated into zones based on occurrence of metamorphic index minerals separated by isograds or faults. Unfortunately, the coverage varies, and so does the certainty of the location of different isograds. Overlapping regional and detailed studies in the Blue Ridge and Inner Piedmont of North Carolina, South Carolina, northeastern Georgia, and eastern Tennessee represent the best coverage, and well delineated isograds. Coverage in

Figure 3–2. Metamorphic isograd map of the southern Appalachian Blue Ridge and Inner Piedmont compiled from various studies including (Hadley and Goldsmith, 1963; Carpenter, 1970; Hadley and Nelson, 1971; Rankin et al., 1972; Espenshade et al., 1975; Goldsmith et al., 1988; Merschat and Wiener, 1988; Steltenpohl and Moore, 1988; Eckert et al., 1989; Hopson et al., 1989; Osberg et al., 1989; Osborne et al., 1989; Butler, 1991; Hatcher and Goldberg, 1991; Nelson et al., 1998; Quinn, 1991; Settles, 2002; Higgins et al., 2003; Merschat, 2003; Tull and Holm, 2005; Hatcher and Merschat, 2006; Hatcher et al., 2007; Tull, 2007; Merschat et al., 2008). Location of zircon rim samples presented in this study are shown in white. Fault and other geologic labels are the same as Figure 3–1.

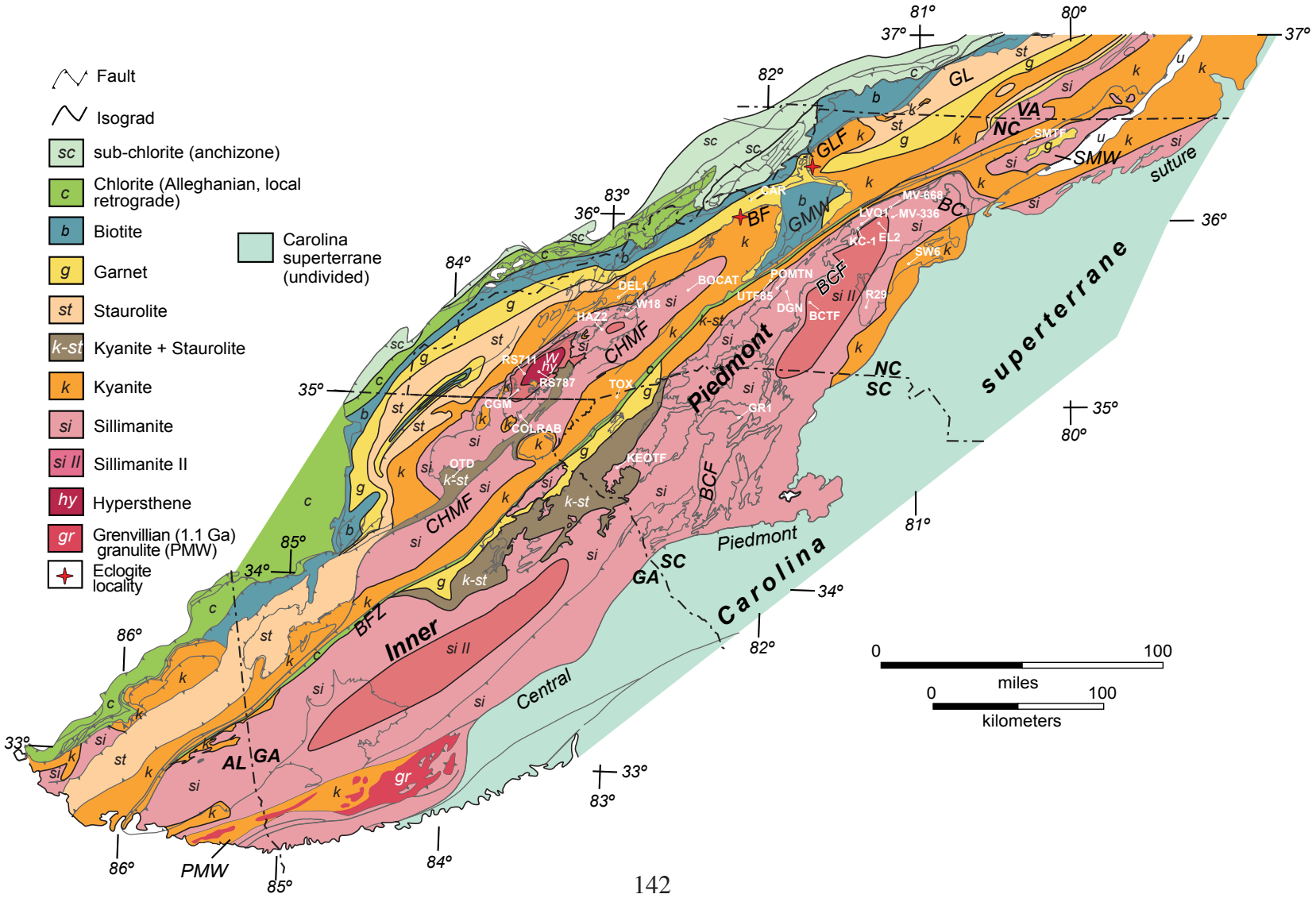
Fault
Isograd
sc sub-chlorite (anchizone)
c Chlorite (Alleghanian, local retrograde)
b Biotite
g Garnet
st Staurolite
k-st Kyanite + Staurolite
k Kyanite
si Sillimanite
si II Sillimanite II
hy Hypersthene
gr Grenvillian (1.1 Ga) granulite (PMW)
Eclogite locality
Carolina superterrane (undivided)
Piedmont
Carolina superterrane
Inner Piedmont
Central Piedmont
suture
BFZ
CHMF
BCF
GLF
SMW
GMW
BF
GL
VA
NC
SC
GA
AL
PMW
CAR
MV-668
LVQ1
MV-336
RC-1
EL2
SW6
SMT1
BC
BOCAT
POMTN
UTF85
DGN
BCTF
R29
DEL1
W18
HAZ2
RS711
RS787
TOX
CGM
COLRAB
GR1
KEOTF
OTD
0 100 miles
0 100 kilometers
81°
80°
37°
82°
83°
36°
84°
35°
34°
85°
86°
33°

Georgia and Alabama varies from detailed studies to reconnaissance, but generally lacks the multiple levels of coverage that exist to the north.

Paleozoic metamorphic grade in the Blue Ridge ranges from sub-greenschist to granulite facies. Hadley and Goldsmith (1963) first recognized a continuous progression of Barrovian isograds increasing from anchizone rocks near the Great Smoky fault to kyanite zone rocks in the western Blue Ridge. Force (1976) and Hatcher and Butler (1979) first recognized granulite facies rocks in the central Blue Ridge, and outlined their distribution based on occurrence of hypersthene (Force, 1976). Eckert et al. (1989) demonstrated the sillimanite isograd crosses the Hayesville fault into the North Carolina central Blue Ridge and surrounds a granulite facies high in the Cartoogechaye terrane. A complete Barrovian facies series progression from chlorite to the hypersthene-in iosgrad is preserved in the western and central Blue Ridge of NC-TN-GA (Eckert et al., 1989; Butler, 1991; Hatcher and Goldberg, 1991). This continuous progression of isograds in the western and central Blue Ridge is broken to the southeast by an abrupt drop across the Soque River fault to staurolite-kyanite grade in the Dahlonega gold belt in northeastern Georgia and extends southwestern North Carolina (Hopson et al., 1989), and a gradual decrease to the southwest by the Murphy syncline. In the western Blue Ridge of southwestern North Carolina and northeastern Georgia, the Murphy syncline folds the garnet to chlorite isograds and preserves chlorite grade rocks of the Mineral Bluff Formation in the axis of the syncline, suggesting post-peak formation of the syncline. At the northeast end of the Murphy syncline, however, isograds cross the axis of the fold. In western Georgia and Alabama the Talladega belt, the southern equivalent of the western Blue Ridge, remains uniformly in the chlorite zone (McClellan et al., 2007).

The eastern Blue Ridge defines a large amphibolite facies domain of kyanite and sillimanite zone rocks from southwest of the Grandfather Mountain window to Alabama. A small area of staurolite-kyanite zone has been recognized in parts of the eastern Blue Ridge/western Tugaloo terrane of southwestern North Carolina and northeastern Georgia (e.g., Stahr, 2007), but is included with the kyanite zone in Figure 3–2. From northwest Georgia into Alabama, kyanite and sillimanite zone rocks of the eastern Blue Ridge are juxtaposed against greenschist facies rocks of the Talladega belt by the Hollins Line fault (Steltenpohl and Moore, 1988). To the southeast across the Goodwater-Enitachopco fault, is a large domain of staurolite-kyanite zone rocks of the Wedowee Group overthrust by kyanite zone rocks of the Alexander City thrust sheet (Steltenpohl and Moore, 1988; Steltenpohl, 2005). The Grandfather Mountain window truncates kyanite zone rocks in the eastern Blue Ridge/western Tugaloo and exposes chlorite and biotite grade rocks

of the western Blue Ridge in several imbricate thrust sheets (Bryant and Reed, 1970). Northeast of the Grandfather Mountain window, grade decreases to garnet and staurolite zones (Rankin et al., 1972; Abbott and Raymond, 1984). Two eclogite localities have been described from the eastern Blue Ridge, located northeast and southwest of the Grandfather Mountain window (Willard and Adams, 1994; Abbot and Raymond, 1997; Abbott and Greenwood, 2001; Fig. 3–2). These small bodies are enclosed in amphibolite facies, kyanite zone rocks of the Ashe/Tallulah Falls Formation, and contain variable amounts of amphibolite facies retrogression (Willard and Adams, 1994; Abbott and Greenwood, 2001).

The Inner Piedmont and Milton terrane is the largest domain of sillimanite grade rocks in the southern Appalachians and extends from the Sauratown Mountains window near the Virginia-North Carolina border to beneath the Coastal Plain in Alabama (Figs. 3–1 and 3–2). The western boundary is marked by the multiply reactivated Brevard fault zone and 3–5 km wide zone of retrograde greenschist facies metamorphism associated with dextral shearing (Hatcher, 2001). The broad migmatitic core remains continuously at sillimanite I or higher along its length (Fig. 3–2), but grade decreases along the flanks of the Inner Piedmont. The western flank decreases from the sillimanite zone southwest of the Sauratown Mountains window in North Carolina to garnet-staurolite zone in the Chauga belt in South Carolina and northeastern Georgia (Fig. 3–2). Sillimanite and kyanite zones occur along the western flank in central Georgia and Alabama. The retrograde chlorite zone associated with the Alleghanian Brevard fault zone truncates the high-grade, staurolite, kyanite, and sillimanite isograds (Fig. 3–2; Bryant and Reed, 1970; Goldsmith et al., 1988; Hatcher, 2001). The eastern flank decreases to kyanite grade in North Carolina, but remains in the sillimanite zone along most of the length adjacent to the central Piedmont suture (Goldsmith et al., 1988; Butler, 1991; Hatcher and Goldberg, 1991; Nelson et al., 1998; Hatcher and Merschat, 2006). The central Piedmont suture consists of several fault segments that often display similar greenschist retrograde assemblages as the Brevard fault zone (Goldsmith et al., 1988; Horton and McConnell, 1991; Hibbard et al., 2002). East of the central Piedmont suture, early Cambrian metamorphism in the Carolina superterrane is considered exotic (~530 Ma, Virgilina; Butler, 1991; Dennis and Wright, 1997b; Hibbard et al., 2002), and these metamorphic zones were not compiled for this study.

Published ^{40}Ar-^{39}Ar, Sm-Nd, Rb-Sr, and U-Pb mineral ages document the complex metamorphic history of the Blue Ridge and Inner Piedmont with mineral ages varying from Ordovician, Devonian, and Mississippian periods. Whole-rock muscovite and

biotite ^{40}Ar-^{39}Ar cooling ages from the western Blue Ridge suggest Ordovician and Mississippian cooling (Connelly and Dallmeyer, 1993; Hames et al., 2007). Muscovite ^{40}Ar-^{39}Ar cooling ages from the Alabama Talladega belt yield ages of 334–320 Ma, consistent with the Mississippian plant fossils reported from the Erin slate (McClellan et al., 2007). Goldberg and Dallmeyer (1997) reported ~460 Ma Sm-Nd and Rb-Sr ages of garnet and hornblende, but ^{40}Ar-^{39}Ar ages of muscovite, biotite, and hornblende yielded Mississippian ages (360–330 Ma) from the Blue Ridge of northwestern North Carolina. North of the Grandfather Mountains window, ^{40}Ar-^{39}Ar ages of hornblende from the Ashe/Tallulah Falls Formation range from 360–327 Ma (Stokes et al., 2008). Hornblende, biotite, and muscovite ^{40}Ar-^{39}Ar ages from the Tugaloo terrane in northeastern Georgia and northwestern South Carolina record late Devonian to Mississippian cooling (360–340 Ma) (Dallmeyer, 1988). Near the Coastal Plain onlap in Alabama, ^{40}Ar-^{39}Ar muscovite and hornblende cooling ages obtained from the Tugaloo terrane range from 347–320 Ma (hornblende) and 333–327 Ma (muscovite) (Steltenpohl and Kunk, 1993; Steltenpohl et al., 2005). Rocks within and framing the Pine Mountain window yielded even younger ^{40}Ar-^{39}Ar ages of hornblende, 300–288 Ma, and muscovite, 285–276 Ma (Steltenpohl and Kunk, 1993).

The few studies reporting zircon or monazite ages indicate 460–450 Ma metamorphism in the western and central Blue Ridge in western North Carolina and eastern Tennessee (Moecher et al., 2004; Miller et al., 2006; Corrie and Kohn, 2007). Steltenpohl et al. (2008) reported a U-Pb age of zircon rim overgrowth of ~300 Ma from the Pine Mountain window, Alabama. The contrasting results between U-Pb ages, ^{40}Ar-^{39}Ar cooling temperatures, and Sm-Nd and Rb-Sr mineral ages suggest a complex, polychronic relationship of overprinting metamorphism in the southern Appalachians (Moecher et al., 2005). To resolve the complex and overprinting metamorphisms of the southern Applachians, more robust geochronometer, like zircon, is required.

SAMPLING AND METHODOLOGY

Sampling and methodology of this study are identical to the procedures of Carrigan et al. (2003) and Bream et al. (2004). Five to ten kilogram rock samples were collected from various ortho- and paragneiss units in the Blue Ridge and Inner Piedmont. Samples were crushed to less than 500 μm, and separated using a water table, heavy liquids, and Frantz magnet, yielding a final zircon concentrate fraction. Zircons were hand-picked (or randomly poured into rows for some detrital samples) and mounted in epoxy. Grains were polished to approximate center and imaged with reflected light and

cathodoluminescence (CL) to distinguish interior features, including oscillatory zoning, cores, rims, inclusions, and fractures.

Rims were analyzed during multiple sessions over seven years using either the Cameca 1270 ion microprobe at UCLA or the Sensitive High Resolution Ion Microprobe-Reverse Geometry (SHRIMP-RG) at Stanford University and U. S. Geological Survey Micro Analysis Center (SUMAC). Zircon standards, AS3 or AS57 (~1099 Ma) at UCLA, and R33 (~419 Ma), VP-10 (~1200 Ma) and RG6 (~1400 Ma) at SUMAC were routinely analyzed. A spot size of 40 μm and primary ion beam energies of 10 kV were utilized with the SHRIMP-RG. CL images acquired prior to ion microprobe analysis were used to recognize potential rims and to determine spot locations. The ion beam often overlapped the epoxy, but cores were avoided. Rim data were reduced and various corrections for common Pb (^{204}Pb-, ^{207}Pb-, and ^{208}Pb-corrected) were calculated using the computer program SQUID v. 1.02 (Ludwig, 2001). Differences in common Pb-corrected ^{206}Pb/^{238}U ages did not vary greater than $\pm 1\sigma$, and ^{204}Pb-corrected ^{206}Pb/^{238}U and ^{207}Pb/^{206}Pb ages are reported. All rims examined in this study are Paleozoic and the ^{206}Pb/^{238}U age was used for all relative probability plots and weighted averages reported.

SAMPLE DESCRIPTION AND ZIRCON MORPHOLOGY

Twenty-five samples from the Blue Ridge and Inner Piedmont (Fig. 3–2) include three Proterozoic (Grenville) basement gneisses, four Paleozoic granitoids, and the remaining eighteen are from various paragneisses that constitute the majority of the Blue Ridge and Inner Piedmont (Table 3–1). Samples are not evenly distributed over the different metamorphic zones, terranes, and belts: a consequence of this study being a derivative of several different geochronologic studies with different goals. All samples used in this study are from amphibolite and granulite facies, and kyanite to sillimanite zones. The western Blue Ridge is poorly represented in this study, because lower grade rocks were sampled for provenance studies (Bream 2002, 2003; Bream et al., 2004; Merschat et al., 2007).

All samples are from kyanite and sillimanite I and II zones, and are variably migmatitic (Table 3–1). The metapsammitic or granitic composition of most samples does not readily yield common metamorphic indicator minerals. Metapsammitic samples contain the general assemblage: quartz + plagioclase + biotite ± muscovite ± potassium feldspar ± garnet, with accessory amounts of sillimanite, kyanite, epidote/clinozoisite, hornblende, rutile, monazite and opaque minerals (magnetite, ilmenite, and iron-sulfides). Orthogneiss samples contained the assemblage: quartz + plagioclase + biotite

± potassium feldspar ± muscovite ± hornblende ± epidote/clinozoisite. Metamorphic assemblages and textures are constrained from additional samples of nearby pelitic rocks and by various detailed studies in the surrounding areas (Griffin, 1974; Hatcher and Butler, 1979; Hatcher, 1980; Eckert 1984; Eckert et al. 1989; Davis, 1993a, 1993b; Miller and Fryer, 1996; Bier et al., 2000; Bier, 2001; Settles, 2002; Merschat, 2003; Moecher et al., 2004; Gatewood, 2007; Hatcher, unpublished mapping). Blue Ridge samples are the most variable in grade and assemblage. Most samples are from sillimanite I and II zones in the central Blue Ridge near the Wayah granulite core (Fig. 3–2). A siliceous marble from the Cowrock terrane, Coweeta Group (CGM) on Chunky Gal Mountain, contains the assemblage: calcite + plagioclase + quartz + garnet + clinopyroxene + biotite.

Pelitic rocks surrounding Inner Piedmont samples contain the typical sillimanite I and II assemblages: garnet + biotite + sillimanite + quartz + muscovite + plagioclase and garnet + biotite + sillimanite + quartz + potassium feldspar + plagioclase + ilmenite + rutile (Bier, 2001; Merschat 2003). Various studies in the Inner Piedmont have reported garnet breaking down to biotite and sillimanite (Davis, 1993a, 1993b; Merschat and Kalbas, 2002; Merschat, 2003).

Migmatite occurs throughout the upper amphibolite facies zones of the Blue Ridge and Inner Piedmont. Types of migmatite structures observed include stromatic (the most abundant), agmatite, and disseminated pods and lenses. Migmatite layering is frequently developed parallel to the dominant foliation in the samples and imply coeval development of migmatite and foliation at near-peak conditions. Late crosscutting migmatite structures are also common. Leucosomes generally consist primarily of quartz + potassium feldspar but may also contain minor amounts of muscovite, biotite, garnet, and hornblende (e.g., Kalbas, 2003; Moecher et al., 2004).

Zircons are subhedral to anhedral and rounded; soccer ball-shaped morphologies, although present, are not common (Fig. 3–3). Metamorphic rims, although observed, are not common to all zircons from a sample. Anhedral, metamict zircons are present, but were generally avoided. Zircon rims occur as 10-40 μm thick roughly concentric bands or as disconnected portions on terminal ends. Widest sections of rims usually occur at the terminal ends of zircons. Most rims are unzoned, bright white or, more commonly, dark gray to black in CL, and truncate and embay the interior oscillatory zoning. Faint, relict zoning, however, can be observed in some grains (Fig. 3–3). Bright white to light gray, faint to unzoned features commonly mark the boundary between metamorphic rim and older core, and are probably related to reabsorption of the core. Few metamorphic

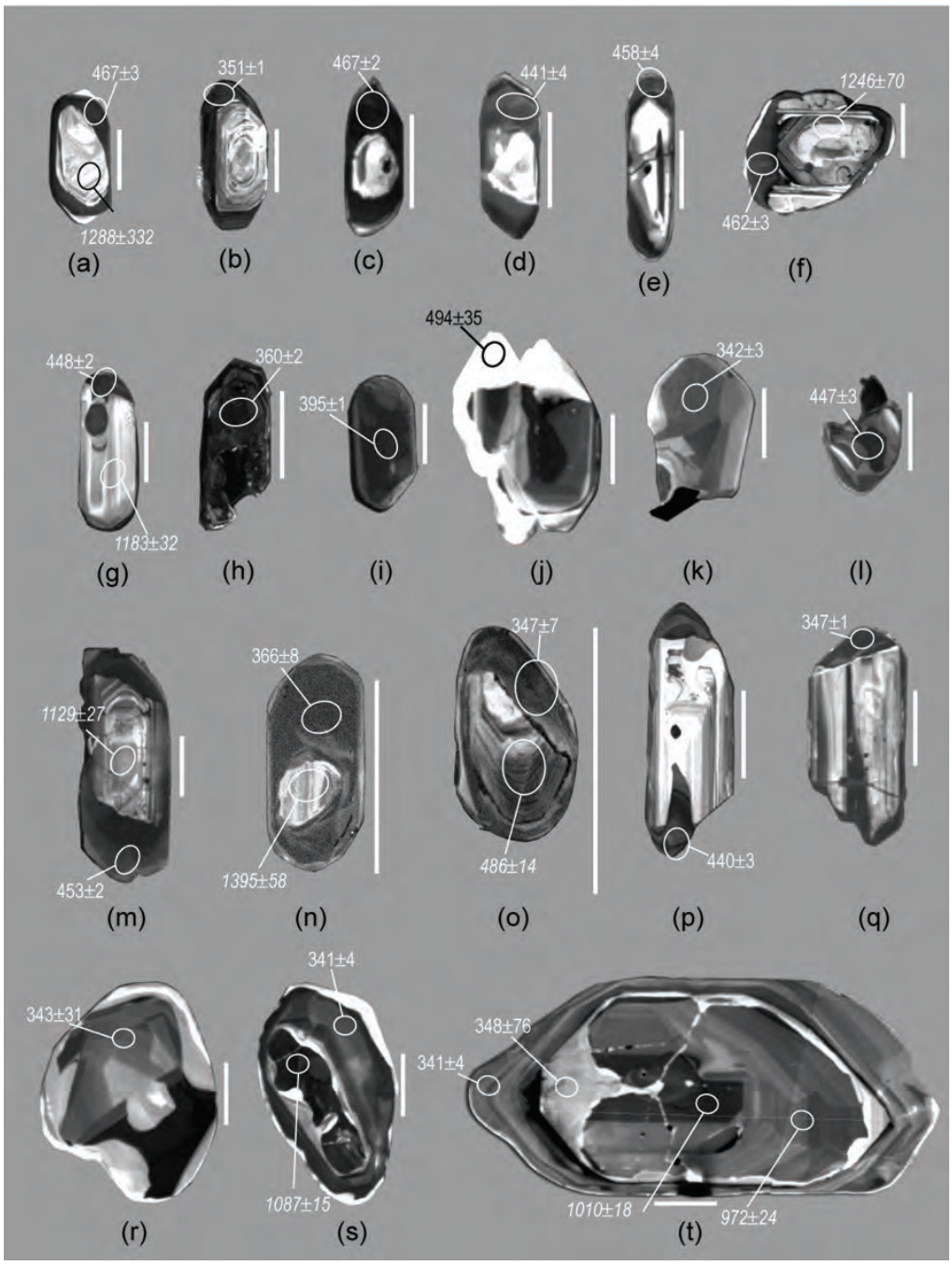

Figure 3–3. CL images of various metamorphic zircon rim morphologies analyzed. Scale bars are 100 mm; italicized ages are Pb/Pb, all others are $^{206}Pb/^{238}U$ ages. (a-e) Dark gray to black roughly concentric metamorphic rims surrounding core. (f-g) Dark unzoned rims that occur only on terminal end. (h-i) Black subhedral metamorphic zircon with faint relict zoning. (j) Anhedral zircon with bright white metamorphic rims from sample W18. (k-l) Part of a soccerball-shaped metamorphic zircon with sector zoning. Black spots are mineral inclusions in the zircon. (m-o) Dark gray, roughly concentric metamorphic rims with faint relict zoning and truncate oscillatory zoning in the core. (p-q) Metamorphic zircon developed only on terminal ends and embays interior. (r-s) Soccerball-shaped metamorphic zircon with sector zoning. An inherited core remains in (s). (t) Large zircon with gray, faintly zoned roughly concentric rim that truncates interior oscillatory zoning. Note the white reabsorption feature between rim and core.

zircons are dark gray to black, unzoned, and lack an older interior or core. Spongy textures, common of hydrothermal zircon (e.g., Corfu et al., 2003) were not observed. Zircon rims are more common in sillimanite zone or higher grade samples, and increasing migmatitic samples (e.g., BCTF, GR1, W18), but no systematic variation exists between rim morphology and metamorphic grade. Multiple zircon morphologies are present in every sample, including dark concentric rims, disconnected tips, and "soccer ball" morphologies. The most homogeneous population of rim morphology observed is from the most migmatitic sample, W18, from the Cartoogechaye terrane in the central Blue Ridge. Most zircons from W18 have bright white, thick-to-thin, unzoned, roughly concentric rims (Fig. 3–3). Similar bright white rims were observed along strike in the Mars Hill terrane and yielded concordant U-Pb ages of ~470 Ma (Ownby et al., 2004). Zones that are bright white in CL are considered to be U-poor. The dominance of white rims in sample W18 may imply some relationship between the amount of migmatization and the reabsorption of U possibly to form new zircon in the leucosomes. Otherwise, no direct relationship exists between grade and rim morphology.

RESULTS

One hundred and twenty-three zircon rims were identified and analyzed from twenty-five samples from the Blue Ridge and Inner Piedmont (Table 3–2). Multiple rims were analyzed from most samples, but often do not yield a coherent age population at 1σ confidence. Analyses vary from concordant to strongly discordant (Fig. 3–4a, b). Th/U ratios range from 1.4 to 0.01, with the majority less than 0.1, and no correlation exists with age (Fig. 3–4c). $^{206}Pb/^{238}U$ ages range from 481–297 Ma with several older ages representing beam overlap with cores and are excluded from further analysis. Relative probability plots constructed using Isoplot (Ludwig, 2003) define multiple peaks between 480–300 Ma (Fig. 3–4d). Removal of ages greater than 10 percent discordant yields more discrete peaks at 465, 450, 430, 396, 376, 364, 348, 328, and 310 Ma (Fig. 3–4d). The peaks at 430 and 310 Ma are defined by only one analysis each, and may not be significant. The relative height of the 380–340 Ma peaks to 460–450 Ma peaks is the result of more analyses within this data set and does not indicate dominance or extent of the 380-340 Ma ages in the orogen.

The multiple peaks observed in the relative probability plots suggest multiple age populations exist. This scatter of ages defining multiple close peaks is also recognized in data from just one sample (Fig. 3–4e). Sample GR1, from the Paris Mountain thrust sheet, Cat Square terrane, contains 22 analyses of zircon rims that range from 399 to 345

Table 3–2. Ion microprobeU-Pb analyses of metamorphic zircons.

Analysis Label	Ref.	Belt	U (in ppm)	Th	Th/U	$^{206}Pb/^{206}Pb$	± 1σ	f206%[2]	$^{238}U/^{206}Pb$	± 1σ	$^{207}Pb/^{206}Pb$	± 1σ	$^{207}Pb/^{235}U$	± 1σ	$^{206}Pb/^{238}U$	± 1σ	$^{238}U/^{206}Pb$	± 1σ	$^{207}Pb/^{206}Pb$	± 1σ	$^{207}Pb/^{235}U$	± 1σ	$^{206}Pb/^{238}U$	± 1σ	error corr.	$^{206}Pb/^{238}U$	± 1σ	$^{207}Pb/^{235}U$	± 1σ	$^{207}Pb/^{206}Pb$	± 1σ	% Conc
GR1-25.1		IP	205.7	50.9	0.25	-0.000041	0.000052	-0.0008									14.8390	0.2162	0.0572	0.0012	0.5314	0.0144	0.0674	0.0010		420	6	433	10	499	47	84
GR1-15.2		IP	63.1	38.1	0.60	0.001206	0.000541	0.0219									15.1130	0.3843	0.0479	0.0093	0.4367	0.0868	0.0662	0.0017		413	10	368	63	93	538	444
GR1-29.1		IP	464.4	155.2	0.33	0.000263	0.000110	0.0048									15.9970	0.3051	0.0558	0.0021	0.4805	0.0210	0.0625	0.0012		391	7	398	15	442	85	88
GR1-32.1		IP	236.3	85.7	0.36	0.000086	0.000117	0.0016									16.3610	0.7068	0.0561	0.0023	0.4725	0.0300	0.0611	0.0026		382	16	393	21	455	95	84
GR1-20.1		IP	260.3	117.0	0.45	0.000206	0.000177	0.0038									17.0740	0.8208	0.0596	0.0037	0.4810	0.0399	0.0586	0.0028		367	17	399	28	588	140	62
GR1-16.2		IP	396.1	6.4	0.02	0.000238	0.000132	0.0043									17.7460	0.6250	0.0517	0.0032	0.4020	0.0303	0.0564	0.0020		353	12	343	22	274	150	129
KEO-6.2		IP	1778.4	15.5	0.01	0.000007	0.000008	0.0001									18.1600	0.1281	0.0521	0.0005	0.3957	0.0051	0.0551	0.0004		346	2	338	4	290	23	119
GR1-6.1		IP	1780.2	47.7	0.03	0.000094	0.000042	0.0017									18.2690	0.2700	0.0559	0.0014	0.4216	0.0131	0.0547	0.0008		344	5	357	9	447	58	77
GR1-26.1		IP	689.2	356.5	0.52	0.000022	0.000018	0.0004									18.7510	0.2273	0.0555	0.0010	0.4083	0.0095	0.0533	0.0007		335	4	348	7	434	42	77
GR1-17.2		IP	384.6	4.6	0.01	0.000317	0.000092	0.0058									18.8720	0.3533	0.0511	0.0022	0.3735	0.0185	0.0530	0.0010		333	6	322	14	246	103	135
OTD-20.2		IP	713.9	1.7	0.00	0.000355	0.000464	0.0064									15.1700	0.6724	0.0653	0.0089	0.5931	0.0882	0.0659	0.0029		412	18	473	58	782	317	53
POMTN-19.1		IP	1820.8	1101.1	0.60	0.000282	0.000074	0.0051	16.12	0.49	0.0572	0.001	0.4895	0.0167	0.0620	0.0019	16.2030	0.4935	0.0531	0.0013	0.4518	0.0190	0.0617	0.0019	0.755	386	11	379	13	333	58	116
BCTF4_sp1.ais		IP						1.4600											0.0482	0.0052	0.4369	0.0492	0.0658	0.0013	0.35	411	8	368	35	106	254	386
BCTF29_sp1.ais		IP						0.1700											0.0538	0.0004	0.4735	0.0043	0.0638	0.0004	0.49	399	3	394	3	364	19	109
BCTF23_sp1.ais		IP						0.1300											0.0545	0.0006	0.4707	0.0086	0.0626	0.0006	0.86	392	4	392	6	392	25	100
BCTF8_sp1.ais		IP						0.1100											0.0543	0.0006	0.4683	0.0080	0.0625	0.0009	0.79	391	5	390	6	384	24	102
BCTF-14 (sq)		IP	1379	1155	0.84	0.001194	0.0003	2.1426	15.79	0.595	0.0765	0.005					16.1356	0.6172	0.0592	0.0071	0.5057	0.0640	0.0620	0.0024	0.30	388	14			574	262	68
BCTF22_sp1.ais		IP						0.1100											0.0546	0.0005	0.4643	0.0056	0.0617	0.0005	0.67	386	3	387	4	395	20	98
BCTF-2 (sq)		IP	1130	6	0.00	<0.000001	<0.000001	0.0000	16.33	0.615	0.0519	0.001					16.3311	0.6149	0.0519	0.0015	0.4385	0.0207	0.0612	0.0023	0.80	383	14			283	65	135
BCTF-4 (sq)		IP	3135	157	0.05	0.000092	0.0000	0.1645	16.34	0.609	0.0556	0.001					16.3704	0.6103	0.0543	0.0010	0.4572	0.0189	0.0611	0.0023	0.90	382	14			383	40	100
BCTF22_sp2.ais		IP						0.4400											0.0540	0.0009	0.4454	0.0084	0.0598	0.0006	0.42	374	4	374	6	373	39	100
BCTF-13 (sq)		IP	1417	9	0.01	<0.000001	<0.000001	0.0000	16.76	0.638	0.0535	0.002					16.7627	0.6377	0.0535	0.0015	0.4402	0.0210	0.0597	0.0023	0.80	374	14			351	65	107
BCTF-7 (sq)		IP	1369	6	0.00	<0.000001	<0.000001	0.0000	16.84	0.636	0.0548	0.001					16.8436	0.6356	0.0548	0.0011	0.4487	0.0191	0.0594	0.0022	0.88	372	14			405	45	92
BCTF19_sp1.ais		IP						0.1500											0.0551	0.0010	0.4450	0.0088	0.0586	0.0007	0.375	367	4	374	6	415	42	88
BCTF21_sp1.ais		IP						0.2100											0.0549	0.0009	0.4431	0.0099	0.0586	0.0010	0.665	367	6	372	7	406	38	90
BCTF26_sp1.ais		IP						0.2200											0.0545	0.0007	0.4397	0.0070	0.0585	0.0006	0.633	366	4	370	5	393	28	93
BCTF3_sp1.ais		IP						0.3100											0.0535	0.0011	0.4286	0.0122	0.0582	0.0009	0.741	364	6	362	9	348	45	105
BCTF35_sp2.ais		IP						0.1300											0.0567	0.0006	0.4496	0.0064	0.0575	0.0007	0.682	361	4	377	4	479	24	75
BCTF-6 (sq)		IP	396	442	1.12	0.000798	0.0003	1.4327	17.40	0.675	0.0626	0.002					17.6537	0.6905	0.0509	0.0047	0.3975	0.0395	0.0566	0.0022	0.394	355	14			236	211	150
BCTF-21 (sq)		IP	1341	32	0.02	<0.000001	<0.000001	0.0000	17.77	0.669	0.0540	0.001					17.7717	0.6688	0.0540	0.0012	0.4186	0.0182	0.0563	0.0021	0.867	353	13			369	49	96
BCTF15_sp2.ais		IP						0.2800											0.0556	0.0011	0.4280	0.0112	0.0558	0.0005	0.708	350	3	362	8	438	46	80
BCTF31_sp1.ais		IP						0.2000											0.0542	0.0010	0.4145	0.0078	0.0554	0.0007	0.349	348	4	352	6	381	42	91
BCTF20_sp1.ais		IP						0.0900											0.0532	0.0004	0.4052	0.0040	0.0552	0.0004	0.538	346	2	345	3	339	19	102
BCTF37_sp2.ais		IP						0.2600											0.0542	0.0009	0.4105	0.0081	0.0549	0.0005	0.559	345	3	349	6	381	37	91
BOCAT12_sp1.ais		eBR						0.4200											0.0539	0.0012	0.4331	0.0101	0.0583	0.0006	0.408	365	4	365	7	366	48	100
CAR-10	1	wBR	681	918	1.39			0.1300	12.91	1.340	.0569	2.360									0.5950	3.0400	0.0770	1.3400	0.440	481.0	6.5			445	60.5	108
CAR-1B	1	WBr	49	1	0.02			-0.3200	13.25	4.670	.0538	8.640									0.5890	9.4700	0.0760	4.6700	0.490	470.0	21.5			468	182.5	100
CGM-22.1R		cBR	364	95	0.27	---	0.0000	0.2414	8.86	0.719	.0644	2.198					8.8633	0.7191	0.0644	2.1977	1.0014	2.3124	0.1128	0.7191	0.311	689.1	4.7			754	46	91
CGM-14.1R		cBR	1234	56	0.05	3.4E-5	63.9611	-0.0755	13.33	0.442	.0557	1.029					13.3383	0.4440	0.0553	1.1875	0.5712	1.2677	0.0750	0.4440	0.350	466.0	2.0			422	27	109
CGM-7.1R		cBR	1244	214	0.18	1.5E-5	57.7359	0.1733	13.45	0.436	.0576	1.000					13.4575	0.4363	0.0574	1.0271	0.5883	1.1159	0.0743	0.4363	0.391	462.1	1.9			508	23	90
CGM-12.1R		cBR	385	54	0.14	---	0.0000	0.0120	13.57	0.804	.0562	1.883					13.5726	0.8037	0.0562	1.8827	0.5714	2.0471	0.0737	0.8037	0.393	458.3	3.6			462	42	99
CGM-3.1		cBR	297	84	0.29	8.3E-5	64.6366	-0.2991	13.55	0.887	.0538	2.046					13.5730	0.8926	0.0526	2.5749	0.5339	2.7252	0.0737	0.8926	0.328	458.3	3.9			310	59	132
CGM-2.1		cBR	464	103	0.23	-2.1E-5	92.5839	0.0131	13.90	0.735	.0560	1.717					13.8909	0.7357	0.0563	1.7789	0.5588	1.9251	0.0720	0.7357	0.382	448.1	3.2			464	39	96
DEL1-44.1		cBR	140	1	0.00	3.1E-4	50.0083	0.0473	13.81	1.167	.0563	2.672					13.8847	1.2008	0.0518	5.2975	0.5143	5.4319	0.0720	1.2008	0.221	448.3	5.2			276	121	138
DEL1-57.1		cBR	362	1	0.00	8.2E-5	57.7386	0.1456	14.11	0.912	.0569	2.009					14.1346	0.9164	0.0557	2.4022	0.5432	2.5711	0.0707	0.9164	0.356	440.7	3.9			440	53	100
DEL1-55.1		cBR	60	0	0.01	4.8E-4	61.9961	0.4567	14.19	2.025	.0593	4.694					14.3161	2.0954	0.0523	9.9070	0.5041	10.1261	0.0699	2.0954	0.207	435.3	8.8			300	226	131
DEL1-41.1		cBR	168	1	0.01	2.6E-4	61.4347	0.8129	15.45	1.475	.0613	3.499					15.5274	1.5031	0.0575	5.5285	0.5106	5.7292	0.0644	1.5031	0.262	402.3	5.9			511	122	73
Dgn_10_sp1		IP				0.000096	0.0000	0.1600			0.0541	0.001	0.3892	0.0067	0.052	0.001			0.0527	0.0008	0.3786	0.0077	0.0521	0.0006	0.712	328	4	326	6	315	33	104
Dgn_8_sp2		IP				0.000635	0.0001	1.0300			0.0555	0.001	0.4278	0.0094	0.056	0.001			0.0462	0.0020	0.3525	0.0169	0.0554	0.0008	0.465	347	5	307	13	7	104	5082
EL-2-1.2R		IP	215	101	0.49	1.9E-4	57.7409	0.8466	15.63	1.098	.0615	2.505					15.6885	1.1166	0.0586	3.8281	0.5153	3.9876	0.0637	1.1166	0.280	398.3	4.3			553	84	72
EL-2-22.1C		IP	889	60	0.07	1.8E-4	45.8946	0.3550	17.34	0.579	.0566	1.393					17.3950	0.5986	0.0540	2.6781	0.4278	2.7442	0.0575	0.5986	0.218	360.3	2.1			370	60	97
GR1-2.1 (sq)		IP	4262	733	0.17	0.000788	0.0001	1.4138	15.26	0.568	0.0685	0.001					15.4782	0.5780	0.0570	0.0022	0.5077	0.0273	0.0646	0.0024	0.694	404	15			491	85	82
HAZ2mss-11.1R		cBR	1763	156	0.09	2.5E-4	13.8691	0.4393	9.42	0.358	.0708	0.530					9.4611	0.3632	0.0672	1.1391	0.9797	1.1956	0.1057	0.3632	0.304	647.7	2.2			845	24	70
HAZ2mss-29.2R		cBR	1053	46	0.05	2.5E-4	25.0032	0.4475	11.92	0.477	.0570	0.950					11.9725	0.4905	0.0534	2.1731	0.6145	2.2278	0.0835	0.4905	0.220	517.1	2.4			344	49	133
HAZ2mss-24.2R		cBR	428	39	0.09	1.5E-4	44.7257	0.2641	13.30	0.731	.0577	1.403					13.3336	0.7410	0.0555	2.3157	0.5744	2.4313	0.0750	0.7410	0.305	466.2	3.3			434	52	107
HAZ2mss-10.1R		cBR	338	31	0.09	7.5E-5	27.8888	0.1350	13.46	0.743	.0559	1.514					13.4803	0.7442	0.0548	1.6634	0.5604	1.8223	0.0742	0.7442	0.408	461.3	3.3			403	37	113
HAZ2mss-33.1R		cBR	581	48	0.09	3.6E-5	0.5226	0.0648	13.74	0.536	.0562	1.089					13.7531	0.5360	0.0557	1.1062	0.5584	1.2292	0.0727	0.5360	0.436	452.5	2.3			440	25	103
HAZ2mss-20.2R		cBR	699	30	0.04	3.8E-5	64.0125	0.0675	13.85	0.498	.0570	1.005					13.8610	0.5001	0.0564	1.1959	0.5613	1.2963	0.0721	0.5001	0.386	449.1	2.2			469	26	95
LVQ1-18.1		IP	701	20	0.03	0.000070	0.0001	0.0013	16.11	0.199	0.0528	0.001	0.452	0.009	0.062	0.001	16.1300	0.2022	0.0518	0.0019	0.4424	0.0177	0.0620	0.0008	0.805	388	5	372	13	275	86	141
LVQ1-13.2		IP	857	22	0.03	0.000041	0.0000	0.0008	16.72	0.160	0.0536	0.001	0.442	0.009	0.060	0.001	16.7280	0.1609	0.0530	0.0012	0.4366	0.0111	0.0598	0.0006	0.664	374	4	368	8	327	52	114
LVQ1-14.1		IP	12298	335	0.03	0.000005	0.0000	0.0001	17.30	0.168	0.0525	0.000	0.418	0.005	0.058	0.001	17.3050	0.1677	0.0524	0.0003	0.4178	0.0049	0.0578	0.0006	0.890	362	3	354	3	305	12	119
LVQ1-4.1		IP	893	30	0.03	0.000087	0.0000	0.0016	17.46	0.186	0.0520	0.001	0.411	0.011	0.057	0.001	17.4820	0.1866	0.0507	0.0015	0.3998	0.0127	0.0572	0.0006	0.761	359	4	342	9	227	67	158
LVQ1-11.2		IP	1324	55	0.04	<0.000001	--	<0.0001	17.93	0.377	0.0526	0.001	0.404	0.010	0.056	0.001	17.9230	0.3765	0.0529	0.0007	0.4069	0.0107	0.0558	0.0012	0.854	350	7	347	8	324	31	108
LVQ1-3.2		IP	1713	66	0.04	0.000033	0.0000	0.0006	18.36	0.233	0.0531	0.001	0.399	0.008	0.054	0.001	18.3710	0.2329	0.0526	0.0009	0.3949	0.0088	0.0544	0.0007	0.850	342	4	338	6	312	38	110
LVQ1-2.1		IP	1544	53	0.03	0.000010	0.0000	0.0002	18.40	0.144	0.0524	0.001	0.393	0.007	0.054	0.000	18.4010	0.1442	0.0523	0.0008	0.3918	0.0070	0.0543	0.0004	0.872	341	3	336	5	298	35	114
LVQ1-21.1		IP	3828	373	0.10	0.000012	0.0000	0.0002	18.75	0.278	0.0526	0.000	0.387	0.007	0.053	0.001	18.7520	0.2784	0.0524	0.0004	0.3852	0.0067	0.0533	0.0008	0.955	335	5	331	5	303	17	111
LVQ1-16.1		IP	1547	158	0.10	0.000046	0.0000	0.0008	18.84	0.156	0.0547	0.001	0.401	0.007	0.053	0.000	18.8550	0.1570	0.0541	0.0011	0.3954	0.0087	0.0530	0.0004	0.850	333	3	338	6	374	44	89
LVQ1-5.1		IP	3523	192	0.05	0.000018	0.0000	0.0003	18.87	0.390	0.0522	0.001	0.382	0.010	0.053	0.001	18.8770	0.3904	0.0520	0.0007	0.3796	0.0098	0.0530	0.0011	0.936	333	7	327	7	284	30	117
LVQ1-20.1		IP	859	34	0.04	0.000010	0.0000	0.0002	19.05	0.231	0.0528	0.001	0.382	0.010	0.052	0.001	19.0560	0.2312	0.0526	0.0012	0.3807	0.0101	0.0525	0.0006	0.817	330	4	328	7	312	51	106
LVQ1-10.2		IP	2345	44	0.02	0.000009	0.0000	0.0002	19.14	0.129	0.0524	0.000	0.378	0.004	0.052	0.000	19.1430	0.1289	0.0523	0.0004	0.3767	0.0041	0.0522	0.0004	0.924	328	2	325	3	299	18	110
R29-18.1R		IP	340	7	0.02	7.4E-5	0.7255	0.1332	13.45	0.771	.0571	1.542					13.4641	0.7711	0.0560	1.5917	0.5739	1.7686	0.0743	0.7711	0.436	461.8	3.4			454	35	102
R29-14.2R		IP	288	15	0.05	---	0.0000	0.0000	14.48	0.859	.0559	1.743					14.4759	0.8587	0.0559	1.7428	0.5323	1.9428	0.0691	0.8587	0.442	430.6	3.6			448	39	96
R29-13.1R		IP	753	31	0.04	---	0.0000	0.0000	14.65	0.666	.0574	1.114					14.6491	0.6663	0.0574	1.1142	0.5406	1.2983	0.0683	0.6663	0.513	425.7	2.7			508	25	81
R29-22.2X		IP	79	3	0.03	---	0.0000	0.0000	14.70	1.615	.0535	3.359					14.6974	1.6154	0.0535	3.3591	0.5015	3.7274	0.0680	1.6154	0.433	424.3	6.6			348	76	118
R29-7.1		IP	512	41	0.08	---	0.0000	0.0000	14.71	0.650	.0567	1.340					14.7096	0.6503	0.0567	1.3400	0.5314	1.4894	0.0680	0.6503	0.437	424.0	2.7			480	30	87
R29-1.1		IP	196	16	0.09	9.2E-5	53.1771	0.1663	16.14	1.096	.0570	2.287					16.1718	1.1000	0.0556	2.6938	0.4741	2.9098	0.0618	1.1000	0.378	386.8	4.1			437	60	87
R29-2.1		IP	678	210	0.32	3.8E-5	64.3728	0.0681	17.77	0.604	.0562	1.288					17.7773	0.6059	0.0556	1.4550	0.4313	1.5761	0.0563	0.6059	0.384	352.8	2.1			437	32	76
R29-12.1		IP	302	108	0.37	---	0.0000	0.0000	18.27	0.900	.0551	1.976					18.2712	0.8996	0.0551	1.9756	0.4158	2.1707	0.0547	0.8996	0.414	343.5	3.0			416	44	79
R29-27.1		IP	285	17	0.06	3.3E-4	24.4467	0.5994	18.21	0.898	.0589	1.889					18.3198	0.9097	0.0541	3.2217	0.4069	3.3477	0.0546	0.9097	0.272	342.6	3.0			374	73	91
R29-28.2R		IP	373	58	0.16	1.2E-4	1.1625	0.2109	18.39	0.821	.0552	1.785					18.4318	0.8209	0.0535	1.8877	0.4001	2.0585	0.0543	0.8209	0.399	340.6	2.7			349	43	97
R29-22.1R		IP	189	56	0.31	8.7E-4	35.3717	1.6045	18.21	1.113	.0628	2.282					18.5050	1.2539	0.0500	10.2011	0.3726	10.2779	0.0540	1.2539	0.122	339.3	4.1			195	237	142

Table 3–2. Continued.

Analysis			U	Th		$^{204}Pb/$			Total $^{238}U/$		$^{207}Pb/$		$^{207}Pb/$		$^{206}Pb/$		Radiogenic Ratios[1] $^{238}U/$		$^{207}Pb/$		$^{207}Pb/$		$^{208}Pb/$		error	Ages (in Ma)[1] $^{208}Pb/$		$^{207}Pb/$		$^{207}Pb/$		%
Label	Ref.	Belt	(in ppm)		Th/U	^{206}Pb	± 1σ	f206%[2]	^{206}Pb	± 1σ	^{206}Pb	± 1σ	^{235}U	± 1σ	^{238}U	± 1σ	^{206}Pb	± 1σ	^{206}Pb	± 1σ	^{235}U	± 1σ	^{238}U	± 1σ	corr.	^{238}U	± 1σ	^{235}U	± 1σ	^{206}Pb	± 1σ	Conc
R29-6.1		IP	172	37	0.22	3.3E-4	38.4393	0.5976	18.47	1.162	.0561	2.507					18.5830	1.1845	0.0513	4.6928	0.3805	4.8400	0.0538	1.1845	0.245	337.9	3.9			254	108	125
RS711-48.1		cBR	409	6	0.02	5.9E-5	62.9585	0.2649	14.16	0.761	0.0578	1.685					14.1760	0.7644	0.0569	1.9612	0.5538	2.1049	0.0705	0.7644	0.363	439.4	3.2			489	43	90
RS787-7.1R		cBR	385	5	0.01	4.0E-5	57.7375	0.0179	13.31	0.713	.0565	1.665					13.3158	0.7138	0.0559	1.7879	0.5792	1.9251	0.0751	0.7138	0.371	466.8	3.2			450	40	104
SMTFB06_sp1.ais		IP						16.5900											0.0402	0.0234	0.3165	0.1930	0.0571	0.0060	0.338	358.1	36.6	279.2	149	-1	0.023	-35810
SW6-11.1		IP	211	10	0.05	---	0.0000	0.0000	19.39	0.995	.0550	2.167					19.3861	0.9949	0.0550	2.1667	0.3909	2.3842	0.0516	0.9949	0.417	324.2	3.1			411	48	73
VM_18_sp2.ais		IP						0.5900											0.0506	0.0022	0.3811	0.0194	0.0546	0.0015	0.542	342.9	9.2	327.9	14.2	222.7	98.8	154
W18-4.1R		cBR	3	0	0.02	---	0.0000	0.0000	12.79	7.194	.0423	15.515					12.7893	7.1940	0.0423	15.5149	0.4565	17.1016	0.0782	7.1940	0.421	485.3	33.6			-206	389	242
MV-668-5.1R	2	IP	917	26	0.03	3.1E-4	25.0027		19.06	0.470	.0538	1.380					19.1670	0.4915	0.0492	2.7806	0.3541	2.8237	0.0522	0.4915	0.174	327.8	1.6	329.6	1.5	159	65	151.6
MV-668-15.1R	2	IP	684	12	0.02	9.2E-5	50.0016		18.37	0.541	.0532	1.574					18.4006	0.5476	0.0519	2.0727	0.3885	2.1438	0.0543	0.5476	0.255	341.1	1.8	341.8	1.8	279	47	118.2
MV-668-11.1R	2	IP	1401	58	0.04	4.7E-5	50.0008		18.24	0.394	.0531	1.120					18.2592	0.3960	0.0525	1.3104	0.3961	1.3690	0.0548	0.3960	0.289	343.7	1.3	343.9	1.3	306	30	111.1
MV-668-9.2R	2	IP	721	9	0.01	1.2E-4	61.7659		18.13	0.553	.0527	1.591					18.1672	0.5688	0.0509	2.6853	0.3864	2.7449	0.0550	0.5688	0.207	345.4	1.9	345.8	1.9	237	62	131.4
MV-668-7.1R	2	IP	1448	20	0.01	1.2E-4	34.8421		18.04	0.377	.0551	1.070					18.0795	0.3848	0.0533	1.6164	0.4065	1.6616	0.0553	0.3848	0.232	347.0	1.3	347.5	1.3	342	37	101.5
MV-668-2.1	2	IP	1137	5	0.00	8.0E-5	40.8264		17.85	0.410	.0534	1.181					17.8788	0.4139	0.0522	1.5166	0.4026	1.5720	0.0559	0.4139	0.263	350.8	1.4	351.4	1.4	295	35	116.0
KC1-4.1R	2	IP	1938	33	0.02	4.4E-5	43.3680		21.16	0.336	.0547	0.854					21.1795	0.3376	0.0541	1.0192	0.3519	1.0737	0.0472	0.3376	0.314	297.4	1.0			374	23	74
KC1-15.1R	2	IP	859	417	0.50	5.9E-4	32.2260		20.27	0.579	.0569	1.542					20.4876	0.6769	0.0482	6.5485	0.3244	6.5834	0.0488	0.6769	0.103	307.2	2.0			109	155	164
KC1-7.1R	2	IP	670	12	0.02	4.4E-4	25.0039		19.95	0.563	.0548	2.169					20.1131	0.5984	0.0483	4.5225	0.3311	4.5619	0.0497	0.5984	0.131	312.8	1.8			114	107	164
KC1-16.1R	2	IP	253	4	0.02	2.1E-3	17.6928		19.52	1.115	.0576	2.869					20.2809	1.3143	0.0262	27.4306	0.1782	27.4620	0.0493	1.3143	0.048	310.3	4.0			-1594	932	714
KC1-8.1R	2	IP	1152	458	0.41	3.1E-4	20.4150		19.45	0.440	.0558	0.959					19.5627	0.4554	0.0512	2.4064	0.3606	2.4491	0.0511	0.4554	0.186	321.4	1.4			248	55	123
KC1-19.1R	2	IP	793	7	0.01	---	0.0000		19.25	0.488	.0547	1.246					19.2537	0.4877	0.0547	1.2464	0.3919	1.3384	0.0519	0.4877	0.364	326.4	1.6			401	28	77
KC1-18.1R	2	IP	1292	9	0.01	---	0.0000		19.06	0.567	.0542	0.894					19.0618	0.5670	0.0542	0.8939	0.3921	1.0585	0.0525	0.5670	0.536	329.6	1.8			380	20	85
KC1-13.1R	2	IP	821	35	0.04	1.0E-4	49.9661		18.16	0.559	.0542	1.245					18.1951	0.5672	0.0527	1.9643	0.3995	2.0446	0.0550	0.5672	0.277	344.9	1.9			317	45	108
KC1-2.1	2	IP	956	4	0.00	1.6E-5	66.1759		18.11	0.426	.0537	1.081					18.1105	0.4267	0.0535	1.1257	0.4073	1.2038	0.0552	0.4267	0.354	346.5	1.4			350	25	99
KC1-11.1R	2	IP	734	8	0.01	2.8E-4	28.8703		17.41	0.494	.0539	1.249					17.5022	0.5162	0.0497	2.9818	0.3916	3.0261	0.0571	0.5162	0.171	358.2	1.8			181	69	149
EL-2-22.1C	2	IP	889	60	0.07	1.8E-4	45.8946		17.34	0.579	.0566	1.393					17.3950	0.5986	0.0540	2.6781	0.4278	2.7442	0.0575	0.5986	0.218	360.3	2.1			370	60	97
EL-2-1.2R	2	IP	215	101	0.47	1.9E-4	57.7409		15.63	1.098	.0615	2.505					15.6885	1.1166	0.0586	3.8281	0.5153	3.9876	0.0637	1.1166	0.280	398.3	4.3			553	84	72
EL-2-2.1C	2	IP	288	77	0.27	1.8E-3	23.5836		15.14	1.038	.0825	2.177					15.6506	1.3189	0.0563	11.8188	0.4958	11.8922	0.0639	1.3189	0.111	399.3	5.1			463	262	84
EL-2-1.1C	2	IP	145	83	0.57	---	0.0000		15.50	1.344	.0521	3.282					15.5020	1.3443	0.0521	3.2820	0.4633	3.5466	0.0645	1.3443	0.379	403.0	5.3			289	75	128
EL-2-8.1C	2	IP	52	29	0.57	1.2E-3	50.0333		15.22	2.295	.0574	5.249					15.5628	2.5653	0.0391	25.2629	0.3465	25.3928	0.0643	2.5653	0.101	401.5	10.0			-410	660	302
WTR29-6R	3	IP	320	26	0.08	---	0.0000		20.26	0.857	.0533	3.346					20.2555	0.8572	0.0533	3.3456	0.3626	3.4536	0.0494	0.8572	0.248	310.6	2.6			341	76	90
WTR29-11R	3	IP	364	25	0.07	---	0.0000		20.12	0.737	.0546	1.920					20.1217	0.7365	0.0546	1.9204	0.3742	2.0568	0.0497	0.7365	0.358	312.7	2.2			396	43	73
WTR29-4.1I	3	IP	312	10	0.03	---	0.0000		19.75	0.795	.0542	2.104					19.7503	0.7945	0.0542	2.1044	0.3785	2.2494	0.0506	0.7945	0.353	318.4	2.5			380	47	81
WTR29-13R	3	IP	454	10	0.02	1.1E-4	50.0024		18.68	0.630	.0530	2.011					18.7202	0.6368	0.0514	2.6040	0.3788	2.6807	0.0534	0.6368	0.238	335.5	2.1			260	60	123
WTR29-5R	3	IP	132	1	0.01	3.0E-4	50.0077		15.96	1.141	.0524	2.960					16.0440	1.1681	0.0480	5.6020	0.4129	5.7225	0.0623	1.1681	0.204	389.8	4.4			101	132	174
WTR29-9R	3	IP	211	3	0.01	8.3E-5	57.7393		15.85	0.968	.0564	2.413					15.8746	0.9715	0.0552	2.7765	0.4796	2.9415	0.0630	0.9715	0.330	393.8	3.7			421	62	93
MV336-5.1C	2	IP	1489	116	0.08	2.3E-5	50.4322		17.23	0.451	.0547	1.085					17.2388	0.4515	0.0544	1.1369	0.4352	1.2233	0.0580	0.4515	0.369	363.5	1.6			388	26	93
MV336-6.1C	2	IP	3068	196	0.06	3.2E-5	44.7220		16.81	0.313	.0546	0.743					16.8204	0.3143	0.0541	0.8454	0.4435	0.9019	0.0595	0.3143	0.348	372.3	1.1			375	19	99
MV336-2.1C	2	IP	4468	230	0.05	---	0.0000		16.69	0.259	.0545	0.614					16.6869	0.2590	0.0545	0.6137	0.4500	0.6661	0.0599	0.2590	0.389	375.2	0.9			390	14	96
MV336-9.1C	2	IP	5251	136	0.03	6.1E-6	64.4018		16.64	0.238	.0540	0.568					16.6459	0.2379	0.0539	0.5793	0.4462	0.6262	0.0601	0.2379	0.380	376.1	0.9			365	13	103
MV336-3.1C	2	IP	146	71	0.49	6.4E-4	50.0126		16.45	1.427	.0580	4.235					16.6403	1.5441	0.0486	11.0518	0.4029	11.1591	0.0601	1.5441	0.138	376.2	5.6			130	260	166
MV336-1C	2	IP	9590	456	0.05	1.4E-5	35.3556		15.82	0.175	.0540	0.407					15.8191	0.1749	0.0538	0.4308	0.4691	0.4649	0.0632	0.1749	0.376	395.1	0.7			364	10	108
MV336-7.1C	2	IP	299	208	0.70	---	0.0000		15.36	0.974	.0550	2.297					15.3633	0.9744	0.0550	2.2970	0.4937	2.4952	0.0651	0.9744	0.391	406.5	3.8			413	51	98
MV336-8.1C	2	IP	177	126	0.72	6.1E-5	99.0000		15.22	1.264	.0530	3.036					15.2393	1.2689	0.0521	3.5302	0.4716	3.7513	0.0656	1.2689	0.338	409.7	5.0			291	81	129

References: 1 - Ownby et al. (2004). 2 - Gatewood (2007). Byars et al. (2008)
[1] 204-corrected data

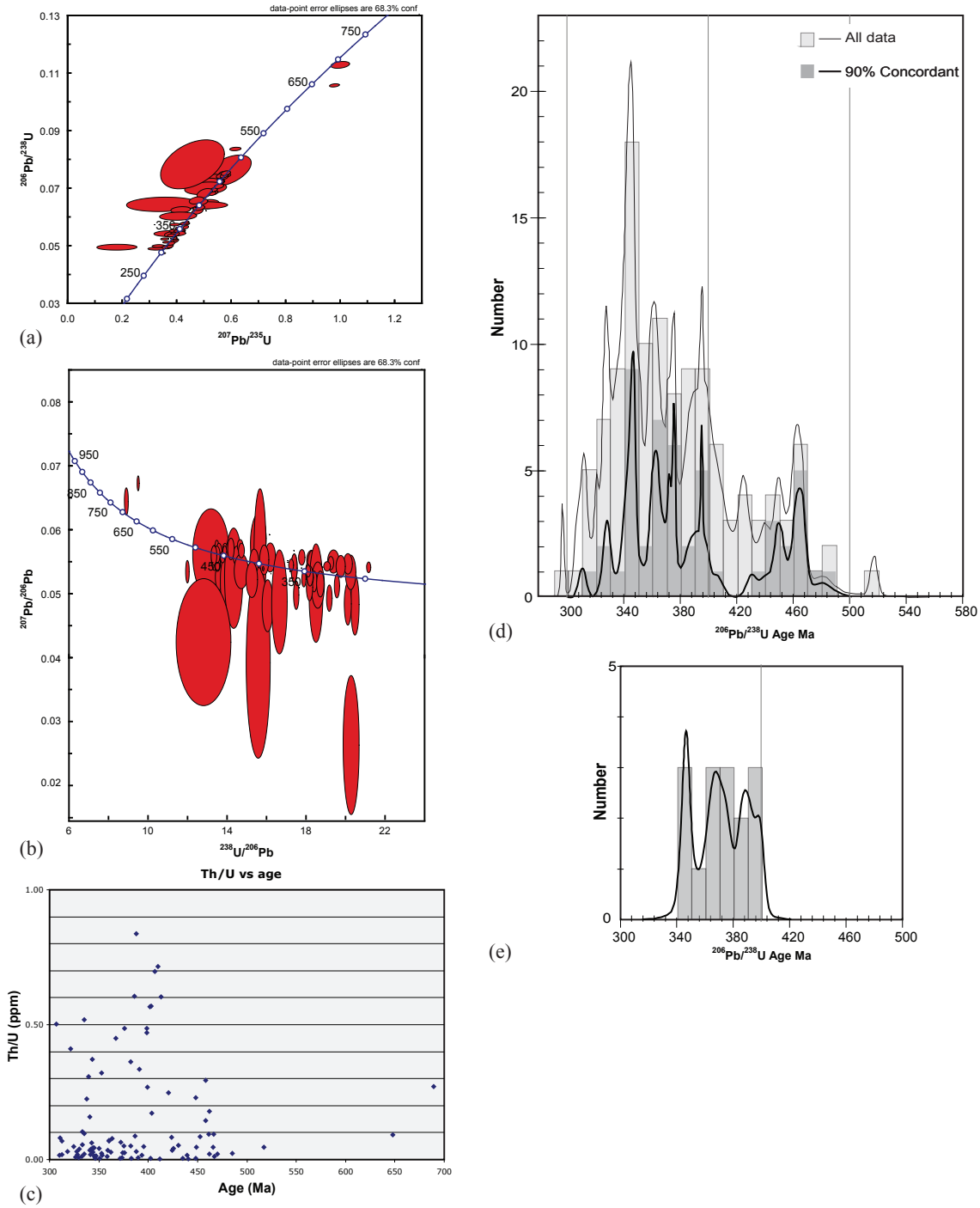

Figure 3–4. Plots of SHRIMP U-Pb metamorphic zircon data. (a) Concordia plot of U-Pb ages, (b) Tera-Wasserburg plot of all rims. (c) Graph of Th/U ratios versus $^{206}Pb/^{238}U$ age of metamorphic zircons. (d) Relative probability plot of all rim data and 90% concordant data. (e) Relative probability plot of 90% concordant metamorphic rim ages from sample GR1.

Ma (and one strongly discordant rim at ~411 Ma). Relative probability plots display multiple peaks at 377, 366, and 345 Ma, and closely overlap the Devonian peaks from the entire data set (Fig. 3–4d & e). Multiple peaks observed in the entire data set between 380–325 Ma are a function of intra-sample variation in addition to any inter-sample variation. Intra-sample variation of ages may be the result of polymetamorphism or multiple zircon-forming reactions during a single prograde event. Outcrop relationships, petrographic, and metamorphic zircon zoning patterns provide critical evidence for multiple processes and reactions for the formation of metamorphic zircon rims.

Zircon Rim Formation, Metamorphism and Deformation

Harley et al. (2007) suggested at least eight separate possibilities for zircon growth during a single prograde metamorphic event. Determination of the processes and reactions involved requires detailed study of zircon textures combined with *in situ* analysis to recognize possible breakdown reactions (Harley et al., 2007). Field and petrographic observations of mineral assemblages and textures have recognized three possible zircon forming processes or reactions. These processes include migmatization, zirconium liberating reactions, and late melts or fluids. All samples are variably migmatitic, and leucosomes commonly parallel the dominant regional foliation defined by high-temperature mineral assemblages. Locally, coarse-grained migmatite leucosomes crosscut the foliation. Both of these migmatite forming events, near-peak development of migmatite (i.e., stromatic, agmatite), or late crosscutting migmatite, can result in the growth of metamorphic rims that may yield different ages (Harley et al., 2007). Several workers have reported the zirconium liberating reaction of garnet breaking down to biotite + sillimanite (Davis, 1993a,b; Bier, 2001; Merschat, 2003; Wilson, 2006). This is a post-peak reaction, that often corresponds to exhumation of a terrain and the highest temperatures obtained along a pressure-temperature path.

Reported ages of crosscutting granitoid dikes and pegmatites from the Blue Ridge and Inner Piedmont bracket the lower bounds of the two sets of peaks (Fig 4d). Crosscutting tonalite-trondhjemite dikes have been documented by various workers in the central and eastern Blue Ridge of North Carolina and Georgia (Hatcher, 1976; Wood and Miller, 1984; C. Miller et al., 2000b). These dikes have been sampled at two locations in the central Blue Ridge of North Carolina and yield U-Pb ages of ~420 Ma (C. Miller et al., 2000b) and ~407 Ma (Mapes, 2002). The country rock from the latter (HAZ2mss) also yielded metamorphic rims of ~450 Ma. A pegmatite mined for zircon near Zirconia, North Carolina, yields an age of ~329 Ma and crosscuts the regional S_2 fabric of the Inner

Piedmont (Bream, 2003; Callahan et al., 2007). Gatewood (2007) reported an age of ~320 Ma for late pegmatitic dikes in the Inner Piedmont. The scatter of ages reported from the samples likely represents formation of zircon rims through different reactions and processes, bracketed by intrusion of post-kinematic granitoids.

DISCUSSION: TECTONIC IMPLICATIONS

This data set of U-Pb ages of zircon rims clearly illustrates: (1) three periods of high-temperature Paleozoic metamorphism have affected the Blue Ridge and Inner Piedmont; (2) U-Pb zircon rim ages, combined with metamorphic isograds and major tectonic boundaries, define five domains of eastward-younging and overlapping Paleozoic metamorphism (Figs. 3–5, 3–6); and (3) critical tectonic implications regarding terrane accretion in the southern Appalachians.

Tectonothermal Events—Three Paleozoic Metamorphisms

Zircon rim data define two broad peaks during the Middle to Upper Ordovician and the Late Devonian to early Pennsylvanian, superposed with several sharper peaks (Fig. 3–4d). These ages are interpreted to correspond to times of near-peak metamorphism based on the high blocking temperature of zircon, and metamorphic grade of the samples. The wide distribution of samples across the Blue Ridge and Inner Piedmont, and consistency of ages, suggest these two sets of peaks correspond to separate Paleozoic orogenies associated with regional metamorphism and deformation in the southern Appalachians (Figs. 3–5, 3–6). Comparison of zircon rim ages with published thermochronologic data, ages of magmatism, foreland sedimentation, and interpreted orogenic events correlates these respective events with the Taconian, Acadian/Neoacadian, and early Alleghanian orogenies. We suggest that the zircon rim ages provide an important constraint on the timing of these three metamorphic events in the southern Appalachian orogen.

The Taconic orogeny in the southern Appalachians likely spanned a period from 480–450 Ma (Drake et al., 1989; Hatcher, 1989; Moecher et al., 2004). Incorporating published ages of metamorphism, magmatism, and Taconian Sevier-Blountian clastic wedge with our zircon rim data, we suggest that peaks at 465 and 450 Ma represent timing of peak Taconian metamorphism and deformation in the southern Appalachians (Fig. 3–7). The younger 430 Ma peak is difficult to explain, but comparison with Middle to Late Ordovician ages from surrounding samples (Fig. 3–5) suggests it does not represent a regional Silurian event corresponding to the Salinic orogeny. Instead

Figure 3–5. Metamorphic isograd map of the Blue Ridge and Inner Piedmont for parts of Georgia, North Carolina, South Carolina, Tennessee, and Georgia; modified from Fig. 3–2. Sources of zircon rim and monazite data are 1–Dennis and Wright (1997a,b). 2–Carrigan et al. (2003). 3–Hibbard et al. (2003). 4–Moecher et al., (2004). 5–Ownby et al. (2004). 6–Berquist et al. (2005). 7–Moecher et al., (2005). 8–B. Miller et al., (2006). 9–Corrie and Kohn (2007). 10–Dennis (2007). 11–Gatewood (2007). 12–Byars et al. (2008). Ar/Ar, Sm/Nd, and Rb/Sr mineral ages are from Dallmeyer et al. (1986), Dallmeyer (1988); Connelly and Dallmeyer, (1993), and Goldberg and Dallmeyer (1997).

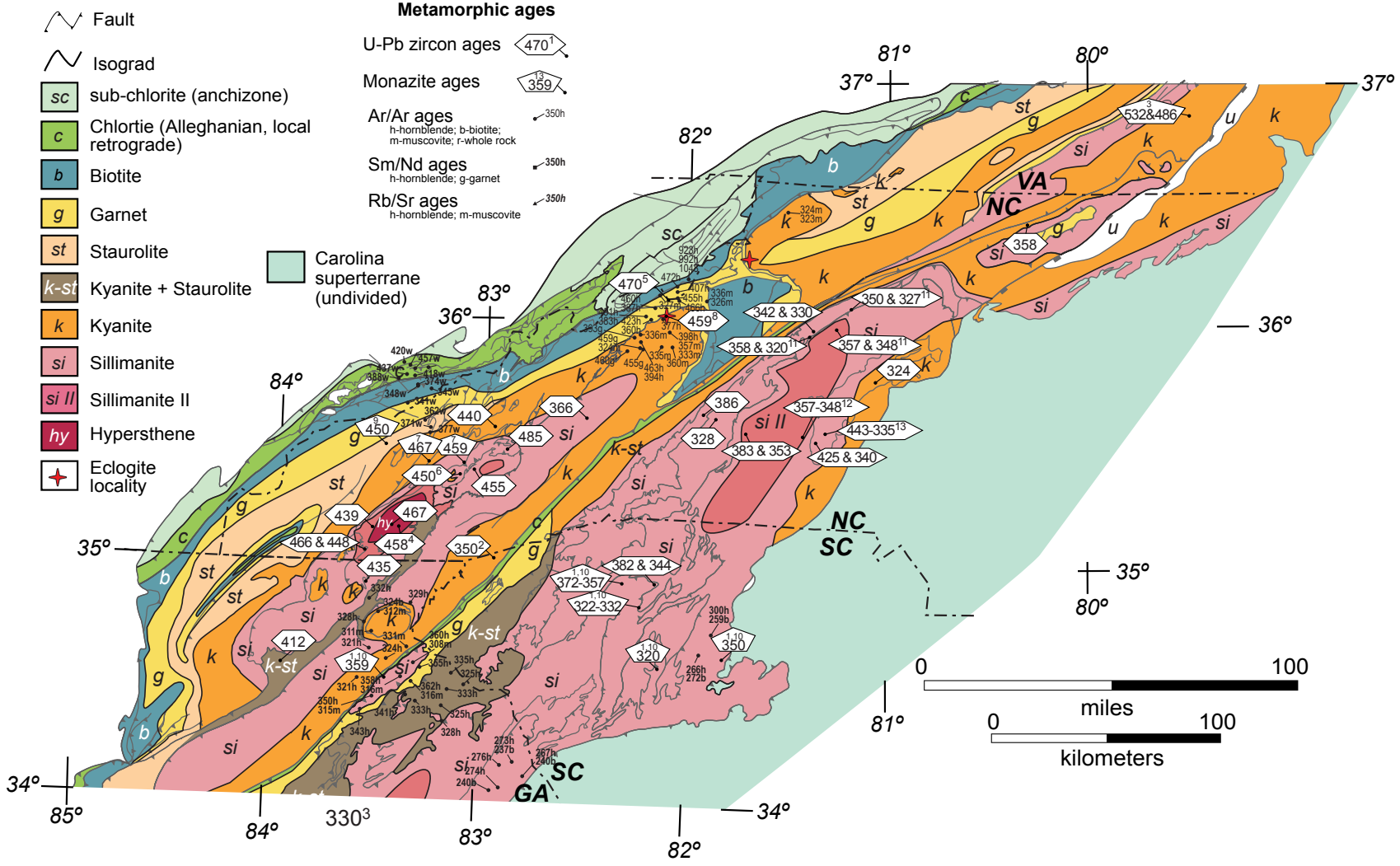
Fault
Isograd
sc sub-chlorite (anchizone)
c Chlortie (Alleghanian, local retrograde)
b Biotite
g Garnet
st Staurolite
k-st Kyanite + Staurolite
k Kyanite
si Sillimanite
si II Sillimanite II
hy Hypersthene
Eclogite locality
Carolina superterrane (undivided)
Metamorphic ages
U-Pb zircon ages
Monazite ages
Ar/Ar ages
h-hornblende; b-biotite; m-muscovite; r-whole rock
Sm/Nd ages
h-hornblende; g-garnet
Rb/Sr ages
h-hornblende; m-muscovite
VA
NC
SC
GA
81°
80°
37°
82°
36°
83°
84°
35°
34°
85°
0
100
miles
kilometers

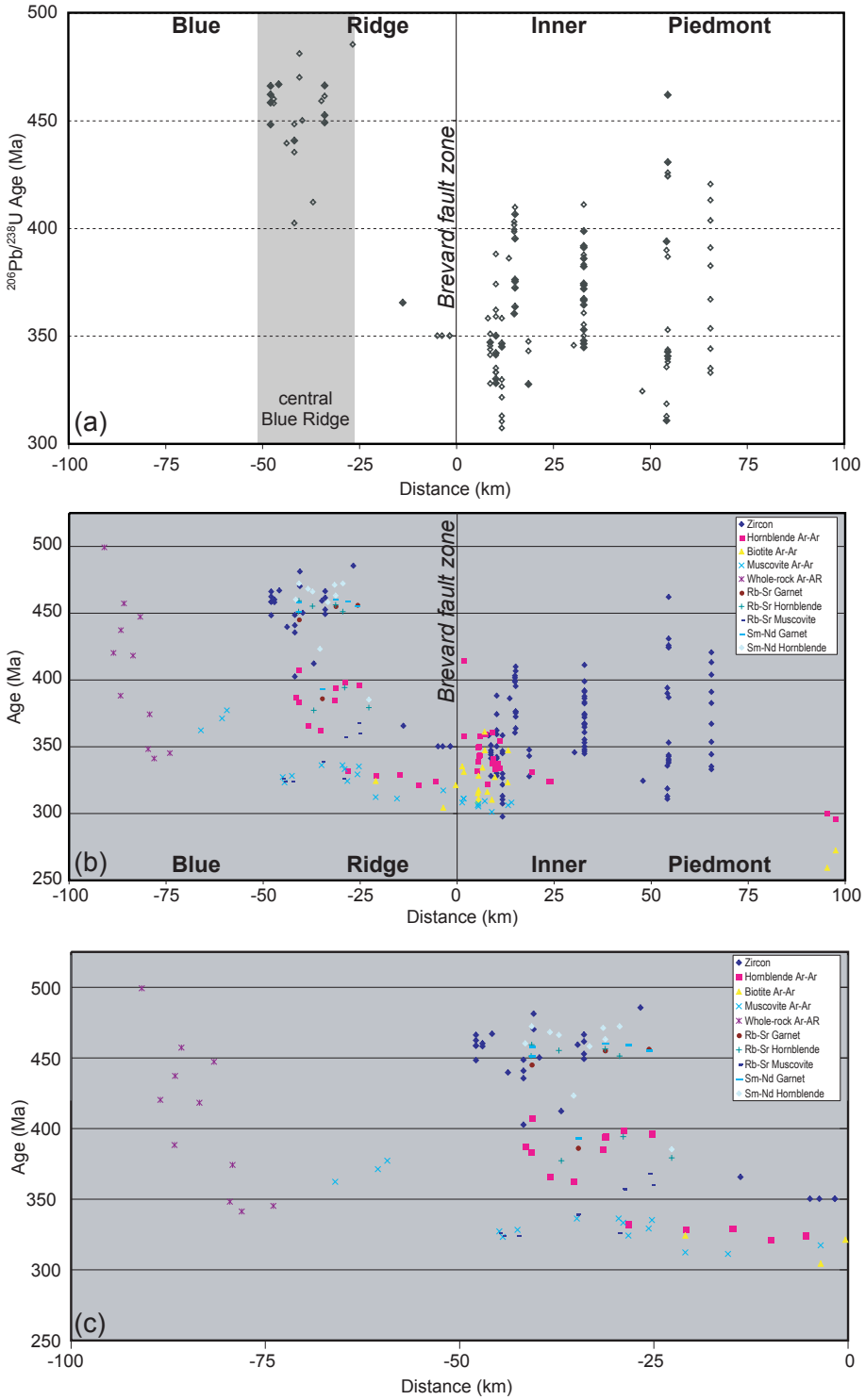

Figure 3–6. Plots of thermochronometers age versus distance from the Brevard fault zone (distance = 0) measured normal to strike of the Brevard fault zone. (a) $^{206}Pb/^{238}U$ zircon rim ages reported in this study. Solid diamonds indicate ±10% discordant and open diamonds indicate greater ±10% discordance. (b) Various published thermochronometers for the Blue Ridge and Inner Piedmont, and (c) only the Blue Ridge. See appendix for list of references.

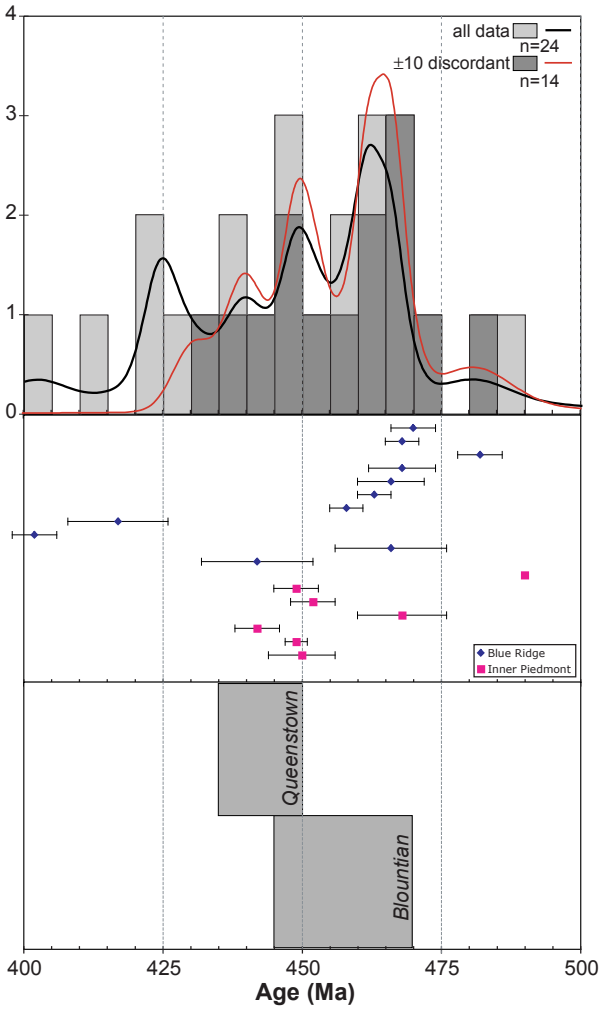

Figure 3–7. Comparison of Ordovician to Silurian U-Pb ages of zircon rims, and magmatism from the Blue Ridge and Inner Piedmont, with reported age of the Sevier-Blountian (southern Appalachians) and Queenstown (central Appalachians) clastic wedges. Age and distribution of Ordovician clastic wedges from Ettensohn (2004).

these rims may represent formation by retrograde reactions or late fluids, as discussed above. Moecher et al. (2004) reported a U-Pb age of ~458 Ma from zircon separated from leucosome associated with granulite facies rocks of the Cartoogechaye terrane at Winding Stair Gap, North Carolina. Although most of our reported ages are from the North Carolina central Blue Ridge, additional published zircon and monazite ages from the western and eastern Blue Ridge support a Middle to Late Ordovician event. In the western Blue Ridge, microdrilled monazite from staurolite to kyanite grade Great Smoky Group yielded TIMS U-Pb age of ~450 Ma (Corrie and Kohn, 2007). Electron microprobe chemical monazite ages from kyanite and sillimanite grade Great Smoky Group rocks also yield ages of ~460 Ma (Moecher et al., 2003, 2005). Miller et al. (2006) reported a U-Pb zircon age of ~459 Ma from the Lick Ridge eclogite in the eastern Blue Ridge/Tugaloo terrane, and interpreted this age to represent peak metamorphism. Sm-Nd and Rb-Sr garnet and hornblende ages from the eastern Blue Ridge near Spruce Pine, North Carolina, are 480–440 Ma, and support the conclusion that a Taconic event affected the eastern Blue Ridge/western Tugaloo terrane. ^{40}Ar-^{39}Ar hornblende, biotite, and muscovite ages, however, yield Devonian to Mississippian cooling ages and imply a younger event (Goldberg and Dallmeyer, 1997; Trupe et al., 2003) (Fig. 3–6). Magmatism in the Blue Ridge and western Inner Piedmont occurs in the range of 465–450 Ma, but no plutons occur in the western Blue Ridge. Middle to Late Ordovician magmatism in the central and eastern Blue Ridge includes the ~468 Ma Persimmon Creek Gneiss in the Cowrock terrane (McDowell et al., 2002), ~466 Ma Whiteside trondhjemite in the Tugaloo terrane (C. Miller et al., 1998; 2000b), and several felsic gneisses from the Dahlonega gold belt in Georgia with reported SHRIMP U-Pb ages of ~468, ~466, ~463, and ~458 Ma (Thomas, 2001). The ~482 Ma Cane Creek gneiss (Settles, 2002; Bream, 2003), from the Dahlonega gold belt in northeastern Georgia is the oldest Blue Ridge Paleozoic intrusion, but still overlaps zircon rim ages reported here. Several 460–450 Ma granitoid intrusions are recognized from the western Inner Piedmont (Bream 2003; Gatewood, 2007); although no Ordovician metamorphic rims were observed from western Inner Piedmont samples. Nevertheless, comparison of zircon rim ages, monazite ages, and granitic magmatism support peak Taconic metamorphism and deformation in the Blue Ridge. Evidence for Taconic metamorphism and deformation in the Inner Piedmont is lacking to nonexistent and only the occurrence of Middle to Late Ordovician magmatism overlaps with metamorphism and deformation in the Blue Ridge at 465–450 Ma (Fig. 3–7).

The Devonian to early Mississippian metamorphic event is defined by peaks at ~396, ~376, ~364, ~348, and ~328 Ma. These ages do not correspond to the described Acadian, 410–380 Ma, (e.g., Osberg et al., 1989), or Alleghanian, 320–260 Ma, events (Hatcher et al., 1989; Hatcher, 2002a), although some overlap occurs with both. Robinson et al. (1998) suggested the term Neoacadian (Quaboagian) to describe a similar ~360 Ma high-temperature event in New England, and this term has been adopted to describe the high temperature event in the southern Appalachians (e.g., Bream, 2002; Hatcher, 2002b; Merschat et al., 2005b; Hatcher and Merschat, 2006; Hatcher et al., 2007; Merschat and Hatcher, 2007). These peaks define a possible ~70 m.y. period of metamorphism, quite a long time for a single event, and make defining a specific period of metamorphism difficult. This event is associated with significant amounts of granitic magmatism in the Inner Piedmont, and overlaps published thermochronometers from the Blue Ridge and Inner Piedmont.

Recent geochronologic and geochemical studies have documented Devonian to Mississippian felsic magmatism in the eastern Blue Ridge and Inner Piedmont. The majority of Devonian-Mississippian granitoids occur in the Cat Square terrane as peraluminous, anatectic granites that range from 407–325 Ma (most between 380–350 Ma). Goldsmith et al. (1988) recognized textural and compositional similarities in the granitoids of the North Carolina Inner Piedmont and correlated numerous disconnected bodies of weakly to moderately foliated, locally megacrystic, peraluminous granites with the Toluca Granite. Mapes (2002) reported a U-Pb age of ~378 Ma for the Toluca Granite. Disconnected bodies of megacrystic Walker Top Granite throughout the northern part of the Cat Square terrane yield U-Pb ages of ~407 Ma (Gatewood, 2007), ~366 Ma (Giorgis et al., 2002; Mapes, 2002), and ~355 Ma (Byars et al., 2008b). Additional plutons in the South Carolina Inner Piedmont yield Late Devonian to Mississippian ages: Gray Court, ~357 Ma, and Reedy River, ~325 Ma (Mapes, 2002). These Cat Square terrane plutons have minimal to no zircon inheritance and yield zircon saturation temperatures in excess of 800 ºC (Mapes, 2002; Miller et al., 2003). Limited Nd-Sm depleted mantle model ages indicate incorporation of 1.6 and 1.2 Ga crust into the Cat Square terrane plutons and are similar model ages for other Inner Piedmont plutons (Fullagar et al., 1997). Oxygen isotopes from the Toluca and Walker Top Granites are identical to those from the surrounding country rocks, implying partial melting of Cat Square terrane metasedimentary units to produce the granites (Mapes, 2002). Granitic magmatism in the Cat Square terrane further supports a 380–350 Ma high-temperature

event that involved partial melting of the metasedimentary rocks, producing anatectic granites, migmatite and zircon rim growth.

Magmatism in the eastern Blue Ridge consists predominantly of granodiorite to trondhjemite plutons that range from 380 to 335 Ma, with most clustered around 335 Ma. Devonian plutons in the eastern Blue Ridge include the Spruce Pine pegmatites, Looking Glass granodiorite, and Pink Beds trondhjemite (Miller et al., 2000b; Mapes, 2002; Miller et al., 2006; Varnell et al., 2008). Mississippian plutons include the ~346 Ma Yonah granite (Mapes, 2002), ~342 Ma Round Mountain granite (Varnell et al., 2008), ~335 Ma Rabun granodiorite (Miller et al., 2006; Stahr, 2007), ~335 Ma Walnut Creek granodiorite (Stahr, 2007), ~334 Ma Mount Airy granodiorite, and ~335 Ma Stone Mountain granodiorite (Miller et al., 2006). Chemistry of all of the granodioritic to trondhjemitic plutons in the eastern Blue Ridge is similar and requires a garnet amphibolite source (Miller et al., 1997), significantly different from the Inner Piedmont, Cat Square terrane plutons.

Thermochronometers from the Georgia, North Carolina, and South Carolina Blue Ridge and Inner Piedmont also support a major Devonian-Mississippian tectonothermal event. ^{40}Ar-^{39}Ar cooling ages from the Georgia and South Carolina Blue Ridge and Inner Piedmont support a 360–340 Ma event (Dallmeyer, 1988; Figs. 3–5, 3–6). Hornblende yielded ^{40}Ar-^{39}Ar ages of 360–340 Ma in and around the Alto allochthon (Dallmeyer, 1988; Fig. 3–5). Additionally, several ^{40}Ar-^{39}Ar studies have documented 380–330 Ma cooling in the eastern and western Blue Ridge (Dallmeyer, 1988; Connelly and Dallmeyer, 1993; Goldberg and Dallmeyer, 1997). Goldberg and Dallmeyer (1997) obtained younger ^{40}Ar-^{39}Ar ages of hornblende, biotite, and muscovite from samples that yielded Ordovician Rb-Sr and Sm-Nd ages, and interpreted the variation to represent polymetamorphism in the Blue Ridge. The youngest ^{40}Ar-^{39}Ar ages reported are ~300 Ma muscovite ages from the easternmost portions of the Inner Piedmont, near the central Piedmont suture in South Carolina, and probably reflect Alleghanian deformation (Dallmeyer et al., 1986). Monazite from the Inner Piedmont has reported U-Pb and chemical ages of ~350 Ma and 330–320 Ma (Dennis and Wright, 1997a, 1997b; Mirante and Patiño-Douce, 2000).

Examination of the zircon rim data, ages of granitic magmatic activity, and other thermochronometers provide significant evidence of the Neoacadian event that affected the eastern Blue Ridge and Inner Piedmont (Fig. 3–8). The thermal affects of this event may have extended westward into parts of the central and western Blue Ridge, although deformation associated with the event is not as intense. Comparison of all the data

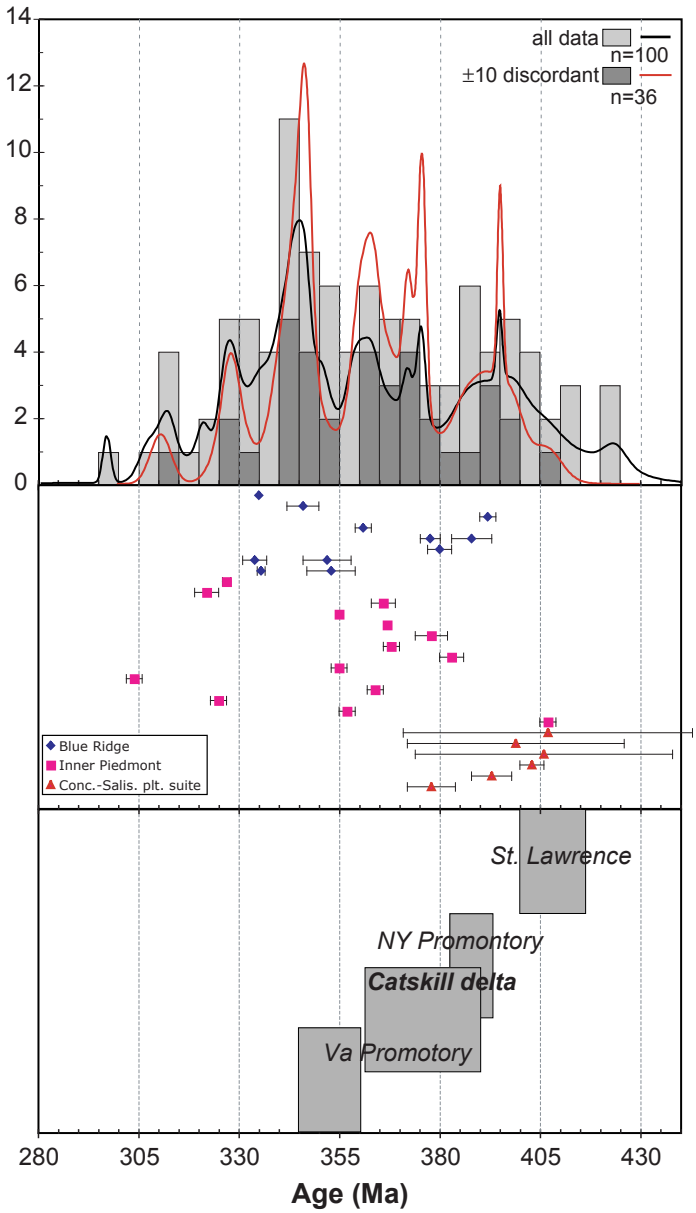

Figure 3–8. Comparison of Silurian to Mississippian U-Pb ages of zircon rims, and magmatism from the Blue Ridge and Inner Piedmont, with reported age of the Catskills delta/Acadian clastic wedge in the New York and Alabama promontories. Constraints on the age and distribution of the clastic wedge data Ettensohn (2004).

suggests this was a major protracted event (407–345 Ma), and peak metamorphism and magmatism likely occurred 375–345 Ma (Fig. 3–8).

Several U-Pb zircon rim ages are younger than ~340 Ma, especially in the Inner Piedmont, and define minor peaks at ~327 and ~310 Ma. Is this just late metamorphic fluids resulting in the growth of new rims, or is it the beginning of another tectonothermal event? Texturally, these youngest zircon rims appear similar to older Devonian and Ordovician rims, and do not display typical spongy textures of hydrothermal zircons. As listed above, 335–320 Ma felsic magmatism occurs in the Blue Ridge and Inner Piedmont Field and structural studies have recognized superposed folds and late foliations interpreted to be early Alleghanian (e.g., Merschat et al., 2005b). Field relationships in the Blue Ridge indicate the ~335 Ma Rabun Granodiorite is truncated by the Chattahoochee fault, implying a late Mississippian ductile deformation in the Blue Ridge (Hatcher et al., 2005; Stahr et al., 2005; and Miller et al., 2006). It is suggested that these late Mississippian to Pennsylvanian ages represent the onset on another moderate to high temperature event that correlates to the beginning of the Alleghanian orogeny. The early Alleghanian orogeny spans from 330–300 Ma, but appears to have more localized affects that produced new fabrics, folds, felsic magmatism, and local areas of greenschist to amphibolite facies metamorphism (Dallmeyer et al., 1986; Merschat et al., 2005b).

Metamorphic Domains

Comparison of thermochronologic data across the Blue Ridge and Inner Piedmont suggests at least two eastward-younging and overlapping Paleozoic metamorphisms (Figs. 3–5, 3–6). Zircon rim data support two general domains: a Middle to Late Ordovician domain in the Blue Ridge overlapped to the east by a Devonian–Mississippian domain extending from eastern Blue Ridge through the Inner Piedmont. ^{40}Ar-^{39}Ar cooling ages, similarly, define an eastward-younging trend, but yield cooling ages significantly younger than zircon rim ages in parts of the Blue Ridge. Integrating U-Pb zircon rim and monazite ages, ^{40}Ar-^{39}Ar cooling ages, metamorphic isograds, distribution of Paleozoic magmatism, and geology; five distinct metamorphic domains can be resolved in the Blue Ridge and Inner Piedmont (Fig. 3–9). Boundaries of the domains are often overprinted by later retrograde shear zones, a metamorphic gradient, or an unrecognized fault. The majority of the domains are fault bounded. The five domains recognized are a Middle to Late Ordovician Taconian core, Devonian to early Mississippian Neoacadian core, late Mississippian to Pennsylvanian, early and late Alleghanian domains, and a domain of polymetamorphism.

Figure 3–9. Metamorphic domains depicting zones of southern Appalachian crust with shared tectonothermal events. Extent of the domains were defined from areas with similar zircon rim ages, continuous of metamorphic isograds, and structural features. Abbreviations of metamorphic minerals and faults are the same as Figs. 3–1, 3–2, and 3–5.

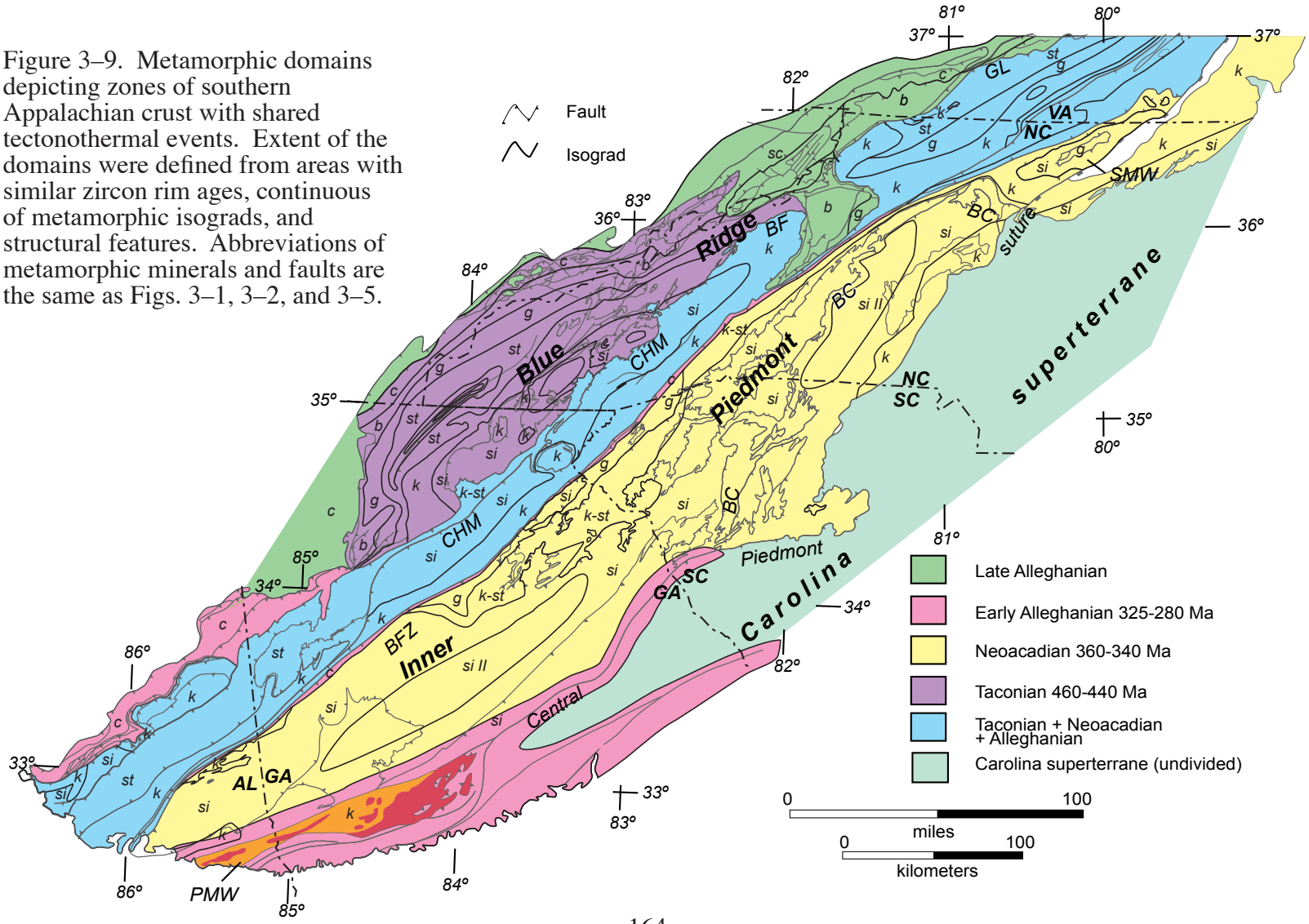

Separation of the southern Appalachians into different metamorphic domains not only attempts to combine areas with the same age of metamorphism, but also similar structural and deformational histories. The domains are also interpreted to contain geologic structures that formed during the same event. The multiple deformations experienced by the southern Appalachians precludes that all structures included in a domain were not formed by or during the same event. Structures in older domains may be superposed by younger structures, but the peak metamorphic assemblage may not be affected. Finally, these domains are not all inclusive, but are an attempt to incorporate existing geochronologic, metamorphic, and structural data. Significant data gaps exist (areas lacking thermochronologic data, specifically U-Pb zircon rim data), and new data may refine these domains.

Taconian core

The Taconian metamorphic core, the oldest domain, occurs in a structural salient in the westernmost part of the Blue Ridge-Piedmont megathrust sheet in the Blue Ridge of eastern Tennessee, northeastern Georgia and western North Carolina (Fig. 3–9). It is almost entirely fault bounded and extends from the Miller Cove and Great Smoky-Cartersville faults to the Chattahoochee-Holland Mountain fault. Laterally, it extends from the junction of the Allatoona and Cartersville-Great Smoky faults near Cartersville, Georgia to west of the Grandfather Mountain window, near the end of the Mars Hill terrane. It contains a continuous Barrovian gradient from greenschist (chlorite grade) to granulite facies. Zircon rim ages range from 480–440 Ma with most around 460 Ma. The Taconian core includes the western Blue Ridge/Laurentian margin, Cartoogechaye, Cowrock and part of the Dahlonega gold belt terranes. Various external and internal Grenville basement massifs are also included within the Taconian core. Middle Ordovician magmatism in the domain is limited to the ~466 Ma Persimmon Creek Gneiss, and several felsic plutonic units in the Georgia Dahlonega gold belt.

Within this continuous section from upper to lower continental crust isograds cross Mesoproterozoic basement massifs, the Greenbrier, Hayesville, Chunky Gal Mountain, and Soque River faults (e.g., Hadley and Goldsmith, 1963; Eckert et al., 1989; Hopson et al., 1989), folded by the Murphy syncline, and truncated along the Great Smoky-Cartersville fault in northeastern Georgia (Tull and Holm, 2005). The present configuration of isograds in this domain is the product of superposed deformations, and structures can be separated into pre-, syn- and post Taconian.

The earliest structures are preserved in the Mesoproterozoic Grenville basement massifs. The affects of Taconian metamorphism on Grenville basement in the western Blue Ridge are not clear, and vary from new crystallization of micas and weak foliation to the development of a gneissic foliation. Several studies have documented crosscutting relationships that indicate the fabrics and structures preserved in several Grenvillian massifs are Mesoproterozoic (Merschat et al., 2005a; Merschat et al., 2006; Hatcher et al., 2006). Ownby et al. (2004) reported U-Pb zircon rim ages of ~470 Ma in the Mars Hill terrane, but hornblende and garnet yield Mesoproterozoic Rb-Sr and Sm-Nd ages from basement rocks north and northwest of the Mars Hill terrane (Goldberg and Dallmeyer, 1997). Much of the ambiguity is likely related to overprinting of high-grade Mesoproterozoic Grenvillian structures by lower grade Taconian metamorphism that was not intense enough to transpose and erase previous fabrics, structures, and mineral assemblages.

Taconian structures can divided into pre- and syn- to post-metamorphic structures. Pre-metamorphic Taconian structures are rare, and the most prominent is the Greenbrier fault, a pre-metamorphic thrust (Hadley and Goldsmith, 1963). The majority of the structures within the domain are syn-metamorphic including multiple foliations and fold generations. The transition from greenschist to upper amphibolite and granulite facies also corresponds to increased structural complexity. Greenschist-facies rocks contain bedding (S_0) with well developed axial planar cleavage (S_1) to tight to closed folds in western part of the domain succumb to multiple foliation and fold generations as grade increases to upper amphibolite to granulite facies (Hatcher and Butler, 1979). The Hayesville, Chunky Gal Mountain, and Shope Fork faults are syn-metamorphic and responsible for juxtaposing the Cartoogechaye and Cowrock terranes against each other and the western Blue Ridge. Zircon rim ages from ~10m below the Chunky Gal Mountain fault (sample CGM) yield a weighted average of ~461 Ma, a maximum age of the amphibolite grade fault. Moecher et al. (2005) reported a monazite chemical age of ~459 Ma from the Hayesville fault hanging wall. These middle Ordovician ages suggest faults are syn- to post-metamorphic Taconian faults.

Superposed on the Taconian and older structures are younger Neoacadian or Alleghanian structures. The western boundary consists of Alleghanian thrust faults including the Cartersville-Great Smoky and Miller Cove faults. Truncation of chlorite and biotite isograds against the simple windows framed by the Great Smoky fault in the western Blue Ridge of eastern Tennessee establishes the relative timing of metamorphism and faulting (Hadley and Goldsmith, 1963). Similarly, Tull and Holm (2005) interpreted

folding of the isograds around the southern end of the Murphy syncline and truncations against the Cartersville fault to be the result of the Blue Ridge-Piedmont megathrust sheet passing over a transverse footwall ramp. In the higher-grade eastern part of the domain, younger structures are manifested as superposed folds, late foliations, slip and crenulations cleavages, and late retrograde shear zones (Hadley and Goldsmith, 1963; Massey and Moecher, 2005; Moecher et al., 2005).

Based on a similar position in a structural salient in the Alabama Piedmont, another Taconian core candidate is the Hollins Line thrust sheet in Alabama. It contains kyanite and sillimanite grade rocks abutted to the southeast by lower grade, staurolite zone rocks of the Goodwater-Enitachopoco thrust sheet. Steltenpohl and Moore (1988) proposed this boundary was a normal fault, and sheared pegmatite along the Goodwater-Enitachopoco fault indicate dextral and normal-slip kinematics (Steltenpohl, 2005). ^{40}Ar-^{39}Ar ages from the Hollins Line thrust sheet are Mississippian (Steltenpohl et al., 2008) and no U-Pb zircon rim or monazite ages from the Hollins Line thrust sheet leave this a suspect area of Taconian metamorphism.

Neoacadian domain

The Inner Piedmont roughly corresponds to the Neoacadian core, the largest domain (Fig. 3–9). It is cored by a broad zone of migmatitic sillimanite I and II zone rocks, flanked on the west by kyanite to garnet grade, and kyanite grade rocks on the east (Butler, 1991; Hatcher and Goldberg, 1991; Hatcher and Merschat, 2006). This domain is bound to the west by the narrow, linear belt of retrograde metamorphism associated with the early Alleghanian reactivation of the Brevard fault zone. The central Piedmont suture marks the eastern boundary until the Georgia-South Carolina border, where a domain of early Alleghanian metamorphism parallels the suture and eventually widens to include the Pine Mountain window and parts of the Alabama Inner Piedmont. U-Pb ages of zircon rims from the Inner Piedmont range from 410 to 300 Ma with prominent peaks at ~396, ~376, ~364, and ~348 Ma (Neoacadian), with lesser peaks at ~328 and ~310 Ma. TIMS U-Pb monazite ages (Dennis and Wright, 1997a, 1997b; Dennis, 2007) and ^{40}Ar/^{39}Ar mineral cooling ages (Dallmeyer, 1988) also support a Late Devonian to Early Mississippian age of metamorphism in this domain. Paleozoic magmatism consists of both Middle Ordovician granitoids in the eastern Tugaloo terrane/western Inner Piedmont and several anatectic granitoids from the Inner Piedmont that range from 407 Ma to 350 Ma, with most ages between 380–350 Ma (Giorgis et al., 2002; Mapes, 2002; Gatewood, 2007; Byars et al., 2008b). Undeformed pegmatite dikes in the western Inner Piedmont

and Cat Square terrane have yielded SHRIMP U-Pb ages of ~325 Ma (Bream, 2003; Gatewood, 2007). All of these support a major ~360 Ma Neoacadian tectonothermal event in the Inner Piedmont. Both the metamorphic and magmatic ages span a 70 m.y. interval, suggesting a protracted event. Intrusion of the ~325 Ma pegmatites bracket the timing of deformation, and possibly represent the "last gasp" of the Neoacadian orogeny.

Structurally the Inner Piedmont can be characterized as a gently dipping stack of northwest- and southwest-vergent type-F thrust sheets (fold-nappes) (Hatcher and Hooper, 1992; Davis, 1993a, 1993b; Merschat et al., 2005b; Hatcher and Merschat, 2006). Goldsmith (1981) first recognized the curved pattern defined by the regional fabric elements, S_2, L_2, and F_2, in the Inner Piedmont. These fabric elements are commonly defined by high-temperature mineral assemblages that contain either sillimanite, hornblende, or kyanite, and the occurrence of migmatite parallel to S_2 suggest these fabrics developed during near-peak metamorphic conditions (Merschat et al., 2005b; Hatcher and Merschat, 2006). Isograds along the western flank are parallel to the gentle to moderate, southeast-dipping regional S_2 foliation and the ductile faults bounding the large type-F thrust sheets. Map-scale truncations of the megacrystic Walker Top granite (~407 and 355 Ma) against the Brindle Creek fault bracket the maximum age of the fault to early Mississippian (Kalbas, 2003; Byars et al., 2008a; Gilliam et al., 2008; Merschat et al., 2008). Merschat et al. (2005b) suggested that the Inner Piedmont thrust stack and the curved L_2 pattern resulted from west- and northwest-directed flow, rooted in the east, was deflected to the southwest by a buttress in the hanging wall of the Neoacadian Brevard fault zone. These regional fabrics, S_2, L_2, and F_2, and map scale faults and folds formed at near-peak conditions at 360–345 Ma.

Unlike the Taconian metamorphic core in the Blue Ridge, older structures formed during an earlier orogeny are difficult to uniquely identify. This is likely the product of the extensive transposition of structures into the Neoacadian fabric, and/or only minor affects of the Taconian metamorphism and deformation in the western Inner Piedmont/ eastern Tugaloo terrane. Younger Alleghanian structures are recognized throughout the Inner Piedmont including late retrograde shear zones like the Brevard fault zone (Hatcher, 2001), and several episodes of folding (e.g., Merschat et al., 2005b).

Mixed Domain

Located between the Taconian and Neoacadian domains, the eastern Blue Ridge represents a middle- to upper-amphibolite facies polymetamorphic domain, bound by the Chattahoochee-Holland Mountain-Burnsville-Gossan-Lead fault to the northwest and the

Brevard fault zone to the southeast. The majority of this domain is kyanite to sillimanite zone, but decreases to staurolite grade in northwestern North Carolina. Unfortunately, only limited data from U-Pb ages of zircon exist from the eastern Blue Ridge, and thermochronologic data support multiple events. Evidence for Middle to Late Ordovician metamorphism and deformation occur in the western parts of the eastern Blue Ridge, yet evidence supporting younger metamorphism and deformation occur across the domain. Miller et al. (2000a, 2006) reported a U-Pb age of ~459 Ma for the Lick Ridge eclogite, suggesting a Taconian event in the eastern Blue Ridge. Further evidence supporting a Taconic tectonothermal event include Middle to Late Ordovician magmatism (Whiteside Granite, Elkahatchie granodiote, Kowaliga, Zanna; Miller et al., 1998; Miller et al., 2000b) and 480–440 Ma Rb/Sr and Sm/Nd ages of garnet and hornblende (Goldberg and Dallmeyer, 1997). Three zircon rim ages from this study range from 360–350 Ma and, combined with ^{40}Ar-^{39}Ar ages of hornblende, biotite, and muscovite, suggest the Neoacadian orogeny also affected the eastern Blue Ridge in Georgia, North Carolina, and South Carolina.

Early and late Alleghanian domains

Zircon rim ages from the Inner Piedmont and ^{40}Ar-^{39}Ar cooling ages of muscovite from across the southern Appalachians record a 330–300 Ma event and suggest a major event affected the orogen (Fig. 3–6). Preserved domains of middle Paleozoic, upper amphibolite to granulite facies metamorphism described above indicate this event was not sufficient to erase previous metamorphisms. Alleghanian structures are documented in all of the middle Paleozoic domains, but metamorphism associated with it is localized. The Alleghanian domains are separated into early and late based on age, metamorphic grade, and structural style. Early Alleghanian domains are characterized by upper greenschist to lower amphibolite facies metamorphism that spanned 325–280 Ma. These domains include a thin, linear belt associated with the Brevard fault zone in the Inner Piedmont, and a larger domain that extends from near Columbia, South Carolina, to Auburn, Alabama, that includes parts of the Inner Piedmont, Pine Mountain Window, Carolina superterrane Modoc shear zone, and Uchee belt. Although these domains are associated with significant amounts of dextral retrogressive shearing, the boundaries of the domains may not be entirely fault bounded. Late Alleghanian domains occur mostly along the westernmost part of the Blue Ridge-Piedmont megathrust sheet and include mostly anchizone to chlorite zone metamorphism, and development of a cleavage and S-C fabric in some shear zones.

Early Alleghanian. A 3–5 km wide zone of retrograde greenschist facies metamorphism along the western edge of the Inner Piedmont represents the early Alleghanian Brevard fault zone (Bryant and Reed, 1970; Hatcher, 2001). The Rosman fault marks the western boundary of this domain, while the eastern limit is a gradational boundary. Neoacadian isograds are truncated by the zone of retrograde greenschist facies metamorphism associated with the Alleghanian dextral reactivation of the Brevard fault (Hatcher, 2001). Interestingly, structures within the Alleghanian Brevard fault zone are parallel to high-temperature Neoacadian structures, S_2, L_2, and F_2, in the Inner Piedmont (Bryant and Reed, 1970; Hatcher, 2001). Relative relationships indicate the Alleghanian Brevard fault zone is younger than 360–345 Ma, age of Neoacadian metamorphism in the Inner Piedmont. Sinha et al. (1988) reported a Rb-Sr age of ~273 Ma from mylonitic Henderson gneiss from this zone.

Mississippian plant fossils from the Erin slate (Gastaldo et al., 1993) and ^{40}Ar-^{39}Ar muscovite ages from the various units of the Talladega belt (McClellan et al., 2007) confirm that the uniformly chlorite grade belt is metamorphosed between 350–320 Ma and represents another early Alleghanian domain (Fig. 3–9). To the northwest, the Talladega fault separates chlorite grade rocks from unmetamphosed rocks the Valley and Ridge. The Hollins line fault juxtaposes amphibolite facies rock of the eastern Blue Ridge to the southeast.

The largest domain of early Alleghanian metamorphism extends from the Georgia–South Carolina border to beneath the Coastal Plain near the Georgia–Alabama border. It is closely related with deformation in the Modoc shear zone (Dallmeyer et al., 1986) and extends southwest into the Uchee belt and Inner Piedmont including the Mountain window (Steltenpohl, 2005; Steltenpohl et al., 2008). Parts of this domain closely correspond to the Modoc shear zone and framing faults of the Pine Mountain window, yet elsewhere the boundaries are loosely defined. Reported ages of deformation vary from 315–295 Ma for the Modoc shear zone (Dallmeyer et al., 1986), to ~300 Ma in the Pine Mountain window and framing faults (Steltenpohl et al., 2008).

Late Alleghanian domains. Late Alleghanian domains are located along the transition from the crystalline terranes of the Blue Ridge-Piedmont megathrust sheet and the eastern Valley and Ridge (Fig. 3–9). Anchizone to greenschist facies (biotite to garnet zones) metamorphism in this domain may be manifested as weakly to well developed cleavage or S-C fabrics in ductile greenschist grade shear zones like Linville Falls or Unaka Mountain faults. These domains are interpreted to be related to emplacement of the Blue

Ridge-Piedmont megathrust sheet at 280–260 Ma. Bryant and Reed (1970) and Boyer and Elliot (1982) interpreted the greenschist to lower amphibolite grade fabrics developed in the rocks of Grandfather Mountain window to be synmetamorphic with thrusting along the Linville Falls fault. The Shady Valley thrust sheet in northeasternmost Tennessee contains cleaved sub-chlorite grade rocks that formed during the same event (King and Ferguson, 1960).

Summary

The proposed metamorphic domains reveal the basic thermal architecture of the southern Appalachian crystalline orogen: regional Paleozoic metamorphism becomes younger toward the east or marginward, and locally overprints and remobilizes the more cratonward, older Paleozoic metamorphism. Structural salients preserve areas of older Paleozoic metamorphism while intervening recesses are overprinted by younger events. The Taconian metamorphic core is located in a structural salient in the Blue Ridge-Piedmont megathrust sheet that also corresponds to the Tennessee salient (embayment). These patterns are not unique and are the expected result of multiple collisional orogenies. Similar patterns are recognized in other parts of the Appalachian orogen (e.g., Robinson et al., 1998) and various ancient and modern orogens. The distribution and timing of regional Paleozoic metamorphism, therefore, provides critical constraints on the timing of terrane accretion.

Constraints on terrane accretion

Different models have been proposed to explain the timing of collision and accretion of southern Appalachians terranes, and regional metamorphism and deformation. Timing of accretion of the Carolina superterrane has been especially controversial and an Ordovician Taconic (Secor et al., 1986; Vick et al., 1987; Hibbard, 2000; Hibbard et al., 2002; Dennis, 2007); Devonian Acadian-Neoacadian (Williams and Hatcher, 1983; Hatcher, 1989; Sinha et al., 1989; Miller et al., 2006; Merschat and Hatcher, 2007); and Pennsylvanian-Permian Alleghanian (Dennis and Wright, 1997b; Steltenpohl et al., 2008) collisions have been proposed, with the strongest evidence supporting a Devonian–Mississippian collision (Merschat et al., 2005b; Hatcher and Merschat, 2006; Merschat and Hatcher, 2007). A common element in all of these models is the juxtaposition of the Carolina superterrane against the Inner Piedmont; therefore, the timing of metamorphism and deformation in the Inner Piedmont is critical to the timing of accretion of the Carolina superterrane and other southern Appalachian terranes. The

U-Pb zircon rim ages presented above, combined with other published thermochronologic ages, provide important data sets to examine the timing of regional metamorphism and terrane accretion in the southern Appalachians.

The oldest shared metamorphic event between terranes is interpreted to mark the time of accretion. Younger metamorphic or deformational events may affect the terranes after they have been accreted, like the Tugaloo terrane. It contains evidence of three tectonothermal events—Taconian, Neoacadian, and Alleghanian—but the oldest regional metamorphism, Middle Ordovician Taconian metamorphism, and associated magmatism are interpreted to correspond to the time of accretion to the eastern Laurentia margin.

In the Blue Ridge the oldest Paleozoic metamorphic event at 460–450 Ma links the terranes of western Blue Ridge/Laurentian margin, Cartoogechaye, Cowrock, Dahlonega gold belt, and Tugaloo terranes. Rb-Sr and Sm-Nd mineral ages, and ~459 Ma eclogite facies metamorphism, in conjunction with Middle Ordovician magmatism in the Tugaloo terrane are interpreted to be the effects of Taconian metamorphism and deformation. Suspect peri-Laurentian terranes (Cartoogechaye, Cowrock, Dahlonega gold belt, and Tugaloo terranes) accreted to Laurentia margin/western Blue Ridge during the Taconic orogeny, resulting in greenschist to upper amphibolite and granulite facies metamorphism. Linking of Taconic metamorphism with deformation in the Carolina Slate belt has been used to support the accretion of the Carolina superterrane to Laurentia during the Taconic orogeny (Vick et al., 1987; Hibbard, 2000; Hibbard et al., 2002). However, the only evidence of the Taconic event in the Inner Piedmont is granitic magmatism in the Tugaloo terrane and thus cannot be linked directly to Ordovician docking of the Carolina superterrane. Metamorphic zircon, monazite and ^{40}Ar-^{39}Ar ages, and the style of deformation in the Inner Piedmont do not support an Ordovician collision of the Carolina superterrane.

Zircon rim ages presented herein confirm that the Inner Piedmont was metamorphosed to upper amphibolite conditions during the Neoacadian orogeny, 360–340 Ma. If the Carolina superterrane was accreted prior to this event (Ordovician), it would have experienced a similar Late Devonian to Mississippian high-temperature tectonothermal event. Evidence of a pervasive Devonian to Mississippian tectonothermal event in the Carolina superterrane is lacking. Dallmeyer et al. (1986) reported discordant ^{40}Ar-^{39}Ar mica and hornblende ages from the western Carolina superterrane (Charlotte and Carolina slate belts) in South Carolina are reset by a Late Devonian tectonothermal event ~360 Ma. ^{40}Ar-^{39}Ar ages of muscovite and hornblende from the Gold Hill-Silver Hill shear zone, the boundary between the Charlotte and Carolina terranes, yield ages

of ~391 and ~358 Ma (e.g., Hibbard et al., 2002, and references therein). Instead, the majority of the Carolina superterrane was affected by a Virgilina metamorphism between 630–535 Ma (Hibbard et al., 2002). Dennis and Wright (1997b) bracketed amphibolite facies metamorphism in the Carolina superterrane at ~535 Ma. A pervasive Neoacadian event is not recognized, suggesting the Carolina superterrane was not part of Laurentia before the Devonian. Instead, localized Devonian metamorphism along the margin is consistent with a 407–360 Ma accretion.

Additional evidence supporting mid-Paleozoic accretion of the Carolina superterrane includes Sr and Nd isotopic data from granitic plutons of the Carolina superterrane and detrital zircons from the Cat Square terrane. Sr and Nd isotopic data from Neoproterozoic, mid-Paleozoic, and Carboniferous granitic rocks of the Carolina superterrane suggest a dominantly juvenile Neoproterozoic source, with minor contributions from 1.0 Ga or older crust (Fullagar et al., 1997). Fullagar et al. (1997) concluded that the middle and late Paleozoic plutons were derived from a juvenile source similar to the Carolina superterrane with minor to no input from Grenvillian source, suggesting a mid- to late Paleozoic accretion of the Carolina superterrane. The Cat Square terrane contains a unique suite of detrital zircons that include peri-Gondwanan 600 and 530 Ma ages and Ordovician to Silurian, 480–430 Ma ages (Bream et al., 2004; Gatewood, 2007). These ages constrain the maximum age of the rocks and provide a link to the Carolina superterrane (Merschat and Hatcher, 2007). A minimum age is constrained by the granitic intrusions in the Cat Square terrane and time of metamorphism. Appearance of peri-Gondwanan detrital zircons in foreland clastic wedges does not occur until the Devonian, supporting a mid-Paleozoic accretion (Thomas et al., 2004; Eriksson et al., 2004; Park et al., 2008).

TECTONIC MODELS

Following successful rifting of Rodinia at the Proterozoic-Paleozoic boundary, the southern Appalachian orogen evolved as an accretionary-collisional orogen, adding new material to its margin until the late Paleozoic assembly of supercontinent Pangea. U-Pb ages of zircon rims suggest the southern Appalachians were affected by three tectonothermal events; a 460–450 Ma Taconian, 360–340 Ma Neoacadian and an early Alleghanian at 330–300 Ma. Both Middle Paleozoic events, Taconian and Neoacadian, resulted in regional upper amphibolite facies metamorphism; however, the duration of the events as recorded by zircon rim ages is significantly different. Nearly half of the Ordovician metamorphic rim data occur within 10 m.y. between 460–450 Ma;

however, Neoacadian data are scattered over ~70 m.y. between 400–330 Ma (Figs. 3–7, 3–8). Dewey (2005) notes that arc-continent collisions are geologically brief (~15 m.y.) compared to longer lasting continent-continent collisions (~50 m.y.). Variation in duration of the two events is quite substantial, suggesting significantly different styles and kinematics existed during these two Middle Paleozoic orogenies.

The Taconic orogeny was the result a continent-arc collision between the various different oceanic- and continental-arc terranes of the Blue Ridge and Inner Piedmont, Cartoogechaye, Cowrock, Dahlonega gold belt and Tugaloo, with the western Blue Ridge/Laurentian margin. Lack of Ordovician plutons in the western Blue Ridge/Laurentian margin and occurrence in terranes to the east suggests east-directed subduction beneath the accreting terranes. The Tugaloo terrane, the structurally highest terrane, contains the most Ordovician plutons, and thus may represent the upper plate during the orogeny.

The Neoacadian orogeny has been described as continent-micro continent collision (Hatcher, 2002b; Merschat et al., 2005b; Hatcher and Merschat, 2006; Merschat and Hatcher, 2007), and is in agreement with the ~70 m.y. span of metamorphic zircon ages. Proposed tectonic models suggest east-directed subduction beneath the Carolina superterrane, resulting in magmas associated with the Concord and Salisbury plutonic suites. By ~400 Ma, the Carolina superterrane had overthrust the Cat Square terrane and most of the Tugaloo terrane, and magmatism in the overlying plate ceased. The thickened crust consisting of the Tugaloo and Cat Square terranes, capped by the Carolina superterrane, was subjected to mid-crustal conditions and regional amphibolite facies metamorphism. Additionally, by ~380 Ma (and possibly as early as ~407 Ma) the mid-crustal conditions produced migmatite and the anatectic granites of the Cat Square terrane. The migmatitic rocks of the Inner Piedmont flowed west and southwestward from beneath the Carolina superterrane as a curved orogenic channel (Hatcher and Merschat, 2006). The channel was buttressed against and partially overrode parts of the eastern Blue Ridge/western Tugaloo terrane. As the footwall of the orogenic channel, rocks of the western Tugaloo terrane were transposed into Neoacadian structures and the growth of higher-pressure (kyanite) amphibolite facies assemblages. The effects of the Neoacadian decreased westward and is expressed in parts of the central and western Blue Ridge as superposed folds, late foliations, and minor shear zones.

Collision of Gondwana with Laurentia began as early as ~330 Ma, and reloaded the amalgamated terranes. Parts of the orogen still warm from the Neoacadian orogeny may have developed younger high temperature assemblages as indicated by the growth

of zircon rims. Areas of Alleghanian metamorphism are mostly related to reorganization of the crust through an anastomosing network of dextral shear zones and accommodating the large amounts of shortening associated with emplacement of the Blue Ridge thrust sheet (Hatcher, 1989). Metamorphism associated with the Alleghanian is mostly greenschist facies, except in the Modoc shear zone which reached amphibolite facies.

The Taconic orogeny, ~460 Ma, resulted from the accretion of peri-Laurentian terranes including the Cartoogechaye, Cowrock, Dahlonega gold belt, and Tugaloo terranes. After assembled, these terranes became the margin of Laurentia until the Devonian collision of the peri-Gondwanan Carolina superterrane. Collision of the Carolina superterrane closed the Rheic ocean, resulting in the addition of the Cat Square terrane, metamorphism, and mobilization of the Inner Piedmont as an orogenic channel (Hatcher and Merschat, 2006; Merschat and Hatcher, 2007). Parts of the Tugaloo terrane were also remobilized during this event.

CONCLUSIONS

1. Ion microprobe analyses of zircon rims can provide critical information regarding the timing of metamorphism in polydeformed high-grade metamorphic terranes.
2. The southern Appalachian orogen was affected by three major Paleozoic tectonothermal events: Middle Ordovician 465–450 Ma, Taconian, Devonian-Mississippian 360–340 Ma, Neoacadian, and late Mississippian-Pennsylvanian 330–300 Ma, Alleghanian orogenies.
3. Five metamorphic domains can be separated using metamorphic isograds, geology and distribution of U-Pb zircon rim ages and other thermochronologic published ages. The Taconian core, ~460 Ma, extends from the Great Smoky fault to the Chattahoochee-Holland Mountain-Burnsville fault, and Gossan Lead fault to the north. A second domain of 360–340 Ma U-Pb zircon rim ages defines the large sillimanite-grade core of the Inner Piedmont. The eastern Blue Ridge, from the Chattahoochee-Holland Mountain-Burnsville-Gossan Lead fault to the Brevard fault zone, defines a domain that was affected by three orogenies, and likely remained at mid-crustal conditions for over 100 m.y. Finally, domains of early and late Alleghanian metamorphism are distributed along retrograde fault zones that bound the domains of older higher-temperature metamorphism.

4. The Taconian core is preserved in a structural salient that closely corresponds to the Tennessee salient. Intervening recesses are overprinted by younger metamorphisms.
5. Terranes of the western, central, and eastern Blue Ridge, including the Tugaloo terrane, were affected by a ~460 Ma Taconian event. The Taconic orogeny is interpreted to be the result of the collision and accretion of the peri-Laurentian terranes of the central and eastern Blue Ridge with the western Blue Ridge/ Laurentian margin.
6. The Inner Piedmont was affected by a ~360 Ma Neoacadian orogeny resulting from the oblique collision of the Carolina superterrane. The Inner Piedmont was underthrust beneath the Carolina superterrane and flowed westward and southwestward as a mid-Paleozoic orogenic channel.

ACKNOWLEDGMENTS

Joe Wooden, Anders Meibom, Frank Mazdab (Stanford University) and Chris Coath (UCLA) provided assistance with the zircon ion microprobe analyses. Allan Patchen provided assistance with obtaining CL images at the University of Tennessee. Heather Byars and Matthew Gatewood are acknowledged for permission to include several zircon rim analyses. Research was funded by NSF grant EAR-9814800 to RDH and EAR-9814801 to CFM; the University of Tennessee Science Alliance Center of Excellence; and U. S. Geological Survey National Cooperative Geologic Mapping Program (EDMAP and FEDMAP components).

REFERENCES CITED

Abbott, R. N., Jr., and Greenwood, J. P., 2001, Retrograde metamorphism of eclogite in the southern Appalachian mountains, U.S.A.—A case involving seamount subduction: Journal of Metamorphic Geology, v. 19, p. 433-443.

Abbott, R. N., Jr., and Raymond, L. A., 1984, The Ashe Metamorphic Suite, northwest North Carolina: Metamorphism and observations on geologic history: American Journal of Science, v. 284, p. 350-375.

Abbott, R. N., Jr., and Raymond, L. A., 1997, Petrology of pelitic and mafic rocks in the Ashe and Alligator Back metamorphic suites, northeast of the Grandfather Mountain window, *in* Stewart, K. G., Adams, M. G., and Trupe, C. H., eds., Paleozoic structure, metamorphism, and tectonics of the Blue Ridge of western North Carolina: Carolina Geological Society Field Trip Guidebook, p. 87-101.

Bentley, R. D. & Neathery, T. N., 1970, Geology of the Brevard zone and related rocks of the Inner Piedmont of Alabama: Alabama Geological Society, Eighth Annual Field Trip Guidebook, 119 p.

Berquist, P. J., 2005, U–Pb geochronology and geochemistry of southern Appalachian basement: Tectonic implications and constraints on age, extent, and origin [M.S. thesis]: Nashville, Tennessee, Vanderbilt University, 91 p.

Bier, S. E., 2001, Geology of the southeastern South Mountains, North Carolina [M.S. thesis]: Knoxville, University of Tennessee, 162 p.

Bier, S. E., Giorgis, S. D., Bream, B. R., Williams, S. T., and Hatcher, R. D., Jr., 2000, Temperature and pressure estimates of Acadian metamorphism in the Inner Piedmont, North Carolina: Geological Society of America Abstracts with Programs, v. 32, no. 2, p. 6.

Boyer, S. E., and Elliot, D., 1982, Thrust systems: The American Association of Petroleum Geologist Bulletin, v. 66, p. 1196-1230.

Bream, B. R., 2002, The southern Appalachian Inner Piedmont: New perspectives based on recent detailed geologic mapping, Nd isotopic evidence, and zircon geochronology, *in* Hatcher, R. D., Jr., and Bream, B. R., eds., Inner Piedmont geology in the South Mountains-Blue Ridge Foothills and the southwestern Brushy Mountains, central-western North Carolina: Carolina Geological Society Guidebook, p. 45-63.

Bream, B. R., 2003, Tectonic implications of geochronology and geochemistry of para- and orthogneisses from the southern Appalachian crystalline core [Ph.D. dissertation]: Knoxville, University of Tennessee, 296 p.

Bream, B. R., Hatcher, R. D., Jr., Miller, C. F., and Fullagar, P. D., 2004, Detrital zircon ages and Nd isotopic data from the southern Appalachian crystalline core, GA-SC-NC-TN: New provenance constraints for Laurentian margin paragneisses, *in* Tollo, R. P., Corriveau, L., McLelland, J., and Bartholomew, M. J., eds., Proterozoic evolution of the Grenville orogen in North America: Geological Society of America Memoir 197, p. 459-475.

Bryant, B., and Reed, J. C., Jr., 1970, Geology of the Grandfather Mountain window and vicinity, North Carolina and Tennessee: U.S. Geological Survey Professional Paper 615, 190 p.

Butler, J. R., 1991, Metamorphism, *in* Horton, J. W., Jr., and Zullo, V. A., eds., The geology of the Carolinas: Knoxville, University of Tennessee Press, p. 127-141.

Byars, H. E., in progress, Geology and geochronology of the west central portion of the Newton Window, Inner Piedmont: Timing and implications for the emplacement of mafic-ultrramafic complexes, the Paleozoic Vale charnockite and megacrystic granites [M.S. thesis]: Knoxville, Tennessee, University of Tennessee, xxx p.

Byars, H. E., Gilliam, W. G., Hatcher, R. D., Jr., Merschat, A. J., and Bier, S. E., 2008a, Tectonic evolution of the Appalachian Inner Piedmont from a new detailed geologic map from the Brevard fault into the Newton Window: Geological Society of America Abstracts with Programs, v. 40, no. 6, p. 157.

Byars, H., Merschat, A. J., Hatcher, R. D., Jr., and Wooden, J., 2008b, Timing and implications for the emplacement of Paleozoic Vale (Cat Square) charnockite and Walker Top Granite, eastern Inner Piedmont: Geological Society of America Abstracts with Programs, v. 40, no. 4, p. 18.

Callahan, J.E., Bream, B.R., Johnson, N.E., and Stepp, J.D., 2007, Geochemistry of megacrystic zircons with distinctive fluorescent zircon populations from the Freeman Mine, North Carolina: Southeastern Geology, v. 45, p. 1-13.

Carpenter, R. H., 1970, Metamorphic history of the Blue Ridge province of Tennessee and North Carolina: Geological Society of America Bulletin, v. 81, p. 749-762.

Carrigan, C. W., Bream, B. R., Miller, C. F., and Hatcher, R. D., Jr., 2001, Ion microprobe analyses of zircon rims from the eastern Blue Ridge and Inner Piedmont, NC-SC-GA: Implication for the timing of Paleozoic metamorphism in the southern Appalachians: Geological Society of America Abstracts with Programs, v. 33, no. 2, p. 7.

Carrigan, C. W., Miller, C. F., Fullagar, P. D., Bream, B. R., Hatcher, R. D., Jr., and Coath, C. D., 2003, Ion microprobe age and geochemistry of southern

Appalachian basement, with implications for Proterozoic and Paleozoic reconstructions: Precambrian Research, v. 120, p. 1-36.

Cherniak, D. J., and Watson, E. D., 2000, Pb diffusion in zircon: Chemical Geology, v. 172, p. 5-24

Cherniak, D. J., and Watson, E. D., 2003, Diffusion in zircon, *in* Hanchar, J. M., and Hoskin, P. W. O., eds., Zircon: Reviews in mineralogy and geochemistry: Washington D.C., v. 53, 113-143.

Connelly, J. B., and Dallmeyer, R. D., 1993, Polymetamorphic evolution of the western Blue Ridge: Evidence from $^{40}Ar/^{39}Ar$ whole-rock slate/phyllite and muscovite ages: American Journal of Science, v. 293, p. 322-359.

Corfu, F., Hanchar, J. M., Hoskin, P. W. O., and Kinny, P., 2003, Atlas of zircon textures, *in* Hanchar, J. M., and Hoskin, P. W. O., eds., Zircon: Reviews in mineralogy and geochemistry: Washington D.C., v. 53, p. 468-500.

Corrie, S. L., and Kohn, M. J., 2007, Resolving the timing of orogenesis in the western Blue Ridge, southern Appalachians, via *in situ* ID-TIMS monazite geochronology: Geology, v. 35, p. 627-630.

Dallmeyer, R. D., 1988, Late Paleozoic tectonothermal evolution of the western Piedmont and eastern Blue Ridge, Georgia: Controls on the chronology of terrane accretion and transport in the southern Appalachian orogen: Geological Society of America Bulletin, v. 100, p. 702-713.

Dallmeyer, R. D., Wright, J. E., Secor, D. T., Jr., and Snoke, A. W., 1986, Character of the Alleghanian orogeny in the southern Appalachians: Part II. Geochronological constraints on the tectonothermal evolution of the east Piedmont in South Carolina: Geological Society of America Bulletin, v. 97, p. 1329-1344.

Davis, T. L., 1993a, Lithostratigraphy, structure, and metamorphism of a crystalline thrust terrane, western Inner Piedmont, North Carolina [Ph.D. dissertation]: Knoxville, University of Tennessee, 245 p.

Davis, T. L., 1993b, Geology of the Columbus Promontory, western Piedmont, North Carolina, southern Appalachians, *in* Hatcher, R. D., Jr., and Davis, T. L., eds., Studies of Inner Piedmont geology with a focus on the Columbus Promontory: Carolina Geological Society Guidebook, North Carolina Geological Survey, p. 17-43.

Dennis, A. J., 2007, Cat Square basin, Catskill clastic wedge: Silurian-Devonian orogenic events in the central Appalachians and the crystalline southern Appalachians, *in* Sears, J. W., Harms, T. A., and Evenchick, C. A., eds., Whence

the Mountains? Inquiries into the evolution of orogenic systems: A volume in honor of Raymond A. Price: Geological Society of America Special Paper, 433, p. 313-329.

Dennis, A. J., and Wright, J. C., 1997a, Middle and late Paleozoic monazite U-Pb ages, Inner Piedmont, South Carolina: Geological Society of America Abstracts with Programs, v. 29, no. 3, p. 12.

Dennis, A. J., and Wright, J. C., 1997b, The Carolina terrane in northwestern South Carolina, U.S.A: Late Precambrian-Cambrian deformation and metamorphism in a peri-Gondwanan oceanic arc: Tectonics, v. 16, p. 460-473.

Dewey, J. F., 2005, Orogeny can be very short: Proceedings of the National Academy of the Sciences, v. 102, p. 15286-15293.

Drake, A. A., Jr., Sinha, A. K., Laird, J., and Guy, R. E., 1989, The Taconic orogen, Chapter 4, *in* Hatcher, R. D., Jr., Thomas, W. A., and Viele, G. W., eds., The Appalachian-Ouachita orogen in the United States: Boulder, Colorado, Geological Society of America, The Geology of North America, v. F-2, p. 101-178.

Eckert, J. O., Jr., 1984, Stratigraphy, structure, and metamorphism of the east half of the Wayah Bald quadrangle, North Carolina: Evidence for Paleozoic granulite facies metamorphism in the southern Appalachians [M.S. thesis]: Columbia, South Carolina, University of South Carolina, 411 p.

Eckert, J. O., Hatcher, R. D., Jr., and Mohr, D. W., 1989, The Wayah granulite-facies metamorphic core, southwestern North Carolina: High-grade culmination of Taconic metamorphism in the southern Blue Ridge: Geological Society of America Bulletin, v. 101, p. 1434-1447.

Eriksson, K. A., Campbell, I. H., Palin, J. M., Allen, M. C., and Bock, B., 2004, Evidence for multiple recycling in Neoproterozoic through Pennsylvanian sedimentary rocks of the central Appalachian basin: Journal of Geology, v. 112, p. 261-276.

Espenshade, G. H., Rankin, D. W., Shaw, K. W., and Neuman, R. B., 1975, Geologic map of the east half of the Winston-Salem quadrangle, North Carolina-Virginia: U.S. Geological Survey Map I-709-B, scale 1:250,000.

Ettensohn, F. R., 2004, Modeling the nature and development of major Paleozoic clastic wedges in the Appalachian basin, USA: Journal of Geodynamics, v. 37, p. 657-681.

Force, E. R., 1976, Metamorphic source rocks of titanium placer deposits—A geochemical cycle: U. S. Geological Survey Professional Paper 959-B, 16 p.

Fullagar, P. D., Goldberg, S. A., and Butler, R. J., 1997, Nd and Sr isotopic characterization of crystalline rocks from the southern Appalachian Piedmont and Blue Ridge, North and South Carolina, *in* Sinha, A. K., Whalen, J. B., and Hogan, J. P., eds., The nature of magmatism in the Appalachian Orogen: Boulder, Colorado, Geological Society of America Memoir 191, p. 165-179.

Gastaldo, R. A., Guthrie, G. M., and Steltenpohl, M. G., 1993, Mississippian fossils from southern Appalachian metamorphic rocks and their implications for Late Paleozoic tectonic evolution: Science, v. 262, p. 732-734.

Gatewood, M. P., 2007, Structure and tectonics of the northeastern Inner Piedmont from detailed geologic mapping, geochronologic, geochemical, and petrologic studies with macro-, meso-, and microstructural analyses of ductile fault zones [M.S thesis]: Knoxville, University of Tennessee, 279 p.

Gilliam, W. G., Byars, H. E., Hatcher, R. D., Jr., and Merschat, A. J., 2008, Tectonic implications of geologic mapping in the western Newton window, Inner Piedmont, NC: Geological Society of America Abstracts with Programs, v. 40, no. 4, p. 18.

Giorgis, S. D., 1999, Inner Piedmont geology of the northwestern South Mountains near Morganton, North Carolina [M.S. thesis]: Knoxville, University of Tennessee, 191 p.

Giorgis, S. D., Mapes, R. W., and Bream, B. R., 2002, The Walker Top Granite: Acadian granitoid or eastern Inner Piedmont basement?, *in* Hatcher, R. D., Jr., and Bream, B. R., eds., Inner Piedmont geology in the South Mountains-Blue Ridge Foothills and the southwestern Brushy Mountains, central-western North Carolina: Carolina Geological Society Guidebook, p. 33-44.

Goldberg, S. A., and Dallmeyer, R. D., 1997, Chronology of Paleozoic metamorphism and deformation in the Blue Ridge thrust complex, North Carolina and Tennessee: American Journal of Science, v. 297, p. 488-526.

Goldsmith, R., 1981, Structural patterns in the Inner Piedmont of the Charlotte and Winston-Salem 2-degree quadrangles, North Carolina and South Carolina, *in* Horton, J. W., Jr., Butler, J. R., and Milton, D. M., eds., Geological investigations of the Kings Mountain belt and adjacent areas in the Carolinas: Carolina Geological Society Field Trip Guidebook, p. 19-27.

Goldsmith, R., Milton, D. J., and Horton, J. W., Jr., 1988, Geologic map of the Charlotte 1-degree x 2-degree quadrangle, North Carolina and South Carolina: U.S. Geological Survey Map I-1251-E, scale 1:250,000.

Griffin, V. S. Jr., 1974, Analysis of the Piedmont in northwest South Carolina: Geological Society of America Bulletin, v. 85, p. 1123-1138.

Hadley, J. B., and Goldsmith, R., 1963, Geology of the eastern Great Smoky Mountains North Carolina and Tennessee: U. S. Geological Survey Professional Paper, 349-B, 117 p.

Hadley, J. B., and Nelson, A. E., 1971, Geologic map of the Knoxville quadrangle, North Carolina, Tennessee, and South Carolina: U. S. Geological Survey Map I–654, scale 1:250,000.

Hames, W. E., Tull, J. F., and McDonald, W., 2007, Laser $^{40}Ar/^{39}Ar$ ages of muscovite from the frontal zone of the western Blue Ridge and Talledega belt, *in* Tull, J. F., ed., Tectonics of the Georgia Blue Ridge: Basement/cover rift architecture, important aspects of overlying drift and clastic wedge facies, and the westernmost accretionary terrane: Georgia Geological Society Guidebook, v. 27, p. 141-155.

Harley, S. L., Kelly, N. M., and Möller, A., 2007, Zircon behavior and the thermal histories of mountain chains: Elements, v. 3, p. 25-30.

Hatcher, R. D., Jr., 1976, Introduction to the geology of the eastern Blue Ridge of the Carolinas and nearby Georgia: Carolina Geological Society Guidebook, 53 p.

Hatcher, R. D., Jr., 1978, Tectonics of the western Piedmont and Blue Ridge: Review and speculation: American Journal of Science, v. 278, p. 276-304.

Hatcher, R. D., Jr., 1980, Geologic map and mineral resources of the Prentiss quadrangle, North Carolina: North Carolina Geological Survey, GM 167–SW, scale 1:24,000.

Hatcher, R. D., Jr., 1987, Tectonics of the southern and central Appalachian internides: Annual Reviews in Earth and Planetary Sciences, v. 15, p. 337-362.

Hatcher, R. D., Jr., 1989, Tectonic synthesis of the U.S. Appalachians, Chapter 14, *in* Hatcher, R. D., Jr., Thomas, W. A., and Viele, G. W., eds., The Appalachian-Ouachita orogen in the United States: Boulder, Colorado, Geological Society of America, The Geology of North America, v. F-2, p. 511-535.

Hatcher, R. D., Jr., 2001, Rheological partitioning during multiple reactivation of the Palaeozoic Brevard fault zone, southern Appalachians, USA, *in* Holdsworth, R. E., Strachan, R. A., Magloughlin, J. F., and Knipe, R. J., eds., The nature and tectonic significance of fault zone weakening: London, Geological Society of London Special Publication 186, p. 255-269.

Hatcher, R. D., Jr., 2002a, Alleghanian (Appalachian) orogeny, a product of zipper tectonics: Rotational transpressive continent-continent collision and closing of ancient oceans along irregular margins, *in* Martínez Catalán, J. R., Hatcher, R. D.,

Jr., Arenas, R., and Díaz García, F., eds., Variscan-Appalachian dynamics: The building of the late Paleozoic basement: Boulder, Colorado, Geological Society of America Special Paper 364, p. 199-208.

Hatcher, R. D., Jr., 2002b, An Inner Piedmont primer, *in* Hatcher, R. D., Jr., and Bream, B. R., eds., Inner Piedmont geology in the South Mountains-Blue Ridge Foothills and the southwestern Brushy Mountains, central-western North Carolina: Carolina Geological Society Guidebook, p. 1-18.

Hatcher, R. D., Jr., and Butler, J. R., 1979, Guidebook for southern Appalachian field trip in the Carolinas, Tennessee, and northeastern Georgia: International Geologic Correlation Program Project 27, University of North Carolina, Chapel Hill, 117 p.

Hatcher, R. D., Jr., and Goldberg, S. A., 1991, The Blue Ridge Geologic Province, *in* Horton, J. W., Jr., and Zullo, V. A., eds., The Geology of the Carolinas—Carolina Geological Society 50th Anniversary Volume: Knoxville, The University of Tennessee Press, p. 11–35.

Hatcher, R. D., Jr., and Hooper, R. J., 1992, Evolution of crystalline thrust sheets in the internal parts of mountain chains, *in* McClay, K. R., ed., Thrust tectonics: London, Chapman and Hall, p. 217–234.

Hatcher, R. D., Jr., and Merschat, A. J., 2006, The Appalachian Inner Piedmont: An exhumed strike-parallel, tectonically forced orogenic channel, *in* Law, R. D., Searle, M., and Godin, L., eds., Channel flow, ductile extrusion and exhumation of lower-mid crust in continental collision zones: London, Geological Society of London Special Publication 268, p. 517-540.

Hatcher, R. D., Jr., Bream, B. R., Miller, C. L., Eckert, J. O., Jr., Fullagar, P. D., and Carrigan, C. W., 2004, Paleozoic structure of internal basement massifs, southern Appalachian Blue Ridge, incorporating new geochronologic, Nd and Sr isotopic, and geochemical data, *in* Tollo, R. P., Corriveau, L., McLelland, J., and Bartholomew, M. J., eds., Proterozoic tectonic evolution of the Grenville orogen in North America: Boulder, Colorado, Geological Society of America Memoir 197, p. 525-547.

Hatcher, R. D., Jr., Merschat, A. J., and Thigpen, J. R., 2005, Blue Ridge Primer, *in* Hatcher, R. D., Jr., and Merschat, A. J., eds., Blue Ridge geology geotraverse east of the Great Smoky Mountains National Park, western North Carolina: Carolina Geological Society Guidebook, North Carolina Geological Survey, p. 1-24.

Hatcher, R. D., Jr., Merschat, A. J., and Raymond, L. A., 2006, Geotraverse: Geology of northeastern Tennessee and the Grandfather Mountain region, *in* Labotka, T. L.,

and Hatcher, R. D., Jr., eds., Geological Society of America Southeastern Section meeting Field Trip Guidebook: Knoxville, Tennessee, University of Tennessee, p. 129-184.

Hatcher, R. D., Jr., Bream, B. R., and Merschat, A. J., 2007, Tectonic map of the southern and central Appalachians: A tale of three orogens and a complete Wilson cycle, *in* Hatcher, R. D., Jr., Carlson, M. P., McBride, J. H., and Martínez Catalán, J. R., eds., 4-D Framework of Continental Crust: Geological Society of America Memoir 200, p. 595–632.

Hibbard, J. P., 2000, Docking Carolina: Geology, v. 28, p. 127-130.

Hibbard, J. P., Stoddard, E. F., Secor, D. T., and Dennis, A. J., 2002, The Carolina zone: overview of Neoproterozoic to Early Paleozoic peri-Gondwanan terranes along the eastern flank of the southern Appalachians: Earth-Science Review, v. 57, p. 299-339.

Hibbard, J. P., Tracy, R. J., and Henika, W. S., 2003, Smith River allochthon: A southern Appalachian peri-Gondwanan terrane emplaced directly on Laurentia?: Geology, v. 31, p. 215-218.

Higgins, M. W., Crawford, T. J., Atkins, R. L., and Crawford, R. F., 2003, Geologic map of the Atlanta 30' x 60' quadrangle, Georgia: U. S. Geologic Survey, Geologic Investigations Series Map I-2602, scale 1:100,000.

Hopson, J. L., Hatcher, R. D., Jr., and Stieve, A. L., 1989, Geology of the eastern Blue Ridge, northeastern Georgia and the adjacent Carolinas, *in* Fritz, W. J., Hatcher, R. D., Jr., and Hopson, J. L., eds., Geology of the eastern Blue Ridge of northeast Georgia and the adjacent Carolinas: Georgia Geological Society Guidebooks, v. 9, p. 1-40.

Horton, J. W., Jr., and McConnell, K. I., 1991, The western Piedmont, *in* Horton, J. W., Jr., and Zullo, V. A., eds., The Geology of the Carolinas—Carolina Geological Society 50th Anniversary Volume: Knoxville, The University of Tennessee Press, p. 36–58.

Horton, J. W., Drake, A. A., Jr., Rankin, D. W., and Dallmeyer, R. D., 1991, Preliminary tectonostratigraphic terrane map of the central and southern Appalachians: U.S. Geological Survey Map I-2163, scale 1:2,000,000.

Kalbas, J. L., 2003, Geology of part of the southwestern Brushy Mountains, Inner Piedmont [M.S. thesis]: Knoxville, University of Tennessee, 208 p.

King, P. B., and Ferguson, H. W., 1960, Geology of northeasternmost Tennessee: U. S. Geological Survey Professional Paper 311, 136 p.

Kish, S. A., 1997, The Cat Square charnockite – A Paleozoic charnockite in the Inner Piedmont of North Carolina: Geological Society Abstracts with Programs, v. 29, no. 3, p 28.

Kohn, M. J., and Malloy, M. A., 2004, Formation of monazite via prograde metamorphic reactions among common silicates: Implications for age determinations: Geochimica et Cosmochimica Acta, v. 68, p. 101-113.

Kunk, M. J., Wintsch, R. P., Naeser, C. W., Naeser, N. D., Southworth, S., Drake, A. A., Jr., and Becker, J. L., 2005, Contrasting tectonothermal domains and faulting in the Potomac terrane, Virginia–Maryland—discrimination by $^{40}Ar/^{39}Ar$ and fission-track thermochronology: Geological Society of America Bulletin, v. 117, p. 1347-1366.

Ludwig, K. R., 2001, Squid v. 1.02, computer program.

Ludwig, K. R., 2003, Isoplot v. 3.0, computer program.

Mapes, R. W., 2002, Geochemistry and geochronology of mid-Paleozoic granitic plutonism in the southern Appalachian Piedmont terrane, North Carolina-South Carolina-Georgia [M.S. thesis]: Nashville, Vanderbilt University, 150 p.

Massey, M. A., and Moecher, D. P., 2005, Deformation and metamorphic history of the western Blue Ridge-eastern Blue Ridge terrane boundary, southern Appalachian orogen: Tectonics, v. 24, p. TC5010, 1-18.

McClellan, E. A., Steltenpohl, M. G., Thomas, C., and Miller, C. F., 2007, Isotopic age constraints and metamorphic history of the Talladega belt: New evidence for timing of arc magmatism and terrane emplacement along the southern Laurentian margin: Journal of Geology, v. 115, p. 541-561.

McDowell, S. M., Miller, C.F., Fullagar, P. D., Bream, B. R., and Mapes, R. W., 2002, The Persimmon Creek Gneiss, eastern Blue Ridge, North Carolina-Georgia: Evidence for the missing Taconic arc?: Southeastern Geology, v. 41, p. 103–117.

Merschat, A. J., 2003, Inner Piedmont tectonics in the southwestern Brushy Mountains, North Carolina: Field and laboratory data revealing 3-D crustal flow and sillimanite I and II metamorphism [M.S. thesis]: Knoxville, University of Tennessee, 198 p.

Merschat, A.J., and Hatcher, R.D., Jr., 2007, The Cat Square terrane: Possible Siluro-Devonian remnant ocean basin in the Inner Piedmont, southern Appalachians, USA, *in* Hatcher, R.D., Jr., Carlson, M.P., McBride, J.H., and Martínez Catalán, J.R., eds., 4-D Framework of Continental Crust: Geological Society of America Memoir 200, p. 553-565.

Merschat, A. J., and Kalbas, J. L., 2002, Geology of the southwestern Brushy Mountains, North Carolina Inner Piedmont: A summary and synthesis of recent studies, *in* Hatcher, R. D., Jr., and Bream, B. R., eds., Inner Piedmont geology in the South Mountains-Blue Ridge Foothills and the southwestern Brushy Mountains, central-western North Carolina: Carolina Geological Society Guidebook, p. 101-126.

Merschat, A. J., Bultman, J. G., and Hatcher, R. D., Jr., 2005a, Polydeformed Proterozoic basement in the Blue Ridge thrust complex of northeast Tennessee–northwest North Carolina: Part 1, Deciphering 1 billion years of southern Appalachian history preserved in an outcrop of middle Proterozoic rocks in the western Blue Ridge, North Carolina: Geological Society of America Abstracts with Programs, v. 37, no. 2, p. 36.

Merschat, A. J., Hatcher, R. D., Jr., and Davis, T. L., 2005b, The northern Inner Piedmont, southern Appalachians, USA: Kinematics of transpression and SW-directed mid-crustal flow: Journal of Structural Geology, v. 27, p. 1252-1281.

Merschat, A. J., Hatcher, R. D., Jr., Gilliam W. G., and Byars, H. E., 2008, Inner Piedmont Geo-Traverse from the Brushy Mountains to Lincolnton, North Carolina: Architecture of the Cat Square and Tugaloo terranes: Geological Society of America Southeastern Section Field Trip Guidebook: Charlotte, North Carolina, 64 p.

Merschat, A. J., Bream, B. R., Hatcher, R. D., Jr., Miller, C. F., and Wooden, J. L., 2007, Provenance and timing of crust formation in the southern Appalachian crystalline core: evidence from detrital zircon studies: Geological Society of America Abstracts with Programs, v. 39, no. 6, p. 341.

Merschat, C. E., and Cattanach, B. L., 2008, Bedrock geologic map of the west half of the Asheville 1:100,000-scale quadrangle, North Carolina and Tennessee: North Carolina Geological Survey, Geologic Map Series 13, scale 1:100,000.

Merschat, C. E., and Wiener, L. S., 1988, Geology of the Sandymush and Canton quadrangles, North Carolina: Raleigh, North Carolina Geological Survey Bulletin 90, 1:24,000 scale, 66 p.

Merschat, C. E., Cattanach, B. L., Carter, M. W., and Wiener, L. S., 2006, Geology of the Mesoproterozoic basement and younger cover rocks in the west half of the Asheville 100,000 quadrangle, North Carolina and Tennessee—An updated look, *in* Labotka, T. L., and Hatcher, R. D., Jr., eds., Geological Society of America Southeastern Section meeting Field Trip Guidebook: Knoxville, Tennessee, University of Tennessee, p. 129-184.

Miller, B. V., Stewart, K. G., Miller, C. F., and Thomas, C. W., 2000a, U-Pb ages from the Bakersville, North Carolina eclogite: Taconian eclogite metamorphism followed by Acadian and Alleghanian cooling: Geological Society of America Abstracts with Programs, v. 32, no. 2, p. 62.

Miller, B. V., Fetter, A. H., and Stewart, K. G., 2006, Plutonism in three orogenic pulses, eastern Blue Ridge Province, southern Appalachians: Geological Society of America Bulletin, v. 118, p. 171-184.

Miller, C. F., Fullagar, P. D., Sando, T. W., Kish, S. A., Solomon, G. C., Russell, G. S., and Steltenpohl, L. F. W., 1997, Low-potassium, trondhjemitic to granodioritic plutonism in the eastern Blue Ridge, southwestern North Carolina-northeastern Georgia, *in* Sinha, A. K., Whalen, J. B., and Hogan, J. P., eds., The nature of magmatism in the Appalachian orogen: Boulder, Colorado, Geological Society of America Memoir 191, p. 235-254.

Miller, C. F., Hatcher, R. D., Jr., Harrison, T. M., Coath, C. D., and Gorisch, E. B., 1998, Cryptic crustal events elucidated through zone imaging and ion microprobe studies of zircon, southern Appalachian Blue Ridge, North Carolina-Georgia: Geology, v. 26, p. 419-422.

Miller, C. F., Hatcher, R. D., Jr., Ayers, J. C., Coath, C. D., and Harrison, T. M., 2000b, Age and zircon inheritance of eastern Blue Ridge plutons, southwestern North Carolina and northeastern Georgia, with implications for magma history and evolution of the southern Appalachian orogen: American Journal of Science, v. 300, p. 142–172.

Miller, C. F., McDowell, S. M., and Mapes, R. W., 2003, Hot and cold granites? Implications of zircon saturation temperatures and preservation of inheritance: Geology, v. 31, p. 529-532.

Miller, J. W. Jr., and Fryer, K. H., 1996, Geology of the Ashe metamorphic suite in the Beaucatcher Mountain road cut, Asheville, North Carolina: Southeastern Geology, v. 36, p. 133-152.

Mirante, D. C., and Patiño-Douce, A. E., 2000, Melting and migmatization in the southern Appalachian Inner Piedmont of northeast Georgia; the Athens gneiss: Geological Society of America Abstracts with Programs, v. 33, p. 297.

Moecher, D. P., Tracy, R. J., and Anderson, E. D., 2003, Taconian metamorphism in eastern Great Smoky Mountains inferred from U–Th–Pb monazite chemical ages: Geological Society of America Abstracts with Programs, v. 35, no. 1, p. 20.

Moecher, D. P., Samson, S. D., and Miller, C. F., 2004, Precise time and conditions of peak Taconian granulite facies metamorphism in the southern Appalachian orogen, USA, with implications for zircon behavior during crustal melting events: Journal of Geology, v. 112, p. 289-304.

Moecher, D. P., Massey, M. A., and Tracy, R. J., 2005, Timing and pattern of metamorphism in the western and central Blue Ridge, TN and NC: Status and outstanding problems, *in* Hatcher, R. D., Jr., and Merschat, A. J., eds., Blue Ridge geology geotraverse east of the Great Smoky Mountains National Park, western North Carolina: Carolina Geological Society Annual Field Trip Guidebook, p. 57-66.

Nelson, A. E., Horton, J. W., and Clarke, J. W., 1998, Geologic map of the Greenville 1ºx2º quadrangle, Georgia, South Carolina, and North Carolina: U.S. Geological Survey Map I-2175, scale 1:250,000.

Osberg, P. H., Tull, J. F., Robinson, P., Hon, R., and Butler, J. R., 1989, The Acadian Orogen Chapter 4, *in* Hatcher, R. D., Jr., Thomas, W. A., and Viele, G. W., eds., The Appalachian Ouachita orogen in the United States: Boulder, Colorado, Geological Society of America, The geology of North America, v. F-2, p. 179-232.

Osborne, W. E., Szabo, M. W., Copeland, C. W., Jr., and Neathery, T. L., 1989, Geologic map of Alabama: Geological Survey of Alabama Special Map 221, scale 1:500,000.

Ownby, S. E., Miller, C. F., Berquist, P. J., Carrigan, C. W., Wooden, J. L., and Fullagar, P. D., 2004, U-Pb geochronology and geochemistry of a portion of the Mars Hill terrane, North Carolina–Tennessee: Constraints on origin, history, and tectonic assembly, *in* Tollo, R. P., Corriveau, L., McLelland, J., and Bartholomew, M. J., eds., Proterozoic evolution of the Grenville orogen in North America: Boulder, Colorado, Geological Society of America Memoir 197, p. 609-632.

Park, H., Rickenbaker, A., Bachmann-Krug, D., Barbeau, D. L., and Gehrels, G. E., 2008, Detrital-zircon geochronology of Acadian foreland basin strat of West Virginia and Virginia: Geological Society of America Abstracts with Programs, v. 40, no. 4, p. 18.

Quinn, M. J., 1991, Two lithotectonic boundaries in western North Carolina: Geologic interpretation of a region surrounding Sylva, Jackson County [unpublished M.S. thesis]: Knoxville, University of Tennessee, 223 p.

Rankin, D. W., Espenshade, G. J., and Neuman, R. B., 1972, Geologic map of the west half of the Winston-Salem quadrangle, North Carolina, Virginia, and Tennessee. U. S. Geological Survey Map I-709-A, scale 1:250,000.

Robinson, P., Tucker, R. D., Bradley, D., Berry, H. N., IV, and Osberg, P. H., 1998, Paleozoic orogens in New England, USA: Geologiska Föreningens Stockholm Forhandlingar, v. 120, p. 119-148.

Robinson, A. C., Yin, A., Manning, C. E., Harrison, T. M., Zhang, S. H., and Wang, Z. F., 2007, Cenozoic evolution of the eastern Pamir: Implications for strain-accommodation mechanisms at the western end of the Himalayan-Tibetan orogen: Geological Society of America Bulletin, V., 119, p. 882-896.

Secor, D. T., Jr., Snoke, A. W., and Dallmeyer, R. D., 1986, Character of the Alleghanian orogeny in the southern Appalachians: Part III. Regional Tectonics: Geological Society of America Bulletin, v. 97, p. 1345-1353.

Settles, D. J., 2002, Defining the Hayesville-Soque River and Allatoona faults and an Ordovician arc assemblage within the central Blue Ridge northwest of Dahlonega, Georgia [unpublished M.S. thesis]: Knoxville, University of Tennessee, 148 p.

Sinha, A. K., Hewitt, D. A., and Rimstidt, J. D., 1988, Metamorphic petrology and strontium isotope geochemistry associated with the development of mylonites: an example from the Brevard fault zone, North Carolina: American Journal of Science, v. 288, p. 115-147.

Sinha, A. K., Hund, E. A., and Hogan, J. P., Paleozoic accretionary history of the North American plate margin (central and southern Appalachians): Constraints from the age, origin, and distribution of granitic rocks, *in* Hillhouse, J. ed., Deep structure and past kinematics of accreted terranes: American Geophysical Union Monograph Series, p. 219-238.

Stahr, D. W., III., 2007, Tectonometamorphic evolution of the eastern Blue Ridge: Differentiating multiple Paleozoic orogenic pulses in the Glenville and Big Ridge quadrangles, southwestern North Carolina [unpublished MS thesis]: Knoxville, Tennessee, University of Tennessee, 263 p.

Stahr, D. W., Miller, C. F., Hatcher, R. D., Jr., Wooden, J., and Fisher, C. M., 2005, Evidence for high-temperature ductile Alleghanian deformation in the eastern Blue Ridge: Implications of new structural, petrologic, and geochronologic data from southwestern North Carolina: Geological Society of America Abstracts with Programs, v. 37, no. 7, p. 72.

Steltenpohl, M. G., 2005, An introduction to the terranes of the southernmost Appalachians of Alabama and Georgia, *in* Steltenpohl, M. G., ed., Southernmost

Appalachian terranes, Alabama and Georgia: Southeastern Section of the Geological Society of America Field Trip Guidebook, p. 1-18.

Steltenpohl, M. G., and Kunk, M. J., 1993, $^{40}Ar/^{39}Ar$ thermochronology and Alleghanian development of the southernmost Appalachian Piedmont, Alabama and southwest Georgia: Geological Society of America Bulletin, v. 105, p. 819-833.

Steltenpohl, M. G., and Moore, W. B., 1988, Metamorphism in the Alabama Piedmont: Geological Survey of Alabama Circular 138, 27 p.

Steltenpohl, M. G., Heatherington, A. L., Mueller, P. M., and Miller, B. V., 2005, New isotopic dates on crystalline rocks from Alabama and Georgia, *in* Steltenpohl, M. G., ed., Southernmost Appalachian terranes, Alabama and Georgia: Southeastern Section of the Geological Society of America Field Trip Guidebook, p. 51-69.

Steltenpohl, M. G., Mueller, P. M., Heatherington, A. L., Hanley, T. B., and Wooden, J. L., 2008, Gondwanan/peri-Gondwanan origin for the Uchee terrane, Alabama and Georgia: Carolina zone or Suwannee terrane(?) and its suture with Grenvillian basement of the Pine Mountain window: Geosphere, v. 4, p. 131-144.

Stokes, R. M., Kunk, M. J., Southworth, S. C., Wintsch, R. P., 2008, Mississippian exhumation and tilting of the Ashe Metamorphic Suite above the Fries Fault, NC: Evidence from amphibole and muscovite $^{40}Ar/^{39}Ar$ age spectrum dating result: Geological Society of America Abstracts with Programs, v. 40, no. 6 p. 204.

Thomas, C. W., 2001, Origins of ultramafic complexes of the eastern Blue Ridge province, southern Appalachians: Geochronological and geochemical constraints [M.S. thesis]: Nashville, Tennessee, Vanderbilt University, 154 p.

Thomas, W. A., Becker, T. P., Samson, S. D., and Hamilton, M. A., 2004, Detrital zircon evidence of a recycled orogenic foreland provenance for Alleghanian clastic-wedge sandstones: Journal of Geology, v. 112, p. 23-37.

Trupe, C. H., Stewart, K. G., Adams, M. G., Waters, C. L., Miller, B. V., and Hewitt, L. K., 2003, The Burnsville fault: Evidence for the timing and kinematics of southern Appalachian Acadian dextral transform tectonics: Geological Society of America Bulletin, v. 115, p. 1365-1376.

Tull, J. F., 2007, Cover stratigraphy and structure of basement culminations, frontal Appalachian Blue Ridge of Georgia: insights into rifted margin architecture *in* Tull, J. F., ed., Tectonics of the Georgia Blue Ridge: Basement/cover rift architecture, important aspects of overlying drift and clastic wedge facies, and the westernmost accretionary terrane: Georgia Geological Society Guidebook, p. 5-54.

Tull, J. F., and Groszos, M. G., 1988, Murphy belt: Stratigraphic complexities and regional correlations, *in* Fritz, W. J., and La Tour, T. E., eds., Geology of the

Murphy belt and related rocks, Georgia and North Carolina: Georgia Geological Society Guidebook, v. 8, p. 35–74.

Tull, J. F., and Holm, C. S., 2005, Structural evolution of a major Appalachian salient-recess junction: Consequences of oblique collisional convergence across a continental transform fault: Geological Society of America Bulletin, v. 117, p. 482-499.

Tull, J. F., Harris, A. G., Repetski, J. E., McKinney, F. K., Garrett, C. B., and Bearce, D. N., 1988, New paleontologic evidence constraining the age and paleotectonic setting of the Talladega slate belt, southern Appalachians: Geological Society of America Bulletin, v. 100, p. 1291-1299.

Varnell, M. G., Hatcher, R. D., Jr., Merschat, A. J., and Wooden, J. L., 2008, Limits on timing of deformation and plutonism in the eastern Blue Ridge, southwestern North Carolina, from Geologic mapping and U-Pb zircon geochronology: Geological Society of America Abstracts with Programs, v. 40, no. 4, p. 28.

Vick, H. K., Channell, J. E. T., and Opdyke, N. D., 1987, Ordovician docking of the Carolina slate belt: Paleomagnetic data: Tectonics, v. 6, p. 573-583.

Wang, Y., Li, Q., and Guosheng, Q., 2006, $^{40}Ar/^{39}Ar$ thermochronological constraints on the cooling and exhumation history of the South Tibetan Detachment System, Nyalam area, southern Tibet, *in* Law, R. D., Searle, M., and Godin, L., eds., Channel flow, ductile extrusion and exhumation of lower-mid crust in continental collision zones: London, Geological Society of London Special Publication 268, p. 327-354.

Willard, R. A., and Adams, M. G., 1994, Newly discovered eclogite in the southern Appalachian orogen, northwestern North Carolina: Earth and Planetary Science Letters, v. 123, p. 61-70.

Williams, H., and Hatcher, R. D. Jr., 1982, Suspect terranes and accretionary history of the Appalachian orogen: Geology, v. 10, p. 530-536.

Williams, H., and Hatcher, R. D., Jr., 1983, Appalachian suspect terranes, *in* Hatcher, R. D., Jr., Williams, H., and Zeitz, I., D., eds., Contributions to the tectonics and geophysics of mountain chains: Geological Society of America Memoir 158, p. 33–53.

Wilson, C. G., 2006, Origin and tectonic evolution of the southern Appalachian Neoacadian crystalline core: Evidence from the geology of the Gilreath 7.5-minute quadrangle, North Carolina [M.S. thesis]: Knoxville, University of Tennessee, 219 p.

Wood, L. F., and Miller, C. F., 1984, Geochemistry and petrogenesis of trondhjemite dikes, Blue Ridge, North Carolina-Georgia: Southeastern Geology, v. 25, no. 1, p. 13-24.

PART IV

Detrital zircon geochronology and provenance of southern Appalachian Blue Ridge and Inner Piedmont crystalline terranes

Part IV was submitted to the upcoming Geological Society of America Memoir "From Rodinia to Pangea: The Lithotectonic Record of the Appalachian Region" edited by Richard P. Tollo, Paul Karabinos, Mervin J. Bartholomew, and James P. Hibbard. This paper represents a collaborative effort to address the provenance of the various metasedimentary terranes of the Blue Ridge and Inner Piedmont through SHRIMP U-Pb zircon geochronology. My coauthors are Robert D. Hatcher, Jr., Brendan R. Bream, Calvin F. Miller, Heather E. Byars, Matthew P. Gatewood, and Joseph L. Wooden. My contributions include sample and data collections, interpretation of the data, and most of the writing.

ABSTRACT

The southern Appalachian crystalline core is comprised of lithotectonic assemblages that are largely metasedimentary in origin. Sixteen paragneiss samples from the Blue Ridge and Inner Piedmont of North Carolina and Georgia, and one Middle Ordovician sample from the Sevier-Blountain clastic wedge in the Tennessee Valley and Ridge were sampled for SHRIMP U–Pb detrital zircon geochronology, whole-rock geochemistry, and zircon trace element analyses. Detrital zircon ages range from Archean (~2.7 Ga) to Middle Paleozoic (~430 Ma) with a notable abundance of Mesoproterozoic zircons, 1.3–0.9 Ga. Many samples also contain moderate populations of slightly older Mesoproterozoic zircons, 1.5–1.3 Ga. Minor populations of Paleoproterozoic, 2.1–1.5 Ga, and Neoproterozoic, 750–700 and 600 Ma, ages occur in several samples; however, detrital Paleozoic zircons of ~500 and 460–430 Ma are restricted to samples from the Cat Square and Smith River allochthon terranes. Depositional periods of the metasedimentary terranes are bracketed by detrital zircon, metamorphic, and magmatic ages, and include: (1) Mesoproterozoic, (2) Neoproterozoic to Middle Ordovician, and (3) Middle Paleozoic times. A xenolith from the ~1.15 Ga Wiley gneiss suggests a post ~1.2 Ga period of sedimentation prior to the ~1.15 Ga Grenvillian magmatic event. Detrital zircon populations of Neoproterozoic to Middle Ordovician and middle Paleozoic terranes suggest a mixed Laurentian provenance with Amazonian and peri-Gondwanan sources deposited in divergent and convergent plate settings, respectively. Blue Ridge and Inner Piedmont detrital zircon ages, whole-rock geochemistry, lithologic assemblages, and field relationships are compatible with deposition of immature clastic material in a rift and passive margin setting for the Neoproterozoic to early Paleozoic. Occurrence of 1.3–0.9 Ga, 1.5–1.3 Ga, and 750–700 Ma detrital zircon populations indicate a dominantly Laurentian provenance for central

Blue Ridge terranes, Cartoogechaye, Cowrock, and Dahlonega gold belt, and the Tugaloo terrane. Minor Paleoproterozoic populations in these terranes suggest input from distal terranes of the Laurentian mid-continent or the Gondwanan Amazonian craton. Transition to a convergent plate margin in the Middle Ordovician resulted in collision of central Blue Ridge and Tugaloo terranes and recycling of material from these terranes into the Mineral Bluff Formation and Sevier Shale. Detrital zircons of ~460 Ma from the Smith River Allochthon suggest it is either a younger and more northerly successor basin or intracontinental rift basin. Ordovician and 600–500 Ma detrital zircons from Cat Square terrane document the first occurrence of peri-Gondwanan material that was deposited in a convergent setting between the Laurentian margin and the accreting Carolina superterrance during the Devonian to Mississippian.

INTRODUCTION

The Appalachian orogen is a complexly assembled mountain chain composed of a foreland fold-thrust belt and composite crystalline core. Within the crystalline core are terranes of known and suspect origin assembled during multiple orogenies over the past billion years (Fig. 4–1; Rodgers, 1970; Hatcher, 1978; Williams and Hatcher, 1982, 1983; Hatcher, 1989; Hatcher et al., 2007a). The southern Appalachians, like the entire orogen, are composed of numerous tectonostratigraphic terranes (Fig. 4–1), and yet their crustal affinity and accretionary history remain controversial (e.g. Hatcher, 1978; Williams and Hatcher, 1983; Hatcher, 1989; Horton et al., 1989; Hibbard, 2000; Hatcher, 2002; Hibbard et al., 2006, 2007). Blue Ridge and Inner Piedmont terranes record the evolution of eastern Laurentia from the Neoproterozoic to Cambrian rifting of the middle Proterozoic supercontinent Rodinia, to early Paleozoic passive margin, transition to a middle Paleozoic collisional orogen, and culminating collision with Gondwana and the formation of supercontinent Pangea at the end of the Paleozoic Era. Unraveling the tectonic history of the southern Appalachian orogen is important to our understanding of the spatial and temporal growth of the entire orogen through time, and how these processes relate to the growth of Laurentia and other continents. Nevertheless, the complex history and paucity of fossils make provenance and chronology of the various southern Appalachian metasedimentary terranes difficult to resolve.

Modern geochemical and geochronologic techniques that have been applied to resolve the tectonic history and affinity of different southern Appalachian terranes

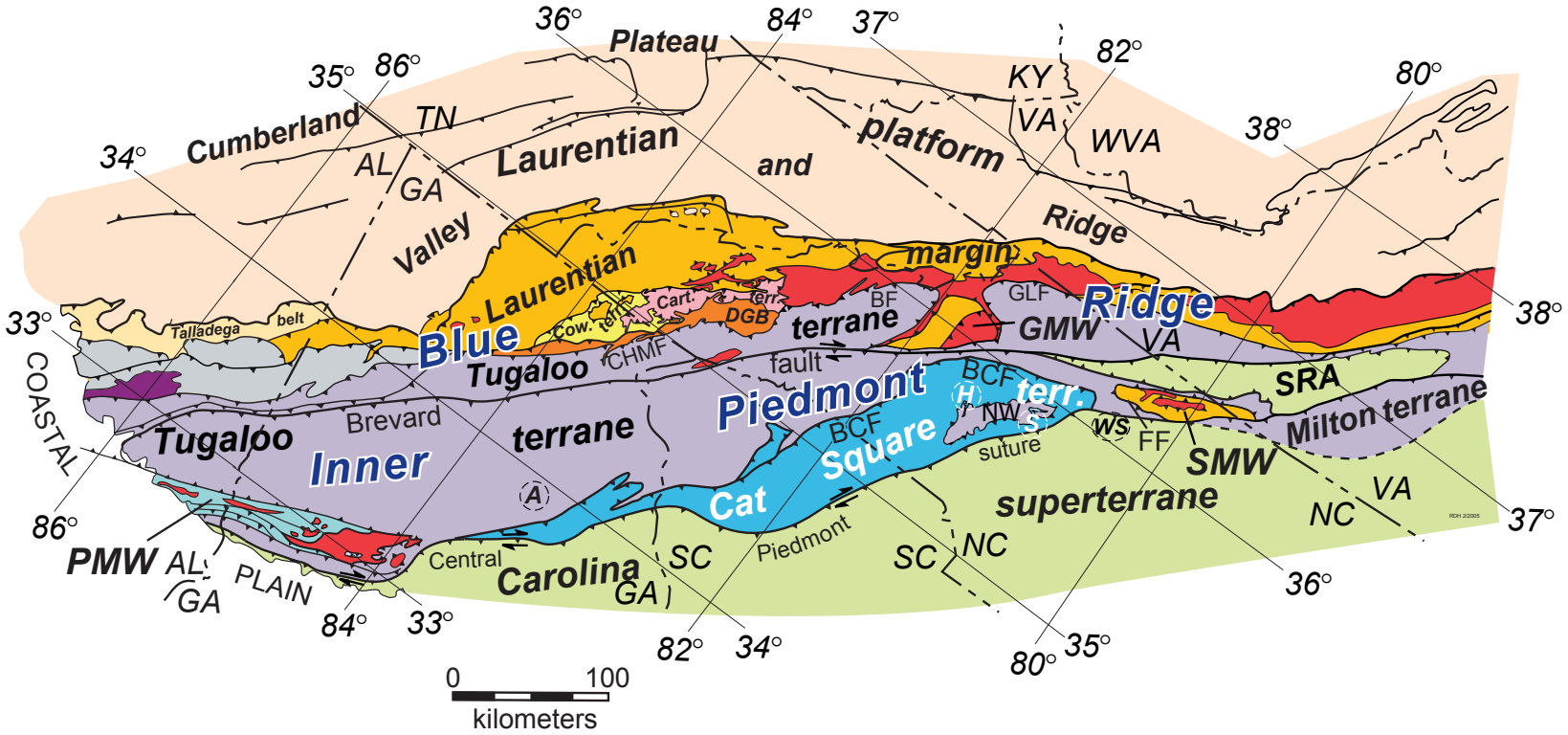

Figure 4–1. Simplified tectonic map of the southern Appalachians showing the location of the Inner Piedmont, and the Tugaloo (lavender) and Cat Square (blue) terranes. The Laurentian platform contains the Alleghanian foreland fold-thrust belt driven in front of the Blue Ridge–Piedmont megathrust sheet, which contains the Laurentian margin (gold with red inliers of Grenvillian, not necessarily Laurentian Grenville, and older inherited crust) and all components to the east. All terranes west of the Cat Square terrane have a Laurentian source (Bream et al., 2004). Cat Square terrane contains Siluro-Devonian metasedimentary rocks with a mixed Laurentian and peri-Gondwanan source. Carolina superterrane is Peri-Gondwanan and exotic to Laurentia. BCF– Brindle Creek fault. BF–Burnsville fault. Cart. terr.–Cartoogechaye terrane. CHMF–Chattahoochee-Holland Mountain fault. Cow. terr.–Cowrock terrane. DGB–Dahlonega gold belt. FF–Forbush fault. GLF–Gossan Lead fault. GMW–Grandfather Mountain window. NW–Newton window. SRA–Smith River allochthon, an outlier of Carolina superterrane rocks. SMW–Sauratown Mountains window. PMW–Pine Mountain window. Light gray–Probable western Tugaloo terrane rocks in Alabama and Georgia. Purple–Ordovician Elkahatchee Quartz Diorite. A–Athens. H–Hickory. S–Statesville. WS–Winston–Salem.

include: common–Pb isotopic studies of Mesoproterozoic metaigneous rocks, whole-rock and trace-element geochemistry of various igneous and metaigneous rocks, whole-rock Sm–Nd model ages, and U–Pb geochronology of different minerals (e.g., zircon, monazite, titanite). Of these, detrital zircon geochronology has been particularly useful to resolve questions regarding provenance of sedimentary rocks (Eriksson et al., 2004; Thomas et al., 2004) and low- to high-grade metasedimentary terranes (Bream et al., 2004; Steltenpohl et al., 2004, 2008; Carter et al., 2006a) because zircon is a common accessory mineral in continental crust, and durable enough to survive sedimentary, metamorphic, and igneous processes (Harley and Kelly, 2007). Detrital zircons can be used to address depositional age, provenance, and paleogeographic histories of different terranes. Individual zircon grain trace-element concentrations provide additional information regarding the igneous or magmatic process by which the zircon formed (Hoskin and Schaltegger, 2003; Grimes et al., 2007).

This study presents whole-rock geochemistry, detrital zircon geochronology, and zircon trace-element data from several key metasedimentary units of the southern Appalachians. The primary focus of this research is to address the crustal evolution of various suspect southern Appalachian terranes within the crystalline core. This is accomplished by: (1) delimiting the depositional age; (2) defining possible source areas; and (3) integrating all possible data into permissible tectonic and paleogeographic reconstructions for various terranes of the southern Appalachian crystalline core.

REGIONAL GEOLOGIC SETTING

The tectonic history of the Appalachians is bracketed by the formation of two supercontinents—Proterozoic Rodinia and the late Paleozoic Pangea—punctuated by middle Paleozoic orogenies (e.g., Hatcher et al., 2007a). Laurentia comprised the core of the Proterozoic supercontinent Rodinia which was joined to other cratons by sinuous Grenvillian, 1.25–0.9 Ga. belts (Hoffman, 1991; Dalziel, 1992; Li et al., 2008). Although numerous configurations have been proposed, the conjugate margin of eastern Laurentia is generally considered to be a combination of the Amazonia, Baltica, Congo, and/or Kalahari cratons (Hoffman, 1991; Dalziel, 1992; Unrug, 1997; Loewy et al., 2003; Tohver et al., 2004; Li et al., 2008). The relative position of Amazonia with eastern Laurentia has been shuffled from locations adjacent to Labrador (Dalziel, 1992, 1994; Tohver et al., 2006), the central Appalachians (Loewy et al., 2003), and the Llano uplift (Tohver et al., 2002). Rifting events at 760–700 Ma and again at 570–560

Ma eventually tore Rodinia apart, causing sediment to be shed into different tectonic locations and basins, and small crustal fragments were set adrift (Thomas, 1991; Unrug, 1997; Aleinikoff et al., 1995). The rifted margin of eastern Laurentia developed into a passive margin, followed by formation of a collisional orogen during the Middle to Late Ordovician and Devonian to Mississippian before amalgamation of Pangea in the Late Carboniferous to Permian (Hatcher et al., 2007a). The Blue Ridge and Inner Piedmont metasedimentary terranes were assembled during these three Paleozoic orogenies (Hatcher, 1978; 1989; Hatcher et al., 2007a).

Blue Ridge and Inner Piedmont terranes consist primarily of metasedimentary sequences deposited on either attenuated or rifted blocks of continental crust, or on oceanic crust. Minor constituents of these terranes may include felsic Paleozoic granitoids, felsic and mafic metavolcanics, and various mafic and ultramafic rocks. These terranes are polydeformed and metamorphosed to low- to high-grade (anchizone and greenschist facies to upper amphibolite facies, locally granulite). They are part of the composite Blue Ridge–Piedmont megathrust sheet, juxtaposed against the Paleozoic Laurentia platform rocks of the foreland fold-thrust belt (Valley and Ridge, see Fig. 4–1) by the Blue Ridge thrust (Hatcher et al., 1989; Hatcher and Hooper, 1992). From Alabama to northern Virginia, the Blue Ridge thrust consists of the Talladega–Emerson, Cartersville, Great Smoky, Iron Mountain–Holston Mountain, and frontal Blue Ridge thrusts (Hatcher, 1987, 1989; Osborne et al., 1989; Hatcher and Goldberg, 1991; Hatcher et al., 2007a; Southworth et al., 2009). The Brevard fault zone separates the steeply dipping structures of the eastern Blue Ridge from the more gently dipping structures of the Inner Piedmont, but is not a suture (Hatcher, 2001; Bream et al., 2004). The Blue Ridge reaches its greatest width in western North Carolina and eastern Tennessee, and is a polydeformed, composite crystalline terrane consisting of a series of thrust sheets juxtaposed during different orogenies. It can be separated into western, central, and eastern belts. The Laurentian affinity of the western Blue Ridge sedimentary cover is widely accepted, but various studies have proposed different nomenclatures and grouping of the central and eastern Blue Ridge and Inner Piedmont terranes. The term Piedmont terrane has been used to collectively refer to all terranes of the central and eastern Blue Ridge and Inner Piedmont (Williams and Hatcher, 1982, 1983; Hibbard et al., 2002; 2007). Other studies have chosen the Brevard fault zone to separate the Blue Ridge and Inner Piedmont terranes (Rankin, 1975; Horton et al., 1989; Raymond et al., 1989). This study uses the terrane nomenclature of Hatcher et al. (2007a), which we feel best incorporates all available data (Fig. 4–2).

Figure 4–2. Tectonic map of part of the Blue Ridge and Inner Piedmont of Georgia, North Carolina, South Carolina and Tennessee with locations of detrital zircon samples analyzed in this study and Bream et al. (2004). Map modified from Hatcher et al. (2004a, 2007a). ACF–Alexander City fault. AF–Allatoona fault. BCF– Brindle Creek fault. BF–Burnsville fault. BFZ–Brevard fault zone. CF–Chattahoochee fault. CPS–central Piedmont suture. Dlg–Looking Glass granodiorite. Dpb–Pink Beds granodiorite. GEF–Goodwater–Enitachopco fault. GLF–Gossan Lead fault. GMW–Grandfather Mountain window. HF–Hayesville fault. HLF–Hollins Line fault. HMF–Holland Mountain fault. Mr–Rabun granodiorite. Mwc–Walnut Creek granodiorite. NW–Newton window. Opc–Persimmon Creek Gneiss. Ow–Whiteside granodiorite. Oh–Henderson Gneiss. PMF–Paris Mountain fault. PMW–Pine Mountain window. SMW–Sauratown Mountains window. SRA–Smith River allochthon. SWL–Stone Wall Line fault. TD–Toxaway dome. TFD–Tallulah Falls dome. TR–Trimont Ridge complex. Cities: Atl–Atlanta. Av–Asheville. Hk–Hickory. W–Waynesville.

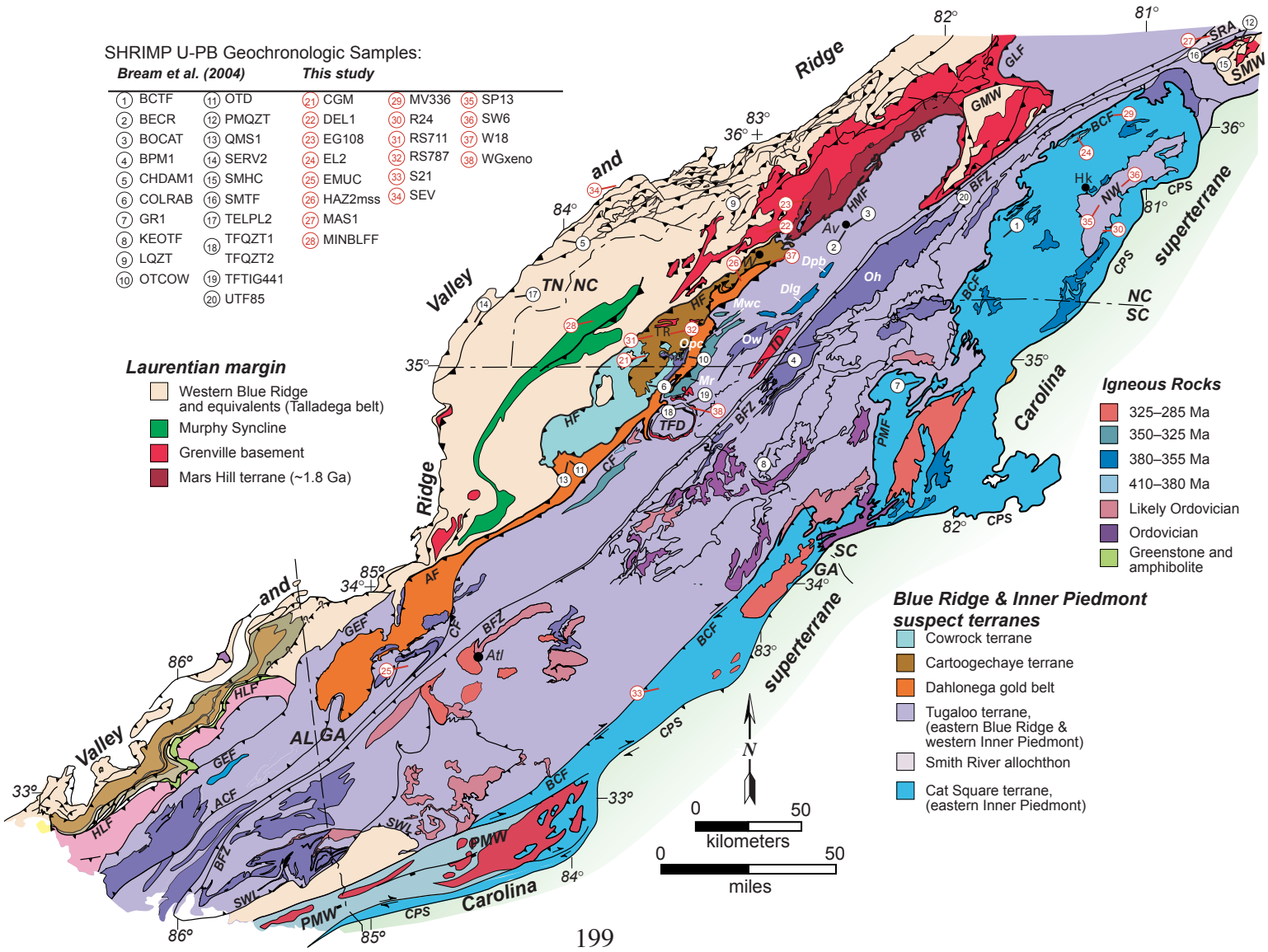
SHRIMP U-PB Geochronologic Samples:
Bream et al. (2004)
This study
1 BCTF
2 BECR
3 BOCAT
4 BPM1
5 CHDAM1
6 COLRAB
7 GR1
8 KEOTF
9 LQZT
10 OTCOW
11 OTD
12 PMQZT
13 QMS1
14 SERV2
15 SMHC
16 SMTF
17 TELPL2
18 TFQZT1
TFQZT2
19 TFTIG441
20 UTF85
21 CGM
22 DEL1
23 EG108
24 EL2
25 EMUC
26 HAZ2mss
27 MAS1
28 MINBLFF
29 MV336
30 R24
31 RS711
32 RS787
33 S21
34 SEV
35 SP13
36 SW6
37 W18
38 WGxeno
Laurentian margin
Western Blue Ridge and equivalents (Talladega belt)
Murphy Syncline
Grenville basement
Mars Hill terrane (~1.8 Ga)
Igneous Rocks
325–285 Ma
350–325 Ma
380–355 Ma
410–380 Ma
Likely Ordovician
Ordovician
Greenstone and amphibolite
Blue Ridge & Inner Piedmont suspect terranes
Cowrock terrane
Cartoogechaye terrane
Dahlonega gold belt
Tugaloo terrane, (eastern Blue Ridge & western Inner Piedmont)
Smith River allochthon
Cat Square terrane, (eastern Inner Piedmont)
Ridge
and
Valley
Ridge
and
Valley
Carolina
superterrane
superterrane
TN
NC
SC
GA
AL
GA
SC
TFD
Atl
Hk
Av
Dpb
Dlg
Oh
Mwc
Ow
Opc
Mr
TR
HF
BF
BFZ
BCF
CPS
HMF
PMF
GLF
GMW
SRA
SMW
NW
CF
AF
GEF
HLF
ACF
SWL
PMW
81°
82°
83°
84°
85°
86°
33°
34°
35°
36°
N
0
50
kilometers
0
50
miles

The oldest basement rocks in the southern Appalachians consist of Proterozoic orthogneisses exposed in several different external and internal massifs (Hatcher, 1984). External massifs (e.g., Watauga and Elk River massifs, Bartholomew and Lewis, 1984) are located in the western Blue Ridge and as defined by Hatcher (1984) are most proximal to the foreland and therefore more likely to have a connection to the underlying subsurface basement. The external basement massifs of the southern Appalachians are lithologically and temporally more diverse than the internal basement massifs which are found in the more internal part of the orogen and as a result are less likely to have direct connections to the basement over which they are thrust. Internal massifs, including the Toxaway dome and those of the Tallulah Falls dome, Pine Mountain, and Sauratown Mountains windows, are small and most are located in the Tugaloo terrane (eastern Blue Ridge and western Inner Piedmont; Fig. 4–2). Recent U–Pb geochronology studies have separated three age groups of Proterozoic basement rocks: (1) 1.8 Ga defined by an upper intercept age from the Mars Hill terrane (Carrigan et al., 2003; Ownby et al., 2004; Berquist et al., 2005); (2) 1.2–1.0 Ga, with most from the southern Appalachians around ~1.15 Ga (Carrigan et al., 2003; Hatcher et al., 2004a); and (3) Neoproterozoic 760–700 Ma (Goldberg et al., 1986; Su et al., 1994; Aleinikoff et al., 1995). The Pb isotopic signatures of Grenville basement of the southern and central Appalachians (Sinha et al., 1996) are more similar to Mesoproterozoic rocks of the Amazonian craton than equivalents in North America (Loewy et al., 2003; Tohver et al., 2004; Fisher et al., 2006, in review). Thus, the Proterozoic basement massifs of the southern and central Appalachians are interpreted to represent a block of Amazonian crust left behind after the break-up of Rodinia. Hatcher et al. (2004a; 2007a) and Fisher et al. (in review) proposed that the New York–Alabama magnetic–gravity lineament is the Grenvillian suture between Laurentia and Amazonia. Therefore, the southern and central Appalachians were assembled on Amazonian Mesoproterozoic rocks. Although these rocks have an Amazonian heritage, they are considered part of Laurentia during the Appalachian tectonic cycle, which is the focus of this paper.

The Laurentian platform consists of largely unmetamorphosed Paleozoic sedimentary rocks of the Cumberland Plateau (undeformed) and Valley and Ridge (foreland fold-thrust belt) (Rodgers, 1953, 1970; Hatcher, 1989; Hatcher et al., 2007a, Fig. 4–1). The base of the platform, Lower Cambrian Rome Formation, rests nonconformably on 1.5-1.3 Ga granite-rhyolite and 1.3–0.9 Ga Grenville province, which is considered Amazonian in the southern and central Appalachians (e.g., Hatcher et al., 2007a). The stratigraphy of the platform is composed of thick carbonate successions

interpreted to represent a stable shelf environments drowned by three periods of siliciclastic sedimentation associated with tectonic activity during the Middle Ordovician, Late Devonian to Mississippian, and Late Mississippian to Permian (Rodgers, 1953, 1970; Shanmugan and Walker, 1983; Hatcher, 1989, Eriksson et al., 2004; Ettensohn, 2004, Thomas et al., 2004). Deformation in the southern and central Appalachian Valley and Ridge occurred during the Alleghanian orogeny by thin-skinned, west-vergent thrusting of unmetamorphosed Paleozoic sedimentary rocks resulting from the collsion of Gondwanaland with Laurentia. A nearly complete section of the Middle Ordovician Sevier-Blountian clastic wedge is exposed in several Tennessee Valley and Ridge thrust sheets (Shanmugan and Walker, 1983).

The western Blue Ridge consists of Laurentian margin rift-related, dominantly clastic metasedimentary rocks deposited nonconformably on Proterozoic igneous and meta-igneous rocks of several external basement massifs (Hadley and Goldsmith, 1963; Rast and Kohles, 1986; Hatcher et al., 2005, 2007a). Sedimentary sequences included in the western Blue Ridge are the Ocoee Supergroup, Grandfather Mountain and Mount Rogers Formations, Cambrian Chilhowee Group, and the Murphy Group. These sequences are thought to be the product of two separate rifting events (Aleinikoff et al., 1995; Brewer and Thomas, 2000). The first stage of rifting (760–700 Ma) is contemporaneous with ~758 Ma felsic volcanism in the Mount Rogers Formation, anorogenic magmatism associated with Crossnore (760–740 Ma) and Robertson River igneous suites, and ~734 Ma intrusion of the Bakersville gabbro dike swarm (Goldberg et al., 1986; Su et al., 1994; Aleinikoff et al., 1995). The second rifting event 572–564 Ma is interpreted as the final opening of Iapetus ocean and followed by deposition of the Chilhowee Group (Aleinikoff et al., 1995; Southworth et al., 2009). Mafic, ultramafic, and Paleozoic intrusive rocks are uncommon in the western Blue Ridge.

The Murphy syncline contains some of the youngest rocks in the western Blue Ridge of Georgia, North Carolina, and Tennessee (Tull et al., 1993; Groszos and Tull, 2007). The Murphy Group rests above the Great Smoky Group (Dean Formation) and consists of the Nantahala Slate-Tusquitte Quartzite, Brasstown Formation, Murphy Marble and Andrews schist and Marble Hill hornblende Schist (Tull and Groszos, 1988). Resting unconformably above these units are phyllites, metasandstone, metasiltstone, schist, and polymictic conglomerates of the Mineral Bluff Formation (Fritz and La Tour, 1987, 1988; Tull and Groszos, 1988; Groszos and Tull, 2007). In the northeastern end of the Murphy syncline, the Mineral Bluff Formation reaches it maximum thickness, ~3000 m, and stratigraphically highest levels (Tull and Groszos, 1988). A single echinoderm

column (class *Crinoidea* or *Rhobifera*) reported from near the base implies a post-Cambrian age for the Mineral Bluff Formation (Tull et al., 1993). The Mineral Bluff Formation has been interpreted as a successor basin (Tull et al., 1993), or Ordovician turbidites shed into part of the Taconic foreland basin (Fritz and La Tour, 1988; Hatcher et al., 2004b, 2005, 2007a).

The Hayesville fault juxtaposes the enigmatic central Blue Ridge terranes against the western Blue Ridge (Hatcher, 1978). These terranes are exposed in an antiform-synform thrust stack consisting of the highest Cartoogechaye, Cowrock, and lowest Dahlonega gold belt terranes. These terranes are dominated by clastic metasedimentary rocks, and the occurrence of mafic and ultramafic bodies in the Cowrock and Cartoogechaye terranes has been cited as evidence of an oceanic origin (Hatcher, 1978; Hatcher et al., 2004a, 2005, 2007a). Mid-ocean floor and suprasubduction zone settings have been suggested for the various mafic and ultramafic rocks distributed throughout central Blue Ridge and Tugaloo terranes based on geochemistry and petrology of the rocks (Thomas, 2001; Raymond et al., 2003; Swanson et al., 2005). The ~1.1 Ga orthogneisses of the Trimont Ridge massif represent the only documented Mesoproterozic basement in the Cartoogechaye terrane (Hatcher et al., 2004a). Bream et al. (2004) reported Paleoproterozoic and Archean detrital zircons from these terranes and suggested a possible Laurentian mid-continent or Gondwanan provenance.

The Tugaloo terrane includes the eastern Blue Ridge and western Inner Piedmont, and is comprised of deep-water, immature clastic rocks of the Ashe–Tallulah Falls Formation (and equivalents in Georgia and Alabama), and associated mafic and ultramafic rocks. It is juxtaposed against both central and western Blue Ridge terranes by the Chattahoochee–Holland Mountain–Burnsville–Gossan Lead fault. The Ashe–Tallulah Falls Formation can be subdivided into a lower metagraywacke-schist-amphibolite member, a middle aluminous schist member, and an upper metagraywacke-schist member. The medium- to high-grade metamorphism and multiple deformations that affected the Tugaloo terrane make interpreting rare primary sedimentary features in the Tallulah Falls Formation difficult. Tugaloo terrane magmatism varies in the eastern Blue Ridge and western Inner Piedmont. Ordovician, Devonian, and Mississippian granodiorite, trondhjemite, and tonalite intrude the eastern Blue Ridge (C. F. Miller et al., 1998, 2000; Thomas, 2001; Mapes, 2002; B. V. Miller et al., 2006; Stahr, 2007); however, only Ordovician granitoids (470–450 Ma) occur in the western Inner Piedmont (Bream, 2003; Gatewood, 2007). Other metasedimentary units recognized in the Tugaloo terrane include the Alligator Back Formation, northwestern North Carolina, and Emuckfaw

Formation, Georgia and Alabama, and are thought to correlate with the Ashe–Talllulah Falls Formation.

The Cat Square terrane is located in the eastern Inner Piedmont and is juxtaposed against the Tugaloo terrane by the Brindle Creek fault. The Siluro-Devonian Cat Square terrane consists of metapsammitic and metapelitic rocks intruded by anatectic Devonian and Mississippian granitoids (Merschat and Hatcher, 2007). Mafic and ultramafic rocks are sparse but generally occur close to the central Piedmont suture (Merschat and Hatcher, 2007). Proterozoic basement rocks common in many of the other terranes have not been recognized in the Cat Square terrane. Detrital zircons from the terrane suggest a mixed peri-Gondwanan and Laurentian affinity (Bream, 2002; Bream et al., 2004). The northern extent of the Cat Square terrane is fairly well documented (Merschat and Kalbas, 2002; Kalbas, 2003; Merschat, 2003; Wilson, 2006; Gatewood, 2007), but the southern end of the terrane is only interpreted from aeromagnetic data and one detrital zircon sample (see discussion below).

The Smith River allochthon is a large synformal structure that overlies the Lynchburg Group and Mesoproterozoic basement to the northwest and Inner Piedmont para- and orthogneisses of the Sauratown Mountains window to the southwest. It consists of a metasedimentary sequence of metagraywackes and schists, and mafic metavolcanics of the Bassett and Fork Mountain Formations intruded by the Martinsville igneous complex (Henika et al., 1996). The crustal affinity of this terrane has been debated: both peri-Gondwanan (Hibbard et al., 2003) and Laurentian (Carter et al., 2006a) affinities have been proposed. The Smith River allochthon is dominated by metagraywacke with minor calc-silicate pods and bands, interlayered with muscovite-biotite schist (Espenshade et al., 1975; Henika et al., 1996).

Appalachian Orogenies

Four orogenies have affected the Blue Ridge and Inner Piedmont, including the Mesoproterozoic Grenville orogeny (1.25–0.9 Ga), Taconic (~460 Ma), Acadian-Neoacadian (~360 Ma), and Alleghanian (~300 Ma) (Butler, 1991; Hatcher and Goldberg, 1991; Hatcher et al., 2007a). Recent geochronologic and geochemical studies, combined with detailed geologic mapping, have shed new light on the nature, extent, and timing of major orogenic events. Evidence of the tectonothermal fingerprint of the Grenville orogeny (1.25–0.9 Ga) exists in the Mesoproterozoic gneisses in the western Blue Ridge and internal massifs of the central and eastern Blue Ridge (Carrigan et al., 2003; Hatcher et al., 2004a; Ownby et al., 2004). Previously, evidence for the Acadian event

in the southern Appalachians was weak (Osberg et al., 1989), and a 480–460 Ma Taconic event was thought to be responsible for most of the penetrative deformation across the interior of the orogen (Drake et al., 1989; Hatcher, 1989). Recent data indicate a ~360 Ma Neoacadian event is more prominent than previously thought, while the Taconian event is now limited to parts of the western and central Blue Ridge (Moecher et al., 2004; Merschat et al., 2008a). Additionally, evidence suggests the Alleghanian orogeny produced a significant tectonothermal event in the Blue Ridge (Hatcher et al., 2005; Miller et al., 2006; Stahr et al., 2006). The effects of these orogenies are not present or manifested in a similar manner in all terranes.

Problems to be Addressed

Bream (2002, 2003), and Bream et al. (2004) documented the dominance of Grenvillian 1.3–0.9 Ga detrital zircons from the western Blue Ridge and eastern Blue Ridge paragneiss samples and suggested that they indicate a Laurentian source, but central Blue Ridge samples contain a unique, possibly Gondwanan, suite (2.1–1.6 Ga and Archean ages). Detrital zircon spectra from the central Blue Ridge terranes may further document a link between Laurentia and the Amazonian craton during the Proterozoic or possibly the early Paleozoic. In the Inner Piedmont, the Cat Square terrane remains an interesting piece of the puzzle. The extent of this terrane has only been delineated in North Carolina and South Carolina, leaving its southern termination or extent speculative at best. The relationship of the Newton antiform, cored by metagraywacke and amphibolite (Goldsmith et al., 1988), and the Cat Square terrane is unclear. Finally, the structural position and lithotectonic units of the Smith River allochthon imply possible connections with Laurentian or peri-Gondwanan terranes, or both, like the Cat Square terrane. These questions and others will be addressed using U–Pb geochronology and geochemistry of carefully selected representative paragneiss samples.

METHODOLOGY

Seventeen clastic sedimentary or paragneiss samples of 5–10 kg were collected from different formations and lithotectonic units of the North Carolina and Georgia Blue Ridge and Inner Piedmont, and Tennessee Valley and Ridge. Samples were prepared for whole-rock geochemistry and detrital zircon geochronology at the University of Tennessee and Vanderbilt University.

Whole-rock geochemistry preparation at the University of Tennessee involved: cut ~1 kg of sample into <0.5 cm thick slabs, crush and combine the slabs, and powder ~40g of sample with an alumina ceramic mill and shatterbox. Each sample powder was then mixed and 20g were separated and sent to Activation Laboratories in Ancaster, Ontario, for whole-rock analysis. Major and trace element geochemistry was obtained using a combination of ICP, INAA, ICP/MS and XRF techniques.

Different stages of detrital zircon sample preparation were carried out at the University of Tennessee, Vanderbilt University, and Stanford University–U. S. Geological Survey Micro Analysis Center (SUMAC) following standard mineral separation techniques. Initial sample crushing occurred in the field and at the University of Tennessee. Any migmatite leucosome fragments observed in the samples were removed during this stage of crushing to decrease the possibility of Paleozoic metamorphic zircons being included with the detrital zircon spectra. Samples were then crushed to <500 μm, and density sorting, using a water table and heavy liquids to remove the majority of less dense phases from the samples. Ferromagnetic minerals were removed using a Frantz magnet and zircons were hand-picked from the final nonmagnetic fraction. Hand-picked zircons were not discriminated on the basis of size or shape. An additional step using methylene iodine was added with several samples to yield a zircon-rich fraction and reduce possible bias associated with hand picking. A minimum of 60–70 zircons per sample were mounted in epoxy and polished to the approximate average center of the grains at SUMAC. Cathodoluminescence (CL) images, acquired using a JEOL 5600 LV scanning electron microscope equipped with a Hamamatsu photo multiplier and reflected light images of the zircon mounts were collected at SUMAC. Reflected light and CL images were used to distinguish interior zoning, inclusions, and fractures. Detrital zircons were analyzed during four visits to the SUMAC SHRIMP Lab in the summers of 2005 and 2007. Routine operating conditions of the SHRIMP-RG similar to those described by Bream et al. (2004) were used. Zircon standards R33 (~419 Ma), VP10 (~1019 Ma), and RG6 (~1440 Ma) provided by the SUMAC were analyzed regularly. Approximately 30–60 grains were analyzed per sample, and data were reduced using the computer program SQUID v. 1.02 (Ludwig, 2001). Common Pb corrections were applied to all analyses during data reduction using SQUID v. 1.02 (Ludwig, 2001). Only ^{204}Pb-corrected ages are reported here, because ^{204}Pb- and ^{207}Pb-corrected ages are identical at $\pm 1\sigma$ error. All relative probability plots with histograms used to graphically display the data were created using Isoplot v. 3.0 (Ludwig, 2003).

Rare-earth element (REE, La, Ce, Nd, Sm, Eu, Gd, Dy, Er, and Yb) and Hf concentrations in zircon were determined by the SHRIMP-RG for every detrital zircon sample analyzed during the summer of 2007. REE data were collected from the same spot as the U-Pb analysis by an additional cycle after the initial four cycles used for U-Pb analysis. SHRIMP-RG operating conditions for REE are similar to U-Pb analysis, and REE data can be measured in sequential analytical session (Mazdab and Wooden, 2006). Zircon trace-element standard MAD (Madagascar green) was provided by SUMAC.

SAMPLE DESCRIPTIONS

Samples in this study were selected based on detailed mapping in the immediate area surrounding, or nearby, each sample locality and their tectonostratigraphic position. As a group, these samples were identified to provide critical information regarding the provenance, paleogeography, and tectonic evolution of the crystalline core of the southern Appalachians. A single unmetamorphosed Paleozoic foreland sample and sixteen paragneiss samples were selected: nine from the Blue Ridge and seven from the Inner Piedmont (Fig. 4–2; Table 4–1). Various units of the western, central, and eastern Blue Ridge, Smith River allochthon, and Cat Square terrane were sampled. A brief description of each sample, including map and stratigraphic relationships, rock types, and mineralogy is provided below.

Valley and Ridge

One Middle Ordovician Sevier Shale sample (SEV) was collected in the Tennessee Valley and Ridge from the immediate footwall of the Great Smoky fault (frontal Blue Ridge boundary). The sample locality is just northwest of Walland, TN on U.S. 321 in the Guess Creek fault hanging wall, a fault block that was unexposed prior to excavation of the roadcut (Fig. 4–2). The Sevier Shale consists mostly of cm-scale turbiditic siltstone and calcareous shale with minor calcareous sandstone, and some conglomerate (Keith, 1895; Rodgers, 1953; Neuman, 1955; Larson et al., 1989). Maximum formation thickness northwest of this locality is ~700 m (2,100 ft) (Neuman, 1955). Graptolites identified from the Sevier shale in the Guess Creek thrust sheet occur in the *Nemagraptus gracilis* Zone or uppermost *Glyptograptus teretiusculus* Zone (Larson et al., 1989), indicating early Llanvirn deposition, ~475 Ma, just above the Middle Ordovician unconformity (Drake et al., 1989).

Table 4–1. Sample descriptions and locations.

Sample	Fig. 2 ID #	Belt	Terrane	Formation or unit name	7.5-minute	County (State)	Latitude (ºN)	Longitude (ºW)
Valley and Ridge								
SEV	34	VR	Laurentian platform	Sevier Shale	Kinzel Springs	Blount (TN)	35.7348	-83.8222
western Blue Ridge								
MinBlff	28	wBR	Laurentian margin	Mineral Bluff Fm.	Murphy	Cherokee (NC)	35.0953	-84.0176
central Blue Ridge								
CGM	21	cBR	Cowrock	Coweeta group	Shooting Creek	Macon (NC)	35.0588	-83.6203
DEL1	22	cBR	Cartoogechaye	Inequigranular migmatite biotite gneiss	Clyde	Haywood (NC)	35.58122	-82.98646
EG108	23	cBR	Cartoogechaye	Earlies Gap biotite gneiss	Canton	Haywood (NC)		
RS711	31	cBR	Cartoogechaye	Rainbow Springs quartzite	Rainbow Springs	Macon (NC)	35.0111	-83.6189
RS 787	32	cBR	Cartoogechaye	felsic gneiss	Rainbow Springs	Macon (NC)	35.0952	-83.5564
W18	37	cBR	Cartoogechaye	Unnamed migmatitic biotite gneiss	Waynesville	Haywood (NC)	35.4709	-82.8850
Dahlonega gold belt (Great Balsam Mountains window)								
HAZ2mss	26	DGB	Dahlonega gold belt	Otto Fm.	Hazelwood	Haywood (NC)	35.4308	-83.0930
eastern Blue Ridge								
Emuc	25	eBR	Tugaloo	Emuckfaw Fm.	Austell	Douglas(GA)	33.7285	-84.7629
WGxeno	38	eBR	Tugaloo	xenolith in Wiley Gneiss	Tiger	Rabun (GA)		
Smith River allochthon								
MAS1	27	IP	Smith River alloc.	Bassett Formation	Mount Airy South	Surry (NC)	36.4073	-80.5643
Newton window								
R24	30	IP	Tugaloo	Tallulah Falls Fm.; mylonitic metagraywacke	Reepsville	Lincoln (NC)	35.5336	-81.2536
SP13	35	IP	Tugaloo	Talulah Falls Fm.	Stony Pint	Irdell (NC)	35.7562	-81.0917
SW6	36	IP	Tugaloo	Tallulah Falls Fm.	Statesville West	Irdell (NC)	35.8038	-80.9217
eastern Inner Piedmont								
EL2	24	IP	Cat Square	unnamed	Ellendale	Alexander (NC)	35.9519	-81.3242
MV-336-MGW	29	IP	Cat Square	unnamed	Moravian Falls	Wilkes (NC)	36.0408	-81.1353
S21	33	IP	Cat Square	unnamed	Stewart	Jasper (GA)	33.3907	-83.7675

NAD27 CONUS coordinates

Blue Ridge

A sample of biotite-grade, interlayered metasandstone, metasiltstone, and phyllite of the Mineral Bluff Formation (MinBlff) from a roadcut on US Highway 19 in Murphy, North Carolina, was obtained for this study (Fig. 4–2). Interlayers of metasandstone, metasiltstone, and phyllite varied from 1 to 20 cm thick, and the sample consists of interlayered phyllite, metasiltstone, and a 3 cm-thick metasandstone layer. Minerals in the phyllite and metasandstone to siltstone are chlorite, biotite, muscovite, quartz, plagioclase, and minor epidote. Zircons separated from the Mineral Bluff Formation, 50–120 μm, were the smallest in this study (Fig. 4–3). The zircons are anhedral, rounded, or broken. Oscillatory and other styles of zoning are preserved in most zircons, and no rims were observed.

Five samples are from the suspect central Blue Ridge terranes in western North Carolina (Fig. 4–2). These samples are upper amphibolite facies, sillimanite grade, and are commonly migmatitic. The occurrence of mafic and ultramafic complexes in the Cowrock and Cartoogechaye terranes suggests these terranes have an oceanic affinity (Hatcher et al., 2005, 2007a). Bream et al. (2004) obtained several Archean and Paleoproterozoic detrital zircons from these terranes, suggesting a possible Laurentian mid-continent or Gondwanan source. Metasandstone and siliceous marble of the Coweeta Group (sample CGM), Cowrock terrane, were sampled at the road-cut exposure of the Chunky Gal Mountain fault as described by Hatcher and Butler (1979) on US 64, west of Franklin, North Carolina. Typical migmatitic biotite gneiss of the Cartoogechaye terrane was sampled at two different locations. Sample W18 is layered migmatitic biotite gneiss consisting of clinozoisite-biotite-quartz-plagioclase from the exposure at the intersection of US 276 and Peace Love Road, east of Waynesville, North Carolina. The second sample, DEL1, is muscovite-bearing, migmatitic, inequigranular garnet-biotite-quartz-plagioclase gneiss (Merschat and Cattanach, 2008) from the road cut on the westbound lane of Interstate 40 at Caldwell Gap, approximately 10 km north of Waynesville, NC. Inequigranular biotite gneiss at Caldwell Gap contains polymineralic porphyroclasts of quartz and feldspar, and euhedral, post-kinematic garnets up to 2 cm in diameter. R. D. Hatcher (unpublished data) mapped bands of isoclinally folded quartzite within the common migmatitic biotite gneiss of the Cartoogechaye terrane in the Rainbow Springs and Shooting Creek 7.5-minute quadrangles. Rainbow Springs quartzite sample, RS711, was obtained from exposure on Middle Ridge above U. S. Forest Service Blye Gap Road. The quartzite is medium-grained with 7–15 cm layers, and contains minor rutile, garnet, muscovite, and biotite. Otto Formation metasandstone



Figure 4–3. Cathodoluminescence images of selected detrital zircons. Ellipses indicate size and location of analyses and 206Pb/207Pb and 206Pb/238U (italics) ages are listed. Scale bars are 100 μm. (a-d) Mineral Bluff Formation, MinBlff. (e-g) Cartoogechaye terrane, W18. (h-j) Cowrock terrane, CGM. (k-l) Dahlonega gold belt, Great Balsams Mountains window, HAZ2mss. (m-o) Tugaloo terrane, Emuckfaw Formation, EMUC. (p-q) Tugaloo terrane, Wiley Gneiss xenolith, WGxeno. (r-s) Tugaloo terrane, Newton window, Tallulah Falls Formation, SP13 and SW6. (t-u) Smith River allochthon, Bassett Formation, MAS1. (v-x) Cat Square terrane, EL2.

and schist, HAZ2mss, from the northernmost part of the Dahlonega gold belt, exposed in the Great Balsam Mountains window is the fifth central Blue Ridge sample. This sample was collected from a large exposure of metagraywacke interlayered with sillimanite-garnet-muscovite-biotite schist at Cove Field Ridge Overlook on the Blue Ridge Parkway. The Otto metagraywacke and schist are migmatitic and intruded by pegmatite and fine- to medium-grained trondhjemite dikes. Zircons separated from these samples are 100–600 μm, rounded, subhedral to anhedral, and display oscillatory, sector, and other complex zoning patterns (Fig. 4–3). Dark gray to black, faintly zoned to unzoned metamorphic rims, 5–40 μm wide, occurred in all of the samples except W18 and DEL1, which contain bright white unzoned rims. Metamorphic rims commonly embay and truncate zoning in the interiors of the zircons. Fractured and annealed zircons are also common in Cartoogechaye samples (e.g., W18).

Two samples, EMUC and WGxeno, are from the Georgia eastern Blue Ridge, western Tugaloo terrane (Fig. 4–2). The western Tugaloo terrane is comprised of the Ashe–Talllulah Falls Formation and equivalents, minor internal basement massifs, Paleozoic granitoid intrusions, and lesser mafic and ultramafic rocks. The Tallulah Falls dome near the Georgia-South Carolina border (Fig. 4–1) is ringed by several Mesoproterozoic basement gneisses: ~1.15 Ga Wiley Gneiss, Sutton Creek Gneiss, and Wolf Creek Gneiss (Hatcher, 1987; Carrigan et al., 2003; Hatcher et al., 2004a). Xenoliths of garnet-biotite schist have been recognized in the field and described in drillcore through the Wiley Gneiss (Hole 4, at depths of 824-827' and 846-853'; Hopson and Hatcher, 1990). Widening of US 23–441 south of Clayton, Georgia, produced several new roadcuts exposing coarse-grained augen Wiley Gneiss. Elliptical to lens-shaped xenoliths (~0.5 x 0.2 m) of garnet-biotite schist are present in a roadcut on the northbound lane near Wiley, Georgia. Several pieces of a xenolith were collected for separation and examination of detrital zircons. This provides a glimpse at the age and provenance of crust the Grenville massifs of the western Tugaloo terrane intruded. Zircons separated from the Wiley Gneiss xenolith are distinctly round, and typical doubly terminated ends were not observed. In CL, these zircons displayed roughly concentric, faintly zoned rims, 10–50 μm thick, that truncate oscillatory zoning in the core (Fig. 4–3). The transition between cores and rims is commonly marked by bright white boundaries.

West of Atlanta, Georgia, the Chattahoochee fault retreats to the southeast and the eastern Blue Ridge(Tugaloo terrane) is comprised of metagraywacke of the Emuckfaw Formation exposed in the Alexander City thrust sheet. Although the distinctive Tallulah Falls Formation stratigraphy has not been mapped in this part of the eastern Blue

Ridge, this unit is considered a southwestern equivalent (Steltenpohl, 2005; Hatcher et al., 2007a). A sample of the Emuckfaw Formation was collected at the roadcut on the entrance ramp from Bill Arp Road onto westbound Interstate 20 west of Douglasville, Georgia. The Emuckfaw consists of typical medium-grained metagraywacke, garnet-muscovite-biotite-quartz-plagioclase gneiss, with minor calc-silicate pods containing epidote-quartz-plagioclase. Subhedral to anhedral, rounded zircons, 100–500 μm long, with oscillatory zoning are common (Fig. 4–3). Some grains display coarse oscillatory zoning or are very light gray to white, but no obvious metamorphic rims were observed.

Inner Piedmont

The composite Inner Piedmont is composed of the eastern Tugaloo terrane (western Inner Piedmont), Cat Square terrane, and Smith River allochthon. Samples from the Inner Piedmont were selected to address questions regarding the spatial extent of the Cat Square terrane and the significance of mid-Paleozoic sedimentation in the crystalline core. Specific objectives include: (1) verify rocks mapped as Cat Square terrane in the Brushy Mountains (Merschat and Kalbas, 2002; Kalbas, 2003; Merschat et al., 2005a; Wilson, 2006; Gatewood, 2007) have similar detrital zircon populations to those reported for the Cat Square terrane to the south (Bream et al., 2001, 2004; Bream, 2002); (2) address the provenance of amphibolite-bearing biotite gneiss of the Newton antiform (Goldsmith et al., 1988); (3) investigate the location of the southern end of the Cat Square terrane; and (4) compare the provenance of the Smith River allochthon, Tugaloo, and Cat Square terranes.

Two samples were collected from texturally and mineralogically identical migmatitic metagraywacke of the Cat Square terrane in the Brushy Mountains. They are located approximately 20 km apart along strike in the limb of the map-scale Poplar Springs sheath fold of the Brindle Creek thrust sheet, Cat Square terrane (Merschat, 2003; Merschat et al., 2005a). These migmatitic metagraywacke samples contain the assemblage biotite-muscovite-quartz-plagioclase with minor sphene, hornblende, clinozoisite, and rutile. The migmatitic metagraywacke samples are from a roadcut along Dover Church Road, near Duck Creek (EL2), and rock exposed in Rocky Creek below East Brocktown Road, ~1.5km south of intersection with Pores Knob Road (MV336mgw). Zircons from these samples vary in size and morphology, but are commonly subhedral and rounded. Oscillatory zoning is preserved in several cores, and 10–30 μm dark gray to black rims are common (Fig. 4–3). A significant amount of sphene is present in MV–336.

Goldsmith et al. (1988) recognized a large doubly plunging antiform in the eastern Inner Piedmont cored by migmatitic metagraywacke with outcrop and map-scale pods of amphibolite. Detailed geologic mapping has documented mylonite and truncations of Devonian Walker Top granite bodies, and Cat Square terrane schist and metagraywacke, confirming that the Newton antiform is a window (Merschat et al., 2005b; Byars et al., 2008; Gilliam et al., 2008). Questions remain, however, regarding the Laurentian, peri-Gondwanan or mixed affinity of the biotite gneiss and amphibolite exposed in the Newton window. Three samples were selected for detrital zircon analysis. Locations sampled include an exposure of metagraywacke on east side of Lookout Shoals Dam spillway (SP13), a sample of the biotite gneiss from the Statesville Martin Marietta Aggregates Quarry (SW6), and biotite gneiss/metagraywacke from the southeastern part of the window (R24). Metagraywacke at Lookout Shoals Dam consists of biotite-quartz-plagioclase gneiss with 1–2 cm bands forming larger 10 cm to >1m–thick layers and meter-size boudins of coarse-grained amphibolite (metagabbro?). Rock from the quarry is dominantly migmatitic biotite gneiss that contains significant interlayers and boudins of amphibolite and garnet-amphibolite. Migmatitic metagraywacke from the southern end of the window (R24) has been mapped as lower Tallulah Falls Formation (Byars et al., 2008). Detrital zircons from all three Newton window samples are subhedral to anhedral and rounded; most display fine and coarse oscillatory zoning, and range from 60–300 μm (R24 and SP13) and 100–600 μm (SW6). Additionally, R24 contains a significant amount of sphene. Unzoned medium gray and white metamorphic rims truncating interior zoning were observed and analyzed in all three samples.

The southern terminus of the Cat Square terrane is largely inferred, and has been suggested to be truncated by the central Piedmont suture near Athens, Georgia (Hatcher, 2002; Merschat et al., 2005a; Hatcher and Merschat, 2006). Several aeromagnetic lineaments connect to lineaments corresponding to the Paris Mountain thrust and the Brindle Creek fault near the North Carolina-South Carolina border (Hatcher et al., 2007a; Merschat et al., 2008b), providing reason to suggest the Cat Square terrane extends further south than Athens, Georgia. A sample of migmatitic metagraywacke (S21) located southeast of the magnetic lineament in Herds Creek ~1 km south of Stewart, Georgia was collected. The metagraywacke consists of sillimanite, garnet, muscovite, biotite, quartz, plagioclase, with minor rutile and epidote. Zircons vary from 100–500 μm, and anhedral to subhedral, rounded and broken. Most display fine to coarse oscillatory zoning with a lesser population of unzoned, black grains. Some grains are

fractured and annealed by darker unzoned zircon in CL. Thin black rims were observed on a few grains, but were not analyzed.

Finally, a metagraywacke of the Bassett Formation from the southern end of the Smith River allochthon near Ararat, North Carolina, was sampled (MAS1). The southern end of the Smith River allochthon in North Carolina consists of banded biotite-plagioclase-K-feldspar-quartz gneiss intercalated with thin calc-silicate (Espenshade et al., 1975). The exposure consists of sillimanite-garnet-muscovite-biotite-quartz-plagioclase gneiss with minor interlayers, <10 cm thick, of garnet-biotite-muscovite schist. The gneissic metagraywacke rock type was sampled. Zircons ranged from 75–150 μm long and were subhedral and rounded. Smaller zircons, <100 μm, often display nearly euhedral terminal ends.

MAJOR AND TRACE ELEMENT WHOLE-ROCK GEOCHEMISTRY

Major-element, whole-rock geochemistry of the thirteen samples from the Valley and Ridge, Blue Ridge, and Inner Piedmont have compositions typical of immature metasedimentary rocks with SiO_2 and Al_2O_3 being the most abundant oxides (Table 4–2), except for the calcareous conglomerate of the Sevier shale (SEV), siliceous marble from the Coweeta Group (CGM), and Rainbow Springs quartzite (RS711). The most abundant oxide in most samples is SiO_2, which ranges from 59–75 weight percent with the outliers of the calcareous conglomerate (SEV, 20.62 weight percent SiO_2), siliceous marble (CGM, 43.09 weight percent SiO_2), and quartzite (RS711, 92.19 weight percent SiO_2). Al_2O_3 varies from 5–18 weight percent and is the second most abundant in all samples, except the calcareous conglomerate (SEV), and siliceous marble (CGM), which contain 41.49, and 23 weight percent CaO, respectively. Transition metals (Fe_2O_3, MnO, MgO, and TiO_2) are characterized by 4–10 weight percent Fe_2O_3, 1–3 weight percent MgO, 0.4–1.4 weight percent TiO_2, and minor MnO ranges from 0.002 to 0.2 weight percent. Excluding the calcareous conglomerate, siliceous marble, and quartzite, CaO, Na_2O, and K_2O contents generally vary between 1–4 weight percent, but are usually similar within each sample.

Trace-element concentrations, determined by several different analytical techniques, are listed in Table 4–3. All samples display similar flat REE patterns with slightly positive Eu anomalies when compared with REE data from North American shale composite (Gromet et al., 1984), and upper continental crust (Taylor and McLennan,

Table 4–2. Whole-rock chemical analyses of weight percent of major oxides and chemical alteration index for metasedimentary samples.

			VALLEY & RIDGE	Western	BLUE RIDGE Central					Eastern		SRA		INNER PIEDMONT Newton window	
Sample ID			SEV	MINBLFF	CGM	DEL 1	Haz2mss	RS711	W18	EMUC	WG xeno	MAS 1	S21	SW6MM	SP13
Analysis Type		Detection Limit													
FUS-ICP															
	SiO_2	0.01	20.62	59.27	43.09	62.17	74.75	92.19	56.56	75.16	60.96	66.78	68.84	61.12	68.75
	Al_2O_3	0.01	1.27	14.79	12.14	15.05	9.98	4.61	17.66	11.07	14.66	15.76	13.69	16.68	13.05
	Fe_2O_3 (T)	0.01	0.55	10.66	7	7.73	4.65	0.29	8.34	3.77	9.98	4.41	5.54	7	6.15
	MnO	0.001	0.015	0.213	0.095	0.151	0.07	0.002	0.109	0.079	0.138	0.066	0.105	0.112	0.084
	MgO	0.01	1.74	2.54	1.6	3.33	1.43	0.1	2.8	1.24	3.43	1.13	1.98	2.32	1.7
	CaO	0.01	41.49	4.31	22.98	3.81	1.56	0.04	5.5	1.62	2.63	3.51	2.57	3.94	2.46
	Na_2O	0.01	0.41	2.84	1.64	2.13	2.26	0.31	3.06	2.97	1.89	4.02	2.57	4.11	2.57
	K_2O	0.01	0.19	0.73	1.31	2.44	2	1.73	2.88	1.89	3.77	2.01	1.99	2.35	2.18
	TiO_2	0.001	0.051	1.4	0.461	1.082	0.846	0.051	1.3	0.559	1.204	0.734	0.938	0.825	1.065
	P_2O_5	0.01	0.04	0.21	0.29	0.23	0.13	0.03	0.54	0.07	0.07	0.28	0.18	0.24	0.18
	LOI	0.01	34.13	1.98	9.21	0.74	0.88	1.04	1.12	0.62	1.71	0.7	1.02	0.92	1.01
	TOTAL		100.49	98.95	99.82	98.87	98.55	100.4	99.87	99.03	100.5	99.4	99.42	99.61	99.2
	CIA		2	54	21	55	54	66	51	53	55	52	56	51	55

Table 4–3. Whole-rock trace element analyses of metasedimentary samples.

			VALLEY & RIDGE	Western	BLUE RIDGE Central					Eastern		SRA		INNER PIEDMONT Newton window	
Sample ID			SEV	MINBLFF	CGM	DEL 1	Haz2mss	RS711	W18	EMUC	WG xeno	MAS 1	S21	SW6MM	SP13
Analysis Type		Detection Limit													
FUS-ICP	Trace Elements (ppm)														
	Be	1	nd	3	3	2	1	nd	2	2	4	3	2	nd	1
	V	5	nd	139	48	132	64	nd	150	42	199	67	79	91	88
	Sr	2	285	185	1206	198	205	23	546	232	176	309	205	510	223
	Y	1	7	56	41	51	44	nd	30	20	66	24	42	43	37
	Ba	1	156	88	321	699	532	406	1622	376	978	568	376	974	642
INAA	Trace Elements (ppm, *-ppb)														
	Sc	0.01	1	17.4	12.6	19.4	9.18	0.64	20.7	6.05	23.1	9.45	12.1	15.9	12.6
	Cr	0.5	4.1	64.3	28.9	108	35.6	5.8	43.7	24.8	125	nd	46.8	87	47.6
	Co	0.1	1.5	34.4	19.4	21.2	10.4	2	17.5	7.1	28.4	8.3	8.6	16.5	13.6
	As	1	1	nd	nd	nd	nd	nd	nd	nd	nd	nd	nd	nd	nd
	Se	0.5	nd	nd	nd	nd	nd	nd	nd	nd	nd	nd	nd	nd	nd
	Br	0.5	0.8	nd	2.4	nd	nd	1	nd	nd	nd	nd	nd	nd	1.5
	Mo	2	nd	—	—	—	—	—	—	—	—	—	—	nd	nd
	Sb	0.1	nd	0.3	nd	0.1	nd	nd	0.1	nd	nd	nd	nd	nd	nd
	W	1	nd	nd	nd	nd	nd	nd	nd	nd	nd	nd	nd	nd	nd
	Ir	1*	nd	nd	nd	nd	nd	nd	nd	nd	nd	nd	nd	nd	nd
	Au	1*	7	nd	1	3	14	nd	4	nd	2	7	3	3	5
	Hg	1	nd	nd	nd	nd	nd	nd	nd	nd	nd	nd	nd	nd	nd
FUS-MS	Trace Elements (ppm)														
	Ga	1	1	27	20	21	15	5	28	15	26	25	22	21	19
	Ge	0.5	nd	2.2	1	1.4	1.1	0.8	1.5	1.2	1.4	1.1	1.4	1.6	1.4
	Rb	2	5	75	45	84	69	35	96	75	127	83	78	49	65
	Zr	1	87	348	157	323	430	149	428	320	338	359	420	313	417
	Nb	0.2	1.7	19.5	10.7	12.8	10.7	0.7	13.8	6.6	16.5	13.8	13.4	7.6	15.2
	Mo	2	—	nd	3	3	nd	2	nd	nd	4	nd	nd	—	—
	In	0.1	nd	nd	nd	nd	nd	nd	nd	nd	nd	nd	nd	nd	nd
	Sn	1	nd	4	3	4	nd	nd	1	2	nd	2	2	nd	nd
	Cs	0.1	nd	11.4	0.3	0.9	0.6	0.1	0.2	2	0.7	1.6	1	0.3	0.5
	La	0.05	5.79	70.3	50.3	47.9	30.5	5.67	69.2	22.9	62.2	49.6	34.5	39.9	38.4
	Ce	0.1	10.4	150	110	104	60.7	7.3	143	50.2	131	74.6	80.9	74.5	78.6
	Pr	0.02	1.36	17.7	13.1	12.3	7.64	1.22	16.3	5.67	14.9	9.9	9.53	8.95	10
	Nd	0.05	5.49	65.9	52.8	49.1	30.3	4.15	65.6	22.2	56.9	36.7	37.3	35.1	38.4
	Sm	0.01	1.02	13.3	10.5	10.2	5.92	0.72	11	4.5	10.6	6.47	7.69	6.97	7.81
	Eu	0.005	0.261	3.27	1.84	2.36	1.44	0.374	3.42	1.18	2.13	2.05	1.79	2.98	1.93
	Gd	0.02	0.97	12	8.8	10	6.39	0.55	8.72	4.25	10.6	6.13	7.5	6.64	6.99
	Tb	0.01	0.16	2.04	1.4	1.66	1.13	0.07	1.2	0.7	1.79	0.88	1.25	1.1	1.19
	Dy	0.02	0.91	11.5	7.69	9.01	6.54	0.29	6.3	3.68	10.6	4.5	6.94	6.71	6.33
	Ho	0.01	0.19	2.06	1.39	1.74	1.42	0.05	1.18	0.72	2.2	0.83	1.41	1.5	1.27
	Er	0.01	0.52	6.03	4.03	5.49	4.74	0.15	3.39	2.19	6.9	2.38	4.54	4.96	4.03
	Tm	0.005	0.077	0.899	0.579	0.836	0.748	0.026	0.47	0.346	1.04	0.326	0.716	0.761	0.601
	Yb	0.01	0.47	5.49	3.53	5.35	4.88	0.2	2.93	2.34	6.38	1.98	4.63	5.14	3.86
	Lu	0.002	0.069	0.835	0.513	0.786	0.756	0.036	0.431	0.362	0.953	0.3	0.692	0.754	0.58
	Hf	0.1	1.4	9.4	4.2	9	10.6	3.6	10.4	7.8	9.1	8.4	11.3	8.5	11.7
	Ta	0.1	nd	1.5	0.8	1	0.6	nd	0.5	0.6	1.2	1.1	1.1	0.2	0.8
	Tl	0.05	nd	0.62	0.35	0.54	0.43	0.16	0.38	0.55	0.91	0.5	0.48	0.33	0.42
	Bi	0.1	nd	1.3	0.6	0.9	0.3	1.8	nd	nd	nd	nd	nd	nd	nd
	Th	0.05	1.07	9.81	9.85	13.1	8.54	1.39	3.76	6.64	18.2	8.11	11.7	1.28	8.15
	U	0.05	0.59	3.23	3.83	4.37	1.09	0.27	0.49	1.6	1.76	2.03	3	0.19	1.07
TD-ICP	Trace Elements (ppm, *-%)														
	S	0.00001*	0.14620	0.189	0.604	0.039	0.002	0.003	0.112	0.004	0.541	0.033	0.01	0.146	0.116
	Ni	1	1	47	16	45	14	2	16	11	69	3	8	39	19
	Cu	1	1	58	41	28	4	4	20	nd	59	6	4	65	20
	Zn	1	nd	134	108	85	69	6	94	60	178	72	65	113	81
	Ag	0.5	nd	nd	nd	nd	nd	nd	nd	nd	nd	0.6	nd	nd	nd
	Cd	0.5	nd	nd	nd	nd	nd	nd	nd	nd	nd	nd	nd	0.7	0.5
	Pb	5	9	27	18	9	5	9	12	15	19	30	6	27	25
Ratios															
	Th/Sc		1.07	0.56	0.78	0.68	0.93	2.17	0.18	1.10	0.79	0.86	0.97	0.08	0.65
	Zr/Sc		87.04	20.00	12.46	16.65	46.84	232.81	20.68	52.89	14.63	37.99	34.71	19.69	33.10
	La/Sc		5.79	4.04	3.99	2.47	3.32	8.86	3.34	3.79	2.69	5.25	2.85	2.51	3.05
	Co/Th		2.57	44.21	29.25	34.30	18.94	3.39	21.26	13.74	46.60	16.41	20.30	17.78	21.75
	Cr/Th		3.81	6.55	2.93	8.24	4.17	4.17	11.62	3.73	6.87	—	4.00	67.97	5.84
	Cr/V		—	0.46	0.60	0.82	0.56	—	0.29	0.59	0.63	—	0.59	0.96	0.54
	V/Ni		—	2.96	3.00	2.93	4.57	—	9.38	3.82	2.88	22.33	9.88	2.33	4.63

1985) (Fig. 4–4). Although they display a similar trend, the quartzite (RS711) and calcareous conglomerate (SEV) have much lower REE concentrations than the other samples and the normalizing standards. The quartzite displays slight depletions in Ce, Dy, Ho, and Er. All other samples have REE concentrations similar to the normalizing standards.

The chemical index of alteration (CIA, CIA= $Al_2O_3/[Al_2O_3+CaO+Na_2O+K_2O]$); Nesbitt and Young, 1982) provides both a measure of the degree of chemical alteration and an approximate composition of the possible source material. CIA values for all samples are between 51 and 56 except the calcareous conglomerate (SEV), and the siliceous marble (CGM), which have values of 2 and 21 (Table 4–2; Fig. 4–5). Expected values of common rock types include: gabbro/basalt, 30–45; granodiorite to granite, 45–55; and average shales, 70–75 (Nesbitt and Young, 1982). Calculated CIA values fall within typical values for felsic plutonic rocks, suggesting these are immature siliciclastic rocks. Two samples, the calcareous conglomerate of the Sevier shale (SEV), and siliceous marble from the Coweeta Group (CGM) plot below the possible composition of gabbro, and are interpreted as either siliceous, chemical sediments, or derived from carbonates. The Mineral Bluff Formation sample, MinBlff, plots near the alteration trend of gabbro, suggestive of a more mafic source. Similarly, Fritz and La Tour (1987, 1988) concluded a non-continental source to explain the low K_2O values observed from several whole rock analyses of Mineral Bluff Formation lithologies. The Rainbow Springs quartzite (RS711) plots close to the advanced weathering trend for granite (Fig. 4–5), indicating the quartzite contains a significant amount of granite in its source area.

Tectonic discrimination diagrams for metagraywackes using different combinations of trace elements Co, Cr, La, Sc, Th, Ti, and Zr have been formulated by Bhatia and Crook (1986), but generally do not yield a consistent tectonic setting for these samples (Fig. 4–6). Most samples either plot in the continental arc field or do not plot within a defined field. No samples plot in the passive margin field. Samples that regularly occur in the continental arc field include DEL1, EMUC, SP13, SW6, and S21. The Mineral Bluff Formation sample, which consists of interlayered phyllite, metasiltstone, and metasandstone, plots in or close to the active continental margin field. Bream (2003) found that most paragneiss samples from the southern Appalachian crystalline core plotted in the continental arc field. This is contrary to the commonly suggested oceanic depositional setting proposed for several terranes (Cartoogechaye, Cowrock, Tugaloo, and Cat Square terranes) based on the occurrence of mafic and ultramafic rocks (Hatcher, 1978; Abbott and Raymond, 1984; Raymond et al., 2003;

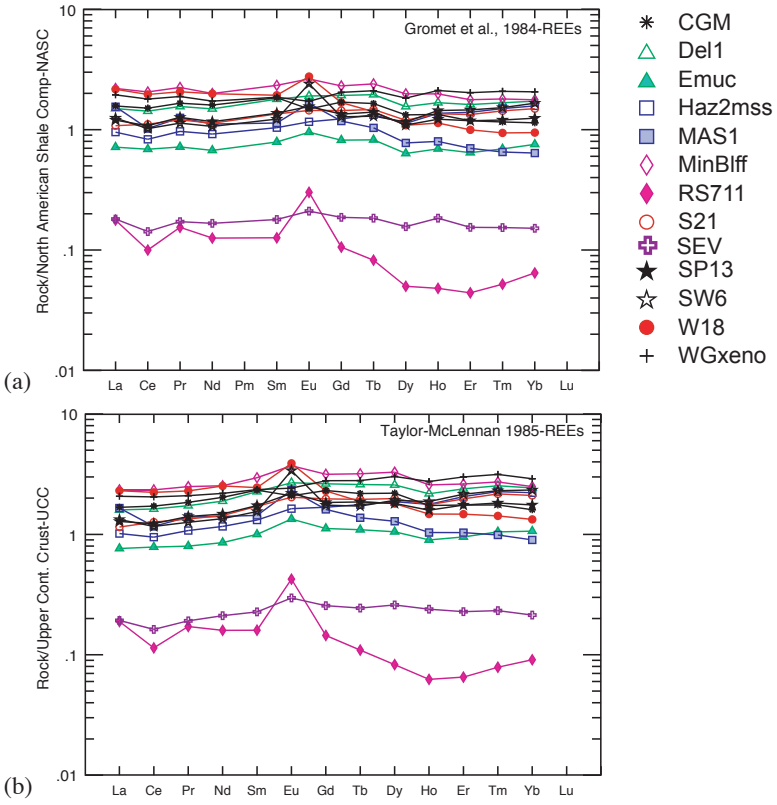

Figure 4–4. Multi-element variation diagrams of REE normalized to (a) North American Shale composite (Gromet et al., 1984), and (b) upper continental crust (Taylor and McLennan, 1985).

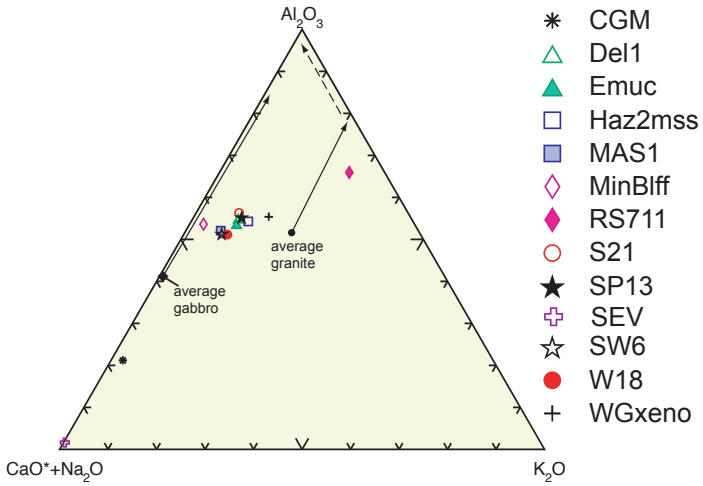

Figure 4–5. CIA ternary plot after Nesbitt and Young (1982). Location and typical weathering profiles of average gabbro and granite are indicated. Advanced weathering trend of granite indicated by dashed arrow.

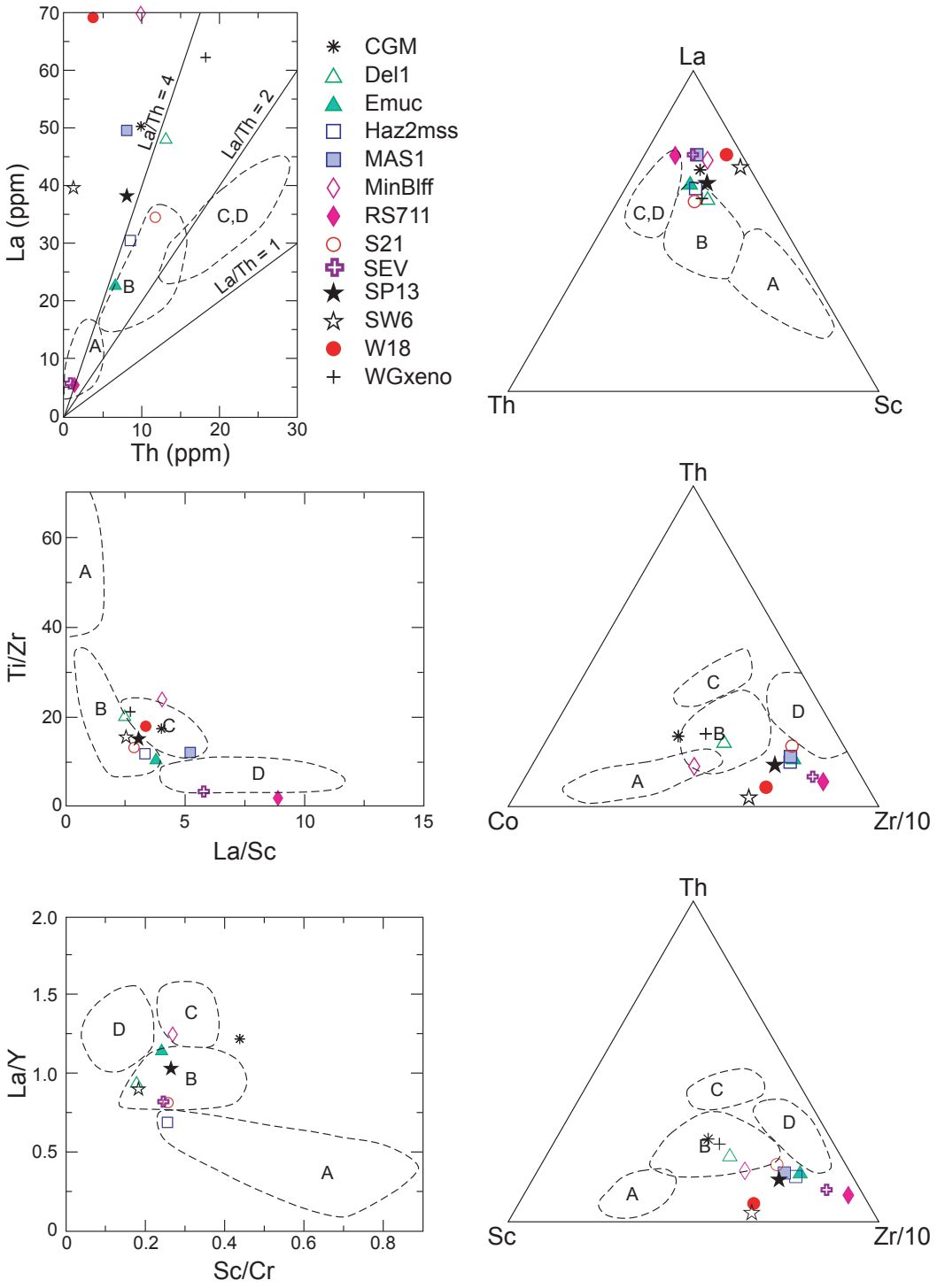

Figure 4–6. Tectonic discriminant diagrams for graywackes from Bhatia and Crook (1986). A–ocean island arcs. B–continental island arcs. C–active continental margin. D–passive continental margin.

Swanson et al., 2005; Hatcher et al., 2007a; Merschat and Hatcher, 2007). However, it is important to note that these diagrams are for greywackes (Bhatia and Crook, 1986), and use with metasedimentary rocks with protoliths other than greywacke may yield questionable results.

DETRITAL ZIRCON GEOCHRONOLOGY

Results from SHRIMP U–Pb analyses of detrital zircons of samples from various metasedimentary terranes from the southern Appalachian Blue Ridge and Inner Piedmont yielded ages that span from the Archean to middle Paleozoic (Appendix III). Relative probability plots with histograms display the multiple age populations observed from each sample (Fig. 4–7). Data used in the relative probability plots and histograms include ^{204}Pb-corrected ^{207}Pb/^{206}Pb ages greater than 700 Ma, and ^{204}Pb-corrected ^{206}Pb/^{238}U ages when ^{207}Pb/^{206}Pb ages are less than 700 Ma. Relative probability plots and histograms were constructed using all of the data and only data ±10 percent discordant (red line and dark gray boxes). Paleozoic metamorphic rims, identified in CL images and typical Th/U ratios less than 0.1, were not included in the relative probability plots. Typically, the samples are dominated by Mesoproterozoic ages (1.3–1.0 Ga), with lesser components of Paleoproterozoic, Neoproterozoic, and Paleozoic ages (Fig. 4–7). The oldest age determined is a single Archean grain of 2.7 Ga from the Mineral Bluff Formation, western Blue Ridge. Neoproterozoic and Paleoproterozoic ages occur in several samples from both the Blue Ridge and Inner Piedmont; however, detrital Paleozoic ages occur only in samples from the Inner Piedmont, including a sample from the Smith River allochthon, and the Cat Square terrane, which yielded a Silurian age (438±5 Ma), the youngest observed. Although these samples display broad similarities, variations in populations exist and are discussed below in more detail.

Valley and Ridge

Sevier Shale detrital zircons (21 of 24 analyses) contain distinctive Grenvillian (1.0 to 1.25 Ga), and pre-Grenvillian components. Pre-Grenvillian ages are dominantly Mesoproterozoic with peaks at ~1.35 and 1.45 Ga, although one Paleoproterozoic grain with a ^{207}Pb/^{206}Pb age of 1.8 Ga was also identified (Fig. 4–7). Errors associated with ages for this sample are suitable for determination of distinct detrital components (1 sigma errors for all analyses fall between 10 and 70 Ma for ^{206}Pb/^{238}U ages and between 25 and 300 Ma for ^{207}Pb/^{206}Pb ages). Three zircons plotted were too reversely discordant

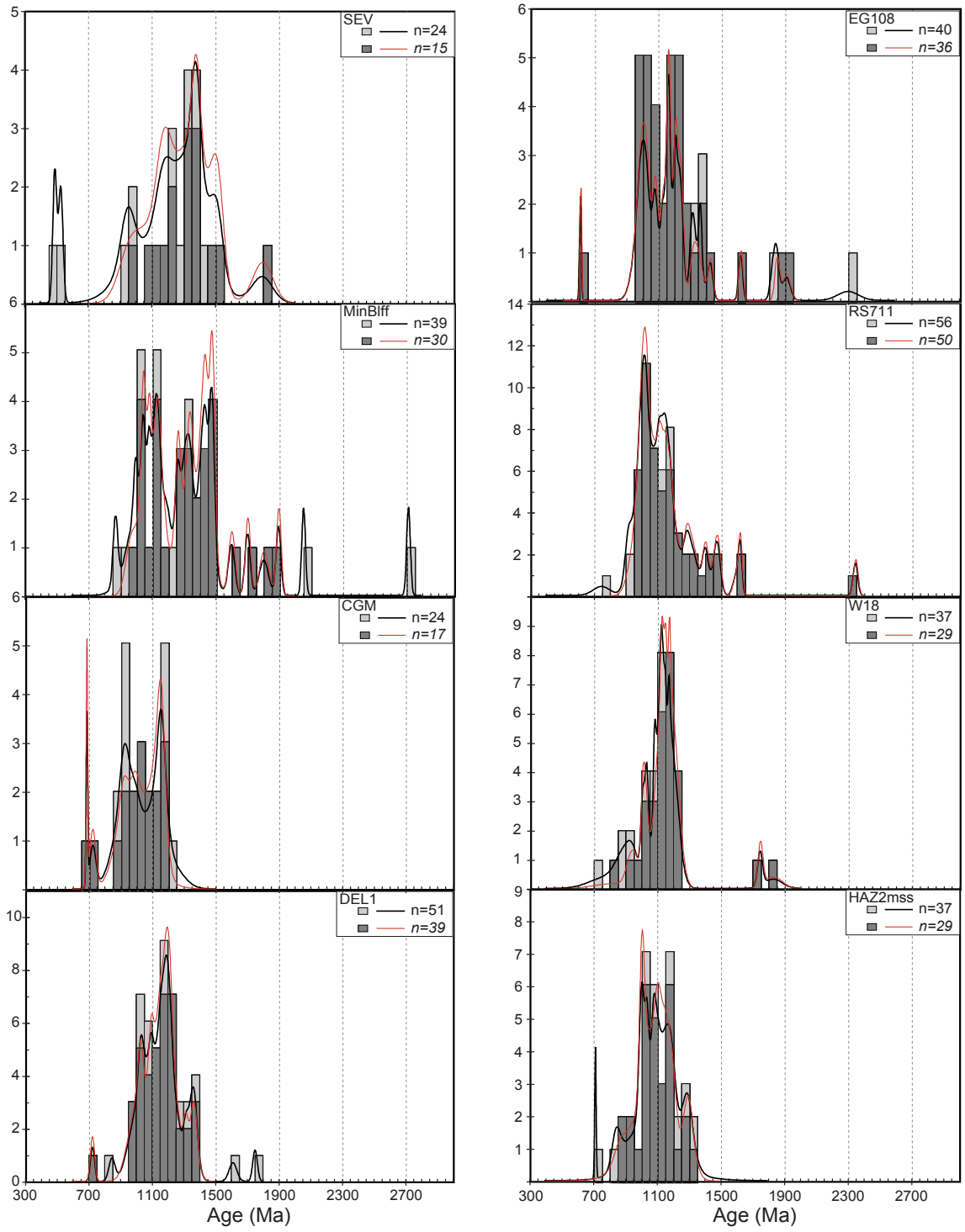

Figure 4–7. Relative probability plots with histograms of U-Pb ages of detrital zircons from 16 paragneiss samples described in this study. Plots were constructed using $^{206}Pb/^{207}Pb$ ages greater than 700 Ma, and $^{206}Pb/^{238}U$ ages when $^{206}Pb/^{207}Pb$ ages are less than 700 Ma. Thicker black line and light gray histograms represent all data, and red line and medium gray histograms represent data ±10 percent discordant.

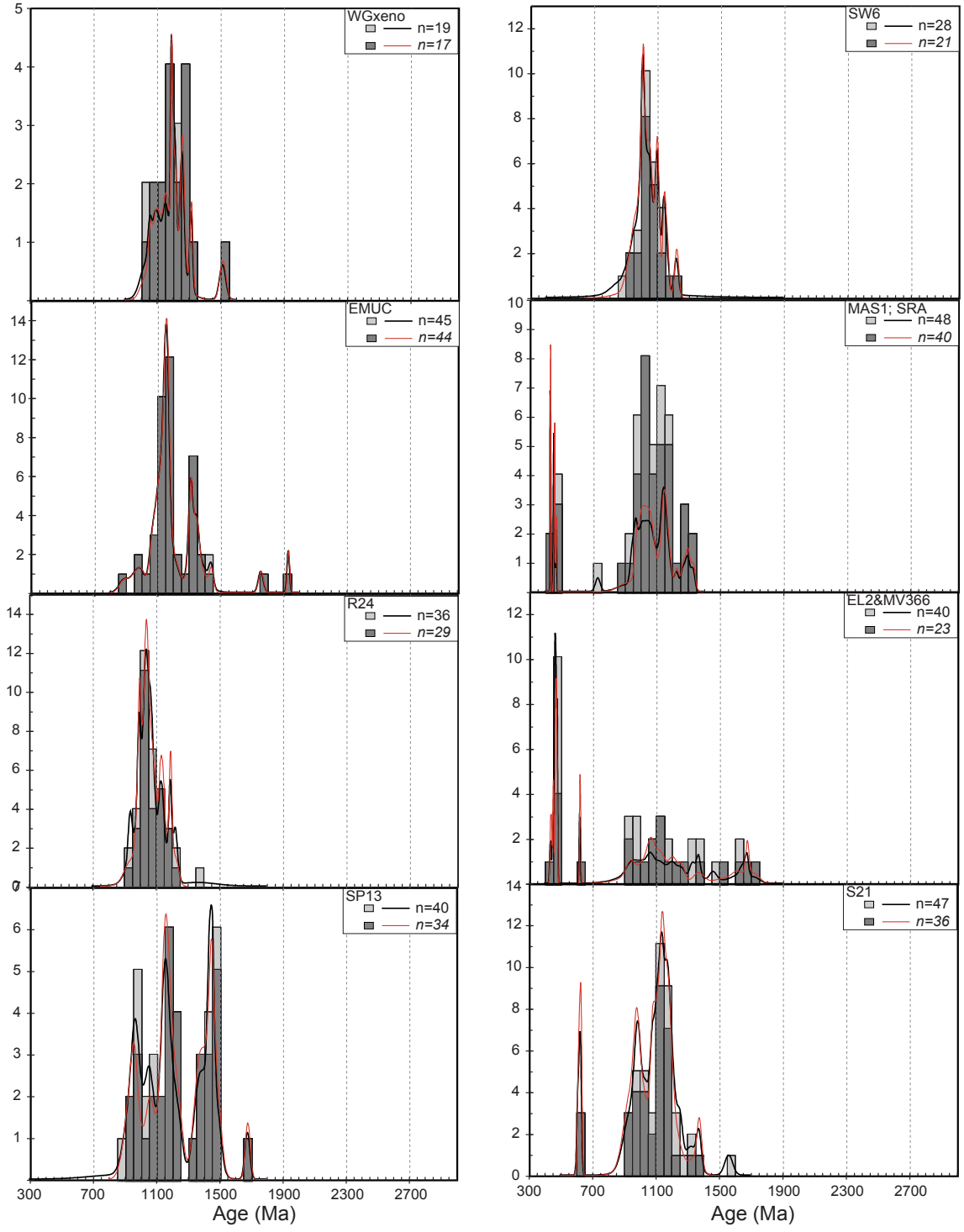

Figure 4–7. Continued.

to be considered reliable (Appendix III); but the $^{206}Pb/^{238}U$ ages are Early Paleozoic for two analyses and ~950 Ma for one of the analyses.

Western Blue Ridge

The single sample from the western Blue Ridge (MinBlff) yielded the most diverse age population of all the samples in this study, including the oldest age, a single 2.7 Ga Archean grain. The typical Mesoproterozoic peaks can be separated into two different groups at 1.2–1.0 Ga, and 1.25–1.5 Ga (Fig. 4–7). Additionally, the several concordant single analyses of Paleoproterozoic ages include 2.0, 1.8, 1.65, and 1.6 Ga grains. Although fossil evidence implies an Ordovician or younger age of the Mineral Bluff Formation, no zircons yielded Paleozoic ages. Discordant Neoproterozoic (~800 Ma) ages represent the youngest zircons from this sample. A thin, discontinuous light gray rim was observed, but it was too narrow to analyze.

Central Blue Ridge

Several samples were analyzed from central Blue Ridge terranes; despite the results of Bream et al. (2004), no Archean ages were observed. The typical Mesoproterozoic peak at 1.3–1.0 Ga was observed in all samples and included some 1.4 Ga ages (Fig. 4–7). Paleoproterozoic ages occurred in all samples except the Dahlonega gold belt from the Great Balsam Mountains window (HAZ2mss) and the Cowrock terrane Coweeta Group siliceous marble (CGM). The Paleoproterozoic ages observed include 2.3, 1.9, 1.8, 1.7, and 1.6 Ga zircons, but these are not common to all samples (Fig. 4–7). Common to all central Blue Ridge samples are Neoproterozoic ages between 900–700 Ma, with analyses of 750–700 Ma occurring in all. These samples yielded abundant Paleozoic metamorphic rims that generally range from 480–440 Ma (Merschat et al., 2008a).

Eastern Blue Ridge

Although the two samples from the eastern Blue Ridge are from fundamentally different stratigraphic horizons, they display similar detrital zircon ages. The xenolith of garnet-biotite schist (WGxeno) from the ~1.15 Ga Wiley Gneiss contains a significant population from 1.3–1.0 Ga and a single analysis at ~1.5 Ga (Fig. 4–7). The sample of metagraywacke and calc-silicate from the Emuckfaw Formation (EMUC) displays a similar span of Mesoproterozoic peaks from 1.4–1.0 Ga, and single analyses of Paleoproterozoic ages at 1.9 and 1.75 Ga (Fig. 4–7). Three Neoproterozoic ages between

950–850 Ma were analyzed from the Emuckfaw sample, and none from the xenolith. No Paleozoic metamorphic rims were present in either sample. Thick gray to white rims analyzed from WGxeno yielded Mesoproterozoic ages close to the age of the Wiley Gneiss 1.15–1.0 Ga.

Inner Piedmont

Smith River allochthon

The single sample from the southwestern end of the Smith River allochthon (MAS1) yielded the typical Mesoproterozoic spectrum with ages between 1.35–1.0 Ga, a single Neoproterozoic age at ~700 Ma, and several Ordovician ages (Fig. 4–7). The Paleozoic ages range from 469–434 Ma and Th/U ratios of 0.2 to >1 are typical of magmatic zircons. No metamorphic rims were observed or measured.

Newton window

Three samples of migmatitic gneiss from the Newton window yielded similar suites of detrital zircon ages (Fig. 4–7). Two samples (R24 and SW6) yielded a roughly Gaussian distribution of ages from 1.25–0.9 Ga, with the largest peak at 1.0 Ga. In sample R24, a single discordant age of 1.35 Ga was analyzed. The third sample (SP13) displays three peaks in the Mesoproterozoic to Neoproterozoic ages 1.5–1.3 Ga, 1.25–1.0 Ga, and 1.05–0.9 Ga, and the oldest zircon analyzed from the Newton window yields an age of ~1.65 Ga. Several late Paleozoic rims were analyzed from these three samples and range from 360–300 Ma (Merschat et al., 2008a).

Cat Square terrane

Two samples (MV336 and EL2) from the Cat Square terrane in the Brushy Mountains were combined because of proximity and limited number of analyses from one sample. In addition to the typical 1.3–1.0 Ga Mesoproterozoic suite of zircons, the sample from the Cat Square terrane in the Brushy Mountains yielded Paleozoic, Neoproterozoic, and Paleoproterozoic ages (Fig. 4–7). Paleoproterozoic ages range from 1.75–1.6 Ga, while Neoproterozoic and Paleozoic ages define three separate peaks at 630 Ma, 468 Ma, and 433 Ma, respectively. Multiple metamorphic rims were observed and analyzed in these two samples, and their U–Pb ages range from 390–325 Ma. The final sample, S21, is from the possible southern continuation of the Cat Square terrane in central Georgia. It also displays the typical Mesoproterozoic suite of zircon ages from 1.3–0.9 Ga. This sample also contains three Neoproterozoic ages at ~630 Ma, and a

single discordant analysis at 1.55 Ga (Fig. 4–7). No Paleozoic metamorphic rims were observed or measured from this sample.

DETRITAL ZIRCON TRACE ELEMENT CONCENTRATIONS

To augment the standard SHRIMP U–Pb detrital zircon geochronology, selected trace elements were measured in zircons from selected samples; five from the Blue Ridge (DEL1, EG108, EMUC, RS711, and WGxeno) and three from the Inner Piedmont (MAS1, S21, and R24). In addition to Th, U, and Pb concentrations measured for all samples, Hf and REE La, Ce, Nd, Sm, Eu, Gd, Dy, Er, and Yb were measured in eight samples (Appendix III). The most abundant trace element is Hf, which varies from 5,000 to 20,000 ppm. U and Th concentrations vary from 23 to 2,000 ppm and <5 to 1,600 ppm, respectively. HREE Gd, Dy, Er, and Yb vary on the order of 10 to 500 ppm with a few concentrations significantly higher. Eu and La typically have concentrations less than 1 ppm, while Nd and Sm vary from 1 to 100 ppm, and Ce varies from 1 to 400 ppm.

Chondrite-normalized REE diagrams were constructed according to age (Fig. 4–8). Three patterns recognized include: (1) steep REE pattern with positive Ce- and negative Eu-anomalies, and HREE values on order of 10^3 to 10^4; (2) steep REE pattern with 10^2 to 10^3 HREEs and no Eu anomaly; and (3) flat HREE pattern on the order of 10^2 to 10^3, positive Ce anomaly, and minor negative Eu anomaly. The majority of the data display REE patterns similar to the first pattern described, including all Paleoproterozoic ages, most Mesoproterozoic ages, and some Neoproterozoic to Paleozoic ages (Fig. 4–8). Variations in this pattern include magnitude of the negative Eu anomaly, HREE concentrations 10^2 to 10^4, and occasionally the magnitude of the positive Ce anomaly. The second and third patterns are not common, and represent only a small portion of the data. The second pattern occurs mostly with the Paleozoic ages and recognized metamorphic Paleozoic rims, but also occurs in some Mesoproterozoic ages. The final flat HREE pattern occurs in Mesoproterozoic ages from EG108 from the central Blue Ridge Cartoogechaye terrane.

Several studies have attempted to link trace element concentrations in zircon with possible protolith composition with only minor success (Hoskin and Ireland, 2000; Grimes et al., 2007). The greatest downfall of using zircon REE concentrations to delimit provenance and protolith composition is the similarity of REE patterns from notably different tectonic environments and protoliths (Hoskin and Ireland, 2000; Hoskin and Schaltegger, 2003). Several patterns, however, are generally considered to be diagnostic

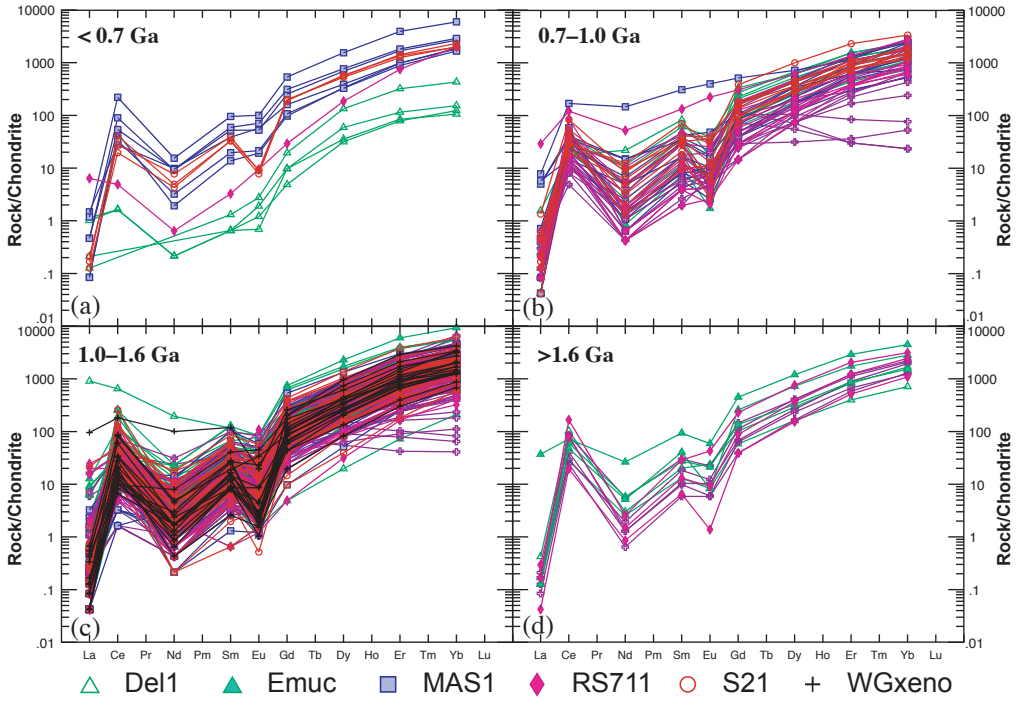

Figure 4–8. Chondrite normalized rare earth element multi-element variation diagrams of zircon separated according to U-Pb and Pb-Pb age. (a) U-Pb < 0.7 Ga. (b) 0.7 Ga < Pb-Pb < 1.0 Ga. (c) 1.0 Ga < Pb-Pb <1.6 Ga. (d) Pb-Pb > 1.6 Ga.

of magmatic, metamorphic, and eclogitic zircons (Hoskin and Schaltegger, 2003; Rubatto and Hermann, 2007). Unmodified magmatic zircons are typically characterized by a steep positive REE pattern with distinct positive Ce and negative Eu anomalies. The majority of the zircons analyzed in this study display a magmatic REE pattern, as described in pattern (1) above. Metamorphic zircons may display an identical pattern to magmatic zircons, especially when formed in equilibrium with melt, or a pattern with a more pronounced positive Ce anomaly and no Eu anomaly (Hoskin and Schaltegger, 2003; Rubatto and Hermann, 2007). Several Paleozoic zircon rims from the central Blue Ridge (DEL1 and RS711) display REE patterns with no Eu anomaly, typical of metamorphic zircons. Metamorphic zircons formed in equilibrium with a melt will have REE patterns that cannot be separated from magmatic zircons (Rubatto and Hermann, 2007). Zircons formed during ecologite facies high-pressure metamorphism have a distinct flat HREE pattern and no Eu anomaly (Hoskin and Schaltegger, 2003; Rubatto and Hermann, 2007), and are similar to pattern (3). Sample EG108 from the Blue Ridge contains four analyses at ~1.0 Ga with diagnostic flat HREE (10^2), positive Ce, and negative Eu patterns (Fig. 4–8). These zircons range in age from 1.02-0.98 Ga and likely formed during high-pressure metamorphism during the Grenville orogeny.

Grimes et al. (2007) used the concentration of U, Hf, Yb, and Gd to separate continental, kimberlitic, and oceanic zircons. Similar ratios and plots were applied to this data set, and all data plot in the fields corresponding to continental crust (Fig. 4–9). Some zircons occur in the kimberlite field within the continental field, but a continental source is more likely and is favored here.

AGE OF DEPOSITION

The lack of biostratigraphic evidence has plagued the understanding of the tectonic affinity and evolution of the southern Appalachian metasedimentary terranes. Of the terranes and formations sampled by this study, biostratigraphy exists for only two samples (MinBlff and SEV) from the Ordovician(?) Mineral Bluff Formation and Sevier Shale. Therefore, the youngest detrital zircon age reported, combined with either the age of metamorphism or oldest intrusive rock, provides limits on the depositional ages of the metasedimentary terranes of the southern Appalachians (Fig. 4–10). It is noted that these depositional ages represent only a maximum age. The limited number of detrital zircons analyzed, or possibly a naturally limited or homogeneous source, can potentially create significant differences between the maximum and actual ages of deposition.

The Mineral Bluff Formation sample is a good example of the large difference between maximum age estimated from detrital zircons and a biostratigraphic age. The youngest detrital zircon dated from the Mineral Bluff Formation, a discordant 850 Ma, is almost 400 m.y. older than the age established by a post-Cambrian echinoderm fossil, which suggests a maximum age of 488 Ma. Correlation of Murphy syncline stratigraphy with the Cambrian Chilhowee, Conasauga, and Knox Groups implies an Ordovician or younger age for the overlying Mineral Bluff Formation (Tull et al., 1993; Hatcher et al., 2005, 2007a).

The youngest detrital zircons measured in most samples are Neoproterozoic (Cryogenian to Ediacaran), except for two samples that contain Paleozoic zircons, and four samples that contain only Mesoproterozoic or older zircons. Based on the youngest detrital zircon ages, age of metamorphism, and/or age of intrusive rocks, this study recognizes three general periods of deposition: (1) Mesoproterozoic; (2) Neoproterozoic to early Paleozoic; and (3) middle Paleozoic (Fig. 4–10). Most samples from the Blue Ridge occur in the Neoproterozoic to early Paleozoic depositional age range, while samples from the Inner Piedmont occur in the Mesoproterozoic, Neoproterozoic to early Paleozoic, and middle Paleozoic depositional ages.

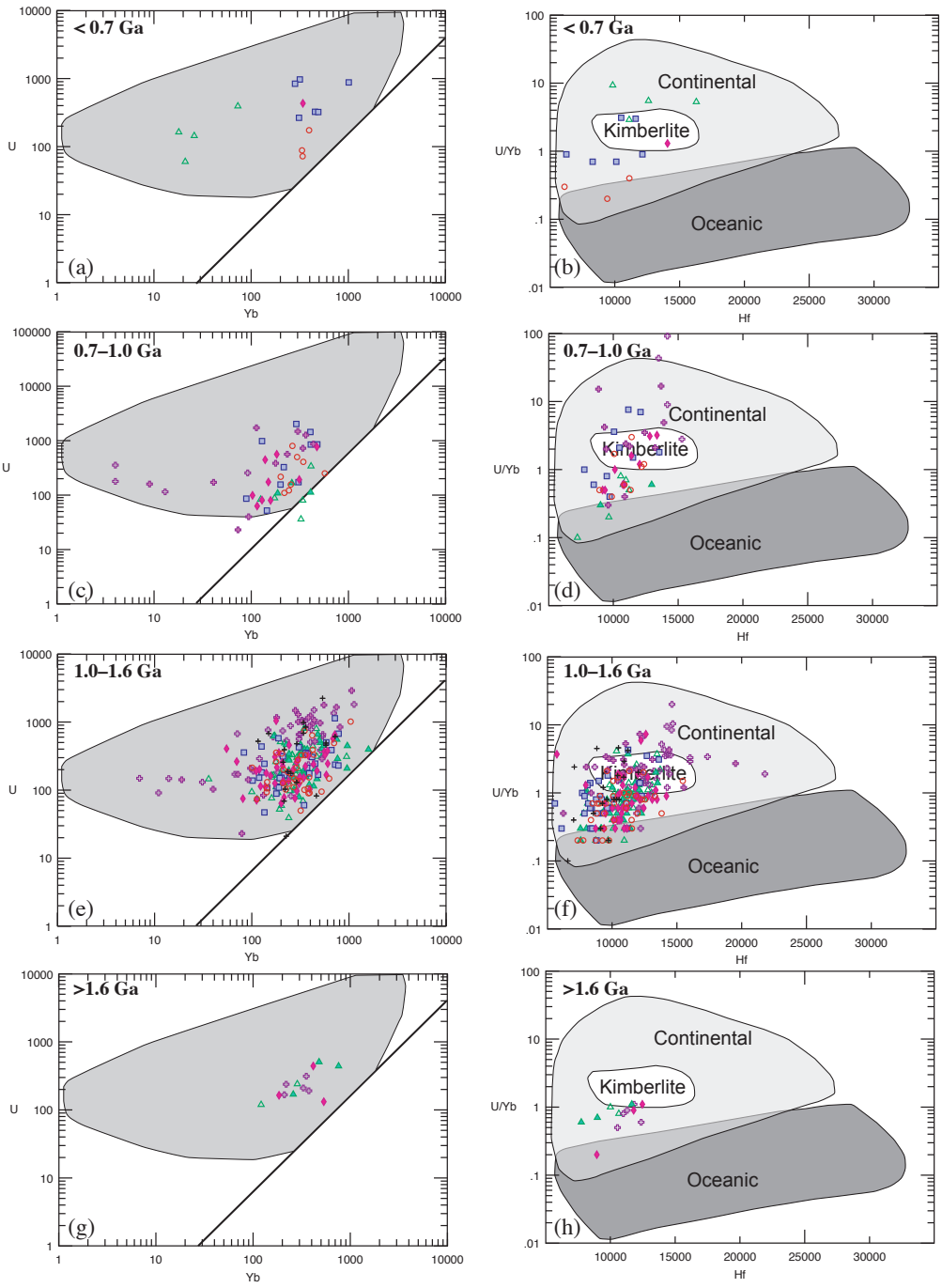

Figure 4–9. Discriminant plots based on Hf, U, and Yb concentrations in zircon (Grimes et al., 2007). Plots are separated according to U-Pb and Pb-Pb ages and symbols are the same as Fig. 8. (a, b) <700 Ma. (c, d) 0.7 Ga-1.0 Ga. (e, f) 1.0-1.6 Ga. (g, h) > 1.6 Ga.

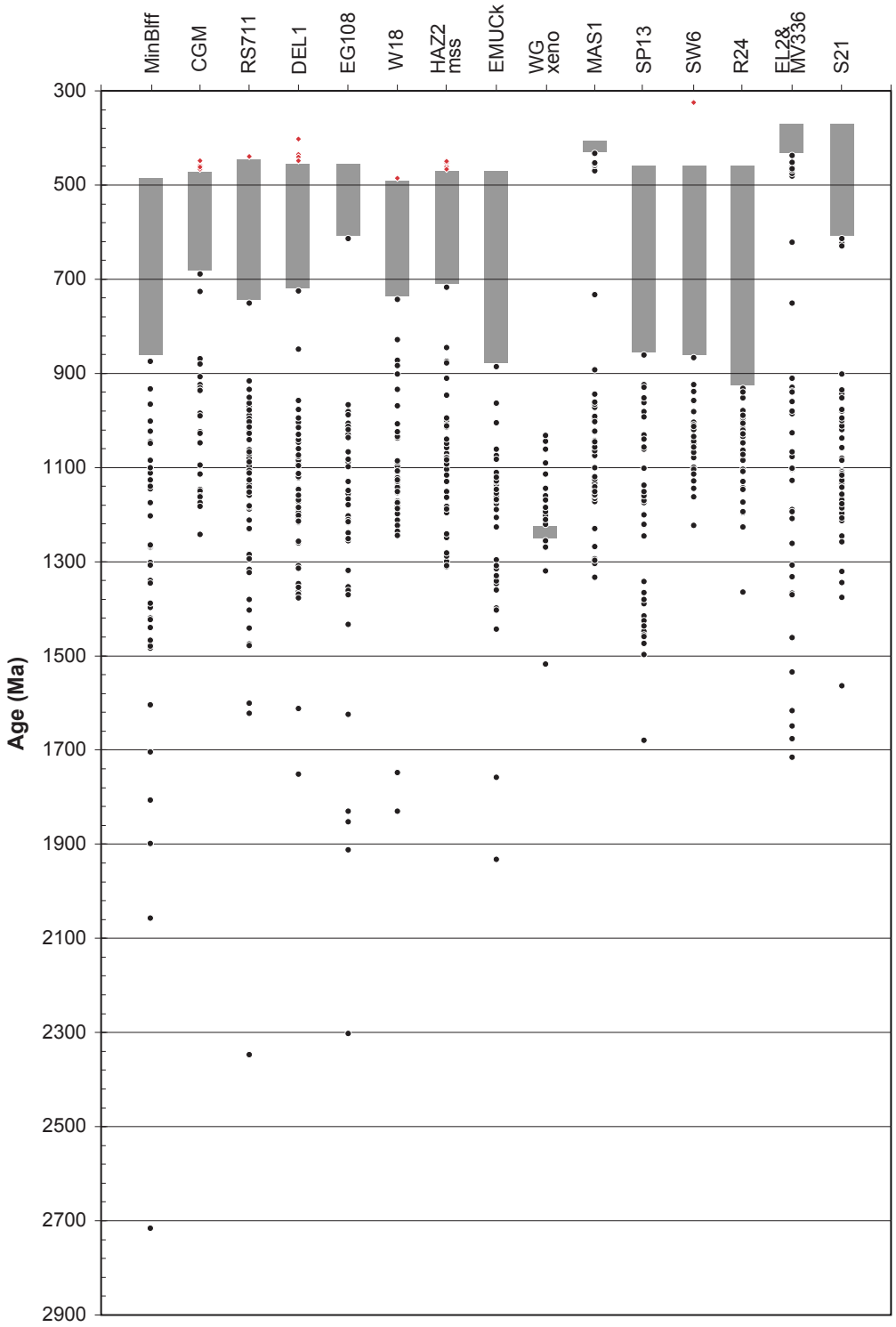

Figure 4–10. Depositional age based on reported U-Pb detrital (circles) and metamorphic zircons (diamonds). Gray boxes indicate possible range of depositional age.

The oldest and probably most poorly constrained group consists of samples containing only Mesoproterozoic or older ages. This group includes several samples from the Tugaloo terrane of the Blue Ridge (EMUC and WGxeno) and Inner Piedmont (R24, SP13, and SW6). The youngest detrital zircon ages from these samples are ~1000 Ma, and ages of intrusive rocks and metamorphism are 700 to 600 m.y. younger. It is possible that younger Neoproterozoic or Paleozoic zircons similar to those found in either groups 2 or 3 were not analyzed or were absent from the source area. Only sample WGxeno, a xenolith from the ~1.15 Ga Wiley Gneiss (Carrigan et al., 2003; Hatcher et al., 2004a), may actually represent Mesoproterozoic sedimentation. Age of deposition for the biotite schist xenolith protolith ranges between ~1.25 Ga and ~1.15 Ga, and loosely corresponds to the interval between the Elzevirian and Grenville orogenies. The other samples included in this group likely belong to a younger group.

Samples grouped in the Neoproterozoic to early Paleozoic contain 900, 800, 700, and 600 Ma detrital zircons. Most samples are from the central Blue Ridge (CGM, DEL1, EG108, HAZ2mss, W18) and generally contain 900, 800, and 700 Ma ages. Included in this group are the samples from the Ordovician(?) Mineral Bluff Formation, discussed above, and Middle Ordovician Sevier shale. Only sample S21, from the Georgia Inner Piedmont, contains ~600 Ma detrital zircons. Central Blue Ridge samples from the Cartoogechaye, Cowrock, and Dahlonega gold belt terranes are bracketed by 465–450 Ma ages of metamorphism (Miller et al., 1998; Moecher et al., 2004; Merschat et al., 2006, 2008a) and documented ages of Ordovician plutonism (Miller et al., 1998, 2000; Thomas, 2001; McDowell et al., 2002; Settles, 2002; Bream, 2003; Miller et al., 2006). Adequate geochronologic data do not exist to bracket the minimum age of S21 from the Georgia Inner Piedmont, but is likely middle Paleozoic based on correlations with ages of plutonism and metamorphism of the North and South Carolina Inner Piedmont (Hatcher and Merschat, 2006; Merschat et al., 2008a).

Only two samples, both from the Inner Piedmont, are considered to have a middle Paleozoic depositional age (Fig. 4–10). Both samples contain Paleozoic and Neoproterozoic zircons, but are different. Samples from the Cat Square terrane in the Brushy Mountains (EL2, MV336) contain several Paleozoic zircon ages between 470–430 Ma. These rocks were intruded by the 407 Ma megacrystic Walker Top Granite (Gatewood, 2007) and metamorphosed to sillimanite grade possibly as early as ~415 Ma (Gatewood, 2007). The youngest detrital zircon analyzed, ~438 Ma, limits deposition to 18–26 m.y. for the Silurian–Devonian Cat Square terrane (Gatewood, 2007, Fig. 4–10). Sample MAS1 from the southern end of the Smith River allochthon contains ~730 Ma

and ~460 Ma detrital zircons. Carter et al. (2006a) reported similar ~460 Ma ages from the northern part of the Smith River allochthon, but concluded these are metamorphic ages. REE trends and Th/U ratios common to magmatic zircon suggest the ~460 Ma are not metamorphic in origin. Instead, the age of the Bassett Formation of the Smith River allochthon is interpreted to be Ordovician to Silurian, bracketed by ~460 Ma detrital zircons and intrusion of the Martinsville Igneous Suite (444–433 Ma, Wilson, 2003; Carter et al., 2006a).

These groups refine previous interpretations of the depositional ages of the terranes based on field relationships and limited geochronology. The Neoproterozoic to Cambrian age suggested for most metasedimentary terranes was loosely demarcated, often bracketed by nonconformable relationships with internal basement massifs, the absence of the bimodal ~730 Ma Crossnore-Robertson River and Bakersville igneous suites, and early isotopic ages of plutons and metamorphism. Although the detrital zircon ages from many of the terranes verify these previous interpretations, the recognition of Siluro-Devonian metasediments of the Cat Square terrane has significantly changed previous interpretations. Regardless, the depositional periods defined by detrital zircon ages for the suspect terranes of the Blue Ridge and Inner Piedmont are close to recognized depositional periods for major sedimentary sequences in the Appalachian platform and rifted margin (Valley and Ridge and western Blue Ridge, respectively; Fig. 4–1).

The earliest Laurentian affinity depositional sequences are associated with the two-phase rifting of Rodinia, recorded in the easternmost thrust sheets of the Valley and Ridge and in the western Blue Ridge (Aleinikoff et al., 1995; Brewer and Thomas, 2000). Two phases of rifting are documented in the western Blue Ridge at 750–700 Ma and ~565 Ma corresponding to the opening of the Iapetus ocean (Aleinikoff et al., 1995; Brewer and Thomas, 2000). Detrital zircons suggest that, during this same time interval, the metasedimentary sequences of the Cartoogechaye, Cowrock, Dahlonega gold belt, and Tugaloo terranes were deposited. The oceanic setting proposed for most of these terranes (e.g., Hatcher, 1978; Hatcher et al., 2004a, 2007a) suggests that deposition was post ~565 Ma.

During the Middle Ordovician the Appalachian platform and rifted margin were drowned by the Sevier-Blountian clastic wedge of the Taconian orogeny (Shanmugam and Walker, 1983; Drake et al., 1989; Ettensohn, 2004; Hatcher, et al., 2004b). The Mineral Bluff Formation and rocks of the Smith River allochthon also represent clastic sedimentation during this time period. Although supported by fossil evidence, the

Ordovician(?) Mineral Bluff Formation corresponds to deposition of several kilometers of clastic turbidite sequences, and has been correlated with the Taconian Blountian clastic wedge in the foreland basin (e.g., Tull et al., 1993; Hatcher et al., 2004b). The Smith River allochthon also contains a significant sequence of interlayered clastic rocks (Henika and Conley, 1973; Henika et al., 1996), but its allochthonous nature has hindered interpretations. The Smith River allochthon is likely younger, 460–440 Ma, than the Mineral Bluff. It may represent a younger and more northerly successor basin or a late rift basin.

Silurian to Devonian sedimentation is not common in the southern Appalachian platform or margin, and adds to the unique nature of the Cat Square terrane. Late Silurian to Mississippian clastic sedimentary rocks exist in the Alabama Talladega belt, and have been correlated with Acadian clastic wedge (Tull et al., 1988; Tull, 2002). Bailey et al. (2008) also documented Late Silurian to Early Devonian deposition of the Arvonia Slate in the Chopawamsic terrane in northern Virginia. In the southern Appalachian platform, however, Silurian to Middle Devonian sedimentation is nearly absent, and often marked by an unconformity that removed much of the stratigraphic record until the Late Devonian (Hatcher et al., 2007a). Northward, Late Silurian to Early Devonian sedimentation becomes more prominent at the base of the Catskill delta/Acadian clastic wedge and turbidite sequences preserved in the Connecticut Valley–Merrimack trough in the New England internides (Ettensohn, 1985, 2004; Hatcher, 1989). The Cat Square terrane, however, was deposited during a ~26 m.y. interval between 433 and 407 Ma, and not on continental crust, so it cannot be a southern continuation of the Acadian clastic wedge, despite its similar age (Merschat and Hatcher, 2007).

PROVENANCE

Detrital zircon ages can be used to link metasedimentary terranes to possible source areas with rocks of similar ages. The SHRIMP U–Pb detrital zircons ages reported in this study have significant implications on the provenance of the different southern Appalachians terranes. Unfortunately, some of the detrital zircon ages do not imply a unique source. The multiple age populations recognized in the samples analyzed in this study require the presence of Paleoproterozoic to Neoproterozoic, and even Paleozoic rocks in the source areas. They are similar to those reported by other detrital zircon geochronologic studies from the crystalline core of the southern Appalachians (Fig. 4–11; Bream, 2003; Bream et al., 2004; Steltenpohl et al., 2004, 2008), and both agree and conflict with different paleogeographic and tectonic models for the Proterozoic

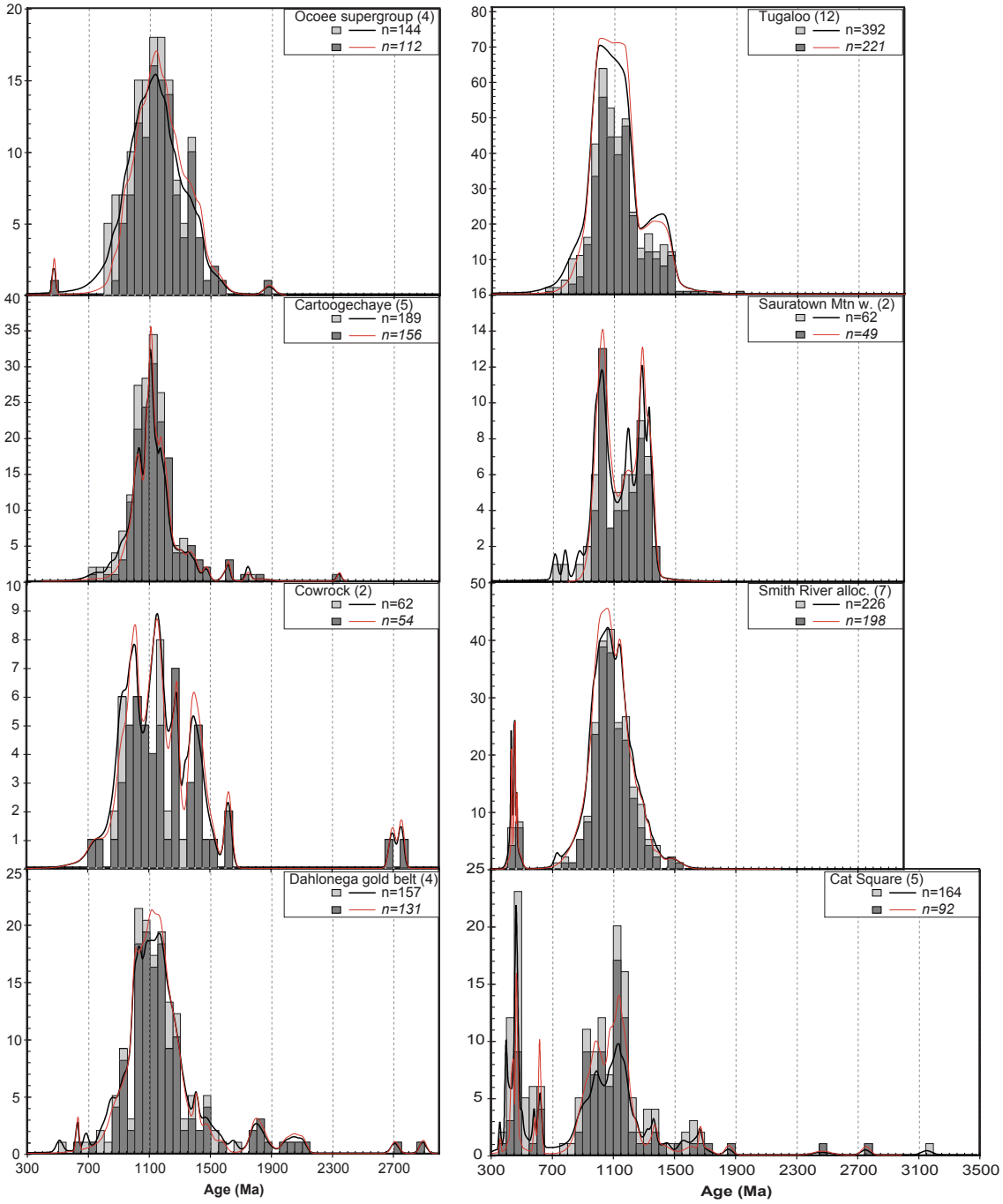

Figure 4–11. Relative probability plots with histograms of U-Pb ages of detrital zircons separated according to terrane. Data compiled from Miller et al. (1998), Bream et al. (2004), and Carter et al. (2006a). Number of samples included in each terrane is shown in parentheses. Plots were constructed using $^{206}Pb/^{207}Pb$ ages greater than 700 Ma, and $^{206}Pb/^{238}U$ ages when $^{206}Pb/^{207}Pb$ ages are less than 700 Ma. Thicker black line and light gray histograms represent all data, and red line and medium gray histograms represent data ±10 percent discordant.

to Paleozoic development of the Appalachians. Common to all samples is the dominance of 1.3–1.0 Ga Mesoproterozoic ages. This age range corresponds to the Grenville-Sunsás orogen, the formation of the Mesoproterozoic supercontinent Rodinia, and likewise constitutes significant portions of crust on several continents (Fig. 4–12; Dalziel, 1992, 1994; Unrug, 1997; Cordani and Teixeira, 2007; Li et al., 2008). A unique source is not implied by this age range; however, the less abundant ages outside of the 1.3–1.0 Ga range are more spatially limited and provide important bearings on provenance and tectonic reconstructions. Finally, the number and variation of grains analyzed per sample (25–60 grains) precludes that the detrital zircon populations are all inclusive. The presence of different ages is significant, but the absence of a certain age population does not entirely rule out its presence in a source area.

Provenance possibilities of the different samples analyzed will be discussed according to terrane and the groups based on depositional ages: Mesoproterozoic, Neoproterozoic to Cambrian, and middle Paleozoic. Emphasis will not be placed on the abundance of 1.3–1.0 Ga zircons, as this prominent age range occurs in all samples and implies a significant Grenville source existed for all samples. Instead, the combination of all ages will be used to interpret the most likely source areas, and whether they are exotic to Laurentia.

The oldest age group consists of three samples that contain only early Neoproterozoic and older ages. Two samples (SW6 and R24) from the Newton window in the Inner Piedmont contain an almost normally distributed set of ages between 1.3–1.0 Ga, with a single analysis at ~1.45 Ga from sample R24 that correlates with either the Laurentian granite-rhyolite or Amazonian Rondonian provinces ages. These two samples are combined with SP13 due to their close proximity and map relationship indicating they are from similar units (Goldsmith et al., 1988; Byars et al., 2008). The final sample, WGxeno, is a xenolith interpreted to represent the Mesoproterozoic or older crust that the ~1.15 Ga Wiley Gneiss intruded. Limited information is provided regarding possible Paleo- to Mesoproterozoic sedimentation in the southern Appalachians from the detrital zircons from the Wiley Gneiss xenolith. The depositional age of the xenolith corresponds to the interval between the Elzevirian and main Grenville orogeny. The abundance of ~1.1 Ga ages are interpreted as being metamorphic, related to the intrusion of the Wiley Gneiss. The few unaffected cores analyzed yielded ages of ~1.5 Ga and 1.3–1.2 Ga and Laurentian, granite-rhyolite and Grenville (Elzevirian) provinces or Amazonian sources are possible. Nd-depleted mantle model age of 1.5 Ga from the Wiley Gneiss is similar to the 1.7–1.5 Ga age range reported for most of the internal basement massifs of the

Figure 4–12. Possible source areas for the different southern Appalachian terranes. References for recognized age divisions of the different cratons are: Laurentian Midcontinent: Hoffman (1988), Whitmeyer and Karlstrom (2005, 2007), Thomas et al. (2004); southern Appalachians; Su et al. (1994), Aleinikoff et al. (1995), Carrigan et al. (2003), Bream, (2003), and Wilson (2003); Amazonia and Kalahari: Loewy et al., (2004), and Cordani and Teixeira (2007); and Carolina superterrane: Samson (1995), McSween and Harvey (1997), Hibbard et al. (2002), and Dennis et al. (2004).

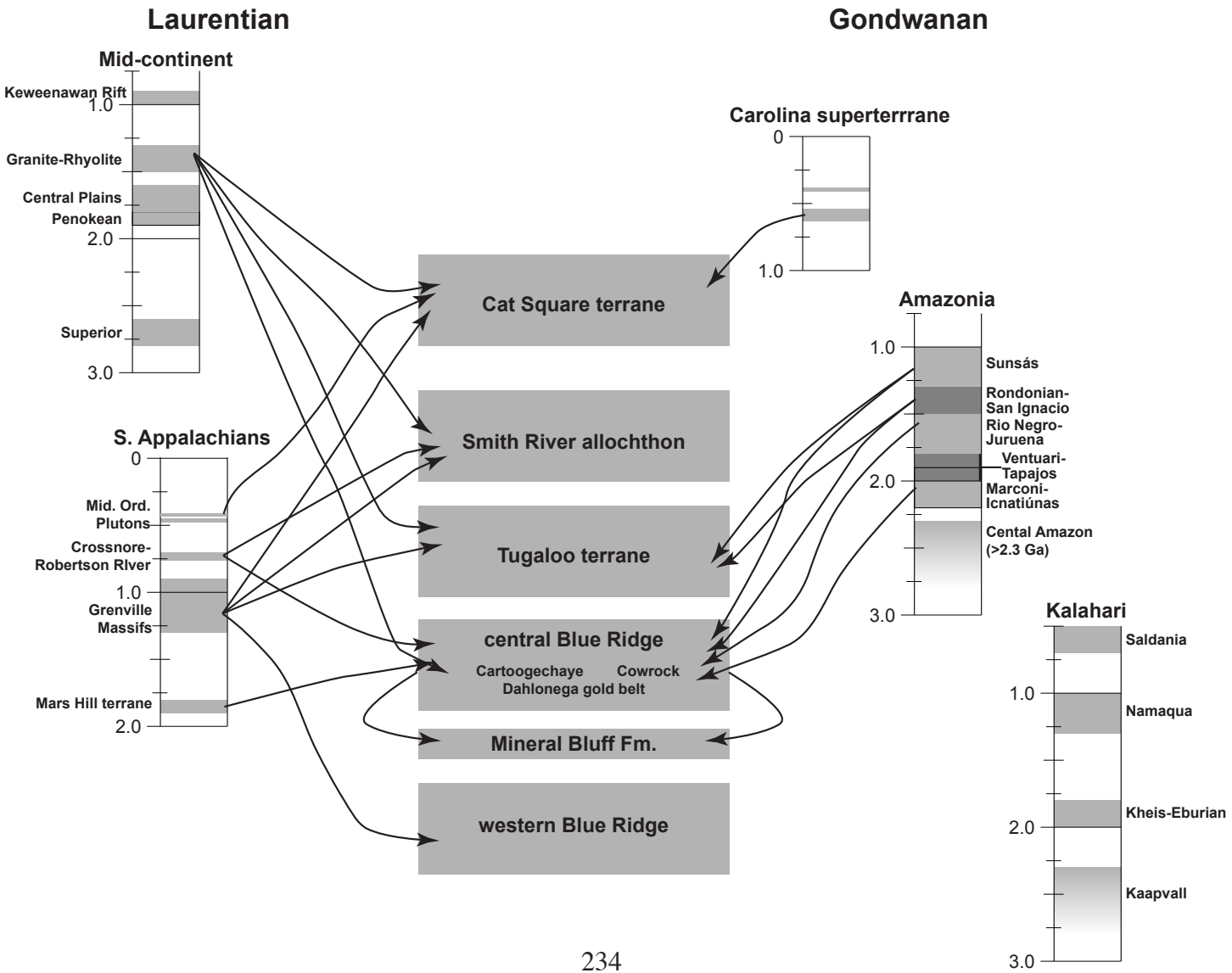
Laurentian
Gondwanan
Mid-continent
Keweenawan Rift
1.0
Granite-Rhyolite
Central Plains
Penokean
2.0
Superior
3.0
S. Appalachians
0
Mid. Ord.
Plutons
Crossnore-
Robertson RIver
1.0
Grenville
Massifs
Mars Hill terrane
2.0
Carolina superterrrane
0
1.0
Amazonia
1.0
Sunsás
Rondonian-
San Ignacio
Rio Negro-
Juruena
Ventuari-
Tapajos
2.0
Marconi-
Icnatiúnas
Cental Amazon
(>2.3 Ga)
3.0
Kalahari
Saldania
1.0
Namaqua
Kheis-Eburian
2.0
Kaapvall
3.0
Cat Square terrane
Smith River allochthon
Tugaloo terrane
central Blue Ridge
Cartoogechaye
Cowrock
Dahlonega gold belt
Mineral Bluff Fm.
western Blue Ridge

Georgia, North Carolina, and South Carolina Blue Ridge, implying they are exotic to Laurentia (Berquist, 2005; Berquist et al., 2005). Source of ~1.5 Ga zircon is likely the Rio Negro-Jurena province of the Amazonian craton and is expected based on similar Pb isotopic ratios of southern and central Appalachian basement and Sunsás basement of Amazonian (Loewy et al., 2003; Tohver et al., 2004; Fisher et al., 2006, in review; Cordani and Teixeira, 2007).

The second group contains the majority of the samples (seven), most of which are from central Blue Ridge terranes. In addition to the 1.3–0.9 Ga zircons, these samples also contain zircon with Paleoproterozoic and Mesoproterozoic ages of 2.3, 1.9–1.8, 1.7, 1.6, and 1.45–1.3 Ga, minor Archean ages, 2.7 Ga, and Neoproterozoic ages of 0.8–0.6 Ga. All samples do not contain the same zircon suites, and differences are interpreted to be related to variations in source material or unrecognized age populations.

Archean and Paleoproterozoic ages are difficult to explain, and generally require a far-traveled sediment from mid-continent regions of either Laurentia or Amazonia. The single Archean zircon age could be sourced from either the Superior province or the Amazonian or Rio de la Plata cratons in South America. Paleoproterozoic zircons present possible links to the Laurentian mid-continent or Amazonia; however, the more common occurrence of Paleoproterozoic orogens (2.2–1.9 Ga Marconi-Icantiúnas; 2.0–1.8 Ga Venruari-Tapajos; and 1.8–1.5 Ga Rio Negro-Juruena; Loewy et al., 2004; Cordani and Teixeira, 2007) favors an Amazonian source. No Laurentian Paleoproterozoic source exists for 2.3–2.0 Ga zircons that occur in several samples from central Blue Ridge terranes. The 1.9–1.8 Ga Penokean and 1.8–1.6 Ga Yavapai-Mazatal provinces are possible Laurentian mid-continent sources. Mesoproterozoic ages of 1.45–1.3 Ga occur in samples SEV, MinBlff, DEL1, EG108, RS711, HAZ2mss, EMUC and S21, and are almost as abundant as 1.3–0.9 Ga zircons. These ages are common to both the Laurentian granite-rhyolite province and Amazonian Rondonian and Sunsás provinces.

Neoproterozoic to early Cambrian ages between 750 and 530 Ma are good indicators of exotic versus Laurentian sources. 600 to 530 Ma rocks are typical of peri-Gondwanan terranes like Carolina and Avalon (e.g., Samson, 1995; Hibbard et al., 2002; Eriksson et al., 2004), and are generally absent from Laurentia. Anorogenic magmatism associated with Crossnore and Robertson River Igneous suites intruded Mesoproterozoic rocks of the western Blue Ridge of northwestern North Carolina and Virginia, and yield U–Pb ages of 750–700 Ma (Su et al., 1994; Tollo and Aleinikoff, 1996). The presence of 750–700 Ma detrital zircons likely indicates a Laurentian Blue Ridge source. Samples containing 750–700 Ma detrital zircons include CGM (Cowrock terrane), DEL1, W18,

RS711 (Cartoogechaye terrane), and HAZ2mss (Dahlonega gold belt). Samples S21 and EG108 contain 600 Ma zircons; however, the latter may represent beam overlap of a core and Paleozoic rim.

Defining a unique provenance for the terranes and samples included in group 2 (Neoproterozoic to early Paleozoic) is difficult. Based on the detrital zircon age populations, a Laurentian and/or Amazonian provenance is possible for most terranes, and a mixed source is most likely. The most abundant ages of 1.3–0.9 Ga and 1.5–1.3 Ga are consistent either a Laurentian (Grenville and granite-rhyolite) or Amazonian (Grenville-Sunsás and Rondonian) source. Whole-rock Pb isotopic data from the metasedimentary terranes of the Blue Ridge and Inner Piedmont are compatible with an Amazonian source (Bream et al., 2008). Paleoproterozoic ages may represent Laurentian mid-continent terranes or Amazonian provinces (Marconi-Icantiúnas; 2.0–1.8 Ga Venruari-Tapajos; and 1.8–1.5 Ga Rio Negro-Juruena). Minor populations of 750–700 Ma detrital zircons suggest a distinct Laurentian source, while 2.3-2.0 Ga imply an Amazonian source. The detrital zircon populations from the Cartoogechaye, Cowrock, Dahlonega gold belt, and Tugaloo terranes cannot be explained by an entirely Laurentian or Amazonian source, and a mixed source is likely and should be expected during rifting.

Despite the ambiguity of the detrital zircon age populations in the Cartoogechaye, Cowrock, Dahlonega gold belt, and Tugaloo terranes and the likelihood of a mixed source resulting from sediment being shed both the Laurentian and Amazonian sides of the opening Iapetus ocean; a strong argument can be made for a largely Laurentian–derived provenance based on the Neoproterozoic geometry of the rifted margin, and the possibility of other Amazonian terranes in the subsurface beneath the Blue Ridge–Piedmont megathrust sheet. Various seismic reflection surveys across the Laurentian Platform (Valley and Ridge) and into the Blue Ridge have documented a gentle southeast-dipping contact between the basement and Lower Cambrian Rome Formation and steep east dipping normal faults (e.g., Harris et al., 1981; Costain et al., 1989; Hatcher et al., 2007b). The gentle southeast–dipping surface suggests no topographic barrier would have separated mid-continent sediment from being transported southeastward to the Iapetan rifted margin. Recent isotopic connections between Appalachian basement units and Amazonian crust (e.g., Loewy et al., 2003; Tohver et al., 2004; Fisher et al., 2006) requires that the post-Rodinian Laurentian margin include a sutured Amazonian belt and that rifting of the Rodinian supercontinent here was almost entirely within the Amazonian crust. Considering the presence of the ~1.8 Ga Mars Hill terrane in the western Blue Ridge and that rifting was entirely within the Amazonian, it is reasonable to suggest that

additional older Amazonian provinces may still exist in the subsurface beneath the Blue Ridge–Piedmont megathrust sheet. The Neoproterozoic to early Cambrian Iapetan rift basins in the southern Appalachians were underlain by Amazonian material; therefore, minor Paleoproterozoic populations in these samples are interpreted here to represent eroded Amazonian material originating from the Laurentian side of the margin rather than from across the growing ocean basin between Laurentia and Amazonia. A definitive answer, if possible, of relative contributions of the Laurentian mid-continent verses Amazonian provenance of 1.5–0.9 Ga may reached by combining U–Pb ages with Hf–Lu ages of zircon.

Other than the Paleozoic ages, the youngest sample group (EL2, MV366, and MAS1) contains a similar detrital zircon age spectrum as observed from the older samples. Both samples contain abundant ages at 1.3–0.9 Ga followed by less abundant ages at 1.4–1.3 Ga, interpreted to represent Laurentian Grenville and granite-rhyolite, or Amazonian Rondonian provinces, respectively. Cat Square terrane sample, EL2, also contains some Paleoproterozoic ages 1.75–1.6 Ga (peak at ~1.7 Ga). Similar to central Blue Ridge and Tugaloo terranes, these ages can represent either a Laurentian, (1.8–1.6 Ga Yavapai and Mazatal provinces), or Gondwanan (1.8–1.5 Ga Amazonian Rio Negro-Jurena province) source. By the Silurian a significant Paleozoic platform covered most of the Laurentian Proterozoic terranes, and paleogeographic studies suggest Gondwanan cratons of Amazonia or Kalahari were not close to Laurentia at this time (Unrug, 1997). Alternative sources of Paleoproterozoic and Mesoproterozoic zircons are the Laurentian mid-continent (2.8–2.6 Ga Superior; 1.9–1.8 Ga Penokean; and 1.5–1.3 Ga granite-rhyolite) or recycling of sediment from already accreted Blue Ridge and Inner Piedmont terranes. No Paleoproterozoic zircons were observed from the Smith River allochthon by Carter et al. (2006a). Slight variations in the Neoproterozoic ages are interpreted to represent Laurentia versus exotic peri-Gondwanan sources. A ~730 Ma zircon from the Smith River allochthon is interpreted as originating from the Crossnore-Robertson River Igneous suite in the Blue Ridge. The ~630 Ma zircon from the Cat Square terrane suggests input from the Carolina or Avalonia superterranes. Although some ~630 Ma sources exist in the Carolina superterrane, they are more common in the Avalon terrane to the north (Samson, 1995; Dennis et al., 2004). Finally, the source for the Ordovician to Silurian ages is the Tugaloo terrane, which contains several Ordovician plutons in the Inner Piedmont of North Carolina (Bream, 2003) and Virginia Piedmont (Wilson, 2003; Sinha et al., in prep.). Several ~430 Ma zircons were present in EL2 and MV366, an age not common to the eastern Tugaloo terrane of the Inner Piedmont in North Carolina and

southward. Late Ordovician to Silurian ages are common in the Tugaloo terrane in the central Appalachians (Wilson, 2001; Sinha et al., in prep.) Both ~630 Ma and ~430 Ma zircons in Cat Square samples (EL2, MV336, and S21) support a more northerly source from the central Appalachians for the northern part of the Cat Square terrane.

PALEOGEOGRAPHY AND TECTONIC MODELS

This data set provides additional implications for tectonic development of the southern Appalachian and paleogeographic reconstructions. Important results include recognition of four different source areas (Fig. 4–12), including possible separation of a central and southern Appalachians source, and separation of different temporal depositional sequences within the crystalline core (Fig. 4–10). These tectonic and paleogeographic constraints are discussed in regard to their broad depositional period and the tectonic evolution of the Appalachians from the Mesoproterozoic supercontinent Rodinia to the Paleozoic Pangea.

Paleoproterozoic to Mesoproterozoic

Detrital zircons from a xenolith in ~1.15 Ga Wiley Gneiss yield a few cores of ~1.5 Ga and 1.3-1.2 Ga. These ages suggest a period of deposition between the Elzevirian and main Grenville orogenies and support other isotopic studies that suggest the southern and central Appalachian Mesoproterozoic basement is Gondwanan (Loewy et al., 2003, 2004; Berquist et al., 2005; Fisher et al., 2006, in review). The presence of ~1.5 Ga zircons suggests a possible Amazonian source, while 1.3-1.2 Ga zircons may have been derived locally. Most of the detrital zircons from the xenolith were reset during intrusion of the magma, and only limited information is preserved.

Neoproterozoic to Early Paleozoic

Tectonic activity during the Neoproterozoic to early Paleozoic consists of a failed rifting event at ~735 Ma followed by successful rifting and opening of the Iapetus ocean at ~565 Ma (Aleinikoff et al., 1995; Brewer and Thomas, 2000). Opening of the Iapetus oceans marks the separation of Laurentia from conjugate Gondwanan cratons including Amazonia; however, a significant portion of Amazonia crust remained behind in Laurentia (Sinha et al., 1996; Loewy et al., 2003; Tohver et al., 2004; Fisher et al., 2006, in review). Most samples from Blue Ridge and Inner Piedmont terranes overlap this period of deposition and have both a Laurentian and Amazonian signature. Limits

on depositional age range from ~700 Ma to ~480 Ma, and the occurrence of mafic and ultramafic bodies throughout these terranes indicate they were deposited on oceanic crust. The age of these units may be further refined to post-Iapetan opening at ~565 Ma and pre-Taconian deformation and magmatism starting in the Early Ordovician, ~480 Ma.

Provenance of the terranes is largely Laurentian, indicated by the combination of 1.4–1.3 Ga, 1.3–0.9 Ga, and 0.73 Ga zircon ages (Figs. 4–11 and 4–12). Minor occurrences of 2.3–1.6 Ga zircons are difficult to explain with a solely Laurentian provenance. Steltenpohl et al. (2004) suggested that 2.4–2.3 Ga zircons from the Hollis Quartzite from one sample in the Pine Mountain window support a Gondwanan provenance. Identical Pb isotopic signatures from Mesoproterozoic (1.3–0.9 Ga) rocks in the central and southern Appalachians and Amazonia suggest part of the 1.3–0.9 Ga Amazonian craton was transferred to Laurentia (Loewy et al., 2004). Oceanic affinity metasedimentary terranes of the central Blue Ridge, Cartoogechaye, and Cowrock rock terranes would have been more proximal to the interior of Amazonia than Laurentia. Therefore, the early rifting stages and opening of the Iapetus ocean likely provided an opportunity for Gondwanan sediment to be shed into the central and eastern Blue Ridge terranes.

The Tugaloo terrane generally displays a bimodal population dominated by 1.3–0.9 Ga and lesser 1.5–1.3 Ga zircons (Bream, 2003; Bream et al., 2004), and lacks many of the Paleoproterozoic and Neoproterozoic ages observed in central Blue Ridge terranes (Figs. 4–11 and 4–12). The relatively restricted provenance of the Tugaloo terrane contrasts with the common Paleoproterozoic, Neoproterozoic, and rare Archean ages observed in the central Blue Ridge terranes (Fig. 4–11). The lack of these ages makes unique correlation to either the Laurentian or Amazonian cratons difficult, although the significant population of 1.5–1.3 Ga zircons suggests a Laurentian granite-rhyolite source. The more outboard location of the Tugaloo terrane may have affected the detrital zircon provenance, and only zircons from the most abundant source area reached the terrane.

Middle Paleozoic

Middle Ordovician sedimentation is widely documented in the Appalachian foreland (e.g., Colton, 1970; Drake et al., 1989). In the southern Appalachian foreland, the Sevier basin developed above the Middle Ordovician Knox unconformity in response to tectonic activity in the hinterland terminating the stable carbonate platform. Detrital zircons from the Sevier Shale (~1.8 and 1.5–1.0 Ga) are similar to other foreland basin

studies in the central and northern Appalachians (Gray and Zeitler, 1997; Cawood and Nemchin, 2001; McLennan et al., 2001; Eriksson et al., 2004). It has been suggested that the near absence of a Paleozoic detrital zircons suggests that the now-eroded equivalent of the western Blue Ridge served as a sedimentary barrier between the accreting Taconic arc and the foreland throughout most of the Appalachians (Eriksson et al., 2004; Thomas et al., 2004). Based of the similar detrital zircon populations, we suggest that central Blue Ridge terranes are a possible source for the Sevier Shale.

The Ordovician(?) Mineral Bluff Formation contains an interesting spectrum of Paleoproterozoic ages that overlap with the combined Paleoproterozoic ages observed in the central Blue Ridge terranes. This spectrum is identical to that reported for the Sevier Shale and Dahlonega gold belt (Bream, 2003; Bream et al., 2004), and could be correlative with the Mineral Bluff Formation based on similar stratigraphic ages and detrital zircon suites. Some studies have suggested that sedimentation in the Dahlonega gold belt was simultaneous with Ordovician volcanism (Settles, 2002); however, other studies correlated Dahlonega gold belt rocks with the Great Smoky Group (Hadley, 1970; Hadley and Nelson, 1971; Nelson, 1991; Hatcher et al., 2007a). Correlation of the Mineral Bluff Formation with Sevier Shale and other parts of the Sevier–Blountian clastic wedge is favored based on stratigraphic position, and detrital zircon suite. The Mineral Bluff Formation may represent turbidites shed into an Ordovician successor basin (Fritz et al., 1985; Fritz and La Tour, 1988; Tull et al., 1993; Groszos and Tull, 2007). Although collisions with peri-Gondwanan terranes have been proposed to explain the Taconic orogeny in the southern Appalachians (Hibbard, 2000; Hibbard et al., 2002), they are not conclusive. Instead, the Paleoproterozoic and rare Archean ages from the Mineral Bluff may have been sourced from the accreting central Blue Ridge terranes (Cartoogechaye, Cowrock, and Tugaloo terranes). Additionally, whole-rock geochemistry of the Mineral Bluff Formation suggests a non-continental source, possibly of basaltic and andesitic composition (Fig. 4–5; Fritz and La Tour, 1987, 1988). No detrital Paleozoic zircons make a strictly volcanogenic source, as suggested by Fritz and La Tour (1987, 1988), unlikely. Instead, the common mafic and ultramafic rocks of the Cartoogechaye, Cowrock, and Tugaloo terranes represent an alternative low-potassium source for the Mineral Bluff Formation. The Cowrock and Cartoogechaye terranes, however, were metamorphosed at upper amphibolite to granulite facies at ~460 Ma (Moecher et al., 2004). This makes a direct link to the terranes difficult, but the data suggest that significant portions of the terranes were exposed at the surface during the Ordovician and provided sediment to the Mineral Bluff Formation. During the Early

Ordovician, the Cartoogechaye and Cowrock terranes were accreted, and exposed portions, including various mafic and ultramafic complexes, were eroded and recycled into the brief Ordovician foreland basin where the Mineral Bluff was deposited. As the Taconic orogeny progressed, the Mineral Bluff Formation was eventually buried and metamorphosed to chlorite and staurolite grade.

The sample from the southern end of the Smith River allochthon (MAS1) may present more complications than possible solutions to Appalachian tectonics. Carter et al. (2006a) dismissed Ordovician ages from one sample from the northern part of the Smith River allochthon as having a metamorphic origin. CL images (Fig. 4–3) and Th/U ratios greater than 0.2 (see Appendix IV) are consistent with our interpretation that the ~460 Ma ages are not metamorphic and should be treated as detrital. Based on the dominance of 1.3–1.0 and 1.4–1.3 Ga zircons, Carter et al. (2006a) suggested a Laurentian source for the terrane, which the ages reported herein also support. The presence of both ~730 Ma and ~460 Ma zircons implies different Laurentian sources. The source of the ~730 Ma zircons is likely the Crossnore and Robertson River igneous suites in the western Blue Ridge, while Ordovician ages likely originate from plutons in the Tugaloo terrane to the east. This suggests that the Smith River allochthon may have represented a basin between the western Blue Ridge and Tugaloo terrane during the Late Ordovician to Early Silurian. Mafic rocks from the Smith River allochthon do share geochemical characteristics with continental rift basalts (Carter et al., 2006b). These suggest that the Smith River allochthon represented a post-Taconian orogeny, Late Ordovician to Early Silurian intracontinental rift basin between the western Blue Ridge and Tugaloo terrane. This basin was subsequently modified and tectonically inverted during the Neoacadian and/or early Alleghanian to rest above the Tugaloo and western Blue Ridge terranes. Although we favor this interpretation, alternative scenarios to explain the Paleozoic detrital zircons include: (1) metamorphic genesis as suggested by Carter et al. (2006a); (2) piggyback basin; and (3) rocks in the southern tip of the Smith River allochthon belong to different terranes and an unrecognized fault exists separating these rocks from older rocks to the north.

Silurian to Devonian

Recent detrital zircon geochronologic studies have documented the existence of Siluro-Devonian metasedimentary rocks in Cat Square terrane in the eastern Inner Piedmont (Bream et al., 2001, 2004; Bream, 2002, 2003). This Siluro-Devonian age establishes that some Inner Piedmont rocks are younger than previously thought, and

thus have significant tectonic implications. Several studies have presented possible tectonic models incorporating the age and provenance of the Cat Square terrane with field relationships, geochronological studies, kinematics, and foreland basin stratigraphy (Bream, 2002; Hatcher, 2002; Merschat and Hatcher, 2004, 2006; Hatcher and Merschat, 2006, Merschat and Hatcher, 2007). Three samples from this study contain 600 and 500 Ma detrital zircons, and of the samples two also contain Paleozoic detrital zircons. These samples corroborate previous studies and contribute additional information regarding Paleozoic sedimentation, paleogeography, and tectonics recorded in the crystalline core of the southern Appalachians.

Recognition of three additional samples with detrital zircon suites similar to the Cat Square terrane further confirms the extent of the terrane, expands its southern limit, and confirms the middle Paleozoic arrival of the Carolina superterrane. The Brushy Mountains samples further confirm the existence of the Cat Square terrane in the northernmost end of Inner Piedmont. The sample from the Georgia Inner Piedmont suggests the Cat Square terrane extends further south than was previously thought. In light of data from these and previous Cat Square terrane samples, the provenance and paleogeographic location of the terrane is further delimited. Previous studies have generally suggested that the 600–500 Ma and possibly some ~430 Ma zircons were sourced from the peri-Gondwanan Carolina superterrane, and the 1.3–0.9 Ga, 1.4–1.3 Ga, and ~460 Ma zircons are from Laurentia (Fig. 4–12; Bream et al., 2001; Bream, 2002, 2003; Hatcher, 2002; Bream et al., 2004; Merschat and Hatcher, 2007). Peri-Gondwanan, 600–500 Ma, detrital zircons from the Cat Square terrane represent the earliest possible Paleozoic connection of the Carolina superterrane with the southern Appalachians. Detrital zircons separated from the clastic wedges of the Appalachian platform do not contain possible peri-Gondwanan detrital zircons until the Devonian or later (Eriksson et al., 2004; Thomas et al., 2004; Park et al., 2008). The structure and tectonics of the Inner Piedmont provide further insight into the nature of the accretion of the Carolina superterrane. The Inner Piedmont is dominated by compressional and transpressional structures formed at amphibolite facies conditions (Davis, 1993; Merschat et al., 2005a; Hatcher and Merschat, 2006), and detailed geologic mapping indicates the contact between the Cat Square and Tugaloo terranes is an amphibolite-facies fault (Giorgis, 1999; Merschat, 2003; Merschat et al., 2005a; Wilson, 2006; Gatewood, 2007; Merschat et al., 2008b). The presence of various mafic and ultramafic bodies in the Cat Square terrane has been used to suggest deposition on oceanic crust (Merschat and Hatcher, 2007; Hatcher et al., 2007a; Merschat et al., 2008b). The paleogeographic

location of the Cat Square basin has been suggested to be in the Pennsylvania embayment from kinematic estimates of SW-directed displacement associated with the Neoacadian Brevard fault zone (Merschat and Hatcher, 2006, 2007). These kinematic estimates are further supported by the more northerly source of ~630 and ~430 Ma zircons from the Avalon and Tugaloo terranes of the central Appalachians. Several ~430 Ma granitic plutons occur in the Tugaloo terrane of the central Appalachians extending as far south as the North Carolina-Virginia border in the Smith River allochthon (Wilson, 2001; Sinha et al., in prep.). Although some ~630 Ma plutons occur in the Carolina superterrane, magmatism of this age is more common to the Avalon terrane (Samson, 1995; Dennis et al., 2004). These ages support a more northerly paleogeographic position of the Cat Square remnant ocean basin. The Carolina superterrane initially collided near the New York promontory and progressively closed the Cat Square basin from north to south. The Carolina superterrane overthrust the Cat Square and Tugaloo terranes, and buried the terranes to midcrustal levels resulting in anatectic melting by ~407 Ma (Merschat and Hatcher, 2007).

Summary

Detrital zircons from the southern Appalachian crystalline core provide significant insight into the sedimentation, paleogeographic, and tectonic history of the southern Appalachian crystalline core. A Laurentian provenance is interpreted for the combination of 1.45–1.3 Ga, 1.3–0.9 Ga, and 750–700 Ma zircons, and their occurrence in most samples from the Blue Ridge and Inner Piedmont suggests a significant Laurentian component. Occurrences of specific Paleoproterozoic (2.4–1.8 Ga) and Neoproterozoic ages (600–500 Ma) are interpreted to indicate the presence of exotic Amazonian and peri-Gondwanan sources during two separate events during the evolution of the southern Appalachians. These events include the rifting of Rodinia, separating Laurentia from various Gondwanan cratons, and the Paleozoic accretion of peri-Gondwanan terranes. The minor exotic Paleoproterozoic populations do not provide significant resolution of the exact location of the Amazonia, and Kalahari cratons with Laurentia. Paleogeographic reconstructions with Amazonia adjacent to Labrador (Dalziel, 1992, 1994) or the Llano uplift (Tohver et al., 2002) are not favored. Instead, Amazonia positioned adjacent to the central and southern Appalachians as proposed by Loewy et al. (2003) and Tohver et al. (2004) provides a likely source of Paleoproterozoic zircons and, therefore, is favored. Peri-Gondwanan zircons, 600–500 Ma, combined with Ordovician zircons from Cat Square terrane samples in the Inner Piedmont, support a Devonian-

Mississippian collision of the Carolina superterrane with Laurentia. Provenance of ~433 Ma detrital zircons from the central Appalachians support kinematic estimates of a paleogeographic location of the Cat Square terrane in the Pennsylvania embayment during the Silurian to Devonian. Collision initiated near the New York promontory and progressed southward, resulting in southwest migration of the clastic wedge and southwest transport of the Cat Square terrane and Inner Piedmont.

Interesting questions remain regarding why the 1.3–0.9 Ga Grenville orogeny remains the most abundant population in almost all samples analyzed. Is it the result of limited provenance, sedimentary or magmatic processes, or a complex combination of all three (Moecher and Samson, 2006)? Grenville rocks were likely exposed during the rifting at ~735 Ma and ~565 Ma, and during the Taconian orogeny. Bream et al. (2004) documented that ε_{Nd} values of metasedimentary terranes of the southern Appalachians are nearly identical to Grenville basement. Eriksson et al. (2004) and Thomas et al. (2004) documented sedimentary recycling in unmetamorphosed rocks of the central Appalachian foreland basin using ε_{Nd} and U–Pb detrital zircon analyses. This study further documents the importance sedimentary recycling of crust during the middle Paleozoic orogenies resulting in the growth of the southern Appalachian orogen. Dominance of Grenville (1.3–0.9 Ga) and Granite-Rhyolite (1.45–1.3 Ga) ages in several terranes suggests these were major crust-forming events that were eroded and recycled into younger parts of the orogen. Younger crust forming events at 750–700 Ma and Ordovician magmatism (480–460 Ma) contribute minor populations, but never reach proportions of the Grenville ages. The amount of intra-terrane recycling is difficult to quantify, as well as how this would affect the observed zircon population. The Mineral Bluff Formation and Cat Square terrane are two examples. Recycling of sediment from accreted central Blue Ridge terranes explains occurrence of Paleoproterozoic and Archean ages from the Mineral Bluff Formation. Similarly, Mesoproterozoic ages observed in the Cat Square terrane are interpreted to be sourced from the Tugaloo terrane, the likely source of Ordovician ages.

CONCLUSIONS

1. Mesoproterozoic zircons are the most abundant in these samples. Abundance of 1.3 to 0.9 Ga zircons in all samples from the Blue Ridge and Inner Piedmont (except the Mesoproterozoic xenolith) indicate Grenville crust remained a prominent source for all southern Appalachian terranes. Detrital zircons cannot address possible sedimentary recycling of crust. Zircons of 1.45–1.3 Ga define

the second-largest population in several samples, and were likely sourced from the Laurentian granite-rhyolite province.

2. Paleoproterozoic ages occurred in several samples, but were often represented by only a few analyses per sample. Zircon ages include ~2.3, ~2.0, ~1.9, ~1.8, ~1.7, and ~1.6 Ga and occurred in several central Blue Ridge and Cat Square terrane samples. The sample from the Mineral Bluff Formation contained all of these Paleoproterozoic ages, and the only Archean zircon (2.7 Ga) analyzed in this study.

3. Neoproterozoic ages occur in several samples and, in addition to the ~0.9 Ga zircons, include ~0.7 and ~0.6 Ga. Most samples from the central Blue Ridge and the sample from the Smith River allochthon contain ~0.73 Ga zircons. Two samples from the Cat Square terrane in the Inner Piedmont contain ~0.6 Ga zircons.

4. Paleozoic (late Ordovician to Silurian) zircons were determined in a sample from the Cat Square terrane (~480, ~460, and ~433 Ma) and the Smith River allochthon (~460 Ma).

5. Depositional ages interpreted from detrital zircons support three periods of sedimentation in the southern Appalachian crystalline core: (1) early Mesoproterozoic; (2) Neoproterozoic to early Paleozoic; and (3) Paleozoic. Evidence of early Mesoproterozoic sedimentation is preserved only as garnet biotite schist xenolith in the ~1.15 Ga Wiley gneiss. Central Blue Ridge terranes and the Tugaloo terrane (eastern Blue Ridge and western Inner Piedmont) were deposited during the Neoproterozoic (0.73 Ga) to early Paleozoic (480 Ma). Paleozoic sequences include those of the Smith River allochthon and the Cat Square terrane, and the Mineral Bluff Formation of the western Blue Ridge.

6. The Cartoogechaye and Cowrock terranes contain Paleoproterozoic zircons possibly derived from a Gondwanan likely Amazonian source, but the occurrence of 1.4–1.3, and 0.73 Ga zircons implies a Laurentia source likely derived from Granite-Rhyolite, Grenville, and Mesoproterozoic and Neoproterozoic igneous rocks of the western Blue Ridge. Amazonian zircons (2.3, 1.9–1.75, and 1.6 Ga)

were contributed during the early stages of rifting and opening of the Iapetus ocean.

7. The Ordovician (?) Mineral Bluff Formation contains the most complete Paleoproterozoic suite of zircons and is the result of sediment recycled from the accreted and uplifted central Blue Ridge terranes.

8. Inner Piedmont samples, and the unique signature of the Cat Square terrane, help delimit terrane boundaries and configurations. The lack of Paleozoic and 600–500 Ma zircons in Newton antiform samples suggest the structure is a window through the Cat Square terrane, exposing the Tugaloo terrane. A sample from the Georgia Inner Piedmont with 0.6 Ga zircons suggests the mixed affinity; Siluro-Devonian Cat Square terrane may extend further south than previously thought.

9. Cat Square terrane provenance requires recycling of Mesoproterozoic rocks from Laurentia and the addition of a peri-Gondwanan source. Plutons in the Tugaloo terrane equivalents in the central Appalachians (Chopawamsic and Potomac terranes) provided the most likely source of ~430 Ma zircons, and support a paleogeographic location of the Cat Square remnant ocean basin in the Pennsylvania embayment.

10. Occurrence of 600–500 Ma peri-Gondwanan zircons in the Siluro-Devonian rocks of the Cat Square terrane, the compressional and transpressional structures of the Inner Piedmont, and timing of metamorphism in the Inner Piedmont support a Devonian to Mississippian accretion of the Carolina superterrane.

ACKNOWLEDGMENTS

Chris Fisher is greatly appreciated for his unselfish assistance during two, week-long zircon separation marathons at Vanderbilt University during 2005. Mary Varnell is also gratefully acknowledged for help during zircon separation sessions in 2007. Frank Mazdab provided assistance with final sample preparation (mounting and polishing) and operating the instruments at SUMAC. Research was funded by the University of Tennessee Science Alliance Center for Excellence, the FEDMAP component of the

National Cooperative Geologic Mapping Program, and National Science Foundation grants EAR-9814800 to RDH and EAR-9814891 to CFM.

REFERENCES CITED

Abbott, R. N., Jr., and Raymond, L. A., 1984, The Ashe Metamorphic Suite, northwest North Carolina: Metamorphism and observations on geologic history: American Journal of Science, v. 284, p. 350–375.

Aleinikoff, J. N., Zartman, R. E., Walter, M., Rankin, D. W., Lyttle, P. T., and Burton, W. C., 1995, U–Pb ages of metarhyolites of the Catoctin and Mount Rodgers Formations, central and southern Appalachians: Evidence for two pulses of Iapetan rifting: American Journal of Science, v. 295, p. 428–454.

Bailey, C., Eriksson, K., Allen, C., and Campbell, I., 2008, Detrital zircon geochronology of the Chopawamsic terrane, Virginia Piedmont: Evidence for a non-Laurentian Provenance: Geological Society of America Abstracts with Programs, v. 40, no. 6, p. 451.

Bartholomew, M. J., and Lewis, S. E., 1984, Evolution of Grenville massifs in the Blue Ridge geologic province, southern and central Appalachians, *in* Bartholomew, M. J., ed., The Grenville event in the Appalachians and related topics: Geological Society of America Special Paper 194, p. 229–254.

Berquist, P. J., 2005, U–Pb geochronology and geochemistry of southern Appalachian basement: Tectonic implications and constraints on age, extent, and origin [M.S. thesis]: Nashville, Tennessee, Vanderbilt University, 91 p.

Berquist, P. J., Fisher, C. M., Miller, C. F., Wooden, J. L., Fullagar, P. D., and Loewy, S. L., 2005, Geochemistry and U–Pb geochronology of Blue Ridge basement, western North Carolina and eastern Tennessee: Implications for tectonic assembly, *in* Hatcher, R. D., Jr., and Merschat, A. J., eds., Blue Ridge geology geotraverse east of the Great Smoky Mountains National Park, western North Carolina: Carolina Geological Society Guidebook, North Carolina Geological Survey, p. 33–44.

Bhatia, M. R., and Crook, K. A. W., 1986, Trace element characteristics of graywackes and tectonic discrimination of sedimentary basin: Contributions to Mineralogy and Petrology, v. 101, p. 361–376.

Bream, B. R., 2002, The southern Appalachian Inner Piedmont: New perspectives based on recent detailed geologic mapping, Nd isotopic evidence, and zircon geochronology, *in* Hatcher, R. D., Jr., and Bream, B. R., eds., Inner Piedmont geology in the South Mountains-Blue Ridge Foothills and the southwestern Brushy Mountains, central-western North Carolina: Carolina Geological Society Guidebook, p. 45–63.

Bream, B. R., 2003, Tectonic implications of geochronology and geochemistry of para- and orthogneisses from the southern Appalachian crystalline core [Ph.D. dissertation]: Knoxville, University of Tennessee, 296 p.

Bream, B. R., Hatcher, R. D., Jr., Miller, C. F., and Fullagar, P. D., 2001, Geochemistry and provenance of Inner Piedmont paragneisses, NC and SC: Evidence for an internal terrane boundary?: Geological Society of America Abstracts with Programs, v. 33, no. 2, p. 65.

Bream, B. R., Hatcher, R. D., Jr., Miller, C. F., and Fullagar, P. D., 2004, Detrital zircon ages and Nd isotopic data from the southern Appalachian crystalline core, Georgia, South Carolina, North Carolina, and Tennessee: New provenance constraints for part of the Laurentian margin, *in* Tollo, R. P., Corriveau, L., McLelland, J., and Bartholomew, M. J., eds., Proterozoic tectonic evolution of the Grenville orogen in North America: Boulder, Colorado, Geological Society of America Memoir 197, p. 459–475.

Bream, B. R., Loewy, S. L., Merschat, A. J., Hatcher, R. D., Jr., and Miller, C. F., 2008, Constraints on Blue Ridge and Inner Piedmont paragneiss provenance: Synthesis of detrital zircon and whole-rock Pb isotopic data: Geological Society of America Abstracts with Programs, v. 40, no. 4, p. 28.

Brewer, M. C., and Thomas, W. A., 2000, Stratigraphic evidence for Neoproterozoic-Cambrian two-phase rifting of southern Laurentia: Southeastern Geology, v. 39, p. 91–106.

Butler, J. R., 1991, Metamorphism, *in* Horton, J. W., Jr., and Zullo, V. A., eds., The geology of the Carolinas: Knoxville, University of Tennessee Press, p. 127–141.

Byars, H. E., Gilliam, W. G., Hatcher, R. D., Jr., Merschat, A. J., and Bier, S. E., 2008, Tectonic evolution of the Appalachian Inner Piedmont from a new detailed geologic map from the Brevard fault into the Newton Window: Geological Society of America Abstracts with Programs, v. 40, no. 6, p. 157.

Carrigan, C. W., Miller, C. F., Fullagar, P. D., Hatcher, R. D., Jr., Bream, B. R., and Coath C. D., 2003, Ion microprobe age and geochemistry of southern Appalachian basement, with implications for Proterozoic and Paleozoic reconstructions: Precambrian Research, v. 120, p. 1–36.

Carter, B. T., Hibbard, J. P., Tubrett, M., and Sylvester P., 2006a, Detrital zircon geochronology of the Smith River allochthon and Lynchburg Group, southern Appalachians: Implications for Neoproterozoic-Early Cambrian paleogeography: Precambrian Research, v. 147, p. 279–304.

Carter, B. T., Loehn, C. W., and Box, G., 2006b, The Smith River allochthon-Lynchburg Group contact, revisited: Does it represent closure of the Iapetus ocean or a Laurentian rift-basin: Geological Society of America Abstracts with Programs, v. 38, no. 3, p. 63.

Cawood, P. A., and Nemchin, A. A., 2001, Paleogeographic development of the east Laurentian margin: Constraints from U-Pb dating of detrital zircons in the Newfoundland Appalachians: Geological Society of America Bulletin, v. 113, p. 1234–1246.

Colton, G. W., 1970, The Appalachian Basin–Its depositional sequences and their geological relationships, *in* Fisher, G. W., Pettijohn, F. J., Reed, J. C., Jr., and Weaver, K. N., eds., Studies of Appalachian geology: Central and southern: New York, Wiley Interscience, p. 5–47.

Cordani, U. G., and Teixeira, W., 2007, Proterozoic accretionary belts in the Amazonia craton, *in* Hatcher, R. D., Jr., Carlson, M. P., McBride, J. H., and Martínez Catalán, J. R., eds., 4-D Framework of Continental Crust: Geological Society of America Memoir 200, p. 297–320.

Costain, J. K., Hatcher, R. D., Jr., and Coruh, C., 1989, Appalachian Ultradeep Core Hole (ADCOH) Project site investigation: Regional seismic lines and geologic interpretation, *in* Hatcher, R. D., Jr., Viele, G. W., and Thomas, W. A., eds., The Appalachian–Ouachita Orogen in the United States: Boulder, Colorado, Geological Society of America, Geology of North America, v. F-2, Plate 8.

Dalziel, I. W. D., 1992, On the organization of American plates in the Neoproterozoic and the breakout of Laurentia: GSA Today, v. 2, p. 240–241.

Dalziel, I. W. D., 1994, Precambrian Scotland as a Laurentia-Gondwana link: Origin and significance of cratonic promontories: Geology, v. 22, p. 589–592.

Davis, T. L., 1993, Geology of the Columbus Promontory, western Piedmont, North Carolina, southern Appalachians, *in* Hatcher, R. D., Jr., and Davis, T. L., eds., Studies of Inner Piedmont geology with a focus on the Columbus Promontory: Carolina Geological Society Guidebook, North Carolina Geological Survey, p. 17–43.

Dennis, A. J., Shervais, J. W., Mauldin, J., Maher, H. D., Jr., and Wright, J. E., 2004, Petrology and geochemistry of Neoproterozoic volcanic arc terranes beneath the Atlantic Coastal Plain, Savannah River Site, South Carolina: Geological Society of America Bulletin, v. 116, p. 572–593.

Drake, A. A., Jr., Sinha, A. K., Laird, J., and Guy, R. E., 1989, The Taconic orogen, Chapter 3, *in* Hatcher, R. D., Jr., Thomas, W. A., and Viele, G. W., eds., The Appalachian-Ouachita orogen in the United States: Boulder, Colorado, Geological Society of America, The Geology of North America, v. F-2, p. 101–177.

Eriksson, K. A., Campbell, I. H., Palin, J. M., Allen, C. M., and Bock, B., 2004, Evidence for multiple recycling in Neoproterozoic through Pennsylvanian sedimentary rocks of the central Appalachian basin: The Journal of Geology, v. 112, p. 261–276.

Espenshade, G. H., Rankin, D. W., Shaw, K. W., and Neuman, R. B., 1975, Geologic map of the east half of the Winston-Salem quadrangle, North Carolina-Virginia: U.S. Geological Survey Map I-709-B, scale 1:250,000.

Ettensohn, F. R., 1985, The Catskill delta complex and the Acadian orogeny: A model, *in* Woodrow, D. L., and Sevon, W. D., eds., The Catskill delta: Boulder, Colorado, Geological Society of America Special Paper 201, p. 39–49.

Ettensohn, F. R., 2004, Modeling the nature and development of major Paleozoic clastic wedges in the Appalachian basin, USA: Journal of Geodynamics, v. 37, p. 657–681.

Fisher, C. M., Loewy, S. L., Miller, C. F., Berquist, P., Van Schmus, W. R., Hatcher, R. D., Jr., Wooden, J. L., and Fullagar, P. D., 2006, An exotic Blue Ridge basement: New isotopic evidence: Geological Society of America Abstracts with Programs, v. 38, no. 3, p. 62.

Fisher, C. M., Loewy, S. L., Miller, C. F., Berquist, P., Van Schmus, W. R., Hatcher, R. D., Jr., Wooden, J. L., and Fullagar, P. D., in review, Whole rock Pb and Sm-Nd isotopic constraints on the growth of the southeastern Laurentia during Grenvillian Orogenesis: Geological Society of America Bulletin.

Fritz, W. J., La Tour, T. E., and Stake, D. S., 1985, Carbonate turbidites in volcaniclastic metasedimentary rocks of the Mineral Bluff Formation, Murphy, North Carolina: Geological Society of America Abstracts with Programs, v. 17, no. 7, p. 587.

Fritz, W. J., and La Tour, T. E., 1987, Chemical variation in the metasedimentary Mineral Bluff Formation, North Carolina: Geological Society of America Abstracts with Programs, v. 19, no. 2, p. 93–94.

Fritz W. J., and La Tour, T. E., 1988, Volcanogenic character of parts of the Mineral Bluff Formation: Evidence from field and geochemical studies, *in* Fritz, W. J., and La

Tour, T. E., eds., Geology of the Murphy belt and related rocks Georgia and North Carolina: Georgia Geological Society Guidebook, v. 8, p. 75–93.

Gatewood, M. P., 2007, Structure and tectonics of the northeastern Inner Piedmont from detailed geologic mapping, geochronologic, geochemical, and petrologic studies with macro-, meso-, and microstructural analyses of ductile fault zones [M.S thesis]: Knoxville, University of Tennessee, 279 p.

Gilliam, W. G., Byars, H. E., Hatcher, R. D., Jr., and Merschat, A. J., 2008, Tectonic implications of geologic mapping in the western Newton window, Inner Piedmont, NC: Geological Society of America Abstracts with Programs, v. 40, no. 4, p. 18.

Giorgis, S. D., 1999, Inner Piedmont geology of the northwestern South Mountains near Morganton, North Carolina [M.S. thesis]: Knoxville, University of Tennessee, 191 p.

Goldberg, S. A., Butler, J. R., and Fullagar, P. D., 1986, The Bakersville dike swarm: Geochronology and petrogenesis of Late Proterozoic basaltic magmatism in the southern Appalachian Blue Ridge: American Journal of Science, v. 286, p. 403–430.

Goldsmith, R., Milton, D. J., and Horton, J. W., Jr., 1988, Geologic map of the Charlotte 1-degree x 2-degree quadrangle, North Carolina and South Carolina: U.S. Geological Survey Map I-1251-E, scale 1:250,000.

Gray, M.B., and Zeitler, P.K., 1997, Comparison of clastic wedge provenance in the Appalachian foreland using U/Pb ages of detrital zircons: Tectonics, v. 16, p. 151–160.

Grimes, C. B., John, B. E., Kelemen, P. B., Mazdab, F. K., Wooden, J. L., Cheadle, M. J., Hangøj, K., and Schwartz, J. J., 2007, Trace element chemistry of zircons from oceanic crust: A method for distinguishing detrital zircon provenance: Geology, v. 35, p. 643–646.

Gromet, L. P., Dymek, R. F., Haskin, L. A., and Korotev, R. L., 1984, The "North American Shale Composite": its compilation, major and trace element characteristics: Geochemica et Cosmochimica Acta, v. 48, p. 2469–2482.

Groszos, M. S., and Tull, J. F., 2007, Stratigraphy and structure of the Murphy belt in the western Blue Ridge of north Georgia, *in* Tull, J. F., ed., Tectonics of the Georgia Blue Ridge: Basement/cover rift architecture, important aspects of overlying drift and clastic wedge facies, and the westernmost accretionary terrane: Georgia Geological Society Field Trip Guidebook, v. 27, p. 61–120.

Hadley, J. B., 1970, The Ocoee series and its possible correlatives, *in* Fisher, G. W., Pettijohn, F. J., Reed, J. C., Jr., and Weaver, K. N., eds., Studies of Appalachian geology, central and southern: New York, Interscience Publisher, p. 247-259.

Hadley, J. B., and Goldsmith, R., 1963, Geology of the eastern Great Smoky Mountains North Carolina and Tennessee: U. S. Geological Survey Professional Paper 349-B, 117 p.

Hadley, J. B., and Nelson, A. E., 1971, Geologic map of the Knoxville quadrangle, North Carolina, Tennessee, and South Carolina: U. S. Geological Survey Miscellaneouse Investigations Series Map I–654, scale 1:250,000.

Harley, S. L., and Kelly, N. M., 2007, Zircon tiny but timely: Elements, v. 3, p. 13-18.

Harris, L. D., Harris, A. G., De Witt, W., Jr., and Bayer, K. C., 1981, Evaluation of southern eastern overthrust belt beneath Blue Ridge–Piedmont thrust: The American Association of Petroleum Geologist Bulletin, v. 65, p. 2497–2505.

Hatcher, R. D., Jr., 1978, Tectonics of the western Piedmont and Blue Ridge: Review and speculation: American Journal of Science, v. 278, p. 276–304.

Hatcher, R. D., Jr., 1984, Southern and central Appalachian basement massifs, *in* Bartholomew, M. J., ed., The Grenville event in the Appalachians and related topics: Boulder, Colorado, Geological Society of America Special Paper 194, p. 149–153.

Hatcher, R. D., Jr., 1987, Tectonics of the southern and central Appalachian internides: Annual Reviews in Earth and Planetary Sciences, v. 15, p. 337–362.

Hatcher, R. D., Jr., 1989, Tectonic synthesis of the U.S. Appalachians, Chapter 14, *in* Hatcher, R. D., Jr., Thomas, W. A., and Viele, G. W., eds., The Appalachian-Ouachita orogen in the United States: Boulder, Colorado, Geological Society of America, The Geology of North America, v. F-2, p. 511–535.

Hatcher, R. D., Jr., 2001, Rheological partitioning during multiple reactivation of the Palaeozoic Brevard fault zone, southern Appalachians, USA, *in* Holdsworth, R. E., Strachan, R. A., Magloughlin, J. F., and Knipe, R. J., eds., The nature and tectonic significance of fault zone weakening: London, Geological Society of London Special Publication 186, p. 255–269.

Hatcher, R. D., Jr., 2002, An Inner Piedmont primer, *in* Hatcher, R. D., Jr., and Bream, B. R., eds., Inner Piedmont geology in the South Mountains-Blue Ridge Foothills and the southwestern Brushy Mountains, central-western North Carolina: Carolina Geological Society Guidebook, p. 1–18.

Hatcher, R. D., Jr., and Butler, J. R., 1979, Guidebook for southern Appalachian field trip in the Carolinas, Tennessee, and northeastern Georgia: International Geologic Correlation Program Project 27, University of North Carolina, Chapel Hill, 117 p.

Hatcher, R. D., Jr., and Goldberg, S. A., 1991, The Blue Ridge Geologic Province, *in* Horton, J. W., Jr., and Zullo, V. A., eds., The Geology of the Carolinas: Knoxville, The University of Tennessee Press, Carolina Geological Society 50th Anniversary Volume, p. 11–35.

Hatcher, R. D., Jr., and Hooper, R. J., 1992, Evolution of crystalline thrust sheets in the internal parts of mountain chains, *in* McClay, K. R., ed., Thrust tectonics: London, Chapman and Hall, p. 217–234.

Hatcher, R. D., Jr., and Merschat, A. J., 2006, The Appalachian Inner Piedmont: An exhumed strike-parallel, tectonically forced orogenic channel, *in* Law, R. D., Searle, M., and Godin, L., eds., Channel flow, ductile extrusion and exhumation of lower-mid crust in continental collision zones: London, Geological Society of London Special Publication 268, p. 517–540.

Hatcher, R. D., Jr., Thomas, W. A., Geiser, P. A., Snoke, A. W., Mosher, S., and Wiltschko, D. V., 1989, Alleghanian orogen, Chapter 5, *in* Hatcher, R. D., Jr., Thomas, W. A., and Viele, G. W., eds., The Appalachian-Ouachita orogen in the United States: Boulder, Colorado, Geological Society of America, The Geology of North America, v. F-2, p. 233–318.

Hatcher, R. D., Jr., Bream, B. R., Miller, C. L., Eckert, J. O., Jr., Fullagar, P. D., and Carrigan, C. W., 2004a, Paleozoic structure of internal basement massifs, southern Appalachian Blue Ridge, incorporating new geochronologic, Nd and Sr isotopic, and geochemical data, *in* Tollo, R. P., Corriveau, L., McLelland, J., and Bartholomew, M. J., eds., Proterozoic tectonic evolution of the Grenville orogen in North America: Boulder, Colorado, Geological Society of America Memoir 197, p. 525–547.

Hatcher, R. D., Jr., Whisner, S. C., Bream, B. R., Miller, C. F., 2004b, Sediments derived from mountain chains do not always land in foredeeps: Southern Appalachian Sevier–Blountain basin dynamics: Geological Society of America Abstracts with programs, v. 36, no. 2, p. 92.

Hatcher, R. D., Jr., Merschat, A. J., and Thigpen, J. R., 2005, Blue Ridge Primer, *in* Hatcher, R. D., Jr., and Merschat, A. J., eds., Blue Ridge geology geotraverse east of the Great Smoky Mountains National Park, western North Carolina: Carolina Geological Society Guidebook, North Carolina Geological Survey, p. 1–24.

Hatcher, R. D., Jr., Bream, B. R., and Merschat, A. J., 2007a, Tectonic map of the southern and central Appalachians: A tale of three orogens and a complete Wilson cycle, *in* Hatcher, R. D., Jr., Carlson, M. P., McBride, J. H., and Martínez Catalán, J. R., eds., 4-D Framework of Continental Crust: Geological Society of America Memoir 200, p. 595–632.

Hatcher, R. D., Jr., Lemiszki, P. J., and Whisner, J. B., 2007b, Character of rigid boundaries and internal deformation of the southern Appalachian foreland fold-thrust belt, *in* Sears, J. W., Harms, T. A., and Evenchick, C. A., eds., Whence the Mountains? Inquiries into the evolution of orogenic systems: A volume in honor of Raymond A. Price: Geological Society of America Special Paper 433, p. 243–276.

Henika, W. S., and Conley, J. F., 1973, Geology of the Snow Creek, Martinsville East, Price, and Spray quadrangles, Virginia: Virginia Division of Mineral Resources Report of Investigations 33, 71 p.

Henika, W. S., Conley, J. F., and Sweet, P. C., 1996, Geology and mineral resources of Henry County and the city of Martinsville, Virginia: Virginia Division of Mineral Resources Publication 137, 22 p.

Hibbard, J. P., 2000, Docking Carolina: Geology, v. 28, p. 127–130.

Hibbard, J. P., Tracy, R. J., and Henika, W. S., 2003, Smith River allochthon: A southern Appalachian peri-Gondwanan terrane emplaced directly on Laurentia?: Geology, v. 31, p. 215–218.

Hibbard, J. P., Stoddard, E. F., Secor, D. T., and Dennis, A. J., 2002, The Carolina zone: overview of Neoproterozoic to Early Paleozoic peri-Gondwanan terranes along the eastern flank of the southern Appalachians: Earth-Science Review, v. 57, p. 299–339.

Hibbard, J. P., van Staal, C. R., Rankin, D. W., and Williams, H., 2006, Lithotectonic map of the Appalachian orogen, Canada–United States of America: Geological Survey of Canada, Map 2096A, Scale 1:1,500,000.

Hibbard, J. P., van Staal, C. R., and Rankin, D. W., 2007, A comparative analysis of pre-Silurian crustal building blocks of the northern and southern Appalachian orogen: American Journal of Science, v. 307, p. 23–45.

Hoffman, P. F., 1988, United Plates of America, the birth of a craton: Early Proterozoic assembly and growth of Laurentia: Annual Reviews in Earth and Planetary Sciences, v. 16, p. 543–603.

Hoffman, P. F., 1991, Did the breakout of Laurentia turn Gondwanaland inside-out?: Science, v. 252, p. 1409–1412.

Hopson, J. L., and Hatcher, R. D., Jr., 1990, ADCOH Appalachian ultradeep core hole (ADCOH) project site investigation: University of Tennessee, Knoxville, Tennessee, 132 p.

Horton, J. W., Jr., Drake, A. A., Jr., and Rankin, D. W., 1989, Tectonostratigraphic terranes and their Paleozoic boundaries in the central and southern Appalachians, *in* Dallmeyer, R. D., ed., Terranes in the circum-Atlantic Paleozoic orogens: Geological Society of America Special Paper 230, p. 213–245.

Hoskin, P. W. O., and Ireland, T. R., 2000, Rare earth element chemistry of zircon and its use as a provenance indicator: Geology, v. 28, p. 627–630.

Hoskin, P. W. O., and Schaltegger, U., 2003, The composition of zircon and igneous and metamorphic petrogenesis, *in* Hanchar, J. M., and Hoskin, P. W. O., eds., Zircon: Washington D.C., Reviews in Mineralogy and Geochemistry, v. 53, p. 27–62.

Kalbas, J. L., 2003, Geology of part of the southwestern Brushy Mountains, Inner Piedmont [M.S. thesis]: Knoxville, University of Tennessee, 208 p.

Keith, A., 1895, Description of the Knoxville sheet: U.S. Geological Survey Geologic Atlas, Folio 16, 6 p.

Larson, K. W., Hatcher, R. D., Jr., Neuman, R. B., and Finney, S. C., 1989, Structure of the Guess Creek fault and Fair Garden anticline, southeastern Tennessee: Relatives of the Great Smoky fault or unrelated structures?: Geological Society of America Abstracts with Programs, v. 21, no. 3, p. 46.

Li, Z. X., Bogdanova, S. V., Collins, A. S., Davidson, A., De Waele, B., Ernst, R. E., Fitzsimons, I. C. W., Fuck, R. A., Gladkochub, D. P., Jacobs, J., Karlstrom, K. E., Lu, S., Natapov, L. M., Pease, V., Pisarevsky, S. A., Thrane, K., and Vernikovsky, V., 2008, Assembly, configuration, and break-up history of Rodinia: A synthesis: Precambrian Research, v. 160, p. 179–210.

Loewy, S. L., Connelly, J. N., Dalziel, I. W. D., Gower, C. F., 2003, Eastern Laurentia in Rodinia: constraints from whole-rock Pb and U/Pb geochronology: Tectonophysics, v. 375, p. 169–197.

Loewy, S. L., Connelly, J. N., and Dalziel, I. W. D., 2004, An orphaned basement block: The Arequipa-Antofalla basement of the central Andean margin of South America: Geological Society of America Bulletin, v. 116, p. 171–187.

Ludwig, K. R., 2001, SQUID v. 1.02, computer program.

Ludwig, K. R., 2003, Isoplot v. 3.00, computer program.

Mapes, R. W., 2002, Geochemistry and geochronology of mid-Paleozoic granitic plutonism in the southern Appalachian Piedmont terrane, North Carolina-South Carolina-Georgia [M.S. thesis]: Nashville, Vanderbilt University, 150 p.

Mazdab, F. K., and Wooden, J. L., 2006, Trace element analysis in zircon by ion microprobe (SHRIMP-RG): technique and applications: 6th Annual V.M. Goldschmidt Conference.

McDowell, S. M., Miller, C.F., Fullagar, P. D., Bream, B. R., and Mapes, R. W., 2002, The Persimmon Creek Gneiss, eastern Blue Ridge, North Carolina-Georgia: Evidence for the missing Taconic arc?: Southeastern Geology, v. 41, p. 103–117.

McLennan, S. M., Bock, B., Compston, W., Hemming, S. R., and McDaniel, D. K., 2001, Detrital zircon geochronology of Taconian and Acadian foreland sedimentary rocks in New England: Journal of Sedimentary Research, v. 71, p. 305–317.

McSween, H. Y., Jr., and Harvey, R. P. 1997, Concord Plutonic Suite: Pre-Acadian gabbro-syenite intrusion in the southern Appalachians, *in* Sinha, A. K., Whalen, J. B., and Hogan, J. P., eds., The nature of magmatism in the Appalachian orogen: Boulder, Colorado, Geological Society of America Memoir 197, p. 221–234.

Merschat, A. J., 2003, Inner Piedmont tectonics in the southwestern Brushy Mountains, North Carolina: Field and laboratory data revealing 3-D crustal flow and sillimanite I and II metamorphism [M.S. thesis]: Knoxville, University of Tennessee, 198 p.

Merschat, A. J., and Hatcher, R. D., Jr., 2004, The Cat Square terrane: A Siluro-Devonian remnant ocean basin in the Inner Piedmont, Southern Appalachians?: 4–D Framework of Continental Crust, 17th International Basement Tectonics Conference, Program with Abstracts, p. 96–97.

Merschat, A. J., and Hatcher, R. D., Jr., 2006, Palinspastic restoration of the southern Appalachian Inner Piedmont: Links between the Acadian clastic wedge and high-temperature deformation in the crystalline core of the southern Appalachians: Geological Society of America Abstracts with Programs, v. 38, no. 3, p. 8.

Merschat, A. J., and Hatcher, R. D., Jr., 2007, The Cat Square terrane: Possible Siluro-Devonian remnant ocean basin in the Inner Piedmont, southern Appalachians, USA, *in* Hatcher, R. D., Jr., Carlson, M. P., McBride, J. H., and Martínez Catalán, J. R., eds., 4-D Framework of Continental Crust: Geological Society of America Memoir 200, p. 553–565.

Merschat, A. J., and Kalbas, J. L., 2002, Geology of the southwestern Brushy Mountains, North Carolina Inner Piedmont: A summary and synthesis of recent studies, *in*

Hatcher, R. D., Jr., and Bream, B. R., eds., Inner Piedmont geology in the South Mountains-Blue Ridge Foothills and the southwestern Brushy Mountains, central-western North Carolina: Carolina Geological Society Guidebook, p. 101–126.

Merschat, A. J., Hatcher, R. D., Jr., and Davis, T. L., 2005a, The northern Inner Piedmont, southern Appalachians, USA: Kinematics of transpression and SW-directed mid-crustal flow: Journal of Structural Geology, v. 27, p. 1252–1281.

Merschat, A. J., Gatewood, M. P., Fisher, C. M., Miller, C. F., Hatcher, R. D., Jr., Wooden, J. L., and Stahr, D. W., III, 2005b, The Newton antiform, NC: A previously unrecognized window through the allochthonous Inner Piedmont thrust stack: Geological Society of America Abstracts with Programs, v. 37, no. 7, p. 20.

Merschat, A. J., Hatcher, R. D., Jr., Miller, C. F., and Wooden, J. L., 2006, Provenance of central and western Blue Ridge paragneisses, southwestern North Carolina: Geological Society of America Abstracts with Programs, v. 38, no. 3, p. 63.

Merschat, A. J., Bream, B. R., Hatcher, R. D., Jr., Miller, C. F., and Carrigan, C. W., 2008a, Delimiting the spatial and extent of superposed metamorphic events of the Blue Ridge and Inner Piedmont with SHRIMP U-Pb ages of zircon rims: Geological Society of America Abstracts with Programs, v. 40, no. 4, p. 19.

Merschat, A. J., Hatcher, R. D., Jr., Gilliam W. G., and Byars, H. E., 2008b, Inner Piedmont Geo-Traverse from the Brushy Mountains to Lincolnton, North Carolina: Architecture of the Cat Square and Tugaloo terranes, Geological Society of America, Southeastern Section Field Trip Guidebook: Knoxville, Tennessee, 64 p.

Merschat, C. E., and Cattanach, B. L., 2008, Bedrock geologic map of the west half of the Asheville 1:100,000-scale quadrangle, North Carolina and Tennessee: North Carolina Geological Survey, scale 1:100,000.

Miller, B. V., Fetter, A. H., and Stewart, K. G., 2006, Plutonism in three orogenic pulses, eastern Blue Ridge Province, southern Appalachians: Geological Society of America Bulletin, v. 118, p. 171–184.

Miller, C. F., Hatcher, R. D., Jr., Harrison, T. M., Coath, C. D., and Gorisch, E. B., 1998, Cryptic crustal events elucidated through zone imaging and ion microprobe studies of zircon, southern Appalachian Blue Ridge, North Carolina-Georgia: Geology, v. 26, p. 419–422.

Miller, C. F., Hatcher, R. D., Jr., Ayers, J. C., Coath, C. D., and Harrison, T. M., 2000, Age and zircon inheritance of eastern Blue Ridge plutons, southwestern North Carolina and northeastern Georgia, with implications for magma history and

evolution of the southern Appalachian orogen: American Journal of Science, v. 300, p. 142–172.

Moecher, D. P., Samson, S. D., and Miller, C. F., 2004, Precise time and conditions of peak Taconian granulite facies metamorphism in the southern Appalachian orogen, USA, with implications for zircon behavior during crustal melting events: Journal of Geology, v. 112, p. 289–304.

Moecher, D. P., and Samson, S. D., 2006, Differential zircon fertility of source terranes and natural bias in the detrital zircon record: Implications for sedimentary provenance analysis: Earth and Planetary Science Letters, v. 247, p. 252–266.

Nelson, A. E., 1991, Geologic map of the Campbell Mountain quadrangle, Lumpkin County, Georgia: U. S. Geological Survey Miscellaneous Field Studies Map MF-2148, scale 1:24,000.

Nesbitt, H. W., and Young, G. M., 1982, Early Proterozoic climates and plate motions inferred from major element chemistry of lutites: Nature, v. 299. p. 715–717.

Neuman, R. B., 1955, Middle Ordovician rocks of the Tellico-Sevier belt eastern Tennessee: U.S. Geological Survey Professional Paper 274-F, 177 p.

Osberg, P. H., Tull, J. F., Robinson, P., Hon, R., and Butler, J. R., 1989, The Acadian Orogen Chapter 4, *in* Hatcher, R. D., Jr., Thomas, W. A., and Viele, G. W., eds., The Appalachian Ouachita orogen in the United States: Boulder, Colorado, Geological Society of America, The geology of North America, v. F-2, p. 179–232.

Osborne, W. E., Szabo, M. W., Copeland, C. W., Jr., and Neathery, T. L., 1989, Geologic map of Alabama: Geological Survey of Alabama Special Map 221, scale 1:500,000.

Ownby, S. E., Miller, C. F., Berquist, P. J., Carrigan, C. W., Wooden, J. L., and Fullagar, P. D., 2004, U-Pb geochronology and geochemistry of a portion of the Mars Hill terrane, North Carolina–Tennessee: Constraints on origin, history, and tectonic assembly, *in* Tollo, R. P., Corriveau, L., McLelland, J., and Bartholomew, M. J., eds., Proterozoic evolution of the Grenville orogen in North America: Boulder, Colorado, Geological Society of America Memoir 197, p. 609–632.

Park, H., Rickenbaker, A., Bachmann-Krug, D., Barbeau, D. L., and Gehrels, G. E., 2008, Detrital-zircon geochronology of Acadian foreland basin strata of west Virginia and Virginia: Geological Society of America Abstracts with Programs, v. 40, no. 4. p. 18.

Rankin, D. W., 1975, The continental margin of eastern North America in the southern Appalachians: The opening and closing of the proto-Atlantic Ocean: American Journal of Science, v. 275-A, p. 298–336.

Rast, N., and Kohles, K. M., 1986, The origin of the Ocoee Supergroup: American Journal of Science, v. 286, p. 593–616.

Raymond, L. A., Yurkovich, S. P., and McKinney, M., 1989, Block-in-matrix structures in the North Carolina Blue Ridge belt and their significance for the tectonic history of the southern Appalachian orogen, *in* Horton, J. W., Jr., and Rast, N., eds., Melanges: Boulder, Colorado, Geological Society of America Special Paper, 228, p. 195–215.

Raymond, L. A., Swanson, S. E., Allan, J. F., and Love, A. B., 2003, Cr-spinel compositions, metadunite petrology, and the petrotectonic history of the Blue Ridge ophiolites, southern Appalachian orogen, USA, *in* Dilek, Y., and Bobinson, P. T., eds., Ophiolites in Earth History: Geological Society of London Special Publication 218, p. 253–277.

Rodgers, J., 1953, Geologic map of East Tennessee with explanatory text: Tennessee Division of Geology Bulletin 58, Part II, 168 p.

Rodgers, J., 1970, The tectonics of the Appalachians: New York, New York, 271 p.

Rubatto, D., and Hermann, J., 2007, Zircon behavior in deeply subducted rocks: Elements, v. 3, p 31–35.

Samson, S. D., 1995, Is the Carolina terrane part of Avalon? *in* Hibbard, J. P., van Staal, C. R., and Cawood, P. A., eds., Current perspectives in the Appalachian-Caledonian orogen: Geological Association of Canada, Special Paper, 41, p. 243–264.

Settles, D. J., 2002, Defining the Hayesville-Soque River and Allatoona faults and an Ordovician arc assemblage within the central Blue Ridge northwest of Dahlonega, Georgia [unpublished M.S. thesis]: Knoxville, University of Tennessee, 148 p.

Shanmugan G., and Walker, K. R., 1983, Anatomy of the Middle Ordovician Sevier shale basin, eastern Tennessee: Sedimentary Geology, v. 34, p. 315–337.

Sinha, A. K., Hogan, J. P., Parks, J. K., 1996, Lead isotope mapping of crustal reservoirs within the Grenville superterrane: I. Central and southern Appalachians, earth processes: reading the isotopic code: American Geophysical Union Monograph 95, p. 293–305.

Sinha, A. K., Thomas, W., Hatcher, R. D., Jr., and Jerden, J. L., in preparation, Correlation of magmatism with pre-collisional depocenters and geometry of rifted

margins: Ordovician to Devonian magmatism associated with Taconic collisional tectonics.

Southworth, S., Aleinikoff, J. N., Bailey, C. M., Burton, W. C., Smoot, J. P., Tollo, R. P., and Crider, E., 2009, Geologic map of the Shenandoah National Park Region, Virginia: U. S. Geological Survey Open-File Report xx, xx p.

Stahr, D. W., III., 2007, Tectonometamorphic evolution of the eastern Blue Ridge: Differentiating multiple Paleozoic orogenic pulses in the Glenville and Big Ridge quadrangles, southwestern North Carolina [unpublished MS thesis]: Knoxville, Tennessee, University of Tennessee, 263 p.

Stahr, D. W., III, Hatcher, R. D., Jr., Miller, C. F., and Wooden, J. L., 2006, Alleghanian deformation in the Georgia and North Carolina eastern Blue Ridge: Insights from pluton ages and fabrics: Geological Society of America Abstracts with Programs, v. 38, no. 3, p. 20.

Steltenpohl, M. G., 2005, An introduction to the terranes of the southernmost Appalachians of Alabama and Georgia, *in* Steltenpohl, M. G., ed., Southernmost Appalachian terranes, Alabama and Georgia: Southeastern Section of the Geological Society of America Field Trip Guidebook, p. 1–18.

Steltenpohl, M. G., Heatherington, A., Mueller, P., Wooden, J. L., 2004, Pre-Appalachian tectonic evolution of the Pine Mountain window in southernmost Appalachians, Alabama and Georgia, *in* Tollo, R. P., Corriveau, L., McLelland, J., and Bartholomew, M. J., eds., Proterozoic tectonic evolution of the Grenville orogen in North America: Boulder, Colorado, Geological Society of America Memoir 197, p. 633–645.

Steltenpohl, M. G., Mueller, P. M., Heatherington, A. L., Hanley, T. B., and Wooden, J. L., 2008, Gondwanan/peri-Gondwanan origin for the Uchee terrane, Alabama and Georgia: Carolina zone or Suwannee terrane(?) and its suture with Grenvillian basement of the Pine Mountain window: Geosphere, v. 4, p. 131–144.

Su, Q., Goldberg, S. A., and Fullagar, P. D., 1994, Precise U-Pb zircon ages of Neoproterozoic plutons in the southern Appalachian Blue Ridge and their implications for the initial rifting of Laurentia: Precambrian Research, v. 68, p. 81–95.

Swanson, S. E., Raymond, L. A., Warner, R. D., Ryan, J. G., Yurkovich, S. P., and Peterson, V. L., 2005, Petrotectonics of mafic and ultramafic rocks in Blue Ridge terranes of western North Carolina and northern Georgia, *in* Hatcher, R. D., Jr., and Merschat, A. J., eds., Blue Ridge geology geotraverse east of the Great

Smoky Mountains National Park, western North Carolina: Carolina Geological Society Guidebook, North Carolina Geological Survey, p. 1–24.

Taylor, S. R., and McLennan, S. M., 1985, The continental crust: its composition and evolution: Blackwell, Oxford, 312 p.

Thomas, C. W., 2001, Origins of ultramafic complexes of the eastern Blue Ridge province, southern Appalachians: Geochronological and geochemical constraints [M.S. thesis]: Nashville, Tennessee, Vanderbilt University, 154 p.

Thomas, W. A., 1991, The Appalachian-Ouachita rifted margin of southeastern North America: Geological Society of America Bulletin, v. 103, p. 415–431.

Thomas, W. A., Becker, T. P., Samson, S. D., and Hamilton, M. A., 2004, Detrital zircon evidence of a recycled orogenic foreland provenance for Alleghanian clastic-wedge sandstones: Journal of Geology, v. 112, p. 23–37.

Tohver, E., van der Pluijm, B. A., Van der Voo, R., Rizzotto, G., Scandolara, J. E., 2002, Paleogeography of the Amazon craton at 1.2 Ga: early Grenvillian collision with the Llano segment of Laurentia: Earth and Planetary Science Letters, v. 199, p. 185–200.

Tohver, E., Bettencourt, J. S., Tosdal, R., Mezger, K., Leite, W. B., and Payolla, B. L., 2004, Terrane transfer during the Grenville orogeny: tracing the Amazonian ancestry of southern Appalachian basement through Pb and Nd isotopes: Earth and Planetary Science Letters, v. 228, p. 161–176.

Tohver, E., Teixeira, W., van der Pluijm, B., Geraldes, M.C., Bettencourt, J.S., and Rizzotto, G., 2006, Restored transect across the exhumed Grenville orogen of Laurentia and Amazonia, with implications for crustal architecture: Geology, v. 34, p. 669–672.

Tollo, R. P., and Aleinikoff, J. N., 1996, Petrology and U-Pb geochronology of the Robertson River Igneous suite, Blue Ridge province, Virginia: evidence for multistage magmatism associated with an early episode of Laurentian rifting: American Journal of Science, v. 296, p. 1045–1090.

Tull, J. F., 2002, Southeastern margin of the middle Paleozoic shelf, southwesternmost Appalachians: Regional stability bracketed by Acadian and Alleghanian tectonism: Geological Society of America Bulletin, v. 114, p. 643–655.

Tull, J. F., and Groszos, M. G., 1988, Murphy belt: Stratigraphic complexities and regional correlations, *in* Fritz, W. J., and La Tour, T. E., eds., Geology of the Murphy belt and related rocks, Georgia and North Carolina: Georgia Geological Society Guidebook, v. 8, p. 35–74.

Tull, J. F., Harris, A. G., Repetski, J. E., McKinney, F. K., Garrett, C. B., and Bearce, D. N., 1988, New paleontologic evidence constraining the age and paleotectonic setting of the Talladega slate belt, southern Appalachians: Geological Society of America Bulletin, v. 100, p. 1291–1299.

Tull, J. F., Ausich, W. I., Groszos, M. S., and Thompson, T. W., 1993, Appalachian Blue Ridge cover sequence ranges at least into the Ordovician: Geology, v. 21, p. 215–218.

Unrug, R., 1997, Rodinia to Gondwana: The geodynamic map of Gondwana supercontinent assembly: GSA Today, v. 7, p. 1–6.

Whitmeyer, S. J., and Karlstrom, K. E., 2005, Proterozoic growth and evolution of southern Laurentia: Visualization and interpretation by digital paleomaps: Geological Society of America Abstracts with Programs, v. 37, no. 7, p. 417.

Whitmeyer, S. J., and Karlstrom, K. E., 2007, Tectonic model for the Proterozoic growth of North America: Geosphere, v. 3, p. 220–259.

Williams, H., and Hatcher, R. D., Jr., 1982, Suspect terranes and accretionary history of the Appalachian orogen: Geology, v. 10, p. 530–536.

Williams, H., and Hatcher, R. D., Jr., 1983, Appalachian suspect terranes, *in* Hatcher, R. D., Jr., Williams, H., and Zeitz, I., D., eds., Contributions to the tectonics and geophysics of mountain chains: Geological Society of America Memoir 158, p. 33–53.

Wilson, C. G., 2006, Origin and tectonic evolution of the southern Appalachian Neoacadian crystalline core: Evidence from the geology of the Gilreath 7.5-minute quadrangle, North Carolina [M. S. Thesis]: Knoxville, University of Tennessee, 219 p.

Wilson, J. R., 2001, U/Pb zircon ages of plutons from the central Appalachians and GIS-based assessment of plutons with comments on their regional tectonic significance [MS thesis]: Virginia Polytechnical Institute, 109 p.

PART V

The Cat Square terrane: Possible Siluro-Devonian remnant ocean basin in the Inner Piedmont, southern Appalachians, USA

This chapter was published in the Geological Society of America Memoir 200. The full citation of the paper is:

Merschat, A. J., and Hatcher, R. D., Jr., 2007, The Cat Square terrane: Possible Siluro-Devonian remnant ocean basin in the Inner Piedmont, southern Appalachians, USA, *in* Hatcher, R. D., Jr., Carlson, M. P., McBride, J. H., and Martínez Catalán, J. R., The 4D Framework of Continental Crust, Geological Society of America Memoir 200, p. 553-565.

As primary author, my contributions included most of the writing, data compilation, and figure construction.

ABSTRACT

The Inner Piedmont is a large, composite, sillimanite-grade terrane that extends from near the Virginia-North Carolina border to central Alabama and consists of the eastern Tugaloo and Cat Square terranes. It is bound to the west by the Brevard fault zone and the east by the central Piedmont suture. It is the core of the Neoacadian (360-350 Ma) orogen in the southern Appalachians and records Late Devonian-Mississippian closure, and high-grade metamorphism (sillimanite I and II) of Siluro-Devonian sediments deposited in the remnant Rheic ocean basin.

The Cat Square terrane is bounded by the younger-over-older Brindle Creek fault to the west and the central Piedmont suture to the east. It consists of a unique sequence of Siluro-Devonian metapsammite and pelitic schist that was intruded by Devonian anatectic granitoids (Toluca Granite, ~378 Ma, and Walker Top Granite, ~366 or ~407 Ma). Rare mafic and ultramafic rocks occur in the eastern Cat Square terrane. Minimum sediment thickness is estimated at 4 km (13,000 ft). Detrital zircons indicate Cat Square terrane rocks have a maximum age of ~430 Ma, with both Laurentian (1.1, 1.4, 1.8, 2.8 Ga) and peri-Gondwanan (500, 600 Ma) affinities. Deposition on oceanic crust explains the existence of several mafic and ultramafic bodies and the absence of continental basement in the Cat Square terrane. The Cat Square terrane petrotectonic assemblage represents a Siluro-Devonian remnant ocean basin between Laurentia and the approaching Carolina superterrane. Metapsammite and pelitic schist may represent turbidites shed from approaching tectonic highlands on both flanks of the closing ocean. Palinspastic restoration of the Inner Piedmont constrains the location of the Cat Square basin to the Pennsylvania embayment, and links the mid-Devonian to Mississippian deformation in the Neoacadian core to the SW-migrating pulses of the diachronous

Acadian-Neoacadian clastic wedge. Location and SW-migration of the clastic wedge in concert with structural patterns in the Inner Piedmont support a transpressive NW-directed collision of the Carolina superterrane with the New York promontory and zippering shut of the basin from NE to SW.

Keywords: Appalachians, Inner Piedmont, remnant ocean basin, Cat Square terrane, transpression, Neoacadian, Acadian clastic wedge

INTRODUCTION

Accretionary margins are the sites of greatest addition of new crust and are therefore important in understanding the 4-D evolution of continental crust. These are sites of accelerated rates and processes, especially during continent-continent and continent-arc collisions. Ingersoll et al. (2003) concluded that few sedimentary systems match the rates and volumes of sediment shed during continent-continent collision (e.g., India and Asia). Sediment shed during collision is transported through major river systems and deposited in deltas, and in remnant ocean basins as part of huge submarine fans that dwarf all other depositional systems on Earth (Graham et al., 1975; Ingersoll et al., 1995, 2003). Ingersoll et al. (1995) defined a remnant ocean basin as a shrinking ocean basin flanked by at least one convergent margin and filled with recycled sediment shed from adjacent uplifted terranes (Fig. 5–1). Remnant ocean basins are destined to become deformed accretionary wedges or are further recycled and eventually preserved in terrigenous clastic wedges (Ingersoll et al., 1995, 2003). Preservation of remnant ocean basins is poor and their recognition is difficult because of complex deformation in suture zones (Ingersoll and Busby, 1995). Recognition of remnant ocean basins, however, is important to understanding the spatial and temporal development of orogens, and processes related to formation of new continental crust. Petrotectonic assemblages are key to identifying deformed remnant ocean basins and unraveling their tectonic evolution.

The Paleozoic Appalachians are a long-lived accretionary-collisional orogen that contains numerous accreted terranes and a complete Wilson cycle (Hatcher, 1978; Williams and Hatcher, 1983; Abbott and Raymond, 1984; Hatcher, 1987, 1989, 2002a; Rankin et al., 1989). Previously, little evidence supported a mid- to late Paleozoic orogeny in the southern Appalachians (Osberg et al., 1989), but recent geochronologic data have yielded overwhelming support for a Neoacadian, 360-350 Ma, tectonothermal event in the southern Appalachians (Dennis and Wright, 1997; Carrigan et al., 2001;

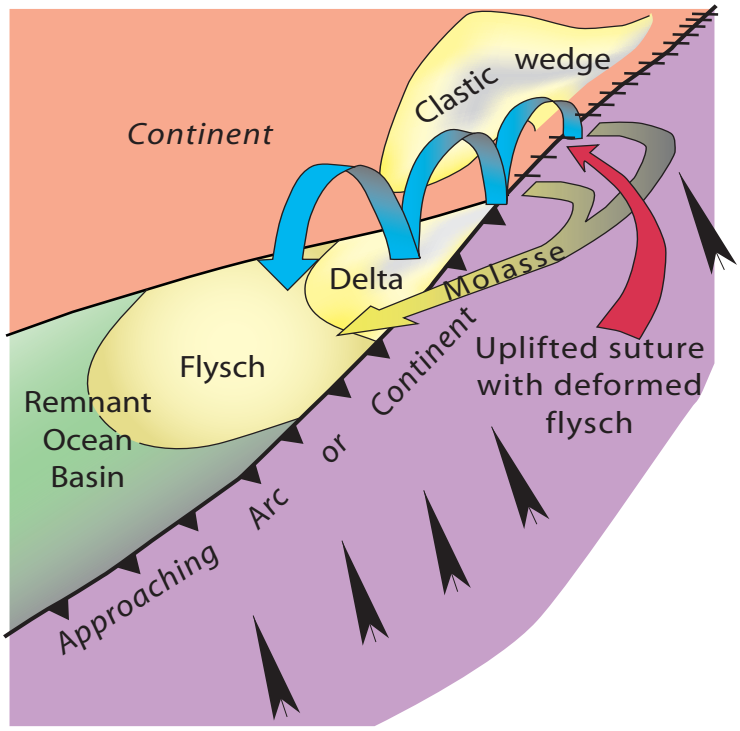

Figure 5–1. Conceptual diagram of a remnant ocean basin after Graham et al. (1975) illustrating the relationships between sequential closure of a remnant ocean basin, longitudinal sediment dispersal between uplifted terranes, and sediment recycling indicated by blue and yellow arrows. Black arrows indicate direction of approaching arc or continent.

Bream, 2002, 2003). One of the most intriguing discoveries is the Cat Square terrane, a Siluro-Devonian terrane in the eastern Inner Piedmont of mixed affinity metasedimentary rocks metamorphosed to upper-amphibolite facies by latest Devonian time (Merschat et al., 2005a). This paper attempts to summarize existing geochronology, geochemistry, map relationships, and petrotectonic assemblage to ascertain the pre-Neoacadian tectonic setting of the Cat Square terrane and the early kinematics of Late Devonian to Mississippian collision of the Carolina superterrane with Laurentia and previously accreted terranes. Based on these data, we speculate that the Cat Square terrane developed as a mid-Paleozoic remnant ocean basin.

TECTONIC SETTING

The Inner Piedmont extends from central Alabama to near the Virginia-North Carolina border (Fig. 5–2). It is bounded to the west by the Brevard fault zone and to the east by the central Piedmont suture. Gently dipping structures and an extensive sillimanite and higher-grade core distinguish the Inner Piedmont from surrounding

Figure 5–2. Simplified tectonic map of the southern Appalachians showing the location of the Inner Piedmont, and the Tugaloo (lavender) and Cat Square (blue-green) terranes. The Laurentian platform contains the Alleghanian foreland fold-thrust belt driven in front of the Blue Ridge-Piedmont megathrust sheet (the Laurentian margin, gold with red inliers of Grenvillian, not necessarily Laurentian Grenville, and older inherited crust), and all components to the east. All terranes west of the Cat Square terrane have a Laurentian source (Bream et al., 2004). Cat Square terrane contains Siluro-Devonian metasedimentary rocks with a mixed Laurentian and Peri-Gondwanan source. Carolina superterrane is Peri-Gondwanan and exotic to Laurentia. BCF– Brindle Creek fault. BF–Burnsville fault. Cart. terr.–Cartoogechaye terrane. CHMF–Chattahoochee-Holland Mountain fault. Cow. terr.–Cowrock terrane. DGB–Dahlonega gold belt. FF–Forbush fault. GLF–Gossan Lead fault. GMW–Grandfather Mountain window. NW–Newton window. SRA–Smith River allochthon, an outlier of Carolina superterrane rocks. SMW–Sauratown Mountains window. PMW–Pine Mountain window. Light gray–Probable western Tugaloo terrane rocks in Alabama and Georgia. Purple–Ordovician Elkahatchee Quartz Diorite. A–Athens. H–Hickory. S–Statesville. WS–Winston–Salem.

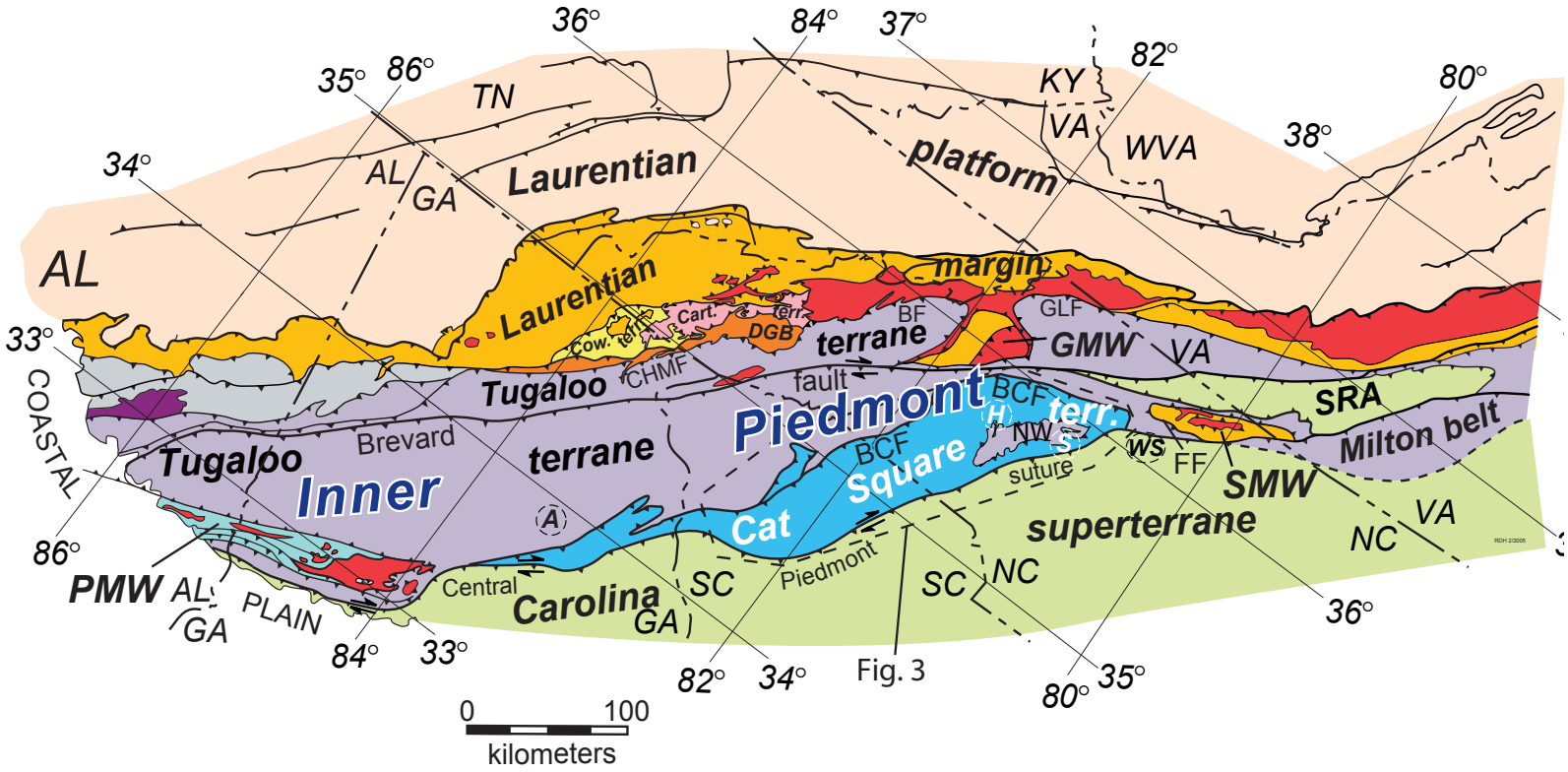
36°
84°
37°
82°
80°
35°
86°
TN
KY
VA
WVA
38°
34°
AL
GA
Laurentian
platform
AL
Laurentian
margin
Cart.
Grr.
DGB
Cow.
BF
GLF
terrane
GMW
VA
33°
COASTAL
Tugaloo
CHMF
fault
Piedmont
BCF
terr.
SRA
Brevard
Tugaloo
terrane
Inner
BCF
Square
NW
SE
WS
FF
suture
SMW
Milton belt
A
Cat
superterrane
NC
VA
86°
PMW
AL
GA
PLAIN
Central
Carolina
SC
GA
Piedmont
SC
NC
84°
33°
82°
34°
Fig. 3
80°
35°
36°
0
100
kilometers

terranes and belts. The Inner Piedmont forms part of the southern Appalachian Neoacadian metamorphic core, a product of Late Devonian-Mississippian oblique collision of the Carolina superterrane (Hatcher, 2002b; Merschat et al., 2005a; Hatcher and Merschat, 2006).

The polydeformed Inner Piedmont is characterized by a gently dipping stack of crystalline Type F thrust sheets (fold nappes; Hatcher and Hooper, 1992) containing various para- and orthogneisses, a curved subhorizontal mineral lineation pattern, and a broad core of migmatitic, sillimanite and higher-grade rocks. The Inner Piedmont thrust stack consists of small-to-large Type F thrust sheets overlain and dwarfed by the much larger Brindle Creek thrust sheet. These thrust sheets nucleated during dextral transpression and record a net displacement of several hundred kilometers, of which 200–400 km are associated with dextral orogen-parallel (SW-directed) displacement along the mid-Paleozoic Brevard fault zone (Merschat et al., 2005a). Metamorphic grade remains sillimanite or higher across the Inner Piedmont core and drops to kyanite and garnet grade along the western flank and kyanite along parts of the eastern flank (Hatcher and Merschat, 2006; their Fig. 10). Paragneisses are pervasively migmatitic, and reached sillimanite I and II grade metamorphism (800–850º C and 5–6 kb; Mirante and Patino Douce, 2000; Merschat, 2003). Numerous studies have demonstrated that the Inner Piedmont is polydeformed and the dominant structural elements are S_2, L_2, and F_2 (e.g., Hopson and Hatcher, 1988; Hatcher, 1993, 2001, 2002b; Merschat et al., 2005a). The gently dipping S_2 foliation distinguishes the Inner Piedmont from other terranes, but recent studies (e.g. Davis, 1993a, 1993b; Hatcher, 2001; Merschat et al., 2005a) have focused on the curved L_2 pattern and its coaxial relationship with F_2, a pattern initially recognized by Goldsmith (1981). Migmatitic layering parallel to S_2 and the dominant fabrics, S_2, L_2, commonly defined by high-grade minerals, hornblende, sillimanite, and kyanite, suggest that deformation occurred at or near peak metamorphic conditions (Davis, 1993a, 1993b; Bier et al., 2002; Merschat et al., 2005a). U-Pb ages of monazite and zircon metamorphic rims suggest Neoacadian (360-350 Ma) timing of metamorphism (Dennis and Wright, 1997; Carrigan et al., 2001; Bream 2003).

The composite Inner Piedmont consists of the eastern Tugaloo and overlying Cat Square terranes (Bream et al., 2001, 2004; Bream, 2002, 2003; Merschat et al., 2005a). The Brindle Creek fault separates the Laurentian-affinity, eastern Tugaloo terrane rocks of the western Inner Piedmont from mixed Laurentian- and Gondwanan-affinity rocks of the eastern Inner Piedmont/Cat Square terrane (Bream, 2002, 2003; Bream et al., 2004) (Fig. 5–2). The eastern Tugaloo terrane consists of Neoproterozic to Cambrian(?) Tallulah

Falls Formation metagraywacke and pelite, overlain by Middle Ordovician amphibolite, quartzite, marble, and felsic metatuff of the Poor Mountain Formation. Various Middle Ordovician to Silurian granitoids intrude the eastern Tugaloo terrane.

CAT SQUARE TERRANE

The Brindle Creek fault extends from south of Athens, Georgia to northwest of Winston-Salem, NC, and is truncated at both ends by the central Piedmont suture (Figs. 5–2 and 5–3). The Brindle Creek thrust sheet is the largest Inner Piedmont thrust sheet with an exposed area of 13,765 km^2. It juxtaposes younger Cat Square terrane rocks against older eastern Tugaloo terrane rocks. Bream et al. (2001, 2004) first suggested the Brindle Creek fault is a terrane boundary to explain contrasting zircon suites. Bream (2002, 2003) and Bream et al. (2001, 2004) recognized four detrital zircons suites from the Cat Square terrane: (1) dominance of Laurentian, 1.1, 1.2, and 1.4 Ga; (2) abundant Paleozoic 430 and 480 Ma; (3) lesser Neoproterozoic peri-Gondwanan 500 and 600 Ma; and (4) a small component of Archean 2.5 and 2.8 Ga zircons. The Cat Square terrane consists of pelitic schist, metapsammite, calc-silicate, minor amphibolite, and ultramafic rocks intruded by mostly anatectic Devonian and Mississippian granitoids (Bier et al., 2002; Merschat and Kalbas, 2002; Merschat et al., 2005a) (Fig. 5–3). Primary sedimentary structures were obliterated by multiple transposition and high metamorphic grade. Schist and metapsammite are interlayered from outcrop to map-scale, but they form separable mappable units throughout the terrane.

Mafic and ultramafic rocks are not common in the Cat Square terrane, but reconnaissance and detailed geologic mapping documents several mafic and lesser ultramafic bodies (e.g., Overstreet et al., 1963; Privett, 1984; Mittwede et al., 1987; Goldsmith et al, 1988; Merschat, 2003; Wilson, 2006). Amphibolites are commonly layered, consisting of alternating dark layers of hornblende, plagioclase, and other minor minerals separated by thin layers of quartz and feldspar. Ultramafic rocks are foliated and altered to chlorite, scapolite, tremolite, serpentine, talc schists with rare olivine and relict pyroxene (Privett, 1984; Mittwede et al., 1987; Goldsmith et al., 1988). These bodies are enveloped in both metapsammite and pelitic schist of the Cat Square terrane. Size of the bodies varies significantly, but the largest mafic and ultramafic bodies occur in the eastern part of the Cat Square terrane near the central Piedmont suture (Fig. 5–3). Several large mafic and ultramafic bodies also occur in the Newton window (Fig. 5–3) near the central Piedmont suture, but recent geochronology suggests this antiformal structure is a window through the Brindle Creek thrust sheet, exposing the eastern Tugaloo terrane (Merschat et

Figure 5–3. Simplified geologic map of the Cat Square terrane from its northern extent to near the Georgia-South Carolina border. Modified from a compilation by Merschat and Hatcher (2003). Dt–Toluca Granite. Dwt–Walker Top Granite with U-Pb ages from Gatewood (2007)[1] ,Giorgis et al., (2002)[2], and Mapes, (2002)[3]. hgu–Hammett Grove metaigneous mafic-ultramafic body. Mc–Cherryville Granite. Mgc–Gray Court granite. Mrr–Reedy River granite. PMF–Paris Mountain thrust sheet, a remnant of the original Brindle Creek thrust sheet that broke through as an out-of-sequence fault. Sm–Sandy Mush granite. tu–Turnersberg ultramafic.

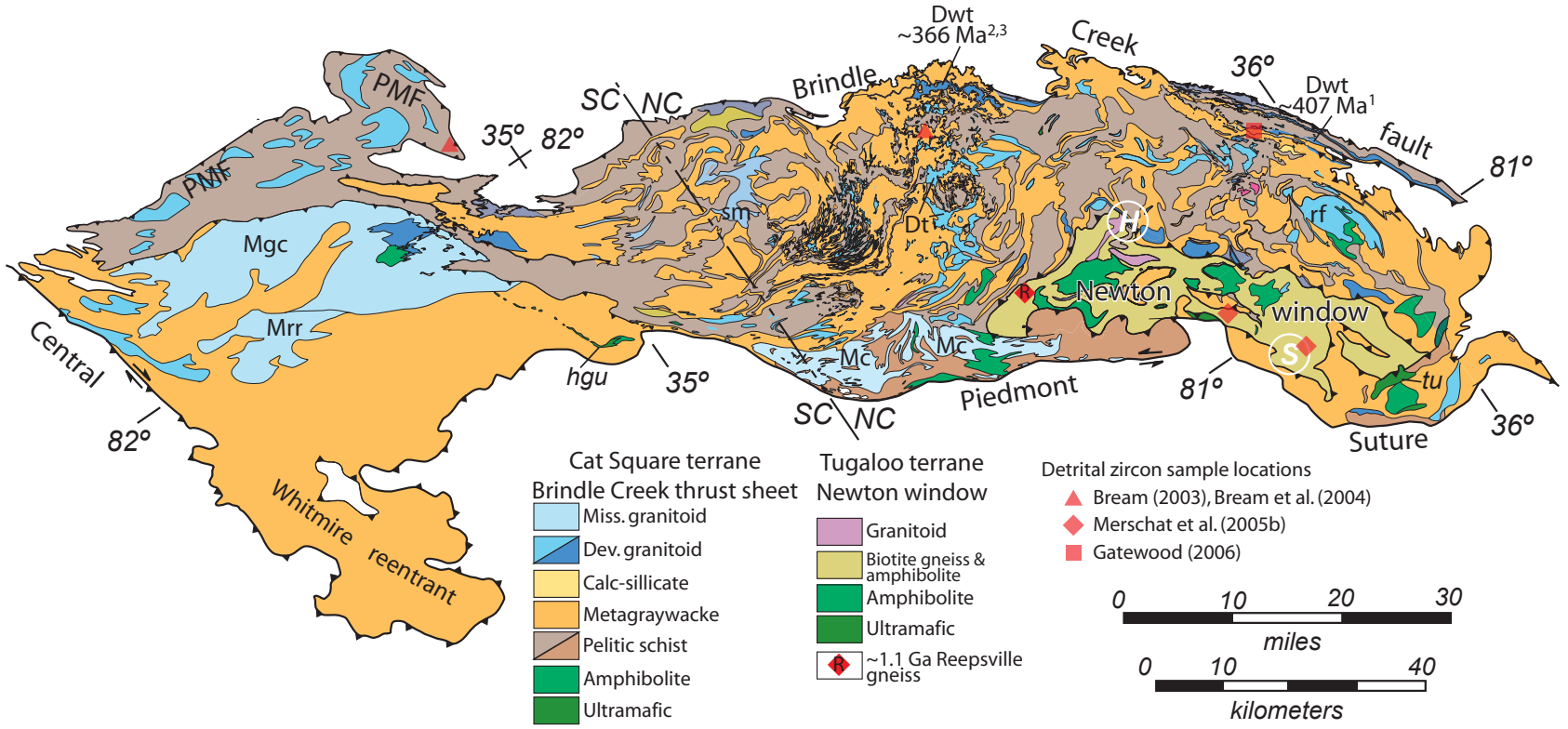
Dwt
~366 Ma2,3
Creek
36°
Dwt
~407 Ma1
fault
81°
PMF
PMF
35°
82°
SC
NC
Brindle
sm
Dt
rf
Mgc
Mrr
Newton
window
Central
hgu
35°
Mc
Mc
81°
tu
36°
82°
SC
NC
Piedmont
Suture
Whitmire reentrant
Cat Square terrane
Brindle Creek thrust sheet
Miss. granitoid
Dev. granitoid
Calc-sillicate
Metagraywacke
Pelitic schist
Amphibolite
Ultramafic
Tugaloo terrane
Newton window
Granitoid
Biotite gneiss & amphibolite
Amphibolite
Ultramafic
~1.1 Ga Reepsville gneiss
Detrital zircon sample locations
Bream (2003), Bream et al. (2004)
Merschat et al. (2005b)
Gatewood (2006)
0 10 20 30
miles
0 10 40
kilometers

al., 2005b). Wilson (2006) reported trace and major element geochemistry of Cat Square terrane amphibolites from the Brushy Mountains are representative of oceanic crust with E-MORB and backarc affinities. The lenticular Hammett Grove meta-igneous suite in the eastern Cat Square terrane in northwestern South Carolina (Fig. 5–3) consists of steatized and serpentinized ultramafic rocks, metapyroxenite, metagabbro, and amphibolite (Mittwede et al., 1987). Based on rock assemblage and chemical composition Mittwede et al. (1987) concluded that the Hammet Grove meta-igneous suite represents a deformed ophiolite emplaced in front of the Carolina superterrane.

Numerous peraluminous Devonian and Mississippian granitoids intrude the Cat Square terrane. Devonian intrusions include the medium- to coarse-grained, weakly to well foliated ~378 Ma Toluca Granite (Mapes, 2002) and disconnected bodies of texturally similar megacrystic granites of the Walker Top plutonic suite yielding ages of ~407 Ma (Brushy Mountains; Gatewood, 2007) and ~366 Ma (South Mountains; Giorgis et al., 2002; Mapes, 2002). Chemistry and isotopic signature of the Toluca and Walker Top Granites indicate that they are anatectic and likely derived from melting Cat Square terrane metapelite and metapsammite protoliths (Giorgis et al., 2002; Mapes, 2002). The ~355 Ma Cherryville Granite, ~357 Ma Gray Court, and ~325 Ma Reedy River granitoids occur along the eastern flank of the Cat Square terrane and have a similar origin (Mapes, 2002). Concordant contacts, lack of contact aureoles, and metamorphic assemblages of country rocks suggest that these are catazonal plutons. Assuming that these Devonian and Mississippian granitoids are anatectic melts and do not add new material to the terrane, a minimum thickness of the Cat Square terrane can be estimated at ~4 km (~13,000 ft) from various small-scale cross sections (Goldsmith et al., 1988; Nelson et al., 1998; Hatcher and Merschat, 2006).

SILURO-DEVONIAN CAT SQUARE REMNANT OCEAN BASIN

Despite the Cat Square terrane being highly deformed and metamorphosed, map relationships combined with geochronology and geochemistry permit a limited reconstruction of the Cat Square basin. Detrital zircons indicate that sediment was derived from both Laurentia and a peri-Gondwanan terrane (Bream et al., 2004). The closest and likeliest peri-Gondwanan source is the Carolina superterrane. Electron-microprobe monazite ages of ~530 Ma link the Smith River allochthon to the Carolina superterrane (Hibbard et al., 2003) (Fig. 5–2). The present structural position of the Smith River allochthon suggests that the Carolina superterrane overrode the Inner Piedmont.

Timing of deposition is bracketed by the youngest detrital zircons, ~430 Ma, and ages of the oldest anatectic Devonian intrusions. Deposition ended prior to ~407 Ma formation of anatectic Walker Top (Brushy Mountains), when the rocks would have been buried 15–20 km. Intrusion of the subduction-related Concord and Salisbury plutonic suites into the Carolina superterrane (McSween et al., 1984; McSween and Harvey, 1997; Esawi, 2004), and the oldest metamorphic rims (~400 Ma) observed on Cat Square terrane detrital zircons (Bream 2002, 2003) support eastward subduction of material beneath the Carolina superterrane during this same interval (430-400 Ma). The entire volume (minimum ~55,059 km^3) of the Cat Square terrane would have been deposited over a 23 m.y. time span (a minimum rate of 0.17 mm/yr).

An enigmatic aspect of the Inner Piedmont is the lack of continental basement on which Inner Piedmont rocks were deposited. The 1,143 ± 33 Ma Forbush Gneiss (Carrigan et al., 2003) exposed in the cores of breached antiforms along the Forbush fault in the southwestern Sauratown Mountains window (McConnell, 1990; Horton and McConnell, 1991) and the 1050±18 Ma Reepsville gneiss exposed in the Newton window (Merschat et al., 2005b) are the only reported continental basement rocks in the Inner Piedmont (Fig. 5–2). Both occur exclusively in the eastern Tugaloo terrane, so they are not basement to the Cat Square terrane. An argument that the older eastern Tugaloo terrane is basement to the Cat Square terrane can be entertained, but the restriction of Devonian magmatism to the Cat Square terrane and truncations of Devonian granitoids against the Brindle Creek fault (e.g. Gatewood et al., 2004; Wilson et al., 2005; Wilson, 2006; Gatewood, 2007) preclude juxtaposition with the eastern Tugaloo/western Inner Piedmont until after ~407 Ma. At Vale, NC, just east of Cat Square crossroads, type locality of the Cat Square terrane (Hatcher, 2002b), a reported charnockite (termed Cat Square charnockite by Kish [1997]) was initially thought to be Grenville basement. Kish (1997), however, reported a U-Pb age of 347-358 Ma and chemistry indicating that the charnockite has a metamorphic origin. Regardless of whether or not the eastern Tugaloo terrane was deposited on continental basement, no evidence supports deposition of Cat Square terrane rocks on continental basement.

We propose that the Cat Square terrane was deposited on oceanic crust, possibly represented by the few large amphibolite bodies throughout the Cat Square terrane. Closely associated altered ultramafic rocks may represent oceanic mantle. Geochemical studies of eastern Inner Piedmont mafic and ultramafic rocks are limited (Mittwede et al., 1987; Wilson, 2006), but generally support a simatic origin. These bodies may constitute pieces of mid- to late-Paleozoic(?) ophiolites on which the Siluro-Devonian Cat Square

terrane metasedimentary rocks were deposited. Emplacement of the mafic and ultramafic bodies likely occurred in an accretionary wedge that developed in front of the Carolina superterrane as the basin closed. The mafic and ultramafic bodies were subsequently modified by high-temperature Neoacadian deformation.

The Devonian to Mississippian Acadian-Neoacadian clastic wedge extends over 1000 km from New England to Alabama, and is 400-700 km wide prograding into the Illinois basin (Dennison, 1985; Ettensohn, 1985, 2004). The Acadian-Neoacadian clastic wedge consists of an aggregate of delta-alluvial complexes that are a mosaic of open-marine, marginal-marine and terrestrial facies (Dennison 1985; Ettensohn, 1985, 2004). Several large and well-documented delta complexes of the Acadian-Neoacadian clastic wedge include the Catskill, Bedford-Berea, Price-Pocono-Grainger, and Borden (Fig. 5–4). The typical unconformity bound lithologic sequence recognized throughout the basin begins with transgressive, shallow marine limestone, overlain by deep water black shale, followed by deep water turbidites, and finally marginal-marine sediments with various red beds (Ettensohn, 2004). The black basinal shales mark periods of subsidence after crustal loading, and are used to track basin subsidence (Ettensohn, 1985). Common to all complexes is a progressive westward and southwestward facies migration indicative of an eastern source that shifted southwestward over time. Dennison (1985) recognized seven to eight lobes of the Catskill delta complex beginning in New York and becoming progressively younger to the southwest. Ettensohn (1985, 2004) proposed four tectophases, or spatially and temporally distinct pulses of sedimentation, during the Acadian-Neoacadian orogeny. The first tectophase was focused in the St. Lawrence Promontory in northern New England during the Early and Middle Devonian, correlating temporally and spatially with the traditional Acadian orogeny (410-380 Ma; Osberg et al., 1989). The second (Middle Devonian) and third (Middle to Late Devonian) tectophases resulted from collisions with the New York and Virginia promontories, respectively. Combined, these two tectophases deposited over 3000 m of sediment in the New York Promontory and over 2400 m in the Virginia Promontory, and represent the Catskill, Bedford-Berea, Price-Pocono, Borden, and Grainger-Ft. Payne delta complexes (Ettensohn, 1985; 2004). In the southern Appalachian foreland these tectophases are represented by the Devonian-Mississippian Chattanooga Shale-Ft. Payne-Grainger Formation unconformably overlying folded and faulted Ordovician and lower Silurian sequences (Hatcher et al., 2005; Hatcher et al., 2007, their Fig. 13). Additional clastics deposited in the southern Appalachian Talladega belt at this time are interpreted as related to the traditional Acadian clastic wedge (Tull, 2002). The final tectophase persisted from

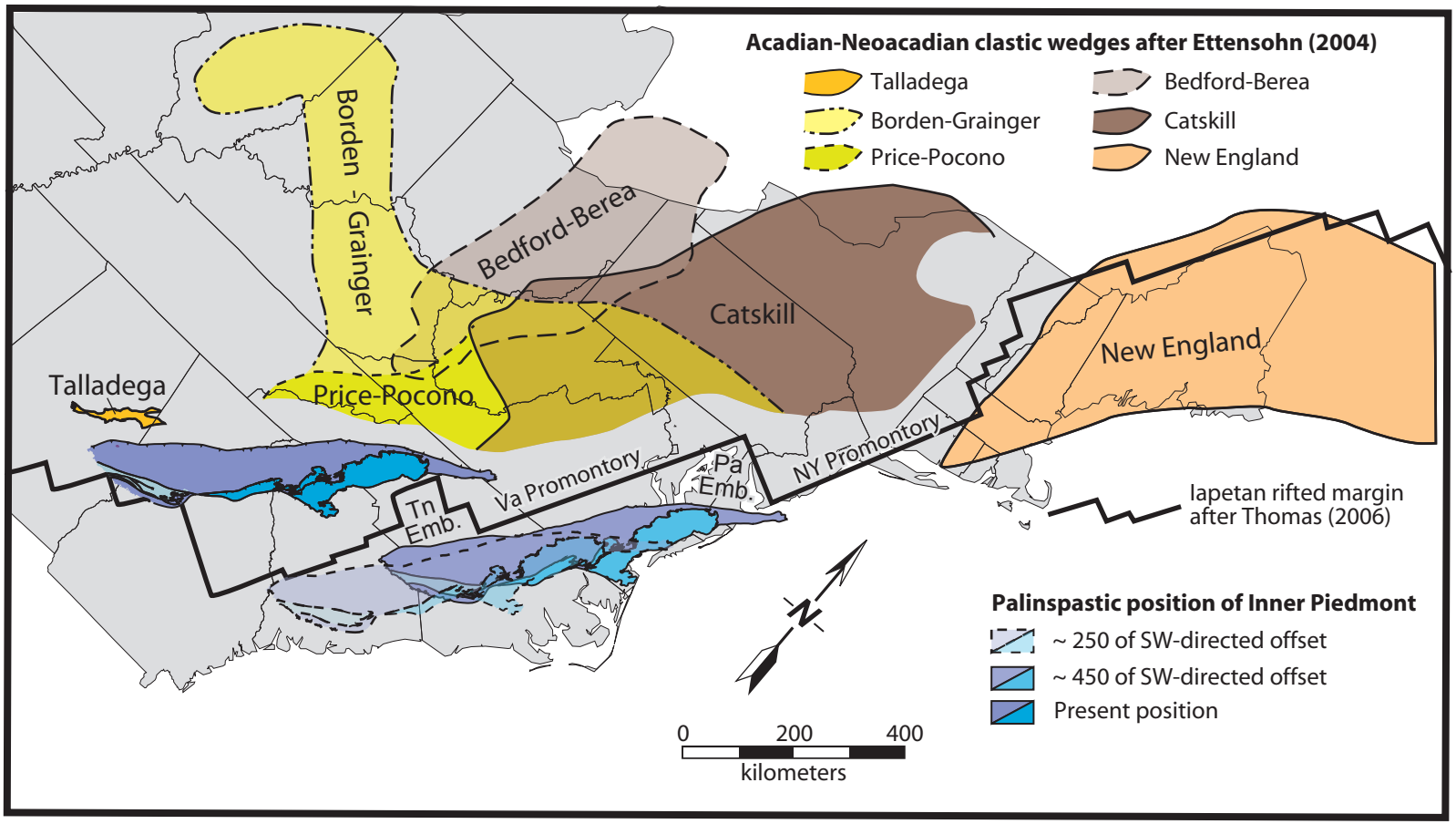

Figure 5–4. Possible palinspastic location of the Inner Piedmont and distribution of major delta complexes of the Acadian-Neoacadian clastic wedge. Locations and shape of clastic wedges after Ettensohn (2004), and Iapten rifted margin from Thomas (2006).

Mississippian to early Pennsylvanian time during which time it migrated southward from its initiation at the Virginia promontory (Ettensohn, 1985, 2004). Tectophases two through four temporally overlap Neoacadian deformation in the Inner Piedmont, but significant lateral offset of the Inner Piedmont from the thickest accumulations in the central Appalachians make correlations difficult (Fig. 5–4). Collectively, southwestward migration of the Acadian-Neoacadian clastic wedge supports an oblique, transpressive, zippered collision of the Avalon-Carolina arc with Laurentia during the Devonian (Dennison, 1985; Ettensohn, 1985, 2004). Collision progressed from NE to SW occurring first in the St. Lawrence promontory, then moving southwestward to the New York and Virginia promontories (Dennison, 1985; Ettenshon, 2004).

Palinspastic restoration of the Inner Piedmont links Devonian-Mississippian high-temperature deformation in the crystalline core with the southwestward-migrating Acadian-Neoacadian clastic wedge in the foreland. The Brevard fault zone has a complex history recording at least two phases of dextral strike-slip activity during the Neoacadian (~360 Ma) and early Alleghanian (~325 Ma; Hatcher, 2001). Merschat et al. (2005a) suggested that the high-temperature mid-Paleozoic Brevard fault zone (Neoacadian) has at least 200 km of SW-directed dextral displacement, and possibly 400 km or greater (Dennis, 2005). SW-directed displacement associated with the early Alleghanian Brevard fault zone has been estimated to be at least 50 km by Hatcher (1989), but may be considerably more when compared with estimates for similar Alleghanian dextral faults (e.g. Bailey et al., 2004). Removal of the SW-directed displacement during Neoacadian and early Alleghanian reactivation of the Brevard fault zone restores the Inner Piedmont to a position in the central Appalachians during the Early Devonian (Fig. 5–4). This palinspastic position provides critical insight into Appalachian tectonics. First, the location of the Cat Square basin was in the Pennsylvania embayment, between the New York and Virginia Promontories, and possibly extended into the Tennessee embayment. Uplifted crust from colliding promontories shed sediment into both the peripheral foreland basin and Cat Square basin. Secondly, this position links mid-Paleozoic deformation in the Inner Piedmont with the prograding Acadian-Neoacadian clastic wedge and its southwestward migration. Structural patterns in the Inner Piedmont and the southwest migrating clastic wedge are consistent with oblique transpressive collision, and sequential NE to SW closure of the basin.

A corollary to our analysis is that the western Tugaloo terrane also had to be transported southwestward by a distance similar to that of the eastern Tugaloo and Cat Square terranes. Otherwise the same stratigraphic sequence (Tallulah Falls-Ashe

Formation) would likely not occur in proximity across the Brevard fault zone (Hatcher, 2002b). Middle Devonian, amphibolite facies, dextral strike-slip kinematics have been documented along the Burnsville fault, bounding the western Tugaloo terrane in northwestern North Carolina (Adams et al, 1995; Trupe et al., 2003) supporting SW-directed transport of the western Tugaloo during the Neoacadian.

Our reconstruction of the Siluro-Devonian Cat Square basin shares several similarities with the remnant-ocean-basin models of Graham et al. (1975) and Ingersoll et al. (1995, 2003) including: (1) shrinking ocean basin; (2) short lifespan; (3) sedimentary petrotectonic assemblage; (4) mixed crustal affinity; and (5) oblique collision and sequential northeast-to-southwest closure of the basin. The Cat Square basin was likely the last remnant of the Rheic ocean separating Laurentia and the approaching Carolina superterrane (Fig. 5–5). The remnant ocean basin existed from, at most, 430 to 407 Ma, and its closure marked the Late Devonian subduction of the Rheic ocean and accretion of the Carolina superterrane to Laurentia. The <25 m.y. duration of the Cat Square basin is consistent with the lifespan of other modern and ancient remnant ocean basins (Ingersoll and Busby, 1995). The Cat Square terrane is the deformed equivalent of the flysch facies and fragments of an ophiolitic suite in an idealized sequence of a closed remnant ocean basin (Ingersoll et al., 1995) (Fig. 5–6). Interlayered pelitic schist and metapsammite are lithologies consistent with sediment derived from uplifted basement terranes (Laurentia) and magmatic arcs (Carolina superterrane) (Ingersoll et al., 1995). Graham et al. (1975) recognized that sequential closure of remnant ocean basins typically causes longitudinal sediment dispersal parallel to the suture and the axis of the basin. Recent models explaining the complex structural patterns in the Inner Piedmont have proposed oblique, NW-directed convergence of the Carolina superterrane (e.g., Merschat et al., 2005a). These are supported by the palispastic position of the Inner Piedmont and the SW-migrating clastic wedge. Oblique collision would produce a diachronous suture that closed from north to south, like a zipper. Sediment would have been dispersed longitudinally southward into the Siluro-Devonian Cat Square basin and would sample both terranes resulting in mixed affinity rocks (Bream et al., 2004). We suggest that the Cat Square terrane represents a Siluro-Devonian remnant ocean basin separating Laurentia from the Carolina superterrane that records the Devonian closing of the Rheic ocean and subduction beneath the Carolina superterrane (Fig. 5–5).

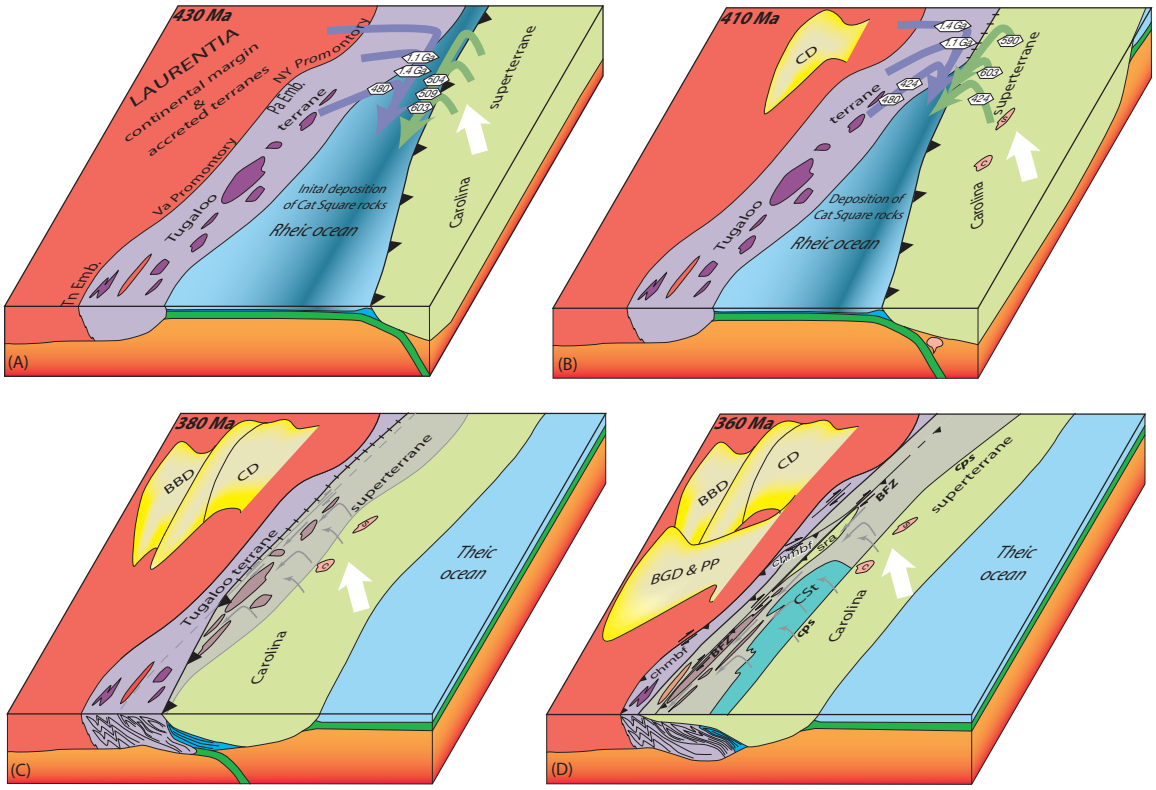

Figure 5–5. Maps representing the sequential tectonic history of the Cat Square terrane. (a) Silurian configuration of Laurentia, Tugaloo terrane with mid-Ordovician plutons (dark purple), and Carolina superterrane separated by Rheic ocean. White arrows indicate motion of the Carolina superterrane. (b) Continued closure of the Rheic ocean and deposition of Cat Square terrane rocks during the Early Devonian. Magmatism in the Carolina superterrane, indicated by the Concord and Salisbury plutonic suites, is the product of subduction of the basin beneath the Carolina superterrane. (c) Closure of the Rheic ocean and suturing of Carolina superterrane by ~380 Ma. Gray lines indicate location of Brevard fault zone and ductile flow of Inner Piedmont material beneath the Carolina superterrane. (d) Neoacadian configuration resulting from dextral transpression. BBD–Bedford-Berea delta. BFZ–Brevard fault zone. BGD–Borden-Grainger delta. c–Concord Plutonic suite. CD–Catskill delta. chmbf–Chattahoochee-Holland Mountain-Burnsville fault. cps–central Piedmont suture. CSt–Cat Square terrane. PP–Price-Pocono delta. s–Salisbury Plutonic suite. sra–Smith River Allochthon.

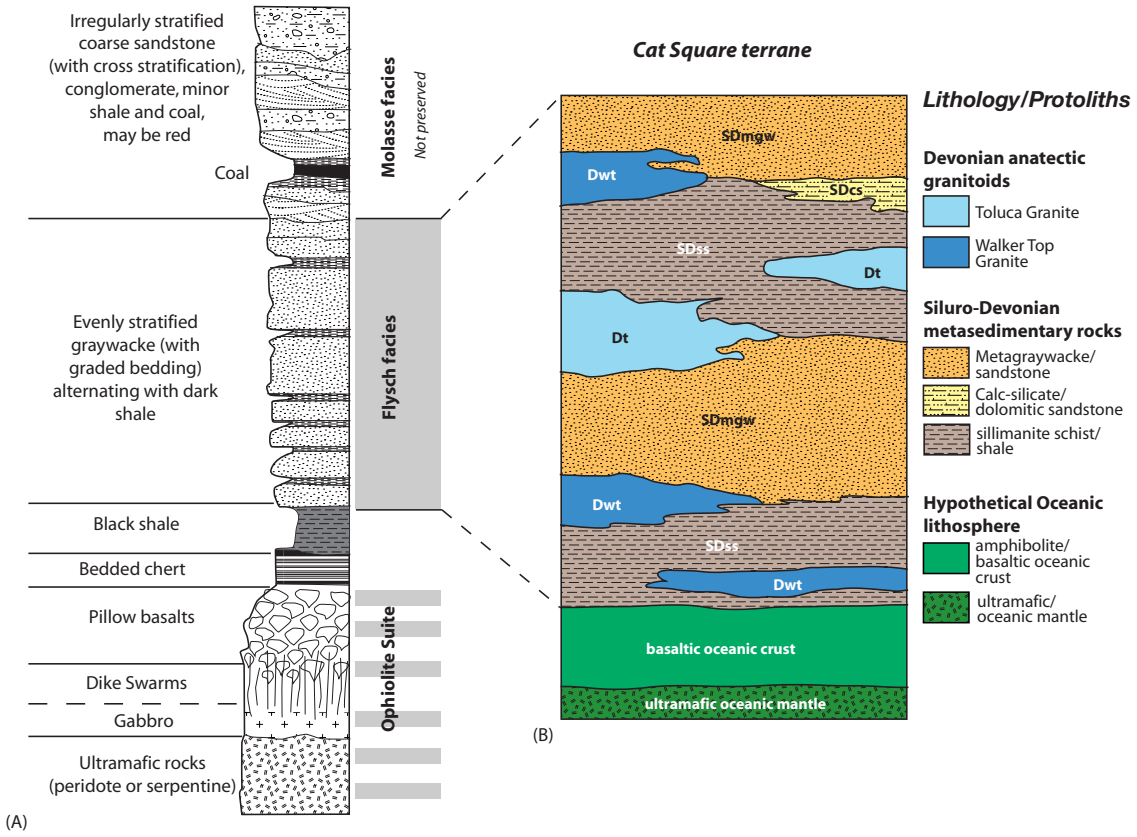

Figure 5–6. (a) Idealized stratigraphic column of a remnant ocean basin (modified from Ingersoll et al., 1995). Gray shading indicates parts of the idealized stratigraphic section likely preserved in the Cat Square terrane. (b) Schematic stratigraphic column highlighting the similarities of the petrotectonic assemblage in the Cat Square terrane and the idealized stratigraphic column of a remnant ocean basin in (a). Rocks of the Cat Square terrane represent the deformed flysch facies and ophiolite suite, respectively. An equivalent proximal molasse facies is not recognized and may never have existed, because the rocks were subducted to midcrustal levels before deposition of the molasse facies. Anatectic Walker Top and Toluca Granites are included because they were derived from metasedimentary rocks of the Cat Square terrane and constrain the minimum age of deposition. SDmgw–metapsammite. SDss–sillimanite schist.

TECTONIC SYNTHESIS

The following tectonic scenario describes the likely evolution and tectonic ramifications of the Cat Square terrane from remnant ocean basin with provenance from approaching terranes to its becoming part of the Inner Piedmont. Deposition of the Cat Square terrane in a remnant ocean basin between Laurentia and approaching Carolina superterrane from 430 to 410 Ma. Palinspastic restoration of the Inner Piedmont northward to the central Appalachians suggests the location of the Cat Square remnant ocean basin was in the Pennsylvania embayment between the New York and Virginia promontories. Eastward subduction of the basin beneath the Carolina superterrane produced Early Devonian magmatism in the Carolina superterrane (Fig. 5–5). The combination of SW-prograding Acadian-Neoacadian clastic wedge and structural patterns in the Inner Piedmont support an oblique, NW-directed transpressive collision initiated in the St. Lawrence promontory and then New York and Virginia promontories. The Cat Square remnant ocean basin was zippered closed from NE to SW and subducted beneath the Carolina superterrane along with part of the Tugaloo terrane and incorporated into the Neoacadian orogen by ~380 Ma (Fig. 5–5b). Metamorphic conditions associated with anatectic formation of the ~378 Ma Toluca Granite require burial of the Cat Square terrane to 15-20 km and temperatures of 800º C, consistent with subduction beneath the Carolina superterrane. Suturing of the Carolina superterrane to Laurentian elements likely produced flysch and molasse that were shed into the central Appalachian foreland basin by ~380 Ma and migrated southwestward into the southern Appalachian foreland basin by ~340 Ma. Peak metamorphic conditions (sillimanite I and II) coeval with peak deformation, D_2 fabrics and structures affected the Cat Square terrane as they became part of the Inner Piedmont by 360-350 Ma. Curved high-temperature NW-rotating to SW-directed flow resulting from oblique convergence of the Carolina superterrane transported Inner Piedmont thrust sheets W and eventually SW several hundred kilometers along the mid-Paleozoic Brevard fault zone (Fig. 5–5c, 5–5d). Hatcher and Merschat (2006) have suggested that the high-temperature curved ductile flow in the Inner Piedmont is a tectonically forced orogenic channel.

CONCLUSIONS

1. The Cat Square terrane consists of pelitic schist, metapsammite, and lesser amphibolite and ultramafic rocks. These rocks were intruded by anatectic Devonian-Mississippian granitoids.

2. The Cat Square terrane was deposited in a Siluro-Devonian remnant ocean basin between eastern Laurentian terranes and the approaching peri-Gondwanan Carolina superterrane.
3. Palinspastic restoration of the Inner Piedmont delimits the location of the Cat Square basin to Pennsylvania embayment between the New York and Virginia Promontories and links uplift as a product of 380–350 Ma deformation in the Inner Piedmont with the Acadian clastic wedge.
4. Southwest migration of the Acadian-Neoacadian clastic wedge and structural patterns in the Inner Piedmont are compatible with oblique NW-directed collision of the Carolina superterrane with the Laurentian margin. Closure of the Cat Square basin zippered shut from NE to SW.
5. The Cat Square terrane is the deformed equivalent of a remnant ocean basin. Rare amphibolite and ultramafic bodies may represent a deformed mid- to late-Paleozoic ophiolite suite consisting of metamorphosed mantle, and oceanic crust overlain by interlayered pelitic and psammitic rocks of the Brindle Creek thrust sheet. Interlayered schist and metapsammite sequences likely represent metamorphosed turbidites (flysch facies) shed from the evolving suture zone between Laurentia and the approaching Carolina superterrane.
6. The tectonic history of the Cat Square terrane provides insight into the brief life span of an ancient remnant ocean basin. The basin existed for less than 25 m.y. before being subducted to mid-crustal depths, metamorphosed to upper amphibolite facies (sillimanite I and II assemblages), and transported ~400 km southwestward from the central to southern Appalachians by 350 Ma during the Neoacadian orogeny. Evolution of the Cat Square terrane from basin to metamorphic core occurred in less than 80 m.y.

ACKNOWLEDGMENTS

U.S. National Science Foundation grants GA–1409, GA–20321, EAR–810852, EAR–8206949, EAR–8417894, and EAR–9004604 to RDH supported much of the field work in the Carolinas and northeast Georgia Inner Piedmont by RDH and graduate students during the 1970s, 1980s, 1990s, and early 2000s. EAR–9814800 supported the detrital zircon SHRIMP geochronology. Additional support during the late 1960s and early 1970s was provided to RDH by the South Carolina Geological Survey, Henry S. Johnson, Jr., and Norman K. Olson, state geologists. Graduate student field work in the late 1990s and 2000s has been supported by the EDMAP component of the

National Cooperative Geologic Mapping Program administered by the U.S. Geological Survey. The University of Tennessee Science Alliance Center of Excellence also has provided considerable support for RDH and students since 1986. Reviews by William R. Dickinson and Raymond V. Ingersoll significantly improved the manuscript. We remain culpable, however, for any errors of fact or interpretation.

REFERENCES CITED

Abbott, R. N., Jr., and Raymond, L. A., 1984, The Ashe Metamorphic Suite, northwest North Carolina: Metamorphism and observations on geologic history: American Journal of Science, v. 284, p. 350-375.

Adams, M. G., Stewart, K. G., Trupe, C. H., and Willard, R. A., 1995, Tectonic significance of high-pressure rocks and dextral strike-slip faulting along the Taconic suture, *in* Hibbard, J. P., van Stall, C. R., and Cawood, P. A., eds., Current perspectives in the Appalachian-Caledonian orogen: Geological Association of Canada, Special Paper 41, p. 21-42.

Bailey, C. M., Francis, B. E., and Fahrney, E. E., 2004, Strain and vorticity analysis of transpressional high-strain zones from the Virginia Piedmont, USA, *in* Alsop, G. I., Holdsworth, R. E., McCaffrey, K. J., W., and Hand M., eds., Flow Processes in faults and shear zones: Geological Society of London, Special Publication 224, p. 249-264.

Bier, S. E., Bream, B. R., and Giorgis, S. D., 2002, Inner Piedmont stratigraphy, metamorphism, and deformation in the Marion-South Mountains area, North Carolina, *in* Hatcher, R. D., Jr., and Bream, B. R., eds., Inner Piedmont geology in the South Mountains-Blue Ridge Foothills and the southwestern Brushy Mountains, central-western North Carolina: Carolina Geological Society Guidebook, p. 65-100.

Bream, B. R., 2002, The southern Appalachian Inner Piedmont: New perspectives based on recent detailed geologic mapping, Nd isotopic evidence, and zircon geochronology, *in* Hatcher, R. D., Jr., and Bream, B. R., eds., Inner Piedmont geology in the South Mountains-Blue Ridge Foothills and the southwestern Brushy Mountains, central-western North Carolina: Carolina Geological Society Guidebook, p. 45-63.

Bream, B. R., 2003, Tectonic implications of geochronology and geochemistry of para- and orthogneisses from the southern Appalachian crystalline core [Ph.D. dissertation]: Knoxville, University of Tennessee, 296 p.

Bream, B. R., Hatcher, R. D., Jr., Miller, C. F., and Fullagar, P. D., 2001, Geochemistry and provenance of Inner Piedmont paragneisses, NC and SC: Evidence for an internal terrane boundary?: Geological Society of America Abstracts with Programs, v. 33, no. 2, p. 65.

Bream, B. R., Hatcher, R. D., Jr., Miller, C. F., and Fullagar, P. D., 2004, Detrital zircon ages and Nd isotopic data from the southern Appalachian crystalline core, GA-

SC-NC-TN: New provenance constraints for Laurentian margin paragneisses, *in* Tollo, R. P., Corriveau, L., McLelland, J., and Bartholomew, M. J., eds., Proterozoic evolution of the Grenville orogen in North America: Geological Society of America Memoir 197, p. 459-475.

Carrigan, C. W., Bream, B. R., Miller, C. F., and Hatcher, R. D., Jr., 2001, Ion microprobe analyses of zircon rims from the eastern Blue Ridge and Inner Piedmont, NC-SC-GA: Implications for the timing of Paleozoic metamorphism in the southern Appalachians: Geological Society of America Abstracts with Programs, v. 33, no. 2, p. 7.

Carrigan, C. W., Miller, C. F., Fullagar, P. D., Bream, B. R., Hatcher, R. D., Jr., and Coath, C. D., 2003, Ion microprobe age and geochemistry of southern Appalachian basement, with implications for Proterozoic and Paleozoic reconstructions: Precambrian Research, v. 120, p. 1-36.

Davis, T. L., 1993a, Lithostratigraphy, structure, and metamorphism of a crystalline thrust terrane, western Inner Piedmont, North Carolina [Ph.D. dissertation]: Knoxville, University of Tennessee, 245 p.

Davis, T. L., 1993b, Geology of the Columbus Promontory, western Piedmont, North Carolina, southern Appalachians, *in* Hatcher, R. D., Jr., and Davis, T. L., eds., Studies of Inner Piedmont geology with a focus on the Columbus Promontory: Carolina Geological Society Guidebook, North Carolina Geological Survey, p. 17-43.

Dennis, A. J., 2005, Middle Paleozoic clastic wedge provenance, dextral collision, and the southern Appalachian Inner Piedmont: the Spechty Kopf and Rockwell Formations of the central Appalachians as tectonic markers: Geological Society of America Abstracts with Programs, v. 37, no. 2., p. 5.

Dennis, A. J., and Wright, J. C., 1997, Middle and late Paleozoic monazite U-Pb ages, Inner Piedmont, South Carolina: Geological Society of America Abstracts with Programs, v. 29, no. 3, p. 12.

Dennison, J. M., 1985, Catskill delta shallow marine strata, *in* Woodrow, D. L., and Sevon, W. D., eds., The Catskill delta: Boulder, Colorado, Geological Society of America Special Paper 201, p. 91-106.

Esawi, E. K., 2004, Evidence from the Farmington pluton for Early Devonian subduction-related magmatism in the Carolina zone of central North Carolina: Journal of Geodynamics, v. 37, p. 531-548.

Ettensohn, F. R., 1985, The Catskill delta complex and the Acadian orogeny: A model, *in* Woodrow, D. L., and Sevon, W. D., eds., The Catskill delta: Boulder, Colorado, Geological Society of America Special Paper 201, p. 39-49.

Ettensohn, F. R., 2004, Modeling the nature and development of major Paleozoic clastic wedges in the Appalachian basin, USA: Journal of Geodynamics, v. 37, p. 657-681.

Gatewood, M. P., 2007, Structure and tectonics of the northeastern Inner Piedmont from detailed geologic mapping, geochronologic, geochemical, and petrologic studies with macro-, meso-, and microstructural analyses of ductile fault zones [M.S thesis]: Knoxville, University of Tennessee, 279 p.

Gatewood, M. P., Merschat, A. J., Wilson, C. G., and Hatcher, R. D., Jr., 2004, Inner Piedmont timing relationships and Neoacadian crustal flow, Brushy Mountains, NC: Results from detailed geologic mapping, structural and petrological analyses: Geological Society of America Abstracts with Programs, v. 36, no. 5, p. 504.

Giorgis, S. D., Mapes, R. W., and Bream, B. R., 2002, The Walker Top Granite: Acadian granitoid or eastern Inner Piedmont basement?, *in* Hatcher, R. D., Jr., and Bream, B. R., eds., Inner Piedmont geology in the South Mountains-Blue Ridge Foothills and the southwestern Brushy Mountains, central-western North Carolina: Carolina Geological Society Guidebook, p. 33-44.

Goldsmith, R., 1981, Structural patterns in the Inner Piedmont of the Charlotte and Winston-Salem 2-degree quadrangles, North Carolina and South Carolina, *in* Horton, J. W., Jr., Butler, J. R., and Milton, D. M., eds., Geological investigations of the Kings Mountain belt and adjacent areas in the Carolinas: Carolina Geological Society Field Trip Guidebook, p. 19-27.

Goldsmith, R., Milton, D. J., and Horton, J. W., Jr., 1988, Geologic map of the Charlotte 1-degree x 2-degree quadrangle, North Carolina and South Carolina: U.S. Geological Survey Map I-1251-E, scale 1:250,000.

Graham, S. A., Dickinson, W. R., and Ingersoll, R. V., 1975, Himalayan-Bengal model for flysch dispersal in the Appalachian–Ouachita system: Geological Society of America Bulletin, v. 86, p. 273-286.

Hatcher, R. D., Jr., 1978, Tectonics of the western Piedmont and Blue Ridge, southern Appalachians: Review and speculations: American Journal of Science, v. 278, p. 276-304.

Hatcher, R. D., Jr., 1987, Tectonics of the southern and central Appalachian internides: Annual Review of Earth and Planetary Science, v. 15, p. 337-362.

Hatcher, R. D., Jr., 1989, Tectonic synthesis of the U.S. Appalachians, Chapter 14, *in* Hatcher, R. D., Jr., Thomas, W. A., and Viele, G. W., eds., The Appalachian Ouachita orogen in the United States: Boulder, Colorado, Geological Society of America, The Geology of North America, v. F-2, p. 511-535.

Hatcher, R. D., Jr., 1993, Perspective on the tectonics of the Inner Piedmont, southern Appalachians, *in* Hatcher, R. D., Jr., and Davis, T. L., eds., Studies of Inner Piedmont geology with a focus on the Columbus Promontory: Carolina Geological Society Guidebook, North Carolina Geological Survey, p. 17-43.

Hatcher, R. D., Jr., 2001, Rheological partitioning during multiple reactivation of the Palaeozoic Brevard fault zone, southern Appalachians, USA, *in* Holdsworth, R. E., Strachan, R. A., Magloughlin, J. F., and Knipe, R. J., eds., The nature and tectonic significance of fault zone weakening: London, Geological Society of London Special Publication 186, p. 255-269.

Hatcher, R. D., Jr., 2002a, Alleghanian (Appalachian) orogeny, a product of zipper tectonics: Rotational transpressive continent-continent collision and closing of ancient oceans along irregular margins, *in* Martínez Catalán, J. R., Hatcher, R. D., Jr., Arenas, R., and Díaz García, F., eds., Variscan-Appalachian dynamics: The building of the late Paleozoic basement: Boulder, Colorado, Geological Society of America Special Paper 364, p. 199-208.

Hatcher, R. D., Jr., 2002b, An Inner Piedmont primer, *in* Hatcher, R. D., Jr., and Bream, B. R., eds., Inner Piedmont geology in the South Mountains-Blue Ridge Foothills and the southwestern Brushy Mountains, central-western North Carolina: Carolina Geological Society Guidebook, p. 1-18.

Hatcher, R. D., Jr., and Hooper, R. J., 1992, Evolution of crystalline thrust sheets in the internal parts of mountain chains, *in* McClay, K. R., ed., Thrust tectonics: London, Chapman and Hall, p. 217-234.

Hatcher, R. D., Jr., and Merschat, A. J., 2006, The Appalachian Inner Piedmont: An exhumed strike-parallel, tectonically forced orogenic channel, *in* Law, R. D., Searle, M., and Godin, L., eds., Channel flow, ductile extrusion and exhumation of lower-mid crust in continental collision zones: London, Geological Society of London Special Publication 268, p. 517-540.

Hatcher, R. D., Jr., Bream, B. R., Merschat, A. J., Mapes, R. W., and Miller, C. F., 2005, Evidence for the (Neo-)Acadian orogeny in the southern Appalachians: Geological Society of America Abstracts with Programs, v. 37, no. 2, p. 5.

Hibbard, J. P., Tracy, R. J., and Henika, W. S., 2003, Smith River allochthon: A southern Appalachian peri-Gondwanan terrane emplaced directly on Laurentia?: Geology, v. 31, p. 215-218.

Hopson, J. L., and Hatcher, R. D., Jr., 1988, Structural and stratigraphic setting of the Alto allochthon, NE Georgia: Geological Society of America Bulletin, v. 100, p. 339-350.

Horton, J. W., and McConnell, K. I., 1991, The western Piedmont, *in* Horton, J. W., and Zullo, V. A., eds., The geology of the Carolinas: Knoxville, Tennessee, University of Tennessee Press, p. 36-58.

Ingersoll, R. V., and Busby, C. J., 1995, Tectonics of sedimentary basins, *in* Busby, C. J., and Ingersoll, R. V., eds, Tectonics of sedimentary basins: Cambridge, Massachusetts, Blackwell Science, p. 1-52.

Ingersoll, R. V., Graham, S. A., and Dickinson, W. R., 1995, Remnant ocean basins, *in* Busby, C. J., and Ingersoll, R. V., eds, Tectonics of sedimentary basins: Cambridge, Massachusetts, Blackwell Science, p. 363-392.

Ingersoll, R. V., Dickinson, W. R., and Graham, S. A., 2003, Remnant-ocean submarine fans: Largest sedimentary systems on Earth, *in* Chan, M. A., and Archer, A. W., eds., Extreme depositional environments: Mega end members in geologic time: Boulder, Colorado, Geological Society of America Special Paper 370, p. 191-208.

Kish, S. A., 1997, The Cat Square charnockite—a Paleozoic charnockite in the Inner Piedmont of North Carolina: Geological Society of America Abstracts with Programs, v. 29, no. 3, p. 28.

Mapes, R. W., 2002, Geochemistry and geochronology of mid-Paleozoic granitic plutonism in the southern Appalachian Piedmont terrane, North Carolina-South Carolina-Georgia [M.S. thesis]: Nashville, Vanderbilt University, 150 p.

McConnell, K. I., 1990, Geology and geochronology of the Sauratown Mountains anticlinorium, northwestern North Carolina [Ph. D. dissertation]: Columbia, South Carolina, University of South Carolina, 232 p.

McSween, H. Y., Jr., and Harvey, R. P. 1997, Concord Plutonic Suite: Pre-Acadian gabbro-syenite intrusion in the southern Appalachians, *in* Sinha, A. K., Whalen,

J. B., and Hogan, J. P., eds., The nature of magmatism in the Appalachian orogen: Boulder, Colorado, Geological Society of America Memoir 197, p. 221-234.

McSween, H. Y., Jr., Sando, T. W., Clark, S. R., Harden, J. T., and Strange, E. A., 1984, The gabbro-metagabbro association of the southern Appalachian Piedmont: American Journal of Science, v. 284, p. 437-461.

Merschat, A. J., 2003, Inner Piedmont tectonics in the southwestern Brushy Mountains, North Carolina: Field and laboratory data revealing 3-D crustal flow and sillimanite I and II metamorphism [M.S. thesis]: Knoxville, University of Tennessee, 198 p.

Merschat, A. J., and Hatcher, R. D., Jr., 2003, Digital geologic map of the northern Inner Piedmont, NC-SC-GA: Geological Society of America Abstracts with Programs, V. 35, no. 1, p. 59-60.

Merschat, A. J., and Kalbas, J. L., 2002, Geology of the southwestern Brushy Mountains, North Carolina Inner Piedmont: A summary and synthesis of recent studies, *in* Hatcher, R. D., Jr., and Bream, B. R., eds., Inner Piedmont geology in the South Mountains-Blue Ridge Foothills and the southwestern Brushy Mountains, central-western North Carolina: Carolina Geological Society Guidebook, p. 101-126.

Merschat, A. J., Hatcher, R. D., Jr., and Davis, T. L., 2005a, The northern Inner Piedmont, southern Appalachians, USA: Kinematics of transpression and SW-directed mid-crustal flow: Journal of Structural Geology, v. 27, p. 1252-1281.

Merschat, A. J., Gatewood, M. P., Fisher, C. M., Miller, C. F., Hatcher, R. D., Jr., Wooden, J. L., and Stahr, D. W., III, 2005b, The Newton antiform, NC: A previously unrecognized window through the allochthonous Inner Piedmont thrust stack: Geological Society of America Abstracts with Programs, v. 37, no. 7, p. 20.

Mirante, D. C., and Patino-Douce, A. E., 2000, Melting and migmatization in the southern Appalachian Inner Piedmont of northeast Georgia; the Athens gneiss: Geological Society of America Abstracts with Programs, v. 33, no. 7, p. 297.

Mittwede, S. K., Ødegård, M., and Sharp, W. E., 1987, Major chemical characteristics of the Hammet Grove meta-igneous suite, northwestern South Carolina: Southeastern Geology, v. 28, p. 49-63.

Nelson, A. E., Horton, J.W., and Clarke, J. W., 1998, Geologic map of the Greenville 1° x 2° quadrangle, Georgia, South Carolina, and North Carolina: U.S. Geological Survey Map I-2175, scale 1:250,000.

Osberg, P. H., Tull, J. F., Robinson, P., Hon, R., and Butler, J. R., 1989, The Acadian orogen, Chapter 4, *in* Hatcher, R. D., Jr., Thomas, W. A., and Viele, G. W., eds.,

The Appalachian-Ouachita orogen in the United States: Boulder, Colorado, Geological Society of America, The Geology of North America, v. F-2, p. 179-232.

Overstreet, W. C., Yates, R. G., and Griffits, W. R., 1963, Geology of the Shelby quadrangle, North Carolina: U.S. Geological Survey Map I-384, scale 1:62,500.

Privett, D. R., 1984, The Turnersberg intrusive: petrogenesis of a metamorphosed alpine ultramafite in the eastern Inner Piedmont Iredell County, North Carolina: Southeastern Geology, v. 25, p. 55-60.

Rankin, D. W., Drake, A. A., Jr., Glover, L. III., Goldsmith, R., Hall, L. M., Murray, D. P., Ratcliff, N. M., Read, J. F., Secor, D. T., Jr., and Stanley, R. S., 1989, Pre-orogenic terranes, *in* Hatcher, R. D., Jr., Thomas, W. A., and Viele, G. W., eds., The Appalachian Ouachita orogen in the United States: Boulder, Colorado, Geological Society of America, The Geology of North America, v. F-2, p. 7-100.

Thomas, W. A., 2006, Tectonic inheritance at a continental margin: GSA Today, v. 16, p. 4-11.

Trupe, C. H., Stewart, K. G., Adams, M. G., Waters, C. L., Miller, B. V., and Hewitt, L. K., 2003, The Burnsville fault: Evidence for the timing and kinematics of southern Appalachian Acadian dextral transform tectonics: Geological Society of America Bulletin, v. 115, p. 1365-1376.

Tull, J. F., 2002, Southeastern margin of the middle Paleozoic shelf, southwesternmost Appalachians: Regional stability bracketed by Acadian and Alleghanian tectonism: Geological Society of America Bulletin, v. 114, p. 643-655.

Williams, H., and Hatcher, R. D., Jr., 1983, Appalachian suspect terranes, *in* Hatcher, R. D., Jr., Williams, H., and Zietz, I., eds., Contributions to the tectonics and geophysics of mountain chains: Geological Society of America Memoir 158, p. 33-53.

Wilson, C. G., 2006, Origin and tectonic evolution of the southern Appalachian Neoacadian crystalline core: Evidence from the geology of the Gilreath 7.5-minute quadrangle, North Carolina [M. S. Thesis]: Knoxville, University of Tennessee, 219 p.

Wilson, C. G., Merschat, A. J., Gatewood, M. P., and Hatcher, R. D., Jr., 2005, Metamorphism, kinematics, and crustal flow of the southern Appalachian orogenic core evidence from detailed geologic mapping in the Brushy Mountains, NC: Geological Society of America Abstracts with Programs, v. 37, no. 2, p. 40.

PART VI

The Appalachian Inner Piedmont: An Exhumed Strike-Parallel, Tectonically Forced Orogenic Channel

This chapter was published in the Geological Society Special Publication 268, Channel Flow, Ductile Extrusion and Exhumation in Contintental Collision Zones. The full citation is:

Hatcher, R. D., and Merschat, A. J., 2006, The Appalachian Inner Piedmont: An Exhumed Strike-Parallel, Tectonically Forced Orogenic Channel, in Law, R. D., Searle, M. P., and Godin, L., eds., Channel Flow, Ductile Extrusion and Exhumation in Contintental Collision Zones: London, U.K., Geological Society Special Publication 268, p. 517-541.

My contributions included: (1) providing detailed geologic mapping, (2) structural analysis, (3) compilation of data from the North Carolina, South Carolina, Georgia, and Alabama Blue Ridge and Inner Piedmont, and (4) partial writing and drafting reposibilities.

ABSTRACT

The Appalachian Inner Piedmont (IP) extends along orogenic strike some 700 km from North Carolina to Alabama. Its physical attributes contrast with those of other Appalachian tectonic elements: gentle dip of dominant foliation; imbricate stack of fold nappes; dominant sillimanite grade metamorphism and near ubiquitous migmatization; heterogeneous, non-plane deformation; and earlier S-foliations transposed to C-foliations southeast of the mid-Paleozoic Brevard fault zone forming a 10-20 km-wide amphibolite grade shear zone along the western flank of the IP. The IP contains W- and SW-directed thrust sheets and mineral stretching lineation, sheath folds on all scales, and other indicators that define a curved crustal flow pattern throughout the belt. Field and modern geochronologic data confirm that the IP is not exotic. It contains a Laurentian component (eastern Tugaloo terrane) and an internal terrane (Cat Square) that contains both Laurentian and Gondwanan detrital zircons, separated by the Brindle Creek fault. Cat Square terrane rocks likely accumulated in a Devonian remnant ocean that closed beginning ~400 Ma.

The complex but consistently asymmetric, NW- to W- to SW-directed flow pattern throughout the IP reflects confinement beneath a >15 km-thick overburden produced during subduction of Cat Square and Laurentian components beneath the approaching Carolina superterrane along the Central Piedmont suture. Oblique NE-to-SW transpressive subduction to >15 km depth initiated partial melting, forcing escape from the collision zone in an along-strike orogenic channel. The IP detached from rocks to the

west of the mid-Paleozoic Brevard fault zone as the collision zone tightened and the IP mass flowed ~200 km southwestward in the channel. The top of the channel is preserved at the NE end of the IP, and the base (Brevard fault zone) is preserved to the W and SW. As an exhumed orogenic channel, the curved IP flow paths may provide insight for middle to lower crustal deformation and flow in modern orogens.

INTRODUCTION

Application of the channel flow concept to the Himalayas originated with Nelson et al. (1996) and was further developed by Grujic et al. (1996, 2002), Clark & Royden (2000), and numerically modeled by Beaumont et al. (2004). INDEPTH seismic imaging of the top of Indian crust beneath southern Tibet (Nelson et al. 1996; Hauck et al. 1998) better defined the the India-beneath-Asia crustal geometry that had been hypothesized for many years. It also revealed several "bright spots" beneath the Tibetan Plateau that were interpreted as low velocity melt zones, suggesting magma exists today beneath the Tibetan Plateau. Clark & Royden (2000) and Burchfiel (2004) presented the case for complex flow beneath the eastern Tibetan Plateau based on real-time GPS data, which indicate a complex movement pattern at the present topographic surface. Gravity driven orogenic channel flow explains four key elements of Himalayan tectonics: 1) synchronous but reversed-sense slip on the Main Central Thrust and South Tibetan Detachment; 2) recognition of a low-velocity middle crust beneath Tibet; 3) down-dip projection of the Greater Himalayan sequence to low–velocity (molten) middle crust beneath Tibet; and 4) strain patterns (Hodges, this volume). Yet another perhaps more important test for the channel flow hypothesis is whether or not it can be exported to other orogens. If the model is only applicable to the Himalaya, its importance for advancing our understanding of collisional tectonics becomes minimal. If it can be recognized in other orogens, however, a major step forward will have been made toward better understanding of processes that affect crustal evolution. Beaumont et al. (2004; this volume) produced alternative models analogous to channel flows that might develop in other tectonic settings recognizing that gravity driven (Himalayan type), tectonically driven, and mixed types of channels are possible.

Beaumont et al. (2004) suggested that natural channels are likely more complex than predicted by numerical models using homogeneous crust, and therefore are difficult to recognize. Application of the channel flow concept, which combines simple shear and Poiseuille flow to orogens (Brunel 1986; England & Houseman 1989; Bird 1991; Mancktelow 1995; Nelson et al. 1996; Clark & Royden 2000; Beaumont et al. 2001,

2004) immediately raises two questions. 1) How would the hypothesized channel beneath the Himalayas and Tibetan Plateau look if the upper crust were removed? 2) Are there places in the world where we can view an exhumed channel to better understand its internal components? The central gneiss belt in the southern Grenville province (Culshaw et al. 1983; Hanmer 1988; Culshaw et al. 1997) may be one case where a mid-crustal channel formed that involved strike-normal flow (Jamieson et al. this volume). Azcárraga et al. (2002), however, have described strike-parallel sheath folds and other fault-related structures near the base of the Cabo Ortegal complex in Spain (Galicia). Our purpose here is to suggest that the Appalachian Inner Piedmont (IP) may represent a tectonically forced, orogenic strike-parallel channel.

Recent tectonic models have hypothesized curved ductile flow in the IP at high metamorphic grade during the Devonian and early Mississippian (Merschat et al. 2005). Flow in the IP, instead of being across orogenic strike, was initially directed towards the north and northwest, then deflected west and southwest parallel to strike. This paper compares observations and data related to mid-Paleozoic high-temperature ductile flow in the southern Appalachian IP to channel flow models to determine if the IP may represent a type of exhumed orogenic channel. If a channel existed during high temperature deformation of the IP, it would have been a net along-strike channel wherein crustal material was extruded at the southwest end of the Appalachian orogen. This may provide insight into the nature of ductile flow beneath the eastern part of the Tibetan Plateau where curved flow trajectories may be present in the middle crust.

Alternative interpretations to the IP being an orogenic channel include: (1) A stack of deep crustal, southwest-vergent, fold-nappe thrust sheets. (2) Stacks of southwest-vergent thrust sheets formed under an orogenic "lid" (Laubscher, 1988), or an infrastructure beneath a suprastructure (Wegmann 1935; Haller 1956; Griffin 1971a). (3) The IP is a crustal-scale ductile shear zone (i.e., a shear zone that encompasses the entire IP thickness) that formed in the mid-crust (Davis et al. 1991, Vauchez et al. 1993). Crustal-scale shear zones (that may have relatively small thickness, but deformed over a large region) have been identified in many places (e.g. Azcárraga et al. 2002; Platt & Behrmann 1986), but these are not comparable in magnitude to the IP structures. (4) The IP may be a "metamorphic core complex" (Coney 1980), like part of the Miocene deformation in Alboran zone in the core of the Betic Cordillera, southeastern Spain (Martínez-Martínez et al. 1997); or a mid-crustal, subhorizontal, extensional shear zone comparable to those in the Archean Abitibi-Wawa orogen in the Superior province in Ontario (Moser et al. 1996). The latter formed at some 30 km beneath an undeformed suprastructure.

This would require that the high temperature IP fabrics be extensional; no mesoscopic extensional shear-sense indicators or map-scale structures have been recognized to date to support this alternative hypothesis. The IP fits alternatives (1) through (3), except the strike-parallel vergence cannot be easily explained with these models. We also consider the IP a shear zone that occupies the entire thickness of the IP (Davis et al. 1991; Hatcher 2001). Our purpose here is to suggest a unified model for IP structure and other IP attributes.

TECTONIC SETTING

The IP extends some 700 km along strike from Winston-Salem, North Carolina, southwestward to the Coastal Plain in Alabama (Fig. 6–1). It has been long recognized for its high metamorphic grade and contrasting structural style with adjacent terranes (King 1955; Bentley & Neathery 1970). The IP is composite and consists of the eastern Tugaloo (western IP) and Cat Square terranes, separated by the Brindle Creek thrust (Fig. 6–1). Eastern Blue Ridge (western Tugaloo terrane) rocks west of the Brevard fault cannot be separated stratigraphically from the rocks in the western IP (eastern Tugaloo terrane), however, because the stratigraphic sequences on either side of this fault are the same (Fig. 6–2). The IP is multiply deformed with shallow-dipping meso- and macroscale structures that contrast with those in adjacent terranes. A gently dipping stack of large, crystalline, Type F thrust sheets (formed by plastic excision of the common limb between a recumbent or reclined antiform and synform—fold nappes) (Hatcher & Hooper 1992; Hatcher 2004), shallow-dipping foliations, map-scale sheath folds, curved mineral stretching lineation pattern, dominance of sillimanite grade rocks and migmatite, and a long, hot thermal history, form the attributes of mid-Paleozoic mid-crustal flow in the IP.

Northwest of the Tugaloo terrane are three terranes in the central Blue Ridge: the Dahlonega gold belt, and Cowrock and Cartoogechaye terranes composed of medium to high-grade metasedimentary, metavolcanic, and ultramafic rocks (Fig. 6–1). Farther west is the Laurentian margin consisting of Grenvillian 1.1 Ga and older basement with a cover of rifted-margin sediments. The IP is bordered in the Carolinas, Georgia, and Alabama to the northwest by the Brevard fault zone and to the southeast by the Central Piedmont suture (Fig. 6–1). East of the IP is the Peri-Gondwanan Carolina superterrane, a 500-650 Ma volcanic arc that was metamorphosed ~550 Ma, intruded by 535 Ma plutons after it was amalgamated with another arc (Dennis & Wright 1997a; Hibbard et al. 2003), and collided with Laurentia during the middle Paleozoic.

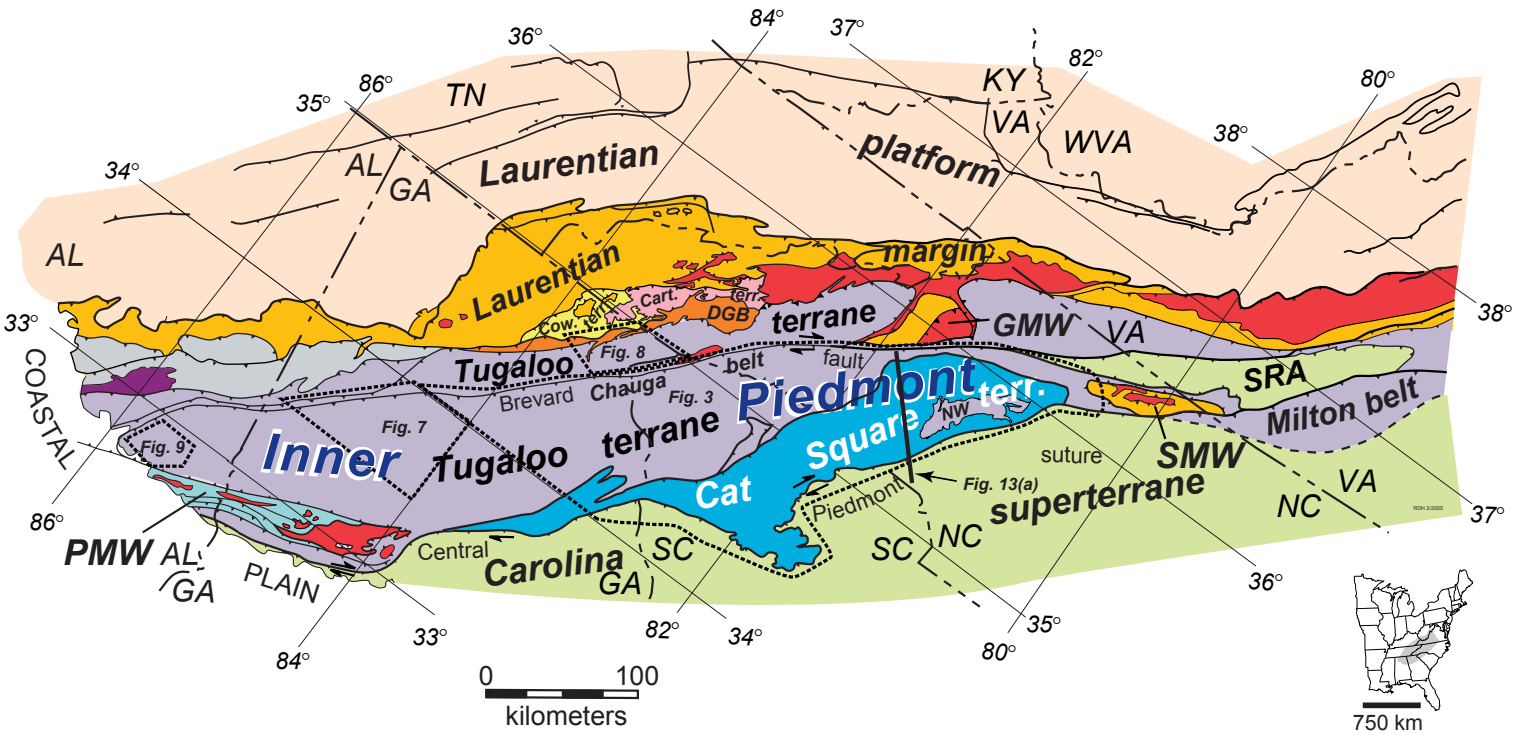

Figure 6–1. Simplified tectonic map of the southern Appalachians showing location of the Inner Piedmont in the Tugaloo (lavender) and Cat Square (blue) terranes. The Laurentian platform (light tan) contains the Alleghanian foreland fold-thrust belt driven in front of the Blue Ridge-Piedmont megatrust sheet, composed of the Laurentian margin (gold with red inliers of Grenvillian—not necessarily Laurentian Grenville, and older inherited crust, Ownby et al. 2004), and all components to the east. All terranes west of the Cat Square terrane have a Laurentian source (Bream et al., 2004). The Cat Square terrane contains Siluro-Devonian metasedimentary rocks with a mixed Laurentian and Peri-Gondwanan source. Carolina superterrane is Peri-Gondwanana and exotic to Laurentia. Cow. Terr.–Cowrock terane. Cart. Terr.–Cartoogechaye terrane. DGB–Dahlonega gold belt. GMW–Grandfather Mountain window. NW–Newton window, predominantly metapsammite, mafic and ultramafic rocks of Tugaloo terrane (Laurentian) affinity. SRA–Smith River allochthon, an outlier of Carolina superterrane rocks. SMW–Sauratown Mountains window. PMW–Pine Mountain window. Light gray–Possible Tugaloo terrane rocks in Alabama and Georgia. Purple (in Alabama)–Ordovician Elkahatchee Quartz Diorite. Dashed boxes indicate locations of smaller figures that detail parts of the IP, as labeled.

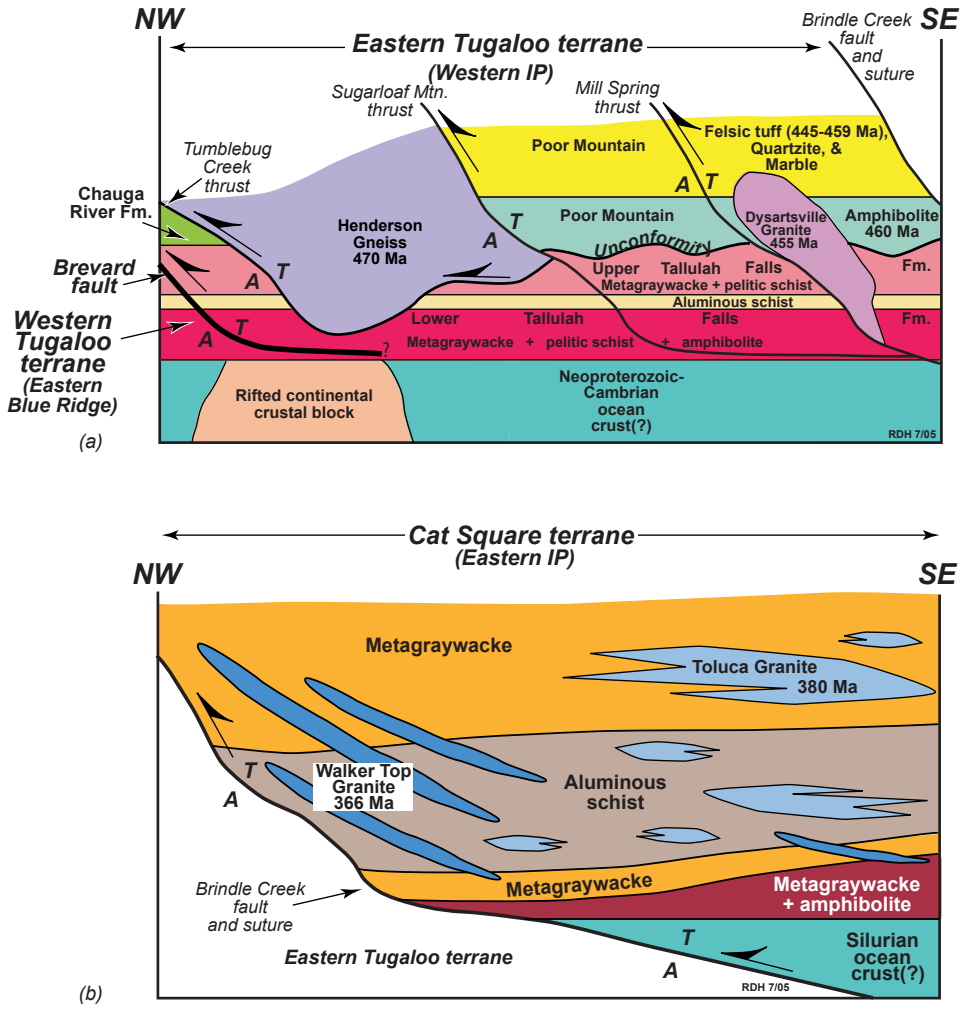

Figure 6–2. Tugaloo and Cat Square terranes lithologic components. (a) Tugaloo terrane sequence showing several Ordovician plutons (purple), possible oceanic and fragmented continental crust upon which the sequences were deposited, Middle Ordovician unconformity, and trajectories of faults that would later propagate through the sequences. (b) Cat Square terrane sequence showing the anatectic Toluca (light blue) and Walker Top (dark blue) granites, and the future trajectory of the Brindle Creek fault.

ATTRIBUTES OF THE INNER PIEDMONT: FACILITATING CONDITIONS OF MID-PALEOZOIC DUCTILE FLOW

Rocks west of the Brevard fault zone in the eastern Blue Ridge (western Tugaloo terrane) contain the same stratigraphic sequence as western IP rocks, with the exception of Middle Ordovician metavolcanic and metasedimentary rocks in the (Fig. 6–2). The dominant assemblage consists of Neoproterozoic-Cambrian(?) deep-water, oceanic, sedimentary, and volcanic rocks (now biotite paragneiss, pelitic and aluminous schist, and amphibolite), metamorphosed to middle and upper amphibolite facies assemblages. These rocks are overlain by Cambrian(?) metasiltstone, quartzite, graphitic schist, and impure, then by Middle Ordovician metavolcanic and metasedimentary rocks (Fig. 6–2). The Middle Ordovician sequence consists of mafic volcanic rocks containing felsic laminae overlain by quartzite-felsic metatuff and relatively pure marble. The felsic metatuff from this sequence has been dated (sensitive high resolution ion microprobe, SHRIMP, U-Pb) at 459 ± 4 and 445 ± 4 Ma (Bream 2003) (Fig. 6–2). The Tugaloo terrane was intruded by Ordovician, Silurian, and Devonian plutons, with some Carboniferous plutons near Atlanta, Georgia. A window of Tugaloo terrane rocks (NW in Fig. 6–1) occurs in the eastern Cat Square terrane in North Carolina, with rocks composed of biotite paragneiss, mafic, and ultramafic rocks. These rocks may be relict early Paleozoic ocean crust and mantle.

The eastern IP (Cat Square terrane) was initially separated from the Tugaloo terrane on the basis of SHRIMP detrital zircon age dates (Bream 2003); otherwise, the two assemblages can only be separated by relative abundances of different lithologies, and some unique sequences to the west. It is bounded to the west by the Brindle Creek thrust and to the SE by the Central Piedmont suture (Fig. 6–1). Cat Square terrane rocks consist of mixed Laurentian-Gondwanan affinity Siluro–Devonian metasedimentary rocks dominated by biotite paragneiss and aluminous schist intruded by Late Devonian and younger anatectic granites, with minor quantities of metabasalt. The Cat Square terrane detrital zircon suite is dominated by Grenvillian 1.1 Ga and older zircons, with additional 600, 500, and 430 Ma. zircons (Bream et al. 2001; Bream 2002, 2003; Bream et al. 2004). The 500-600 Ma zircons were probably shed from the approaching Carolina superterrane, while the older zircons were probably derived from Laurentia (Bream 2003; Merschat et al. 2005). The 430 Ma zircons (unknown source) delimit the maximum age of Cat Square terrane rocks (Bream et al. 2004), but otherwise have an unknown source. Cat Square plutons are all late Devonian and younger and appear to be dominantly anatectic (Mapes 2002).

The Brevard fault separates the eastern from the western Tugaloo terrane, but the Brevard played a key mechanical and kinematic role in the deformational history of the IP (Hatcher 2001; Merschat et al. 2005). A zone of strongly aligned foliations and lineations along the western flank of the IP defines the mid–Paleozoic Brevard fault zone, which consists of a 15 to 20 km wide amphibolite grade dextral shear zone that dips 10 to 45º SE (Hatcher 2001). It is characterized by strongly aligned mylonitic foliation (S_2) striking NE, dipping SE, and a subhorizontal NE–SW– trending mineral lineation (L_2), with a top-to-the-SW shear sense, and was active from at least 360 to 350 Ma (Davis et al. 1991; Davis 1993a,b; Vauchez et al. 1993; Hatcher 2001; Merschat et al. 2005). The primary characteristics of the IP that separate it from Blue Ridge rocks to the west (west of the Brevard fault) are the gentle dip of foliation throughout the IP (Fig. 6–3a and 6–3b), and the curved subhorizontal mineral lineation (Fig. 6–3c and 6–3d). Several studies have demonstrated that the IP is multiply deformed and the dominant structural elements are S_2, $L_{2,}$ and F_2 (e.g. Hopson & Hatcher 1988; Hatcher 2001; Merschat et al. 2005). The dominant S_2 foliation throughout the IP dips gently and becomes strongly NE-SW oriented along the western flank of the IP (Fig. 6–3a). S_2 is defined by parallel alignment of phyllosilicates, quartz ribbons, and other nonequant minerals. Transposed compositional layering and new migmatitic layering parallel to S_2 is axial planar to recumbent to reclined, isoclinal to tight, gently plunging F_2 folds. The high–temperature mineral stretching lineation, L_2, (see Merschat et al. 2005, *their* Fig. 8b) varies in degree of development with rock type and is defined by elongate sillimanite, hornblende, quartz rods, streaked muscovite, or mantled feldspars. Throughout most of the IP L_2 is subhorizontal and coaxial with F_2. Goldsmith (1981) was the first to recognize this arcuate pattern defined by L_2 mineral lineations and F_2 fold hinges. From SE to NW the pattern curves from N-S to NW-SE to E-W to NE-SW (Fig. 6–3c). As stated by Merschat et al. (2005 in press), this mineral lineation, which yields the flow pattern critical to our interpretation, formed during peak metamorphism and has been dated (zircon rims) at 350-360 Ma by Bream et al. (2001) and Bream (2002, 2003). Field and geochronologic relationships clearly indicate that this lineation formed during one event, and the curved pattern is ***not*** the product of overprinting during separate events.

Griffin (1969, 1971a, 1971b, 1974b) was the first to recognize the fold-nappe (Type F of Hatcher & Hooper 1992; Hatcher 2004) structural style in the IP, and concluded these nappes are northwest vergent. The westernmost of these thrust sheets in NE Georgia, South Carolina, and adjacent North Carolina—the Six Mile thrust sheet and Walhalla nappe (Griffin 1969, 1974b, *his* Fig. 13)—place migmatitic rocks at upper

Figure 6–3. Pattern of dominant (S_2) foliation and lineation in the northern Inner Piedmont. (a) Histogram of 4,587 dip measurements of dominant foliation in the northern Inner Piedmont. (b) Form-line map of S_2 foliation in the northern Inner Piedmont. Form lines are parallel to strike; teeth on form lines indicate dip direction. Density of form lines indicates density of data coverage used in map compilation. Based on 4,587 measurements from Hadley & Nelson (1971), Rankin et al. (1972), Espenshade et al. (1975), Heyn (1984), Goldsmith et al. (1988), Nelson et al. (1998), and Hatcher (unpublished data). New data collected after this map was compiled reinforce the broad patterns depicted in this map. (c) Histogram of 764 mostly mineral elongation lineations in the northern IP. Note the dominance of gentle plunges. (d) Distribution of measured lineations (filtered to create cartographic spacing) illustrating the vortex-like pattern in the northern IP. Arrowhead indicates direction of plunge; arrowhead on both ends of line indicates horizontal lineation. Line on each measurement indicates trend. Sources of lineation data are Grant (1958), Hadley & Nelson (1971), Lemmon & Dunn (1973a, 1973b), Griffin (1974a), Whisonant (1979), Conley & Drummond (1981), Goldsmith (1981), Hatcher & Acker (1984), Heyn (1984), Hopson (1984), Willis (1984), Dennis (1989), McConnell (1990), Liu (1991), Davis (1993a), Maybin (1995, 1997), Niewendorp & Maybin (1994a, 1994b), Yanagihara (1994), Niewendorp (1995a, 1995b, 1996, 1997), West (1996, 1997, unpublished data), Curl (1998), Nelson et al. (1998), J.M. Garihan (unpublished data), R.D. Hatcher, Jr (unpublished data), and W.M. Schwerdtner (unpublished data). From Merschat & Hatcher (2005 in press.) Additional measurements added to this data set since the original compilation was made reinforce the curved pattern illustrated by the data (see Figs. 6–7 and 6–12).

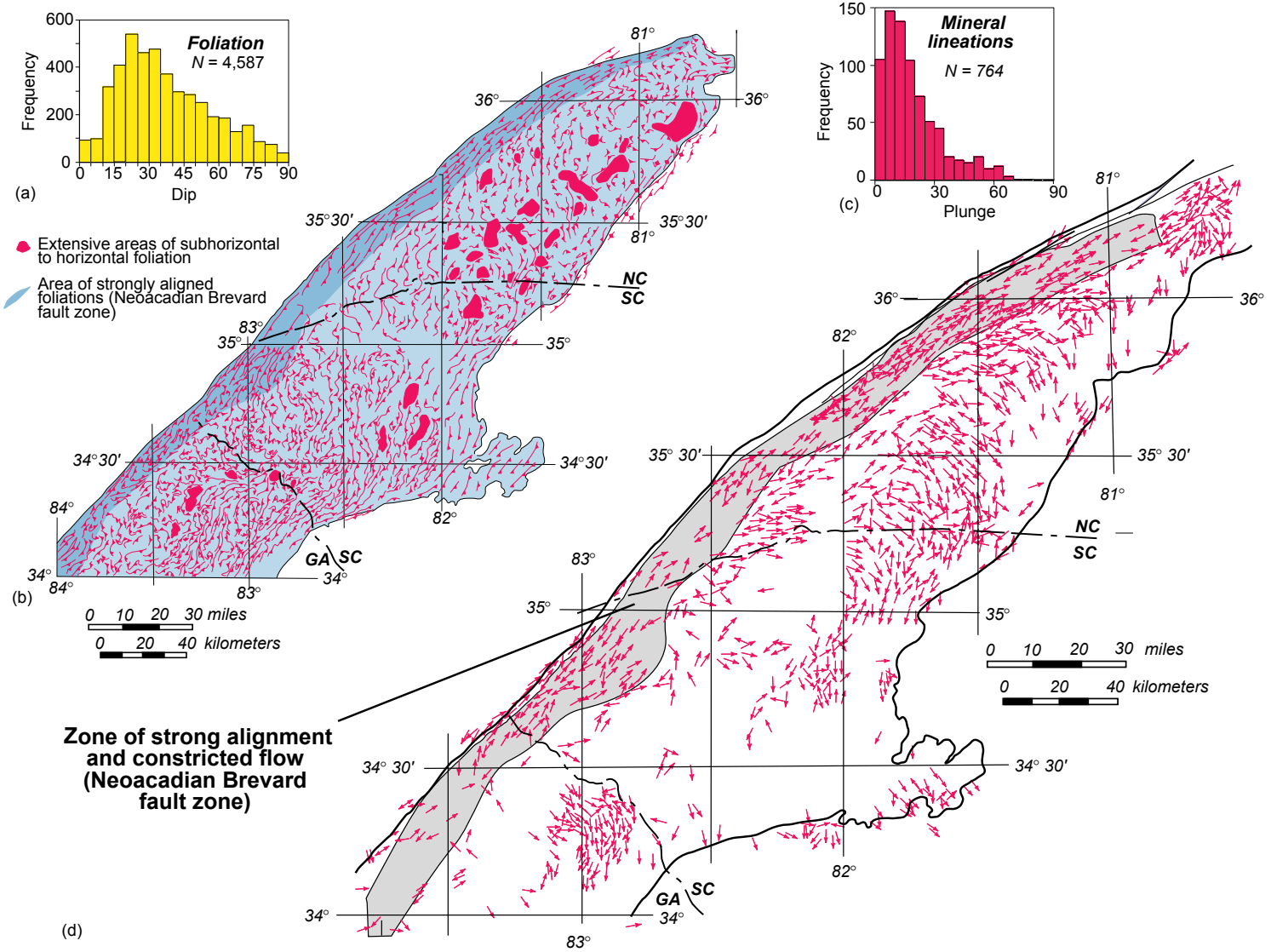
Foliation
N = 4,587
Frequency
Dip
(a)
Extensive areas of subhorizontal to horizontal foliation
Area of strongly aligned foliations (Neoacadian Brevard fault zone)
Mineral lineations
N = 764
Plunge
(c)
NC
SC
GA
SC
(b)
0 10 20 30 miles
0 20 40 kilometers
Zone of strong alignment and constricted flow (Neoacadian Brevard fault zone)
(d)

kyanite or sillimanite grade over lower grade garnet to staurolite grade rocks of the Chauga belt (Hatcher 1972) (Fig. 6–1). Griffin (1974b) depicted the imbricate structure of the western IP in South Carolina in a 3-D block model similar to our modern block model for the northern IP. We similarly interpret the thrust sheets as an infrastructure and the Carolina superterrane a suprastructure above the IP, as the Cat Square and Tugaloo terranes were subducted beneath the Carolina superterrane during mid-Paleozoic time (Fig. 6–4; Merschat et al. 2005). Our block model differs from Griffin's principally in recognizing the southwest vergence of thrust sheets and macroscale sheath folds. The Brevard fault zone constitutes the lower boundary to the IP, while the central Piedmont suture and obducted Carolina superterrane comprises the upper boundary. We infer that the Carolina superterrane collided obliquely and thus diachronously from north to south with the IP so that flow in the migmatitic mass could escape toward the southwest as it was buttressed against the underlying Brevard fault zone. Oblique, zippered northeast-to-southwest collision of Carolina terrane would imply that progressive younging of deformation and metamorphism should also occur. Modern age dates do not exist in western Georgia and Alabama to test this implication, but faults framing the east end of the Pine Mountain window have yielded 330 and 303 Ma ages (Student & Sinha 1992), and these faults truncate IP structures and mesofabrics.

Another fundamental structural characteristic recently documented in the IP is both map- and meso-scale sheath folds (see Merschat et al. 2005, *their* Figs. 8c, 8d, and 11). Because of the small size of exposures throughout most of the IP, we have observed only a few large mesoscale sheath folds (e.g., Fig. 6–5a and Merschat et al. 2005, *their* Figs. 8, 9, and 11), but smaller mesoscale sheath folds are fairly common. Sheath folds that have been observed mostly have southwest-directed transport confirmed independently by numerous shear sense indicators and map patterns (Merschat et al. 2005). In addition, map-scale southwest-directed sheath folds exist in the western IP in South Carolina, and were mapped as southwest-directed thrusts that repeat the Chauga belt sequences (see Merschat et al. 2005, *their* Fig. 9).

Ideally, if the IP is an orogenic channel, the base of the channel should record top-to-the-southwest shear sense and the top should record top-to-the-northeast shear sense. Detailed geologic mapping by Heyn (1984) along the southwest margin of the Sauratown Mountains window in North Carolina (Fig. 6–1) where it meets the lower boundary of the IP reveals top-to-the-southwest shear sense. Similarly, shear-sense indicators at the southwest end of the IP reveal top-to-the-southwest transport (Steltenpohl et al. 1990; Steltenpohl et al. 2005). Detailed geologic mapping and collection of mesofabric data

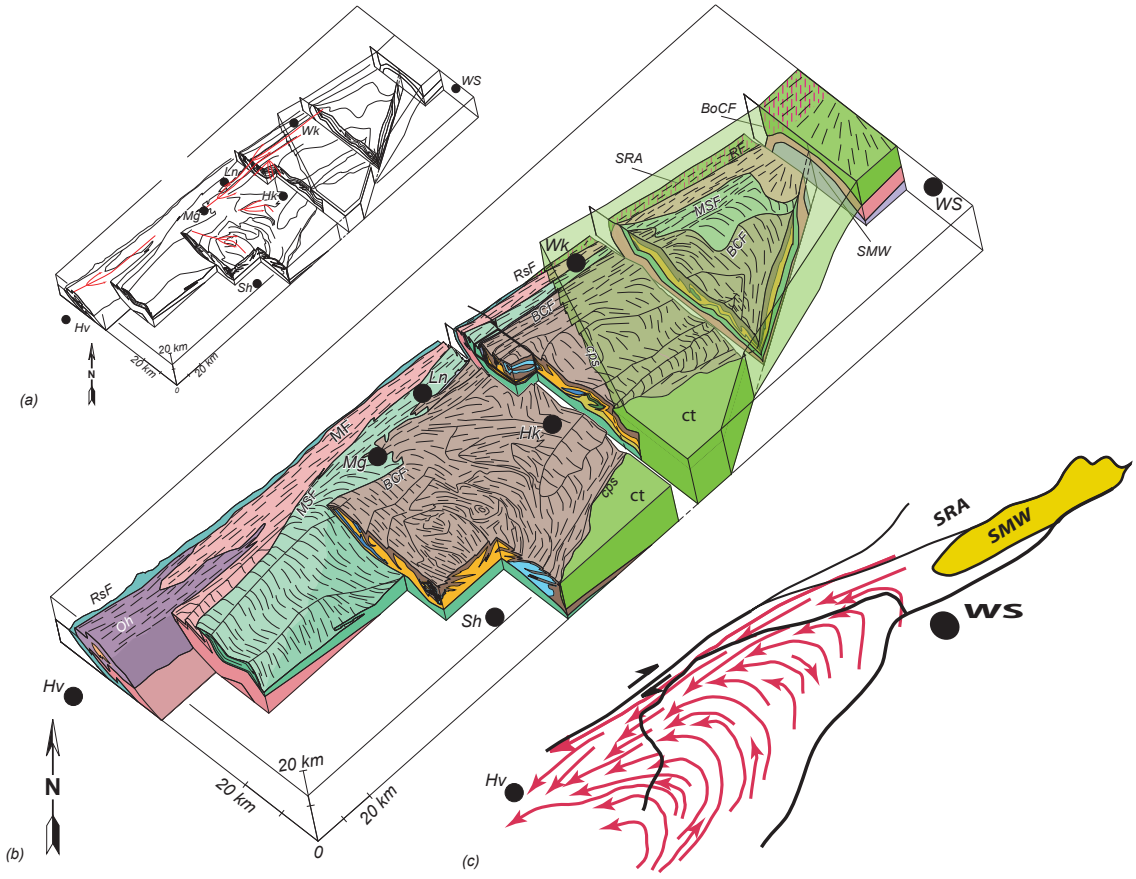

Figure 6–4. 3D structure of part of the northern IP. (a) 3D block diagram depicting the structure of part of the northern IP from near Hendersonville, NC to the Sauratown Mountains window. Red lines are map-scale sheath folds. Vertical exaggeration in (a) and (b) 1.3:1:1 (X:Y:Z). Towns: Hk—Hickory; Hv—Hendersonville; Ln—Lenoir; Mg—Morganton; Sh—Shelby; Wk—Wilkesboro; WS—Winston-Salem. (b) More detailed 3D block diagram of area in (a) showing major tectonic units. Trends on block surface drawn from lineations. BCF—Brindle Creek fault; BoCF—Bowens Creek fault; cps—Central Piedmont suture; ct—Carolina terrane; MSF—Mill Spring fault; MF—Marion fault; Oh—Henderson Gneiss; RF—Ridgeway fault; RsF—Rosman fault; SMW—Sauratown Mountains window; SRA—Smith River allochthon. Town abbreviations sames as in (a). (c) Flow model for the northern Inner Piedmont based on detailed geologic mapping and lineation data of the kind displayed in Figure 6–3. WS–Winston-Salem. Hv–Hendersonville.

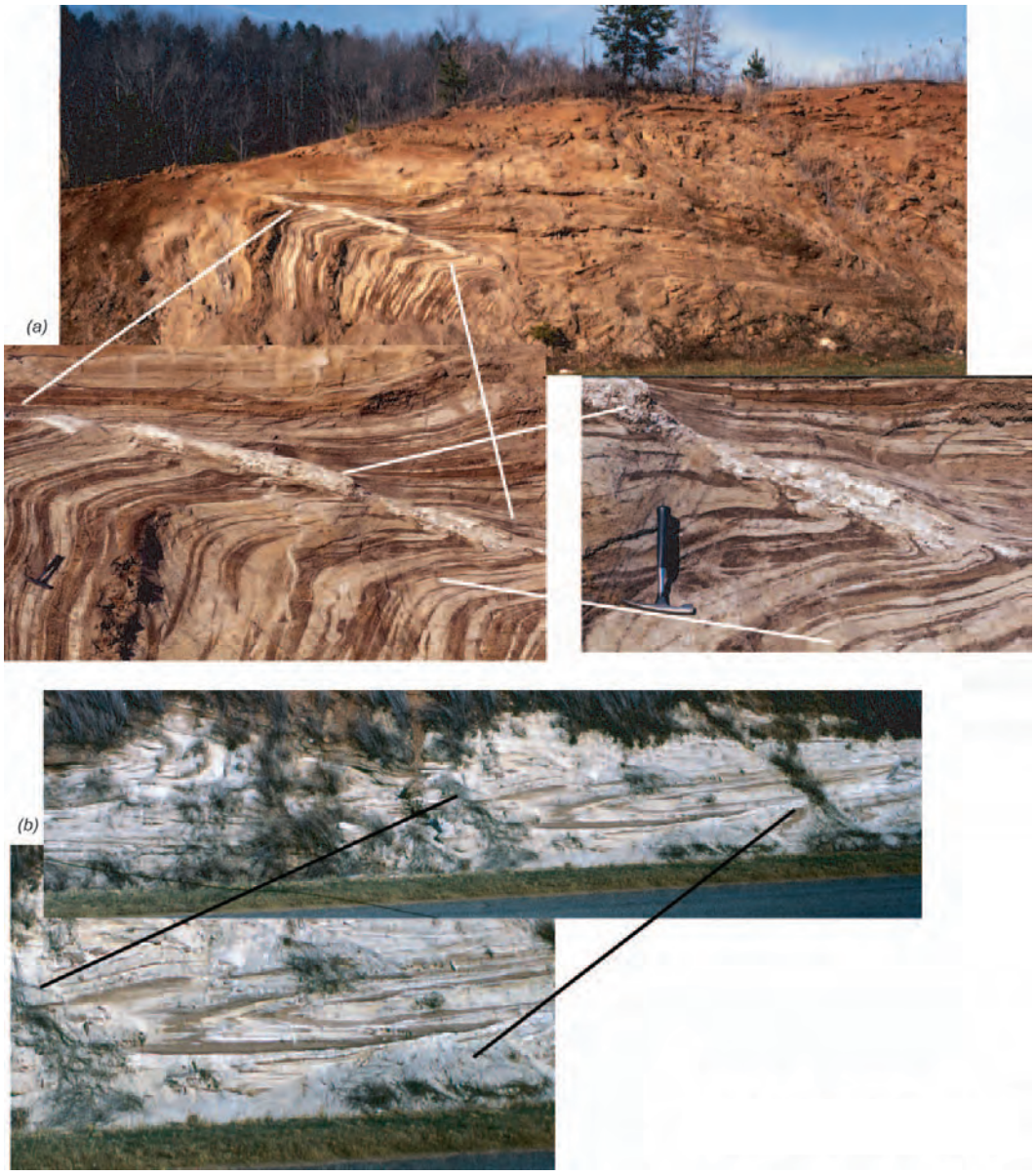

Figure 6–5. Folded stromatic migmatite in saprolite exposures in northwestern South Carolina. (a) Northwest-vergent F_3 folds (or NW limb of a larger sheath fold) on U.S. 76 2 km west of Westminster, South Carolina. Cut is ~6 m high; view is toward the northeast. Pegmatite related to decompression melting(?) along a small fault (note drag folds) cuts folds in the westernmost part of the exposure. Insets, with hammer for scale, show details of structures. Lenticular amphibolite layers probably are modified elliptical or anvil sections through mesoscopic sheath folds. (b) Isoclinal recumbent F_2 folds near Coneross Creek ~4 km north of Townville. Exposure is ~3 m high; view is toward the northeast. Inset shows complete transposition in hinge of one of the folds. Plunge is <5° south. Dark-colored layers are weathered amphibolite; light-colored layers are weathered granitoid melt. Fold hinges in both (a) and (b) are nearly normal to the roadcuts.

(Hatcher unpublished) along the northwest flank of the Sauratown Mountains window in North Carolina, however, reveals top-to-the-northeast shear sense along the fault at the base of the overlying Smith River allochthon.

The combination of the gentle dip of foliation and shallow plunge of the mineral stretching lineation in the IP led us to construct a model for flow with vortex-like trajectories that range from northwest to north along the Central Piedmont suture, to west-directed in the central IP, then strongly southwest-directed from several km southeast of the Brevard fault zone buttress (Fig. 6–6). New mineral lineation data from the Atlanta area (Higgins et al. 2003) (Fig. 6–7) reproduce the same pattern that we have recognized farther north in NE Georgia (Fig. 6–8), but data from the IP in Alabama available only in fabric diagrams (Bentley and Neathery 1970; Neilson 1988; Fig. 6–9) reveal a strongly northeast-southwest alignment. Southwest-directed flow also propagated into the eastern Blue Ridge northwest of the Brevard fault zone, because the lineation in this area also trends NE-SW and plunges gently with shear sense indicators again indicating southwest-directed transport (Figs. 6–7 and 6–8). This overprint into the eastern Blue Ridge, however, gives way to contrasting Blue Ridge structural regimes a few kilometers west of the Brevard fault zone (e.g. Hatcher et al. 2004) (Fig. 6–8).

Metamorphic isograd maps of the IP (Fig. 6–10) reveal a metamorphic core of pervasively migmatitic sillimanite and higher grade rocks throughout the central IP, decreasing to kyanite grade in the southeastern IP in North Carolina, and to kyanite, staurolite, or garnet grade in the western IP in northwest South Carolina and northeast Georgia (Fig. 6–10). Recent estimates of P-T conditions during peak metamorphism by Mirante & Patino-Douce (2000), Bier (2001), Bier et al. (2002), and Merschat (2003) indicate the core of the Inner Piedmont consistently reached 750-850° C and pressures of 500-800 MPa. The IP thus reached sillimanite I, sillimanite II, and possibly hornblende granulite facies conditions. Classic migmatite structures described in other orogens (e.g., Mehnert 1968) are abundant here: stromatic migmatite is most common (Fig. 6–5), but agmatite (Fig. 6–11), diatexite, and other varieties are also present (Williams 2000). In addition, Cat Square terrane granitoids mostly have an anatectic origin, including the 378 Ma Toluca and 366 Ma Walker Top Granite bodies (Giorgis et al. 2002; Mapes 2002). A phenomenon first noted by Griffin (1969) immediately beneath the Six Mile thrust sheet in northwestern South Carolina is a zone of excessive melting producing what might be called “super migmatite.” A zone of much more extensive melting and super migmatite occurs beneath the Brindle Creek thrust sheet in North and South Carolina (Giorgis 1999; Williams 2000; Bier et al. 2002; Merschat et al. 2005).

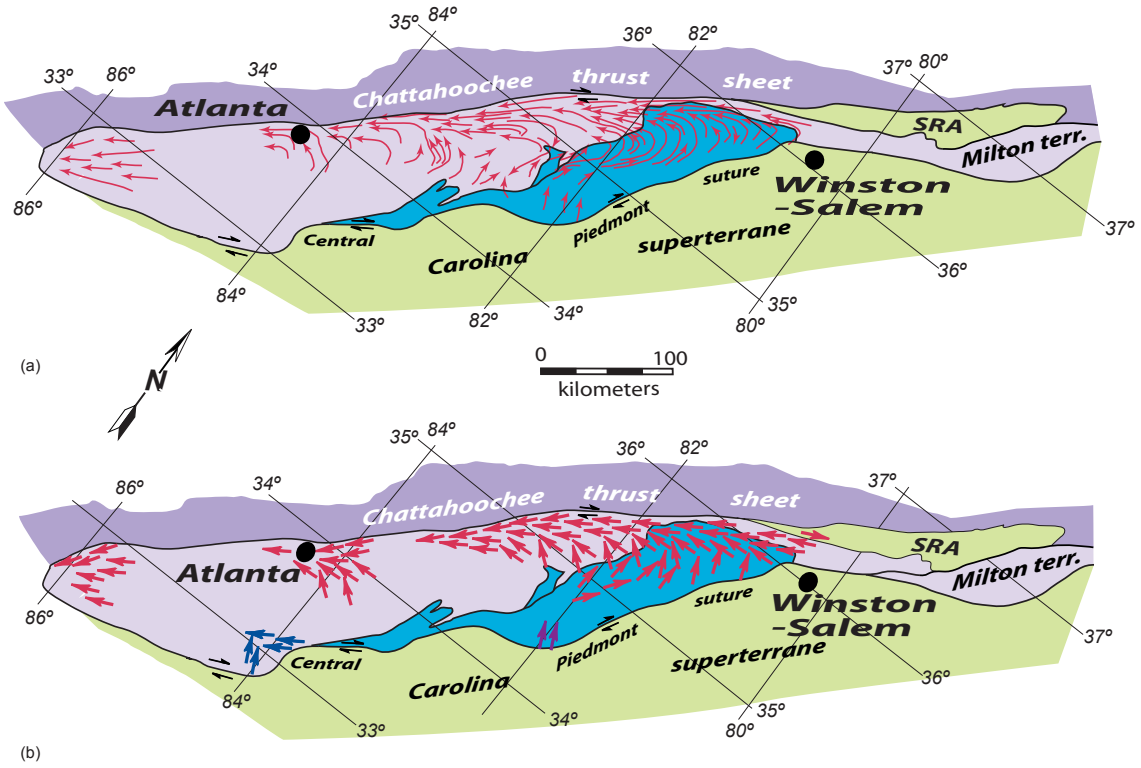

Figure 6–6. Ductile flow orientation and shear-sense data from the Inner Piedmont. (a) Flow model for the southern Appalachian Inner Piedmont based on available data. (b) Same base map as in (a) with shear-sense data, where it is known. Arrowheads indicate top direction. Red arrows are shear-sense indicators formed during the Neoacadian event (350-360 Ma). Purple arrows in South Carolina are high temperature shear-sense indicators that could have formed during either the Neoacadian or early Alleghanian (from West 1997). Blue arrows in western Georgia represent high temperature Alleghanian shear-sense indicators (from Hooper et al. 1997, and references therein). Each arrow represents at least 10 measurements, most represent several 10s of measurements. Measurements in Alabama are from Steltenpohl et al. (1990), Steltenpohl (2005), and Hatcher (unpublished data). Measurements in northern Georgia are from Higgins et al. (2003). Measurements in northeastern Georgia and the Carolinas are from data in or cited in Hopson & Hatcher (1988), Merschat et al. (2005 in press), W. M. Schwerdtner (unpublished) and Hatcher (unpublished).

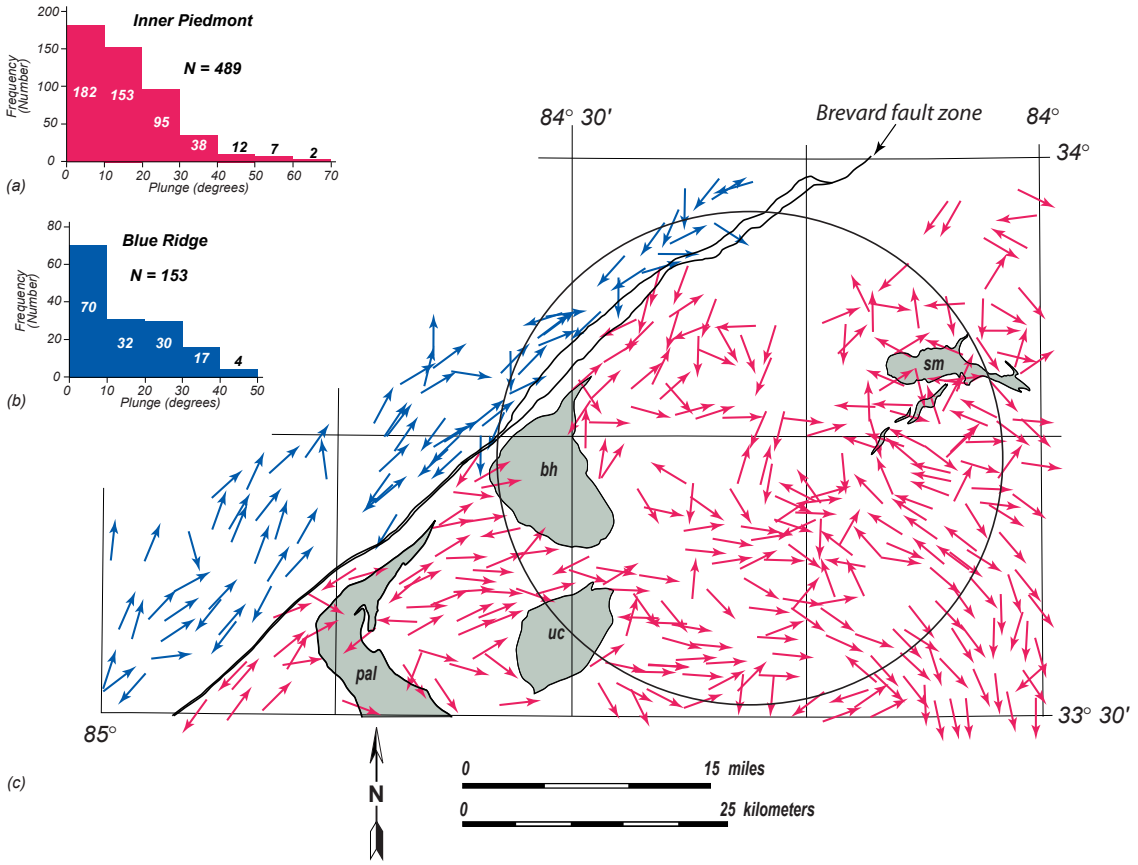

Figure 6–7. Mineral stretching lineation and tight fold pattern in the eastern Blue Ridge and western Inner Piedmont near Atlanta, Georgia (after Higgins et al. 2003). (a) Frequency distribution of plunges of 489 mineral stretching lineations and hinges of tight folds in the Inner Piedmont. (b) Frequency distribution of plunges of 153 mineral stretching lineations and hinges of tight folds in the eastern Blue Ridge (western Tugaloo terrane). (c) Map of eastern Blue Ridge (blue) and Inner Piedmont (red) mineral stretching lineations and tight folds. Arrows point in direction of plunge. Double-ended arrows indicate horizontal lineations. Late Carboniferous plutons (little internal deformation): pal–Palisades. uc–Union City. bh–Ben Hill. sm–Stone Mountain. Circle is approximate location of Atlanta.

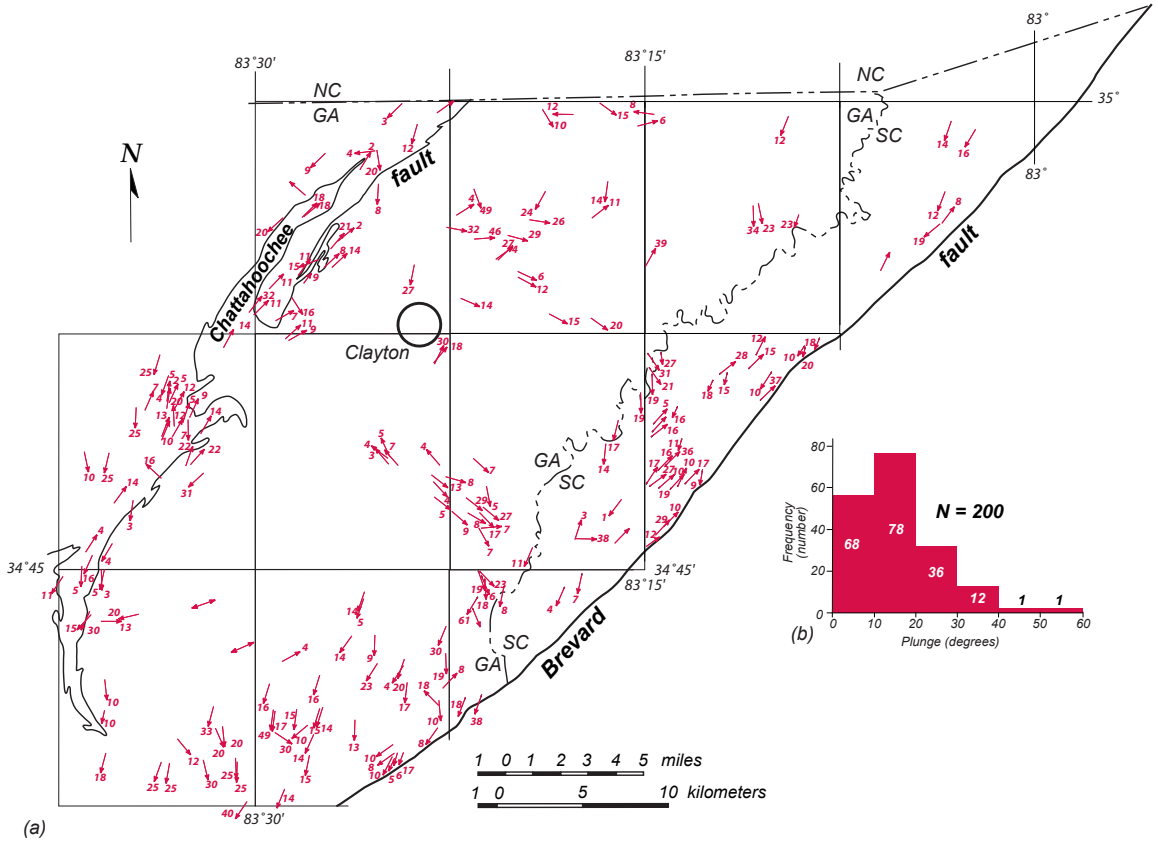

Figure 6–8. Orientation of mineral stretching lineations and fold hinges. (a) Mineral stretching lineations and hinges of tight folds in the western Tugaloo terrane (eastern Blue Ridge) of northeastern Georgia and northwestern South Carolina. Note that lineations are strongly aligned NE-SW for a short distance northwest of the Brevard fault zone, but become aligned with Blue Ridge structures farther west. Arrows point in plunge direction, with number indicating plunge value; double-ended arrows indicate horizontal lineations. (b) Frequency distribution of plunge of 200 mineral stretching lineations and hinges of tight folds. Note that >50% plunge <20°. See Hatcher et al. (2004) *their* Figure 2 for detailed geologic map. Data compiled from Stieve (1989), Hopson (1994), and Hatcher (unpublished).

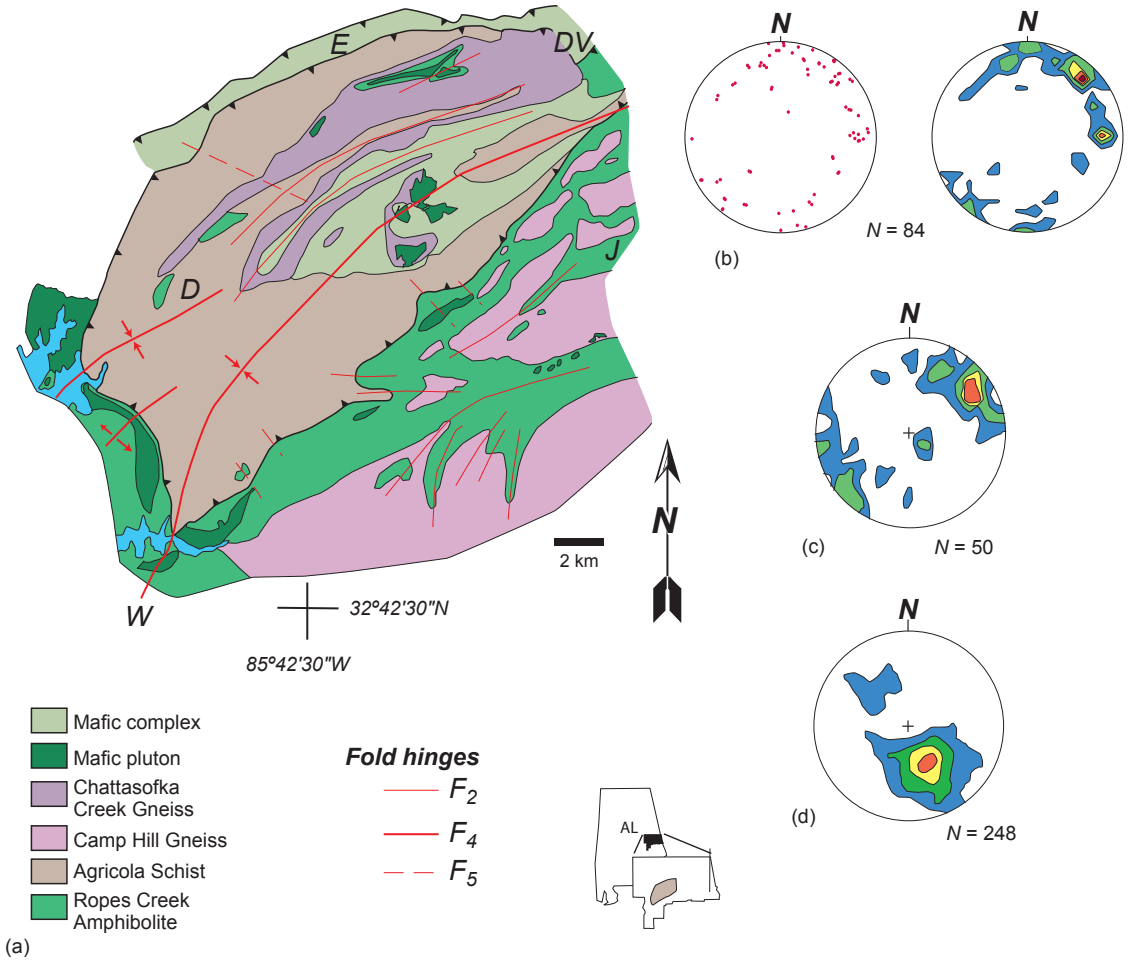

Figure 6–9. Geologic map and orientations of lineations and tight folds in the southwestern Inner Piedmont of Alabama (after Bentley & Neathery 1970 and Neilson 1988). (a) Geologic map (after Neilson 1988). C–Camp Hill. D–Dadeville. DV–Dudleyville. J–Judson. W–Walnut. (b) Mineral stretching lineations and tight folds from the Inner Piedmont (Bentley & Neathery ¢1970). Left is a point diagram; right is contoured data. (c) Contoured lineation data from Neilson (1988). (d) Contoured poles to S_2 foliations (from Neilson 1988). All contours are 2% per 1% area.

Figure 6–10. Neoacadian metamorphic isograd map of the Tugaloo and Cat Square terranes, the Dahlonega gold belt, and the Pine Mountain (PMW, AL-GA) and Sauratown Mountains (SMW, NC-VA) windows. CHM–Chattahoochee-Holland Mountain fault. GL–Gossan Lead fault. BFZ–Brevard fault zone. BC–Brindle Creek fault. Modified from metamorphic maps by Steltenpohl et al. (1988), Butler (1991), Hatcher & Goldberg (1991), and mineral assemblages in Bentley & Neathery (1970), Neilson (1988), Hooper & Hatcher (1992), and Higgins et al. (2003).

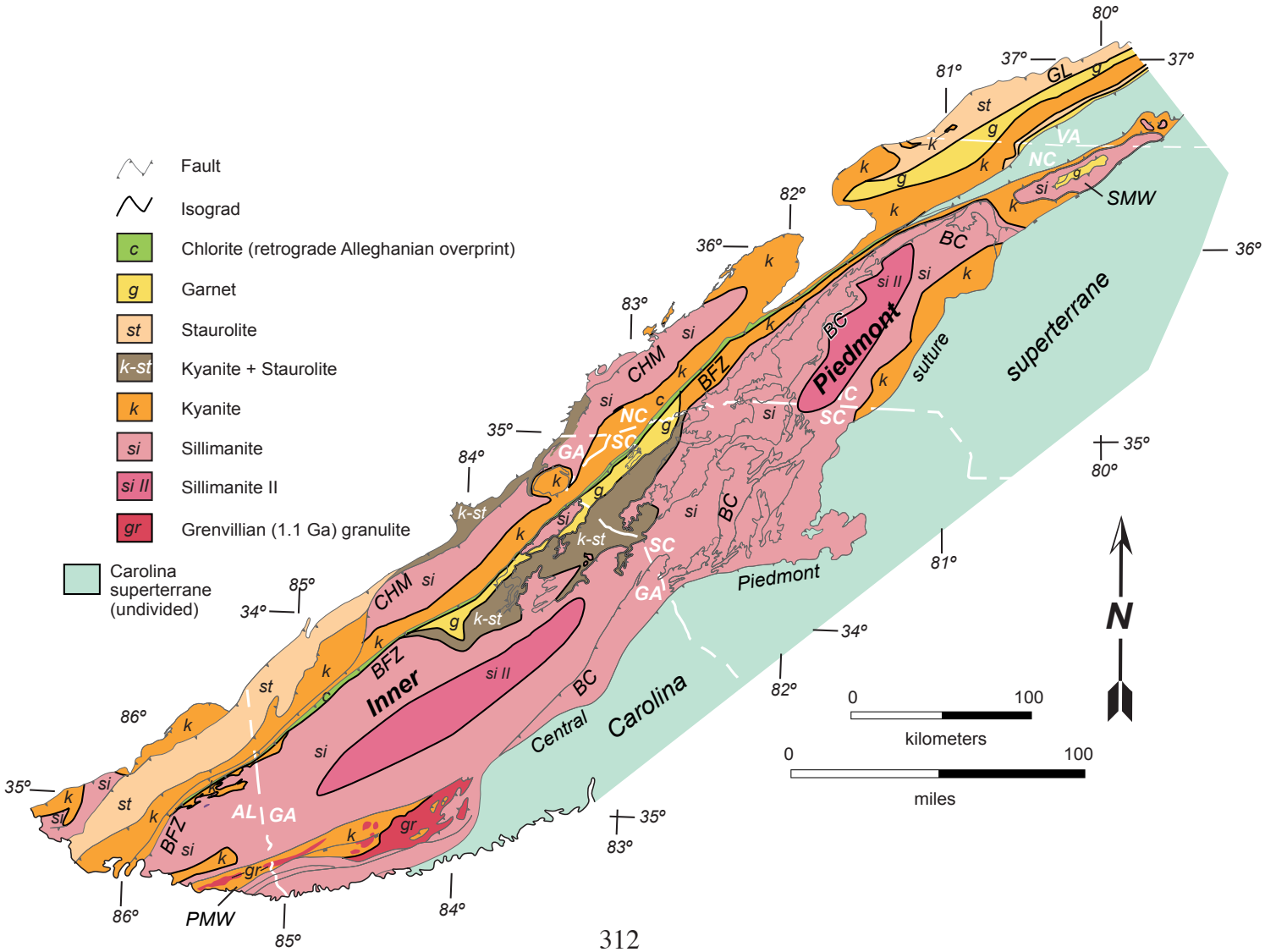
Fault
Isograd
c
Chlorite (retrograde Alleghanian overprint)
g
Garnet
st
Staurolite
k-st
Kyanite + Staurolite
k
Kyanite
si
Sillimanite
si II
Sillimanite II
gr
Grenvillian (1.1 Ga) granulite
Carolina superterrane (undivided)
Inner
Piedmont
Central
Carolina
superterrane
suture
Piedmont
BC
BFZ
CHM
GA
SC
NC
AL
GA
PMW
SMW
GL
VA
N
0
100
kilometers
0
100
miles
80°
81°
82°
83°
84°
85°
86°
37°
36°
35°
34°



Figure 6–11. Agmatite (blocky migmatite) in saprolite 1 km east of Old Pickens, South Carolina. Exposure is ~3 m high; view is toward the north. Reddish-brown material (paleosome) is weathered amphibolite and biotite gneiss (paleosome); light-colored material is granitic leucosome (neosome).

Metamorphism of IP rocks was a protracted event that spanned 30 m.y., bracketed by intrusion of the Toluca Granite (378 Ma) and reported metamorphic ages (365, 345, and 330 Ma; Fig. 6–12). Mapes (2002) concluded from geochemical–tectonic discriminant analysis that both the Toluca and Walker Top Granites are anatectic melts of Cat Square terrane metasedimentary rocks. Calculated zircon saturation temperatures (Mapes 2002) indicate Cat Square terrane rocks reached 800º C or greater by ~378 Ma. Bream (2003) reported three metamorphic peaks at 365, 345, and 330 Ma from U-Pb ion microprobe ages of zircon rims in the northern IP and eastern Blue Ridge in the Carolinas and Georgia. Dennis & Wright (1997a) reported 360 Ma and 320 Ma U-Pb monazite ages from five samples across the South Carolina IP. Kish (1997) reported a U-Pb age of 357-348 Ma for the Cat Square charnockite. Biotite and hornblende $^{40}Ar/^{39}Ar$ plateau ages from the Georgia IP suggest high-grade metamorphism and a thermal overprint in the Carolina superterrane occurred at ~350-360 Ma (Dallmeyer et al. 1986; Dallmeyer 1989). Overlapping metamorphic mineral ages and P-T estimates suggest the IP remained hot until at least 345 Ma, cooled, and was reheated to high grade again 330-320 Ma (Fig. 6–12). Late Silurian (~415 Ma) magmatism in the Carolina superterrane (Samson & Secor

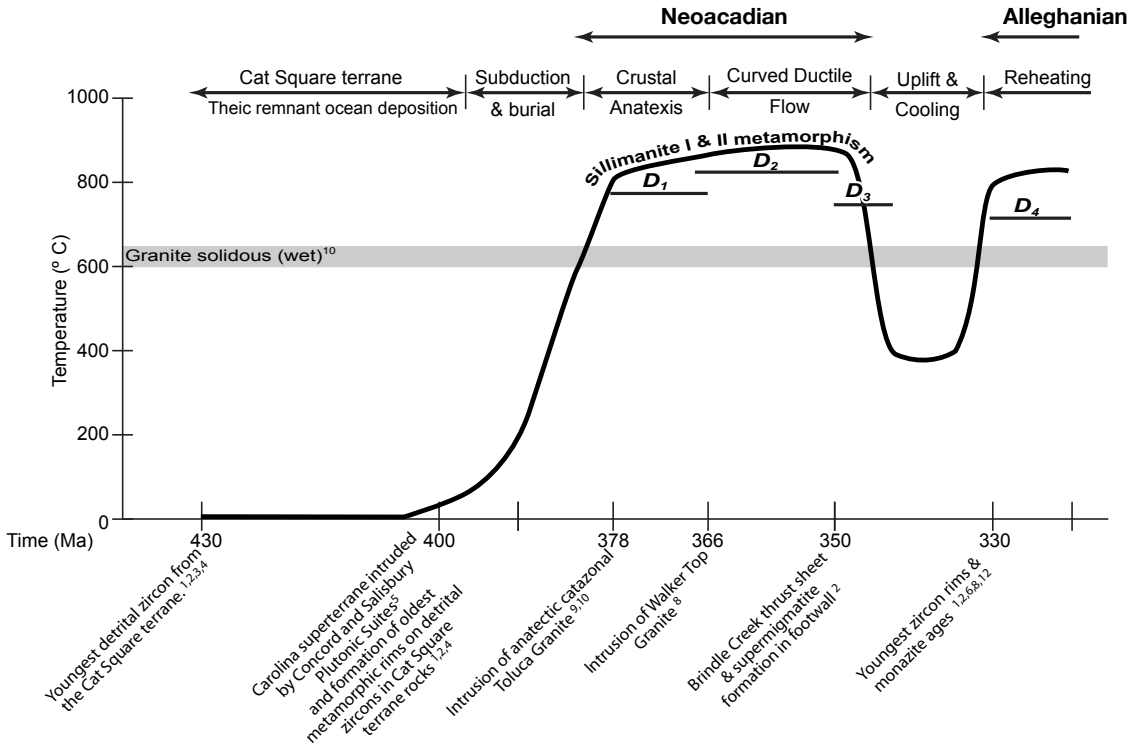

Figure 6–12. Tectonothermal time line for the Inner Piedmont. Data sources: 1–Bream (2002). 2–Bream (2003). 3–Bream et al. (2001). 4–Bream et al. (2004). 5–McSween et al. (1984, 1991). 6–Carrigan et al. (2001). 7–Davis (1993a). 8–Dennis & Wright (1997a, 1997b). 9–Giorgis et al. (2002). 10–Luth et al. (1964). 11–Mapes (2002). 12–Mapes et al. (2001). 13–Mirante & Patino-Douce (2000).

2000) not only indicates that the superterrane had been assembled, but it may mark the initiation of B subduction of Rheic ocean crust prior to A subduction of Tugaloo terane.

Mechanical components of the IP thus include the Mid-Paleozoic Brevard fault and Central Piedmont suture (upper and lower boundaries), plastic rheology of the lithologic assemblage of quartzofeldspathic, pelitic, Ordovician granitoids (Tugaloo terrane), volcanic rocks, and minor quartzite and ultramafic rocks; free water from relict and metamorphic reactions; migmatite; and anatectic melt-generated plutons. Metamorphic mineral assemblages require burial depths of 15 to 18 km (see Merschat et al., 2005, their Fig. 6–4b). Limited estimated heat production values in Tugaloo terrane metagraywacke, pelite, amphibolite, and granitoids range from 0.7–4.7 $\mu W/m^3$ (Costain & Decker 1987). Young (mostly Alleghanian) granitoids in the Carolina superterrane have high heat production values in the range of 1 to 4 $\mu W/m^3$ (Costain et al. 1986), corresponding to higher U and Th values (McSween et al. 1991). The anatectic Toluca and Walker Top plutons have low to moderate U contents of 0.85–2.2 ppm and high Th contents of 10.6–47.8 ppm (Mapes 2002). Calculated zircon saturation temperatures of 773–913° C for the

Toluca Granite and 830–881° C for the Walker Top Granite are consistent with calculated peak metamorphic temperatures (Merschat et al. 2005). IP rocks consist of ~50% by volume metagraywacke, 30% pelitic (including aluminous) schist, 10% granitoids (as plutons), 5–7% amphibolite, and the remainder other rock types.

APPLICATION OF THE CHANNEL FLOW CONCEPT TO THE INNER PIEDMONT

Discovery of the north-dipping, north-vergent South Tibetan Detachment led to an initial interpretation that the Himalayas were undergoing extensional collapse (Burchfiel &Royden 1985; England & Houseman 1989). Recognition of the possible coupled kinematic and mechanical relationship between the South Tibetan Detachment, the migmatites of the Greater Himalayan sequence beneath, and the Main Central Thrust below (Brunel 1986), raised the possibility that channel flow (involving components of simple shear and Poiseiulle flow), may be a mechanism for crustal deformation. If so, extrusion of formerly partially melted crust that lies between the two faults would have occurred as a product of India's collision with southern Asia. Mineral stretching lineations, shear-sense indicators, and quartz c-axis fabrics all support southward transport of the Asian Plate during head-on collision with India (Brunel 1986).

Several important assumptions must be made before the channel flow concept can be applied to crustal deformation anywhere. The principal assumption is that viscous—fluid—rheology is involved and that the principles of fluid mechanics describing channel (Poiseiulle) flow, probably more *apropos* 3D flow between two rigid plates (Prandtl flow; Acheson 1990), are applicable here. An additional component of simple shear at the boundaries is required, because both Poiseiulle and Prandl flow require zero velocity at all boundaries. If these assumption are valid and crustal rocks contain the threshold amounts of melt for fluid behavior to occur ($\geq$ 1 per cent; Jamieson et al. 2004), numerous intriguing possibilities arise for understanding the behavior of migmatite terranes.

The Appalachian IP doubtlessly contained sufficient melt to have become mobilized in a viscous state during the mid-Paleozoic (Figs. 6–5 and 6–11), producing the complex flow pattern we have identified (Hatcher 2001; Merschat et al. 2005). It was, however, tectonically driven rather than gravity driven, involving a viscosity $>10^{19}$ Pa s, as in one of Beaumont's et al. (this volume) models of large hot orogens. The complex flow pattern observed in the Appalachian IP (Fig. 6–6; Merschat et al., 2005) raises the possibility that flow may have been initially confined from the northeast and less

confined toward the southwest because of oblique subduction, producing a channel composed of stacks of southwest-directed imbricate thrusts that were directed along strike into what is now Alabama. If so, this provides an opportunity to observe and better understand an exhumed along-strike channel at various depths of erosion. Portions near the upper boundary of the proposed channel are exposed at the northeast end of the IP immediately northwest of the Sauratown Mountains window (Fig. 6–1). The southwest end in Alabama represents the lowest part of the channel, as suggested by the strong northeast-southwest alignment of the mineral stretching lineation across the IP (Fig. 6–3). With that possibility, we may be able to better understand the process of generation of a southwest-directed, tectonically driven mid-Paleozoic channel. If the Appalachian IP is an exhumed mid-Paleozoic channel consisting of numerous Type F imbricates, it compares favorably with the 2D Beaumont et al. (2004, their Fig. 14) model HT–HET in which they introduced initial anisotropies and produced a series of imbricates as it deformed over a simulated 20-m.y. time span (Fig. 6–13). Deformation in the IP, however, occurred in a state of 3D heterogeneous strain, and the migmatitic IP became an along-strike channel with SW-directed flow a product of oblique collision between Carolina superterrane to the east and various components of the remnant Theic ocean and the Laurentian margin to the west. These were subducted beneath Carolina to depths sufficient to melt and begin detachment and southwestward transport in a channel (Fig. 6–14).

Carolina superterrane likely began to subduct the remnant Theic(?) ocean, then Cat Square terrane, followed by the Tugaloo terrane, during the Late Devonian (~408 Ma; Fig. 6–12). By ~380 Ma anatectic melting produced the Toluca granitoids, and by 365 to 355 Ma Carolina had subducted the Tugaloo and Cat Square terranes to depths of 15-20 km, indicated by metamorphic mineral assemblages (Figs. 6–10 and 6–12). Anatectic melting produced the Walker Top granitoid suite at 366 $\pm$ 4 Ma (Giorgis et al. 2002; Mapes 2002). Water was released from hydrous minerals via dehydration reactions (e.g., muscovite breakdown), as the threshold of wholesale migmatization was reached at upper kyanite to sillimanite I zone conditions from 360 to 355 Ma (Dennis & Wright 1997a; Bream 2003). The flow regime developed producing the Type F imbricate thrust stack at or near peak metamorphic conditions, confined above by the Carolina superterrane suprastructure and detaching below on the mid-Paleozoic Brevard fault zone. Initial melting and southwestward escape of IP nappes occurred over a 25- to 30-m.y. time span. Cat Square and Tugaloo terrane rocks cooled to temperatures below the blocking temperatures of monazite and zircon and remained cool for the next 30 m.y.; then they

Figure 6–13. Comparison of a cross section (a) through part of the Inner Piedmont in North Carolina with Beaumont et al. (2004, *their* Fig. 14) model HT–HET (b). Configurations of deep Inner Piedmont structure and mid-Paleozoic Brevard fault zone were extrapolated from surface geologic maps in Goldsmith et al. (1988) and Bier et al. (2002, their Fig. 2). Colors in (a): Red–Lower Tallulah Falls-Ashe Formation metagraywacke, amphibolite, and pelitic schist. Pink–Upper Tallulah Falls-Ashe Formation metagraywacke and pelitic schist. Yellow–Aluminous schist marker that separates upper from lower Tallulah Falls-Ashe Formation units. Purple–Ordovician plutons. Green and yellow (adjacent)–Poor Mountain Formation Amphibolite (green) and quartzite (yellow). Orange–Metagraywacke in Brindle Creek Thrust sheet. Brown–Sillimanite schist in Brindle Creek thrust sheet. Dark blue–Devonian and Mississippian plutons in Cat Square terrane and Carolina superterrane. Blue-Green–Possible ocean crust in Brindle Creek thrust sheet. Cross-section location is shown in Figure **6–**1. Colors in (b) represent materials of higher (blue, yellow, and lower viscosity (pink and red).

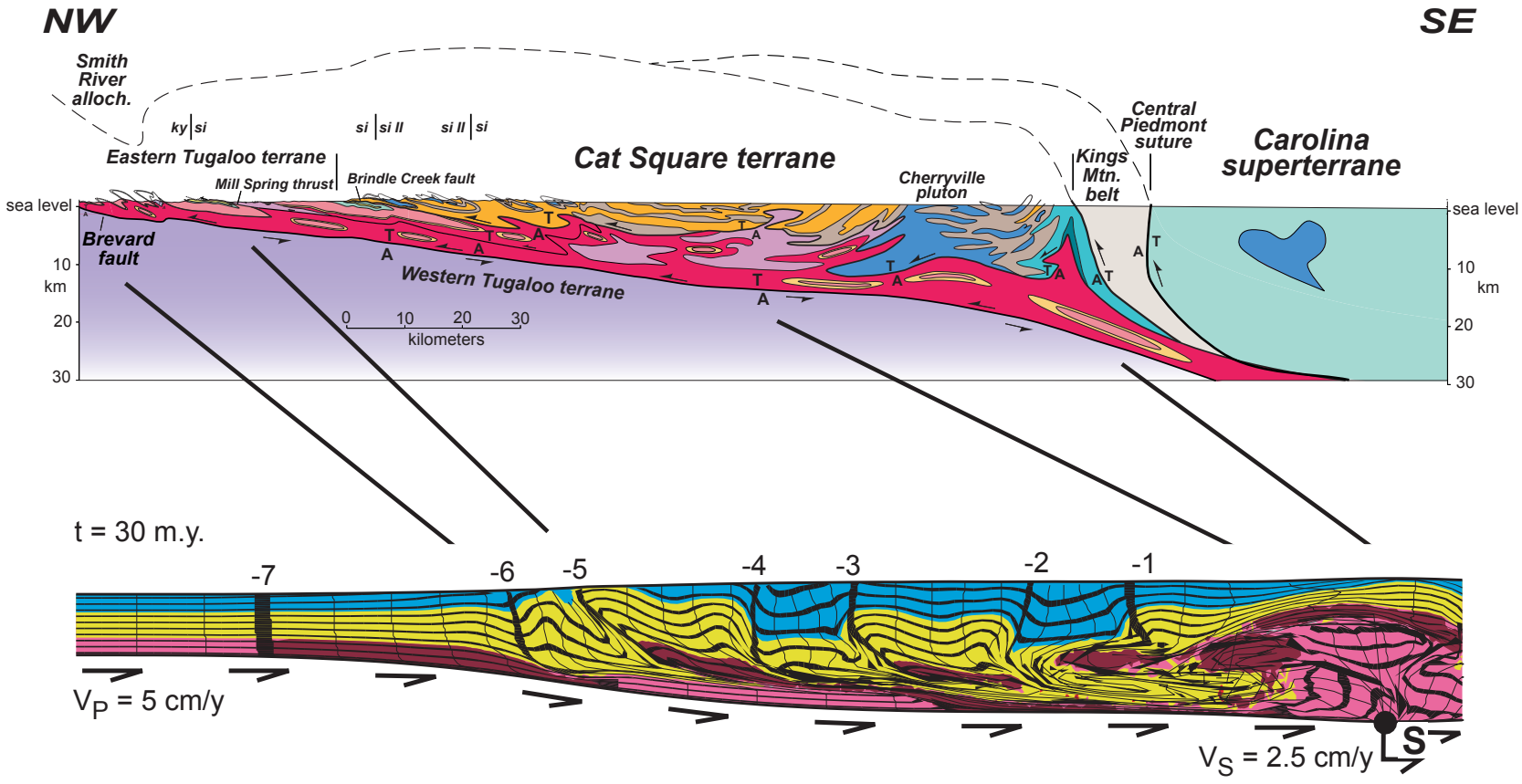
NW
SE
Smith River alloch.
ky | si
si | si II
si II | si
Eastern Tugaloo terrane
Mill Spring thrust
Brindle Creek fault
Cat Square terrane
Cherryville pluton
Kings Mtn. belt
Central Piedmont suture
Carolina superterrane
sea level
Brevard fault
10
km
20
30
Western Tugaloo terrane
0 10 20 30
kilometers
t = 30 m.y.
-7
-6
-5
-4
-3
-2
-1
V_P = 5 cm/y
V_S = 2.5 cm/y

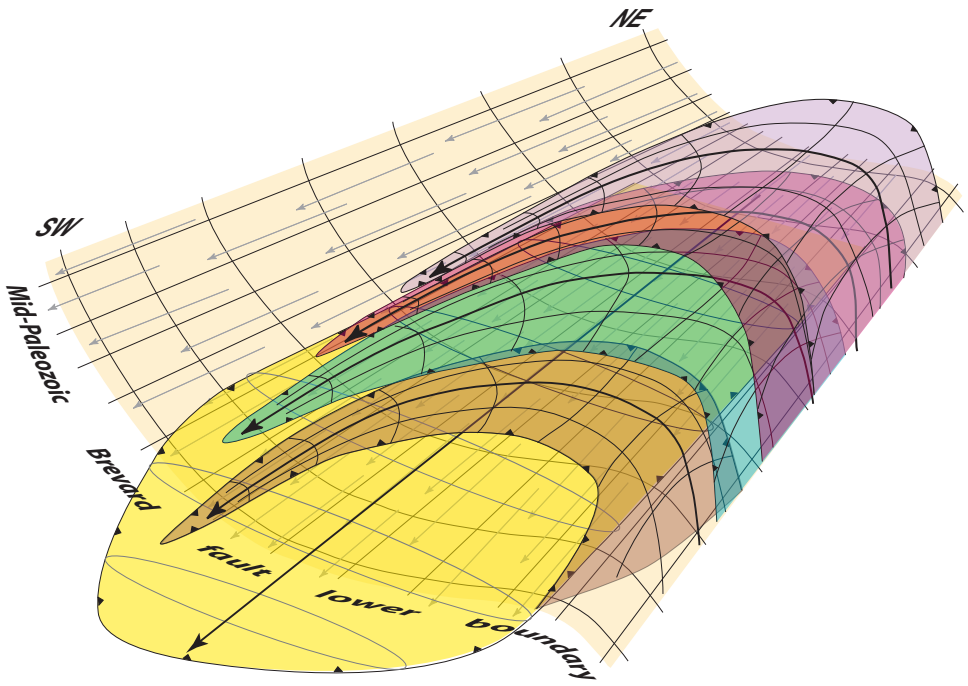

Figure 6–14. Relationships in 3D between a stack of four hot imbricate Type F thrust sheets that are deflected SW by confinement beneath the overriding Carolina superterrane (removed) and the mid-Paleozoic Brevard fault zone lower boundary. The lowest sheet (in gold) may not have been deflected, but is forced SW by confinement between the overlying thrust sheets and the underlying Brevard fault zone.

were heated again between 325 and 320 Ma (Dennis & Wright 1997b; Bream 2003) during the early Alleghanian. The oldest direct thermal connection between the Carolina superterrane suprastructure and the Cat Square and Tugaloo terrane infrastructure consists of the 420 to 380 Ma Silurian-Devonian plutonic suite that occurs in all of these terranes (McSween et al. 1984, 1991; Miller et al. 2000; Samson & Secor 2000). In addition to the plutons, a 360 Ma thermal overprint is also recorded in $^{40}Ar/^{39}Ar$ plateau ages in the western Carolina superterrane (Dallmeyer et al. 1986). Monazite ages from the Smith River allochthon (Fig. 6–1) link it to the peri–Gondwanan Carolina superterrane (Hibbard et al. 2003) and support the hypothesis that the Carolina superterrane overrode the IP.

Significant differences exist between our proposed IP channel and Tertiary to Holocene channel hypothesized beneath Tibet and extruding between the Himalayan Main Central thrust and the South Tibetan Detachment. Flow in the IP is curved, instead of involving up-dip and across-strike extrusion, as in the Himalayas, so it was directed southwestward subparallel to strike, consistent with oblique collision. Abundant shear sense data throughout the central and western IP document the observed flow pattern (Merschat et al. 2005). Ideally, the Central Piedmont suture, by analogy with the South

Table 6–1. Hypothetical subduction zone parameters required for different dip*

Dip	$t_{subduction\ initiation\ (m.y.)}$	$t_{melting\ (°C)}$	$x_{subduction\ (km)}$	***Subduction direction***
20°	385	383	52.6	Head-on
10°	387	382	104	Oblique
5°	393	383	206.5	Oblique

*Subduction rate = 2 cm/y; required (estimated) depth from metamorphic assemblage = 18 km; required depth for minimum melting = ~7 km; Toluca Granite crystallized ~380 Ma. ***t*** = time. ***x*** = distance

Tibetan Detachment, should be a normal fault if the IP were gravity-driven. Evidence of down-to-the-southeast transport along the Central Piedmont suture has not been observed (e.g., West 1998), and is clearly dextral—not sinistral—in central Georgia east of the Pine Mountain window (Fig. 6–1; Hooper et al. 1997).

There are, however, important similarities with the Himalayan-Tibetan channel. A prolonged thermal history occurred in the IP within ~30 m. y. following burial and subduction of IP constituents beneath the Carolina superterrane beginning ~400 Ma, with first melting at ~385 Ma culminating with peak metamorphism, a melt-weakened middle crust, and flow at 360 to 355 Ma (Table 6–1). Despite the differences cited above, the IP channel as defined herein compares favourably with the Beaumont et al. (2004, their Fig. 14) tectonically driven $\eta > 10^{19}$ Pa s model, H-HET and the large, hot orogens model in Beaumont et al. (this volume). It also fits most of the other criteria in terms of position in the crust, availability of water for extensive melting in the subducted mass, forming a series of thrust nappes that are west-, then SW-directed. The rheological state of melting and southwest-directed flow in a tectonically driven channel had to have been induced by oblique subduction, burial, and radioactive decay yielding the high temperatures and moderate pressures, coupled with available free water (both primary and from metamorphic reactions). The major conclusion from this discussion is that the Appalachian IP may be an exhumed tectonically forced orogenic channel, in the context of the Beaumont et al. (in review) large hot orogen's concept. Tests of our hypothesis might consist of: (1) 3D finite-element or numerical models incorporating the physical parameters discussed above for the IP. Difficulties with this approach lie in the limited capabilities of 3D modeling these techniques. (2) Collecting additional modern geochronologic data throughout the IP, but particularly in Georgia and Alabama, to additionally corroborate (or revise) the 350-360 Ma age of peak metamorphism and

coeval formation of fabric elements at all scales. This would augment the data of Dennis & Wright (1997a, 1997b), Bream et al. (2001), Mapes (2002), and Bream (2003). (3) Additional detailed field studies should be conducted along the Central Piedmont suture to collect new shear-sense data. Herein the difficulty lies in the reactivation of suitably oriented segments of the suture as a thrust (in South Carolina, West 1998), and in dextral strike slip (in central Georgia, Hooper & Hatcher 1988), where detailed studies already exist. Even so, large areas of the IP and its boundaries remain mapped only by reconnaissance wherein little shear-sense data were collected.

An average heat production of ~2 $\mu W/m^3$ like that assumed by Beaumont et al. (2004, in review this volume) in their models, would probably be appropriate for the IP. If we assume initial subduction was head-on, the subduction zone had a dip of 20° and a subduction rate of 2 cm/y, subduction could have begun as recently as 385 Ma under hydrous conditions for the Toluca Granite to crystallize at 380 Ma. For reasons stated above, subduction more likely was oblique, so if the dip was 10°, subduction could have begun as late as 387 Ma, or if the dip was 5°, subduction could have begun as early as 393 Ma (Table 6–1). The latter possibility seems more reasonable in light of the post-430 Ma time of deposition of Cat Square terrane sediments, likely oblique subduction closing the Rheic ocean and the time needed for burial to reach melting temperature.

The resulting tectonically driven IP channel would have been SW-directed parallel to the strike of the orogen, because of confinement beneath the overriding Carolina superterrane and buttressing by the underlying mid-Paleozoic Brevard fault and western Tugaloo terrane to the west (Fig. 6–15). These formed a closed system above and below that apparently remained open to the SW.

CONCLUSIONS

1. The IP is an exhumed, tectonically forced, strike-parallel orogenic channel that formed as a product of Late Devonian to early Mississippian (390-350 Ma) oblique subduction of previously assembled, dominantly Laurentian terranes beneath the Carolina superterrane.
2. This channel has an upper boundary consisting of the overlying Carolina superterrane, a lower boundary consisting of the mid-Paleozoic Brevard fault zone, and less confinement toward the southwest permitting along-strike, southwest-directed extrusion of partially melted, mid-crustal material.

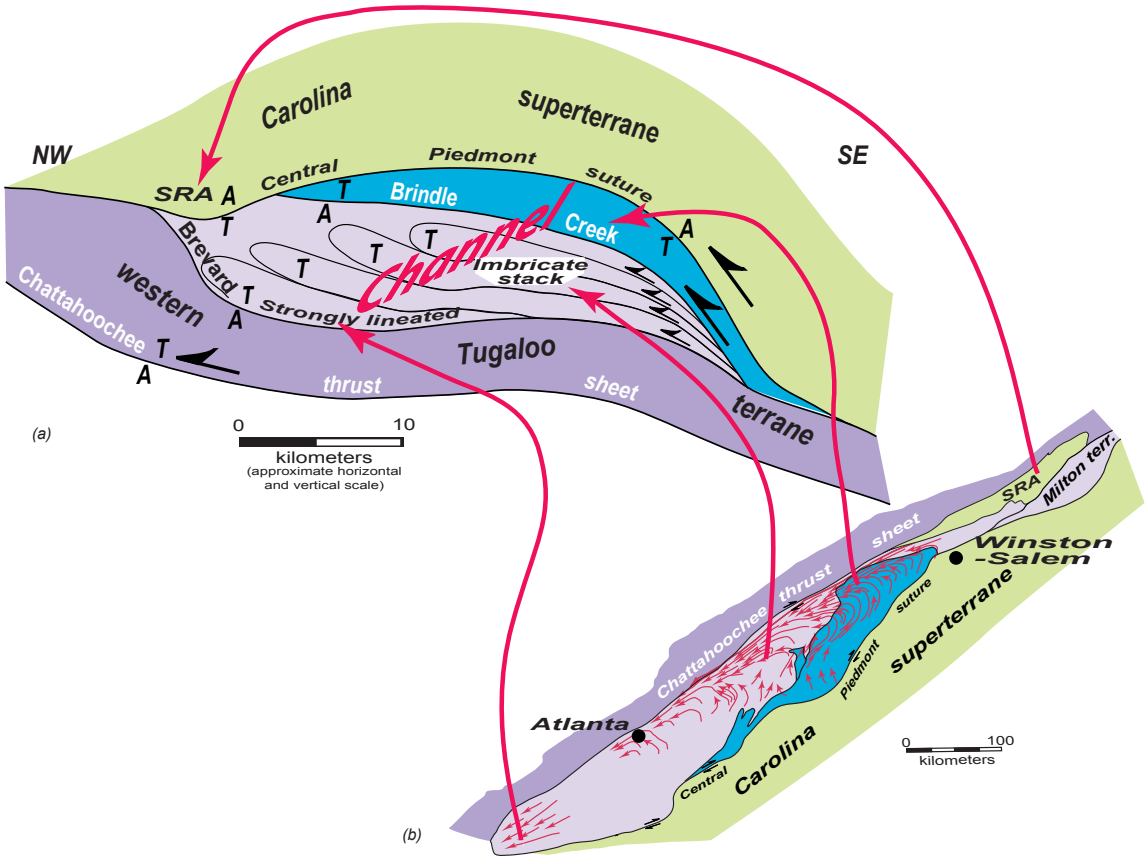

Figure 6–15. Composite cross-section cartoon (a) showing the relationships between different components of the Inner Piedmont channel now exposed at different erosion levels in different parts of the Inner Piedmont and adjacent terranes. Purple–Western Tugaloo terrane (Chattahoochee thrust sheet) west of and below the mid-Paleozoic Brevard fault zone. Lavender and blue–Eastern Tugaloo and Cat Square terranes, the components of the Inner Piedmont along-strike channel. Light green–Carolina superterrane and Smith River allochthon (SRA), Peri–Gondwanan overriding plate.

3. Attributes that permit our primary conclusions are: contrasting structural style with adjacent terranes, prolonged thermal activity at middle to upper amphibolite facies conditions, extensive migmatization, southwest-directed hot Type F imbricate thrust sheets, curved flow, and gentle dip of meso- to macroscale planar structures.
4. Orogenic channels can form in transpressional regimes, but they produce more complex flow patterns than gravity-driven channels in head-on collision zones.
5. The IP provides unique insights into the complexities of an exhumed, tectonically driven orogenic channel. Because of the possible along-strike exposure of all levels of the channel, it is particularly important in understanding heterogeneous, non-plane channel flow at different structural levels.

ACKNOWLEDGMENTS

U.S. National Science Foundation grants GA–1409, GA–20321, EAR–810852, EAR–8206949, EAR–8417894, EAR–9004604, and EAR–9814800 supported a great deal of field work in the Carolinas and northeast Georgia Inner Piedmont by RDH and graduate students during the 1970s, 1980s, 1990s, and early 2000s. Additional support during the late 1960s and early 1970s was provided by the South Carolina Geological Survey, Henry S. Johnson, Jr. and Norman K. Olson, state geologists. Field work in the late 1990s and early 2000s has been supported by the EDMAP program administered by the U.S. Geological Survey. The University of Tennessee Science Alliance Center of Excellence has provided considerable support for RDH and students since 1986. Chris Beaumont (Dalhousie University) has kindly shared the graphics of several of his finite-element models with us. He and his colleagues' models have provided additional impetus for attempting to apply the channel flow concept to the Appalachian Inner Piedmont.

Finally, RDH enjoyed numerous debates with Doug Nelson, to whom this volume is dedicated, about southern Appalachian tectonics prior to his INDEPTH success (e.g., Nelson 1988; Hatcher & Hooper 1988). These debates were at times heated, but we always remained on friendly terms—the way scientific debate should be conducted. Doug is missed.

REFERENCES CITED

Acheson, D. J. 1990. Elementary fluid dynamics. Oxford, Oxford University Press, 397 p.

Azcárraga, J., Abalos, B., & Gil Ibarguchi, J. I. 2002. On the relationship between kilometer-scale sheath folds, ductile thrusts and minor structures in the basal high-pressure units of the Cabo Ortegal complex (NW Spain). Journal of Structural Geology 24, 1971-1989.

Beaumont, C., Jamieson, R. A., Nguyen, M. H. & Lee, B. 2001. Himalayan tectonics explained by extrustion of a low-viscosity crustal channel coupled to focused surface denudation. Nature, 414, 738-742.

Beaumont, C., Jamieson, R. A., Nguyen, M. H. & Medvede, S. 2004. Crustal channel flows: 1. Numerical models with applications to the tectonics of the Himalayan-Tibetan orogen. Journal of Geophysical Research, 109, doi: 10.1029/2003JB002809.

Beaumont, C., Nguyen, M. H., Jamieson, R. A., & Ellis, S. this volume. Crustal flow modes in large hot orogens. In: Law, R. D., Searle, M. , Macloughlin, J. F., Knipe, R. J. (eds) The nature and significance of fault zone weakening. Geological Society of London Special Publication 186, 255–269.

Bentley, R. D. & Neathery, T. N. 1970. Geology of the Brevard zone and related rocks of the Inner Piedmont of Alabama. Alabama Geological Society, Eight Annual Field Trip Guidebook, 119 p.

Bier, S. E. 2001. Geology of the southeastern South Mountains, North Carolina. M.S. thesis, Knoxville, University of Tennessee 162 p. http://carolinageologicalsociety.org/cgscdguide.htm.

Bier, S. E., Bream, B. R. & Giorgis, S. D. 2002. Inner Piedmont stratigraphy, metamorphism, and deformation in the Marion-South Mountains area, North Carolina. In: Hatcher, R. D. Jr. & Bream, B. R. (eds) Inner Piedmont geology in the South Mountains-Blue Ridge Foothills and the southwestern Brushy Mountains, central-western North Carolina. Carolina Geological Society Guidebook, 65-100.

Bird, P. 1991. Lateral extrusion of lower crust from under high topography in the isostatic limit. Journal of Geophysical Research, 96, 10275-10286.

Bream, B. R. 2002. The southern Appalachian Inner Piedmont: New perspectives based on recent detailed geologic mapping, Nd isotopic evidence, and zircon geochronology. In: Hatcher, R. D. Jr. & Bream, B. R. (eds) Inner Piedmont geology in the South Mountains-Blue Ridge Foothills and the southwestern

Brushy Mountains, central-western North Carolina. Carolina Geological Society Guidebook, 45-63. http://carolinageologicalsociety.org/cgscdguide.htm.

Bream, B. R. 2003. Tectonic implications of geochronology and geochemistry of para- and orthogneisses from the southern Appalachian crystalline core. Ph.D. dissertation, Knoxville, University of Tennessee, 296 p.

Bream, B. R., Hatcher, R. D. Jr., Miller, C. F. & Fullagar, P. D. 2001. Geochemistry and provenance of Inner Piedmont paragneisses, NC and SC: Evidence for an internal terrane boundary? Geological Society of America Abstracts with Programs, 33, 65.

Bream, B. R., Hatcher, R. D. Jr., Miller, C. F. & Fullagar, P. D. 2004. Detrital zircon ages and ND isotopic data from the southern Appalachian crystalline core, GA-SC-NC-TN: New provenance constraints for Laurentian margin paragneisses. In: Tollo, R. P., Corriveau, L., McLelland, J., Bartholomew, M. J. (eds) Proterozoic evolution of the Grenville orogen in North America. Geological Society of America Memoir 197. 459–475.

Brunel, M. 1986. Ductile thrusting in the Himalayas: Shear sense criteria and stretching lineations. Tectonics, 5, 247-265.

Burchfiel, B. C. 2004. New tecnology; new geological challenges. GSA Today, 14/2, 4-10.

Burchfiel, B. C. & Royden, L. H. 1985. North-south extension within the convergent Himalayan region. Geology, 13, 679-682.

Butler, J. R. 1991. Metamorphism. In: Horton, J. W. Jr. & Zullo, V. A. (eds) The Geology of the Carolinas, Carolina Geological Society Fiftieth Anniversary Volume. University of Tennessee Press, 127-142.

Carrigan, C. W., Bream, B. R., Miller, C. F. & Hatcher, R. D. Jr. 2001. Ion Microprobe analyses of zircon rims from the eastern Blue Ridge and Inner Piedmont, NC-SC-GA. Geological Society of America Abstracts with Programs, 33/2, 7.

Clark, M. K. & Royden, L. H. 2000. Topographic ooze: Building the eastern margin of Tibet by lower crustal flow. Geology 28, 703-706.

Coney, P. J. 1980. Cordilleran metamorphic core complexes: An overview. In: Crittenden, M. D. Jr., Coney, P. J., and Davis, G. H. (eds) Cordilleran metamorphic core complexes. Geological Society of America Memoir 153, 7-34.

Conley, J. F. & Drummond, K. M. 1981. Geologic map and mineral resources summary of the northeast 1/4 of the Marion quadrangle, North Carolina. North Carolina Geological Survey GM 210-NE, scale 1/24,000.

Costain, C. K. & Decker, E. R. 1987. Heat flow at the proposed Appalachian ultradeep core hole (ADCOH) site. In: Hopson, J. L. & Hatcher, R. D. Jr. (eds) Appalachian ultradeep core hole project site investigation: Data set I. ADCOH Project Publication 5, University of Tennessee Department of Geological Sciences Studies in Geology 17, 137 p.

Costain, J. K., Speer, J. A., Glover, L., Perry, L., Dashevsky, S. & Mckinney, M. 1986. Heat flow in the Piedmont and Atlantic Coastal Plain of the southeastern United States. Journal of Geophysical Research, 91, 2123–2135.

Culshaw, N. G., Davidson, A. & Nadeau, L. 1983. Structural subdivisions of the Grenville province in the Parry Sound-Algonquin region. Geological Survey of Canada Paper 83–1B, 243–252.

Culshaw, N. G., Jamieson, R. A., Ketchum, J. W. F., Wodica, N., Corrigan, D. & Reynolds, P. H. 1997. Transect across the northwestern Grenville orogen, Georgian Bay, Ontario: Polystage convergence and extension in the lower orogenic crust. Tectonics, 16, 966–982.

Curl, D. C. 1998. Stratigraphy and structure of Wellford and Reidville quadrangles in part of the eastern Inner Piedmont, near Spartanburg, South Carolina. M.S. thesis, Knoxville, University of Tennessee, 129 p.

Dallmeyer, R. D. 1989. Late Paleozoic thermal evolution of crystalline terranes within portions of the U.S., Appalachian orogen. In: Hatcher, R. D. Jr., Thomas, W. A., and Viele, G. W. (eds) The Appalachian–Ouachita orogen in the United States, The Geology of North America F-2. Boulder Colorado, 417-444.

Dallmeyer, R. D., Wright, J. E., Secor, D. T. Jr. & Snoke, A. W. 1986. Character of the Alleghanian orogeny in the southern Appalachians: Part II. Geochronological constraints on the tectonothermal evolution of the eastern Piedmont in South Carolina. Geological Society of America Bulletin, 97, 1382–1392.

Davis, T. L., Hatcher, R. D., Jr., Liu, Angang, and Tabor, J. R. 1991. Southern Appalachian western Inner Piedmont: A progressive crustal–scale shear zone Geological Society of America Abstracts with Programs (Annual Meeting), 23, A138.

Davis, T. L. 1993a. Lithostratigraphy, structure, and metamorphism of a crystalline thrust terrane, western Inner Piedmont, North Carolina. Ph.D. dissertation, Knoxville, University of Tennessee, 245 p..

Davis, T. L. 1993b. Geology of the Columbus Promontory, westernPiedmont, North Carolina, southern Appalachians. In: Hatcher Jr., R. D. & Davis, T. L. (eds)

Studies of Inner Piedmont Geology with a Focus on the Columbus Promontory. Carolina Geological Society Guidebook. North Carolina Geological Survey, 17–43. http://carolinageologicalsociety.org/cgscdguide.htm.

Davis, T. L., Hatcher, R. D. Jr., Liu, Angang & Tabor, J. R. 1991. Southern Appalachian western Inner Piedmont: A progressive crustal–scale shear zone. Geological Society of America Abstracts with Programs (Annual Meeting), 23, A138.

Dennis, A. J. 1989. Tectogenesis of an accreted terrane: the Carolina arc in the Paleozoic. Ph.D. dissertation, Columbia, University of South Carolina.

Dennis, A. J. & Wright, J. E. 1997a. The Carolina terrane in northwestern South Carolina, U.S.A.: Late Precambrian-Cambrian deformation and metamorphism in a peri-Gondwanan oceanic arc. Tectonics, 16, 460-473.

Dennis, A. J. & Wright, J. E. 1997b. Middle and Late Paleozoic monazite U-Pb ages, Inner Piedmont, South Carolina. Geological Society of America Abstracts with Programs, 29/3, 12.

England, P. & Houseman, G. 1989. Extension during continental convergence, with application to the Tibetan Plateau. Journal of Geophysical Research, 94/B12, 17,561-17,579.

Espenshade, G. H., Rankin, D. W., Shaw, K. W. & Neuman, R. B., 1975, Geologic map of the east half of the Winston-Salem quadrangle, North Carolina–Virginia. U.S. Geological Survey Map I-709-B, scale 1:250,000.

Giorgis, S. D. 1999. Inner Piedmont geology of the northwestern South Mountains near Morganton, North Carolina. M.S. thesis, Knoxville, University of Tennessee, 186 p.

Giorgis, S. D., Mapes, R. W. & Bream, B. R. 2002. The Walker Top Granite: Acadian granitoid or eastern Inner Piedmont basement? In: Hatcher, R. D. Jr. & Bream, B. R. (eds) Inner Piedmont geology in the South Mountains-Blue Ridge Foothills and the southwestern Brushy Mountains, central-western North Carolina. Carolina Geological Society Guidebook, 33-43. http://carolinageologicalsociety.org/cgscdguide.htm.

Goldsmith, R. 1981. Structural patterns in the Inner Piedmont of the Charlotte and Winston-Salem 2-degree quadrangles, North Carolina and South Carolina. In: Horton Jr., J. W., Butler, J. R., Milton, D.M. (eds) Geological Investigations of the Kings Mountain Belt and Adjacent Areas in the Carolinas. Carolina Geological Society Field Trip Guidebook, 9–27. http://carolinageologicalsociety.org/cgscdguide.htm.

Goldsmith, R., Milton, D. J. & Horton, J. W. Jr. 1988. Geologic map of the Charlotte 1-degree x 2-degree quadrangle, North Carolina and South Carolina. U.S. Geological Survey Map I-1251-E, scale 1:250,000.

Grant, W. H. 1958. The geology of Hart County, Georgia. Georgia State Division of Conservation Geological Survey, Bulletin 67, 75 p.

Griffin, V. S. Jr. 1969. Migmatitic Inner Piedmont belt of northwestern South Carolina. South Carolina Division of Geology, Geology Notes, 13, 87-104.

Griffin, V. S. Jr. 1971a. Stockwork tectonics in the Appalachian Piedmont of South Carolina and Georgia. Geologischen Rundschau, 60, 868-886.

Griffin, V. S. Jr. 1971b. The Inner Piedmont belt of the southern crystalline Appalachians. Geological Society of America Bulletin, 82, 1885-1898.

Griffin, V.S. Jr. 1974a. Geology of the Walhalla quadrangle, S.C. South Carolina Division of Geology MS-19, 53p., scale 1:24,000.

Griffin, V. S. Jr., 1974b. Analysis of the Piedmont in northwest South Carolina. Geological Society of America Bulletin, 85, 1123-1138.

Grujic, D., Casey, M., Davidson, C., Hollister, L. S., Kundig, R., Pavlis, T. & Schmid, S. 1996. Ductile extrusion of the Higher Himalayan crystallines in Bhutan: evidence from quartz microfabrics. Tectonophysics, 260, 21-43.

Grujic, D., Hollister, L. S. & Parrish, R. R. 2002. Himalayan metamorphic sequence as an orogenic channel: Insight from Bhutan. Earth and Planetary Science Letters, 198, 177-191.

Hadley, J. B. & Nelson, A. E. 1971. Geology of the Knoxville 1 x 2 degree quadrangle, North Carolina, Tennessee, and South Carolina. U.S. Geological Survey Map I-654, scale 1:250,000.

Haller, J. 1956. Probleme der Tiefentektonik: Bauformen im Migmatit-Stockwerk der ostgrönländischen Kaledonien. Geologischen Rundschau, 45, 159–167.

Hanmer, S. 1988. Ductile thrusting at mid-crustal level, southwestern Grenville province. Canadian Journal of Earth Science, 25, 1049–1059.

Hatcher, R. D. Jr. 1972. Developmental model for the southern Appalachians. Geological Society of America Bulletin, 83, 2735-2760.

Hatcher, R. D. Jr. 1978. Tectonics of the western Piedmdont and Blue Ridge: Review and speculation. American Journal of Science, 278, 276-304.

Hatcher, R. D. Jr. 1993. Perspective on the tectonics of the Inner Piedmont, southern Appalachians. In: Hatcher, R. D. Jr. & Davis, T. L. (eds) Studies of Inner Piedmont geology with a focus on the Columbus Promontory. Carolina

Geological Society guidebook, North Carolina Geological Survey, 17-43. http://carolinageologicalsociety.org/cgscdguide.htm.

Hatcher, R. D. Jr. 2001. Rheological partitioning during multiple reactivation of the Paleozoic Brevard Fault Zone, Southern Appalachians, USA. In: Holdsworth, R. E., Strachan, R. A., Macloughlin, J. F., Knipe, R. J. (eds) The nature and significance of fault zone weakening. Geological Society of London Special Publication 186, 255–269.

Hatcher, R. D. Jr. 2002. An Inner Piedmont primer. In: Hatcher, R. D. Jr. & Bream, B. R. (eds) Inner Piedmont geology in the South Mountains-Blue Ridge Foothills and the southwestern Brushy Mountains, central-western North Carolina. Carolina Geological Society Guidebook, 1-18. http://carolinageologicalsociety.org/cgscdguide.htm.

Hatcher, R. D. Jr. 2004. Properties of thrusts and the upper bounds for the size of thrust sheets. In: McClay, K. R. (ed) Thrust tectonics and hydrocarbon systems. American Association of Petroleum Geologists Memoir 82, 18-29.

Hatcher, R. D. Jr. & Acker, L. L. 1984. Geology of the Salem quadrangle, South Carolina. South Carolina Geological Survey, MS-26, 23p., scale 1/24,000.

Hatcher, R. D. Jr. & Goldberg, S. A. 1991. The Blue Ridge Geologic Province. In: Horton, J. W. Jr. & Zullo, V. A. (eds), The Geology of the Carolinas—Carolina Geological Society 50th Anniversary Volume. Knoxville, TN, The University of Tennessee Press, 11–35.

Hatcher, R. D. Jr. & Hooper, R. J. 1992. Evolution of crystalline thrust sheets in the internal parts of mountain chains. In: McClay, K. R. (ed) Thrust Tectonics. London, Chapman and Hall, 217–234.

Hatcher, R. D. Jr. Bream, B. R., Miller, C. L., Eckert, J. O. Jr. Fullagar, P. D. & Carrigan, C. W. 2004. Paleozoic Structure of Southern Appalachian Blue Ridge Grenvillian Internal Basement Massifs. In: Tollo, R. P., Corriveau, L., McLelland, J. & Bartholomew, M. J. (eds) Proterozoic evolution of the Grenville orogen in North America. Boulder, Colorado, Geological Society of America Memoir 197, 525–547.

Hauck, M. L., Nelson, K. D., Brown, L. D., Zhao, W. & Ross, A. R. 1998. Crustal structure of the Himalayan orogen at ~90° east longitude from Project INDEPTH deep reflection profiles. Tectonics, 17, 481-500.

Heyn, T. 1984. Stratigraphic and structural relationships along the southwestern flank of the Sauratown Mountains anticlinorium. M.S. thesis, Columbia, University of South Carolina, 192 p.

Hibbard, J. P., Stoddard, E. F., Secor, D. T. & Dennis, A. J. 2002. The Carolina Zone: overview of Neoproterozoic to Early Paleozoic peri-Gondwanan terranes along the eastern flank of the southern Appalachians. Earth-Science Reviews, 57, 299-339.

Hibbard, J. P., Tracy, R. J. & Henika, W. S. 2003. Smith River allochthon: A southern Appalachian peri-Gondwanan terrane emplaced directly on Laurentia? Geology, 31, 215-218.

Higgins, M. W., Crawford, T. J., Atkins, R. L. & Crawford, R. F. 2003. Geologic map of the Atlanta 30' x 60' quadrangle, Georgia. U.S. Geological Survey Geologic Investigations Series Map I-2062, scale 1:100,000.

Hooper, R. J. & Hatcher, R. D. Jr. 1988. The Pine Mountain terrane, a complex window in the Georgia and Alabama Piedmont: Evidence from the eastern termination: Reply: Geology, 16, 1049–1050.

Hooper, R. J. & Hatcher, R. D. Jr. 1992. The origin of the Pine Mountain window: An internal basement massif within the Piedmont of Alabama and Georgia. In: Mason, R. (ed) International Basement Tectonics, Association Publication 7, Basement Tectonics 7. Netherlands, Kluwer Academic Publishers, 375–383.

Hooper, R. J., Hatcher, R. D., Jr., Troyer, P. K., Dawson, R. J. & Redmond, C. G. 1997. The character of the Avalon terrane in central Georgia. In: Glover, L. III & Gates, A. E. (eds) Central and southern Appalachian sutures: Results of the EDGE Project and related studies. Geological Society of America Special Paper 314, 1-14.

Hopson, J.L. 1984. Stratigraphy and structure of the Alto allochthon, Ayersville quadrangle, Georgia. M.S. thesis, Columbia, University of South Carolina, 151 p.

Hopson, J. L. 1994. Structure of part of the Blue Ridge, northeastern Georgia and North Carolina. Ph.D. dissertation, Knoxville, University of Tennessee. 350 p.

Hopson, J. L. & Hatcher, R. D. Jr. 1988. Structural and stratigraphic setting of the Alto allochthon, northeast Georgia. Geological Society of America Bulletin, 100, 339–350.

Jamieson, R. A., Beaumont, C. & Medvedov, S. 2004. Crustal channel flows: 2. Numerical models with implications for metamorphism in the Himalayan-Tibetan orogen. Journal of Geophysical Research, 109, doi: 10.1029/2003JB002809.

King, P. B. 1955. A geologic section across the southern Appalachians: An outline to the geology in the segment in Tennessee, North Carolina, and South Carolina. In: Russell, R. J. (ed) Guides to southeastern geology. New York, Geological Society of America, 332-373.

Kish, S. 1997. The Cat Square charnockite—a Paleozoic charnockite in the Inner Piedmont of North Carolina. Geological Society of America Abstracts with Programs, 29/3, 28.

Laubscher, H. P., 1988, Material balance in Alpine orogeny. Geological Society of America Bulletin, 100, 1313–1328.

Lemmon, R. E. & Dunn, D. E. 1973a. Geologic map and mineral resources of the Bat Cave quadrangle, North Carolina. North Carolina Geological Survey GM 202-NW, scale 1/24000.

Lemmon, R. E. & Dunn, D. E. 1973b. Geologic map and mineral resources of the Fruitland quadrangle, North Carolina. North Carolina Geological Survey GM 202-NW, scale 1/24000.

Liu, A. 1991. Structural geology and deformation history of the Brevard fault zone, Chauga belt, and Inner Piedmont, northwestern South Carolina and adjacent areas. PhD dissertation, Knoxville, University of Tennessee, 200 p.

Luth, W. D., Jahns, R. H. & Tuttle, O. F. 1964. The granite system at pressures of 4 to 10 kilobars. Journal of Geophysical Research 69, 759–773.

Mancktelow, N. S. 1995. Nonlithostatic pressure during sediment subduction and the development and exhumation of high pressure metamorphic rocks. Journal of Geophysical Research, 100, 571-583.

Mapes, R. W. 2002. Geochemistry and geochronology of mid-Paleozoic granitic plutonism in the southern Appalachian Piedmont terrane, North Carolina-South Carolina-Georgia. M.S. thesis, Nashville, Vanderbilt University, 150 p.

Mapes, R. W., Miller, C. F., Fullagar, P. D. & Bream, B. R. 2001. Nature and origin of Acadian plutonism, Piedmont terane, NC-GA. Geological Society of America Abstracts with Programs, 33/6, 92.

Martizez-Martinez, J. M., Soto, J. I., and Balanyá 1997. Crustal decoupling and intracrustal flow beneath domal exhumed core complexes, Betics (SE Spain). Terra Nova 9, 223-227.

Maybin, A. H. III. 1995. Geologic map of the Simpsonville, Quadrangle, South Carolina. South Carolina Geological Survey Open File Map 92, scale 1:24,000.

Maybin, A. H. III. 1997. Geologic map of the Pelham quadrangle, South Carolina. South Carolina Geological Survey Open File Map, scale 1/24,000.

McConnell, K. I. 1990. Geology and geochronology of the Sauratown Mountains anticlinorium, northwestern North Carolina. Ph.D. dissertation, Columbia, University of South Carolina, 232 p.

McSween, H. Y. Jr., Sando, T W., Clark, S. R., Harden, J. T. & Strange, E. A. 1984. The gabbro-metagabbro association of the southern Appalachian Piedmont. American Journal of Science, 284, 437–461.

McSween, H. Y. Jr., Speer, J A. & Fullagar, P. D. 1991. 7. Plutonic rocks. In: Horton, J. W. Jr. & Zullo, V. A. (eds) The Geology of the Carolinas—Carolina Geological Society 50th Anniversary Volume. Knoxville, TN, The University of Tennessee Press, 109–126.

Mehnert, K. R. 1968. Migmatites and the origin of granitic rocks. Amsterdam, Elsevier, 393 p.

Merschat, A. J. 2003. Inner Piedmont tectonics in the southwestern Brushy Mountains, North Carolina: Field and laboratory data revealing 3-D crustal flow and sillimanite I and II metamorphism. M.S. thesis, Knoxville, University of Tennessee, 198 p.

Merschat, A. J., Hatcher, R. D. Jr. & Davis, T. L., 2005. The northern Inner Piedmont, southern Appalachians, USA: Kinematics of transpression and SW-directed mid-crustal flow. Journal of Structural Geology, 27, 1252–1281.

Miller, C. F., Hatcher, R. D., Jr., Ayers, J. C., Coath, C. D., and Harrison, T. M., 2000, Age and zircon inheritance of eastern Blue Ridge plutons, southwestern North Carolina and Northeastern Georgia, with implications for magma history and evolution of the southern Appalachian orogen: American Journal of Science, v. 300, p. 142–172.

Mirante, D. C. & Patino-Douce, A. E. 2000. Melting and migmatization in the southern Appalachian Inner Piedmont of northeast Georgia; the Athens gneiss. Geological Society of America Abstracts with Programs, 33, 297.

Moser, D. E., Heaman, L. M., Krogh, T E.,& Hanes, J.A. 1996. Intracrustal extension of an Archean orogen revealed using single-grain U-Pb geochronology. Tectonics 15/5, 1093-1109.

Neilson, M. J. 1988. The structure and stratigraphy of the Tallassee Synform, Dadeville Belt, Alabama: Southeastern Geology, 29/1, 41-50.

Nelson, A. E., Horton, J. W. & Clarke, J. W. 1998. Geologic map of the Greenville 1° x 2° quadrangle, Georgia, South Carolina, and North Carolina. U.S. Geological Survey Map I-2175, scale 1:250,000.

Nelson, K. D. 1988. The Pine Mountain terrane, a complex window in the Georgia and Alabama Piedmont: Evidence from the eastern termination: Comment. Geology, v. 16, p. 1049.

Nelson, K. D., Zhao, W., Brown, L. D., Kuo, J., Che, J., Liu, X., Klemperer, S. L., Makovsky, Y., Meissner, R., Mechie, J., Kind, R., Wenzel, F., Ni, J., Nabelek, J., Chen, L., Tan, H., Wie, W., Jones, A. G., Booker, J., Unsworth, M., Kidd, W. S. F., Hauck, M., Alsdorf, D., Ross, A., Cogan, M., Wu, C., Sandvol, E. A. & Edwards, M. 1996. Partially molten middle crust beneath southern Tibet; synthesis of Project INDEPTH results. Science, 274, 1684-1688.

Niewendorp, C. A. 1995a. Geology of the Bush River quadrangle, South Carolina. South Carolina Geological Survey Open File Map 84, scale 1/24,000.

Niewendorp, C. A. 1995b. Geology of the Joanna quadrangle, South Carolina. South Carolina Geological Survey Open File Map 85, scale 1/24,000.

Niewendorp, C. A. 1996. Geology of the Laurens North quadrangle, South Carolina. South Carolina Geological Survey Open File Map 89, scale 1/24,000.

Niewendorp, C. A. 1997. Geology of the Paris Mountain Quadrangle, South Carolina. South Carolina Geological Survey Open File Map 99, scale 1:24,000.

Niewendorp, C. A. & Maybin, A. H. III. 1994a. Geology of the Laurens South quadrangle, South Carolina. South Carolina Geological Survey Open File Map 77, scale 1/24,000.

Niewendorp, C. A. & Maybin, A. H. III. 1994b. Geology of the Cross Hill quadrangle, South Carolina. South Carolina Geological Survey Open File Map 78, scale 1/24,000.

Ownby, S. E., Miller, C. F., Berquist, P. J., Carrigan, C. W., Wooden, J. L. & Fullagar, P. D. 2004. U-Pb geochronology and geochemistry of a portion of the Mars Hill terrane, North Carolina–Tennessee: Constraints on origin, history, and tectonic assembly. In: Tollo, R. P., Corriveau. L., McLelland, J. & Bartholomew, M. J. (eds) Proterozoic tectonic evolution of the Grenville orogen in North America. Boulder, Colorado, Geological Society of America Memoir 197, 609-632.

Platt, J. P., & Behrmann, J. H., 1986. Structureees and fbrics in a crustal-scale shear zone, Betic Cordillera, SE Spain. Journal of Structural Geology 8, 15-33.

Rankin, D. W., Espenshade, G. J. & Neuman, R. B. 1972. Geologic map of the west half of the Winston-Salem quadrangle, North Carolina, Virginia, and Tennessee. U.S. Geological Survey Map I-709-A, scale 1:250,000.

Samson, S. D. & Secor, D. 2000. New U-Pb geochronological evidence for a Silurian magmatic event in central South Carolina. Geological Society of America Abstracts with Programs, 32/2, A71.

Steltenpohl, M. G. & Moore, W. B. 1988. Metamorphism in the Aabama Piedmont. Geological Survey of Alabama, Mineral Resources Circular 138, 27 p.

Steltenpohl, M. G., Kish, S. A. & Neilson, M. J. 1990. Geology of the southern Inner Piedmont, Alabama and southwest Georgia. Alabama Geological Survey & Alabama Geological Society Guidebook for Field Trip VII, 138 p.

Steltenpohl, M. G. (ed) 2005. Southernmost Appalachian terranes, Alabama and Georgia. Southeastern Section Geological Society of America Field Trip guide. Alabama Geological Society, 162 p.

Stieve, A. L. 1989. The structural evolution and metamorphism of the southern portion of the Tallulah Falls Dome, northeast Georgia. Ph.D. dissertation, Columbia, University of South Carolina, 207 p.

Student, J. J. & Sinha, A. K. 1992. Carboniferous U-Pb ages of zircons from the Box Ankle and Ocmulgee faults, central Georgia: Implications for accretionary models: Geological Society of America Abstracts with Programs, 24/2, 69.

Vauchez, A., Babaie, H. A. & Babaei, A. 1993. Orogen-parallel tangential motion in the Late Devonian-Early Carboniferous southern Appalachians internides. Canadian Journal of Earth Sciences, 30, 1297-1305.

Wegmann, C. E. 1935. Zur Deutung der Migmatite. Geologicschen Rundschau, 26, 20–350.

West, T. E., Jr. 1996. Geology of the Shoals Junction quadrangle, South Carolina. South Carolina Geological Survey Open File Map 88, scale 1/24,000.

West, T. E., Jr. 1997. Structural studies along the Carolina–Inner Piedmont terrane boundary in South Carolina and Georgia: implications for the tectonics of the southern Appalachians. Ph.D. dissertation, Columbia, University of South Carolina.

West, T. 1998. Structural analysis of the Carolina-Inner Piedmont terrane boundary: Implications for the age and kinematics of the central Piedmont suture, a terrane boundary that records Paleozoic Laurentia-Gondwana interactions. Tectonics, 17. 379–394.

Whisonant, J. S. 1979. Geologic map of the SE 1/4 of the Marion quadrangle, North Carolina. North Carolina Geological Survey GM 210-SE, scale 1/24,000.

Williams, S. T. 2000. Structure, stratigraphy, and migmatization in the southwestern South Mountains, North Carolina. M.S. thesis, Knoxville, University of Tennessee, 111 p.

Willis, J. D. 1984. Geology of the Cross Anchor area—the boundary between the Carolina terrane and Inner Piedmont in northwestern South Carolina. M.S. thesis, Columbia, University of South Carolina, 61 p.

Yanagihara, G. M. 1994. Structure, stratigraphy, and metamorphism of a part of the Columbus Promontory, western Inner Piedmont, North Carolina. M.S. thesis, Knoxville, University of Tennessee, 214 p.

PART VII

Inner Piedmont Geo-traverse from the Brushy Mountains to Lincolnton, North Carolina: Architecture of the Cat Square and Tugaloo Terranes

Part II consists of a slightly modified version of the guidebook from a field trip organized by my coauthors and myself for the 57th annual meeting of the Southeastern Section of the Geological Society of America in April 2008. Stop descriptions are excluded from this version. A full reference and link to a digital copy of the entire guidebook is listed below.

Merschat, A. J., Hatcher, R. D., Jr., Byars, H. E., and Gilliam, W. G., 2008, Inner Piedmont geo-traverse from the Brushy Mountains to Lincolnton, North Carolina: Architecture of the Cat Square and Tugaloo terranes: Geological Society of America Southeastern Section, Field trip guidebook, 64 p. http://segsa2008.uncc.edu/fieldtrips.html

The field trip traversed the Inner Piedmont from northwest to southeast, beginning in the Brushy Mountains, Day 1, and ending near Lincolnton, North Carolina, Day 2. Sixteen stops were selected to highlight the geology of the Inner Piedmont with special emphasis on the tectonics of the Cat Square terrane. My contributions included: (1) writing most of the guide; a summary of recent work and new data; (2) stop descriptions for Day 1 in the Brushy Mountains; and (3) assistance with trip logistics. New material added to this version includes a dectritpion of the petrography and geochemistry of Newton window amphibolites and geochronology of the Reepsville gneiss.

INTRODUCTION

One of the most significant recent developments in southern Appalachian geology is the recognition of the sillimanite grade, mixed Laurentian and peri-Gondwanan affinity, Siluro-Devonian metasedimentary Cat Square terrane in the southeastern Inner Piedmont (IP) (Fig. 7–1). The existence of these young rocks in the orogen has important tectonic implications regarding sedimentation, timing of metamorphism, terrane accretion, and our understanding of the development of the orogen as a whole. These tectonic implications, however, must be consistent with field observations regarding the nature of terrane boundaries, comparison of lithostratigraphy with other terranes, contact relationships with intrusive bodies, and deformational and metamorphic histories.

The objective of this field trip is to examine the key elements—boundaries, rock types, plutons, metamorphism, and structures—of the Cat Square terrane in a northwest-to-southeast traverse across the North Carolina IP. We will examine the different lithostratigraphies of the Tugaloo and Cat Square terranes, rocks of the Brindle Creek fault zone that bounds the Cat Square terrane, evidence of the close temporal relationship of Devonian plutonism and metamorphism in the IP, and the significance of the Newton window in the eastern IP. On Day 1 we will depart Morganton, drive to Lenoir, and begin

Figure 7–1. (a) Index map of the U.S. (b) Tectonic map of the southern Appalachians showing the location of the Inner Piedmont and major tectonostratigraphic terranes. DGB–Dahlonega gold belt. GMW–Grandfather Mountain window. PMW–Pine Mountain window. SMW–Sauratown Mountains window. SRA–Smith River allochthon. Chatt. F.– Chattahoochee fault. Dark purple– Elkahatchee pluton (Middle Ordovician). Yellow, pink, light orange, and brown–internal Blue Ridge terranes. Red–Grenville and pre-Grenville basement. (c) Tectonic map of the Inner Piedmont in the Carolinas and northern Georgia, compiled and modified from Rankin et al. (1972), Espenshade et al. (1975), Goldsmith et al. (1988), Hopson and Hatcher (1988), Hatcher and Hooper (1992), Nelson et al. (1998), and Fig. 1 in Hatcher (2002, and sources cited therein). Faults and thrust sheets: AA–Alto allochthon. AnF–Anderson. BCF–Brindle Creek. BFZ–Brevard. FF–Forbush. MF–Marion. MSF–Mill Spring. PMF–Paris Mountain. RF–Ridgeway. RsF–Rosman fault. SMtF–Sugarloaf Mountain fault. SMW–Sauratown Mountains window. SNF–Six Mile–Seneca. SRA–Smith River allochthon. WLF–Walhalla. Named Ordovician (purple) and Ordovician(?) (lighter purple) granitoids: Och–Caesars Head. Od–Dysartsville. Oh–Henderson. Ot–Toccoa. an–Antreville. st–Starr. Others in the western Inner Piedmont (probably Ordovician) are colored lighter shades of purple. Silurian granitoid: Sbc–Brooks Crossroads. Devonian and Devonian(?) plutons (light blue): rf–Rocky Face. Dt–Toluca. Dwt–Walker Top. sm–Sandy Mush. Darker blue–Mississippian plutons: Mc–Cherryville. Mgc–Gray Court. Mrr–Reedy River. Pennsylvanian plutons: Pe–Elberton. Ppm–Pacolet Mills (in Carolina terrane). Towns: An–Anderson. Gr–Greenville. Gs–Gainesville. Gw–Greenwood. Hk–Hickory. Hv–Hendersonville. Ln–Lenoir. Mg–Morganton. Sh–Shelby. Sp–Spartanburg. Wk–Wilkesboro. WS–Winston-Salem.

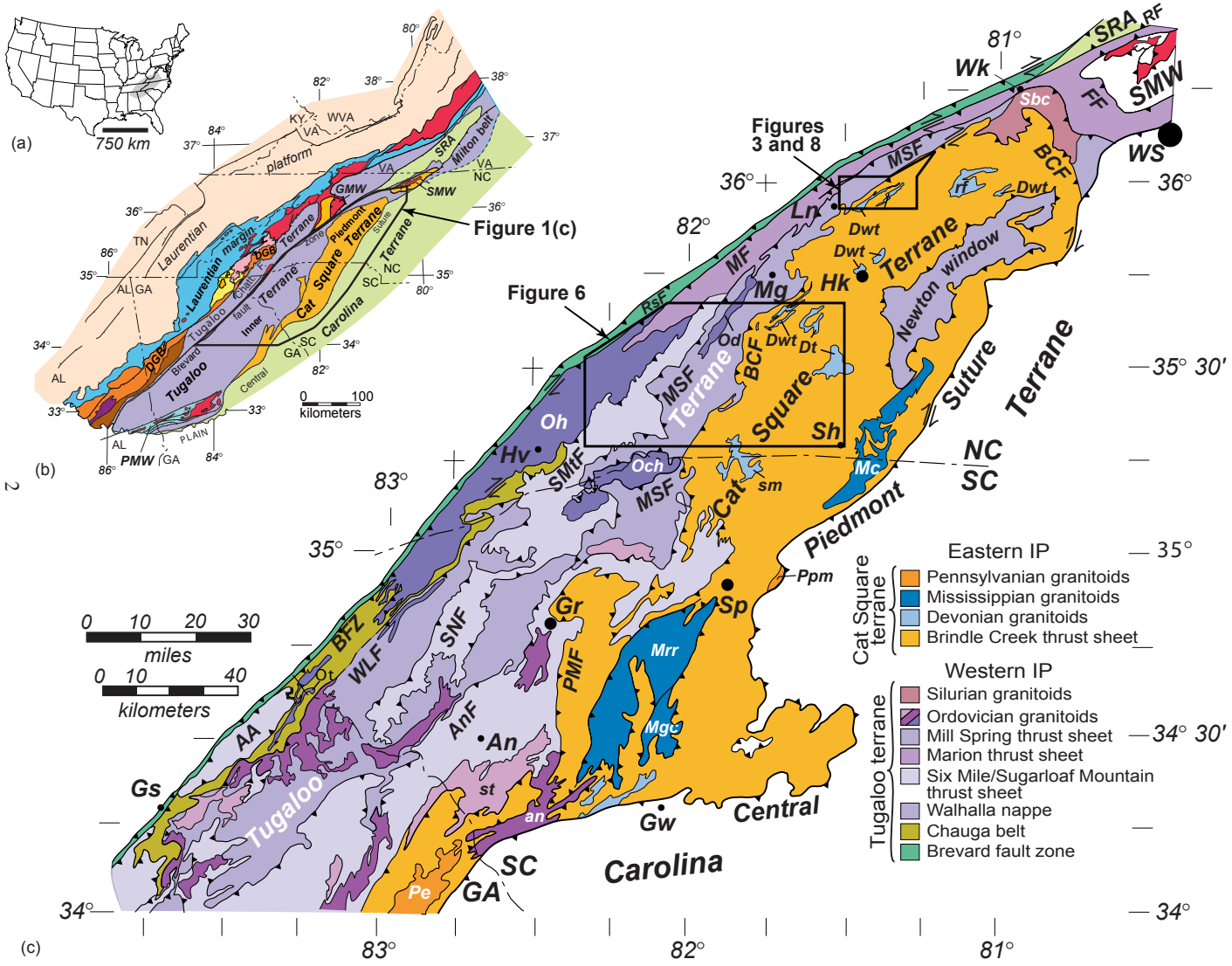
(a)
750 km
(b)
Figure 1(c)
Figure 6
Figures 3 and 8
(c)
0 100 kilometers
0 10 20 30 miles
0 10 40 kilometers
Eastern IP
Cat Square terrane
Pennsylvanian granitoids
Mississippian granitoids
Devonian granitoids
Brindle Creek thrust sheet
Western IP
Tugaloo terrane
Silurian granitoids
Ordovician granitoids
Mill Spring thrust sheet
Marion thrust sheet
Six Mile/Sugarloaf Mountain thrust sheet
Walhalla nappe
Chauga belt
Brevard fault zone
Laurentian margin
platform
Milton belt
Inner Piedmont Terrane
Cat Square Terrane
Carolina Terrane
Tugaloo Terrane
Central Piedmont Suture
Newton window
Eastern Piedmont
Central Carolina
Tugaloo
Wk
Sbc
FF
SMW
WS
SRA
RF
MSF
BCF
MF
Ln
Dwt
Mg
Hk
RSF
Od
Dt
Oh
Hv
SMtF
Och
Sh
Mc
NC
SC
Cat
sm
Ppm
Sp
Gr
Mrr
Mgc
PMF
SNF
BFZ
WLF
AA
Ot
AnF
An
st
an
Gs
Gw
Pe
GA
SC
81°
82°
83°
34°
35°
36°
34° 30'
35° 30'

the trip in the western IP to examine Tugaloo terrane rocks, then traverse the Brindle Creek fault zone into the Cat Square terrane. We will then move southeast into the Cat Square terrane to examine relationships between metamorphism, migmatites, granitoids, and other rock units in the internal portion of the Cat Square terrane before returning to Morganton. Day 2 will focus on the Newton window: the Brindle Creek fault framing the window and the differences between Tugaloo terrane rocks in the window and surrounding Cat Square terrane rocks. Exposures will include the Brindle Creek fault, the Vale charnockite xenolith in Walker Top Granite, and Tugaloo terrane rocks inside the Newton window. The field trip will conclude with a stop in Cat Square, North Carolina, and a drive to Charlotte in time for the welcoming party (beer!).

TECTONIC SETTING AND ATTRIBUTES OF THE NORTHERN IP

The IP extends some 700 km along strike from Winston-Salem, North Carolina, southwestward to the Coastal Plain in Alabama (Fig. 7–1b) and has been long recognized for its high metamorphic grade and contrasting structural style with adjacent terranes (King, 1955; Bentley and Neathery, 1970). It is separated from the eastern Blue Ridge (western Tugaloo terrane) to the northwest by the Brevard fault zone and from the exotic Carolina superterrane (Secor et al., 1983) to the southeast by the central Piedmont suture (Hatcher and Zietz, 1980; Williams and Hatcher, 1983). The composite IP consists of the eastern Tugaloo (western IP) and Cat Square terranes, separated by the Brindle Creek fault (Fig. 7–1). Metamorphic grade remains at or above first sillimanite across the broad core of the IP, decreasing to kyanite and locally garnet grade on the eastern and western flanks (Butler, 1991; Hatcher and Merschat, 2006).

The IP is polydeformed with shallow-dipping meso- and macroscale structures that contrast with those in adjacent terranes. A gently dipping stack of large, crystalline, Type F thrust sheets (formed by plastic excision of the common limb between a recumbent or inclined antiform and synform—fold nappes; Hatcher and Hooper, 1992; Hatcher, 2004), shallow-dipping foliations, map-scale sheath folds, curved mineral stretching lineations, dominance of sillimanite grade rocks and migmatite, and a long, hot thermal history, comprise the attributes of the mid-Paleozoic IP.

Several studies have demonstrated that the IP is multiply deformed (Table 7–1) and the dominant structural elements are S_2, $L_{2,}$ and F_2 (e.g., Hopson and Hatcher 1988; Hatcher, 2001; Merschat et al., 2005a). The dominant S_2 foliation throughout the IP dips gently and becomes strongly NE-SW oriented along the western flank of the IP (Fig. 7–2). S_2 is defined by parallel alignment of phyllosilicates, quartz ribbons, and other

Table 7–1. Tectonic summary for the northern IP.

EVENTS	STRUCTURES			METAMORPHIC CONDITIONS	REGIONAL EVENTS	OROGENY & TIMING
	Fabrics	Folds	Faults	Z | PP | Gs | A | G		
D_1	S_1 Early foliation preserved in amphibolite and calc-silicate boudins	F_1 Intrafolial folds and isoclinal folds preserved in boudins	———	M_1 Moderate to high pressure and temperature	Initial collision and subduction of IP beneath Carolina terrane	Pre- to early Acadian post ~410 Ma
D_2	S_2 Penetrative foliation L_2 Mineral lineation; curving pattern, trends NE-SW, E-W, & NW-SE	F_2 Inclined to recumbent, tight to isoclinal passive and flexural flow folds, and sheath folds; curving pattern trends NE-SW, E-W, & NW-SE	Initial NW and then SW deflected movement of IP faults	M_2 Peak metamorphism, upper amphibolite facies, sillimanite I & II grade	Continued subduction, emplacement of crystalline thrust sheets, and SW deflection along Neoacadian BFZ, channel flow	Neoacadian 360–345 Ma
D_3	S_3 Rare secondary foliation L_3 Mineral and intersection lineations	F_3 Inclined to upright, closed to open folds, trend NNE-SSW, N, & NW	Continued NW and SW movement on IP faults	M_3 Decreasing P-T conditions, high to moderate pressure and temperature	Initial subduction beneath Africa, final emplacement and exhumation of IP thrust sheets	Early Alleghanian 330–325 Ma
D_4	S-C and related fabrics in BFZ, & CPS Mineral lineations in BFZ, intersections in IP	F_4 Upright, open folds, trend NW-SE, & NE; crenulations plunge SE, & NE	Ductile reactivation of BFZ & CPS	Low pressure and temperature – greenschist facies (retrogressive)	Initial emplacement of the composite Blue Ridge-IP thrust sheet and exhumation	Alleghanian ~300 Ma
D_5	Joints Mineralized (?)	Regional broad, open folds, most trend NE & NW	Brittle movements associated with the Rosman fault of the BFZ	Brittle conditions	Continued emplacement and exhumation of the composite Blue Ridge-IP thrust sheet	Late Alleghanian ~260 Ma
$D_{6...}$	Filled joints Unfilled joints	Regional broad, open folds, trend NE	Meso- and macroscale normal faults	M_4 Brittle conditions	Rifting — — ? — — Uplift	Mesozoic extension — ? — Cenozoic uplift

Shaded curve under metamorphic conditions represents changes in P-T conditions, identifying peak conditions in each event.
Metamorhpic facies: *Z*–Zeolite, *PP*–Prehnite-Pumpellyite, *Gs*–Greenschist, *A*–Amphibolite, *G*–Granulite
BFZ—Brevard fault zone. CPS—central Piedmont suture.

Figure 7–2. Pattern of dominant (S_2) foliation and lineation in the northern Inner Piedmont. (a) Histogram of 4,587 dip measurements of dominant foliation in the northern Inner Piedmont. (b) Form-line map of S_2 foliation in the northern Inner Piedmont. Form lines are parallel to strike; teeth on trend lines indicate dip direction. Density of form lines indicates density of data coverage used in map compilation. New data collected after this map was compiled reinforce the broad patterns depicted on this map. (c) Histogram of 764 mostly mineral lineations in the northern IP. Note the dominance of gentle plunges. (d) Distribution of measured lineations (filtered to create spacing). Arrowhead indicates direction of plunge; arrowhead on both ends of line indicates horizontal lineation. Line on each measurement indicates trend. Additional measurements added to this data set since the original compilation was made (see Figs. **7-**7 and **7-**12) reinforce the curved pattern illustrated by the data. Sources of foliation and lineation data are listed in Hatcher (2001, 2002) and Merschat et al., (2005a).

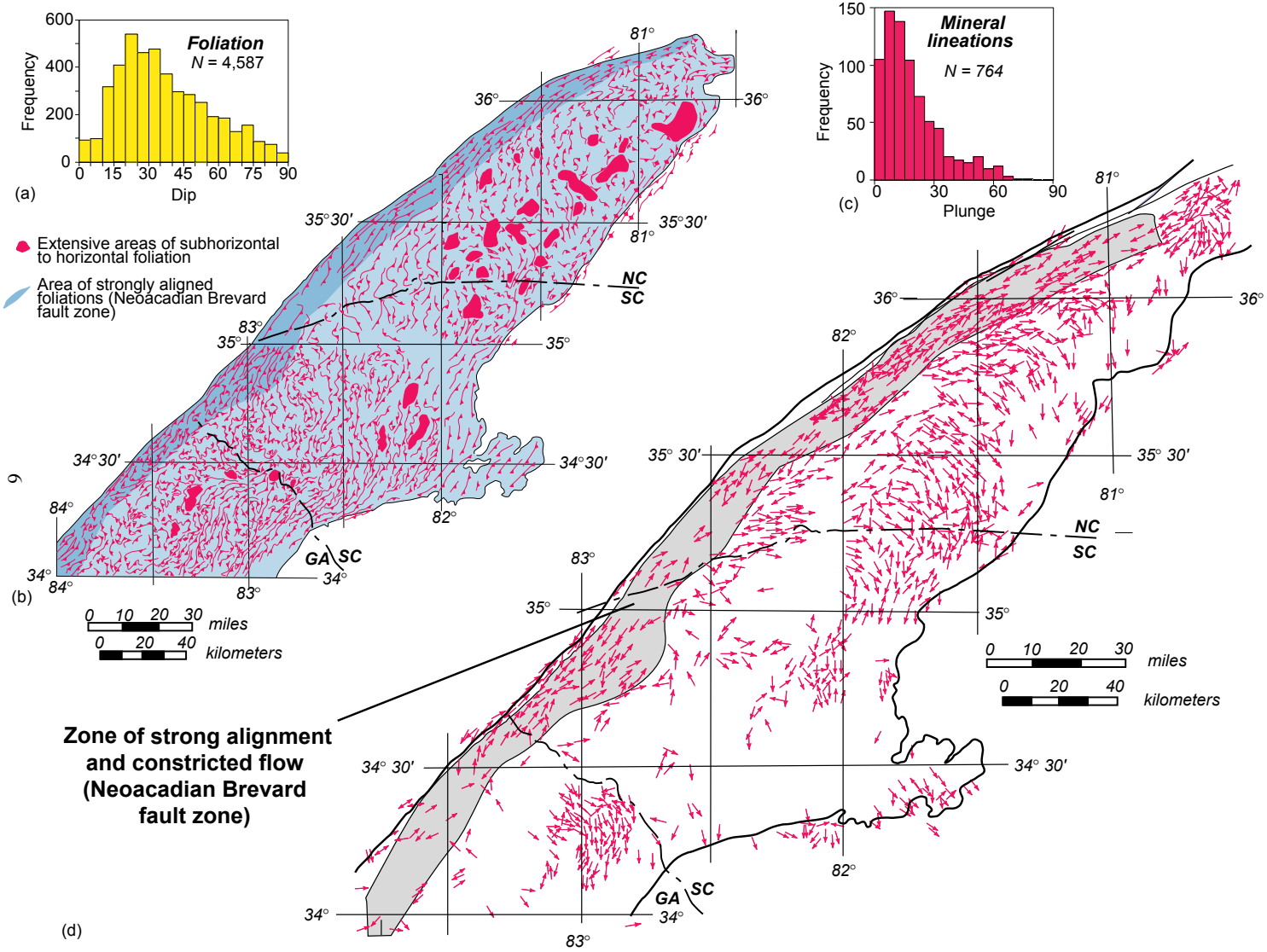
Foliation
N = 4,587
Frequency
Dip
(a)
Extensive areas of subhorizontal to horizontal foliation
Area of strongly aligned foliations (Neoacadian Brevard fault zone)
Mineral lineations
N = 764
Plunge
(c)
NC
SC
GA
SC
(b)
(d)
miles
kilometers
Zone of strong alignment and constricted flow (Neoacadian Brevard fault zone)

nonequant minerals. Transposed compositional layering and new migmatitic layering parallel to S_2 are axial planar to recumbent to reclined, isoclinal to tight, gently plunging F_2 folds. The high–temperature mineral stretching lineation, L_2, (see Merschat et al., 2005a, *their* Fig. 8b) varies in degree of development with rock type and is defined by elongate sillimanite, hornblende, quartz rods, streaked muscovite, or mantled feldspars. Throughout most of the IP, L_2 is subhorizontal and coaxial with F_2. Goldsmith (1981) was the first to recognize this arcuate pattern defined by L_2 mineral lineations and F_2 fold hinges. From southeast to northwest the pattern curves from N-S to NW-SE to E-W to NE-SW (Fig. 7–3c). As stated by Merschat et al. (2005a), this mineral lineation formed during peak metamorphism and has been dated (zircon rims) at 360-350 Ma by Bream et al. (2001) and Bream (2002, 2003). Field and geochronologic relationships indicate that L_2 formed during one event, and the curved pattern is ***not*** the product of overprinting polydeformation.

Another fundamental structural characteristic recently documented in the IP is both map- and meso-scale sheath folds (Fig. 7–3; see also Merschat et al., 2005a, *their* Figs. 8c, 8d, and 11). Because of the small size of exposures throughout most of the IP, we have observed only a few large mesoscale sheath folds (e.g., Fig. 7–3 and Merschat et al., 2005a, *their* Figs. 8, 9, and 11), but smaller mesoscale sheath folds are fairly common. Sheath folds that have been observed mostly have southwest-directed transport confirmed independently by numerous shear sense indicators and map patterns (Merschat et al., 2005a). In addition, map-scale southwest-directed sheath folds exist in the western IP in South Carolina, and were mapped as southwest-directed thrusts that repeat the Chauga belt sequences (see Merschat et al., 2005a, *their* Fig. 9).

The Brevard fault separates the eastern from the western Tugaloo terrane, but the Brevard played a key mechanical and kinematic role in the deformational history of the IP (Hatcher, 2001; Merschat et al., 2005a). The Brevard fault records three deformational events, a mid-Paleozoic high-temperature event, followed by greenschist grade dextral shearing, and late brittle thrusting of the northwest boundary associated with the Rosman fault (Horton and Butler, 1986; Hatcher, 2001). A zone of strongly aligned foliations and lineations along the western flank of the IP defines the mid–Paleozoic Brevard fault zone, which consists of a 15 to 20 km wide amphibolite grade dextral shear zone that dips 10 to 45° SE (Hatcher, 2001). It is characterized by strongly aligned mylonitic foliation (S_2) striking NE, dipping SE, and a subhorizontal NE–SW– trending mineral lineation (L_2), with a top-to-the-SW shear sense, and was active from at least 360 to 350 Ma (Fig. 7–2; Davis et al., 1991; Davis, 1993a, b; Vauchez et al., 1993; Hatcher, 2001;

Figure 7–3. Simplified geologic maps of (a) northwestern IP and (b) part of the SW BM showing structures in the Brindle Creek fault hanging wall and Walker Top and Toluca Granite bodies dismembered by SW-thrusted sheath folds. BCF–Brindle Creek fault. BWSF–Big Warrior sheath fold. ESF–Ellendale sheath fold. MSF-–Mill Spring fault. PSSF–Poplar Springs sheath fold. RsF–Rosman fault. SRA–Smith River allochthon.

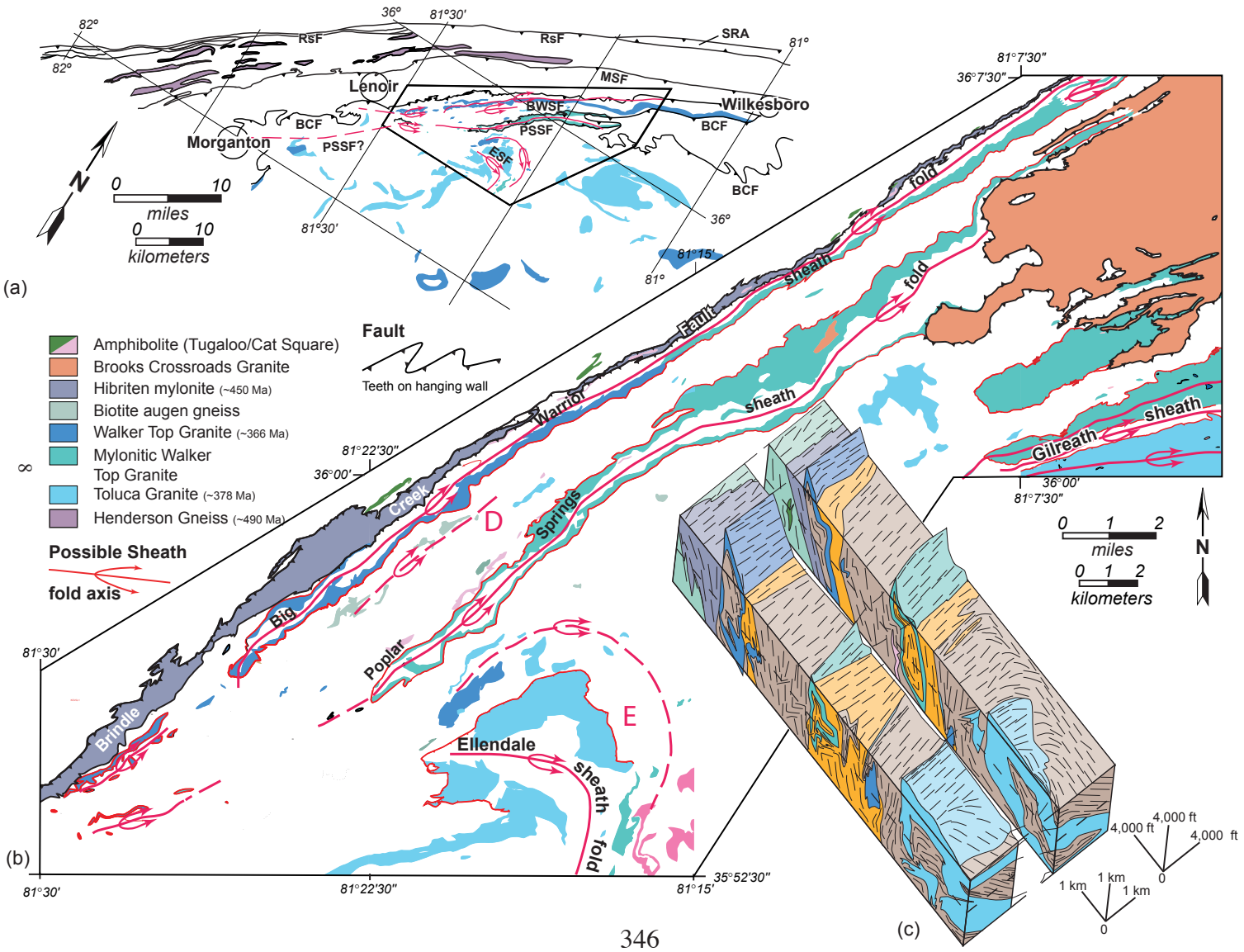
(a)
82°
36°
81°30′
81°
RsF
SRA
MSF
BWSF
PSSF
PSSF?
BCF
FSF
Lenoir
Wilkesboro
Morganton
0 10
miles
0 10
kilometers
81°15′
Amphibolite (Tugaloo/Cat Square)
Brooks Crossroads Granite
Hibriten mylonite (~450 Ma)
Biotite augen gneiss
Walker Top Granite (~366 Ma)
Mylonitic Walker Top Granite
Toluca Granite (~378 Ma)
Henderson Gneiss (~490 Ma)
Fault
Teeth on hanging wall
Possible Sheath
fold axis
Fault
Warrior
Creek
Springs
Big
Poplar
Brindle
Ellendale
sheath
fold
D
E
81°22′30″
36°00′
81°30′
35°52′30″
81°15′
(b)
81°7′30″
36°7′30″
36°00′
0 1 2
miles
0 1 2
kilometers
N
(c)
4,000 ft
1 km
0

Merschat et al., 2005a). Estimates for the net SW-directed displacement associated with the mid–Paleozoic Brevard fault zone range from 200-400 km from bulk strain estimates for restoring the Henderson gneiss, and integrating shear strain estimates typical of sheath folds (γ =10-20) over the width of the Neoacadian Brevard fault zone.

The IP consists of a stack of gently dipping crystalline thrust sheets (Griffin, 1971; Goldsmith et al., 1988; Higgins et al., 1988; Horton and McConnell, 1991). Griffin (1969, 1971, 1974) was the first to recognize the fold-nappe structural style in the IP, but concluded these nappes are northwest vergent. Griffin (1971) suggested that the IP is the autochthonous core of a high-grade, west-verging nappe complex, but other interpretations favor allochthonous crystalline thrust sheets (e.g., Hatcher, 1972, 1974, 1978; Goldsmith et al., 1988; Higgins et al., 1988; Hatcher and Hooper, 1992; Nelson et al., 1998). Hatcher and Hooper (1992) and Hatcher (2004) concluded the IP thrusts are Type-F thrusts: plastic, lobate, fold-derived thrusts with penetrative mesofabrics that evolved entirely beneath the ductile-brittle transition, similar to those in the Parry Sound region of the southern Grenville province in Ontario (Hanmer, 1988), the Cabo Ortegal complex in northwestern Spain (Azcárraga et al., 2002), the Moine nappes in the northern Scottish Caledonides (Alsop and Holdsworth, 1999, 2002), and the Pennine Alpine nappes (Trümpy, 1960, 1980; Merle et al., 1989). Seven major faults occur in the northern IP (Fig. 7–1c), and additional thrust sheets have been recognized in the IP farther south in Georgia (Higgins et al., 1988).

Griffin (1974) suggested the IP represented the high-grade mobile infrastructure below a suprastructure represented by the Carolina superterrane. Recent studies integrating the key elements of the IP have reached similar conclusions. Merschat et al. (2005a) and Hatcher and Merschat (2006) concluded that the IP represents an exhumed mid-Paleozoic, southwest-directed, orogenic channel forced from beneath the Carolina superterrane. Although similar to the infrastructure-suprastructure model of Griffin (1974), we infer that the Carolina superterrane collided obliquely and thus diachronously from north to south with the IP so that flow in the migmatitic mass could escape toward the southwest, as it was buttressed against the underlying Brevard fault zone (Fig. 7–4). Oblique, zippered northeast-to-southwest collision of Carolina superterrane would imply that progressive younging of deformation and metamorphism should also occur. Modern age dates do not exist in western Georgia and Alabama to test this implication, but faults framing the east end of the Pine Mountain window have yielded 330 and 303 Ma ages (Student and Sinha 1992), and these faults truncate IP structures and mesofabrics.

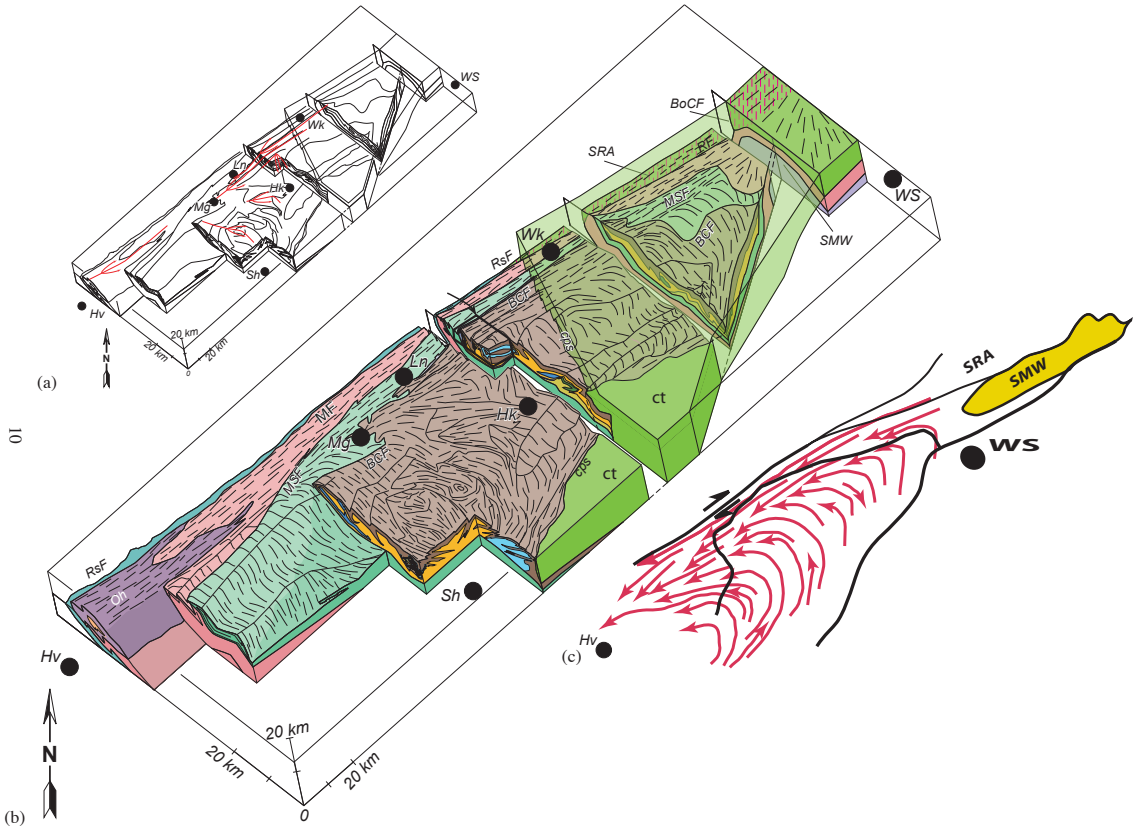

Figure 7–4. 3D sturcture of part of the northern Inner Piedmont. (a) 3D block diagram depicting the structure of part of the northern IP from near Hendersonville, NC to the Sauratown Mountains window. Red lines are map-scale sheath folds. Vertical exaggeration in (a) and (b) 1.3:1:1 (X:Y:Z). Towns: Hk—Hickory; Hv—Hendersonville; Ln—Lenoir; Mg—Morganton; Sh—Shelby; Wk—Wilkesboro; WS—Winston-Salem. (b) More detailed 3D block diagram of area in (a) showing major tectonic units. Trends on block surface drawn from lineations. BCF—Brindle Creek fault; BoCF—Bowens Creek fault; cps—Central Piedmont suture; ct—Carolina terrane; MSF—Mill Spring fault; MF—Marion fault; Oh—Henderson Gneiss; RF—Ridgeway fault; RsF—Rosman fault; SMW—Sauratown Mountains window; SRA—Smith River allochthon. Town abbreviations sames as in (a). (c) Flow model for the northern Inner Piedmont based on detailed geologic mapping and lineation data of the kind displayed in Figure **7**-2. WS–Winston-Salem. Hv–Hendersonville.

METAMORPHISM

Metamorphic grade increases from garnet (in South Carolina) and staurolite–kyanite (in North Carolina) near the BFZ to sillimanite and higher grade across the broad core of the IP (Reed and Bryant, 1964; Bryant and Reed, 1970; Butler, 1991; Bier et al., 2002), locally decreasing to staurolite or garnet grade along the southeast flank (Goldsmith et al., 1988; Butler, 1991) (Fig. 7–5). IP rocks are pervasively migmatitic, except along the flanks. P-T estimates range from 500º C to 800º C and 3-7 kbar (Davis, 1993a; Mirante and Patino-Douce, 2000; Bier et al., 2002; Merschat, 2003). Single continuous garnet zoning profiles and an increase in temperature from garnet cores to rims from both the western and eastern IP indicate a single prograde metamorphic event affected the IP (Davis, 1993a; Bier et al., 2002; Merschat and Kalbas, 2002). Retrograde greenschist facies assemblages resulted from Alleghanian reactivation of the Brevard fault zone (Reed and Bryant, 1964; Bryant and Reed, 1970; Hatcher, 2001).

Hopson and Hatcher (1988) documented fault-related inversion of metamorphic isograds beneath the Alto allochthon in northeast Georgia and northwestern South Carolina. Rocks of the Brindle Creek fault footwall are intensely migmatitic up to 7 km west of the trace of the fault (Giorgis, 1999; Merschat and Kalbas, 2002). Hatcher (2002) and Merschat and Kalbas (2002) speculated the sheet was emplaced hot and the additional heat and crustal thickening summed to produce the intense footwall migmatization. Griffin (1969) observed a similar phenomenon locally beneath the Six Mile thrust sheet in northwestern South Carolina.

Using conventional (TIMS) U-Pb dating methods, Dennis and Wright (1997a, b) reported monazite ages of ~360 Ma and ~325 Ma from a sample traverse across the South Carolina IP. Mirante and Patino-Douce (2000) reported an electron microprobe U-Pb monazite age of ~330 Ma for IP metamorphism near Athens, Georgia. Carrigan et al. (2001) reported a summed probability age of ~352 Ma for ion microprobe zircon rims from the IP and eastern Blue Ridge (Fig. 7–5). A 342 Ma U-Pb ion microprobe age records growth of metamorphic zircon rims and coeval migmatite generation in intermediate and mafic metaigneous rocks in the Brindle Creek footwall near Lenoir, North Carolina (Fig. 7–5) (Kalbas et al., 2002; Bream, 2003). Similarly, Gatewood (2007) reported SHRIMP U/Pb zircon rim ages of ~364 and 345 Ma from the Hibriten mylonite. Robinson et al. (1998) proposed the term Neoacadian for a 366-355 Ma thermal event in New England, which has been adopted for the 360-345 Ma high temperature event in the southern Appalachians (e.g. Kohn, 2001; Hatcher, 2002). The

Figure 7–5. Metamorphic isograd map of the northern Inner Piedmont and U-Pb ages of metamorphic zircons. (a) Summed probability of zircon rim ages from the IP and one sample from the eastern Blue Ridge (Bream, 2003). (b) Isograd map of the Neoacadian core of the southern Appalachians modified from Hatcher and Merschat (2006). Sources of data are Dennis and Wright (1997a,b)[1], Kish (1997)[2], Mirante and Patino-Douce (2000)[3], Mapes (2002)[4], Bream (2003)[5], Hibbard et al. (2003)[6], Merschat et al. (2005b)[7], and Dennis (2007)[8].

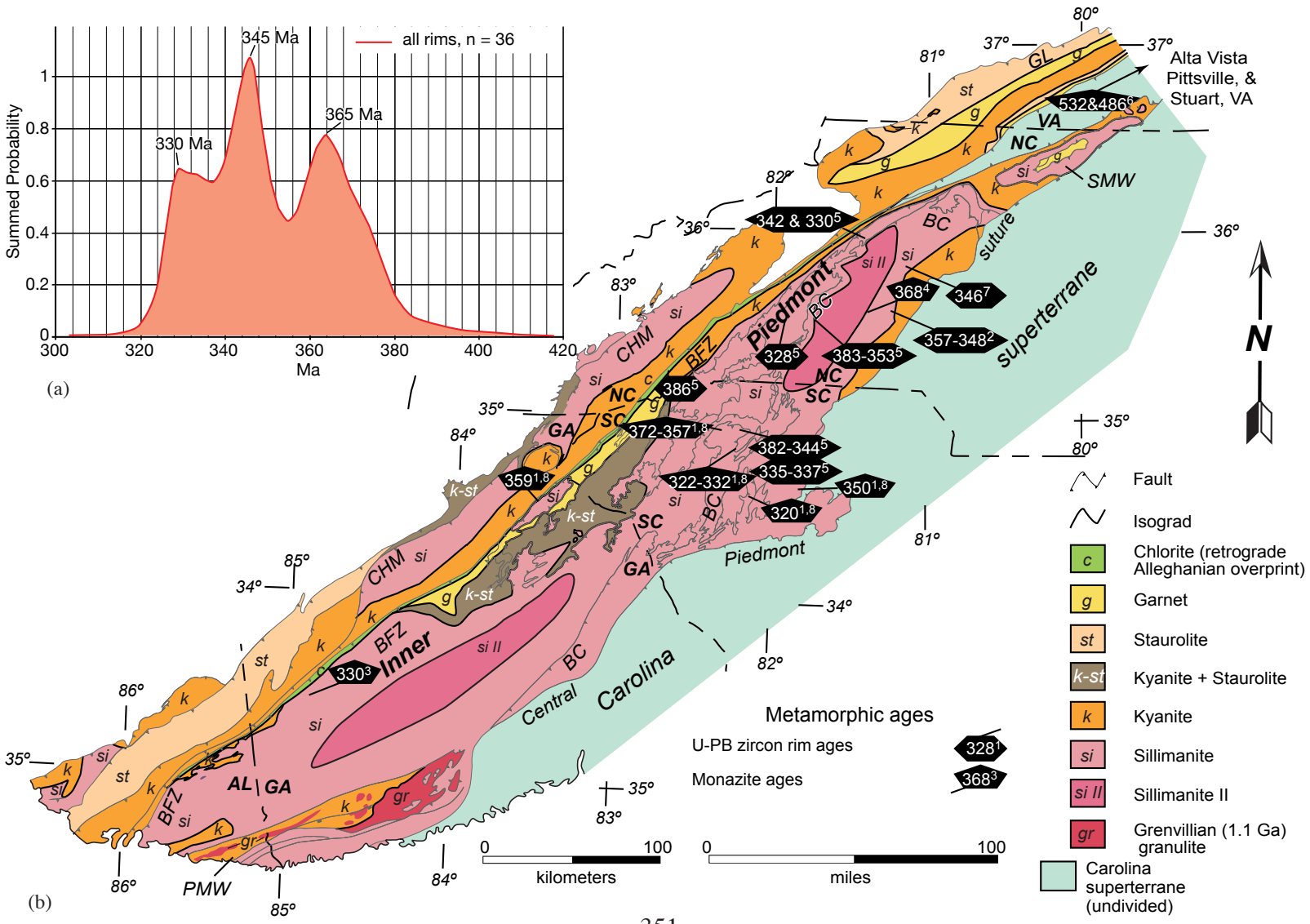
345 Ma
all rims, n = 36
330 Ma
365 Ma
Summed Probability
Ma
(a)
(b)
Alta Vista
Pittsville, &
Stuart, VA
532&4866
342 & 3305
368⁴
346⁷
328⁵
383-353⁵
357-348²
386⁵
372-357¹,⁸
382-344⁵
335-337⁵
322-332¹,⁸
350¹,⁸
320¹,⁸
359¹,⁸
330³
Piedmont
superterrane
Carolina
Central
Inner
Piedmont
suture
BFZ
CHM
BC
NC
SC
GA
AL
GA
SMW
PMW
VA
GL
Metamorphic ages
U-PB zircon rim ages
Monazite ages
3281
3683
Fault
Isograd
Chlorite (retrograde Alleghanian overprint)
Garnet
Staurolite
Kyanite + Staurolite
Kyanite
Sillimanite
Sillimanite II
Grenvillian (1.1 Ga) granulite
Carolina superterrane (undivided)
kilometers
miles
N

330-325 Ma ages are Alleghanian, recording the earliest thermal events connecting the Tugaloo, Cat Square, and Carolina terranes (Dennis and Wright, 1997a, b).

INNER PIEDMONT TERRANES: CONTRASTING LITHOSTRATIGRAPHIES AND MAGMATISM

The Brindle Creek fault extends from northwest of Winston-Salem, North Carolina to south of Athens, Georgia (Fig. 7–1c). Reconnaissance mapping, detrital zircon geochronology, and aeromagnetic data suggest the Brindle Creek fault may extend into Alabama (Hatcher et al., 2007). It separates the IP into two contrasting lithologic assemblages: the western and eastern IP (Bream and Hatcher, 2002). Dominance of biotite gneiss/metagraywacke in the western IP versus aluminous schist and biotite gneiss in the eastern IP can be easily recognized on most geologic maps (e.g., Reed, 1964; Bryant and Reed,1970; Brown et al., 1985; Goldsmith et al., 1988). Magmatism in the IP is also partitioned across the Brindle Creek fault: Ordovician-Silurian magmatism dominates to the west and Devonian to Mississippian magmatism dominates to the east (Mapes, 2002; Mapes et al., 2002; Bream, 2003) (Table 7–2). Finally, contrasting detrital zircon populations support different provenances of the Cat Square and Tugaloo terranes (Bream et al., 2001, 2004)(Table 7–2).

Western IP –Tugaloo terrane

Western IP rocks are part of the Tugaloo terrane, the western boundary of which is the Chattahoochee fault in the eastern Blue Ridge (Fig. 7–1b). The BFZ is located within this terrane, and was a suitably oriented crustal weak zone during Neoacadian deformation that was reactivated in the Alleghanian (Hatcher, 2001). The crustal affinity of the IP has long been debated, with some concluding the BFZ is a suture, making the IP a suspect (Williams and Hatcher, 1983) or an exotic terrane (e.g., Rankin, 1975; Horton and McConnell, 1991; Hibbard, 2000). Detrital zircon data indicate Laurentian affinity of eastern Blue Ridge and western IP rocks, indicating the BFZ likely is not a suture (Bream et al., 2000, 2001; Bream 2003). Identical stratigraphic sequences (Tallulah Falls Formation rocks) on both sides of the BFZ also preclude it being a suture (Hopson and Hatcher, 1988; Hatcher, 2001, 2002; Hatcher et al., 2007).

Western IP thrust sheets contain the Laurentian affinity, Neoproterozoic to Cambrian(?) Tallulah Falls and Chauga River Formations unconformably overlain by Middle Ordovician Poor Mountain Formation, traceable from near Gainesville, Georgia to northeast of Lenoir, North Carolina (Bream, 2002; Hatcher, 2002; Bream et al., 2004).

Table 7–2. Summary of recent SHRIMP U-Pb magmatic, metamorphic, and detrital zircon geochronology.

Terrane	Tectonic belt/structure	Sample	Location	Ages*	Source
Tugaloo	Western Inner Piedmont	Zirconia pegmatite	35.233ºN 82.446ºW	~327 Ma	Bream, 2003
		Hibriten mylonite (KC-1)	35.907ºN 81.491ºW	~442 or ~433 Ma	Gatewood, 2007
		Hibriten mylonite (MV-688)	36.073ºN 81.196ºW	~449 Ma	Gatewood, 2007
		Poor Mountain metatuff	35.605ºN 81.955ºW	~451 Ma (all) or 444 Ma	Bream, 2003
		Toccoa granitoid	Hanson quarry	~449 Ma	Bream, 2003
		Lenoir Quarry Migmatite	35.931ºN 81.479ºW	~450 Ma *(342 & 330 Ma)*	Bream, 2003
		Dysartsville Tonalite	35.549ºN 81.962ºW	~468 Ma	Bream, 2003
		Chauga River Formation Brevard-Poor Mountain transitional member (SC), detrital	34.916ºN 82.914ºW	1.0, 1.1, 1.2, 1.3, 1.4, 1.5, 1.6, & 1.7 Ga	Bream et al., 2004
		Tallulah Falls Fm. metagraywacke (NC), detrital	35.644ºN 81.987ºW	1.1 ,1.2, 1.3, 1.4, & 1.5 Ga	Bream et al., 2004
		Tallulah Falls Fm. alum. schist (SC), detrital	34.696ºN 82.879ºW	1.0, 1.1, 1.2, 1.3, & 1.4 Ga	Bream et al., 2004
	Sauratown Mountains window	Tallulah Falls Fm. metagraywacke (NC), detrital	35.336ºN 84.296ºW	1.0, 1.1, 1.2, & 1.3 Ga	Bream et al., 2004
		Grassy Creek gneiss	36.348ºN 80.453ºW	~1,165 Ma	Carrigan et al., 2003
		Forbush gneiss	36.258ºN 80.633ºW	~1,143 Ma	Carrigan et al., 2003
	Newton window	Tallulah Falls Fm. (?) metagraywacke (NC) SW6	35.8038ºN 80.9217ºW	0.9, 1.0, 1.1, & 1.2 Ga	Merschat et al., 2005b
		Tallulah Falls Fm. (?) metagraywacke (NC) SP13	35.756ºN 81.092ºW	0.9, 1.0, 1.1, 1.2, 1.4, 1.5, & 1.7	Merschat et al., 2005b
		Reepsville gneiss	35.516ºN 81.354ºW	~1,050 Ga *(410, 350)*	Merschat et al., 2005b
	Smith River allochthon	Bassett Fm. Metagraywacke (NC), detrital	36.407ºN 80.564ºW	0.47, 0.7, 1.0, 1.1, 1.2, & 1.3 Ga	Merschat et al.., 2007

Table 7–2. Continued.

Terrane	Tectonic belt/structure	Sample	Location	Ages (Ma)*	Source
Cat Square	Laurens thrust sheet	Reedy River granite	34.611ºN 82.3ºW	~325 Ma	Mapes, 2002
		Gray Court granite	34.912ºN 81.783ºW	~357 Ma	Mapes, 2002
	Brindle Creek thrust sheet	Granitoid dike cutting Walker Top	36.045ºN 81.100ºW	~323 Ma	Gatewood, 2007
		Cherryville Granite (NC)	35.273ºN 81.445ºW	~355 Ma	Mapes, 2002
		Granitic Gneiss cutting Walker Top	36.077ºN 81.151ºW	~360 Ma	Gatewood, 2007
		Vale Walker Top Granite	35.540ºN 81.398ºW	~355 Ma	Byars et al., 2008
		Vale charnockite xenolith	35.540ºN 81.398ºW	~367 Ma	Byars et al., 2008
		Walker Top Granite, South Mountains	35.61ºN 81.753ºW	~366 Ma	Giorgis et al., 2002; Mapes, 2002
		Toluca Granite, South Mountains	35.521ºN 81.525ºW	~378 Ma	Mapes, 2002
			35.640ºN 81.668ºW	~383 Ma	Mapes, 2002
		Walker Top Granite, Brushy Mountains	36.031ºN 81.236ºW	~407 Ma	Gatewood, 2007
		Unnamed metagraywacke, Brushy Mountains (NC), detrital	35.952ºN 81.324ºW	0.43, 0.46, 0.6, 1.0, 1.1, 1.2, 1.3, 1.5, 1.6, & 1.7 Ga	Gatewood, 2007
		Unnamed metagraywacke, Brushy Mountains (NC), detrital	36.041ºN 81.135ºW	0.44, 1.3 Ga	Gatewood, 2007
		Unnamed metagraywacke, South Mountains (NC), detrital	35.539º N 81.702ºW	0.43, 0.5, 0.6, 1.0, 1.1, 1.2, & 1.4 Ga	Bream et al., 2004
	Paris Mountain thrust sheet	Unnamed metagraywacke, Paris Mountain (SC), detrital	34.917ºN 82.139ºW	0.43, 0.5, 0.6, 1.0, 1.1, 1.2, 1.4, 1.9, 2.5, & 2.8 Ga	Bream et al., 2004
		Unnamed metagraywacke, Stewart (GA), detrital	33.391ºN 83.768ºW	0.6,0.9, 1.0, 1.1, 1.2, 1.3, 1.4, & 1.6 Ga	Merschat, unpub. data

*Detrital zircon ages listed in Ga. Metamorphic ages are in parentheses and italicized.

The Tallulah Falls Formation consists of lower metagraywacke-amphibolite and upper metagraywacke units separated by a mappable aluminous schist unit (Hatcher, 1978, 1993). The Tallulah Falls Formation is overlain by graphitic phyllite and quartzite, muscovite-chlorite phyllite, impure marble and more chlorite-muscovite phyllite unique to the BFZ and phyllonitic metasiltstone southeast of the BFZ: the Chauga River Formation (Hatcher, 1969, 2002). These units yield only 1.1 Ga and older detrital zircons (Bream, 2002, 2003; Bream et al., 2004) (Table 7–2). Laminated to massive amphibolite (MORB to island-arc basalt composition) are overlain by quartzite-felsic tuff and marble of the Middle Ordovician Poor Mountain Formation, the youngest known unit in the western IP (Hatcher 1969, 2002). New 460-440 Ma ion microprobe zircon ages on the amphibolite and felsic tuff (Bream, 2003), the absence of older zircons, and northeastward decreased thickness of Chauga River metasiltstone, suggest the Poor Mountain rests unconformably atop the Tallulah Falls and Chauga River Formations (Hatcher, 2002).

Tallulah Falls Formation rocks were intruded by the ~490 Ma (Carrigan et al., 2001) Henderson Gneiss (biotite-K-feldspar quartz monzonite augen gneiss) (Fig. 7–6), and plagioclase-dominant 470-460 Ma granitoids, including the Dysartsville Tonalite, Sugarloaf Mountain granitoid gneiss, and Toccoa granitoid (Bream, 2002, 2003; Bream et al., 2004) (Table 7–2). These plutons occur intermittently from NE Georgia to north of Lenoir, North Carolina (Reed and Bryant, 1964; Bryant and Reed, 1970; Harper and Fullagar, 1981; Hatcher, 1993; Bream, 2003).

Cat Square terrane-Eastern IP

Eastern IP-Cat Square terrane rocks consist of aluminous schist and metagraywacke intruded by Devonian to Carboniferous granitoids. Minor calc-silicate bodies have been mapped in the Brushy Mountains (Merschat, 2003; Gatewood, 2007). Detrital zircons from the Cat Square terrane consist of : (1) dominance of Laurentian 1.4, 1.2, and 1.1 Ga; (2) abundant early Paleozoic 480, 460, and 430 Ma; (3) lesser Neoproterozoic peri-Gondwanan 600 and 500 Ma; and (4) minor Archean 2.8 and 2.5 Ga zircons (Table 7–2; Bream et al., 2001, 2004; Bream, 2003; Gatewood, 2007) (Table 7–2). A maximum age of Cat Square terrane metasedimentary rocks is ~430 Ma, the youngest detrital zircons (Bream, 2002; Bream et al., 2004; Gatewood, 2007). Early Paleozoic zircons (480-460 Ma) are consistent with a Laurentian source from either the southern or central Appalachians; however, ~430 Ma plutons are common in the central Appalachians and suggest a possible northerly source for the Cat Square terrane (Sinha et

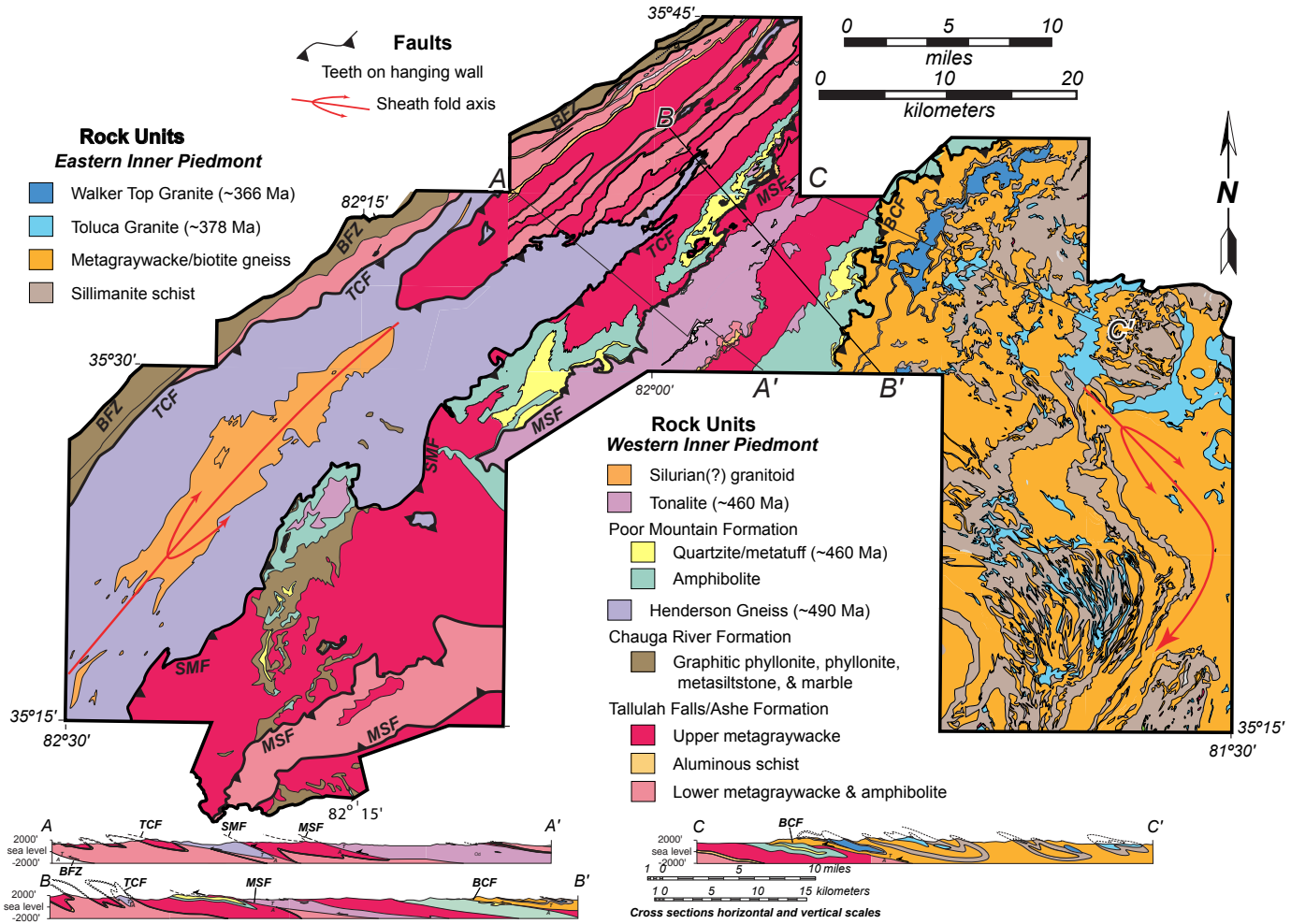

Figure 7–6. Simplified detailed geologic map of the South Mountains–Columbus Promontory region modified from Bier et al. (2000). Data from Overstreet et al. (1963), Davis (1993a), Yanagihara (1994), Bream (1999), Giorgis (1999), Hill (1999), Williams (2000), and Bier (2001). Abbreviations: BCF–Brindle Creek fault. BFZ–Brevard fault zone. MSF–Mill Spring fault. SMF–Sugarloaf Mountain fault. TCF–Tumblebug Creek fault.

al., in prep.). Recognition of 600 and 500 Ma zircons in the Cat Square terrane requires input from an exotic peri-Gondwanan source, mostly likely the Carolina superterrane (Bream, 2002; Hatcher, 2002; Bream et al., 2004). Based on the occurrence of 600, 500, and 400 Ma detrital zircons (in addition to 1.2-1.1 Ga detrital zircons) in biotite gneiss, Bream et al. (2001, 2004) concluded that the Brindle Creek fault is a terrane boundary separating Neoproterozic to early Paleozoic Laurentian affinity rocks of the western IP-Tugaloo terrane from suspect middle Paleozoic rocks of the eastern IP-Cat Square terrane (Bream et al., 2001; Bream and Hatcher, 2002; Hatcher, 2002; Bream et al., 2004).

Ultramafic and mafic bodies are uncommon, but have been recognized in the Cat Square terrane (Goldsmith et al. 1988; Giorgis, 1999; Merschat 2003). Several small pods of altered ultramafic rocks (talc-chlorite schist) occur near the Brindle Creek fault in the South and Brushy Mountains (Giorgis, 1999; Merschat, 2003; Wilson, 2006). The largest mafic and ultramafic bodies occur near the central Piedmont suture. Two of the larger bodies include the Turnersburg ultramafic, northeast of Statesville, North Carolina (Privett, 1984; Goldsmith et al., 1988), and the Hammett Grove mafic-ultramafic body in South Carolina (Mittwede et al., 1987). The Hammett Grove mafic-ultramafic body was interpreted as a deformed ophiolite from rock assemblage and chemical composition (Mittwede et al., 1987). The lack of continental basement, presence of ultramafic and mafic bodies, and mixed provenance suggest the Cat Square terrane was deposited on oceanic crust in a basin between Laurentian and the Carolina superterrane (Merschat and Hatcher, 2007).

The Devonian and Carboniferous Toluca (378 Ma, Mapes, 2002), Walker Top (366 Ma, Giorgis et al., 2002; Mapes, 2002), and Cherryville Granites (375 Ma, Mapes, 2002) intruded the Cat Square terrane. The Toluca and Cherryville Granites are massive, equigranular, medium- to coarse-grained, foliated, and have concordant to subconcordant contacts. The Walker Top Granite is porphyritic with microcline megacrysts 1-8 cm long, and common myrmekite rims, in a dark gray, medium- to coarse-grained matrix of biotite, quartz, K-feldspar, and plagioclase (Giorgis et al., 2002; Mapes et al., 2002). SHRIMP U/Pb ages obtained for the Walker Top include ~407 Ma in the Brushy Mountains (Gatewood, 2007), ~366 Ma in the South Mountains (Giorgis et al., 2002; Mapes, 2002), and ~367 Ma for Vale charnockite and ~355 Ma for enclosing granite (Byars et al., 2008) (Table 7–2). Chemically, all are intraplate, anatectic granites (Giorgis et al., 2002; Mapes, 2002). The Toluca and Walker Top Granites have oxygen isotope signatures identical to surrounding Cat Square terrane paragneisses, suggesting these are anatectic melts of the surrounding Cat Square terrane country rocks (Mapes, 2002). Devonian

magmatism constrains the minimum age of the Cat Square terrane, by which time the rocks were deposited and subducted to mid-crustal levels associated with intrusion of Walker Top and Toluca Granites accompanied by upper amphibolite metamorphism and deformation (Fig. 7–7).

NATURE OF THE TUGALOO-CAT SQUARE CONTACT: THE BRINDLE CREEK FAULT

Siluro-Devonian Cat Square terrane overlies the Neoproterozoic to Ordovician Tugaloo terrane, creating both a simple and complex relationship of younger-over-older rocks. This relationship is similar to the Salinic basins in New England, with Silurian and Devonian rocks deposited unconformably on the Laurentian margin (e.g., Osberg et al., 1989; Robinson et al., 1998). Other important characteristics of this boundary include lack of sedimentary structures and fossils, no metamorphic discontinuity, truncation of both Tugaloo and Cat Square terrane units, mylonite of variable thickness, and a significant change in lithostratigraphies and provenance. Although several of these characteristics are non-unique, limitation of Devonian plutonism to the Cat Square terrane, the association of mylonite with the contact, and truncation of units support the contact is a fault. A simple interpretation that the contact is an unconformity (Dennis, 2007) ignores most of the data based on detailed geologic mapping in the South and Brushy Mountains that have documented mylonite, and several map-scale truncations associated with the contact (Giorgis, 1999; Williams, 2000; Kalbas, 2003; Merschat, 2003; Wilson, 2006; Gatewood, 2007). For the reasons cited below, we maintain that the contact between the Cat Square and Tugaloo terranes is a fault, the Brindle Creek fault. It has been mapped at 1:24,000 or larger scale in the Brushy and South Mountains. Preliminary results from detailed geologic mapping in the Newton-Lincolnton area also have recognized mylonite associated with the contact, and truncations of hanging-wall plutons similar to those recognized in the South and Brushy Mountains.

South Mountains

Giorgis (1999) first recognized the Brindle Creek fault to explain map-scale truncations of synforms of migmatitic Poor Mountain Quartzite in the Mill Spring thrust sheet and significant changes in lithostratigraphy (Fig. 7–6). The Brindle Creek fault was placed at the contact between the migmatitic biotite-hornblende gneiss of the Poor Mountain Formation, and migmatitic metagraywacke with common amphibolite pods

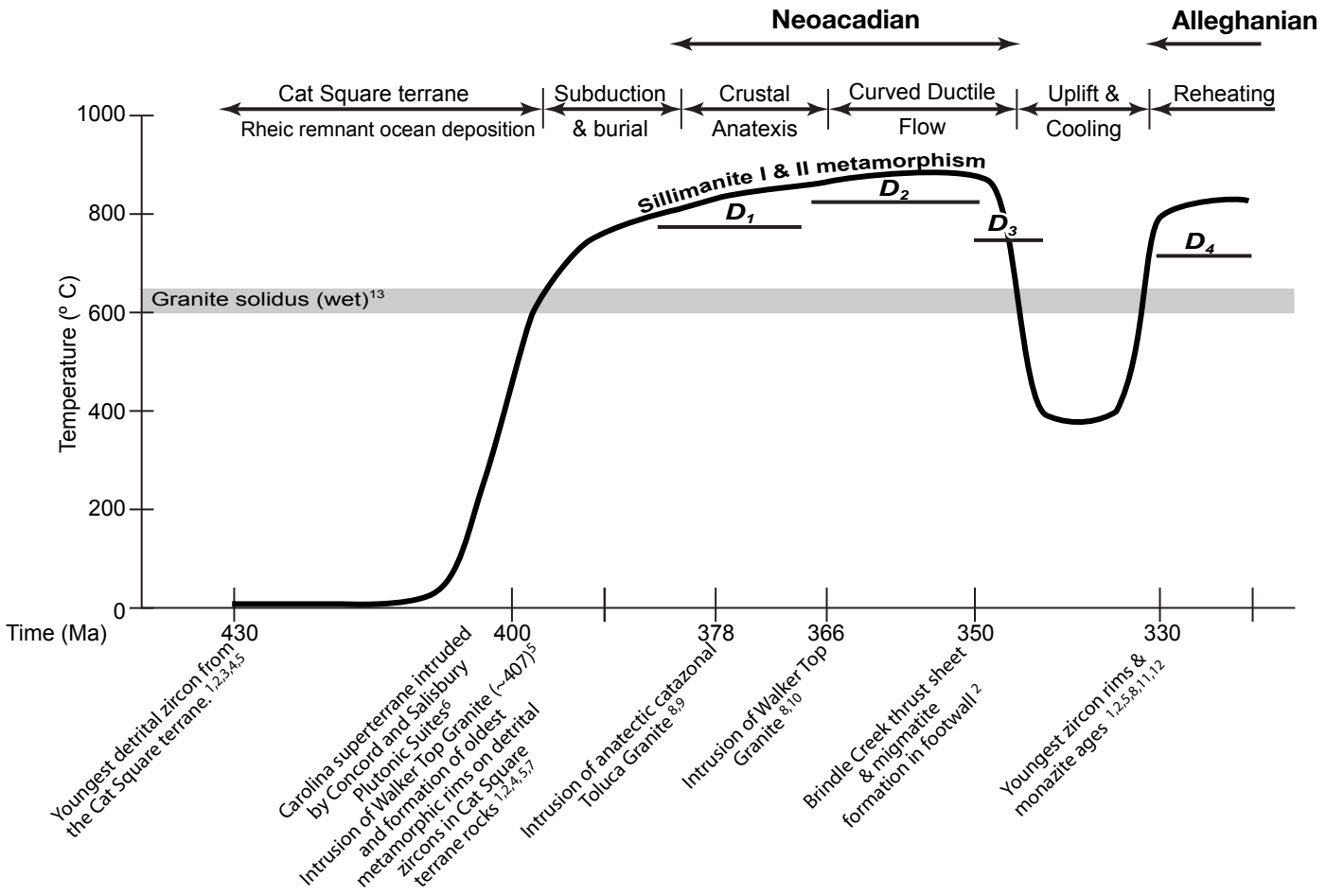

Figure 7–7. Tectonothermal time line for the Inner Piedmont. Data sources: 1–Bream (2002). 2–Bream (2003). 3–Bream et al. (2001). 4–Bream et al. (2004). 5 –Gatewood (2007). 6–McSween et al. (1984, 1997). 7–Carrigan et al. (2001). 8–Mapes (2002). 9–Mapes et al. (2002). 10–Giorgis et al. (2002). 11–Dennis & Wright (1997a, 1997b). 12–Mirante & Patino-Douce (2000). 13–Luth et al. (1964).

then interpreted as lower Tallulah Falls Formation (Giorgis, 1999; Williams, 2000). The gentle 10-15º SE dip of the fault led Giorgis (1999) to interpret it as a northwest-verging thrust. The significance of the Brindle Creek fault was not understood until Bream et al. (2000, 2001, 2004) reported the distinct 600, 500, and 460 Ma and common Laurentian detrital zircon population from a metagraywacke from the Brindle Creek thrust sheet in the South Mountains, and suggested it is a separate suspect terrane.

Brushy Mountains

Several key map relationships have been recognized in the Brushy Mountains that indicate the contact is a fault, and delimit its kinematics and timing (Fig. 7–8). Mapping in the Brushy Mountains began in January, 2001, and benefited from previous mapping in the South Mountains and Columbus Promontory, and an explosion of modern SHRIMP U/Pb geochronology (e.g., Bream et al., 2000, 2001). Merschat and Kalbas (2002) placed the Brindle Creek fault at the base of a dark gray to black, fine- to medium-grained inequigranular, porphyroclastic garnet-biotite-K-feldspar-quartz-plagioclase mylonite gneiss that often contains abundant amphibolite pods, lenses and boudins. Kalbas (2003) named the unit the Hibriten gneiss for exposures from Hibriten Mountain east of Lenoir, North Carolina, and the unit has been traced ~44 km (27 mi) northeast along the northwestern flank of the Brushy Mountains (Figs. 7–3 and 7–8). Samples of the unit on Hibriten Mountain and near Moravian Falls, North Carolina, yielded SHRIMP U/PB ages of ~449, ~445, and ~435 Ma, identical to the age of the Lenoir Quarry Migmatite (Gatewood, 2007). The porphyroclastic texture, common amphibolite boudins, and pervasive S-C fabric suggest the protolith for Hibriten mylonite is the Lenoir Quarry Migmatite. Moreover, Gatewood (2007) separated zones of mylonite and ultramylonite in the Hibriten gneiss, described microstructures typical of amphibolite grade deformation, and abundant dextral, top-to-the-SW shear sense. The Hibriten mylonite mapped in the Brindle Creek fault zone in the Brushy Mountains correlates with the inequigranular biotite gneiss unit of Goldsmith et al. (1988) that can be used to locate the Brindle Creek fault across the Charlotte 1º x 2º sheet.

A late F_5 dome of the Brindle Creek fault in the northeastern Brushy Mountains created a reentrant into the thrust and reveals key map relationships (Figs. 7–3 and 7–8; Wilson, 2006; Gatewood, 2007). This dome folds the Brindle Creek fault and exposes granitic gneiss of the Ordovician Brooks Crossroads pluton of the Mill Spring thrust sheet in its core. Wilson (2006) and Gatewood (2007) mapped a thin band of Hibriten mylonite along the Brindle Creek fault around the reentrant. The Poplar Springs map-scale sheath

Figure 7–8. Simplified detailed geologic map of the Brushy Mountains, North Carolina. Geology mapped by Kalbas (2003), Merschat (2003), Wilson (2006), and Gatewood (2007). Field trip stops are indicated. BCF–Brindle Creek fault, BWSF–Big Warrior Creek sheath fold, ESF–Ellendale sheath fold, GSF–Gilreath sheath fold, MSF–Mill Spring fault, PSSF–Poplar Spring sheath fold, and TCF–Tumblebug Creek fault.

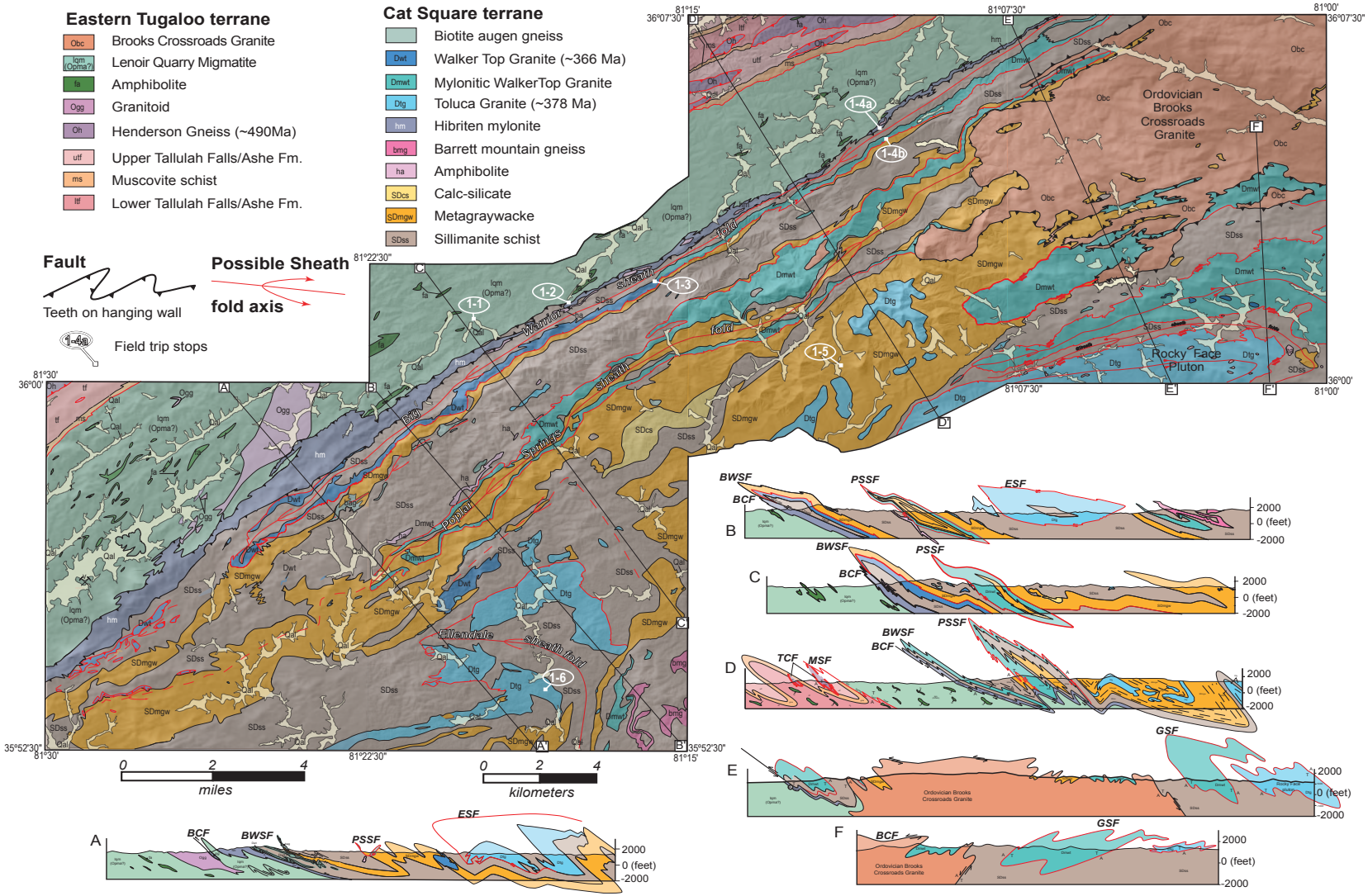
Eastern Tugaloo terrane
Obc Brooks Crossroads Granite
lqm (Opma?) Lenoir Quarry Migmatite
fa Amphibolite
Ogg Granitoid
Oh Henderson Gneiss (~490Ma)
utf Upper Tallulah Falls/Ashe Fm.
ms Muscovite schist
ltf Lower Tallulah Falls/Ashe Fm.
Cat Square terrane
Biotite augen gneiss
Dwt Walker Top Granite (~366 Ma)
Dmwt Mylonitic WalkerTop Granite
Dtg Toluca Granite (~378 Ma)
hm Hibriten mylonite
bmg Barrett mountain gneiss
ha Amphibolite
SDcs Calc-silicate
SDmgw Metagraywacke
SDss Sillimanite schist
Fault
Teeth on hanging wall
Possible Sheath fold axis
1-4a Field trip stops
Ordovician Brooks Crossroads Granite
Rocky Face Pluton
Warrior
Sheath fold
Ellendale
Sprucy
Poplar
81°15'
81°07'30"
81°00'
36°07'30"
36°00'
81°30'
81°22'30"
35°52'30"
0 2 4
miles
kilometers
BWSF
BCF
PSSF
ESF
TCF
MSF
GSF
2000
0 (feet)
-2000

fold outlined by the ~407 Ma megacrystic Walker Top Granite truncates against the Brindle Creek fault (Figs. 7–3 and 7–8), and suggests emplacement of the thrust sheet is post ~407 Ma. In the southwestern Brushy Mountains, the northwest limb of the Big Warrior Creek sheath fold outlined by ~407 Ma Walker Top Granite is excised against the Brindle Creek fault. These map truncations provide critical evidence of the post ~407 Ma timing of emplacement of the Brindle Creek thrust sheet. Map geometries, kinematic indicators, and microstructural evidence all support that the Brindle Creek fault was an amphibolite grade, dextral shear zone during the Neoacadian orogeny.

Newton Window

The Newton antiform (NA), recognized by Goldsmith et al. (1988), is a broad NE-SW-trending, doubly plunging antiform in the eastern IP between Hickory and Statesville, North Carolina (Figs. 7–1, and 7–9). It exposes a unique assemblage of biotite gneiss, biotite–hornblende gneiss, amphibolite, and ultramafic rocks that dip gently to steeply NW beneath typical Cat Square terrane rocks (Fig. 7–9). Truncations of Siluro-Devonian paragneisses and bodies of ~366 Ma (or ~407 Ma) Walker Top Granite occur along the NW boundary of the NA. The rocks dip southeast beneath the central Piedmont suture on the southeast flank of the NA. Inside the window biotite gneiss with amphibolite interlayers and boudins dominate and surround larger bodies of amphibolite and altered ultramafic rocks. Lesser amounts of pelitic schist and metagraywacke occur locally. Possible tectonic settings of the NA are: (1) mid-Paleozoic ophiolites associated with Devonian docking of the Carolina superterrane; (2) a window through the Brindle Creek thrust sheet exposing rocks of the Tugaloo terrane; or (3) a previously unidentified terrane. Geochemistry and of selected mafic bodies, detrital zircon geochronology of NA paragneisses and detailed geologic mapping are examined to provide a preliminary assessment the tectonic significance and history of the NA.

Amphibolites in the NA occur as both map scale bodies and smaller mesoscopic layers or boudins. Recent detailed geologic mapping has revealed that some of the amphibolite bodies recognized by Goldsmith et al. (1988) are not as extensive as indicated (Byars, in progress). Texturally, the amphibolites vary from fine- to medium-grained, laminated to layered and locally coarse-grained, and weakly foliated. Common mineral assemblages include hornblende + plagioclase ± garnet ± epidote + quartz and lesser amounts of biotite, sphene, clinopyroxene, calcite, sericite, and opaques (Table 7–3). Hornblende, typically pleochroic pale to dark green and greenish brown, defines the S_2 foliation, and often an L_2 lineation. Garnet varies in both abundance and occurrence.

Figure 7–9. Geologic map and cross section of the Newton window, modified from Rankin et al. (1972) and Goldsmith et al. (1988). Location of SHRIMP samples are indicated with red triangle and amphibolite whole-rock geochemistry samples are indicated with a red diamond.

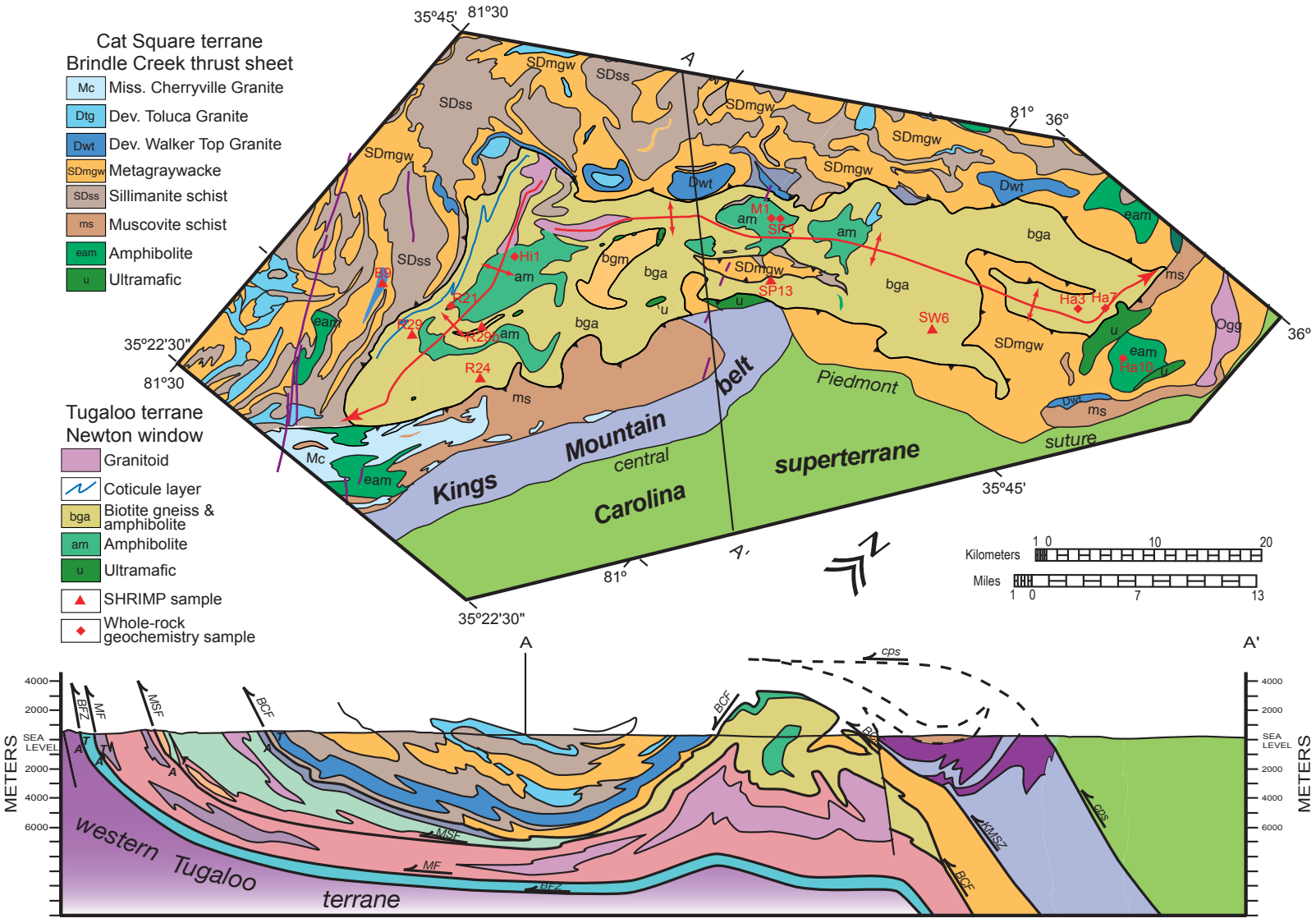
Cat Square terrane
Brindle Creek thrust sheet
Mc Miss. Cherryville Granite
Dtg Dev. Toluca Granite
Dwt Dev. Walker Top Granite
SDmgw Metagraywacke
SDss Sillimanite schist
ms Muscovite schist
eam Amphibolite
u Ultramafic
Tugaloo terrane
Newton window
Granitoid
Coticule layer
bga Biotite gneiss & amphibolite
am Amphibolite
u Ultramafic
SHRIMP sample
Whole-rock geochemistry sample
35°45'
81°30
81°
36°
35°22'30"
A
A'
Kings Mountain belt
central Carolina superterrane
Piedmont suture
Kilometers
Miles
western Tugaloo terrane
METERS
SEA LEVEL
BFZ
MF
MSF
BCF
KMSZ
cps

Table 7–3. Locations and descriptions of amphibolite

Terrane	Sample	Location	Field occurrence and Outcrop Description	Mineralogy	Textures
Cat Square	Ha10	35.8875ºN 80.7576ºW	Map body, medium-grained amphibolite	Plag(An_{75-63}), hbl, gar, clinozoisite, sericite	Garnet reaction rims dissect sample; Sericite replacing plag
Tugaloo- Newton window	Ha7	35.9081ºN 80.8064ºW	Boudin in metagraywacke	Hbl, plag (An_{60-54}), qtz, gar, sphene, epidote, clinozoisite, opaques	Subhedral gar with curved inclusion trail
	Ha3	35.898ºN 80.826ºW	Map body, fine-grained, garnet–epidote amphibolite	Hbl, epidote, gar, qtz, clinozoisite, plag	Anhedral embayed garnet
	M1	35.7875ºN 81.1275ºW	Map body, migmatitic, 1 to 3 cm thick, layered amphibolite	Hbl, plag (An_{28}) gar, qtz, clinozoisite & layered clinopyroxene, gar, plag (An_{55-45}), qtz, cc, opaques	Symplectic epidote/clinozoisite-plag; subdedral gar with multiple zircon inclusions
	SW6mm	35.800ºN 80.922ºW	boudin/layer (uncertain), coarse-grained migmatitic garnet amphibolite	Bi, hbl, plag (An_{67}), qtz, opaques, qtz	Gar, 0.25 - 2 cm dia. anhedral, embayed with inclusions of hbl, plag, opaques, bi
	Hi1	35.6321ºN 81.3072ºW	Map body	Hbl, plag (An_{52}), symplectitite, epidote/clinozoixite, qtz, opaques	Symplectic intergrowth of epidote and plag
	R21	35.5636ºN 81.3444ºW	50 cm interlayer of migmatitic amphibolite	Hbl, symplectitec, plag (An_{30}), qtz, opaques	Symplectic intergrowth of epidote and plag cuts foliation
	SP13	35.756ºN 81.092ºW	1 to 1.5 m thick boudins of weakly foliated, coarse-grained amphibolite in metagraywacke	Hbl, qtz, opaques, cc, zircon	~0.5 cm poikilolitic hbl porphyroclasts
	SP3	35.7965ºN 81.1197ºW	Map body, medium-grained, layered amphibolite	Hbl, symplectite, plag (An_{37}), epidote, gar, qtz, sphene	Symplectic intergrowth of epidote and plag; gar subhedral and embayed

Mineral abbreviations are bi–biotite, cc–calcite, gar–garnet, hbl–hornblende, qtz–quartz, and plag–plagioclase.

Most samples contains subhedral, 0.1-0.5 cm diameter garnets; however, sample SW6mm contains 1-2cm diameter garnets with inclusions of hornblende, plagioclase, biotite and opaques. Preserved in some garnets are curvi-linear inclusion trails that define an earlier foliation, S_1, oblique to the dominant foliation in the sample. Symplectic intergrowths of epidote and plagioclase are common in several samples. Orientation of the symplectic epidote grains obliquely cut the dominant S_2 foliation defined by hornblende. Epidote-plagioclase symplectites are likely forming by the breakdown of hornblende in the presence of a metamorphic fluid.

Samples of both map-scale and mesoscopic boudins and interlayers of amphibolite were collected for whole-rock and trace element geochemistry (Fig. 7–9 and Table 7–4). Trace element discriminant diagrams were used to determine possible tectonic environments in which the mafic samples formed. Unfortunately, results from tectonic discriminant diagrams using Zr and Ti with combinations of Sr, and Y did not reveal a consistent tectonic environment. Most samples overlapped the MORB and island arc tholeiite fields and, to a lesser amount, the calc-alkaline fields (Fig. 7–10). Low Zr values (~6 ppm) of Ha7 and Ha10 resulted in the samples plotting outside of the defined discriminant fields. Samples M1 and SP3, which are from the same map body (Fig. 7–9), consistently plotted in the MORB and overlapping MORB, island arc and calc-alkali basalt fields (Fig. 7–10). Tectonic discriminant diagrams based on La-Y-Nb and Th-Hf-Ta similarly displayed little consistency except for M1 and SP3 which plotted in MORB fields (Fig. 7–11). Tectonic discriminant diagrams do not support an intracontinental rift setting for amphibolites of the NA, as might be implied in some tectonic models (Dennis, 2007). Kalbas (2003) and Wilson (2006) recognized that Poor Mountain amphibolite generally overlapped the MORB and island arc fields similar to the samples from the NA. The limited number of samples and inconsistencies between the different discriminant diagrams hinders recognizing definite tectonic setting of the NA amphibolites, although a MORB to island arc setting is preferred. NA amphibolites may be correlative to the Poor Mountain amphibolite in the western IP, Tugaloo terrane.

The distinct detrital zircon suite of the Cat Square terrane creates another simple test of the above possibilities of the NA. Detrital zircons were separated from two paragneisses from the NA (SP13 and SW6) and analyzed using the SHRIMP-RG. Zircon U-Pb ages reveal peaks at 1.2, 1.15, 1.0 Ga (Grenvillian), and 1.4 Ga (granite-rhyolite province?) implying a Laurentian provenance, and distinctly different from the Cat Square terrane (Merschat et al., 2005b) (Table 7–2 and Fig. 7–12). An additional sample from near Reepsville, North Carolina, interpreted as a biotite orthogneiss, yielded a U-

Table 7–4. Whole-rock major and trace element data of selected ampibolites and the Reepsville gneiss from the Newton window and Cat Square terrane. nd–Below detection limit.

			Newton Window amphibolite									Reepsville gneiss	
Sample ID			Ha7	Ha10**	Ha3	M1 SW6mm		Hi1	R21	SP13	SP3	R29A	R29B
Analysis Type	Detection Limit												
FUS-ICP													
	SiO_2	0.01	51.55	47.24	50.46	48.26	42.84	53.81	49.75	54.56	49.81	70.46	63.16
	Al_2O_3	0.01	14.35	15.62	13.07	13.23	12.58	15.01	15.9	9.86	12.76	13.91	14.35
	Fe_2O_3 (T)	0.01	11.02	10.79	15.26	15.29	18.56	11.56	12.76	8.41	15.93	3	7.19
	MnO	0.001	0.173	0.189	0.204	0.227	0.371	0.178	0.217	0.154	0.203	0.023	0.063
	MgO	0.01	6.24	9.34	6.47	7.06	6.31	4.78	5.21	11.46	6.2	0.86	2.51
	CaO	0.01	9.95	14.06	11.84	11.38	8.59	8.72	9.82	10.87	9.84	1.8	3.24
	Na_2O	0.01	1.46	0.9	0.83	1.84	1.93	2.72	2.93	0.91	2.14	3.06	2.77
	K_2O	0.01	1.32	0.03	0.15	0.21	2.06	0.57	1.02	0.56	0.35	4.48	3.71
	TiO_2	0.001	1.35	0.638	0.314	1.184	3.635	0.609	0.723	0.402	1.072	0.639	1.58
	P_2O_5	0.01	0.13	0.07	0.04	0.11	1.37	0.05	0.08	0.05	0.12	0.18	0.71
	LOI	0.01	1.46	0.3	0.81	0.99	0.77	1.43	0.86	1.88	0.87	0.7	nd
	TOTAL		98.99	99.19	99.44	99.78	99.01	99.44	99.27	99.14	99.31	99.12	99.29
	Trace Elements (ppm)												
	Ba	1	239	50	18	74	839	57	193	207	68	1260	1495
	Be	1	2	nd	nd	1	2	nd	nd	nd	1	nd	1
	Sr	2	301	107	144	81	207	110	115	77	87	550	376
	V	5	324	284	358	432	224	274	313	202	435	38	103
	Y	1	31	14	28	30	70	25	27	15	25	6	29
INAA	Trace Elements (ppm, *-ppb)												
	As	1	nd	nd	nd	nd	nd	nd	nd	nd	nd	nd	nd
	Au	1*	nd	4	7	nd	4	nd	5	nd	nd	nd	nd
	Br	0.5	nd	1.1	nd	nd	nd	nd	nd	nd	nd	nd	nd
	Co	0.1	47	46.8	62.9	59.5	51.4	48.7	38.6	47.2	57.2	6.8	15.5
	Cr	0.5	326	246	18.4	67.4	182	13.2	13.9	1070	56.5	6.9	43.3
	Hg	1	nd	nd	nd	nd	nd	nd	nd	nd	nd	nd	nd
	Ir	1*	nd	nd	nd	nd	nd	nd	nd	nd	nd	nd	nd
	Mo	2	nd	nd	nd	nd	nd	nd	nd	nd	nd	nd	nd
	Sb	0.1	nd	nd	nd	nd	nd	nd	nd	nd	0.2	nd	nd
	Sc	0.01	42.9	57.3	62	55.3	36.9	44.7	51.8	61.2	52.1	2.89	11.2
	Se	0.5	nd	nd	nd	nd	nd	nd	nd	nd	nd	nd	nd
	W	1	nd	nd	nd	nd	nd	nd	nd	nd	nd	nd	nd
FUS-MS	Trace Elements (ppm)												
	Bi	0.1	0.2	nd	nd	nd	nd	nd	nd	nd	nd	nd	nd
	Ce	0.1	35.7	3.1	6.5	9.5	94.3	11.2	14.2	18.8	10.5	138	194
	Cs	0.1	0.1	nd	nd	nd	0.2	nd	nd	nd	nd	0.3	0.8
	Dy	0.02	4.96	2.49	5.57	4.21	10.8	3.69	4.12	2.24	3.43	1.46	6.71
	Er	0.01	2.92	1.58	3.43	2.95	6.48	2.47	2.58	1.46	2.56	0.42	2.4
	Eu	0.005	1.41	0.704	2.03	0.988	4.04	0.75	0.935	0.564	0.803	2.15	3.41
	Ga	1	20	15	14	17	23	16	18	11	17	19	24
	Gd	0.02	5.34	1.87	6.39	3.16	12.6	3.12	3.38	1.92	2.75	4.76	12.9
	Ge	0.5	1.6	1.8	2.1	1.7	2.2	1.7	2.1	1.6	1.8	0.9	1.2
	Hf	0.1	4	0.3	0.2	1.9	7.3	2.1	1.2	2.1	1.7	5.9	9.8
	Ho	0.01	0.99	0.54	1.09	0.93	2.18	0.81	0.86	0.48	0.8	0.2	1.03
	In	0.1	nd	nd	nd	nd	nd	nd	nd	nd	nd	nd	nd
	La	0.05	17.9	1.92	36.4	3.98	41.5	4.12	5.88	9.88	4.79	99.3	108
	Lu	0.002	0.378	0.223	0.532	0.46	0.874	0.39	0.359	0.228	0.42	0.046	0.216
	Nb	0.2	6.6	nd	0.3	4.3	30.7	1.8	1.4	3.9	5.6	3.7	15.1
	Nd	0.05	21.2	4.93	54	7.77	56.5	8.61	9.56	9.14	6.99	59.1	97.1
	Pr	0.02	4.73	0.82	14.6	1.41	12.2	1.67	1.87	2.2	1.43	18.4	26.3
	Rb	2	32	3	4	2	37	3	9	6	5	94	147
	Sm	0.01	5.18	1.71	11.2	2.54	13.1	2.56	2.93	2.01	2.12	7.62	17.1
	Sn	1	3	2	2	2	4	4	2	6	2	nd	nd
	Ta	0.1	0.4	nd	nd	0.2	1.8	nd	nd	0.3	0.3	nd	0.5
	Tb	0.01	0.89	0.37	1.05	0.63	2	0.59	0.64	0.35	0.52	0.39	1.57
	Th	0.05	3.83	< 0.05	0.13	0.34	2.7	0.88	0.67	4.05	0.56	19.5	12.7
	Tl	0.05	0.33	nd	nd	nd	0.17	nd	0.1	nd	nd	0.67	1.06
	Tm	0.005	0.416	0.227	0.538	0.45	0.915	0.377	0.38	0.226	0.391	0.054	0.3
	U	0.05	1.06	nd	nd	0.1	0.55	0.19	0.19	0.56	0.13	0.35	0.96
	Yb	0.01	2.52	1.43	3.56	2.91	5.73	2.48	2.32	1.48	2.64	0.33	1.69
	Zr	1	137	6	6	59	307	69	30	73	55	211	376
TD-ICP	Trace Elements (ppm, *-%)												
	Ag	0.5	nd	nd	nd	nd	nd	nd	nd	nd	nd	nd	nd
	Cd	0.5	1.4	nd	nd	0.9	2	0.8	0.6	nd	1.1	nd	nd
	Cu	1	107	93	82	251	23	54	19	44	90	24	17
	Ni	1	81	65	52	57	52	11	10	102	49	6	22
	Pb	5	9	nd	nd	nd	nd	nd	nd	nd	nd	32	39
	S	0.001*	0.193	0.012	nd	0.256	0.121	0.013	0.01	0.108	0.048	0.008	0.013
	Zn	1	122	47	77	82	136	68	82	45	91	57	133

** Ha10 is from the Cat Square terrane.

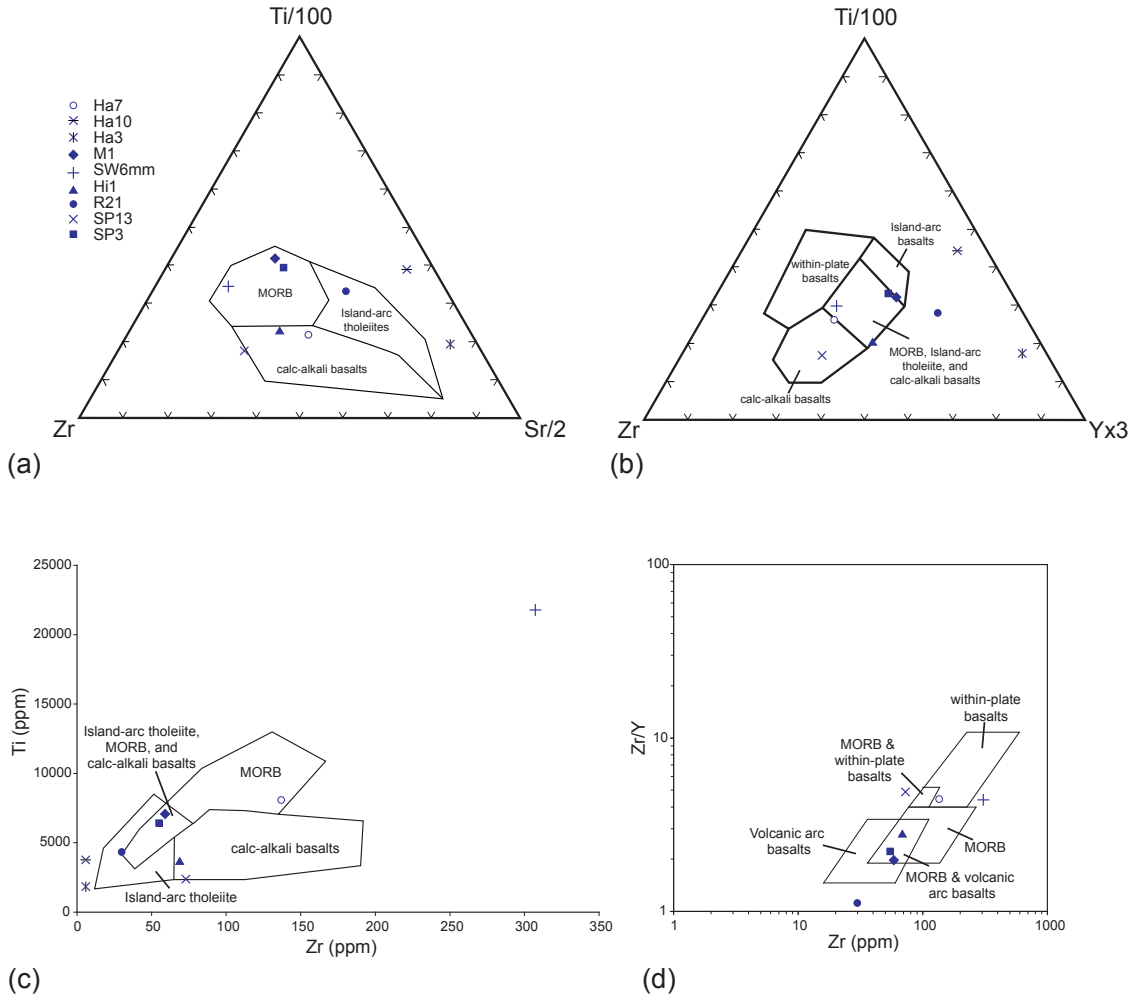

Figure 7–10. Tectonic discriminant diagrams for mafic rocks based on trace elements Zr, Ti, Sr, and Y. (a) Zr-Ti-Sr, (b) Zr-Ti-Y, and (c) Zr-Ti variation diagrams of Pearce and Cann (1973), and (d) Zr/Y-Zr discriminant diagram of Pearce and Norry (1979). Symbols listed in (a) are the same for the other plots.

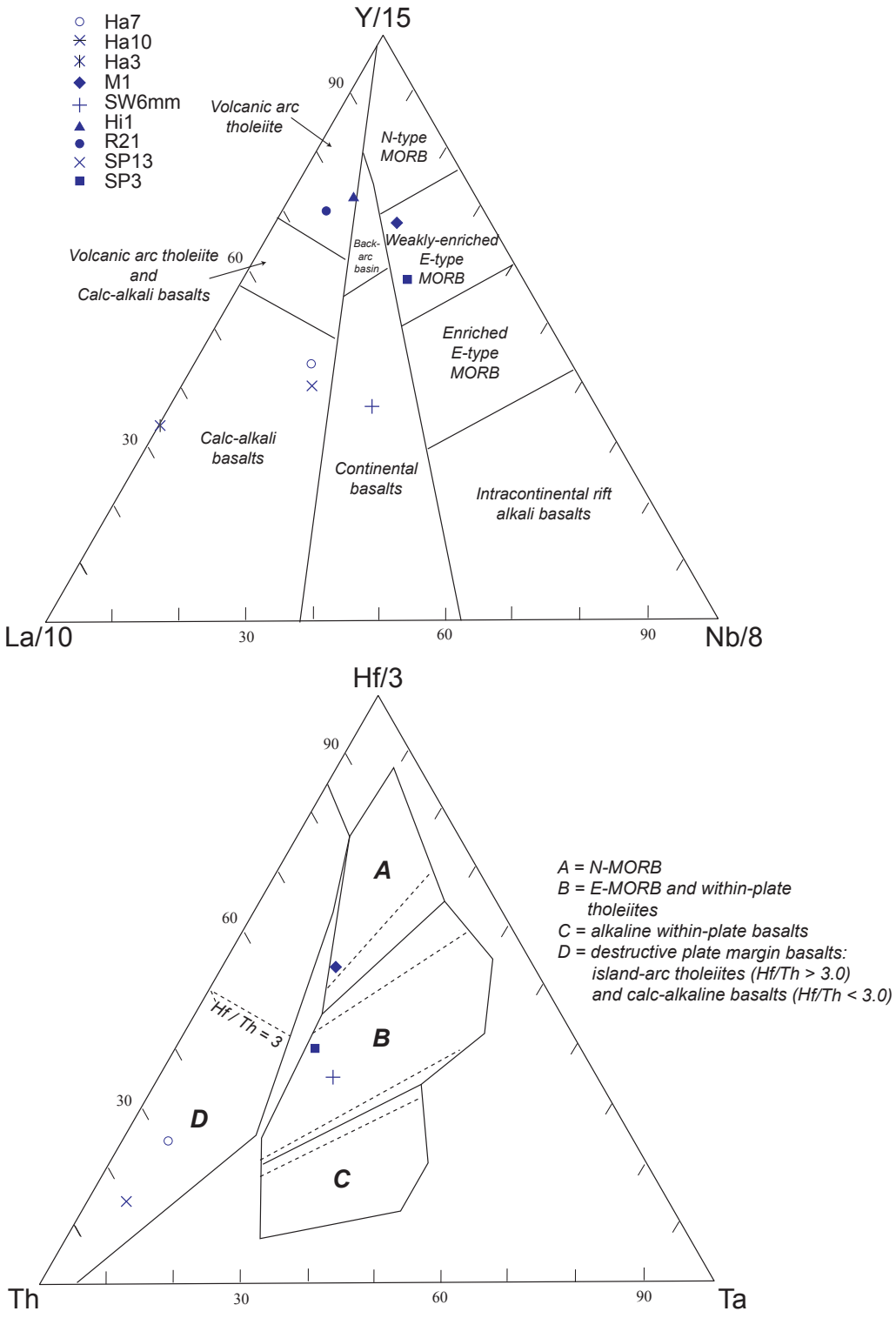

Figure 7–11. Tectonic discrimant diagrams for mafic rocks using REE (a) La-Y-Nb (Cabanis and Lecolle, 1989), and (b) Th-Hf-Ta (Wood, 1980). Symbols are the same as Fig. **7-**10.

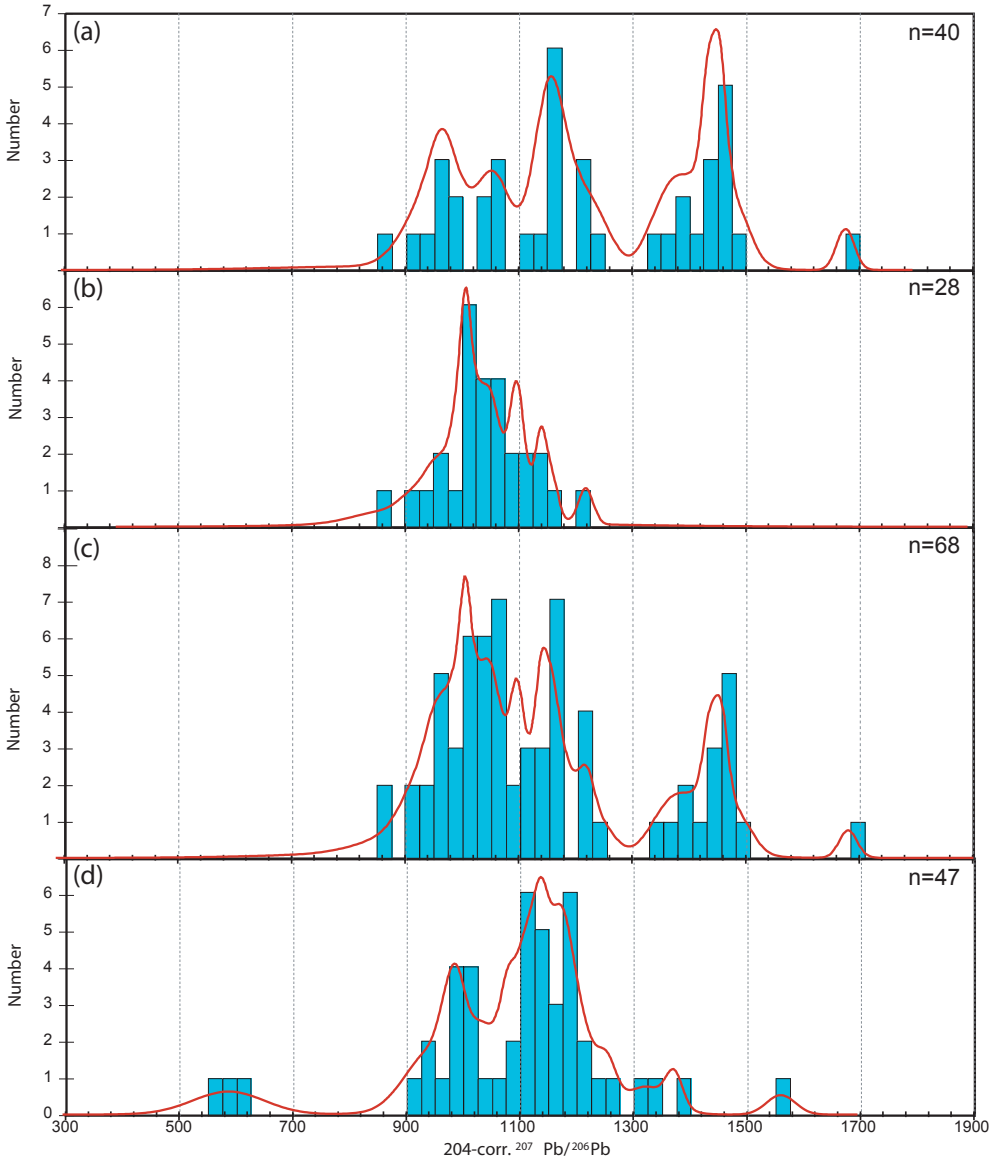

Figure 7–12. Relative probability plots and histograms of 204-corrected $^{207}Pb/^{206}Pb$ SRHIMP ages of detrital zircons from different IP paragneisses: (a) SP13, Newton window; (b) SW6, Newton window; (c) SP13 and SW6 combined; and (d) S21, Cat Square terrane(?), Georgia IP.

Pb age of 1051±18 Ma with metamorphic rims of ~350 Ma and may be a fragment of Grenville crust (Table 7–5 and Fig. 7–13). The Laurentian affinity provenance of the NA rocks and the presence of Grenville basement have striking similarities with the rocks of the Tugaloo terrane.

Similar lithostratigraphies and amphibolite geochemistry, detrital zircon populations, and possible Grenville basement permit correlation of NA rocks with the Tugaloo terrane. Occurrence and truncations of mylonitic megacrystic Walker Top Granite along the boundary of the NA suggest the boundary is a fault. Thus NA is a window through the Brindle Creek thrust sheet and should be called the Newton window (Merschat et al., 2005b). Recognition of the Newton window further supports the allochthonous nature of the Cat Square terrane restoring to a position at least 40 km east of the NA.

Southern Termination

The southern termination of the Brindle Creek fault is uncertain, and is often interpreted to truncate against the central Piedmont suture south of Athens, Georgia (e.g. Hatcher, 2002; Merschat and Hatcher, 2007). Examination of aeromagnetic maps of Alabama and Georgia reveal a lineament that can be traced north into South Carolina and North Carolina where the lineament closely corresponds to the Brindle Creek fault (Hatcher et al., 2007) (Fig. 7–14). Bently et al. (1974) identified this lineament and named it the Indian Springs fault. A sample of metagraywacke from near Stewart, Georgia, located just southeast of the lineament, contains 600 Ma detrital zircons similar to the Cat Square terrane assemblage (Merschat et al., 2007) (Fig. 7–14). Combined, these suggest the Cat Square terrane may extend significantly further south than previously thought, although additional detailed geologic mapping is required.

TECTONIC SYNTHESIS

The following tectonic scenario describes the likely evolution and tectonic ramifications of the Cat Square terrane from remnant ocean basin with provenance from approaching terranes to its becoming part of the IP (Merschat and Hatcher, 2007): (1) Deposition of the Cat Square terrane in a remnant ocean basin between Laurentia and approaching Carolina superterrane from 430 to 410 Ma. Palinspastic restoration of the IP northward to the central Appalachians suggests the location of the Cat Square remnant ocean basin was in the Pennsylvania embayment between the New York and Virginia promontories (Fig. 7–15). This restored position links foreland sedimentation with

Table 7–5. U-Pb SHRIMP-RG analytical data for zircons from the Reepsville gneiss. Gray shading

Spot Name	204 /206	% err	% comm 206	ppm U	ppm Th	232Th /238U	204corr 206Pb /238U Age	1s err	207corr 206Pb /238U Age	1s err	204corr 207Pb /206Pb Age	1s err	% Dis-cor-dant	Total 238 /206	% err	Total 207 /206	% err	238/ 206r	% err	207r /206r	% err	207r /235	% err	206r /238	% err	err corr
R29-6.1	3.3E-4	38	**0.60**	**172**	**37**	0.22	**337.9**	**3.9**	**338.7**	**3.9**	**254**	**108**	-25	18.47	1.2	.0561	2.5	18.58	1.2	.0513	4.7	0.38	4.8	.0538	1.2	.245
R29-28.2R	1.2E-4	1	**0.21**	**373**	**58**	0.16	**340.6**	**2.7**	**340.5**	**2.8**	**349**	**43**	3	18.39	0.8	.0552	1.8	18.43	0.8	.0535	1.9	0.40	2.1	.0543	0.8	.399
R29-22.1R	8.7E-4	35	**1.60**	**189**	**56**	0.31	**339.3**	**4.1**	**340.6**	**3.8**	**195**	**237**	-42	18.21	1.1	.0628	2.3	18.51	1.3	.0500	10.2	0.37	10.3	.0540	1.3	.122
R29-27.1	3.3E-4	24	**0.60**	**285**	**17**	0.06	**342.6**	**3.0**	**342.3**	**3.1**	**374**	**73**	9	18.21	0.9	.0589	1.9	18.32	0.9	.0541	3.2	0.41	3.3	.0546	0.9	.272
R29-12.1	---	0	**0.00**	**302**	**108**	0.37	**343.5**	**3.0**	**342.8**	**3.1**	**416**	**44**	21	18.27	0.9	.0551	2.0	18.27	0.9	.0551	2.0	0.42	2.2	.0547	0.9	.414
R29-2.1	3.8E-5	64	**0.07**	**678**	**210**	0.32	**352.8**	**2.1**	**351.9**	**2.1**	**437**	**32**	24	17.77	0.6	.0562	1.3	17.78	0.6	.0556	1.5	0.43	1.6	.0563	0.6	.384
R29-1.1	9.2E-5	53	**0.17**	**196**	**16**	0.09	**386.8**	**4.1**	**386.2**	**4.2**	**437**	**60**	13	16.14	1.1	.0570	2.3	16.17	1.1	.0556	2.7	0.47	2.9	.0618	1.1	.378
R29-7.1	---	0	**0.00**	**512**	**41**	0.08	**424.0**	**2.7**	**423.3**	**2.7**	**480**	**30**	13	14.71	0.7	.0567	1.3	14.71	0.7	.0567	1.3	0.53	1.5	.0680	0.7	.437
R29-13.1R	---	0	**0.00**	**753**	**31**	0.04	**425.7**	**2.7**	**424.6**	**2.8**	**508**	**25**	19	14.65	0.7	.0574	1.1	14.65	0.7	.0574	1.1	0.54	1.3	.0683	0.7	.513
R29-22.2X	---	0	**0.00**	**79**	**3**	0.03	**424.3**	**6.6**	**425.3**	**6.8**	**348**	**76**	-18	14.70	1.6	.0535	3.4	14.70	1.6	.0535	3.4	0.50	3.7	.0680	1.6	.433
R29-14.2R	---	0	**0.00**	**288**	**15**	0.05	**430.6**	**3.6**	**430.4**	**3.7**	**448**	**39**	4	14.48	0.9	.0559	1.7	14.48	0.9	.0559	1.7	0.53	1.9	.0691	0.9	.442
R29-18.1R	7.4E-5	1	**0.13**	**340**	**7**	0.02	**461.8**	**3.4**	**461.9**	**3.5**	**454**	**35**	-2	13.45	0.8	.0571	1.5	13.46	0.8	.0560	1.6	0.57	1.8	.0743	0.8	.436
R29-26.1	3.4E-6	1	**0.01**	**2338**	**107**	0.05	**838.9**	**2.0**	**834.2**	**2.1**	**982**	**8**	17	7.20	0.3	.0719	0.4	7.20	0.3	.0719	0.4	1.38	0.5	.1390	0.3	.550
R29-10.1	8.6E-5	33	**0.15**	**934**	**127**	0.14	**842.4**	**3.1**	**837.0**	**3.3**	**1007**	**17**	20	7.15	0.4	.0740	0.6	7.16	0.4	.0727	0.9	1.40	0.9	.1396	0.4	.417
R29-20.1	2.0E-5	54	**0.03**	**755**	**180**	0.25	**847.0**	**3.6**	**840.7**	**3.8**	**1035**	**15**	22	7.12	0.4	.0741	0.7	7.12	0.4	.0738	0.7	1.43	0.9	.1404	0.4	.526
R29-18.2C	1.5E-4	28	**0.25**	**1227**	**259**	0.22	**845.9**	**2.9**	**842.1**	**3.0**	**964**	**22**	14	7.11	0.4	.0733	0.5	7.13	0.4	.0712	1.1	1.38	1.1	.1402	0.4	.325
R29-15.1	1.0E-5	54	**0.02**	**706**	**187**	0.27	**864.5**	**4.6**	**861.5**	**4.7**	**956**	**15**	11	6.97	0.6	.0711	0.7	6.97	0.6	.0710	0.7	1.40	0.9	.1435	0.6	.615
R29-5.1	7.1E-5	26	**0.12**	**1348**	**286**	0.22	**887.3**	**2.7**	**883.7**	**2.9**	**990**	**13**	12	6.77	0.3	.0732	0.5	6.78	0.3	.0721	0.6	1.47	0.7	.1476	0.3	.453
R29-19.1R	---	0	**0.00**	**1148**	**79**	0.07	**895.0**	**2.9**	**892.5**	**3.0**	**964**	**11**	8	6.71	0.3	.0712	0.5	6.71	0.3	.0712	0.5	1.46	0.6	.1489	0.3	.545
R29-25.1	4.0E-5	69	**0.07**	**662**	**113**	0.18	**901.2**	**3.9**	**898.1**	**4.0**	**990**	**18**	10	6.66	0.5	.0727	0.7	6.66	0.5	.0721	0.9	1.49	1.0	.1500	0.5	.458
R29-29.1	2.0E-4	58	**0.34**	**99**	**49**	0.51	**904.3**	**10.2**	**900.2**	**10.5**	**1016**	**59**	12	6.62	1.2	.0759	1.8	6.64	1.2	.0731	2.9	1.52	3.2	.1506	1.2	.381
R29-3.1	---	0	**0.00**	**1022**	**556**	0.56	**908.4**	**3.2**	**905.1**	**3.4**	**1001**	**12**	10	6.61	0.4	.0725	0.6	6.61	0.4	.0725	0.6	1.51	0.7	.1513	0.4	.552
R29-16.1	---	0	**0.00**	**1189**	**398**	0.35	**910.3**	**3.0**	**907.1**	**3.2**	**998**	**11**	10	6.59	0.4	.0724	0.6	6.59	0.4	.0724	0.6	1.51	0.7	.1517	0.4	.540
R29-8.1	2.3E-5	38	**0.04**	**694**	**82**	0.12	**925.9**	**4.0**	**921.3**	**4.2**	**1047**	**18**	13	6.47	0.5	.0745	0.9	6.47	0.5	.0742	0.9	1.58	1.0	.1545	0.5	.452
R29-22.3C	5.7E-5	27	**0.10**	**466**	**255**	0.57	**930.3**	**4.8**	**927.3**	**5.0**	**1010**	**18**	9	6.44	0.6	.0737	0.8	6.44	0.6	.0729	0.9	1.56	1.1	.1552	0.6	.524
R29-28.1	2.9E-5	44	**0.05**	**576**	**152**	0.27	**952.2**	**5.3**	**946.9**	**5.6**	**1087**	**15**	14	6.28	0.6	.0761	0.7	6.28	0.6	.0757	0.8	1.66	1.0	.1592	0.6	.618
R29-13.2C	1.8E-5	50	**0.03**	**535**	**157**	0.30	**962.2**	**4.7**	**959.7**	**4.9**	**1027**	**16**	7	6.21	0.5	.0737	0.8	6.21	0.5	.0735	0.8	1.63	1.0	.1610	0.5	.551
R29-9.1	---	0	**0.00**	**666**	**227**	0.35	**969.4**	**4.2**	**966.0**	**4.4**	**1056**	**14**	9	6.16	0.5	.0745	0.7	6.16	0.5	.0745	0.7	1.67	0.8	.1623	0.5	.568
R29-17.1	1.3E-5	77	**0.02**	**1081**	**269**	0.26	**976.1**	**3.3**	**975.0**	**3.5**	**1004**	**12**	3	6.12	0.4	.0728	0.5	6.12	0.4	.0726	0.6	1.64	0.7	.1635	0.4	.536
R29-4.1	-1.5E-5	111	**-0.03**	**364**	**117**	0.33	**977.8**	**5.8**	**975.8**	**6.1**	**1027**	**23**	5	6.11	0.6	.0733	1.1	6.11	0.6	.0735	1.1	1.66	1.3	.1638	0.6	.489
R29-19.2C	3.8E-5	34	**0.06**	**362**	**138**	0.39	**984.0**	**6.8**	**983.8**	**7.1**	**989**	**20**	0	6.06	0.7	.0726	0.9	6.06	0.7	.0721	1.0	1.64	1.2	.1649	0.7	.614
R29-22.4I	4.5E-5	54	**0.08**	**266**	**199**	0.77	**995.1**	**6.6**	**996.0**	**7.0**	**972**	**24**	-2	5.99	0.7	.0721	1.0	5.99	0.7	.0715	1.2	1.65	1.4	.1669	0.7	.526
R29-11.1	5.0E-5	4	**0.08**	**675**	**250**	0.38	**1009.0**	**5.2**	**1008.9**	**5.5**	**1013**	**14**	0	5.90	0.6	.0737	0.7	5.90	0.6	.0730	0.7	1.70	0.9	.1694	0.6	.631
R29-21.1	-1.7E-5	82	**-0.03**	**531**	**171**	0.33	**1012.1**	**4.8**	**1009.7**	**5.0**	**1070**	**16**	6	5.88	0.5	.0748	0.7	5.88	0.5	.0750	0.8	1.76	0.9	.1700	0.5	.545
R29-23.1	---	0	**0.00**	**367**	**165**	0.47	**1020.2**	**5.8**	**1016.8**	**6.1**	**1098**	**18**	8	5.83	0.6	.0761	0.9	5.83	0.6	.0761	0.9	1.80	1.1	.1715	0.6	.572
R29-12.2C	1.4E-5	0	**0.02**	**787**	**331**	0.43	**1034.1**	**4.1**	**1034.3**	**4.3**	**1029**	**12**	0	5.75	0.4	.0738	0.6	5.75	0.4	.0736	0.6	1.76	0.7	.1740	0.4	.572
R29-6.2C	1.2E-5	86	**0.02**	**680**	**186**	0.28	**1037.3**	**4.4**	**1037.2**	**4.6**	**1039**	**14**	0	5.73	0.5	.0741	0.6	5.73	0.5	.0739	0.7	1.78	0.8	.1746	0.5	.558
R29-24.1	---	0	**0.00**	**104**	**62**	0.62	**1050.2**	**10.9**	**1051.7**	**11.5**	**1015**	**33**	-3	5.65	1.1	.0730	1.6	5.65	1.1	.0730	1.6	1.78	2.0	.1769	1.1	.571
R29-14.1C	-1.2E-5	82	**-0.02**	**680**	**381**	0.58	**1080.7**	**4.4**	**1079.9**	**4.6**	**1099**	**13**	2	5.48	0.4	.0760	0.6	5.48	0.4	.0761	0.6	1.92	0.8	.1825	0.4	.567

Errors are 1σ unless otherwise specified

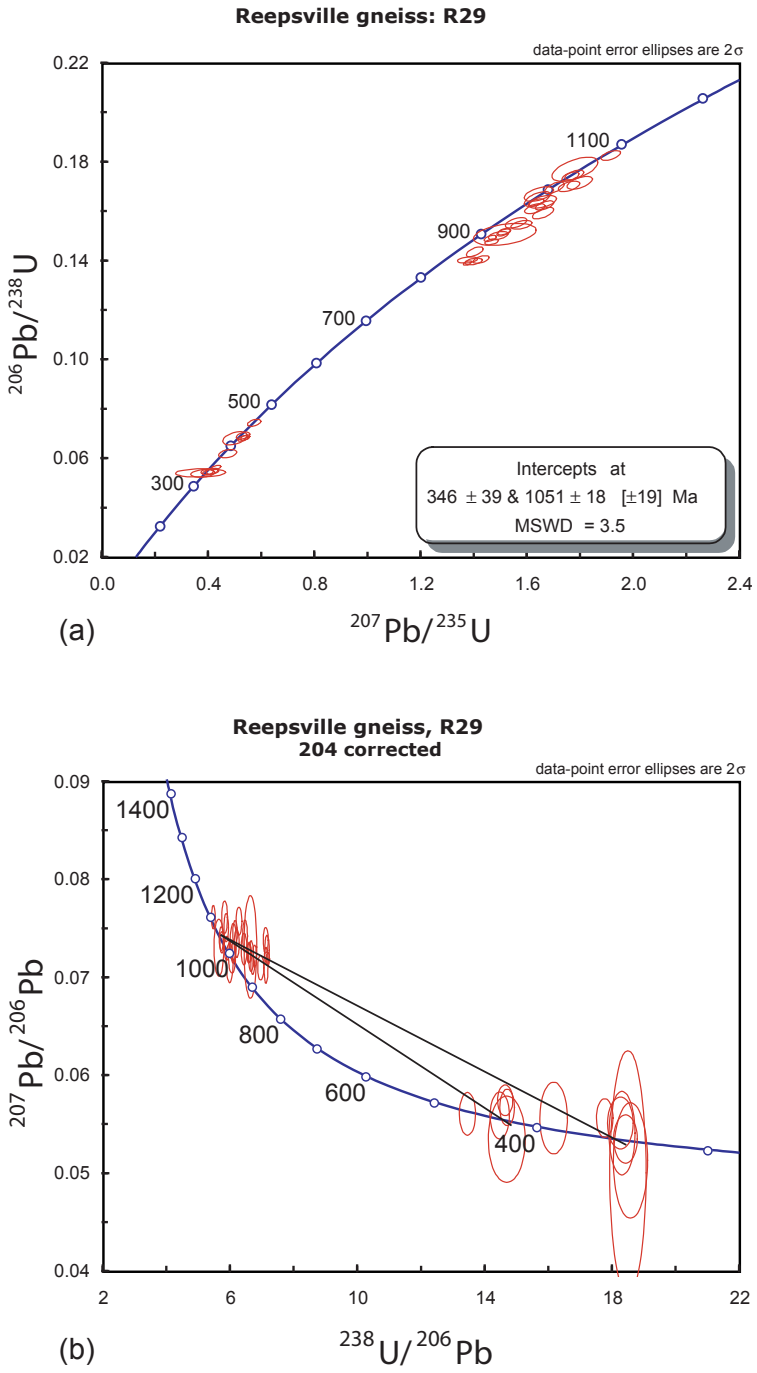

Figure 7–13. Concordia diagrams of 204-corrected SHRIMP U-Pb data from the Reepsville gneiss. (a) Conventional U/Pb concordia diagram with calculated concordia ages of the Reepsville gneiss at 1051±18 Ma and younger metamorphism at 346±39 Ma. (b) Tera-Wasserburg concordia diagram of Reepsville gneiss with two possible episodes of Paleozoic metamorphism and possible chords drawn from magmatic age of ~1051 Ma.

Figure 7–14. Possible location of the southern termination of the Brindle Creek fault. (a) Aeromagnetic map (D. L. Daniels, unpub. data) of part of the southern Appalachian Blue Ridge and Piedmont in AL, GA, SC, and NC. Note the very linear feature and curved anomalies to the NW of it in the IP (yellow arrow). The small red arrows are measurements of mesoscopic mineral stretching lineations whose curved pattern (Hatcher, 2001) is remarkably similar to that of the magnetic anomalies; there may be other possibilties. Irregular red line in SW and S parts of the map is the edge of the Coastal Plain. (b) Simplified tectonic map of part of the Tugaloo and adjacent terranes showing the location of the southern continuation of the Brindle Creek fault and Cat Square terrane. This projection is based solely on identification of a possible major fault in the aeromagnetic data in Figure 2(a). Curved dark blue lines in the IP represent magnetic lineaments. Red arrows track orientations of mineral lineations and interpreted crustal flow pattern in the IP (Hatcher and Merschat, 2006). Red bodies–Grenvillian basement. Lime green bodies–mafic rocks. Light green inside Pine Mountain window–Paleozoic cover rocks. Orange inside Dahlonega gold belt–metasandstone and pelitic schist. Yellow inside Tallulah Falls dome–quartzite. Light and dark green in Carolina superterrane–low and high grade rocks, respectively. Lavender in Tugaloo terrane–variously migmatitic metasandstone, pelitic schist, and mafic metavolcanic rocks. Dgb–Dahlonega gold belt. Aa–Alto allochthon. TFd–Tallulah Falls dome. MSf–Mill Spring fault. SMf–Six Mile fault. BAf–Box Ankle fault. DROw–Dog River-Opelika window. Fs–Forsyth. Plutons: Dark purple–Ordovician granitoids. Light purple–Ordovician(?) granitoids. Medium blue–Devonian granitoids. Darker blue-green–Mississippian plutons. Orange–Pennsylvanian granitoids. Red star in the southern Stewart quad is the location of a SHRIMP age date on detrital zircons. Modified from Hatcher et al. (2007).

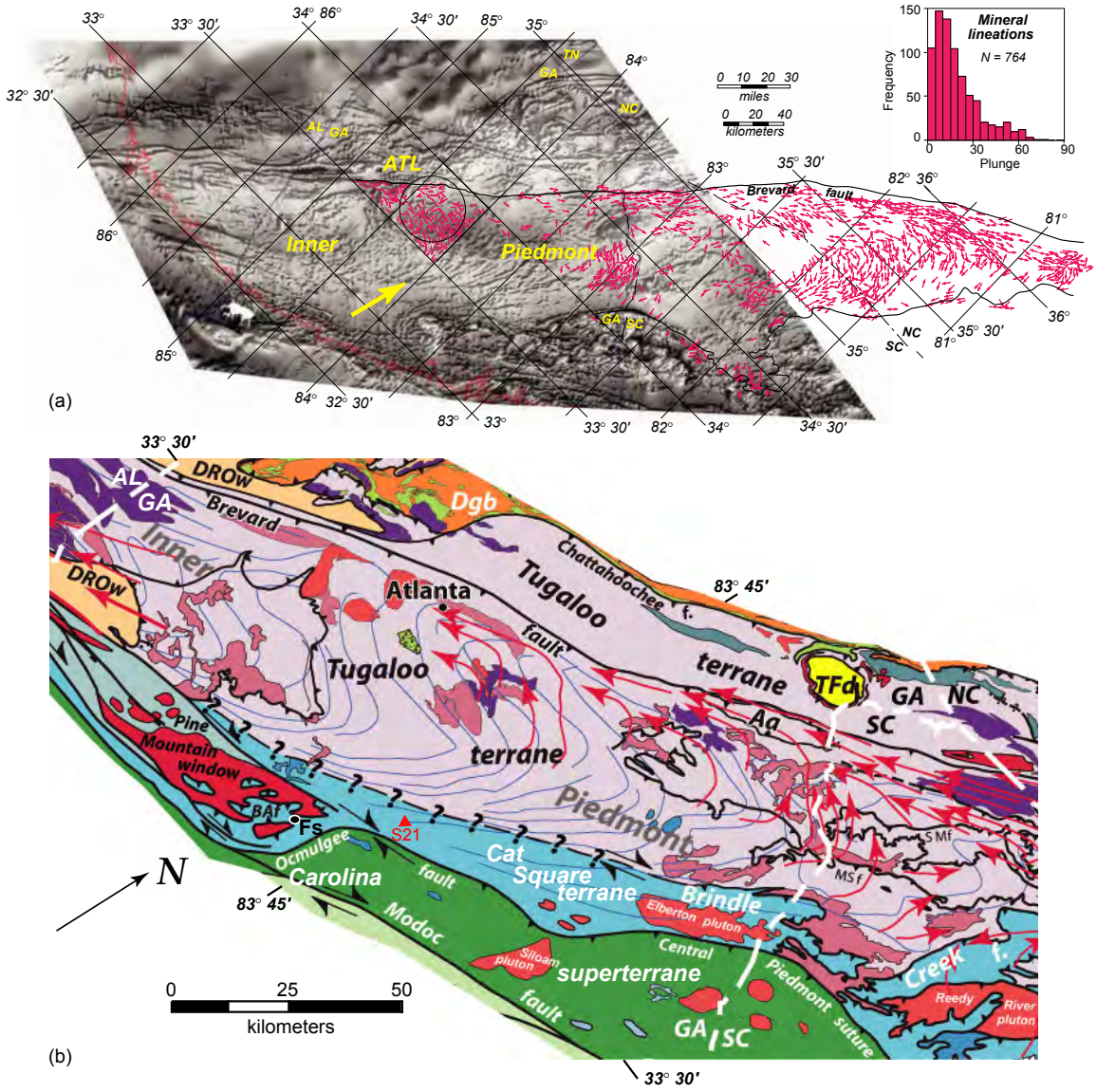
(a)
ATL
Inner
Piedmont
Brevard fault
Mineral lineations
N = 764
Frequency
Plunge
0 10 20 30
miles
0 20 40
kilometers
(b)
AL GA
DROw
Brevard
Inner
Dgb
Chattahoochee f.
Atlanta
Tugaloo
fault
terrane
TFd
GA NC SC
Aa
Pine Mountain window
BAT
Fs
S21
Piedmont
Ocmulgee fault
Carolina terrane
Cat Square terrane
Brindle
Elberton pluton
Modoc fault
Silo Creek pluton
Central Piedmont suture superterrane
Reedy River pluton
GA SC
N
83° 45′
33° 30′
0 25 50
kilometers

Figure 7–15. Maps representing the sequential tectonic history of the Cat Square terrane modifed from Merschat and Hatcher (2007). (a) Silurian configuration of Laurentia, Tugaloo terrane with mid-Ordovician plutons (dark purple), and Carolina superterrane separated by Rheic ocean. White arrows indicate motion of the Carolina superterrane. (b) Continued closure of the Rheic ocean and deposition of Cat Square terrane rocks during the Early Devonian. Magmatism in the Carolina superterrane, indicated by the Concord and Salisbury plutonic suites, is the product of subduction of the basin beneath the Carolina superterrane. (c) Closure of the Rheic ocean and suturing of Carolina superterrane by ~380 Ma. Gray lines indicate location of Brevard fault zone and ductile flow of Inner Piedmont material beneath the Carolina superterrane. (d) Neoacadian configuration resulting from dextral transpression. BBD–Bedford-Berea delta. BFZ–Brevard fault zone. BGD–Borden-Grainger delta. c–Concord Plutonic suite. CD–Catskill delta. chmbf–Chattahoochee-Holland Mountain-Burnsville fault. cps–central Piedmont suture. CSt–Cat Square terrane. PP–Price-Pocono delta. s–Salisbury Plutonic suite. sra–Smith River Allochthon.

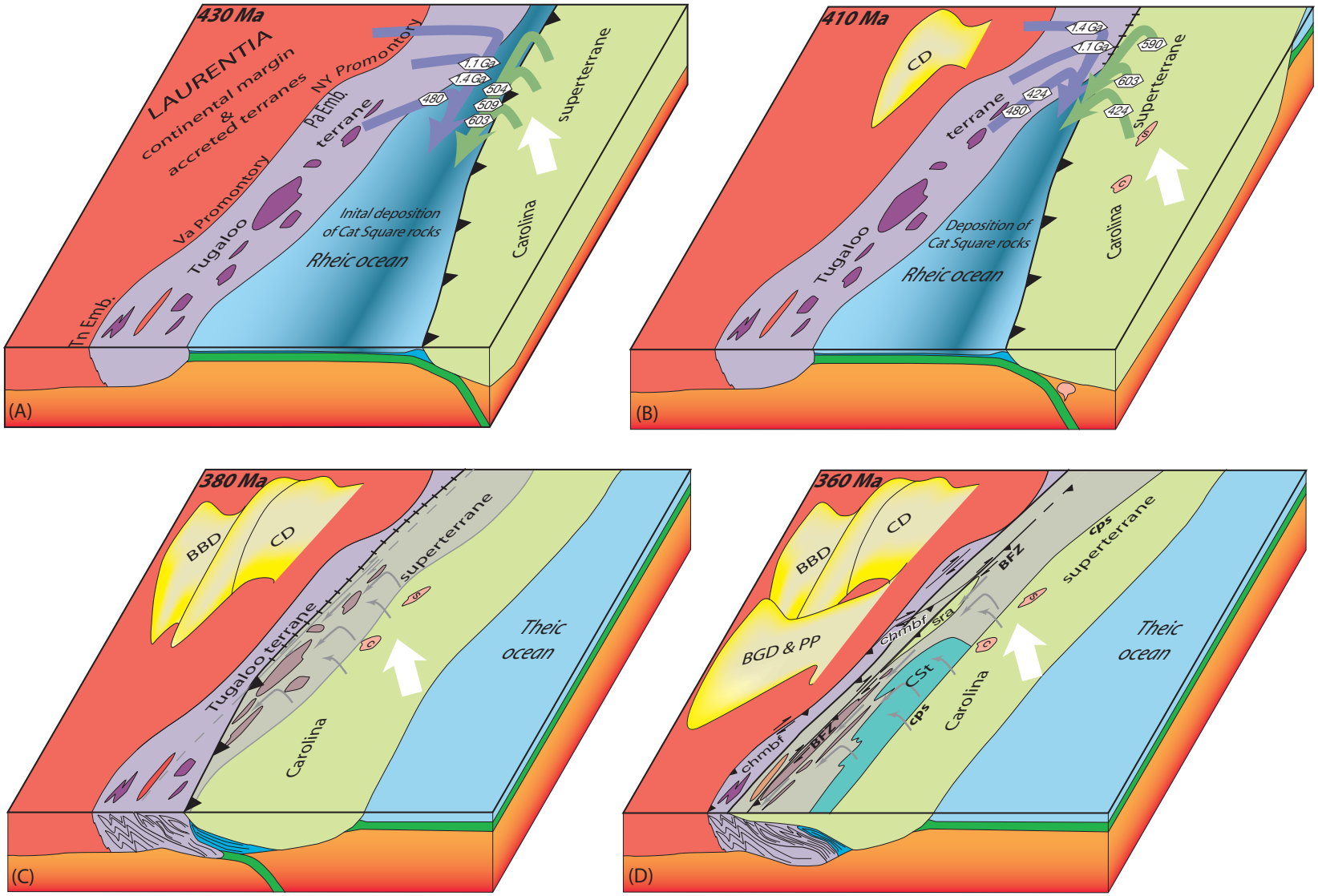
430 Ma
LAURENTIA
continental margin
&
accreted terranes
NY Promontory
Pa Emb.
terrane
Va Promontory
Tugaloo
Tn Emb.
Inital deposition
of Cat Square rocks
Rheic ocean
Carolina
superterrane
1.1 Ga
1.4 Ga
480
504
509
603
(A)
410 Ma
CD
terrane
Tugaloo
Deposition of
Cat Square rocks
Rheic ocean
Carolina
Superterrane
1.4 Ga
1.1 Ga
590
603
424
480
424
(B)
380 Ma
BBD
CD
superterrane
Tugaloo terrane
Carolina
Theic
ocean
(C)
360 Ma
BBD
CD
BGD & PP
BFZ
cps
superterrane
chmbf
sra
CSt
cps
BFZ
chmbf
Carolina
Theic
ocean
(D)

deformation in the IP and provides a possible source for the ~430 Ma detrital zircons to be derived from the central Appalachian Blue Ridge and Piedmont. (2) Eastward subduction of the basin beneath the Carolina superterrane produced Early Devonian magmatism in the Carolina superterrane (Fig. 7–15a). The combination of SW-prograding Acadian-Neoacadian clastic wedge and structural patterns in the IP support an oblique, NW-directed transpressive collision initiated in the St. Lawrence promontory and then the New York and Virginia promontories. (3) The Cat Square remnant ocean basin was zippered closed from NE to SW and subducted beneath the Carolina superterrane, along with part of the Tugaloo terrane and incorporated into the Neoacadian orogen by ~380 Ma (Fig. 7–15b). Metamorphic conditions associated with anatectic formation of the ~378 Ma Toluca Granite require burial of the Cat Square terrane to 15-20 km and temperatures of 800º C, consistent with subduction beneath the Carolina superterrane. (4) Suturing of the Carolina superterrane to Laurentian elements likely produced flysch and molasse that were shed into the central Appalachian foreland basin by ~380 Ma and migrated southwestward into the southern Appalachian foreland basin by ~340 Ma. Peak metamorphic conditions (sillimanite I and II) coeval with peak deformation, D_2 fabrics and structures affected the Cat Square terrane as they became part of the IP by 360-350 Ma. Curved high-temperature NW-rotating to SW-directed flow resulting from oblique convergence of the Carolina superterrane transported IP thrust sheets W and eventually SW several hundred kilometers along the mid-Paleozoic BFZ (Figs. 7–15c and 7–15d). Hatcher and Merschat (2006) have suggested that the high-temperature curved ductile flow in the IP is a tectonically forced orogenic channel.

ACKNOWLEDGMENTS

Funding for detailed geologic mapping in the South and Brushy Mountains, and the Newton-Lincolnton area were provided by grants from the EDMAP component of the National Cooperative Geologic Mapping Program, administered by the U.S. Geological Survey (to RDH). Several U.S. National Science Foundation grants (to RDH) have supported earlier detailed geologic mapping in the IP of North Carolina, South Carolina, Georgia, and Alabama. U/Pb zircon geochronology was funded by an NSF grant (to RDH), UT Science Alliance, and USGS FEDMAP. Andrew Wunderlich is acknowledged for his GIS assistance and help with several figures. Nancy Meadows is greatly acknowledged and appreciated for her help and special ability to resolve logistical problems. We remain culpable for all errors of fact or interpretation.

REFERENCES CITED

Alsop, G. I., and Holdsworth, R. E., 1999, Vergence and facing patterns in large-scale sheath folds: Journal of Structural Geology, v. 21, 1335-1349.

Alsop, G. I., and Holdsworth, R. E., 2002, The geometry and kinematics of flow perturbation folds: Tectonophysics, v. 350, p. 99-125.

Azcárraga, J., Ábalos, B., and Ibarguchi, J. I. G., 2002, On the relationship between kilometer-scale sheath folds, ductile thrusts and minor structures in the basal high-pressure units of the Cabo Ortegal complex (NW Spain): Journal of Structural Geology, v. 24, p. 1971-1989.

Bently, R. D., and Neathery, 1970, Geology of the Brevard zone and related rocks of the Inner Piedmont of Alabama: Alabama Geological Society, Eighth Annual Field Trip Guidebook

Bently, R. D., Higgins, M. W., Pickering, S. M., Jr., Grant, W. H., Zietz, I., and Neathery, T. L., 1974, Preliminary interpretation of an aeromagnetic map of most of the central and southern Georgia Piedmont: Geological Society of America Abstracts with Programs, v. 6, no. 4, p. 333-334.

Bier, S. E., 2001, Geology of the southeastern South Mountains, North Carolina [M.S. thesis]: Knoxville, University of Tennessee, 162 p.

Bier, S. E., Bream, B. R., and Giorgis, S. D., 2002, Inner Piedmont stratigraphy, metamorphism, and deformation in the Marion-South Mountains area, North Carolina, *in* Hatcher, R. D., Jr., and Bream, B. R., eds., Inner Piedmont geology in the South Mountains-Blue Ridge Foothills and the southwestern Brushy Mountains, central-western North Carolina: Carolina Geological Society Guidebook, p. 65-100.

Bream, B. R., 1999, Geology of the Glenwood and Sugar Hill quadrangles, North Carolina, and the structure of the northeast end of the Henderson Gneiss [M.S. thesis]: Knoxville, University of Tennessee, 155 p.

Bream, B. R., 2002, The southern Appalachian Inner Piedmont: New perspectives based on recent detailed geologic mapping, Nd isotopic evidence, and zircon geochronology, *in* Hatcher, R. D., Jr., and Bream, B. R., eds., Inner Piedmont geology in the South Mountains-Blue Ridge Foothills and the southwestern Brushy Mountains, central-western North Carolina: Carolina Geological Society Guidebook, p. 45-63.

Bream, B. R., 2003, Tectonic implications of geochronology and geochemistry of para- and orthogneisses from the southern Appalachian crystalline core [Ph.D. dissertation]: Knoxville, University of Tennessee, 296 p.

Bream, B. R., and Hatcher, R. D., Jr., 2002, Southern Appalachian terranes amended: Timing of accretion and delimiting provenance from new detritral zircon and Nd isotopic data: Geological Society of America Abstracts with Programs v. 34, p. 41.

Bream, B. R., Hatcher, R. D., Jr., Miller, C. F., and Fullagar, P. D., 2000, Paragneiss geochemistry and preliminary ion microprobe geochronology of detrital zircons from the southern Appalachian crystalline core: Geological Society of America Abstracts with Programs, v. 32, no. 7, p. 31.

Bream, B. R., Hatcher, R. D., Jr., Miller, C. F., and Fullagar, P. D., 2001, Geochemistry and provenance of Inner Piedmont paragneisses, NC and SC: Evidence for an internal terrane boundary?: Geological Society of America Abstracts with Programs, v. 33, no. 2, p. 65.

Bream, B. R., Hatcher, R. D., Jr., Miller, C. F., and Fullagar, P. D., 2004, Detrital zircon ages and Nd isotopic data from the southern Appalachian crystalline core, GA-SC-NC-TN: New provenance constraints for Laurentian margin paragneisses, *in* Tollo, R. P., Corriveau, L., McLelland, J., and Bartholomew, M. J., eds., Proterozoic evolution of the Grenville orogen in North America: Geological Society of America Memoir 197, p. 459-475.

Brown, P. M., Burt, E. R., II, Carpenter, P.A., Enos, R. M., Flynt, B. J., Jr., Gallagher, P. E., Horrman, C. W., Merschat, C. E., Wilson, W. F., and Parker, J. M., III, 1985, Geologic map of North Carolina: North Carolina Geological Survey, scale 1:500,000.

Bryant, B., and Reed, J. C., Jr., 1970, Geology of the Grandfather Mountain window and vicinity, North Carolina and Tennessee: U.S. Geological Survey Professional Paper 615. 190 p.

Butler, J. R., 1991, Metamorphism, *in* Horton, J. W., Jr., and Zullo, V. A., eds., The geology of the Carolinas: Knoxville, University of Tennessee Press, p. 127-141.

Byars, H. E., Merschat, A. J., Hatcher, R. D., Wooden, J. L., 2008, Timing and implications for the emplacement of the Paleozoic Vale (Cat Square) charnockite and Walker Top Granite, eastern Inner Piedmont, North Carolina: Geological Society of America Abstracts with Programs, v. 40, no. 4, p. 18.

Cabanis, B., and Lecolle, M., 1989, Le diagramme La/10-Y/15-Nb/8: un outil pour la discrimination des series volcaniques et la mise en evidence des processus de mélange et/ou de contamination crustale: C. R. Academy of Science Series II. v. 309, p. 2023-2029.

Carrigan, C. W., Bream, B. R., Miller, C. F., and Hatcher, R. D., Jr., 2001, Ion microprobe analyses of zircon rims from the eastern Blue Ridge and Inner Piedmont, NC-SC-GA: Implications for the timing of Paleozoic metamorphism in the southern Appalachians: Geological Society of America Abstracts with Programs, v. 33, no. 2, p. 7.

Carrigan, C. W., Miller, C. F., Fullagar, P. D., Bream, B. R., Hatcher, R. D., Jr., and Coath, C. D., 2003, Ion microprobe age and geochemistry of southern Appalachian basement, with implications for Proterozoic and Paleozoic reconstructions: Precambrian Research, v. 120, p. 1-36.

Davis, T. L., 1993a, Lithostratigraphy, structure, and metamorphism of a crystalline thrust terrane, western Inner Piedmont, North Carolina [Ph.D. dissertation]: Knoxville, University of Tennessee, 245 p.

Davis, T. L., 1993b, Geology of the Columbus Promontory, western Piedmont, North Carolina, southern Appalachians, *in* Hatcher, R. D., Jr., and Davis, T. L., eds., Studies of Inner Piedmont geology with a focus on the Columbus Promontory: Carolina Geological Society Guidebook, North Carolina Geological Survey, p. 17-43.

Davis, T. L., Hatcher, R. D., Jr., Liu, A., Tabor, J. R., 1991, Southern Appalachian western Inner Piedmont: A progressive crustal-scale shear zone: Geological Society of America Abstracts with Programs, v. 23, p. 138.

Dennis, A. J., 2007, Cat Square basin, Catskill clastic wedge: Silurian-Devonian orogenic events in the central Appalachians and the crystalline southern Appalachians, *in* Sears, J. W., Harms, T. A., and Evenchick, C. A., eds., Whence the Mountains? Inquiries into the evolution of orogenic systems: A volume in honor of Raymond A. Price: Geological Society of America Special Paper 433, p. 313-329.

Dennis, A. J., and Wright, J. C., 1997a, Middle and late Paleozoic monazite U-Pb ages, Inner Piedmont, South Carolina: Geological Society of America Abstracts with Programs, v. 29, no. 3, p. 12.

Dennis, A. J., and Wright, J. C., 1997b, The Carolina terrane in northwestern South Carolina, U.S.A: Late Precambrian-Cambrian deformation and metamorphism in a peri-Gondwanan oceanic arc: Tectonics, v. 16, p. 460-473.

Espenshade, G. H., Rankin, D. W., Shaw, K. W., and Neuman, R. B., 1975, Geologic map of the east half of the Winston-Salem quadrangle, North Carolina-Virginia: U.S. Geological Survey Map I-709-B, scale 1:250,000.

Gatewood, M. P., 2007, Structure and tectonics of the northeastern Inner Piedmont from detailed geologic mapping, geochronologic, geochemical, and petrologic studies with macro-, meso-, and microstructural analyses of ductile fault zones [M.S thesis]: Knoxville, University of Tennessee, 279 p.

Giorgis, S. D., 1999, Inner Piedmont geology of the northwestern South Mountains near Morganton, North Carolina [M.S. thesis]: Knoxville, University of Tennessee, 191 p.

Giorgis, S. D., Mapes, R. W., and Bream, B. R., 2002, The Walker Top Granite: Acadian granitoid or eastern Inner Piedmont basement?, *in* Hatcher, R. D., Jr., and Bream, B. R., eds., Inner Piedmont geology in the South Mountains-Blue Ridge Foothills and the southwestern Brushy Mountains, central-western North Carolina: Carolina Geological Society Guidebook, p. 33-44.

Goldsmith, R., 1981, Structural patterns in the Inner Piedmont of the Charlotte and Winston-Salem 2-degree quadrangles, North Carolina and South Carolina, *in* Horton, J. W., Jr., Butler, J. R., and Milton, D. M., eds., Geological investigations of the Kings Mountain belt and adjacent areas in the Carolinas: Carolina Geological Society Field Trip Guidebook, p. 19-27.

Goldsmith, R., Milton, D. J., and Horton, J. W., Jr., 1988, Geologic map of the Charlotte 1-degree x 2-degree quadrangle, North Carolina and South Carolina: U.S. Geological Survey Map I-1251-E, scale 1:250,000.

Griffin, V. S. Jr., 1969, Migmatitic Inner Piedmont belt of northwestern South Carolina: South Carolina Division of Geology Geologic Notes, v. 13, p. 87-104.

Griffin, V. S., Jr., 1971, The Inner Piedmont belt of the southern crystalline Appalachians: Geological Society of America Bulletin, v. 82, p. 1885-1898.

Griffin, V. S., Jr., 1974, Analysis of the Piedmont in northwest South Carolina: Geological Society of America Bulletin, v. 85, p. 1123-1138.

Hanmer, S., 1988, Ductile thrusting at mid-crustal level, southwestern Grenville province: Canadian Journal of Earth Science, v. 25, p. 1049–1059.

Harper, S. B., and Fullagar, P. D., 1981, Rb-Sr ages of granitic gneisses of the Inner Piedmont belt of northwestern North Carolina and southwestern South Carolina: Geological Society of America Bulletin, v. 92, p. 864-872.

Hatcher, R. D., Jr., 1969, Stratigraphy, petrology, and structure of the low rank belt and part of the Blue Ridge of northwestern South Carolina: South Carolina Division of Geology Geologic Notes, v. 13, p. 105-141.

Hatcher, R. D., Jr., 1972, Developmental model for the southern Appalachians: Geological Society of America Bulletin, v. 82, p. 2735-2760.

Hatcher, R. D., Jr., 1974. Introduction to the tectonic history of northeast Georgia: Georgia Geological Society Guidebook 13-A, 59 p.

Hatcher, R. D., Jr., 1978, Tectonics of the western Piedmont and Blue Ridge, southern Appalachians: Review and speculations: American Journal of Science, v. 278, p. 276-304.

Hatcher, R. D., Jr., 1993, Perspective on the tectonics of the Inner Piedmont, southern Appalachians, *in* Hatcher, R. D., Jr., and Davis, T. L., eds., Studies of Inner Piedmont geology with a focus on the Columbus Promontory: Carolina Geological Society Guidebook, North Carolina Geological Survey, p. 17-43.

Hatcher, R. D., Jr., 2001, Rheological partitioning during multiple reactivation of the Palaeozoic Brevard fault zone, southern Appalachians, USA, *in* Holdsworth, R. E., Strachan, R. A., Magloughlin, J. F., and Knipe, R. J., eds., The nature and tectonic significance of fault zone weakening: London, Geological Society of London Special Publication 186, p. 255-269.

Hatcher, R. D., Jr., 2002, An Inner Piedmont primer, *in* Hatcher, R. D., Jr., and Bream, B. R., eds., Inner Piedmont geology in the South Mountains-Blue Ridge Foothills and the southwestern Brushy Mountains, central-western North Carolina: Carolina Geological Society Guidebook, p. 1-18.

Hatcher, R. D., Jr., 2004, Properties of thrusts and the upper bounds for the size of thrust sheets, *in* McClay, K. R., ed., Thrust tectonics and hydrocarbon systems: American Association of Petroleum Geologists, Memoir 82, p. 18-29.

Hatcher, R. D., Jr., and Hooper, R. J., 1992, Evolution of crystalline thrust sheets in the internal parts of mountain chains, *in* McClay, K. R., ed., Thrust tectonics: London, Chapman and Hall, p. 217-234.

Hatcher, R. D., Jr., and Merschat, A. J., 2006, The Appalachian Inner Piedmont: An exhumed strike-parallel, tectonically forced orogenic channel, *in* Law, R. D., Searle, M., and Godin, L., eds., Channel flow, ductile extrusion and exhumation

of lower-mid crust in continental collision zones: London, Geological Society of London Special Publication 268, p. 517-540.

Hatcher, R. D., Jr., and Zietz, I., 1980, Tectonic implications of regional aeromagnetic and gravity data from the southern Appalachians, *in* Wones, D., ed., Proceedings, The Caledonides in the USA, IGCP Project 27-Caledonide orogen, 1979 Meeting: Blacksburg, Virginia Polytechnic Institute and State University, Department of Geological Sciences, Memoir 2, p. 235-244.

Hatcher, R. D., Jr., Bream, B. R., and Merschat, A. J., 2007, Tectonic map of the southern and central Appalachians: A tale of three orogens and a complete Wilson cycle, *in* Hatcher, R. D., Jr., Carlson, M. P., McBride, J. H., and Martínez Catalán, J. R., eds., 4-D Framework of Continental Crust: Geological Society of America Memoir 200, p. 595–632.

Hibbard, J., 2000, Docking Carolina: Mid Paleozoic accretion in the southern Appalachians: Geology, v. 28, p. 127-130.

Hibbard, J. P., Tracy, R. J., and Henika, W. S., 2003, Smith River allochthon: A southern Appalachian peri-Gondwanan terrane emplaced directly on Laurentia?: Geology, v. 31, p. 215-218.

Higgins, M. W., Atkins, R. L., Crawford, T. J., Crawford, R. F., III, Brooks, R., and Cook, R. R., 1988, The structure, stratigraphy, tectonostratigraphy, and evolution of the southernmost part of the Appalachian orogen: U.S. Geological Survey Professional Paper 1475. 173 p.

Hill, J. C., 1999, Geology of the Marion East quadrangle, North Carolina, and the stratigraphy of the Tallulah Falls Formation in the Chauga belt [M.S. thesis]: Knoxville, University of Tennessee, 188 p.

Hopson, J. L., and Hatcher, R. D., Jr., 1988, Structural and stratigraphic setting of the Alto allochthon, NE Georgia: Geological Society of America Bulletin, v. 100, p. 339-350.

Horton, J. W., Jr., and Butler, J. R., 1986, The Brevard fault zone at Rosman, Translyvania County, North Carolina, *in* Neathery, T. L., ed., Centennial Field Guide Volume 6, Southeastern Section of the Geological Society of America: Boulder, Colorado, Geological Society of America, p. 251–256.

Horton, J. W., and McConnell, K. I., 1991, The western Piedmont, *in* Horton, J. W., and Zullo, V. A., eds., The geology of the Carolinas: Knoxville, Tennessee, University of Tennessee Press, p. 36-58.

Kalbas, J. L., 2003, Geology of part of the southwestern Brushy Mountains, Inner Piedmont [M.S. thesis]: Knoxville, University of Tennessee, 208 p.

Kalbas, J. L., Bream, B. R., Hatcher, R. D., Jr., and Maybin, A. H., 2002, Evidence for mafic Ordovician magmatism in the Brushy Mountains, western Inner Piedmont of North Carolina: Geological Society of America Abstracts with Programs, v. 34, no. 2, p. 119.

King, P. B., 1955, A geologic cross section across the southern Appalachians, an outline of the geology in the segment in Tennessee, North Carolina, and South Carolina, *in* Russell, R. J., ed., Guides of southeastern geology: Geological Society of America Annual Meeting, p. 332-373.

Kish, S. A., 1997, The Cat Square charnockite—a Paleozoic charnockite in the Inner Piedmont of North Carolina: Geological Society of America Abstracts with Programs, v. 29, no. 3, p. 28.

Kohn, M. J., 2001, Timing of arc accretion in the southern Appalachians: Perspectives from the Laurentian margin: Geological Society of America Abstracts with Programs, v. 33, no. 6, p. 262.

Luth, W. D., Jahns, R. H., and Tuttle, O. F., 1964, The granite system at pressures of 4 to 10 kilobars: Journal of Geophysical Research, v. 69, p. 759-773.

Mapes, R. W., 2002, Geochemistry and geochronology of mid-Paleozoic granitic plutonism in the southern Appalachian Piedmont terrane, North Carolina-South Carolina-Georgia [M.S. thesis]: Nashville, Vanderbilt University, 150 p.

Mapes, R. W., Maybin, A. H., III, Miller, C. F., Fullagar, P. D., and Bream, B. R., 2002, Geochronology and geochemistry of mid Paleozoic granitic magmatism, central and eastern Inner Piedmont, North Carolina and South Carolina: Geological Society of America Abstracts with Programs, v. 34, no. p. A-94.

McSween, H. Y., Jr., and Harvey, R. P. 1997, Concord Plutonic Suite: Pre-Acadian gabbro-syenite intrusion in the southern Appalachians, *in* Sinha, A. K., Whalen, J. B., and Hogan, J. P., eds., The nature of magmatism in the Appalachian orogen: Boulder, Colorado, Geological Society of America Memoir 197, p. 221-234.

McSween, H. Y., Jr., Sando, T. W., Clark, S. R., Harden, J. T., and Strange, E. A., 1984, The gabbro-metagabbro association of the southern Appalachian Piedmont: American Journal of Science, v. 284, p. 437-461.

Merle, O., Cobbold, P. R., and Schmid, S., 1989, Tertiary kinematics in the Lepontine dome, *in* Coward, M. P., Dietrich, D., and Park., R. G., eds., Alpine tectonics: Geological Society of London Special Publication 45, p. 113–134.

Merschat, A. J., 2003, Inner Piedmont tectonics in the southwestern Brushy Mountains, North Carolina: Field and laboratory data revealing 3-D crustal flow and sillimanite I and II metamorphism [M.S. thesis]: Knoxville, University of Tennessee, 198 p.

Merschat, A. J., and Kalbas, J. L., 2002, Geology of the southwestern Brushy Mountains, North Carolina Inner Piedmont: A summary and synthesis of recent studies, *in* Hatcher, R. D., Jr., and Bream, B. R., eds., Inner Piedmont geology in the South Mountains-Blue Ridge Foothills and the southwestern Brushy Mountains, central-western North Carolina: Carolina Geological Society Guidebook, p. 101-126.

Merschat, A. J., and Hatcher, R. D., Jr., 2007, The Cat Square terrane: Possible Siluro-Devonian remnant ocean basin in the Inner Piedmont, southern Appalachians, USA, in Hatcher, R. D., Jr., Carlson, M. P., McBride, J. H., and Martínez Catalán, J. R., eds., 4-D Framework of Continental Crust: Geological Society of America Memoir 200, p. 553–565.

Merschat, A. J., Hatcher, R. D., Jr., and Davis, T. L., 2005a, The northern Inner Piedmont, southern Appalachians, USA: Kinematics of transpression and SW-directed mid-crustal flow: Journal of Structural Geology, v. 27, p. 1252-1281.

Merschat, A. J., Gatewood, M. P., Fisher, C. M., Miller, C. F., Hatcher, R. D., Jr., Wooden, J. L., and Stahr, D. W., III, 2005b, The Newton antiform, NC: A previously unrecognized window through the allochthonous Inner Piedmont thrust stack: Geological Society of America Abstracts with Programs, v. 37, no. 7, p. 20.

Merschat, A. J., Bream, B. R., Hatcher, R. D., Jr., Miller, C. F., and Wooden, J. L., 2007, Provenance and timing of crust formation in the southern Appalachian crystalline core: evidence from detrital zircon studies: Geological Society of America Abstracts with Programs, v. 39, no. 6, p. 341.

Mirante, D. C., and Patino-Douce, A. E., 2000, Melting and migmatization in the southern Appalachian Inner Piedmont of northeast Georgia: the Athens gneiss: Geological Society of America Abstracts with Programs, v. 33, no. 7, p. 297.

Mittwede, S. K., Ødegård, M., and Sharp, W. E., 1987, Major chemical characteristics of the Hammett Grove meta-igneous suite, northwestern South Carolina: Southeastern Geology, v. 28, p. 49-63.

Nelson, A. E., Horton, J. W., and Clarke, J. W., 1998, Geologic map of the Greenville 1° x 2° quadrangle, Georgia, South Carolina, and North Carolina: U.S. Geological Survey Map I-2175, scale 1:250,000.

Osberg, P. H., Tull, J. F., Robinson, P., Hon, R., and Butler, J. R., 1989, The Acadian orogen, Chapter 4, *in* Hatcher, R. D., Jr., Thomas, W. A., and Viele, G. W., eds., The Appalachian-Ouachita orogen in the United States: Boulder, Colorado, Geological Society of America, The Geology of North America, v. F-2, p. 179-232.

Overstreet, W. C., Yates, R. G., and Griffits, W. R., 1963, Geology of the Shelby quadrangle, North Carolina: U.S. Geological Survey Map I-384, scale 1:62,500.

Pearce, J. A., and Cann, J. R., 1973, Tectonic setting of basic volcanic rocks determined using trace element analyses: Earth and Planetary Science Letters, v. 19, p. 290-300.

Pearce, J. A., and Norry, M. J., 1979, Petrogenetic implications of Ti, Zr, Y and Nb variations in volcanic rocks: Contributions to Mineralogy and Petrology, v. 69, p. 33-47.

Privett, D. R., 1984, The Turnersberg intrusive: Petrogenesis of a metamorphosed alpine ultramafite in the eastern Inner Piedmont, Iredell County, North Carolina: Southeastern Geology, v. 25, p. 55-60.

Rankin, D. W., 1975, The continental margin of eastern North America in the southern Appalachians: The opening and closing of the proto-Atlantic Ocean: American Journal of Science, v. 275-A, p. 298-336.

Rankin, D. W., Espenshade, G. J., and Neuman, R. B., 1972, Geologic map of the west half of the Winston-Salem quadrangle, North Carolina, Virginia, and Tennessee: U.S. Geological Survey Map I-709-A, scale 1:250,000.

Reed, J. C., 1964, Geology of the Lenoir quadrangle, North Carolina: U. S. Geological Survey Map I-709-A, scale 1:62,500.

Reed, J. C., Jr., and Bryant, B., 1964, Evidence for strike-slip faulting along the Brevard zone in North Carolina: Geological Society of America Bulletin, v. 75. p. 1177-1196.

Robinson, P., Tucker, R. D., Bradley, D., Berry, H. N., IV, and Osberg, P. H., 1998, Paleozoic orogens in New England, USA: Geologiska Föreningens Stockholm Forhandlingar, v. 120, p. 119-148.

Secor, D. T., Samson, S. L., Snoke, A. W., and Palmer, A. R., 1983, Confirmation of the Carolina Slate Belt as an exotic terrane: Science, v. 221, p. 649-651.

Sinha, A. K., Thomas, W., Hatcher, R. D., Jr., and Jerden, J. L., *in preparation*, Correlation of magmatism with pre-collisional depocenters and geometry of rifted

margins: Ordovician to Devonian magmatism associated with Taconic collisional tectonics.

Student, J. J. and Sinha, A. K. 1992. Carboniferous U-Pb ages of zircons from the Box Ankle and Ocmulgee faults, central Georgia: Implications for accretionary models: Geological Society of America Abstracts with Programs, v. 24, no. 2, 69.

Trümpy, R., 1960, Paleotectonic evolution of the central and western Alps: Geological Society of America Bulletin, v. 71, p. 843-908.

Trümpy, R., 1980, Geology of Switzerland, a guide-book. Part A: An outline of the geology of Switzerland: Basel, Wepf & Co. 104 p.

Vauchez, A., Babaie, H. A., and Babaei, A., 1993, Orogen-parallel tangential motion in the Late Devonian – Early Carboniferous southern Appalachians internides: Canadian Journal of Earth Sciences, v. 30, p. 1297-1305.

Williams, S. T., 2000, Structure, stratigraphy, and migmatization in the southwestern South Mountains, North Carolina [M.S. thesis]: Knoxville, University of Tennessee, 111 p.

Williams, H., and Hatcher, R. D., Jr., 1983, Appalachian suspect terranes, *in* Hatcher, R. D., Jr., Williams, H., and Zietz, I., eds., Contributions to the tectonics and geophysics of mountain chains: Geological Society of America Memoir 158, p. 33-53.

Wilson, C. G., 2006, Origin and tectonic evolution of the southern Appalachian Neoacadian crystalline core: Evidence from the geology of the Gilreath 7.5-minute quadrangle, North Carolina [M.S. thesis]: Knoxville, University of Tennessee, 219 p.

Wood, D. A., 1980, The application of a Th-Ha-Ta diagram to problems of tectonomagmatic classification and to establishing the nature of crustal contamination of bsaltic lavas of the British Tertiary volcanic province: Earth and Planetary Science Letters, v. 50, p. 11-30.

Yanagihara, G. M., 1994, Structure, stratigraphy, and metamorphism of a part of the Columbus Promontory, western Inner Piedmont, North Carolina [M.S. thesis]: Knoxville, University of Tennessee, 214 p.

APPENDICES

APPENDIX I

Structural Measurements and Outcrop Descriptions from the Waynesville 7.5-minute Quadrangle

Note: Stations correspond to locations shown in Plate 2. Lithologic descriptions are in field shorthand.

ABBREVIATIONS

Minerals

BI	-	Biotite
CHL	-	Chlorite
E	-	Epidote
FELD	-	Feldspar
GAR	-	Garnet
H	-	Hornblende
KY	-	Kyanite
M	-	Muscovite
QTZ	-	Quartz
SIL	-	Sillimanite
TM	-	Tourmaline

Rock Types

AM	-	Amphibolite
CALC-SI	-	Calc-silicate
GG	-	Granitic gneiss
GTD	-	Granitoid
LEUCO	-	Leucocratic
(M)	-	Mylonite
MGW	-	Metagraywacke
(P)	-	Protomylonite
PEG	-	Pegmatite
QTZITE	-	Quartzite

Textures

INEQ	-	Inequigranular
MEGAC	-	Megacrystic
MIG	-	Migmatitic
MYLO	-	Mylonitic
P	-	Porphyroblastic

			Foliation		Lineation		Fold Axis		Axial Surface		IL	Fold	Fold	Crenulation Axis		Joint		Joint	
Station	Quad	Lithology	Strike	Dip	Plunge	Trend	Plunge	Trend	Strike	Dip	Angle	Genr.	Verg.	Plunge	Trend	Strike	Dip	Strike	Dip
1	W	MIG. MGW	N85W	45NE															
2	W	MGW & MS-BI SCHIST	N 58W	39SW															
3	W	MGW & MS-BI SCHIST	N56W	60SW	4	N65W													
4	W	MS-BI SCHIST	N80W	27NE															
5	W	SAP & INTRLD MS-BI SCHIS	N72E	88NW															
6	W	GAR-MS-BI SCHIST	N45W	55NE														N75E	37NW
7	W	MGW INTRLD SCHIST	N55E	32NW														N23W	87NE
8	W	MGW-MIG LYRS 1/2CM	N40W	25NE			14	N74W	N75W	10NE	0								
9	W	MIG BI GN W/ AM	N68E	65SE			7	N50E	N56E	65NW	0-10	F2							
10	W	MIG BI-PLAG GN	N50W	26NE			12	S74E	N12W	12NE	0								
11	W	MIG. BI-PLAG GN					10	N35W			0	F2, SHEATH							
12	W	MIG. BI-PLAG GN	N 85E	44NW															
13	W	BI-QTZ-FELD GN	N38W	38NE															
14	W	MIG. BI-PLAG GN	N10E	28SE			28	S80E	N12E	25SE	10-30					N27W	77SW		
15	W	MIG BI-PLAG GN	N2W	28NE															
16	W	MIG AM	N60E	85SE															
17	W	MIG. BI-PLAG GN	N61E	20SE												N12E	88SE		
18	W	MIG. INEQ. BI-PLAG GN	N29E	48SE			21	N28E	N28E	26SE	0-70					N12E	51SE		
19	W	MIG. INEQ. BI GN	N11W	66NE															
20	W	BI-PLAG GN	N 55E	51SE															
21	W	MIG. INEQ. BI-PLAG GN	N14E	75SE															
22	W	SAP-MIG. BI GN	N75W	68SW															
23	W	MIG. INEQ BI-PLAG GN	N24E	78SE															
24	W	MI. INEQ. BI-PLAG GN	N24E	75SE															
25	W	MIG. BI GN	N 11W	38NE			2	S15W	N15E	17SE	10-30	F2							
26	W	MIB. BI-PLAG GN	N40W	65NE															
27	W	MIG. BI-PLAG GN	N70E	25SE															
28	W	MIG. BI GN	N80E	26SE															
29	W	MIG. BI-PLAG GN	N26E	56SE															
30	W	MIG. BI-PLAG GN	N45E	49NW														N58W	85NE
31	W	MIG. BI-PLAG GN					25	N55E	N35S	48SE	20-100								
32	W	MIG. BI-PLAG GN	N87E	81SE												N40E	73NW		
33	W	MIG. INEQ-BI-PLAG GN	N45E	73SE															
34	W	MIG.INEQ-BI-PLAG GN	N96E	69SE			19	N6E	N40E	40SE	10-70		NW						
35	W	MIG. BI-PLAG GN	N75E	60NW			7	N65E	N65E	90	70-90								
36	W	MIG. BI-GN	N81E	44NW															
37	W	MIG. BI-PLAG GN	N84E	65SE					N44W	42NE	90					N30W	80SW	N24E	66SE
38	W	MIG. BI-GAR-PLAG GN	N76E	66SE												N8W	39NE	N40E	72SE
39	W	MIG. AM & MIG BI-PLAG GN	N87E	77SE	8	S69E													
40	W	MIG AM	N70E	54NW	54	N44E	46	N85E	N85E	71NW	0								
41	W	FLOAT MIG AM																	
42	W	MIG. BI-PLAG GN	N74E	39SE												N69E	77NW	N50E	70NW
43	W	MIG. INEQG GAR-BI-PLAG G	N21E	31SE															
44	W	MIG BI-PLAG GN & AM	N70W	40NE															
45	W	MIG. BI-PLAG GN	N21W	68NE															
46	W	MIG. BI-PLAG GN	N80W	39NE												N7E	78SE		
47	W	MIG. GAR-BI-PLAG GN	N78W	79NE			80	N80E	N80E	18NW	0-10	VERGE SW							
48	W	MIG. BI-PLAG GN	N36W	61NE												N54W	90		
49	W	?MIG. INEQ BI-PLAG GN	N80W	50NE												N-S	85SE		
50	W	INEQ-GAR-BI-PLAG-QTZ GN	N25W	85SW															
51	W	INEQ-GAR-BI-PLAG-QTZ GN	N18W	41NE															
52	W	LYRD MIG. BI-PLAG GN	N88W	45NE															
53	W	MIG. BI GN	N15W	46NE															
54	W	LYRD MIG. BI-PLAG GN	N87W	47SW															
55	W	SAP-MIG. BI-PLAG GN	N18E	56NW															
56	W	SAP-MIG. BI-PLAG GN	N32W	39NE															
57	W	LYRD MIG. BI-PLAG GN					13	S84E	N84W	55NE	70								
58	W	LYRD MIG. BI-PLAG GN	N46W	15NE			15	N59E	N59W	~15NE	0-10					N64E	72SE		
59	W	SAP. MIG. AMP &PODS OF ?	N50E	30SE															
60	W	SAP. MIG. BI-PLAG GN	N71E	67SE															
61	W	?. MIG. BI-PLAG GN &AMP P	N79E	32SE															
62	W	MIG. BI-PLAG GN	N69W	29NE															
63	W	SAP-MGW WITH MS	N12E	31SE															
64	W	SAP-MGW	N30E	38SE															
65	W	MGW-MS PRESENT	N68W	27NW															
66	W	MGW	N88E	90SE															
67	W	MIG. MGW	N78E	70NW												N70E	86NW		
68	W	MIG. CG MGW	N11E	36SE															
69	W	MIG. MGW-MS	N80W	33NE												N80E	78SE		
70	W	MGW	N72W	54NE												N48E	66NW		
71	W	LYRD MIG. BI-PLAG GN	N51E	40NW												N62W	55SW		
72	W	LYRD MIG &MEG BI-PLAG G	N41E	26SE			30	N10E	N30E	16NW	10-30								
73	W	LYRD MIG. BI-PLAG GN	N70W	20NE												N34W	79NE		
74	W	LYRD MIG. BI-PLAG GN	N68E	47NW												N5W	56NE		
75	W	LYRD MIG. BI-PLAG GN	N56W	48NE															
76	W	LYRD MIG. BI-PLAG GN	N68W	60NE			9	S82E	N82W	31NE	10-0					N88E	72SE		
77	W	LYRD MIG. BI-PLAG GN	N70W	52NE			41	N45E	N70W	52NE	0-10					N5E	70NW		
78	W	MGW BI-PLAG GN	N19E	58SE															
79	W	MIG. -MGW	N78W	47NE															
80	W	GAR-MS-BI SCHIST	N78W	26SW												N54E	73SE		
81	W	MIG. GAR-BI-MS-SCHIST	N28E	67NW												N56W	57NE		
82	W	MIG. INEQ BI GN	N28W	66NE			32	N29W	N29W	75SW	0-10					N3W	90		
83	W	MIG. BI-PLAG GN	N26W	61NE															
84	W	MIG. H-BI-PLAG GN					10	N32E	N32E	28SE	70								
85	W	SAP MIG. BI GN	N66W	24NE												N49W	78SW		
86	W	MIG. BI-PLAG GN	N10W	61NE															
87	W	MIIG. MEG BI-PLAG GN	N50E	78NW															
88	W	MIG. BI-PLAG GN	N48E	68SE												N35W	72NW		
89	W	YRD MIG. HORN-BI-PLAG G	N74E	82NW			65	S81W	N81E	86NW	10-20								
90	W	MIG. BI-PLAG GN	N76W	69NE															
91	W	INEQ. MIG. BI-PLA GN	N84W	85NE															
92	W	LYRD. MIG. BI GN	N73W	64NE			26	N30W	N34W	50NE	100								
93	W	LYRD. MIG. BI GN	N58W	25NE															
94	W	LYRD. MIG. BI GN	N85W	25NE												N16E	79NW		
95	W	MIG. TO GG - ?	N82E	27NW			27	N72W	N72W	50NE	10					N62W	84NE	N62E	72NW
96	W	LYRD. MIG. BI -PLAG GN	N73W	32NE			37	N70E								N74E	9NW	N89W	33NE
97	W	LYRD. MIG.BI-PLAG GN	N20E	42SE	38	N88E										N24W	65NE		
98	W	LYRD. MIG. BI-PLAG GN	N55W	35SW															
99	W	LYRD. MIG BI-PLAG GN	N81W	19SW			18	S82E	N82W	30NE	0-30					N83W	80NE	N34E	54NW
100	W	LYRD. MIG. BI-PLAG GN	N35W	44NE			24	S75E	N75W	44NE	30					N23W	56N		
101	W	LYRD. MIG. BI-PLAG GN	N10W	26NE			18	S85E	N85W	66NE	50-60								
102	W	MIG BI-MS-SCHIST	N88W	5NE															
103	W	IG. BI-M SCHIST WITH P OF	N29W	45NE															
104	W	MG SCHIST	N10E	20NW															
105	W	MS-SCHIST & MGH	N20W	30NE															
106	W	MIG. BI GN	N75E	58SE															
107	W	LYRD MIG. BI-PLAG GN	N85E	50SE			7	N88W	N78W	35SW	0-30					N20W	70SW		
108	W	G BI-PLAG GN LENS LYRD M	N78W	15NE															
109	W	MIG. BI-PLAG GN	N85E	29SE															
110	W	MIG. AM -LENS PIE SHAPED	N62E	31SE															
111	W	MIG. AM & MIG BI-PLAG GN	N29W	41NE															
112	W	LYRD MIG. BI-PLAG GN	N66W	28NE															
113	W	LYRD MIG. BI-PLAG GN	N88W	44NE												N60W	18SW		
114	W	LYRD MIG. BI-PLAG GN	N66W	43NE															

			Foliation		Lineation		Fold Axis		Axial Surface		IL	Fold	Fold	Crenulation Axis		Joint		Joint	
Station	Quad	Lithology	Strike	Dip	Plunge	Trend	Plunge	Trend	Strike	Dip	Angle	Genr.	Verg.	Plunge	Trend	Strike	Dip	Strike	Dip
115	W	LYRD MIG. BI-PLAG GN	N90E	88NW															
116	W	G. BI-PLAG GN &MIG. AM &AM PODS					10	N75E	N75E	30NW	10-30								
117	W	IG. BI-PLAG GN TOAM SCHI	N83W	52SW															
118	W	. AM WITH QTZ-FELD LAY	N87E	55W												N70W	54SW	N15W	70NE
119	W	MIG. AM	N70W	54NE			27	S83E	N83W	53NE	10-20								
120	W	LYRD MIG. BI-GN	N72E	56NW												N28W	75SW	N18W	88NE
121	W	MIG. BI-PLAG GN	N89W	81NE															
122	W	LYRD MIG. BI-PLAG GN	N84E	30NW															
123	W	LYRD. MIG. BI-PLAG GN	N88W	59NE												N5W	88NE		
124	W	LYRD MIG. BI-PLAG GN	N80E	25NW			11	N20E	N70E	27NW	30-50								
125	W	LYRD MIG. BI-PLAG GN	N70W	63NW															
126	W	MIG. BI-PLAG GN	N75E	12NW												N20W	80SW		
127	W	LYRD MIG. BI-PLAG GN	N88E	80NW												N55W	75SW		
128	W	LYRD MIG. BI-PLAG GN	N81E	75NW															
129	W	LYRD MIG. BI-PLAG GN	N71W	23NE			29	N55E	N55E	49SE	50-70					N68W	69SW	N61E	81NW
130	W	RD MIG. BI-PLAG GN TO BI	N24E	58SE															
131	W	LYRD MIG. BI-PLAG GN	N24E	76SE			28	N43E	N43E	90	80								
132	W	MIG. BI-PLAG-QTZ GN	N44W	58NW												N17E	88NW		
133	W	LYRD MIG. BI-PLAG GN	N75E	18NW												N50E	85NW	N55W	68SW
134	W	LYRD MIG. BI-PLAG GN	N50E	40SE												N70W	79SW		
135	W	LYRD MIG. BI-PLAG GN	N55E	62NW												N75W	72SW	N10E	75SE
136	W	LYRD MIG. BI-PLAG GN	N80E	70NW												N60W	78SW		
137	W	MIG. BI GN	N70E	54NW												N52E	E54NW		
138	W	MIG. BI-PLAG GN	N80W	58NE												N5W	88SW		
139	W	LYRD MIG BI-PLAG GN	N11E	55SE															
140	W	MIG BI-PLAG GN	N30E	66SE															
141	W	GAR MS	N69W	64NE															
142	W	INTLRD CALC-SI & SCHIST	N70W	34NE															
143	W	MGW	N80W	54NE															
144	W	S SCHIST WITH CG MS FLAK	N60W	42NE			40	N88E	N88E	84NW	120-150								
145	W	GAR-BI-MS SCHIST	N70W	56NE															
146	W	GAR-SIL-BI-MS SCHIST	N52W	57NE			22	S48E	N48W	70NE	50-70								
147	W	GAR-BI-MS SCHIST	N70E	70SE															
148	W	GAR-BI-MS SCHIST	N58E	45SE															
149	W	S SCHIST -YELLOW-SULFUR	N40E	75SE			49	N60E	N60E	20SE	120-050					N20E	32NW	N45W	20SW
150	W	-MS SCHIST WITH MGW & (	N10E	31SE												N71W	74SW		
151	W	GAR-BI-MS SCHIST	N4E	79NW															
152	W	GAR-BI-MS SCHIST	N31E	61SE												N55W	69SW		
153	W	GAR-BI-MS SCHIST	N42E	64SE															
154	W	GAR-BI-MS SCHIST	N80E	73NW															
155	W	GAR-BI-MS SCHIST	N80E	74NW												N48W	62NE		
156	W	GAR-BI-MS SCHIST	N75E	54NW															
157	W	MIG. AM	N81E	28SE												N60W	58SW		
158	W	SIL-GAR-BI SCHIST	N52W	80NE	21	N34W										N50E	76SE		
159	W	MGW GAR-BI SCHIST	N45W	65SW												N15E	76NW		
160	W	GAR-MS-BI SCHIST	N39W	49NE															
161	W	MS-GAR-BI SCHIST	N17E	30SE												N49W	85SW		
162	W	MGW & MGW-SCHIST IN FI	N70E	64NW															
163	W	SAP BI-MS SCHIST	N31E	54NW															
164	W	SAP BI-MS SCHIST	N80W	18NE															
165	W	BI-MS SCHIST &MIG MGW	N80W	60SW															
166	W	MIG MGW	N79W	73SW												N73E	80NW	N50E	77SE
167	W	FG SCHISTOSE MGW	N61E	60NW															
168	W	MS-H SCHIST	N79E	24SE															
169	W	MIG MGW & BI-MS SCHIST	N80E	62NW															
170	W	MGW &MS-BI SCHIST	N78E	25SE															
171	W	MIG MS-BI SCHIST	N55E	65NW															
172	W	RY MIG MGW &MS-BI SCH	N83W	63NE															
173	W	SIL-QTZ-GAR-BI-MS SCHIST	N63W	70NE															
174	W	MGW & MINOR MS-BI SCH	N86W	78NE															
175	W	MS-BI SCHIST	N54E	30NW															
176	W	GAR-BI-SIL SCHIST	N86W	32NE												N75W	60SW		
177	W	MS -BI SCHIST	N80E	52NW												N45W	77NE	N85E	62SE
178	W	MIG BI-GNEISS	N75E	45SE															
179	W	LYRD MIG BI-PLAG GN	N38E	55SE															
180	W	LYRD MIG BI-PLAG GN	N76W	49SW															
181	W	LYRD MIG BI-PLAG GN	N48E	44SE	38	N78E													
182	W	LYRD MIG BI-PLAG GN	N50E	71SE			10	N80E	N80E	25NW	0-20					N40E	85NW	N80W	72NE
183	W	LYRD MIG BI-PLAG GN & AM	N18E	30SE															
184	W	G AM & LYRD MIG BI-PLAG	N55W	42NE			32	S55E	N50W	72NE	0-90					N45E	69NW		
185	W	LYRD MIG BI-PLAG GN	N80W	58NE															
186	W	) MIG BI-PLAG GN & LENS (	N12E	92SE															
187	W	LYRD MIG BI-PLAG GN	N41E	40SE			12	N78E	N78E	31NW	80-110					N5E	64SE		
188	W	MIG BI-PLAG GN	N82E	89SE															
189	W	LYRD MIG BI-PLAG GN	N27E	32SE												N39E	68SE		
190	W	LYRD MIG BI-PLAG GN	N35E	38NW															
191	W	FOLD IN LYRD MIG BI-PLAG GN					17	S41W	N41E	72SE	100-90								
192	W	LYRD MIG GAR-BI-PLAG GN	N25E	65SE												N40W	66SW	N52E	22SE
193	W	MIG BI-GN & MGW	N5W	51NE												N44E	48NW		
194	W	SAP-LYRD MIG BI-PLAG GN	N65E	41NW															
195	W	LYRD MIG BI-PLAG GN	N64E	36NW												N30E	86SE		
196	W	SAP MIG. BI GN	N70W	76NE															
197	W	MEG-MEG BI-PLAG GN	N64W	35NE												N58E	83SE		
198	W	INEQ BI-PLAG GN	N20W	60SW												N64E	74SE		
199	W	LYRD MIG BI-PLAG GN	N70E	80SE															
200	W	LYRD MIG BI-PLAG GN	N49E	76SE															
201	W	LYRD MIG BI-PLAG GN	N68E	74SE															
202	W	LYRD MIG BI-PLAG GN	N50E	81SE															
203	W	GAR -BI-MS SCHIST	N49E	60NW															
204	W	GAR-MS-BI SCHIST	N66E	55NW												N54W	90		
205	W	SIL-GAR-BI-MS-QTZ SCHIST	N65E	50SE												N30W	88SW		
206	W	SIL-GAR-MS-BI SCHIST	N83E	21SE												N80E	21SES	N15E	77NW
207	W	GAR-BI-MS-SIL SCHIST	N68E	88NW												N15E	64SE	N52W	82NE
208	W	MG MS-BI GTD	N68E	88NW												N15E	69SE	N52W	82NW
209	W	MS-QTZ SCHIST	N10E	70SE												N65E	74SE		
210	W	FG MGW	N65E	74SE												N38W	69NE		
211	W	BI-GAR-SIL-MS SCHIST	N64E	72NW												N23W	80SW		
212	W	-QTZ SCHIST TO META SIL	N75E	83NW															
213	W	MGW SCHIST	N54E	22SE															
214	W	MIG BI-PLAG GN	N38E	78SE															
215	W	MIG LYRD. BI-PLAG GN	N60E	62NW												N28W	81NE		
216	W	LYRD MIG. BI-PLAG GN	N64E	70NW															
217	W	LYRD MIG. BI-PLAG GN	N22E	73NW															
218	W	LYRD MIG. BI-PLAG GN	N20E	37NW			21	N24W	N24W	38SW	70								
219	W	LYRD MIG. BI-PLAG GN	N60E	72SE															
220	W	LYRD MIG. BI-PLAG GN	N68E	39NW															
221	W	LYRD MIG. BI-PLAG GN	N72E	63NW															
222	W	YRD WITH MINOR GAR-BI-(	N68E	57NW												N77W	60SW		
223	W	SIL-GAR-BI SCHIST & MGW	N69E	70NW												N57W	87SW		
224	W	MGW	N58E	79NW															
225	W	GAR-BI SCHIST & MGW	N31E	62NW												N46W	85NE		
226	W	MGW	N64E	80NW												N28W	84NE	N33E	34SE
227	W	RD MIG BI-PLAG GN TO A M	N69E	40NW			22	N55W	N55W	48SW	0-20								
228	W	IG BI-PLAG GN & MGW BI-I	N40E	44NW												N36W	84NE		

			Foliation		Lineation		Fold Axis		Axial Surface		IL	Fold	Fold	Crenulation Axis		Joint		Joint	
Station	Quad	Lithology	Strike	Dip	Plunge	Trend	Plunge	Trend	Strike	Dip	Angle	Genr.	Verg.	Plunge	Trend	Strike	Dip	Strike	Dip
229	W	LYRD MIG BI-PLAG GN	N66E	69NW															
230	W	THIN LYRD MGW	N61E	67NW															
231	W	THIN LYRD MGW - MS -QTZ	N50E	71NW															
232	W	MS-SCHIST & MS-GG	N60E	60NW															
233	W	ULFIDE & SIL-GAR-BI SCHI	N50E	54NW												N88E	60NW	N54W	79NE
234	W	AG-FELD GN/MGW WITH IN	N52E	57NW												N58W	72SW		
235	W	HINLY LYRD MS-QTZ-SCHI	N58E	85SE															
236	W	MGW	N25E	65SE															
237	W	LYRD MIG BI-PLAG GN	N60E	79SE															
238	W	LYRD MIG BI-PLAG GN	N54E	53SE															
239	W	LYRD MIG BI-PLAG GN	N44W	53NE															
240	W	AP LYRD MGW / BI-PLAG G	N50E	73NW															
241	W	MGW	N10W	71NE												N79W	55SW		
242	W	MGW	N65W	50NW															
243	W	GAR-MS SCHIST	N28E	38SE															
244	W	LYRD MIG. BI-PLAG GN	N48W	47NE															
245	W	LYRD MIG BI-PLAG GN	N25W	47NE															
246	W	IIG BI-PLAG GN & INEQ BI-P	N20W	49NE												N37W	87SW		
247	W	LYRD MIG BI-PLAG GN	N20E	70SE															
248	W	BI-PLAG GN	N20W	85NE												N2E	62NW		
249	W	BI-PLAG GN	N12E	85SE															
250	W	BI-PLAG GN	N10E	44SE															
251	W	R-BI-MS SCHIST WITH 30%	N48W	57NE												N82E	69SE		
252	W	MGW INTRLD GA-BI-MS SC	N74W	68NE			20	N64E	N69E	65NW	0					N25W	56SW	N75E	38SE
253	W	MGW	N32W	68NE												N62E	88SE	N88W	83NE
254	W	MGW	N81W	49SW			10	S58E	N58W	10NE	120								
255	W	GAR-BI-MS SCHIST	N88E	58SE															
256	W	R-BI-MS SCHIST WITH CG	N69W	82NE															
257	W	GAR-BII-MS SCHIST	N72W	68NE															
258	W	MGW	N62W	44NE															
259	W	GAR-BI-MS SCHIST	N88E	60SW															
260	W	I-QTZ SCHIST TO THINLY L	N56W	60SW															
261	W	MGW & GAR-BI-MS SCHIST	N84W	78SW															
262	W	MGW	N85W	35SW															
263	W	GW & MINOR GAR-BI SCHI	N79W	69SW															
264	W	MIG MGW	N88W	71NE															
265	W	GAR-BI-MS SCHIST	N88E	84NW															
266	W	GAR-BI-MS SCHIST	N60E	65NW			14	S50W	N45E	66NW	0-10					N65E	80SE		
267	W	MGW	N23W	40SW															
268	W	GW GAR-P-SIL-MS-BI SCHI	N71E	82SE	23	N83E										N24W	72NE		
269	W	MGW	N82W	82SW															
270	W	MGW	N81E	65NW															
271	W	MGW	N88W	69NE															
272	W	MGW	N88E	56SE															
273	W	LYRD MIG BI-PLAG GN	N81E	85NW												N40W	76NE		
274	W	LYRD MIG BI-GN	N70E	74NW															
275	W	LYRD MIG BI-PLAG GN	N64E	75NW															
276	W	LYRD MIG BI-PLAG GN	N72W	68NE															
277	W	LYRD MIG BI-PLAG GN	N75W	72NE															
278	W	LYRD MIG BI-PLAG GN	N88W	72SW															
279	W	LYRD MIG BI-PLAG GN	N86W	73NE															
280	W	OVERTURNED OPEN FOLD	N68W	52NE			30	N80E	N80E	35SE	120-100					N14W	44SW		
281	W	LYRD MIG BI-PLAG GN	N85E	72SE															
282	W	LYRD MIG BI-PLAG GN	N80E	68NW															
283	W	LYRD MIG BI-PLAG GN	N80W	75NE			35	N85E	N88E	17SE	120								
284	W	LYRD MIG BI-PLAG GN	N65W	66NE												N56E	78SE		
285	W	LYRD MIG BI-PLAG GN	N82E	54NW															
286	W	GAR-BI-MS-SIL SCHIST	N71E	58NW															
287	W	GW & SOME GAR-TO-M SCH	N82W	40NE															
288	W	LYRD MIG BI-PLAG GN	N76W	81NE															
289	W	LYRD MIG BI-PLAG GN	N80E	62NW			19	N79E	N74E	29SE	130					N78E	49NW	N38E	26SE
290	W	LYRD MIG BI-PLAG GN	N75W	52NE															
291	W	LYRD MIG BI-PLAG GN	N65W	58NE															
292	W	LYRD MIG BI-PLAG GN	N82E	62NW															
293	W	LYRD MIG BI-PLAG GN	N70W	65NE															
294	W	LYRD MIG BI-PLAG GN	N71E	78NE															
295	W	LYRD MIG BI-PLAG GN	N85W	82NE															
296	W	LYRD MIG BI-PLAG GN	N62W	58NE															
297	W	LYRD MIG BI-PLAG GN	N56W	69NE															
298	W	LYRD MIG BI-PLAG GN	N86W	93NE			23	S75E	N75W	50NE	0								
299	W	LYRD MIG BI-PLAG GN	N89E	68NW															
300	W	LYRD MIG BI-PLAG GN	N60W	70NE															
301	W	MGW & GAR-BI-SIL SCHIST	N68E	48NW															
302	W	LYRD MIG BI-PLAG GN	N86E	88SE															
303	W	LYRD MIG BI-PLAG GN	N85E	62NW												N0E	82NW		
304	W	MGW	N72E	60NW															
305	W	GAR-BI-MS SCHIST & MGW	N80E	86SE															
306	W	SIL-MS-BI SCHIST	N51W	40NW															
307	W	MIG MS SCHIST	N69W	71NE															
308	W	SAP LYRD MIG BI-PLAG GN	N10E	51SE															
309	W	LYRD MIG BI-PLAG GN	N85W	78NE															
310	W	MGW -LAYERING	N81E	67NW												N15E	59NW	N40W	88SW
311	W	GAR-BI-MS SCHIST	N79W	44NE															
312	W	GAR-BI -MS-SIL SCHIST	N55E	72NW												N70W	88SW		
313	W	MS-GAR-BI-SIL SCHIST	N57E	23SE															
314	W	GAR-BI-MS-SIL SCHIST	N73E	69SE															
315	W	MGW	N18E	60NW															
316	W	W INTERLAYERD WITH SCI	N60E	50NW												N38E	75SE		
317	W	F.G. MS-QTZ SCHIST	N5E	82NW															
318	W	GAR-BI-MS-SIL SCHIST	N59E	92NW			25	N90E	N40E	32SE	120								
319	W	GAR-BI -SIL SCHIST	N50E	84SE												N46W	W88SW		
320	W	GAR-BI-MS SCHIST	N41E	50NW															
321	W	GAR-BI-SIL SCHIST	N78E	79NW															
322	W	MGW & GAR-BI-SIL SCHIST	N50E	69NW												N42W	71SW	N80E	50SE
323	W	MIG GAR-BI-MS-SIL SCHIST	N60E	72NW												N31W	85SW		
324	W	GAR-BI-MS-SIL SCHIST	N42E	68NW															
325	W	MGW WITH MM SCHIST	N30E	75NW												N59W	77SW		
326	W	W MINOR SCHIST INTERLAY	N42E	70NW	29	S51W										N53W	88SW		
327	W	BI-SIL SCHIST &MGW	N45E	76NW															
328	W	GAR-BI-SIL SCHIST	N43E	64NW	11	N20E													
329	W	MGW TO GAR-BI-SIL SCHIS	N29E	83NW												N30W	60NE	N72W	71SW
330	W	GAR-MS-SIL SCHIST	N48E	39SE															
331	W	MS-BI SCHIST	N45E	76NW															
332	W	MS-BI-SIL SCHIST	N72E	61SE															
333	W	D, BI-MS-SIL SCHIST CUT B	N55E	76NW												N31E	25SE	N65E	72NW
334	W	MGW	N72W	49SW															
335	W	GAR-MS-BI-SIL SCHIST	N44E	75NW												N72W	76NE		
336	W	GAR-BI-SIL SCHIST	N78E	79NW															
337	W	MGW & GAR-BI-SIL SCHIST	N66E	45NW												N54W	77SW		
338	W	GAR-BI-SIL SCHIST	N44E	87NW												N52W	70SW		
339	W	GAR-BI-SIL SCHIST	N45E	66NW	55	N38W													
340	W	MGW	N78E	69NW												N10E	79NW		
341	W	GAR-BI-MS-SIL SCHIST	N42E	68NW												N74W	80NE		
342	W	MGW TO GAR-BI-SIL SCHIS	N68E	52NW												N48E	39SE	N88W	57SW

			Foliation		Lineation		Fold Axis		Axial Surface		IL	Fold	Fold	Crenulation Axis		Joint		Joint	
Station	Quad	Lithology	Strike	Dip	Plunge	Trend	Plunge	Trend	Strike	Dip	Angle	Genr.	Verg.	Plunge	Trend	Strike	Dip	Strike	Dip
343	W	GAR-BI SCHIST	N80E	78SE												N54W	66SW		
344	W	LYRD MIG BI-PLAG GN	N28E	75NW															
345	W	LYRD MIG BI-PLAG GN	N52E	72NW												N55W	85SW		
346	W	MGW	N71E	59NW															
347	W	GW WITH TIGHT TO OPEN FOLD					66	N84E	N84E	40SE	60								
348	W	LYRD MIG BI-PLAG GN	N31E	36SE															
349	W	LYRD MIG BI-PLAG GN	N16E	66SE															
350	W	LYRD MIG BI-PLAG GN	N19E	61SE															
351	W	LYRD MIG BI-PLAG GN	N61E	90NW															
352	W	LYRD MIG BI-PLAG GN	N78W	71NE												N21E	60SE		
353	W	LYRD MIG BI-PLAG GN	N55E	66NW															
354	W	LYRD MIG BI-PLAG GN	N78W	76NE															
355	W	LYRD MIG BI-PLAG GN					42	N30E	N30E	64SE	90								
356	W	LYRD MIG BI-PLAG GN	N41E	84SE															
357	W	LYRD MIG BI-PLAG GN	N65E	72SW															
358	W	LYRD MIG BI-PLAG GN	N78W	64SW															
359	W	MIG AM	N60W	62SW															
360	W	LYRD MIG BI-PLAG GN	N72E	73NW												N2W	76NE		
361	W	G BI-PLAG GN TO A MEG BI	N65E	62NW												N19E	78NW		
362	W	RD MIG BI-PLAG GN WITH	N85W	75NE															
363	W	LYRD MIG BI-PLAG GN	N62E	70SW															
364	W	MIG AM & MIG BI-PLAG GN	N50W	67NE															
365	W	LYRD MIG BI-PLAG GN	N88E	62SE															
366	W	RD MIG GAR-AM & BI-PLAG	N84E	65NW												N0E	79SE		
367	W	LYRD MIG BI-PLAG GN	N84E	23SE			15	S51E	N51W	66NE	110								
368	W	LYRD MIG BI-PLAG GN	N55E	52SE			25	N55E	N55E	22SE	0	F2				N56W	85SW	N30E	36SE
369	W	LYRD MIG BI-PLAG GN	N56E	58SE															
370	W	LYRD MIG BI-PLAG GN	N80W	66SW															
371	W	LYRD MIG BI-PLAG GN	N85E	98SE															
372	W	LYRD MIG BI-PLAG GN	N88W	78SW												N61E	71NW	N86W	81NE
373	W	LYRD MIG BI-PLAG GN	N84W	62NE												N5W	78NE		
374	W	LYRD MIG BI-PLAG GN	N63E	62NW															
375	W	M & LYRD MIG GAR- BI-PL	N88E	88SE															
376	W	-BEARING MGW TO META	N31E	55SE												N63W	79NE	N59E	16SE
377	W	GAR-BI-QTZ MGW-LYRD	N14E	77SE												N85W	67NE	N62W	88SW
378	W	GAR-MS-BI-SIL SCHIST	N48W	41NE												N36W	86SW		
379	W	GAR-MS-BI-SIL SCHIST	N36E	81SE												N54W	72NE		
380	W	MGW & MS-GAR-BI SCHIST	N32E	65SE												N28W	60SW	N24E	15SE
381	W	GAR-BI-SIL SCHIST & MGW	N22E	62SE															
382	W	GAR-MS-SCHIST	N28E	57SE															
383	W	GAR-BI-MS-SIL SCHIST	N21E	65SE			56	N33E	N31E	71SE	50-60								
384	W	GAR-MS-SIL SCHIST	N24E	48SE															
385	W	GAR-SIL-MS SCHIST	N35E	71SE															
386	W	GAR-MS-SIL SCHIST	N50E	69NW	75	N51W										N41W	64SW	N42W	70NE
387	W	GAR-MS-SIL SCHIST	N39E	67NW															
388	W	GAR-MS-SIL SCHIST					44	N40E	N40E	84SE	10-20								
389	W	MGW & PART MS-GAR SCHIS	N74W	31NE															
390	W	QTZ WITH MGW LAYERING	N14W	33NE												N71E	78NW		
391	W	-BI-MS SCHIST WITH PEG P	N46W	27NE															
392	W	GAR-BI-SIL SCHIST	N24W	27NE												N75W	81SW	N30E	56NW
393	W	GAR-BI-SIL SCHIST	N61W	55NE															
394	W	GAR-BI-MS-SIL SCHIST	N14W	17NE															
395	W	GAR-MS-BI SCHIST	N81E	75NW															
396	W	GAR-BI-MS-SIL SCHIST	N68E	43NW												N20W	78NE		
397	W	SULFIDIC-GAR-BI-AM MGW	N45E	62NW	14	S50W													
398	W	GAR-BI-MS-SIL SCHIST	N54E	68NW															
399	W	MGW	N86W	69NE												N12W	72SW		
400	W	MGW	N80E	75SW												N16E	82NW		
401	W	FG MGW	N11E	68NW															
402	W	GAR-BI-MS-SIL SCHIST	N45E	32NW															
403	W	GAR-MS SCHIST	N47W	30NW												N45W	83SW		
404	W	MGW TO METACGL	N41E	72SE			39	N41E	N41E	72SE	0								
405	W	CG MGW TO A METACGL	N14E	44SE												N3W	6NE	N66E	75SE
406	W	LD MGW-GAR-MS-BI-SIL SC	N82E	61NW			32	S42W	N58E	74NW	70					N81W	48SW		
407	W	G MGW WITH CG MS FLAK	N52E	85NW												N55W	83NE		
408	W	GAR-SIL-MS SCHIST	N87E	50NW												N46W	24SW		
409	W	AR-MS SCHIST & GAR-QTZ	N81W	53NE															
410	W	MS-BI SCHIST	N74E	52NW															
411	W	GAR-MS-QTZ SCHIST	N84E	38SE															
412	W	BI SCHIST & MGW DUT BY	N27W	62SW															
413	W	GAR-BI-MS SCHIST	N45E	64SE															
414	W	RK GREY MGW W MS FLAK	N49E	87NW			14	N46E	N46E	44SE	80-90								
415	W	GAR-MS-SIL SCHIST	N58E	78NW															
416	W	RK GREY MGW W MS FLAK	N39E	85NW			33	N24E	N24E	68SE	100					N71W	49SW		
417	W	BI-MS-QTZ-FELD LEUCOSO	N31E	82NW															
418	W	MGW & MS-GAR-BI SCHIST	N47E	58NW															
419	W	MIG MGW	N36E	76NW															
420	W	MGW	N65E	41NW															
421	W	MGW & PEG DIKES	N31E	76NW			20	N18E	N18E	70SE	50					N57W	54SW		
422	W	MIG MGW	N18E	78SE															
423	W	MGW	N38E	48NW															
424	W	MGW	N24E	40SE												N70W	81NE		
425	W	MIG MGW	N74E	77NW												N66W	74SW		
426	W	GAR-BI-MS SCHIST	N12E	60SE															
427	W	GAR-MS SCHIST	N10E	46SE															
428	W	MS SCHIST	N45E	51NW															
429	W	MS SCHIST	N54W	48NE			61	N20E	N20E	66SE	20								
430	W	MGW	N60E	77SE															
431	W	GAR-BI-MS SCHIST	N44E	71SE												N57W	58NW		
432	W	MGW	N3E	77SE															
433	W	GAR-BI-MS SCHIST	N32E	75SE															
434	W	R-BI-MS SCHIST W/ MS FLA	N21E	72SE												N70W	63SW	N87W	24SW
435	W	MGW	N41E	85SE															
436	W	GAR-BI-MS SCHIST	N29E	70SE												N55W	88NE		
437	W	MGW & MINOR GAR-BI-MS S	N42E	88NW															
438	W	GAR-BI-MS SCHIST	N31E	75NW															
439	W	GAR-BI-MS SCHIST	N58E	60NW															
440	W	GAR-BI-MS SCHIST	N16E	61NW															
441	W	GAR-BI-MS SCHIST	N21E	62SE															
442	W	GAR-BI-MS SCHIST	N58E	84NW															
443	W	TRLD MGW-GAR-BI-MS SCH	N50E	75NW															
444	W	MIG MGW	N60E	59NW			44	S60W	N61E	59NW	10					N52W	85SW		
445	W	GW & INTRLD GAR-MS- SCH	N16E	81SE												N90E	67S		
446	W	MIG MGW	N31E	72SE												N70W	84SW		
447	W	GAR-BI-MS SCHIST	N31E	64NW															
448	W	THINLY LYRD MGW	N27E	65NW															
449	W	MGW & MINOR SIL LYRS	N42E	71SE			21	N39E	N39E	70SE	20					N55W	75NE		
450	W	MIG MGW	N35E	79SE												N32W	56SW	N50E	90SE
451	W	MIG MGW	N32E	63SE												N51W	90SW		
452	W	MIG. BI-GNEISS	N80W	39SW												N15E	17SE		
453	W	LYRD BI GN	N33W	52SW															
454	W	MIG BI GN	N85W	85NE															
455	W	LYRD MIG BI-PLAG GN	N22E	27SE												N49E	86SE		
456	W	T FOLD IN LYRD MIG BI-PLA	N82W	42NE			13	N80W	N80W	17SW	30-40								

			Foliation		Lineation		Fold Axis		Axial Surface		IL	Fold	Fold	Crenulation Axis		Joint		Joint	
Station	Quad	Lithology	Strike	Dip	Plunge	Trend	Plunge	Trend	Strike	Dip	Angle	Genr.	Verg.	Plunge	Trend	Strike	Dip	Strike	Dip
457	W	LYRD MIG BI-PLAG GN	N10W	55NE			21	S42W	N42E	41NW	110								
458	W	GAR-BI-MS SCHIST	N25E	72NW												N61W	54SW		
459	W	GAR-BI-MS SCHIST	N31E	80NW															
460	W	MG QTZITE	N29W	63NE												N55E	72SE		
461	W	LIGHTLY MIG GAR-MS SCHI	N60E	59NW												N80W	44SW		
462	W	GAR-BI-MS SCHIST	N36E	75NW			27	N11W	N11W	54NE	80								
463	W	MGW - LYRD	N24E	66SE												N64W	89NE		
464	W	MIG MGW	N25E	71SE												N59W	81SW		
465	W	MGW-MIG	N40E	72SE															
466	W	R-BI-MS SCHIST W MS FLA	N10E	70NW															
467	W	GAR-BI-MS SCHIST	N50E	80NW															
468	W	MIG MGW	N21E	78SE												N55W	84SW		
469	W	MGW W MINOR CALC-SI	N29E	62SE												N79W	76SW		
470	W	MGW	N65E	62SE															
471	W	GAR-BI-MS SCHIST	N44E	74SE												N20W	59SW		
472	W	GAR-BI-MS SCHIST	N62E	75SE															
473	W	MIG MGW	N32E	65NW															
474	W	MGW	N31E	87SW															
475	W	MGW	N25E	41NW															
476	W	BI-MS SCHIST W CG MS FL	N15E	81NW															
477	W	GAR-BI-MS SCHIST	N22E	71SE															
478	W																		
479	W	MGW	N70E	61NW															
480	W	MGW	N76E	86NW															
481	W	GAR-BI-MS SCHIST	N70W	55NE															
482	W	FG MS SCHIST	N20E	55NW												N30E	90		
483	W	MGW	N50E	64NW															
484	W	MIG MGW	N25E	76SE			14	S26W	N26E	75NW	60					N90E	85SE	N58W	15SW
485	W	MIG MGW	N74E	74SE															
486	W	CG BI-GG	N25E	86NW															
487	W	MIG MGW	N70E	46SE															
488	W	MGW	N22E	88SE												N56W	83NE		
489	W	MGW	N25E	61NW															
490	W	GA-MS-BI-SIL SCHIST	N48E	84NW															
491	W	MIG MGW	N79E	60NW			42	N53E	N55E	90SE	70								
492	W	GAR-BI-MS SCHIST	N21W	44NW															
493	W	/ INTRLS OF GAR-BI-MS-SIL	N39E	71SE			53	N20E	N20E	90	120-80								
494	W	MIG MGW	N31E	70SE	32	N40E										N64E	75SE	N72W	10NE
495	W	MIG MGW	N20E	66SE			32	N31E	N31E	90SE									
496	W	GAR-BI-MS SCHIST	N78E	58NW															
497	W	GAR-BI-MS SCHIST	N65E	50NW												N45W	75SW	N28W	20SW
498	W	MS SCHIST	N58E	57SE															
499	W	MS SCHIST	N59E	50SE															
500	W	MS SCHIST	N51E	79NW												N20W	79SW		
501	W	GAR-BI-MS-SIL SCHIST	N48E	71NW															
502	W	GAR-BI-MS-SIL SCHIST	N68W	85NE															
503	W	GAR-BI-MS-SIL SCHIST	N69E	70NW															
504	W	MS-CHL SCHIST &GAR-BI-SI	N14W	62SW															
505	W	MIG MGW	N40E	40SE												N57W	56SW		
506	W	MIG MGW	N21E	62SE															
507	W	GAR-BI-MS-SIL SCHIST	N75W	53NE															
508	W	MGW	N5E	50SE			50	N39E	N5E	50SE	0								
509	W	MS-GAR-BI-SIL SCHIST	N50E	81SE															
510	W	MS-SIL-GAR SCHIST	N50E	51SE															
511	W	IS-GAR-BI-SIL SCHIST & MG	N26E	47SE															
512	W	GAR-BI-MS SCHIST	N51E	45SE															
513	W	MIG GAR-BI-MS-SIL SCHIST	N60E	74NW															
514	W	MGW	N41E	76SE															
515	W	MIG MS-BI-SIL SCHIST	N73E	77SE															
516	W	FG MS SCHIST	N78E	52NW			25	N61E	N61E	61SE	120								
517	W	MGW & MINOR SCHIST	N16E	45NW												N58W	36SW	N57E	70SE
518	W	SAP MIG MS SIL GAR SCHIS	N61E	64SE												N2W	80NE		
519	W	GAR-BI-MS SCHIST	N78E	57NW															
520	W	MIG GAR-BI-MS SCHIST	N67W	48NE												N30E	45SE		
521	W	MIG GAR-BI-MS SCHIST & PE	N85E	48NW															
522	W	MIG MS SCHIST	N72W	50NW															
523	W	SAP-MIG BI-PLAG GN	N62E	42NW															
524	W	SILICEOUS BRECCIA			35	S44E													
525	W	MIG BI-PLAG GN	N71W	42NE															
526	W	MIG H-BI-PLAG GN	N70W	51SW															
527	W	SILICEOUS BRECCIA	N71E	74SE															
528	W	MIG BI-PLAG GN	N81E	36SE															
529	W	MIG BI-PLAG GN	N65E	40SE															
530	W	MIG BI-PLAG GN	N40E	42SE															
531	W	MIG BI-PLAG GN	N32W	82SW			38	N52W	N52W	86NE	0-10					N10E	81NW		
532	W	LYRD MEG BI-PLAG GN	N41E	20SE												N48W	81NE	N74W	23SW
533	W	LYRD MEG BI-PLAG GN	N72E	43SE			22	N85E	N85E	9SE	10-20					N32W	88NE	N89W	79NW
534	W	LYRD MEG BI-PLAG GN	N63W	71NE															
535	W	LYRD MEG BI-PLAG GN	N71W	67NE	11	S82E	10	N70E	N70E	55NW						N88W	26SW		
536	W	LYRD MEG BI-PLAG GN	N65E	64SE															
537	W	LYRD MEG BI-PLAG GN	N85W	46SW															
538	W	LYRD MEG BI-PLAG GN	N82E	88NW			5	S85E	N85E	55SE	70								
539	W	MIG BI GN	N81W	85NE															
540	W	MIG BI GN	N86E	63SE															
541	W	GAR-BI-PLAG GN	N65W	62NE															
542	W	GAR-BI-SIL SCHIST	N82W	74SW															
543	W	GAR-AM	N88E	90SE															
544	W	GAR-AM MIG	N88E	90SE															
545	W	UCO MS-GAR-BI-QTZ FELD	N68E	48NW												N38E	72SE	N17W	75SW
546	W	MIG BI-PLAG GN			76	S89E													
547	W	MS SCHIST	N12E	82SE															
548	W	MIG BI-PLAG GN	N89E	65NW															
549	W	MIG GAR-BI GG	N1W	43NE															
550	W	MI BI-PLAG GN	N46E	62SE															
551	W	NEISS SAP, GAR-MS-BI-QTZ	N40W	17NE															
552	W	NEISS SAP, GAR-MS-BI-QTZ	N3E	29SE															
553	W	MIG MGW-LUECO	N82W	57NE															
554	W	MIG MGW	N65W	37NE															
555	W	MIG BI GN TO MGW	N65E	58SE												N61W	79SW		
556	W	BI-PLAG GN TO MEG BI-PLA	N72E	35SE															
557	W	MIG BI-PLAG GN	N66E	68SE															
558	W	INEQ BI GN/MGW	N11W	21NE			1	N81W	N81W	15SW	70-80								
559	W	MIG-MEG BI-PLAG GN	N25W	22NE												N8W	25SW		
560	W	LEUCO- MIG BI GG	N10W	12NE												N80E	86SE		
561	W	BI-PLAG GN TO ALMOST SC	N15E	81SE												N71W	90SW		
562	W	LYRD MIG BI-PLAG GN	N30E	82SE			13	N30E	N30E	72NW	0-10								
563	W	LYRD MIG BI-PLAG-H GN	N28E	80SE			13	N30E	N30E	72	0-10								
564	W	MIG AM	N90E	66SE	21	S79E										N5E	58SE		
565	W	INTRLD MIG BI-PLAG GN	N85E	70NW															
566	W	MIG BI-PLAG GN	N82W	64SW															
567	W	MIG BI-PLAG GN	N64E	82NW			74	N31E	N31E	81SE	0								
568	W	YRD MIG H-GAR-BI-PLAG G	N65E	46NW			6	S62W	N62E	32NW	100					N63E	79SE	N84E	85NW
569	W	MIG BI-PLAG GN	N50E	21SE												N85W	77SW		
570	W	MIG BI-PLAG GN	N50E	21SE			11	N85E	N88E	35SE	100-30					N10W	80SW		

			Foliation		Lineation		Fold Axis		Axial Surface		IL	Fold	Fold	Crenulation Axis		Joint		Joint	
Station	Quad	Lithology	Strike	Dip	Plunge	Trend	Plunge	Trend	Strike	Dip	Angle	Genr.	Verg.	Plunge	Trend	Strike	Dip	Strike	Dip
571	W	MIG BI-PLAG GN	N76E	72SE															
572	W	MIG BI-PLAG GN	N73E	84SE															
573	W	LYRD MIG BI-PLAG GN	N25E	45SE												N78W	86SW		
574	W	MIG BI-PLG GN	N70E	47SE															
575	W	MS QTZITE	N65E	60SE															
576	W	MIG BI-PLAG GN	N78E	26SE															
577	W	MIG BI-PLAG GN	N22E	14SE												N34W	85NE		
578	W	MIG BI-PLAG GN	N10E	15SE	11	S78E										N50E	85NW		
579	W	MIG BI-PLAG GN	N1E	21SE												N54W	75SW		
580	W	INTRLD GAR-BI-MS SCHIST	N13E	30SE												N50W	90SW		
581	W	THINLY LYRD MGW	N31E	58SE															
582	W	THINLY LYRD MGW	N25W	32NE												N18E	67NW	N47W	17SW
583	W	META CGL	N52E	23NW															
584	W	LYRD MIG BI GN	N88W	27NE															
585	W	MIG H GN	N52W	26NE															
586	W	MIG MGW	N31W	13NE			6	39E	N9W	35NE	10-70								
587	W	LYRD MIG BI-QTZ-PLAG GN	N32W	39NE															
588	W	MIG MGW	N81E	44SE															
589	W	MIG MGW	N68E	28SE												N47W	81NE		
590	W	MIG-BI GN	N70W	57NE															
591	W	SAP-MIG BI GN	N88E	76NW															
592	W	SAP-MIG-BI GN	N81E	61SE															
593	W	MIG BI GN	N64E	51SE			14	N76E	N76E	29SE	30								
594	W	LYRD MIG BI GN	N75W	65SW															
595	W	SAP AM	N60E	26SE															
596	W	MS SCHIST TO GAR SCHIST	N30W	40NE															
597	W	MIG MS SCHIST	N15E	32SE															
598	W	LYISH BR MG TO CG H BI-QT	N32W	68NE															
599	W	SAP MIG-BI GN & AM	N42E	78SE															
600	W	MIG BI-GTD	N88W	84NE															
601	W	SAP- MIG-BI GN	N84W	74SW															
602	W	ITLY MIG CG P GA-MS-BI S	N73E	34SE												N78W	85NE		
603	W	IDE STAINED GAR-MS-BI SC	N40E	51SE															
604	W	IDE STAINED GAR-MS-BI SC	N52E	16SE															
605	W	MS-GAR-BI SCHIST W CG M	N25E	70SE															
606	W	-BII-QTZ & INTRLD W GAR	N52E	30SE												N84E	78SE		
607	W	QTZ INTRLD W MS SCHIST	N88E	59SE															
608	W	TRLD MGW GAR-MS-BI SCH	N7E	15SE	15	N62E													
609	W	RLD GAR-BI-SIL SCHIST &	N88E	63SE															
610	W	HTLY MIG MS-GAR-SIL SCHIST														0E	90SE		
611	W	-SIL-GAR-BI-QTZ-FELD SCH	N78W	57SW												N54W	65NE		
612	W	MS-GAR-BI-SIL GN/ SCHIST	N70E	59SE															
613	W	O MG W INTRLS OF MS-GAR	N40E	79SE															
614	W	G MS?-SIL-GAR-BI GELD-GN	N81W	64SW															
615	W	MIG BI-PLAG GN	N67W	54NE															
616	W	LYRD MIG BI-PLAG GN	N41E	55SE			10	N82E	N82E	20NW	30-60								
617	W	LYRD MIG-BI-PLAG GN	N74E	75SE			22	N80E	N80E	30SE	30-50					N45E	72NW		
618	W	GAR-MS-BI SCHIST	N57E	43SE															
619	W	MIG BI-PLAG GN	N58E	31SE															
620	W	GAR-BI-QTZ-PLAG GN -MGW	N62E	1SE															
621	W	MIG CALC-SI -GAR-MS MGW	N70E	92SE															
622	W	W - FG TO MG GAR-BI-FELD	N68E	16SE															
623	W	MIG MGW	N66E	23SE	14	S27W													
624	W	OLIATED GG-MS-BI GG TO	N59E	78NW															
625	W	MIG BI GN	N85E	50SE															
626	W	FG TO MG BI-QTZ & MIG BI-PLAG GN																	
627	W	MYLO MIG BI GN	N65E	33SE															
628	W	MYLO BI GN	N27E	61SE	49	N75E													
629	W	MIG BI GM & BI GG	N33E	71NW															
630	W	AGMATITE W/ BI GN & BI GG	N56W	83NE															
631	W	MIG GAR-MS-FELD-QTZ GN	N37E	47SE	5	N40E										N52W	83SW		
632	W	INTRLD MIG MGW	N58E	68SE												N57W	86SW		
633	W	MIG QT-MS SCHIST	N45E	39SE															
634	W	MIG MS-BI-QTZ GN - MGW	N50E	15SE			7	N79W	N79W	15NE	70					N30W	85SW	N15W	47SW
635	W	INTRLD MIG MGW - MS-QTZ	N38W	26NE															
636	W	MIG MGW & QTZ	N30E	47SE												N51W	76SW		
637	W	LEUCO MIG FELSIC GN	N30W	42NE												N85E	75SW		
638	W	LEUCO MIG MYLO	N15W	40NE															
639	W	MIG MGW W MS & MIG -BI-I	N61E	44SE												N82W	88SW	N55E	84SE
640	W	MIG BI-PLAG GN	N53W	59NE															
641	W	LUECO MIG MGW	N65W	45NE															
642	W	MIG BI-PLAG GN	N59E	70SE															
643	W	MIG BI-PLAG GN & AM LYR	N69W	32SW															
644	W	I & MIG BI-PLAG GN - CALC	N85W	59SW												N45E	80NW		
645	W	DARK MIG BI-PLAG GN	N52E	35SE			20	N80E	N80E	60SE	0-70					N18E	22SE		
646	W	MIG BI-PLAG GN	N37E	46SE															
647	W	MIG BI-PLAG GN					26	N25W	N25W	43SW	30-90								
648	W	INTRLD MIG BI-PLAG GN	N82E	11NW															
649	W	MIG BI-PLAG GN	N40E	42SE												N75E	72NW		
650	W	MIG BI-PLAG GN	N18E	42SE			37	S10E	N67W	30SW	0-50								
651	W	SAP MIG BI-PLAG GN	N15W	62NE												N40W	52NE		
652	W	REFOLD IN MIG BI-PLAG GN	N78W	82NE			56	N55E	N55E	90SE	90-100								
653	W	MIG BI-PLAG GN	N77W	57NE															
654	W	MIG BI-PLAG GN	N61E	55SE															
655	W	MIG BI-PLG GN	N79W	83NE															
656	W	MIG BI-PLAG GN	N71E	68SE															
657	W	IIG MGW W GAR-BI-PLAG G	N48E	23SE															
658	W	MIG MGW	N20E	16SE			5	N55E	N20E	16SE	0					N10W	85SW		
659	W	MIG BI GN	N72E	84NW			60	S85E	N51E	66SE	30-40								
660	W	GAR-BI GN	N84E	76SE															
661	W	SAP MIG BI-PLAG GN	N58E	49SE															
662	W	MIG BI-PLAG GN & GAR AM	N72E	75NW															
663	W	- WEAKLY TO MOD FOLDE	N44W	50SW															
664	W	MIG MGW	N55W	55NE															
665	W	MIG MGW	N50W	76NE															
666	W	P MIG BI-PLAG GN & MIG A	N16E	79SE															
667	W	MIG BI-PLAG GN -SAP RED	N45E	81SE															
668	W	M - MIG BI-PLAG GN & GAR	N52E	64SE															
669	W	ED TIGHTLY FOLDED M-MI	N22W	27SW			14	S52W	N55E	34SE	70					N41E	54SE	N30W	84NE
670	W	LYRD MIG GAR-BI-PLAG GN	N45E	85SE												N37E	73NE	N8W	29SW
671	W	G AR-BI-PLAG GN & AM	N71W	62SW															
672	W	MIG BI-PLAG GN	N60W	67SW															
673	W	MIG BI-PLAG GN	N70W	48SW															
674	W	LOAT MIG CG GAR-AM TO GN																	
675	W	SAP MIG BI GN	N44E	80NW															
676	W	YLO MEGAC BI GN & GAR A	N33E	58SE												N72W	68SW		
677	W	MIG GAR-BI-PLAG GN	N21E	36SE	32	N34E													
678	W	LYRD MIG BII-PLAG GN	N61W	62SW															
679	W	LYRD MIG BI-PLAG GN	N19W	39SW															
680	W	NTRLD MIG BI-PLAG GN & A	N16W	56NE															
681	W	GN W/ RECLINED TO RECUMBENT FOLD					11	N4W	N1W	21SW	70					N67E	82SE		
682	W	MPLEX FOLD - MIG BI-PLAG GN					13	S38E	N33W	35SW	100					N54E	81SE	N32W	87SW
683	W	MIG BI-PLAG GN	N52W	76NE															
684	W	MIG BI-PLAG GN	N2W	41SW	11	N45E										N80E	79SE	N55W	61SW

			Foliation		Lineation		Fold Axis		Axial Surface		IL	Fold	Fold	Crenulation Axis		Joint		Joint	
Station	Quad	Lithology	Strike	Dip	Plunge	Trend	Plunge	Trend	Strike	Dip	Angle	Genr.	Verg.	Plunge	Trend	Strike	Dip	Strike	Dip
685	W	SAP MIG BI-PLAG GN	N57W	55SW															
686	W	MIG BI-PLAG GN	N28W	86SW															
687	W	MIG BI-PLAG GN	N69W	71SW															
688	W	MIG BI-PLAG GN & MIG AM	N47E	56NW															
689	W	MIG BI GN W/ AM BOUDINS	N71E	63SE															
690	W	MIG BI-PLAG GN	N85E	66NW															
691	W	MIG BI-PLAG GN	N58W	74NE															
692	W	MIG BI-PLAG GN	N18W	42NE															
693	W	MIG BI-PLAG GN W PEG	N56W	52NW															
694	W	G BI-PLAG GN W SOME CG	N71W	32NE															
695	W	MIG BI-PLAG GN	N25W	34NE			23	S69E	N66W	48NE	30					N76E	72SE		
696	W	IIG BI-PLAG GN & INTRLD A	N32E	46SE															
697	W	AM - SAP	N61W	66SW															
698	W	MIG BI GN	N10W	64NE															
699	W	SAP - AM	N55E	15SE															
700	W	AP - MIG BI GN W INTRLS A	N10W	64NE															
701	W	AM & MIG BI-PLAG GN INT	N52W	51NE															
702	W	AM & MINOR MIG BI-PLAG	N40E	62SE															
703	W	M & MGW - MS-QTZ-FELD G	N40E	50SE															
704	W	MS & MGW W BI GTD DIKE	N33E	48NW															
705	W	MIG BI GN	N60E	40SE															
706	W	BI GN /MGW	N59E	55SE															
707	W	MIG AM & BI GN /MGW	N72E	54NW															
708	W	BI GN/MGW W MINOR AM	N45W	70NE															
709	W	MIG AM - CG	N68E	80NW												N15W	87SW		
710	W	CG AM	N48E	65NW															
711	W	MS/ PEG/ FOLDED	N55E	54SE															
712	W	MIG BI GN	N82E	80SE															
713	W	GAR-BI-MS SCHIST	N79W	76SW															
714	W	GAR-BI-MS-SIL SCHIST	N86E	64SE															
715	W	MIG BI-PLAG GN	N82E	78SE															
716	W	LYRD MIG BI-PLAG GN	N82E	70SE												N15W	74SW		
717	W	MIG BI-PLAG GN	N52E	61SE															
718	W	LYRD MIG BI-PLAG GN	N65E	34SE			7	S86E	N77E	30SE	30					N18W	89SW		
719	W	LYRD MIG BI-PLAG GN	N85E	57NW															
720	W	GAR-BI-MS-SIL SCHIST	N89W	62SW															
721	W	GAR-BI-MS SCHIST TO MGW	N65E	68SE															
722	W	INEQ MGW	N82E	76SE															
723	W	MIG MGW	N75W	61SW															
724	W	MIG GAR-BI-MS-SIL SCHIST	N79E	65SE															
725	W	MIG GAR-BI-MS-SIL SCHIST	N70E	70SE															
726	W	MIG BI-PLAG GN	N65E	70SE															
727	W	MIG BI-PLAG GN	N61E	84SE															
728	W	MIG BII-PLAG GN	N82E	67NW															
729	W	MIG BI GN	N58E	86SE															
730	W	MGW W GAR-MS-BI	N70E	87SE															
731	W	GAR-BI-SIL SCHIST	N55E	85SE															
732	W	MIG BI GN	N55E	87SE															
733	W	GAR-BI-SIL SCHIST W CG M	N71E	72SE															
734	W	RLD MGW - GAR-BI-SIL SCI	N29W	75SW															
735	W	MS-GAR-BI-SIL SCHIST	N60W	32SW															
736	W	LD MGW - GAR-MS-BI-SIL SC	N80E	90SE	31	S78E													
737	W	GAR-BI -SIL SCHIST	N70E	65NW															
738	W	MGW	N72E	74SE															
739	W	MIG MGW	N75W	38NE												N78E	89SE		
740	W	MGW & GAR-MS-BI-SIL SCI	N71W	98NE															
741	W	FUR - GAR-BI-SIL SCHIST TO	N64W	32NE															
742	W	GAR-BI-MS-SIL SCHIST	N60W	72NE															
743	W	MGW	N52W	51NE															
744	W	GAR-BI-MS-SIL SCHIST	N25W	47NE															
745	W	MGW	N82E	54NW															
746	W	W & INTRLD GAR-BI-SIL SCI	N68W	34NE															
747	W	W & INTRLD GAR-BI-SIL SCI	N88E	50NW												N20E	64NW		
748	W	GAR-MS-BI-SIL SCHIST	N71E	49NW												N75E	82NW		
749	W	MGW	N79W	34NE															
750	W	MGW	N85W	58NE															
751	W	GAR-BI-MS-SIL SCHIST	N52W	40NE															
752	W	GAR-BI-MS-SIL SCHIST	N74E	22SE															
753	W	GAR-BI-SIL SCHIST W FELD	N80E	67NW	12	N80W													
754	W	GAR-SIL-MS SCHIST	N81E	60SE															
755	W	GAR-MS-SIL SCHIST	N80E	75SE															
756	W	QTZ-FELD-MS SCHIST	N31E	65NW															
757	W	-BI-MS SCHIST INTRLD W M	N2W	70SW															
758	W	GAR-BI-MS SCHIST & MGW	N30E	65SE															
759	W	AR-BI-MS-SIL SCHIST - MG	N45E	31SE												N24W	81SW		
760	W	W TO BLACK STAIN COTIC	N35E	60SE															
761	W	A APLETTE & GAR-QTZ GN	N40W	32NE															
762	W	MGW WMS - MS-QTZ-GELI	N70E	42SE															
763	W	GAR-QTZ GN / COTICLE	N70W	45SW															
764	W	MYLO GAR-BI-MS SCHIST	N42E	35SE															
765	W	MIG BI GN	N80E	81NW															
766	W	MYLO GAR-BI-MS P SCHIST	N22E	63SE															
767	W	MIG GAR-BI-PLAG GN	N76W	78NE												N12E	85NW	N64E	62SE
768	W	MIG BI-PLAG GN	N79E	44SE												N43E	83NW		
769	W	MIG BI-PLAG GN	N82E	69SE															
770	W	FLOAT - MIG BI-PLAG GN																	
771	W	MIG BI-PLAG GN	N72E	35SE												N12E	88SE		
772	W	MIG GAR-BI-PLAG GN	N77E	10SE			15	S81E	N71E	25S	0-10					N34W	78SW	N27E	64NW
773	W	MYLO MIG BI GN	N26E	30SE	26	N86E													
774	W	MIG BI-PLAG GN	N72E	25SE												N18W	37SE	N0W	79SW
775	W	MIG BI-PLAG GN	N54E	40SE												N29W	88NE		
776	W	MIG GAR-BI -PLAG GN	N89W	28SW															
777	W	MIG BI-PLAG GN	N88W	61SW															
778	W	MIG AM	N86E	81SE															
779	W	MIG BI-PLAG GN	N63E	16SE												N12E	85NW		
780	W	MIG BI-PLAG GN	N31E	56SE															
781	W	MIG BI-PLAG GN	N88W	71NE			6	S75E	N60W	50SW	0-10					N40E	85NW		
782	W	MIG BI-PLAG GN	N86W	59SW			5	S77E	N85E	43SE						N15W	86SW		
783	W	MIG BI GN W AM LENS	N36W	31NE															
784	W	MIG BI GN TO A MG MGW	N66W	73NE												N47E	72NW		
785	W	INEQ MIG BI GN	N81W	79NE															
786	W	MIG BI-PLAG GN	N52W	45NE															
787	W	MIG BI GN	N82E	82NW			15	S83E	N82E	84SE	30-85					N25E	28SE	N82W	40SW
788	W	MIG BI GN W/ AM PODS					19	N59E	N47E	63SE	70-90								
789	W	IG MGW & GAR-MS-BI SCHI	N72W	69NE												N24E	66SE	N84W	34SW
790	W	MIG BI-PLAG GN	N82W	75NE															
791	W	MIG MGW	N11W	50NE												N69E	60SE		
792	W	MGW - MS-SCHIST IN FLOA	N17W	25NE															
793	W	MIG MGW	N71W	70NE															
794	W	LYRD MIG MGW	N88E	62NW															
795	W	MIG BI GN	N87E	39NW												N76E	50SE	N13E	85W
796	W	MIG BI-PLAG GN & AM	N74W	44NE															
797	W	MIG BI-PLAG GN	N15W	56SW															
798	W	MIG BI-PLAG GN	N87E	34SE															

			Foliation		Lineation		Fold Axis		Axial Surface		IL	Fold	Fold	Crenulation Axis		Joint		Joint	
Station	Quad	Lithology	Strike	Dip	Plunge	Trend	Plunge	Trend	Strike	Dip	Angle	Genr.	Verg.	Plunge	Trend	Strike	Dip	Strike	Dip
799	W	MIG BI-PLAG GN	N61E	44SE															
800	W	EAKLY FOLIATED LEUCO I	N21W	51SW												N60W	90SW		
801	W	MIG BI-PLAG GN - AM	N27W	27NE															
802	W	CO MIG - MIG BI-QTZ-FELD	N65W	62NE												N40W	88SW		
803	W	LUECO MIG MGW	N40E	85NW															
804	W	LEUCO MIG BI GTD TO MG	N65E	70SE															
805	W	SAP - AM - LYRD M MGW	N16W	44NE															
806	W	MGW	N64E	46SE															
807	W	MIG MGW - MIG BI GN	N76W	55SW															
808	W	MIG AM - LEUCO MIG BI GN	N80W	65SW															
809	W	LEUCO MGW	N84W	75SW															
810	W	MIG BI GN	N81E	46SE															
811	W	LEUCO MIG MGW	N84E	30SE															
812	W	MIG BI-PLAG GN	N64E	41SE															
813	W	MIG BI-PLAG GN	N6W	45NE															
814	W	MIG BI-PLAG GN W AM POD	N62W	22NE															
815	W	MIG BI-PLAG GN W AM LEN	N67E	39SE															
816	W	MIG BI-PLAG GN	N16W	36NW															
817	W	GREY - MG TO FG - MIG M	N23W	23NE															
818	W	INTRLD AM - MIG MGW	N65W	66NE															
819	W	MIG BI-PLAG GN	N39E	66NW															
820	W	MIG BI-PLAG GN	N49E	77NW															
821	W	QTZ-FELD-BI SCHIST -MYL	N67E	70SE	8	S68W													
822	W	MIG BI-PLAG GN	N51E	63NW												N59E	85NW	N58E	61SE
823	W	SAP - MIG BI-PLAG GN	N40E	74SE															
824	W	MIG BI-PLAG GN	N35E	65SE			15	N31E	N41E	71SE	20								
825	W	G BI-PLAG GN TO AN INEQ	N40W	45NE												N48W	90SW		
826	W	MIG BI-PLAG GN	N75E	85NW															
827	W	MIG BI-PLAG GN	N48E	38SE															
828	W	MIG BI-PLAG GN	N45E	89NW															
829	W	MIG BI-PLAG GN	N88W	48SW												N14E	79SE		
830	W	MIG BI-PLAG GN	N72W	45SW												N2W	73NE	N82W	51NE
831	W	MIG BI-PLAG GN	N88E	51SE															
832	W	AG GN W FOLDS AND SHEA	N60W	59SW			13	N80E				SHEATH FOLD				N74W	78NE	N24E	68SE
833	W	MIG BI-PLAG GN	N88W	59SW															
834	W	MIG BI-PLAG GN	N75E	80NW															
835	W	MIG BI-PLAG GN	N69E	23SE			15	S46E	N42E	32SE	30								
836	W	MIG BI-PLAG GN	N60W	68SW															
837	W	MIG BI-PLAG GN	N22E	35NW															
838	W	MIG BI GN	N22W	25SW												N31E	79SE		
839	W	MIG BI GN	N42W	42SW															
840	W	MIG BI GN	N86E	22SE															
841	W	MIG BI GN	N60E	57SE															
842	W	MIG BI GN	N87E	46SE															
843	W	MIG BI GN	N80E	33SE															
844	W	MIG BI GN	N62E	21SE												N44W	58SW		
845	W	MIG BI GN	N81E	16SE												N46W	88NE		
846	W	MIG BI GN	N70E	75SE												N78E	77NW		
847	W	MIG BI GN	N67E	55SE												N16W	85SW		
848	W	MIG BI GN	N85E	41SE															
849	W	N W LARGE VW SIZED AM	N70W	33SW												N71W	57NE	N6E	90SE
850	W	MGW W AM FLOAT	N78W	56NE															
851	W	MIG BI GN	N30E	50SE															
852	W	MIG BI GN	N27W	31NE															
853	W	MIG BI GN	N33W	15NE															
854	W	LEUCO FG-MG TRONJ GTD	N72W	60NE															
855	W	FG-MG BI TRONJ	N71E	48SE												N71E	25NW		
856	W	MIG AM INTRLD W BI GN	N65E	46SE															
857	W	IG AM INTRLD W MIG BI G	N44E	39SE												N20E	87SE	N85W	60NE
858	W	MIG BI GN & MIG AM	N42E	19SE												N85E	58NW		
859	W	MIG BI GN	N28E	25SE															
860	W	MIG MGW	N27W	30NW															
861	W	MIG MGW	N62E	90SE															
862	W	MIG AM W/ TRONJ DIKE	N64W	45NE	21	N64E													
863	W	GAR-BI-MS SCHIST	N69E	46SE															
864	W	AR-BI-MS SCHIST TO A MIG	N77E	76SE															
865	W	AM	N79W	79NE															
866	W	RLD MGW & GAR-MS-BI SCI	N42E	73SE															
867	W	MGW	N22E	54NW															
868	W	AR AM - W/ SHEATH FOLDS	N88W	65SW			31	S60E	N82W	57SW	0-10	HEATH FOLD				N20E	70SE		
869	W	AM	N38E	54SE															
870	W	MGW - MIG	N26E	27SE												N62W	27SW		
871	W	MIG MGW	N30E	57SE												N81W	72NE		
872	W	MGW LAYERING	N51E	21SE												N74W	79SW		
873	W	INTRLS OF GAR-BI-MS-SIL	N56E	34SE												N53W	75SW	N88W	78SW
874	W	GAR-BI-MS SCHIST	N52W	37NE															
875	W	GAR-BI-MS SCHIST	N43E	76NW												N43W	86NE		
876	W	INTRLD MGW & SCHIST	N56E	52NW															
877	W	INTRLD MGW & SCHIST	N72W	48NE			5	S71E	N85W	61NE	90								
878	W	MIG GAR-BI-MS SCHIST	N38W	46NE															
879	W	TO SEMI SCHIST; MGW HAS	N24E	50SE															
880	W	GAR-MS SCHIST	N41W	46NE															
881	W	MIG GAR-MS SCHIST	N81W	52SW															
882	W	GAR-BI-MS SCHIST	N52E	54SE															
883	W	MIG MGW	N71W	61NE												N16E	70SE		
884	W	W INTRLS OF GAR-BI-MS S	N60W	47NE															
885	W	BI-MS-QTZ SCHIST; MS WA	N63W	47NE															
886	W	GAR-BI-MS SCHIST	N78W	68SW															
887	W	INTLRLD MIG & SCHIST	N71W	56NE															
888	W	MGW	N15W	46NE															
889	W	MGW	N79W	51NE												N9E	89NW		
890	W	MGW	N75E	76NW	26	N50E										N65W	70SW		
891	W	MIG BI GN	N85E	70NW															
892	W	MIG BI GN	N62E	51NW												N69E	53NW		
893	W	IG BI GN TO AM MEGAC BI	N89E	44NW												N25W	67NE		
894	W	MIG BI GN	N80E	51NW												N30W	82SW		
895	W	IG BI GN & AM MEGAC BI	N85W	42NE												N80E	61SE	N8E	51SE
896	W	& MEGAC BI GN W PODS & I	N64W	42NE												N57E	67SE		
897	W	MIG BI GN	N71E	81NW															
898	W	MIG BI GN	N62W	62NE															
899	W	MIG MGW	N44W	68NE															
900	W	MIG MGW & MS-BI SCHIST	N68W	61NE															
901	W	MIG AM	N36W	36NE															
902	W	MIG BI GN	N15W	20NE												N85E	81SE	N19E	79SE
903	W	MIG AM	N12E	43SE															
904	W	MIG AM	N78W	29NE															
905	W	MIG BI GN & MIG AM	N45W	45NE												N3W	75SW		
906	W	MIG BI GN	N88E	55SE															
907	W	MIG BI GN	N75E	59SE															
908	W	NTRLD GAR-AM - MIG BI G	N88W	60SW															
909	W	FG LEUCO GTD	N26E	56SE															
910	W	GAR-BI-MS-SIL SCHIST	N70E	31NW			18	N9W	N9W	90	150-130					N78E	55SE		
911	W	MGW	N85E	24SE															
912	W	MGW	N85W	37SW															

			Foliation		Lineation		Fold Axis		Axial Surface		IL	Fold	Fold	Crenulation Axis		Joint		Joint	
Station	Quad	Lithology	Strike	Dip	Plunge	Trend	Plunge	Trend	Strike	Dip	Angle	Genr.	Verg.	Plunge	Trend	Strike	Dip	Strike	Dip
913	W	MGW	N43E	33SE															
914	W	GAR-BI-MS SCHIST	N29E	54SE															
915	W	MIG GAR-MS SCHIST	N48W	78NE															
916	W	MIG AM	N70E	39SE															
917	W	MIG BI GN	N63E	29SE												N16W	82SW		
918	W	FLOAT - GAR-BI-MS SCHIST	N77W	45NE												N31E	75NW		
919	W	GAR-BI-MS SCHIST - MIG	N56E	60SE												N15E	55SE		
920	W	MIG BI GN	N25W	70NE															
921	W	IIG BI GN & LENS OF GAR A	N26W	19NE												N66E	85SE		
922	W	MIG AM & BI GN	N48E	52NW															
923	W	MIG BI GN & AM	N35E	75SE															
924	W	MIG BI GN & AM	N89W	69NE															
925	W	MIG AM	N88W	65NE															
926	W	AM	N81W	79SW															
927	W	MIG AM & MINOR MIG BI GI	N3E	60SE												N75E	82SE		
928	W	GAR-BI-MS SCHIST	N78E	24NW												N54E	85SE		
929	W	MIG GAR-BI-MS SCHIST	N37E	21NE															
930	W	CHL-MS-QTZ SCHIST	N68W	72NE															
931	W	GAR-BI-MS SCHIST	N88E	68NW															
932	W	MIG AM & BI GN	N74E	21NW															
933	W	MIG AM	N65W	57SE															
934	W	MS-GAR SCHIST	N64E	61NW															
935	W	MGW	N46W	35NE												N66E	81SE		
936	W	GAR-BI-MS SCHIST - MGW	N81E	35NW															
937	W	GAR-BI-MS SCHIST	N81W	67NE												N78E	87SE		
938	W	GAR-MS BI SCHIST - MIG	N75W	68NE															
939	W	MGW	N50W	36NE															
940	W	AR-BI-MS SCHIST CUT BY PI	N80E	44NW															
941	W	MIG BI GN	N85W	67NE															
942	W	GAR-MS-BI SCHIST	N47E	60NW															
943	W	AM W ROTATED GAR (DEX	N75W	26NE															
944	W	MIG MS-BI SCHIST & MGW	N11W	76NE															
945	W	MGW/2MG	N65E	46SE															
946	W	MGW/2MG	N66E	36SE												N11E	76SE		
947	W	BI-MS SCHIST - CG MS	N71E	45SE												N2E	69SE		
948	W	AR-BI-MS SCHIST W CG MS	N71E	84NW															
949	W																		
950	W	INTRLD MIG MGW	N52E	43SE															
951	W	MGW/2MG	N80E	33SE															
952	W	MIG GAR AM	N52E	68SE			6	S65E	N85W	49NE	0-10								
953	W	GAR BI SCHIST	N76E	61SE	8	58E													
954	W	GAR-BI SCHIST W CG MS	N85W	42NE															
955	W	KY-GAR-BI-MS SCHIST	N85E	38NW												N55E	69NW		
956	W	CK MN STAINED, COTICULI	N32E	54SE															
957	W	MN STAINED, MIG TO CG BI	N32E	42SE															
958	W	CG BI-MS GG	N82E	63SE															
959	W	MIG BI-MS SCHIST	N88E	81SE															
960	W	BI-MS SCHIST - MIG MGW	N82E	85SE															
961	W	GAR AM & MIG BI-GN	N32E	62SE															
962	W	D BII-MS SCHIST & MIG MS	N9W	40NE															
963	W	MS-BI SCHIST W QTZ VEIN	N52E	64SE															
964	W	GAR-BI-MS-SIL SCHIST	N46E	64SE															
965	W	GAR-MS-QTZ SCHIST	N42E	59SE															
966	W	SIL-MS SCHIST	N68W	44SW												N30E	72SE		
967	W	GAR-MS-SIL SCHIST	N50E	75SE															
968	W	MS SCHIST	N52W	35SW															
969	W	GAR-BI-SIL SCHIST	N77W	40SW	5	S72E										N74W	87SW		
970	W	MIG GAR-MS-SIL SCHIST	N72W	30SW												N81E	77NW		
971	W	MIG BI GN	N15W	57SW															
972	W	MIG BI GN	N50W	80SW															
973	W	MIG BI GN	N70W	61SW															
974	W	FOLIATED QTZ VEIN	N78E	33SE															
975	W	MIG BI GN	N78E	60NW															
976	W	BI GN TO A MEGAC BI-PLA	N11E	29SE			15	N50W	N38W	15NW	10					N50E	88NW	N56W	85NE
977	W	LYRS MIG BI GN	N16E	43SE			10	N0E	N5W	70NE	90								
978	W	MS SCHIST	N30W	50NW															
979	W	GAR-BI-MS-SIL SCHIST	N85E	73NW												N15W	82NE		
980	W	IIG BI GN TO A MEGAC BI G	N65E	82NW															
981	W	MGW & BI-GAR-MS QTZITE	N76W	43NE												N11E	78NW		
982	W	MIG GAR-BI-SIL SCHIST	N43W	22NE												N46W	84NE		
983	W	D MIG MGW & GAR-BI-SIL S	N70W	19NE															
984	W	QTZ-MS SCHIST	N88E	60NW															
985	W	INTRLD MS SCHIST & MGW	N35W	15SW															
986	W	GAR-BI-SIL SCHIST	N45E	42SE															
987	W	MGW	N50W	33NE															
988	W	GAR-BI-MS-SIL SCHIST	N65W	70NE															
989	W	GAR-BI-SIL SCHIST	N88E	63NW															
990	W	GAR-BI-SIL SCHIST	N5E	25SE												N44W	73SW		
991	W	MGW	N37W	29NE															
992	W	D MGW & GAR-MS-BI-SIL S	N10W	11NE												N21E	74NW	N84W	83SW
993	W	GAR-MS-BI-SIL SCHIST	N85E	30SE															
994	W	MGW	N84E	20SE												N20W	50NE		
995	W	MGW	N50E	27SE															
996	W	GAR-MS SCHIST	N75W	59SW															
997	W	/ QTZ GRAINS ARE FLATTI	N20E	20SE															
998	W	MGW	N68E	21SE												N26W	85SW	N68E	90SE
999	W	MGW	N21E	11SE															
1000	W	MGW	N50W	44NE															
1001	W	/ INTRLS OF GAR-MS-BI-SII	N60E	53NW															
1002	W	MGW	N66E	30SE															
1003	W	GAR-BI-MS-SIL SCHIST	N65W	36NE												N77W	62SW		
1004	W	GAR-BI-MS-SIL SCHIST	N75W	52NE															
1005	W	QTZ-MS SCHIST	N69E	42SW															
1006	W	GAR-BI-MS-SIL SCHIST	N25W	41NE															
1007	W	GAR-BI-MS SCHIST & GN	N35E	26NW	32	S72E										N26E	52NW		
1008	W	SAP - MIG-BI-QTZ-FELD GN	N80W	35NE															
1009	W	GAR-MS-BI SCHIST	N71W	52NE												N81E	55SE		
1010	W	MIG BI GN	N89W	70NE			46	N31E	N35W	46NE	120								
1011	W	AM	N65W	64SW															
1012	W	GAR-BI-SIL SCHIST TO MGW	N72W	31NE															
1013	W	MGW TO MOSTLY MEGAC	N79E	28NW												N34W	62SW		
1014	W	INTRLD MGW	N77E	57SE															
1015	W	INTRLD MEGAC	N50E	60NW															
1016	W	MGW	N87W	55NE															
1017	W	MGW - GAR-BI-SIL SCHIST	N80E	39NW															
1018	W	GAR-BI-MS-SIL SCHIST	N50W	77NE															
1019	W	MGW	N86E	56SE															
1020	W	RLD MGW & GAR-BI-SM SCI	N48W	32SW															
1021	W	GAR-BI-MS SCHIST	N72E	56NW															
1022	W	GAR-BI-MS SCHIST	N72E	56NW															
1023	W	GAR-BI-MS SCHIST	N46E	37NW															
1024	W	GAR-BI-SIL SCHIST & MGW	N65E	55NW												N20E	84SE		
1025	W	BI-SIL SCHIST TO GN W LOT	N86E	39NW															
1026	W	MGW	N76E	33NW															

			Foliation		Lineation		Fold Axis		Axial Surface		IL	Fold	Fold	Crenulation Axis		Joint		Joint	
Station	Quad	Lithology	Strike	Dip	Plunge	Trend	Plunge	Trend	Strike	Dip	Angle	Genr.	Verg.	Plunge	Trend	Strike	Dip	Strike	Dip
1027	W	MS-BI-SIL SCHIST INTRLD W	N78W	83NE															
1028	W	MGW	N81W	50NE												N28W	81NE		
1029	W	GAR-BI-MS-SIL SCHIST	N72W	39NE															
1030	W	LYRD MGW	N84W	64NE															
1031	W	GAR-BI-MS-SIL SCHIST	N80E	50NW															
1032	W	GAR-MS-BI-SIL SCHIST	N69W	62NE															
1033	W	GAR-MS-BI-SIL SCHIST	N66W	52NE															
1034	W	GAR-MS-BI-SIL SCHIST	N78W	82NE	12	S88E													
1035	W	GAR-BI-MS-SIL SCHIST	N83E	38NW												N20E	57NW		
1036	W	MGW	N62W	68NE															
1037	W	MGW	N66E	72SE															
1038	W	THIN INTRLS OF GAR-MS-B	N60W	67NE			31	N32W	N60W	67NE	6-10								
1039	W	BI-MS-SIL SCHIST INTRLD W	N47W	50NE															
1040	W	MGW	N51W	41NE															
1041	W	MGW - MIG	N58W	56NE															
1042	W	NTRLD MGW & MS-BI SCHIS	N67W	47NE															
1043	W	MGW & MS-BI-SIL SCHIST	N25W	61NE															
1044	W	GAR-MS-BI SIL SCHIST - MG	N50W	79NE															
1045	W	GAR-MS-BI-SIL SCHIST	N40W	35NE	26	S55E													
1046	W	MS-SIL SCHIST CUT BY BI G	N64W	55NE															
1047	W	GAR-BI-MS-SIL SCHIST	N45W	44NE															
1048	W	MIG GAR-MS-BI-SIL SCHIS	N59W	66NE															
1049	W	GAR-BI-SIL SCHIST	N55W	36NE															
1050	W	GR-BI-MS-SIL SCHIST	N65W	52NE															
1051	W	GAR-BI-MS-SIL SCHIST	N79W	30NE															
1052	W	GAR-BI-MS-SIL SCHIST	N70W	30NE												N53E	52NW	N35E	63NW
1053	W	MGW	N72W	40NE															
1054	W	MGW	N75W	56NE															
1055	W	GAR-BI-MS-SIL SCHIST	N80W	28SW															
1056	W	GAR-BI-MS-SIL SCHIST	N78W	43NE															
1057	W	PEG QTZ -PROSPECT																	
1058	W	LD GR-MS-BI-SIL SCHIST M	N72E	34SE												N00NW	73SW		
1059	W	MGW	N34W	32NE															
1060	W	GAR-BI-SIL SCHIST	N73E	32SE															
1061	W	GAR-BI-QTZ-FELD GN	N75E	9SE												N80E	87NW	N16W	87NE
1062	W	GAR-BI-MS-SIL SCHIST	N85E	32SE												N25W	85SW		
1063	W	GAR-BI-SIL SCHIST	N50W	42NE															
1064	W	GAR-BI-SIL SCHIST	N50E	73NW															
1065	W	MIG MGW	N88W	21NE	8	N80W										N16E	86SE		
1066	W	GAR-BI-SIL SCHIST	N53E	29SE															
1067	W	GAR-BI-MS-SIL SCHIST	N62W	15NE															
1068	W	MIG GAR-BI-MS-SIL SCHIS	N42E	32SE												N76E	88SE		
1069	W	W W INTRLS OF GAR-BI-SIL	N20E	34SE												N17E	21NW		
1070	W	GAR-BI-SIL SCHIST	N55W	24NE															
1071	W	GAR-BI-SIL SCHIST					15	N77E	N72E	90	130								
1072	W	MGW	N00E	33SE															
1073	W	MGW	N26W	20NE															
1074	W	GAR-BI-SIL SCHIST	N10W	18NE															
1075	W	GR-BI-SIL SCHIST TO GN	N20E	27SE															
1076	W	GAR-BI-SIL SCHIST	N11E	32SE															
1077	W	MGW W INTRLS OF GA-BI-S	N11E	30SE	30	N85E										N39E	75NW		
1078	W	RLD MGW- GAR-BI-SIL SCH	N65W	38NE												N27W	81SW		
1079	W	GAR-BI-SIL SCHIST	N58W	19NE															
1080	W	BI-SIL SCHIST W INTRLS OF	N77W	20NE															
1081	W	GAR-BI-SIL SCHIST & MGW	N13W	30NE												N86E	79SE		
1082	W	ULFIDIC- GAR-BI-SIL SCHIS	N55W	46NE															
1083	W	SULFIDIC-GAR-BI-SIL SCHIS	N58W	17NE															
1084	W	GAR-BI-MS-SIL SCHIST	N35E	20NW															
1085	W	MIG GAR-MS-BI-SIL SCHIST	N28W	60NE	31	N8W										N44W	33SW		
1086	W	SULFIDIC- GAR-BI SCHIST	N46W	16NE															
1087	W	D SULFIDIC- GAR-BI-MS-SIL	N15W	66NE			24	N30W	N12W	61NE									
1088	W	W(GAR-BI-QTZ) & GAR-BI-SI	N50W	24NE															
1089	W	IGW W INTRLS OF MS SCHIS	N45W	38NE															
1090	W	V MINOR INTRLS OF SIL-MS	N38E	56SE															
1091	W	RLS OF GAR-BI-MS-SIL SCH	N56E	79NW															
1092	W	GAR-BI-MS-SIL SCHIST	N10W	40NE															
1093	W	IDIC MIG GAR-MS-BI-SIL SC	N38E	24SE															
1094	W	VE MGW W INTRLS OF MS S	N60E	55SE															
1095	W	LFIDIC GAR-BI-MS-SIL SCH	N24W	40NE															
1096	W	GAR-BI-MS- SIL SCHIST	N10E	32SE												N81W	74NE		
1097	W	GAR-MS-BI-SIL SCHIST	N12E	42SE															
1098	W	GAR-BI-MS-SIL SCHIST	N80W	45NE												N33W	38SW		
1099	W	GAR-MS-BI-SIL SCHIST	N8W	31NE												N47E	70NW	N18W	83SW
1100	W	GAR-MS-BI-SIL SCHIST	N33W	36NE															
1101	W	DIC MGW & GAR-MS-BI-SIL	N7E	49NW															
1102	W	GAR-MS-SIL-BI SCHIST	N53E	26SE															
1103	W	GAR-BI-MS SCHIST	N53E	26SE															
1104	W	INTRLD MGW	N6W	64NE															
1105	W	GAR-BI-MS SCHIST	N00E	48SE															
1106	W	GAR-SIL-BI-MS SCHIST	N8W	29NE			17	N70E	N66E	55NW	0								
1107	W	GAR-BI-MS-SIL SCHIST	N34W	27NE															
1108	W	GAR-BI-MS SCHIST	N45W	56NE															
1109	W	GAR-BI-MS-SIL SCHIST	N30E	40SE															
1110	W	K THINLY LAYERED GAR-BI	N70E	61NW															
1111	W	GAR-MS-BI-SILSCHIST	N74E	50NW															
1112	W	RLD MGW & GAR-BI-SM SCI	N61E	80NW			43	S14W	N5W	67NE	85								
1113	W	GAR-BI-MS-SIL SCHIST	N62E	27NW															
1114	W	/ INTRLS OF GAR-BI-MS SIL	N80E	77NW															
1115	W	INTRLD W GAR-BI-MS-SIL S	N57E	51SW												N36W	73SW	N24E	73NW
1116	W	MGW	N88E	60NW															
1117	W	INTRLD MGW	N23E	75NW															
1118	W	MGW	N37W	30NE															
1119	W	V INTRLD W GAR-MS-SIL SC	N28W	32NE															
1120	W	MGW	N73E	55NW															
1121	W	GAR-BI-MS-SIL SCHIST	N84E	67NW			21	N45E	N34E	35SE	170-150					N26W	82NE		
1122	W	GAR-BI-MS-SIL SCHIST	N60W	44NE															
1123	W	GAR-BI-MS-SIL SCHIST	N53E	42SE															
1124	W	GAR-BI-MS-SIL SCHIST	N68E	33SE															
1125	W	GAR-BI-MS-SIL SCHIST	N68W	42NE															
1126	W	GAR-BI-MS-SIL SCHIST	N50W	61NE															
1127	W	GAR-BI-MS-SIL SCHIST	N61W	58NE															
1128	W	GAR-BI-MS-SIL SCHIST	N71W	48NE															
1129	W	GAR-MS-BI-SIL SCHIST	N54W	46NE												N21E	57NW		
1130	W	GAR-MS-BI-SIL SCHIST	N48W	39NE															
1131	W	GAR-BI-SIL SCHIST	N84E	54NW	18	N77W										N52W	66SW		
1132	W	BI-MS-SIL SCHIST & MINOR	N69E	33NW															
1133	W	GAR-BI-MS-SIL SCHIST	N80W	79NE															
1134	W	GAR-BI-SIL SCHIST	N68W	54NE															
1135	W	GAR-BI-MS-SIL SCHIST	N84W	37NE															
1136	W	GAR-BI-MS-SIL SCHIST	N44W	41NE															
1137	W	GAR-BI-MS-SIL SCHIST	N40W	42NE												N78W	75NE		
1138	W	GAR-BI-MS-SIL SCHIST	N57W	44NE															
1139	W	GAR-BI-SIL SCHIST	N45E	39SE															
1140	W	MGW & MINOR SCHIST	N60E	17NW															

			Foliation		Lineation		Fold Axis		Axial Surface		IL	Fold	Fold	Crenulation Axis		Joint		Joint	
Station	Quad	Lithology	Strike	Dip	Plunge	Trend	Plunge	Trend	Strike	Dip	Angle	Genr.	Verg.	Plunge	Trend	Strike	Dip	Strike	Dip
1141	W	GAR-BI-MS SCHIST & MGW	N52W	28NE															
1142	W	AR-BI-MS-SIL SCHIST & BI G	N68W	47NE															
1143	W	IS-BI-SIL SCHIST W PODS O	N26E	62NW															
1144	W	GW & GAR-BI-MS-SIL SCHI	N73E	47NW												N86W	61SW		
1145	W	AR-BI-MS-SIL SCHIST & MG	N89E	35SE															
1146	W	GAR-BI-MS-SIL SCHIST	N85W	02NE															
1147	W	SIL SCHIST	N18E	76NW															
1148	W	SIL SCHIST	N80E	52NW															
1149	W	MGW	N80W	19NE															
1150	W	MGW & SIL SCHIST	N60E	68NW															
1151	W	MGW	N50W	56NE															
1152	W	LFIDIC GAR-MS-BI-SIL SCH	N60W	46NE												N64W	74SW		
1153	W	CG MS FLAKES I INTRLS OI	N60W	59NE															
1154	W	MGW	N70W	56NE															
1155	W	MGW	N66W	54NE															
1156	W	INTRLD SCHIST & MGW	N60W	47NE												N55W	68SW		
1157	W	MGW & INTRLS OF SCHIST	N60W	32NE															
1158	W	GAR-MS SCHIST	N10W	42NE															
1159	W	RLD GAR-BI-MS SCHIST & M	N45W	67NE															
1160	W	MIG MS SCHIST	N60E	56NW															
1161	W	GAR-BI-MS-SIL SCHIST	N54W	40NE															
1162	W	GAR-MS SCHIST	N36W	36NE															
1163	W	GAR-BI-MS-SIL SCHIST	N36E	40SE															
1164	W	GAR-BI-MS SCHIST	N10W	44NE															
1165	W	IG QTZ-MS SCHIST TO A MG	N11E	40SE												N14E	61NW		
1166	W	GAR-BI-MS-SIL SCHIST	N45W	50NE															
1167	W	MGW	N19E	65NW															
1168	W	FG MS-QTZ MGW TO SCHIS	N13E	66SE															
1169	W	LFIDIC GAR-BI-MS-SIL SCH	N71W	31NE												N17E	57NW		
1170	W	MIG GAR-MS-BI-SIL SCHIST	N36W	33NE															
1171	W	FG MGW	N35E	53SE															
1172	W	MGW	N9W	36NE															
1173	W	FG SIL-MS-QTZ SEMI-SCHIS	N22W	82NE															
1174	W	GAR-BI-MS-SIL SCHIST	N12W	31NE															
1175	W	GAR-BI-MS-SIL SCHIST	N8W	80NE															
1176	W	GAR-BI-MS-SIL SCHIST	N13W	42NE															
1177	W	MGW & MS-QTZ SEMI-SCHIS	N25W	37NE															
1178	W	GAR-MS-SIL SCHIST	N63W	37NE															
1179	W	GAR-QTZ GN/CALC-SI	N31E	62SE															
1180	W	GW & GAR-BI-MS-SIL SCHI	N24W	60NE															
1181	W	GAR-BI-MS-SIL SCHIST	N10E	55NW															
1182	W	MGW & SIL SCHIST	N3W	78SW															
1183	W	GAR-BI-MS SCHIST	N12W	59NE															
1184	W	R-MS-SCHIST W CG MS FLA	N26W	57NE												N32E	71NW		
1185	W	GAR-BI-MS-SIL SCHIST	N7W	40NE															
1186	W	W & SOME GAR-BI-SIL SCH	N50W	38NE												N50E	90SE		
1187	W	MGW	N8W	42NE															
1188	W	GAR-BI-MS-SIL SCHIST	N10W	59NE															
1189	W	GAR-BI-MS-SIL SCHIST	N60W	02NE															
1190	W	MGW -GAR-BI-MS SCHIST	N6W	32NE															
1191	W	GAR-BI-MS-SIL SCHIST	N0W	51NE															
1192	W	GAR-BI-MS-SIL SCHIST	N4W	66NE															
1193	W	MGW	N23E	48SE															
1194	W	MGW	N43E	61SE															
1195	W	MIG MGW	N34E	55SE															
1196	W	MGW W MOSTLY BI	N9E	50SE												N42E	78NW		
1197	W	Y LYRD CG GAR-MS-BI-SIL	N11E	50SE												N71E	61NW	N10W	90SE
1198	W	MGW	N35E	69NW															
1199	W	LYRD GAR-BI-MS-SIL SCHIS	N32E	60SE			49	S84E	N37E	60SE	30								
1200	W	MIG GAR-BI-MS SCHIST	N45E	68SE															
1201	W	LYRD MGW TO GAR-BI-MS S	N46E	68SE															
1202	W	MGW	N32E	84NW															
1203	W	FG TO MG BI-QTZ-FELD GN	N32E	90SE												N27W	83SW		
1204	W	BI-QTZ-FELD GN	N45E	62NW															
1205	W	BI-QTZ-FELD GN/MGW	N10W	59NE															
1206	W	G GAR-BI-MS SCHIST TO MG	N33W	40NE															
1207	W	GAR-BI-QTZ-FELD GN/MGW	N17E	70SE															
1208	W	GAR-BI-MS-SIL SCHIST	N42E	76SE															
1209	W	RD MGW TO FG GAR-BI-MS	N10E	78SE															
1210	W	NTRLD FG GAR-BI-MS SCHIS	N15E	60SE															
1211	W	THINLY LYRD MGW	N27E	60SE												N75E	85SE		
1212	W	BI GN TO GAR-BI-MS SHIST	N22E	62SE															
1213	W	AR-BI-MS-SIL SCHIST & MG	N50E	82NW															
1214	W	BI DOMINANT MGW	N3E	38SE															
1215	W	MGW	N64E	54NW															
1216	W	GAR-BI-MS-SIL SCHIST	N44E	69NW															
1217	W	FG MS-SIL SCHIST	N36E	65SE															
1218	W	THINLY LYRD MGW	N23E	70SE															
1219	W	MGW	N55E	45NW															
1220	W	MIG MGW CUT BY PEG	N20E	45SE															
1221	W	MIG BI GN/MGW					18	N20E	N28E	72SE	70								
1222	W	MIG MGW					5	N35E	N35E	90	120								
1223	W	MIG MGW & MS-BI SCHIST	N29E	81NW															
1224	W	MIG MGW	N45E	77SE			28	N25E	N22E	73NW	20					N58W	84NE	N54E	52SE
1225	W	GAR-BI-QTZ-FELD GN/MGW	N51E	51SE												N47W	82SW		
1226	W	MGW GAR-BI-MS SCHIST	N84E	42SE															
1227	W	MG TO CG BI QTZITE	N55E	70SE															
1228	W	MGW	N31E	51SE															
1229	W	GAR-BI-MS-SIL SCHIST	N10W	55NE			13	N49E	N45E	75SE	120					N22E	81SE		
1230	W	MIG BI GN/MGW	N29W	71NE															
1231	W	MIG BI-QTZ-FELD GN /MGW	N20E	52NW															
1232	W	MIG BI-QTZ-FELD GN /MGW	N15E	62NW															
1233	W	MIG BI-QTZ-FELD GN /MGW	N30W	16NE												N15E	83NW		
1234	W	MIG BI-QTZ-FELD GN	N50W	62SW															
1235	W	MIG BI-QTZ-FELD GN/ MGW	N30W	49NE															
1236	W	BI GN - MGW	N44W	29NE															
1237	W	MIG MGW - BI-QTZ-FELD GI	N71W	35NE												N10W	21SW		
1238	W	MGW - BI-QTZ-FELD GN	N48W	30NE												N41W	48SW	N32E	58SE
1239	W	MGW	N25W	37NE															
1240	W	MIG MGW	N29W	24NE															
1241	W	GAR-MS-BI-SIL SCHIST	N61E	68SE															
1242	W	GAR-MS-BI-SIL SCHIST	N23W	63NE															
1243	W	MGW	N5W	86NE															
1244	W	MGW	N83W	58NE															
1245	W	MIG MGW	N62W	71NE															
1246	W	MIG MGW	N82W	28NE															
1247	W	MIG MGW	N60W	64NE															
1248	W	MGW	N70W	57NE															
1249	W	MGW	N64W	50NE															
1250	W	MIG MGW/BI GN	N44E	62NW			14	N35E	N42E	62NW	0								
1251	W	MS-BI PEG DIKE CUT MGW	N25W	53NE												N50E	86NW		
1252	W	MGW	N28E	83SE															
1253	W	MIG MGW	N36E	66SE															
1254	W	GAR-BI-MS SCHIST	N38E	73SE															

Station	Quad	Lithology	Foliation		Lineation		Fold Axis		Axial Surface		IL	Fold	Fold	Crenulation Axis		Joint		Joint	
			Strike	Dip	Plunge	Trend	Plunge	Trend	Strike	Dip	Angle	Genr.	Verg.	Plunge	Trend	Strike	Dip	Strike	Dip
1255	W	GAR-BI-MS-SIL SCHIST	N25E	51SE															
1256	W	MIG MGW	N55E	82NW	49	S60W													
1257	W	i FG TO MG GAR-BI-MS SCI	N41E	83SE															
1258	W	GAR-BI-MS SCHIST	N43E	76SE															
1259	W	-MS SCHIST - UP-RIGHT OPE	N41E	64SE			19	N51E	N52E	88NW	130								
1260	W	GAR-BI-MS SCHIST	N51E	69NE															
1261	W	GAR-BI-MS SCHIST	N15E	22SE															
1262	W	GAR-BI-MS SCHIST	N88E	32W															
1263	W	MGW	N65E	53NW												N35W	82SW		
1264	W	MIG MGW	N27E	77SE															
1265	W	GAR-MS-BI SCHIST	N35W	28SE															
1266	W	MGW	N39E	66SE															
1267	W	MGW	N42E	54SE															
1268	W	MGW	N15E	48SE															
1269	W	MGW	N11E	71SE															
1270	W	MGW	N22E	66SE															
1271	W	MGW	N30E	75SE															
1272	W	GAR-BI-MS SCHIST	N55E	70NW															
1273	W	GAR-BI-MS-SIL SCHIST	N70E	48SE															
1274	W	GAR-BI-MS SCHIST	N88E	28NW															
1275	W	MGW	N45E	60SE															
1276	W	MGW	N66E	85SE															
1277	W	MIG MGW	N37E	73SE															
1278	W	MIG MGW	N51E	75SE															
1279	W	MIG MGW	N24E	75SE															
1280	W	MIG MGW	N35E	67SE												N70W	82NE		
1281	W	IGW INTRLD W GAR-MS-BI	N31E	80NW															
1282	W	GAR-MS-SIL SCHIST	N36E	69SE															
1283	W	MIG MGW	N42E	72SE															
1284	W	GAR-BI-MS SCHIST	N37E	58NW															
1285	W	MIG MGW	N25E	70NW															
1286	W	GAR-BI-MS SCHIST	N46E	51SE															
1287	W	GAR-BI-MS-SIL SCHIST	N42E	74SE												N12W	81NE		
1288	W	MIG MGW	N25E	68SE															
1289	W	MIG MGW	N21E	62SE															
1290	W	MIG MGW	N37E	63SE															
1291	W	MIG MGW	N23E	72SE															
1292	W	MIG MGW	N35E	84SE															
1293	W	MIG MGW	N38E	76SE															
1294	W	GAR-MS-SIL SCHIST	N30E	73SE															
1295	W	GAR-MS-SIL SCHIST	N30E	44NW															
1296	W	GAR-BI-MS-SIL SCHIST	N56E	62NW															
1297	W	GAR-BI-MS-SIL SCHIST	N39E	88NW												N75W	89NE		
1298	W	GAR-BI-MS-SIL SCHIST	N32E	72NW															
1299	W	GAR-BI-MS-SIL SCHIST	N10E	63NW															
1300	W	MIG MGW	N42E	71NW															
1301	W	MIG MGW	N44E	73NW															
1302	W	GAR-BI-MS SCHIST	N43E	78NW															
1303	W	MGW	N28E	55SE															
1304	W	MIG GAR-BI-MS-SIL SCHIST	N74E	78NW															
1305	W	MIG GAR-BI-MS-SIL SCHIST	N51E	84SE												N60W	82NE		
1306	W	MGW & SCHIST	N58E	78NW															
1307	W	MGW W INTRLS OF AN INE	N48E	71NW															
1308	W	MIG MGW W CG MS FLAKES	N27E	72NW															
1309	W	GAR-BI-MS-SIL SCHIST	N39E	71NW															
1310	W	-BI-MS SHIST W CG MS FLA	N53E	87NW															
1311	W	GAR-BI-MS-SIL SCHIST	N32W	51NE															
1312	W	MIG MGW	N17E	69SE															
1313	W	MIG MGW	N31W	61NE															
1314	W	-BI-MS SCHIST & INTRLD M	N10W	61NE															
1315	W	-BI-MS SCHIST W CG MS DI	N24E	71SE															
1316	W	GAR-BI-MS-SIL SCHIST	N67E	84NW															
1317	W	GAR-BI-MS-SIL SCHIST	N54E	62NW															
1318	W	GAR-BI-MS-SIL SCHIST	N25E	86NW	21	S33W													
1319	W	GAR-BI-MS-SIL SCHIST	N41E	68NW															
1320	W	MS-BI-SIL-QTZITE/MGW	N48E	70SE															
1321	W	IGW W INTRLD MS-BI-SIL S	N119E	54SE			62	N33E	N19E	54SE	0					N76E	63SE		
1322	W	MIG MGW					68	N29E	N15E	78SE	20-90	F3							
1323	W	GAR-BI-MS-SIL SCHIST	N19E	65SE															
1324	W	MIG MGW	N5E	54SE															
1325	W	MIG MGW	N22E	67SE															
1326	W	MIG MGW	N29E	81NW															
1327	W	MIG MGW	N21E	49SE												N62E	74SE		
1328	W	GAR-BI-MS SCHIST	N15E	49SE															
1329	W	-BI-MS SCHIST W CG MS FL	N42E	75SE															
1330	W	-BI-MS SCHIST W CG MS FL	N27E	75SE															
1331	W	GAR-BI-MS SCHIST & MGW	N21E	64SE															
1332	W	-BI-MS SCHIST W CG MS FL	N32E	60NW															
1333	W	GAR-BI-MS SCHIST	N45E	80NW															
1334	W	GAR-MS-BI SCHIST	N45E	85SE															
1335	W	GAR-BI-MS SCHIST	N47E	25SE															
1336	W	GAR-BI-MS SCHIST	N64E	85NW															
1337	W	GAR-BI-MS SCHIST	N28E	52NW												N60E	80SE		
1338	W	GAR-BI-MS SCHST	N32E	52NW															
1339	W	GAR-BI-MS SCHIST	N21E	85NW															
1340	W	GAR-BI-MS SCHIST	N22E	80NW												N41W	86SW		
1341	W	GAR-BI-MS SCHIST CG MS	N41E	75NE															
1342	W	GAR SCHIST	N40E	78SE															
1343	W	GAR-MS-BI SCHIST	N38E	70SE															
1344	W	GAR SCHIST	N42E	55SE															
1345	W	MIG GAR-BI-MS-SIL SCHIST	N43E	71NW															
1346	W	MIG GAR-BI-MS-SIL SCHIST	N54E	42NW															
1347	W	MIG GAR-BI-MS-SIL SCHIST	N28E	81NW															
1348	W	MIG GAR-BI-MS-SIL SCHIST	N40E	62NW															
1349	W	MGW	N45E	66NW															
1350	W	GAR-BI-MS SCHIST	N28E	70SE												N70W	80SW		
1351	W	GAR-BI-MS SCHIST	N10E	79NW															
1352	W	GAR-BI-MS SCHIST	N45E	86NW															
1353	W	MGW	N45E	61NW												N29W	85SW		
1354	W	MGW	N37E	87NW															
1355	W	MGW	N22E	82NW															
1356	W	MGW	N18E	47SE															
1357	W	MIG MGW	N10E	33SE															
1358	W	MIG MGW	N12E	55SE															
1359	W	GAR-BI-MS SCHIST	N27E	92NW															
1360	W	MGW & SCHIST CALC-SI	N86E	82NW															
1361	W	GAR-BI-MS SCHIST	N35E	51NW															
1362	W	) BI GN / MGW - BI-QTZ-FEL	N10E	55NW															
1363	W	GAR-BI-MS SCHIST	N41E	60NW															
1364	W	INEQ BI-QTZ-PLAG GN	N23E	25NW															
1365	W	GAR-BI-MS SCHIST	N36E	82NW															
1366	W	MIG MGW	N50E	69NW															
1367	W	GAR-BI-MS SCHIST	N60E	50NW															
1368	W	GAR-BI-MS SCHIST	N35E	85NW															

			Foliation		Lineation		Fold Axis		Axial Surface		IL	Fold	Fold	Crenulation Axis		Joint		Joint	
Station	Quad	Lithology	Strike	Dip	Plunge	Trend	Plunge	Trend	Strike	Dip	Angle	Genr.	Verg.	Plunge	Trend	Strike	Dip	Strike	Dip
1369	W	GAR-BI-MS SCHIST	N30E	75NW															
1370	W	IGW & INTRLD GAR-BI-MS S	N30E	83SE															
1371	W	GAR-BI-MS SCHIST	N50E	79NW															
1372	W	GAR-BI-MS SCHIST	N48E	88SE															
1373	W	GAR-BI-MS SCHIST	N42E	77SE															
1374	W	GAR-BI-MS SCHIST	N44E	90SE															
1375	W	MIG MGW	N41R	74NW			37	N56E	N46E	60NW	20								
1376	W	MIG MGW					30	N45E	N34E	49SE	0-70								
1377	W	MIG MGW	N46E	55NW															
1378	W	MIG MGW	N55E	79NW															
1379	W	MIG MGW	N50E	90NW															
1380	W	RLD MIG MGW & GAR-BI SC	N42E	61NW															
1381	W	MIG GAR-BI-MS SCHIST	N25E	60SE															
1382	W	PEG & MS-BI SCHIST	N45E	88SE															
1383	W	MGW	N46E	65NW															
1384	W	RLD MIG MGW & GAR-BI SC	N65E	46NW															
1385	W	GAR-BI-MS-SIL SCHIST	N58E	75SE															
1386	W	GAR-BI-MS-SIL SCHIST	N38E	78NW															
1387	W	GAR-BI-MS-SIL SCHIST	N48E	70SE															
1388	W	MIG MGW					66	N9E	N40E	69SW	10								
1389	W	GAR-BI-MS-SIL SCHIST	N33E	68SE															
1390	W	GAR-BI-MS SCHIST	N60E	80NW															
1391	W	GAR-BI-MS SCHIST	N64E	54SE															
1392	W	MYLO MGW	N12E	82NW															
1393	W	MIG MGW	N40E	67MW												N84E	62SE		
1394	W	MIG MGW	N40E	65SE															
1395	W	MIG MGW	N43E	52SE															
1396	W	RLD MGW & GAR-BI-MS SCI	N47E	41NW												N22W	88NE		
1397	W	MIG GAR-BI-PLAG SCHIST	N46E	80SE															
1398	W	MIG MGW	N30E	80NW															
1399	W	MIG MGW	N60E	52NW															
1400	W	THINLY LYRD MGW	N30E	65NW															
1401	W	THINLY LYRD MIG MGW	N32E	67SE															
1402	W	MIG MGW	N42E	69NW															
1403	W	GAR-BI-MS SCHIST	N30E	72NW															
1404	W	MIG MGW	N44E	86NW															
1405	W	W W INTRLS OF GAR-BI-MS	N41E	75SE															
1406	W	W W INTRLS OF GAR-BI-MS	N50E	76NW												N31W	87NE		
1407	W	MIG MGW & GAR-BI SCHIST	N42E	59SE															
1408	W	MGW TO A SEMI-SCHIST	N62E	73SE												N35W	72NE		
1409	W	MIG BI GN/MGW	N58E	77SE															
1410	W	IGW & INTRLD GAR-BI-MS S	N46E	84NW															
1411	W	MIG MGW	N30E	31NW															
1412	W	MIG MGW	N38E	80NW															
1413	W	IG MGW CUT BY 2 PEG DIK	N76E	80SE			53	N31E	N45E	64NW	0-70	F2							
1414	W	MIG MGW	N34E	73NW	19	N40E	19	N40E	N34E	73NW	0								
1415	W	MIG MGW	N48E	87SE															
1416	W	GAR-BI-MS SCHIST	N40E	78NW												N54W	80SW		
1417	W	MIG MGW	N68E	74NW	65	N42E	65	N42E	N68E	74W	0-30								
1418	W	MIG MGW	N44E	43SE															
1419	W	I-MS SCHIST & INTRLD MIG	N62E	76SE															
1420	W	MIG MGW	N39E	90SE															
1421	W	MIG MGW	N11E	66NW															
1422	W	MIG MGW	N10E	79SE															
1423	W	MIG MGW	N22E	78NW															
1424	W	GAR-BI-MS SCHIST	N16E	81NW															
1425	W	GW TO A GAR-BI-MS SEMI-S	N22E	69NW															
1426	W	IGW & INTRLS GAR-BI-MS S	N17E	88NW															
1427	W	MGW	N38E	69NW															
1428	W	SEMI SCHIST TO MGW	N55E	88SE															
1429	W	MGW	N37E	46NW															
1430	W	MIG MGW	N22E	65NW															
1431	W	MIG MGW	N45E	82NW															
1432	W	MIG MGW	N48E	65NW															
1433	W	SCHIST TO SEMI-SCHIST &	N45E	70NW												N50W	74NE		
1434	W	MIG GAR-BI-MS SCHIST	N39E	70NW												N50W	85W		
1435	W	AR-BI-MS SEMI-SCHIST TO	N52E	69NW												N40W	84NE		
1436	W	R-BI-MS SEMI-SCHIST TO M	N48E	77SE															
1437	W	MIG MGW	N54E	77NW															
1438	W	GAR-BI-MS SCHIST	N52E	68W															
1439	W	GAR-BI-MS SEMI-SCHIST	N58E	40NW															
1440	W	GAR-BI-MS SCHIST	N42E	76SE															
1441	W	GAR-BI-MS SCHIST - MGW	N26E	69NW															
1442	W	MIG GAR MGW	N52E	51SE															
1443	W	GAR-BI-MS SCHIST	N44E	82SE															
1444	W	INTRLD MGW & CALC-SI	N39E	90SE	39	S51W													
1445	W	AR-MS TO GAR-BI-MS SCHI	N36E	85SE												N59W	89SW		
1446	W	GAR-BI-MS SCHIST	N48E	78SE															
1447	W	MIG MGW	N35E	80NW															
1448	W	GAR-BI-MS SCHIST	N45E	60SE															
1449	W	METACGL & MS SCHIST	N57E	34SE															
1450	W	IG GAR-BI-MS SCHIST & PE	N41E	67SE															
1451	W	MIG MGW	N50E	55SE															
1452	W	GAR-BI-MS SCHIST	N41E	75SE												N60W	67SW		
1453	W	GAR-BI-MS SCHIST	N31E	47SE															
1454	W	MIG MGW	N37E	57SE															
1455	W	GAR-BI-MS SCHIST	N20E	64SE															
1456	W	GAR-BI-MS SCHIST	N42E	83SE															
1457	W	MIG MGW	N46E	89SE															
1458	W	GAR-BI-MS SCHIST	N51E	80SE															
1459	W	MIG MGW	N35E	86SE															
1460	W	GAR-BI-MS SCHIST	N46E	47SE															
1461	W	GAR-BI-MS SCHIST	N21E	60SE															
1462	W	MIG MGW	N48E	71SE															
1463	W	MGW & MIG GAR-BI-MS SC	N51E	82NW															
1464	W	GAR-BI-MS SCHIST	N29E	72NW															
1465	W	MIG MGW	N42E	81SE															
1466	W	R-BI-MS SCHIST & MINOR M	N55E	83SE															
1467	W	IG MGW & GAR-BI-MS SCHI	N34E	75SE															
1468	W	IGW & MINOR GAR-BI-MS S	N46E	81SE															
1469	W	IGW & MINOR GAR-BI-MS S	N23E	69SE															
1470	W	MIG MGW	N44E	83NW												N65W	88NE		
1471	W	GAR-BI-MS SCHIST - MIG	N61E	64NW			3	N42E	N50E	70SE	0-90								
1472	W	THINLY LYRD MIG MGW	N35E	80SE															
1473	W	MIG MGW	N21E	66SE												N57W	70SW		
1474	W	MIG MGW	N34E	70SE															
1475	W	GAR-BI-MS SCHIST	N85E	55SE															
1476	W	GAR-BI-MS SCHIST & MGW	N52E	87SE															
1477	W	GAR-BI-MS SCHIST	N45E	45SE															
1478	W	MIG MGW	N58W	76SW															
1479	W	GAR-BI-MS SCHIST - MIG	N22E	76SE															
1480	W	IGW & INTRLD GAR-BI-MS S	N51E	83SE															
1481	W	MIG GAR-BI-MS SCHIST	N47E	84SE															
1482	W	MIG MGW	N43E	84SE															

			Foliation		Lineation		Fold Axis		Axial Surface		IL	Fold	Fold	Crenulation Axis		Joint		Joint	
Station	Quad	Lithology	Strike	Dip	Plunge	Trend	Plunge	Trend	Strike	Dip	Angle	Genr.	Verg.	Plunge	Trend	Strike	Dip	Strike	Dip
1483	W	) GAR-BI-MS SCHIST & MGW	N25W	46NE												N50W	64SW		
1484	W	GAR-BI-MS SCHIST & MGW	N15E	56SE												N70W	46SW		
1485	W	GAR-BI-MS SCHIST	N75W	68NE												N56W	38SW		
1486	W	FG GAR-BI-MS SCHIST	N52E	70SE												N70W	85NE		
1487	W	GAR-BI-MS SCHIST	N32E	65NW												N65W	86SW		
1488	W	MIG GAR-BI-MS SCHIST	N59E	68NW															
1489	W	I-MS SCHIST & CONTACT W	N80E	68NW															
1490	W	GAR-BI-MS SCHIST	N45E	84NW															
1491	W	BI SCHIST TO A GAR-BI-MS S	N50E	61NW															
1492	W	MGW	N20E	58SE															
1493	W	MIG MGW	N14E	40SE															
1494	W	FG TO MG SEMI SCHIST	N3E	67SE															
1495	W	GAR-BI-MS SCHIST	N11E	70SE															
1496	W	MIG GAR-BI-MS SCHIST	N36E	86SE			20	N30E	N26E	55SE	100								
1497	W	GAR-BI-MS SCHIST	N10E	69NW															
1498	W	GAR-BI-MS SCHIST	N18E	70SE												N81E	71SE		
1499	W	GAR-BI-MS SCHIST	N23E	72NW												N71W	81NE		
1500	W	MIG GAR-BI-MS SCHIST	N12E	65NW															
1501	W	GAR-BI-MS SCHIST	N12E	66SE															
1502	W	MIG GAR-BI-MS SCHIST	N36E	70SE															
1503	W	GAR-BI-MS SCHIST	N28E	76SE															
1504	W	GAR-BI-MS SCHIST & MGW	N45E	85SE															
1505	W	MGW	N25E	66SE															
1506	W	RLD MGW & GAR-BI-MS SCI	N28E	76SE															
1507	W	GAR-BI-MS SCHIST	N15E	73SE												N0W	80SW		
1508	W	LYRD MGW	N2W	41NE												N51W	69SW		
1509	W	MIG MGW	N27W	66NE															
1510	W	-BI-MS SCHIST TO SEMI-SC	N59W	39NE															
1511	W	MIG MGW	N1E	52SE												N85E	83SE		
1512	W	MIG MGW TO A METACGL	N69E	49SE												N70E	88NW		
1513	W	MIG MGW	N11W	52NE															
1514	W	MIG MGW	N14E	61SE															
1515	W	MIG MGW W METACGL LYR	N15W	51NE															
1516	W	MIG MGW W METACGL LYR	N75W	32NE															
1517	W	Y SCHIST - KY ALTERED T	N58W	44NE															
1518	W	R-BI-MS SEMI-SCHIST TO M	N84W	66NE															
1519	W	MIG MGW	N10E	70NW	38	N68E										N16E	87SE		
1520	W	MASSIVE MIG MGW	N85W	70NE												N41W	78NE	N58W	37NE
1521	W	R-MS SCHIST TO SEMI-SCH	N10E	26SE															
1522	W	MIG MGW TO A SEMI-SCHIS	N76E	58NW															
1523	W	MIG MGW	N42E	82SE															
1524	W	CALC-SI & MGW	N84W	57NE												N25W	88NE		
1525	W	GAR-BI-MS SCHIST	N24E	48SE															
1526	W	GAR-BI-MS SCHIST	N28E	76SE															
1527	W	GAR-BI-MS SCHIST	N9E	74SE															
1528	W	RLD MIG MGW & GAR-BI SC	N31E	73SE															
1529	W	MGW	N25E	79NW															
1530	W	MIG MGW	N52E	66SE												N53E	35NW		
1531	W	IG MGW & GAR-BI-MS SCHI	N27E	46SE															
1532	W	IGW & INTRLD GAR-BI-MS S	N33E	82SE															
1533	W	Y LYRD MIG GAR-BI-MS-Q	N30E	86SE															
1534	W	MGW	N18E	82NW															
1535	W	INOR INTRLS OF GAR-BI-M	N35E	84SE															
1536	W	R-BI-MS SCHIS W MS FLAK	N27E	65SE															
1537	W	MGW	N20E	81SE															
1538	W	Y LYRD FG MGW & INTRLS	N37E	85NW															
1539	W	MGW TO A GAR-BI SCHIST	N42E	79SE															
1540	W	GAR-BI-MS SHIST	N58E	75NW															
1541	W	MGW	N21W	24NE															
1542	W	R-BI-MS SEMI-SCHIST & MG	N22E	78SE															
1543	W	MGW	N43E	84NW															
1544	W	MGW	N65E	47NW															
1545	W	MGW	N23E	45SE												N10W	82SW	N79W	64SW
1546	W	MGW	N44E	68NW															
1547	W	MGW & GAR-BI-MS SCHIST	N72E	24NW															
1548	W	MGW & GAR-BI-MS SCHIST	N12E	62SE															
1549	W	MG MGW	N38E	62SE															
1550	W	GAR-BI-MS SCHIST	N38E	74SE															
1551	W	RLD GAR-BI-MS SCHIST & M	N17E	52SE															
1552	W	MGW	N24E	87SE															
1553	W	GAR-BI-MS SCHIST & PEG	N13E	55SE															
1554	W	MGW	N42E	78NW															
1555	W	GAR-BI-MS SCHIST	N60E	84SE															
1556	W	GAR-BI-MS SCHIST	N32E	85SE															
1557	W	MGW TO A BI SCHIST	N44E	60SE															
1558	W	THINLY LYRD MGW	N11E	82SE															
1559	W	-BI-MS SCHIST TO SEMI-SC	N22E	73SE															
1560	W	GAR-BI-MS SCHIST	N45E	85SE															
1561	W	MGW	N8W	65SW															
1562	W	MIG MGW	N16E	63SE															
1563	W	GAR-BI-MS-SIL SCHIST	N7E	53SE															
1564	W	GAR-BI-MS-SIL SCHIST	N18E	60SE												N70W	81SE		
1565	W	GAR-BI-MS SCHIST & MGW	N25E	64W															
1566	W	MGW	N20E	76SE															
1567	W	GAR-BI-MS SCHIST	N3E	68NW															
1568	W	GAR-BI-MS SCHIST	N35E	77NW															
1569	W	MGW	N42E	63SE												N42W	81SW		
1570	W	MGW	N42E	70SE															
1571	W	-BI-MS SCHIST TO SEMI-SC	N23E	81SE															
1572	W	IG MGW & GAR-BI-MS SCHI	N21E	62NW															
1573	W	GAR-BI-MS SCHIST	N27E	74SE												N9W	37SW		
1574	W	MGW	N4W	86NE															
1575	W	W W INTRLD GAR-BI-MS SC	N12W	72NE															
1576	W	MGW & CG BI-MS GTD	N5W	49NE															
1577	W	MGW	N41W	56NE															
1578	W	MGW	N24W	65NE															
1579	W	MGW & BI-QTZ-FELD GN	N20W	54NE															
1580	W	MGW	N22E	89SE															
1581	W	MGW & GAR-BI-MS SCHIST	N68W	57NE															
1582	W	GAR-BI-MS SCHIST	N23E	47NE															
1583	W	GAR-BI-MS SCHIST	N21E	56SE															
1584	W	GAR-BI-MS SCHIST	N22E	61SE															
1585	W	MGW	N28E	53SE															
1586	W	GAR-BI-MS SCHIST	N18E	77SE															
1587	W	GW TO A GAR-BI SEMI-SCHI	N30E	45SE															
1588	W	GAR-BI-MS SCHIST	N15W	47NE												N65E	85SE		
1589	W	MGW	N23W	53NE															
1590	W	GAR-BI-MS SCHIST	N17W	40NW															
1591	W	LIATED CG GTD - MINOR M	N53E	63SE												N42W	62SW	N55W	26NE
1592	W	EAKLY FOLIATED CG P BI G	N71W	36NE															
1593	W	W & MINOR GAR-BI-MS SCI	N54E	50SE															
1594	W	LFIDIC GAR-BI-MS-SIL SCH	N71W	80SW												N82E	70NW		
1595	W	BI-MS SCHIST - GAR-BI-SIL S	N15E	50SE	37	S55E													
1596	W	GAR-BI-SIL SCHIST	N67W	60NE															

Station	Quad	Lithology	Foliation		Lineation		Fold Axis		Axial Surface		IL	Fold	Fold	Crenulation Axis		Joint		Joint	
			Strike	Dip	Plunge	Trend	Plunge	Trend	Strike	Dip	Angle	Genr.	Verg.	Plunge	Trend	Strike	Dip	Strike	Dip
1597	W	MGW	N67W	68NE															
1598	W	GAR-BI-SIL SCHIST	N71W	62SE												N54W	57SW	N32E	65SE
1599	W	MGW	N68E	48NW															
1600	W	MGW	N12W	59SW															
1601	W	MGW	N78E	84NW															
1602	W	AR-BI-QTZ-SIL SCHIST & MG	N81W	30SW															
1603	W	GAR-BI-MS-SIL SCHIST	N18E	56SE															
1604	W	MGW	N44W	62NE															
1605	W	GAR-BI-QTZ-FELD-SIL SCH	N38E	35SE												N54E	84SE		
1606	W	GAR-BI-SIL SCHIST/GN	N38E	80SE															
1607	W	MGW	N33E	49SE												N45W	83SW		
1608	W	GAR-BI-SIL SCHIST	N25W	58NE															
1609	W	MGW	N12E	61SE															
1610	W	GAR-BI-SIL SCHIST & MGW	N36E	55SE															
1611	W	MGW	N42E	70SE															
1612	W	GAR-BI-SIL SCHIST	N56E	72NW	28	N71E													
1613	W	MGW	N21E	50SE															
1614	W	MGW	N17E	61NW															
1615	W	MGW	N77E	51SE															
1616	W	MGW	N13E	45SE															
1617	W	MGW	N24E	51SE															
1618	W	GAR-BI-MS-SIL SCHIST	N17E	84NW															
1619	W	GAR-BI-MS SCHIST & MGW	N15E	58SE															
1620	W	LYRD MGW	N36E	84NW	50	N20E													
1621	W	MGW	N19E	75SE															
1622	W	LYRD MIG MGW	N28E	74SE															
1623	W	R-BI-MS SEMI-SCHIST TO M	N10E	53SE												N52E	72NW		
1624	W	MGW	N32E	83SE															
1625	W	W W MINOR GAR-BI-MS SCI	N35E	45SE												N75W	60SW		
1626	W	MGW	N61E	54SE															
1627	W	MGW	N56E	53SE												N61W	62NE		
1628	W	MGW	N25E	45SE															
1629	W	MGW	N3E	49SE															
1630	W	MGW	N22E	66SE															
1631	W	RD MGW - MS-GAR-BI-QTZ	N15E	34SE															
1632	W	MGW	N66E	53SE												N36W	82NE		
1633	W	MGW	N2W	58NE															
1634	W	THINLY LYRD MGW	N19E	77SE															
1635	W	MGW TO GAR-BI-QTZ-SIL G	N20W	69NE															
1636	W	MS-TALC-TREM SCHIST	N27E	46SE															
1637	W	R-BI-MS SCHIST & MINOR M	N15W	84NE															
1638	W	GAR-BI-MS SEMI-SCHIST T	N6E	60SE															
1639	W	GAR-BI-MS SCHIST	N14W	63NE															
1640	W	MGW	N20W	79NE															
1641	W	LFIDIC GAR-BI-MS-SIL SCH	N11W	55NE	45	S70E										N57E	56NW	N63W	53SW
1642	W	MS-SIL SCHIST W INTRLS (	N5E	90SE															
1643	W	MGW	N12E	54SE															
1644	W	LYRD MGW	N20W	70NE												N76E	80SE		
1645	W	GAR-BI-MS SCHIST	N21E	42SE															
1646	W	R-BI-MS SCHIST TO GN - MG	N8W	70NE															
1647	W	LFIDIC GAR-BI-MS-SIL SCH	N27W	54NE												N81E	78SE	N2W	76SW
1648	W	GAR-BI-MS-SIL SCHIST	N15E	68SE															
1649	W	MIG MGW	N19E	51SE												N59W	88SW		
1650	W	MGW	N7E	67SE															
1651	W	GAR-BI-MS-SIL SCHIST	N16E	36SE															
1652	W	AR-BI-MS-SIL SCHIST - MG	N12E	45SE															
1653	W	MGW	N24E	43SE															
1654	W	GAR-BI-MS-SIL SCHIST	N34W	29NE															
1655	W	GAR-BI-MS-SIL SCHIST	N21W	38NE															
1656	W	MGW	N10W	77NE															
1657	W	MGW	N87W	48NE															
1658	W	MGW	N30W	53NE															
1659	W	-BI-MS-SIL SCHIST & MIG M	N63W	58NE															
1660	W	MGW	N50W	74SW												N81E	32SE		
1661	W	W & MINOR GAR-BI-MS SCI	N85W	54NE															
1662	W	GAR-BI-MS SCHIST	N15E	55SE															
1663	W	THINLY LYRD MGW	N85W	72NE															
1664	W	MGW	N70E	86NW															
1665	W	MGW	N10E	65SE															
1666	W	MGW	N45W	60NE												N54E	78SE		
1667	W	MGW - GAR-BI-MS-SIL SCHIS	N66W	70NE															
1668	W	GAR-BI-MS SCHIST	N10W	41NE															
1669	W	W INTRLD W GAR-BI-MS SC	N38E	72NW															
1670	W	MGW	N53W	78NW															
1671	W	GAR-BI-MS-SIL SCHIST	N78W	58NE															
1672	W	AR-BI-MS-SIL SCHIST & MG	N42W	75NE															
1673	W	GAR-BI-MS-SIL SCHIST	N50W	51NE															
1674	W	GAR-BI-MS SCHIST	N89W	66NE												N16E	87NW		
1675	W	-MS-QTZ SCHIST W CG MS I	N87E	77SE															
1676	W	MGW	N75W	51NE															
1677	W	AR-BI-MS-SIL SCHIST & MG	N80W	67NE															
1678	W	GAR-BI-MS SCHIST	N50W	64NE															
1679	W	MGW & GAR-BI-MS SCHIST	N42W	70NE															
1680	W	MIG BI-PLAG GN	N5E	72SE															
1681	W	MIG BI-PLAG GN	N30W	65NE															
1682	W	BI-MS SCHIST W CG MS FL	N27W	47NE															
1683	W	MIG BI-PLAG GN TO BI GG	N25W	40NE															
1684	W	MIG BI GN	N16W	25NE												N44E	85SE		
1685	W	MIG BI GN	N14W	40NE															
1686	W	MIG BI GN	N42W	55NE															
1687	W	MIG BI GN	N35W	65SW															
1688	W	MGW	N2E	68NW															
1689	W	GAR-BI-MS SCHIST	N28W	64SW															
1690	W	MGW	N82W	58SW															
1691	W	MGW	N68W	78NE															
1692	W	GAR-BI-SIL SCHIST	N86E	76NW	47	N68E													
1693	W	MGW	N54W	60SW															
1694	W	MIG MGW TO A MCGL	N62W	68NE															
1695	W	MGW	N26W	70NE															
1696	W	GAR-BI-SIL SCHIST & MGW	N79W	74SW	56	S28E										N86W	86SW		
1697	W	MGW W CALC-SI INTRLS	N27W	42NE															
1698	W	MGW	N62W	55NE												N10W	83SW		
1699	W	GAR-BI-MS-SIL SCHIST	N50W	56NE															
1700	W	MGW	N80W	73NE												N72W	58NE		
1701	W	MGW	N65W	71NE															
1702	W	GAR-BI-MS SCHIST & MGW	N40W	59NE															
1703	W	MGW	N85W	48SW															
1704	W	GL INTRLD W QTZ GRANUI	N39E	65SE												N48W	79NE		
1705	W	MGW & GAR-BI-MS SCHIST	N46E	72SE															
1706	W	MGW	N37E	59SE															
1707	W	MGW	N36E	64SE															
1708	W	R-BI-MS SCHIST & MINOR M	N22E	76SE															
1709	W	GAR-BI-MS SCHIST					19	N11W	N5W	84SW	90								
1710	W	MIG - GAR-BI-MS-SIL SCHIS	N37E	86NW												N27E	88SE		

			Foliation		Lineation		Fold Axis		Axial Surface		IL	Fold	Fold	Crenulation Axis		Joint		Joint	
Station	Quad	Lithology	Strike	Dip	Plunge	Trend	Plunge	Trend	Strike	Dip	Angle	Genr.	Verg.	Plunge	Trend	Strike	Dip	Strike	Dip
1711	W	MGW	N20E	73SE															
1712	W	IGW & GAR-BI-MS-SIL SCHIS	N8W	44SW															
1713	W	MGW	N9W	56NE															
1714	W	TALC TREMOLITE SCHIST	N32E	24NW															
1715	W	CHLORITE SCHIST	N53E	44NW															
1716	W	MGW	N20E	53SE												N66W	54SE		
1717	W	GAR-BI-MS SCHIST	N10E	39SE															
1718	W	THINLY LYRD MGW	N60E	34SE															
1719	W	MIG BI GN	N62E	63SE															
1720	W	MIG BI GN	N74E	37SE			32	S52E	N32E	32SE	100-50								
1721	W	MIG BI GN	N48E	47SE												N18W	72SW	N81E	79SE
1722	W	SAP - MIG MGW W/ AM POD	N75W	49NE															
1723	W	DARK GREY MGW	N42E	85SE															
1724	W	DARK GREY MIG MGW	N45E	83SE												N75W	83SW		
1725	W	W & MINOR GAR-BI-MS SCI	N46E	82SE															
1726	W	MIG MGW	N42E	90SE															
1727	W	MIG MGW	N77E	80NW			32	N42E	N61E	71NW	10-30								
1728	W	IIG MGW & INTRLD MIG H-(	N32E	90SE															
1729	W	MGW	N10E	76SE												N82W	83NE		
1730	W	MGW	N16E	82SE															
1731	W	MGW	N10E	72NW															
1732	W	MGW	N80W	52NE															
1733	W	MIG BI GN	N20E	75SE															
1734	W	MIG BI GN	N30E	46SE															
1735	W	SAP - GAR-BI-MS SCHIST	N78W	75NE															
1736	W	IIG GAR-BI-MS SCHIST - MG	N26E	74SE															
1737	W	MGW	N39W	49NE															
1738	W	MGW	N2W	74NE															
1739	W	MGW	N8W	57NE															
1740	W	MGW	N16E	46SE												N68W	74SW		
1741	W	MGW	N5W	52NE												N80E	90		
1742	W	MGW	N5E	51NW												N90E	76NW		
1743	W	MGW	N34W	56SW															
1744	W	MGW	N51E	32SE															
1745	W	MGW	N62W	62SW															
1746	W	DARK GREY MIG MGW	N24W	67SW															
1747	W	DARK GREY MIG MGW	N70W	46SW															
1748	W	DARK GREY INEQ MIG MGV	N34W	56NE															
1749	W	MIG GAR-BI-MS SCHIST	N32W	81NE															
1750	W	GAR-BI-MS SCHIST	N70E	42SE															
1751	W	GAR-BI-MS SCHIST	N60E	72NW															
1752	W	MIG INEQ MGW	N40W	70SW															
1753	W	MIG GAR-BI-MS SCHIST	N82W	41NE															
1754	W	FLOAT- KY-GBM SCHIST																	
1755	W	KY-GAR-BI-MS SCHIST	N75E	50SE															
1756	W	MGW	N65E	78SE															
1757	W	2 MICA MGW	N65E	60NW															
1758	W	GAR-BI-MS SCHIST	N23E	52NW															
1759	W	IG GAR-BI-MS SCHIST & MG	N10W	60SW															
1760	W	GAR-BI-MS SCHIST	N38E	90SE															
1761	W	AR-BI-MS SCHIST & MIG MG	N57W	53NE															
1762	W	MIG MGW	N27W	76NE															
1763	W	MGW	N13W	77NE												N76E	86SE		
1764	W	MIG BI GN W AM PODS	N50E	89NW															
1765	W	INTRLD MIG FELD GN	N42W	23NE			15	S21E	N19W	25NE	0								
1766	W	MIG BI GN	N15W	81NE	35	N9W													
1767	W	LYRD MIG BI GN	N39W	70NE															
1768	W	TYLO MIG GAR-BI-MS SCHIS	N18E	50SE															
1769	W	MIG BI GN W AM LENSES	N10W	22NE															
1770	W	MIG AM & BI GNEISS					33	N70E				SHEATH FOLD							
1771	W	BI-FELD GN TO FELD MGW	N37E	79SE															
1772	W	MIG MGW	N47E	83NW															
1773	W	MIG MGW	N56W	42NE															
1774	W	MIG MGW	N77W	42NE												N82E	84SE		
1775	W	MIG MGW	N70W	28NE															
1776	W	MIG MGW TO MGW	N33W	24NE															
1777	W	MIG MGW	N28W	32NE															
1778	W	MIG MGW TO MGW	N45W	59NE															
1779	W	GAR-BI-MS SCHIST	N38W	28NE												N74E	84NW		
1780	W	MYLO MGW	N55W	42NE															
1781	W	GAR-BI-SIL SCHIST	N38W	78NE												N76E	77NW		
1782	W	GAR-BI-SIL SCHIST	N88W	68SW	7	N83E													
1783	W	MGW	N52W	52NE															
1784	W	MIG - MIG MGW	N85W	90NE												N39E	79SE		
1785	W	MGW	N52W	78NW															
1786	W	GAR-BI SCHIST	N70W	27NE															
1787	W	MGW	N70W	58NE															
1788	W	MGW & GAR-BI-MS SCHIST	N54W	36NE															
1789	W	GAR-BI-SIL SCHIST	N48W	78NE															
1790	W	GAR-BI-SIL SCHIST	N88W	53NE															
1791	W	GAR-BI-SIL SCHIST	N69W	69NE															
1792	W	GAR-BI-MS SCHIST	N85W	81NE															
1793	W	MIG BI GN W PODS OF AM	N88E	68SE															
1794	W	MGW	N11W	38NE												N71E	88SE	N37W	84SW
1795	W	GAR-BI-MS-SIL SCHIST	N58E	23NW												N48W	58SW		
1796	W	MGW - MIG W CALC SI POD	N65W	49NE															
1797	W	GAR-BI-MS-SIL SCHIST	N78W	61NE															
1798	W	MGW	N77W	40NE															
1799	W	MGW	N78E	32NW												N24E	75NW	N89E	65SE
1800	W	ALTERED ULTRAMAFIC	N37W	67SW												N12W	50NE	N52E	32SE
1801	W	MGW & GAR-BI-MS SCHIST	N52W	49NE															
1802	W	MGW	N79E	26SE															
1803	W	GAR-BI-MS SCHIST & MGW	N52W	40SW															
1804	W	MGW	N88W	16NE															
1805	W	MGW	N74W	30NE															
1806	W	MGW & GAR-BI-MS SCHIST	N88E	34NW															
1807	W	MGW & INTRLD SCHIST	N54W	37NE															
1808	W	MGW	N75W	58SW															
1809	W	MGW	N18W	38SW															
1810	W	GAR-BI-MS SCHIST	N77W	40SW												N12W	81NE		
1811	W	MGW	N46W	51SW															
1812	W	GAR-BI-MS-SIL GN	N68W	53SW	16	S58E										N19E	72SE		
1813	W	MIG MGW	N29W	65SW															
1814	W	IGW TO A GAR-BI-MS-SIL G	N58W	42SW															
1815	W	-BI-MS SIL SCHIST & GAR M	N64W	48SW												N39E	79NW		
1816	W	GAR-BI-MS-SIL SCHIST	N84E	86SE															
1817	W	MGW	N55E	56SE															
1818	W	GAR-BI-MS-SIL SCHIST	N62W	62SW															
1819	W	MIG MGW	N65W	86NE															
1820	W	MGW	N34W	80NE															
1821	W	AR-BI-MS-SIL-KF GN - SIL 2 (	N65W	67SW												N8E	81NW		
1822	W	GAR-BI-MS-SIL SCHIST	N87W	86NE															
1823	W	MGW	N59W	53NE															
1824	W	GAR-BI-MS-SIL SCHIST	N75W	62SW															

			Foliation		Lineation		Fold Axis		Axial Surface		IL	Fold	Fold	Crenulation Axis		Joint		Joint	
Station	Quad	Lithology	Strike	Dip	Plunge	Trend	Plunge	Trend	Strike	Dip	Angle	Genr.	Verg.	Plunge	Trend	Strike	Dip	Strike	Dip
1825	W	MIG MGW	N71W	53SW															
1826	W	GAR-BI-MS-SIL SCHIST	N64W	36SW															
1827	W	AR-BI-MS SCHIST & MIG MG	N87E	26SE															
1828	W	GAR-BI-MS-SIL SCHIST	N40W	51SW															
1829	W	GAR-BI-MS-SIL SCHIST	N60W	38SW	6	N72W										N58E	75NW	N59E	85SE
1830	W	S SCHIST TO MGW TO A GAI	N44W	60SW															
1831	W	MS PEG IN GBM SCHIST & M	N31W	54SW												N88E	54NW	N5E	82NW
1832	W	GAR-BI-MS-SIL 2 GN	N62W	37NE	22	N52W													
1833	W	MIG GAR-BI-MS-SIL SCHIST	N51W	56NE															
1834	W	GAR-BI-MS SCHIST	N88E	39SE															
1835	W	MGW	N41W	40SW												N42E	70NW		
1836	W	MGW	N65W	30NE															
1837	W	MGW	N65W	37SW															
1838	W	IIG MGW TO A MIG BI SCHIS	N79W	34SW															
1839	W	GAR-BI-MS-SIL 2 GN	N80E	15SE															
1840	W	GAR-BI-MS-SIL 2 GN	N41W	44SW	13	S33E													
1841	W	GAR-BI-MS-KF-SIL 2 GN	N32W	53SW															
1842	W	GAR-BI-MS-? SIL GN	N76W	75SW															
1843	W	GAR-BI-MS-? SIL GN	N59W	53SW												N45E	76SE		
1844	W	GAR-BI-MS-? SIL GN	N54W	63NE												N58E	65SE		
1845	W	GAR-BI-KF-SIL GN	N80E	72SE															
1846	W	GAR-BI-MS-KF-SIL GN	N54W	38NE												N45W	84SW	N40E	76SE
1847	W	GAR-BI-MS-SIL GN	N80E	68SE												N37W	77NE		
1848	W	W & GAR-BI-MS-KF-SIL SCI	N36W	55NE												N15W	60SW		
1849	W	GAR-BI-MS SCHIST	N30W	37NE															
1850	W	MIG MGW	N36W	31NE												N42E	81NW		
1851	W	MIG MGW	N48W	25NE															
1852	W	MS-KF-SIL SCHIST W MGW	N78W	44NE															
1853	W	GAR-BI-MS GG TO A PEG	N62W	45NE															
1854	W	MGW	N75W	72NE															
1855	W	MGW & QTZ MS PEG	N36W	86SE															
1856	W	MGW	N65W	40SW															
1857	W	GAR-BI-MS-SIL SCHIST	N87W	77NE															
1858	W	GAR-BI-MS-KY SCHIST	N68W	40NE												N60E	85NW		
1859	W	MGW W CALC-SI	N79W	50NE	25	N52E										N25E	27SE		
1860	W	AR-BI-MS-SIL SCHIST & MIG	N43W	49NE												N56W	51SW	N66E	60SE
1861	W	MGW & CALC-SI	N89E	70NW															
1862	W	MGW	N88E	44NW															
1863	W	MGW	N31W	29NE															
1864	W	MGW - MIG MGW	N40W	92NE												N51E	84SE		
1865	W	MIG MGW	N10E	11SE															
1866	W	IG MGW & GAR-BI-MS SCHI	N11E	47SE															
1867	W	MIG MGW	N53W	80SW															
1868	W	MIG GAR-BI-MS SCHIST	N35W	76NE															
1869	W	GAR-BI-MS-KY SCHIST	N85E	50SE															
1870	W	GAR-BI-MS-KY SCHIST	N46W	62NE	17	N14W										N70E	68SE	N30W	59NE
1871	W	GAR-BI-MS-SIL SCHIST	N38W	53SW	13	S31E										N65W	65NE		
1872	W	GAR-BI-MS-KF-SIL 2 GN	N85E	37SE												N69W	87SW		
1873	W	GAR-BI-KF-SIL 2 GN	N49W	27SW															
1874	W	AR-BI-MS-SIL SCHIST & MG	N9W	47NE												N17W	85SW	N88E	74SE
1875	W	GW & GAR-BI-MS-KF-SIL 2 G	N21W	52SW	16	N35W													
1876	W	MGW & GAR-BI-KF-SIL GN	N0W	35SW												N48E	62SE	N34W	79NE
1877	W	GAR-BI GG & MGW	N50W	32SW															
1878	W	MGW	N68W	65SW												N12E	77SE		
1879	W	R-BI-MS SCHIST TO A MIG M	N86E	78SE															
1880	W	MIG MGW	N54W	21NE												N62W	88SW		
1881	W	/ W CALC-SI & GAR-BI-MS-S	N74W	36NE												N35W	58SW		
1882	W	MIG MGW	N86W	33NE												N35E	74SE		
1883	W	MGW	N72W	34NE															
1884	W	MIG GAR-BI-MS-SIL SCHIST	N59W	47SW															
1885	W	-BI-MS-SIL SCHIST & BI-MS	N44W	45NE															
1886	W	CG GAR-BI-MS SCHIST	N60W	86NE															
1887	W	MIG MGW & BI GTD	N75W	50NE															
1888	W	FG GAR-BI-MS SCHIST	N82E	35NW															
1889	W	MIG MGW	N61W	65NE															
1890	W	BI GG	N76W	61NE															
1891	W	BI-MS PEG	N41W	78NE															
1892	W	BI-MS PEG	N64W	82SW												N31E	62SE		
1893	W	GAR-BI-MS-SIL SCHIST	N44W	69NE															
1894	W	GAR-BI-KF-SIL GN	N37W	62SW	18	N54W										N4E	82SE		
1895	W	MGW	N76W	74SW												N29E	71NW		
1896	W	GAR-BI-KF-SIL GN	N67W	63SW	11	S75E													
1897	W	MIG MGW	N56W	56SW															
1898	W	MIG MGW	N11E	84NW															
1899	W	MIG MGW	N34W	32NE															
1900	W	MIG MGW	N74W	61SW															
1901	W	MIG MGW	N79W	61NE															
1902	W	GAR-BI-MS-SIL SCHIST	N87W	52NE												N36W	31SW		
1903	W	GAR-BI-MS-SIL SCHIST	N64W	47NE															
1904	W	MIG MGW & GAR-BI-MS-SIL	N76W	55NE															
1905	W	GAR-BI-MS-SIL SCHIST	N88E	46SE															
1906	W	R-BI-MS-SIL SCHIST & MIG M	N54W	51NE															
1907	W	SIL BEARING MGW	N66W	58NE												N27E	68NW		
1908	W	GAR-BI-SIL GN TO MGW	N11E	56SE															
1909	W	MGW	N39W	76NE															
1910	W	MIG MGW	N11W	48NE															
1911	W	MGW	N88E	40SE															
1912	W	GW INTRLD W GAR-BI-MS S	N47W	35NE												N26E	81NW	N2E	73SE
1913	W	MIG MGW	N50W	56NE															
1914	W	MGW & GAR-BI-MS SCHIST	N46W	82SW															
1915	W	GAR-BI-MS-SIL SCHIST	N26E	35SE															
1916	W	MGW	N41W	46SW												N36E	68SE		
1917	W	R-BI-MS-SIL SCHIST TO SIL 2 GN														N36W	68SW		
1918	W	GAR-BI-KF-SIL 2 GN	N17W	52SW												N80W	81SW		
1919	W	MIG MGW	N88W	59NE												N17W	86NE		
1920	W	MGW	N83W	87NE															
1921	W	AR-BI-MS-SIL SCHIST & MG	N40W	54SW															
1922	W	MGW	N48W	35SW												N16W	70NE		
1923	W	MGW	N63W	61SW												N27E	71SE		
1924	W	MGW	N71W	39SW												N23W	48SW		
1925	W	GW - INTRLD GAR-BI-KF-SIL	N54W	60SW															
1926	W	GAR-BI-KF-SIL GN	N64W	60SW															
1927	W	W INTRLD W GAR-BI-MS SC	N63W	71SW															
1928	W	MYLONITIC MIG. MGW	N88E	52NW	52	N12E													
1929	W	ITIC MIG. BI-PLAG-QUARTZ	N68E	83NW															
1930	W	FELSIC BI GNEISS	N89E	62NW	45	N61W													
1931	W	LONITIC MIG BI-PLAG-GNE	N64E	64NW															
1932	W	MIG. BI-PLAG GNEISS	N64E	73NW															
1933	W	MGW	N14E	82NW															
1934	W	MGW TO MIG. MGW	N66E	79NW															
1935	W	YLONITIC GAR-BI-MS SCHI	N73E	80SE															
1936	W	GBM-SIL. SCHIST	N79W	43NE															
1937	W	MGW & GAR-BI-MS SCHIST	N78E	62NW															
1938	W	MIG. BI-PLAG GNEISS	N51E	89SE															

			Foliation		Lineation		Fold Axis		Axial Surface		IL	Fold	Fold	Crenulation Axis		Joint		Joint	
Station	Quad	Lithology	Strike	Dip	Plunge	Trend	Plunge	Trend	Strike	Dip	Angle	Genr.	Verg.	Plunge	Trend	Strike	Dip	Strike	Dip
1939	W	MIG. BI-PLAG GNEISS	N41E	69NW															
1940	W	MS GRANITIC GNEISS TO AI	N44E	56NW															
1941	W	MGW & GBM SCHIST	N32E	85SE															
1942	W	MIG. BI GNEISS	N38E	49SE															
1943	W	MIG. BI GNEISS	N15W	76NE															
1944	W	GNEISS WITH AM PODS & AC	N24E	38SE															
1945	W	MIG BI GNEISS	N3E	32SE															
1946	W	BI GTD	N82E	77NW															
1947	W	LONITIC MS-FELD-QTZ-GNI	N89E	21SE	11	S44W													
1948	W	G BI GNEISS TO FELSIC GNE	N76W	81SW															
1949	W	MGW	N10W	73SW															
1950	W	MGW	N6E	61NW			15	N10W	N4W	44SW	0-10								
1951	W	GAR-GI-FELD-SIL2 GNEISS	N52W	57NE															
1952	W	GNEISS- GAR-BI-SIL-FELD G	N41W	60NE												N50E	89SE		
1953	W	MGW & SIL2 GNEISS	N16W	49SW	7	N32W													
1954	W	MGW WITH KY & SIL	N29W	57SW															
1955	W	GW TO SCHISTOSE MGW, MI	N56W	43SW												N54E	60SE	N25W	73SW
1956	W	SCHISTOSE MGW	N22W	33SW												N74E	82NW	N41W	81NE
1957	W	MIG MGW/GNEISSIC MGW	N34W	26SW															
1958	W	MGW	N41W	34SW															
1959	W	MGW	N46W	29SW															
1960	W	MGW	N53W	52SW			12	N48W	N81W	30NE	90-100								
1961	W	MGW	N49W	35SW															
1962	W	MGW	N20E	56NW															
1963	W	NGW	N14W	35SW															
1964	W	GAR-BI-MS-SIL SCHIST	N72W	68SW															
1965	W	MGW	N30W	53SW															
1966	W	MGW	N81E	38NW															
1967	W	R-BI-SIL-FELD GNEISS & M	N24W	37SW															
1968	W	BI GNEISS TO MASSIVE SC	N59E	87SE															
1969	W	GAR-BI-MS-SIL2 GNEISS	N84W	32NE															
1970	W	MGW	N81W	37NE															
1971	W	MS-GAR-BI-FELD-SIL GNEIS	N73W	47NE															
1972	W	GAR-BI-FELD-SIL2 GNEISS	N76W	39NE															
1973	W	GAR-BI-FELD-SIL2 GNEISS	N46W	39SW															
1974	W	GAR-BIFELD-SIL2 GNEISS	N82W	78SW															
1975	W	GAR-BI-FELD-SIL2 GNEISS	N31W	23SW												N44W	68SW	N79E	85NW
1976	W	MGW & TDJ	N15W	31SW															
1977	W	GAR-BI-FELD-SIL2 GNEISS	N22W	27SW															
1978	W	GAR-BI-FELD-SIL2 GNEISS	N14W	27NE															
1979	W	MGW & SIL2 GNEISS	N36W	68NE															
1980	W	IIG GAR-BI-FELD-SIL2 GNEI	N46W	40SW															
1981	W	MGW & MIG SIL2 GNEISS	N49W	52SW															
1982	W	GAR-BI-FELD-SIL2 GNEISS	N36W	49SW															
1983	W	MGW	N47W	78SW															
1984	W	MGW	N78W	60SW															
1985	W	R-BI-FELD-SIL2 GNEISS & M	N69W	51NE															
1986	W																		
1987	W																		
1988	W																		
1989	W																		
1990	W																		
1991	W																		
1992	W																		
1993	W																		
1994	W																		
1995	W																		
1996	W																		
1997	W																		
1998	W																		
1999	W																		
2000	W																		
2001	W																		
2002	W																		
2003	W																		
2004	W																		
2005	W																		
2006	W																		
2007	W																		
2008	W																		
2009	W																		
2010	W																		
2011	W																		
2012	W																		
2013	W																		
2014	W																		
2015	W																		
2016	W																		
2017	W																		
2018	W																		
2019	W																		
2020	W																		
2021	W																		
2022	W																		
2023	W																		
2024	W																		
2025	W																		
2026	W																		
2027	W																		
2028	W																		
2029	W																		
2030	W																		
2031	W																		
2032	W																		
2033	W																		
2034	W																		
2035	W																		
2036	W																		
2037	W																		
2038	W																		
2039	W																		
2040	W																		
2041	W																		
2042	W																		
2043	W																		
2044	W																		
2045	W																		
2046	W																		
2047	W																		
2048	W																		
2049	W																		
2050	W																		
2051	W																		
2052	W																		

APPENDIX II

Structural Measurements and Outcrop Descriptions from the Sam Knob 7.5-minute Quadrangle

Note: Stations correspond to locations shown in Plate 2. Lithologic descriptions are in field shorthand.

ABBREVIATIONS

Minerals

BI	-	Biotite
CHL	-	Chlorite
E	-	Epidote
FELD	-	Feldspar
GAR	-	Garnet
H	-	Hornblende
KY	-	Kyanite
M	-	Muscovite
QTZ	-	Quartz
SIL	-	Sillimanite
TM	-	Tourmaline

Rock Types

AM	-	Amphibolite
CALC-SI	-	Calc-silicate
GG	-	Granitic gneiss
GTD	-	Granitoid
LEUCO	-	Leucocratic
(M)	-	Mylonite
MGW	-	Metagraywacke
(P)	-	Protomylonite
PEG	-	Pegmatite
QTZITE	-	Quartzite

Textures

INEQ	-	Inequigranular
MEGAC	-	Megacrystic
MIG	-	Migmatitic
MYLO	-	Mylonitic
P	-	Porphyroblastic

			Foliation		Lineation		Fold Axis		Axial Surface		IL	Fold	Fold	Crenulation Axis		Joint		Joint	
Station	Quad	Lithology	Strike	Dip	Plunge	Trend	Plunge	Trend	Strike	Dip	Angle	Genr.	Verg.	Plunge	Trend	Strike	Dip	Strike	Dip
1	SK	MGW W GAR-BI-QTZ-FELD	N37E	50NW												N47W	82SW		
2	SK	MGW & GAR-BI-MS SCHIST	N5E	83SE															
3	SK	GAR RICH MGW	N49W	66SW															
4	SK	GAR-BI-MS SCHIST TO MGW	N27W	47NE															
5	SK	GAR-BI-QTZ-FELD GN/MGW	N5W	58NE															
6	SK	MGW & GAR-BI-MS SCHIST	N16W	57NE															
7	SK	W - MIG W GAR-BI-PLAG-Q	N5W	43SW															
8	SK	TRLD MGW & CG BI-MS SCH	N35W	43NE															
9	SK	MIG GAR-MS-BI-SIL SCHIST	N11E	51SE															
10	SK	BI-MS-SIL SCHIST W MGW	N43E	71SE	57	N42E													
11	SK	GAR-BI-SIL SCHIST	N61E	44NW															
12	SK	MGW - BI-QTZ-FELD GN	N75W	43SW															
13	SK																		
14	SK	MIG MGW	N28E	80NW			30	S47E	N42E	83NW	0					N65E	85NW		
15	SK	MIG MGW/BI GN	N41E	79SE															
16	SK	MIG BI GN/MGW	N20E	62NW			23	N10E	N10E	90SE	40					N55W	85NE		
17	SK	CHIST & SOME GAR-MS-SIL	N5E	75SE	20	S20W													
18	SK	LYRD SULFIDIC MGW	N38E	76NW															
19	SK	MGW - MS-BI-QTZ-FELD GN	N38E	72NW															
20	SK	MIG BI GN/MGW	N62E	44NW															
21	SK	REY MIG MGW/BI-FELD-QT	N30E	75NW															
22	SK	S SIL SCHIST TO A GAR-BI-S	N35E	73NW															
23	SK	DK GREY MIG MGW	N62E	44NW															
24	SK	BI-MS-CHL SCHIST	N41E	73SE															
25	SK	GAR-BI-MS-CHL SCHIST	N35E	60SE															
26	SK	MIG MGW - MS-GAR-BI-FEL	N65E	35NW															
27	SK	DK GREY MIG MGW	N35E	59NW															
28	SK	DK GREY MIG MGW	N39E	78NW															
29	SK	MIG MGW	N36E	47SE															
30	SK	DK GREY MIG MGW	N42E	50NW												N24W	72NE		
31	SK	DK GREY MGW	N59E	5NW															
32	SK	GAR-BI-MS SCHIST	N54E	74NW															
33	SK	GAR-BI-MS SCHIST	N45E	79NW	14	N35E													
34	SK	GAR-BI-MS SCHIST	N44E	80NW												N60W	86SW		
35	SK	MIG INEQ MGW	N51E	51NW															
36	SK	DK GREY MIG MGW	N47E	67NW												N20W	89NE		
37	SK	MIG MGW - BI-QTZ GN	N84E	57NW															
38	SK	T QUARTZ TOURMALINE SCHIST																	
39	SK	DK GREY MIG MGW	N54E	35NW															
40	SK	DK GREY MIG MGW	N56E	51NW															
41	SK	MIG MGW	N32E	72SES															
42	SK	MIG MGW	N32E	72NW															
43	SK	MIG MGW	N58E	55NW															
44	SK	MIG MGW	N52E	60NW												N56W	60SW		
45	SK	MIG MGW	N42E	82NW												N35W	85SW	N18E	65NW
46	SK	MIG MGW - DK GN	N17E	42NW															
47	SK	MIG MGW	N29E	53NW															
48	SK	DK GREY MIG MGW	N38E	68SE															
49	SK	DK GREY MIG MGW - BI RIC	N35E	36NW															
50	SK	DK MIG MGW - BI RICH	N42E	31NW															
51	SK	MGW - MS-GAR-BI-QTZ GN	N44E	84SE															
52	SK	MGW & GAR-BI-MS SCHIST	N24E	57NW															
53	SK	MIG MGW	N56E	45NW															
54	SK	ETAPYX W LARGE CHL FLA	N10E	50SE															
55	SK	SULFIDIC FG AM	N30E	35NW															
56	SK	MGW	N30E	63NW															
57	SK	DK GREEN H-CHL SCHIST	N5E	46NW															
58	SK	MIG MGW	N38E	56NW												N55W	75NE		
59	SK	MGW	N39E	38NW															
60	SK	MIG MGW	N42E	90W															
61	SK	SAP MIG MGW	N18E	77SE															
62	SK	DK GREY MGW - BI RICH	N17E	58SE															
63	SK	MGW - BI RICH	N58E	89NW															
64	SK	MGW & PEG	N5E	69SE															
65	SK	MGW	N58E	62NW															
66	SK	MGW - BI RICH	N48E	77NW															
67	SK	BI-MS-SIL SCHIST INTRLD W	N46E	81NW												N46E	81NW	N60E	60NW
68	SK	MGW	N61E	34NW															
69	SK	IGW & MINOR MIG BI GAR S	N51E	54NW	37	N25E	N27E	65NW	70-30				SE						
70	SK	AR-BI-MS SCHIST & GAR MG	N31E	90															
71	SK	MGW	N75E	72NW															
72	SK	MGW - MS	N11E	90															
73	SK	MGW - MS	N34E	83SE															
74	SK	GAR-BI-MS-SIL SCHIST	N42E	77NW															
75	SK	GAR-BI-MS SCHIST & MGW	N50E	80NW															
76	SK	Y LYRD AM GN - SLIGHTLY	N33E	66SE												N64W	45SW		
77	SK	GAR-BI-SIL SCHIST	N70E	55NW															
78	SK	MGW	N42E	78NW															
79	SK	MGW - W MS	N85E	72NW												N69E	88SE	N25W	83SW
80	SK	GAR-BI-MS-SIL SCHIST	N46E	62NW	22	N62W													
81	SK	GAR-BI-SIL SCHIST	N80W	75NE															
82	SK	GAR-BI-SIL SCHIST	N58E	66NW															
83	SK	MGW - DK GREY MGW	N26W	64NE															
84	SK	AR-BI-SIL SCHIST - SULFIDI	N19W	40NE												N64E	87NW		
85	SK	GAR-BI-MS SCHIST	N89W	46NE												N46E	67NW		
86	SK	MGW - DK GREY MIG	N36E	65NW															
87	SK	DARK GARY MIG. MGW	N38E	72NW												N23W	76NE		
88	SK	RLD MGW & GAR-BI-MS SCI	N28E	86NW			67	S72W	N28E	73NW	70								
89	SK	AR-BI-MS-SIL SCHIST & MG	N22E	48NW															
90	SK	MGW	N32E	73NW															
91	SK	GAR-BI-MS SCHIST	N21E	72NW															
92	SK	MIG MGW	N38E	83NW															
93	SK	LY LYRD MGW - SLIGHTLY	N27E	87NW															
94	SK	MIG GAR-BI-MS SCHIST	N5E	31NW															
95	SK	MIG MGW	N37E	74NW												N85W	82SW		
96	SK	MGW	N32E	83NW															
97	SK	MGW	N34E	90															
98	SK	MGW	N40E	64NW												N62E	76NW		
99	SK	THINLY LYRD MGW	N13E	35NW															
100	SK	MGW W MINOR PODS OF AM	N39E	59NW															
101	SK	MIG GAR-BI-MS SCHIST	N48E	51NW															
102	SK	IGW MIG GAR-BI-MS SCHIS	N31E	38NW															
103	SK	GAR-BI-MS SCHIST	N52E	53NW															
104	SK	W & SOME GAR-BI-MS SCI	N19E	42NW															
105	SK	MYLO MGW	N43E	68NW															
106	SK	MGW	N37E	84SE															
107	SK	MGW	N44E	77NW															
108	SK	GAR-BI-MS SCHIST	N42E	80NW															
109	SK	MGW	N41E	66NW												N76E	73NW	N80E	12SE
110	SK	GAR-BI-MS SCHIST	N32E	83NW															
111	SK	MGW	N43E	76NW															
112	SK	GAR-BI-MS SCHIST	N15E	83SE															
113	SK	MGW	N33E	70NW															
114	SK	MGW	N34E	85SE												N71E	64SE		

			Foliation		Lineation		Fold Axis		Axial Surface		IL	Fold	Fold	Crenulation Axis		Joint		Joint	
Station	Quad	Lithology	Strike	Dip	Plunge	Trend	Plunge	Trend	Strike	Dip	Angle	Genr.	Verg.	Plunge	Trend	Strike	Dip	Strike	Dip
115	SK	MGW	N34E	90															
116	SK	MGW	N11E	90SE															
117	SK	MGW TO BI GN	N11E	90SE															
118	SK	MGW TO A DK GREY MGW	N51E	76NW															
119	SK	MGW	N46E	62NW															
120	SK	DK GREY BI RICH MIG MGW	N26E	63NW															
121	SK	DK MIG MGW	N25E	81NW															
122	SK	DK MIG MGW TO MGW	N26E	77SE															
123	SK	MIG MGW - DK GREY	N90E	81SE															
124	SK	MIG MGW - THINLY LYRD	N71W	72NE															
125	SK	MIG DK MGW	N58W	49NE															
126	SK	MIG MGW	N70E	81NW															
127	SK	DK MIG MGW	N76E	73NW															
128	SK	DK MIG MGW	N50E	74NW															
129	SK	DK MIG MGW	N20E	56SE												N87E	71NW		
130	SK	DK MIG MGW	N35E	62NW															
131	SK	K MIG MGW - ISOCLINAL FO	N494E	71NW			23	N40E	N49E	71NW	0-10								
132	SK	DK MIG MGW	N54E	71NW															
133	SK	MIG MGW - OPEN FOLD	N49E	74NW			45	N49E	N35E	90	100-120								
134	SK	MIG MGW	N40R	63NW															
135	SK	MIG MGW	N39E	74NW															
136	SK	MIG MGW	N27E	80SE			32	N32E	N30E	75SE	0-10								
137	SK	MYLO MIG MGW	N41E	70NW															
138	SK	MYLO MIG MGW	N46E	82SE															
139	SK	MIG MGW - SLIGHTLY MYL	N32E	71NW															
140	SK	MIG MGW - SLIGHTLY MYL	N47E	60NW															
141	SK	MIG MGW	N34E	58NW															
142	SK	O CHL-GAR-BI SCHIST & MI	N44E	71NW															
143	SK	SCHIST & MIG MGW & INTI	N65E	78NW			33	N48E	N45E	66NW	0-10								
144	SK	MIG BI GN	N35E	51NW															
145	SK	MIG MGW - DK GN	N16E	56NW															
146	SK	BI MGW - W INTRLS OF CA	N39E	84SE			47	N38E	N49E	82NW	0-10								
147	SK	MGW	N64E	80SE															
148	SK	MGW	N42E	64SE												N56W	78SW		
149	SK	GAR-BI-MS SCHIST	N12E	73NW															
150	SK	W & GAR-BI-MS SCHIST INT	N10E	56NW															
151	SK	R-BI-MS SCHIST & MINOR M	N14E	78SE															
152	SK	MGW & GAR-BI-MS SCHIST	N10E	75SE			15	N30E	N20E	61NW	0-30								
153	SK	GW - GAR-BI-MS-QTZ-FELD	N0E	59SE															
154	SK	MGW - MIG - SLIGHTLY MYL	N89E	26NW															
155	SK	W - INTRLD W MS-GAR-BI SC	N17W	63NE												N84W	90		
156	SK	MIG BI GN - VERY FOLDED	N12E	64SE			54	N58E	N36E	70SE	100-10								
157	SK	GAR-BI SCHIST	N36E	72SE												N76W	76SW		
158	SK	MIG MGW - DK GREY	N15E	73SE															
159	SK	MGW	N20W	82SW															
160	SK	MIG - GAR-BI-MS SCHIST	19W40N	86SW															
161	SK	MGW	N10E	73NW															
162	SK	MGW	N15E	89NW															
163	SK	MGW & INTRLS OF GAR-BI-M	N18E	87NW															
164	SK	DK GREY BI RICH MGW	N74E	58NW															
165	SK	MGW & SCHIST	N6W	72NE			32	N10E	N5E	70SE	30								
166	SK	MGW	N22E	68SE															
167	SK	GAR-BI-MS SCHIST & MGW	N46E	74SE															
168	SK	R-BI-MS SCHIST & INTRLD M	N18E	85NW															
169	SK	GAR-BI SCHIST & MS PEG	N40E	61SE															
170	SK	GAR-BI-MS SCHIST & MGW	N10E	84NW															
171	SK	MGW	N10E	88SE															
172	SK	MGW	N0W	82NW															
173	SK	MGW	N19E	82SE															
174	SK	GW & W INTRLS GAR-BI-MS	N47E	67NW												N59W	53SW		
175	SK	DK GREY MGW	N76W	59NE															
176	SK	MGW	N35E	65NW															
177	SK	MGW/BI GN	N26E	54NW															
178	SK	MGW	N45E	75NW															
179	SK	MGW W CALC-SI LYRS	N12E	54SE			17	N15E	N27E	69SE	0-90					N36W	72SW	N51E	89SE
180	SK	BI MGW & CALC-SI	N46E	63NW												N16W	68NE		
181	SK	MGW - CALC-SI	N50E	58NW															
182	SK	H MGW	N56E	65NW															
183	SK	MIG BI MGW	N51E	73NW															
184	SK	R-BI-MS SCHIST & MIG BI M	N53E	74NW												N72W	65SW		
185	SK	MIG BI-MGW	N41E	78NW															
186	SK	MIG MGW W MCGL	N54E	51NW	15	N44E													
187	SK	MIG MGW	N73E	62NW															
188	SK	MIG MGW W GTD DIKE	N12E	90															
189	SK	DK GREY MGW	N22E	62NW															
190	SK	DK GREY MIG MGW	N71E	60NW															
191	SK	DK GREY MGW	N22E	70NW			36	N5W	N70W	43NE	0					N11E	88SE		
192	SK	MIG BI MGW	N54E	74NW															
193	SK	DK GREY MIG MGW	N80E	68NW												N6W	82NE		
194	SK	MIG MGW	N68E	62NW															
195	SK	GAR-BI SCHIST	N42E	68NW												N60W	90		
196	SK	GAR-BI SCHIST	N31E	75NW															
197	SK	GAR-BI-CHL SCHIST TO GN	N30E	45NW															
198	SK	MIG MGW & BI SCHIST	N30E	87NW															
199	SK	MIG BI-GAR SCHIST	N56E	62NW			29	S70W	N58E	73NW	0								
200	SK	A LOT OF GAR-BI-MS SCH	N30E	65SE															
201	SK	MGW & GAR-BI-MS SCHIST	N50E	75SE															
202	SK	MGW & GAR-BI-MS SCHIST	N11E	77SE															
203	SK	DK MGW	N19E	53SE												N74E	88NW		
204	SK	GAR-BI-MS SCHIST	N37E	82SE															
205	SK	R-BI-MS SCHIST & INTRLD M	N20E	70SE															
206	SK	GAR-BI-MS SCHIST	N12E	77SE															
207	SK	MGW & GAR-BI-MS SCHIST	N25E	85SE															
208	SK	MS SCHIST - SLIGHTLY MIG	N22E	58SE															
209	SK	MASSIVE DK GREY MGW	N31E	66SE															
210	SK	SIVE MGW - H-GAR-BI-MS S	N55E	62SE															
211	SK	MGW - GAR-BI-MS SCHIST	N20E	62SE															
212	SK	IG GAR-BI-MS SCHIST & MG	N11E	50SE															
213	SK	MGW	N80E	55NW															
214	SK	-QTZ-FELD GN -BI RICH MG	N36E	71SE															
215	SK	R-BI-MS SCHIST - VERY MS I	N78E	60SE															
216	SK	MYLO MGW	N38E	62NW															
217	SK	MYLO MGW	N24E	72NW															
218	SK	MGW / BI GN	N83E	50SE												N90E	90		
219	SK	MGW	N80E	68NW															
220	SK	MGW	N10E	55NW															
221	SK	BI-QTZ-FELD GN W A FEW A	N10E	32NW												N15W	60SW		
222	SK	MGW & GAR-BI-MS SCHIST	N20W	69NW	30	N42W													
223	SK	GAR-BI-MS SCHIST	N15E	60NW															
224	SK	GAR-BI-MS SCHIST	N14E	70NW															
225	SK	GAR-BI-MS SCHIST & MS PE	N41E	40NW															
226	SK	MGW	N81E	27NW															
227	SK	MGW W SCHIST INTRLD	N44E	46SE															
228	SK	LO MEG GN INTRLD W FG M	N44E	77SE															

			Foliation		Lineation		Fold Axis		Axial Surface		IL	Fold	Fold	Crenulation Axis		Joint		Joint	
Station	Quad	Lithology	Strike	Dip	Plunge	Trend	Plunge	Trend	Strike	Dip	Angle	Genr.	Verg.	Plunge	Trend	Strike	Dip	Strike	Dip
229	SK	MYLO MGW	N47E	77SE															
230	SK	GAR-BI-MS SCHIST	N58E	69NW															
231	SK	DK GREY MIG FG MGW	N40E	75SE															
232	SK	FELSIC MGW	N49E	74NW															
233	SK	GREY MGW SLIGHTLY MY	N31E	70SE												N41W	54SW		
234	SK	GAR-BI-MS SCHIST	N52E	75NW															
235	SK	MYLO INEQ MGW	N32E	84SE															
236	SK	DK GREY MGW	N48E	90												N47W	80SW		
237	SK	MGW	N31E	59SE															
238	SK	MGW INTRLD W SCHIST	N50E	73NW															
239	SK	DK GREY MGW	N41E	64SE															
240	SK	MGW	N48E	68SE															
241	SK	MIG MGW	N29E	82NW															
242	SK	W INTRLD W FELD-BI SCH	N42E	80NW															
243	SK	MYLO MIG MGW	N40E	75NW															
244	SK	DK GREY MGW	N43E	78NW															
245	SK	DK GREY MGW	N55E	88NW															
246	SK	MYLO DK GREY MGW	N45E	80NW															
247	SK	MIG MGW	N48E	69NW															
248	SK	G WAVY GAR-BI-MS SCHIS	N38E	77NW															
249	SK	H MGW & GAR-BI-MS SCHI	N50E	67NW	25	N25E													
250	SK	MIG DK GREY MGW	N70E	58NW															
251	SK	MYLO. DK GREY MIG MGW	N25E	75NW	68	N34W										N53W	71SW		
252	SK	GAR-BI-MS SCHIST	N41E	75NW															
253	SK	W INTRLD W GAR-BI-MS SC	N56E	75NW												N42W	86NE		
254	SK	MYLO MEG MIG MGW	N69E	72SE															
255	SK	GAR-BI-MS SCHIST	N55E	85NW															
256	SK	MGW - SLIGHTLY MYLO	N42E	79NW												N48W	82NE		
257	SK	MGW	N52E	87NW															
258	SK	LO GAR-BI-MS SCHIST & M	N48E	85NW															
259	SK	MYLO INEQ MGW	N39E	78NW															
260	SK	MGW	N38E	88NW															
261	SK	MGW - GAR-BI-MS SCHIST	N68E	90SE															
262	SK	MGW - GAR-BI-MS SCHIST	N39E	85NW															
263	SK	MGW	N51E	80NW															
264	SK	MIG MGW	N27E	88NW															
265	SK	DK GREY MIG MGW	N48E	70SE															
266	SK	G GAR-BI-MS SCHIST TO MG	N37E	73NW												N64W	90NE		
267	SK	YLO MG GAR-BI-MS SCHIS	N34E	80SE															
268	SK	MIG MGW	N53E	75NW												N45W	88SW		
269	SK	DK GREY MIG MGW	N40E	40SE			30	N38E	N34E	62SE	10								
270	SK	DK GREY MIG MGW	N47E	76SE															
271	SK	DK GREY MIG MGW	N54E	59NW															
272	SK	MIG MGW - CONTAINS FELI	N47E	83NW															
273	SK	MGW	N51E	43NW												N44W	85SW		
274	SK	DK GREY MIG MGW	N38E	90SE															
275	SK	MIG MGW	N38E	80SE															
276	SK	MYLO MGW - THINLY LYRI	N55E	70SE															
277	SK	MIG MGW	N25E	46SE															
278	SK	MIG MGW	N50W	63NE															
279	SK	& GAR-BI-MS SCHIST W QT	N78E	72SE	34	S76W													
280	SK	YLO MGW - TOP-DOWN-TO	N53E	61SE	42	N76E										N59W	90		
281	SK	MIG MGW	N50E	81SE															
282	SK	W & INTRLD GAR-BI-MS SCI	N54E	67SE															
283	SK	MIG MGW	N38E	71SE															
284	SK	DK GREY MIG MGW	N35E	77SE															
285	SK	MGW	N61E	70NW															
286	SK	DK GREY FG MIG MGW	N65E	76SE															
287	SK	DK GREY MIG MGW	N38E	80SE															
288	SK	GAR-BI-MS SCHIST & MGW	N52E	77SE															
289	SK	& INTRLD SIL-GAR-BI-MS S	N51E	78NW															
290	SK	MYLO MGW	N49E	32NW															
291	SK	W - W INTRLS OF GAR-BI-M	N40E	86NW												N22W	82SW		
292	SK	MGW & GAR-BI-MS SCHIST	N32E	73NW															
293	SK	MYLO MGW	N48E	73NW															
294	SK	GAR-BI-MS SCHIST	N50E	64SE															
295	SK	GAR-BI-MS SCHIST	N14E	87NW															
296	SK	MGW	N35E	72SE															
297	SK	W & MINOR GAR-BI-MS SCH	N20E	76NW															
298	SK	DK GREY MIG MGW	N44W	85SW															
299	SK	MCGL	N31E	46SE															
300	SK	MIG DK GREY MGW	N74E	78NW															
301	SK	MIG DK GREY MGW	N60E	60NW															
302	SK	MGW	N46E	58NW															
303	SK	SIL-GAR-BI-MS SCHIST	N9E	68NW															
304	SK	MGW	N9E	65SE															
305	SK	MYLO MCGL & MGW	N31E	90SE															
306	SK	GAR-BI-MS SCHIST & MGW	N28E	75SE															
307	SK	RLD GAR-BI-MS SCHIST & M	N27E	60SE															
308	SK	MGW & GAR-BI-MS SCHIST	N32E	72SE															
309	SK	THINLY LYRD MGW	N32E	78SE															
310	SK	MGW W PODS OF CALC-SI	N63E	64NW															
311	SK	MGW	N70E	67NW															
312	SK	MGW	N50E	75SE															
313	SK	DRK GRAY MGW	N17E	70SE															
314	SK	R-BI-MS SCHIST & MINOR M	N43E	77NW															
315	SK	MGW & GAR-BI-MS SCHIST	N28E	47SE															
316	SK	MGW	N23E	73NW															
317	SK	MGW	N0E	60SE															
318	SK	MGW	N23E	63SE															
319	SK	MGW	N20E	72SE															
320	SK	GAR-BI-MS SCHIST	N59E	73NW															
321	SK	MGW	N38E	77NW															
322	SK	MGW	N43E	73NW												N34W	50SW		
323	SK	MGW	N39E	65NW															
324	SK	DK GREY MGW	N59E	82NW															
325	SK	MGW	N51E	50NW												N59E	83SE		
326	SK	- INTRLD W MS-GAR-BI SC	N62E	64NW															
327	SK	DK GREY MIG MGW	N30E	80NW															
328	SK	MIG MGW	N36E	74NW	55	N18E										N46W	83SW		
329	SK	MIG MGW	N31E	72SE															
330	SK	MIG MGW	N78E	63NW															
331	SK	MIG MGW	N8W	63SW												N73E	88SE		
332	SK	MIG MGW	N29E	69SE												N10W	64SW	N47W	77SW
333	SK	MIG MGW	N28E	72SE															
334	SK	MIG MGW	N30E	84NW			50	S38W	N47E	75SE	30					N79E	81NW		
335	SK	MIG MGW	N10E	84NW			60	S20E	N35E	72SE	30								
336	SK	MIG MGW	N20E	78SE															
337	SK	G MGW & GAR-BI-SIL SCHI	N48E	52NW															
338	SK	MGW	N42E	75NW			36	N45E	N31E	70SE	70					N73W	78SW		
339	SK	AR-BI-SIL SCHIST & MIG G	N57E	58NW															
340	SK	MIG MGW	N60E	79NW															
341	SK	MIG MGW	N17E	81SE												N52W	76NE		
342	SK	MIG MGW	N54E	66NW															

			Foliation		Lineation		Fold Axis		Axial Surface		IL	Fold	Fold	Crenulation Axis		Joint		Joint	
Station	Quad	Lithology	Strike	Dip	Plunge	Trend	Plunge	Trend	Strike	Dip	Angle	Genr.	Verg.	Plunge	Trend	Strike	Dip	Strike	Dip
343	SK	MIG MGW	N52E	65NW															
344	SK	MIG MGW	N84W	51NE															
345	SK	MIG MGW	N25W	51NE															
346	SK	MIG MGW	N24E	65NW															
347	SK	MIG MGW	N26E	60SE															
348	SK	MIG MGW	N30E	68SE															
349	SK	MIG MGW	N42E	66SE															
350	SK	MIG MGW	N62E	82SE															
351	SK	MIG MGW	N35E	47SE															
352	SK	MIG MGW	N57E	53SE												N40W	62SW		
353	SK	AR-BI-MS SCHIST W CG MS I	N31E	64NW															
354	SK	MIG MGW	N13W	87NE															
355	SK	MIG MGW	N40E	45SE												N42W	70SW		
356	SK	MIG MGW	N35W	78NE															
357	SK	MIG MGW	N51W	49SW												N20E	56SE		
358	SK	MIG MGW	N60E	58NW															
359	SK	MIG MGW	N32E	52W															
360	SK	IIST - MAY CONTAIN KY RE	N10W	66NE															
361	SK	MIG MGW	N2E	59SE												N89W	78NE		
362	SK	MIG MGW	N84W	54NE			22	S21W	N25E	68SE	0-30								
363	SK	MIG MGW	N31E	66SE			22	S21W	N25E	68SE	0-30								
364	SK	MIG MGW	N58W	72NE															
365	SK	MIG MGW	N33E	54SE															
366	SK	MGW	N26E	61SE												N49W	58NE		
367	SK	GAR-BI-MS SCHIST - MGW	N21E	86SE															
368	SK	MIG MGW	N27E	49NW												N64W	79SW		
369	SK	MIG MGW	N24E	51NW												N64W	72SW	N48E	51SE
370	SK	MIG MGW	N80E	56NW															
371	SK	MIG MGW	N46E	82NW												N75W	83SW		
372	SK	MGW - CG MS FLAKES	N36E	69NW															
373	SK	MGW	N44E	88NW															
374	SK	MGW	N35E	85NW															
375	SK	MYLO MIG MGW	N32E	85SE															
376	SK	GAR-BI-MS SCHIST	N44E	83SE															
377	SK	GAR-BI-MS SCHIST	N28E	87SE															
378	SK	MGW	N10E	78SE															
379	SK	GAR-BI-MS SCHIST - MGW	N80W	61NE															
380	SK	MIG MGW	N90E	60NW															
381	SK	MIG MGW	N87W	50NE															
382	SK	MIG MGW	N89E	62NW															
383	SK	MIG MGW	N71E	60NW															
384	SK	MIG MGW	N41E	60SE															
385	SK	MINOR INTRLS OF GAR-BI-M	N26E	69SE															
386	SK	MIG MGW	N48E	85SE															
387	SK	MIG MGW	N78E	50NW															
388	SK	MIG MGW & FG BI GTD	N49E	58NW			24	N73E	N71E	52NW	40-60								
389	SK	MIG MGW	N52E	57NW												N54W	88SW		
390	SK	MIG MGW	N74E	72NW															
391	SK	MIG MGW	N74E	77NW															
392	SK	MIG MGW	N82W	47NE															
393	SK	MIG MGW	N65E	85NW															
394	SK	MIG MGW	N28W	43NE															
395	SK	MIG MGW	N33W	77NE															
396	SK	MIG MGW	N5W	82NE															
397	SK	MIG MGW	N29E	78SE												N88W	83SW		
398	SK	MIG MGW	N77E	79NW			43	N35E	N40E	63W	0-80								
399	SK	MIG MGW	N24E	76NW															
400	SK	MIG MGW	N46E	83NW															
401	SK	MIG MGW	N39E	81NW															
402	SK	MGW - GAR-BI SCHIST	N25E	71SE															
403	SK	MIG MGW	N22E	79NW															
404	SK	MIG MGW	N25E	43SE															
405	SK	MIG MGW	N29E	82SE															
406	SK	MIG MGW	N85E	80NW												N64E	90SE		
407	SK	IS SCHIST - FG + SIL INTRLI	N21E	70SE															
408	SK	MIG MGW	N80E	67NW															
409	SK	MIG MGW & SCHIST	N24E	67NW															
410	SK	MIG MGW	N81E	60NW															
411	SK	MIG MGW	N40E	79NW															
412	SK	MIG MGW	N69E	61NW															
413	SK	MIG MGW	N46E	78NW			35	N26E	N41E	82NW	0-30								
414	SK	MIG MGW	N69E	67NW															
415	SK	MIG MGW	N71E	57NW															
416	SK	MIG MGW	N53E	72NW												N2W	65NE		
417	SK	MIG MGW	N67E	69NW															
418	SK	MIG MGW	N32E	80NW															
419	SK	MIG MGW	N36E	77NW															
420	SK	MIG MGW	N45E	65NW															
421	SK	MIG MGW	N86E	53NW															
422	SK	MIG MGW	N45E	67NW															
423	SK	MIG MGW & SCHIST	N34E	84SE															
424	SK	G BI-MS SCHIST & MIG MG	N60E	62NW															
425	SK	LY LYRD BI-MS SCHIST TO	N49E	83NW															
426	SK	MIG MGW	N32E	88SE															
427	SK	GW & GAR-BI-MS SCHIST T	N72E	73NW															
428	SK	/ TO SCHIST - GAR-BI-MS SC	N36E	57NW															
429	SK	MGW - SCHIST	N28E	83NW															
430	SK	GAR-BI-MS SCHIST & MGW	N42E	72NW															
431	SK	GAR-BI-MS SCHIST	N52W	28NE															
432	SK	GAR-BI-MS SCHIST	N43E	67NW										9	S42W				
433	SK	MGW	N68E	57NW															
434	SK	TRLS OF GAR-BI-MS SCHIST	N61E	18NW															
435	SK	MIG MGW/ 2M	N2E	40SE															
436	SK	MIG MGW	N12E	65SE															
437	SK	IG MGW - 2 M - CALC-SI PO	N21E	66NW			24	N13E	N2E	75NW	90-120								
438	SK	MIG MGW	N38E	53NW															
439	SK	GAR-BI-MS SCHIST - MGW	N32E	35NW															
440	SK	GAR-BI-MS SCHIST	N55E	52NW															
441	SK	MGW	N75E	56NW															
442	SK	GAR-BI-MS SCHIST	N48E	68NW															
443	SK	MGW & GAR-BI-MS SCHIST	N41E	59SE												N31E	56NW	N84W	64SW
444	SK	MGW	N28E	66NW															
445	SK	IG MGW - LOTS OF AM FLO	N88W	77NE															
446	SK	) GAR-BI-MS SCHIST & MIG	N37E	59NW															
447	SK	MIG MGW W AM LYRS	N42E	38NW															
448	SK	MIG MGW	N33W	55NE															
449	SK	MIG MGW	N12E	29SE												N74E	69NW		
450	SK	IS SCHIST TO MGW - FG SEI	N18E	33SE												N66W	68SW		
451	SK	MGW	N70E	35SE															
452	SK	MGW	N6W	55NE															
453	SK	MGW	N58W	66NE															
454	SK	MGW & MYLO MGW	N36W	50NE															
455	SK	GAR AM - AM	N39W	61NE															
456	SK	GAR-BI-MS SCHIST	N2W	62NE															

			Foliation		Lineation		Fold Axis		Axial Surface		IL	Fold	Fold	Crenulation Axis		Joint		Joint	
Station	Quad	Lithology	Strike	Dip	Plunge	Trend	Plunge	Trend	Strike	Dip	Angle	Genr.	Verg.	Plunge	Trend	Strike	Dip	Strike	Dip
457	SK	-BI-MS SCHIST W CG MS FL	N39E	84NW	17	N40E													
458	SK	MS SCHIST W MGW & CALC	N21E	52SE	6	N27E	14	N21E	N42E	33NW	90					N39E	80SE		
459	SK	REY MGW -GAR-BI-QTZ-FEI	N68E	42NW												N45W	85SW		
460	SK	MIG MGW - STAINED BLACI	N48E	59NW															
461	SK	MIG MGW W REFOLDS	N62E	42NW			28	N38W	N31E	42NW	0					N32W	90		
462	SK	IGW - QTZ VEIN- ISOCLINAL	N68E	48NW			16	N21E	N31E	55NW	0								
463	SK	IIG MGW W ISOCLINAL FOL	N39E	30NW			14	N72E	N54E	76NW	0								
464	SK	DK GREY MGW	N47E	38NW															
465	SK	GAR-BI-MS SCHIST	N41E	60SE															
466	SK	MIG MGW	N62E	52NW															
467	SK	MIG MGW	N32E	50NW			25	N36E	N55E	50NW	0								
468	SK	AKLY FOLIATED CG MS-BI (	N32E	74SE															
469	SK	CHIST -MIG CALC-SI -MAY	N57E	58SE															
470	SK	MIG MGW	N45E	47NW															
471	SK	MYLO GAR-BI-MS SCHIST	N48E	49NW															
472	SK	MIG MGW	N31E	62NW															
473	SK	MIG MGW	N43E	38NW			6	S43W	N44W	16SW	120								
474	SK	MGW INTRLD W MS-BI PEG	N42E	54NW															
475	SK	MIG MGW W AM LYRS	N52E	30NW															
476	SK	MIG MGW	N54E	47NW															
477	SK	MGW & GAR-BI-MS SCHIST	N48E	90															
478	SK	MIG MGW	N41E	71NW															
479	SK	MIG MGW	N70W	55NE															
480	SK	GAR-BI-MS SCHIST & MGW	N22E	69SES															
481	SK	MIG MGW	N29E	63NW															
482	SK	MGW	N6E	57NW															
483	SK	MGW & SCHIST	N18E	94NW															
484	SK	MIG MGW	N36E	32NW															
485	SK	MIG MGW	N52E	61NW															
486	SK	GAR-BI-MS SCHIST & CHL	N82E	50NW															
487	SK	MIG MGW	N46E	56NW															
488	SK	MIG MGW	N54E	60NW															
489	SK	MIG MGW	N72E	53NW															
490	SK	MIG MGW	N42E	88SE															
491	SK	MGW	N55W	44NE															
492	SK	MGW - 2M GN	N69E	69NW															
493	SK	AR-BI-MS SCHIST - SIL? - K	N30E	32NW															
494	SK	MGW	N63E	80NW															
495	SK	MGW	N62E	42NW															
496	SK	MGW - MIG MGW	N32E	68SE															
497	SK	MIG MGW W INTRLD AM	N27E	52NW															
498	SK	MIG MGW & INTRLD AM	N3E	27SE												N62S	81NW		
499	SK	MIG MGW & AM	N22E	17NW															
500	SK	MIG MGW	N16E	60NW															
501	SK	MIG MGW W AM INTRLD	N38E	89NW															
502	SK	MIG MGW	N52W	79NE															
503	SK	MIG MGW	N42E	41NW															
504	SK	MYLO MIG MGW	N48E	51SE	23	N62E													
505	SK	MIG MGW W AM PODS	N12E	32NW															
506	SK	MIG MGW - SCHIST	N45E	76NW															
507	SK	MIG MGW	N36E	57NW															
508	SK	MIG MGW W AM PODS	N38E	59NW			16	N36E	N9W	12NE	90								
509	SK	MIG MGW W AM	N30E	59SE	29	N36E													
510	SK	MIG MGW	N10W	57NE												N36E	44NW		
511	SK	MIG MGW	N40E	60NW															
512	SK	MIG MGW	N27W	64NE															
513	SK	MIG MGW	N33W	74NE															
514	SK	GAR-BI-MS SCHIST	N83E	61NW															
515	SK	GAR-BI-MS SCHIST	N83E	71NW															
516	SK	CG BI-MS GTD	N55E	60SE															
517	SK	MGW	N68W	44NE															
518	SK	I-MS SCHIST - SIL? - W MS F	N88E	48NW															
519	SK	GAR-BI-MS SCHIST TO MGW	N82W	65NE															
520	SK	MIG MGW	N82E	55NE															
521	SK	MIG MGW	N36E	90SE															
522	SK	MIG MGW	N70E	64NW															
523	SK	MYLO GAR-BI-MS SCHIST	N55E	76NW															
524	SK	GAR-BI-MS SCHIST & MGW	N62E	76NW												N32W	88SW		
525	SK	MGW & SCHIST	N48E	63NW															
526	SK	MGW	N61E	71NW												N40W	82SW		
527	SK	MGW - FG BI-MS GG	N61E	40NW															
528	SK	BI-MS GG - FG H GTD	N36E	77NW															
529	SK	MIG MGW -SLIGHTLY MYL(	N14E	36SE															
530	SK	MIG MGW	N50W	32NE															
531	SK	MG CONTAINS GAR-MODEF	N52E	52NW															
532	SK	GAR-BI-MS SCHIST & MGW	N46E	62NW															
533	SK	MS SCHIST TO GAR-MS-QTZ	N56E	62NW															
534	SK	MYLO GAR-BI SCHIST	N75W	70NE															
535	SK	GAR-BI SCHIST	N32W	47NW															
536	SK	MIG GAR-BI-MS SCHIST	N56E	85SE															
537	SK	MIG MGW	N32E	81SE															
538	SK	MIG MGW	N52E	84SE															
539	SK	MIG MGW	N30E	46NW												N75W	79SW		
540	SK	MIG MGW	N31E	89NW															
541	SK	GAR-BI-MS SCHIST & MGW	N35E	65NW												N47W	87NE		
542	SK	MIG MGW	N48E	79SE															
543	SK	MIG MGW	N56E	73NW															
544	SK	MIG MGW	N36W	56NE															
545	SK	MIG MGW	N33E	74SE															
546	SK	MIG MGW	N22E	79NW															
547	SK	GAR-BI-MS SCHIST & MGW	N51E	74SE															
548	SK	MGW & GAR-BI-MS SCHIST	N25E	85NW															
549	SK	MYLO GAR-BI-MS SCHIST	N41E	68NW															
550	SK	IIG MGW - GAR-BI-MS SCHIS	N64E	79NW															
551	SK	TYLO MIG GAR-BI-MS SCHIS	N47E	73NW															
552	SK	MGW TO MIG MGW	N33E	64NW															
553	SK	MIG MGW	N42E	76NW															
554	SK	MIG MGW	N42E	76NW															
555	SK	MIG MGW TO A MGW	N30E	68NW															
556	SK	MINOR INTRLS OF GAR-BI	N32E	77NW															
557	SK	GW & INTRLD GAR-BI-MS S	N34E	83NW															
558	SK	MGW	N31E	79NW															
559	SK	MIG MGW	N36E	71SE															
560	SK	MIG MGW	N36E	84SE															
561	SK	MIG MGW	N31E	73SE															
562	SK	GAR-BI-MS SCHIST	N29E	68SE															
563	SK	MS SCHIST W CG MS FLAK	N34E	40NW															
564	SK	BI-MS SCHIST W CG MS FL	N52E	88NW															
565	SK	MIG MGW	N37E	84NW															
566	SK	MIG MGW	N5E	51SE												N43W	78SW		
567	SK	MIG MGW	N33E	80SE															
568	SK	MIG MGW	N11E	74SE															
569	SK	W W CALC-SI PODS - QTZ-G	N42E	68SE															
570	SK	MIG MGW	N37E	66SE															

			Foliation		Lineation		Fold Axis		Axial Surface		IL	Fold	Fold	Crenulation Axis		Joint		Joint	
Station	Quad	Lithology	Strike	Dip	Plunge	Trend	Plunge	Trend	Strike	Dip	Angle	Genr.	Verg.	Plunge	Trend	Strike	Dip	Strike	Dip
571	SK	MIG MGW	N24E	80SE															
572	SK	MGW	N40E	82SE															
573	SK	MGW & MIG GAR-BI-MS SC	N27E	77SE			14	N47E	N47E	72SE	0-90								
574	SK	MGW	N34E	61NW															
575	SK	MIG MGW	N50E	79NW												N50W	90		
576	SK	BI-MS SCHIST W CG MS FL/	N62E	76SE															
577	SK	GAR-BI-MS SCHIST	N34E	75SE															
578	SK	MIG MGW	N20E	76SE															
579	SK	MIG MGW	N30E	50SE															
580	SK	D MIG GAR-BI-MS SCHIST &	N29E	86SE												N43W	86NE		
581	SK	MGW & LEUCO MIG GAR-B	N31E	78NW												N70W	87NE		
582	SK	MIG MGW-LOCALLY LOOI	N32E	90SE															
583	SK	GAR-BI-MS SCHIST & MGW	N30E	72NW												N65E	67SW		
584	SK	MIG MGW & MIG MGW &	N30E	82NW															
585	SK	- MIG TO CG MS-BI-FELD-Q	N32E	81NW												N65W	79SW		
586	SK	INTRLD MIG MGW	N34E	77NW															
587	SK	MGW - GAR-BI-MS SCHIST	N9E	80SE												N61W	87NE		
588	SK	MIG MGW & MINOR SCHIST	N52E	88NW															
589	SK	GAR-BI-MS SCHIST W MS FL	N38E	74NW															
590	SK	R-BI-MS SCHIST W MS FLA	N42E	65NW												N61W	71SW		
591	SK	MIG MGW	N33E	76NW															
592	SK	GAR-BI-MS SCHIST	N30E	67NW															
593	SK	GAR-BI-MS SCHIST	N41E	72NW															
594	SK	W TO AN INEQ MGW TO M	N28E	84NW															
595	SK	/ MS FLAKES - CONTAINS (	N30E	79NW															
596	SK	MIG MGW & CALC SILYS &	N72E	84NW															
597	SK	MIG MGW & GAR-BI-MS-CH	N42E	85SE															
598	SK	CO MIG MGW - SLIGHTLY M	N29E	24SE												N33W	83SW		
599	SK	IIG MGW & GAR-BI-MS-SIL	N29E	83SE															
600	SK	MIG MGW	N31E	65NW															
601	SK	MIG MGW	N35E	58NW															
602	SK	AR-BI-MS SCHIST & CG MS I	N38E	46NW															
603	SK	MIG MGW	N54E	59NW															
604	SK	MIG MGW	N21E	66NW												N57W	82NE		
605	SK	MGW & MINOR AM MS FL/	N47E	64NW															
606	SK	MIG MGW	N43E	59NW															
607	SK	MIG MGW	N32E	60NW												N68W	83SW	N55W	75SW
608	SK	MGW - 2 MICA GN	N62E	28NW															
609	SK	MGW	N54E	17NW															
610	SK	MGW/MIG MGW					22	N27E	N21E	69SES	150					N56W	52SW	N40E	86SE
611	SK	MIG MGW	N31E	74NW			34	N53E	N35E	76SE	30-50								
612	SK	MIG MGW	N48E	74NW															
613	SK	MIG MGW W H	N47E	52NW												N48W	80NW		
614	SK	MIG MGW	N31E	62SE												N45W	76SW		
615	SK	GAR-BI-MS SCHIST - W SIL	N17E	68SE															
616	SK	MGW	N28E	67SE															
617	SK	MGW - MASSIVE LYRS	N64E	39NE												N86W	60SW		
618	SK	MGW - MINOR SCHIST	N38E	45SE															
619	SK	MIG GAR-BI-MS SCHIST	N17E	72SE															
620	SK	MGW & GAR-BI-MS SCHIST	N36E	449NW															
621	SK	MIG MGW	N22E	64NW															
622	SK	GAR-BI-MS SCHIST	N10E	72NW															
623	SK	MS SCHIST - ? KY REPLACE	N85E	74NW															
624	SK	W - LOT OF AM & MGW FL(	N39E	86SE															
625	SK	MIG MGW	N41E	68SE															
626	SK	MGW - LOT OF AM FLOAT	N30E	64NW															
627	SK	MGW & GAR-BI-MS SCHIST	N25E	32NW															
628	SK	MIG INEQ MGW	N40E	83SE															
629	SK	MIG BI SHIST	N21E	81SE															
630	SK	MGW	N18W	42NE															
631	SK	GAR-BI-MS SCHIST	N26E	70SE															
632	SK	MIG MGW	N50E	62SE															
633	SK	MGW	N62E	38NW															
634	SK	MIG MGW					44	N4E	N4E	90	90								
635	SK	MIG MGW & MIG GAR-BI S	N35E	71NW															
636	SK	LFIDIC MIG GAR-BI-MS SCH	N51E	52NW												N30W	73NE		
637	SK	MIG MGW	N41E	79NW															
638	SK	MIG MGW	N44E	69NW			62	N52E	N50E	66NW	0-35					N8W	69SW		
639	SK	SULFIDIC GAR-BI-MS SCHIS	N51E	74NW															
640	SK	R-BI-MS SCHIST - MS & QTZ	N54E	63NW	90	N489E													
641	SK	MIG MGW & SCHIST	N38E	47NW															
642	SK	MIG MGW	N72E	62NW															
643	SK	GAR-BI-MS SCHIST & MGW	N54E	39NW															
644	SK	IG MGW & GAR-BI-MS SCHI	N30E	80NW												N50W	55NW	N70W	85NE
645	SK	LYRD MIG MGW	N51E	67NW															
646	SK	MGW TO INEQ MIG MGW	N41E	88NW															
647	SK	INEQ CG MIG MGW/BI GN	N37E	68NW															
648	SK	MIG MGW & GAR-BI-MS SC	N50E	58NW															
649	SK	MGW - GAR-BI-MS SCHIST	N55E	82NW															
650	SK	CG INEQ MIG BI GN	N37E	67NW															
651	SK	MIG GAR-BI-MS SCHIST	N50E	69NW															
652	SK	A INEQ BI GN - GAR-BI-MS	N38E	54NW															
653	SK	MGW	N39E	71NW															
654	SK	IIG MGW - GAR-BI-MS SCHIS	N47E	88SE															
655	SK	MIG MGW	N74E	44NW															
656	SK	MIGMA - INEQ MIG MGW	N50E	77NW															
657	SK	GAR-BI-MS SCHIST	N39E	83NW															
658	SK	A MG GAR-BI-MS SCHIST	N38E	66NW												N70W	82NE	N74E	72NW
659	SK	MIG MGW	N34E	78NW															
660	SK	MIG MGW & AM	N40E	78NW															
661	SK	MIG MGW - MIGMA - INEQ	N42E	68NW															
662	SK	MIGMA - INEQ MIG MGW	N38E	62NW															
663	SK	INEQ BI GN/MGW & SCHIST	N25E	79NW															
664	SK	MIG MGW	N48E	86NW												N55W	88NE	N66W	86NE
665	SK	MIGMA - MIG INEQ MGW	N32E	83NW															
666	SK	MIGMA - MIG INEQ MGW	N30E	66NW												N90E	83SE		
667	SK	MIGMA - MIG INEQ MGW	N31E	83NW															
668	SK	MIG MGW TO MG MIG MGW	N41E	72NW															
669	SK	MIG MGW/MIGMA	N33E	81NW															
670	SK	MIG MGW - MIGMA	N27E	67NW															
671	SK	MIGMA - MIG MGW/BI GN	N43E	59NW															
672	SK	MIGMA - MIG MGW	N28E	80NW															
673	SK	MIGMA	N46E	88SE															
674	SK	MIGMA - BI GN	N34E	72NW															
675	SK	MIGMA	N32E	81SE															
676	SK	MIGMA	N34E	85SE			33	S52W	N54E	76SE	0-30								
677	SK	MIGMA	N33E	77NW															
678	SK	MIGMA	N42E	87NW															
679	SK	MIG MGW TO MIGMA	N42E	78NW															
680	SK	GA-BI-MS SCHIST - MG - SIL	N61E	65NW															
681	SK	MIG GAR-BI-MS SCHIST	N30E	71NW															
682	SK	R-BI-MS SCHIST - PEG DIKE	N49E	35NW															
683	SK	MIG MGW	N15E	20NW															
684	SK	MIG MGW	N84E	39NW												N5W	78NE		

Station	Quad	Lithology	Foliation		Lineation		Fold Axis		Axial Surface		IL	Fold	Fold	Crenulation Axis		Joint		Joint	
			Strike	Dip	Plunge	Trend	Plunge	Trend	Strike	Dip	Angle	Genr.	Verg.	Plunge	Trend	Strike	Dip	Strike	Dip
685	SK	MIG MGW	N84E	25NW															
686	SK	MIG MGW	N84E	46NW												N0E	76SE		
687	SK	IG MGW - LOTS OF AM FLO	N31W	50NW															
688	SK	IG MGW - LOTS OF AM FLO	N52E	4NW			28	S37W	N42E	69NW	120					N80E	84SE		
689	SK	MGW	N0E	64SE												N78W	74NE		
690	SK	MGW - LOTS OF AM FLOAT	N65W	42NE															
691	SK	GREY MGW - LOTS OF AM FI	N22W	24NE															
692	SK	MIG MGW					28	N89E	N51W	47NE	90-70					N10E	78SE		
693	SK	MGW	N41E	58NW															
694	SK	IG MGW - LOTS OF AM FLO	N60E	24NW															
695	SK	MGW & AM FLOAT	N34E	27SE															
696	SK	MGW	N21E	37SE															
697	SK	MGW	N38E	90SE															
698	SK	MIG MGW & AM FLOAT	N33E	72NW															
699	SK	MGW	N58E	39NW															
700	SK	MIG MGW	N68W	42NE												N17E	85NW		
701	SK	MIG MGW	N51E	88SE												N81E	87SE		
702	SK	MIG MGW	N9E	79NW												N28E	86NW		
703	SK	MGW	N44W	67NE															
704	SK	MIG MGW	N40E	70NW															
705	SK	MGW	N58E	83NW															
706	SK	MGW & AM FLOAT	N38E	55SE															
707	SK	GAR-BI-MS SCHIST	N10W	40NE															
708	SK	MGW	N68W	12NE															
709	SK	MGW & GAR-BI-MS SCHIST	N48E	24SE															
710	SK	GAR-BI-MS SCHIST	N18E	50SE															
711	SK	GAR-BI-MS SCHIST	N18E	72SE												N13E	90SE		
712	SK	GAR-BI-MS SCHIST	N34E	73NW															
713	SK	MGW - 2 MS GN	N74E	22NW															
714	SK	MGW & GAR-BI-MS SCHIST	N44E	24NW															
715	SK	MIG MGW	N15E	53SE															
716	SK	LYRD MIG MGW - SLIGHTL	N74E	24NW															
717	SK	GAR-BI-MS SCHIST	N20E	74SE															
718	SK	MGW & AM LYRS & AM FL	N38W	17NE															
719	SK	MGW	N32E	56NW															
720	SK	MGW MIG	N32E	76NW												N61W	69SW		
721	SK	AM	N51E	88SE															
722	SK	MGW W SMALL AM PODS	N59E	66SE															
723	SK	MIG MGW	N46E	66SE	14	N51E													
724	SK	MGW	N34E	68NW															
725	SK	LO MIG MGW & FELD-BI SC	N84E	25NW	14	N51E													
726	SK	FLOAT																	
727	SK	DUNITE W QTZ VEIN	N50E	44NW												N50W	67SW		
728	SK	GAR-BI-MS SCHIST	N34E	72NW															
729	SK	MGW & GAR-BI-MS SCHIST	N47E	50NW															
730	SK	MGW & GAR-BI-MS SCHIST	N40E	47NW															
731	SK	MIG MGW	N61E	80NW															
732	SK	MIG MGW	N31E	66NW															
733	SK	MIG MGW	N32E	8SE															
734	SK	MIG MGW	N27E	66NW															
735	SK	MIG MAG - CHL-MS SCHIST	N63E	72NW															
736	SK	AG-CHL-MS SCHIST & MINO	N81E	52NW															
737	SK	MIG MGW	N67E	31NW															
738	SK	GAR-BI-MS SCHIST	N31E	51NW															
739	SK	MIG MGW - ALMOST FLOAT	N29E	6NW												N2W	84SW	N40E	90SE
740	SK	MGW & GAR-BI-MS SCHIST	N48E	0NW															
741	SK	MGW W MINOR SCHIST IN	N29E	30NW												N74E	75SE		
742	SK	MIG MGW	N38E	39NW															
743	SK	MIG MGW	N34E	11NW												N50E	75NW	N70W	50SW
744	SK	MIG MGW	N72E	24NW												N80E	79NW	N1E	76NW
745	SK	R-BI-MS SCHIST - MAY CON	N47E	60NW															
746	SK	MIG MGW	N54E	43NW															
747	SK	MIG MGW	N49E	41NW															
748	SK	MIG MGW & AM FLOAT	N83E	38NW															
749	SK	MGW	N10E	25SE			32	N80E	N75E	51SE	70								
750	SK	MGW	N9E	65NW															
751	SK	MGW	N31E	18SE												N3W	78NE		
752	SK	MGW	N28E	51SE															
753	SK	THINLY LYRD MGW	N12E	31SE												N32E	70NW	N71W	86NE
754	SK	MGW	N15E	56SE															
755	SK	MGW	N18E	59SE															
756	SK	GAR-BI-MS SCHIST W AM	N10E	78SE			7	S50W	N60E	74SE	0-20								
757	SK	MGW	N6W	30NE												N29W	90SW		
758	SK	INOR INTRLS SCHIST LOCA	N32W	29NE			11	N19E	N2W	53NE	70-120								
759	SK	MGW	N42W	25NE															
760	SK	MIG MGW	N30E	45SE															
761	SK	MGW - LOCALLY AN AGMA	N66W	10NE												N40W	88SW		
762	SK	V - MIG MGW CUT BY CG BI	N32E	74SE												N50E	76SE		
763	SK	MGW	N38E	32SE															
764	SK	MGW	N37E	71SE															
765	SK	MGW	N50E	46NW															
766	SK	MGW	N10W	72NE															
767	SK	G GAR-BI-MS SCHIST TO MG	N22E	16SE															
768	SK	MGW - GAR-BI-MS SCHIST	N24E	88NW															
769	SK	MIG MGW	N10E	69NW															
770	SK	MIG MGW	N53W	46SW															
771	SK	MIG MGW - 2M GN	N43W	17SW												N65E	75NW		
772	SK	MIG MGW	N72W	82NE															
773	SK	MIG MGW & AM	N25E	68NW															
774	SK	IG MGW & GAR-BI-MS SCHI	N34E	82SE															
775	SK	MIG MGW	N12W	48SW															
776	SK	MIGMA TO MIG MGW	N44E	84NW															
777	SK	MIG PROCLASTIC MS-BI-PL	N36E	68NW															
778	SK	MIGMA - INEQ BI GN	N35E	62NW															
779	SK	MIG MGW	N38E	78NW															
780	SK	GAR-BI-MS SCHIST	N40E	68NW															
781	SK	GAR-BI-MS SCHIST	N56E	50NW															
782	SK	MIG MGW TO INEQ BI GN	N32E	88SE												N62W	73NW	N75E	52NW
783	SK	MIG MGW	N42E	55NW															
784	SK	MIG MGW	N38E	68NW															
785	SK	MIG MGW					89	N31E	90	0-10		F2, SHEATH							
786	SK	MIG MGW	N15E	75NW															
787	SK	MIG MGW	N25E	84SE															
788	SK	MIG MGW	N20E	82NW															
789	SK	MIG MGW	N27E	88SE															
790	SK	MIG MGW	N35E	89NW															
791	SK	MIG MGW	N30E	78NW															
792	SK	MIG MGW	N60E	82NW															
793	SK	MIG MGW - MIGA	N26E	85W															
794	SK	MIG MGW	N21E	81NW															
795	SK	MIG MGW & AM PODS	N48E	69NW															
796	SK	MIG MGW	N22E	79NW															
797	SK	MIGMA - INEQ BI GN	N27E	82NW															
798	SK	IGMA - INEQ BI GN/MIG MG	N54E	62NW			24	N31E	N36E	69NW	0-30								

			Foliation		Lineation		Fold Axis		Axial Surface		IL	Fold	Fold	Crenulation Axis		Joint		Joint	
Station	Quad	Lithology	Strike	Dip	Plunge	Trend	Plunge	Trend	Strike	Dip	Angle	Genr.	Verg.	Plunge	Trend	Strike	Dip	Strike	Dip
799	SK	MIG MGW - INEQ BI GN	N38E	82NW															
800	SK	MGW - INEQ BI GN	N20E	80NW															
801	SK	GW & GAR-BI-MS SCHIST TO	N36E	72NW												N36W	90NW		
802	SK	MIG MGW TO MIGMA	N22E	85NW															
803	SK	MIG MGW	N28E	78NW															
804	SK	MIG MGW	N31E	84NW															
805	SK	MIG MGW TO MIGMA	N34E	82NW															
806	SK	MIG MGW/MIGMA	N28E	83NW															
807	SK	MIG MGW/MIGMA	N50E	55NW															
808	SK	MIG MGW/MIGMA	N26E	88NW															
809	SK	IIG MGW - GAR-BI-MS SCHIS	N39E	82SE												N67W	80NE		
810	SK	MIG MGW	N39E	87NW															
811	SK	R-BI-MS SCHIST & MGW INT	N49E	80NW															
812	SK	MIG MS-CHL SCHIST	N50E	52NW			16	N51E	N52E	65SE	90-120								
813	SK	INEQ MIG MGW	N52E	78NW												N35E	75SE	N12W	56SW
814	SK	MIG GAR-BI-MS SCHIST	N34E	68SE															
815	SK	MA - GAR-BI-MS SCHIST &	N34E	65NW															
816	SK	MIGMA - MGW & BI GTD	N19E	52SE															
817	SK	MIG MGW -BI DOMINANT	N58E	37NW															
818	SK	MIG MGW	N15E	9SE												N70E	15NW		
819	SK	MIGMA & GAR-BI-MS SCHIS	N38E	74NW															
820	SK	MIG GAR-BI-MS SCHIST	N49E	67NW												N41W	89SW		
821	SK	MG P MS-BI GN	N26E	72SE															
822	SK	AINED TO MASSIVE GAR-M	N54E	66NW															
823	SK	G EVEN GRAINED MS-BI GTD														N75E	66NW	N15W	74NE
824	SK	I MS GTD - WEAKLY FOLIA	N31E	30SE												N42W	75NE		
825	SK	GAR-BI-MS SCHIST	N52E	70SE															
826	SK	MG CHL-MS SCHIST	N43E	75NW															
827	SK	MIG MGW & MS SCHIST	N46E	81NW															
828	SK	BI-MS GTD TO A MS-BI GG	N54E	74SE															
829	SK	/ LENSES & PODS OF BI GN	N61E	65NW															
830	SK	BI GG & MIG BI GN	N76W	42SES															
831	SK	I GG & BI-MS GTD W BI GN	N50E	70NW															
832	SK	FG FOLIATED BI GTD TO GG	N58E	72NW															
833	SK	LIATED MS-BI GTD W BI GN	N86E	71NW												N13E	57NW		
834	SK	MIG BI GN - BI GTD	N60E	72NW															
835	SK	INTRLD MIG MGW - BI GTD	N77E	43NW												N10E	56SE		
836	SK	MIG MGW TO MIG GAR-BI-M	N72W	25NE												N76E	86NW		
837	SK	LFIDIC MIG GAR-BI-MS SCH	N74W	40NW															
838	SK	W/2M GN W MS PEG - SULFI	N85E	36NW															
839	SK	SULFIDIC MGW	N64E	30NW												N57E	81NW	N74W	84SW
840	SK	// INTRLD GAR-BI-MS SCHIS	N63E	42NW												N28W	86SW		
841	SK	MGW	N32E	48NW															
842	SK	- MYLO & MODERATELY L	N10E	42NW	19	N15W										N62E	83SE		
843	SK	CG FOLIATED BI GTD	N72E	22NW												N22W	83NE		
844	SK	BI GTD	N74E	24NW															
845	SK	BI GTD - FG TO CG	N74E	22NW															
846	SK	G - WEAK TO MODERATE I	N55E	36NW															
847	SK	MGW	N54E	38NW															
848	SK	MGW	N60W	44NE															
849	SK	CG MS-GAR-BI GTD W THIN	N3W	41SW			39	N24E	N20E	68SE	0-20								
850	SK	FOLIATED CG BI GTD	N2W	38SW															
851	SK	FOLIATED CG BI GTD	N21E	32SE															
852	SK	BI GTD	N63E	35NW															
853	SK	BI GG TO GTD	N85W	28NW															
854	SK	CG BI GTD	N85E	44NW															
855	SK	MGW	N5E	50SE															
856	SK	-MS SCHIST - MGW CUT BY	N55W	38SE															
857	SK	GMA TO BI GG W BI GN LEN	N30E	76NE															
858	SK	GTD INTRLD W BI QTZ W L	N55E	42NW															
859	SK	MGW & MIG MGW TO BI GG	N28E	56NW	10	N9W										N5W	85NE		
860	SK	GW & INTRLD GAR-BI-MS S	N48W	24NW															
861	SK	BI GTD	N50W	52NE															
862	SK	G GAR-BI-MS SCHIST W BI	N7W	55SW												N65W	87SW		
863	SK	AR-BI-MS SCHIST - MGW - S	N20E	77NW												N50E	72NE		
864	SK	A - MIG MGW - AGMATITE &	N29E	61SE															
865	SK	MIG MGW	N19E	72NW															
866	SK	MIG GAR-BI-MS SCHIST	N31E	38NW															
867	SK	MIG MGW & BI-QTD PODS	N37E	37SE															
868	SK	MGW	N14E	46NW												N15E	81SE		
869	SK	MGW & GAR-BI-MS SCHIST	N31E	59SE												N45W	84SW		
870	SK	MGW - GAR-BI-MS SCHIST	N44E	66NW												N20W	79NE		
871	SK	GAR-BI-MS SCHIST - MGW	N27E	60SE															
872	SK	GAR-BI-MS SCHIST	N43E	37NW															
873	SK	LYRD MGW	N46W	30NE												N19E	79NW		
874	SK	GAR-BI-MS SCHIST	N31E	67SE															
875	SK	MGW	N21E	80NW															
876	SK	BI GTD - MGW IN FLOAT	N31E	61SE															
877	SK	MIG GAR-BI-MS SCHIST	N47E	20NW															
878	SK	GAR-BI-MS SCHIST - MGW	N20E	78SE															
879	SK	MAG-CHL-MS SCHIST	N38E	84SE															
880	SK	MIG MAG-CHL-MS SCHIST	N39E	82NW															
881	SK	QTZ-TM SCHIST & CHL-H-MS SCHIST																	
882	SK	GW & MIG CHL-H-MS SCHIST					22	N84E	N69E	56SE	0								
883	SK	MIG MGW & MIG BI SCHIST	N29E	45NW												N22E	83NW		
884	SK	MIG MGW	N86W	32NE			29	N34E	N65E	82NW	110								
885	SK	MIG MGW - INEQ MGW	N82E	35NW															
886	SK	MIG MGW	N60E	21NW															
887	SK	MIG MGW	N21W	35NE															
888	SK	MIG MGW	N4W	51NE															
889	SK	MIG MGW	N22E	51SE												N70W	90SW		
890	SK	MIG MGW	N13E	29SE															
891	SK	MIG MGW	N11E	19SE															
892	SK	MGW	N60W	21NE												N12W	50SW	N15W	89NE
893	SK	MGW	N38W	37NE															
894	SK	MGW TO MIG MGW	N73W	38NE															
895	SK	MIG MGW	N71W	41NE															
896	SK	GAR-BI-MS SCHIST - SIL?	N52E	49NW															
897	SK	MGW & AM INTRLS	N35E	52NW															
898	SK	MGW	N56E	57NW															
899	SK	MGW	N12E	69SE															
900	SK	MGW	N24E	59SE															
901	SK	GAR-BI-MS SCHIST - SIL?	N4W	32NE															
902	SK	MCGL? - CONTAINS PODS O	N28E	53NW															
903	SK	LEUCO MS-BI GTD	N30E	36SE															
904	SK	MGW	N20E	80SE															
905	SK	MIG MGW	N33E	53SE															
906	SK	MGW	N15E	47SE															
907	SK	MIG MGW					21	N35E	N29E	79SE	80								
908	SK	MIG MGW & FOLD TRDJ	N44E	52NW			11	S31W	N30E	65NW	10								
909	SK	GAR-BI-MS SCHIST	N61E	52NW															
910	SK	GAR-BI-MS SCHIST & MGW	N31E	45SE															
911	SK	MGW	N58E	47NW															
912	SK	MIG	N32E	52NW															

			Foliation		Lineation		Fold Axis		Axial Surface		IL	Fold	Fold	Crenulation Axis		Joint		Joint	
Station	Quad	Lithology	Strike	Dip	Plunge	Trend	Plunge	Trend	Strike	Dip	Angle	Genr.	Verg.	Plunge	Trend	Strike	Dip	Strike	Dip
913	SK	MIG MGW	N32E	68N															
914	SK	MGW	N34E	79NW															
915	SK	GAR-BI-MS SCHIST	N6E	57SE															
916	SK	MGW & GAR-BI-MS SCHIST	N12E	85NW															
917	SK	GAR-BI-MS SCHIST	N78E	74SE															
918	SK	GW & SOME GAR-BI-MS SCH	N22E	68SE															
919	SK	GW & MINOR GAR-BI-MS S	N12E	65SE															
920	SK	MGW	N27E	72SE															
921	SK	MGW	N21E	67SE															
922	SK	MIG MGW	N18E	25SE															
923	SK	GAR-BI-MS SCHIST	N12E	82SE															
924	SK	MGW	N21E	84SE															
925	SK	GAR-BI-MS SCHIST	N5E	56SE															
926	SK	MIG MGW	N11E	72NW															
927	SK	AR-BI-MS SCHIST & INTRLI	N40E	38SE															
928	SK	MIG GAR-BI-MS SCHIST	N11E	56SE															
929	SK	MIG MGW	N12E	62SE															
930	SK	GAR-BI-MS SCHIST	N8E	41NW															
931	SK	MIG MGW	N20W	74SW												N89W	66NE		
932	SK	MGW	N40E	62SE															
933	SK	MGW	N49W	52SW															
934	SK	MIG MGW	N32E	84NW															
935	SK	- AGMATITE + PODS OF CAI	N27E	78SE															
936	SK	W PODS & BOUDENS OF AM & CALC-SI					15	S5W	N12E	69SE	0	F2							
937	SK	- CG AM CUT BY BI-GTD D	N60W	57NE															
938	SK	FROM MASSIVE TO WEAK	N44W	64NE															
939	SK	PODS & GAR-BI-MS SCHIST	N70W	70SW															
940	SK	MIG AM & MIG MGW	N12E	71NW															
941	SK	MIG MGW & PODS OF AM	N28E	71NW															
942	SK	IG MGW & GAR-BI-MS SCHI	N21E	65SE															
943	SK	MIG MGW	N31E	62SE															
944	SK	IS SCHIST & MINOR MGW &	N14E	72SE															
945	SK	MIG MGW	N44E	55SE															
946	SK	MGW & GAR-BI-MS SCHIST	N58E	44NW															
947	SK	MIG MGW	N62E	50NW												N24W	49NE		
948	SK	MIG MGW W F2 REFOLDS F	N41E	53NW			32	S34W	N29E	46NW	0-20	F2				N72E	32SE		
949	SK	IG MGW TO INEQ MIG MG	N47E	56NW															
950	SK	G MGW - ALMOST MIG MS	N56E	66NW															
951	SK	BI-MS SCHIST - SLIGHTLY M	N49E	58NW															
952	SK	MIG MGW	N51E	66NW															
953	SK	MIG MGW	N68E	64SE															
954	SK	MIG MGW	N45E	67NW															
955	SK	MIG MGW	N48E	61NW															
956	SK	MIG MGW	N39E	71SE			22	N28E	N20E	72SE	0-70					N86W	78NE		
957	SK	MIG MGW	N42E	71NW												N81E	79NW	N56W	87NE
958	SK	MIG MGW	N58E	50NW												N87E	79NW	N56W	87NE
959	SK	MIG MGW	N67E	47NW															
960	SK	AR-BI-MS SCHIST W INTRLS	N46E	75NW												N59W	73SW		
961	SK	IG GAR-BI-MS SCHIST & MC	N60E	50NW															
962	SK	MIG MGW	N60E	56NW															
963	SK	-INEQ MIG BI SCHIST TP M	N50E	50NW															
964	SK	YRD MGW - MINOR GAR-BI	N75E	42NW															
965	SK	GAR-BI-MS SCHIST	N60E	58NW															
966	SK	GAR-BI-MS SCHIST	N20E	59NW															
967	SK	MIG MGW	N46E	50NW															
968	SK	IG INEQ BI SCHIST - MIG MC	N56E	63NW															
969	SK	HIST & MGW - FLOAT MAG	N32E	55NW															
970	SK	MIG MGW	N49E	52NW												N10W	62SW		
971	SK	MIG MGW	N42E	48NW															
972	SK	MIG MGW	N41E	45NW															
973	SK	MS-CHL SCHIST & MIG MGW	N41E	72NW															
974	SK	IS SCHIST & INTRLD W MIG	N44E	71NW	7	N54E													
975	SK	MIG MGW	N36E	80NW												N39W	75SW		
976	SK	MIG MGW	N33E	81NW															
977	SK	MIG GAR-BI-MS SCHIST	N36E	74NW												N48W	84NE		
978	SK	THINLY LYRD GAR-BI-MS	N47E	71NW												N56W	72NE		
979	SK	GAR-BI-MS SCHIST	N38E	73NW															
980	SK	AR-BI-MS SCHIST & MIG MC	N30E	90SE												N69W	88NE		
981	SK	GAR-BI-MS SCHIST	N34E	66SE															
982	SK	MIG MGW	N55E	85NW															
983	SK	G MGW TO GAR-BI-MS SCH	N33E	73NW															
984	SK	INEQ MIG MGW	N46E	72NW															
985	SK	MGW	N32E	60NW															
986	SK	MIG GAR-BI-MS SCHIST	N31E	66NW															
987	SK	MIG GAR-BI-MS SCHIST	N31E	75NW															
988	SK	MIG GAR-BI-MS SCHIST	N36E	74SE															
989	SK	MAG BEARING GAR-CHL-MS SCHIST																	
990	SK	-BI-MS SCHIST W INTRLS M	N45E	59NW												N47W	72SW		
991	SK	MIG MAG-MS-CHL SCHIST	N49E	59NW												N62W	72NE		
992	SK	MGW & MIG MS-MAG SCHIS	N40E	76NW															
993	SK	MAG-MS-CHL-SCHIST & M	N5E	50NW															
994	SK	AG MGW & MAG-MS-CHL S	N52E	71NW	46	N84W										N31W	78SW	N58W	66SW
995	SK	GAR-MAG-CHL-BI-MS SCI	N82E	58NW															
996	SK	MIG MAG-MS SCHIST	N54E	52NW															
997	SK	MIG MAG-MS SCHIST	N53E	75NW															
998	SK	MIG MAG-BI-MS-CHL SCHIS	N40E	69NW															
999	SK	MAG-MS-CHL SHIST & MIG	N82E	58NW												N50W	86NE		
1000	SK	MIG MGW & MAG-MS SCHIS	N42E	69NW												N42W	84SW		
1001	SK	MIG MGW & MAG-MS SCHIS	N68E	48NW															
1002	SK	MS-CHL-MAG SCHIST	N41E	64NW															
1003	SK	MIG MAG-MS-CHL SCHIST	N75E	65NW															
1004	SK	MIG MAG-MS-CHL-BI SCHIS	N66E	69NW												N18E	37SE	N50W	85SW
1005	SK	MS SCHIST	N71E	80NW															
1006	SK	MIG MAG-MS SCHIST	N68E	67NW															
1007	SK	MIG MS SCHIST	N62E	58NW															
1008	SK	MIG MGW	N55E	68NW															
1009	SK	O CG WEAKLY FOLIATED B	N60E	84NW															
1010	SK	GAR-BI-MS SCHIST	N20E	79NW															
1011	SK	MIG MS-MAG SCHIST	N63E	62NW			29	N55E	N63E	45NW	70-80								
1012	SK	MIG MGW	N48E	70NW															
1013	SK	GAR-BI-MS SCHIST	N61E	66NW															
1014	SK	I-MS SCHIST W LOTS OF MS	N65E	72NW															
1015	SK	I-MS SCHIST W LOTS OF MS	N35E	75NW															
1016	SK	GAR-BI-MS SCHIST	N60E	71NW															
1017	SK	MYLO INEQ BI GN	N18E	59SE															
1018	SK	GAR-BI-MS SCHIST	N36E	88SE															
1019	SK	LD INEQ MIG BI SCHIST & C	N44E	54NW															
1020	SK	IG MGW - AGMATITE & LYR	N42E	65NW												N7E	56SE		
1021	SK	AR-BI-MS SCHIST & MIG MC	N25E	58NW															
1022	SK	MIG MGW	N28E	67NW															
1023	SK	MS-CHL-MAG SCHIST	N15E	67NW															
1024	SK	MIG MS-CHL-MAG SCHIST	N72E	53NW															
1025	SK	MIG MGW	N42E	46NW												N54E	62NW		
1026	SK	MIG MGW	N35E	65NW												N71W	42SW		

			Foliation		Lineation		Fold Axis		Axial Surface		IL	Fold	Fold	Crenulation Axis		Joint		Joint	
Station	Quad	Lithology	Strike	Dip	Plunge	Trend	Plunge	Trend	Strike	Dip	Angle	Genr.	Verg.	Plunge	Trend	Strike	Dip	Strike	Dip
1027	SK	MIG MGW	N41E	64NW															
1028	SK	MIG MGW	N42E	68NW															
1029	SK	MIG MGW	N42E	53NW															
1030	SK	MIG MGW	N0E	58NW															
1031	SK	MIG MGW	N32E	65NW															
1032	SK	GAR-BI-MS SCHIST & MGW	N37E	82NW															
1033	SK	MIG GAR-BI-MS SCHIST	N45E	61NW												N60W	87SW		
1034	SK	MIG MGW	N36E	61NW															
1035	SK	BEARING MG BI GTD & SC	N59E	61NW															
1036	SK	IG MAG-H-BI-CHL-MS SCHI	N50E	87NW															
1037	SK	ARING BI GTD & MIG MGW	N34E	78NW															
1038	SK	MGW, MAG GTD, & MIG MA	N54E	75NW															
1039	SK	I GTD W ? & MAG-MS-CHL S	N37E	67NW															
1040	SK	GTD & MIG MEGAC BI GN/M	N38E	63NW															
1041	SK	G MGW & MAG-GAR-MS SCI	N17E	57SE															
1042	SK	MIG MS SCHIST & MIG MGW	N658E	62NW															
1043	SK	MIG MS SCHIST	N43E	62NW															
1044	SK	MS-BI-CHL SCHIST W MINOR	N43E	62NW															
1045	SK	MIG MGW W LATE ? GAR	N75E	60NW												N50W	50SW		
1046	SK	MIG MS-CHL SCHIST	N64E	52NW															
1047	SK	MIG MGW	N62E	76NW															
1048	SK	BI GTD TO GG	N65E	66NW															
1049	SK	GAR-BI-MS GTD	N70E	58NW															
1050	SK	BI GTD & MIG MGW	N62E	52NW															
1051	SK	G MGW & MIG MS-MAG SCI	N52E	73NW												N21W	79SW		
1052	SK	MGW & MIG MS SCHIST &	N62E	75NW															
1053	SK	MIG MGW	N40E	58NW															
1054	SK	MIG MGW	N87E	60NW															
1055	SK	MIG GAR-BI-MS SCHIST - SIL	N71E	59NW															
1056	SK	CHL-BI-MS SCHIST	N49E	61NW															
1057	SK	MIG MS SCHIST	N45E	72NW															
1058	SK	MIG MS SCHIST - MAG	N48E	71NW															
1059	SK	MIG MS-MAG SCHIST -PEG-	N25E	45NW															
1060	SK	MIG MGW	N65E	40NW															
1061	SK	MGW - GAR-MS-BI-QTZ-FEL	N27E	70SE															
1062	SK	GAR-BI-MS SCHIST	N44E	71NW															
1063	SK	MIG MGW - 2 MS GN	N80W	33NE															
1064	SK	MGW - GAR-BI-MS SCHIST	N22E	72SE															
1065	SK	GAR-BI-MS SCHIST	N36E	58SE															
1066	SK	MGW TO MIG MGW	N36E	71NW															
1067	SK	MGW	N34E	85NW															
1068	SK	MGW	N32E	84SE															
1069	SK	MGW TO MIG MGW	N21E	64SE															
1070	SK	MGW TO MIG MGW	N30E	68SE															
1071	SK	MIG MGW	N45E	56NW															
1072	SK	MIG MGW	N42E	85SE															
1073	SK	MGW	N32E	68SE															
1074	SK	MGW	N43E	77SE															
1075	SK	MGW	N10W	62NE															
1076	SK	MGW	N21E	57SE															
1077	SK	GAR-BI-MS SCHIST	N70E	49NW															
1078	SK	MGW & GAR-BI-MS SCHIST	N84E	49NW												N50E	90SE		
1079	SK	MIG MGW W 2MG	N62E	66SE															
1080	SK	S & PODS OF GAR AM - FLO	N32E	78SE															
1081	SK	MGW - 2MG	N32E	76SE															
1082	SK	MIG MGW - AM FLOAT	N29E	69SE												N48W	77NE		
1083	SK	AR-BI-MS SCHIST - AM FLO	N31E	62SE															
1084	SK	GAR-BI-MS SCHIST & MGW	N36E	72SE															
1085	SK	MIG MGW	N34E	72SE															
1086	SK	MIG MGW	N8E	58SE															
1087	SK	MIG MGW	N31E	62SE															
1088	SK	MIG MGW & GAR AM	N48E	52NW															
1089	SK	MGW	N88E	74NW												N20W	68SW		
1090	SK	MIG MGW	N41E	68NW															
1091	SK	D W BI-GAR SCHIST & SCHI	N46E	46NW															
1092	SK	G MAG BEARING BI-MS SCH	N51E	61NW															
1093	SK	MS-CHL-MAG SCHIST	N44E	74NW															
1094	SK	MIG MGW TO BI GG	N48E	82NW															
1095	SK	MIG MGW W MAG	N38E	84NW															
1096	SK	MIG MGW	N58E	71NW															
1097	SK	MIG GAR-BI-MS SCHIST	N30E	80NW															
1098	SK	MGW - GAR-BI-MS SCHIST	N12E	62NW															
1099	SK	ALLY FOLDED MIG MGW - A	N51E	70NW			34	N71E	N81E	70NW	0-10								
1100	SK	MIG MGW	N57E	68NW												N22W	80NW		
1101	SK	MIG MGW	N69E	76NW															
1102	SK	MIG MGW	N59E	60NW															
1103	SK	A - AGMATITE - MGW - 80%	N66E	71NW															
1104	SK	MIG GAR-BI-MS SCHIST - SIL	N64E	75NW															
1105	SK	MIG MGW	N52E	66NW															
1106	SK	D MIG MGW & MAG BEARIN	N41E	69NW												N32W	76SW	N90E	88SE
1107	SK	MIG MGW W MAG	N53E	84NW															
1108	SK	IG MGW - LYRS OF MIGMA (	N69E	68NW												N6E	72NW	N62W	75SW
1109	SK	MIG MGW	N47E	82NW															
1110	SK	MIG MGW	N34E	79NW															
1111	SK	GAR-BI-MS SCHIST	N42E	82NW															
1112	SK	IGMA GN - BI GTD - BI SCHI	N29E	82NW															
1113	SK	G BEARING MIGMA GN & M	N20E	81SE															
1114	SK	GAR-BI-MS SCHIST	N58E	78NW															
1115	SK	MIG MGW	N45E	67NW															
1116	SK	MIG MGW	N41E	85SE															
1117	SK	MIG MGW	N65E	81SE															
1118	SK	MIG MGW	N62E	51NW															
1119	SK	MIG MGW - TO MIGMA GN	N54E	87NW															
1120	SK	IG MGW & MIG - W AM POI	N52E	81NW			17	N40E	N46E	75NW	0-30								
1121	SK	MIG MGW	N31E	73NW															
1122	SK	MIG MGW	N36E	47NW															
1123	SK	MIG MGW & MIG GN	N44E	79NW															
1124	SK	MIG MGW	N62E	65NW												N60W	82NW		
1125	SK	MIG MGW	N50E	73NW															
1126	SK	MIG MGW	N52E	70NW															
1127	SK	A GN - BI GTD - LYRS OF MI	N52E	52NW															
1128	SK	MIG MAG-CHL-MS-BI SCHIS	N53E	65NW															
1129	SK	MAG-CHL-MS SCHIST	N45E	60NW	14	N34E													
1130	SK	MIG MGW	N56E	61NW			43	N27E	N52E	60NW	0-10								
1131	SK	MIG MGW	N39E	61NW															
1132	SK	MIGMA GN - GTD - MIG BI G	N62E	65NW			40	N21E	N44E	63NW	0								
1133	SK	MIG MGW	N46E	71NW															
1134	SK	MIG GAR-BI-MS SCHIST	N11E	35SE															
1135	SK	MIG GAR-BI-MS SCHIST	N68E	57NW															
1136	SK	MGW & PEG - 2MG	N36E	70NW															
1137	SK	IGW & INTRLD GAR-BI-MS S	N35E	82NW															
1138	SK	MGW - 2MG	N33E	79NW															
1139	SK	MIG MGW	N46E	74SE			9	N41E	N38E	74SE	0								
1140	SK	GAR-BI-MS SCHIST	N42E	77SE												N54W	52NE		

			Foliation		Lineation		Fold Axis		Axial Surface		IL	Fold	Fold	Crenulation Axis		Joint		Joint	
Station	Quad	Lithology	Strike	Dip	Plunge	Trend	Plunge	Trend	Strike	Dip	Angle	Genr.	Verg.	Plunge	Trend	Strike	Dip	Strike	Dip
1141	SK	MGW - MINOR GAR-BI-MS S	N52E	62NW															
1142	SK	MIG MGW	N52E	73NW															
1143	SK	GAR-BI-MS-SIL SCHIST	N43E	70SE															
1144	SK	R-BI-MS SCHIST & MINOR M	N46E	66SE															
1145	SK	MIG MGW TO MEGAC MGW	N57E	77NW															
1146	SK	W & MINOR GAR-BI-MS SCI	N60E	54NW															
1147	SK	IIG MGW TO INEQ MIG MG	N46E	83NE															
1148	SK	MIG MGW	N54E	71NW															
1149	SK	FG BI GTD	N51W	77NW															
1150	SK	IIG MGW W CG FELD-BI GT	N42E	73NW															
1151	SK	MIG MGW	N46E	72NW															
1152	SK	MIG MGW	N61E	72NW															
1153	SK	FG MS-CHL SCHIST	N55E	86NW															
1154	SK	GAR-BI-MS SCHIST	N64E	81SE															
1155	SK	MIG MGW	N54E	75NW												N52W	81SW		
1156	SK	MIG MGW	N61E	52NW															
1157	SK	GAR-BI-MS SCHIST	N59E	58NW															
1158	SK	MIG MGW	N34E	65NW															
1159	SK	GAR-BI-MS-SIL SCHIST	N59E	76NW															
1160	SK	GAR-BI-MS SCHIST	N37E	67NW															
1161	SK	MIG MGW	N54E	67NW												N75W	80SW		
1162	SK	IIG MGW TO LOCALLY INE	N58E	85NW															
1163	SK	MIG MGW TO SCHIST	N52E	84NW															
1164	SK	GAR-BI-MS SCHIST	N59E	65SE															
1165	SK	MIG MGW	N39E	90															
1166	SK	MIG MGW	N52E	71SE															
1167	SK	GAR-BI-MS SCHIST	N53E	80SE															
1168	SK	MIG MGW	N54E	77SE															
1169	SK	IG MGW & GAR-BI-MS SCH	N46E	83NW															
1170	SK	MYLO MIG MGW	N51E	74NW												N27W	75NE		
1171	SK	AR-BI-MS SCHIST & MINOR	N52E	59NW															
1172	SK	MIG GAR-BI-MS SCHIST	N44E	68SE															
1173	SK	MIG MGW	N47E	89NW															
1174	SK	MIG MGW - MYLO/INEQ	N45E	79NW															
1175	SK	MIG MGW W BI GTD	N50E	63SE															
1176	SK	MIG MGW	N51E	67NW															
1177	SK	MIG MGW	N56E	81NW												N29W	67NE		
1178	SK	D MIG MGW & GAR-BI-MS S	N33E	88NW															
1179	SK	R-BI-MS SCHIST W AM FLO	N42E	64SE															
1180	SK	GAR-BI-MS SCHIST	N32E	69SE															
1181	SK	GAR-BI-MS SCHIST	N48E	83NW												N54W	84NE		
1182	SK	MIG MGW	N55E	57SE															
1183	SK	SOME INTRLS OF GAR-BI-M	N26E	35SE															
1184	SK	MIG GAR-BI-MS SCHIST	N47E	57SE															
1185	SK	R-BI-MS SCHIST - MINOR M	N52E	58SE												N44W	86SW		
1186	SK	MGW	N47E	87NW															
1187	SK	AR-BI-MS SCHIST & AM POI	N36E	78NW															
1188	SK	GAR-BI-MS SCHIST W AM I	N60E	77SE															
1189	SK	MIG BI SCHIST	N41E	71SE															
1190	SK	IG GAR-BI-MS SCHIST & MC	N47E	79SE															
1191	SK	MIG MGW	N48E	79NW															
1192	SK	MIG MGW	N37E	69NW															
1193	SK	MIG MGW	N54E	66SE															
1194	SK	GAR-BI-MS SCHIST	N51E	67SE												N16W	78SW		
1195	SK	LYRS OF QTZ-GAR-H - POD	N44E	56NW															
1196	SK	MIG MGW TO MEGAC	N25E	71SE															
1197	SK	IIG MGW TO INEQ MIG MG	N47E	74NW															
1198	SK	MIG MGW	N37E	65NW															
1199	SK	MIG MGW	N47E	73NW															
1200	SK	AM - SOME GAR	N49E	57SE															
1201	SK	GAR-BI-MS SCHIST	N40E	61SE															
1202	SK	GAR-BI-MS SCHIST & MIG M	N38E	84NW												N60W	81NE		
1203	SK	MIG MGW	N49E	61NW			53	N44E	N49E	0-20									
1204	SK	GAR-BI-MS SCHIST	N46E	63NW															
1205	SK	INLY LYRD GAR-BI-MS SCH	N41E	81NW															
1206	SK	GAR-BI-MS SCHIST	N37E	80NW												N62W	74NE		
1207	SK	MGW	N43E	80NW															
1208	SK	GAR-BI-MS SCHIST	N44E	68NW															
1209	SK	GAR-BI-MS SCHIST	N48E	47NW															
1210	SK	GAR-BI-MS SCHIST	N47E	70NW															
1211	SK	MS SCHIST & MGW W POD	N25E	71NW															
1212	SK	AR-BI-MS SCHIST & MIG MC	N35E	82NW															
1213	SK	MIG MGW	N43E	63NW															
1214	SK	MIG MGW	N41E	62NW															
1215	SK	GAR-BI-MS SCHIST	N40E	69NW															
1216	SK	NTRLD MIB GAR-BI-MS SCI	N35E	67NW															
1217	SK	MIG MGW	N45E	89NW															
1218	SK	MIG MGW	N39E	61NW			4	N44E	N45E	62NW	0-10	F2				N44W	79NE		
1219	SK	MIG MGW	N72E	45NW			15	S35W	N42E	61SE	90-100	F3				N38E	66SE		
1220	SK	MIG MGW					80	N28E	N22E	82SE	70	F3							
1221	SK	IG AM - BOUDEN IN MIG MC	N37E	49NW															
1222	SK	MGW W PODS & BOUDENS (	N44E	69NW												N70E	34SE	N65W	67NE
1223	SK	MIG MGW	N44E	73NW															
1224	SK	MIG MGW	N46E	47NW															
1225	SK	MIG MGW	N44E	51NW												N28E	28SE		
1226	SK	MIG MGW	N37E	66NW															
1227	SK	IG MGW - QTZ FILLED JOIN	N48E	42NW												N47E	82SE		
1228	SK	W CALC SI & MIG GAR-BI	N77E	33NW												N49W	87SW		
1229	SK	MIG MGW	N47E	50NW															
1230	SK	MIG MGW	N40E	82NW															
1231	SK	MIG MGW	N27E	62SE															
1232	SK	MIG MGW	N20E	87SE															
1233	SK	GW & GAR-BI-MS SCHIST I	N60E	41NW	8	N18E										N72E	83SE	N43W	82SW
1234	SK	MIG MGW	N44E	76NW															
1235	SK	G MAG-GAR-MS SCHIST TO	N36E	71NW															
1236	SK	MG MIG MAG SCHIST	N30E	68NW															
1237	SK	MIG MGW	N38E	72NW												N84W	82SW		
1238	SK	MIG GAR-BI-MS SCHIST	N35E	64NW															
1239	SK	IGW & GAR-BI-MS SCHIST I	N20E	80NW															
1240	SK	CG BI-MS GG	N38E	80NW															
1241	SK	IATED MS-BI GTD & INTRLS	N33E	64NW															
1242	SK	MIG GAR-BI-MS SCHIST	N26E	79SE															
1243	SK	MIG MGW	N26E	72NW															
1244	SK	MIG MGW	N41E	64NW			17	S9W	N17E	53NW	0-10								
1245	SK	MIG MGW	N40E	88NW															
1246	SK	MIG MGW	N34E	68NW												N52W	74SW		
1247	SK	IG GAR-BI-MS SCHIST & MC	N50E	61NW															
1248	SK	MG MS-BI GG	N36E	66NW															
1249	SK	MIG MGW	N59E	72NW															
1250	SK	GAR-BI SCHIST	N36E	69NW															
1251	SK	MGW TO MIG MGW	N45E	51NW												N35W	75SW		
1252	SK	MS-BI GG - SLIGHTLY MYL	N38E	77NW															
1253	SK	MIG MGW	N37E	52NW															
1254	SK	MIG MGW	N58E	32NW															

			Foliation		Lineation		Fold Axis		Axial Surface		IL	Fold	Fold	Crenulation Axis		Joint		Joint	
Station	Quad	Lithology	Strike	Dip	Plunge	Trend	Plunge	Trend	Strike	Dip	Angle	Genr.	Verg.	Plunge	Trend	Strike	Dip	Strike	Dip
1255	SK	MIG MGW	N44E	65NW															
1256	SK	BI-MS SCHIST & SOME LYRI	N42E	68NW												N70W	78NE		
1257	SK	MIG MGW	N38E	58NW															
1258	SK	MIG MGW	N71E	58NW															
1259	SK	R-BI-MS SCHIST & INTRLD M	N32E	66NW															
1260	SK	IGW & INTRLD GAR-BI-MS S	N18E	66NW															
1261	SK	MIG MGW	N55E	64NW															
1262	SK	GAR-BI-MS SCHIST	N37E	74SE												N88W	83SW		
1263	SK	MIG MGW	N30E	60NW															
1264	SK	MINOR LYRS OF F-GAR-B	N34E	59NW															
1265	SK	MIG MGW	N33E	78SE												N44W	87SW		
1266	SK	THINLY LYRD MIG MGW	N45E	76SE															
1267	SK	CG -MG FOLIATED BI GTD	N57E	63NW															
1268	SK	MIG MGW	N44E	67NW															
1269	SK	MIG MGW	N40E	86NW															
1270	SK	GAR-BI-MS SCHIST	N51E	40NW															
1271	SK	MIG BI SCHIST	N42E	79NW															
1272	SK	MIG MGW	N48E	65SE															
1273	SK	MIG MGW	N44E	62NW															
1274	SK	MIG MGW	N36E	67SE															
1275	SK	MIG GAR-BI-MS SCHIST	N54E	73SE															
1276	SK	MIG GAR-BI-MS SCHIST	N37E	52NW															
1277	SK	BI-MS SCHIST TO MIG INEQ	N36E	67NW															
1278	SK	GAR-BI-MS SCHIST	N38E	60NW															
1279	SK	MIG MGW	N46E	79NW															
1280	SK	MIG GAR-BI-MS SCHIST	N47E	62SE															
1281	SK	MGW & MIG GAR-BI-MS SC	N45E	72NW															
1282	SK	GW & LYRD GAR-BI-MS SC	N39E	75NW															
1283	SK	MIG MGW	N34E	87NW															
1284	SK	MGW	N45E	76NW															
1285	SK	D GAR-BI-MS SCHIST & MI	N47E	77NW															
1286	SK	MIG MGW	N53E	82NW															
1287	SK	MIG MGW	N48E	68NW															
1288	SK	MIG MGW	N42E	84NW															
1289	SK	RD MGW & GAR-BI-MS SCH	N48E	78SE															
1290	SK	RD MGW & GAR-BI-MS SCH	N38E	78SE															
1291	SK	MIG MGW	N48E	84NW															
1292	SK	GW W GAR-BI-MS SCHIST INTRLD					14	S25W	N15E	77NW	50-10								
1293	SK	GAR-BI-MS SCHIST & PEG I	N14W	34NE												N65W	62SW	N65E	75SE
1294	SK	MIG MGW & INEQ MIG MGW	N52E	74NW															
1295	SK	IG MGW W SOME MINOR G	N54E	74NW															
1296	SK	MIG MGW	N47E	67NW															
1297	SK	MIG MGW	N33E	51SE															
1298	SK	GW W GAR-BI-MS SCHIST I	N33E	77NW															
1299	SK	GAR-BI-MS SCHIST	N45E	66SE															
1300	SK	MIG INEQ MGW	N58E	75NW															
1301	SK	MIG MGW	N47E	80NW															
1302	SK	R-BI-MS SCHIST & MINOR M	N36E	78NW															
1303	SK	MS SCHIST W MINOR LYRS	N65E	67SE															
1304	SK	MIG MGW	N44E	76SE															
1305	SK	MIG GAR-BI-MS SCHIST	N52E	76SE															
1306	SK	INTRLS MGW & SCHIST	N48E	68SE															
1307	SK	INEQ MIG MGW	N27E	76SE															
1308	SK	MGW	N47E	77NW															
1309	SK	GAR-BI-MS SCHIST & MGW	N65E	80SE															
1310	SK	MIG CHL-MS-MAG SCHIST	N54E	66NW															
1311	SK	ONSISTS OF QTZ-PLAG-BI	N88E	67SE															
1312	SK	P BI GTD	N31E	39SE															
1313	SK	MS SCHIST & MGW/BI GN -	N54E	34NW															
1314	SK	MIG MGW	N43E	65SE			28	N38E	N57E	45NW	40		NW			N32W	81SW		
1315	SK	LO MIG MGW - INEQ MIG M	N52E	50NW															
1316	SK	GAR-BI-MS SCHIST	N23E	57NW															
1317	SK	GAR-BI-MS SCHIST	N51E	52NW															
1318	SK	OURMALINE SCHIST & GAR-BI-MS SCHIST																	
1319	SK	QTZITE ? & QTZ VIEN INTRL	N14E	61NW															
1320	SK																		
1321	SK	MIG MGW	N9W	39NE															
1322	SK	GAR-BI-MS SCHIST - SIL?	N42E	45SE															
1323	SK	GAR-BI-MS SCHIST	N41E	40NW															
1324	SK	MIG MGW	N21W	17NW															
1325	SK	THINLY LYRD MGW	N19W	24NE															
1326	SK	INTRLD MIG MGW	N19E	22SE												N19E	72NW		
1327	SK	MGW	N25E	52SE															
1328	SK	THINLY LYRD MGW	N22E	49SE															
1329	SK	MYLO MGW	N23E	60SE															
1330	SK	BI GAR SCHIST	N45E	68SE															
1331	SK	MGW	N38E	65SE												N62E	78NW		
1332	SK	MIG FELD MGW	N66E	73NW												N52W	56SW		
1333	SK	MIG P SCHIST - MGW	N62E	61NW												N37W	68NE		
1334	SK	W 2MG & MINOR GAR-BI-M	N71E	74NW												N33W	76SW		
1335	SK	GAR-BI SCHIST & MGW	N58E	40NW															
1336	SK	W INTRLD W GAR-BI-MS SC	N42E	68SE	10	N39E													
1337	SK	MIG MGW	N49E	51NW												N46E	67SE		
1338	SK	GAR-BI-MS SCHIST & MIGM	N76E	43NW															
1339	SK	MGW	N53E	72NW												N47W	51NE	N58E	44SE
1340	SK	CG INEQ MIG MGW	N71E	53NW												N57W	56SW		
1341	SK	CG INEQ MIG MGW	N38E	66NW												N34W	77NE		
1342	SK	CG INEQ MIG MGW	N56E	56NW															
1343	SK	R-BI-MS SCHIST & INTRLD M	N37E	71NW												N47W	57NE		
1344	SK	MGW	N77E	42NW			49	S12W	N28E	74SE	70-30					N40W	36SW		
1345	SK	MIG MGW	N81E	57SE															
1346	SK	MIG MGW	N72E	74SE												N74W	41NE		
1347	SK	E - CG BI GG TO GTD & SC	N46E	59SE															
1348	SK	D MIG MGW TO LYRD MIG I	N44E	34NW															
1349	SK	RD MIG MGW TO MIG BI SCI	N38E	64NW															
1350	SK	RD MIG MGW TO MIG BI SCI	N39E	72SE															
1351	SK	MIG GAR-BI SCHIST	N66E	68NW															
1352	SK	MIG MGW	N57E	56NW												N24W	72NE		
1353	SK	GAR-BI-MS SCHIST - SIL?	N47E	72NW															
1354	SK	SCHIST & MIG MGW - NEW	N62E	73NW															
1355	SK	GAR-BI-MS SCHIST	N48E	63NW															
1356	SK	MGW - INTRLD W BI GN & L	N50E	48NW												N23W	73NE		
1357	SK	W & INEQ MIGMA - SLIGHTI	N31E	56NW			17	S68W	N59E	45SE	50-60					N10W	52NE		
1358	SK	RANO MIG MGW & CROSS C	N80W	32NE												N90E	56SE		
1359	SK	GAR-BI-MS SCHIST - MIGM	N53E	81NW															
1360	SK	MIG MGW	N48E	37NW			11	S64W	N68E	29NW	0-10					N36W	72NE		
1361	SK	MIG MGW	N57E	48NW															
1362	SK	MIG MGW W CG MS FLAKES	N46E	33NW												N37W	58NE		
1363	SK	MIG MGW	N42E	34NW															
1364	SK	SIVE TOURMALINE SCHIST w/ QTZ VEINS																	
1365	SK	QTZ & BI SCHIST	N43E	78NW															
1366	SK	MIG MGW	N51E	76NW															
1367	SK	MIG MGW & PEG	N41E	77NW															
1368	SK	MIG MGW	N42E	68NW	46	N13E													

			Foliation		Lineation		Fold Axis		Axial Surface		IL	Fold	Fold	Crenulation Axis		Joint		Joint	
Station	Quad	Lithology	Strike	Dip	Plunge	Trend	Plunge	Trend	Strike	Dip	Angle	Genr.	Verg.	Plunge	Trend	Strike	Dip	Strike	Dip
1369	SK	MIG MGW	N41E	81NW															
1370	SK	MIG MGW & INEQ MIG MGW	N49E	73NW															
1371	SK	AR-QTZ GN - SCHIST - CALC	N24W	21NE															
1372	SK	MGW & MIG MGW	N38E	53SE															
1373	SK	MIG MGW TO MIG BI SCHIS	N40E	82SE	26	S22W	26	S22W	N51E	42NW	90	F3							
1374	SK	S-SIL SCHIST & MGW - CON	N68W	46SW															
1375	SK	GAR-BI-MS SCHISTOSE MGV	N67E	29SE												N85E	86NW		
1376	SK	GAR-BI-MS-SIL SCHIST & I	N20W	58NE	26	S34E										N71E	83SE	N42W	55SW
1377	SK	I-MS-SIL SCHIST & SCHISTO	N5E	58SE															
1378	SK	GAR-BI-MS SCHIST - MIGM/	N11E	64NW												N34W	72SW		
1379	SK	I MGW - SOME SULFIDIC ST	N39E	74NW															
1380	SK	D GN MGW & SULFIDIC STA	N50E	61SE															
1381	SK	FIDIC MGW - GAR-QTZ-FELI	N53E	68SE												N85W	69SW	N2W	67SW
1382	SK	MINOR GAR-BI-MS SCHIST	N19W	42NE												N28E	78NW	N72W	75SW
1383	SK	GAR-BI-MS SCHIST - MIGM/	N76E	59SE															
1384	SK	SCHISTOSE MGW	N34E	47SE															
1385	SK	MINOR GAR-BI-MS SCHIST	N57E	83SE												N34W	63SW		
1386	SK	TRLS OF GAR-BI-MS SCHIST	N45E	65SE												N30W	70SW		
1387	SK	STOSE MGW - GAR-BI-MS SCHIST	N28E	67SE															
1388	SK	GAR-BI-MS SCHIST	N85E	81SE															
1389	SK	GAR-BI-MS SCHISTOSE MGV	N54E	54SE												N71W	65SW	N90E	58NW
1390	SK	STOSE MGW TO MGW - CO	N33E	43SE	12	S3W										N6W	54SW		
1391	SK	& MINOR GAR-BI-MS SCHI	N58E	57SE															
1392	SK	MGW	N27E	60SE															
1393	SK	MGW TO GN MGW	N40E	71SE															
1394	SK	LFIDIC MIG GAR-BI-MS SCH	N75W	62NE															
1395	SK	GAR-BI-MS-SIL SCHIST	N22E	34NW															
1396	SK	SCHISTOSE MGW TO MGW	N38E	69SE															
1397	SK	IGW - GAR-BI-MS-QTZ-FELI	N52E	86SE												N28W	75NE	N69E	42SE
1398	SK	G MS-BI-GAR GG TO GTD	N50E	82SE															
1399	SK	MIG MGW W SOME BI GTD	N51E	80NW												N20W	84SW		
1400	SK	MINOR INTLYRS OF GAR-B	N64E	56NW												N59W	47SW		
1401	SK	MIG GAR-BI-MS QTZ-FELD G	N75E	76NW												N5W	68SW		
1402	SK	BI-MS-SIL SCHIST - SLIGHTL	N71W	48NE												N53W	68SW	N87E	78SE
1403	SK	ULFIDIC MGW TO LYRD MG	N58W	51NE															
1404	SK	BI-MS-SIL SCHIST TO SCHIS	N43W	16NE															
1405	SK	GAR-BI-MS-SIL SCHIST	N39W	39NE	16	S55E													
1406	SK	GAR-BI-MS SCHIST	N37W	37NE												N54E	84SE		
1407	SK	& MINOR GAR-BI-MS-SIL S	N84W	36SW												N55E	39NW		
1408	SK	INED MGW CUT BY SEVER/	N23W	54SW															
1409	SK	SIVE SCHISTOSE MGW TO M	N56E	44SE												N41E	76NW	N9W	88SW
1410	SK	MGW	N66E	56NW															
1411	SK	CONTAINS CHL W INTRLS	N61E	67NW															
1412	SK	DK GREY MIG MGW	N59E	57NW			28	N59W	N81E	45NW	0-10	F2							
1413	SK	DK GREY MIG MGW	N37E	61NW															
1414	SK	MIG MGW	N51E	70NW															
1415	SK	MIG MGW	N58E	32NW															
1416	SK	MGW - VERY QTZ RICH - QT	N31E	73SE															
1417	SK	G MGW TO LYRD MIG BI SCI	N31E	71NW															
1418	SK	MIG MGW	N60E	70NW												N52W	81NE		
1419	SK	DK GREY MIG MGW/GN	N19E	47NW															
1420	SK	GTD GN W INTRLS OF BI GN	N53E	53NW															
1421	SK	MS GG & THIN LYRS OF BI	N64E	31NW															
1422	SK	MIG, SLIGHTLY MYLO MGW	N32E	50NW															
1423	SK	MIG BI GG - INTRLD W BI GI	N10W	62NE															
1424	SK	MYLO MGW	N62E	41NW															
1425	SK	MIG DK GREY MGW	N84W	21NE															
1426	SK	MIGMA	N47E	37NW															
1427	SK	- MOSTLY MIG MGW TO MI	N13E	52NW															
1428	SK	MIG MGW	N14E	52NW															
1429	SK	GW/2MG TO SCHISTOSE MG	N42E	52NW															
1430	SK	MGW - MIG MGW, P	N66E	26NW															
1431	SK	W PEG LYRS, BI GTD & MS	N68W	37NE			38	N30E	N36E	86NW	150								
1432	SK	MIG MGW	N70E	32NW												N48W	81SW		
1433	SK	MGW	N41E	74NW															
1434	SK	MGW & GAR-BI-MS SCHIST	N33E	55NW															
1435	SK	MGW	N51E	33NW															
1436	SK	MGW - MIG MGW	N63E	57NW															
1437	SK	MIG MYLO MGW	N43E	61NW															
1438	SK	MIG MYLO MGW	N54E	56NW															
1439	SK	MGW/GN - DK GREY	N20E	82NW															
1440	SK	MIG MYLO MGW	N81E	40NW															
1441	SK	MIG MGW	N62E	52NW															
1442	SK	IS SCHIST +ST + KY + SIL - A	N79W	32NE															
1443	SK	MGW	N74E	46NW															
1444	SK	MIG MGW	N61W	28NE															
1445	SK	MIG MGW	N64W	42NE															
1446	SK	MIG MGW	N35W	47NE															
1447	SK	MIG MGW & INTRLS OF AM	N3W	51NE															
1448	SK	MIG MGW	N39W	55NE															
1449	SK	MIG MGW	N56W	38NE															
1450	SK	MIG MGW	N57E	64NW															
1451	SK	DIOP-QTZ- CALC-SI	N67E	56NW															
1452	SK	QTZITE	N53E	73NE															
1453	SK	MIG MGW	N45E	46NW			28	N23E	N45E	46NW	0-10								
1454	SK	W & MIG INTRLD BI-PLAG	N67E	43NW												N27E	75SE		
1455	SK	GAR-BI-MS SCHIST - SIL?	N52E	56NW															
1456	SK	MGW	N76E	72NW															
1457	SK	AM	N72E	70SE															
1458	SK	GAR AM	N30E	80NW															
1459	SK	-BI-MS SCHIST - KY? - GAR	N71E	31NW															
1460	SK	-BI-MS SCHIST - KY? - GAR	N73E	47NW															
1461	SK	AR-BI-MS SCHIST - GAR RIC	N66W	54NW															
1462	SK	AR-BI-MS SCHIST - GAR RIC	N81E	31NW															
1463	SK	SCHIST TO SCHISTOSE MGW	N84E	37NW												N75E	59SE		
1464	SK	MGW	N79E	39NW															
1465	SK	TOSE MGW TO GAR-BI-MS S	N71E	52NW															
1466	SK	CHIST INTRLD W MGW - CO	N85W	56NW															
1467	SK	MGW	N68E	52NW															
1468	SK	MGW	N88E	26NW			36	N37W	N48E	45NW	30								
1469	SK	MGW	N82E	24NW															
1470	SK	MIG GMW	N36W	29NE												N76E	73SE		
1471	SK	MGW	N12E	64SE															
1472	SK	MGW - BI-QTZ-FELD GN	N34E	74SE															
1473	SK	MGW	N14E	52NW															
1474	SK	MGW	N29E	76SE												N44W	79NE		
1475	SK	-MS SCHIST TO A SCHISTOS	N29E	74SE															
1476	SK	MGW	N88E	78NW															
1477	SK	MGW - SCHIST	N2E	68SE															
1478	SK	MGW	N35E	84SE															
1479	SK	MGW	N57W	40NE															
1480	SK	MGW	N638E	57NW												N24W	82SW		
1481	SK	MGW	N78E	69NW															
1482	SK	MIG MGW	N45E	72NW															

			Foliation		Lineation		Fold Axis		Axial Surface		IL	Fold	Fold	Crenulation Axis		Joint		Joint	
Station	Quad	Lithology	Strike	Dip	Plunge	Trend	Plunge	Trend	Strike	Dip	Angle	Genr.	Verg.	Plunge	Trend	Strike	Dip	Strike	Dip
1483	SK	MIG MGW - DK GREY	N51E	45NW															
1484	SK	TRLD MS-CHL SCHIST & MG	N42E	61NW															
1485	SK	THINLY LYRD MIG MGW	N46E	660NW												N23W	85SW		
1486	SK	DK GREY MIG MGW	N34E	56NW															
1487	SK	DK GREY MIG MGW	N52E	58NW															
1488	SK	DK GREY MIG MGW	N32E	39NW															
1489	SK	GREY THINLY LYRD MIG M	N35E	71NW												N51W	58NE		
1490	SK	CHIST INTRLD W PODS & LI	N72E	52NW			37	N47E	N53E	80SE	90					N49W	80SW		
1491	SK	CHL SCHIST W INTRLS OF M	N0E	57SE	1	S27W	48	N55E	N55E	90SE	90-10								
1492	SK	GAR-BI-MS SCHIST	N24W	44NE															
1493	SK	MGW	N74W	62NE															
1494	SK	MIG MGW	N71E	41NW															
1495	SK	MIG MGW	N85E	48NW															
1496	SK	MIG MGW	N81E	45NW															
1497	SK	GAR-BI-MS SCHIST - FLOAT	N52E	32NW															
1498	SK	SCHISTOSE MGW	N69E	41NW															
1499	SK	GAR-BI-MS-SIL SCHIST	N82W	58NE															
1500	SK	MIG MGW	N80E	58NW															
1501	SK	MIG MGW	N12W	65NE															
1502	SK	G MGW - BLOCKS OF AM FLA	N64E	40NW															
1503	SK	CG GAR-BI-MS SCHIST	N58E	53NW															
1504	SK	CG MIG GAR-BI-MS SCHIST	N43E	20NW															
1505	SK	CG GAR-BI-MS SCHIST	N71E	39NW												N71W	71NE		
1506	SK	SCHISTOSE MGW	N60E	28NW															
1507	SK	MIG GAR-BI-MS SCHIST	N72E	56NW															
1508	SK	BI-MS SCHIST TO GN - GAR	N58E	36NW															
1509	SK	GAR-BI-MS SCHIST	N71E	42NW															
1510	SK	GAR-BI-MS SCHIST	N48E	58NW															
1511	SK	MIG MGW	N85E	50NW															
1512	SK	SIL-GAR-BI-MS SCHIST	N32E	60NW															
1513	SK	RLD GAR-BI-MS SCHIST & M	N64E	48NW	32	N29E													
1514	SK	RLD GAR-BI-MS SCHIST & M	N36E	21NW															
1515	SK	MIG MGW	N45E	53NW															
1516	SK	MGW	N7E	67SE															
1517	SK	QTZITE TO FELD-GAR MGW	N45W	37NE															
1518	SK	QTZITE TO QTZ RICH MGW	N2E	33SE												N68E	87SE		
1519	SK	MGW TO QTZITE	N73E	42NW															
1520	SK	MIG MGW	N46E	72NW															
1521	SK	MIG MGW	N28E	63NW															
1522	SK	IG MGW TO SCHISTOSE MG	N16E	40SE															
1523	SK	MIG GAR-BI-MS SCHIST - SIL	N48E	46NW															
1524	SK	NTRLD MIG MGW - GAR-BI-S	N76E	3NW			23	N46E	N43E	43SE	50								
1525	SK	MGW	N24E	52NW															
1526	SK	GAR-BI-MS SCHIST - SIL?	N21E	72NW															
1527	SK	MIG MGW	N21E	72NW															
1528	SK	MGW	N15W	42NE															
1529	SK	GAR-BI-MS SCHIST	N35E	62NW															
1530	SK	GAR-BI-MS SCHIST - SIL?	N38E	43SE															
1531	SK	MIG MGW	N43E	68NW												N65W	63SW		
1532	SK	MGW	N34E	73SE															
1533	SK	MGW	N27E	68SE												N54W	85SW		
1534	SK	LT GREY MGW - QTZITE(?)	N32E	80SE															
1535	SK	GAR-BI-MS SCHIST	N43E	38NW															
1536	SK	MGW & GAR-BI-MS SCHIST	N85W	44NW															
1537	SK	GAR-BI-MS SCHIST	N44E	60NW															
1538	SK	GAR-BI-MS SCHIST	N42E	77NW	21	S32W													
1539	SK	MYLONITIC MIG MGW	N71W	53NE															
1540	SK	GW INTRLD W GAR-BI-MS S	N54W	33NE												N24W	81SW		
1541	SK	MIG MGW - SLIGHTLY MYLO	N61E	42NW															
1542	SK	MIG MGW TO MIG BI GN	N71W	82NE			20	N68W	N76W	82NW	0								
1543	SK	MYLO - MIG MGW	N42E	73NW															
1544	SK	SAP - MYLO - MIG MGW	N72W	31NE															
1545	SK	TYLO - MIG MGW - MIG BI G	N50E	47NW															
1546	SK	SAP - DK GREY BI-MS MGW	N41E	82NW												N45W	79SW		
1547	SK	MGW	N65E	79SE															
1548	SK	MIG MGW	N74W	76NE												N21E	83NW		
1549	SK	THIN LYRS OF GAR-BI-MS	N79W	63NE															
1550	SK	CG MS-BI GTD - SIL?	N78E	76NW															
1551	SK	V W N LENSES OF GAR-BI-M	N70E	50NW															
1552	SK	MIG MGW	N47E	53NW															
1553	SK	MGW	N65W	50NE															
1554	SK	MIG GAR-BI-MS SCHIST	N71E	62NW															
1555	SK	W - GAR-BI-MS SCHIST - SIL	N87E	32NW															
1556	SK	W & INTRLD GAR-BI-MS SCI	N43E	42NW															
1557	SK	GAR-BI-MS SCHIST	N52E	41NW															
1558	SK	SCHISTOSE MGW - GTD	N40W	44NE															
1559	SK	MIG MGW	N40W	32NE												N61E	85SE		
1560	SK	MIG MGW W ? FOLD	N68E	47NW			36	N44E	N31E	67SE	20-10								
1561	SK	MIG MGW	N78E	56NW															
1562	SK	MGW W GAR CLUSTER	N82W	48NE															
1563	SK	MGW	N86E	23SE															
1564	SK	MIG MGW	N60W	43NE															
1565	SK	MIG MGW	N86E	31NW															
1566	SK	MIG MGW	N87E	42NW															
1567	SK	MGW - MIG MGW	N68E	55NW															
1568	SK	MIG MGW	N82W	36NE															
1569	SK	THINLY LYRD MIG MGW	N85W	55NE												N4W	58SW		
1570	SK	MILKY QTZ VEIN	N42E	87NW															
1571	SK	MIG MGW	N31E	79NW															
1572	SK	MIG MGW	N72E	68NW															
1573	SK	SAP - MIG MGW	N54E	55NW															
1574	SK	GAR-BI-MS SCHIST	N63E	58NW															
1575	SK	GAR-BI-MS SCHIST & MGW	N65E	52NW															
1576	SK	MGW & GAR-BI-MS SCHIST	N85W	63NW															
1577	SK	MIG MGW	N41E	58NW															
1578	SK	BI-MS-SIL-CHL SCHIST - FI	N58E	45NW															
1579	SK	FOLIATED MS-BI GTD TO GO	N78E	71NW															
1580	SK	FOLIATED MG BI-MS GTD	N76E	58NW															
1581	SK	MGW	N65E	64NW															
1582	SK	GW & GAR-BI-MS SCHIST I	N80E	65NW															
1583	SK	MS SCHIST - CRENULITE MS	N41E	44NW	25	N64E													
1584	SK	GAR-BI-MS GTD TO GN	N54E	75SE															
1585	SK	GAR-BI-MS SCHIST TO GN	N81E	63NW															
1586	SK	GAR-BI-MS SCHIST & GTD	N77W	30NE															
1587	SK	FELSIC MGW	N89W	44NE															
1588	SK	MIG MGW	N75E	33NW															
1589	SK	MGW TO QTZITE	N68E	57NW															
1590	SK	RLD MGW & GAR-BI-MS SCI	N76E	41NW	19	N21E													
1591	SK	MGW	N71E	48NW															
1592	SK	MS-BI SCHIST	N71E	36NW															
1593	SK	GAR-BI-MS SCHIST	N64E	67NW															
1594	SK	R-BI-MS SCHIST W QTZ LEN	N50E	43NW															
1595	SK	MGW	N81E	35NW															
1596	SK	MGW	N32E	32NW															

			Foliation		Lineation		Fold Axis		Axial Surface		IL	Fold	Fold	Crenulation Axis		Joint		Joint	
Station	Quad	Lithology	Strike	Dip	Plunge	Trend	Plunge	Trend	Strike	Dip	Angle	Genr.	Verg.	Plunge	Trend	Strike	Dip	Strike	Dip
1597	SK	MIG MGW	N73E	55NW															
1598	SK	MGW & MS-BI SCHIST	N69E	31NE												N75E	62SE		
1599	SK	V TO INTRLD GAR-BI-MS SC	N69E	59NW															
1600	SK	R-BI-MS TO BI-MS SCHIST -	N78E	59NW															
1601	SK	ST-SIL-GAR-BI-MS SCHIST	N64E	56NW															
1602	SK	MGW & MS-BI SCHIST	N56E	45NW															
1603	SK	MGW - FG TO MG BI GTD	N57E	47NW															
1604	SK	CONTACT - MGW & BI GTD	N40E	56NW															
1605	SK	MGW - SCHIST	N71E	54NW															
1606	SK	MGW	N62E	32NW															
1607	SK	G WEAKLY FOLIATED BI GT	N53E	34NW															
1608	SK	FG TO MG BI GTD	N42E	76NW															
1609	SK	BI GTD	N32E	62NW															
1610	SK	-DEXTRAL SHEAR SENSE -	N63E	53NW															
1611	SK	MS SCHIST	N85E	25NW															
1612	SK	BI GTD	N21E	25NW															
1613	SK	BI GTD W SCREENS OF MS	N53E	52NW															
1614	SK	MIG MGW	N89E	67SE															
1615	SK	CONTACT OF BI GTD SIL.	N59E	36NW															
1616	SK	EAKLY FOLIATED FG BI GT	N37E	78NW															
1617	SK	MYLO MGW	N46E	31NW												N89W	63SW		
1618	SK	MGW	N46E	41NW															
1619	SK	MIG MGW & SCHIST	N47E	83NW															
1620	SK	GAR-BI-MS SCHIST	N73E	72SE															
1621	SK	MIG MGW	N62E	38NW															
1622	SK	MIG MGW	N81E	31NW															
1623	SK	MIG MGW	N56E	67NW															
1624	SK	GW INTRLD W GAR-BI-MS S	N55E	32NW															
1625	SK	MIG MGW	N49E	46NW															
1626	SK	MGW	N79E	55NW															
1627	SK	BI GTD - GG & MIG MGW	N74E	67NW															
1628	SK	BI GTD	N86W	62NE															
1629	SK	FOLIATED CALC-SI & MGW	N71E	26NW															
1630	SK	SOME INTRLS OF GAR-BI-M	N62W	30NE												N61E	70SE	N36W	57SW
1631	SK	AM	N66W	44NE															
1632	SK	BEARING GAR-BI-MS SCHI	N83W	34NE															
1633	SK	MGW & INTRLS OF GAR-BI	N62E	40NW															
1634	SK	INTRLS OF GAR-BI-MS SCHI	N72E	42NW															
1635	SK	TYLO MIG MGW - S -C FABR	N81E	26NW												N48E	79SE		
1636	SK	W W LENS SHAPED LEUCO	N55E	44NW															
1637	SK	MIG MGW - MYLO - TOPS TO	N47E	59NW												N51W	90NE	N33E	64SE
1638	SK	MS SCHIST W SOME STREA	N37E	70NW															
1639	SK	MGW	N64E	48NW															
1640	SK	-MS SCHIST W THIN LYRS (	N90E	61SE															
1641	SK	MIG MGW	N77E	57NW												N11W	46SW		
1642	SK	MGW	N72E	42NW															
1643	SK	MGW	N87E	78NW															
1644	SK	RICH MIG GAR-BI-MS SCHI	N52E	72NW															
1645	SK	MIG MGW	N73E	54NW			67	N61E	N73E	54NW	0	F2	SE						
1646	SK	IG MGW - LT GRAY QTZITE	N60E	66NW															
1647	SK	MIG MGW	N38E	82NW															
1648	SK	MIG MGW	N68E	59NW															
1649	SK	W THIN LYRS OF GAR-BI-M	N54E	69NW															
1650	SK	MGW	N70E	80NW															
1651	SK	MIG MGW	N61E	55NW			56	N16E	N55E	66NW	0-10								
1652	SK	GW & GAR-BI-MS SCHIST -	N58E	54NW															
1653	SK	MIG MGW TO MYLO MGW	N51E	50NW															
1654	SK	MIG MGW	N69E	63NW															
1655	SK	MIG MGW & QTZITE	N43E	66NW															
1656	SK	MIG MGW	N81W	58NE												N60E	79SE		
1657	SK	IG GAR-BI-MS SCHIST & MG	N63E	64NW			24	N60E	N63E	64NW	0								
1658	SK	MIG MGW	N71E	52NW												N29W	57NE	N54E	56NW
1659	SK	MIG MGW	N71W	48NE															
1660	SK	MIG MGW	N56E	61NW															
1661	SK	MIG MGW	N81W	52NE															
1662	SK	MIG MGW	N62E	67NW															
1663	SK	MYLO WHISPY MIG MGW	N63E	66NW			23	N21E	N24E	51NW	80-90								
1664	SK	MIG MGW	N68W	44NE															
1665	SK	MIG MGW	N78E	47NW															
1666	SK	MIG MGW	N61E	60NW															
1667	SK	MASSIVE MGW	N54E	49NW												N36E	70NW		
1668	SK	MIG MGW	N71E	41NW															
1669	SK	MIG MGW	N79E	57NW															
1670	SK	MIG MGW	N38W	78NE												N71E	57SE	N46W	87SW
1671	SK	W THIN INTRLS OF GAR-BI	N7W	37NE															
1672	SK	MIG MGW	N34W	84NE															
1673	SK	PY MIG MGW - TOPS TO TH	N41E	63NW			66	N28E	N36E	80NW	0-20	F2	SE						
1674	SK	LYRD AM	N75W	39NE															
1675	SK	MIG MGW	N83E	42NW															
1676	SK	MIG MGW	N65W	39NE															
1677	SK	AM	N66E	73NW															
1678	SK	MIG MGW	N72E	44NW															
1679	SK	MIG MGW & AM	N77E	53NW												N24E	50NW		
1680	SK	-BI-MS SCHIST INTRLD W M	N80E	42NW															
1681	SK	MIG MGW	N54E	34NW												N71W	75NE	N39E	84SE
1682	SK	MIG MGW	N82E	33NW															
1683	SK	MGW W AM BOUDENS	N49E	58NW															
1684	SK	-MS SCHIST TO SCHISTOSE	N62E	37NW															
1685	SK	W - CONTAINS PRISMATIC	N49E	43NW															
1686	SK	MIG MGW	N85E	41NW															
1687	SK	AR-BI-MS SCHIST - MS REPL	N64E	59NW															
1688	SK	Y GAR-BI-MS SCHIST - MINO	N51E	48NW												N6E	84SE	N76W	86SW
1689	SK	LEY GAR-BI-MS SCHIST & M	N52E	63NW															
1690	SK	MGW	N41E	73NW															
1691	SK	IG MGW - GAR-BI-MS SCHIS	N40E	73NW															
1692	SK	MIG MGW	N43E	59NW															
1693	SK	MGW	N48E	30NW															
1694	SK	MGW	N77E	56NW															
1695	SK	RY GAR-BI-MS SCHIST & MG	N64E	65NW															
1696	SK	AR-BI-MS SCHIST & MINOR	N67E	50NW															
1697	SK	TOSE MGW TO GAR-BI-MS S	N21E	50NW															
1698	SK	WHISPY MIG MGW - MYLO	N25E	58NW															
1699	SK	MIG MGW	N48E	62NW												N74W	77SW		
1700		MIG MGW & GAR-BI-MS SCHI	N51E	64NW			64	N31E	N51E	64NW	0-10	F2							
1701	SK	MIG MGW	N51E	26NW															
1702	SK	MIG GAR-BI-MS-SIL SCHIST	N21E	34NW															
1703	SK	GAR-BI-MS SCHIST - SCALE	N48E	79NW															
1704	SK	GAR-BI-MS SCHIST - SCALE	N55E	29NW															
1705	SK	MIG MGW - SLIGHTLY MYL	N85E	69NW															
1706	SK	MIG MGW	N62E	48NW															
1707	SK	GAR-BI-MS SCHIST	N61E	57NW															
1708	SK	DK GREEN AM	N71E	87NW															
1709	SK	AM - MAY CONTAIN PYX	N21E	46SE															
1710	SK	AM	N54W	35NE															

			Foliation		Lineation		Fold Axis		Axial Surface		IL	Fold	Fold	Crenulation Axis		Joint		Joint	
Station	Quad	Lithology	Strike	Dip	Plunge	Trend	Plunge	Trend	Strike	Dip	Angle	Genr.	Verg.	Plunge	Trend	Strike	Dip	Strike	Dip
1711	SK	QTZ VEIN - PEG W MS	N80W	52NE															
1712	SK	MIG MGW & BI GTD TO GG	N54E	48NW															
1713	SK	MIG MGW	N56W	33NE															
1714	SK	MIG MGW	N39W	36NW															
1715	SK	MGW & MINOR SCHIST IN	N5W	53NE															
1716	SK	AM	N10W	68NE															
1717	SK	FLOAT - DK GREEN AM																	
1718	SK	MIG MGW	N34E	39NW															
1719	SK	MGW	N36W	51NE															
1720	SK	MGW	N49W	52NE															
1721	SK	SIVE DK GREEN AM TO GAI	N39W	55NE												N7W	76NE		
1722	SK	FG MS SCHIST & MGW	N36E	59NW															
1723	SK	MS SCHIST & MGW	N17E	70NW															
1724	SK	AM	N62E	44SE															
1725	SK	EATHERED DK GREEN CPX	N88W	43NW															
1726	SK	MYLO MGW	N51E	84NW															
1727	SK	MIG MGW	N52E	77NW															
1728	SK	MIG MGW	N51E	33NE															
1729	SK	MIG MGW	N32E	40NW															
1730	SK	MIG MGW	N299E	52NW															
1731	SK	LOAT - MGW & MINOR AM	N28E	77NW															
1732	SK	BI GTD TO PEG	N48E	68NW															
1733	SK	MGW	W24E	33NW															
1734	SK	MIG MGW W LYRS OF BI GT	N71E	42NW															
1735	SK	MIG MGW	N54E	41NW															
1736	SK	MINOR MGW INTRLD W PEG	N68E	43NW															
1737	SK	GAR-BI-MS SCHIST	N85E	37NW															
1738	SK	BI-MS SCHIST	N81E	40NW															
1739	SK	W W THIN INTRLS OF BI-MS	N86E	61NW															
1740	SK	MIG MGW	N74E	51NW															
1741	SK	MGW W INTRLS OF BI-MS S	N81E	44NW												N4W	68SW	N52E	56NW
1742	SK	MIG MGW	N81W	33NE															
1743	SK	ETRIC LEUCO PODS SUGGES	N88E	52NW															
1744	SK	MIG MGW	N88E	68NW															
1745	SK	MIG MGW	N88W	62NE															
1746	SK	GAR-BI-MS SCHIST	N51E	52NW															
1747	SK	MIG MGW	N76E	42NW			36	N11E	N16E	87NW	150								
1748	SK	GAR-BI-MS SCHIST	N57E	42NW	20	N39E													
1749	SK	SOME INTRLS OF GAR-BI-M	N61E	61NW															
1750	SK	AM	N52E	46NW															
1751	SK	MIG MGW	N67E	59NW												N32W	83SW	N10E	68SE
1752	SK	MIG MGW	N68E	57NW															
1753	SK	GAR-BI-MS SCHIST - SIL?	N84E	52NW															
1754	SK	MGW	N87E	45NW															
1755	SK	WHISPY - FOLDS VERGE TO	N78E	67NW															
1756	SK	ATTENED GAR - SINISTRAL	N27E	50NW	28	S61W	10	N11E	N48E	70NW	0-10	F2	SE						
1757	SK	GAR-BI-MS SCHIST	N59E	55NW															
1758	SK	MIG MYLO MIGMA	N68E	50NW															
1759	SK	- CONTAINS SOME FLATTE	N60E	56NW	14	N40E													
1760	SK	MIG MGW	N64E	63NW															
1761	SK	MYLO MIG MGW	N44E	66NW															
1762	SK	GAR-B-MS SCHIST	N53E	75SE															
1763	SK	GAR-BI-MS SCHIST	N66E	52NW															
1764	SK	MIG MGW - ALMOST INEQ M	N62E	68NW															
1765	SK	MIG MGW	N56E	73NW															
1766	SK	FOLDS IN MGW	N59E	77SE			47	N70E	N59E	77SE	70	F3							
1767	SK	GAR-BI-MS SCHIST	N67E	60NW															
1768	SK	-BI GTD - SLIGHTLY FOLIAT	N66E	80SE															
1769	SK	MIG MGW	N67E	76NW															
1770	SK	IS SCHIST TO SCHISTOSE M	N63E	67NW															
1771	SK	MIG MGW - QTZ RICH	N59E	74NW															
1772	SK	DK GRAY QTZ RICH MGW	N59E	74NW															
1773	SK	DK GRAY QTZ RICH MGW	N34E	62NW															
1774	SK	MGW	N48E	66NW															
1775	SK	BI-MS SCHIST - SIL? - INTR	N48E	75NW	8	S55W													
1776	SK	MS-BI SCHIST TO MGW	N54E	65NW															
1777	SK	BI-MS SCHIST TO FG MS-BI S	N37E	66NW															
1778	SK	IIG MGW - QTZ RICH - SLIG	N37E	75NW															
1779	SK	MIG MGW	N40E	58NW												N15W	50SW		
1780	SK	IAG BERING CHL-MS SCHIS	N38E	56NW															
1781	SK	PEG TO GTD - CONTAINS M	N72E	34NW															
1782	SK	FELD LENSES - LYRS ARE F	N47E	63NW	19	N56E	54	N31W	N45E	73NW	0-10								
1783	SK	MIG MGW - SLIGHTLY MYL	N42E	50NW															
1784	SK	MIG MGW - MYLO	N49E	75NW															
1785	SK	R-BI-MS SCHIST TO MS SCH	N47E	75NW															
1786	SK	RLD MGW & GAR-BI-MS SC	N56E	72NW															
1787	SK	GAR-BI-MS-SIL SCHIST	N43E	65NW															
1788	SK	AR-BI-MS-ST SCHIST & MG	N61E	56NW															
1789	SK	MGW	N52E	61NW															
1790	SK	BI GG	N66E	47NW															
1791	SK	W MAG BERING LEUCO - W	N59E	50NW															
1792	SK	MIG MGW	N46E	60NW	15	N31E													
1793	SK	MIG MGW	N45E	49NW															
1794	SK	SLIGHTLY MYLO - TOP TO	N49E	57NW												N38W	84NE	N4W	79SW
1795	SK	MIG MGW	N53E	57NW															
1796	SK	GAR-BI-MS SCHIST	N52E	71NW															
1797	SK	G MGW - DK GRAY - QTZ RI	N40E	69NW															
1798	SK	MIG MGW	N54E	77NW															
1799	SK	MIG MGW	N57E	58NW															
1800	SK	GAR-BI-MS SCHIST - SIL?	N46E	67NW															
1801	SK	RLD GAR-BI-MS SCHIST & M	N54E	53NW	9	S38W													
1802	SK	MIG MGW	N57E	65NW															
1803	SK	SCHIST- FOLLOWED BY MIG	N74E	67NW															
1804	SK	MIG MGW	N42E	67NW															
1805	SK	MIG MGW	N46E	74NW															
1806	SK	MIG MGW	N34E	62NW															
1807	SK	MIG MGW	N37E	67NW															
1808	SK	MIG MGW	N49E	56NW															
1809	SK	MIG MGW	N66E	52NW															
1810	SK	GW W TIGHT TO ISOCLINAL					50	N24E	N26E	57NW	0-30	F3							
1811	SK	MASSIVE MIG MGW	N50E	60NW															
1812	SK	MIG MGW - MS VEIN	N54E	48NW															
1813	SK	MIG MGW	N36E	65NW															
1814	SK	MIG MGW	N31E	53NW															
1815	SK	MIG MGW	N46E	44NW															
1816	SK	MIG MGW	N42E	62NW															
1817	SK	GAR-BI-MS SCHIST	N52E	47NW															
1818	SK	MYLO MIG MGW	N47E	72NW															
1819	SK	GAR-BI-MS SCHIST	N51E	63NW															
1820	SK	MIG MGW	N51E	62NW															
1821	SK	MIG MGW	N56E	48NW															
1822	SK	GAR-BI-MS SCHIST & MGW	N48E	46NW															
1823	SK	MIG MGW	N48E	78NW															
1824	SK	D MIG MGW & GAR-BI-MS S	N11E	63NW															

			Foliation		Lineation		Fold Axis		Axial Surface		IL	Fold	Fold	Crenulation Axis		Joint		Joint	
Station	Quad	Lithology	Strike	Dip	Plunge	Trend	Plunge	Trend	Strike	Dip	Angle	Genr.	Verg.	Plunge	Trend	Strike	Dip	Strike	Dip
1825	SK	MIG MGW	N49E	65NW												N54W	57NE		
1826	SK	GAR-BI-MS SCHIST	N42E	52SE															
1827	SK	GAR-BI-MS SCHIST	N55E	64NW															
1828	SK	MYLO BI GG	N69E	81NW															
1829	SK	MIG MGW	N56E	797NW															
1830	SK	GAR-BI-MS SCHIST & MGW	N51E	51NW															
1831	SK	MIG MGW	N67E	55NW															
1832	SK	GAR-BI-MS SCHIST	N30E	44SE															
1833	SK	GAR-BI-MS SCHIST	N31E	84NW															
1834	SK	GAR-BI-MS SCHIST	N42E	63NW															
1835	SK	MIG MGW	N74E	46NW															
1836	SK	MAG-MS-CHL SCHIST - MGW	N49E	48NW															
1837	SK	L-MS SCHIST & THIN MGW	N66E	55NW															
1838	SK	W - W INTRLS OF CHL-MS-B	N80E	34NW															
1839	SK	MIG MGW W DK CHL	N67E	79NW	42	N34W										N60E	39NW		
1840	SK	NTRLD GAR-BI-MS SCHIST -	N43E	37NW															
1841	SK	MIG MGW	N47E	69NW															
1842	SK	MIG MGW	N48E	46NW			13	N46E	N29E	76NW	20	F3	SE						
1843	SK	MS CHL SCHIST	N39E	35NW															
1844	SK	BI-MS CG GTD TO PEG	N46E	54NW												N46E	54NW		
1845	SK	MIG MGW	N67E	47NW															
1846	SK	BI GTD & CG MS-BI GTD	N49E	60NW															
1847	SK	MIG MGW & SCHIST	N36E	51NW															
1848	SK	MIG MGW & SCHIST	N59E	77NW															
1849	SK	MIG MGW	N67E	64NW															
1850	SK	MIG MGW	N52E	53NW															
1851	SK	MGW - MINOR MS SCHIST IN	N67E	68NW															
1852	SK	MASSIVE MIG MGW	N48E	47NW															
1853	SK	MASSIVE MIG MGW	N59E	60NW															
1854	SK	CG BI-MS SCHIST - SIL? - ST	N79E	59NW															
1855	SK	MIG MGW	N75E	57NW															
1856	SK	MIG MGW	N56W	61NE															
1857	SK	MIG MGW	N31E	53NW															
1858	SK	MIG MGW	N80E	60NW															
1859	SK	MIG MGW	N61W	43NE															
1860	SK	MIG MGW	N74E	52NW															
1861	SK	DOMINANT DK TO MED GR	N52E	72NW												N20W	75NE		
1862	SK	GRAY QTZITE & GAR-BI SCI	N77E	52NW															
1863	SK	AM	N83E	38NW															
1864	SK	MIG MGW	N64E	58NW															
1865	SK	MIG MGW & MINOR SCHIST	N41E	67NW															
1866	SK	MYLO MIG MGW - DEXTRAL	N69E	59NW															
1867	SK	MIG MGW & FG-MG BI GTD	N44E	64NW															
1868	SK	MGW CUT BY MG BI-GTD	N50E	46NW			33	N80W	N68E	52NW	0-10	F2							
1869	SK	MIG MGW	N71E	71NW															
1870	SK	MIG MGW & GTD SILLS	N66E	45NW															
1871	SK	MIG MGW	N67E	50NW															
1872	SK	MIG MGW	N494E	60NW															
1873	SK	BI-MS SCHIST TO SCHISTOSE	N36W	65NE															
1874	SK	MGW	N54E	52SE															
1875	SK	MGW TO SCIHSTOSE MGW	N32E	55SE															
1876	SK	MGW	N14E	60SE															
1877	SK	MIG MGW	N58E	67SE															
1878	SK	G MGW W GAR-BI-MS AM PO	N33E	29NW															
1879	SK	MIG MGW	N65E	54NW															
1880	SK	AR-BI-MS SCHIST & SCHIST	N87E	47SE															
1881	SK	MIG MGW	N0E	78SE															
1882	SK	G MGW CUT BY MS BERING	N64E	55SE															
1883	SK	MIG MGW	N14E	47NW															
1884	SK	MS SCHIST & MGW	N60E	75NW															
1885	SK	CG MGW TO METACGL	N85E	75NW															
1886	SK	- INEQ - SLIGHTLY MYLO I	N71E	67NW															
1887	SK	MIG MGW	N20E	83SE															
1888	SK	MIG MGW	N38E	64NW															
1889	SK	MIG MGW	N10E	65SE															
1890	SK	MIG MGW	N49E	65NW															
1891	SK	MIG MGW	N55E	67NW												N61W	74NW		
1892	SK	MGW TO GNESSIC MGW	N26E	84NW												N22E	63NW		
1893	SK	AR-BI-MS SCHIST - ROCKS A	N61E	81SE															
1894	SK	- GAR-BI-MS-SIL SCHIST M	N21E	84NW												N4W	35SW	N14E	83SE
1895	SK	MGW CUT BY BI GTD	N46E	74SE												N45W	87SW		
1896	SK	C-SI PODS & INTRUDED BY	N55E	76NW															
1897	SK	MIG MGW & GTD	N85E	42NW															
1898	SK	W, CONTAINS SMALL PODS	N45E	880NW												N51W	76NE	N35E	69NW
1899	SK	INEQ MIG MGW - TOPS TO I	N41E	71NW												N29W	65SW	N13E	70NW
1900	SK	GAR-BI-MS SCHIST - INTR	N54E	87SE															
1901	SK	MYLO MGW TO METACGL	N68E	84SE															
1902	SK	MYLO INEQ MIG MGW	N57E	81NW															
1903	SK	CONTAINING GAR-MS-BI-G	N85E	75SE															
1904	SK	SLICKENSIDES - THE WHOL	N48E	88SE	74	S65W	20	S42W	N44E	88SE	10-90	TO CLOSED FOLD				N32E	74SE		
1905	SK	TO AUGEN GN - SINISTRAL	N41E	71NW															
1906	SK	MIG INEQ MGW	N57E	61SE															
1907	SK	MIG INEQ MGW	N72E	85NW												N18E	66NW	N42W	69SW
1908	SK	MIG MGW	N56E	83NW												N34E	76NW		
1909	SK	CG MS FLAKES - LOOKS SLI	N81W	67NE															
1910	SK	K GRAY FG MGW - QTZ RIC	N59E	70NW															
1911	SK	AY MIG MGW TO QTZ RICH	N38E	66NW															
1912	SK	MIG MGW	N46E	55NW												N23W	82NE		
1913	SK	G MGW - GAR-BI-MS-SIL SCI	N38E	68NW															
1914	SK	MIG MGW	N66E	63NW															
1915	SK	MIG MGW	N35E	79NW															
1916	SK	MIG MGW	N53E	53NW															
1917	SK	MIG GAR-BI-MS SCHIST - SIL	N32E	45NW															
1918	SK	MIG GAR-BI-MS SCHIST	N50E	47NW															
1919	SK	MIG MGW	N26E	82NW															
1920	SK	K-SPAR , POT-ASH, SUGGE	N26E	82NW															
1921	SK	MIG MGW	N39E	72NW												N36W	80NE		
1922	SK	MIG MGW	N28E	58NW															
1923	SK	IG GAR-BI-MS SCHIST & MG	N45E	49NW															
1924	SK	MIG MGW	N34E	48NW															
1925	SK	MGW W UP RIGHT F3 TIGHT	N46E	83NW			23	N43E	N46E	83NW	30-50	F3							
1926	SK	MIG MGW	N37E	57NW															
1927	SK	MIG MGW	N52E	69NW															
1928	SK	MIG MGW	N29E	60NW															
1929	SK	MIG MGW	N10E	51NE															
1930	SK	GAR-BI-MS SCHIST - MIGM/	N44E	75NW															
1931	SK	MIG MGW	N36E	66NW															
1932	SK	GAR-BI-MS SCHIST	N59E	64NW															
1933	SK	MIG MGW	N37E	52NW															
1934	SK	GAR-BI-MS SCHIST	N23E	65NW															
1935	SK	MIG MGW	N36E	61NW															
1936	SK	MIG MGW	N32E	80NW															
1937	SK	R-BI-MS SCHIST - MIGMA -	N54E	73NW															
1938	SK	G TO MGW - FLOAT IS GAB	N44E	76NW															

			Foliation		Lineation		Fold Axis		Axial Surface		IL	Fold	Fold	Crenulation Axis		Joint		Joint	
Station	Quad	Lithology	Strike	Dip	Plunge	Trend	Plunge	Trend	Strike	Dip	Angle	Genr.	Verg.	Plunge	Trend	Strike	Dip	Strike	Dip
1939	SK	BI-MS SCHIST & MGW - CON	N49E	68NW															
1940	SK	MIG MGW	N40E	52NW															
1941	SK	MIG MGW	N34E	60NW															
1942	SK	MIG MGW	N36E	68NW															
1943	SK	MIG MGW	N40E	82NW															
1944	SK	MIG MGW	N46E	57NW															
1945	SK	MIG MGW	N51E	68NW															
1946	SK	MIG MGW	N42E	62NW															
1947	SK	LIGHTLY MYLO - DEXTRAL	N48E	73NW															
1948	SK	MIG MGW	N51E	59NW															
1949	SK	GAR-BI-MS SCHIST & MGW	N51E	58NW															
1950	SK	IS-CHL-MAG(MINOR) SCHIS	N58E	49NW	12	N47E													
1951	SK	MS-CHL SCHIST	N55E	75NW															
1952	SK	W - FLOAT - MS-CHL-MAG	N68E	66NW															
1953	SK	MS-CHL SCHIST	N44E	68NW															
1954	SK	- MAG SCHIST W THIN INTE	N56E	62NW															
1955	SK	MS-CHL-MAG SCHIST	N54E	39NW															
1956	SK	MIG MGW - PEG	N57E	56NW															
1957	SK	GAR-BI-MS GTD TO LOCAI	N3E	29SE												N20W	66SW	N84E	87SE
1958	SK	CG TO PEG MS-BI GTD	N6E	42NW															
1959	SK	BI GTD & BI GN	N76E	67NW												N25E	78SE	N65W	82NE
1960	SK	RLD MS-BI GG & CG MS-BI	N34W	39SW															
1961	SK	MIGMA TO MS-GAR-BI GG	N79W	48NW															
1962	SK	MIGMA TO MS-BI GG	N71E	47NW			34	N34E	N71E	47NW	30	F3							
1963	SK	ORMED BY SHEARING OUT	N80W	43NE	39	N6E													
1964	SK	IGG & THIN INTRLS OF FG	N43W	34NE	33	N44E										N52E	83NW		
1965	SK	YLO BIGG & THIN LYRS OF	N72E	29NW															
1966	SK	FG MIG/BI GG	N75E	34NW												N22W	80SW		
1967	SK	GAR-BI MS SCHIST	N60E	45NW															
1968	SK	FG MIG/BI GG	N46E	50NW															
1969	SK	FG MIG/BI GG	N70E	35NW															
1970	SK	FG MIG/BI GG	N58E	48NW															
1971	SK	-QTZ GN - VERY LT GRAY I	N84E	36NW															
1972	SK	WHITE MS-FELD-QTZ GN - V	N39E	43NW															
1973	SK	ITE TO MS-BI GG - VERY L	N63E	43NW															
1974	SK	FOLIATED BI GTD	N51W	57NE															
1975	SK	INEQ BI GN	N66E	49NW															
1976	SK	MYLO INEQ BI GN/ MGW	N57W	60NE															
1977	SK	MIG MGW	N58E	58NW															
1978	SK	GAR-BI-MS SCHIST	N51E	58NW															
1979	SK	TOSE MGW TO GAR-BI-MS S	N52W	24NE															
1980	SK	MYLO INEQ MIG MGW	N24E	29NE												N84E	80SE		
1981	SK	SCHISTOSE MGW	N86E	34NW															
1982	SK	MIG MGW	N12E	18SE															
1983	SK	MIG MGW	N36W	58NE															
1984	SK	MIG MGW	N44W	18NE															
1985	SK	MIG MGW	N48E	42NW															
1986	SK	MIG MGW	N72E	54NW															
1987	SK	MIG MGW	N55E	34NW															
1988	SK	MIG MGW	N35E	51SE															
1989	SK	MIG MGW	N57E	52SE															
1990	SK	MIG MGW	N42E	52SE															
1991	SK	MIG MGW	N51W	22NE															
1992	SK	MIG MGW	N0E	52SE															
1993	SK	MIG MGW	N50W	25NE															
1994	SK	MIG MGW	N63W	32NE															
1995	SK	MIG MGW	N16E	63SE															
1996	SK	MIG MGW W AM PODS	N33E	83SE															
1997	SK	MIG MGW	N29E	75NW															
1998	SK	MIG MGW	N73E	65NW															
1999	SK	AM PODS - GIVING DEXTRA	N47E	76NW															
2000	SK	MIG MGW	N54E	51NW															
2001	SK	WEAKLY FOLIATED MS-BI	N59E	29NW															
2002	SK	G TO CG WEAKLY FOLIATE	N66W	32NE															
2003	SK	BI SCHIST - NEAR GTD IS STI	N19E	43SE	17	N36E	18	N31E	N44E	56NW	60-70	F3-4		20	N42E				
2004	SK	ONTACT - BI GTD & MIG MG	N16W	22NE															
2005	SK	GAR-BI-MS SCHIST	N20E	58NW															
2006	SK	GAR-BI-MS SCHIST & GTD	N66W	26NE															
2007	SK	MGW	N89E	46NW															
2008	SK	MIG MGW	N19W	12NE															
2009	SK	MIG MGW	N86E	25NW															
2010	SK	MIG MGW	N55W	58NW												N23W	68SW		
2011	SK	ACT W MIG MGW - FOLIATI	N52W	66NE															
2012	SK	MIG MGW	N81E	26NW															
2013	SK	GAR-BI-MS SCHIST & MGW	N37W	30NE															
2014	SK	I BI GTD - WEAKLY FOLIA	N58W	28NE															
2015	SK	MIG MGW	N81E	26NW															
2016	SK	SCHIST - FOLIATION IN MI	N74W	25NW	11	N66E													
2017	SK	BI GTD - WEAKLY FOLIAT	N31W	20NE															
2018	SK	MIG MGW	N78W	43NE															
2019	SK	MIG MGW	N88W	33NE												N69W	34NE	N76W	22NE
2020	SK	WEAKLY FOLIATED BI GTI	N86E	36NW															
2021	SK	TACT -MIG MGW & BI GTD	N79E	32NW															
2022	SK	ACT - MIG MGW & BI GTD	N81W	32NE															
2023	SK	MIG MGW	N83W	73NE															
2024	SK	ONTACT - MIG MGW & BI GT	N86E	13NW															
2025	SK	MGW	N60E	37NW															
2026	SK	MIG MGW	N79W	28NE															
2027	SK	KY-ST-GAR-BI-MS SCHIST	N76E	10NW															
2028	SK	MIG MGW	N87W	39NE															
2029	SK	& CRENULATED GAR-BI-M	N53E	59NW	13	N47E													
2030	SK	MIG MGW	N84W	37NE			8	N62E	N72E	41NW	0-10	F2							
2031	SK	MIG MGW	N25W	37NE															
2032	SK	MIG MGW	N62E	69NW															
2033	SK	MIG MGW	N51E	51NW															
2034	SK	MIG MGW	N48E	30NW															
2035	SK	R-BI-MS SCHIST ~ 1-9CM TI	N42E	78NW												N48W	81NE		
2036	SK	BECOMING QTZ & FELD RI	N39E	80NW															
2037	SK	IC MGW - INTRUDED BY SE	N58E	70NW												N39E	88SE	N63E	83SE
2038	SK	EG DIKES - DIKES OCCUR I	N42E	76NW												N66W	78SW	N58E	86SE
2039	SK	V - LT GRAY W SULFIDIC ST	N56E	78NW			30	N58E	N46E	75NW	0-30		SE			N58W	76SW	N29W	48NE
2040	SK	S OF GAR-BI-MS SCHIST -TO	N51E	88NW															
2041	SK	MGW & MS SCHIST	N58E	71NW												N56W	78SW		
2042	SK	IC MGW W INTRLS OF GAI	N56E	81NW															
2043	SK	GW & GAR-BI-MS SCHIST -	N54E	78NW															
2044	SK	MGW TO MIG MGW	N49E	76NW															
2045	SK	MYLO GAR-BI-MS SCHIST	N44E	82NW												N87E	76NW		
2046	SK	MYLO MIG MGW	N42E	83NW															
2047	SK	MGW	N44E	75NW															
2048	SK	INTRLD MGW & SCHIST	N42E	74NW															
2049	SK	MIG MGW	N42E	75NW															
2050	SK	SENSE & ISOCLINAL FOLDS	N58E	72NW															
2051	SK	DK GRAY MIG MGW	N30E	72NW															
2052	SK	UT BY SEVERAL PEG DIKE	N52E	81NW												N42E	72NW		

			Foliation		Lineation		Fold Axis		Axial Surface		IL	Fold	Fold	Crenulation Axis		Joint		Joint	
Station	Quad	Lithology	Strike	Dip	Plunge	Trend	Plunge	Trend	Strike	Dip	Angle	Genr.	Verg.	Plunge	Trend	Strike	Dip	Strike	Dip
2053	SK	YLO MGW - SULFIDIC STAIN	N66E	83NW															
2054	SK	LD MGW- GAR-BI-MS-SIL SC	N35E	77NW															
2055	SK	MYLO MIG MGW	N83W	47NE															
2056	SK	GAR-BI-MS SCHIST & MGW	N54E	55NW															
2057	SK	- LAYRING ALMOST BECOM	N56E	53NW															
2058	SK	G MGW - MORE MEGAC & L	N80E	36NW															
2059	SK	MIG MGW	N65E	72NW															
2060	SK	MIG MGW	N58E	60NW			42	N40E	N70E	67NW	90-120	F3	SE						
2061	SK	MIG MGW - SLIGHTLY MYL	N64E	51NW															
2062	SK	IIG MGW - GAR-BI-MS SCHIS	N74W	62NE															
2063	SK	MGW TO GAR-BI-MS SCHIS	N77W	48NE															
2064	SK	MIG GNEISSIC MGW	N84E	59NW															
2065	SK	MIG GNEISSIC MGW	N57E	44NW			35	S60W	N58E	67NW	0-10	F2	SE			N85E	60NW		
2066	SK	MYLO MIG MGW	N69E	56NW															
2067	SK	RALLEL TO FOLIATION & D	N74E	56NW	22	N65E										N48W	80SW		
2068	SK	SSIC MGW & MS-CHL SCHIS	N75E	58NW															
2069	SK	AR-BI-CHL SCHIST W INTR	N88W	76NE															
2070	SK	MIG GNEISSIC MGW	N53E	52NW															
2071	SK	MIG GNEISSIC MGW	N69E	68NW															
2072	SK	IIG GNEISSIC MGW & MAG	N65E	58NW															
2073	SK	MIG MGW TO METACGL	N73E	72NW	31	N73E													
2074	SK	IS SCHIST & MINOR INTRLS	N59E	76NW												N20W	81SW	N77E	57SE
2075	SK	ST - CONTAINS ENOUGH M	N54E	76NW															
2076	SK	OF MAG BERING MS SCHIS	N51E	64NW															
2077	SK	MIG MGW & MS SCHIST	N62E	78NW															
2078	SK	MIG GNEISSIC MGW	N52E	68NW															
2079	SK	MIG GNEISSIC MGW	N64E	60NW															
2080	SK	MIG GNEISSIC MGW	N67E	62NW			30	N62E	N77E	53NW	0								
2081	SK	MIG GNEISSIC MGW	N65E	81NW															
2082	SK	MIG GNEISSIC MGW	N53E	57NW															
2083	SK	MAG-MS SCHIST - INTRLD	N74E	74NW															
2084	SK	IC MGW INTRLD W MAG-M	N79E	56NW															
2085	SK	MIG GNEISSIC MGW	N71W	36NE															
2086	SK	RLD GAR-BI-MS SCHIST & M	N71W	59NE															
2087	SK	RLD MAG-GAR-BI-MS SCHIS	N70E	49NW			45	N31E	N35E	73NW	70-90	F2-3	SE	14	N41E				
2088	SK	MS SCHIST & INTRLS OF MI	N62E	71NW															
2089	SK	MIG MAG-BI-MS SCHIST	N82E	51NW															
2090	SK	IIG MGW & MAG-MS SCHIS	N72E	47NW															
2091	SK	NTRLD MIG MGW & MAG-M	N82E	64NW															
2092	SK	MIG MAG-MS-BI SCHIST	N47E	54NW															
2093	SK	MIG GNEISSIC MGW	N75E	56NW												N21W	39SW	N32E	57NW
2094	SK	MIG GNEISSIC MGW	N54E	58NW												N35W	84NE		
2095	SK	MIG GNEISSIC MGW	N48E	57NW												N40W	89NE		
2096	SK	MIG GNEISSIC MGW	N58E	58NW															
2097	SK	MIG GNEISSIC MGW	N26E	74SE															
2098	SK	GAR-BI-MS SCHIST	N49E	48NW															
2099	SK	GAR-BI-MS SCHIST & MGW	N65E	70NW															
2100	SK	MIG GNEISSIC MGW	N63E	70NW												N40W	87NE		
2101	SK	GAR-BI-MS SCHIST & MGW	N79W	72NE															
2102	SK	MGW W MINOR INTRLS OF	N54E	55NW															
2103	SK	TOSE MGW TO GAR-BI-MS S	N66E	68NW															
2104	SK	RLD MGW & GAR-BI-MS SC	N36E	79SE															
2105	SK	MIG GNEISSIC MGW	N54E	71NW															
2106	SK	MIG GNEISSIC MGW	N72E	42NW															
2107	SK	MIG GNEISSIC MGW	N39E	42NW															
2108	SK	MGW	N71W	50NE															
2109	SK	BI-MS SCHIST - (+-)CHL(+-)M	N41E	61NW	8	N40E										N2W	86NE	N54E	88NW
2110	SK	SCALEY GAR-BI-MS SCHIST	N65E	61NW	44	N58E													
2111	SK	SIC MGW - F2 TIGHT FOLD I	N52E	40NW			24	N47E	N43E	74NW	70-90	F2	SE						
2112	SK	MGW & GAR-BI-MS SCHIST	N66E	46NW															
2113	SK	TOSE MGW TO GAR-BI-MS S	N68E	60NW															
2114	SK	DS & MINOR INTRLS OF SL	N78W	42NE															
2115	SK	GAR-BI-MS SCHIST	N63E	77NW															
2116	SK	GAR-BI-MS SCHIST	N72W	40NE															
2117	SK	R-BI-MS SCHIST TO SCHIST	N86E	62NW															
2118	SK	MIG GNEISSIC MGW	N47E	45NW															
2119	SK	10 CM THICK LAYERS OF G	N60E	30NW															
2120	SK	AR-BI-MS SCHIST W MGW L	N58E	39NW															
2121	SK	MIG GNEISSIC MGW	N71E	40NW															
2122	SK	MIG GNEISSIC MGW	N53E	69NW															
2123	SK	METACGL	N39E	67NW															
2124	SK	MIG MGW	N58E	75NW															
2125	SK	MIG MGW & METACGL	N70E	71NW															
2126	SK	GAR-BI-MS SCHIST	N61E	57NW															
2127	SK	MIG MGW	N67E	74NW															
2128	SK	MIG MGW	N56E	57NW															
2129	SK	MIG GNEISSIC MGW	N79E	69NW															
2130	SK	MIG MGW	N74E	48NW															
2131	SK	TRAL - TOP TO NE - INEQ M	N67E	51NW															
2132	SK	BERING GAR-BI-MS SCHIST	N72E	39NW															
2133	SK	OF MORE MYLO MAG-GAR-	N75E	66NW															
2134	SK	MIG GNEISSIC MGW	N83E	61NW															
2135	SK	MIG GNEISSIC MGW	N53E	57NW															
2136	SK	LY MYLO - GRADES INTO M	N55E	62NW															
2137	SK	O - SHEAR SENSE NOT OBSI	N63E	40NW															
2138	SK	MGW - 30% LEUCO - MORE	N83E	40NW															
2139	SK	ROTOMYLONITIC MIG MGW	N64E	47NW															
2140	SK	TE TO COARSE MYLO - MIG	N56E	63NW															
2141	SK	MIG GNEISSIC MGW	N44E	52NW															
2142	SK	IIG GAR-BI-MS SCHIST - MG	N53E	42NW												N60E	62SE	N52W	69SW
2143	SK	LENS & PODS OF MIGMA	N51E	73NW									NW	18	N39E				
2144	SK	MAG BERING CHL-MS SC	N59E	65NW			38	N54E	N66E	72NW	10-60	F2	SE						
2145	SK	MGW BERING CHL-MS SCI	N47E	52NW															
2146	SK	MIG GNEISSIC MGW	N52E	64NW															
2147	SK	MIG GNEISSIC MGW	N42E	53NW															
2148	SK	MIG GNEISSIC MGW	N48E	67NW															
2149	SK	MS SCHIST - CG GAR-BI-MS	N47E	40NW															
2150	SK	MIG GAR-BI-MS SCHIST	N45E	53NW															
2151	SK	MIG MGW	N54E	50NW															
2152	SK	MIG GNEISSIC MGW	N47E	59NW												N55W	90SW		
2153	SK	CG GAR-BI-MS SCHIST	N76E	41NW															
2154	SK	MIG GNEISSIC MGW	N54E	56NW															
2155	SK	MIG MGW	N63E	47NW															
2156	SK	AR-BI-MS-(KY OR SIL) SCHI	N20E	57SE															
2157	SK	MIG MGW	N36E	73NW															
2158	SK	GAR-BI-MS SCHIST	N61E	53SE															
2159	SK	MIG MGW	N65E	40NW															
2160	SK	MIG GAR-BI-MS SCHIST	N39E	48SE															
2161	SK	G MS SCHIST W MGW INTR	N78E	39NW															
2162	SK	BERING MS SCHIST W INTR	N66E	32NW															
2163	SK	/ & INTRLS OF MAG BERING	N68E	49NW															
2164	SK	Y MYLO INTRLS OF MIG M	N68E	35NW															
2165	SK	IAG BERING CHL-MS SCHIS	N77E	37NW															
2166	SK	MIG GNEISSIC MGW	N59E	49NW															

			Foliation		Lineation		Fold Axis		Axial Surface		IL	Fold	Fold	Crenulation Axis		Joint		Joint	
Station	Quad	Lithology	Strike	Dip	Plunge	Trend	Plunge	Trend	Strike	Dip	Angle	Genr.	Verg.	Plunge	Trend	Strike	Dip	Strike	Dip
2167	SK	MIG GNEISSIC MGW	N73E	77NW															
2168	SK	BI GTD	N58E	59NW															
2169	SK	PEG IN MIG GNEISSIC MGW	N76E	53NW															
2170	SK	MIG GNEISSIC MGW	N63E	42NW															
2171	SK	MIG GNEISSIC MGW	N78E	51NW															
2172	SK	LIATION - TDJ DIKE WEAKL	N72E	48NW												N47W	87SW	N41W	67NE
2173	SK	MIG MGW & PEG	N73W	48NE															
2174	SK	MIG GNEISSIC MGW	N69E	81NW															
2175	SK	MIG MGW	N72E	66NW															
2176	SK	BI-MS SCHIST TO SCHISTOSE	N45E	69NW															
2177	SK	MAG-CHL-MS SCHIST	N52E	77NW															
2178	SK	SOME LYRS ~20-50% CHL	N72E	54NW										15	N58E				
2179	SK	IAG BERING CHL-MS SCHIS	N59E	51NW															
2180	SK	E MIG GAR-BI-MS SCHIST	N63E	72NW												N6W	63SW		
2181	SK	FG GAR-BI-MS SCHIST	N60E	72SE															
2182	SK	GAR-BI-MS SCHIST	N51E	89NW															
2183	SK	TE & GAR-BI-MS SCHIST NE	N41E	70NW												N46W	73NE	N69W	72SW
2184	SK	D MIG GAR-BI-MS SCHIST &	N43E	72NW			37	N42E	N49E	81NW	0-30	F2	SE						
2185	SK	MIG GNEISSIC MGW	N61E	71NW															
2186	SK	MIG MGW - W FOLDED LINE	N55E	75NW	10	S36W													
2187	SK	IG MGW & GAR-BI-MS SCHI	N51E	81NW															
2188	SK	AR-BI-MS SCHIST - F2 TIGH	N44E	61NW			19	S43W	N49E	51NW	0-30	F2	SE			N54W	85SW		
2189	SK	LC-SI & MINOR GAR-BI-MS	N54E	54NW															
2190	SK	MIG MGW TO QTZITE	N60E	66NW															
2191	SK	YROBLAST OF MS - LATH S	N84E	68NW															
2192	SK	MIG GNEISSIC MGW	N71E	38NW															
2193	SK	IISTOSIC MGW & GAR-BI-M	N44E	67NW															
2194	SK	MGW TO GAR-BI-MS SCHIS	N61E	59NW															
2195	SK	C MGW & MIG MGW & GAR	N73E	58NW												N31E	61SE	N32W	68SW
2196	SK	W & GAR-BI-MS SCHIST - ISO	N72E	60NW			26	S69W	N81E	95NW	30-10	F2-3	SE						
2197	SK	IISTOSE MGW & GAR-BI-MS	N62E	41NW															
2198	SK	TOSE MGW & GAR-BI-MS S	N42E	74NW															
2199	SK	TOSE MGW W CACL-SILICA	N48E	58NW															
2200	SK	IISTOSE MGW& MIG GNEISS	N49W	31NW												N63E	69SE	N50W	87SW
2201	SK	K GRAY MIG GNEISSIC MG	N25E	58NW															
2202	SK	K GRAY MIG GNEISSIC MG	N29E	51NW												N52W	79NE		
2203	SK	K GRAY MIG GNEISSIC MG	N60E	52SE															
2204	SK	K GRAY MIG GNEISSIC MG	N39E	26NW												N50W	80NE	N50E	76SE
2205	SK	YLO MIG INEQ GNEISSIC MG	N48E	69NW															
2206	SK	ISSIC MGW - LARGE SCALE					10	N32E	N30E	75NW	50-10	F2	SE						
2207	SK	NEISSIC MGW W MAG & QT	N48E	42NW															
2208	SK	BI GG & MIG MGW	N44E	50NW															
2209	SK	GAR-BI-MS SCHIST	N51E	75NW															
2210	SK	MIG GNEISSIC MGW	N61E	53NW															
2211	SK	MIG GAR-BI-MS SCHIST	N52E	70NW															
2212	SK	-4 FOLD IN MIG MAG BERIN	N30E	85NW			17	N22E	N30E	85NW	70-90	F3-4	SE						
2213	SK	SCHIST & GRADES INTO MIG	N72W	38NE			22	N21E	N24E	76NW	90-100	F3	SE						
2214	SK	OR INTRLS OF MAG BERIN	N63E	57NW															
2215	SK	OR INTRLS OF MAG BERIN	N34E	51NW															
2216	SK	MIG GNEISSIC MGW	N54E	55NW															
2217	SK	IAG BERING MS-CHL SCHIS	N41E	31NW															
2218	SK	MAG BERING MS SCHIST &	N37E	48NW															
2219	SK	MAG-CHL-MS SCHIST	N45E	40NW															
2220	SK	ISSIC MGW W FOLDED F2 C	N39E	66NW			29	S32W	N35E	69NW	0-10	F2	SE						
2221	SK	MS SCHIST - F2 ISOCLINE FO	N41E	49NW			13	N44E	N41E	72NW	0-30	F2	SE			N41E	54NW		
2222	SK	MIG GNEISSIC MGW	N68W	22NE															
2223	SK	MIG GNEISSIC MGW	N76E	53NW															
2224	SK	MIG GNEISSIC MGW	N66E	73SE															
2225	SK	CHL-MS SCHIST W QTZ BO	N68E	55SE															
2226	SK	IAG BERING MS SCHIST - M	N79E	68NW															
2227	SK	MAG BERING CHL-MS SCH	N77E	46NW															
2228	SK	MIG GNEISSIC MGW	N40E	39NW															
2229	SK	MIG MGW	N65E	59NW															
2230	SK	MIG GNEISSIC MGW	N26W	56SW												N55E	90SE		
2231	SK	MIG GNEISSIC MGW	N37E	64NW												N48E	83SE		
2232	SK	MIG GNEISSIC MGW	N18E	72NW															
2233	SK	MIG GNEISSIC MGW	N74E	58NW															
2234	SK	MIG GNEISSIC MGW	N30E	72NW															
2235	SK	GAR-BI-MS SCHIST	N21E	57NW															
2236	SK	MGW	N48E	58NW															
2237	SK	MG - MS-BI GG	N56E	62NW															
2238	SK	MG - MS-BI GG	N74E	46NW															
2239	SK	BI GG W SMALL XENOLITHS	N62E	47NW												N16W	79SW		
2240	SK	BI GG - QTZ - SOME LENSES	N82E	58NW															
2241	SK	I-MS SCHIST - KY LOOKS R	N68E	76NW															
2242	SK	MA - LG MS - MIG GNEISSIC	N65E	78NW															
2243	SK	MIG GNEISSIC MGW	N39E	82NW															
2244	SK	MIG GNEISSIC MGW	N60E	60SE															
2245	SK	MIG GAR-BI-MS SCHIST	N50E	75NW															
2246	SK	FOLIATED BI GTD	N79E	60NW															
2247	SK	MIG MGW	N53E	49NW															
2248	SK	MGW & PEG	N72E	32NW												N8W	87SW		
2249	SK	MIG MGW	N42E	77NW															
2250	SK	MIG MGW	N40E	86SE															
2251	SK	GAR-BI-MS SCHIST & MGW	N56E	60NW															
2252	SK	G BERING MIG GNEISSIC M	N42W	50NE															
2253	SK	AR-BI-MS SCHIST & MIG G	N57E	66NW															
2254	SK	MIG MGW TO BI SCHIST	N18E	58SE															
2255	SK	EAKLY FOLIATED CG BI GT	N34E	67NW															
2256	SK	MIG MGW	N54E	46SE															
2257	SK	GW & MINOR GAR-BI-MS SC	N73E	47NW												N24W	80SW	N80E	72SE
2258	SK	MIG MGW	N84E	50NW												N5E	49SE		
2259	SK	G MGW TO GAR-BI-SM SCH	N81E	50NW															
2260	SK	GAR-BI-MS SCHIST - MGW	N58E	64NW															
2261	SK	QTZITE TO MGW	N69E	88NW															
2262	SK	NEISSIC MGW & GAR-BI-MS	N58E	64NW															
2263	SK	AR-BI-MS SCHIST & MIG GN	N67E	84NW			14	N54E	N70E	75SE	30	F2-3	NE						
2264	SK	CTACULAR FOLDS - BUT OI	N62E	69NW												N53E	49SE	N28E	76NW
2265	SK	LFIDIC MGW & GAR-BI-MS	N46E	45NW															
2266	SK	MIG GNEISSIC MGW	N63E	51NW															
2267	SK	CHISTOSE MGW & MINOR S	N61E	89SE												N27W	49SW		
2268	SK	-BI-MS SCHIST & INTRLD M	N71E	67NW															
2269	SK	MIG MGW	N37E	74SE															
2270	SK	MIG GNEISSIC MGW	N87E	53NW															
2271	SK	MIG GNEISSIC MGW	N24E	55SE															
2272	SK	MIG GNEISSIC MGW	N58E	62NW												N37W	86SW		
2273	SK	MIG GNEISSIC MGW	N56E	66NW															
2274	SK	MIG GNEISSIC MGW	N61E	64NW															
2275	SK	MIG GNEISSIC MGW	N49E	77SE												N43W	89SW		
2276	SK	MGW - TIGHT NEARLY UPRI	N61E	50NW			4	N65E	N78E	80NW	30-70	F2-3	SE						
2277	SK	MIG GNEISSIC MGW	N64E	49NW															
2278	SK	/ & QTZITE - F3 TIGHT TO O	N72E	83NW			41	N64E	N72	83NW	90-10	F3	SE						
2279	SK	MIG MGW	N42E	37SE															
2280	SK	GAR-BI-MS SCHIST	N29E	73NW															

			Foliation		Lineation		Fold Axis		Axial Surface		IL	Fold	Fold	Crenulation Axis		Joint		Joint	
Station	Quad	Lithology	Strike	Dip	Plunge	Trend	Plunge	Trend	Strike	Dip	Angle	Genr.	Verg.	Plunge	Trend	Strike	Dip	Strike	Dip
2281	SK	MIG MGW	N39E	71SE															
2282	SK	MIG MGW	N28E	58SE															
2283	SK	MIG GNEISSIC MGW	N68E	54NW															
2284	SK	MIGMGW	N22E	69SE															
2285	SK	MIG GNEISSIC MGW	N50E	69SE															
2286	SK	IC MGW - ISOCLINAL TO TI	N44E	70NW			34	N22E	N29E	78NW	0-30	F2							
2287	SK	-BI-MS SCHIST - MIG GNEIS	N41E	79SE															
2288	SK	EISSIC MGW W LOTS OF BI	N81E	67NW															
2289	SK	EISSIC MGW W LOTS OF BI	N72E	69NW															
2290	SK	YLO TO INEQ - CONTAINS L	N4E	79NW															
2291	SK	LING MS-BI SCHIST & MIG G	N44E	69NW															
2292	SK	GNEISSIC MGW W BI, MAG	N20E	61NW															
2293	SK	G MS-BI SCHIST & MIG MG	N50E	45NW															
2294	SK	I-CHL BERING MIG GNEISSI	N33E	74NW															
2295	SK	MIG GNEISSIC MGW TO INE	N52E	65NW															
2296	SK	GAR MGW - SLIGHTLY MY	N50E	33NW															
2297	SK	MGW- DEXTRAL TOP TO N	N48E	58NW															
2298	SK	MYLO MIG GNEISSIC MGW	N41E	52NW															
2299	SK	MYLO MIG GNEISSIC MGW	N42E	52NW															
2300	SK	MIG MYLO QTZITE MGW	N41E	46NW															
2301	SK	YLO - ALMOST AUGEN GN	N51E	73NW															
2302	SK	G MGW TO GAR-BI-SM SCH	N52E	49NW															
2303	SK	MGW - SLIGHTLY MYLO	N31E	40NW															
2304	SK	GAR-BI-MS SCHIST & INTL	N67E	62NW															
2305	SK	BERING - MS SCHIST W M	N54E	68NW			24	N50E	N54E	89SE	50	F3	NE						
2306	SK	MIG GNEISSIC MGW	N67E	61NW															
2307	SK	CHIST (+- CHL) - MIG VERY	N50E	50NW															
2308	SK	MIG GNEISSIC MGW	N72E	34NW															
2309	SK	GAR-BI-MS SCHIST	N56E	52NW															
2310	SK	MIG MGW	N43E	50NW															
2311	SK	MIG GNEISSIC MGW	N73E	60NW															
2312	SK	SIC MGW - INTRLS OF MS-C	N54E	53NW															
2313	SK	MIG MGW	N46E	63NW															
2314	SK	MIG MGW	N53E	47NW															
2315	SK	MIG GNEISSIC MGW	N44E	62NW															
2316	SK	ISSIC MGW - MINOR SCHIS	N34E	46NW															
2317	SK	CHISTOSE MGW TO MINOR	N32E	61NW															
2318	SK	ISTOSE MGW W CG MS FLA	N68E	55NW															
2319	SK	MIG MGW	N36E	56NW															
2320	SK	-BI-MS SCHIST TO SCHISTO	N36E	60NW															
2321	SK	I-MS SCHIST TO SCHISTOSI	N37E	55NW															
2322	SK	GW & MINOR GAR-BI-MS S	N26E	56NW												N54W	74NE		
2323	SK	MIG MGW - GNEISSIC MGW	N66E	84NW												N50W	64SW		
2324	SK	IG MGW TO SCHISTOSE MG	N34E	67NW															
2325	SK	MIG MGW	N44E	64NW															
2326	SK	D MGW INTRLD W MIG MA	N47E	62NW															
2327	SK	MAG BERING MS SCHIST &	N51E	74NW															
2328	SK	G MAG BERING MS-CHL SCH	N29E	67NW															
2329	SK	AG BERING MS-CHL SCHIST	N44E	67NW	76NW														
2330	SK	AG BERING MS-CHL SCHIST	N44E	76NW															
2331	SK	G MAG BERING MS-CHL SCH	N15E	80NW															
2332	SK	G GAR-MS SCHIST - MINOR	N39E	77NW															
2333	SK	MIG MGW - CONTAINS MS	N11E	70NW															
2334	SK	G-MS-BI SCHIST & INTRLD M	N75E	57MW															
2335	SK	MIG GNEISS - ALMOST MGW	N52E	61NW															
2336	SK	ICK QTZ-FELD-MAG LEUCO W 1/4 TO 2CM MAG CLUSTERS																	
2337	SK	MIG GNEISSIC MGW	N24E	58NW															
2338	SK	MIG MGW	N26E	52NW												N58W	71NE		
2339	SK	NEISSIC MGW TO SCHISTOS	N38E	51NW															
2340	SK	NTRLD MGW - GAR-BI-MS S	N33E	64NW															
2341	SK	MIG GNEISSIC MGW	N24E	53NW															
2342	SK	QTZITE TO GG - MINOR SCH	N58E	52NW												N0E	73SE		
2343	SK	MIG GNEISSIC MGW	N30E	36NW															
2344	SK	NEISSIC MGW & SCHISTOSE	N28E	50NW												N23W	74SW		
2345	SK	& LEUCO - SOME AGMATITI	N56E	54SE															
2346	SK	I GTD - CONTAINS XENOLIT	N62E	73NW												N28W	88SW	N24E	89SE
2347	SK	MIG GNEISSIC MGW	N24E	58NW															
2348	SK	SIC MGW - INTRLD GAR-BI	N42E	60NW															
2349	SK	G MAG BERING MS-CHL SCH	N73E	62NW															
2350	SK	MIG MS-CHL MG SCHIST	N51E	57NW															
2351	SK	INEQ GNEISSIC MGW	N32E	69NW												N0W	70NW		
2352	SK	DK GRAY MIG MGW	N11E	48SE															
2353	SK	MIG GNEISSIC MGW	N34E	54SE															
2354	SK	SHEAR ZONES - FOLDS AR	N56E	65NW															
2355	SK	MIG GNEISSIC MGW	N46E	52NW															
2356	SK	W INTRLD W MAG BERING	N36E	66NW															
2357	SK	G CHL-MS SCHIST - MAG FA	N29E	66NW															
2358	SK	TO SCHISTOSE MGW TO IN	N42E	59NW										3	N33E				
2359	SK	HIST & MIG MGW - MGW C	N37E	56NW															
2360	SK	G MGW W CG MS & BI FLA	N26E	77NW												N56E	74NW	N4W	73NE
2361	SK	IIG MGW & SCHISTOSE MG	N43E	62SE															
2362	SK	GREENISH GRAY FG SERICITE - CHL SCHIST																	
2363	SK	MIG GNEISSIC MGW	N33E	63NW															
2364	SK	G-MS-BI SCHIST & DK GRA	N44E	39NW															
2365	SK	CG MAG BERING CHL-MS SC	N21E	67NW															
2366	SK	& CRENULATED MAG BER	N27E	84NW										9	S43W	N14W	71NE		
2367	SK	RLD MIG & FG MAG-MS SCH	N36E	78SE										14	S62W	N47W	68SW		
2368	SK	IC MGW W - 1/4 - 1/2 CM RE	N57E	30NW												N32W	57NE		
2369	SK	ASSIVE MIG MGW - DK GR	N58E	47NW															
2370	SK	W W MINOR CHL-MS SCHIS	N76E	56NW															
2371	SK	IIG MGW TO CHL-SERICITE	N44E	40SE												N38W	86SW		
2372	SK	G MAG BERING MS-CHL SCH	N64E	56NW												N38W	86SW		
2373	SK	G MAG BERING MS-CHL SCH	N74E	54NW															
2374	SK	MIG GAR-BI-MS SCHIST	N10E	62NW															
2375	SK	MYLO GAR-BI-MS SCHIST &	N46E	68NW															
2376	SK	MIG MGW	N46E	79NW												N34W	83SW		
2377	SK	MIG MGW W MINOR CHL	N39E	69NW															
2378	SK	MIG MGW - PIN STRIPED	N42E	47NW															
2379	SK	MIG MGW	N34E	81NW															
2380	SK	ES - GAR-BI-MS SCHIST & SO	N58E	68NW			37	N73E	N75E	72NW	70	F3	SE						
2381	SK	ALTERED TO KY) & SCHIST	N71E	56NW															
2382	SK	MIG GNEISSIC MGW	N54E	41NW															
2383	SK	ING CHL-MS SCHIST INTRL	N16E	81SE															
2384	SK	TRLD MGW & MAG-MS-CHL	N79E	34NW															
2385	SK	GAR-BI-MS SCHIST	N42E	39NW															
2386	SK	GW & INTRLD GAR-BI-MS S	N56E	47NW															
2387	SK	G MAG BERING MS-CHL SCH	N38E	77NW															
2388	SK	S-CHL SCHIST - MINOR MA	N61E	66NW															
2389	SK	MIG GNEISSIC MGW	N63E	50NW												N29W	79NE		
2390	SK	MIG GNEISSIC MGW	N34E	87NW															
2391	SK	MIG GNEISSIC MGW	N38E	77NW												N40W	71SW		
2392	SK	MIG MGW	N81W	58NE															
2393	SK	AR-BI-MS SCHIST & SCHIST	N81E	60SE												N24E	83SE	N50E	77SE
2394	SK	RENULATED FG MS SCHIS	N33E	62NW										5	N41E				

			Foliation		Lineation		Fold Axis		Axial Surface		IL	Fold	Fold	Crenulation Axis		Joint		Joint	
Station	Quad	Lithology	Strike	Dip	Plunge	Trend	Plunge	Trend	Strike	Dip	Angle	Genr.	Verg.	Plunge	Trend	Strike	Dip	Strike	Dip
2395	SK	W INTRLD W GAR-BI-MS SC	N28E	74SE															
2396	SK	FOLD IN SHEAR ZONE - MI	N38E	80SE			40	S18W	N23E	83SE	0		SE						
2397	SK	MGW -MYLO & FG GN - TRI	N32S	85NW												N32W	78NW	N32W	76SW
2398	SK	MIG GNEISSIC MGW	N37E	88NW															
2399	SK	G - PTYGMATIC MIG LYRS	N40E	83NW															
2400	SK	// TO MIG MGW - SCHIST LY	N36E	61SE												N59W	86SW		
2401	SK	ISTRAL TOP TO NW SHEAR	N40E	84NW			38	N44E	N61E	80NW	50-90	F3	NW			N81E	65NW		
2402	SK	MIG GNEISSIC MGW	N56E	81SE															
2403	SK	CRYSTALS ~ 2-3 CM LONG	N56E	76NW			36	N26E	N41E	80NW	20	F2-3	SE			N65W	79SW		
2404	SK	LEUCO & MAG BERING CHL	N48E	79NW															
2405	SK	IVE GNEISSIC MAG BERING	N9E	83SE												N68E	55SE	N42E	79NW
2406	SK	EISSIC MGW TO MASSIVE M	N60E	52NW												N46E	59SE	N74E	54SE
2407	SK	SSIVE MAG-CHL BERING M	N13E	85NW												N28E	76SE	N49W	78SW
2408	SK	ING CHL-MS SCHIST & LES	N64E	67NW															
2409	SK	AG BERING CHL-MS SCHIS	N42E	71SE															
2410	SK	QTZ RICH MGW & CHL-MS	N24E	32NW	19	S35W													
2411	SK	-MS SCHIST W CRENULATI	N50E	27NW										5	S46W				
2412	SK	NEISSIC MGW W CHL-MS S	N53E	62NW															
2413	SK	MGW & INTRLD MS-CHL SC	N21E	86NW															
2414	SK	D CRENULATIONS - MGW &	N14E	67SE										12	S21W				
2415	SK	MGW & MINOR SCHIST	N49E	38NW															
2416	SK	IIST & SCHISTOSE MGW - M	N33E	46SE															
2417	SK	MS-CHL SCHIST	N17E	42SE															
2418	SK	ON DETERMINED BY MIG L	N38E	58SE			10	N62E	N37E	45SE	20-70	F3-4							
2419	SK	AG BERING CHL-MS SCHIST	N38E	55SE															
2420	SK	MIG MS CHL SCHIST & MGW	N22E	58SE															
2421	SK	IS CHL SCHIST & CG MS GT	N36E	53NW															
2422	SK	W OVERLIES SCHIST - SPET	N49E	46NW															
2423	SK	C GRAAY MIG GNEISSIC MG	N56W	50NE												N71E	80SE	N74E	60NW
2424	SK	SHEAR SENSE IN SMALL -	N85W	58NE	11	N84E										N47W	87SW		
2425	SK	-10CM LENS POCKS WEATH	N58E	61NW															
2426	SK	RY FROM 5 CM TO 3 M - CON	N58E	51NW												N48W	86SW	N16E	36NW
2427	SK	W SUPERIMPOSED BY CLOS	N61E	78NW			36	N56E	N61E	78NW	70					N4W	59SW		
2428	SK	MGW W ZONES OF PEG & SI	N55E	54NW															
2429	SK	CONTAINS SOME CHL - CG	N41E	48NW															
2430	SK	EISSIC MIG MGW TO MYLO	N52E	44NW															
2431	SK	YLO INEQ MIG MGW - TOP T	N84E	56NW															
2432	SK	MIG GNEISSIC MGW	N50E	55NW												N28W	82SW	N88W	63NW
2433	SK	TION DEVELOPED IN FOLD	N42E	56NW			11	N38E	N47E	57NW	0-20	F2-3				N18W	47NE	N66W	54NE
2434	SK	K GRAY MIG GNEISSIC MG	N52E	62NW															
2435	SK	GNEISSIC MGW INTRLD W C	N48E	35NW															
2436	SK	- SHEAR - PRE F3-4 TIGHT T	N14E	33SE			12	N54E	N73E	22NW	30-70	F3-4	NW						
2437	SK	BERING CHL-MS SCHIST - M	N45E	56SE															
2438	SK	G MAG BERING CHL-MS SCH	N49E	67SE															
2439	SK	G MAG BERING CHL-MS SCH	N30E	65SE			3	N28E	N27E	48SE	60-70	F3-4	NW			N31W	68NE		
2440	SK	L-MS SCHIST & MIG MGW T	N63E	28NW										5	S28W	N26E	57SE		
2441	SK	G CHL-MS SCHIST -MAG BER	N63W	42NE												N56E	82SE		
2442	SK	HL-MS SCHIST & INTRLS OF	N35E	77NW															
2443	SK	MIG GNEISSIC MGW	N54E	23NW															
2444	SK	G GNEISSIC MGW - MAG BER	N51E	32NW												N45W	87SW		
2445	SK	D W MIG MGW & CHL-MS SC	N57E	36NW												N27W	72SW		
2446	SK	T MGW W INTRLS OF MIG C	N72E	28NW												N23E	67SE		
2447	SK	MIG GNEISSIC MGW	N18E	32NW															
2448	SK	W TRD SCHIST PODS & LOT	N85E	60SE															
2449	SK	G MAG BERING CHL-MS SCH	N80W	42NE															
2450	SK	G CHL-MS SCHIST & MIG MG	N60E	43NW															
2451	SK	SSIC MIG MGW & CHL-MS S	N50W	15NE												N7E	78NW		
2452	SK	G MS-CHL SCHIST & MIG MG	N46E	22NW															
2453	SK	DK GNEISSIC MIG MGW	N24W	16NE															
2454	SK	MS SCHIST W MIG GNEISSI	N66E	5SE	58	S29E	12	N67E	N48E	34SE	0-80	F2-3	NW						
2455	SK	BI-MS SCHIST TO CHL-MS SC	N88E	34SE												N47W	72NE	N54W	83SW
2456	SK	ING CHL-MS SCHIST & INTL	N72E	44SE															
2457	SK	AG BERING CHL-MS SCHIST	N38E	34SE															
2458	SK	AG BERING CHL-MS SCHIST	N44E	83SE												N71E	78NW	N28W	43NE
2459	SK	D MIG MGW & MIG CHL-MS	N39E	57NW															
2460	SK	-MS SCHIST & GREENISH M	N39E	29NW															
2461	SK	MGW & MINOR CHL-MS SC	N41E	45NW															
2462	SK	MIG GNEISSIC MGW	N34E	29NW															
2463	SK	MIG GNEISSIC MGW	N85E	25NW												N50E	84SE	N42W	80NE
2464	SK	SSIC MGW - 1/4 CM BAND OF	N37E	15NW												N41E	83NE		
2465	SK	MGW	N25E	78NW															
2466	SK	MGW - MIG GNEISSIC MGW	N82W	65NE															
2467	SK	MIG MGW	N46E	75SE												N44E	90SE		
2468	SK	MIG MGW	N41E	23SE												N62W	72SE		
2469	SK	D ~ // TO FOLIATION - AGM	N39E	79NW			12	S33W	N39E	80NW	0-80		NW			N52W	82SW		
2470	SK	R-BI-MS SCHIST & INEQ MY	N46E	66NW															
2471	SK	- LINEATION DEFINED BY I	N36E	79NW	16	S38W										N62W	85NE		
2472	SK	QTZ-FELD GN & MIG GNEIS	N34E	83NW															
2473	SK	MIG MGW TO MIG GNEISSI	N33E	78NW															
2474	SK	MIG MGW	N33E	76NW															
2475	SK	MIG FG MGW - SMALL SLID	N43E	72NW															
2476	SK	SSIC MGW - SEVERAL SMA	N54E	60NW															
2477	SK	MIG MGW	N52E	60NW															
2478	SK	ULFIDE STAINED - SULFIDI	N49E	76NW	13	N58E										N12E	51NW	N62E	81SE
2479	SK	I GG TO PEG DIKES - // TO F	N42E	72NW												N61W	73SW	N38W	69SW
2480	SK	RLD W INEQ BI GG - BI GG I	N39E	69NW															
2481	SK	OR CHL - CONTACT W MIG	N42E	72NW												N84W	88SW		
2482	SK	INOR GAR MGW - GRADES I	N41E	84NW												N19W	84SW		
2483	SK	VISIBLE - SHEAR TOP TO NE	N51E	66NW			13	N41E	N54E	78NW	0-10	F2	SE						
2484	SK	MIG GNEISSIC MGW	N24E	77NW															
2485	SK	MIG MS SCHIST	N66E	54NW															
2486	SK	SCHISTOSE MGW - SIL? & M	N46E	66NW												N28W	55SW		
2487	SK	GAR-BI-MS SCHIST	N64E	62NW															
2488	SK	MAG BERING MS-CHL SCHIS	N47E	53NW															
2489	SK	G MAG BERING CHL-MS SCH	N40E	51SE															
2490	SK	GW - MINOR CHL-MS SCHIS	N47E	57NW															
2491	SK	S SCHIST - MAKES ANTIFOR	N52E	57SE			1	S51W	N51E	90	122	F4							
2492	SK	MAG BERING CHL-MS SCHIS	N51E	65NW										13	N21E				
2493	SK	MIG GNEISSIC MGW	N72E	62NW												N31E	57SW		
2494	SK	MIG GNEISSIC MGW	N88E	26NW															
2495	SK	MG TO CG MS-BI GTD	N66E	83NW															
2496	SK	MS PEG PROSPECT PIT																	
2497	SK	MIG MGW	N68E	57NW															
2498	SK	MIG MGW	N62E	56NW															
2499	SK	MIG MGW	N77E	43NW															
2500	SK	MIG MGW	N62E	37NW															
2501	SK	MIG MGW	N66E	67NW															
2502	SK	R-BI-MS SCHIST & CRENUL	N74E	59NW										26	N68E				
2503	SK	MIG MGW	N79E	34NW															
2504	SK	THINLY LYRD - SLIGHTLY	N67E	59NW												N39W	67SW		
2505	SK	GAR-BI-MS-SIL SCHIST	N10E	75SE															
2506	SK	GAR-BI-MS-SIL SCHIST	N41E	54NW	6	N43E								6	N43E				
2507	SK	FLOAT HAS ~ 2 CM APPEAR	N51E	77NW															
2508	SK	MGW	N31E	77NW															

Station	Quad	Lithology	Foliation		Lineation		Fold Axis		Axial Surface		IL	Fold	Fold	Crenulation Axis		Joint		Joint	
			Strike	Dip	Plunge	Trend	Plunge	Trend	Strike	Dip	Angle	Genr.	Verg.	Plunge	Trend	Strike	Dip	Strike	Dip
2509	SK	GAR-BI-MS SCHIST	N79E	69SE															
2510	SK	HINLY LYRD SCHISTOSE MG	N63E	52NW															
2511	SK	THINLY SCHISTOSE MGW	N49E	54NW															
2512	SK	MYLO SCHISTOSE MGW	N44E	69NW															
2513	SK	GAR-BI-MS SCHIST	N47E	61NW															
2514	SK	GAR-BI-MS SCHIST	N48E	66NW															
2515	SK	LY LYRD SLIGHTLLY MYLO	N43E	51NW			58	S63W	N54E	68NW	30-Oct	F3	NW						
2516	SK	LY LYRD SLIGHTLLY MYLO	N44E	68NW															
2517	SK	MIG MGW	N76W	33NE															
2518	SK	W - FOLIATION IN BI GTD IS	N82W	32NE															
2519	SK	EAKLY FOLIATED MS-BI G	N47W	45NE															
2520	SK	IG MGW TO SCHISTOSE MG	N73E	36NW															
2521	SK	MS-BI GTD	N42W	37NE												N69W	85NE	N17W	55NE
2522	SK	MS-BI GTD	N47W	32NE															
2523	SK	MS-BI GTD	N11E	50NW															
2524	SK	MS-BI GTD	N25W	26SW															
2525	SK	MS-BI GTD TO GG	N62E	22SE															
2526	SK	I-MS SCHIST - MAYBE XENO	N62E	45NW															
2527	SK	CG MS SCHIST	N77E	42NW															
2528	SK	MS-BI GTD	N44E	52NW															
2529	SK	MS-BI SCHIST	N42E	38NW															
2530	SK	ES LARGE EXFOLIATION C	N42E	49NW															
2531	SK	MIG MGW	N59W	80NE															
2532	SK	EAKLY FOLIATED MS-BI G	N42E	70NW															
2533	SK	TO MIG GN & MINOR MIG	N42E	77NW															
2534	SK	GAR-BI-MS SCHIST	N44E	65SE															
2535	SK	MG BI GTD - WEAKLY FOL	N50E	57SE															
2536	SK	W & MINOR GAR-BI-MS SCI	N43E	68NW															
2537	SK	MIG MYLO MGW	N50E	73NW															
2538	SK	MIG MGW	N55E	73NW															
2539	SK	GAR-BI-MS SCHIST	N57E	63NW															
2540	SK	GNEISSIC MGW - F3 TIGHT	N67E	67NW			25	N17E	N22E	82NW	100-90	F3	SE						
2541	SK	MGW & GAR-BI-MS SCHIST	N71E	81SE															
2542	SK	MIG MGW	N51E	74NW															
2543	SK	MIG MGW	N43E	63NW															
2544	SK	GAR-BI-MS SCHIST & MINOR	N53E	63NW															
2545	SK	GAR-BI-MS SCHIST & MINOR	N50E	74NW															
2546	SK	W & GAR + BI - MELASOME	N39E	75NW															
2547	SK	MIG MGW	N58E	80SE															
2548	SK	MIG MGW - CG	N38E	59NW															
2549	SK	MIG MGW	N48E	64NW															
2550	SK	MIG GNEISSIC MGW	N48E	52NW															
2551	SK	GAR-BI-MS-QTZ-FELD-PLA	N45E	37SE												N5E	78NW	N69E	74SE
2552	SK	V PODS OF GAR-QTZ LEUCO	N67E	57SE															
2553	SK	TO 1M THICK - THIS STUFF	N30E	53SE												N40W	76SW	N36E	85SE
2554	SK	S LIKE BEDDING - RARE - I	N12W	42SW															
2555	SK	INTRLD MGW	N44E	43SE												N37E	47NW	N27E	72SE
2556	SK	GRAY MAG BERING MIG M	N68E	60NW												N61W	74NE		
2557	SK	ERING MIG MS-CHL SCHIST	N56E	77NW			20	N51E	N56E	85NW	0-10		SE						
2558	SK	ERING CHL-MS SCHIST & CH	N68E	47NW												N64W	88NE		
2559	SK	ERING CHL-MS SCHIST & CH	N42E	50NW															
2560	SK	M - 1M) - MIG MGW W MINO	N67E	67NW												N48W	85SW		
2561	SK	TZ-FELD GNEISS - THIS MS	N68E	39NW	0	N51E										N48W	88NE		
2562	SK	- 2 - 3CM LONG GAR - LOCA	N63E	67NW															
2563	SK	N F3-4 FOLDS - FOLD CHL-Q	N39E	40NW	39	N14W	17	N64E	N79E	33NW	10-100	F3-4	SE						
2564	SK	G MGW & MIG MS-CHL SCH	N67E	33NW															
2565	SK	NW DIPPING DEXTRAL SHE	N56E	70NW															
2566	SK	MIG MGW	N19E	40NW			18	N82W	N0E	20NW	30-10		NE						
2567	SK	GAR-BI-MS SCHIST TO MIG	N53W	20NE												N29W	85SW		
2568	SK	MIG MGW	N16E	45NW												N29W	88SW		
2569	SK	MIG MGW	N36E	52NW			37	N22E	N19E	62SE	150								
2570	SK	R-BI-MS SCHIST & MINOR M	N26E	58NW	3	N34E							NE						
2571	SK	EISS - MAG BERING METAI	N19E	40SE															
2572	SK	LC-CHL-TR SCHIST - METAI	N15W	67SW															
2573	SK	MIG MGW	N49E	48NW															
2574	SK	MIG MGW	N47E	47NW															
2575	SK	MIG MGW	N57E	67NW															
2576	SK	MIG MGW	N41E	55NW															
2577	SK	RUNCATED BY GG MS-GG L	N77E	42NW	34	N47W	28	N38E	N52E	77NW	70-100	F3				N39W	67SW	N31E	81NW
2578	SK	L SCHIST - VERY MIGMATTI	N48E	67NW			37	N42E	N31E	74NW	70-50	F1-2-3 S2							
2579	SK	MIG MGW	N47E	68NW															
2580	SK	PEN F3 FOLD - PIC OF BOUD	N47E	76NW			32	N23E	N24E	78SE	70-120	F3							
2581	SK	MIG MGW	N51E	50NW															
2582	SK	GAR-BI-MS SCHIST	N61E	71NW															
2583	SK	BI-MS SCHIST & SCHISTOSE	N52E	68NW															
2584	SK	MIG MGW	N50E	34NW															
2585	SK	MIG MGW	N52E	36NW															
2586	SK	BI-MS SCHIST TO SCHISTOSI	N51E	48NW															
2587	SK	MIG MGW	N48E	52NW															
2588	SK	MIG MGW	N21E	53SE															
2589	SK	MIG MGW	N84E	69NW			24	N64E	N60E	76SE	70	F3	NE						
2590	SK	TOSE MGW & INTRLD W GA	N47E	78NW															
2591	SK	F3 FOLD IN CHL-GAR-BI-MS	N58E	64SE			28	N51E	N58E	64SE	70-90	F3							
2592	SK	MGW	N76E	25SW															
2593	SK	MIG GAR-BI-MS SCHIST	N36E	66NW															
2594	SK	BI-MS SCHIST TO SCHISTOSI	N22E	82NW															
2595	SK	R-BI-MS SCHIST TO SCHISTO	N46E	69NW															
2596	SK	MGW - SCHISTOSE MGW	N59E	47NW															
2597	SK	W TO SCHISTOSE MGW - F3	N53E	48NW			11	S81W	N66E	56NW	0-10	F2	SE						
2598	SK	LONG GROVES - 2 CM DIAM	N41E	35NW															
2599	SK	S SCHIST - SIL MAY BE REP	N51E	65NW															
2600	SK	F3 FOLDS DOMINATE - DOES	N25E	86NW			24	N16E	N25E	86NW	30-70	F3	NE			N68E	82NW		
2601	SK	- LG MS FLAKES MAY BE A	N29W	12NE															
2602	SK	MS CHL SCHIST	N80W	30NE															
2603	SK	BI-MS SCHIST & SCHISTOSE	N58E	84NW															
2604	SK	MIG MGW	N77E	66NW															
2605	SK	SAP - MIG MGW	N78E	75NW															
2606	SK	SAP - MIG MGW	N76E	79NW															
2607	SK	SAP - BI GTD & MIG MGW	N61E	61NW															
2608	SK	CM) LAYER OF BI SCHIST	N71E	57NW															
2609	SK	MIG INEQ MGW	N69E	70NW															
2610	SK	MIG MGW	N81E	50NW															
2611	SK	MIG MGW	N51E	47NW															
2612	SK	MIG MGW	N67E	44NW															
2613	SK	MIG MGW	N57E	51NW															
2614	SK	MIG MGW	N68E	46NW															
2615	SK	MGW & SCHISTOSE MGW	N50E	56NW															
2616	SK	MIG MS SCHIST & MGW	N54E	29NW															
2617	SK	MIG MGW	N59E	78NW															
2618	SK	SAP MIG MGW	N42W	54NE															
2619	SK	MIG MGW	N53E	79NW															
2620	SK	FG BI GTD	N79E	52NW															
2621	SK	MIG MGW	N75E	46NW															
2622	SK	MIG MGW	N66E	46NW															

			Foliation		Lineation		Fold Axis		Axial Surface		IL	Fold	Fold	Crenulation Axis		Joint		Joint	
Station	Quad	Lithology	Strike	Dip	Plunge	Trend	Plunge	Trend	Strike	Dip	Angle	Genr.	Verg.	Plunge	Trend	Strike	Dip	Strike	Dip
2623	SK	MIG MGW	N46E	61NW															
2624	SK	MIG MGW	N449E	55NW															
2625	SK	MIG MGW	N44E	58NW															
2626	SK	GAR-BI-MS SCHIST	N51E	79NW															
2627	SK	MIG MGW	N88E	64NW															
2628	SK	- CHL-TALC-TR SCHIST - METAPYX																	
2629	SK	L-TALC-TR SCHIST - METAI	N71E	30SE															
2630	SK	MGW	N70W	37NE															
2631	SK	GAR-BI-MS SCHIST & MGW	N50W	52NE															
2632	SK	MIG MGW	N26E	82NW															
2633	SK	MIG MGW	N73E	72NW															
2634	SK	MIG MGW	N79W	50NE															
2635	SK	MIG MGW	N82E	50SE															
2636	SK	MIG MGW	N64W	49NW															
2637	SK	MIG MGW	N64W	26NE															
2638	SK	MGW - MIG LYR // TO FOLIA	N68E	35NW	27	65NW													
2639	SK	MIG MGW	N61E	37NW												N78E	82NW		
2640	SK	THINLY LYRD MIG MGW	N62E	50NW															
2641	SK	MIG MGW	N71E	37NW															
2642	SK	MIG MGW	N72E	59NW															
2643	SK	MIG MGW	N64E	34NW															
2644	SK	MIG MGW	N66E	36NW												N39W	82SW	N49E	66SE
2645	SK	MIG MGW	N54E	56NW															
2646	SK	OLIATED BI GTD & MIG MG	N49E	44NW												N23W	77NE		
2647	SK	YS - SCHIST LYRS ARE MYL	N54E	45NW										3	S50W				
2648	SK	MIG MGW	N56E	46NW															
2649	SK	GAR-BI-MS SCHIST	N62E	47					N51E	13SE	30-100	F4		17	N54E				
2650	SK	MIGM MGW	N58E	57NW															
2651	SK	MIG MGW	N12E	66NW															
2652	SK	MIG MGW	N71W	60NE															
2653	SK	MIG MGW	N79E	37NW												N39W	61SW	N60E	47NW
2654	SK	MIG MGW	N86E	37NE															
2655	SK	MIG MGW	N89W	56NE															
2656	SK	IG MGW & GAR-BI-MS SCHI	N72E	49NW															
2657	SK	GAR-BI-MS SCHIST - DEXTR	N72E	48NW															
2658	SK	MIG MGW	N81E	33NW															
2659	SK																		

APPENDIX III

SHRIMP-RG U-Pb Analyses and Trace Element Concentrations of Detrital Zircons

Table A3–1. SHRIMP U-Pb analyses of detrital zircons from the southern Appalachian Valley and Ridge, Blue Ridge, and Inner Piedmont.

						Totals				Radiogenic Ratios[1]									Ages (Ma)[1]				
Spot Name	% comm 206	ppm U	ppm Th	Th/U	$^{232}Th/^{238}U$	$^{238}U/^{206}Pb$	% err	$^{207}Pb/^{206}Pb$	% err	$^{238}U/^{206}Pb$	% err	$^{207}Pb/^{206}Pb$	% err	$^{207}Pb/^{235}U$	% err	$^{206}Pb/^{238}U$	% err	err corr	$^{206}Pb/^{238}U$	± 1σ	$^{207}Pb/^{206}Pb$	± 1σ	% Discord.
CGM-1.1	0.00	25	16	0.634	0.66	8.38	2.8	.0635	5.5	8.38	2.8	.0635	5.5	1.04	6.2	.1193	2.8	.459	***726.4***	***19.5***	**725**	**116**	0
CGM-10.1	0.20	268	86	0.323	0.33	5.24	0.8	.0788	1.6	5.24	0.8	.0786	1.6	2.07	1.8	.1907	0.8	.429	***1125.2***	***8.1***	**1162**	**33**	3
CGM-11.1	0.06	149	54	0.364	0.38	6.68	1.1	.0695	1.8	6.69	1.1	.0680	2.4	1.40	2.7	.1494	1.1	.408	***897.4***	***9.2***	**869**	**51**	-3
CGM-12.1R	0.01	385	54	0.140	0.14	13.57	0.8	.0562	1.9	13.57	0.8	.0562	1.9	0.57	2.0	.0737	0.8	.393	***458.3***	***3.6***	**462**	**42**	1
CGM-13.1	0.52	609	207	0.340	0.35	7.19	0.6	.0713	1.0	7.20	0.6	.0699	1.3	1.34	1.4	.1389	0.6	.402	***838.6***	***4.5***	**924**	**27**	10
CGM-14.1R	-0.08	1234	56	0.045	0.05	13.33	0.4	.0557	1.0	13.34	0.4	.0553	1.2	0.57	1.3	.0750	0.4	.350	***466.0***	***2.0***	**422**	**27**	-9
CGM-15.1	-0.22	101	76	0.750	0.78	5.71	1.3	.0722	2.1	5.73	1.3	.0684	3.6	1.64	3.9	.1744	1.3	.350	***1036.2***	***12.9***	**879**	**75**	-15
CGM-16.1	1.21	34	33	0.958	0.99	6.03	2.3	.0818	3.4	6.03	2.3	.0818	3.4	1.87	4.1	.1658	2.3	.550	***988.7***	***20.7***	**1242**	**67**	26
CGM-17.1	-0.80	124	83	0.669	0.69	5.31	1.2	.0703	3.2	5.31	1.2	.0703	3.2	1.83	3.4	.1884	1.2	.338	***1112.5***	***11.9***	**936**	**66**	-16
CGM-18.1	0.70	368	293	0.795	0.82	7.83	0.7	.0707	1.3	7.83	0.7	.0701	1.4	1.23	1.5	.1276	0.7	.465	***774.4***	***5.2***	**931**	**28**	20
CGM-19.1	0.06	304	68	0.223	0.23	5.11	0.7	.0787	1.6	5.12	0.7	.0780	1.8	2.10	1.9	.1954	0.7	.376	***1150.7***	***7.6***	**1146**	**35**	0
CGM-2.1	0.01	464	103	0.223	0.23	13.90	0.7	.0560	1.7	13.89	0.7	.0563	1.8	0.56	1.9	.0720	0.7	.382	***448.1***	***3.2***	**464**	**39**	4
CGM-20.1	0.95	296	122	0.411	0.42	6.05	0.8	.0797	1.8	6.09	0.8	.0742	2.6	1.68	2.7	.1643	0.8	.285	***980.4***	***7.1***	**1048**	**53**	7
CGM-21.1	0.74	53	36	0.680	0.70	5.88	1.7	.0789	2.7	5.91	1.8	.0735	5.2	1.71	5.5	.1691	1.8	.325	***1007.2***	***16.6***	**1028**	**105**	2
CGM-22.1R	0.24	364	95	0.261	0.27	8.86	0.7	.0644	2.2	8.86	0.7	.0644	2.2	1.00	2.3	.1128	0.7	.311	***689.1***	***4.7***	**754**	**46**	9
CGM-22.2C	-0.21	55	39	0.708	0.73	5.33	1.7	.0748	2.9	5.34	1.7	.0734	3.6	1.90	4.0	.1874	1.7	.437	***1107.2***	***17.6***	**1024**	**72**	-8
CGM-23.1	-0.13	137	88	0.641	0.66	5.61	1.1	.0735	1.7	5.63	1.1	.0720	2.2	1.76	2.4	.1778	1.1	.452	***1054.8***	***10.7***	**985**	**44**	-7
CGM-24.1	0.38	34	32	0.927	0.96	5.88	2.2	.0760	5.2	5.88	2.2	.0760	5.2	1.78	5.7	.1700	2.2	.385	***1012.0***	***20.4***	**1095**	**105**	8
CGM-25.1	0.26	111	98	0.886	0.92	5.25	1.2	.0792	1.8	5.27	1.2	.0767	2.4	2.01	2.7	.1898	1.2	.448	***1120.3***	***12.5***	**1114**	**48**	-1
CGM-26.1	0.95	174	124	0.715	0.74	5.80	1.0	.0810	1.5	5.81	1.0	.0794	1.8	1.88	2.1	.1721	1.0	.476	***1023.5***	***9.4***	**1182**	**36**	16
CGM-27.1	0.13	449	601	1.338	1.38	5.11	0.6	.0793	0.9	5.12	0.6	.0785	1.0	2.12	1.1	.1954	0.6	.518	***1150.7***	***6.2***	**1160**	**19**	1
CGM-28.1	0.22	230	167	0.724	0.75	6.65	0.9	.0709	1.4	6.67	0.9	.0693	1.9	1.43	2.1	.1500	0.9	.420	***900.9***	***7.3***	**907**	**39**	1
CGM-3.1	-0.30	297	84	0.285	0.29	13.55	0.9	.0538	2.0	13.57	0.9	.0526	2.6	0.53	2.7	.0737	0.9	.328	***458.3***	***3.9***	**310**	**59**	-32
CGM-4.1	-0.73	64	53	0.825	0.85	5.38	1.6	.0703	2.6	5.38	1.6	.0703	2.6	1.80	3.1	.1858	1.6	.531	***1098.7***	***16.5***	**937**	**53**	-15
CGM-5.1	-0.46	80	39	0.485	0.50	4.35	1.4	.0820	3.9	4.37	1.4	.0791	4.5	2.50	4.7	.2289	1.4	.294	***1328.6***	***16.7***	**1174**	**89**	-12
CGM-6.1	-0.32	174	130	0.743	0.77	4.77	1.0	.0787	1.4	4.78	1.0	.0781	1.5	2.26	1.7	.2094	1.0	.550	***1225.5***	***10.7***	**1150**	**29**	-6
CGM-7.1R	0.17	1244	214	0.172	0.18	13.45	0.4	.0576	1.0	13.46	0.4	.0574	1.0	0.59	1.1	.0743	0.4	.391	***462.1***	***1.9***	**508**	**23**	10
CGM-8.1	0.06	296	393	1.326	1.37	5.90	0.7	.0733	1.2	5.91	0.7	.0722	1.4	1.68	1.6	.1692	0.7	.460	***1007.9***	***6.9***	**991**	**29**	-2
CGM-9.1	0.55	100	44	0.434	0.45	5.92	1.3	.0771	2.1	5.93	1.3	.0760	2.3	1.77	2.6	.1687	1.3	.498	***1005.2***	***12.1***	**1095**	**45**	9
DEL1-1.1	0.05	299	110	0.369	0.38	5.10	0.6	.0787	0.9	5.10	0.6	.0784	0.9	2.12	1.1	.1961	0.6	.535	***1154.1***	***6.3***	**1157**	**19**	0
DEL1-10.1	0.06	35	23	0.655	0.68	8.40	1.9	.0640	3.7	8.40	1.9	.0640	3.7	1.05	4.2	.1191	1.9	.468	***725.2***	***13.3***	**742**	**78**	2
DEL1-11.1	0.07	608	204	0.335	0.35	5.81	0.4	.0739	0.7	5.81	0.4	.0736	0.7	1.75	0.8	.1721	0.4	.508	***1023.9***	***4.1***	**1030**	**15**	1
DEL1-12.1	-0.02	39	33	0.844	0.87	5.75	1.7	.0736	2.6	5.75	1.7	.0736	2.6	1.76	3.1	.1738	1.7	.534	***1033.1***	***15.9***	**1029**	**53**	0
DEL1-13.1	0.73	161	38	0.235	0.24	6.72	0.8	.0747	1.4	6.72	0.8	.0747	1.4	1.53	1.6	.1488	0.8	.512	***894.0***	***6.9***	**1060**	**28**	19
DEL1-14.1	0.17	320	129	0.404	0.42	5.43	0.6	.0771	0.9	5.44	0.6	.0767	1.0	1.94	1.2	.1839	0.6	.518	***1088.5***	***6.2***	**1112**	**20**	2
DEL1-15.1	0.37	428	119	0.279	0.29	5.30	0.5	.0797	0.7	5.30	0.5	.0797	0.7	2.07	0.9	.1885	0.5	.561	***1113.3***	***5.0***	**1189**	**14**	7
DEL1-16.1	0.07	295	324	1.097	1.13	4.83	0.6	.0813	0.8	4.83	0.6	.0807	0.9	2.30	1.1	.2070	0.6	.541	***1212.7***	***6.7***	**1214**	**19**	0
DEL1-17.1	-0.14	79	35	0.443	0.46	5.69	1.2	.0730	1.9	5.70	1.2	.0717	2.1	1.73	2.4	.1754	1.2	.489	***1041.8***	***11.5***	**976**	**43**	-6
DEL1-18.1	0.20	192	52	0.268	0.28	4.99	0.7	.0808	1.1	5.00	0.8	.0803	1.1	2.22	1.4	.2001	0.8	.556	***1176.1***	***8.1***	**1205**	**22**	3
DEL1-19.1	0.34	147	67	0.453	0.47	4.84	0.8	.0833	1.2	4.84	0.8	.0826	1.3	2.35	1.5	.2065	0.8	.544	***1210.4***	***9.2***	**1260**	**25**	4

Table A3–1. Continued.

						Totals				Radiogenic Ratios[1]									Ages (Ma)[1]				
Spot Name	% comm 206	ppm U	ppm Th	Th/U	$^{232}Th/^{238}U$	$^{238}U/^{206}Pb$	% err	$^{207}Pb/^{206}Pb$	% err	$^{238}U/^{206}Pb$	% err	$^{207}Pb/^{206}Pb$	% err	$^{207}Pb/^{235}U$	% err	$^{206}Pb/^{238}U$	% err	err corr	$^{206}Pb/^{238}U$	± 1σ	$^{207}Pb/^{206}Pb$	± 1σ	% Discord.
DEL1-2.1	1.70	509	85	0.167	0.17	7.03	0.5	.0813	0.8	7.04	0.5	.0795	1.1	1.56	1.2	.1420	0.5	.419	***855.9***	***3.9***	**1184**	**21**	38
DEL1-20.1	0.19	190	116	0.613	0.63	4.80	0.8	.0825	1.1	4.80	0.8	.0825	1.1	2.37	1.4	.2084	0.8	.575	***1220.2***	***8.7***	**1257**	**22**	3
DEL1-21.1	1.08	50	14	0.285	0.29	5.45	1.5	.0843	2.1	5.46	1.5	.0826	2.5	2.09	2.9	.1831	1.5	.509	***1083.8***	***14.6***	**1261**	**48**	16
DEL1-22.1	0.06	351	264	0.754	0.78	4.42	0.5	.0854	0.7	4.42	0.6	.0849	0.8	2.65	1.0	.2261	0.6	.555	***1313.8***	***6.5***	**1314**	**16**	0
DEL1-23.1	0.11	145	41	0.281	0.29	5.40	0.9	.0769	1.3	5.41	0.9	.0752	1.8	1.91	2.1	.1847	0.9	.433	***1092.6***	***8.9***	**1074**	**37**	-2
DEL1-24.1	0.30	166	65	0.392	0.41	5.16	0.8	.0802	1.5	5.16	0.8	.0802	1.5	2.14	1.7	.1938	0.8	.485	***1141.7***	***8.5***	**1203**	**29**	5
DEL1-25.1	2.31	239	204	0.853	0.88	4.12	0.6	.1071	0.8	4.12	0.6	.1071	0.8	3.58	1.0	.2425	0.6	.630	***1399.4***	***8.1***	**1751**	**15**	25
DEL1-26.1	0.36	73	18	0.243	0.25	6.19	1.2	.0741	2.0	6.20	1.2	.0726	2.3	1.62	2.6	.1612	1.2	.475	***963.7***	***11.1***	**1004**	**47**	4
DEL1-28.1	0.11	314	190	0.605	0.63	4.85	0.6	.0813	0.8	4.86	0.6	.0808	0.9	2.29	1.1	.2058	0.6	.551	***1206.6***	***6.6***	**1216**	**18**	1
DEL1-29.1	0.83	162	99	0.613	0.63	4.93	0.8	.0864	1.2	4.93	0.8	.0864	1.2	2.42	1.5	.2028	0.8	.573	***1190.4***	***9.1***	**1347**	**23**	13
DEL1-3.1	-0.07	129	37	0.285	0.29	4.77	0.9	.0807	1.3	4.77	0.9	.0807	1.3	2.33	1.6	.2095	0.9	.577	***1226.2***	***10.3***	**1214**	**26**	-1
DEL1-30.1	0.78	379	164	0.434	0.45	6.78	0.6	.0748	1.0	6.79	0.6	.0742	1.1	1.51	1.3	.1473	0.6	.477	***886.0***	***5.0***	**1047**	**22**	18
DEL1-31.1	0.71	138	26	0.185	0.19	4.75	1.0	.0871	1.4	4.75	1.0	.0871	1.4	2.53	1.8	.2106	1.0	.582	***1232.0***	***11.5***	**1363**	**28**	11
DEL1-32.1	-0.04	104	41	0.395	0.41	4.17	1.1	.0878	1.5	4.17	1.1	.0878	1.5	2.90	1.8	.2397	1.1	.618	***1385.1***	***14.2***	**1377**	**28**	-1
DEL1-33.1	0.55	89	30	0.336	0.35	6.89	1.3	.0726	2.1	6.89	1.3	.0726	2.1	1.45	2.5	.1451	1.3	.518	***873.4***	***10.6***	**1002**	**44**	15
DEL1-34.1	0.01	425	115	0.270	0.28	5.09	0.5	.0785	0.9	5.09	0.5	.0785	0.9	2.13	1.0	.1964	0.5	.539	***1156.2***	***5.8***	**1159**	**17**	0
DEL1-35.1	0.31	72	35	0.490	0.51	5.84	1.3	.0756	2.0	5.84	1.3	.0756	2.0	1.78	2.4	.1711	1.3	.542	***1018.4***	***12.3***	**1085**	**41**	7
DEL1-36.1	0.28	150	40	0.265	0.27	5.37	0.9	.0785	1.4	5.37	0.9	.0780	1.5	2.00	1.7	.1862	0.9	.537	***1101.0***	***9.4***	**1146**	**29**	4
DEL1-37.1	-0.11	76	56	0.729	0.75	6.07	1.3	.0710	2.1	6.07	1.3	.0710	2.1	1.61	2.5	.1648	1.3	.522	***983.5***	***11.7***	**957**	**43**	-3
DEL1-38.1	0.22	771	192	0.249	0.26	5.63	0.4	.0762	0.6	5.63	0.4	.0760	0.6	1.86	0.8	.1775	0.4	.537	***1053.5***	***4.0***	**1096**	**13**	4
DEL1-39.1	0.12	141	32	0.226	0.23	4.44	0.9	.0856	1.3	4.45	0.9	.0847	1.4	2.63	1.7	.2249	0.9	.548	***1307.6***	***11.0***	**1308**	**28**	0
DEL1-4.1	0.95	169	41	0.242	0.25	6.25	0.8	.0786	1.2	6.25	0.8	.0786	1.2	1.74	1.5	.1600	0.8	.539	***957.0***	***7.0***	**1163**	**24**	21
DEL1-40.1	-0.07	138	34	0.247	0.26	4.80	0.9	.0803	1.4	4.81	0.9	.0795	1.5	2.28	1.8	.2080	0.9	.530	***1218.4***	***10.5***	**1185**	**30**	-3
DEL1-41.1	0.81	168	1	0.005	0.01	15.45	1.5	.0613	3.5	15.53	1.5	.0575	5.5	0.51	5.7	.0644	1.5	.262	***402.3***	***5.9***	**511**	**122**	27
DEL1-42.1	0.11	498	129	0.259	0.27	5.61	0.5	.0755	0.8	5.61	0.5	.0753	0.8	1.85	1.0	.1783	0.5	.535	***1057.5***	***5.0***	**1076**	**16**	2
DEL1-43.1	0.35	250	41	0.164	0.17	4.45	0.7	.0874	0.9	4.45	0.7	.0874	0.9	2.71	1.2	.2247	0.7	.600	***1306.7***	***8.2***	**1369**	**18**	5
DEL1-44.1	0.05	140	1	0.004	0.00	13.81	1.2	.0563	2.7	13.88	1.2	.0518	5.3	0.51	5.4	.0720	1.2	.221	***448.3***	***5.2***	**276**	**121**	-38
DEL1-45.1	-1.42	330	233	0.706	0.73	5.05	0.6	.0673	1.0	5.05	0.6	.0673	1.0	1.84	1.1	.1980	0.6	.548	***1164.5***	***6.7***	**848**	**20**	-27
DEL1-46.1	-0.01	66	55	0.833	0.86	4.87	1.4	.0802	1.9	4.87	1.4	.0802	1.9	2.27	2.4	.2054	1.4	.585	***1204.0***	***15.4***	**1202**	**38**	0
DEL1-47.1	0.16	165	56	0.339	0.35	5.13	0.9	.0793	1.3	5.13	0.9	.0789	1.4	2.12	1.6	.1948	0.9	.553	***1147.1***	***9.4***	**1169**	**27**	2
DEL1-48.1	0.12	196	200	1.017	1.05	4.95	0.9	.0805	1.2	4.96	0.9	.0800	1.3	2.23	1.6	.2018	0.9	.554	***1185.1***	***9.3***	**1196**	**26**	1
DEL1-49.1	0.26	472	120	0.254	0.26	5.53	0.5	.0772	1.0	5.54	0.5	.0770	1.0	1.92	1.1	.1806	0.5	.464	***1070.4***	***5.2***	**1122**	**20**	5
DEL1-50.1	0.23	289	138	0.476	0.49	6.14	0.7	.0733	1.1	6.14	0.7	.0730	1.1	1.64	1.3	.1628	0.7	.522	***972.2***	***6.2***	**1015**	**23**	4
DEL1-51.1	0.50	94	24	0.260	0.27	6.07	1.2	.0759	1.9	6.07	1.2	.0759	1.9	1.72	2.2	.1647	1.2	.538	***983.1***	***11.0***	**1092**	**38**	11
DEL1-52.1	1.09	117	61	0.519	0.54	3.95	1.0	.1001	1.2	3.95	1.0	.0993	1.3	3.47	1.7	.2531	1.0	.615	***1454.5***	***13.3***	**1612**	**24**	11
DEL1-53.1	0.23	57	19	0.331	0.34	5.24	1.5	.0790	2.2	5.24	1.5	.0790	2.2	2.08	2.7	.1908	1.5	.573	***1125.6***	***16.0***	**1172**	**44**	4
DEL1-54.1	0.39	276	66	0.239	0.25	5.50	0.7	.0784	1.1	5.51	0.7	.0769	1.3	1.93	1.5	.1816	0.7	.468	***1075.7***	***7.0***	**1120**	**27**	4
DEL1-55.1	0.46	60	0	0.005	0.01	14.19	2.0	.0593	4.7	14.32	2.1	.0523	9.9	0.50	10.1	.0699	2.1	.207	***435.3***	***8.8***	**300**	**226**	-31
DEL1-56.1	0.44	149	47	0.313	0.32	5.48	1.0	.0790	1.5	5.49	1.0	.0779	1.7	1.96	2.0	.1823	1.0	.515	***1079.4***	***10.1***	**1145**	**34**	6
DEL1-57.1	0.15	362	1	0.003	0.00	14.11	0.9	.0569	2.0	14.13	0.9	.0557	2.4	0.54	2.6	.0707	0.9	.356	***440.7***	***3.9***	**440**	**53**	0
DEL1-6.1	0.65	108	58	0.538	0.56	5.23	1.0	.0825	1.5	5.25	1.0	.0805	2.1	2.11	2.4	.1906	1.0	.440	***1124.5***	***10.7***	**1209**	**42**	8
DEL1-7.1	0.44	329	104	0.317	0.33	6.14	0.6	.0750	0.9	6.15	0.6	.0740	1.1	1.66	1.2	.1625	0.6	.471	***970.8***	***5.3***	**1040**	**22**	7
DEL1-8.1	-0.24	87	50	0.581	0.60	5.54	1.1	.0731	1.8	5.55	1.1	.0723	1.9	1.80	2.2	.1803	1.1	.500	***1068.5***	***10.9***	**994**	**39**	-7
DEL1-9.1	0.16	151	103	0.685	0.71	4.38	0.8	.0867	1.1	4.38	0.8	.0867	1.1	2.73	1.3	.2281	0.8	.603	***1324.7***	***9.7***	**1354**	**21**	2

Table A3–1. Continued.

						Totals				Radiogenic Ratios[1]									Ages (Ma)[1]				
Spot Name	% comm 206	ppm U	ppm Th	Th/U	^{232}Th/ ^{238}U	^{238}U/ ^{206}Pb	% err	^{207}Pb/ ^{206}Pb	% err	^{238}U/ ^{206}Pb	% err	^{207}Pb/ ^{206}Pb	% err	^{207}Pb/ ^{235}U	% err	^{206}Pb/ ^{238}U	% err	err corr	^{206}Pb/ ^{238}U	± 1σ	^{207}Pb/ ^{206}Pb	± 1σ	% Discord.
EG108C-1	0.01	870	12	0.014	0.01	5.21	0.4	.0774	0.6	5.21	0.4	.0773	0.6	2.05	0.7	.1918	0.4	.539	***1131.3***	***4.0***	**1130**	**12**	0
EG108C-10.1	-0.02	1002	20	0.020	0.02	5.02	0.4	.0789	0.6	5.02	0.4	.0788	0.6	2.17	0.7	.1993	0.4	.564	***1171.8***	***4.1***	**1166**	**11**	0
EG108C-11.1	0.51	456	97	0.212	0.22	4.32	0.6	.0903	0.9	4.32	0.6	.0903	0.9	2.89	1.0	.2317	0.6	.556	***1343.5***	***7.0***	**1433**	**16**	7
EG108C-12.1	0.00	90	153	1.710	1.77	5.89	1.3	.0729	2.0	5.89	1.3	.0718	2.3	1.68	2.6	.1697	1.3	.486	***1010.2***	***11.8***	**981**	**46**	-3
EG108C-13.1	0.23	143	153	1.070	1.11	5.86	1.0	.0749	1.6	5.86	1.0	.0749	1.6	1.76	1.8	.1705	1.0	.536	***1015.1***	***9.3***	**1066**	**31**	5
EG108C-14.1	-0.22	165	4	0.025	0.03	5.74	0.9	.0720	1.5	5.74	0.9	.0720	1.5	1.73	1.7	.1742	0.9	.497	***1035.0***	***8.3***	**986**	**31**	-5
EG108C-15.1	0.08	581	56	0.097	0.10	6.08	0.5	.0724	1.0	6.08	0.5	.0721	1.1	1.63	1.2	.1643	0.5	.429	***980.9***	***4.5***	**988**	**21**	1
EG108C-16.1	-0.04	1031	25	0.024	0.03	4.68	0.4	.0818	0.5	4.68	0.4	.0817	0.5	2.41	0.6	.2138	0.4	.566	***1249.1***	***4.1***	**1238**	**10**	-1
EG108C-17.1	-0.14	113	137	1.220	1.26	5.84	1.1	.0721	1.7	5.84	1.1	.0713	1.9	1.68	2.1	.1712	1.1	.503	***1018.7***	***10.1***	**966**	**38**	-5
EG108C-18.1	0.03	201	122	0.606	0.63	2.90	0.8	.1173	1.4	2.90	0.8	.1171	1.4	5.57	1.6	.3452	0.8	.480	***1911.9***	***12.8***	**1912**	**25**	0
EG108C-19.1	0.31	242	59	0.243	0.25	10.01	1.0	.0628	1.9	10.02	1.0	.0616	2.3	0.85	2.5	.0998	1.0	.382	***613.2***	***5.6***	**660**	**50**	8
EG108C-2.1	-0.09	351	135	0.385	0.40	5.79	0.6	.0727	1.0	5.79	0.6	.0727	1.0	1.73	1.2	.1726	0.6	.520	***1026.5***	***5.9***	**1006**	**21**	-2
EG108C-20.1	0.34	174	188	1.079	1.11	6.24	0.9	.0738	1.4	6.24	0.9	.0738	1.4	1.63	1.6	.1604	0.9	.530	***958.9***	***7.7***	**1036**	**28**	8
EG108C-21.1	0.07	304	197	0.649	0.67	3.51	0.6	.1002	0.7	3.51	0.6	.1000	0.7	3.93	0.9	.2851	0.6	.654	***1616.8***	***8.6***	**1624**	**13**	0
EG108C-22.1	0.15	610	37	0.060	0.06	4.95	0.5	.0807	0.7	4.95	0.5	.0806	0.7	2.24	0.8	.2021	0.5	.556	***1186.5***	***4.9***	**1211**	**13**	2
EG108C-23.1	0.03	181	109	0.603	0.62	5.93	0.9	.0729	1.4	5.93	0.9	.0729	1.4	1.70	1.7	.1687	0.9	.516	***1004.7***	***8.0***	**1012**	**29**	1
EG108C-24.1	0.02	662	35	0.053	0.05	4.67	0.5	.0824	0.7	4.67	0.5	.0824	0.7	2.44	0.8	.2143	0.5	.570	***1251.7***	***5.2***	**1256**	**13**	0
EG108C-25.1	-0.34	747	23	0.030	0.03	4.72	0.4	.0790	0.6	4.72	0.4	.0787	0.7	2.30	0.8	.2120	0.4	.533	***1239.2***	***4.8***	**1165**	**13**	-6
EG108C-26.1	0.27	1779	102	0.057	0.06	5.31	0.3	.0788	0.5	5.31	0.3	.0788	0.5	2.05	0.5	.1885	0.3	.524	***1113.1***	***2.9***	**1167**	**9**	5
EG108C-27.1	0.71	471	124	0.264	0.27	4.97	0.6	.0851	0.7	4.97	0.6	.0851	0.7	2.36	0.9	.2013	0.6	.599	***1182.5***	***6.0***	**1318**	**14**	11
EG108C-28.1	-0.08	669	78	0.116	0.12	5.68	0.5	.0736	0.9	5.68	0.5	.0736	0.9	1.79	1.0	.1762	0.5	.468	***1046.1***	***4.5***	**1029**	**18**	-2
EG108C-29.1	0.39	658	29	0.043	0.04	5.21	0.4	.0805	0.7	5.21	0.4	.0807	0.7	2.14	0.8	.1920	0.4	.547	***1132.4***	***4.5***	**1215**	**13**	7
EG108C-3.1	-0.11	291	33	0.113	0.12	4.83	0.6	.0798	1.3	4.84	0.6	.0783	1.6	2.23	1.7	.2068	0.6	.377	***1211.6***	***7.0***	**1155**	**31**	-5
EG108C-30.1	1.35	165	105	0.637	0.66	3.42	0.9	.1122	1.0	3.42	0.9	.1119	1.0	4.51	1.3	.2924	0.9	.658	***1653.3***	***12.5***	**1830**	**18**	11
EG108C-31.1	0.53	81	43	0.529	0.55	4.61	1.4	.0870	1.9	4.61	1.4	.0870	1.9	2.60	2.3	.2167	1.4	.588	***1264.6***	***15.7***	**1361**	**36**	8
EG108C-32.1	-0.91	188	94	0.501	0.52	2.82	0.8	.1133	0.9	2.82	0.8	.1133	0.9	5.55	1.2	.3552	0.8	.697	***1959.5***	***14.0***	**1853**	**15**	-5
EG108C-33.1	-0.20	127	175	1.372	1.42	5.62	1.0	.0729	1.6	5.63	1.0	.0718	1.9	1.76	2.2	.1775	1.0	.478	***1053.5***	***10.0***	**979**	**39**	-7
EG108C-34.1	0.13	144	201	1.394	1.44	6.02	1.0	.0732	1.6	6.02	1.0	.0732	1.6	1.68	1.9	.1661	1.0	.525	***990.8***	***9.2***	**1019**	**33**	3
EG108C-35.1	0.23	569	87	0.153	0.16	5.02	0.5	.0808	0.7	5.02	0.5	.0808	0.7	2.22	0.9	.1991	0.5	.546	***1170.4***	***5.1***	**1216**	**14**	4
EG108C-36.1	-0.34	373	250	0.670	0.69	4.07	0.6	.0869	0.8	4.07	0.6	.0852	1.0	2.88	1.2	.2455	0.6	.511	***1415.0***	***7.6***	**1320**	**19**	-7
EG108C-37.1	0.05	544	137	0.252	0.26	4.88	0.5	.0805	0.8	4.88	0.5	.0802	0.8	2.27	1.0	.2048	0.5	.531	***1201.2***	***5.7***	**1203**	**16**	0
EG108C-38.1	-0.03	237	128	0.542	0.56	5.40	0.8	.0757	1.5	5.40	0.8	.0757	1.5	1.93	1.6	.1852	0.8	.473	***1095.2***	***7.9***	**1088**	**29**	-1
EG108C-39.1	0.36	748	40	0.054	0.06	5.46	0.4	.0785	0.6	5.46	0.4	.0781	0.7	1.97	0.8	.1831	0.4	.526	***1083.7***	***4.2***	**1149**	**13**	6
EG108C-4.1	0.13	657	433	0.659	0.68	4.75	0.4	.0825	0.8	4.75	0.4	.0822	0.8	2.39	0.9	.2105	0.4	.469	***1231.2***	***4.9***	**1251**	**16**	2
EG108C-40.1	0.15	304	238	0.784	0.81	5.50	0.7	.0765	1.0	5.50	0.7	.0761	1.0	1.91	1.2	.1818	0.7	.532	***1076.7***	***6.5***	**1099**	**21**	2
EG108C-5.1	0.28	186	111	0.596	0.62	4.41	0.8	.0873	1.1	4.41	0.8	.0867	1.2	2.71	1.5	.2265	0.8	.567	***1316.4***	***10.0***	**1353**	**24**	3
EG108C-6.1	1.32	1300	105	0.081	0.08	5.27	0.3	.0875	0.5	5.27	0.3	.0874	0.5	2.29	0.6	.1897	0.3	.536	***1119.7***	***3.2***	**1370**	**10**	22
EG108C-7.1	5.16	234	102	0.436	0.45	3.24	0.7	.1462	3.8	3.24	0.7	.1462	3.8	6.21	3.9	.3082	0.7	.176	***1732.0***	***10.4***	**2302**	**66**	33
EG108C-8.1	0.13	769	65	0.084	0.09	5.60	0.4	.0757	0.7	5.60	0.4	.0755	0.7	1.86	0.8	.1785	0.4	.515	***1059.0***	***4.0***	**1082**	**14**	2
EG108C-9.1	0.31	1440	60	0.042	0.04	5.28	0.3	.0794	0.5	5.28	0.3	.0793	0.5	2.07	0.6	.1892	0.3	.559	***1117.2***	***3.3***	**1179**	**9**	6
EL-2-30.1C	-0.12	222	71	0.322	0.33	14.27	1.1	.0547	2.6	14.24	1.1	.0563	3.4	0.55	3.6	.0702	1.1	.311	***437.5***	***4.7***	**464**	**76**	6
EL-2-7.1C	0.11	489	334	0.683	0.71	13.77	0.7	.0568	1.7	13.78	0.7	.0561	1.9	0.56	2.0	.0725	0.7	.372	***451.5***	***3.3***	**457**	**41**	1
EL-2-31.1C	-0.06	484	595	1.229	1.27	13.42	0.7	.0558	1.7	13.46	0.8	.0536	2.7	0.55	2.8	.0743	0.8	.272	***462.0***	***3.4***	**356**	**61**	-30
EL-2-35.2C	0.72	264	215	0.814	0.84	13.29	1.0	.0622	2.3	13.35	1.1	.0585	3.8	0.60	3.9	.0749	1.1	.269	***465.7***	***4.7***	**548**	**82**	15

Table A3–1. Continued.

						Totals				Radiogenic Ratios[1]									Ages (Ma)[1]				
Spot Name	% comm 206	ppm U	ppm Th	Th/U	^{232}Th/ ^{238}U	^{238}U/ ^{206}Pb	% err	^{207}Pb/ ^{206}Pb	% err	^{238}U/ ^{206}Pb	% err	^{207}Pb/ ^{206}Pb	% err	^{207}Pb/ ^{235}U	% err	^{206}Pb/ ^{238}U	% err	err corr	^{206}Pb/ ^{238}U	± 1σ	^{207}Pb/ ^{206}Pb	± 1σ	% Discord.
EL-2-39.1R	0.05	287	32	0.112	0.12	13.32	0.9	.0567	2.1	13.33	0.9	.0556	2.4	0.58	2.6	.0750	0.9	.358	***466.2***	***4.2***	**438**	**54**	-6
EL-2-2.2R	0.38	812	79	0.097	0.10	13.22	0.6	.0594	1.3	13.25	0.6	.0577	1.8	0.60	1.9	.0755	0.6	.310	***469.1***	***2.6***	**520**	**39**	10
EL-2-23.1C	0.48	235	87	0.369	0.38	13.21	1.1	.0603	2.4	13.31	1.1	.0539	5.6	0.56	5.8	.0751	1.1	.198	***467.0***	***5.1***	**365**	**127**	-28
EL-2-17.1C	-0.23	126	98	0.773	0.80	13.17	1.5	.0547	3.4	13.27	1.5	.0482	7.2	0.50	7.4	.0753	1.5	.205	***468.2***	***6.8***	**107**	**170**	-338
EL-2-39.2C	-0.12	559	232	0.416	0.43	13.07	0.7	.0556	1.5	13.07	0.7	.0556	1.5	0.59	1.6	.0765	0.7	.405	***475.2***	***3.0***	**437**	**33**	-9
EL-2-35.1R	1.85	631	90	0.143	0.15	12.71	0.7	.0717	2.2	13.00	0.7	.0533	5.8	0.57	5.9	.0769	0.7	.126	***477.6***	***3.4***	**341**	**132**	-40
EL-2-37.1R	-0.23	1109	123	0.111	0.11	12.92	0.5	.0548	1.1	12.92	0.5	.0545	1.1	0.58	1.2	.0774	0.5	.380	***480.5***	***2.2***	**392**	**26**	-23
EL-2-33.1C	0.12	796	780	0.98	1.01	9.87	0.5	.0615	1.1	9.88	0.5	.0608	1.2	0.85	1.4	.1012	0.5	.395	***621.6***	***3.2***	**632**	**27**	2
EL-2-37.2C	0.81	136	241	1.771	1.83	7.74	1.2	.0718	4.0	7.74	1.2	.0718	4.0	1.28	4.2	.1293	1.2	.293	***783.8***	***9.0***	**980**	**81**	20
EL-2-19.1C	2.46	1474	303	0.206	0.21	7.09	0.4	.0872	0.6	7.09	0.4	.0874	0.6	1.70	0.7	.1410	0.4	.526	***850.4***	***3.0***	**1370**	**12**	38
EL-2-18.1C	2.37	907	230	0.253	0.26	7.07	0.5	.0866	0.8	7.07	0.5	.0857	0.9	1.67	1.0	.1414	0.5	.477	***852.5***	***3.8***	**1332**	**17**	36
EL-2-4.1C	0.54	322	110	0.343	0.35	6.92	0.8	.0724	2.5	6.93	0.8	.0711	2.8	1.41	2.9	.1443	0.8	.273	***869.0***	***6.3***	**960**	**56**	9
EL-2-6.1C	-0.42	56	31	0.55	0.57	6.44	1.9	.0667	3.1	6.42	1.9	.0694	4.7	1.49	5.0	.1557	1.9	.375	***932.8***	***16.4***	**910**	**96**	-2
EL-2-21.1C	0.50	504	176	0.348	0.36	6.26	0.6	.0749	1.0	6.26	0.6	.0749	1.0	1.65	1.2	.1597	0.6	.531	***955.2***	***5.6***	**1067**	**20**	10
EL-2-38.1C	-0.02	364	41	0.112	0.12	6.19	0.7	.0711	1.2	6.20	0.7	.0704	1.3	1.57	1.5	.1614	0.7	.485	***964.5***	***6.6***	**940**	**27**	-3
EL-2-36.1C	0.25	17	14	0.79	0.82	5.94	3.3	.0746	5.0	6.05	3.5	.0581	18.0	1.32	18.3	.1652	3.5	.190	***985.4***	***31.8***	**533**	**393**	-85
EL-2-32.1C	0.83	89	35	0.395	0.41	5.84	1.5	.0798	2.2	5.84	1.5	.0798	2.2	1.89	2.7	.1713	1.5	.561	***1019.2***	***14.2***	**1193**	**44**	15
EL-2-14.1C	0.58	130	49	0.374	0.39	5.83	1.2	.0779	1.9	5.84	1.2	.0763	2.5	1.80	2.7	.1712	1.2	.446	***1019.0***	***11.5***	**1102**	**49**	8
EL-2-27.1C	0.30	207	98	0.475	0.49	5.74	0.9	.0762	1.5	5.75	0.9	.0753	1.8	1.81	2.0	.1740	0.9	.469	***1034.0***	***9.0***	**1076**	**36**	4
EL-2-25.1C	0.04	233	72	0.307	0.32	5.74	0.9	.0741	1.5	5.75	0.9	.0734	1.6	1.76	1.8	.1740	0.9	.510	***1033.9***	***8.8***	**1026**	**32**	-1
EL-2-15.1C	0.00	77	73	0.95	0.98	5.70	1.5	.0685	2.5	5.73	1.5	.0643	4.2	1.55	4.5	.1746	1.5	.342	***1037.6***	***14.8***	**751**	**90**	-38
EL-2-29.1C	0.11	49	40	0.806	0.83	5.54	2.0	.0759	3.1	5.54	2.0	.0763	3.1	1.90	3.7	.1805	2.0	.543	***1069.6***	***19.7***	**1104**	**62**	3
EL-2-12.1C	-0.13	80	53	0.67	0.69	5.46	1.5	.0745	2.6	5.49	1.5	.0703	4.4	1.76	4.7	.1821	1.5	.325	***1078.4***	***15.1***	**937**	**91**	-15
EL-2-10.1C	0.58	17	7	0.396	0.41	5.28	3.3	.0815	4.8	5.35	3.4	.0701	13.0	1.81	13.5	.1870	3.4	.255	***1104.9***	***34.9***	**930**	**268**	-19
EL-2-13.1C	0.08	252	152	0.604	0.62	5.25	0.9	.0777	1.3	5.26	0.9	.0772	1.3	2.03	1.6	.1902	0.9	.554	***1122.4***	***9.1***	**1128**	**26**	0
EL-2-3.1C	0.41	319	194	0.608	0.63	5.02	0.7	.0822	1.0	5.02	0.7	.0827	1.1	2.27	1.3	.1992	0.7	.548	***1170.9***	***7.9***	**1261**	**22**	7
EL-2-34.1C	0.10	135	24	0.178	0.18	4.90	1.2	.0808	1.7	4.91	1.2	.0797	1.9	2.24	2.3	.2039	1.2	.519	***1196.1***	***12.9***	**1189**	**38**	-1
EL-2-28.1C	-0.23	254	197	0.775	0.80	4.63	0.8	.0808	1.2	4.63	0.8	.0805	1.2	2.39	1.5	.2159	0.8	.566	***1260.1***	***9.5***	**1208**	**24**	-4
EL-2-9.1C	2.03	425	156	0.368	0.38	4.37	0.7	.1018	0.9	4.37	0.7	.1014	1.0	3.20	1.2	.2290	0.7	.561	***1329.1***	***7.8***	**1649**	**18**	19
EL-2-24.1C	0.28	156	78	0.503	0.52	4.25	1.1	.0893	1.4	4.26	1.1	.0873	1.8	2.82	2.1	.2346	1.1	.521	***1358.5***	***13.2***	**1366**	**34**	1
EL-2-26.1C	0.00	86	28	0.321	0.33	3.91	1.4	.0872	1.8	3.92	1.4	.0847	2.5	2.97	2.9	.2548	1.4	.499	***1463.1***	***19.0***	**1308**	**49**	-12
EL-2-5.2R	1.02	725	214	0.295	0.30	3.74	0.5	.1031	0.5	3.74	0.5	.1028	0.6	3.79	0.7	.2675	0.5	.639	***1528.2***	***6.5***	**1675**	**11**	9
EL-2-20.1C	0.80	98	21	0.218	0.22	3.69	1.3	.1023	1.5	3.70	1.3	.0996	2.0	3.71	2.4	.2703	1.3	.551	***1542.5***	***17.9***	**1617**	**37**	5
EL-2-11.1C	-0.10	62	30	0.483	0.50	3.68	1.6	.0953	3.9	3.68	1.6	.0953	3.9	3.57	4.3	.2718	1.6	.380	***1550.1***	***22.3***	**1534**	**74**	-1
EL-2-5.1C	0.91	59	58	0.988	1.02	3.53	1.6	.1062	1.8	3.54	1.6	.1051	2.0	4.10	2.5	.2827	1.6	.638	***1605.0***	***23.1***	**1716**	**36**	6
EL-2-16.1C	-1.22	170	96	0.565	0.58	3.43	1.0	.0917	1.2	3.43	1.0	.0917	1.2	3.68	1.5	.2914	1.0	.644	***1648.5***	***14.5***	**1461**	**22**	-13
EMUC-1.1	0.02	452	223	0.493	0.51	5.66	0.5	.0749	0.8	5.66	0.5	.0747	0.8	1.82	1.0	.1767	0.5	.537	***1048.7***	***5.0***	**1061**	**16**	1
EMUC-10.1	0.02	517	271	0.524	0.54	4.67	0.5	.0849	0.7	4.67	0.5	.0847	0.7	2.50	0.9	.2142	0.5	.578	***1250.9***	***5.8***	**1309**	**14**	5
EMUC-12.1	0.07	194	64	0.332	0.34	5.31	0.8	.0780	1.2	5.31	0.8	.0774	1.3	2.01	1.5	.1882	0.8	.528	***1111.5***	***8.1***	**1130**	**25**	2
EMUC-13.1	0.01	733	238	0.325	0.34	4.62	0.4	.0851	0.5	4.62	0.4	.0850	0.6	2.54	0.7	.2164	0.4	.586	***1262.6***	***4.6***	**1315**	**11**	4
EMUC-14.1	0.07	192	73	0.379	0.39	5.23	0.8	.0782	1.2	5.23	0.8	.0776	1.3	2.04	1.5	.1912	0.8	.530	***1127.6***	***8.1***	**1136**	**25**	1
EMUC-15.1	0.00	324	141	0.435	0.45	5.16	0.6	.0785	0.9	5.16	0.6	.0785	0.9	2.10	1.1	.1939	0.6	.538	***1142.4***	***6.2***	**1160**	**18**	2
EMUC-16.1	0.00	907	135	0.149	0.15	5.06	0.4	.0787	0.5	5.06	0.4	.0787	0.5	2.14	0.7	.1975	0.4	.561	***1162.0***	***3.9***	**1165**	**11**	0
EMUC-17.1	3.55	488	277	0.567	0.59	4.57	0.5	.1193	0.9	4.74	0.5	.0889	2.5	2.59	2.6	.2112	0.5	.203	***1235.1***	***5.9***	**1403**	**49**	14

Table A3–1. Continued.

						Totals				Radiogenic Ratios[1]									Ages (Ma)[1]				
Spot Name	% comm 206	ppm U	ppm Th	Th/U	$^{232}Th/^{238}U$	$^{238}U/^{206}Pb$	% err	$^{207}Pb/^{206}Pb$	% err	$^{238}U/^{206}Pb$	% err	$^{207}Pb/^{206}Pb$	% err	$^{207}Pb/^{235}U$	% err	$^{206}Pb/^{238}U$	% err	err corr	$^{206}Pb/^{238}U$	± 1σ	$^{207}Pb/^{206}Pb$	± 1σ	% Discord.
EMUC-18.1	0.02	433	450	1.038	1.07	4.56	0.5	.0851	0.7	4.56	0.5	.0850	0.7	2.57	0.9	.2192	0.5	.588	***1277.7***	***6.0***	**1315**	**14**	3
EMUC-19.1	0.00	233	165	0.708	0.73	5.57	0.7	.0752	1.1	5.57	0.7	.0752	1.1	1.86	1.4	.1795	0.7	.548	***1064.2***	***7.3***	**1075**	**23**	1
EMUC-2.1	0.00	560	231	0.413	0.43	4.97	0.5	.0782	0.7	4.97	0.5	.0782	0.7	2.17	0.8	.2013	0.5	.564	***1182.5***	***4.9***	**1151**	**13**	-3
EMUC-20.1	0.08	122	71	0.587	0.61	6.18	1.0	.0718	1.6	6.18	1.0	.0712	1.7	1.59	2.0	.1617	1.0	.508	***966.2***	***9.2***	**963**	**35**	0
EMUC-21.1	0.04	218	68	0.311	0.32	5.59	0.7	.0773	1.1	5.60	0.7	.0770	1.2	1.90	1.4	.1787	0.7	.536	***1060.0***	***7.2***	**1120**	**23**	6
EMUC-22.1	0.10	102	50	0.491	0.51	4.44	1.0	.0850	1.4	4.44	1.0	.0841	1.5	2.61	1.8	.2250	1.0	.555	***1308.3***	***12.1***	**1296**	**30**	-1
EMUC-23.1	0.00	187	88	0.470	0.49	5.24	0.8	.0782	1.2	5.24	0.8	.0782	1.2	2.06	1.4	.1908	0.8	.555	***1125.8***	***8.3***	**1152**	**24**	2
EMUC-24.1	0.00	188	58	0.307	0.32	6.37	0.8	.0686	1.4	6.37	0.8	.0686	1.4	1.49	1.6	.1571	0.8	.515	***940.4***	***7.3***	**886**	**29**	-6
EMUC-25.1	0.00	138	42	0.306	0.32	5.18	0.9	.0797	1.4	5.18	0.9	.0797	1.4	2.12	1.7	.1932	0.9	.564	***1138.8***	***9.7***	**1189**	**27**	4
EMUC-26.1	0.00	379	107	0.283	0.29	5.07	0.6	.0786	0.8	5.07	0.6	.0786	0.8	2.14	1.0	.1971	0.6	.563	***1159.5***	***6.1***	**1163**	**17**	0
EMUC-27.1	0.00	177	102	0.575	0.59	5.35	0.8	.0766	1.2	5.35	0.8	.0766	1.2	1.97	1.5	.1870	0.8	.548	***1105.3***	***8.2***	**1110**	**25**	0
EMUC-28.1	0.00	193	188	0.971	1.00	3.31	0.8	.1075	0.9	3.31	0.8	.1075	0.9	4.48	1.1	.3019	0.8	.664	***1700.7***	***11.3***	**1758**	**16**	3
EMUC-29.1	0.00	358	175	0.488	0.50	4.46	0.6	.0870	0.8	4.46	0.6	.0870	0.8	2.69	1.0	.2244	0.6	.593	***1305.2***	***6.9***	**1360**	**15**	4
EMUC-3.1	0.00	89	41	0.457	0.47	4.61	1.2	.0861	1.8	4.61	1.2	.0861	1.8	2.58	2.1	.2171	1.2	.545	***1266.6***	***13.4***	**1341**	**35**	6
EMUC-30.1	0.00	313	495	1.581	1.63	5.62	0.6	.0755	1.0	5.62	0.6	.0755	1.0	1.85	1.2	.1779	0.6	.548	***1055.6***	***6.2***	**1082**	**20**	2
EMUC-31.1	0.08	177	83	0.470	0.49	4.75	0.9	.0863	1.3	4.76	0.9	.0856	1.4	2.48	1.7	.2102	0.9	.559	***1230.1***	***10.4***	**1329**	**27**	8
EMUC-32.1	0.48	522	72	0.139	0.14	5.44	0.5	.0813	0.7	5.46	0.5	.0773	1.3	1.95	1.4	.1831	0.5	.366	***1083.8***	***5.0***	**1129**	**25**	4
EMUC-33.1	0.00	165	62	0.378	0.39	5.28	0.8	.0766	1.3	5.28	0.8	.0766	1.3	2.00	1.5	.1895	0.8	.552	***1118.5***	***8.6***	**1111**	**25**	-1
EMUC-34.1	0.07	321	163	0.510	0.53	5.12	0.6	.0795	0.9	5.12	0.6	.0789	1.0	2.12	1.1	.1952	0.6	.523	***1149.3***	***6.2***	**1170**	**19**	2
EMUC-35.1	0.03	694	171	0.247	0.25	5.32	0.4	.0791	0.6	5.32	0.4	.0788	0.6	2.04	0.8	.1878	0.4	.541	***1109.4***	***4.2***	**1168**	**13**	5
EMUC-36.1	0.00	442	302	0.682	0.70	5.06	0.5	.0792	0.8	5.06	0.5	.0792	0.8	2.16	0.9	.1975	0.5	.562	***1161.8***	***5.6***	**1177**	**15**	1
EMUC-37.1	0.00	174	58	0.335	0.35	4.28	0.9	.0887	1.2	4.28	0.9	.0887	1.2	2.86	1.5	.2339	0.9	.607	***1355.0***	***10.8***	**1398**	**22**	3
EMUC-38.1	0.00	126	49	0.387	0.40	5.26	1.0	.0804	1.4	5.26	1.0	.0804	1.4	2.11	1.7	.1900	1.0	.569	***1121.4***	***10.1***	**1206**	**28**	8
EMUC-39.1	0.00	136	42	0.312	0.32	4.89	0.9	.0812	1.3	4.89	0.9	.0812	1.3	2.29	1.6	.2043	0.9	.578	***1198.6***	***10.2***	**1226**	**26**	2
EMUC-4.1	0.01	569	277	0.487	0.50	2.88	0.4	.1185	0.4	2.88	0.4	.1184	0.4	5.66	0.6	.3469	0.4	.703	***1919.7***	***7.2***	**1932**	**8**	1
EMUC-40.1	0.04	223	166	0.746	0.77	6.23	0.8	.0730	1.2	6.24	0.8	.0727	1.2	1.61	1.5	.1604	0.8	.520	***958.9***	***6.7***	**1005**	**25**	5
EMUC-41.1	0.04	603	216	0.358	0.37	5.62	0.5	.0783	0.7	5.62	0.5	.0780	0.7	1.91	0.8	.1778	0.5	.534	***1054.9***	***4.4***	**1147**	**14**	9
EMUC-42.1	0.06	275	99	0.361	0.37	5.45	0.7	.0771	1.0	5.45	0.7	.0766	1.1	1.94	1.3	.1835	0.7	.525	***1086.0***	***6.7***	**1111**	**22**	2
EMUC-43.1	0.08	109	38	0.352	0.36	5.24	1.1	.0778	1.6	5.25	1.1	.0771	1.7	2.03	2.0	.1906	1.1	.542	***1124.5***	***11.1***	**1125**	**33**	0
EMUC-44.1	0.00	364	342	0.940	0.97	5.22	0.6	.0785	0.9	5.22	0.6	.0785	0.9	2.08	1.0	.1917	0.6	.565	***1130.3***	***6.1***	**1161**	**17**	3
EMUC-45.1	0.00	439	165	0.376	0.39	5.12	0.5	.0782	0.7	5.12	0.5	.0782	0.7	2.11	0.9	.1954	0.5	.574	***1150.8***	***5.5***	**1153**	**15**	0
EMUC-46.1	0.00	516	115	0.223	0.23	5.31	0.5	.0783	0.7	5.31	0.5	.0783	0.7	2.03	0.8	.1883	0.5	.562	***1112.4***	***4.8***	**1154**	**14**	4
EMUC-5.1	0.28	625	351	0.562	0.58	4.02	0.4	.0932	0.5	4.03	0.4	.0908	0.7	3.11	0.8	.2483	0.4	.492	***1429.5***	***5.4***	**1443**	**14**	1
EMUC-6.1	0.00	123	53	0.433	0.45	6.09	1.1	.0712	1.7	6.09	1.1	.0712	1.7	1.61	2.0	.1642	1.1	.521	***980.1***	***9.6***	**964**	**35**	-2
EMUC-7.1	0.27	227	123	0.541	0.56	5.21	0.7	.0791	1.1	5.22	0.7	.0768	1.6	2.03	1.8	.1915	0.7	.418	***1129.3***	***7.6***	**1117**	**32**	-1
EMUC-8.1	0.15	220	91	0.414	0.43	4.56	0.8	.0871	1.0	4.56	0.8	.0858	1.3	2.59	1.5	.2191	0.8	.506	***1277.3***	***8.8***	**1334**	**25**	4
EMUC-9.1	0.02	513	389	0.759	0.78	4.35	0.5	.0865	0.7	4.35	0.5	.0864	0.7	2.74	0.9	.2297	0.5	.590	***1333.0***	***6.3***	**1347**	**14**	1
HAZ2mss-1.1	0.00	109	64	0.583	0.60	4.26	1.2	.0794	1.3	4.26	1.2	.0794	1.3	2.57	1.7	.2349	1.2	.686	***1360.3***	***14.6***	**1182**	**25**	-13
HAZ2mss-10.1R	0.14	338	31	0.092	0.09	13.46	0.7	.0559	1.5	13.48	0.7	.0548	1.7	0.56	1.8	.0742	0.7	.408	***461.3***	***3.3***	**403**	**37**	-13
HAZ2mss-10.2C	0.17	112	38	0.343	0.35	5.04	1.3	.0836	3.2	5.04	1.3	.0822	3.6	2.25	3.8	.1982	1.3	.352	***1165.8***	***14.3***	**1249**	**70**	7
HAZ2mss-11.1R	0.44	1763	156	0.089	0.09	9.42	0.4	.0708	0.5	9.46	0.4	.0672	1.1	0.98	1.2	.1057	0.4	.304	***647.7***	***2.2***	**845**	**24**	30
HAZ2mss-12.1	0.00	179	46	0.258	0.27	6.10	1.1	.0728	1.3	6.10	1.1	.0728	1.3	1.65	1.7	.1638	1.1	.654	***978.1***	***10.0***	**1009**	**26**	3
HAZ2mss-13.1	0.03	1436	171	0.119	0.12	6.20	0.4	.0732	0.5	6.21	0.4	.0729	0.6	1.62	0.7	.1611	0.4	.528	***963.1***	***3.4***	**1011**	**13**	5
HAZ2mss-14.1	0.25	178	89	0.502	0.52	5.75	0.9	.0727	1.2	5.76	0.9	.0706	1.5	1.69	1.8	.1735	0.9	.492	***1031.2***	***8.3***	**946**	**31**	-8

Table A3–1. Continued.

						Totals				Radiogenic Ratios[1]									Ages (Ma)[1]				
Spot Name	% comm 206	ppm U	ppm Th	Th/U	$^{232}Th/^{238}U$	$^{238}U/^{206}Pb$	% err	$^{207}Pb/^{206}Pb$	% err	$^{238}U/^{206}Pb$	% err	$^{207}Pb/^{206}Pb$	% err	$^{207}Pb/^{235}U$	% err	$^{206}Pb/^{238}U$	% err	err corr	$^{206}Pb/^{238}U$	± 1σ	$^{207}Pb/^{206}Pb$	± 1σ	% Discord.
HAZ2mss-15.1	0.00	176	27	0.150	0.16	6.02	0.8	.0754	1.8	6.02	0.8	.0754	1.8	1.73	2.0	.1661	0.8	.435	***990.3***	***7.8***	**1079**	**35**	9
HAZ2mss-16.1	0.08	941	10	0.010	0.01	6.02	0.4	.0732	0.6	6.02	0.4	.0725	0.6	1.66	0.8	.1661	0.4	.522	***990.3***	***3.6***	**1001**	**13**	1
HAZ2mss-17.1	0.00	47	18	0.374	0.39	4.68	1.6	.0848	2.0	4.68	1.6	.0848	2.0	2.50	2.6	.2138	1.6	.625	***1248.9***	***18.2***	**1311**	**39**	5
HAZ2mss-18.1	0.00	248	110	0.443	0.46	5.56	0.7	.0763	1.0	5.56	0.7	.0763	1.0	1.89	1.2	.1799	0.7	.583	***1066.7***	***7.1***	**1104**	**20**	3
HAZ2mss-19.1	0.09	100	34	0.340	0.35	5.41	1.4	.0804	1.5	5.41	1.4	.0796	1.6	2.03	2.2	.1848	1.4	.646	***1093.3***	***14.0***	**1188**	**33**	9
HAZ2mss-2.1	0.00	107	30	0.278	0.29	4.57	1.0	.0843	1.3	4.57	1.0	.0843	1.3	2.54	1.7	.2187	1.0	.623	***1275.2***	***12.0***	**1299**	**25**	2
HAZ2mss-20.1	0.00	87	34	0.391	0.40	5.26	1.2	.0794	1.6	5.26	1.2	.0794	1.6	2.08	2.0	.1900	1.2	.603	***1121.2***	***12.5***	**1183**	**32**	5
HAZ2mss-20.2R	0.07	699	30	0.043	0.04	13.85	0.5	.0570	1.0	13.86	0.5	.0564	1.2	0.56	1.3	.0721	0.5	.386	***449.1***	***2.2***	**469**	**26**	5
HAZ2mss-21.1	0.59	118	30	0.257	0.27	5.78	1.0	.0791	1.4	5.82	1.0	.0742	2.3	1.76	2.5	.1719	1.0	.412	***1022.4***	***9.9***	**1047**	**47**	2
HAZ2mss-21.2R	0.01	854	34	0.039	0.04	6.29	0.5	.0757	0.7	6.29	0.5	.0756	0.7	1.66	0.8	.1590	0.5	.589	***951.4***	***4.3***	**1084**	**13**	14
HAZ2mss-22.1	0.12	66	50	0.761	0.79	5.03	1.3	.0760	1.8	5.03	1.3	.0751	2.0	2.06	2.4	.1987	1.3	.563	***1168.6***	***14.2***	**1070**	**39**	-8
HAZ2mss-23.1	0.01	971	228	0.235	0.24	6.61	0.5	.0740	0.5	6.61	0.5	.0739	0.5	1.54	0.7	.1512	0.5	.639	***907.9***	***3.8***	**1039**	**11**	14
HAZ2mss-24.1C	0.13	80	22	0.274	0.28	5.03	1.2	.0849	1.6	5.04	1.2	.0838	1.6	2.29	2.0	.1986	1.2	.596	***1167.8***	***12.9***	**1288**	**32**	10
HAZ2mss-24.2R	0.26	428	39	0.092	0.09	13.30	0.7	.0577	1.4	13.33	0.7	.0555	2.3	0.57	2.4	.0750	0.7	.305	***466.2***	***3.3***	**434**	**52**	-7
HAZ2mss-25.1C	2.38	345	167	0.485	0.50	6.43	0.7	.0892	2.9	6.59	0.8	.0694	6.7	1.45	6.7	.1518	0.8	.121	***911.1***	***6.9***	**910**	**137**	0
HAZ2mss-26.1C	0.00	97	38	0.395	0.41	6.86	1.2	.0683	1.8	6.86	1.2	.0683	1.8	1.37	2.1	.1458	1.2	.546	***877.2***	***9.5***	**877**	**37**	0
HAZ2mss-27.1R	0.00	504	36	0.070	0.07	5.56	0.6	.0746	2.7	5.56	0.6	.0746	2.7	1.85	2.7	.1800	0.6	.216	***1067.0***	***5.8***	**1058**	**54**	-1
HAZ2mss-27.2C	3.28	85	49	0.574	0.59	5.01	1.2	.1121	1.4	5.18	1.4	.0847	7.2	2.25	7.4	.1931	1.4	.185	***1138.3***	***14.2***	**1308**	**140**	15
HAZ2mss-28.1C	0.10	101	45	0.445	0.46	5.50	1.3	.0843	3.1	5.51	1.3	.0835	3.2	2.09	3.5	.1816	1.3	.374	***1075.7***	***12.9***	**1281**	**63**	19
HAZ2mss-29.1C	0.06	429	41	0.095	0.10	8.50	0.7	.0661	1.0	8.50	0.7	.0656	1.1	1.06	1.3	.1176	0.7	.553	***716.8***	***4.8***	**793**	**22**	11
HAZ2mss-29.2R	0.45	1053	46	0.044	0.05	11.92	0.5	.0570	0.9	11.97	0.5	.0534	2.2	0.61	2.2	.0835	0.5	.220	***517.1***	***2.4***	**344**	**49**	-33
HAZ2mss-3.1	0.00	67	46	0.687	0.71	4.76	1.4	.0800	1.7	4.76	1.4	.0800	1.7	2.32	2.2	.2101	1.4	.617	***1229.3***	***15.3***	**1196**	**34**	-3
HAZ2mss-30.1C	-0.05	262	134	0.513	0.53	5.54	0.8	.0814	2.0	5.54	0.8	.0818	2.0	2.04	2.2	.1806	0.8	.384	***1070.2***	***8.2***	**1241**	**39**	16
HAZ2mss-31.1C	0.01	305	156	0.511	0.53	5.61	0.6	.0769	1.0	5.61	0.6	.0768	1.1	1.89	1.3	.1783	0.6	.502	***1057.6***	***6.1***	**1116**	**22**	6
HAZ2mss-32.1C	0.13	154	69	0.447	0.46	5.02	0.8	.0807	1.1	5.03	0.8	.0796	1.3	2.18	1.6	.1988	0.8	.533	***1169.1***	***8.9***	**1188**	**26**	2
HAZ2mss-33.1R	0.06	581	48	0.083	0.09	13.74	0.5	.0562	1.1	13.75	0.5	.0557	1.1	0.56	1.2	.0727	0.5	.436	***452.5***	***2.3***	**440**	**25**	-3
HAZ2mss-33.2C	0.16	204	82	0.403	0.42	5.54	0.8	.0786	1.0	5.55	0.8	.0773	1.4	1.92	1.6	.1801	0.8	.484	***1067.5***	***7.4***	**1129**	**27**	6
HAZ2mss-34.1C	0.00	71	27	0.375	0.39	6.04	1.6	.0742	1.8	6.04	1.6	.0742	1.8	1.70	2.4	.1657	1.6	.646	***988.2***	***14.3***	**1048**	**37**	6
HAZ2mss-34.2C	0.00	108	35	0.325	0.34	5.91	1.2	.0753	2.0	5.91	1.2	.0753	2.0	1.76	2.3	.1691	1.2	.530	***1007.3***	***11.5***	**1078**	**40**	7
HAZ2mss-4.1	0.06	272	100	0.368	0.38	4.97	0.7	.0791	1.9	4.97	0.7	.0787	1.9	2.18	2.0	.2011	0.7	.327	***1181.5***	***7.2***	**1164**	**38**	-1
HAZ2mss-5.1	0.29	134	50	0.375	0.39	6.37	1.0	.0747	1.5	6.39	1.0	.0723	2.5	1.56	2.7	.1566	1.0	.368	***937.9***	***8.7***	**995**	**51**	6
HAZ2mss-6.1	0.00	278	74	0.265	0.27	5.71	0.8	.0759	2.4	5.71	0.8	.0759	2.4	1.83	2.5	.1751	0.8	.321	***1040.3***	***7.8***	**1092**	**48**	5
HAZ2mss-7.1	0.03	241	69	0.288	0.30	4.79	0.7	.0784	1.0	4.79	0.7	.0781	1.0	2.25	1.2	.2087	0.7	.602	***1221.8***	***8.2***	**1151**	**19**	-6
HAZ2mss-8.1	-0.01	413	119	0.289	0.30	5.98	0.7	.0729	1.3	5.98	0.7	.0730	1.3	1.68	1.5	.1672	0.7	.467	***996.7***	***6.3***	**1014**	**26**	2
HAZ2mss-9.1	0.20	52	26	0.501	0.52	6.16	1.6	.0699	2.4	6.17	1.6	.0682	2.9	1.52	3.3	.1621	1.6	.497	***968.5***	***14.8***	**874**	**59**	-10
MAS1-1.1	0.90	140	30	0.214	0.22	5.89	0.9	.0801	1.4	5.91	0.9	.0769	2.4	1.80	2.5	.1693	0.9	.363	***1008.0***	***8.6***	**1120**	**47**	11
MAS1-10.1	-0.16	144	86	0.597	0.62	5.61	1.2	.0733	1.9	5.61	1.2	.0733	1.9	1.80	2.3	.1782	1.2	.523	***1057.1***	***11.6***	**1022**	**39**	-3
MAS1-11.1	-0.35	211	88	0.416	0.43	5.37	0.8	.0734	1.3	5.37	0.8	.0734	1.3	1.88	1.6	.1861	0.8	.536	***1100.0***	***8.5***	**1024**	**27**	-7
MAS1-12.1	0.50	2621	182	0.069	0.07	9.95	0.3	.0644	0.6	9.96	0.3	.0637	0.7	0.88	0.8	.1004	0.3	.387	***616.6***	***1.8***	**732**	**15**	19
MAS1-13.1	0.04	329	182	0.552	0.57	13.67	0.8	.0564	1.9	13.67	0.8	.0564	1.9	0.57	2.0	.0732	0.8	.401	***455.2***	***3.6***	**469**	**41**	3
MAS1-14.1	0.01	1201	116	0.096	0.10	13.57	0.4	.0563	0.9	13.58	0.4	.0559	1.0	0.57	1.1	.0736	0.4	.374	***458.0***	***1.8***	**448**	**23**	-2
MAS1-15.1	0.61	265	75	0.285	0.29	5.81	0.8	.0783	1.3	5.82	0.8	.0772	1.5	1.83	1.7	.1719	0.8	.465	***1022.6***	***7.5***	**1126**	**30**	10
MAS1-16.1	0.07	296	331	1.117	1.15	5.19	0.7	.0781	1.0	5.19	0.7	.0781	1.0	2.07	1.2	.1925	0.7	.552	***1135.1***	***7.2***	**1149**	**21**	1
MAS1-17.1	-0.02	304	104	0.343	0.35	5.53	0.7	.0750	1.1	5.53	0.7	.0750	1.1	1.87	1.3	.1809	0.7	.536	***1072.1***	***6.7***	**1068**	**22**	0

Table A3–1. Continued.

						Totals				Radiogenic Ratios[1]									Ages (Ma)[1]				
Spot Name	% comm 206	ppm U	ppm Th	Th/U	$^{232}Th/^{238}U$	$^{238}U/^{206}Pb$	% err	$^{207}Pb/^{206}Pb$	% err	$^{238}U/^{206}Pb$	% err	$^{207}Pb/^{206}Pb$	% err	$^{207}Pb/^{235}U$	% err	$^{206}Pb/^{238}U$	% err	err corr	$^{206}Pb/^{238}U$	± 1σ	$^{207}Pb/^{206}Pb$	± 1σ	% Discord.
MAS1-18.1	0.49	228	80	0.350	0.36	4.83	0.8	.0846	1.1	4.83	0.8	.0840	1.2	2.40	1.4	.2071	0.8	.553	***1213.2***	***8.8***	**1294**	**23**	7
MAS1-19.1	-0.06	109	182	1.664	1.72	6.14	1.0	.0710	1.6	6.15	1.0	.0688	2.5	1.54	2.7	.1625	1.0	.367	***970.6***	***8.8***	**892**	**51**	-8
MAS1-2.1	-0.03	851	355	0.417	0.43	4.72	0.4	.0815	0.6	4.73	0.4	.0813	0.6	2.37	0.7	.2116	0.4	.498	***1237.5***	***4.1***	**1229**	**12**	-1
MAS1-20.1	0.13	217	155	0.712	0.74	5.17	0.7	.0787	1.0	5.17	0.7	.0787	1.0	2.10	1.2	.1934	0.7	.556	***1139.9***	***6.9***	**1166**	**19**	2
MAS1-21.1	-0.01	410	120	0.291	0.30	5.92	0.5	.0726	0.8	5.93	0.5	.0724	0.9	1.68	1.0	.1687	0.5	.509	***1005.2***	***4.7***	**996**	**17**	-1
MAS1-22.1	-0.11	294	84	0.287	0.30	4.36	0.6	.0849	1.0	4.36	0.6	.0845	1.0	2.67	1.2	.2295	0.6	.492	***1331.7***	***6.9***	**1303**	**20**	-2
MAS1-23.1	0.34	408	370	0.906	0.94	13.70	0.6	.0588	1.4	13.73	0.6	.0573	1.9	0.58	2.0	.0728	0.6	.303	***453.2***	***2.7***	**502**	**42**	11
MAS1-24.1	0.14	177	62	0.352	0.36	5.81	0.7	.0744	1.2	5.82	0.7	.0741	1.2	1.76	1.4	.1719	0.7	.508	***1022.6***	***7.0***	**1043**	**25**	2
MAS1-25.1	0.99	1433	181	0.126	0.13	6.68	0.3	.0769	1.2	6.69	0.3	.0762	1.2	1.57	1.3	.1495	0.3	.222	***898.1***	***2.3***	**1100**	**25**	22
MAS1-26.1	0.14	60	17	0.278	0.29	5.80	1.4	.0745	2.2	5.80	1.4	.0745	2.2	1.77	2.6	.1725	1.4	.517	***1025.7***	***12.8***	**1056**	**45**	3
MAS1-27.1	-0.07	412	276	0.671	0.69	13.24	0.7	.0558	1.5	13.24	0.7	.0554	1.6	0.58	1.7	.0755	0.7	.376	***469.2***	***3.0***	**427**	**36**	-9
MAS1-28.1	0.43	1098	358	0.326	0.34	6.98	0.3	.0713	0.6	6.98	0.3	.0713	0.6	1.41	0.7	.1434	0.3	.490	***863.7***	***2.7***	**965**	**12**	12
MAS1-29.1	0.22	225	56	0.249	0.26	5.38	0.7	.0779	1.0	5.38	0.7	.0775	1.1	1.98	1.3	.1858	0.7	.511	***1098.8***	***6.8***	**1133**	**23**	3
MAS1-3.1	-0.16	594	192	0.323	0.33	4.48	0.4	.0830	0.6	4.48	0.4	.0829	0.7	2.55	0.8	.2234	0.4	.569	***1299.7***	***5.3***	**1267**	**13**	-2
MAS1-30.1	0.74	1833	112	0.061	0.06	7.92	0.3	.0707	0.5	7.92	0.3	.0705	0.5	1.23	0.5	.1263	0.3	.468	***766.6***	***1.8***	**944**	**10**	23
MAS1-31.1	0.09	1123	1317	1.172	1.21	14.40	0.4	.0562	0.8	14.40	0.4	.0561	0.9	0.54	0.9	.0694	0.4	.383	***432.7***	***1.5***	**456**	**19**	5
MAS1-32.1	0.73	392	66	0.167	0.17	5.94	0.5	.0785	1.9	5.95	0.5	.0782	1.9	1.81	2.0	.1682	0.5	.259	***1002.0***	***4.8***	**1151**	**38**	15
MAS1-33.1	0.03	463	59	0.127	0.13	5.57	0.5	.0751	1.9	5.57	0.5	.0749	1.9	1.85	2.0	.1794	0.5	.241	***1063.8***	***4.6***	**1065**	**38**	0
MAS1-34.1	0.03	397	278	0.701	0.72	5.49	0.5	.0756	0.8	5.49	0.5	.0752	0.9	1.89	1.0	.1820	0.5	.514	***1078.0***	***5.1***	**1074**	**17**	0
MAS1-35.1	-0.03	67	30	0.448	0.46	5.97	1.3	.0722	2.1	5.98	1.3	.0706	2.6	1.63	2.9	.1672	1.3	.445	***996.8***	***12.0***	**946**	**53**	-5
MAS1-36.1	0.33	209	34	0.164	0.17	6.24	0.7	.0737	1.1	6.24	0.7	.0733	1.1	1.62	1.3	.1602	0.7	.496	***957.6***	***5.8***	**1023**	**23**	7
MAS1-37.1	0.16	213	75	0.353	0.36	5.13	0.7	.0793	1.0	5.13	0.7	.0790	1.1	2.12	1.3	.1950	0.7	.547	***1148.4***	***7.2***	**1173**	**21**	2
MAS1-38.1	0.11	195	192	0.985	1.02	5.83	0.7	.0741	1.2	5.83	0.7	.0741	1.2	1.75	1.4	.1715	0.7	.523	***1020.4***	***6.9***	**1044**	**24**	2
MAS1-39.1	0.06	191	92	0.481	0.50	5.74	0.7	.0743	1.2	5.74	0.7	.0743	1.2	1.78	1.4	.1743	0.7	.528	***1035.8***	***7.0***	**1049**	**24**	1
MAS1-4.1	0.92	1075	146	0.136	0.14	8.02	0.3	.0719	0.6	8.02	0.3	.0711	0.7	1.22	0.8	.1246	0.3	.431	***757.1***	***2.4***	**961**	**15**	27
MAS1-40.1	0.20	308	88	0.285	0.29	5.21	0.6	.0790	0.9	5.22	0.6	.0785	0.9	2.08	1.1	.1917	0.6	.529	***1130.8***	***5.9***	**1160**	**18**	3
MAS1-41.1	-0.01	1247	123	0.098	0.10	6.10	0.3	.0717	0.5	6.10	0.3	.0715	0.5	1.62	0.6	.1640	0.3	.502	***978.7***	***2.6***	**972**	**10**	-1
MAS1-42.1	0.32	116	79	0.681	0.70	5.42	0.9	.0784	1.5	5.42	0.9	.0784	1.5	2.00	1.7	.1846	0.9	.541	***1092.3***	***9.5***	**1158**	**29**	6
MAS1-43.1	0.52	538	115	0.213	0.22	4.86	0.4	.0845	0.6	4.86	0.4	.0842	0.7	2.39	0.8	.2056	0.4	.547	***1205.4***	***4.7***	**1297**	**13**	8
MAS1-44.1	0.15	218	77	0.351	0.36	5.97	0.7	.0736	1.1	5.98	0.7	.0722	1.5	1.66	1.7	.1672	0.7	.420	***996.4***	***6.5***	**992**	**31**	0
MAS1-45.1	0.16	429	185	0.431	0.45	5.26	0.5	.0783	0.7	5.26	0.5	.0781	0.7	2.05	0.9	.1901	0.5	.538	***1122.1***	***4.9***	**1149**	**15**	2
MAS1-46.1	0.39	498	257	0.516	0.53	4.61	0.4	.0859	0.6	4.62	0.4	.0858	0.6	2.56	0.7	.2167	0.4	.568	***1264.3***	***4.8***	**1334**	**12**	5
MAS1-47.1	0.28	136	43	0.315	0.33	5.88	0.8	.0752	1.4	5.89	0.8	.0741	1.6	1.74	1.8	.1699	0.8	.477	***1011.3***	***7.9***	**1045**	**32**	3
MAS1-48.1	-0.20	195	44	0.228	0.24	5.66	0.7	.0727	1.2	5.66	0.7	.0724	1.2	1.76	1.4	.1767	0.7	.517	***1049.0***	***7.0***	**997**	**24**	-5
MAS1-5.1	0.10	729	169	0.232	0.24	5.26	0.4	.0779	0.6	5.26	0.4	.0779	0.6	2.04	0.8	.1901	0.4	.557	***1121.7***	***4.4***	**1143**	**13**	2
MAS1-6.1	0.39	633	51	0.081	0.08	6.48	0.5	.0730	0.9	6.49	0.5	.0726	0.9	1.54	1.0	.1541	0.5	.494	***924.1***	***4.5***	**1002**	**19**	8
MAS1-7.1	0.13	1066	157	0.147	0.15	14.33	0.4	.0566	1.0	14.35	0.4	.0556	1.3	0.53	1.4	.0697	0.4	.319	***434.2***	***1.9***	**435**	**29**	0
MAS1-8.1	0.55	548	44	0.080	0.08	5.82	0.5	.0777	0.8	5.82	0.5	.0777	0.8	1.84	1.0	.1718	0.5	.535	***1022.0***	***5.0***	**1140**	**17**	12
MAS1-9.1	0.28	75	53	0.706	0.73	5.10	1.3	.0805	1.9	5.11	1.3	.0786	2.5	2.12	2.8	.1955	1.3	.469	***1151.3***	***13.9***	**1162**	**49**	1
MINBLFF-1.1C	0.09	312	211	0.675	0.70	3.89	0.7	.0930	0.9	3.90	0.7	.0928	0.9	3.28	1.2	.2567	0.7	.620	***1472.7***	***9.6***	**1483**	**18**	1
MINBLFF-10.1C	0.39	148	97	0.654	0.68	5.53	1.1	.0782	1.7	5.54	1.1	.0762	2.3	1.90	2.6	.1804	1.1	.432	***1069.2***	***10.9***	**1100**	**46**	3
MINBLFF-11.1C	0.24	107	27	0.254	0.26	3.10	1.2	.1120	1.3	3.11	1.2	.1104	1.6	4.90	2.0	.3219	1.2	.588	***1798.9***	***18.3***	**1806**	**29**	0
MINBLFF-12.1C	0.61	267	142	0.532	0.55	5.55	0.8	.0799	1.2	5.55	0.8	.0791	1.2	1.96	1.5	.1801	0.8	.537	***1067.5***	***7.7***	**1174**	**24**	10
MINBLFF-13.1C	1.28	737	380	0.516	0.53	5.90	0.5	.0831	0.8	5.92	0.5	.0802	1.2	1.87	1.3	.1689	0.5	.403	***1005.9***	***4.8***	**1203**	**23**	20

Table A3–1. Continued.

						Totals				Radiogenic Ratios[1]									Ages (Ma)[1]				
Spot Name	% comm 206	ppm U	ppm Th	Th/U	$^{232}Th/^{238}U$	$^{238}U/^{206}Pb$	% err	$^{207}Pb/^{206}Pb$	% err	$^{238}U/^{206}Pb$	% err	$^{207}Pb/^{206}Pb$	% err	$^{207}Pb/^{235}U$	% err	$^{206}Pb/^{238}U$	% err	err corr	$^{206}Pb/^{238}U$	± 1σ	$^{207}Pb/^{206}Pb$	± 1σ	% Discord.
MINBLFF-14.1C	-0.11	938	31	0.033	0.03	5.43	0.4	.0749	0.6	5.44	0.4	.0743	0.7	1.88	0.8	.1840	0.4	.510	***1088.7***	***4.2***	**1049**	**14**	-4
MINBLFF-15.1C	-0.18	110	52	0.469	0.48	5.43	1.2	.0744	1.9	5.44	1.2	.0733	2.1	1.86	2.4	.1840	1.2	.506	***1088.6***	***12.3***	**1023**	**42**	-6
MINBLFF-16.1C	0.31	435	158	0.364	0.38	4.05	0.6	.0922	0.7	4.07	0.6	.0883	2.5	2.99	2.6	.2455	0.6	.252	***1415.3***	***8.2***	**1388**	**47**	-2
MINBLFF-17.1C	-0.38	168	94	0.561	0.58	3.80	1.0	.0909	1.2	3.81	1.0	.0887	1.8	3.21	2.0	.2627	1.0	.476	***1503.5***	***13.0***	**1397**	**34**	-7
MINBLFF-18.1C	0.08	686	385	0.562	0.58	4.59	0.5	.0837	0.7	4.60	0.5	.0828	0.8	2.48	0.9	.2175	0.5	.544	***1268.6***	***5.7***	**1265**	**15**	0
MINBLFF-19.1C	0.05	421	194	0.462	0.48	5.14	0.6	.0784	1.2	5.14	0.6	.0779	1.2	2.09	1.4	.1944	0.6	.444	***1145.4***	***6.5***	**1145**	**25**	0
MINBLFF-2.1C	0.38	384	63	0.163	0.17	4.09	0.7	.0922	0.8	4.09	0.7	.0926	0.9	3.12	1.1	.2444	0.7	.597	***1409.4***	***8.3***	**1479**	**17**	5
MINBLFF-20.1C	-0.11	216	81	0.376	0.39	3.94	0.8	.0906	1.0	3.95	0.8	.0899	1.1	3.14	1.4	.2533	0.8	.583	***1455.6***	***10.6***	**1423**	**22**	-2
MINBLFF-21.1C	0.42	858	338	0.394	0.41	5.46	0.4	.0789	0.7	5.47	0.5	.0777	0.8	1.96	1.0	.1827	0.5	.474	***1081.9***	***4.5***	**1139**	**17**	5
MINBLFF-22.1C	0.18	282	44	0.155	0.16	5.41	0.8	.0774	1.2	5.46	0.8	.0702	3.1	1.77	3.2	.1833	0.8	.252	***1085.0***	***8.0***	**933**	**63**	-14
MINBLFF-23.1C	-0.43	198	150	0.759	0.78	3.77	0.9	.0910	1.2	3.78	0.9	.0897	1.4	3.27	1.7	.2646	0.9	.567	***1513.5***	***12.6***	**1420**	**26**	-6
MINBLFF-24.1C	0.84	2104	169	0.080	0.08	7.16	0.3	.0740	0.5	7.17	0.3	.0726	0.7	1.40	0.8	.1395	0.3	.399	***841.7***	***2.4***	**1002**	**14**	19
MINBLFF-25.1C	-0.19	328	113	0.345	0.36	5.61	0.7	.0731	1.2	5.63	0.7	.0713	1.7	1.75	1.8	.1777	0.7	.413	***1054.5***	***7.3***	**965**	**34**	-8
MINBLFF-26.1C	0.59	519	181	0.349	0.36	5.89	0.6	.0776	0.9	5.89	0.6	.0772	1.1	1.81	1.2	.1698	0.6	.463	***1010.9***	***5.2***	**1126**	**21**	11
MINBLFF-27.1C	0.52	454	256	0.563	0.58	4.27	0.6	.0910	0.8	4.27	0.6	.0907	0.8	2.93	1.0	.2343	0.6	.588	***1356.8***	***7.0***	**1440**	**15**	6
MINBLFF-28.1R	1.53	82	96	1.175	1.21	11.88	2.0	.0700	4.0	12.11	2.3	.0544	17.8	0.62	18.0	.0826	2.3	.129	***511.5***	***11.4***	**386**	**400**	-25
MINBLFF-29.1C	0.77	793	294	0.370	0.38	4.60	0.4	.0892	0.6	4.61	0.5	.0861	0.9	2.57	1.0	.2167	0.5	.435	***1264.4***	***5.2***	**1339**	**18**	6
MINBLFF-3.1C	0.51	1949	281	0.144	0.15	7.81	0.3	.0691	0.6	7.82	0.3	.0682	0.7	1.20	0.8	.1278	0.3	.408	***775.5***	***2.4***	**874**	**15**	13
MINBLFF-30.1C	0.08	504	84	0.166	0.17	5.34	0.6	.0770	0.9	5.35	0.6	.0766	0.9	1.98	1.1	.1871	0.6	.528	***1105.5***	***5.8***	**1111**	**18**	1
MINBLFF-31.1C	0.09	1108	325	0.293	0.30	5.52	0.4	.0759	0.6	5.52	0.4	.0756	0.6	1.89	0.7	.1810	0.4	.530	***1072.5***	***3.8***	**1084**	**12**	1
MINBLFF-32.1	-0.26	121	41	0.342	0.35	4.15	1.1	.0864	1.5	4.16	1.1	.0844	1.9	2.80	2.3	.2405	1.1	.508	***1389.4***	***14.3***	**1302**	**38**	-6
MINBLFF-33.1	0.46	308	122	0.396	0.41	4.09	0.7	.0929	0.9	4.09	0.7	.0925	0.9	3.11	1.2	.2442	0.7	.601	***1408.6***	***8.8***	**1477**	**18**	5
MINBLFF-34.1	0.25	519	361	0.697	0.72	5.93	0.6	.0747	0.9	5.94	0.6	.0743	1.0	1.72	1.1	.1685	0.6	.507	***1003.7***	***5.3***	**1048**	**19**	4
MINBLFF-35.1	-0.08	105	119	1.134	1.17	4.17	1.2	.0875	1.6	4.19	1.2	.0830	2.8	2.73	3.0	.2384	1.2	.399	***1378.3***	***15.0***	**1269**	**54**	-8
MINBLFF-36.1	0.30	202	113	0.560	0.58	4.44	0.9	.0871	1.2	4.46	0.9	.0829	2.1	2.56	2.3	.2241	0.9	.403	***1303.5***	***11.1***	**1267**	**42**	-3
MINBLFF-37.1	0.46	163	178	1.092	1.13	5.56	1.0	.0786	1.5	5.59	1.0	.0741	2.7	1.83	2.9	.1788	1.0	.361	***1060.6***	***10.1***	**1045**	**54**	-1
MINBLFF-38.1	0.32	217	92	0.422	0.44	3.00	0.8	.1160	0.8	3.00	0.8	.1162	0.8	5.35	1.2	.3337	0.8	.702	***1856.2***	***13.2***	**1899**	**15**	2
MINBLFF-39.1	9.29	278	66	0.237	0.24	2.83	0.7	.1903	0.6	2.84	0.7	.1870	0.7	9.07	1.0	.3517	0.7	.709	***1942.7***	***11.9***	**2716**	**12**	40
MINBLFF-4.1C	1.61	931	654	0.702	0.73	4.73	0.4	.0944	0.8	4.78	0.5	.0863	1.4	2.49	1.4	.2092	0.5	.314	***1224.6***	***5.1***	**1345**	**27**	10
MINBLFF-5.1C	1.02	773	499	0.646	0.67	5.05	0.5	.0868	0.7	5.06	0.5	.0846	0.9	2.30	1.1	.1975	0.5	.461	***1161.6***	***5.2***	**1307**	**18**	13
MINBLFF-6.1C	-0.05	167	52	0.309	0.32	3.52	0.9	.0989	1.1	3.52	0.9	.0989	1.1	3.87	1.4	.2840	0.9	.655	***1611.3***	***13.5***	**1604**	**20**	0
MINBLFF-7.1C	4.21	434	94	0.216	0.22	3.79	0.6	.1273	0.6	3.79	0.6	.1270	0.7	4.61	0.9	.2636	0.6	.672	***1508.1***	***8.1***	**2057**	**12**	36
MINBLFF-8.1C	0.39	292	81	0.278	0.29	3.39	0.7	.1054	0.8	3.39	0.7	.1044	0.9	4.24	1.2	.2947	0.7	.625	***1665.0***	***10.6***	**1704**	**17**	2
MINBLFF-9.1C	1.35	154	73	0.475	0.49	4.09	1.0	.1000	1.3	4.13	1.1	.0920	2.6	3.07	2.8	.2422	1.1	.378	***1397.9***	***13.4***	**1467**	**49**	5
R24-14.1	0.84	23	7	0.3	0.31	6.23	2.2	.0698	3.9	6.29	2.3	.0628	8.9	1.38	9.2	.1591	2.3	.246	***951.6***	***19.9***	**703**	**189**	-35
R24-23.1	0.15	158	97	0.617	0.64	6.28	0.8	.0714	1.4	6.29	0.8	.0701	1.6	1.54	1.8	.1590	0.8	.443	***951.3***	***7.2***	**932**	**34**	-2
R24-9.1	0.00	1514	36	0.024	0.02	7.38	0.3	.0704	0.6	7.38	0.3	.0704	0.6	1.32	0.6	.1356	0.3	.470	***819.6***	***2.3***	**940**	**11**	13
R24-2.1	0.00	41	14	0.337	0.35	5.68	1.5	.0718	3.7	5.68	1.5	.0718	3.7	1.74	4.0	.1761	1.5	.382	***1045.8***	***14.9***	**979**	**76**	-7
R24-6.1	0.03	720	75	0.105	0.11	6.34	0.4	.0723	0.6	6.34	0.4	.0721	0.7	1.57	0.7	.1577	0.4	.487	***944.0***	***3.2***	**989**	**13**	5
R24-31.1	0.01	1701	240	0.141	0.15	6.14	0.2	.0724	0.4	6.14	0.2	.0723	0.4	1.62	0.5	.1629	0.2	.503	***972.9***	***2.2***	**995**	**9**	2
R24-32.1	0.00	1280	95	0.074	0.08	6.15	0.3	.0726	0.5	6.15	0.3	.0726	0.5	1.63	0.6	.1625	0.3	.500	***970.5***	***2.6***	**1002**	**10**	3
R24-15.1	0.00	174	140	0.804	0.83	6.22	0.9	.0727	1.5	6.22	0.9	.0727	1.5	1.61	1.7	.1609	0.9	.504	***961.6***	***7.6***	**1006**	**30**	4
R24-28.1	0.06	140	88	0.629	0.65	5.87	0.9	.0737	1.4	5.87	0.9	.0731	1.5	1.72	1.7	.1703	0.9	.503	***1013.8***	***8.2***	**1018**	**31**	0
R24-8.1	0.00	103	67	0.655	0.68	5.99	1.0	.0733	1.7	5.99	1.0	.0733	1.7	1.68	2.0	.1668	1.0	.511	***994.6***	***9.3***	**1021**	**34**	3

Table A3–1. Continued.

						Totals				Radiogenic Ratios[(1)]									Ages (Ma)[(1)]				
Spot Name	% comm 206	ppm U	ppm Th	Th/U	$^{232}Th/^{238}U$	$^{238}U/^{206}Pb$	% err	$^{207}Pb/^{206}Pb$	% err	$^{238}U/^{206}Pb$	% err	$^{207}Pb/^{206}Pb$	% err	$^{207}Pb/^{235}U$	% err	$^{206}Pb/^{238}U$	% err	err corr	$^{206}Pb/^{238}U$	± 1σ	$^{207}Pb/^{206}Pb$	± 1σ	% Discord.
R24-21.1	0.01	889	436	0.49	0.51	6.28	0.4	.0736	0.9	6.29	0.4	.0735	0.9	1.61	1.0	.1591	0.4	.381	***951.7***	***3.2***	**1027**	**18**	7
R24-30.1	0.03	390	102	0.261	0.27	7.19	0.5	.0738	1.0	7.19	0.5	.0735	1.0	1.41	1.1	.1390	0.5	.471	***839.0***	***4.2***	**1028**	**20**	18
R24-10.1	0.00	585	90	0.154	0.16	6.03	0.4	.0737	0.7	6.03	0.4	.0737	0.7	1.69	0.8	.1659	0.4	.510	***989.6***	***3.7***	**1034**	**14**	4
R24-12.1	0.01	1010	219	0.216	0.22	5.84	0.3	.0739	0.5	5.84	0.3	.0738	0.6	1.74	0.6	.1712	0.3	.505	***1018.8***	***3.1***	**1035**	**11**	2
R24-27.1	0.00	141	81	0.574	0.59	5.73	0.8	.0740	1.4	5.73	0.8	.0740	1.4	1.78	1.6	.1746	0.8	.520	***1037.5***	***8.1***	**1041**	**28**	0
R24-35.1	0.00	2825	232	0.082	0.08	5.21	0.2	.0742	0.6	5.21	0.2	.0742	0.6	1.96	0.6	.1919	0.2	.308	***1131.7***	***1.9***	**1046**	**11**	-8
R24-11.1R	0.00	23	6	0.266	0.27	6.20	2.3	.0742	3.9	6.20	2.3	.0742	3.9	1.65	4.5	.1614	2.3	.509	***964.4***	***20.4***	**1047**	**78**	8
R24-20.1	0.01	947	364	0.384	0.40	6.26	0.3	.0743	0.7	6.26	0.3	.0742	0.7	1.63	0.8	.1597	0.3	.432	***954.9***	***3.1***	**1047**	**15**	9
R24-7.1	0.01	1151	701	0.609	0.63	6.09	0.3	.0748	1.1	6.09	0.3	.0747	1.1	1.69	1.2	.1642	0.3	.254	***980.2***	***2.7***	**1062**	**23**	8
R24-17.1	0.00	88	44	0.5	0.52	6.73	1.3	.0748	2.3	6.73	1.3	.0748	2.3	1.53	2.7	.1486	1.3	.495	***892.9***	***10.9***	**1063**	**46**	16
R24-4.1	0.01	1486	279	0.187	0.19	6.16	0.2	.0751	0.9	6.16	0.2	.0750	0.9	1.68	0.9	.1624	0.2	.263	***969.8***	***2.2***	**1068**	**18**	9
R24-16.1	0.00	1013	666	0.658	0.68	6.28	0.4	.0750	0.6	6.28	0.4	.0750	0.6	1.65	0.7	.1593	0.4	.496	***953.1***	***3.2***	**1069**	**13**	11
R24-25.1	0.03	1379	242	0.175	0.18	6.67	0.3	.0754	0.7	6.67	0.3	.0751	0.7	1.55	0.8	.1499	0.3	.439	***900.3***	***2.8***	**1072**	**14**	16
R24-24.1	0.00	875	476	0.544	0.56	5.70	0.4	.0755	1.0	5.70	0.4	.0755	1.0	1.82	1.0	.1753	0.4	.342	***1041.4***	***3.4***	**1081**	**20**	4
R24-29.1	0.00	206	139	0.675	0.70	6.04	0.7	.0756	1.1	6.04	0.7	.0756	1.1	1.73	1.3	.1655	0.7	.522	***987.1***	***6.3***	**1085**	**23**	9
R24-1.1	0.00	186	122	0.654	0.68	5.50	0.7	.0763	1.1	5.50	0.7	.0763	1.1	1.91	1.3	.1818	0.7	.534	***1076.6***	***6.9***	**1104**	**22**	2
R24-22.1	0.00	166	88	0.532	0.55	5.50	0.8	.0765	1.6	5.50	0.8	.0765	1.6	1.92	1.8	.1818	0.8	.451	***1076.7***	***7.8***	**1108**	**31**	3
R24-26.1	0.00	1681	743	0.442	0.46	5.72	0.3	.0773	0.5	5.72	0.3	.0773	0.5	1.86	0.6	.1749	0.3	.531	***1038.8***	***2.8***	**1129**	**9**	8
R24-36.1	0.05	478	477	0.997	1.03	5.33	0.5	.0783	0.8	5.33	0.5	.0778	0.8	2.01	1.0	.1875	0.5	.521	***1107.7***	***5.2***	**1143**	**17**	3
R24-33.1	0.00	1176	80	0.068	0.07	5.68	0.3	.0780	0.5	5.68	0.3	.0780	0.5	1.89	0.6	.1760	0.3	.531	***1045.1***	***3.0***	**1146**	**10**	9
R24-3.1	0.01	1059	794	0.75	0.77	5.39	0.3	.0792	0.8	5.39	0.3	.0791	0.8	2.02	0.8	.1856	0.3	.355	***1097.7***	***2.9***	**1174**	**15**	6
R24-5.1	0.06	1761	1465	0.832	0.86	5.11	0.2	.0803	0.4	5.11	0.2	.0798	0.4	2.15	0.5	.1957	0.2	.513	***1152.0***	***2.5***	**1193**	**8**	3
R24-13.1	0.05	838	534	0.637	0.66	4.96	0.4	.0804	0.5	4.96	0.4	.0800	0.6	2.22	0.7	.2015	0.4	.520	***1183.3***	***3.8***	**1196**	**11**	1
R24-19.1	0.00	296	300	1.013	1.05	5.22	0.6	.0812	1.0	5.22	0.6	.0812	1.0	2.15	1.2	.1917	0.6	.543	***1130.7***	***6.5***	**1225**	**19**	8
R24-18.1	0.00	1157	732	0.633	0.65	5.58	0.3	.0812	0.6	5.58	0.3	.0812	0.6	2.01	0.7	.1793	0.3	.472	***1063.2***	***3.2***	**1226**	**12**	13
R24-34.1	0.04	992	470	0.474	0.49	6.87	0.4	.0876	5.9	6.87	0.4	.0872	6.0	1.75	6.0	.1456	0.4	.062	***876.1***	***3.0***	**1365**	**115**	36
RS711-1	0.71	182	40	0.222	0.23	10.04	0.9	.0660	1.9	10.06	0.9	.0643	2.5	0.88	2.6	.0994	0.9	.335	***610.9***	***5.1***	**750**	**52**	23
RS711-10.1	0.11	166	68	0.414	0.43	5.96	0.9	.0734	1.5	5.98	0.9	.0712	2.1	1.64	2.2	.1673	0.9	.384	***997.3***	***8.0***	**963**	**42**	-3
RS711-11.1	0.70	69	23	0.337	0.35	5.74	1.3	.0793	2.2	5.74	1.3	.0793	2.2	1.91	2.6	.1742	1.3	.507	***1035.0***	***12.4***	**1181**	**43**	14
RS711-12.1	0.00	60	30	0.491	0.51	5.57	1.3	.0748	2.2	5.59	1.3	.0721	3.0	1.78	3.3	.1790	1.3	.404	***1061.3***	***12.9***	**989**	**61**	-7
RS711-13.1	0.45	73	29	0.397	0.41	5.16	1.2	.0813	2.0	5.16	1.2	.0813	2.0	2.17	2.4	.1936	1.2	.525	***1141.0***	***13.1***	**1230**	**40**	8
RS711-14.1	-0.20	236	133	0.563	0.58	4.99	0.6	.0776	1.1	4.99	0.6	.0776	1.1	2.14	1.2	.2002	0.6	.525	***1176.6***	***7.0***	**1136**	**21**	-3
RS711-15.1	0.31	145	87	0.604	0.62	5.32	0.8	.0791	1.3	5.32	0.8	.0785	1.4	2.03	1.6	.1879	0.8	.503	***1110.2***	***8.4***	**1159**	**28**	4
RS711-16.1	-0.18	353	187	0.529	0.55	5.65	0.5	.0728	0.9	5.65	0.5	.0728	0.9	1.78	1.1	.1768	0.5	.495	***1049.7***	***5.2***	**1009**	**19**	-4
RS711-17.1	0.37	194	33	0.169	0.17	6.26	0.8	.0740	1.5	6.26	0.8	.0730	1.6	1.61	1.8	.1597	0.8	.439	***954.9***	***7.1***	**1014**	**33**	6
RS711-17.1R	0.13	434	58	0.133	0.14	6.21	0.5	.0722	0.9	6.22	0.5	.0717	1.0	1.59	1.1	.1609	0.5	.422	***961.7***	***4.3***	**978**	**21**	2
RS711-19.1	0.18	108	32	0.292	0.30	4.81	0.9	.0823	1.6	4.82	0.9	.0806	2.0	2.31	2.2	.2075	0.9	.422	***1215.7***	***10.5***	**1212**	**40**	0
RS711-20.1	-0.23	170	41	0.239	0.25	4.84	0.7	.0787	1.2	4.84	0.7	.0784	1.2	2.23	1.4	.2066	0.7	.526	***1210.6***	***8.1***	**1157**	**24**	-4
RS711-21.1	0.76	217	80	0.367	0.38	4.30	0.7	.0925	1.0	4.30	0.7	.0925	1.0	2.97	1.2	.2327	0.7	.580	***1348.8***	***8.4***	**1478**	**18**	10
RS711-22.1	0.27	63	23	0.360	0.37	4.09	1.2	.0915	1.7	4.09	1.2	.0907	1.8	3.06	2.2	.2445	1.2	.547	***1410.3***	***15.1***	**1440**	**35**	2
RS711-23.1	0.65	185	65	0.350	0.36	4.77	0.7	.0864	1.1	4.78	0.7	.0853	1.2	2.46	1.4	.2094	0.7	.512	***1225.5***	***8.3***	**1323**	**24**	8
RS711-24.1	0.13	155	77	0.497	0.51	5.95	0.8	.0736	1.5	5.96	0.8	.0726	1.7	1.68	1.9	.1679	0.8	.437	***1000.7***	***7.6***	**1003**	**34**	0
RS711-25.1	0.41	100	23	0.233	0.24	4.63	1.0	.0859	1.5	4.64	1.0	.0850	1.7	2.53	1.9	.2157	1.0	.509	***1258.9***	***11.3***	**1316**	**32**	5
RS711-26.1	0.69	146	102	0.699	0.72	4.24	0.8	.0927	1.1	4.24	0.8	.0924	1.2	3.00	1.4	.2357	0.8	.565	***1364.3***	***9.8***	**1475**	**22**	8

Table A3–1. Continued.

						Totals				Radiogenic Ratios[1]									Ages (Ma)[1]				
Spot Name	% comm 206	ppm U	ppm Th	Th/U	$^{232}Th/^{238}U$	$^{238}U/^{206}Pb$	% err	$^{207}Pb/^{206}Pb$	% err	$^{238}U/^{206}Pb$	% err	$^{207}Pb/^{206}Pb$	% err	$^{207}Pb/^{235}U$	% err	$^{206}Pb/^{238}U$	% err	err corr	$^{206}Pb/^{238}U$	± 1σ	$^{207}Pb/^{206}Pb$	± 1σ	% Discord.
RS711-27.1	-0.45	220	102	0.463	0.48	5.23	0.7	.0736	1.3	5.23	0.7	.0733	1.4	1.93	1.5	.1910	0.7	.481	***1126.9***	***7.7***	**1022**	**27**	-9
RS711-28.1	0.14	130	34	0.259	0.27	6.06	0.9	.0730	1.7	6.06	0.9	.0730	1.7	1.66	1.9	.1650	0.9	.483	***984.5***	***8.5***	**1015**	**34**	3
RS711-29.1	0.42	73	57	0.781	0.81	5.86	1.2	.0764	2.0	5.86	1.2	.0764	2.0	1.80	2.4	.1706	1.2	.503	***1015.2***	***11.2***	**1106**	**41**	9
RS711-2C	-0.25	80	55	0.686	0.71	5.64	1.3	.0724	2.4	5.64	1.3	.0724	2.4	1.77	2.7	.1773	1.3	.479	***1052.3***	***12.6***	**996**	**48**	-5
RS711-2R	0.00	350	138	0.394	0.41	5.72	0.6	.0739	1.0	5.73	0.6	.0735	1.0	1.77	1.2	.1746	0.6	.469	***1037.7***	***5.3***	**1027**	**21**	-1
RS711-3	0.90	221	56	0.251	0.26	6.60	0.9	.0766	1.7	6.60	0.9	.0766	1.7	1.60	1.9	.1516	0.9	.470	***909.8***	***7.7***	**1111**	**34**	22
RS711-30.1	-0.14	152	66	0.431	0.45	5.04	0.8	.0776	1.4	5.05	0.8	.0772	1.4	2.11	1.7	.1982	0.8	.504	***1165.5***	***8.9***	**1126**	**29**	-3
RS711-31.1	0.01	1017	177	0.174	0.18	5.79	0.3	.0735	0.7	5.79	0.3	.0735	0.7	1.75	0.8	.1727	0.3	.438	***1026.7***	***3.2***	**1028**	**14**	0
RS711-32.1	0.75	128	91	0.707	0.73	3.87	0.9	.0987	1.1	3.87	0.9	.0987	1.1	3.52	1.5	.2587	0.9	.638	***1483.0***	***12.4***	**1600**	**21**	8
RS711-33.1	0.11	316	209	0.660	0.68	5.18	0.6	.0785	0.9	5.18	0.6	.0778	1.0	2.07	1.2	.1930	0.6	.522	***1137.5***	***6.7***	**1142**	**21**	0
RS711-34.1	0.32	253	190	0.750	0.78	5.27	0.7	.0794	1.1	5.27	0.7	.0794	1.1	2.08	1.3	.1896	0.7	.555	***1119.1***	***7.3***	**1183**	**21**	6
RS711-35.1	0.74	442	99	0.224	0.23	5.91	0.6	.0787	1.1	5.92	0.6	.0782	1.2	1.82	1.3	.1690	0.6	.428	***1006.6***	***5.2***	**1152**	**23**	14
RS711-36.1	0.17	367	162	0.441	0.46	4.58	0.6	.0846	0.8	4.58	0.6	.0837	0.9	2.52	1.1	.2182	0.6	.520	***1272.6***	***6.4***	**1284**	**18**	1
RS711-37.1	0.06	300	60	0.199	0.21	5.74	0.7	.0743	1.1	5.74	0.7	.0740	1.1	1.78	1.3	.1742	0.7	.522	***1035.4***	***6.4***	**1040**	**22**	0
RS711-38.1	-0.09	122	63	0.517	0.53	5.38	1.1	.0754	1.6	5.38	1.1	.0754	1.6	1.93	2.0	.1859	1.1	.550	***1099.4***	***11.0***	**1080**	**33**	-2
RS711-39.1	-0.20	311	174	0.558	0.58	5.65	0.7	.0727	1.1	5.65	0.7	.0727	1.1	1.77	1.3	.1769	0.7	.538	***1050.3***	***6.6***	**1007**	**22**	-4
RS711-4	0.10	253	21	0.083	0.09	5.18	0.7	.0785	1.4	5.18	0.7	.0785	1.4	2.09	1.6	.1930	0.7	.421	***1137.5***	***6.9***	**1159**	**29**	2
RS711-40.1	0.18	132	51	0.386	0.40	4.91	1.0	.0814	1.4	4.91	1.0	.0814	1.4	2.28	1.7	.2036	1.0	.573	***1194.4***	***10.6***	**1230**	**27**	3
RS711-41.1	-0.14	79	35	0.444	0.46	5.76	1.3	.0725	2.0	5.77	1.3	.0714	2.2	1.71	2.6	.1734	1.3	.499	***1030.6***	***12.2***	**970**	**46**	-6
RS711-42.1	-0.05	93	50	0.541	0.56	5.18	1.2	.0772	1.8	5.19	1.2	.0748	2.6	1.99	2.9	.1926	1.2	.406	***1135.3***	***12.2***	**1064**	**53**	-6
RS711-43.1	0.28	130	41	0.315	0.33	5.28	1.0	.0791	1.5	5.29	1.0	.0783	1.7	2.04	1.9	.1891	1.0	.517	***1116.3***	***10.3***	**1153**	**33**	3
RS711-44.1	0.23	75	27	0.356	0.37	4.33	1.2	.0879	1.5	4.33	1.2	.0879	1.5	2.80	1.9	.2308	1.2	.609	***1338.9***	***14.2***	**1380**	**29**	3
RS711-45.1	0.21	97	41	0.422	0.44	6.66	1.1	.0708	1.9	6.66	1.1	.0708	1.9	1.47	2.2	.1502	1.1	.507	***902.0***	***9.5***	**951**	**39**	5
RS711-46.1	0.25	624	122	0.195	0.20	5.55	0.4	.0770	0.6	5.55	0.4	.0767	0.7	1.90	0.8	.1801	0.4	.535	***1067.5***	***4.2***	**1113**	**13**	4
RS711-47.1	0.00	232	123	0.529	0.55	4.11	0.7	.0889	0.9	4.11	0.7	.0889	0.9	2.98	1.1	.2431	0.7	.615	***1402.8***	***8.4***	**1403**	**16**	0
RS711-48.1	0.26	409	6	0.016	0.02	14.16	0.8	.0578	1.7	14.18	0.8	.0569	2.0	0.55	2.1	.0705	0.8	.363	***439.4***	***3.2***	**489**	**43**	11
RS711-49.1	0.08	163	158	0.969	1.00	5.49	0.8	.0761	1.3	5.49	0.8	.0761	1.3	1.91	1.5	.1822	0.8	.552	***1079.1***	***8.4***	**1097**	**26**	2
RS711-5	0.03	548	249	0.453	0.47	5.92	0.5	.0729	0.8	5.92	0.5	.0726	0.8	1.69	1.0	.1688	0.5	.480	***1005.5***	***4.3***	**1003**	**17**	0
RS711-50.1	0.06	267	50	0.188	0.19	5.61	0.7	.0750	1.0	5.61	0.7	.0748	1.0	1.84	1.2	.1782	0.7	.530	***1057.0***	***6.4***	**1062**	**21**	1
RS711-51.1	0.42	197	96	0.486	0.50	5.81	0.8	.0767	1.2	5.82	0.8	.0751	1.6	1.78	1.8	.1719	0.8	.427	***1022.3***	***7.3***	**1071**	**33**	5
RS711-52.1	-0.06	260	127	0.490	0.51	4.89	0.8	.0796	1.1	4.89	0.8	.0796	1.1	2.25	1.3	.2046	0.8	.567	***1200.2***	***8.4***	**1188**	**22**	-1
RS711-53.1	1.83	729	244	0.334	0.35	9.99	0.4	.0750	0.7	10.05	0.4	.0702	1.4	0.96	1.5	.0995	0.4	.279	***611.7***	***2.4***	**934**	**29**	53
RS711-54.1	0.51	429	230	0.537	0.55	3.68	0.5	.1000	0.6	3.68	0.5	.0999	0.6	3.74	0.8	.2714	0.5	.644	***1548.0***	***6.7***	**1622**	**11**	5
RS711-55.1	0.56	546	94	0.172	0.18	7.67	0.5	.0700	0.8	7.67	0.5	.0696	0.9	1.25	1.0	.1303	0.5	.468	***789.6***	***3.5***	**916**	**18**	16
RS711-56.1	0.42	391	16	0.042	0.04	5.91	0.5	.0761	0.9	5.91	0.5	.0758	0.9	1.77	1.0	.1691	0.5	.516	***1007.1***	***5.0***	**1089**	**18**	8
RS711-6	0.16	185	58	0.312	0.32	6.02	0.8	.0735	1.8	6.02	0.8	.0735	1.8	1.68	1.9	.1660	0.8	.416	***990.1***	***7.4***	**1027**	**35**	4
RS711-7	0.38	118	57	0.483	0.50	4.73	1.0	.0846	1.5	4.73	1.0	.0841	1.6	2.45	1.9	.2112	1.0	.534	***1235.2***	***11.2***	**1294**	**31**	5
RS711-8	0.21	160	146	0.909	0.94	2.29	0.8	.1503	0.8	2.30	0.8	.1501	0.8	9.01	1.1	.4357	0.8	.678	***2331.1***	***15.2***	**2347**	**14**	1
RS711-9.1	0.30	109	39	0.363	0.38	5.95	1.0	.0749	2.2	5.95	1.0	.0749	2.2	1.74	2.4	.1681	1.0	.430	***1001.5***	***9.6***	**1067**	**43**	7
RS787-1	-0.05	196	188	0.958	0.99	5.78	0.9	.0732	1.5	5.78	0.9	.0724	1.6	1.73	1.8	.1729	0.9	.496	***1028.1***	***8.5***	**997**	**32**	-3
RS787-2.1	-0.08	162	98	0.603	0.62	4.02	0.9	.0898	1.2	4.02	0.9	.0890	1.3	3.06	1.6	.2489	0.9	.580	***1432.5***	***12.2***	**1405**	**25**	-2
RS787-3.1	0.05	334	5	0.015	0.01	12.09	0.8	.0579	1.7	12.06	0.8	.0597	2.4	0.68	2.5	.0829	0.8	.312	***513.6***	***3.9***	**593**	**52**	15
RS787-4.1	0.10	294	178	0.607	0.63	5.74	0.7	.0746	1.6	5.74	0.7	.0742	1.6	1.78	1.8	.1743	0.7	.393	***1035.5***	***6.7***	**1048**	**33**	1
RS787-5.1	0.92	265	144	0.545	0.56	5.21	0.7	.0848	1.8	5.21	0.7	.0845	1.8	2.24	1.9	.1920	0.7	.360	***1132.3***	***7.3***	**1305**	**35**	15

Table A3–1. Continued.

						Totals				Radiogenic Ratios[1]									Ages (Ma)[1]				
Spot Name	% comm 206	ppm U	ppm Th	Th/U	^{232}Th/ ^{238}U	^{238}U/ ^{206}Pb	% err	^{207}Pb/ ^{206}Pb	% err	^{238}U/ ^{206}Pb	% err	^{207}Pb/ ^{206}Pb	% err	^{207}Pb/ ^{235}U	% err	^{206}Pb/ ^{238}U	% err	err corr	^{206}Pb/ ^{238}U	± 1σ	^{207}Pb/ ^{206}Pb	± 1σ	% Discord.
RS787-6.1	-0.16	61	35	0.571	0.59	4.61	1.6	.0816	2.3	4.61	1.6	.0816	2.3	2.44	2.8	.2169	1.6	.558	***1265.6***	***18.0***	**1235**	**46**	-2
RS787-7.1R	0.02	385	5	0.012	0.01	13.31	0.7	.0565	1.7	13.32	0.7	.0559	1.8	0.58	1.9	.0751	0.7	.371	***466.8***	***3.2***	**450**	**40**	-4
RS787-7.2C	0.05	93	44	0.474	0.49	6.09	1.4	.0722	4.1	6.11	1.4	.0695	4.9	1.57	5.1	.1637	1.4	.271	***977.0***	***12.5***	**914**	**100**	-6
RS787-8.1	-0.02	91	34	0.374	0.39	10.51	1.4	.0594	3.3	10.51	1.4	.0594	3.3	0.78	3.6	.0951	1.4	.401	***585.7***	***8.0***	**581**	**71**	-1
RS787-9.1	-0.55	99	23	0.233	0.24	5.73	1.3	.0694	2.0	5.73	1.3	.0694	2.0	1.67	2.4	.1744	1.3	.524	***1036.3***	***12.0***	**911**	**42**	-12
S21-1.1	0.00	144	45	0.311	0.32	5.16	0.9	.0764	1.3	5.16	0.9	.0764	1.3	2.04	1.6	.1937	0.9	.557	***1141.2***	***9.4***	**1107**	**27**	-3
S21-10.1	0.00	170	56	0.329	0.34	5.60	0.9	.0774	1.4	5.60	0.9	.0774	1.4	1.90	1.7	.1785	0.9	.545	***1058.6***	***9.1***	**1132**	**29**	7
S21-11.1	0.00	1129	654	0.579	0.60	5.58	0.4	.0778	0.6	5.58	0.4	.0778	0.6	1.92	0.7	.1791	0.4	.554	***1061.9***	***3.6***	**1141**	**11**	7
S21-12.1	0.00	143	74	0.516	0.53	6.35	1.2	.0725	2.2	6.35	1.2	.0725	2.2	1.57	2.5	.1575	1.2	.471	***942.8***	***10.3***	**1000**	**45**	6
S21-13.1	0.00	555	158	0.285	0.29	6.58	0.5	.0718	0.9	6.58	0.5	.0718	0.9	1.51	1.0	.1520	0.5	.530	***912.4***	***4.5***	**980**	**17**	7
S21-14.1	0.00	900	262	0.291	0.30	7.05	0.4	.0723	0.7	7.05	0.4	.0723	0.7	1.41	0.8	.1418	0.4	.512	***854.9***	***3.3***	**995**	**14**	16
S21-15.1	0.06	250	67	0.268	0.28	6.50	0.9	.0696	1.4	6.50	0.9	.0691	1.5	1.47	1.8	.1538	0.9	.499	***922.3***	***7.5***	**902**	**31**	-2
S21-16.1	0.04	710	122	0.171	0.18	7.15	0.5	.0796	0.7	7.16	0.5	.0792	0.8	1.53	0.9	.1397	0.5	.504	***843.0***	***3.6***	**1177**	**16**	40
S21-17.1	0.22	548	272	0.497	0.51	5.86	0.6	.0802	1.8	5.88	0.6	.0784	2.0	1.84	2.1	.1702	0.6	.269	***1013.2***	***5.2***	**1156**	**40**	14
S21-18.1	0.09	168	78	0.463	0.48	6.75	1.1	.0724	1.7	6.76	1.1	.0717	1.9	1.46	2.1	.1479	1.1	.493	***889.2***	***8.8***	**977**	**38**	10
S21-19.1	0.00	224	84	0.376	0.39	5.91	0.8	.0804	1.2	5.91	0.8	.0804	1.2	1.87	1.4	.1691	0.8	.556	***1007.3***	***7.5***	**1207**	**24**	20
S21-2.1	0.00	296	57	0.192	0.20	5.95	0.7	.0772	1.0	5.95	0.7	.0772	1.0	1.79	1.2	.1682	0.7	.542	***1002.2***	***6.2***	**1128**	**20**	13
S21-20.1	0.22	120	47	0.392	0.41	5.07	1.0	.0818	1.5	5.08	1.0	.0800	2.0	2.17	2.3	.1969	1.0	.456	***1158.7***	***10.9***	**1197**	**40**	3
S21-21.1	0.00	98	42	0.422	0.44	10.01	1.3	.0605	2.7	10.01	1.3	.0605	2.7	0.83	3.0	.0999	1.3	.452	***614.0***	***7.9***	**622**	**57**	1
S21-22.1	0.00	156	43	0.273	0.28	5.67	1.0	.0806	1.5	5.67	1.0	.0806	1.5	1.96	1.8	.1764	1.0	.550	***1047.4***	***9.3***	**1213**	**29**	16
S21-23.1	0.09	159	61	0.384	0.40	5.54	0.9	.0763	1.3	5.54	0.9	.0756	1.5	1.88	1.7	.1805	0.9	.528	***1069.6***	***8.9***	**1085**	**29**	1
S21-24.1	0.17	100	52	0.522	0.54	5.17	1.1	.0810	1.6	5.18	1.1	.0796	2.0	2.12	2.3	.1932	1.1	.501	***1138.7***	***11.9***	**1186**	**39**	4
S21-25.1	0.22	105	64	0.612	0.63	5.25	1.1	.0792	1.7	5.26	1.2	.0773	2.1	2.03	2.4	.1900	1.2	.483	***1121.4***	***11.9***	**1130**	**42**	1
S21-26.1	0.00	102	40	0.389	0.40	5.23	1.1	.0776	1.7	5.23	1.1	.0776	1.7	2.04	2.0	.1911	1.1	.555	***1127.1***	***11.5***	**1137**	**33**	1
S21-27.1	0.00	113	111	0.980	1.01	5.75	1.1	.0771	1.7	5.75	1.1	.0771	1.7	1.85	2.0	.1738	1.1	.545	***1033.1***	***10.5***	**1124**	**34**	9
S21-28.1	0.00	409	111	0.271	0.28	6.80	0.6	.0738	1.1	6.80	0.6	.0738	1.1	1.50	1.2	.1471	0.6	.504	***884.6***	***5.2***	**1037**	**22**	17
S21-29.1	0.12	83	32	0.386	0.40	6.18	1.3	.0739	2.0	6.19	1.3	.0729	2.2	1.62	2.6	.1615	1.3	.505	***965.3***	***11.6***	**1011**	**45**	5
S21-3.1	0.11	109	33	0.305	0.31	6.85	1.1	.0717	1.9	6.86	1.1	.0708	2.1	1.42	2.3	.1459	1.1	.482	***877.7***	***9.3***	**952**	**42**	8
S21-30.1	0.00	117	39	0.335	0.35	4.96	1.1	.0852	1.6	4.96	1.1	.0852	1.6	2.37	1.9	.2018	1.1	.581	***1184.8***	***12.0***	**1320**	**30**	11
S21-31.1	0.06	142	42	0.294	0.30	4.39	1.0	.0973	1.3	4.39	1.0	.0968	1.3	3.04	1.7	.2277	1.0	.600	***1322.3***	***12.0***	**1563**	**25**	18
S21-32.1	0.46	125	47	0.374	0.39	6.36	1.2	.0743	1.9	6.39	1.2	.0705	3.4	1.52	3.6	.1565	1.2	.341	***937.5***	***10.7***	**943**	**69**	1
S21-33.1	0.00	371	117	0.315	0.33	4.37	0.6	.0877	0.8	4.37	0.6	.0877	0.8	2.77	1.0	.2289	0.6	.601	***1329.0***	***6.9***	**1376**	**15**	4
S21-34.1	0.00	236	55	0.236	0.24	5.36	0.7	.0789	1.1	5.36	0.7	.0789	1.1	2.03	1.3	.1864	0.7	.563	***1102.0***	***7.6***	**1169**	**22**	6
S21-35.1	0.12	146	65	0.441	0.46	5.56	1.0	.0738	1.5	5.56	1.0	.0728	1.7	1.81	2.0	.1798	1.0	.499	***1065.9***	***9.7***	**1009**	**35**	-5
S21-36.1	0.00	81	59	0.735	0.76	9.85	1.5	.0590	3.0	9.85	1.5	.0590	3.0	0.83	3.4	.1016	1.5	.452	***623.5***	***9.1***	**567**	**66**	-9
S21-37.1	0.17	195	120	0.616	0.64	9.74	1.0	.0607	2.0	9.76	1.0	.0593	2.5	0.84	2.7	.1025	1.0	.378	***629.1***	***6.1***	**579**	**54**	-8
S21-38.1	0.05	362	145	0.402	0.42	5.13	0.6	.0800	0.9	5.13	0.6	.0796	0.9	2.14	1.1	.1948	0.6	.548	***1147.2***	***6.3***	**1187**	**18**	3
S21-39.1	0.10	391	69	0.177	0.18	6.41	0.6	.0776	0.9	6.42	0.6	.0768	1.1	1.65	1.2	.1558	0.6	.490	***933.1***	***5.2***	**1117**	**21**	20
S21-4.1	0.00	151	71	0.470	0.49	5.15	0.9	.0793	1.7	5.15	0.9	.0793	1.7	2.12	2.0	.1942	0.9	.462	***1144.0***	***9.5***	**1181**	**34**	3
S21-40.1	0.08	207	68	0.331	0.34	5.03	0.8	.0802	1.2	5.03	0.8	.0796	1.3	2.18	1.5	.1988	0.8	.541	***1168.9***	***8.6***	**1186**	**25**	1
S21-41.1	0.00	372	77	0.206	0.21	5.68	0.6	.0765	2.2	5.68	0.6	.0765	2.2	1.86	2.2	.1762	0.6	.275	***1046.0***	***6.0***	**1109**	**43**	6
S21-42.1	0.00	275	132	0.478	0.49	6.99	0.8	.0702	1.3	6.99	0.8	.0702	1.3	1.38	1.5	.1430	0.8	.516	***861.9***	***6.1***	**935**	**26**	8
S21-43.1	0.00	193	177	0.916	0.95	7.10	0.9	.0746	1.5	7.10	0.9	.0746	1.5	1.45	1.7	.1408	0.9	.523	***848.9***	***7.1***	**1057**	**29**	25
S21-44.1	0.00	174	80	0.460	0.48	5.54	0.9	.0771	1.3	5.54	0.9	.0771	1.3	1.92	1.6	.1805	0.9	.554	***1069.5***	***8.8***	**1125**	**27**	5

Table A3–1. Continued.

						Totals				Radiogenic Ratios[(1)]									Ages (Ma)[(1)]				
Spot Name	% comm 206	ppm U	ppm Th	Th/U	$^{232}Th/^{238}U$	$^{238}U/^{206}Pb$	% err	$^{207}Pb/^{206}Pb$	% err	$^{238}U/^{206}Pb$	% err	$^{207}Pb/^{206}Pb$	% err	$^{207}Pb/^{235}U$	% err	$^{206}Pb/^{238}U$	% err	err corr	$^{206}Pb/^{238}U$	± 1σ	$^{207}Pb/^{206}Pb$	± 1σ	% Discord.
S21-45.1	0.00	450	102	0.226	0.23	6.34	0.6	.0717	0.9	6.34	0.6	.0717	0.9	1.56	1.1	.1578	0.6	.532	***944.4***	***5.1***	**979**	**19**	4
S21-46.1	0.05	309	70	0.227	0.23	5.20	0.6	.0789	0.9	5.20	0.6	.0785	0.9	2.08	1.1	.1921	0.6	.545	***1132.9***	***6.4***	**1160**	**19**	2
S21-47.1	0.00	124	140	1.129	1.17	5.86	1.0	.0732	1.6	5.86	1.0	.0732	1.6	1.72	1.9	.1706	1.0	.532	***1015.5***	***9.6***	**1019**	**33**	0
S21-5.1	-0.02	842	640	0.761	0.79	5.53	0.4	.0753	0.6	5.53	0.4	.0754	0.6	1.88	0.7	.1810	0.4	.536	***1072.3***	***3.8***	**1080**	**12**	1
S21-6.1	0.07	115	50	0.436	0.45	5.19	1.1	.0826	1.6	5.19	1.1	.0820	1.7	2.18	2.0	.1925	1.1	.527	***1135.0***	***11.1***	**1245**	**34**	10
S21-7.1	0.00	239	179	0.751	0.78	5.79	0.8	.0767	1.2	5.79	0.8	.0767	1.2	1.83	1.5	.1727	0.8	.545	***1026.9***	***7.6***	**1113**	**25**	8
S21-8.1	0.04	445	336	0.756	0.78	5.20	0.5	.0829	0.8	5.20	0.5	.0825	0.8	2.19	1.0	.1922	0.5	.548	***1133.3***	***5.5***	**1258**	**16**	11
S21-9.1	0.00	55	12	0.221	0.23	4.39	1.5	.0863	2.0	4.39	1.5	.0863	2.0	2.71	2.5	.2277	1.5	.606	***1322.2***	***18.3***	**1344**	**39**	2
SEV-1.1	0.00	179	171	0.952		5.13	0.13	0.087	0.0	5.14	0.1	0.0851	0.00	2.28	0.1	0.1944	0.0	0.692	***1145***	***26***	**1317**	**80**	13
SEV-2.1	0.00	134	119	0.890		5.69	0.12	0.072	0.0	5.71	0.1	0.0693	0.00	1.67	0.1	0.1751	0.0	0.576	***1040***	***21***	**909**	**112**	-14
SEV-3.1	0.01	201	63	0.315		5.42	0.07	0.080	0.0	5.45	0.1	0.0748	0.00	1.89	0.1	0.1835	0.0	0.523	***1086***	***13***	**1063**	**83**	-2
SEV-4.1	0.00	482	318	0.661		5.13	0.05	0.091	0.0	5.15	0.0	0.0881	0.00	2.36	0.0	0.1942	0.0	0.722	***1144***	***9***	**1384**	**33**	17
†SEV-5.1	0.02	111	71	0.639		11.40	0.30	0.058	0.0	11.60	0.3	0.0440	0.01	0.52	0.1	0.0862	0.0	0.140	***533***	***14***	**0**	**0**	–
SEV-6.1	<0.0001	61	26	0.419		5.52	0.12	0.076	0.0	5.51	0.1	0.0778	0.00	1.95	0.1	0.1815	0.0	0.550	***1075***	***21***	**1142**	**118**	6
SEV-7.1	0.00	140	83	0.593		5.49	0.12	0.082	0.0	5.50	0.1	0.0807	0.00	2.02	0.1	0.1820	0.0	0.651	***1078***	***23***	**1213**	**99**	11
SEV-8.1	0.00	91	62	0.688		5.17	0.13	0.087	0.0	5.19	0.1	0.0836	0.01	2.22	0.2	0.1927	0.0	0.314	***1136***	***28***	**1284**	**157**	12
†SEV-9.1	0.02	273	152	0.558		12.30	0.31	0.061	0.0	12.51	0.3	0.0479	0.01	0.53	0.1	0.0799	0.0	0.091	***496***	***12***	**95**	**266**	-423
SEV-10.1	0.01	156	78	0.499		4.79	0.10	0.090	0.0	4.82	0.1	0.0854	0.00	2.45	0.1	0.2076	0.0	0.523	***1216***	***23***	**1326**	**93**	8
SEV-11.1	0.00	140	57	0.406		3.95	0.09	0.093	0.0	3.95	0.1	0.0929	0.00	3.24	0.1	0.2531	0.0	0.729	***1454***	***28***	**1486**	**49**	2
SEV-12.1	0.00	62	36	0.585		4.36	0.10	0.087	0.0	4.37	0.1	0.0851	0.00	2.69	0.1	0.2291	0.0	0.519	***1330***	***28***	**1318**	**95**	-1
SEV-13.1	0.00	326	104	0.320		5.08	0.06	0.080	0.0	5.08	0.1	0.0792	0.00	2.15	0.1	0.1967	0.0	0.811	***1157***	***13***	**1177**	**44**	2
SEV-14.1	0.00	39	21	0.527		4.93	0.18	0.087	0.0	4.94	0.2	0.0855	0.00	2.39	0.2	0.2025	0.0	0.348	***1189***	***40***	**1327**	**105**	10
SEV-1 (sq)	0.63	92	39	0.428		4.25	0.17	0.093	0.0	4.28	0.2	0.0883	0.00	2.85	0.2	0.2338	0.0	0.605	***1355***	***49***	**1388**	**101**	2
SEV-2 (sq)	0.00	57	15	0.263		3.14	0.13	0.110	0.0	3.14	0.1	0.1101	0.00	4.83	0.3	0.3184	0.0	0.762	***1782***	***64***	**1801**	**64**	1
SEV-3 (sq)	0.30	296	75	0.254		3.91	0.15	0.097	0.0	3.92	0.1	0.0946	0.00	3.32	0.1	0.2549	0.0	0.891	***1463***	***50***	**1520**	**36**	4
SEV-4 (sq)	0.00	60	25	0.423		4.15	0.17	0.087	0.0	4.15	0.2	0.0875	0.00	2.91	0.2	0.2412	0.0	0.764	***1393***	***50***	**1371**	**65**	-2
SEV-5 (sq)	0.00	105	81	0.773		5.50	0.22	0.080	0.0	5.50	0.2	0.0801	0.00	2.01	0.1	0.1820	0.0	0.739	***1078***	***39***	**1200**	**71**	10
SEV-6 (sq)	0.00	113	55	0.491		5.88	0.23	0.071	0.0	5.88	0.2	0.0710	0.00	1.67	0.1	0.1701	0.0	0.770	***1013***	***37***	**958**	**67**	-6
†SEV-7 (sq)	1.05	48	18	0.373		6.21	0.27	0.069	0.0	6.27	0.3	0.0603	0.01	1.32	0.2	0.1594	0.0	0.372	***953***	***39***	**614**	**237**	-55
SEV-8 (sq)	0.00	467	132	0.282		4.69	0.18	0.088	0.0	4.69	0.2	0.0880	0.00	2.59	0.1	0.2131	0.0	0.938	***1246***	***43***	**1383**	**27**	10
SEV-9 (sq)	2.44	65	34	0.528		4.22	0.17	0.100	0.0	4.32	0.2	0.0809	0.01	2.58	0.2	0.2315	0.0	0.476	***1342***	***50***	**1220**	**150**	-10
SEV-10 (sq)	4.59	247	97	0.393		4.98	0.19	0.126	0.0	5.22	0.2	0.0899	0.01	2.38	0.2	0.1917	0.0	0.410	***1130***	***41***	**1423**	**166**	21
SP13-1.1R	0.00	121	76	0.630	0.65	4.10	1.0	.0923	1.2	4.10	1.0	.0923	1.2	3.10	1.6	.2438	1.0	.644	***1406.2***	***13.2***	**1474**	**23**	5
SP13-1.2C	0.00	237	249	1.048	1.08	3.65	0.8	.1030	0.8	3.65	0.8	.1030	0.8	3.89	1.1	.2740	0.8	.674	***1561.0***	***10.7***	**1680**	**16**	8
SP13-10.1	0.25	90	42	0.466	0.48	6.45	1.3	.0732	1.9	6.46	1.3	.0711	2.1	1.52	2.5	.1547	1.3	.510	***927.2***	***10.9***	**961**	**43**	4
SP13-11.1	0.03	288	124	0.429	0.44	5.15	0.7	.0792	2.0	5.15	0.7	.0789	2.1	2.11	2.2	.1942	0.7	.316	***1144.2***	***7.2***	**1170**	**41**	2
SP13-12.1	0.00	129	57	0.438	0.45	4.32	1.0	.0883	1.2	4.32	1.0	.0883	1.2	2.82	1.6	.2316	1.0	.635	***1342.9***	***12.2***	**1390**	**23**	3
SP13-13.1	0.00	228	68	0.299	0.31	5.12	0.8	.0789	1.0	5.12	0.8	.0789	1.0	2.12	1.3	.1954	0.8	.595	***1150.5***	***7.9***	**1169**	**20**	2
SP13-14.1	0.13	1446	173	0.120	0.12	7.03	0.3	.0729	0.8	7.04	0.3	.0718	1.0	1.41	1.0	.1420	0.3	.325	***855.9***	***2.6***	**981**	**19**	15
SP13-15.1	0.04	246	187	0.760	0.78	5.59	0.8	.0751	1.1	5.59	0.8	.0747	1.1	1.84	1.3	.1790	0.8	.564	***1061.4***	***7.4***	**1061**	**22**	0
SP13-16.1	0.00	170	14	0.081	0.08	8.60	1.2	.0722	1.6	8.60	1.2	.0722	1.6	1.16	2.0	.1163	1.2	.610	***709.3***	***8.4***	**993**	**33**	40
SP13-17.1	0.07	103	41	0.400	0.41	4.53	1.1	.0885	1.4	4.53	1.1	.0879	1.5	2.67	1.8	.2206	1.1	.607	***1285.1***	***12.9***	**1380**	**28**	7

Table A3–1. Continued.

						Totals				Radiogenic Ratios[1]									Ages (Ma)[1]				
Spot Name	% comm 206	ppm U	ppm Th	Th/U	$^{232}Th/^{238}U$	$^{238}U/^{206}Pb$	% err	$^{207}Pb/^{206}Pb$	% err	$^{238}U/^{206}Pb$	% err	$^{207}Pb/^{206}Pb$	% err	$^{207}Pb/^{235}U$	% err	$^{206}Pb/^{238}U$	% err	err corr	$^{206}Pb/^{238}U$	± 1σ	$^{207}Pb/^{206}Pb$	± 1σ	% Discord.
W18-33.1C	0.43	249	142	0.573	0.59	5.01	0.6	.0856	0.8	5.03	0.7	.0819	1.8	2.25	1.9	.1989	0.7	.347	***1169.3***	***7.1***	**1244**	**35**	6
W18-34.1C	0.00	217	120	0.553	0.57	4.96	0.7	.0777	0.9	4.96	0.7	.0777	0.9	2.16	1.1	.2015	0.7	.598	***1183.2***	***7.3***	**1138**	**18**	-4
W18-35.1C	0.06	366	129	0.352	0.36	5.46	0.5	.0783	0.7	5.47	0.5	.0778	0.8	1.96	1.0	.1829	0.5	.543	***1082.9***	***5.3***	**1142**	**16**	5
W18-36.1C	0.06	434	112	0.257	0.27	6.13	0.5	.0777	0.7	6.13	0.5	.0772	0.7	1.74	0.9	.1632	0.5	.565	***974.3***	***4.4***	**1126**	**14**	16
W18-4.1R	0.00	3	0	0.023	0.02	12.79	7.2	.0423	15.5	12.79	7.2	.0423	15.5	0.46	17.1	.0782	7.2	.421	***485.3***	***33.6***	**-206**	**389**	-142
W18-5.1C	0.00	272	88	0.325	0.34	4.97	0.6	.0794	2.1	4.97	0.6	.0794	2.1	2.20	2.2	.2014	0.6	.279	***1182.7***	***6.6***	**1182**	**42**	0
W18-6.1C	0.10	106	274	2.593	2.68	7.64	1.1	.0693	1.7	7.65	1.1	.0685	1.9	1.24	2.2	.1308	1.1	.499	***792.3***	***8.0***	**884**	**39**	12
W18-7.1C	0.00	686	92	0.134	0.14	5.32	0.5	.0801	0.8	5.32	0.5	.0801	0.8	2.08	0.9	.1881	0.5	.505	***1110.8***	***4.8***	**1199**	**16**	8
W18-8.1C	0.06	441	184	0.417	0.43	5.49	0.5	.0801	0.7	5.50	0.5	.0796	0.7	2.00	0.9	.1819	0.5	.555	***1077.2***	***4.8***	**1186**	**14**	10
W18-9.1C	0.04	260	163	0.628	0.65	5.95	0.7	.0741	1.0	5.95	0.7	.0737	1.0	1.71	1.2	.1681	0.7	.549	***1001.7***	***6.2***	**1034**	**21**	3
WGxeno-1.1	0.18	616	102	0.166	0.17	5.37	0.4	.0777	1.0	5.37	0.4	.0779	1.0	2.00	1.1	.1861	0.4	.374	***1100.4***	***4.1***	**1144**	**20**	4
WGxeno-10.1	0.04	234	43	0.186	0.19	5.03	0.6	.0791	2.1	5.03	0.6	.0789	2.1	2.16	2.2	.1986	0.6	.291	***1168.0***	***6.9***	**1169**	**42**	0
WGxeno-11.1	-0.06	579	233	0.402	0.42	4.59	0.4	.0826	1.6	4.59	0.4	.0825	1.6	2.48	1.6	.2179	0.4	.247	***1270.5***	***4.6***	**1256**	**31**	-1
WGxeno-12.1	-0.03	861	392	0.455	0.47	4.37	0.3	.0854	0.4	4.37	0.3	.0852	0.5	2.69	0.6	.2289	0.3	.577	***1328.6***	***3.9***	**1320**	**9**	-1
WGxeno-13.1	0.14	854	170	0.199	0.21	4.73	0.3	.0827	0.5	4.74	0.3	.0824	0.5	2.40	0.6	.2112	0.3	.554	***1235.0***	***3.8***	**1256**	**10**	2
WGxeno-14.1	-0.02	772	302	0.392	0.40	4.59	0.4	.0830	0.5	4.59	0.4	.0830	0.5	2.50	0.6	.2181	0.4	.576	***1271.8***	***4.1***	**1269**	**10**	0
WGxeno-15.1	-0.20	1227	240	0.195	0.20	4.71	0.3	.0802	0.4	4.71	0.3	.0802	0.4	2.35	0.5	.2122	0.3	.565	***1240.4***	***3.4***	**1202**	**9**	-3
WGxeno-16.1	0.33	495	104	0.210	0.22	5.69	0.4	.0767	0.7	5.69	0.4	.0767	0.7	1.86	0.8	.1756	0.4	.529	***1043.0***	***4.3***	**1113**	**14**	7
WGxeno-17.1	0.29	26	16	0.619	0.64	4.82	1.9	.0830	2.8	4.82	1.9	.0830	2.8	2.37	3.4	.2073	1.9	.568	***1214.2***	***21.5***	**1269**	**55**	5
WGxeno-18.1	-0.17	88	35	0.402	0.42	5.55	1.0	.0736	1.6	5.55	1.0	.0736	1.6	1.83	1.9	.1802	1.0	.537	***1068.3***	***10.0***	**1032**	**32**	-3
WGxeno-19.1	1.34	362	84	0.232	0.24	6.50	0.5	.0805	0.7	6.50	0.5	.0805	0.7	1.71	0.9	.1538	0.5	.588	***922.2***	***4.5***	**1210**	**14**	31
WGxeno-2.1	0.37	167	54	0.326	0.34	5.20	0.7	.0805	1.1	5.20	0.7	.0795	1.2	2.11	1.4	.1922	0.7	.492	***1133.1***	***7.2***	**1185**	**24**	5
WGxeno-3.1	-0.29	223	76	0.342	0.35	4.81	0.6	.0785	0.9	4.81	0.6	.0785	0.9	2.25	1.1	.2078	0.6	.558	***1217.3***	***7.0***	**1159**	**19**	-5
WGxeno-4.1	-0.34	699	204	0.292	0.30	5.18	0.4	.0749	0.6	5.18	0.4	.0747	0.7	1.99	0.8	.1929	0.4	.530	***1137.2***	***4.3***	**1062**	**13**	-7
WGxeno-5.1	0.02	619	250	0.403	0.42	5.38	0.4	.0763	0.6	5.38	0.4	.0758	0.7	1.94	0.8	.1857	0.4	.516	***1098.2***	***4.0***	**1091**	**13**	-1
WGxeno-6.1	0.05	132	64	0.487	0.50	3.79	0.8	.0945	1.0	3.79	0.8	.0945	1.0	3.44	1.3	.2641	0.8	.621	***1510.6***	***11.1***	**1518**	**20**	0
WGxeno-7.1	0.17	1076	483	0.448	0.46	4.93	0.3	.0811	0.5	4.93	0.3	.0809	0.5	2.26	0.6	.2028	0.3	.550	***1190.2***	***3.4***	**1220**	**9**	3
WGxeno-8.1	-0.58	103	87	0.843	0.87	4.75	1.0	.0768	1.4	4.77	1.0	.0741	2.3	2.14	2.5	.2098	1.0	.393	***1227.8***	***11.1***	**1044**	**47**	-15
WGxeno-9.1	0.02	2822	577	0.205	0.21	4.93	0.2	.0799	0.3	4.93	0.2	.0799	0.3	2.23	0.3	.2027	0.2	.558	***1189.8***	***2.0***	**1194**	**5**	0

Errors are 1σ unless otherwise specified.

[1] 204-corrected

Discordance calculated using $((^{207}Pb/^{206}Pb - ^{206}Pb/^{238}U)/^{207}Pb/^{206}Pb)*100$

Table A3–2. Detrital zircon trace element concentrations from selected samples.

	Age																
	207/206	206/238	208/232	Th ppm	U ppm	La ppm	Ce ppm	Nd ppm	Sm ppm	Eu ppm	Gd ppm	Dy ppm	Er ppm	Yb ppm	Hf ppm	Ce/Ce*	Eu/Eu*
DEL1-1.1	**1157**	**1235**	**1197**	114	311	0.02	17	1.5	3.9	0.60	33	144	267	466	11110	94	0.16
DEL1-10.1	**742**	**698**	**712**	24	36	0.37	11	10.2	12.6	0.95	69	158	214	325	7229	5	0.10
DEL1-11.1	**1030**	**1085**	**1041**	209	629	0.01	16	0.5	1.1	0.18	9	42	83	172	13471	175	0.17
DEL1-12.1	**1029**	**1038**	**1025**	33	39	0.09	13	5.9	9.5	2.39	54	135	172	240	9687	18	0.32
DEL1-13.1	**1060**	**848**	**1154**	39	165	0.02	30	0.4	1.1	0.39	10	43	84	168	11416	242	0.37
DEL1-14.1	**1112**	**1038**	**1252**	133	328	214.86	397	91.0	17.8	1.92	40	89	142	261	12082	1	0.22
DEL1-15.1	**1189**	**1136**	**1120**	123	443	0.25	18	1.5	2.7	0.58	21	91	175	316	11287	19	0.24
DEL1-16.1	**1214**	**1380**	**1287**	336	310	0.15	155	10.7	19.2	4.85	126	395	617	945	10094	121	0.30
DEL1-17.1	**976**	**1047**	**1072**	37	83	0.03	10	0.9	1.8	0.40	13	46	73	125	10975	60	0.25
DEL1-18.1	**1205**	**1222**	**1176**	53	200	0.03	5	1.3	2.7	0.31	22	77	124	205	10191	24	0.12
DEL1-19.1	**1260**	**1158**	**1153**	69	151	0.03	40	0.8	2.0	0.55	17	70	134	252	11091	215	0.29
DEL1-2.1	**1184**	**923**	**1305**	89	536	0.12	9	1.3	3.4	0.55	31	134	262	491	11094	17	0.17
DEL1-20.1	**1257**	**1205**	**1163**	118	193	0.08	35	2.3	4.2	1.21	30	102	176	306	10650	68	0.33
DEL1-21.1	**1261**	**1076**	**1175**	15	52	0.03	6	0.5	1.7	0.33	15	58	110	193	9135	39	0.20
DEL1-22.1	**1314**	**1292**	**1274**	272	359	0.03	51	1.0	2.1	0.77	17	66	141	315	11939	239	0.39
DEL1-23.1	**1074**	**1061**	**1099**	41	148	0.02	7	0.9	2.1	0.25	20	74	128	215	10986	47	0.12
DEL1-24.1	**1203**	**1110**	**1170**	67	170	0.02	19	0.8	2.2	0.23	20	84	155	285	11637	128	0.11
DEL1-25.1	**1751**	**1310**	**1650**	206	240	0.10	63	1.4	3.1	1.38	21	74	136	285	10655	127	0.52
DEL1-26.1	**1004**	**980**	**1087**	18	76	0.03	2	0.5	1.4	0.22	13	53	91	160	7798	16	0.16
DEL1-28.1	**1216**	**1297**	**1258**	197	328	0.15	18	5.4	6.2	0.49	32	94	152	261	9803	18	0.11
DEL1-29.1	**1347**	**1110**	**1291**	101	164	0.04	11	0.8	1.6	0.42	13	52	95	162	10462	48	0.28
DEL1-3.1	**1214**	**1280**	**1176**	38	132	0.02	11	0.5	1.6	0.10	15	73	138	240	10986	87	0.06
DEL1-30.1	**1047**	**984**	**1051**	163	375	0.04	21	0.2	0.5	0.19	5	32	101	326	12759	149	0.38
DEL1-31.1	**1363**	**1353**	**1266**	27	145	0.01	4	0.0	0.1	0.09	1	5	12	36	10344	197	0.68
DEL1-32.1	**1377**	**1530**	**1529**	43	111	0.02	9	0.5	1.3	0.15	11	51	97	178	11260	77	0.12
DEL1-33.1	**1002**	**944**	**992**	31	94	0.01	11	0.6	1.4	0.17	9	39	61	100	11926	101	0.14
DEL1-34.1	**1159**	**1230**	**1164**	119	443	0.02	20	1.3	3.7	0.24	37	156	274	424	12241	133	0.06
DEL1-35.1	**1085**	**1064**	**1007**	36	74	0.02	10	0.8	1.8	0.21	12	44	68	113	10672	88	0.13
DEL1-36.1	**1146**	**1104**	**1143**	41	154	0.02	8	0.4	1.3	0.12	11	49	90	161	11403	71	0.09
DEL1-37.1	**957**	**978**	**978**	58	80	0.06	26	4.2	7.3	1.92	43	133	205	339	9652	50	0.33
DEL1-38.1	**1096**	**1060**	**1109**	198	797	0.11	17	1.1	2.7	0.24	29	138	264	462	12689	35	0.08
DEL1-39.1	**1308**	**1271**	**1231**	33	145	0.02	13	0.3	0.8	0.15	8	39	88	190	10899	142	0.18
DEL1-4.1	**1163**	**985**	**974**	42	174	0.09	11	0.8	2.0	0.11	19	76	137	231	9193	29	0.05
DEL1-40.1	**1185**	**1151**	**1166**	35	141	0.04	7	0.5	1.4	0.11	14	63	117	209	10858	37	0.07
DEL1-41.1	**511**	**284**	**779**	1	163	0.24	1	0.1	0.1	0.04	2	9	14	18	9840	1	0.28
DEL1-42.1	**1076**	**1042**	**1041**	132	511	0.19	21	1.4	2.1	0.69	14	50	94	197	11884	27	0.38
DEL1-43.1	**1369**	**1375**	**1359**	42	260	0.01	9	0.3	0.8	0.06	8	40	84	177	12646	109	0.07
DEL1-44.1	**276**	**421**	**1298**	1	144	0.05	0	0.0	0.1	0.11	2	15	19	26	12599	3	0.66
DEL1-45.1	**848**	**1185**	**1057**	240	339	0.06	19	2.2	5.6	0.32	46	158	257	412	10573	45	0.06
DEL1-46.1	**1202**	**1360**	**1271**	57	69	0.08	9	4.0	7.6	1.10	50	158	227	337	10939	16	0.17
DEL1-47.1	**1169**	**1202**	**1189**	58	171	0.05	9	2.3	4.9	0.26	37	140	225	344	9678	25	0.06
DEL1-48.1	**1196**	**1337**	**1259**	204	203	0.06	80	2.1	3.4	1.08	22	86	155	300	11311	196	0.37
DEL1-49.1	**1122**	**1153**	**1071**	123	489	0.15	8	0.8	1.4	0.13	12	56	115	218	13717	15	0.09
DEL1-50.1	**1015**	**1055**	**1017**	142	301	0.03	35	0.9	2.4	0.30	22	83	152	291	13038	185	0.13
DEL1-51.1	**1092**	**1025**	**1083**	25	97	0.02	7	1.1	2.4	0.44	19	71	134	248	10025	41	0.20
DEL1-52.1	**1612**	**1471**	**1601**	62	119	0.03	17	1.2	2.0	0.48	12	41	66	121	10004	82	0.29
DEL1-53.1	**1172**	**1272**	**1244**	20	59	0.04	8	0.6	1.6	0.14	14	61	111	202	10951	38	0.09
DEL1-54.1	**1120**	**1130**	**1194**	68	287	0.03	6	0.7	1.8	0.09	16	73	130	227	13078	35	0.05
DEL1-55.1	**300**	**330**	**1440**	0	60	0.27	1	0.1	0.1	0.07	1	8	13	21	11112	2	0.52
DEL1-56.1	**1145**	**1204**	**1140**	49	154	0.02	5	1.0	2.7	0.49	23	92	160	263	9855	31	0.19
DEL1-57.1	**440**	**535**	**1482**	1	392	0.03	0	0.0	0.2	0.16	4	34	53	73	16287	5	0.60
DEL1-6.1	**1209**	**1074**	**1159**	59	110	0.07	51	1.4	3.3	0.94	25	93	163	280	10799	130	0.31
DEL1-7.1	**1040**	**966**	**1010**	107	338	0.02	9	0.6	2.3	0.11	26	122	236	403	12487	79	0.04
DEL1-8.1	**994**	**963**	**977**	51	88	0.02	15	1.2	2.5	0.44	18	63	103	174	11222	109	0.19
DEL1-9.1	**1354**	**1403**	**1368**	108	158	0.04	23	0.7	1.8	0.61	14	56	113	230	11182	108	0.36
EG108C-1	**1127**	**1036**	**1077**	13	881	0.05	1	0.2	0.6	0.11	12	87	134	250	14101	7	0.13

Table A3–2. Continued.

	Age																
	207/206	206/238	208/232	Th ppm	U ppm	La ppm	Ce ppm	Nd ppm	Sm ppm	Eu ppm	Gd ppm	Dy ppm	Er ppm	Yb ppm	Hf ppm	Ce/Ce*	Eu/Eu*
EG108C-10.1	**1186**	**1274**	**1177**	23	1033	0.06	1	0.2	0.6	0.06	11	98	179	352	16021	5	0.07
EG108C-11.1	**1422**	**1052**	**1800**	98	434	0.03	10	0.9	2.3	0.88	21	94	169	311	12511	51	0.38
EG108C-12.1	**1008**	**998**	**972**	167	91	0.02	13	1.5	4.2	0.23	19	23	13	11	14592	64	0.08
EG108C-13.1	**1022**	**1087**	**1016**	170	148	0.02	12	1.7	4.7	0.28	24	32	17	14	14689	58	0.08
EG108C-14.1	**1032**	**729**	**1003**	5	171	0.06	1	0.5	0.7	0.13	6	27	40	67	12250	5	0.19
EG108C-15.1	**1007**	**1034**	**903**	63	602	0.12	7	0.9	2.0	0.19	14	42	67	166	14281	14	0.11
EG108C-16.1	**1248**	**1318**	**1190**	28	1066	0.07	2	0.3	0.8	0.07	13	109	182	327	16016	6	0.06
EG108C-17.1	**988**	**1075**	**997**	151	115	0.05	12	1.6	4.3	0.24	21	27	14	13	14176	40	0.08
EG108C-18.1	**1901**	**2365**	**2054**	137	210	0.03	51	0.6	1.6	0.59	14	67	148	329	12378	327	0.38
EG108C-19.1	**709**	**648**	**640**	67	256	0.12	6	1.2	2.6	0.37	20	49	48	92	15294	12	0.16
EG108C-2.1	**983**	**927**	**1014**	146	355	0.03	13	1.6	4.9	0.24	24	18	5	4	14179	53	0.07
EG108C-20.1	**1040**	**1073**	**997**	211	183	0.02	25	0.8	2.3	0.33	19	61	103	186	13175	166	0.15
EG108C-21.1	**1645**	**1865**	**1881**	218	313	0.05	52	2.6	4.6	1.29	30	102	184	353	11305	132	0.33
EG108C-22.1	**1230**	**1141**	**1538**	40	619	0.03	3	0.2	0.5	0.13	7	65	181	534	14253	26	0.22
EG108C-23.1	**997**	**892**	**972**	115	179	0.01	9	0.7	2.7	0.18	15	14	5	4	13492	86	0.09
EG108C-24.1	**1244**	**1165**	**1258**	38	661	0.04	3	0.4	1.2	0.21	13	76	147	316	13642	17	0.16
EG108C-25.1	**1167**	**1057**	**1052**	24	742	0.05	1	0.2	0.7	0.09	10	68	111	208	14518	8	0.11
EG108C-26.1	**1147**	**1131**	**1079**	111	1817	0.29	7	0.5	1.4	0.29	18	147	443	1129	13450	9	0.18
EG108C-27.1	**1319**	**1559**	**1320**	144	507	0.07	20	2.4	4.2	1.02	31	108	193	402	12891	44	0.27
EG108C-28.1	**1023**	**1039**	**836**	85	673	0.05	4	0.4	1.8	0.18	18	56	47	71	14224	22	0.09
EG108C-29.1	**1188**	**1095**	**1436**	30	655	0.25	5	0.8	1.1	0.38	10	62	127	306	13225	7	0.34
EG108C-3.1	**1202**	**920**	**875**	35	290	1.40	8	0.6	1.7	0.23	14	51	76	120	8665	4	0.15
EG108C-30.1	**1834**	**1709**	**1816**	114	167	0.04	25	0.6	1.5	0.35	13	59	111	210	11000	118	0.24
EG108C-31.1	**1357**	**1301**	**1347**	46	82	0.02	7	0.8	2.4	0.66	26	93	158	253	12202	57	0.25
EG108C-32.1	**1848**	**2045**	**2102**	102	191	0.04	18	0.9	2.8	0.71	23	104	200	375	10554	77	0.27
EG108C-33.1	**1000**	**1099**	**1048**	193	131	0.04	16	2.0	5.4	0.39	27	37	27	31	14028	56	0.10
EG108C-34.1	**1023**	**1012**	**989**	222	149	0.02	11	1.0	3.3	0.11	14	14	7	7	14622	76	0.05
EG108C-35.1	**1235**	**1036**	**1048**	93	566	0.15	12	1.3	2.7	0.52	18	69	138	306	12348	19	0.23
EG108C-36.1	**1353**	**1551**	**1455**	277	386	0.03	61	1.3	3.1	0.95	26	120	246	507	11687	289	0.32
EG108C-37.1	**1202**	**941**	**996**	145	534	0.11	6	1.1	3.1	0.23	19	83	129	228	14244	12	0.09
EG108C-38.1	**1081**	**1016**	**1061**	138	237	0.03	15	0.6	2.4	0.21	25	117	222	382	12343	90	0.08
EG108C-39.1	**1158**	**1166**	**1397**	45	780	0.03	4	0.5	1.2	0.23	13	99	191	408	14422	25	0.17
EG108C-4.1	**1241**	**1062**	**1096**	465	658	0.24	22	2.7	5.2	0.38	43	165	297	538	11275	20	0.08
EG108C-40.1	**1109**	**1148**	**1044**	264	314	0.05	12	1.3	3.4	0.38	20	61	106	206	12536	39	0.14
EG108C-5.1	**1359**	**1352**	**1315**	115	181	0.01	47	0.7	2.0	0.75	18	87	185	386	11888	434	0.38
EG108C-6.1	**1363**	**1193**	**1005**	117	1351	3.86	23	11.1	5.6	1.33	17	66	166	697	21792	2	0.41
EG108C-7.1	**2202**	**1879**	**1891**	111	238	0.02	15	0.3	0.9	0.34	8	42	96	219	11831	153	0.38
EG108C-8.1	**1068**	**893**	**998**	69	764	0.14	4	0.7	1.6	0.17	19	102	124	147	13823	8	0.10
EG108C-9.1	**1160**	**1237**	**1184**	67	1500	1.45	30	2.6	1.8	0.48	11	61	156	437	17362	8	0.32
EMUC-1.1	**1065**	**1088**	**1065**	215	408	0.02	46	1.1	2.7	0.51	25	123	254	530	10796	264	0.19
EMUC-10.1	**1304**	**1230**	**1224**	256	453	3.01	73	7.1	4.1	0.79	28	129	276	550	11651	9	0.22
EMUC-12.1	**1124**	**1119**	**1128**	61	172	0.02	22	0.3	0.9	0.14	8	40	91	198	12007	218	0.15
EMUC-13.1	**1304**	**1285**	**1290**	229	658	0.03	15	0.9	3.0	0.08	34	150	283	477	13511	85	0.02
EMUC-14.1	**1139**	**1101**	**1080**	70	171	0.04	6	1.8	4.3	0.19	36	131	220	355	10383	22	0.05
EMUC-15.1	**1161**	**1166**	**1165**	135	290	0.02	32	0.6	1.5	0.37	11	54	108	239	10021	248	0.27
EMUC-16.1	**1152**	**1119**	**1125**	128	801	0.11	8	0.8	2.8	0.56	29	108	186	345	11809	18	0.19
EMUC-17.1	**1944**	**1283**	**1572**	266	439	8.78	44	12.3	14.3	3.42	92	304	480	758	7756	2	0.29
EMUC-18.1	**1325**	**1295**	**1297**	440	395	0.11	48	6.2	15.1	5.02	153	580	991	1586	8728	54	0.32
EMUC-19.1	**1064**	**1048**	**1036**	159	208	0.66	19	10.7	19.7	2.18	138	438	658	955	7575	5	0.13
EMUC-2.1	**1151**	**1162**	**1146**	220	497	0.03	24	2.3	5.5	0.15	48	183	316	506	11042	104	0.03
EMUC-20.1	**984**	**969**	**960**	70	112	0.08	17	5.4	9.3	2.30	56	172	255	408	9008	24	0.31
EMUC-21.1	**1114**	**1008**	**1042**	64	193	0.09	22	0.7	1.8	0.22	18	89	166	274	9198	62	0.12
EMUC-22.1	**1310**	**1286**	**1287**	48	91	0.02	12	0.6	1.4	0.25	12	48	94	185	9221	115	0.19
EMUC-23.1	**1148**	**1053**	**1097**	83	164	0.03	15	0.8	2.5	0.23	24	99	185	322	11138	85	0.09
EMUC-24.1	**912**	**886**	**943**	55	167	0.01	17	0.6	1.6	0.10	17	78	148	262	12958	198	0.06
EMUC-25.1	**1168**	**1162**	**1135**	41	124	0.01	12	0.7	1.7	0.08	15	65	120	217	10984	141	0.05

Table A3–2. Continued.

	207/206	Age 206/238	208/232	Th ppm	U ppm	La ppm	Ce ppm	Nd ppm	Sm ppm	Eu ppm	Gd ppm	Dy ppm	Er ppm	Yb ppm	Hf ppm	Ce/Ce*	Eu/Eu*
EMUC-26.1	**1162**	**1111**	**1141**	103	341	0.01	17	0.6	1.4	0.09	14	63	127	242	11768	186	0.06
EMUC-27.1	**1113**	**972**	**977**	97	157	0.05	9	2.0	4.1	0.32	39	144	237	360	10786	26	0.08
EMUC-28.1	**1743**	**1646**	**1601**	176	169	0.04	37	2.7	4.2	1.23	28	83	144	259	9000	105	0.34
EMUC-29.1	**1339**	**1207**	**1215**	161	307	0.03	39	2.6	6.4	1.12	62	219	357	522	9497	133	0.17
EMUC-3.1	**1355**	**1199**	**1251**	39	79	0.04	9	0.8	2.2	1.19	21	92	174	306	9190	38	0.53
EMUC-30.1	**1062**	**1053**	**1032**	466	274	0.47	65	9.3	10.2	4.53	55	112	150	242	8001	25	0.58
EMUC-31.1	**1322**	**1193**	**1214**	78	155	0.02	17	0.9	2.1	0.59	17	63	131	256	10183	125	0.30
EMUC-32.1	**1221**	**1049**	**1319**	71	463	2.20	20	2.2	2.1	0.68	10	44	87	226	13375	4	0.44
EMUC-33.1	**1100**	**1069**	**1077**	59	146	0.04	16	4.0	8.1	1.47	64	222	340	469	7561	40	0.20
EMUC-34.1	**1190**	**1173**	**1182**	159	289	1.51	30	4.1	7.3	2.48	57	219	410	762	10890	7	0.37
EMUC-35.1	**1163**	**1088**	**1168**	163	619	0.33	15	0.5	0.6	0.37	4	22	57	168	11223	19	0.74
EMUC-36.1	**1169**	**1106**	**1140**	289	396	0.06	28	2.4	3.8	1.23	24	81	165	351	11211	67	0.39
EMUC-37.1	**1381**	**1351**	**1317**	55	153	0.03	25	1.5	3.6	0.21	28	93	162	267	8290	122	0.06
EMUC-38.1	**1157**	**1198**	**1184**	47	114	0.01	5	1.0	3.7	0.22	37	155	266	433	11417	45	0.06
EMUC-39.1	**1200**	**1251**	**1258**	40	120	0.02	22	1.3	3.4	0.90	34	144	252	390	8021	117	0.25
EMUC-4.1	**1932**	**2039**	**1931**	264	505	0.03	29	2.4	6.2	0.48	53	184	288	477	11656	123	0.08
EMUC-40.1	**1007**	**976**	**978**	161	201	0.01	47	1.1	2.2	0.89	18	79	163	347	9879	488	0.43
EMUC-41.1	**1150**	**1028**	**1074**	206	537	1.53	27	2.5	3.9	0.70	30	133	259	498	11795	7	0.20
EMUC-42.1	**1119**	**1089**	**1104**	97	249	0.05	17	0.5	1.5	0.09	15	76	154	285	11303	74	0.06
EMUC-43.1	**1131**	**1168**	**1133**	38	99	0.08	15	1.1	2.4	0.43	21	86	155	277	10296	36	0.18
EMUC-44.1	**1161**	**1166**	**1141**	330	328	0.04	115	3.3	5.9	3.17	43	124	186	315	7980	346	0.60
EMUC-45.1	**1159**	**1315**	**1230**	161	398	0.01	22	1.0	2.5	0.24	23	105	198	372	12073	211	0.10
EMUC-46.1	**1150**	**1159**	**1141**	111	465	0.02	19	0.2	0.4	0.16	5	33	107	318	10646	245	0.36
EMUC-5.1	**1482**	**1463**	**1428**	335	554	0.57	46	4.5	8.1	2.24	58	207	394	750	8112	19	0.31
EMUC-6.1	**953**	**898**	**928**	50	108	0.01	25	0.4	1.1	0.22	10	44	91	187	10756	271	0.21
EMUC-7.1	**1178**	**1054**	**1039**	117	203	0.35	17	2.6	5.6	0.51	46	168	281	444	9817	12	0.10
EMUC-8.1	**1357**	**1225**	**1264**	87	195	2.06	22	1.7	1.9	0.94	15	53	109	240	9610	6	0.53
EMUC-9.1	**1317**	**1279**	**1283**	364	446	0.01	159	1.1	2.6	0.84	30	152	404	962	12261	1805	0.29
MAS1-1.1	**1120**	**928**	**927**	24	113	0.06	6	0.7	1.3	0.23	12	52	100	181	8428	24	0.18
MAS1-10.1	**1022**	**894**	**876**	66	109	0.02	15	2.7	4.9	1.01	28	81	119	190	9720	61	0.26
MAS1-11.1	**1024**	**1052**	**1028**	69	166	0.01	16	0.6	1.9	0.27	17	70	126	216	10101	176	0.14
MAS1-12.1	**732**	**520**	**534**	141	2027	1.85	104	68.2	47.3	23.15	106	183	188	291	12103	8	0.99
MAS1-13.1	**469**	**443**	**430**	145	265	0.02	28	0.9	2.1	1.11	20	85	162	311	12131	209	0.52
MAS1-14.1	**448**	**451**	**335**	93	971	0.35	17	4.6	5.9	3.31	33	99	163	317	10491	10	0.72
MAS1-15.1	**1126**	**925**	**875**	62	213	0.36	12	3.0	5.7	0.57	44	152	249	371	8308	8	0.11
MAS1-16.1	**1149**	**1125**	**1128**	262	237	0.06	8	6.0	15.7	3.41	110	339	494	720	8334	14	0.25
MAS1-17.1	**1068**	**1024**	**1014**	83	244	0.01	24	0.4	1.1	0.63	8	35	65	135	9657	402	0.65
MAS1-18.1	**1294**	**1232**	**963**	65	182	0.01	12	0.1	0.2	0.07	2	13	41	126	12093	235	0.33
MAS1-19.1	**892**	**887**	**906**	143	86	0.02	28	0.7	1.2	0.61	8	30	51	89	7760	210	0.57
MAS1-2.1	**1229**	**1185**	**1147**	280	675	0.02	23	2.0	5.1	0.67	49	219	437	782	9083	124	0.13
MAS1-20.1	**1166**	**1113**	**1071**	124	176	0.02	18	1.5	3.5	0.94	30	120	219	390	9332	111	0.27
MAS1-21.1	**996**	**929**	**929**	94	326	0.01	36	0.3	0.9	0.15	8	41	96	216	11517	597	0.17
MAS1-22.1	**1303**	**1229**	**1233**	66	230	0.01	1	1.5	4.7	0.12	49	242	469	778	11156	9	0.02
MAS1-23.1	**502**	**404**	**427**	293	325	0.11	55	4.3	8.0	3.04	52	175	278	454	10115	70	0.45
MAS1-24.1	**1043**	**879**	**896**	49	138	0.01	9	0.6	1.3	0.20	10	37	61	102	8316	114	0.16
MAS1-25.1	**1100**	**822**	**982**	143	1135	0.77	10	6.8	9.9	2.97	61	223	383	716	10507	3	0.37
MAS1-26.1	**1056**	**853**	**874**	13	47	0.01	16	0.5	1.3	0.50	10	39	74	135	8471	271	0.41
MAS1-27.1	**427**	**407**	**402**	216	322	0.11	33	4.4	9.1	4.10	64	195	301	491	8289	42	0.52
MAS1-28.1	**965**	**708**	**761**	279	849	0.11	15	3.2	5.8	1.24	35	122	217	410	10471	21	0.26
MAS1-29.1	**1133**	**1002**	**980**	44	178	0.09	12	1.0	2.3	0.25	20	84	152	248	8157	27	0.11
MAS1-3.1	**1267**	**1511**	**1193**	117	353	0.01	19	0.8	2.3	0.43	22	98	193	361	7688	159	0.19
MAS1-30.1	**944**	**712**	**652**	88	1444	1.20	25	7.0	5.2	1.00	17	67	149	406	10054	6	0.32
MAS1-31.1	**456**	**367**	**387**	1033	878	0.28	135	7.2	14.6	5.82	110	392	650	1011	6265	79	0.44
MAS1-32.1	**1151**	**918**	**941**	52	306	0.04	2	0.8	2.2	0.25	22	103	206	417	11086	9	0.11
MAS1-33.1	**1065**	**944**	**904**	45	357	0.01	7	0.1	0.4	0.17	4	21	41	83	11237	196	0.37
MAS1-34.1	**1074**	**991**	**1005**	219	313	0.08	21	2.7	3.8	2.60	22	67	112	209	8975	40	0.86

Table A3–2. Continued.

	207/206	Age 206/238	208/232	Th ppm	U ppm	La ppm	Ce ppm	Nd ppm	Sm ppm	Eu ppm	Gd ppm	Dy ppm	Er ppm	Yb ppm	Hf ppm	Ce/Ce*	Eu/Eu*
MAS1-35.1	**946**	**880**	**886**	23	52	0.01	12	0.5	1.3	0.27	10	43	80	145	9721	200	0.22
MAS1-36.1	**1023**	**836**	**753**	25	152	0.14	6	1.2	1.7	0.36	10	35	64	119	8096	11	0.26
MAS1-37.1	**1173**	**1098**	**1103**	59	168	0.04	6	4.1	8.0	1.59	50	169	289	481	6098	18	0.24
MAS1-38.1	**1044**	**904**	**912**	150	152	0.03	21	4.9	8.2	1.26	45	115	148	202	8766	56	0.20
MAS1-39.1	**1049**	**950**	**953**	72	150	0.01	13	1.0	2.2	0.55	18	66	111	194	9203	144	0.27
MAS1-4.1	**961**	**685**	**453**	117	855	1.19	22	6.9	6.4	2.81	22	91	194	478	13544	5	0.73
MAS1-40.1	**1160**	**1028**	**1084**	70	245	0.41	17	5.0	8.2	0.79	55	196	312	449	7869	9	0.11
MAS1-41.1	**972**	**911**	**878**	96	982	1.36	9	2.3	2.5	0.61	20	87	102	129	11156	3	0.27
MAS1-42.1	**1158**	**961**	**1015**	61	89	0.01	10	0.9	2.1	0.38	17	62	106	179	8886	140	0.19
MAS1-43.1	**1297**	**1164**	**1057**	92	427	0.01	6	0.5	1.9	0.28	21	102	186	305	12149	72	0.13
MAS1-44.1	**992**	**939**	**968**	61	173	0.17	23	2.3	4.7	0.90	33	109	182	306	8488	27	0.22
MAS1-45.1	**1149**	**1069**	**1089**	145	339	0.01	50	0.9	1.7	0.41	13	68	164	377	7878	601	0.26
MAS1-46.1	**1334**	**1054**	**1099**	201	387	0.05	24	3.0	7.4	0.47	62	240	431	660	9608	61	0.07
MAS1-47.1	**1045**	**922**	**969**	34	108	0.01	31	0.4	0.8	0.45	6	29	69	144	5587	461	0.61
MAS1-48.1	**997**	**1012**	**944**	35	156	0.01	19	0.6	1.6	0.47	14	57	107	200	9497	329	0.30
MAS1-5.1	**1143**	**1156**	**1015**	133	577	0.55	15	2.0	1.3	0.70	7	39	92	188	13607	9	0.70
MAS1-6.1	**1002**	**913**	**752**	41	504	0.01	17	0.2	0.8	0.37	12	92	227	584	12289	224	0.35
MAS1-7.1	**435**	**389**	**417**	123	839	0.02	20	1.5	3.0	1.24	22	83	146	283	11609	108	0.46
MAS1-8.1	**1140**	**1001**	**1007**	35	437	0.04	2	0.6	2.4	0.15	20	43	56	126	12683	8	0.07
MAS1-9.1	**1162**	**1101**	**1069**	42	60	0.04	6	4.0	7.2	1.53	47	151	227	345	8799	16	0.25
R24-1.1	**1110**	**1067**	**1049**	134	190	0.02	12	0.5	1.2	0.45	10	39	62	104	12303	102	0.39
R24-10.1	**990**	**886**	**893**	92	563	0.09	12	0.6	1.0	0.41	8	45	103	235	10966	35	0.43
R24-11.1R	**1023**	**854**	**915**	7	23	0.01	8	0.2	0.6	0.21	5	20	39	79	11174	103	0.38
R24-12.1	**1024**	**887**	**908**	235	1009	0.04	11	0.5	1.5	0.54	14	60	132	301	9526	55	0.36
R24-13.1	**1201**	**1221**	**1188**	575	844	1.69	21	3.3	7.4	1.79	60	229	447	808	8395	5	0.26
R24-14.1	**917**	**791**	**904**	7	23	0.02	8	0.2	0.6	0.25	5	19	37	73	9607	81	0.45
R24-15.1	**993**	**868**	**868**	148	172	0.02	8	0.3	0.6	0.49	6	19	28	41	9318	87	0.80
R24-16.1	**1046**	**822**	**985**	713	1011	0.05	18	0.6	2.0	0.74	24	99	178	329	10876	77	0.33
R24-17.1	**1050**	**785**	**805**	45	84	0.04	11	0.3	1.0	0.57	8	35	68	132	12062	64	0.61
R24-18.1	**1212**	**1065**	**1072**	792	1166	0.06	49	0.6	1.2	0.91	9	34	73	180	12306	182	0.82
R24-19.1	**1205**	**1011**	**1032**	311	288	0.37	44	14.5	15.3	4.77	78	176	303	528	6240	17	0.42
R24-2.1	**986**	**963**	**960**	15	40	0.02	9	0.3	0.7	0.33	6	24	46	94	10879	100	0.49
R24-20.1	**1035**	**926**	**995**	394	957	0.03	18	1.0	3.1	0.82	29	119	230	427	11347	92	0.26
R24-21.1	**999**	**796**	**844**	457	868	0.11	24	0.9	2.7	1.15	29	117	227	437	9446	53	0.39
R24-22.1	**1073**	**927**	**980**	97	171	0.02	16	0.5	1.2	0.37	9	26	40	72	12469	142	0.35
R24-23.1	**954**	**1012**	**954**	106	160	0.02	22	0.7	1.3	0.47	6	8	6	9	13685	197	0.53
R24-24.1	**1061**	**1035**	**1073**	510	872	0.06	19	0.6	2.3	0.72	25	104	201	392	9681	72	0.29
R24-25.1	**1035**	**665**	**927**	243	1294	0.02	9	0.2	0.9	0.22	11	61	142	300	14396	94	0.22
R24-26.1	**1106**	**995**	**1018**	782	1649	0.05	33	0.6	2.8	0.32	41	194	402	743	11528	148	0.09
R24-27.1	**1054**	**972**	**994**	88	142	0.02	17	0.6	1.4	0.54	8	16	15	19	12138	126	0.48
R24-28.1	**1022**	**1021**	**1026**	96	142	0.04	11	0.3	0.9	0.44	7	28	48	92	10425	69	0.55
R24-29.1	**1077**	**979**	**1007**	151	209	0.01	13	0.5	1.2	0.52	11	43	64	97	11892	135	0.42
R24-3.1	**1174**	**987**	**1030**	858	1068	0.04	26	0.7	2.6	0.64	32	130	244	440	8009	120	0.22
R24-30.1	**978**	**688**	**757**	108	385	0.15	9	0.5	0.8	0.68	8	37	84	178	11256	21	0.85
R24-31.1	**988**	**939**	**949**	261	1724	0.03	5	0.2	0.4	0.29	3	18	43	113	8858	55	0.76
R24-32.1	**983**	**820**	**987**	101	1269	0.07	5	0.7	0.9	0.50	8	56	140	364	12421	17	0.56
R24-33.1	**1154**	**984**	**1262**	92	1233	0.03	6	0.2	0.5	0.17	7	45	138	402	13108	47	0.29
R24-34.1	**1268**	**958**	**1020**	496	968	0.04	27	0.8	2.6	0.49	32	134	276	505	10884	123	0.17
R24-35.1	**1051**	**1154**	**1137**	256	2902	0.12	10	0.7	0.9	0.33	10	98	342	1066	19527	23	0.34
R24-36.1	**1167**	**1157**	**1120**	555	520	0.01	37	1.2	3.3	0.62	33	136	245	445	15529	308	0.18
R24-4.1	**1062**	**826**	**878**	298	1481	0.07	18	0.4	1.3	0.43	13	54	125	281	11046	67	0.32
R24-5.1	**1202**	**1081**	**1095**	1584	1775	0.27	36	1.2	3.6	1.07	41	167	312	552	9757	41	0.27
R24-6.1	**989**	**873**	**783**	82	726	0.10	7	0.5	0.8	0.41	6	31	96	340	13227	19	0.60
R24-7.1	**1031**	**925**	**927**	758	1159	0.05	22	0.4	2.2	0.64	24	111	213	382	10094	108	0.27
R24-8.1	**1049**	**917**	**925**	72	103	0.05	12	0.4	1.2	0.50	9	26	31	40	10940	56	0.46
R24-9.1	**916**	**658**	**805**	37	1483	0.09	3	0.2	0.3	0.42	3	27	98	301	13899	13	1.41

Table A3–2. Continued.

	Age																
	207/206	206/238	208/232	Th ppm	U ppm	La ppm	Ce ppm	Nd ppm	Sm ppm	Eu ppm	Gd ppm	Dy ppm	Er ppm	Yb ppm	Hf ppm	Ce/Ce*	Eu/Eu*
RS711-1	**750**	**677**	**1052**	42	193	0.11	19	4.9	7.3	1.71	38	121	180	312	10849	24	0.31
RS711-10.1	**963**	**1071**	**1028**	71	174	0.03	32	0.3	0.6	0.25	5	29	64	150	12031	241	0.43
RS711-11.1	**1181**	**1044**	**1063**	24	71	0.02	14	0.6	1.1	0.28	8	35	59	112	11176	116	0.28
RS711-12.1	**989**	**1113**	**1066**	31	63	0.03	53	0.8	1.4	0.66	10	35	59	115	9170	262	0.55
RS711-13.1	**1230**	**1191**	**1160**	30	75	0.02	7	0.3	0.6	0.22	6	23	43	81	12776	58	0.35
RS711-14.1	**1136**	**1264**	**1194**	137	245	0.19	14	3.8	9.0	1.20	69	248	390	604	10446	13	0.15
RS711-15.1	**1159**	**1200**	**1159**	91	152	0.02	13	0.9	2.7	0.55	24	100	190	342	10404	75	0.21
RS711-16.1	**1009**	**1104**	**1039**	192	366	0.03	28	3.3	7.8	0.74	53	187	323	558	11521	90	0.11
RS711-17.1	**1014**	**925**	**962**	34	202	0.04	33	0.3	0.7	0.22	5	27	54	120	10929	221	0.36
RS711-17.1R	**978**	**922**	**961**	59	446	0.02	10	0.2	0.6	0.12	6	31	63	139	13367	128	0.18
RS711-19.1	**1212**	**1218**	**1223**	33	112	0.01	6	0.4	1.0	0.10	9	40	74	138	12192	67	0.09
RS711-20.1	**1157**	**1286**	**1189**	42	178	0.02	8	0.9	1.8	0.10	14	49	83	141	7968	59	0.06
RS711-21.1	**1478**	**1498**	**1443**	82	224	0.03	11	1.0	2.4	0.54	21	94	190	356	11126	58	0.23
RS711-22.1	**1440**	**1325**	**1371**	23	64	0.03	16	0.7	2.1	0.13	17	69	125	201	8735	97	0.06
RS711-23.1	**1323**	**1358**	**1466**	67	193	4.76	12	5.6	5.6	0.80	42	169	289	468	10676	1	0.16
RS711-24.1	**1003**	**1007**	**1004**	80	162	0.10	15	0.8	1.8	0.36	13	52	88	156	10619	34	0.22
RS711-25.1	**1316**	**1318**	**1357**	24	103	0.04	6	3.0	6.2	1.01	45	158	247	396	9378	17	0.18
RS711-26.1	**1475**	**1432**	**1391**	106	152	0.03	62	0.9	2.2	0.52	16	72	150	308	10730	328	0.27
RS711-27.1	**1022**	**1230**	**1059**	99	216	0.03	18	0.9	2.2	0.18	16	64	107	181	11777	97	0.09
RS711-28.1	**1015**	**984**	**985**	34	133	0.02	8	0.7	2.0	0.34	18	71	119	208	10783	66	0.17
RS711-29.1	**1106**	**1089**	**1049**	59	76	0.05	11	3.7	7.0	1.50	44	132	184	278	10239	25	0.26
RS711-2C	**996**	**916**	**922**	55	80	0.06	28	2.4	4.4	1.49	26	70	99	158	9357	63	0.43
RS711-2R	**1027**	**980**	**998**	141	356	0.05	36	1.2	2.3	0.67	15	58	99	190	10465	122	0.34
RS711-3	**1111**	**799**	**810**	57	226	0.10	15	0.4	1.0	0.10	9	49	103	208	13373	45	0.10
RS711-30.1	**1126**	**1171**	**1156**	67	155	0.02	14	1.3	3.3	0.43	29	119	207	314	9505	74	0.13
RS711-31.1	**1028**	**1011**	**1027**	182	1044	0.10	17	0.3	0.8	0.18	8	39	84	178	12226	56	0.22
RS711-32.1	**1600**	**1548**	**1486**	94	132	0.04	102	1.2	4.4	2.48	47	193	339	534	8956	423	0.52
RS711-33.1	**1142**	**1238**	**1142**	214	328	0.10	26	4.7	9.1	2.84	56	183	307	567	10849	35	0.38
RS711-34.1	**1183**	**1085**	**1081**	194	257	0.51	22	2.2	2.3	1.01	15	51	94	206	10814	13	0.53
RS711-35.1	**1152**	**1022**	**1117**	103	458	3.63	22	3.7	3.9	6.29	21	65	115	242	11992	3	2.13
RS711-36.1	**1284**	**1254**	**1240**	167	377	0.45	29	1.5	2.6	1.17	23	117	282	601	10030	21	0.46
RS711-37.1	**1040**	**987**	**979**	62	308	0.04	29	0.2	0.4	0.18	4	22	58	173	10667	220	0.42
RS711-38.1	**1080**	**1142**	**1078**	65	126	0.04	23	1.0	2.0	0.74	15	55	93	173	9437	94	0.40
RS711-39.1	**1007**	**1086**	**1022**	179	321	0.01	44	0.4	1.6	0.36	15	80	180	381	13468	472	0.23
RS711-4	**1159**	**1242**	**1204**	22	263	0.02	4	0.0	0.1	0.07	1	8	27	70	5741	121	0.74
RS711-40.1	**1230**	**1301**	**1228**	53	137	0.03	14	0.9	2.3	0.35	20	79	136	239	11115	74	0.16
RS711-41.1	**970**	**1064**	**1018**	36	81	0.03	10	0.9	2.0	0.31	15	52	78	129	10736	48	0.17
RS711-42.1	**1064**	**1175**	**1149**	52	97	0.03	9	1.2	3.0	0.36	26	104	177	291	11146	44	0.13
RS711-43.1	**1153**	**1132**	**1101**	42	133	0.03	9	0.6	1.5	0.10	14	65	122	213	12449	56	0.07
RS711-44.1	**1380**	**1478**	**1397**	27	78	0.01	8	0.6	1.6	0.29	13	58	113	215	10095	80	0.19
RS711-45.1	**951**	**868**	**850**	42	99	0.03	6	0.8	1.7	0.22	12	42	64	103	10119	39	0.15
RS711-46.1	**1113**	**1161**	**1085**	127	652	0.04	3	0.8	3.0	0.07	36	208	412	714	14192	13	0.02
RS711-47.1	**1403**	**1487**	**1434**	127	240	0.02	24	2.0	4.0	0.79	30	117	233	432	10456	115	0.22
RS711-48.1	**489**	**490**	**483**	7	432	1.51	3	0.3	0.5	0.55	6	47	124	341	14066	2	1.02
RS711-49.1	**1097**	**1148**	**1104**	162	167	0.04	52	2.0	4.6	1.08	40	154	305	585	10927	168	0.24
RS711-5	**1003**	**1083**	**1022**	256	570	0.03	78	0.7	2.3	0.34	24	143	332	684	13097	477	0.14
RS711-50.1	**1062**	**1021**	**1083**	52	275	0.02	8	0.7	1.8	0.09	19	87	165	299	11880	55	0.04
RS711-51.1	**1071**	**998**	**1037**	98	202	5.82	28	4.9	3.3	0.27	18	72	142	268	12118	2	0.11
RS711-52.1	**1188**	**1187**	**1105**	125	254	0.07	38	2.0	4.1	1.39	30	101	171	288	10414	85	0.38
RS711-53.1	**934**	**634**	**839**	256	769	6.90	74	24.3	20.3	12.96	63	157	224	474	11395	3	1.10
RS711-54.1	**1622**	**1646**	**1596**	237	442	0.07	48	0.7	2.0	0.53	18	93	204	416	12469	161	0.27
RS711-55.1	**916**	**776**	**841**	97	562	0.05	10	0.2	0.3	0.15	3	19	59	183	12816	64	0.47
RS711-56.1	**1089**	**1044**	**916**	17	406	0.03	4	0.2	0.8	0.66	7	20	30	55	12607	31	0.86
RS711-6	**1027**	**1029**	**1022**	59	191	0.01	9	0.3	0.6	0.14	6	25	50	111	12755	115	0.22
RS711-7	**1294**	**1336**	**1195**	59	124	0.02	9	0.9	2.9	0.61	29	117	202	307	10548	58	0.20
RS711-8	**2347**	**2595**	**2323**	149	164	0.01	12	0.4	1.0	0.08	8	39	85	185	11799	130	0.08

Table A3–2. Continued.

	Age																
	207/206	206/238	208/232	Th ppm	U ppm	La ppm	Ce ppm	Nd ppm	Sm ppm	Eu ppm	Gd ppm	Dy ppm	Er ppm	Yb ppm	Hf ppm	Ce/Ce*	Eu/Eu*
RS711-9.1	**1067**	**1061**	**1050**	41	114	0.03	10	0.5	1.1	0.13	9	37	65	123	11964	72	0.12
S21-1.1	**1097**	**1114**	**1068**	42	127	0.37	9	0.7	1.6	0.11	14	63	120	209	11057	9	0.07
S21-10.1	**1112**	**997**	**1037**	52	148	0.06	13	1.9	4.8	0.94	41	171	338	626	9255	33	0.20
S21-11.1	**1141**	**1085**	**1084**	629	1015	0.08	50	4.9	10.0	0.17	88	346	632	1040	11289	75	0.02
S21-12.1	**982**	**791**	**851**	68	122	0.03	28	1.5	3.2	0.33	28	90	148	244	11335	123	0.11
S21-13.1	**964**	**990**	**966**	153	501	0.14	21	2.1	4.4	0.41	33	116	185	296	10067	29	0.10
S21-14.1	**974**	**807**	**874**	250	801	0.32	51	4.5	4.9	2.13	20	71	117	265	11413	32	0.65
S21-15.1	**914**	**904**	**901**	63	217	0.01	17	0.9	2.3	0.16	21	74	125	201	12181	264	0.07
S21-16.1	**1164**	**774**	**1058**	117	636	5.04	34	8.2	6.9	2.16	34	119	208	419	10092	3	0.43
S21-17.1	**1188**	**1080**	**1172**	261	491	0.13	18	4.1	9.2	1.20	78	265	438	701	8491	22	0.14
S21-18.1	**988**	**871**	**892**	78	156	0.04	12	2.9	5.3	0.75	37	110	163	255	10858	37	0.16
S21-19.1	**1195**	**1076**	**1082**	80	200	0.02	60	0.6	1.5	0.33	11	52	101	212	11823	418	0.25
S21-2.1	**1124**	**961**	**997**	54	261	0.02	11	0.2	0.7	0.03	8	45	96	178	15457	141	0.04
S21-20.1	**1234**	**1128**	**1097**	45	106	0.01	11	0.4	1.1	0.26	9	37	71	143	10139	120	0.25
S21-21.1	**599**	**603**	**598**	40	88	0.04	25	2.3	5.0	0.45	39	147	225	334	6117	83	0.10
S21-22.1	**1206**	**935**	**1242**	40	138	0.18	16	1.3	2.7	0.45	23	94	169	286	9389	21	0.17
S21-23.1	**1129**	**1205**	**1150**	60	147	0.03	25	0.6	1.6	0.20	15	67	131	273	13824	145	0.12
S21-24.1	**1213**	**1199**	**1171**	51	91	0.04	7	2.9	4.8	0.95	32	119	220	393	8733	22	0.23
S21-25.1	**1172**	**1169**	**1152**	62	95	0.14	29	8.3	13.0	3.28	78	227	335	522	9762	27	0.31
S21-26.1	**1133**	**1084**	**1120**	38	90	0.02	12	3.4	7.1	1.75	55	179	272	383	7776	54	0.27
S21-27.1	**1125**	**997**	**1033**	106	101	0.04	44	2.3	5.3	1.51	35	114	197	348	9363	145	0.33
S21-28.1	**1031**	**653**	**813**	103	354	0.02	11	0.5	1.2	0.11	11	49	91	178	12419	95	0.09
S21-29.1	**1043**	**1034**	**986**	31	74	0.03	11	0.8	1.6	0.48	11	38	64	113	9016	59	0.35
S21-3.1	**1006**	**837**	**898**	30	93	0.01	9	0.4	1.0	0.09	9	40	78	142	11102	105	0.09
S21-30.1	**1293**	**1203**	**1246**	38	105	0.01	22	0.5	1.5	0.34	19	92	197	378	11528	233	0.19
S21-31.1	**1520**	**1310**	**1433**	39	124	0.02	14	0.4	1.4	0.18	13	63	125	239	11960	118	0.13
S21-32.1	**1028**	**928**	**951**	44	110	0.04	8	1.1	2.8	0.36	27	96	169	270	10165	30	0.13
S21-33.1	**1370**	**1326**	**1290**	112	332	0.02	22	0.9	2.7	0.20	31	145	269	433	12545	138	0.07
S21-34.1	**1193**	**1120**	**1149**	54	213	0.01	19	0.1	0.1	0.09	2	10	30	101	11322	519	0.57
S21-35.1	**1039**	**1101**	**1033**	62	131	0.01	7	0.1	0.3	0.18	3	21	53	144	13301	161	0.53
S21-36.1	**603**	**650**	**650**	57	72	0.03	12	2.0	5.1	0.54	41	134	207	339	9421	45	0.11
S21-37.1	**623**	**583**	**612**	115	174	0.05	17	3.6	6.0	0.52	40	141	235	395	11123	39	0.10
S21-38.1	**1186**	**1190**	**1177**	141	326	0.13	17	2.0	4.0	0.70	33	127	216	355	11174	26	0.19
S21-39.1	**1083**	**950**	**1007**	66	345	0.06	13	0.8	1.9	0.15	16	64	113	204	10459	43	0.08
S21-4.1	**1175**	**1139**	**1147**	68	136	0.03	31	0.9	2.3	0.50	21	85	162	313	11506	158	0.22
S21-40.1	**1157**	**1148**	**1152**	66	184	0.04	16	0.5	1.4	0.13	14	67	131	235	12321	93	0.09
S21-41.1	**1093**	**891**	**1023**	72	325	0.03	6	0.9	2.4	0.16	22	94	178	324	10904	33	0.07
S21-42.1	**919**	**904**	**972**	128	251	0.10	18	5.8	10.8	1.72	79	254	382	571	9883	22	0.18
S21-43.1	**1040**	**875**	**984**	170	173	0.07	75	2.6	4.3	1.65	27	85	144	254	8869	153	0.47
S21-44.1	**1121**	**1085**	**1065**	76	154	0.02	20	1.4	3.6	0.77	30	128	233	388	8369	112	0.22
S21-45.1	**994**	**985**	**1024**	98	408	0.11	18	0.6	1.5	0.65	15	74	166	343	12368	45	0.42
S21-46.1	**1156**	**1140**	**1155**	68	277	0.06	22	1.0	2.1	0.32	20	90	172	297	10093	73	0.15
S21-47.1	**998**	**975**	**974**	134	110	0.05	33	4.0	6.2	2.34	35	92	129	219	8935	76	0.48
S21-5.1	**1060**	**1050**	**1037**	607	743	0.06	158	2.2	2.9	1.05	18	65	146	349	9601	406	0.44
S21-6.1	**1235**	**1226**	**1211**	48	102	0.04	11	1.9	3.5	1.62	21	70	117	223	8822	39	0.57
S21-7.1	**1105**	**1007**	**1006**	171	213	0.03	88	2.2	3.9	1.91	28	92	163	287	9531	366	0.56
S21-8.1	**1252**	**1026**	**1116**	317	390	0.16	35	1.7	3.4	1.32	30	124	239	423	9073	49	0.40
S21-9.1	**1323**	**1434**	**1362**	12	50	0.00	15	0.6	1.7	0.43	17	103	208	318	7340	303	0.25
WG-1.1	**1144**	**978**	**1030**	79	481	0.02	8	0.3	1.3	0.11	13	67	141	291	10901	80	0.08
WG-10.1	**1169**	**1110**	**1091**	35	187	0.01	10	0.5	1.4	0.13	14	63	123	235	9597	146	0.09
WG-11.1	**1256**	**1268**	**1231**	183	456	0.04	5	1.4	4.3	0.15	41	189	349	578	10538	20	0.04
WG-12.1	**1320**	**1285**	**1264**	308	678	0.11	37	1.1	1.3	0.50	9	34	66	149	10490	77	0.43
WG-13.1	**1256**	**1228**	**1149**	136	686	0.00	8	0.6	2.5	0.13	25	103	196	341	12017	231	0.05
WG-14.1	**1269**	**1190**	**1192**	239	611	0.03	21	1.2	3.9	0.14	42	245	481	720	10153	90	0.03
WG-15.1	**1202**	**1140**	**1126**	191	977	0.08	13	0.8	1.8	0.10	17	83	178	339	10923	36	0.05
WG-16.1	**1113**	**902**	**963**	82	392	0.10	8	0.8	1.2	0.17	9	52	108	216	10424	18	0.15

Table A3–2. Continued.

	Age															
	207/206	**206/238**	**208/232**	**Tb ppm**	**U ppm**	**La ppm**	**Ce ppm**	**Nd ppm**	**Sm ppm**	**Eu ppm**	**Gd ppm**	**Dy ppm**	**Er ppm**	**Yb ppm**	**Hf ppm**	**Ce/Ce***	**Eu/Eu***
WG-17.1	**1269**	**1115**	**1111**	13	21	0.03	6	3.7	6.2	2.61	36	104	154	226	6580	18	0.53
WG-18.1	**1032**	**989**	**1014**	28	69	0.01	17	0.4	1.2	0.27	12	55	112	215	9114	358	0.21
WG-19.1	**1210**	**1057**	**1078**	60	257	0.00	7	0.4	1.3	0.06	14	64	122	210	9319	163	0.04
WG-2.1	**1185**	**977**	**988**	42	130	0.02	9	0.8	2.2	0.25	21	90	173	290	7032	52	0.11
WG-3.1	**1159**	**1090**	**1088**	60	176	0.02	4	0.8	2.5	0.17	23	91	159	253	9262	36	0.07
WG-4.1	**1062**	**965**	**978**	154	521	0.03	12	0.2	0.4	0.09	4	21	50	116	8822	108	0.22
WG-5.1	**1091**	**1073**	**1100**	197	491	0.03	50	2.1	4.1	1.35	29	113	224	580	10362	206	0.38
WG-6.1	**1518**	**1388**	**1409**	50	103	0.01	6	0.8	2.2	0.51	18	72	128	220	8552	75	0.24
WG-7.1	**1220**	**1013**	**1058**	379	844	0.16	53	2.3	2.9	1.97	18	68	153	358	7086	66	0.82
WG-8.1	**1044**	**1122**	**1353**	68	82	22.72	111	46.7	18.3	1.13	53	156	284	462	9704	2	0.11
WG-9.1	**1194**	**1079**	**1079**	456	2229	0.13	20	0.8	1.9	0.12	20	109	255	535	11217	41	0.06

Vita

Arthur James Merschat was born September 24, 1978, in Asheville, North Carolina, the second and youngest son of Carl and Holley Merschat. He grew up in Barnardsville, NC, a small town tucked away in the Blue Ridge Mountains of western North Carolina. His youth was spent playing sports: football, baseball, basketball, wrestling, racquetball, tennis, and any other possible sport. After graduating from North Buncombe High School in 1996, Arthur attended Appalachian State University in Boone, North Carolina. He majored in geology and took advantage of the opportunity to walk-on and play football for the Mountaineers. Arthur graduated with a B.S. in Geology in the spring of 2000 and enrolled that fall at the University of Tennessee to pursue an M.S. in Geology. His research was focused on the tectonics of the southern Appalachians under the supervision of Dr. Robert D. Hatcher Jr. In April, 2002, Arthur married Carrie C. Brown, the wonderful girl he met at Appalachian State University. He received his M.S. in December, 2003 from the University of Tennessee, and chose to continue his research on the tectonics of the southern Appalachians and pursue a Ph.D. in Geology under the guidance of Dr. Hatcher. Arthur will receive his Ph.D. in geology in August, 2009.